Direct Design of Reinforced and Partially Prestressed Concrete Beams for Combined Torsion, Bending and Shear

UNIVERSITY
of
GLASGOW

By

Ali Said Mohammed Alnuaimi

B.Sc. M.Sc.

A thesis submitted for the Degree of Doctor of Philosophy

Department of Civil Engineering

University of Glasgow

November 1999

Dedication

This work is dedicated to my beloved wife who gave unlimited moral support and encouragement during this research. Her assistance was the deriving force behind the completion of this study.

Acknowledgement

This work was carried out by the author under a scholarship from the government of Oman represented by Sultan Qaboos University. The author would like to acknowledge and appreciate that.

The author is indebted to his supervisor Dr. P. Bhatt for his invaluable guidance, advice, constant encouragement, and for always finding time to read through and for suggesting corrections to the manuscripts throughout the work.

The author expresses his deep gratitude to Dr. T. J. A. Agar for his interest and valuable suggestions during useful discussions.

Grateful thanks are extended to Professor N. Bicanic, head of the department for making laboratory and office facilities available.

Many thanks also to Mr. Alan Burnett and his team specially Mr. S. Mclean, Mr. R. Thornton, Mr. W. Thomson, Mr. A. Yuill, Mr. R. McCaskie and Mr. I. Gardener without whom the laboratory investigations could not have been successfully carried out.

Thanks go to Mr. McColl, computer manager of the department for his support in making computational program facilities available.

The author is also grateful to his friends in the Department of Civil Engineering in the University of Glasgow, specially Dr. B. Zhang, research assistant, Dr. X. W. Gao, research assistant, Mr. Lee Cunningham, Ph.D. student, for their friendship and discussions.

Finally, special thanks and appreciation go to my wife, children and parents for their endless patience, encouragement and support during the course of study.

Table of contents

Summary

This thesis presents experimental and computational results on reinforced and partially prestressed concrete hollow and solid beams subjected to combined bending moment, torsion and shear force. The beams were designed using the direct design method which is based on the theory of plasticity. Nielsen's 2-D yield criterion for reinforced concrete subjected to in-plane forces was the basis of the design of reinforcement. Elastic stress distribution was used for the design of hollow beams and the partially prestressed solid beams while the design of reinforced solid beams was based on a stress distribution obtained from a detailed study of the stress distribution using non-linear analysis. The main variables studied were the ratio of torsion to bending moment and the ratio of maximum shear stress due to torsion to the maximum shear stress due to shear force.

The experimental work consisted of testing eleven reinforced and partially prestressed hollow beams, and six reinforced and partially prestressed solid beams. The beam outer dimensions were 300x300mm and 3800mm long. Hollow beams had a wall thickness of 50mm. Average concrete cube strength was 46N/mm^2. The average yield strength of the reinforcement was 490N/mm^2. 5mm diameter prestressing wires with an yield strength of 1570N/mm^2 were used.

The computational work involved non-linear analysis using 2-D finite element program for the analysis of the hollow beams and 3-D program for the analysis of the solid beams. The concrete model in the 2-D program was based on work of Kupfer-Hilsdorf and in the 3-D program was based on work of Kotsovos.

Good agreement was achieved between the experimental and design values as well as between the experimental and non-linear analysis in most cases. Large variations in the ratio of torsion to bending moment and the ratio of shear stress due to torsion to shear stress due to shear force did not cause major differences between the design and experimental and computational failure loads. In the case of large torsion, however, some beams failed at about 10% below design load and some stirrups did not reach yield strength.

1: Introduction

1.1: Problem statement

The present procedures and code recommendations for the design of concrete structures (specially for shear and torsion) have been developed largely on the basis of test data on specific types of members. Design equations are an outcome of test results. The code design procedures for combined loading is conservatively done by designing for each force separately and the results are summed together algebraically.

In practice, structures are generally subjected to bending combined with torsion and/or shear. Consequently, there is interaction between these forces which determine the strength of the structure. Several interaction theories based on ultimate strength criterion have been developed by various researchers. But the general approach adopted for the development of interaction equations is still based on the experimental results as follows:

1. Identify the parameters affecting the problem.
2. Study experimentally the effects of the parameters.
3. Develop design equations based on the experimental results to define interaction curves.

This approach has certainly contributed greatly to the understanding of the problem. However, its weakness lies in the fact it is difficult to extend it to more generalised stress situations since this can be done only if the design procedures are based on sound theoretical principals.

A proper design procedure should consider the interaction between bending, torsion and shear in the structure and ensure that the ultimate and serviceability limit states are satisfied. To be applicable for any stress field, it should be based on well established theories like, say, the theory of plasticity. In addition, it should be able to optimise the usage of material and be easy to apply.

1.2: Proposed solution

In the present investigation, a procedure called the "Direct Design Method" was adopted for the design of reinforced and partially prestressed hollow and solid beams subjected to combined loading of bending, torsion and shear. The basis of this method is the lower bound theorem of the theory of plasticity. In this approach,

a section is designed to resist a given set of stresses using elastic or plastic stress distributions and a 2-D yield criterion for "in-plane forces". In this work, the section was then tested to verify the basic assumptions adopted in the design. In addition a 2-D finite element program for the hollow beams and a 3-D one for solid beams were used for the non-linear analysis to further check the validity of the assumptions made.

1.3: Scope of work

In this research eleven hollow beams and six solid ones were designed using the direct design method and experimentally tested. Elastic stress distribution was used in the design of hollow beams and the partially prestressed solid beams while plastic stress distribution was used for the design of all reinforced solid beams, except one beam. A 2-D finite element program based on Kupfer-Hilsdorf model for concrete yield criterion was used for the non-linear analysis of hollow beams. Model parameters were based on a parametric study using the 2-D program. In the case of solid beams, a 3-D finite element program based on Kotsovos' concrete model was used for a computational study before the selection of stress distribution used for the design of solid beams. This was done to study the effect of the concrete core on beam strength and behaviour. Based on the findings, the solid beams were designed and tested. The 3-D program was then used for the non-linear analysis of the solid beams.

1.4: Thesis layout

Chapter 2 focuses on the literature review of the analytical models used for the design of reinforced beams subjected to combined loading. Chapter 3 discusses the development of the Direct Design Method. Chapter 4 describes the test rig, monitoring, loading and testing procedure of reinforced and partially prestressed beams. Chapter 5 presents the test results of the hollow beams. Chapter 6 discusses the material behaviour and modelling used in the finite element programs. In chapter 7 the 2-D finite element program is discussed. Chapter 8 gives details of a parametric study carried out to develop a general computational model for hollow beams. A comparison between experimental and computational results of hollow beams is shown in chapter 9. In chapter 10 theoretical investigation on the stress distribution in solid beams is carried out. The results of the investigation were used

in the design and test of solid beams described in chapter 11. Chapter 12 gives conclusions and recommendations. Appendix A has a numerical design example using the truss analogy. Appendix B contains comparison between experimental and computational steel strain ratios for hollow and solid beams. Appendix C contains examples on the effect of the centre line of shear flow on the steel requirement.

2: Analytical models for combined loading in reinforced concrete beams

2.1: Introduction

Considerable research has been done in an effort to develop methods for predicting the behaviour of reinforced concrete beams in pure torsion and in torsion combined with flexure and/or shear. In studying torsion, elasticity theory was used by some researchers in the first half of this century [Cowan (1965)] for the analysis of reinforced concrete beams, while others adopted the plastic theory approach [Nadai (1950)]. Analytical models were developed for the design of reinforced beams. These models enabled researchers and engineers to gain a better understanding of actual structural behaviour and minimise the usage of existing empirical design equations. In this chapter a brief review of previous investigations and analytical models for fully reinforced beams (having longitudinal and transverse steel) subjected to combined load of torsion, bending and shear is presented.

2.2: Combined load in reinforced concrete beams

In rectangular sections, normal stress is caused by axial force or bending moment while shear stress due to shear force is mainly parallel to the direction of the shear force and the shear stress due to torsion circulates around the section in different directions (Fig. 2.1). The side of the section where the shear stresses are additive is critical in design. In general longitudinal and transverse reinforcements are required to resist all load conditions except in the case of pure bending where longitudinal reinforcement alone is required. It is worth mentioning that concrete strength plays a significant role in the cracking strength of a member. High strength concrete gives larger cracking torque. Also, the concrete cover affects the cracking strength. For two beams of same overall dimensions, the one with smaller cover results in a bigger torque capacity due to the longer lever arm.

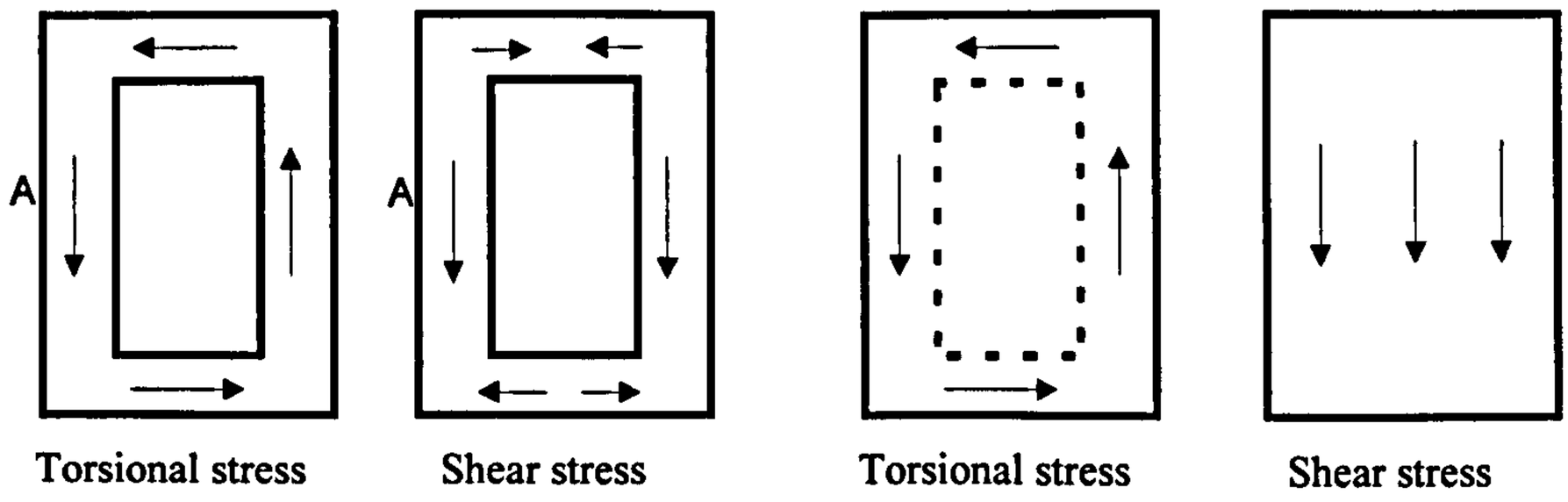

Fig. 2.1: Applied stresses due to torsion and shear force in a rectangular section

2.2.1: Pre-cracking strength

Before cracking, load is resisted mainly by concrete and steel is virtually unstressed. Cracks start when the maximum principal tensile stress reaches the tensile strength of the concrete. This behaviour is true even for beams having steel in both directions. Because of this, reinforced concrete beams before cracking stage can be treated as plain concrete ones using equations developed by many researchers and available in the literature [e.g. Hsu (1984)].

2.2.2: Post-cracking behaviour

Many models have been developed for predicting the behaviour of members with both longitudinal and transverse steel subjected to combined loading. These models can be categorised under two groups, the skew-bending theory and the space truss theory. In recent years, the space truss theory has dominated the research field in both design and non-linear analysis. A brief discussion of some significant developments in these theories with more emphasise towards the truss theory is presented here.

2.2.2.1: Skew-Bending Theory

Lessig (1958) proposed an approach of analysis for under-reinforced beams where the equilibrium conditions for an observed skew-bending type of failure mechanism is assumed. Inclined tension crack spiral round three faces of the beam. On the fourth side, the ends of the crack are joined by a compression zone. At failure, reinforcement is assumed to be yielding on the three sides. She presented the first two modes of failure shown in figure 2.2. Mode 1 failure happens when bending moment is predominant, tension cracks appear first on the bottom and then spreads to the side faces. The compression zone is located at the top face. Failure occurs by yielding of both bottom and transverse steels. Mode 2 failure happens when torsion and shear are predominant, and cracks appear first at an angle of about 45° to the longitudinal axis of the beam, on the vertical face in which the shear stresses due to torsion and shear are additive. These cracks later spread to the bottom and top faces. The compression zone is located along the other face where the shear stresses are subtractive.

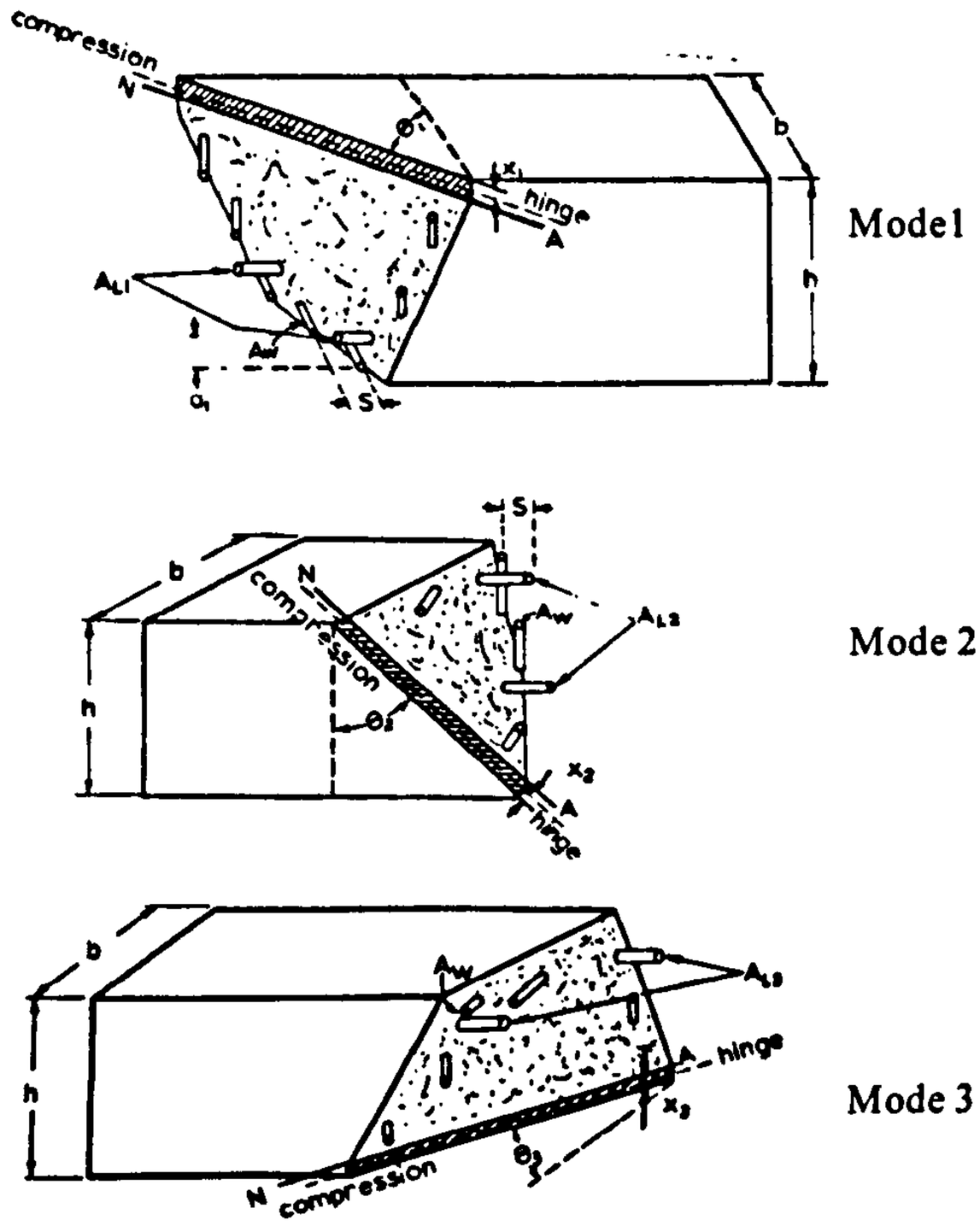

Fig. 2.2: Modes of failure

The following assumptions were made in Lessig's theory:

1. Both longitudinal and transverse steels yield at failure and no compressive reinforcement is considered.
2. Concrete resists no tension.
3. Stirrups are equally spaced.
4. No aggregate interlock or dowel action of reinforcement is considered.
5. The ratio of torsion to bending moment remains constant within the failure zone.

It should be noted that the assumptions of both longitudinal and transverse steels yield at failure and the angle of inclination is 45° require equal amount of steel in each direction.

Collins et al. (1968) discovered mode 3 failure (Fig. 2.2) and extended the analysis to a more general case of un-symmetrically reinforced members where the top longitudinal steel is significantly less than the bottom longitudinal steel and subjected to large torque and small bending moment. Cracks are initiated at the top and side faces and the compression zone is at the bottom face. Failure occurs when both top and transverse steels yield.

Elfren et al. (1974) presented interaction surface (Fig. 2.3) for three modes of failure similar to the modes discussed above. Mode *t* represents the failure mode when the concrete compression zone is in the top of the beam due to positive bending dominance. For negative or small moment the compression zone is formed in the bottom of the beam and the mode of failure is called mode *b*. Mode *s* is decisive for beams subjected to high shear stresses from both torsion and vertical shear. The compression zone forms in the vertical side where the shear stresses are subtractive.

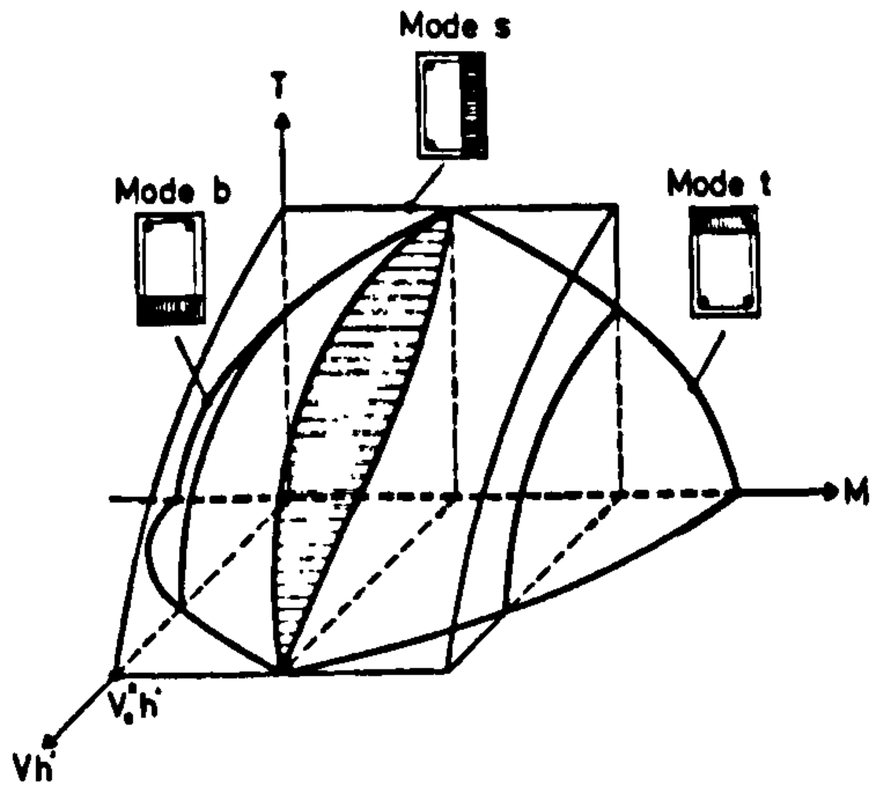

Fig. 2.3: Interaction surface for modes s, b and t [Elfren et al. (1974)]

It should be noted that the above discussed skew-bending theories were based on equilibrium of forces at assumed continuous failure surface. They can predict the ultimate strength of under reinforced members where steel is assumed to yield at failure.

Ewida and McMullen (1981) presented a non-dimensionalised torsion-shear-flexure interaction equations for under-reinforced, partially over-reinforced, and completely over-reinforced beams. Their model predicts different curves for under reinforced and completely over-reinforced beams subjected to combined loading of torsion and shear (Fig. 2.4). The under-reinforced beams fail due to steel yielding while the completely over-reinforced ones fail due to concrete crushing. The strength of a beam is defined as the smallest of the three strengths computed according to the three modes of failure. The non-dimensionalised interaction surface proposed by Ewida and McMullen for torsion-shear-flexure is shown in figure 2.5. In this figure:

M_u = ultimate flexural moment in combined loading.

M_{uo} = ultimate flexural moment in pure bending.

V_u = ultimate shear force in combined loading.

V_{uo} = ultimate shear force in pure shear.

T_u = ultimate torque in combined loading.

T_{uo1} = ultimate torque in pure torsion for mode 1.

T_{uo2} = ultimate torque in pure torsion for mode 2.

$r = T_{uo2} / T_{uo1}$

n = 1.2 for beams under-reinforced in torsion-shear.

n = 1.75 for beams partially over-reinforced in torsion-shear.

n = 3.0 for beams completely over-reinforced in torsion-shear.

The power n, greater than 1 applied to the normalised shear term only, suggests that a small change in torque affects the shear strength more than the other way round. Similarly the power value 2 used for the normalised torsion and shear in the case of bending presence shows that the torsion and shear strengths can be increased by the presence of bending and not the other way round.

More can be found about skew-bending theory in the literature i.e. Goode and Helmy (1968).

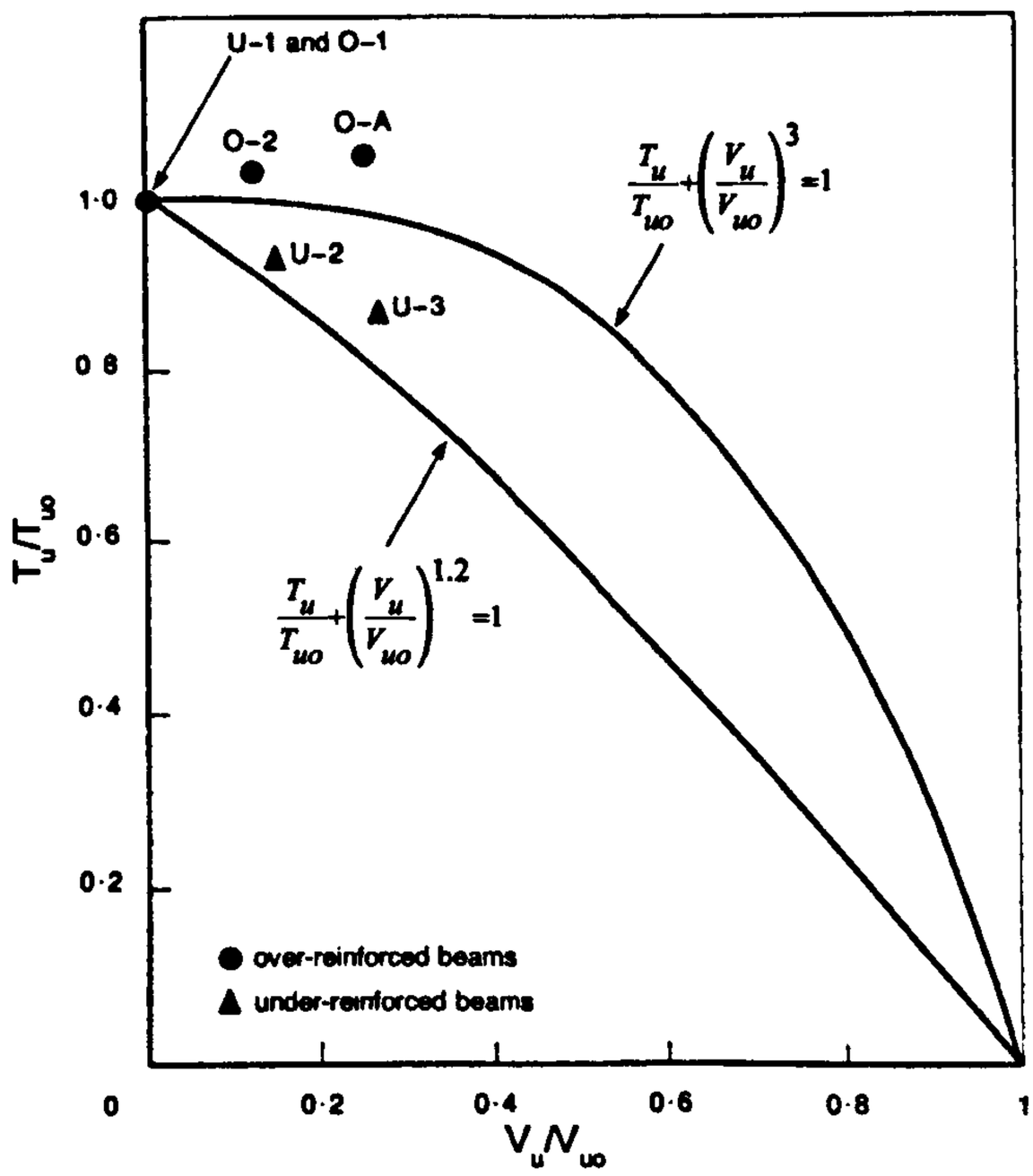

Fig. 2.4: Torsion-shear interaction diagrams for under-reinforced and completely over-reinforced beams [Ewida and McMullen (1981)]

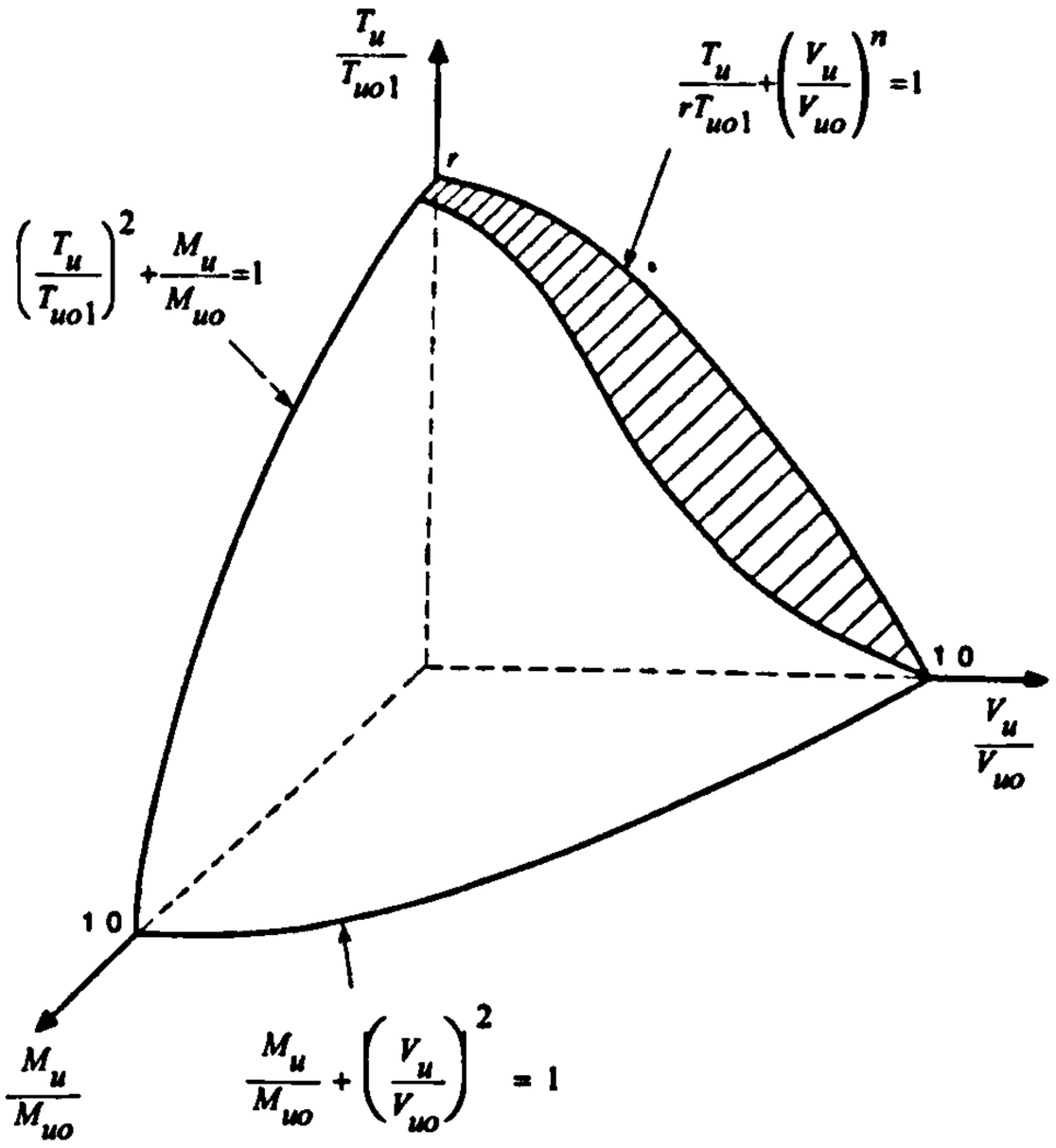

Fig. 2.5: Torsion-shear-flexure interaction surface [Ewida and McMullen (1981)]

2.2.2.2: The space-truss analogy

45° Truss Model: Ritter (1899) and Morsch (1902) were the pioneers who introduced the truss analogy to analyse cracked reinforced beams subjected to shear. However, Rausch (1929) was the first to apply the truss analogy to beams subjected to torsion.

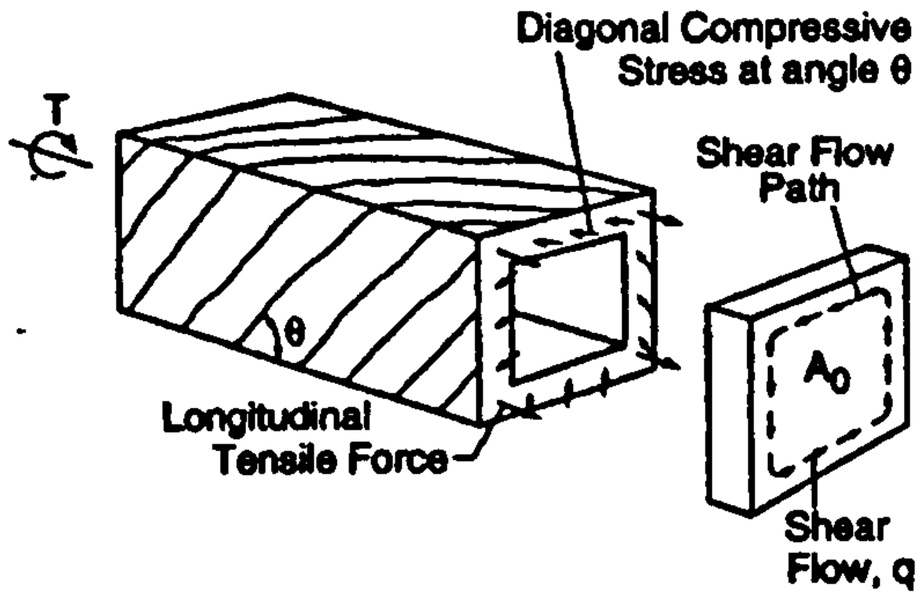

Fig. 2.6: Rectangular beam under torsion

These models were based on the following assumptions (Fig. 2.6):

1. The space truss is made up of 45° diagonal concrete struts, longitudinal bars, and hoop bars connected at the joints by hinges.
2. The diagonal concrete member carries only axial compression; i.e. shear resistance by aggregate interlock is neglected.

3. The longitudinal and transverse bars carry only axial load i.e. dowel action resistance is ignored.
4. For a solid section, the concrete core does not contribute to the ultimate torsional resistance.
5. In the case of pure torsion, the path of the shear flow coincides with the centreline of the closed stirrup.

These models assume that the volume of all longitudinal steel within the stirrup spacing is equal to the volume of one complete stirrup. This is so called the equal volume principal which allows the concrete to form 45° inclined struts which might be possible in the case of shear or torsion. Test results [i.e. Hsu (1968), Mattock (1968) and Osburn et al. (1969)] revealed that the 45° model is quite conservative, particularly for beams with small amounts of web reinforcement.

Many models have been proposed using the truss analogy after the above models were developed. A brief discussion of a few significant changes is presented here.

Variable Angle Truss Model: Lampert and Thurlimann (1971) generalised the space truss model for under reinforced members subjected to torsion or to combined torsion and bending. They assumed that the angle of inclination of the concrete struts is constant for each side and may deviate from 45°. In the walls governing the failure, both longitudinal and transverse steel reach yield at failure. They assumed an elastic-perfectly plastic stress-strain curve for reinforcement. The 45° model became a special case of their model when equal volume reinforcement is provided. They also assumed that the shear flow uses a path defined by a line connecting the centres of the longitudinal corner bars enclosed by the stirrups. In this model the superposition approach of steel required to resist torsion and that required to resist bending was adopted. In the tensile zone the two longitudinal steel components are added, whereas in the flexural compression zone, the longitudinal torsional reinforcement can be reduced by an amount corresponding to the flexural compressive force as shown in figure 2.7. They presented interaction curves for rectangular sections subjected to combined torsion and bending. Figure 2.8 shows these curves for $Z_{fu}/Z_{fo} = 3$ (solid line) and $Z_{fu}/Z_{fo} = 1$ (dashed line), where Z_{fu} and Z_{fo} = yield force in the bottom and top longitudinal reinforcement respectively. It can be seen that the torsional strength of a section, reinforced for bending (Z_{fu} >

Z_{fo}), can be increased by the simultaneous application of a bending moment as at point A at which all reinforcements of the section yield. For a section reinforced for pure torsion ($Z_{fu} = Z_{fo}$), the maximum torque occurs when the bending moment equal to zero. In this case, both top and bottom reinforcement and the stirrups yield.

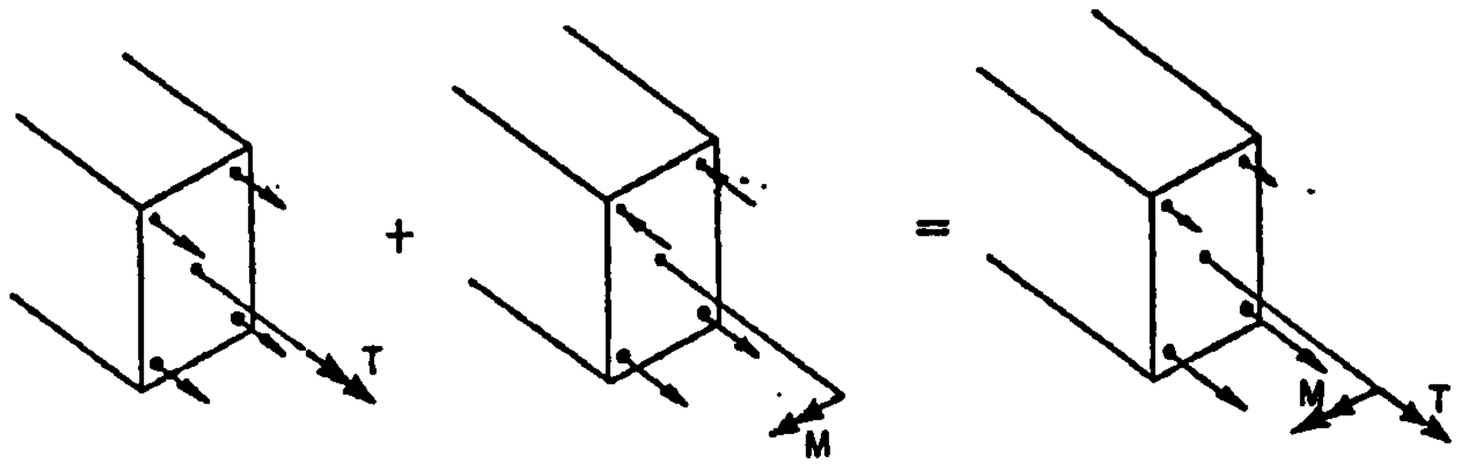

Fig. 2.7: Superposition of forces in longitudinal reinforcement

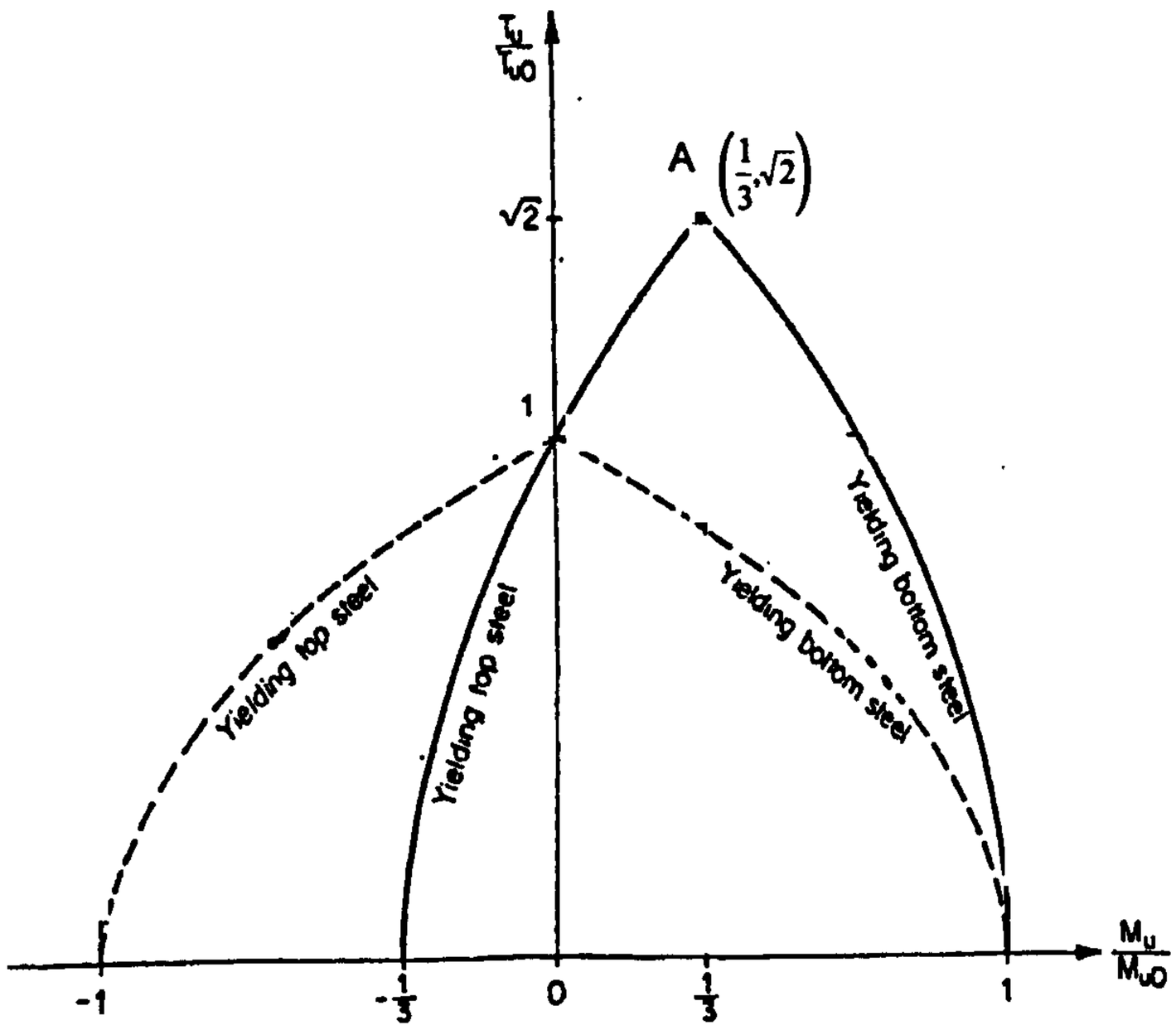

Fig. 2.8: Interaction surface for torsion-bending in a rectangular cross-section [Lampert and Thurlimann (1971)]. M_u, T_u = ultimate bending and torsional moments in combined loading receptively. M_{uo}, T_{uo} = ultimate bending and torsional moments for pure bending and pure torsion receptively.

Compression Field Theory: Collins and Mitchell (1980) suggested a compatibility relationship which links the strains in the concrete diagonals, the longitudinal steel and the transverse steel as given by equation 2.1.

$$\tan^2\theta = \frac{\varepsilon_l + \varepsilon_d}{\varepsilon_t + \varepsilon_d} \qquad 2.1$$

where:

θ = the angle of inclination of the diagonal struts

ε_l = longitudinal tensile strain

ε_t = transverse tensile strain

ε_d = diagonal compressive strain

They used this equation for the prediction of the equilibrium equations of the truss, and the stress-strain relationships of concrete and steel in reinforced concrete members subjected to shear or torsion. Thus the compression field theory can predict the angle of inclination of the diagonal compression.

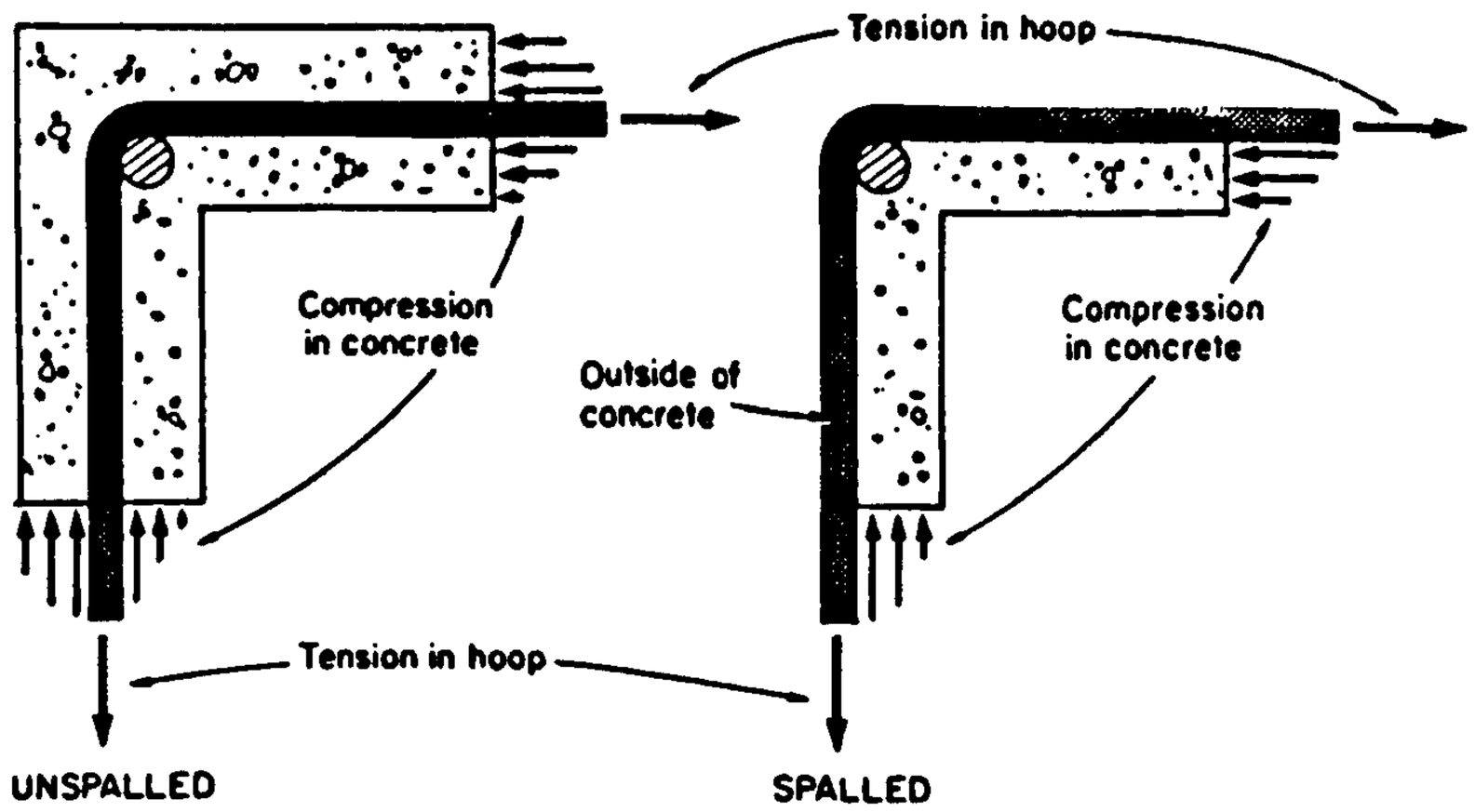

(a): Spalling of concrete cover due to torsion

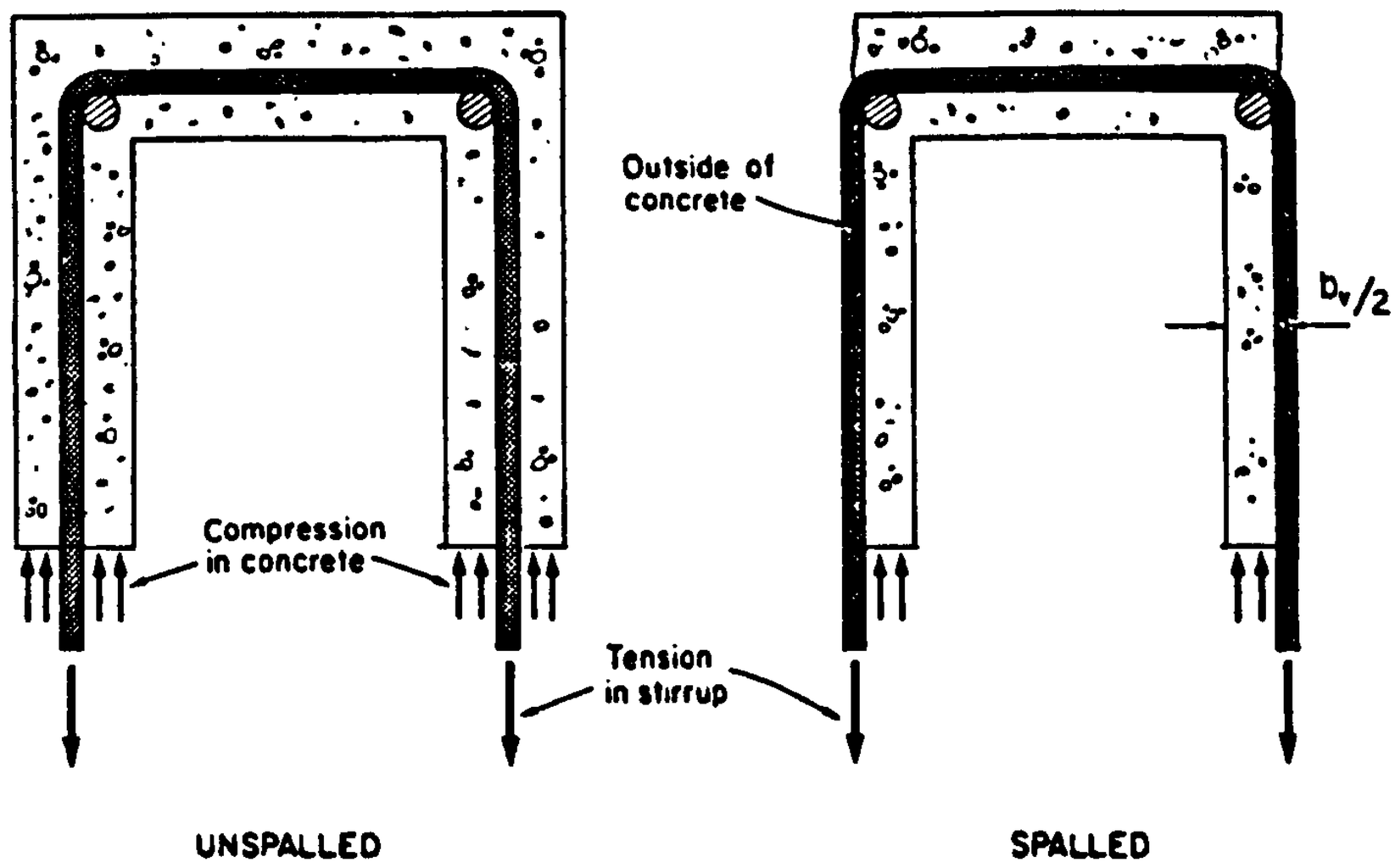

(b): Spalling of concrete cover due to shear

Fig. 2.9: Spalling of concrete

In this theory it was assumed that the compression in the concrete tends to push off the concrete while the tension in the stirrups holds it on (Fig 2.9). Since concrete is weak in tension, the concrete outside of the stirrups spalls off. Because of this spalling it was assumed that the effective outer surface of the concrete coincides with the stirrup centreline. The compression field theory assumes that diagonal compressive stresses can be transmitted through cracked concrete by means of aggregate interlock and dowel action of reinforcement crossing the crack. For the usage of this theory in the design of reinforced or prestressed members, reader is referred to the reference quoted above.

Modified Truss Model: Ramirez and Breen (1991) suggested a concrete contribution to be added to the truss action to compensate for the difference between the test results and the conservative truss model. This is to account for the shear carried by the un-cracked concrete, aggregate interlock, and dowel action. Figure 2.10a shows the concrete contribution for reinforced members in shear. The vertical axis represents the concrete contribution in terms of nominal shearing stresses v_c. The horizontal axis represents the shear stress level v produced by the applied loading. For example when the applied load causes shear stress less than $2\sqrt{f_c'}$, the contribution v_c is constant ($=2\sqrt{f_c'}$) while when it causes shear stress equal $6\sqrt{f_c'}$ the contribution becomes zero.

In the case of prestressed members, the presence of the prestressing force enhances the effect of the aggregate interlock and un-cracked concrete resistance to shear. A constant concrete contribution which is a function of the level of prestress and extreme tension fibre stresses such as shown in figure 2.10b was proposed. The total available shear capacity of this modified model is:

$$v_{MTM} = v_{Truss} + v_c \qquad 2.2$$

Ramirez and Breen tried their model on 59 reinforced concrete beams and 77 pretensioned concrete beams. The model provided generally conservative values in reinforced and prestressed beams as can be seen in figure 2.11.

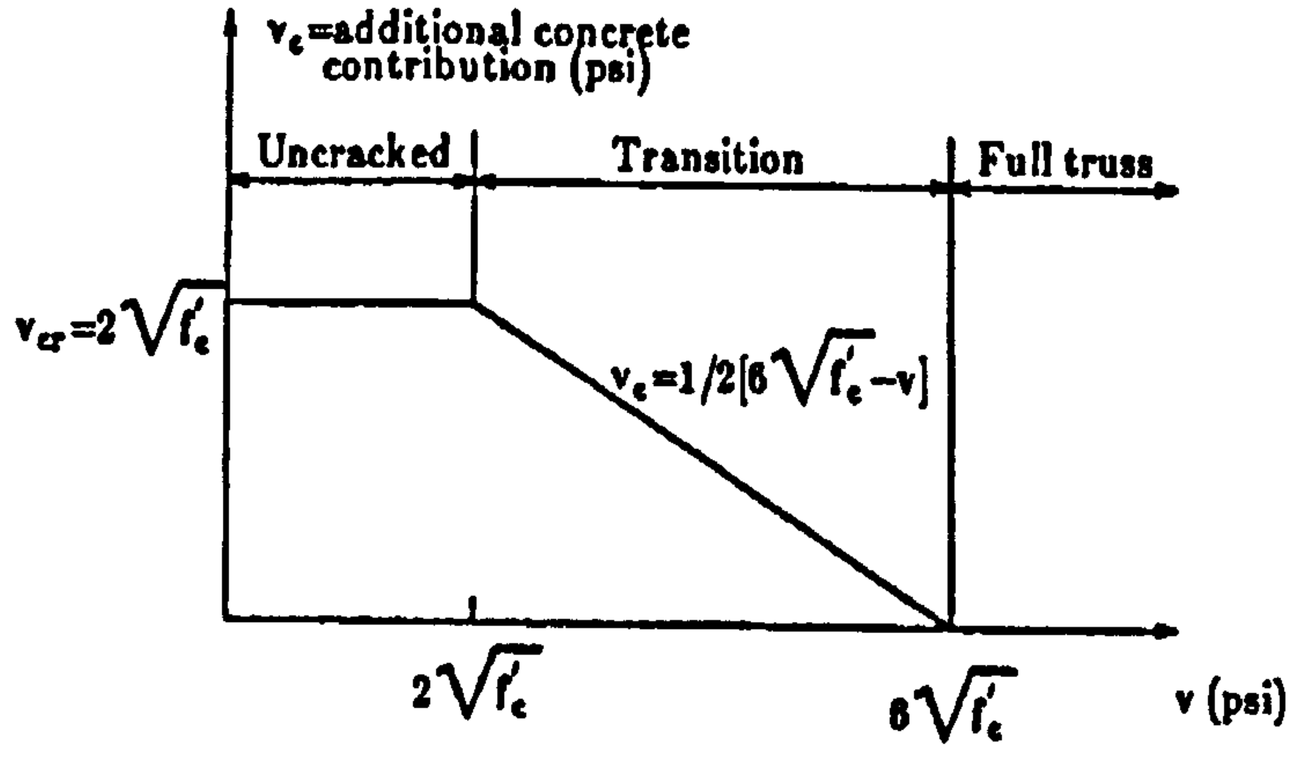

Fig. 2.10 (a): Concrete contribution for reinforced concrete beam

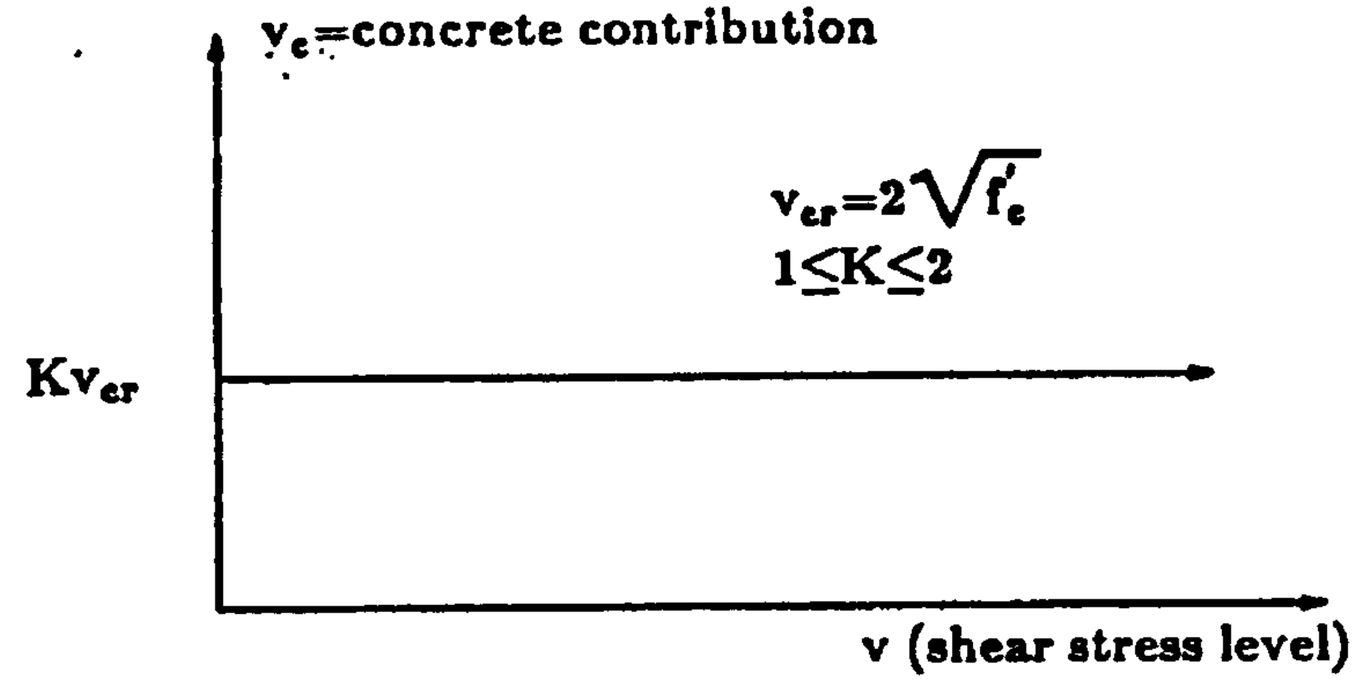

Fig. 2.10 (b): concrete contribution for prestresed concrete beam

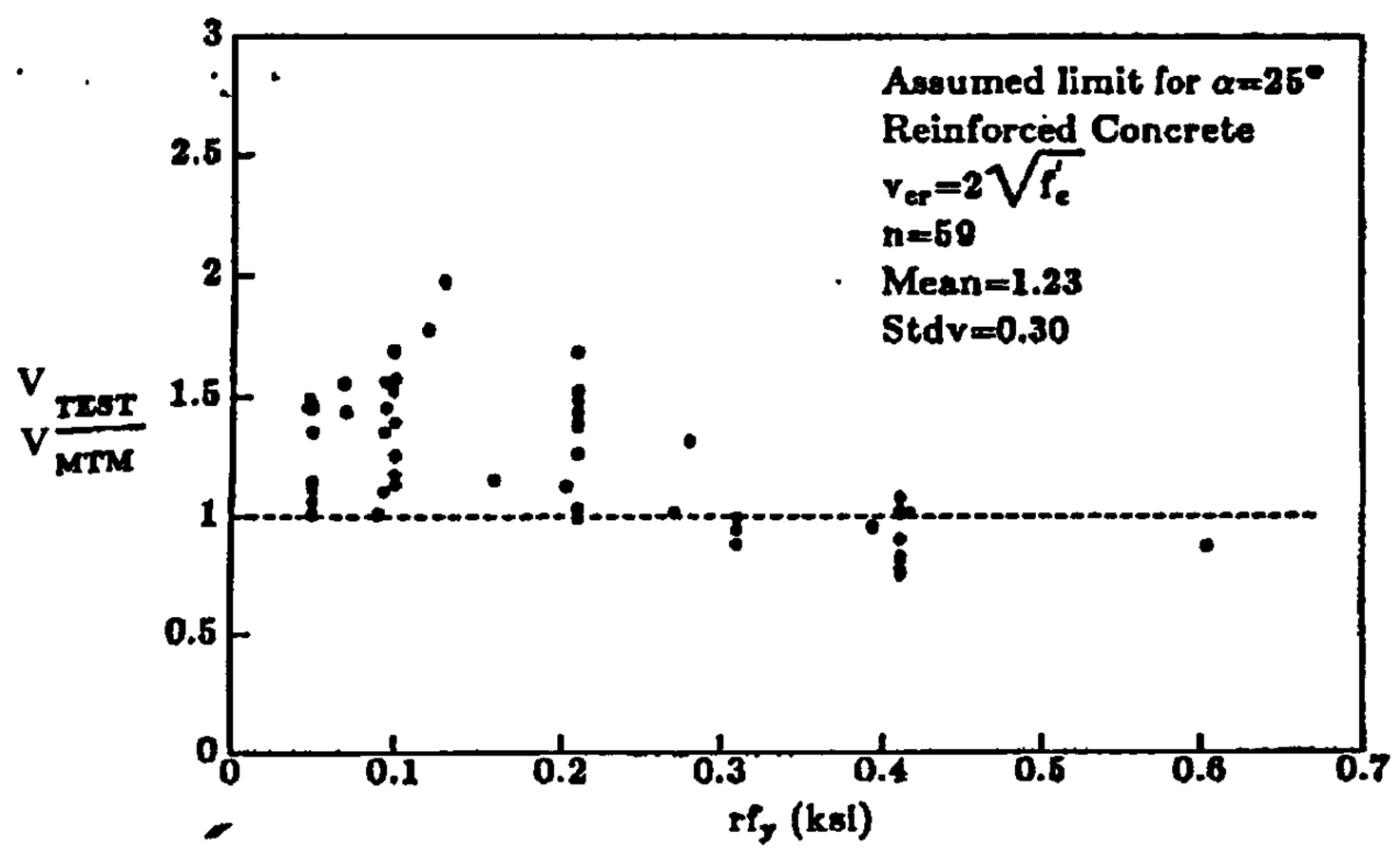

Fig. 2.11 (a): Evaluation with reinforced concrete beams with concrete contribution of Fig. 2.10 (a)

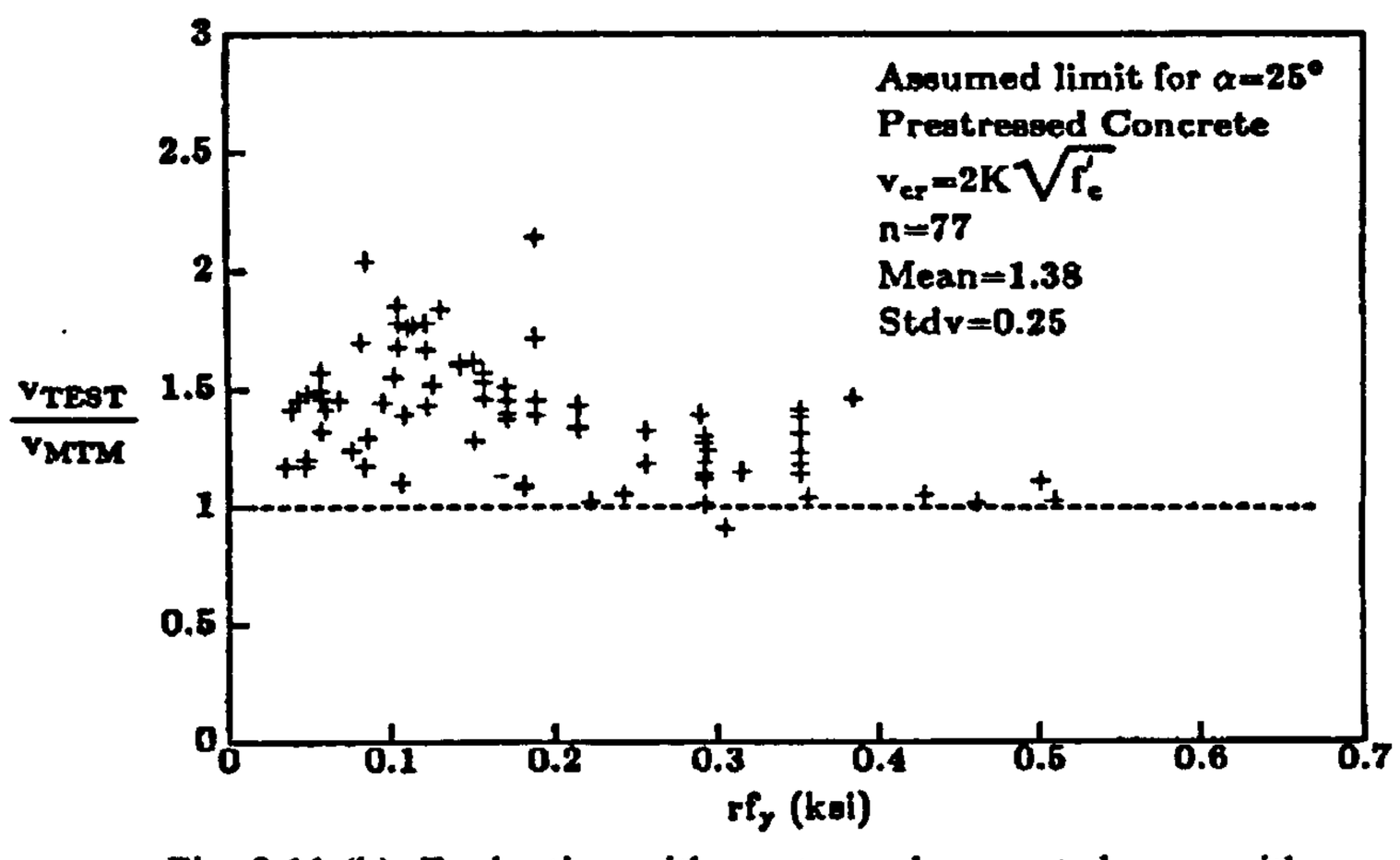

Fig. 2.11 (b): Evaluation with prestressed concrete beams with constant concrete contribution of Fig. 2.10 (b)

Modified Compression Field Theory: Vecchio and Collins (1986, 1988) developed the modified compression field theory to analyse reinforced concrete elements subjected to in-plane shear and normal stresses (Fig. 2.12a).

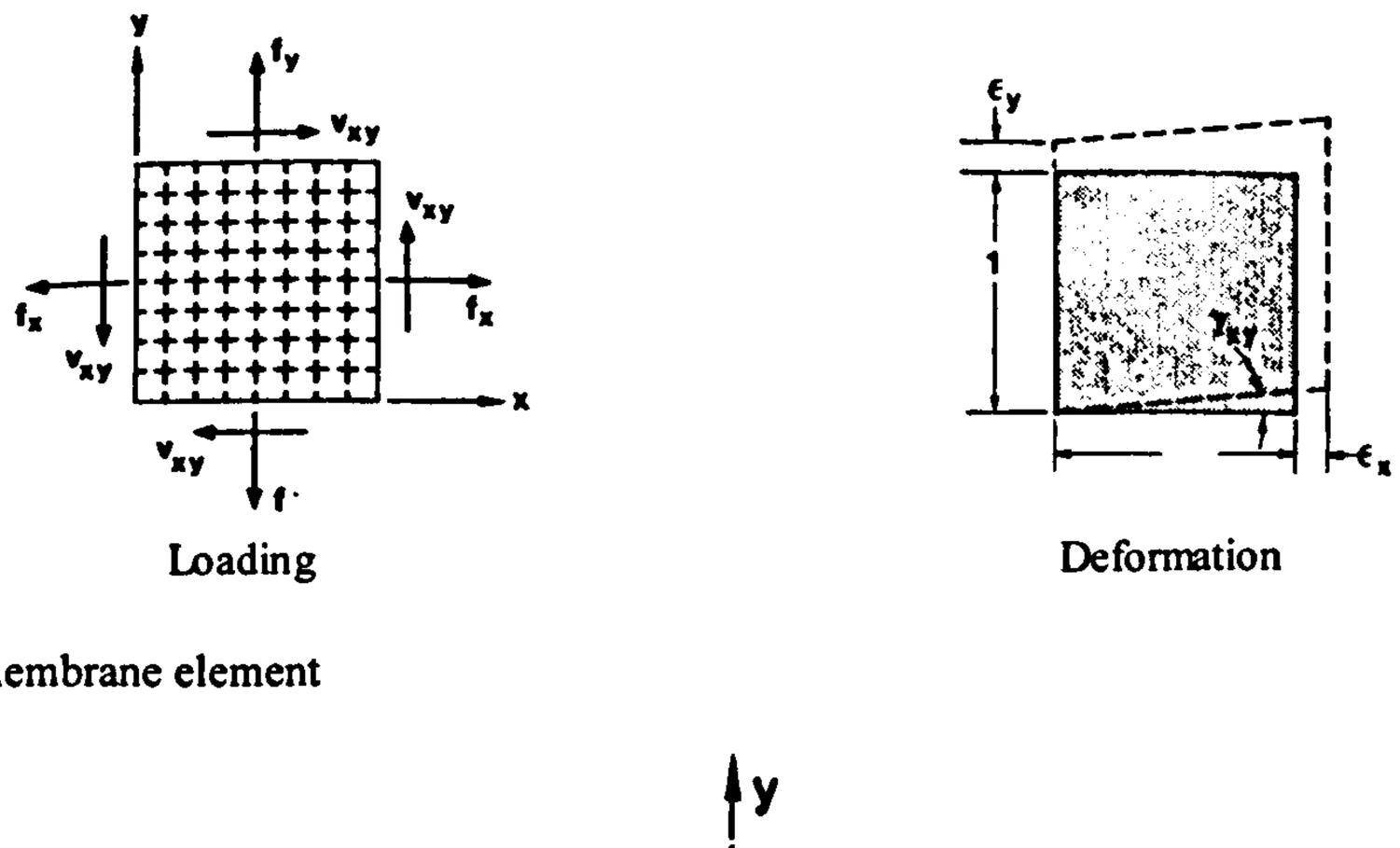

Fig. 2.12: Average stresses and strains in concrete element (Modified Compression Field Theory)

This theory was based on the assumption that the reinforcement is uniformly distributed. This is to ensure well distributed cracks. While the original compression field theory ignored tension in the cracked concrete, in this modified model, concrete between cracks is assumed to resist tensile stresses. The average stresses

and average strains (Fig. 2.12b-d) were used in formulating the equilibrium, compatibility and stress-strain relationships. The post cracking behaviour was given in a form of compression softening and tension stiffening of concrete in the stress-strain relationships (Fig. 2.13).

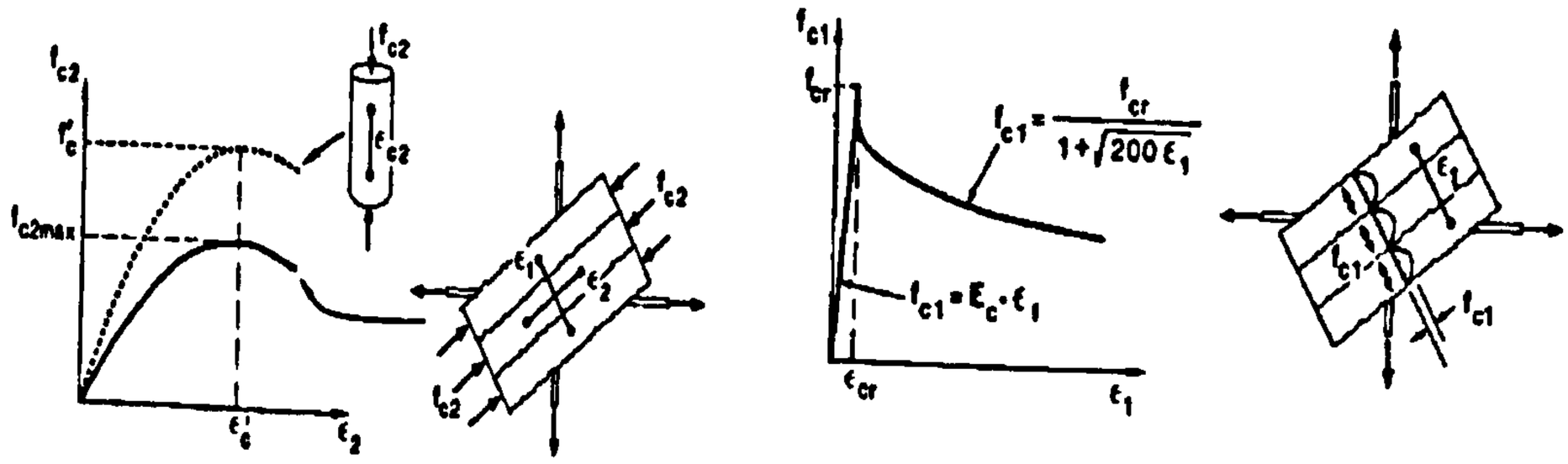

(a): Stress-strain relationship for cracked concrete in compression

(b): Stress-strain relationship for cracked concrete in tension

Fig. 2.13: Stress-strain relationships (Modified Compression Field Theory)

Softened Truss Model: Hsu (1988, 1991) presented a unified model for shear and torsion. Figure 2.14 shows an orthogonally reinforced concrete element subjected to in-plane shear and normal stresses. σ_l and σ_t are the applied normal stresses and τ_{lt} is the applied shear stress. After cracking, a truss action is formed with the compression diagonal struts oriented in the d-axis which is inclined at an angle α to the longitudinal steel. This direction is also assumed to be the direction of the principal compressive stress and strain. Taking the direction perpendicular to the d-axis as r-axis, the $d-r$ co-ordinate system is formed which represent the principal stress and strain. The direction of the initial crack is determined by the direction of the principal tensile stress σ_r that existed before cracking. With increased loading, the new cracks change their direction based on the direction of the principal tensile stresses in the concrete at the new applied load level. After cracking, the direction of the $d-r$ co-ordinate system is dependent on the relative amount of stresses in the longitudinal to transverse reinforcement. Stress-strain relationships similar to what was proposed in the modified compression field theory were presented (Fig. 2.15). More can be found about the truss analogy and its applications in the literature i.e. Karlsson and Elfgren (1972), Mitchell and Collins (1974), Hsu and Mo (1985),

Belarbi and Hsu (1990), Stevens et al. (1991), MacGregor and Ghoneim (1995), Pang and Hsu (1996), Asghar and Almughrabi (1996), and Ali and White (1999).

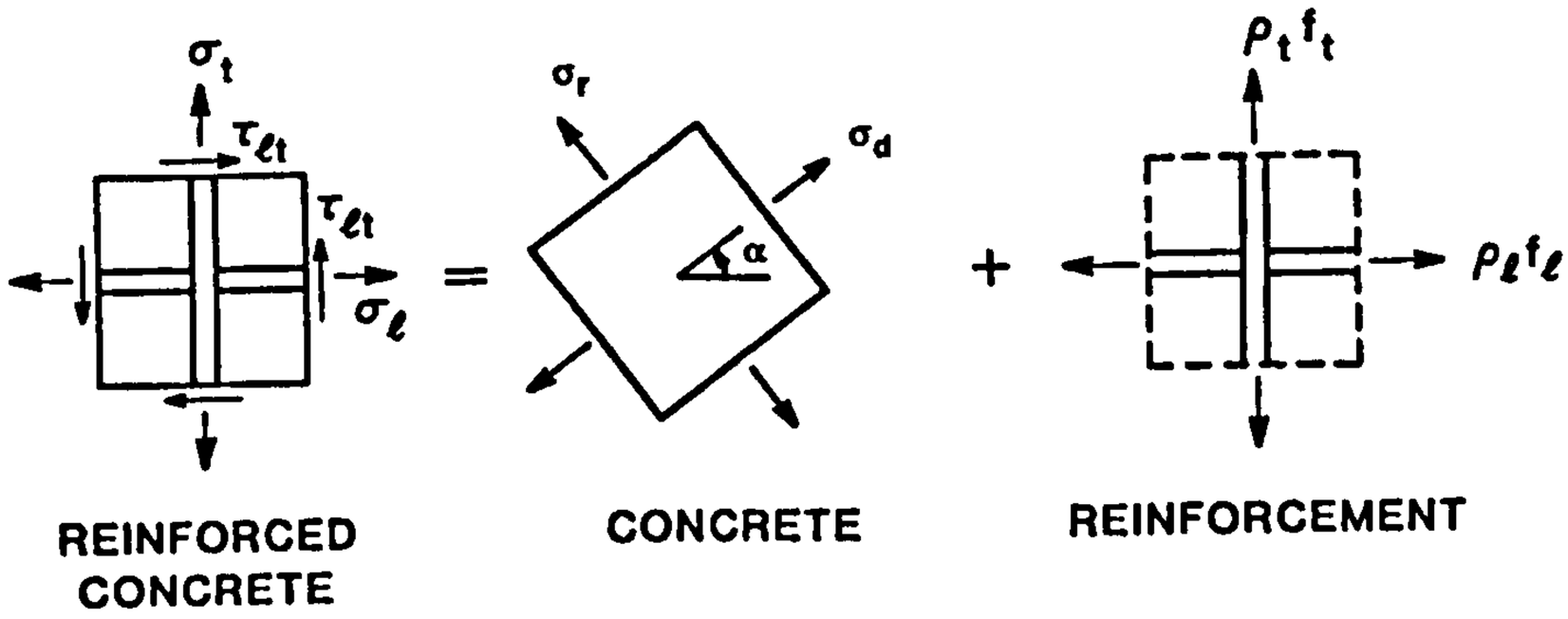

Fig. 2.14: Stress condition in reinforced concrete element (Softened Truss Model)

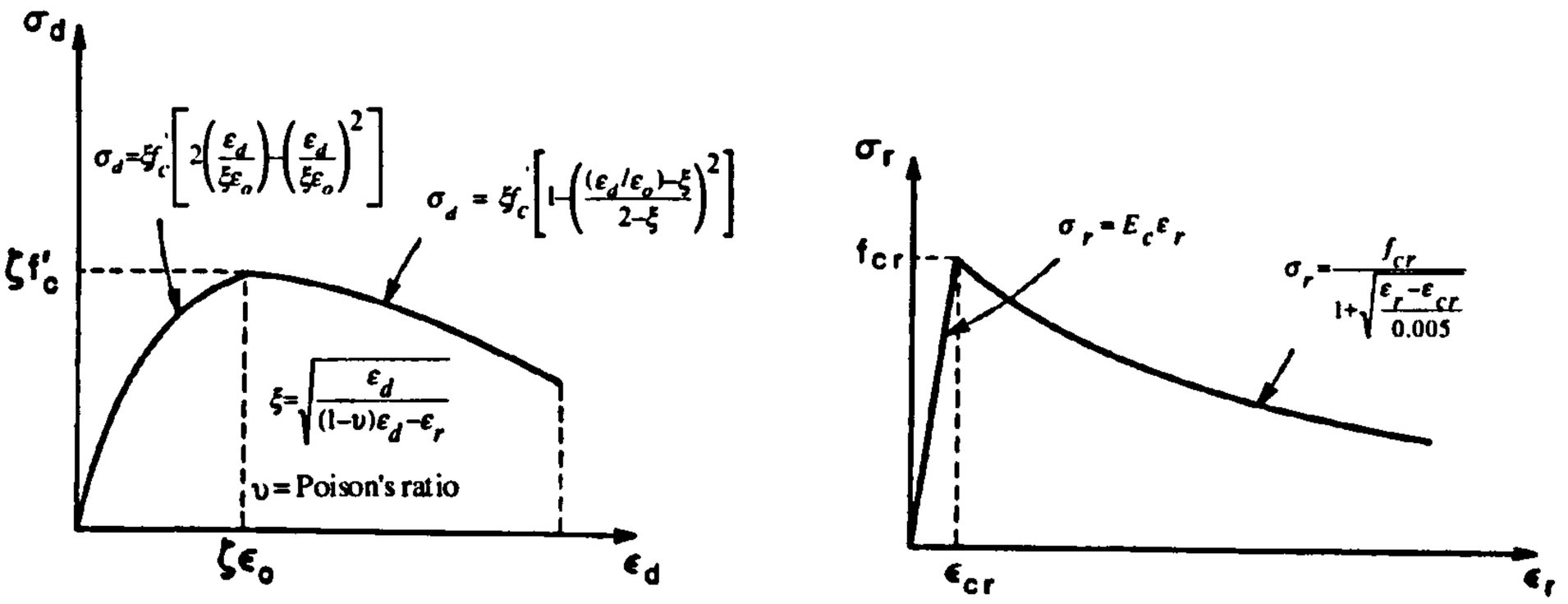

(a): Compression stress-strain relationship (b): Tensile stress-strain relationship

ε_d, ε_r = Average principal strains in the d and r directions respectively. ε_o = Strain at the maximum compressive stress (taken as 0.002). ε_{cr} = strain at tensile cracking of concrete.

Fig. 2.15: Stress-strain relationships for reinforced concrete (Softened Truss Model)

2.3: Comments on the comparison between skew-Bending and truss theories

Kuyt (1971) made a theoretical comparison between the truss analogy and the ultimate equilibrium method (skew-bending) for under-reinforced beams. He stated: "... the latter method will give the same results as the truss theory, provided that proper assumptions are made with respect to the form of the failure surfaces and the magnitude of the stirrup stresses at the smaller and the larger sides of the beam respectively". In a final observations he said: "... it may be stated that calculations based on the truss analogy are preferable, because they rest on a more definite basis with regard to the internal equilibrium of the beam as a whole."

Thurlimann (1979), in his comment on the two theories said: " In many cases they lead to the same results." However, he preferred the truss analogy because it is applicable to any type of cross section, allows a uniform treatment of combined load cases, can be used to determine the warping resistance of thin walled reinforced concrete beams with open cross sections, and torsional stiffness members after cracking.

Hsu (1988) stated: " It is agreed by researchers in recent years that the truss model theory provides a more promising way to treat shear and torsion".

2.4: Derivation of force equations using the space-truss analogy

1. Pure torsion

For a rectangular beam subjected to pure torsion, tension cracks spiral around the beam with a constant angle θ as shown in figure 2.6. After cracking, the beam can be idealised as a space truss consisting of longitudinal bars in the corners, closed stirrups and concrete compression diagonals which spiral around the member between the torsional cracks as shown in figure 2.16a.

Using the thin-walled member analogy the shear stress τ due to torsion can be calculated from:

$$\tau = \frac{T}{2A_o t} \qquad 2.3$$

where:

T = torque

A_o = area enclosed by the centre line of the wall thickness

t = thickness of the wall

The shear force per unit length of perimeter, at any point on the perimeter of the shell is referred to as shear flow $q = \tau t$ and from equation 2.3:

$$q = \tau t = \frac{T}{2A_o} \qquad 2.4$$

Figure 2.16b shows a portion of vertical side 2 of space truss. The diagonal compressive force D_2 is resolved into a vertical force V_2 balanced by the stirrups and a horizontal force N_2 resisted by the longitudinal steel. The total shear force due to torsion in a given side of the tube is q times the length of this side. Thus, the shear force in side 2 with depth y_o is:

$$V_2 = qy_o = \frac{T}{2A_o} y_o \qquad 2.5$$

Similar forces act on all four sides to cause a torque about the axis of the member to resist the applied torque.

$$V_2 = D_2 \sin\theta \qquad 2.6$$

$$N_2 = \frac{V_2}{\tan\theta} \qquad 2.7$$

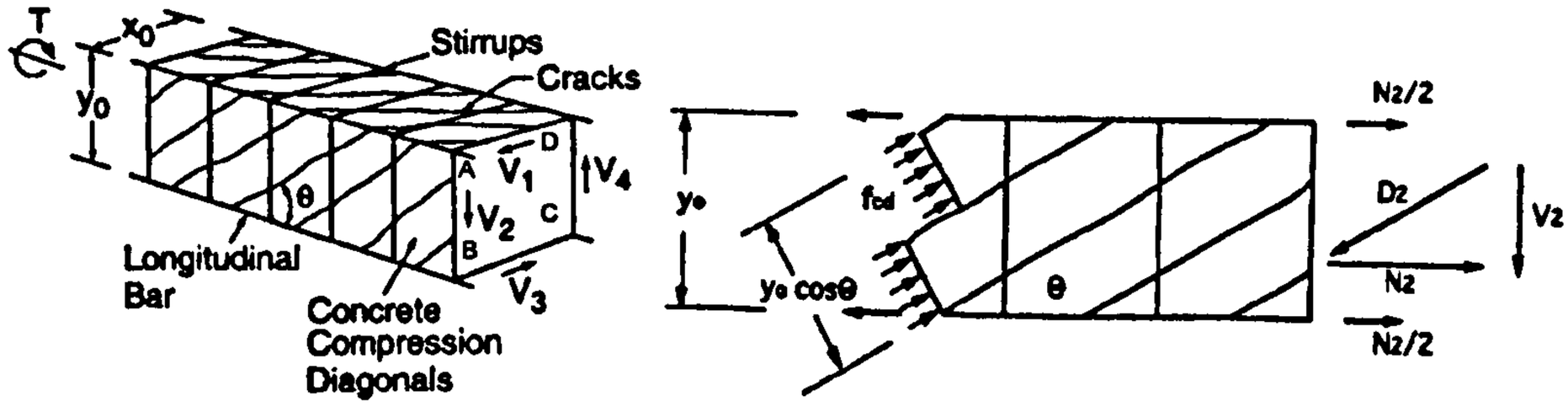

(a): Space truss

(b): Portion of vertical side 2 of space truss

(c): Resolution of shear force in side 2 of space truss

Fig. 2.16: Space truss analogy

It can be seen that if a low angle of inclination of the diagonal struts is used, smaller vertical force and accordingly less transverse reinforcement but larger normal force and more longitudinal reinforcement will be required. The horizontal force N_2 acts at the mid-height of side 2 and, therefore, it is divided equally between the top and bottom bars in this side. For a beam with only corner reinforcement, the forces at each corner will be as follows:

$$A = \frac{N_2}{2} + \frac{N_1}{2}$$

$$B = \frac{N_2}{2} + \frac{N_3}{2}$$

$$C=\frac{N_3}{2}+\frac{N_4}{2}$$

$$D=\frac{N_4}{2}+\frac{N_1}{2}$$

where the corners A, B, C and D are as shown in figure 2.16a and N_i represents the normal force in i^{th} side.

2. Pure bending

In this case the compression diagonals are replaced by a compression block across the width parallel to the chords and only longitudinal steel is required. If concrete alone is resisting the compression and steel is taking the tension, failure happen by either steel yielding or concrete crushing with vertical cracks to the beam axis. The cracks first appear at the bottom face and then spread to the side faces.

3. Combined shear and torsion

The shear stress situation is as shown in figure 2.1. The forces due to torsion are calculated as in case 1 above and the forces due to shear force are calculated using either elastic or plastic stress distribution. As an example, for a hollow section the stresses in the top and bottom flanges can be considered as torsional shear stress alone using equation 2.3. In the side where the stresses are added the net shear stress is the result from equation 2.3 plus $V/2ht$, where V is the applied shear force, h is the depth of the web and t is its thickness. In the side where the stresses are subtractive the net shear stress is the result from equation 2.3 minus $V/2ht$.

4. Combined bending and torsion

Torsion leads to axial force N which must be resisted by longitudinal reinforcement and a transverse force V which must be resisted by stirrups. The bending moment causes two equal but opposite axial forces. In the tension side the axial force from the torsion is added to the one from bending and in the compression zone the forces are subtracted (Fig. 2.7). This leads to a reduction in the longitudinal reinforcement required to resist torsion in the compression region. The smaller the ratio of torsion to bending the steeper the cracks will be with respect to the beam axis.

5. Combined bending, torsion and shear

In this case, the vertical forces are algebraically added as described in case 3 and the horizontal forces are added as in case 4. For under reinforced beams, failure may happen by one of three distinct failure modes. First, yielding of bottom longitudinal steel and stirrups on the side where shear stresses are additive. In this mode rotation will take place about the top horizontal axis (similar to skew-bending mode 1). Second, yielding of the top stringer and the web reinforcement on the side where shear stresses due to torsion and shear force are additive. The rotation will take place at the bottom horizontal axis (similar to skew-bending mode 3). Third, yielding of the top and bottom longitudinal reinforcement and transverse steel in one side of beam where shear stresses are additive. Rotation will take place along the axis in the other side of the beam where the shear stresses are subtractive (similar to skew-bending mode 2). The inclination of the cracks in this load combination depends upon torsion-shear and torsion-flexure ratios.

Appendix A presents a numerical design example for combined load of bending, torsion and shear using the truss analogy. It can be seen that the smaller the angle of the diagonals the larger the amount of the longitudinal steel and the smaller amount of the transverse steel. This is considered to be a more economical design as the transverse steel is more expensive.

3: Direct Design Method

3.1: Introduction

In this chapter the 'Direct Design Method' is introduced. This method satisfies the conditions of the classical theory of plasticity and reduces the ductility demand of the structure.

3.2: Aim of structural design

The aim of structural design is to produce economical structures to resist, with adequate safety and durability, all loads and deformations likely to occur during construction and use of the structure. A structure or part of a structure is defined as unfit for use when it reaches a limit state beyond which it ceases to satisfy the functions and conditions for its existence. There are two limit states that the structure has to satisfy during its existence:

Ultimate limit state: The structure must resist safely maximum loads likely to occur before collapse. The collapse of the structure or part of it, may arise from rupture of one or more critical sections, from the loss of equilibrium (transformation into a mechanism) or from buckling due to elastic or plastic instability.

Serviceability limit state: The structure must not suffer from excessive deformations, cracking and vibration ...etc. under service load conditions.

3.3: Basic conditions of the classical theory of plasticity

To overcome the problem of using empirical equations in the design, one should go to basic theories of mechanics. A well known theory dealing with structure's ultimate load carrying capacity is the theory of plasticity. This theory requires the structure to satisfy three basic conditions at ultimate load:

Equilibrium condition: Internal stresses must equilibrate external applied loads.

Yield criterion: At no point in the structure should the set of stresses violate the yield criterion for the material.

Mechanism condition: Under ultimate load the structure should develop sufficient plastic regions or hinges to transform it into a mechanism.

Unfortunately the theory of plasticity assumes unlimited ductility of material. This means that the regions which yield early in the structure need to continue to deform without any reduction in their strength. Obviously, this is not the case with reinforced concrete and even less with prestressed concrete. Therefore, this theory

has to be used with caution when dealing with concrete structures. What is needed is that the difference between the load at which first yielding occurs at any point and the ultimate load of the whole structure is made as small as possible. This will reduce the load range during which sections that yield early are required to deform at constant 'stress' without losing their strength due to strain softening of concrete. From the above discussion, it is clear that two issues have to be addressed: one is to produce design equations for concrete structures based on sound theoretical principals using the theory of plasticity, and second is to reduce the ductility demand made by the theory of plasticity. Before discussing the direct design method, yield criteria for reinforced concrete to resist applied in-plane stresses is developed.

3.4: Design of orthogonal tension reinforcement to resist in-plane forces

3.4.1: Assumptions

Nielsen (1971, 1974, 1979, 1984) derived a yield criterion for reinforced concrete which he used for derivation of design equations for orthogonal tension reinforcement to resist in-plane forces. He based his work on the following assumptions:

1. Reinforcing bars are assumed to exhibit perfectly elastic-plastic behaviour (Fig. 3.1) and positioned symmetrically with reference to the middle plane of the section in two orthogonal directions.
2. The steel bars are conservatively considered to resist only uniaxial stresses in the original direction of the bar as shown in figure 3.2.
3. Kinking of bars across cracks and dowel action of bars in resisting shear forces are neglected.
4. Spacing of bars in both orthogonal directions is considered to be very small compared to the over all dimension of the section, therefore, reinforcing steel is considered in terms of area per unit length.
5. Concrete is assumed to be perfectly plastic and, conservatively, resists no tension. The square yield criterion is adopted as shown in figure 3.3.
6. Ultimate failure occurs by unrestricted plastic flow and not by buckling of section. Instability or bond failures are assumed to be prevented by proper detailing of steel and choice of section.

7. If both principal in-plane forces were compressive, concrete of sufficient strength precludes the use of compression reinforcement.

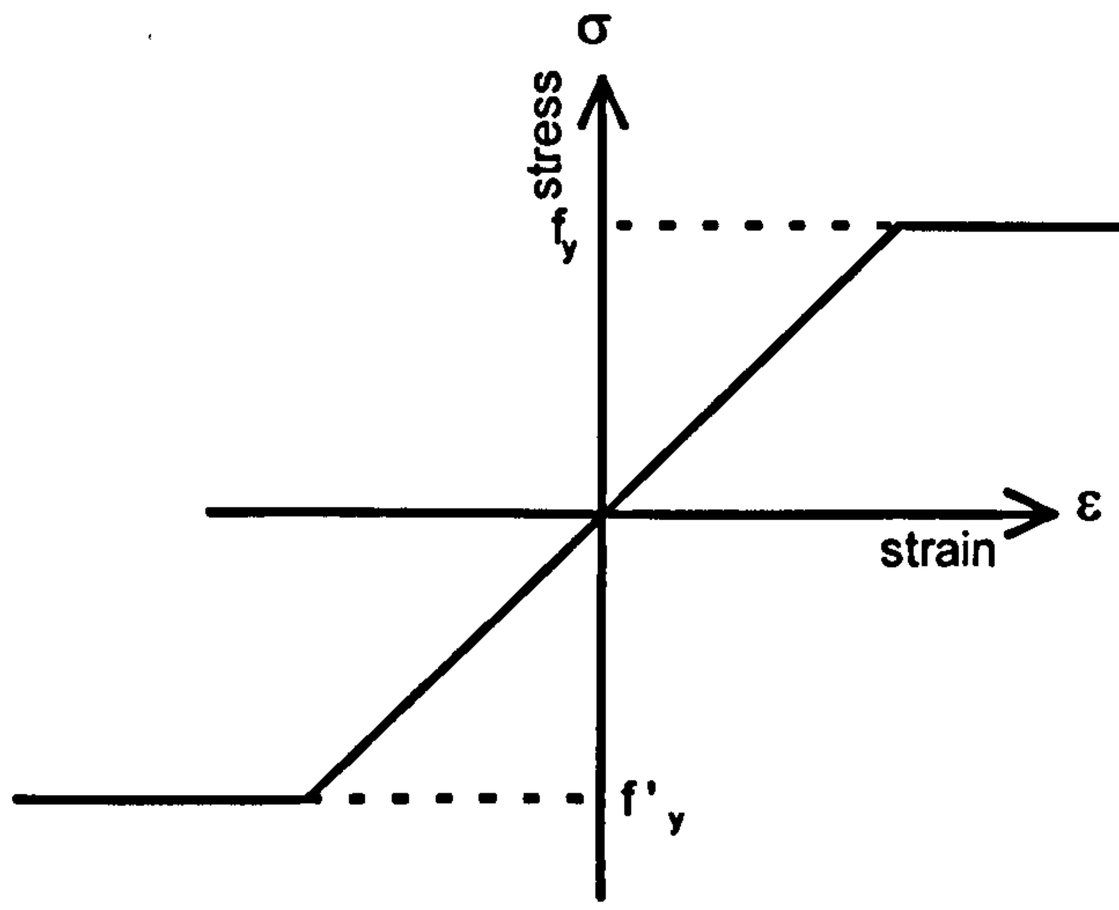

Fig. 3.1: Stress-strain curve in a reinforcing bar

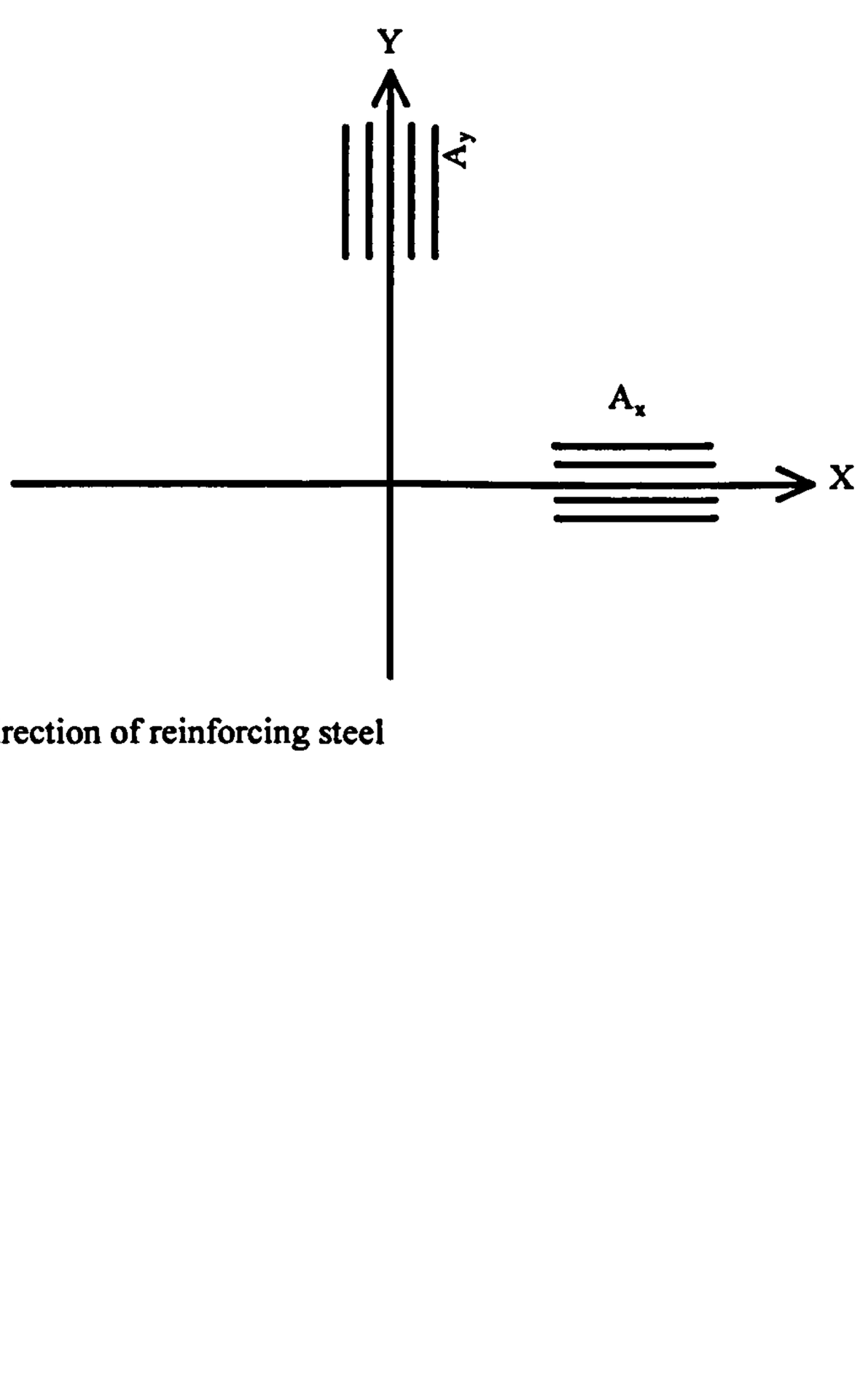

Fig. 3.2: Direction of reinforcing steel

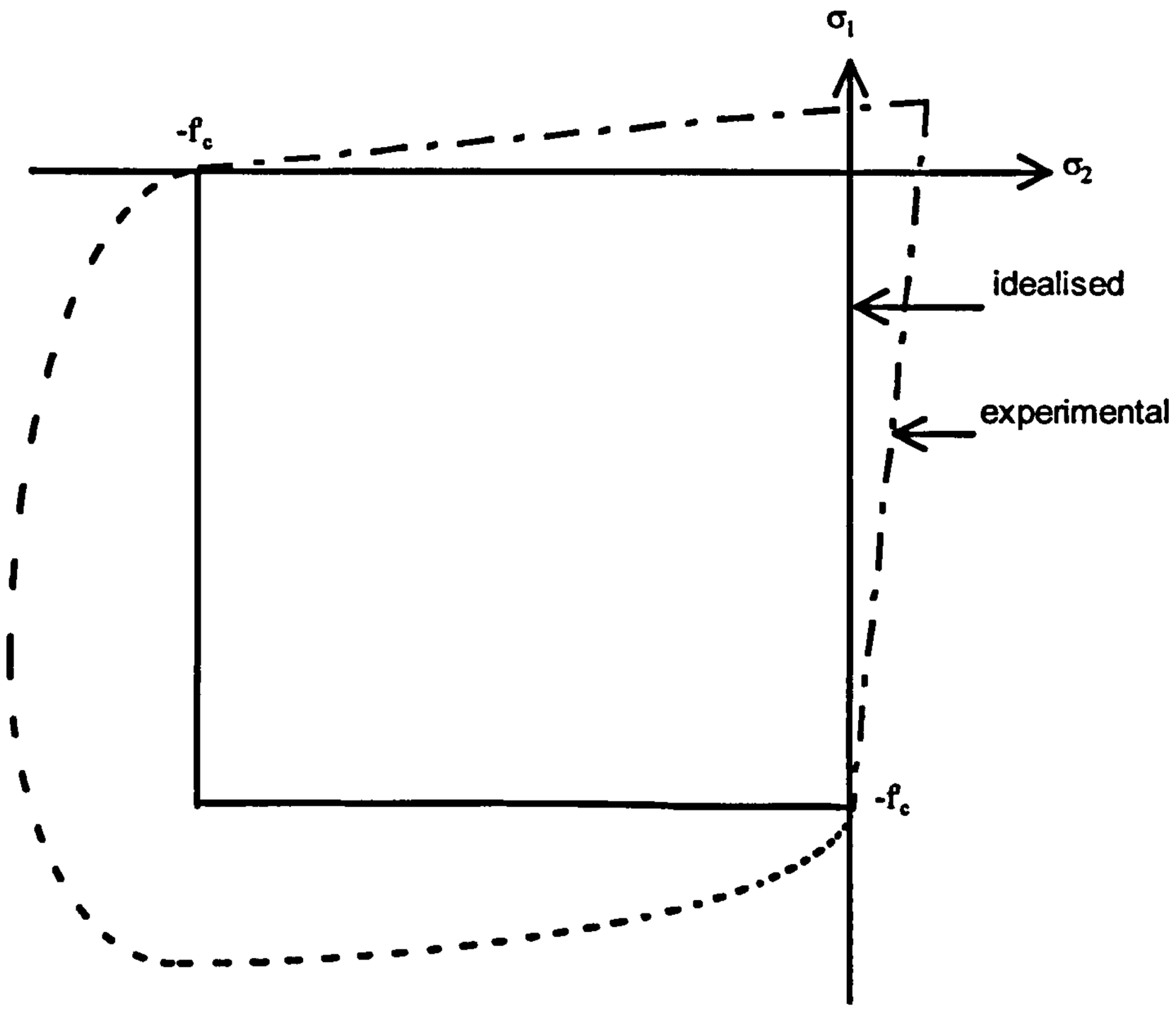

Fig. 3.3: Yield criterion for concrete in in-plane stress

3.4.2: Applied in-plane loads and resisting stresses

Let a set of applied stresses σ_x, σ_y and τ_{xy} act on a reinforced concrete element (Fig. 3.7) with thickness t. The stresses are resisted by concrete and steel in two orthogonal directions as shown in figure 3.4.

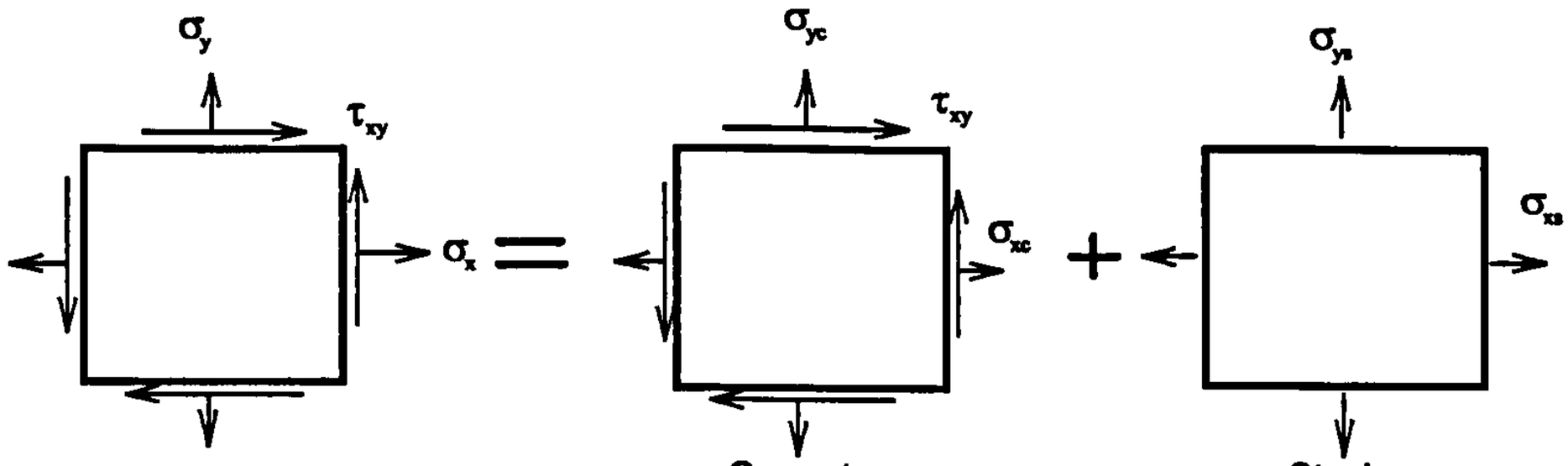

Fig. 3.4: Concrete and steel resistance to applied load

Where:

σ_x, σ_y = applied normal stresses in x and y directions.

τ_{xy} = applied shear stress.

σ_{xc}, σ_{yc} = normal stresses in concrete in x and y directions.

σ_{xs}, σ_{ys} = steel stresses in x and y directions.

3.4.3: Equilibrium condition

Concrete:

Let the principal stresses in concrete σ_1 and σ_2 as shown in figure 3.5a and $\sigma_1 > \sigma_2$.

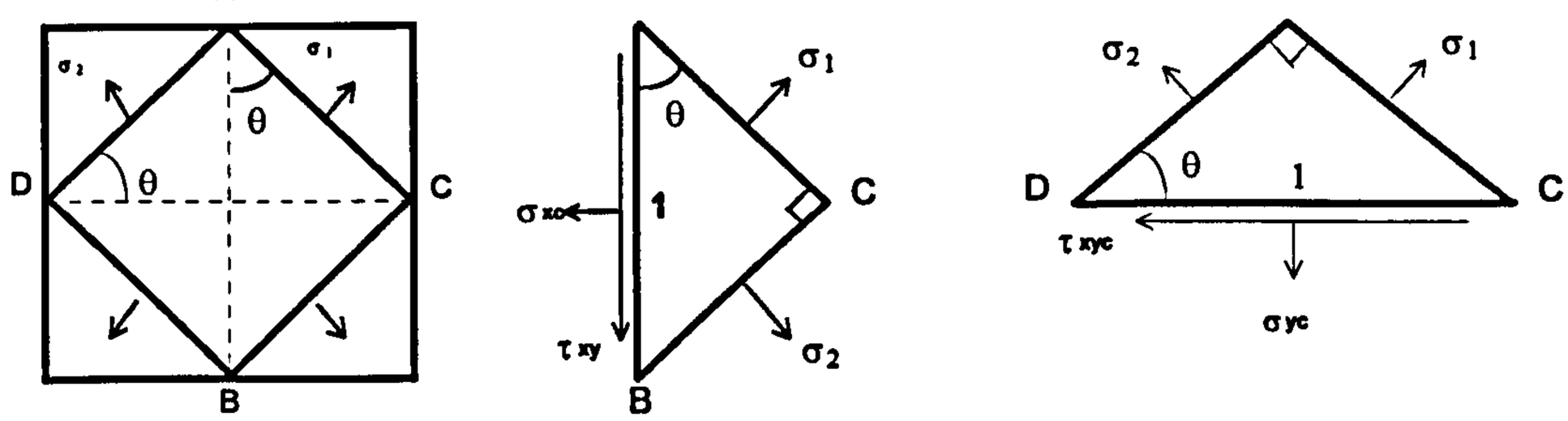

(a) (b) (c)

Fig. 3.5: Concrete resistance to applied load

From figure 3.5b:

$$\sigma_{xc} = \sigma_1 \cos^2\theta + \sigma_2 \sin^2\theta \qquad 3.1a$$

$$\tau_{xyc} = (\sigma_1 - \sigma_2)\sin\theta\cos\theta \qquad 3.1b$$

and from figure 3.5c:

$$\sigma_{yc} = \sigma_1 \sin^2\theta + \sigma_2 \cos^2\theta \qquad 3.1c$$

Steel:

Let A_x and A_y be the steel areas per unit width in x and y directions respectively, and t is the thickness of the element. From figure 3.6:

$$\sigma_{xs} = A_x . f_x / t \qquad 3.1d$$

$$\sigma_{ys} = A_y . f_y / t \qquad 3.1e$$

Equilibrium combined stresses:

$$\sigma_x = \sigma_{xc} + \sigma_{xs} = \sigma_1 \cos^2\theta + \sigma_2 \sin^2\theta + A_x . f_x / t \qquad 3.2a$$

$$\sigma_y = \sigma_{yxc} + \sigma_{ys} = \sigma_1 \sin^2\theta + \sigma_2 \cos^2\theta + A_y . f_y / t \qquad 3.2b$$

$$\tau_{xy} = \tau_{xyc} = (\sigma_1 - \sigma_2)\sin\theta\cos\theta \qquad 3.2c$$

Where θ is the inclination of the major principal concrete stress σ_1 to the x axis.

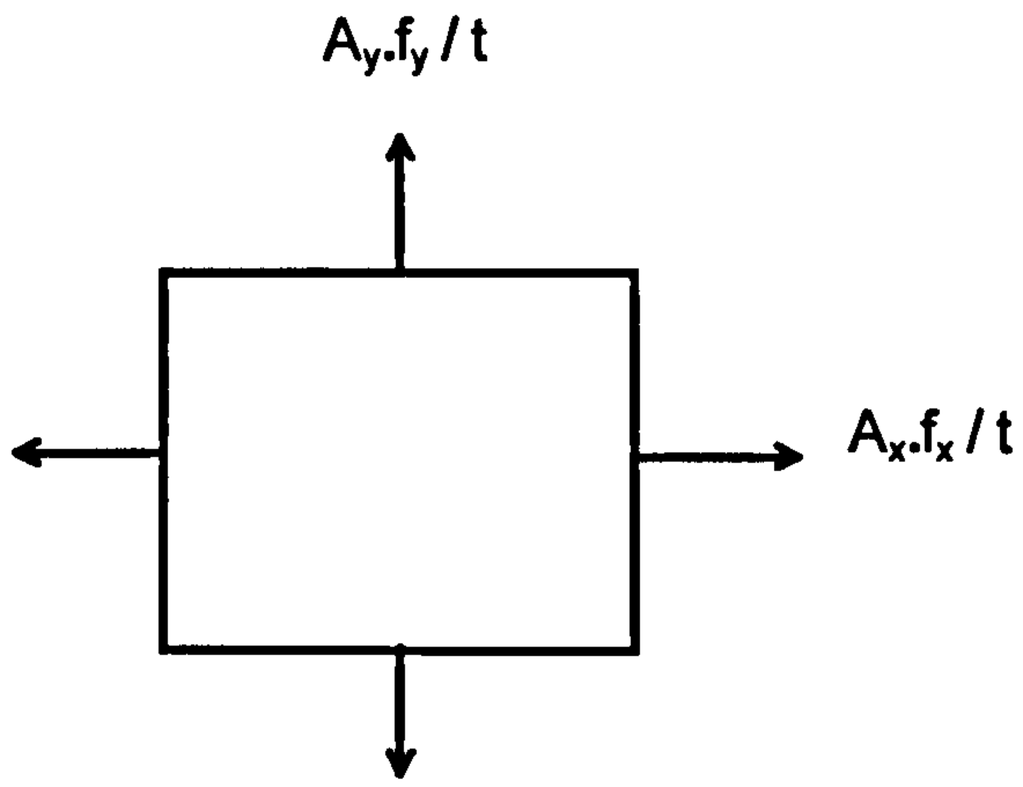

Fig. 3.6: Steel resistance to applied load

3.4.4: Yield criterion

Let $N_x = \sigma_x.t$, $N_y = \sigma_y.t$ and $N_{xy} = \tau_{xy}.t$ be the applied in-plane forces per unit length on a element with thickness t as shown in figure 3.7. Also, the resisting forces are $N_1 = \sigma_1.t$, $N_2 = \sigma_2.t$, $N_x^s = A_x.f_x$ and $N_y^s = A_y.f_y$. Then equations 3.2 can be written as:

$$N_x = \sigma_x.t = (N_1 \cos^2\theta + N_2 \sin^2\theta) + N_x^s$$

$$N_y = \sigma_y.t = (N_1 \sin^2\theta + N_2 \cos^2\theta) + N_y^s$$

$$N_{xy} = \tau_{xy}.t = (N_1 - N_2)\sin\theta\cos\theta$$

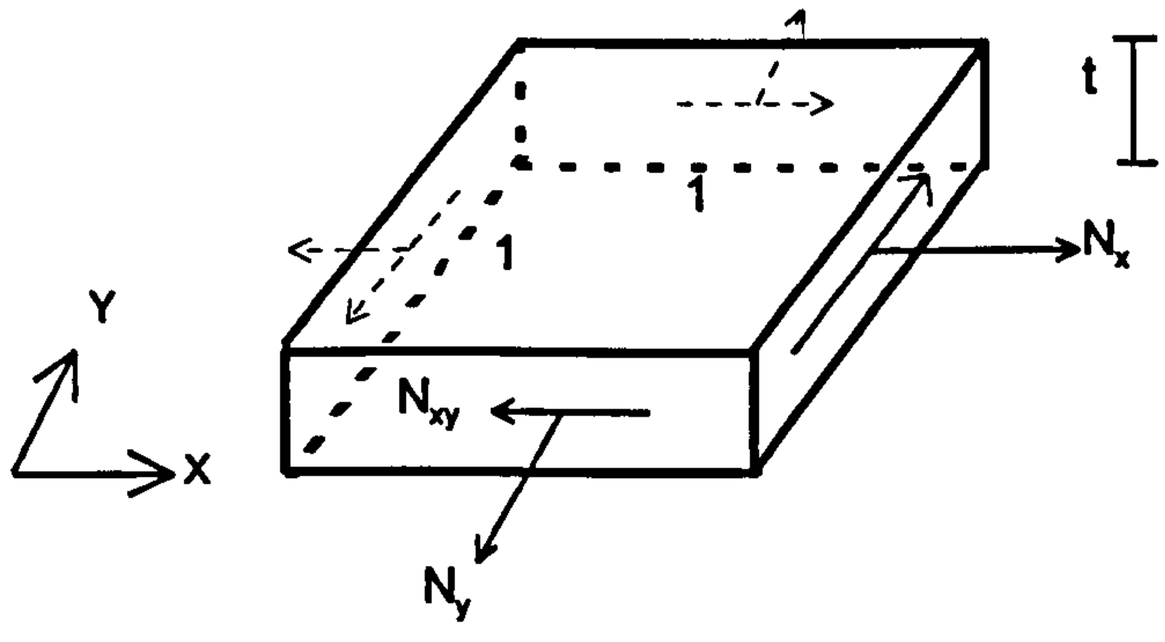

Fig. 3.7: In-plane forces on an element

Since concrete is considered to carry no tensile stress, $\sigma_1 = 0$. The above equations become:

$$N_x = N_2 \sin^2\theta + N_x^s$$

$$N_y = N_2 \cos^2\theta + N_y^s$$

$$N_{xy} = -N_2 \sin\theta\cos\theta$$

or

$$N_x^s - N_x = -N_2 \sin^2\theta \qquad 3.3a$$

$$N_y^s - N_y = -N_2 \cos^2\theta \qquad 3.3b$$

$$N_{xy} = -N_2 \sin\theta\cos\theta \qquad 3.3c$$

Eliminating θ and N_2 from the above equations leads to the yield criterion equation for reinforced concrete element under in-plane loads:

$$(N_x^s - N_x)(N_y^s - N_y) - N_{xy}^2 = 0 \qquad 3.4$$

3.4.5: Design equations

Based on the magnitude of the applied in-plane forces, optimum reinforcement solution requires steel in one or both directions or no steel at all. This leads to four possible sets of design equations for different cases. All of these design equations are derived from the above yield criterion (Eq. 3.4) for orthogonal tension reinforcement as follows:

Case 1: Only Y steel is required:

$$N_x^s = 0 \quad \text{and} \quad N_y^s \neq 0$$

Then Eq. 3.4 gives:

$$N_y^s = N_y - \frac{N_{xy}^2}{N_x} \qquad 3.5a$$

And Eq. 3.3a and Eq. 3.3c lead to:

$$N_2 = N_x + \frac{N_{xy}^2}{N_x} \qquad 3.5b$$

It is clear from Eq. 3.5a that if $N_y^s = 0$ then:

$$N_x . N_y = N_{xy}^2 \qquad 3.5c$$

Case 2: Only X steel is required:

$$N_y^s = 0 \text{ and } N_x^s \neq 0$$

Then Eq. 3.4 gives:

$$N_x^s = N_x - \frac{N_{xy}^2}{N_y} \qquad 3.6a$$

And Eq. 3.3b leads to:

$$N_2 = N_y + \frac{N_{xy}^2}{N_y} \qquad 3.6b$$

if $N_x^s = 0$ then: $N_x . N_y = N_{xy}^2$

Case 3: X and Y steels required:

$$N_x^s \neq 0 \quad \text{and} \quad N_y^s \neq 0$$

Then Eq. 3.4 gives:

$$N_y^s = N_y + \frac{N_{xy}^2}{N_x^s - N_x}$$

or

$$N_x^s + N_y^s = N_x^s + N_y + \frac{N_{xy}^2}{N_x^s - N_x}$$

Minimising the sum of steel in both directions:

$$\frac{d}{dN_x^s}\left(N_x^s + N_y^s\right) = \frac{d}{N_x^s}\left(N_x^s + N_y + \frac{N_{xy}^2}{N_x^s - N_x}\right) = 0$$

or

$$1 - \frac{N_{xy}^2}{\left(N_x^s - N_x\right)^2} = 0$$

This leads to:

$$N_x^s - N_x = \pm\left|N_{xy}\right|$$

As $N_x^s > 0$, then:

$$N_x^s = N_x + \left|N_{xy}\right| \qquad 3.7a$$

Substituting Eq. 3.7a into Eq. 3.4:

$$N_y^s = N_y + \left|N_{xy}\right| \qquad 3.7b$$

Substituting eq. 3.7a and 3.7b into 3.3a and 3.3b respectively:

$$N_2 = -2\left|N_{xy}\right| \qquad 3.7c$$

If $N_x^s = 0$ then Eq. 3.7a gives $N_x = \left|N_{xy}\right|$ 3.7d

and if $N_y^s = 0$ then Eq. 3.7b gives $N_y = -\left|N_{xy}\right|$ 3.7e

Case 4: No steel is required:

When σ_1 and σ_2 are both compressive, it is assumed that concrete alone will resist the applied loads and, therefore, no steel is required. This leads to:

$$N_x^s = 0 \qquad 3.8a$$

$$N_y^s = 0 \qquad 3.8b$$

$$\left.\begin{matrix} N_1 \\ N_2 \end{matrix}\right\} = \frac{N_x + N_y}{2} \pm \sqrt{\frac{(N_x - N_y)^2}{4} + N_{xy}^2} \qquad 3.8c$$

If in any of the above cases $|\sigma_2| > f_c'$ then the section has to be redesigned or the concrete strength has to be increased.

3.4.6: Boundary curves

In order to know the regions in which each set of equations is used, the boundary curves separating the cases were established using for horizontal axis $\left(N_x / |N_{xy}|\right)$ and for vertical axis $\left(N_y / |N_{xy}|\right)$. All boundary curves are derived by equating the design equations of the two adjacent cases. As an example the curves separating case 3 from cases 1 and 2 is derived as follows:

All points on the curve between cases 1 and 3 must have equal values of reinforcement using both set of equations. Thus:

$$N_x^s(1) = N_x^s(3) \rightarrow 0 = N_x + |N_{xy}| \rightarrow N_x = -|N_{xy}| \rightarrow \frac{N_x}{|N_{xy}|} = -1$$

Which is the equation of straight line parallel to the y axis at -1 on the x axis.

Similarly all points on the curve between cases 3 and 2 must have equal values of reinforcement using both sets of equations. Thus:

$$N_y^s(2) = N_y^s(3) \rightarrow 0 = N_y + |N_{xy}| \rightarrow \frac{N_y}{|N_{xy}|} = -1$$

Which is the equation of straight line parallel to the x axis at -1 on the y axis.

All other boundaries are determined in a similar way. Figure 3.8 shows boundary graph for Nielsen's orthogonal tension reinforcement.

3.5: Orthogonal compression and Skew reinforcement

Clark (1976) derived equations for the case of compression reinforcement in one or both directions including steel in skew directions.

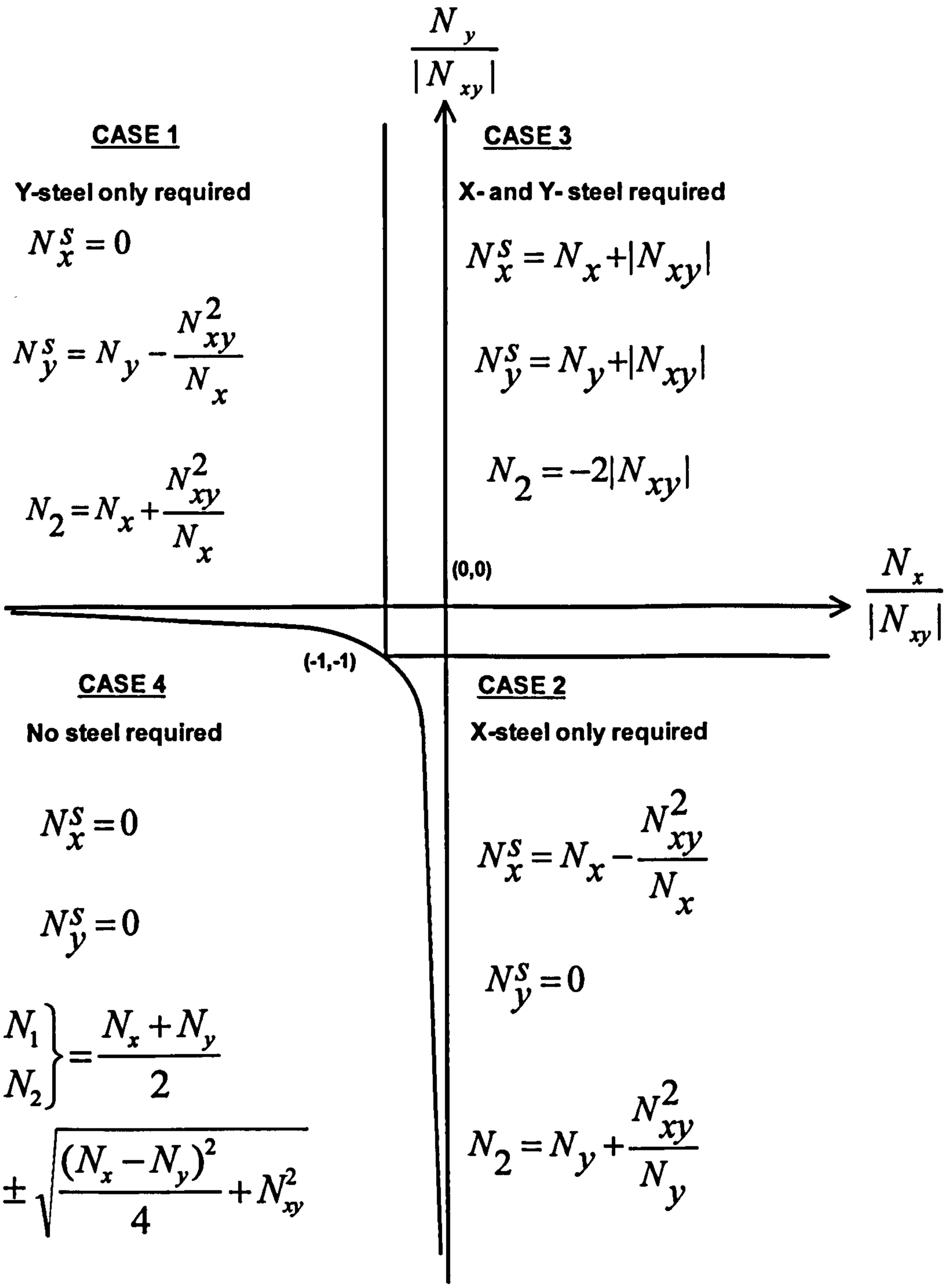

Fig. 3.8: Boundary graph for Nielsen's design equations

When the works of Nielsen and Clark are combined together, nine sets of design equations for skew or orthogonal tension and/or compression reinforcement required to resist a given triad of in-plane forces can be found. The equations are based on the assumptions made in sub-section 3.4.1 except that the reinforcement can be positioned in two non-orthogonal directions by replacing y axis by α which make an

angle θ with the x direction. Compression reinforcement is also assumed to be perfectly plastic and to yield at stress of f_s' in compression. Table 3.1 shows the nine possible cases of orthogonal reinforcement to resist in-plane forces. In this table σ_1 is given as zero when tension reinforcement is provided because the concrete must be cracked, and $\sigma_2 = f_c'$ when compression reinforcement is provided so as to make optimum use of the concrete.

Table 3.1 Summary of possible combinations of reinforcement

Case	Reinforcement description	Known values	Method of solution
1	Both tension	$f_x=f_\alpha=f_s$, $\sigma_1=0$	Minimisation of $(\rho_x+\rho_\alpha)$
2	No x , α tension	$f_\alpha=f_s$, $\rho_x=0$, $\sigma_1=0$	Direct solution
3	No α , x tension	$f_x=f_s$, $\rho_\alpha=0$, $\sigma_1=0$	Direct solution
4	Both compression	$f_x=f_\alpha=f_s'$, $\sigma_2=f_c'$	Minimisation of $(\rho_x+\rho_\alpha)$
5	No x , α compression	$f_\alpha=f_s'$, $\rho_x=0$, $\sigma_2=f_c'$	Direct solution
6	No α , x compression	$f_x=f_s'$, $\rho_\alpha=0$, $\sigma_2=f_c'$	Direct solution
7	x tension, α compression	$f_x=f_s$, $f_\alpha=f_s'$, $\sigma_1=0$, $\sigma_2=f_c'$	Direct solution
8	x compression, α tension	$f_x=f_s'$, $f_\alpha=f_s$, $\sigma_1=0$, $\sigma_2=f_c'$	Direct solution
9	No reinforcement	$\rho_x=\rho_\alpha=0$	Direct solution

Table 3.2 shows a summary of the design equations for orthogonal reinforcement, principal stresses and their angle θ for each case. Table 3.3 shows the boundary equations separating these design sets. Figure 3.9 shows boundary curves and regions for orthogonal reinforcement. For more detailed information the reader is referred to Nielsen (1984) and Clark (1976).

3.6: Direct design method

The yield criterion in equation 3.4 and the design equations proposed by Nielsen (Fig. 3.8) suggest an approach to ultimate limit state design as follows:

1. At any point calculate a set of stress in equilibrium with external loads. The stress distribution can be derived from elastic or plastic analysis as long as it maintains equilibrium with external load.
2. Calculate required steel areas using Nielsen's equations.

In this research these rules were applied to the design of hollow and solid reinforced and partially prestressed concrete beams. This procedure is called the Direct Design Method because the area of reinforcement is directly calculated from the stress field using Nielsen's equations.

Table 3.2 Design equations for orthogonal reinforcement

Case	ρ_x	ρ_y	σ_1	σ_2	$\tan\theta$
1	$\frac{1}{f_s}\left(\sigma_x+\lvert\tau_{xy}\rvert\right)$	$\frac{1}{f_s}\left(\sigma_y+\lvert\tau_{xy}\rvert\right)$	0	$-2\lvert\tau_{xy}\rvert$	$-\frac{\tau_{xy}}{\lvert\tau_{xy}\rvert}$
2	0	$\frac{1}{f_s}\left(\sigma_y-\frac{\tau_{xy}^2}{\sigma_x}\right)$	0	$\sigma_x+\frac{\tau_{xy}^2}{\sigma_x}$	$\frac{\sigma_x}{\tau_{xy}}$
3	$\frac{1}{f_s}\left(\sigma_x-\frac{\tau_{xy}^2}{\sigma_y}\right)$	0	0	$\sigma_y+\frac{\tau_{xy}^2}{\sigma_y}$	$\frac{\tau_{xy}}{\sigma_y}$
4	$\frac{1}{f_s'}\left(\sigma_{xf}-\lvert\tau_{xy}\rvert\right)$	$\frac{1}{f_s'}\left(\sigma_{yf}-\lvert\tau_{xy}\rvert\right)$	$f_c'+2\lvert\tau_{xy}\rvert$	f_c'	$-\frac{\tau_{xy}}{\lvert\tau_{xy}\rvert}$
5	0	$\frac{1}{f_s'}\left(\sigma_{yf}-\frac{\tau_{xy}^2}{\sigma_{xf}}\right)$	$\sigma_x+\frac{\tau_{xy}^2}{\sigma_{xf}}$	f_c'	$-\frac{\tau_{xy}}{\sigma_{xf}}$
6	$\frac{1}{f_s'}\left(\sigma_{xf}-\frac{\tau_{xy}^2}{\sigma_{yf}}\right)$	0	$\sigma_y+\frac{\tau_{xy}^2}{\sigma_{yf}}$	f_c'	$-\frac{\sigma_{yf}}{\tau_{xy}}$
7	$\frac{1}{f_s}\left[\sigma_x-\frac{f_c'}{2}(1-\beta)\right]$	$\frac{1}{f_s'}\left[\sigma_y-\frac{f_c'}{2}(1+\beta)\right]$	0	f_c'	$\frac{2\tau_{xy}}{f_c'(1+\beta)}$
8	$\frac{1}{f_s'}\left[\sigma_x-\frac{f_c'}{2}(1+\beta)\right]$	$\frac{1}{f_s}\left[\sigma_y-\frac{f_c'}{2}(1-\beta)\right]$	0	f_c'	$\frac{2\tau_{xy}}{f_c'(1-\beta)}$
9	0	0	$\frac{\sigma_x+\sigma_y+\sqrt{(\sigma_x-\sigma_y)^2+4\tau_{xy}^2}}{2}$	$\frac{\sigma_x+\sigma_y-\sqrt{(\sigma_x-\sigma_y)^2+4\tau_{xy}^2}}{2}$	$\frac{\sigma_x-\sigma_y-\sqrt{(\sigma_x-\sigma_y)^2+4\tau_{xy}^2}}{2\tau_{xy}}$

where: $\rho_x=A_x/t$, $\rho_\alpha=A_\alpha/t$, $\sigma_{xf}=\sigma_x-f_c'$, $\sigma_{yf}=\sigma_y-f_c'$ and $\beta=\sqrt{1-\frac{4}{f_c'^2}\left(\tau_{xy}+\sigma_y\cot\alpha\right)}$

Table 3.3: Boundary curves for orthogonal reinforcement

Curve	Equation	Curve	Equation
1	$\frac{\sigma_y}{\lvert\tau_{xy}\rvert}=+\infty$	7	$\frac{\sigma_x}{\lvert\tau_{xy}\rvert}=\frac{1}{2}\left(\frac{f_c'}{\lvert\tau_{xy}\rvert}-\sqrt{\left(\frac{f_c'}{\lvert\tau_{xy}\rvert}\right)^2-4}\right)$
2	$\frac{\sigma_x}{\lvert\tau_{xy}\rvert}=\frac{1}{2}\left(\frac{f_c'}{\lvert\tau_{xy}\rvert}+\sqrt{\left(\frac{f_c'}{\lvert\tau_{xy}\rvert}\right)^2-4}\right)$	8	$\frac{\sigma_x}{\lvert\tau_{xy}\rvert}=-1$
3	$\frac{\sigma_y}{\lvert\tau_{xy}\rvert}=-1$	9	$\frac{\sigma_{xf}}{\lvert\tau_{xy}\rvert}\frac{\sigma_{yf}}{\lvert\tau_{xy}\rvert}=1$
4	$\frac{\sigma_y}{\lvert\tau_{xy}\rvert}=\frac{f_c'}{\lvert\tau_{xy}\rvert}+1$	10	$\frac{\sigma_x}{\lvert\tau_{xy}\rvert}\frac{\sigma_y}{\lvert\tau_{xy}\rvert}=1$
5	$\frac{\sigma_y}{\tau_{xy}}=\frac{1}{2}\left(\frac{f_c'}{\lvert\tau_{xy}\rvert}-\sqrt{\left(\frac{f_c'}{\lvert\tau_{xy}\rvert}\right)^2-4}\right)$	11	$\frac{\sigma_x}{\lvert\tau_{xy}\rvert}=\frac{f_c'}{\lvert\tau_{xy}\rvert}+1$
6	$\frac{\sigma_y}{\lvert\tau_{xy}\rvert}=-\infty$	12	$\frac{\sigma_x}{\lvert\tau_{xy}\rvert}=\frac{1}{2}\left(\frac{f_c'}{\lvert\tau_{xy}\rvert}+\sqrt{\left(\frac{f_c'}{\lvert\tau_{xy}\rvert}\right)^2-4}\right)$

3.6.1: Satisfaction of the conditions of the theory of plasticity

The direct design approach satisfies the conditions of plasticity theory as follows:

Equilibrium condition: The internal stresses which are used in the design are in equilibrium with the external applied loads.

Yield criterion: Stresses will not violate the yield criterion of the material because the yield criterion is used to determine the steel areas.

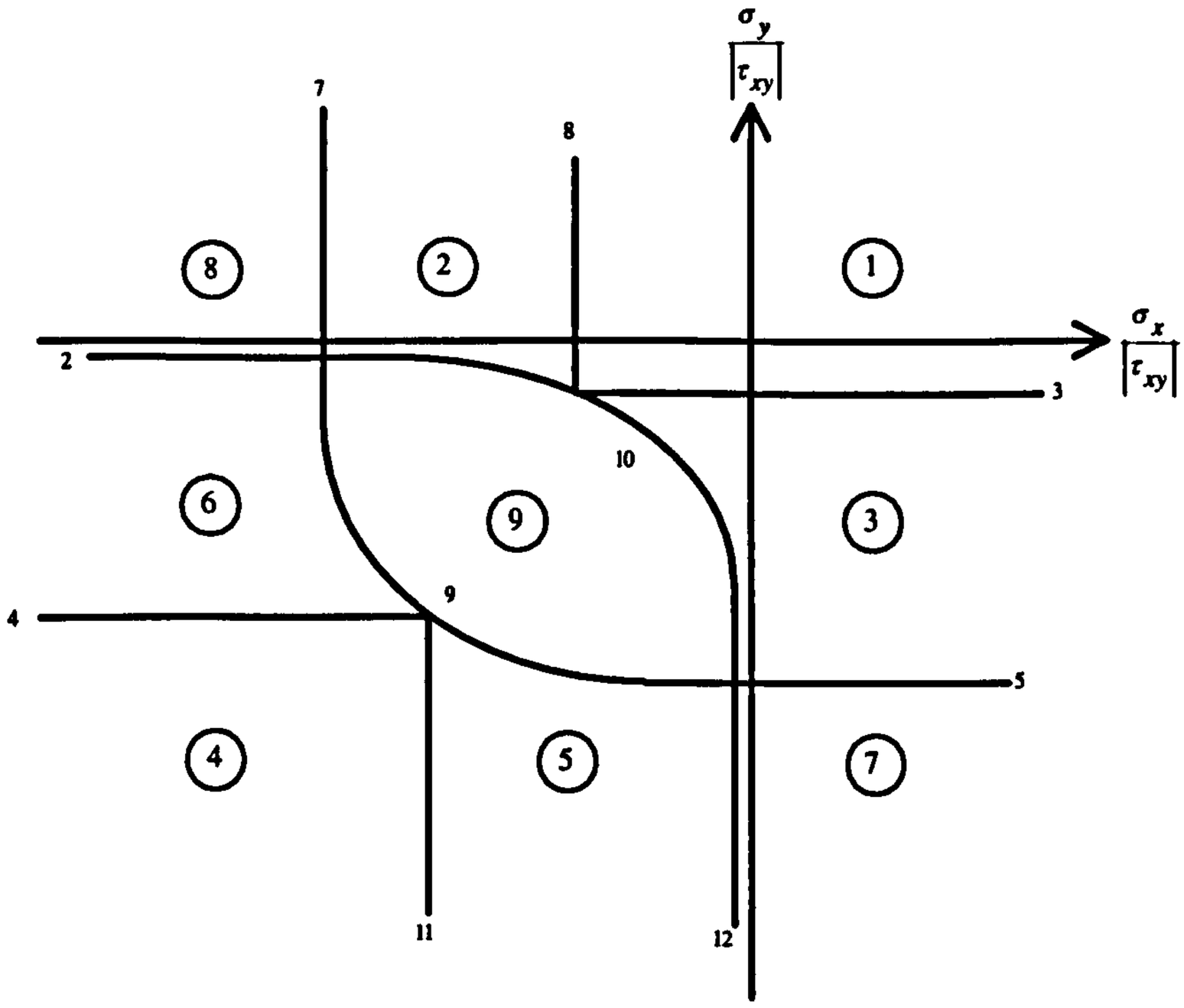

Figure 3.9: Case boundary graph for orthogonal reinforcement

Plain numerals represent boundary curve Nos. while ringed numerals represent case Nos.

Mechanism condition: Under ultimate load, the structure will develop sufficient plastic hinges to transform it into a mechanism because the resisting forces are exactly equal to the applied loads and therefore, theoretically, all points of the structure will yield simultaneously. Practically, however, this is not possible because it is difficult to provide exactly the required reinforcement for each point in the structure.

3.6.2: Reduction of ductility demand

When applying the theory of plasticity to reinforced or prestressed concrete structures, it is important to realise that they have limited ductility. Direct design method, in addition to the satisfaction of the conditions in sub-section 3.6.1 also

reduces the ductility demand made by the theory of plasticity. This is achieved by the 'simultaneous' yielding of all points in the structure. In other words the difference between the first yield load and ultimate load will be as small as practicable.

3.6.3: Multiple load cases

The previous design equations apply when the structure is subjected to a stress field resulting from a single load case. That means one in-plane force triad $\left(N_{xi}, N_{yi}, N_{xyi}\right)$ and one corresponding reinforcement $\left(N_{xi}^{s}, N_{yi}^{s}\right)$ for every point *i* in the structure due to the single applied load case.

In practice, structures are designed for multiple load cases as shown in figure 3.10. These load cases are possible load combinations that the structure might be subjected to during its existence. The economic solution is the one which gives safe design with least reinforcement. An advantage of the direct design method is that it can also handle this multiple load cases easily as follows:

1. For every point *i* in the structure under each load case *j* calculate $\left(N_{xij}, N_{yij}, N_{xyij}\right)$ and corresponding $\left(N_{xij}^{s}, N_{yij}^{s}\right)$.
2. Select the largest N_{xij}^{s} from all load cases and use it in the yield criterion (Eq. 3.4) to find the minimum N_{yij}^{s} which satisfy this equation. Find $N_{xij}^{s} + N_{yij}^{s}$.
3. Select the largest N_{yij}^{s} from all load cases and use it in the yield criterion (Eq. 3.4) to find the minimum N_{xi}^{s} which satisfy this equation. Find $N_{xij}^{s} + N_{yij}^{s}$.
4. The least reinforcement $(N_{xij}^{s} + N_{yij}^{s})$ from steps 2 and 3 is the optimal reinforcement at point *i*.

Of course if the largest N_{xij}^{s} from step 2 and the largest N_{yij}^{s} from step 3 are used, the structure will be safe but steel reinforcement is not economical.

It has to be observed that with above procedures used for designing reinforcement, at ultimate load, not all points yield simultaneously for all load cases. Thus the structure might not become a mechanism and the true ultimate load can be larger than the design load.

3.6.4: Comparison between the direct design method and the truss analogy

As discussed in section 2.3 of chapter 2, the truss analogy has received more attention and given preference over the skew-bending method. Therefore, here a comparison between the truss analogy and the direct design method is made. Table 3.4 shows the required reinforcement for hollow beams based on the direct design method and in the truss analogy for hollow beams. Detailed design procedure using the direct design method is presented in chapter 5, while for the truss analogy the example in appendix A was followed. Elastic stress distribution was used in the case of the direct design method. Three angles for the compressive diagonals as recommended by several researchers were used in the case of truss analogy. It can be seen that the direct design approach leads to steel requirement close to the truss analogy when the angle of inclination of the diagonals is 45°. Less longitudinal but more transverse steel is required by the direct design method than the truss analogy when the angle is 26.57°. When the angle is 63.43° the direct design method requires much less transverse reinforcement but slightly more longitudinal reinforcement than the truss analogy.

From this comparison it is possible to say that although the direct design method does not necessarily lead to less reinforcement but it is more systematic and not relying on the selection of the angle of inclination of the compressive diagonals.

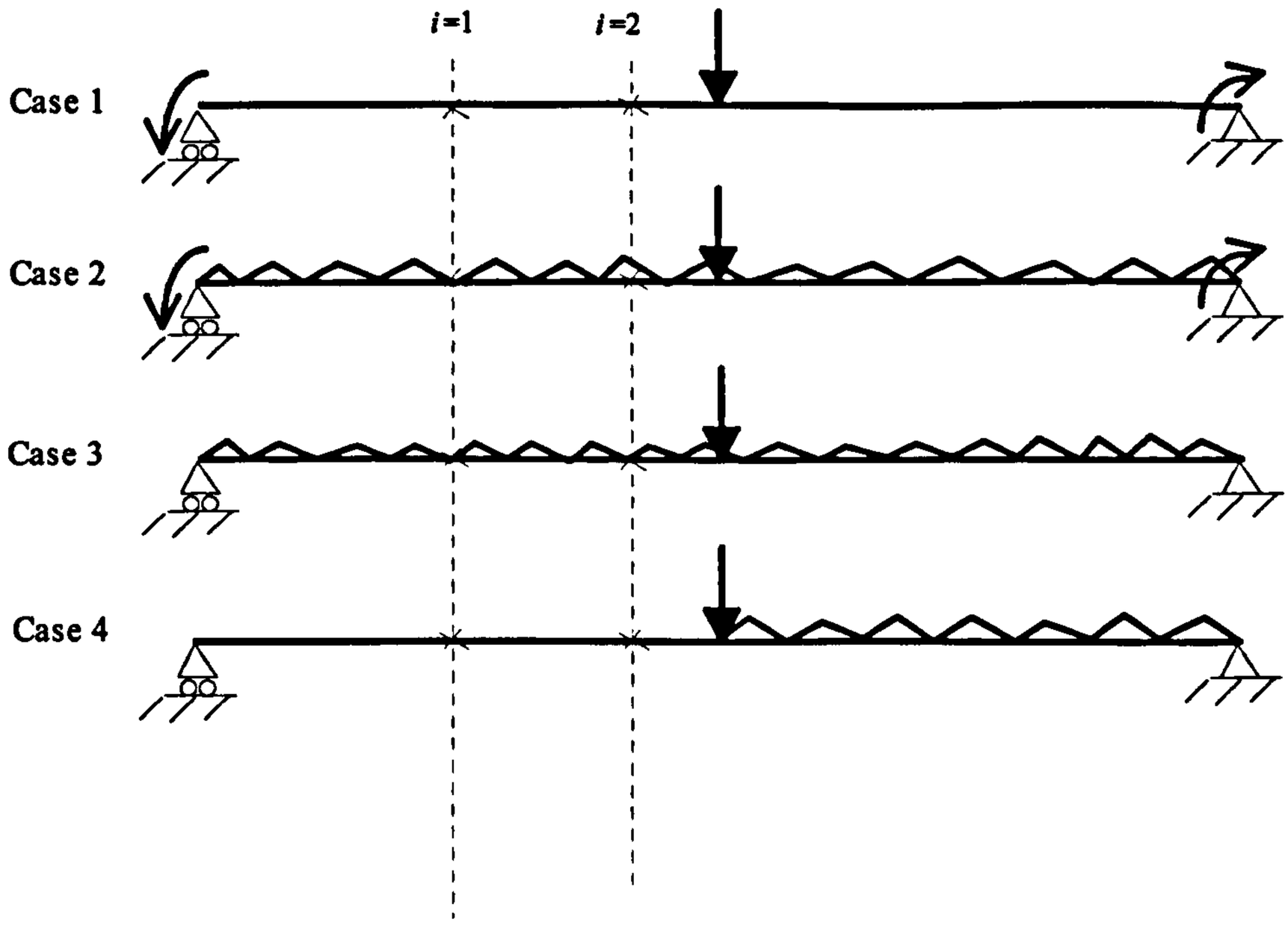

Fig. 3.10: Multiple load cases

Table 3.4: Steel requirement using the direct design method and the truss analogy

Applied load			Direct Design Method		Truss Analogy					
					$\alpha = 26.57°$		$\alpha = 45.00°$		$\alpha = 63.43°$	
M	V	T	A_s	A_{sv}	A_s	A_{sv}	A_s	A_{sv}	A_s	A_{sv}
kN.m.	kN.	kN.m.	mm^2	mm^2/m	mm^2	mm^2/m	mm^2	mm^2/m	mm^2	mm^2/m
14.89	21.08	13	253	299	416	146	226	292	171	585
68.89	81.08	13	745	559	759	266	655	532	604	1065
14.89	21.08	39	475	715	1248	354	624	708	312	1417

3.6.5: Previous usage

The direct design method has been successfully used for the design of different structures such as: design of reinforced slabs and slab-beam systems [Hago (1982)], design of shear wall-slab junctions subjected to gravity and wind loading [Memon (1984)], design of T-section shear walls [El-Nuonu (1985)], design of reinforced beams subjected to bending and torsion [Ebireri (1985)], design of reinforced concrete skew slabs [Abdel-Hafez (1986)], design of reinforced and partially prestressed concrete beams subjected to multiple combinations of bending and torsion [Moussa (1988)], design of reinforced and partially prestressed beams subjected to combined load of bending and torsion [Saadi (1988)], and design of deep beams and slabs [Bensalem (1993)]. Also, comparison between non-linear analysis and direct design method in reinforced concrete beams subjected to combined load of bending, torsion and shear [El-Hussein (1994)].

3.7: Beam design

3.7.1: Hollow beams

The main stress conditions in the thin-walled concrete beams, due to combined loading of torsion, bending and shear, are those of direct stresses in the plates of box girder as shown in figure 3.11. The forces involved in out-of-plane bending are very small and can be ignored. At any point in the cross-section a biaxial state of stress is maintained. At the top and bottom flanges, normal stress due to bending is combined with the shear stress due to torsion. This can be used to calculate the required reinforcement in the flanges. Similarly, in the webs, the normal stress due to bending is combined with the net shear stress due to shear force and torsion. This can be used to calculate the required reinforcement in the webs. This suggests that the design equations derived above can be used in the direct design procedure to calculate the required reinforcement at each section. This procedure is used in

chapter five for the design of reinforced and partially prestressed concrete hollow beams. The minimum wall thickness for torsional resistance in hollow beams as suggested by Thurlimann (1979) is 1/6 the diameter of the largest circle inscribed into the perimeter connecting the corner longitudinal bars as in figure 3.12. This is based on tests which revealed that the torsional strength of beams relies on the outer concrete shell of about this value. In this study, the wall thickness was conservatively taken as 1/6 of the outer dimension of the tested beam.

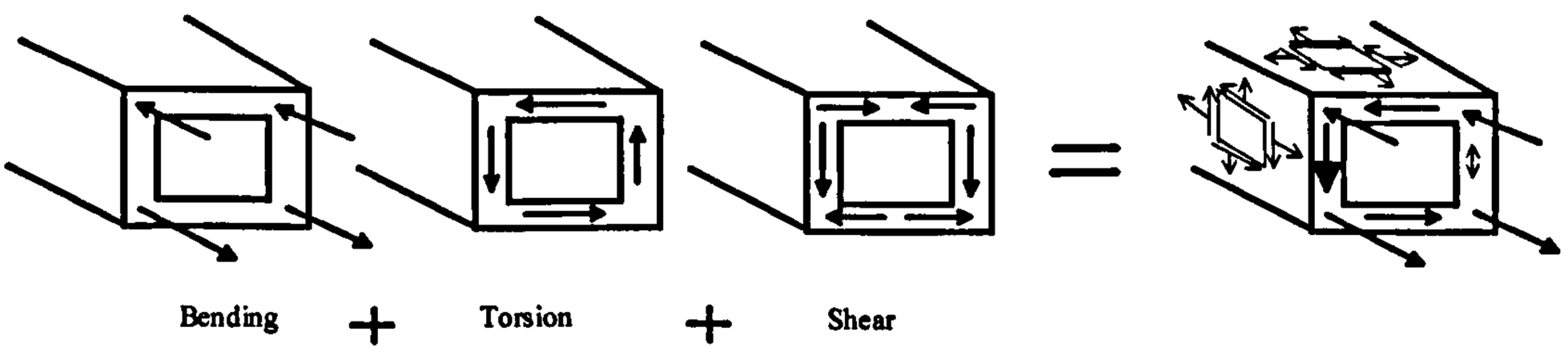

Fig. 3.11: Stresses in a hollow section

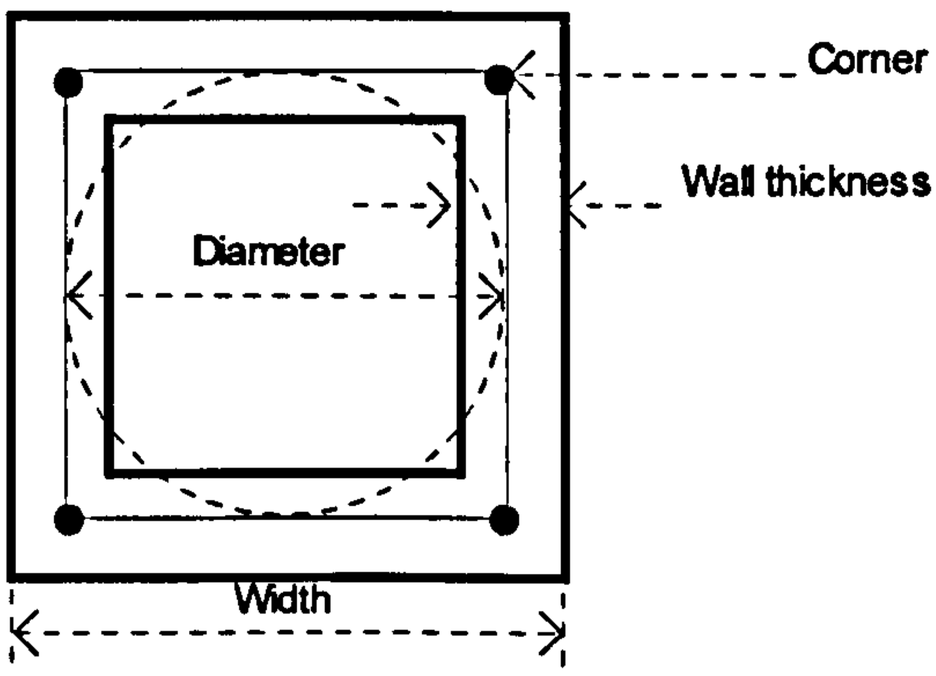

Fig. 3.12: Circle connecting the centre line of corner bars

3.7.2: Solid beams

In solid beams subjected to torsion, bending and shear the general state of stress is tri-axial. However, torsional shear stress is concentrated in the outer periphery and the shear stress due to shear force is minimal in the top and bottom strips. Therefore, if the torsional resistance of the core and the direct shear resistance of top and bottom strips are ignored, a bi-axial state of stress is formed in every part of the beam similar to hollow beams. More about the design of solid beams is presented in chapters ten and eleven.

4: Experimental set-up

4.1: Introduction

The aim of this chapter is to explain the experimental set up used to study the strength and behaviour characteristics of rectangular reinforced and partially prestressed hollow and solid beams subjected to combined loading of torsion, bending moment and shear force.

The investigation of the beams was carried out to study the followings:

- Load-displacement relationship.
- Strain distribution in steel and concrete.
- Load-twist relationship.
- Failure characteristics.
- Crack pattern and crack propagation.

4.2: Description of testing rig

The 'test rig' shown in figure 4.1a is a three-dimensional frame designed to allow application of torsion, bending moment and shear force. The beam was 300x300mm cross-section and 3.8m length. It was simply supported by a set of two perpendicular rollers at each support as shown in figure 4.1b. The lower roller allows axial displacement and the upper one allows rotation about a horizontal axis at the soffit level of the beam. The diameter of each roller was 100mm and the length was 300mm. The rollers were separated by 300x300x20mm steel plates. Similar plates were used between the rollers and the beam soffit and the support.

Torsion was applied by means of torsion arm fixed to each end of the beam. The torsion arm was made of rectangular steel sections as shown in figure 4.1c. The net torsion lever arm was 1.3m. A rectangular frame with adjustment screws fixed to a 25mm steel plates was built in the torsion arm to fix it to the beam. The adjustment screws allow for variations of specimen sizes within the frame. 2mm thick plastic sheets were used as soft contact between the beam and the steel plates and to prevent local stress concentration. Bending moment and shear force were applied at the mid-span across the beam width at the top face as shown in figure 4.1d. Using cement plaster a 300x100x30mm steel plate was placed on the top face at mid-span. A set of a pin and a roller system was installed below the load cell. The pin prevented rigid body motion and the roller allowed rotation about horizontal beam axis. At each

load point a hydraulic jack and a load cell were installed. The jack was operated using a manual hydraulic pump and the load cell was connected to a data logger for recording the applied load. This support and loading arrangement allowed full rotation about the centre line of the beam soffit and displacement in the beam axial direction.

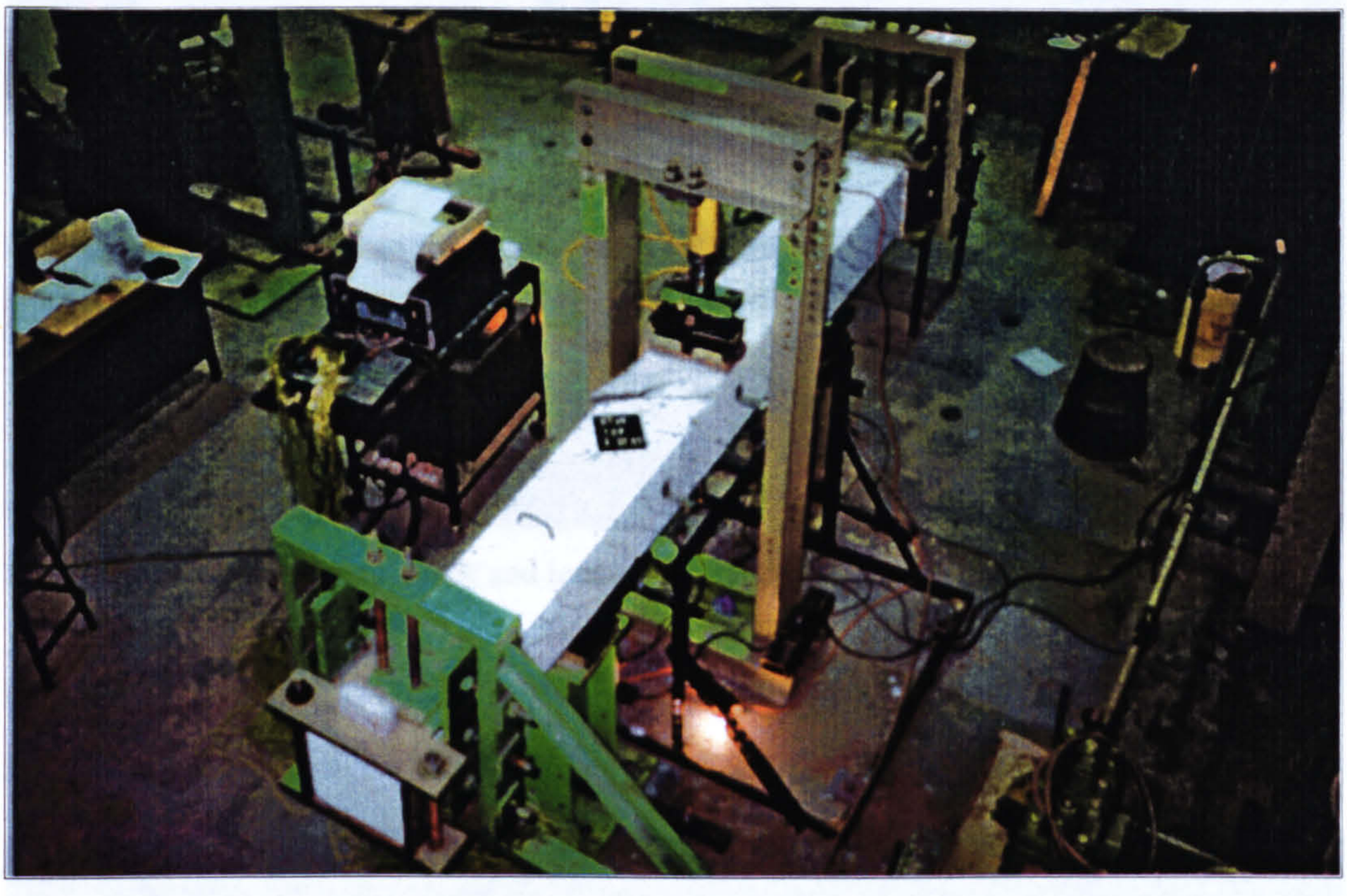

Fig. 4.1a: Test rig with a typical beam installation

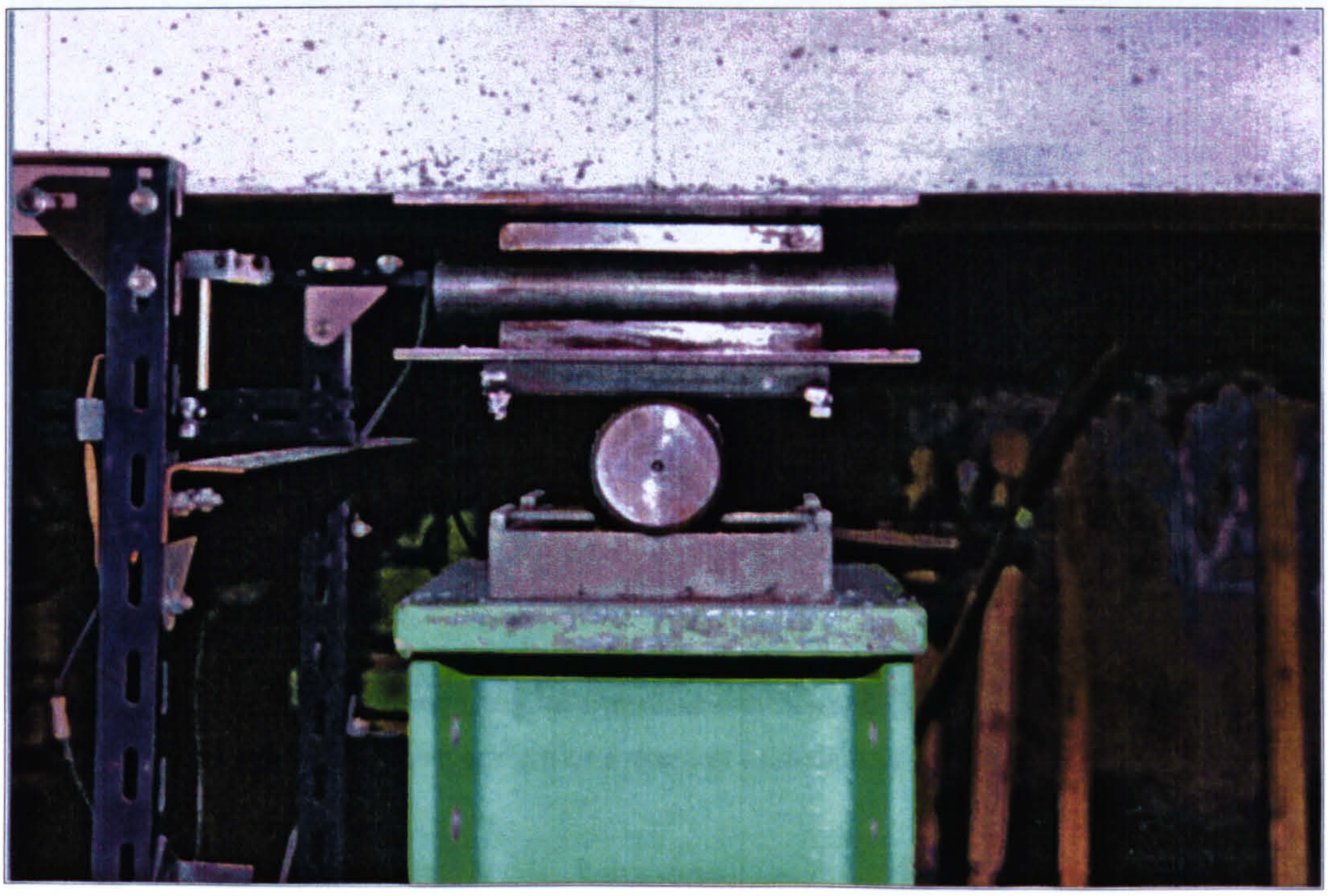

Fig. 4.1b: Set of perpendicular rollers

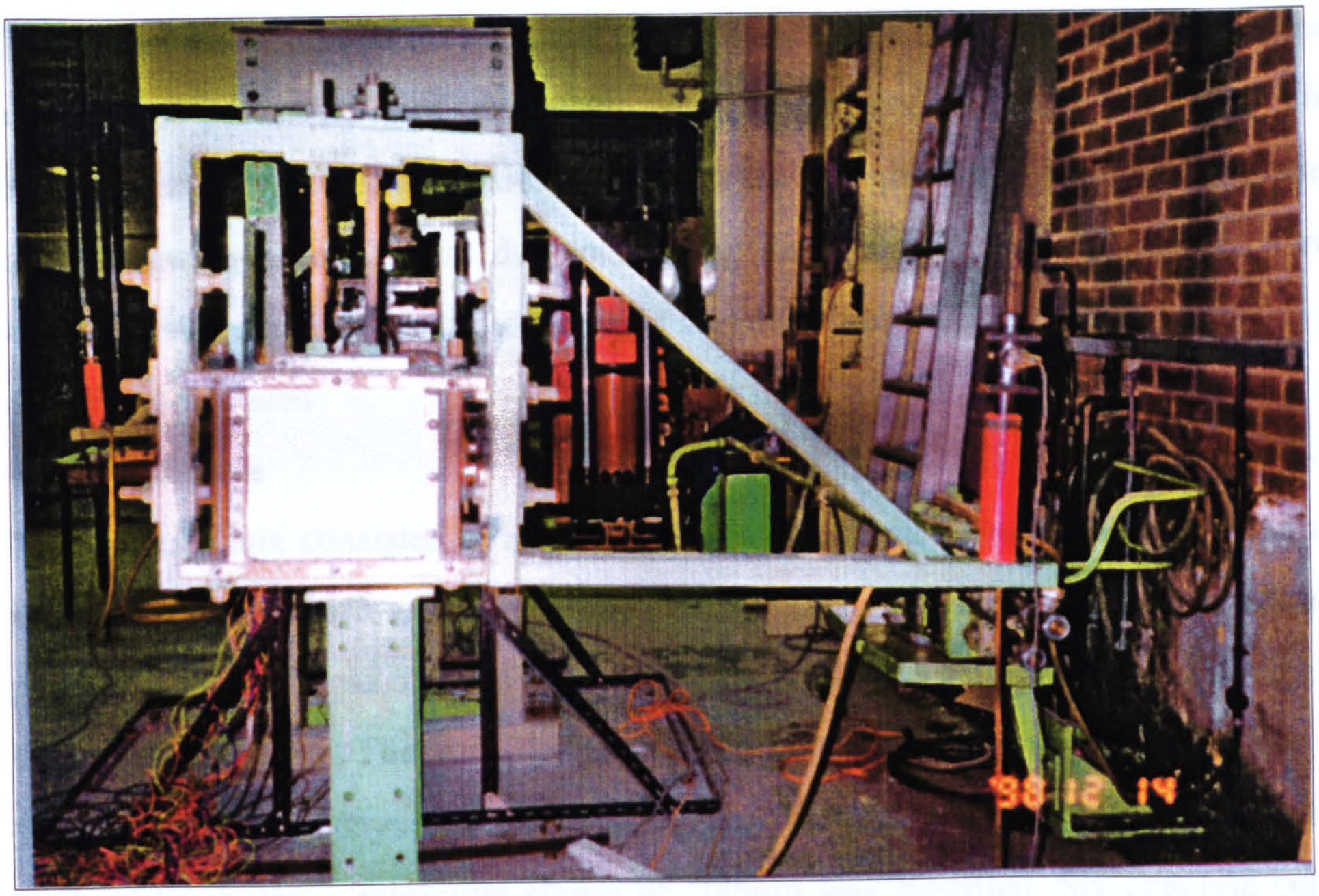

Fig. 4.1c: Torsion arm with a jack and load cell installed

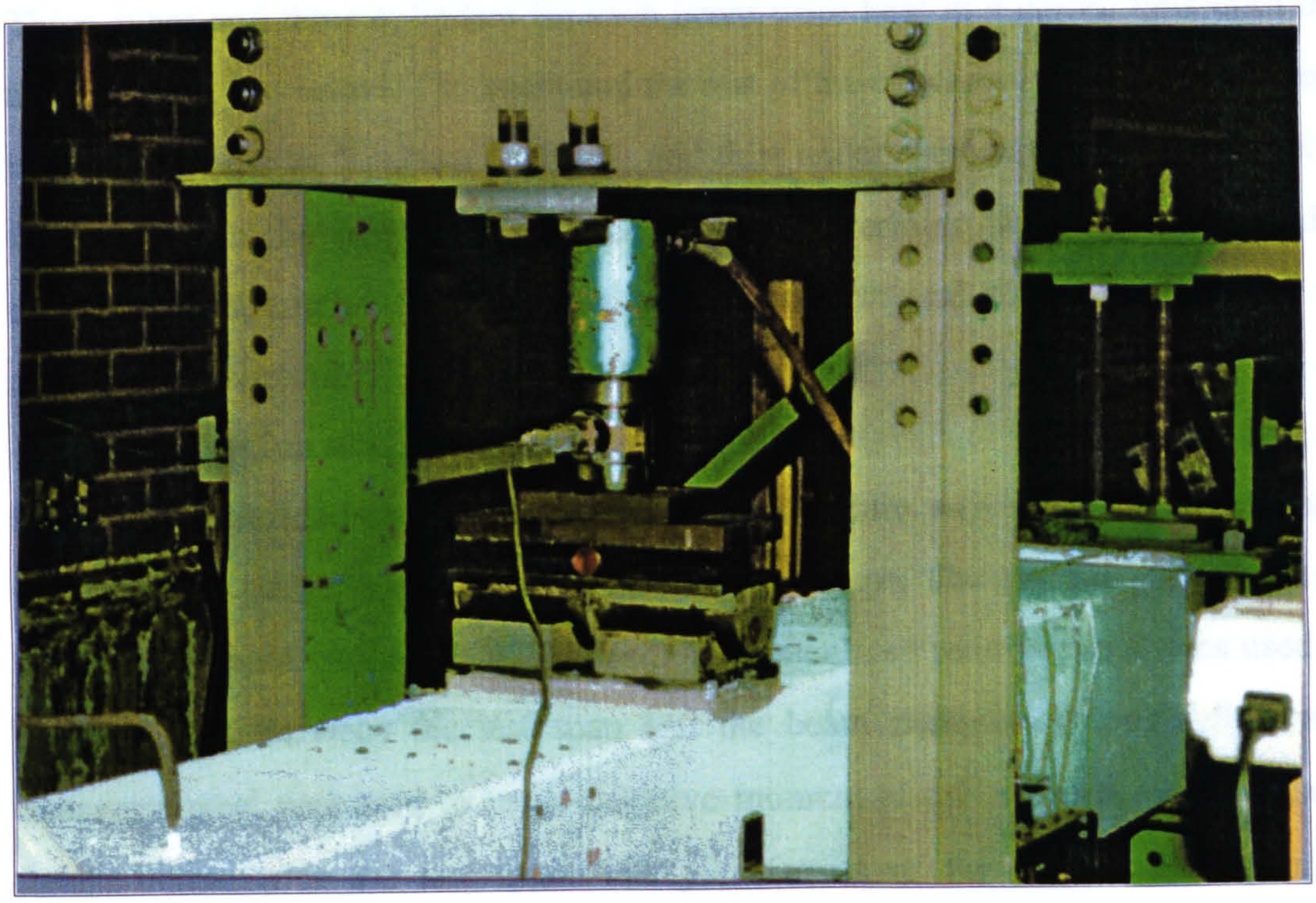

Fig. 4.1d: Jack, load cell and pin and roller system at mid-span of top face

The model was mounted on two steel stools fixed to the concrete floor at a distance of 1.8m a part. The torsional arms were at the ends of the specimen. This arrangement gave constant torsional shear stress over the entire length of the beam and maximum normal stress due to bending and shear stress due to shear force occurred near the mid-span. The test span was 1.2m long centred at mid-span.

4.3: Material used

4.3.1: Concrete

The concrete mix consisted of Rapid Hardening Portland Cement, 10mm uncrushed gravel and sand from Lanarkshire. The manual 'Design of Normal Concrete Mixes' published by the Department of Environment UK in 1988 was used for the design of the concrete mixes. The mix design was based on an average cube strength of 40N/mm^2 at seven days. To ensure adequate flow of fresh concrete into the thin walls of the beam, a minimum slump of 100mm was specified. Six concrete cubes (100mm) and six cylinders (150x300mm) were cast for each beam from the concrete used for the beam. A vibrating table was used for compacting the samples while the beam was vibrated using an external vibrator attached to the shuttering. Three cubes and three cylinders for each beam were kept in a curing tank until the day the beam was tested. The beam and the rest of the cubes and cylinders were kept under damp hessian for about four days and then under room condition. All samples were tested on the day the beam was tested to determine the cube and cylinder compressive strengths, split cylinder tensile strength and the static modulus of elasticity of concrete.

4.3.2: Reinforcing steel

High yield deformed bars of diameter 8, 10 and 12mm were used for longitudinal reinforcement while 8mm bar was used for the stirrups. The average yield stress of the reinforcement was about 490N/mm^2. The calculated reinforcement was used in the test span. Between the test span and the beam ends, more longitudinal and transverse steel was used to resist negative moment at the supports and to ensure failure occurred in the test span. The yield stress of the bars was determined according to the British standard. Using a proof strain of 0.2%, the mean tensile stress was used in the design of reinforcement.

4.3.3: Prestressing wires

In partially prestressed beams, 5mm diameter wires were used. The yield strength of the wires was 1570N/mm^2. Only two wires in the bottom flange were strain gauged with minimal number of strain gauges to minimise the possibility of reducing the wire effective diameter. The wires were prestressed one day before casting and released at least three days after casting. The force and strain in each wire was continuously monitored from the time the wire was stressed until just before moving the beam to the test rig. After the beam was installed on the rig, the wires were hooked again to the data logger for strain measurement. The pre-testing strain was added to the strain measured during testing.

4.4: Mould and specimen construction

The form work for hollow reinforced beams was made up of two parts, an internal core and an open external box. The internal core was made up of four 100x50x3800mm steel hollow sections covered with a 2mm thick plywood as shown in figure 4.2a. The steel sections were connected by screwed rods only at the ends to maintain relative position of the sections and to allow easy dismantling (Fig. 4.2b). The external dimensions of the internal core were 200x200x3800mm. The external box was made of 20mm thick marine plywood strengthened by 50x50mm horizontal and vertical wooden battens. The internal dimensions of the external box were 300x300x3800mm. The initial preparation for construction of the specimen consisted of erecting the internal steel rectangular section to form a steel skeleton. The 2mm thick plywood was lightly glued to the skeleton and painted using oil paint. The reinforcing bars and stirrups were then placed in position and tied around the internal core. Plastic spacers were used to maintain reinforcement in position. Care was taken not to damage the strain gauges or the electrical wires. The external box was cleaned and coated with a demoulding oil. The internal core encased with the steel cage was placed inside the box. Finally, the end caps were screwed to the ends of the box to ensure correct position of the internal core and made ready for concrete casting. The concrete was mixed using a rotating drum with a special mixer. The concrete was shovelled into the mould and samples were taken. A few hours after casting, the beam was covered with damp hessian. Next day the samples were demoulded and some of them were put in a water tank while the rest were kept

with the beam. After three days of wet curing, the internal steel skeleton was carefully dismantled and withdrawn, leaving the plywood still in place. The plywood sheets were then leavered off. To avoid local distortion during torsional loading, the outer 600mm of each end was filled with concrete to make it solid. After about seven days, the beam was carefully taken out of the external box. On the following day, the beam was cleaned, painted and marked. The beam was then installed on the rig, hooked to the data logger and made ready for testing. In the case of partially prestressed beams, the beams were pretensioned using a simple rig developed in the laboratory. The rig consisted of four 50x100x5000mm longitudinal hollow steel sections and two 50x100x1000mm transverse hollow sections and two 50x100x500mm vertical hollow sections at each end to hold the longitudinal ones in position. Two 50x100x1000mm sliding hollow sections were used at each end for positioning the prestressing wires. This rig formed an external frame which contained the external wooden box and the core as can be seen in figure 4.2c. The wires were tensioned using a simple arrangement of two nuts with ball bearings such that the wire could be stressed by a pair of spanners tightening the nuts. The ball bearings prevented the twisting of the wires while tensioning. The force in the wires was measured using a simple load cell developed for this purpose as shown in figure 4.2d.

4.5: Instrumentation

All the models were instrumented to measure the load and both global and local deformations.

4.5.1: Loads

Torsion, bending and shear loads were applied using manually operated hydraulic pumps connected to hydraulic jacks. The load cells were used to measure the load at each jack location. The load cells were connected to a data logger for data acquisition.

Figure 4.3 shows the loading arrangement for beams under combined loading of torsion, bending and shear including self weight of beam and torsion arms.

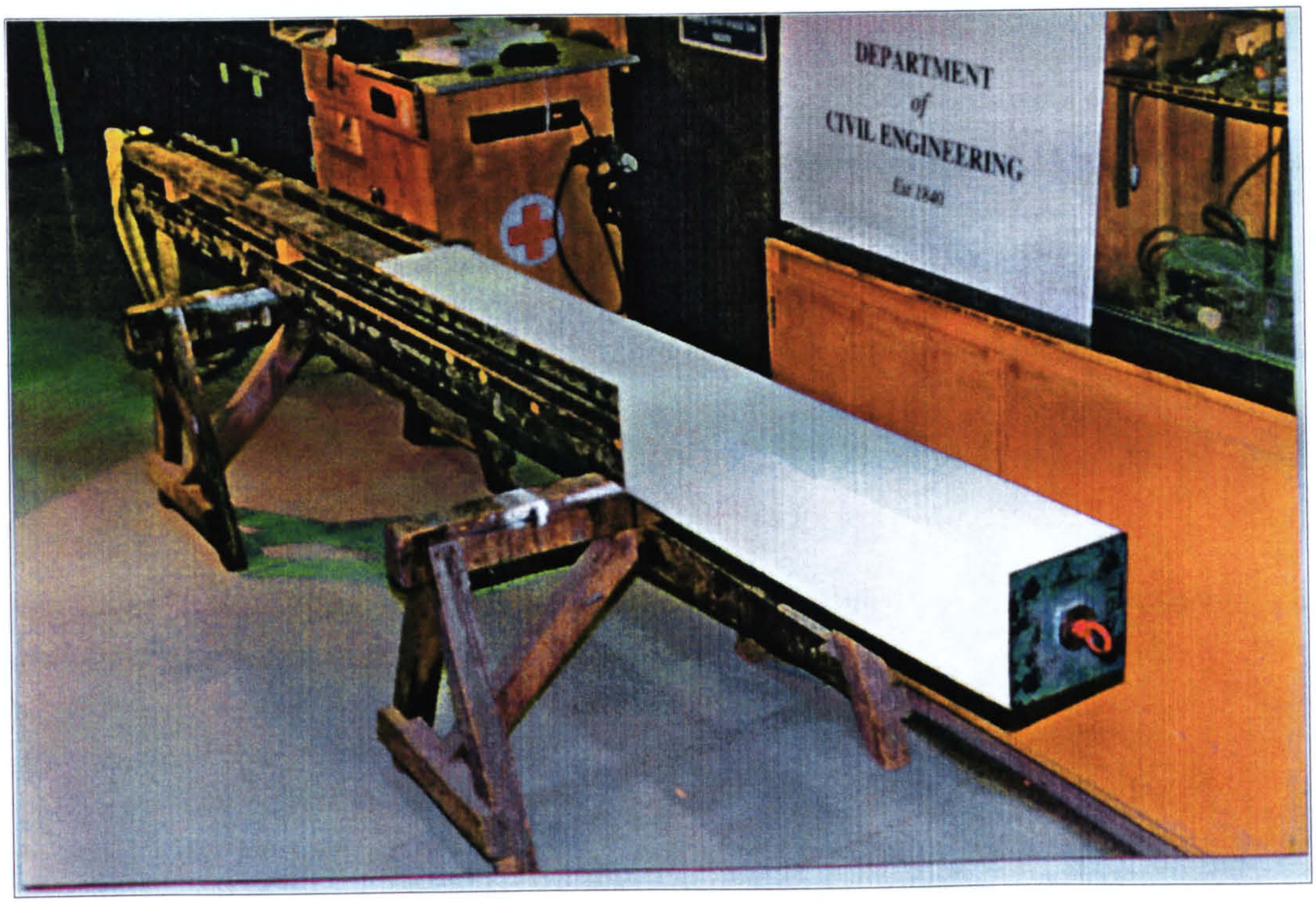

Fig. 4.2a: Internal steel box partially covered by plywood

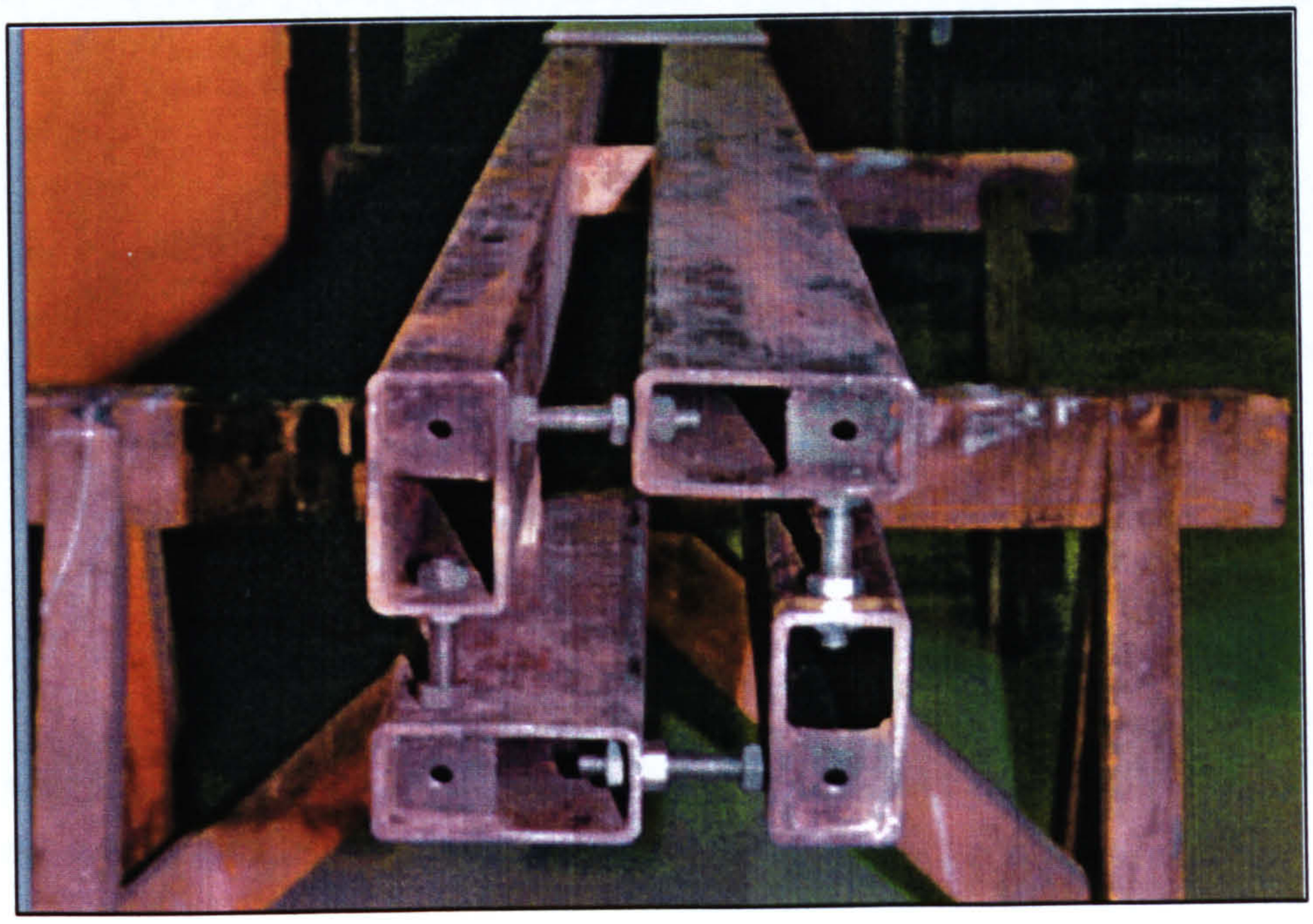

Fig. 4.2b: Internal steel box cross-section

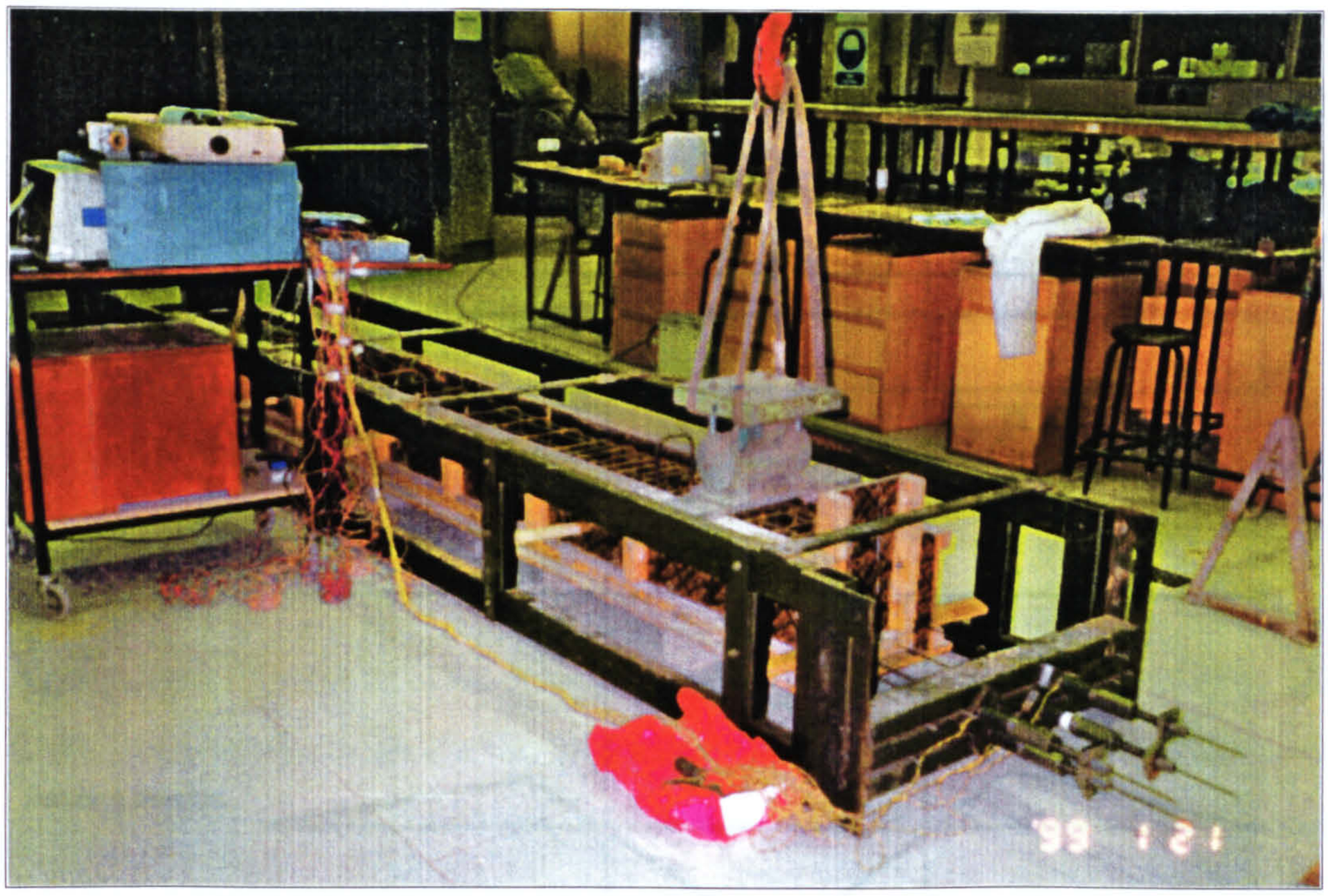

Fig. 4.2c: Pretensioning rig, sliding sections, load cells, data logger, external wooden box and vibrator

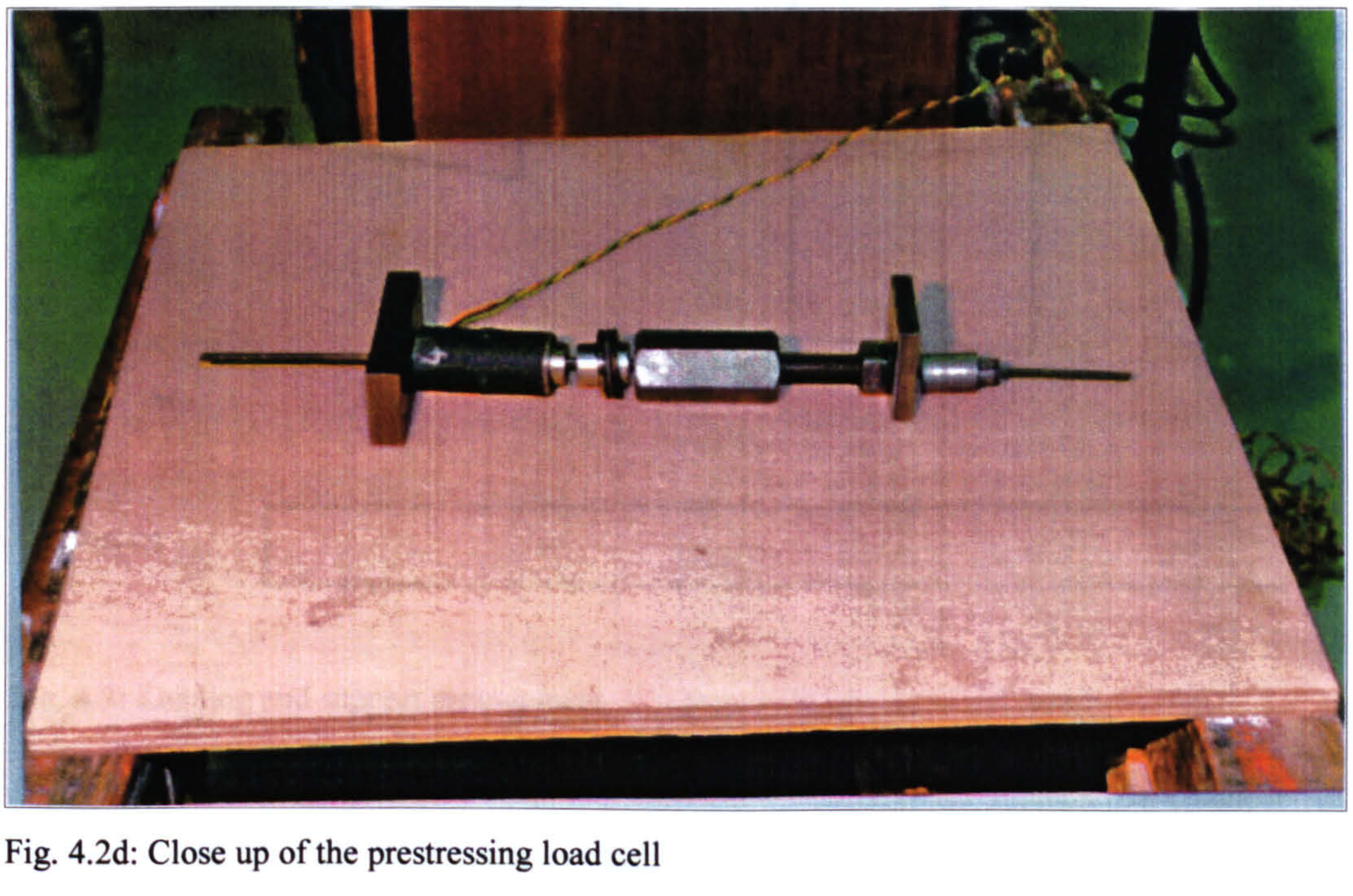

Fig. 4.2d: Close up of the prestressing load cell

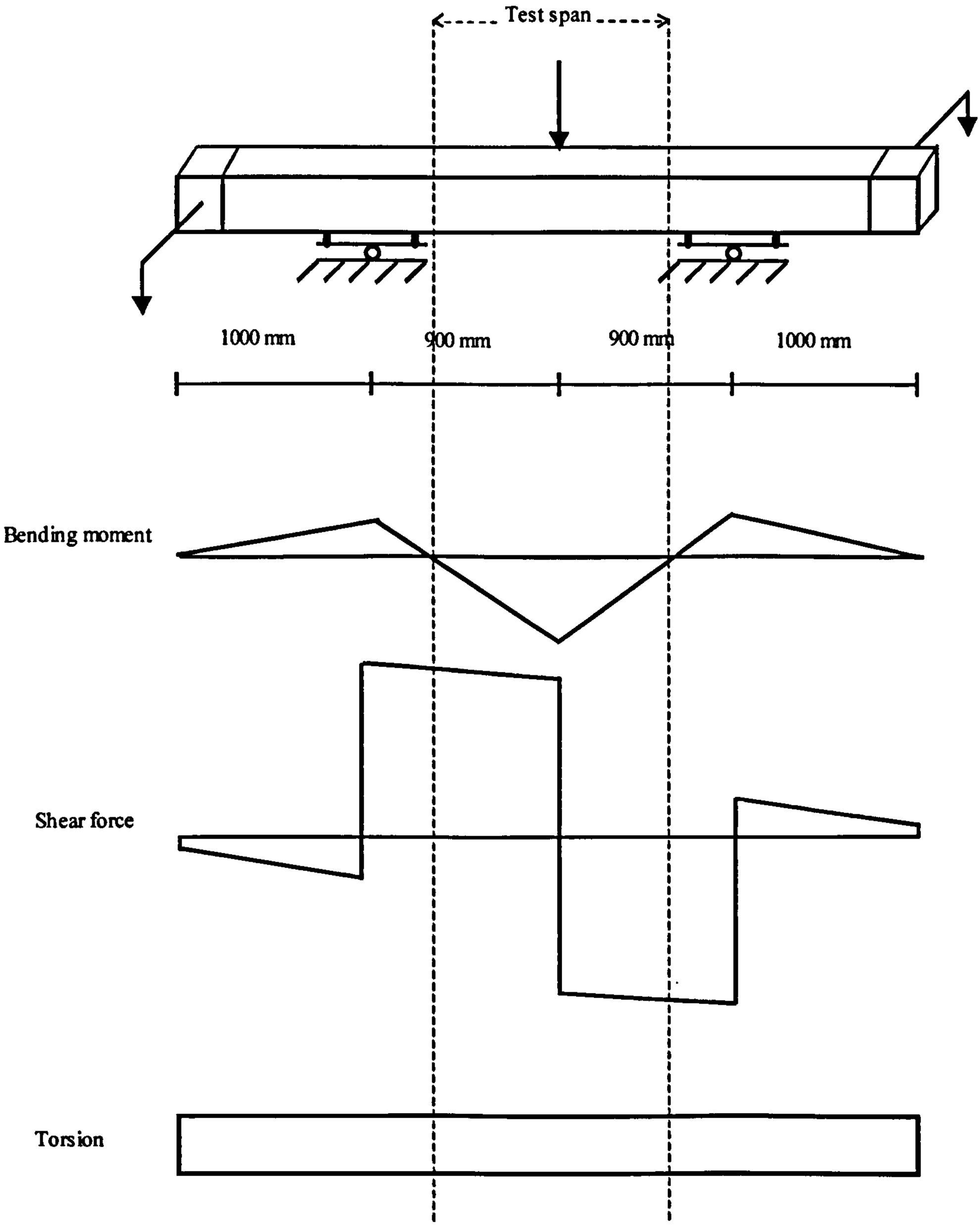

Fig. 4.3: Loading and support arrangement

4.5.2: Global deformations

Global deformations comprises of twist and displacement. They were measured at various points within the test span by means of electrical displacement transducers. To facilitate recording of results, linear voltage displacement transducers (LVDT) were used in conjunction with an automatic data storing and processing system.

4.5.2.1: Displacement

The vertical displacement of the beam was measured by means of transducers located on the centreline of the bottom face as shown in figure 4.4a.

4.5.2.2: Twist

For the measurement of twist, three transducers were located on the centreline of the front and back faces as shown in figures 4.4b-c. Rotation at any of the vertical sections was obtained by dividing the vertical difference in displacement between directly opposite transducers by the distance between these points as shown in figure 4.5a. Using the notations in this figure the angle of twist is equal to $(d_r+d_f)/L_h$. In the tested beams, the relative twist is the difference between the angle of twist θ_2 caused by the displacements in transducers 6 and 9 (Fig. 4.4) and the angle of twist θ_1 caused by the displacements in transducers 4 and 7. The rate of twist $\psi = (\theta_2 - \theta_1)/a$, where a is the distance between the two sections (Fig. 4.5b).

4.5.3: Local deformation

4.5.3.1: Strains

Strain in the longitudinal and transverse steel was measured by means of 6mm long electrical resistance strain gauges type EA.06-240LZ-120 connected to a linear voltage processing data logger. The preparation of the strain gauge installation area required the surface to be filed and smoothened with sand paper. Care was taken not to remove excessive area of steel during this operation. The surface was then treated with M-prep conditioner and M-prep neutraliser 5A to remove dirt and obtain a shining surface. The strain gauge and its terminal were stuck to the steel surface using M-bond 200 adhesive. Three 0.5mm diameter wires were carefully soldiered to the terminal and the strain gauge. These wires were connected to the data logger for measuring strain. The strain gauge and the terminal surfaces were cleaned using M-line rosin solvent applied with a small fine brush.

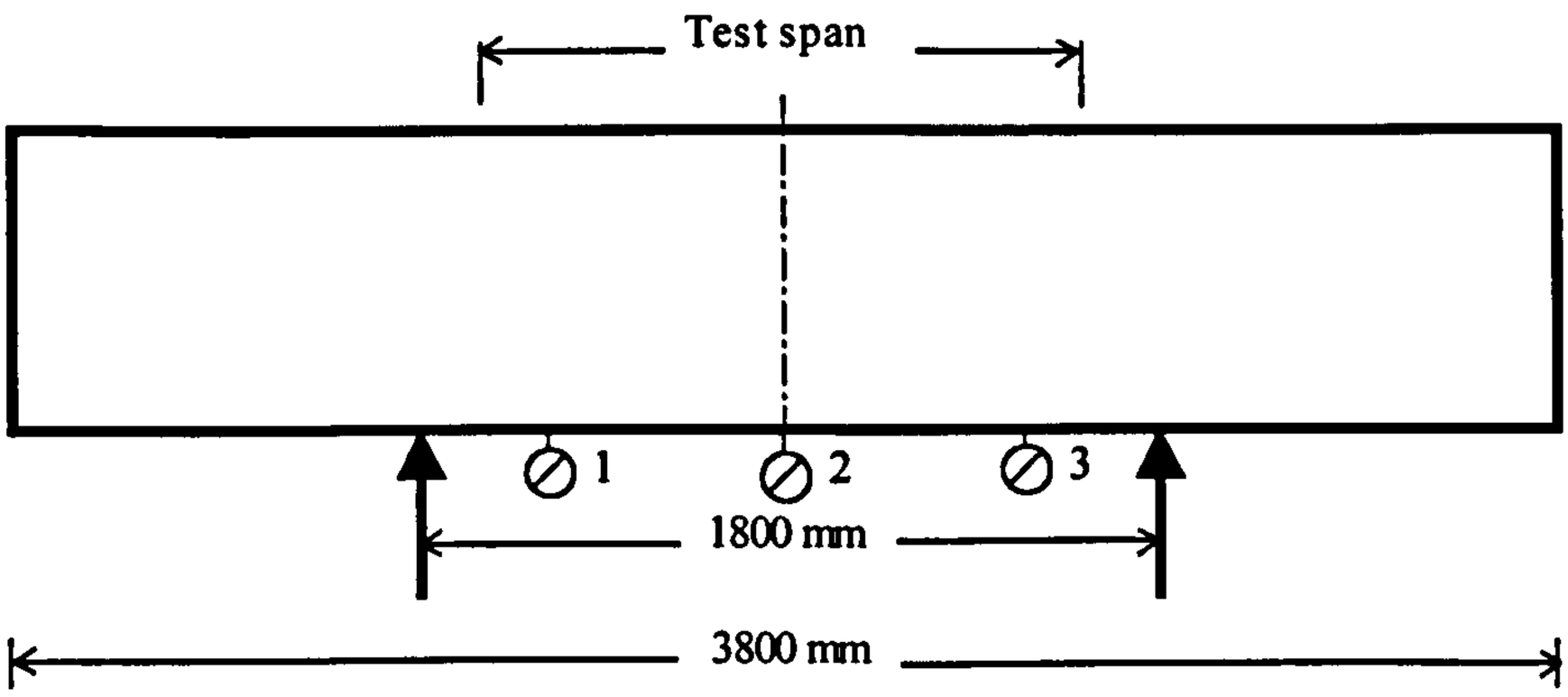

(a): LVDT at the bottom face

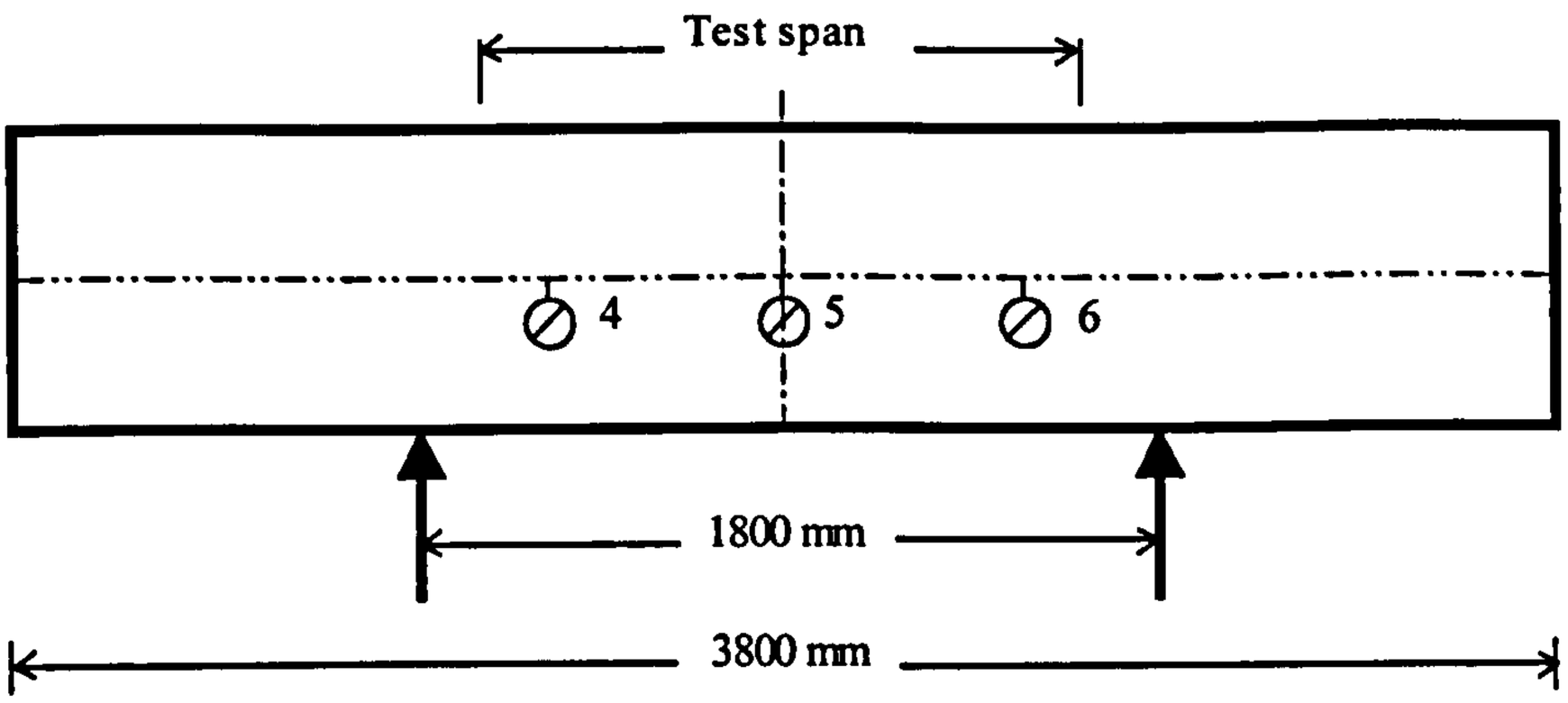

(b): LVDT at the front face

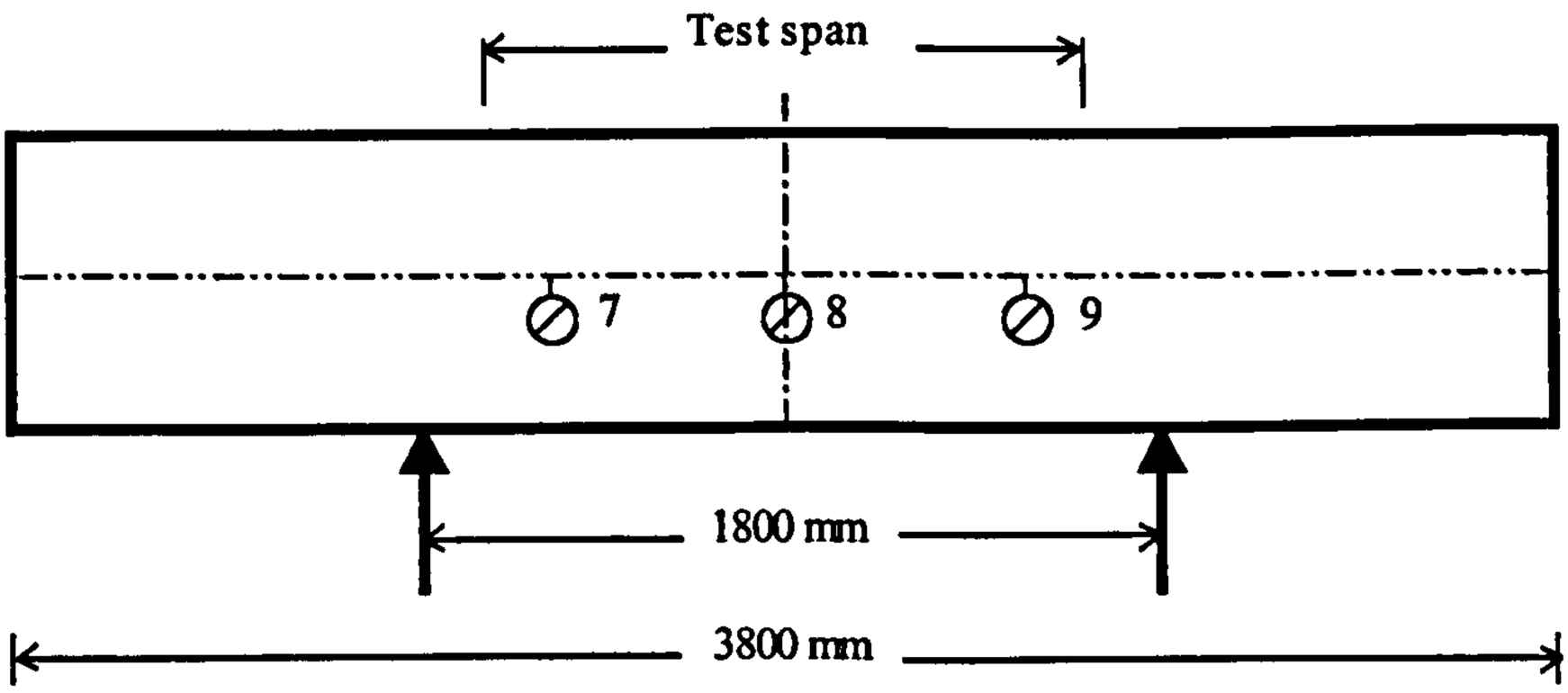

(c): LVDT at the back face

Fig. 4.4: Location of transducers

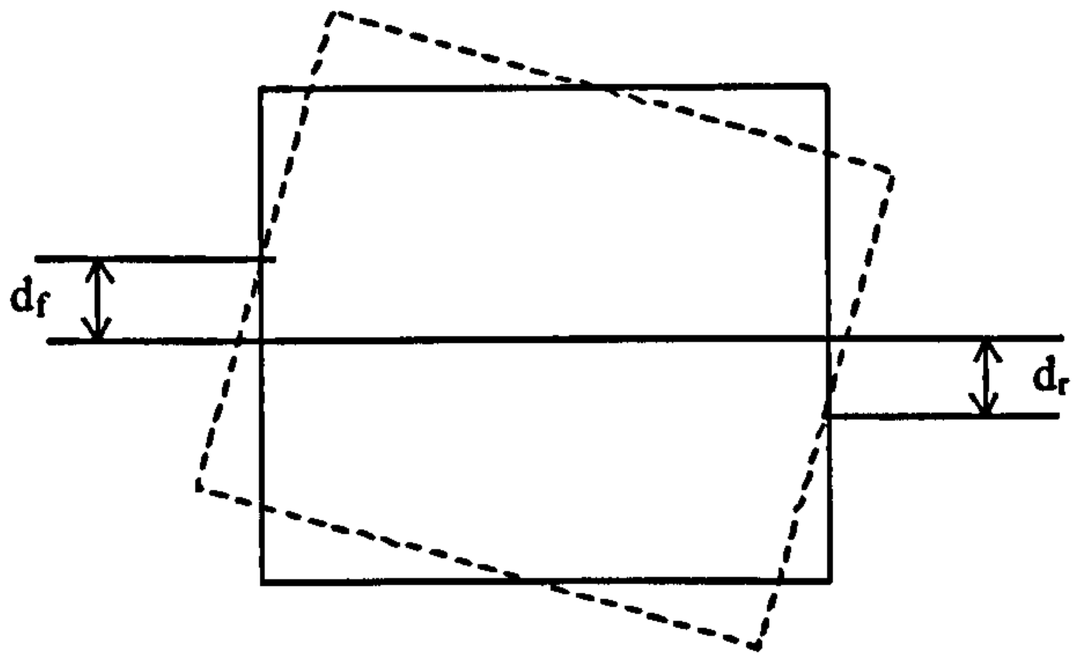

(a): Angle of twist at a section $\theta_t = (d_f+d_r)/L_h$

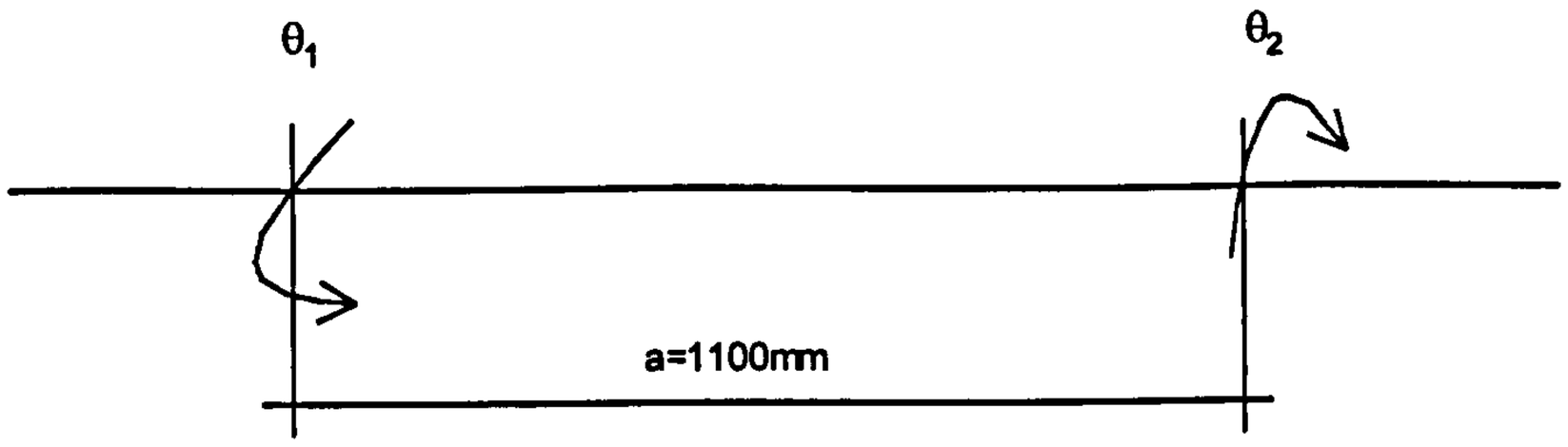

(b): Rate of twist $\psi = (\theta_2 - \theta_1)/a$

Fig. 4.5: Deformation of beam section due to torsion

For the protection of the gauge and terminal against moisture and mechanical damage during casting, first M-coat D air drying acrylic coating was applied and after drying a quick set epoxy adhesive resin was used. To measure strain in the bars, a pair of strain gauges was fixed on directly opposite faces of the bar. Accordingly, the axial strain recorded at each load stage was taken as the average reading of both gauges. A maximum of 5 pairs of strain gauges were fixed to each of maximum four longitudinal bars in each reinforced beam. In the partially prestressed beams, a maximum of three pairs of strain gauges were fixed to each of two wires in every partially prestressed beam. In the stirrups, two pairs of strain gauges were fixed to each of maximum five stirrups in each beam. Locations of strain gauges will be shown in chapters 5 and 11.

DEMEC gauges were used for measuring concrete surface strains. Since the average strains rather than the very localised ones of a cracked beam are continuous and related to one another in various directions by compatibility requirements, the average concrete strain in this study was measured over a gauge length of 100mm.

This gauge length was assumed to be sufficiently long to include several cracks. Figure 4.6 shows locations at which horizontal and vertical concrete strains were measured on three faces of the beam within the test span.

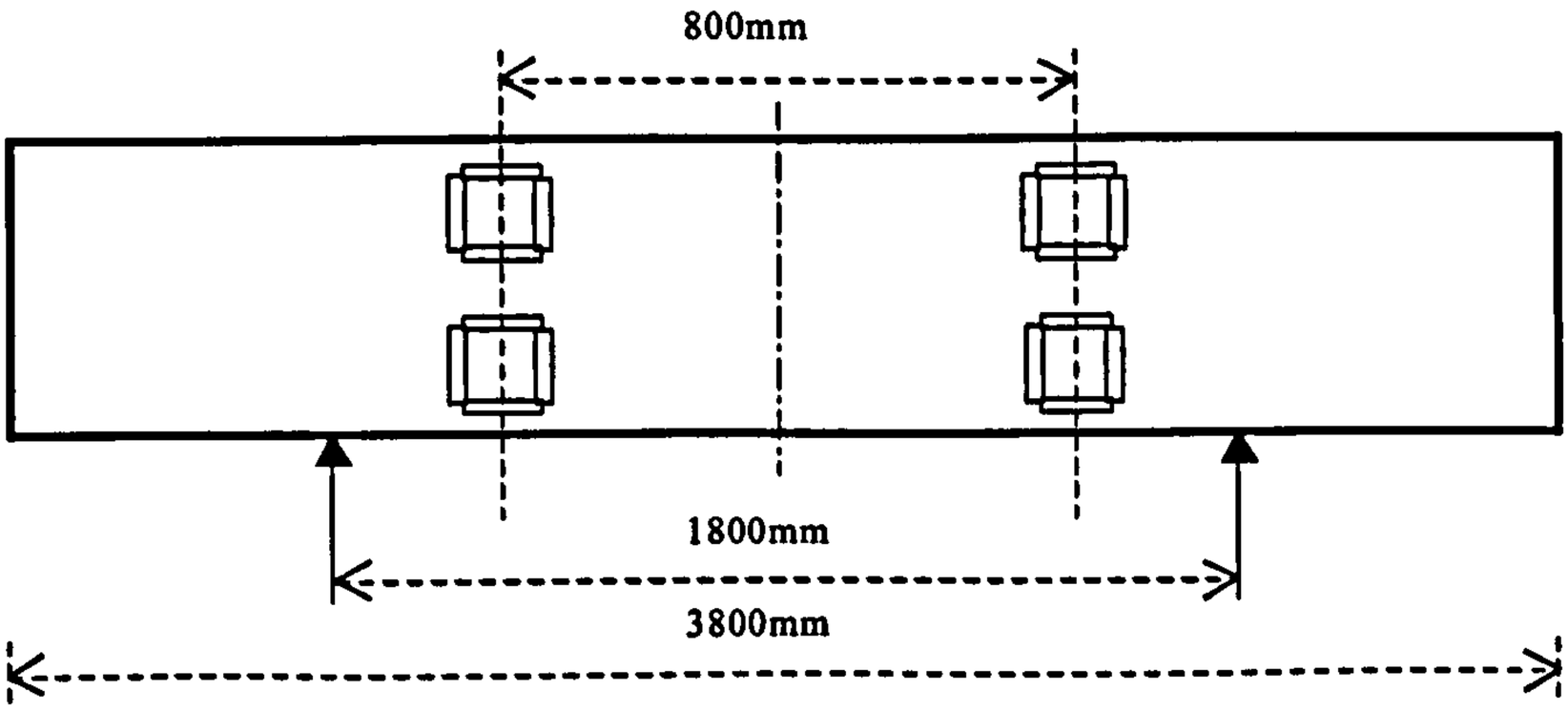

Fig. 4.6: DEMEC gauge locations on the front, top and rear faces

4.5.3.2: Crack width

All cracks were marked at each load stage and given the increment number. Crack widths were measured by means of a crackwidth measuring microscope (measuring to 0.02mm). At least two prominent cracks were selected on each face of the beam. The object of crackwidth measurement was to obtain a quantitative measure of the severity of the crack instead of arbitrary description and for the purpose of monitoring the trend of crack development.

4.6: Test procedure

For each experiment, the design load was divided into ten equal load increments. The first step was to zero all load cells and record instrument readings with minimum possible loads on the model. Flexural loads were normally applied before torsional load at each load level. To allow for stable deformation to take place after each load increment, an interval of about one minute was used before recording the instrument readings. After the steel strains and displacement readings were recorded, cracks were marked and DEMEC readings were taken before the next load was applied. The beam was considered to have collapsed when it could resist no more load. This usually happened after a major crack spiralled around the beam cross-section near the mid-span dividing the beam into two parts connected by the longitudinal reinforcement.

4.7: Data acquisition

All strain gauges, LVDTs and load cells were connected to a SOLARTRON ORION data logger. The strain gauge readings were in micro strains positive when elongation and negative when contraction, the displacement readings were in millimetre positive when downward and negative when upward and the loading was measured in kilo Newton. The DEMECs readings were taken using a digital signal conditioning box.

4.8: Test program

In this research seventeen reinforced and partially prestressed beams were tested. There were eleven hollow beams and six solid ones as shown in table 4.1.

The test results for hollow beams are discussed in chapters five and nine and for the solid ones are discussed in chapters ten and eleven.

Table 4.1 Design load combinations for tested beams

Beam No.	T_d kN.m.	V_d kN.	M_d kN.m.	τ_{tor}/τ_{shr} Ratio.	T_d/M_d Ratio.
Group A: Reinforced hollow beams.					
BTV1	13	21.08	14.89	2.28	0.87
BTV2	13	41.08	32.89	1.17	0.40
BTV3	13	61.08	50.89	0.79	0.26
BTV4	13	81.08	68.89	0.59	0.19
BTV5	26	21.08	14.89	4.56	1.75
BTV6	26	41.08	32.89	2.34	0.79
BTV7	39	21.08	14.89	6.84	2.62
BTV8	39	41.08	32.89	3.51	1.19
Group B: Partially prestressed hollow beams.					
BTV9	18	61.08	50.89	1.09	0.35
BTV10	26	21.08	14.89	4.56	1.75
BTV11	39	21.08	14.89	6.84	2.62
Group C: Reinforced solid beams.					
BTV12	13	61.08	50.89	0.79	0.26
BTV13	26	61.08	50.89	1.39	0.51
BTV14	13	61.08	50.89	0.69	0.26
BTV15	39	41.08	32.89	3.04	1.19
Group D: Partially prestressed solid beams.					
BTV16	13	61.08	50.89	0.69	0.26
BTV17	39	41.08	32.89	3.04	1.19

5: Experimental investigation of hollow beams

5.1: Introduction

In this chapter experimental investigation of hollow beams designed using elastic stress distribution combined with the direct design method is presented. All beams were subjected to a combined load of torsion, bending and shear. The beams were constructed and tested following the procedure discussed in the preceding chapter. Beams were 3.8m long with a test span of 1.2m centred at mid-span. The external dimension of the cross-section was 300x300mm with a 50mm wall thickness. Experimental observation is presented here while comparison between the experimental and computational results is discussed in chapter nine. Appendix B shows a complete set of strain gauge readings compared with computed strains.

5.2: Design stress distribution

Since the direct design method requires a stress field to be used for the calculation of reinforcement, it is worth discussing the stress distribution which gives the least required reinforcement for the geometry of the beam and load combinations used in this research. For this purpose, the required reinforcement for three typical reinforced and partially prestressed beams using elastic and plastic stress distributions are compared. The yield strength for unstressed longitudinal and transverse steel was arbitrarily taken as 500N/mm^2. In partially prestressed beams, two pairs of prestressing wires were assumed, each wire stressed to 20kN axial force. The eccentricity for each pair was 125 and 75mm and the yield stress f_{py} of the wire was taken as 1570N/mm^2.

5.2.1: Elastic stress distribution (Fig. 5.1a)

In elastic stress distribution, the normal stress due to bending σ_{xb} at any point of the beam section is given by equation 5.1 and the shear stress τ_{shr} due to shear force is calculated using equation 5.2. Equation 5.3 is used for the torsional shear stress τ_{tor}.

$$\sigma_{xb}=My/I \qquad 5.1$$

$$\tau_{shr}=VQ/(Ib) \qquad 5.2$$

$$\tau_{tor}=T/(2tA_o) \qquad 5.3$$

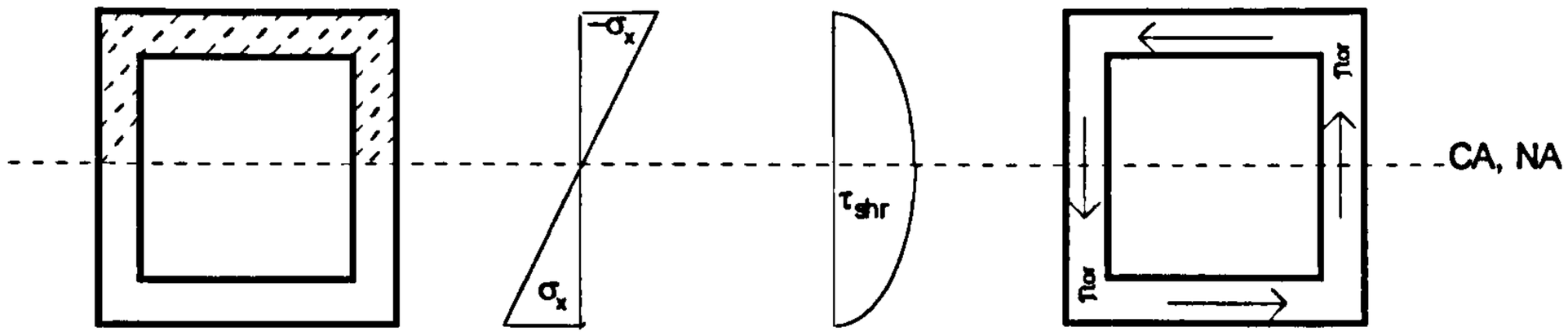

(a): Elastic stress distribution (Reinforced or partially prestressed beams)

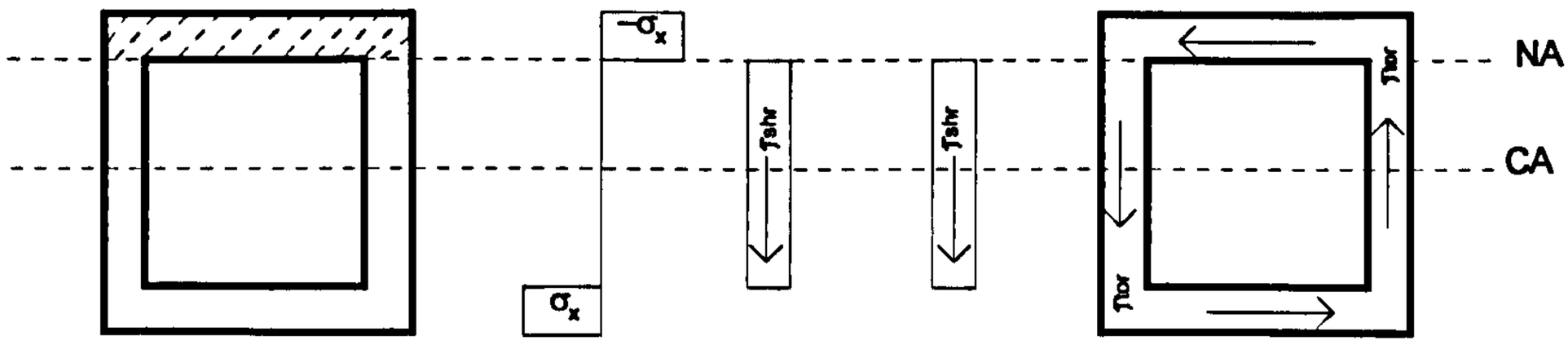

(b): Plastic stress (Reinforced beams)

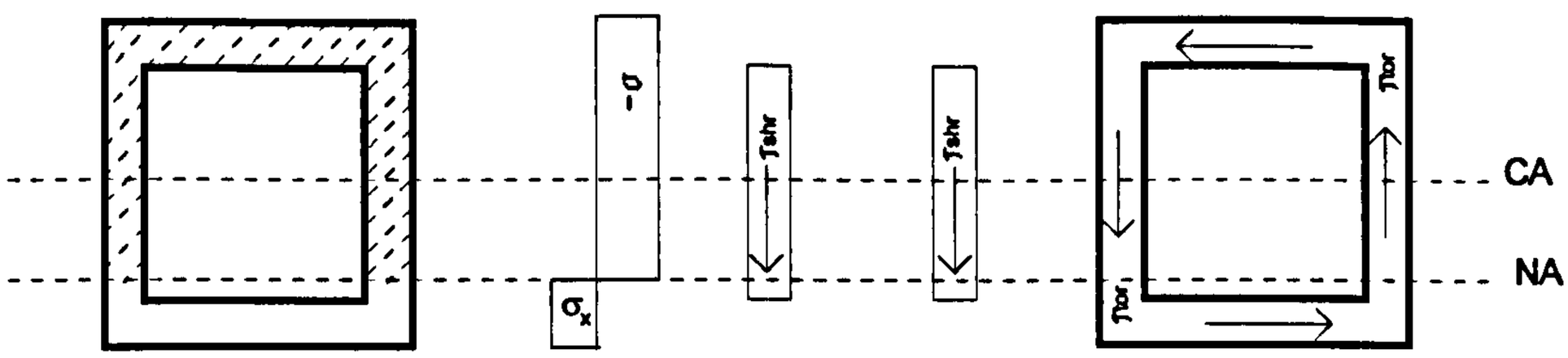

(c): plastic stress (partially prestressed beams)

Fig. 5.1: Design stress distribution in hollow beams (CA = Centroidal axis, NA = Neutral axis)

Where:

M, T and V = bending moment, torsion and shear force respectively.

y = the distance from the centroidal axis to the centroid of the partial area.

I = Centroidal moment of inertia of the hollow section.

$Q = \int_{area} ydA$. The statical moment of area about the neutral axis of the area above the section where the shear stress is required..

b = breadth of the solid section (300mm in the flanges and 2x50mm in the webs).

t = the thickness in which the torsional shear stress is circulating (50mm).

A_o = The area enclosed by the centre line of the wall thickness of the hollow section.

The normal stress and the shear stress due to shear force from equations 5.1 and 5.2 are uniformly distributed across the width of the flanges and the webs and vary through the depth. The shear stress due to torsion is assumed to be circulating in the

50mm thick flanges and webs. The net shear stress is the algebraic sum of the shear stress due to shear force and the shear stress due to torsion.

In the partially prestressed beams the net axial force induces normal compressive stress as in equation 5.4 and normal stress due to bending caused by the eccentricities of each axial force as in equation 5.5.

$$\sigma_{xa}=\Sigma P_i/A_c \qquad 5.4$$

$$\sigma_{xe}= (\Sigma P_i e_i)y/I \qquad 5.5$$

where:

σ_{xa} = normal compressive stress due to total axial force.

ΣP_i = total axial force after all losses.

A_c = cross-sectional area of the beam.

σ_{xe} = normal stress due to all eccentric axial forces.

P_i, e_i = axial force and its eccentricity of individual wire.

The net normal stress is the algebraic sum of the stresses due to prestressing σ_{xa} and σ_{xe} and the normal stress due to applied bending moment σ_{xb}.

5.2.2: Plastic stress distribution (Fig. 5.1b-c)

Bending moment is resisted by constant normal stress in the top and bottom flanges. Similarly, shear stresses due to shear force is assumed to be constant and act in the webs only. The torsion is resisted by constant shear flow in all the sides of the beam. In the case of partially prestressed beams, the assumptions are similar except that constant normal stress acts in the webs as well to account for the presence of axial force

Table 5.1 shows the required longitudinal and transverse reinforcement. In this table A_{sx}^E and A_{sx}^P are the required longitudinal reinforcement due to elastic and plastic stress distributions respectively and A_{sy}^E and A_{sy}^P are required transverse reinforcement due to elastic and plastic stress distributions respectively. It is clear from this table that the elastic stress distribution requires less longitudinal and transverse reinforcement than the plastic stress distribution. This is due to the shorter lever arm in the case of plastic stress distribution in the partially prerstressed beams which leads to larger tensile force for the same bending moment. Therefore, the elastic stress distribution is used in the design of hollow beams in this research.

Table 5.1: Required reinforcement using elastic and plastic stress distributions

Load	T	M	V	T/M	A_{sx}^E	A_{sy}^E	A_{sx}^P	A_{sy}^P
Beam	kNm	kNm	kN	Ratio	mm^2	mm^2/m	mm^2	mm^2/m
Reinforced beams								
M1	13	36	40	0.36	430	381	434	408
M2	39	36	40	1.08	659	797	725	824
M3	39	18	20	2.17	624	711	624	724
Partially prestressed beams								
M4	13	36	40	0.36	183	381	228	420
M5	39	36	40	1.08	415	797	414	1334
M6	39	18	20	2.17	357	711	289	1184

5.3: Design Examples

Using the elastic stress distribution, a typical design example for a reinforced beam and another for partially prestressed beam are presented. The beam section is divided into 50x50mm cells as in figure 5.2 and the torsion, bending moment and shear force at a cross-section are calculated. From these applied loads the resisting normal and shear stresses are calculated. These stresses are used in Nielsen's equations for the calculation of required reinforcement. In the case of partially prestressed beams, normal stresses due to prestressing forces are added to the stress from applied bending moment.

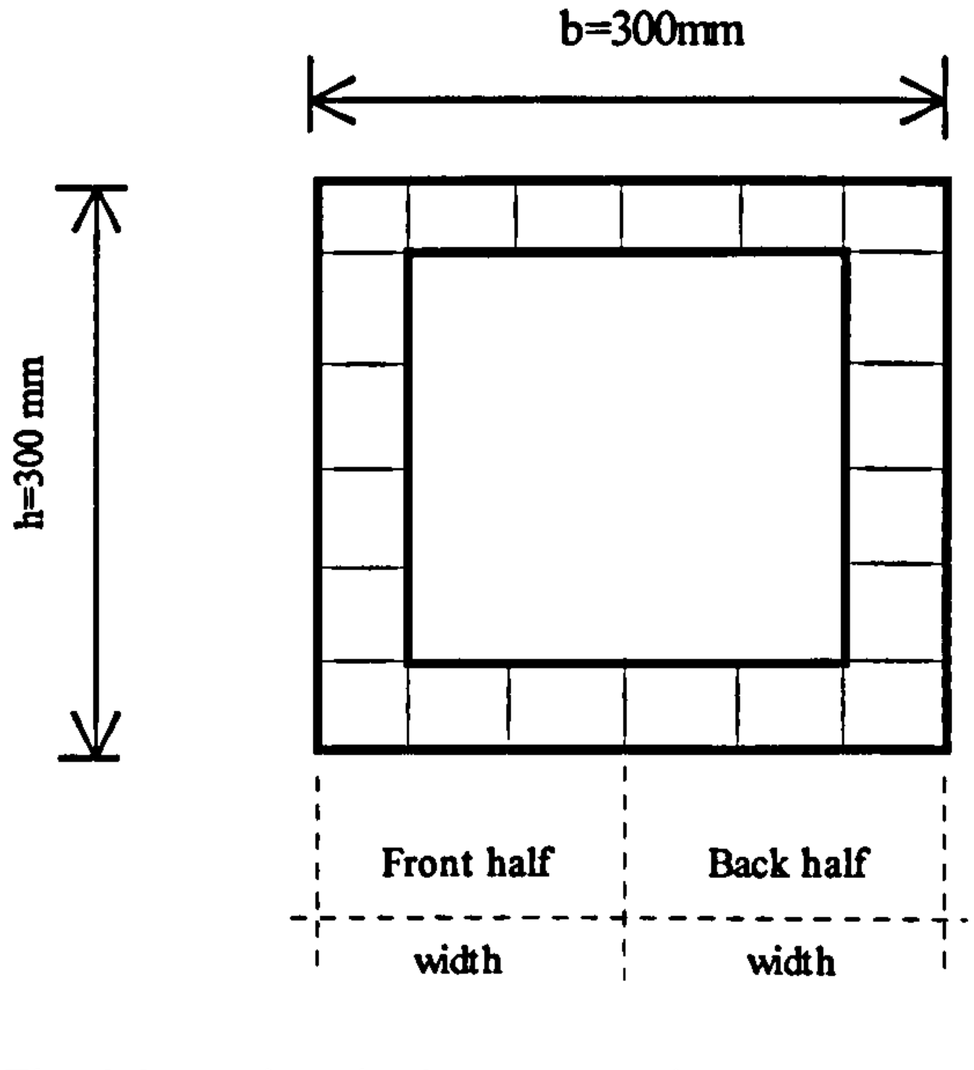

Fig. 5.2: Regions in the cross section

- **Reinforced concrete beam:** Calculate required reinforcement for a hollow section to resist 13kNm torsion, 36kNm bending moment and 40kN shear force. The cross-section is 300x300mm with a 200x200mm hollow core. The steel yield

stress for the longitudinal f_y and transverse f_{yv} reinforcement is 500N/mm^2 and the concrete cube compressive strength f_{cu} is 40N/mm^2.

Solution:

1. Calculate the normal stress σ_x using equation 5.1 (Table 5.2a).
2. Calculate the shear stress due to shear force τ_{shr} using equation 5.2 (Table 5.2b).
3. Calculate the shear stress due to torsion τ_{tor} using equation 5.3 (Table 5.2c).
4. Add the shear stresses from table 5.2b and table 5.2c to get the net shear stress τ (Table 5.2d).
5. Calculate the ratio of σ_x/τ (Table 5.2e).
6. Select Nielsen's design case (Fig. 3.8) based on the ratios in step 5 (Table 5.2f).
7. Use the corresponding Nielsen's equation (Fig. 3.8) to calculate the forces per unit length N_x^s and N_y^s in x and y or z directions respectively (Tables 5.2g and 5.2j). Also, check that the compressive principal stress does not exceed the value of the concrete cube strength. If it does, the wall thickness or the concrete cube strength has to be increased. This was not necessary in this case.
8. In each cell, the required longitudinal reinforcement A_x and transverse reinforcement A_t to resist the forces in step 7 are finally calculated as follows (Tables 5.2h and 5.2k):

   $A_x = (N_x^s / f_y)t$, where t is the thickness of the cell. A_x is in mm^2.

   $A_t = (N_y^s / f_{yv})1000$. A_t is in mm^2/m.

- **Partially prestressed beam:** Calculate required reinforcement for a partially prestressed beam with same loads and material as described above. For prestressing, four 5mm diameter wires were used, each stressed to a net force of 20kN after losses. The eccentricity for the first pair was 125mm and for the second pair was 75mm. The yield strength of the wires f_{py} was 1570N/mm^2.

Solution:

1. Calculate normal stress due to applied bending moment σ_{xb} using equation 5.1 (Table 5.3a).
2. Calculate normal stress due to axial compressive force σ_{xa} using equation 5.4 (Table 5.3b).

3. Calculate the normal stress due to eccentricities σ_{xe} using equation 5.5 (Table 5.3c).
4. Calculate the normal stress σ_{xtrn} at transfer (Table 5.3d). That is when only prestress forces act. The tensile stress at the top of the beam (if any) should be negligible or reinforcement should be provided. Also check that the compressive stress at the bottom does not exceed the concrete compressive strength, otherwise concrete strength or cross-section dimension should be increased.

Table 5.2: Design calculation for reinforced beam

σ_x	σ_x	σ_x	σ_x	σ_x	σ_x
N/mm²	N/mm²	N/mm²	N/mm²	N/mm²	N/mm²
-8.31	-8.31	-8.31	-8.31	-8.31	-8.31
-4.98					-4.98
-1.66					-1.66
1.66					1.66
4.98					4.98
8.31	8.31	8.31	8.31	8.31	8.31

a: Normal stress due to bending

τ_{shr}	τ_{shr}	τ_{shr}	τ_{shr}	τ_{shr}	τ_{shr}
N/mm²	N/mm²	N/mm²	N/mm²	N/mm²	N/mm²
0.25	0.25	0.25	0.25	0.25	0.25
1.55					1.55
1.73					1.73
1.73					1.73
1.55					1.55
0.25	0.25	0.25	0.25	0.25	0.25

b: Shear stress due to shear force

τ_{tor}	τ_{tor}	τ_{tor}	τ_{tor}	τ_{tor}	τ_{tor}
N/mm²	N/mm²	N/mm²	N/mm²	N/mm²	N/mm²
-2.08	-2.08	-2.08	-2.08	-2.08	-2.08
2.08					-2.08
2.08					-2.08
2.08					-2.08
2.08					-2.08
2.08	2.08	2.08	2.08	2.08	2.08

c: Shear stress due to torsion

τ	τ	τ	τ	τ	τ
N/mm²	N/mm²	N/mm²	N/mm²	N/mm²	N/mm²
-2.08	-2.08	-2.08	-2.08	-2.08	-2.08
3.63					-0.53
3.81					-0.35
3.81					-0.35
3.63					-0.53
2.08	2.08	2.08	2.08	2.08	2.08

d: Net shear stress

σ_x/τ	σ_x/τ	σ_x/τ	σ_x/τ	σ_x/τ	σ_x/τ
Ratio	Ratio	Ratio	Ratio	Ratio	Ratio
-3.99	-3.99	-3.99	-3.99	-3.99	-3.99
-1.37					-9.34
-0.44					-4.76
0.44					4.76
1.37					9.34
3.99	3.99	3.99	3.99	3.99	3.99

e: ratio of normal stress to shear stress

Selection of Nielsen's design cases					
case	case	case	case	case	case
1	1	1	1	1	1
1					1
3					1
3					3
3					3
3	3	3	3	3	3

f: Design case

Nx^s	Nx^s	Nx^s	Nx^s	Nx^s	Nx^s
N/mm	N/mm	N/mm	N/mm	N/mm	N/mm
0	0	0	0	0	0
0					0
107					0
274					101
431					276
519	519	519	519	519	519

g: Forces in the longitudinal direction

A_x	A_x	A_x	A_x	A_x	A_x
mm²	mm²	mm²	mm²	mm²	mm²
0	0	0	0	0	0
0					0
11					0
27					10
43					28
52	52	52	52	52	52

h: Longitudinal reinforcement

Longitudinal

Front	Back
mm²	mm²
0	0
0	0
11	0
27	10
43	28
156	156
A_{sx}^{f}	A_{sx}^{b}
237	193

Ny^s	Ny^s	Ny^s	Ny^s	Ny^s	Ny^s
N/mm	N/mm	N/mm	N/mm	N/mm	N/mm
26	26	26	26	26	26
132					3
191					4
191					17
181					27
104	104	104	104	104	104

j: Forces in the transverse direction

A_t	A_t	A_t	A_t	A_t	A_t
mm²/m	mm²/m	mm²/m	mm²/m	mm²/m	mm²/m
52	52	52	52	52	52
264					6
381					7
381					35
363					53
208	208	208	208	208	208

k: Transverse reinforcement

Transverse

Front	Back	Top
mm²	mm²	mm²
		52
264	6	
381	7	
381	35	Bot.
363	53	mm²
		208
A_{sy}^{f}	A_{sy}^{b}	
381	35	

Table 5.3: Design calculation for partially prestressed beam

σ_{xb}	σ_{xb}	σ_{xb}	σ_{xb}	σ_{xb}	σ_{xb}
N/mm²	N/mm²	N/mm²	N/mm²	N/mm²	N/mm²
-8.31	-8.31	-8.31	-8.31	-8.31	-8.31
-4.98					-4.98
-1.66					-1.66
1.66					1.66
4.98					4.98
8.31	8.31	8.31	8.31	8.31	8.31

a: Normal stress due to bending

σ_{xa}	σ_{xa}	σ_{xa}	σ_{xa}	σ_{xa}	σ_{xa}
N/mm²	N/mm²	N/mm²	N/mm²	N/mm²	N/mm²
-1.60	-1.60	-1.60	-1.60	-1.60	-1.60
-1.60					-1.60
-1.60					-1.60
-1.60					-1.60
-1.60					-1.60
-1.60	-1.60	-1.60	-1.60	-1.60	-1.60

b: Normal stress due to axial force

σ_{xe}	σ_{xe}	σ_{xe}	σ_{xe}	σ_{xe}	σ_{xe}
N/mm²	N/mm²	N/mm²	N/mm²	N/mm²	N/mm²
1.15	1.15	1.15	1.15	1.15	1.15
0.69					0.69
0.23					0.23
-0.23					-0.23
-0.69					-0.69
-1.15	-1.15	-1.15	-1.15	-1.15	-1.15

c: Normal stress due to eccentricity (1)

σ_{xe}	σ_{xe}	σ_{xe}	σ_{xe}	σ_{xe}	σ_{xe}
N/mm²	N/mm²	N/mm²	N/mm²	N/mm²	N/mm²
0.69	0.69	0.69	0.69	0.69	0.69
0.42					0.42
0.14					0.14
-0.14					-0.14
-0.42					-0.42
-0.69	-0.69	-0.69	-0.69	-0.69	-0.69

c: Normal stress due to eccentricity (2)

σ_{xtm}	σ_{xtm}	σ_{xtm}	σ_{xtm}	σ_{xtm}	σ_{xtm}
N/mm²	N/mm²	N/mm²	N/mm²	N/mm²	N/mm²
0.25	0.25	0.25	0.25	0.25	0.25
-0.49					-0.49
-1.23					-1.23
-1.97					-1.97
-2.71					-2.71
-3.45	-3.45	-3.45	-3.45	-3.45	-3.45

d: Transfer normal stress

σ_{xser}	σ_{xser}	σ_{xser}	σ_{xser}	σ_{xser}	σ_{xser}
N/mm²	N/mm²	N/mm²	N/mm²	N/mm²	N/mm²
-8.06	-8.06	-8.06	-8.06	-8.06	-8.06
-5.48					-5.48
-2.89					-2.89
-0.31					-0.31
2.28					2.28
4.86	4.86	4.86	4.86	4.86	4.86

e: Service normal stress

τ_{shr}	τ_{shr}	τ_{shr}	τ_{shr}	τ_{shr}	τ_{shr}
N/mm²	N/mm²	N/mm²	N/mm²	N/mm²	N/mm²
0.25	0.25	0.25	0.25	0.25	0.25
1.55					1.55
1.73					1.73
1.73					1.73
1.55					1.55
0.25	0.25	0.25	0.25	0.25	0.25

f: Shear stress due to shear force

τ_{tor}	τ_{tor}	τ_{tor}	τ_{tor}	τ_{tor}	τ_{tor}
N/mm²	N/mm²	N/mm²	N/mm²	N/mm²	N/mm²
-2.08	-2.08	-2.08	-2.08	-2.08	-2.08
2.08					-2.08
2.08					-2.08
2.08					-2.08
2.08					-2.08
2.08	2.08	2.08	2.08	2.08	2.08

g: Shear stress due to torsion

τ	τ	τ	τ	τ	τ
N/mm²	N/mm²	N/mm²	N/mm²	N/mm²	N/mm²
-2.08	-2.08	-2.08	-2.08	-2.08	-2.08
3.63					-0.53
3.81					-0.35
3.81					-0.35
3.63					-0.53
2.08	2.08	2.08	2.08	2.08	2.08

h: Net shear stress

σ_{xmax}/τ	σ_{xmax}/τ	σ_{xmax}/τ	σ_{xmax}/τ	σ_{xmax}/τ	σ_{xmax}/τ
Ratio	Ratio	Ratio	Ratio	Ratio	Ratio
-3.9	-3.9	-3.9	-3.9	-3.9	-3.9
-1.5					-10.3
-0.8					-8.3
-0.1					-0.9
0.6					4.3
2.3	2.3	2.3	2.3	2.3	2.3

j: ratio of normal stress to shear stress

Selection of Nielsen's design cases					
case	case	case	case	case	case
1	1	1	1	1	1
1					1
3					1
3					3
3					3
3	3	3	3	3	3

k: Design case

N_x^a	N_x^a	N_x^a	N_x^a	N_x^a	N_x^a
N/mm	N/mm	N/mm	N/mm	N/mm	N/mm
0	0	0	0	0	0
0					0
46					0
175					2
295					141
347	347	347	347	347	347

m: Forces in the longitudinal direction

A_x	A_x	A_x	A_x	A_x	A_x
mm²	mm²	mm²	mm²	mm²	mm²
0	0	0	0	0	0
0					0
5					0
18					0
3					-13
35	8	35	35	8	35

n: Longitudinal reinforcement

N_y^a	N_y^a	N_y^a	N_y^a	N_y^a	N_y^a
N/mm	N/mm	N/mm	N/mm	N/mm	N/mm
27	27	27	27	27	27
120					3
191					2
191					17
181					27
104	104	104	104	104	104

p: Forces in the transverse direction

A_t	A_t	A_t	A_t	A_t	A_t
mm²/m	mm²/m	mm²/m	mm²/m	mm²/m	mm²/m
54	54	54	54	54	54
240					5
381					4
381					35
363					53
208	208	208	208	208	208

q: Transverse reinforcement

A_{sx}^t	A_{sx}^b
102	65

A_{sy}^t	A_{sy}^b
381	35

5. Calculate the service normal stress σ_{xser} (Table 5.3e). That is when all loads are simultaneously applied.
6. Calculate the shear stress due to shear force τ_{shr} using equation 5.2 (Table 5.3f).
7. Calculate the shear stress due to torsion τ_{tor} using equation 5.3 (Table 5.3g).
8. Calculate the net shear stress τ (Table 5.3h).
9. The ratio of σ_{xser}/τ is given in table 5.3j.
10. Select Nielsen's design case (Fig. 3.8) based on the ratios in step 9 (Table 5.3k).
11. Use the corresponding Nielsen's equations (Fig. 3.8) to calculate the forces per unit length N_x^s and N_y^s in x and y or z directions respectively (Tables 5.3m and 5.3p). Also, check that the compressive principal stress is not exceeding the value of the concrete cube strength. If it does the wall thickness or the concrete cube strength has to be increased.
12. The required reinforcement to resist the forces in step 11 are finally calculated as follows (Tables 5.3n and 5.3q):

$A_x = (N_x^s / f_y)t$, where t is the thickness of the cell. A_x is in mm^2.

$A_t = (N_y^s / f_{yv})1000$. A_t is in mm^2/m.

In the cells were the prestressing wires are present the prestressing wires are assumed to act as unstressed steel with a yield stress equal to the difference between the yield stress f_{py} and the stress at service f_{pe} (Fig. 5.3) using the following equation:

$$tN_x^s = A_x f_y + A_{xp}(f_{py} - f_{pe})$$

or

$$A_x = [(N_x^s - \frac{A_{xp}}{t}(f_{py} - f_{pe})) / f_y]t$$

where:

A_{xp} = area of prestressing wire.

f_{py} = yield strength of the prestressing wire.

f_{pe} = effective prestress stress in the wire at service.

t = thickness of the cell.

A_x = additional unstressed steel required.

f_y = yield stress of unstressed steel.

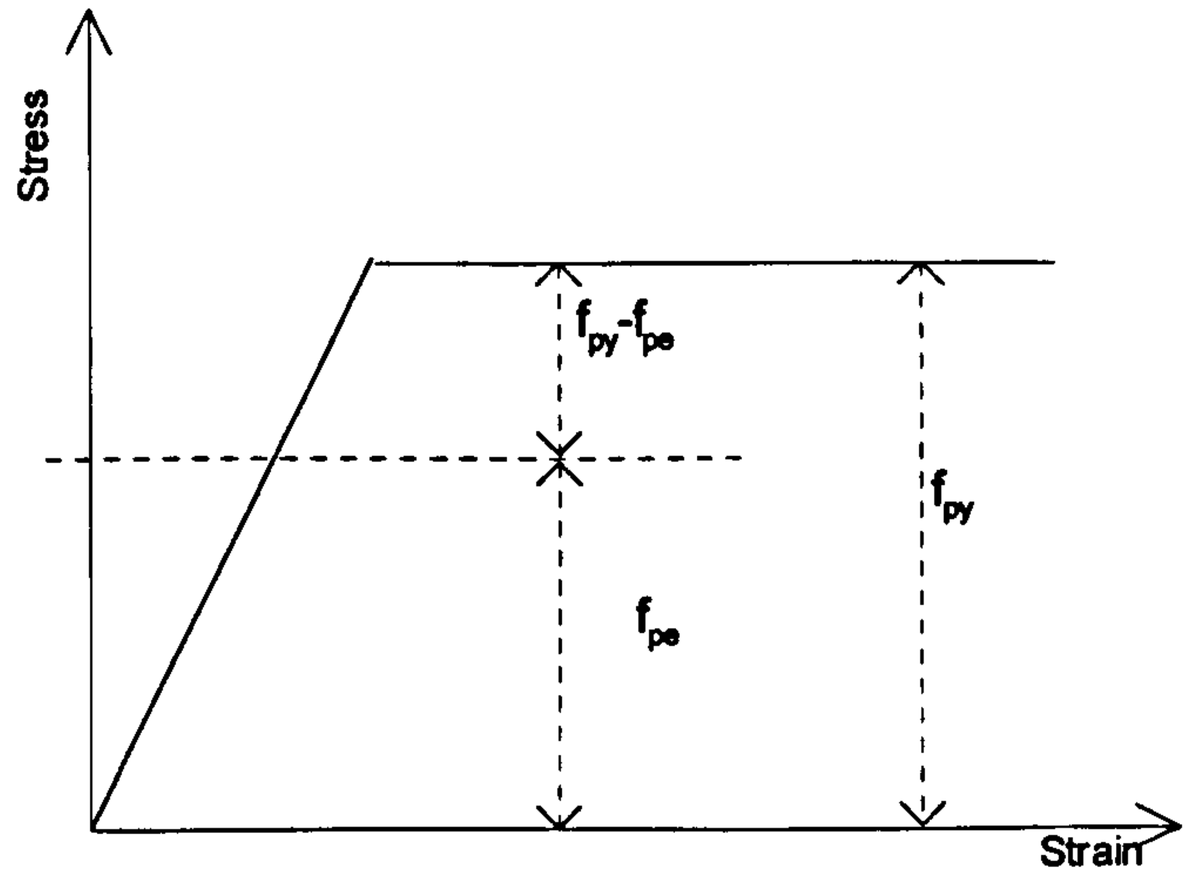

Fig. 5.3: Transfer and service stresses in a prestressing wire

The above calculated values of A_x and A_t are the required reinforcement for each cell in the x and y or z directions respectively.

5.4: Required and provided reinforcement

Due to the loading and support arrangement, torsion is constant along the beam length while the bending moment and shear force vary along the beam as shown in figure 4.3 of chapter 4. In addition, at any cross-section, the normal stress is uniformly distributed across the width of the flanges and the webs. However, in the webs the shear stresses, to the right of mid-span, are additives in the front web and subtractive in the back web. On the other hand, in the webs to the left of mid-span, shear stresses are additives in the back web and subtractive in the front web. The theoretically required longitudinal and transverse reinforcement is naturally larger in the region where the stresses are added than where they are subtracted.

The theoretically required reinforcement is practically difficult to provide exactly for the following reasons:

1. In the front web of the beam, the reinforcement to the right of the mid-span is larger than the reinforcement to the left. In the back web, this situation is reversed.
2. The reinforcement is largest at mid-span and decreases towards the supports.
3. The reinforcement for the top and bottom flanges are constant across the width and vary along the span.

4. The transverse reinforcement in the front and back webs vary with the depth and the location along the span.
5. Commercially available bar sizes do not always fit the exact steel requirement.

For these reasons the largest required reinforcement was provided in the hollow beams for the whole cross-section in the whole test span. The term 'largest' corresponds to the steel area calculated at mid-span section and to the location where the shear stresses are added. Providing the largest reinforcement, of course, leads to some sections being over designed.

In tables 5.2-3, A_{sx}^{f} is the summation of the required longitudinal reinforcement in the front half of the beam width where the shear stresses are added and A_{sx}^{b} is the summation of the longitudinal reinforcement in the back half where the stresses are subtracted. A_{sy}^{f} is the largest required leg area in the front web and A_{sy}^{b} is the required leg area in the corresponding cell in the back web at the same level. In the hollow beams studied in this research, A_{sx}^{f} was provided for both half widths of the beam as longitudinal reinforcement and A_{sy}^{f} was used as stirrup leg area for the whole cross-section. This reinforcement was provided in whole test span. Outside the test span, more reinforcement was provided to resist the negative moment above the supports and to ensure failure in the test span.

5.5: Test beams

Table 5.4 shows the hollow beams tested in this research. The main variables studied were the ratio of the maximum elastic shear stress τ_{tor} due to torsion to the maximum elastic shear stress τ_{shr} due to shear force and the ratio of the ultimate design torsion T_d to bending moment M_d. The ratio τ_{tor}/τ_{shr} varied between 0.59 to 6.84 and the ratio T_d/M_d varied between 0.26 to 2.62. This large variation of the ratios allowed examining the applicability of the direct design method in designing hollow beams with different load combinations. All beams were designed using elastic stress distribution combined with the direct design method as explained in the previous examples. The centre line of wall thickness coincides with line passing between the stirrup leg and the corner longitudinal bars.

Longitudinal and transverse reinforcement in the 600mm region to the right of mid-span were strain gauged. In this region the shear stresses are added in the front web and subtracted in back web. This leads to small negative load factor value when there is no external load applied. The strain gauges and their locations are shown in table 5.5 and in figure 5.4.

Table 5.4: Tests on hollow beams

Beam	T_d	τ_{tor}	M_d	V_d	τ_{shr}	τ_{tor}/τ_{shr}	T_d/M_d
No.	kNm	N/mm^2	kNm	kN	N/mm^2	Ratio	Ratio
Group A: Reinforced concrete hollow beams							
BTV1	13	2.08	14.89	21.08	0.91	2.28	0.87
BTV2	13	2.08	32.89	41.08	1.78	1.17	0.40
BTV3	13	2.08	50.89	61.08	2.64	0.79	0.26
BTV4	13	2.08	68.89	81.08	3.51	0.59	0.19
BTV5	26	4.16	14.89	21.08	0.91	4.56	1.75
BTV6	26	4.16	32.89	41.08	1.78	2.34	0.79
BTV7	39	6.24	14.89	21.08	0.91	6.84	2.62
BTV8	39	6.24	32.89	41.08	1.78	3.51	1.19
Group B: Partially prestressed concrete hollow beams							
BTV9	18	2.88	50.89	61.08	2.64	1.09	0.35
BTV10	26	4.16	14.89	21.08	0.91	4.56	1.75
BTV11	39	6.24	14.89	21.08	0.91	6.84	2.62

Table 5.5: Location of strain gauges (To be read in conjunction with Fig. 5.4)

Space	a	b	c	d	e	f	g	h	j	k
Beam	mm	mm	mm	mm	mm	mm	mm	mm	mm	mm
BTV1	134	173	173	173	-	220	173	173	173	-
BTV2	60	120	120	120	-	120	120	120	120	-
BTV3	46.5	93	93	93	-	93	93	93	93	-
BTV4	84	84	84	84	84	126	84	84	84	84
BTV5	46	92	92	92	92	92	92	92	92	92
BTV6	40	80	80	80	80	80	80	80	80	80
BTV7	99	66	66	66	66	132	66	66	66	66
BTV8	90	60	60	60	60	120	60	60	60	60
BTV9	120	60	-	-	-	60	120	120	120	-
BTV10	93	93	-	-	-	46	93	93	93	-
BTV11	170	68	-	-	-	136	68	68	68	-

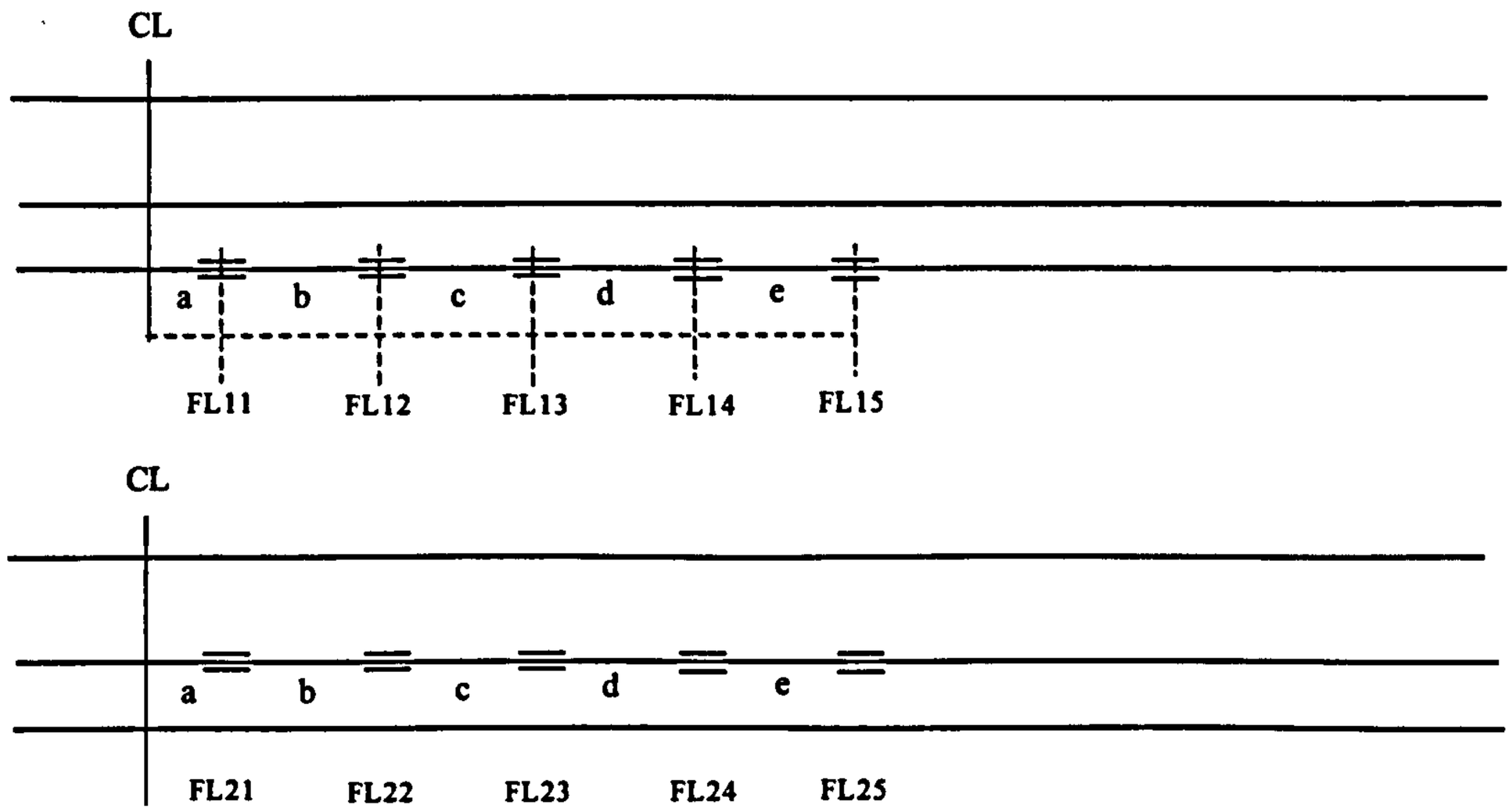

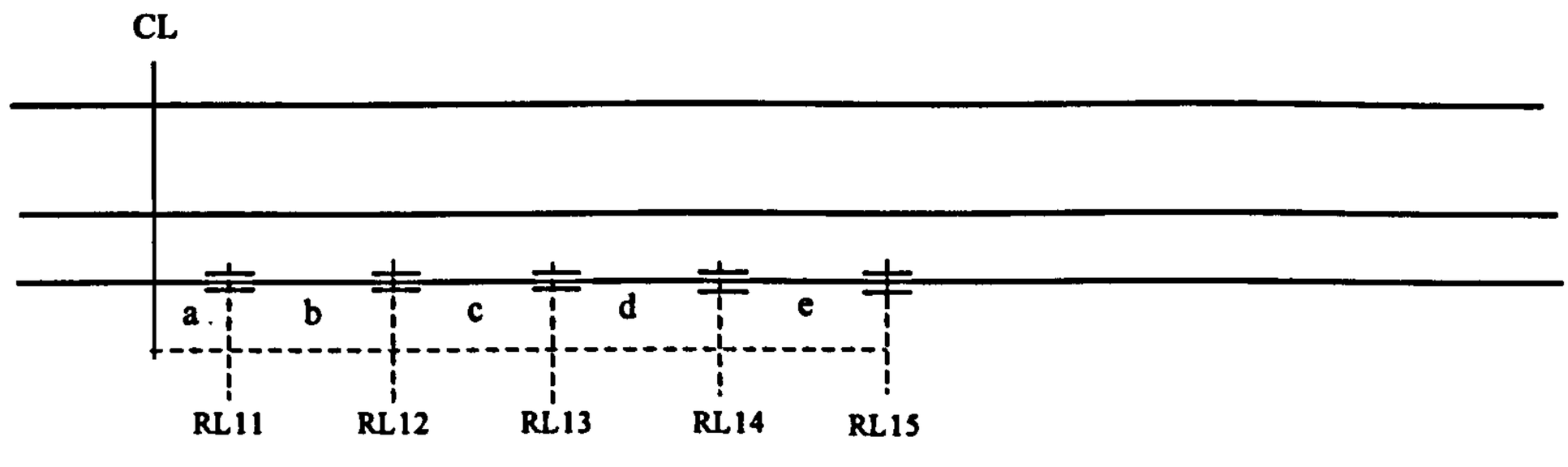

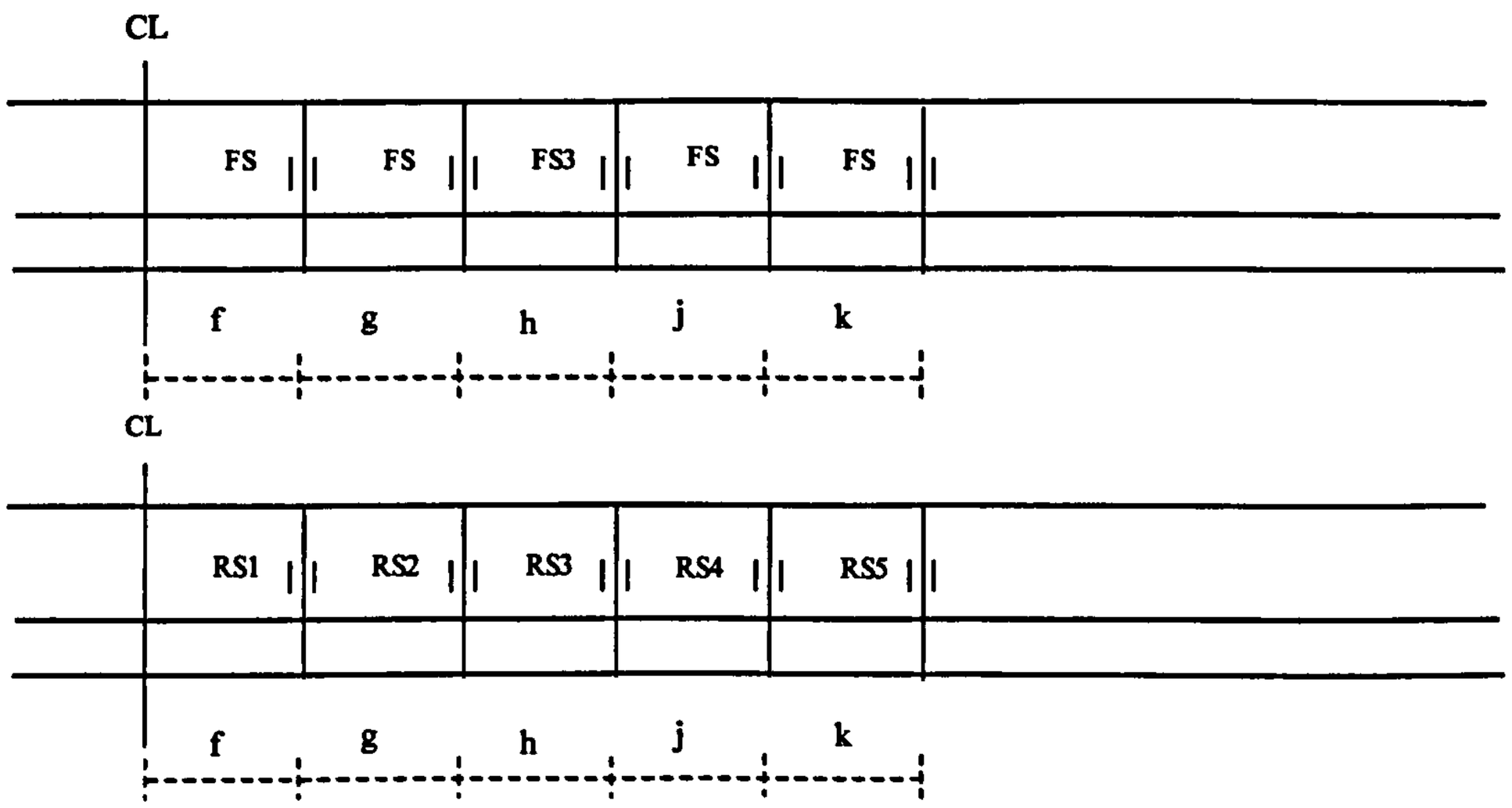

Fig. 5.4: Legend for strain gauge location

The first letter denotes web (F = Front web, R = Back web), the second letter denotes the type of reinforcement (L = Longitudinal, S = Stirrup), the first numeral in the longitudinal steel denotes the layer level (1 = the bottom layer, 2 = second bottom layer) and the numeral in the stirrup and the second numeral in the longitudinal steel represent the horizontal location (1 = closest to mid-span). For example, FL13 = Front web, Longitudinal steel, at the bottom layer and at the third location from the mid-span and RS1 = Back web, Stirrup, at the first location from the mid-span. Figure 5.5 shows typical arrangement of reinforcement.

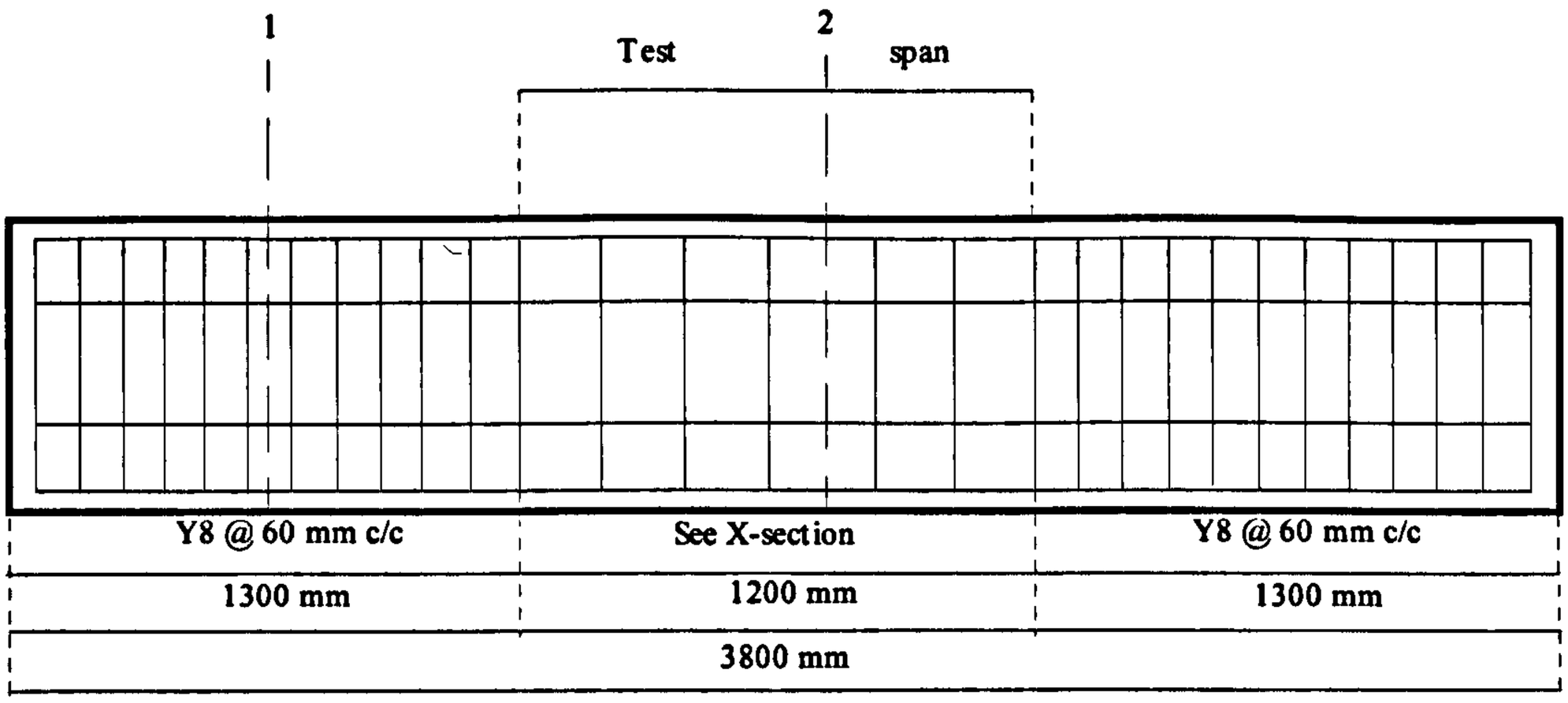

Fig. 5.5: Typical arrangement for reinforcement

Fig. 5.6: (a): Typical vertical distance between reinforcement layers (b): Strain gauge locations

Figure 5.6a shows the vertical distances between layers of longitudinal reinforcement. Stirrup strain gauge was at mid depth of the beam. Figure 5.6b shows the relationship between the location and notation of the strain gauges. Figure 5.7 shows the reinforcement provided for each beam. With the exception of beams BTV7, BTV8 and BTV11 the stirrup spacing in the regions outside the test-span was 60mm. The solid circles in this figure represent the longitudinal bars or prestressing wires which were strain gauged while the hollow circles represent the rest. Although in some cases the design required no longitudinal reinforcement in the top flange, two 8mm diameter bars were provided for stirrup anchorage. Table

5.6 shows the measured average material properties. The concrete compressive strengths of cube f_{cu} and of cylinder f'_c in this table are for the samples cured under the same conditions as for the beam. f_y and f_{yv} are the yield strength of the longitudinal and transverse reinforcement while f_{yp} is the yield strength of prestressing wires.

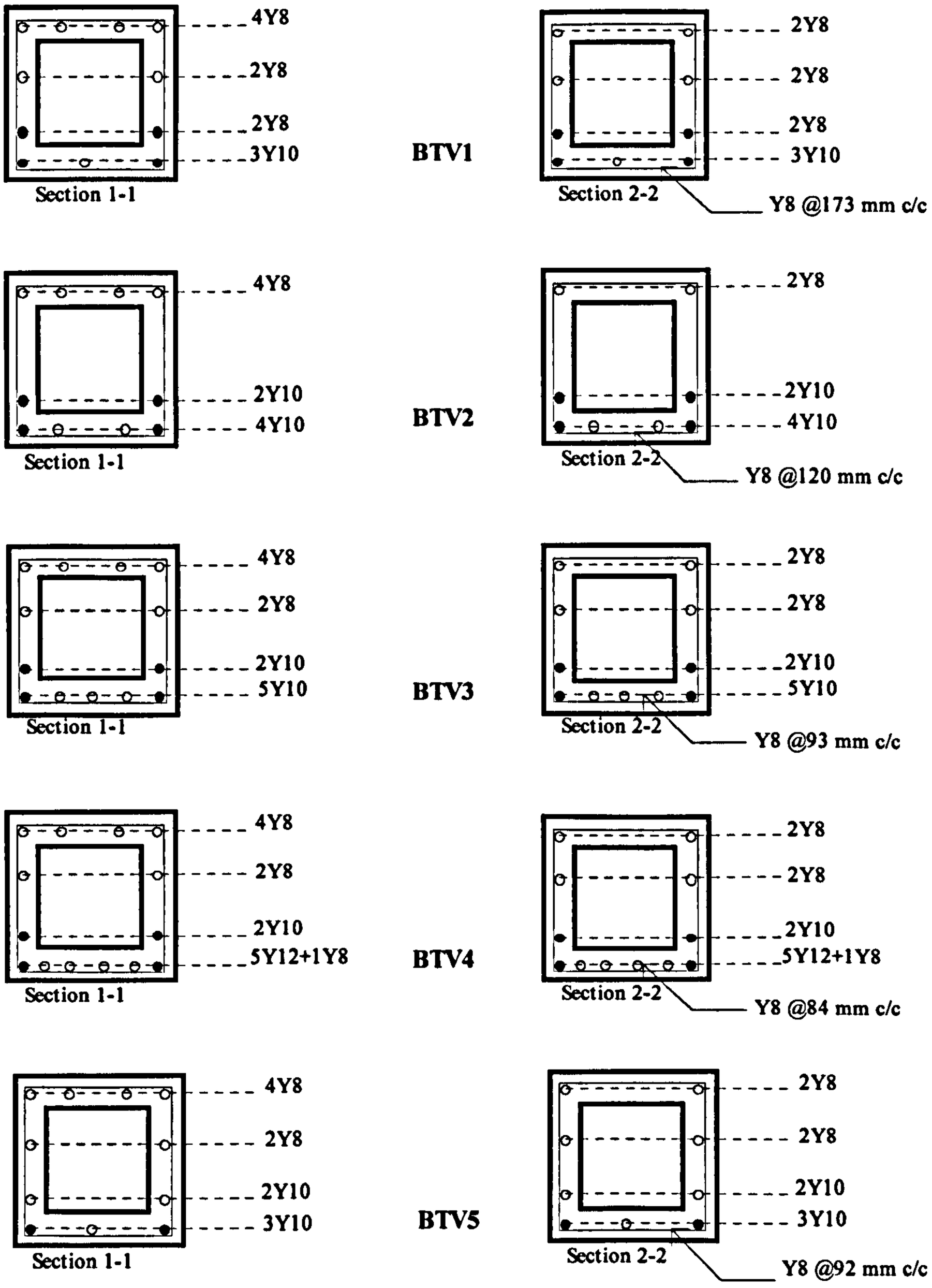

Fig. 5.7 Provided reinforcement

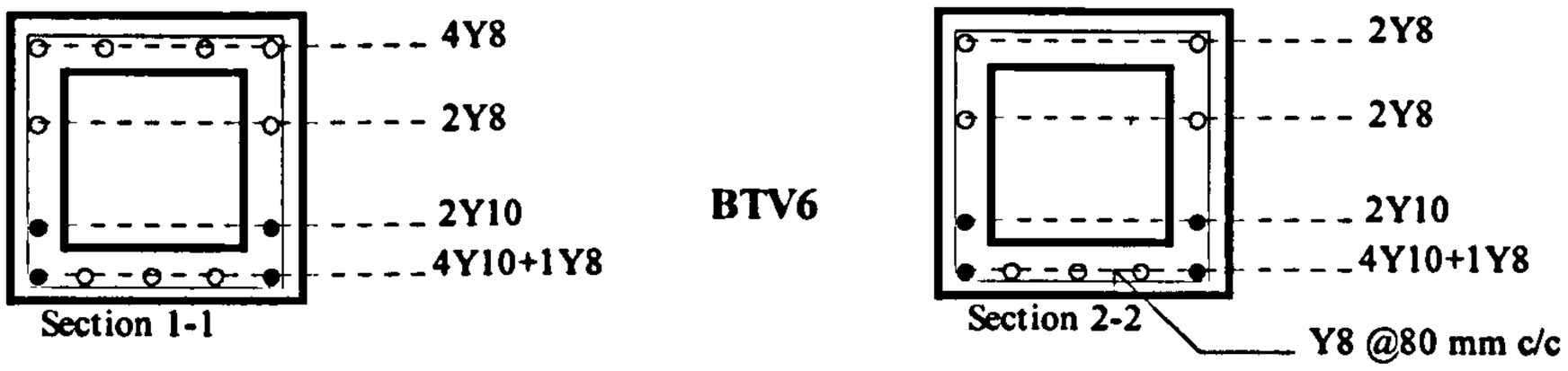

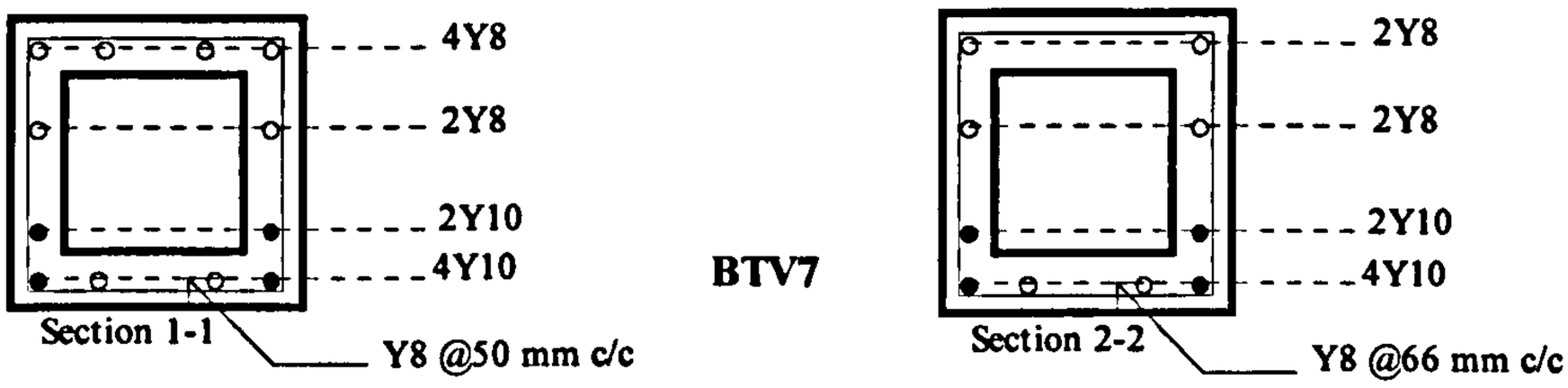

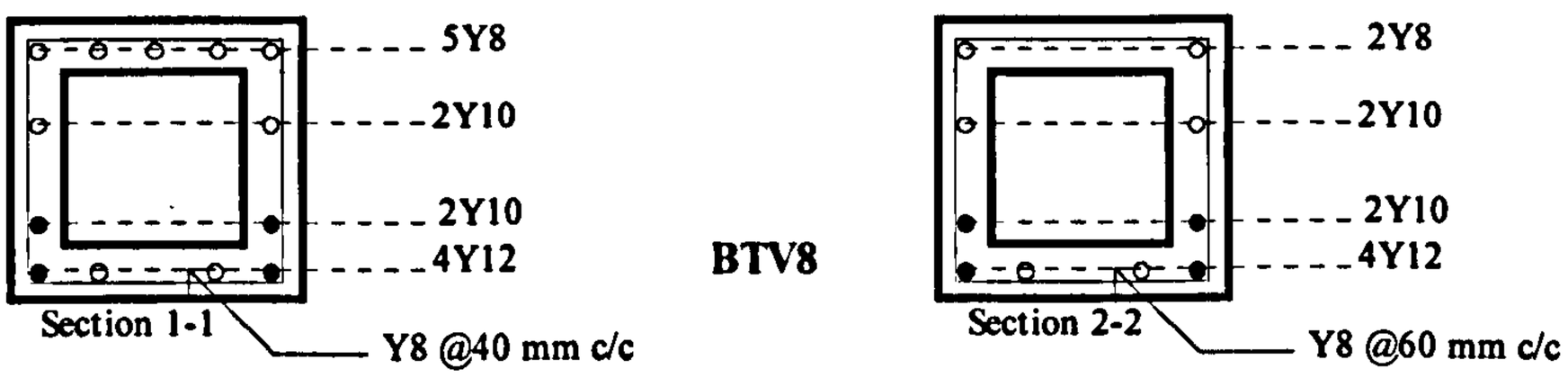

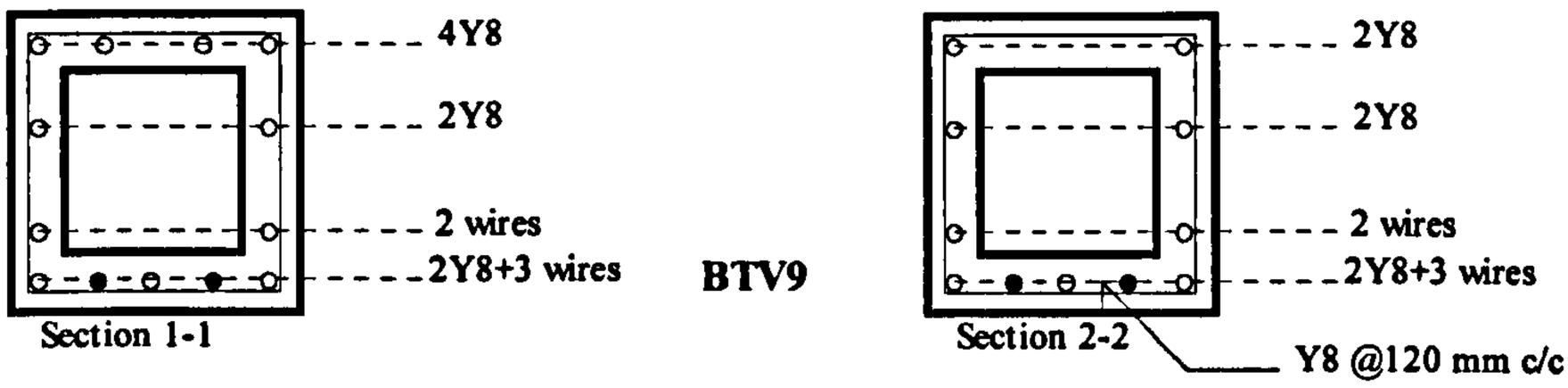

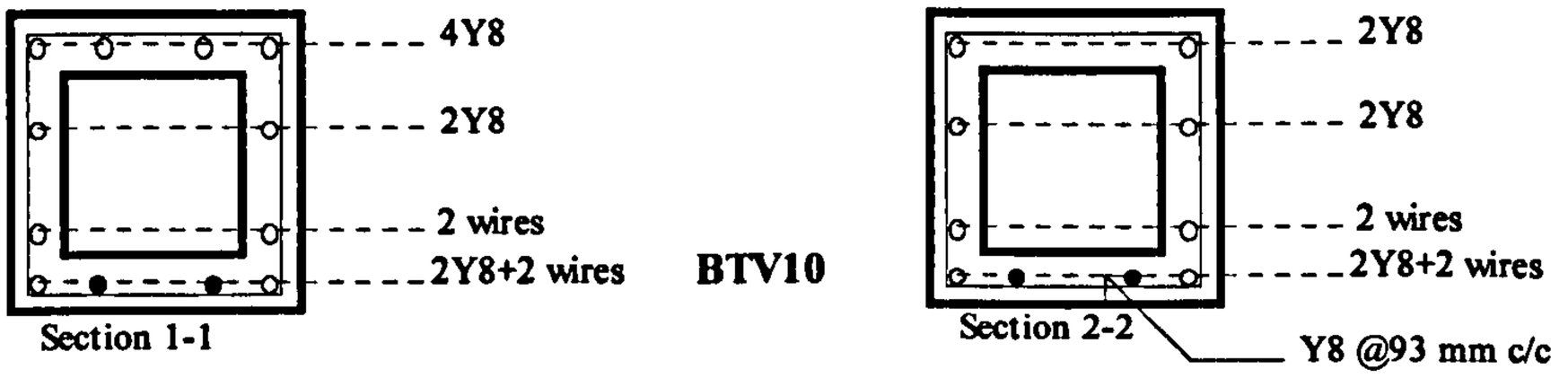

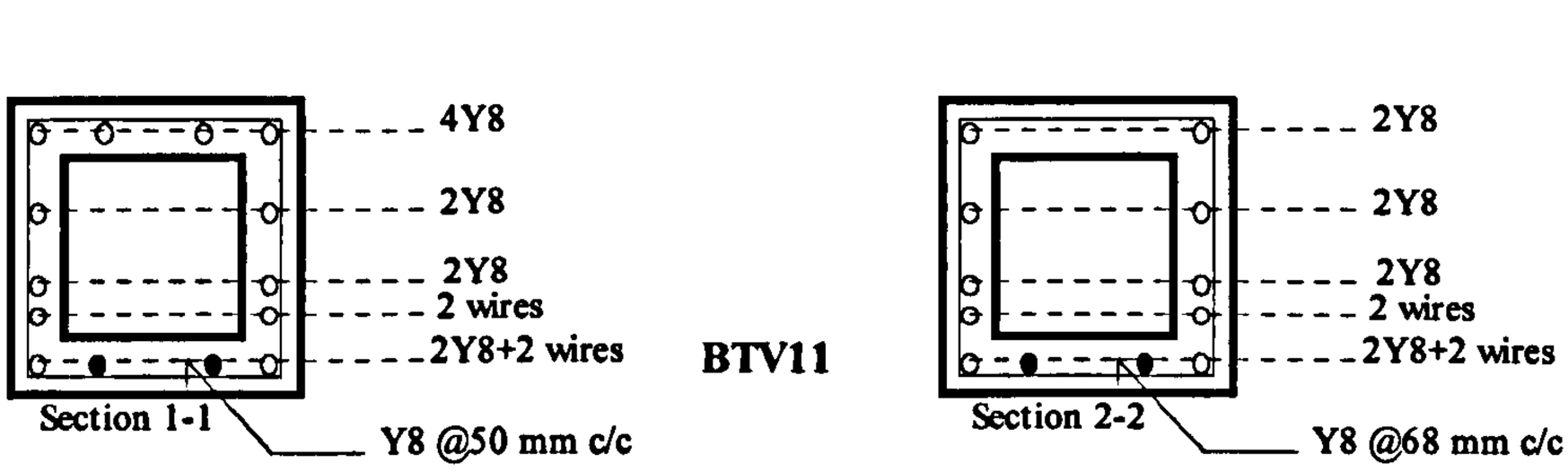

Fig. 5.7: Continued

Table 5.6: Average material properties

Beam No.	f_{cu} N/mm^2	f'_c N/mm^2	f_y N/mm^2	f_{yv} N/mm^2	f_{py} N/mm^2	Age days
Group A: Reinforced concrete hollow beams						
BTV1	39	33	495	516	-	10
BTV2	37	24	490	472	-	7
BTV3	38	27	490	472	-	7
BTV4	42	33	480	472	-	7
BTV5	35	27	490	472	-	8
BTV6	35	28	490	472	-	7
BTV7	54	34	500	472	-	7
BTV8	53	36	500	472	-	8
Group B: Partially prestressed hollow beams						
BTV9	61	46	500	472	1570	13
BTV10	48	39	500	472	1570	10
BTV11	44	36	500	472	1570	13

5.6: Experimental observations

This section summaries the observed behaviour in the test span region of the tested hollow beams at significant stages in the behaviour. The angle of crack is measured from the horizontal axis. Vertical displacement is measured at the mid-span of the bottom flange (location 2 in figure 4.4a of chapter 4). Strain in the bottom layer of the longitudinal steel and prestressing wires and in the transverse steel, in front and back webs over the 600mm region to the right of mid-span are presented. The strain gauge location is as shown in figure 5.4 and table 5.5. As the two strain gauged prestressing wires were located in the bottom flange, the one close to the front web is called the front side and the one close to the back web is called the rear side. The quoted load is a percentage of the design load, and the average strain ratio in the reinforcement is the average of the maximum measured strain to the yield strain. The load factor L.F. = $(M_e/M_d + T_e/T_d)/2$ including the self weight, where M_e and T_e are the experimental failure loads of bending and torsion respectively.

BTV1: T_d=13kNm, M_d=14.89kNm, V_d=21.08kN, T_d/M_d=0.87, τ_{tor}/τ_{shr}=2.28

The first few cracks were noticed at 30% of load at the bottom of the webs near mid-span and in the upper half of the webs half way between the mid-span and the supports. The cracks at the bottom of the webs were almost vertical and the ones in the upper half of the webs were inclined at 50°.

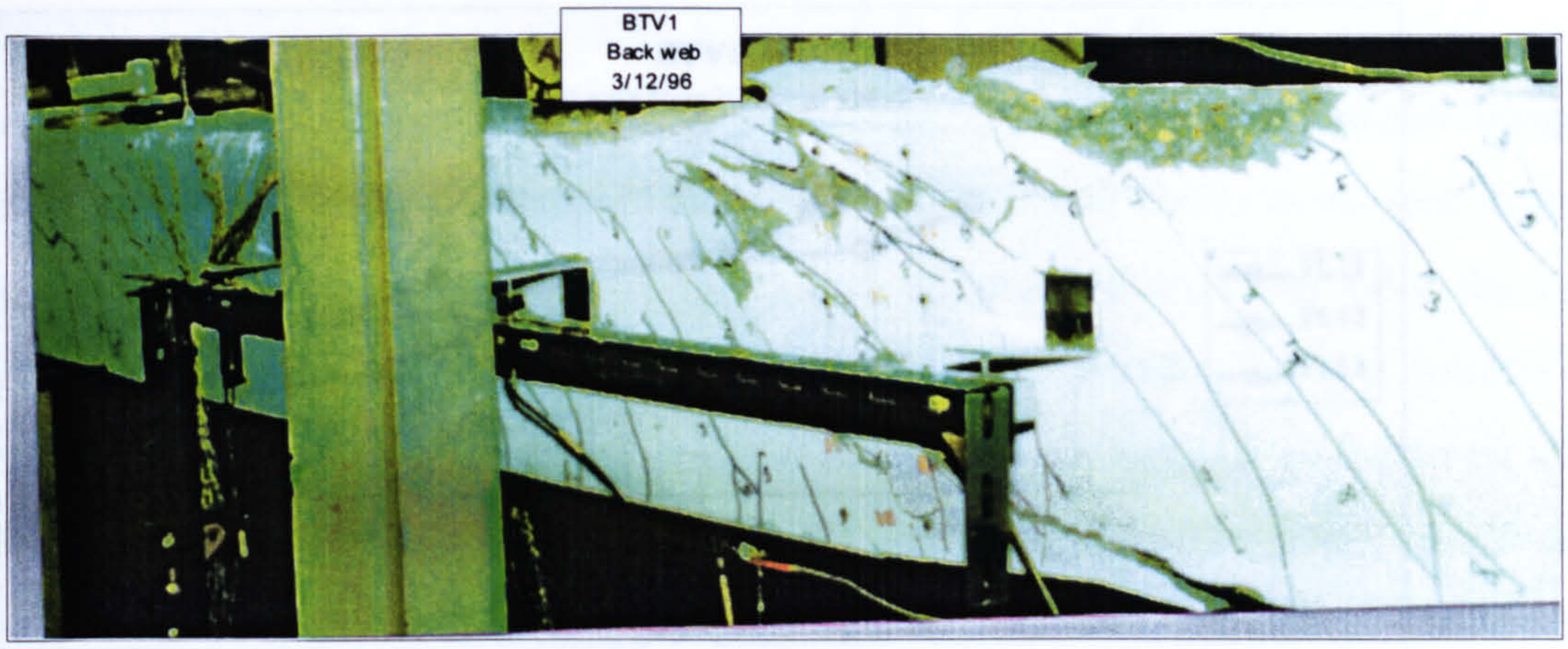

Fig. 5.8: Crack development in the back web (BTV1)

At 40% of load, the first crack at the bottom flange was noticed joining the vertical cracks in the webs at an angle of about 60°. At about 80% of load, cracks started in the top flange joining the inclined cracks in the webs at an angle of about 45°. The average crack width at this stage was 0.5mm. Failure happened at 104% of load by a major (45°) inclined crack starting at about 700mm to the right of mid-span on the front web and spiralling round the beam. A few additional large cracks were also present in the top part of the front web with the same inclination as the major crack. Figure 5.8 shows crack development at the back web of the beam. The displacement is shown in figure 5.9, and figure 5.10 shows the steel strain. The average strain ratio reached in the front web was 0.73 and in the back web 0.31. In the stirrups, the average strain ratio in the front web was 0.85 and in the back web was 0.43.

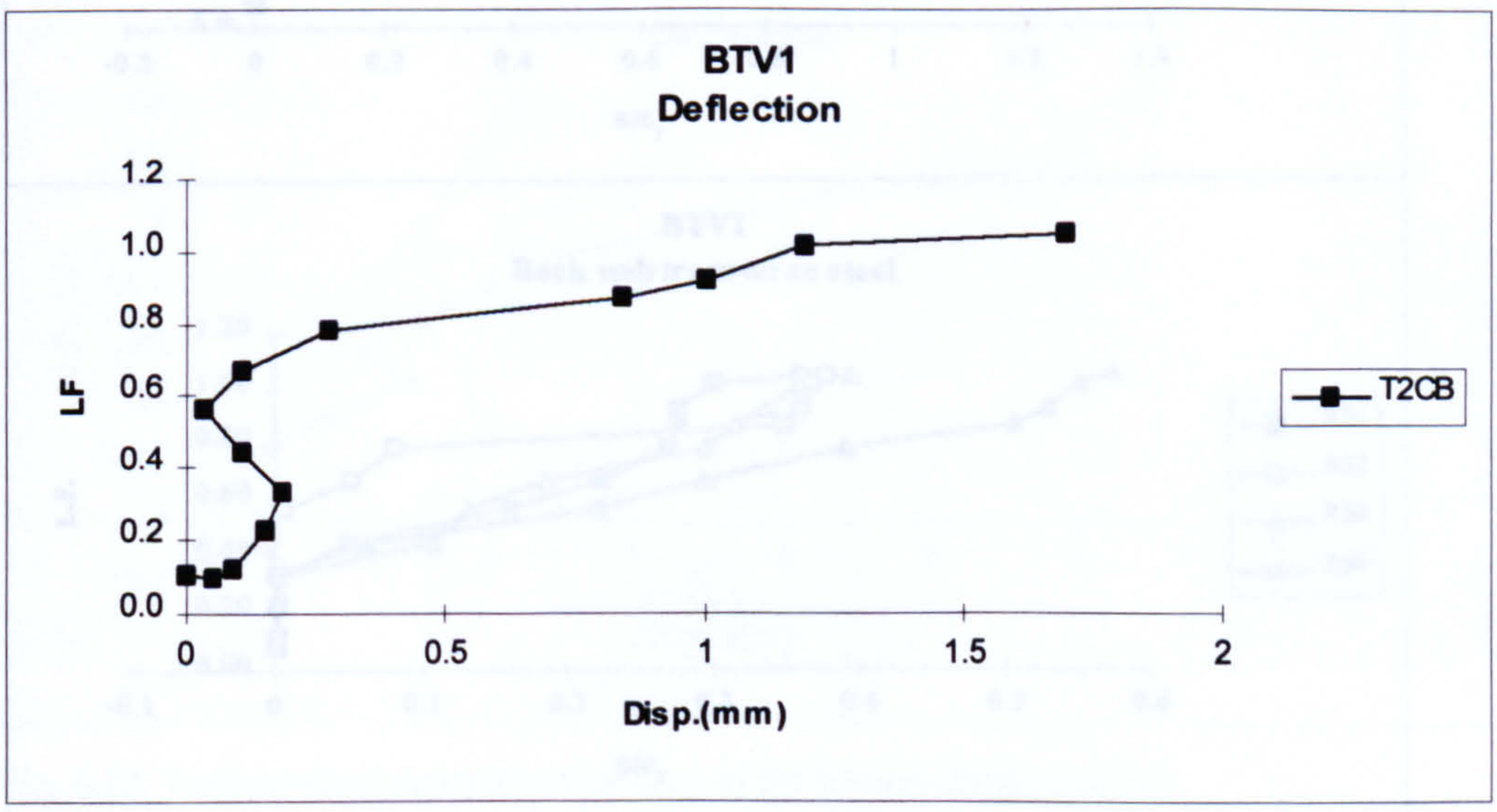

Fig. 5.9: Vertical displacement at mid-span of the bottom flange (BTV1)

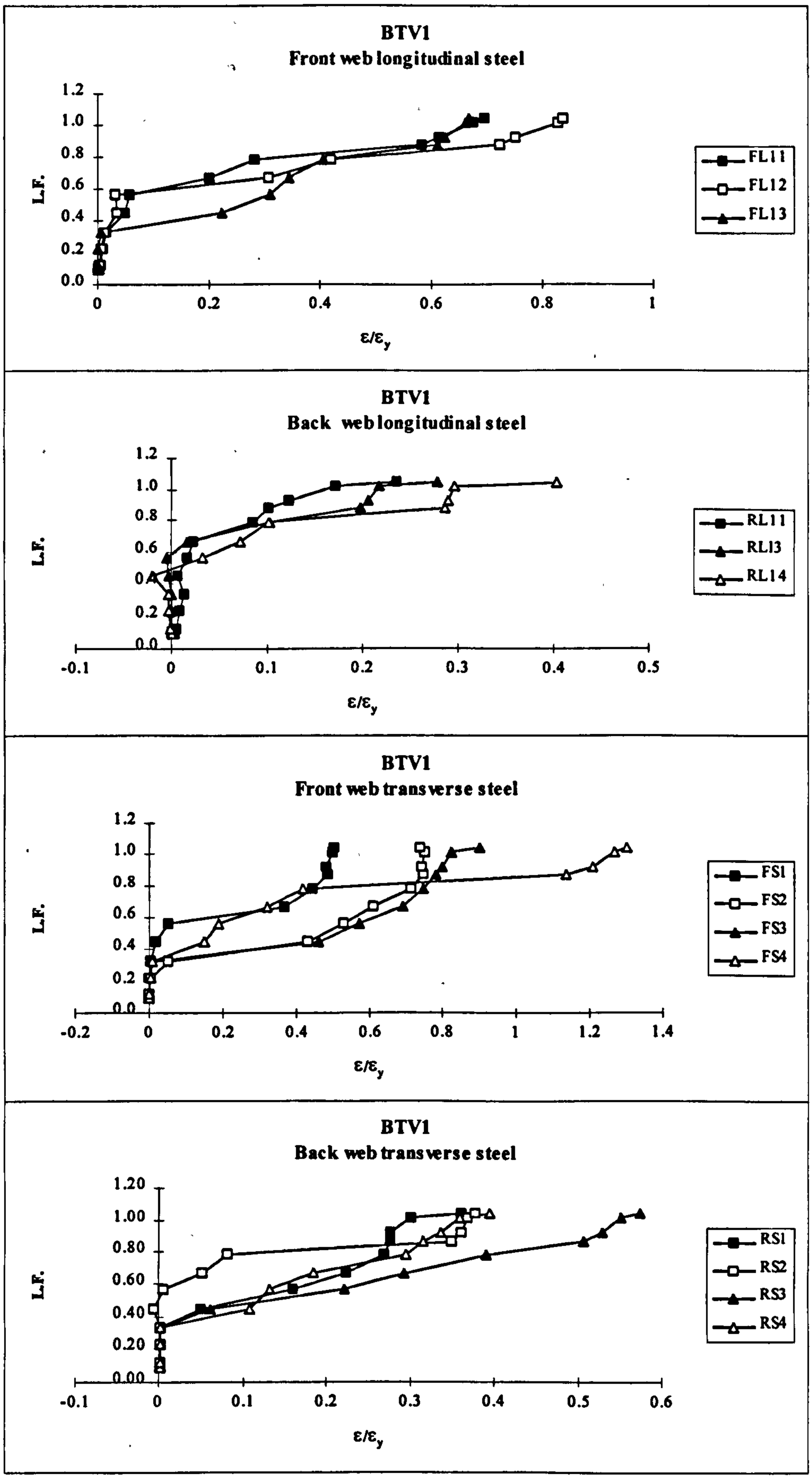

Fig. 5.10: Strain ratios in the steel (BTV1)

BTV2: T_d=13kNm, M_d=32.89kNm, V_d=41.08kN, T_d/M_d=0.40, τ_{tor}/τ_{shr}=1.17

At 50% of load, a single almost vertical crack was first noticed at the bottom flange near mid-span. With the increase of the load, 60° inclined cracks developed in the bottom flange and webs. At about 90% of load, 45° inclined cracks started in the top flange as an extension of the cracks in webs. Failure happened at 122% of load by a major 60° inclined crack starting at about 600mm to the right of mid-span on the front web and spiralling round the beam. The average crack width at this load level was 0.6mm. Figure 5.11 shows crack development at the front web of the beam. The displacement is shown in figure 5.12 and figure 5.13 shows the steel strain. The average strain ratio in the front web longitudinal steel was 1.16 and in the back web was 0.59. In the stirrups, the average strain ratio in the front web was 0.68 and in the back web was 0.20.

Fig. 5.11: Crack development in the front web (BTV2)

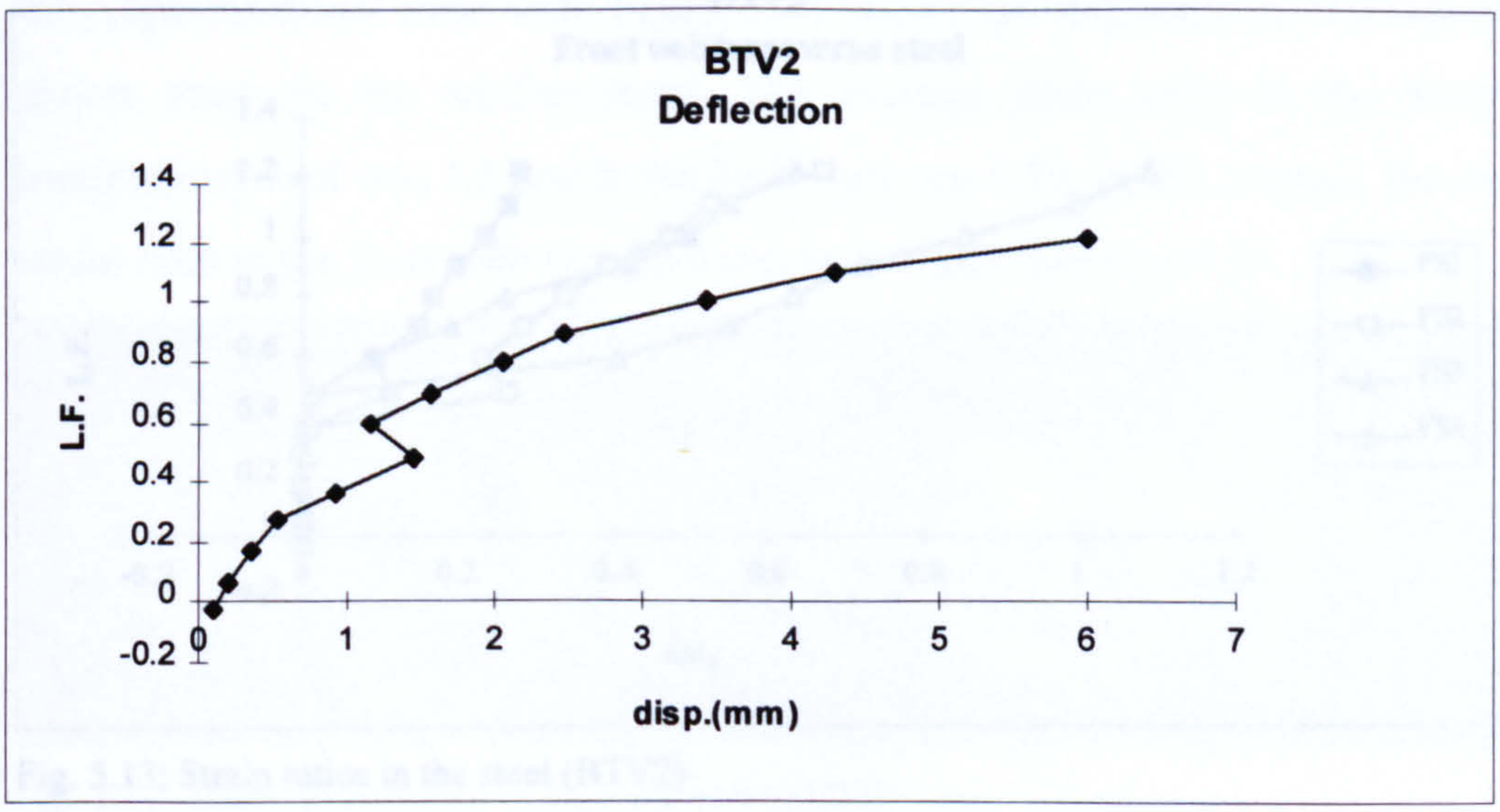

Fig. 5.12: Vertical displacement at mid-span of the bottom flange (BTV2)

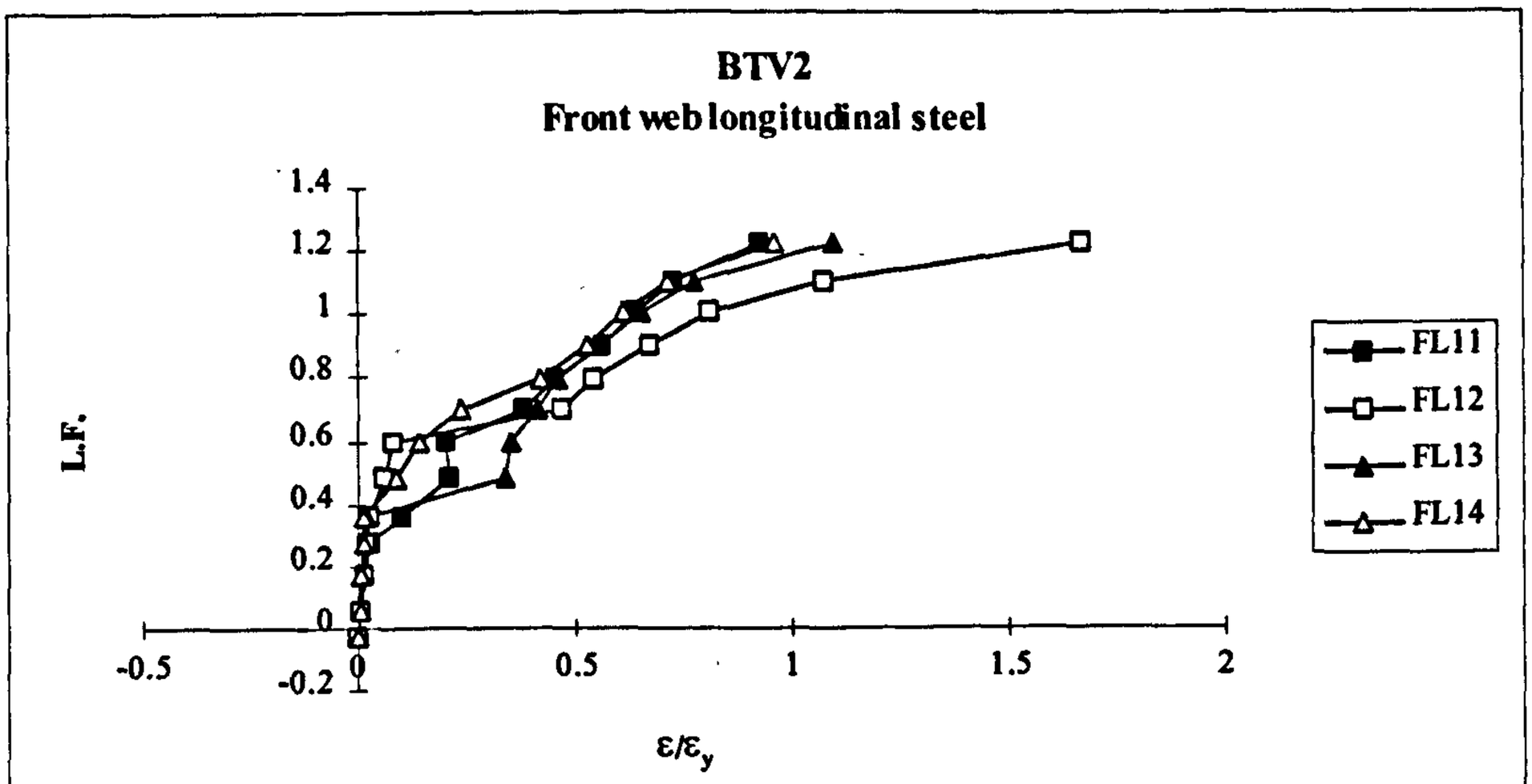

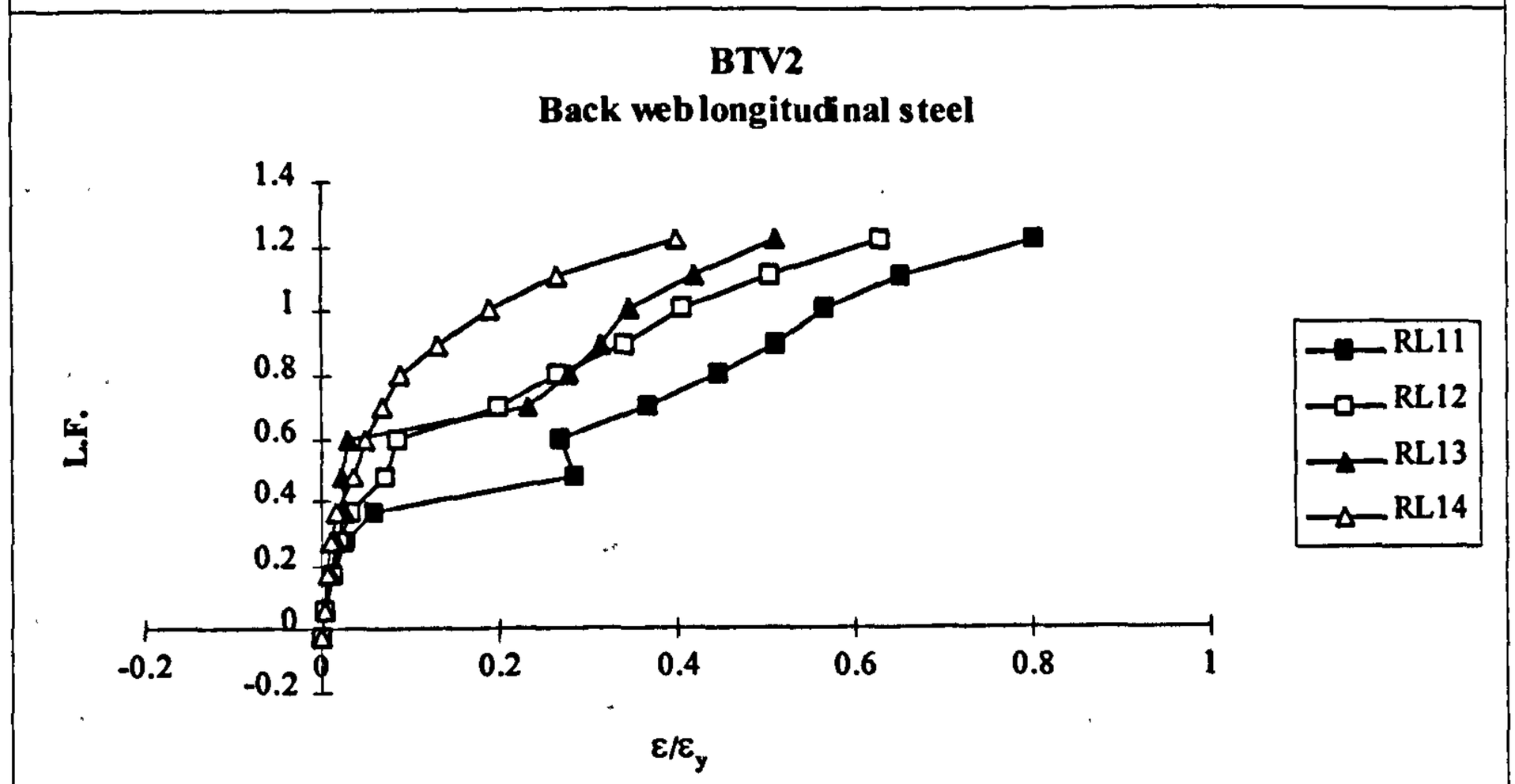

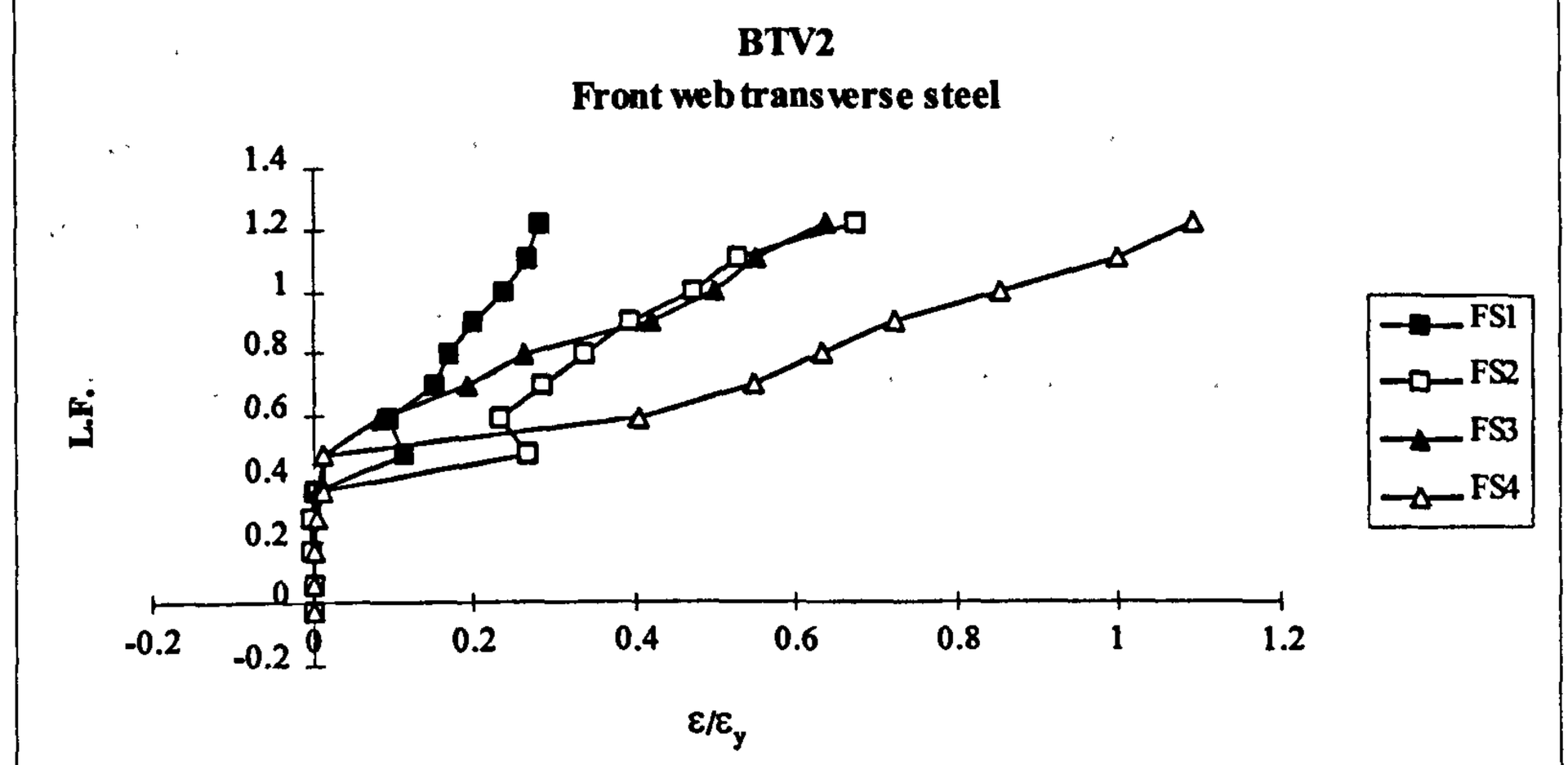

Fig. 5.13: Strain ratios in the steel (BTV2)

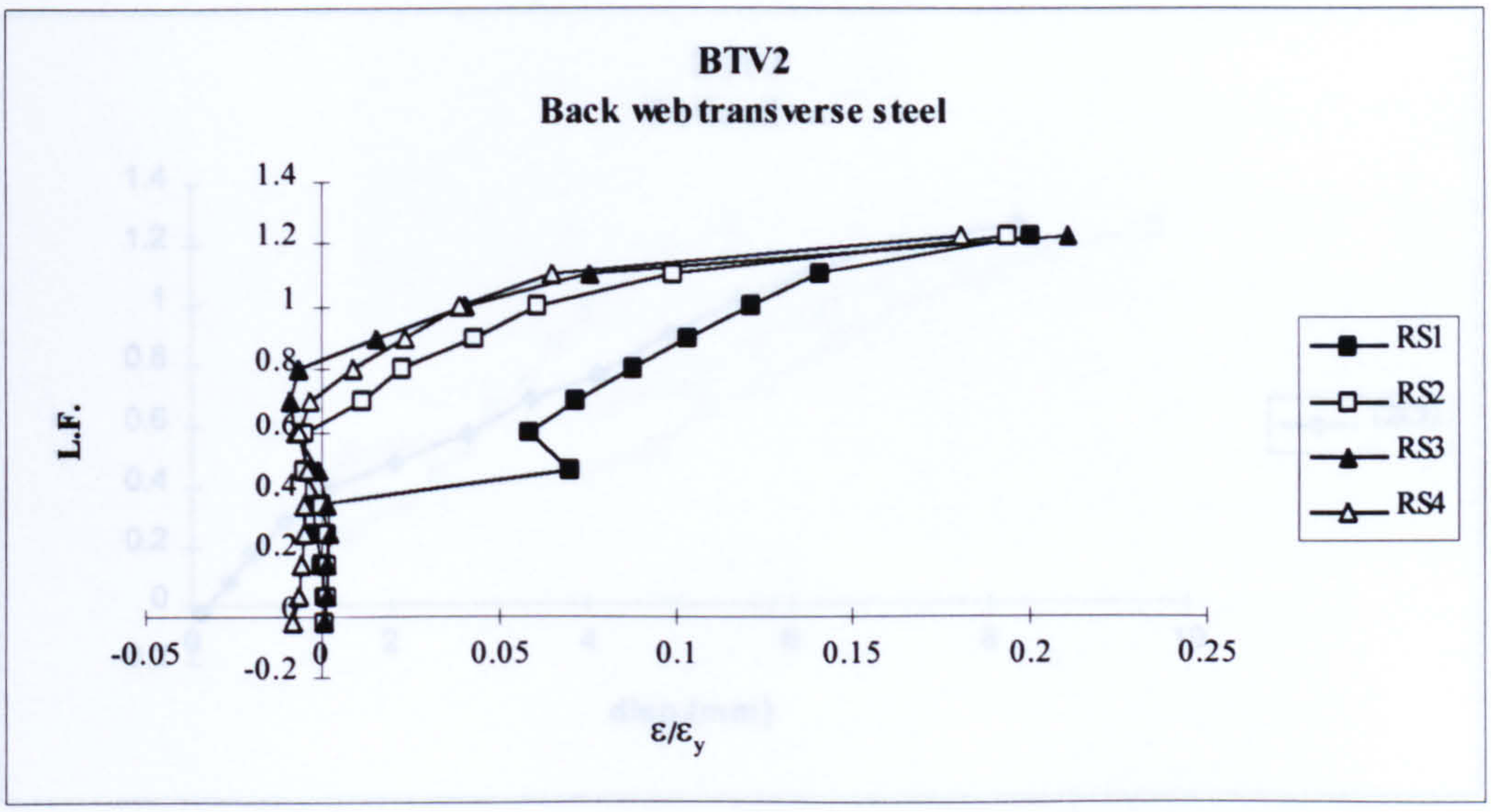

Fig. 5.13: Continued

BTV3: T_d=13kNm, M_d=50.89kNm, V_d=61.08kN, T_d/M_d=0.26, τ_{tor}/τ_{shr}=0.79

At 40% of load, almost vertical cracks were first noticed in the bottom flange and the webs near mid-span. Inclined cracks developed after this load level in the bottom flange and webs. At about 90% of load, 50° inclined cracks started in the top flange joining the cracks in the webs. The average crack width at this stage was 0.7mm. Displacement limit of span/250 was reached at 120% of load. Failure happened at 126% of load by two 60° inclined parallel major cracks starting at about 500mm to the right of mid-span on the front web. Figure 5.14 shows crack development in the front web. Figure 5.15 shows the displacement and figure 5.16 shows strain in the reinforcement. The average strain ratio in the front web longitudinal steel was 1.2 and in the back web was 0.76. In the stirrups, the average strain ratio in the front web was 0.69 and in the back web was 0.13.

Fig. 5.14: Crack development in the front web (BTV3)

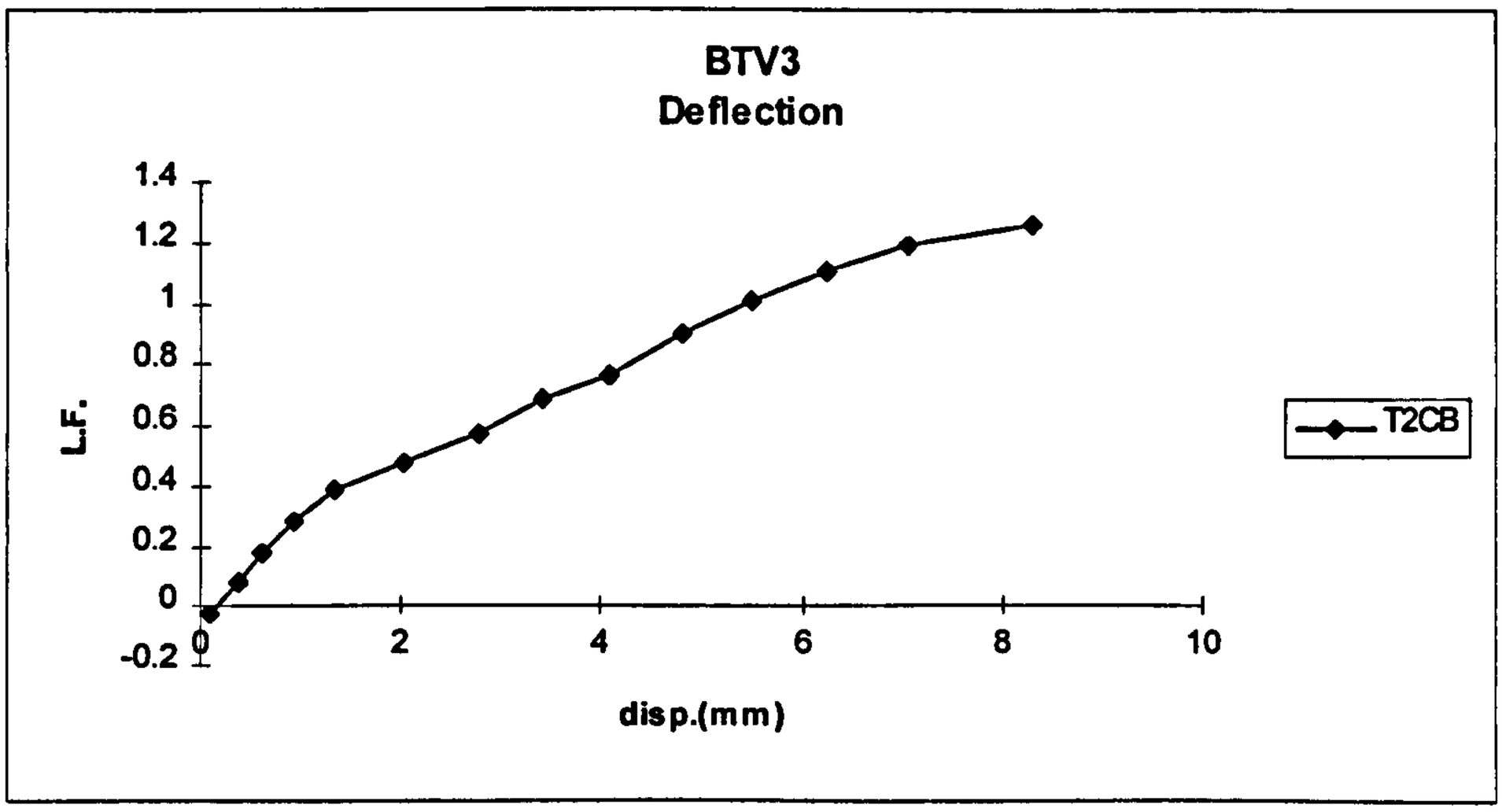

Fig. 5.15: Vertical displacement at mid-span of the bottom flange (BTV3)

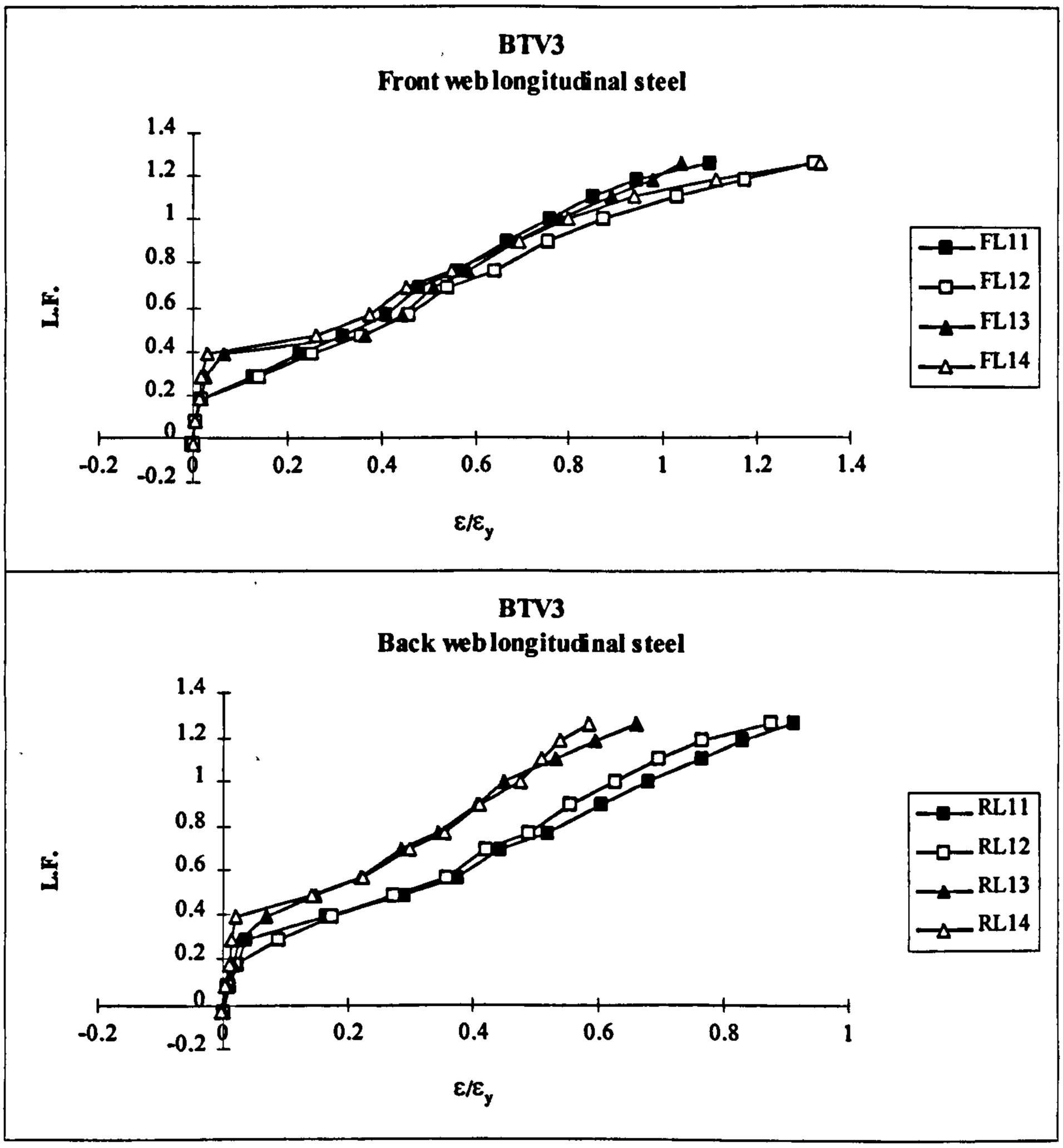

Fig. 5.16: Strain ratios in the steel (BTV3)

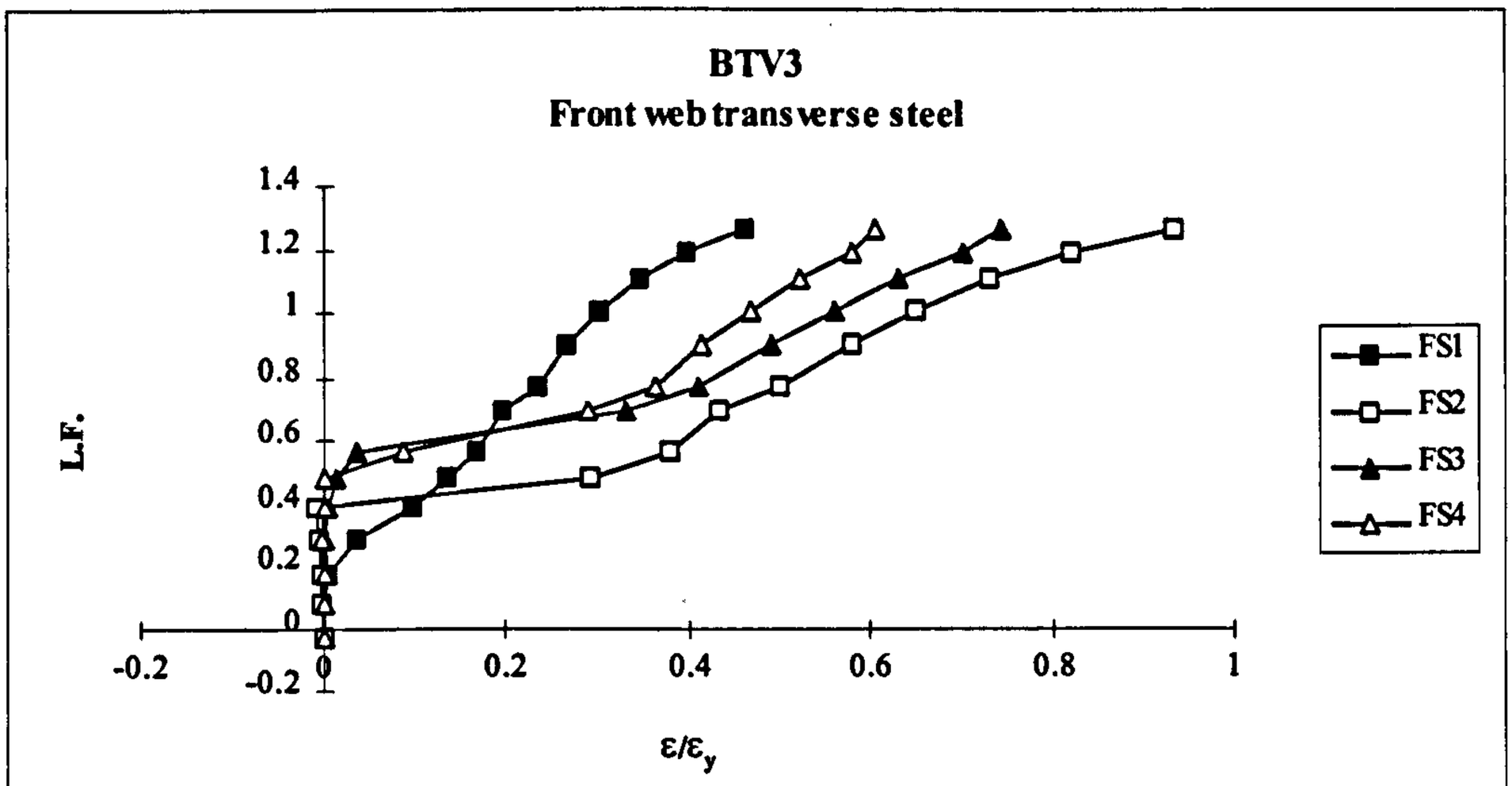

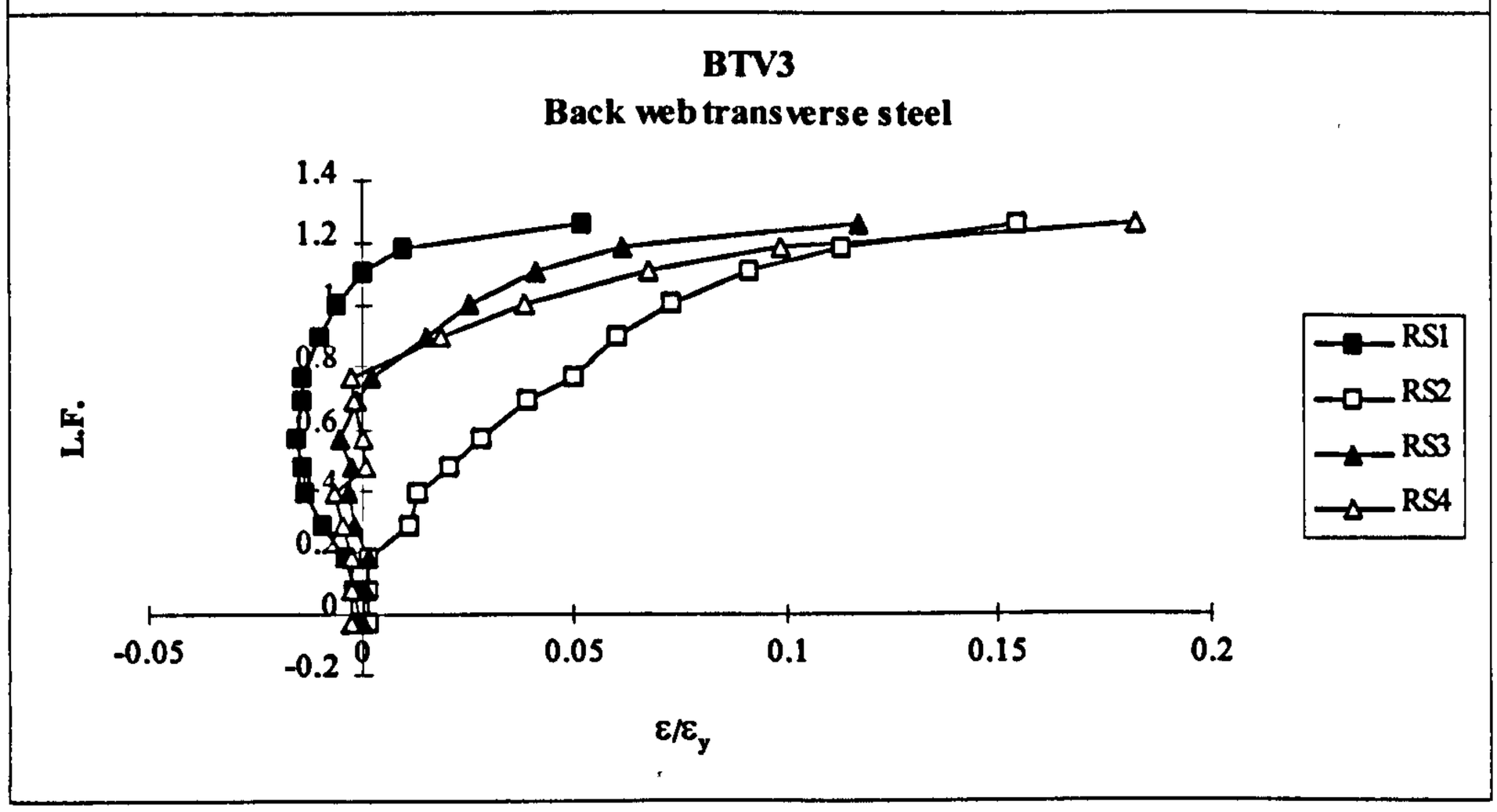

Fig. 5.16: Continued

BTV4: T_d=13kNm, M_d=68.89kNm, V_d=81.08kN, T_d/M_d=0.19, τ_{tor}/τ_{shr}=0.59

At 40% of load, vertical cracks started in the bottom flange and webs near mid-span. With increase of load, 60° inclined cracks developed in the bottom flange and webs. At about 80% of load, 50° inclined cracks started in the top flange joining the cracks in the webs. The average crack width at this stage was 0.5mm. Displacement limit of span/250 was reached at 100% of load. Failure happened at 106% of load by a major crack starting at about 500mm to the left of mid-span on the back web. Figure 5.17 shows crack development at the back web. Figure 5.18 shows the displacement and figure 5.19 shows strain in the reinforcement. The average strain ratio in the front web was 1.12 and in the back web was 0.60. In the stirrups, the average strain ratio in the front web was 0.67 and in the back web was 0.12.

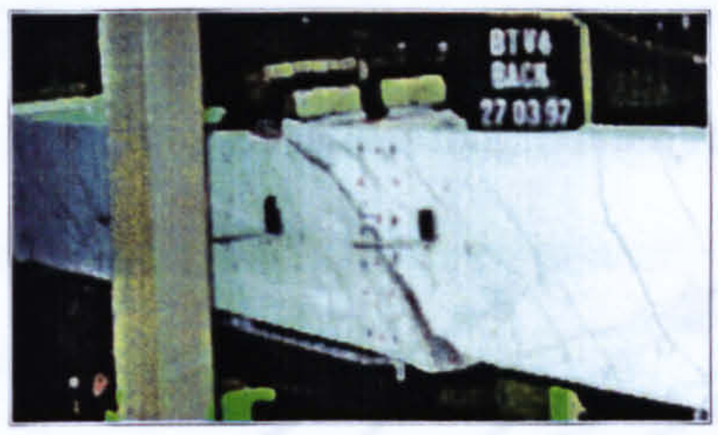

Fig. 5.17: Crack development in the back web (BTV4)

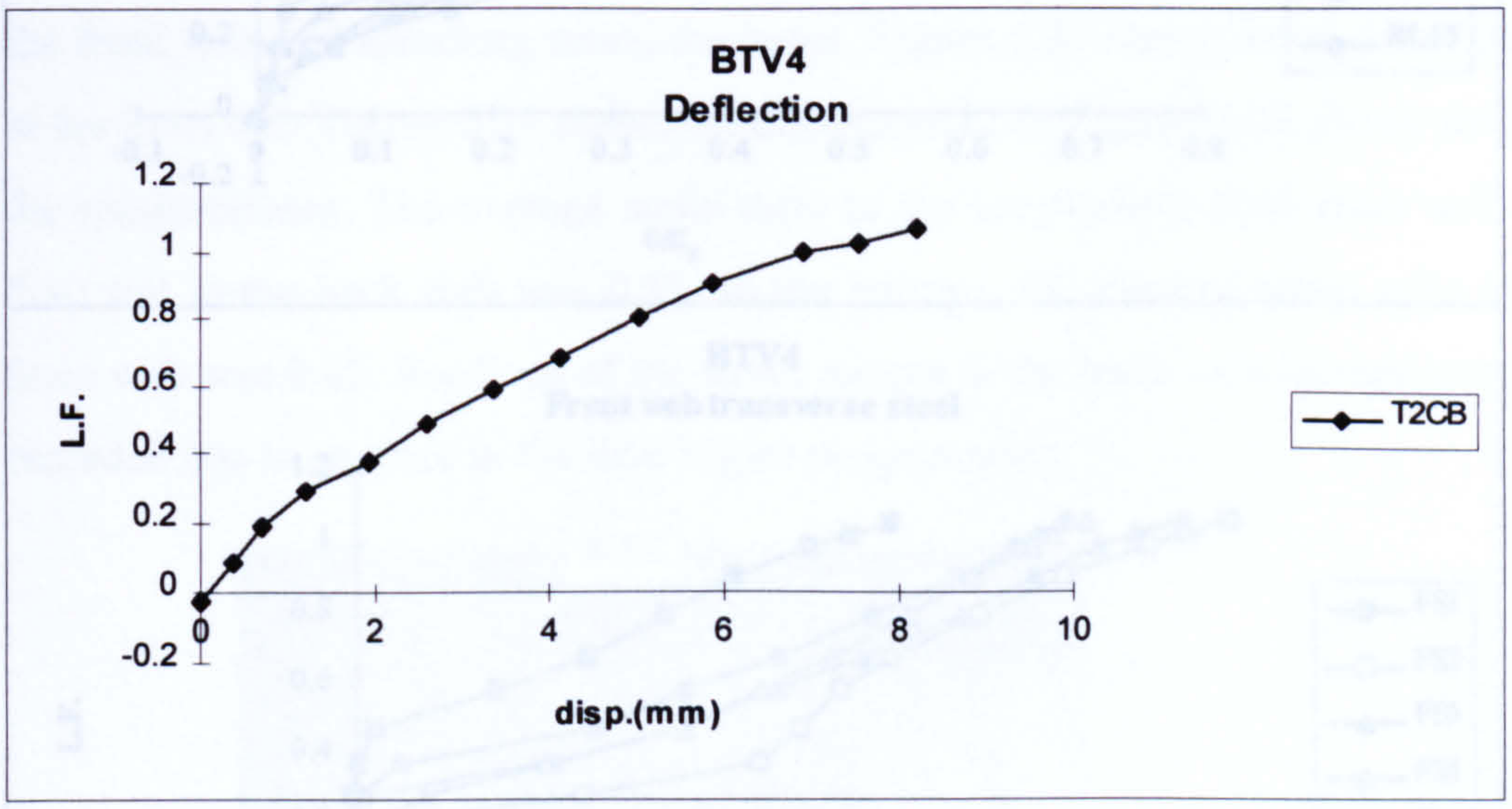

Fig. 5.18: Vertical displacement at mid-span of the bottom flange (BTV4)

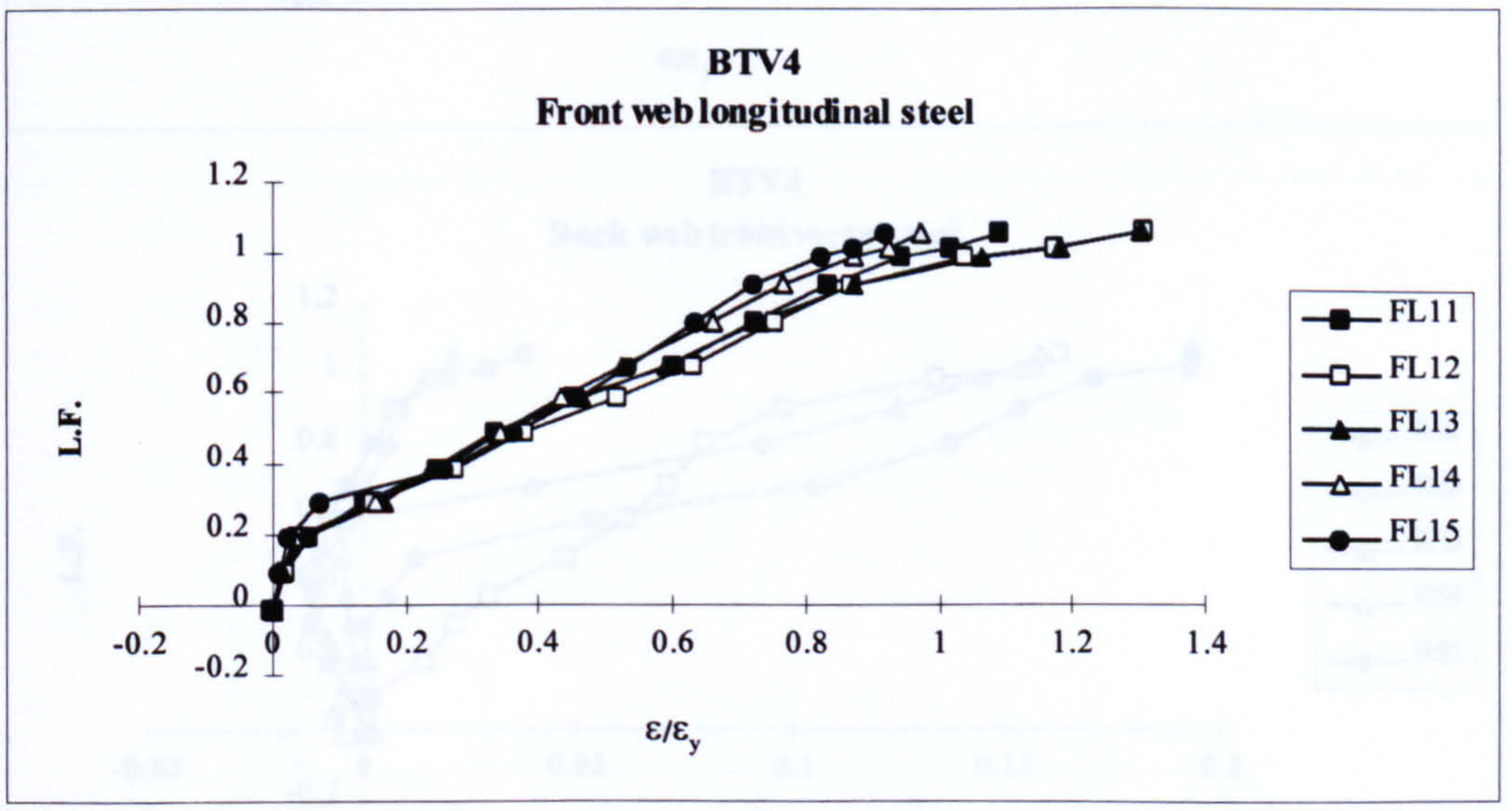

Fig. 5.19: Strain ratios in the steel (BTV4)

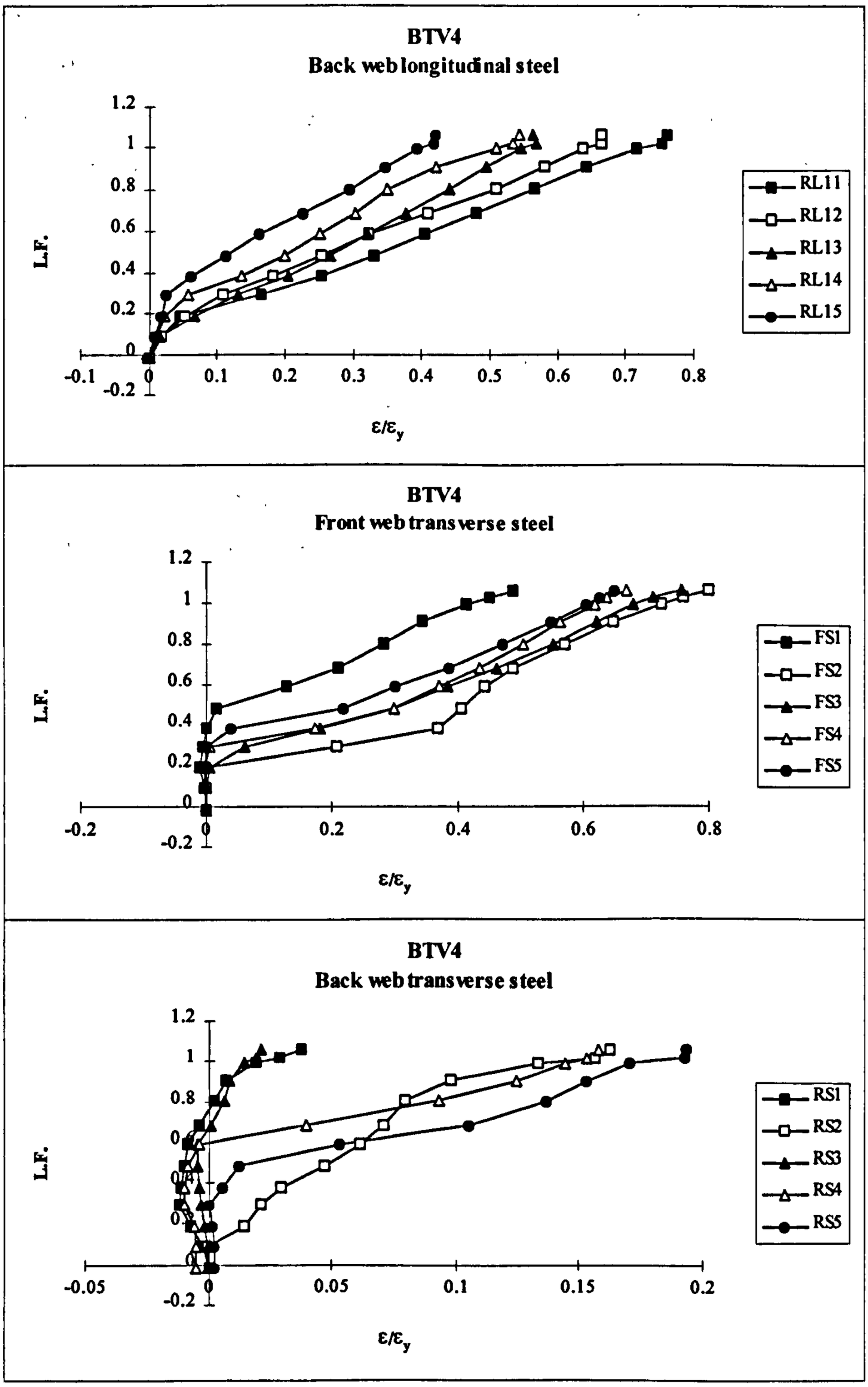

Fig. 5.19: Continued (BTV4)

BTV5: T_d=26kNm, M_d=14.89kNm, V_d=21.08kN, T_d/M_d=1.75, τ_{tor}/τ_{shr}=4.56

At 30% of load, 50° inclined cracks started in the webs half way between mid-span and supports. At 40% of load, cracks appeared in the bottom flange near mid-span and at 50% of load, cracks were observed in the top flange. The average crack width at this load level was 0.5mm. Displacement limit of span/250 was reached at 90% of load. Failure happened at 102% of load, by a major inclined (50°) crack starting in the front web and spiralling round the beam. Figure 5.20 shows crack development at the front web. Figure 5.21 shows the displacement and figure 5.22 shows strain in the reinforcement. The average strain ratio in the longitudinal steel front web was 0.80 and in the back web was 0.55. In the stirrups, the average strain ratio in the front web was 0.82. Readings of the strain gauges in the back web stirrups were not recorded due to an error in the data logger programming.

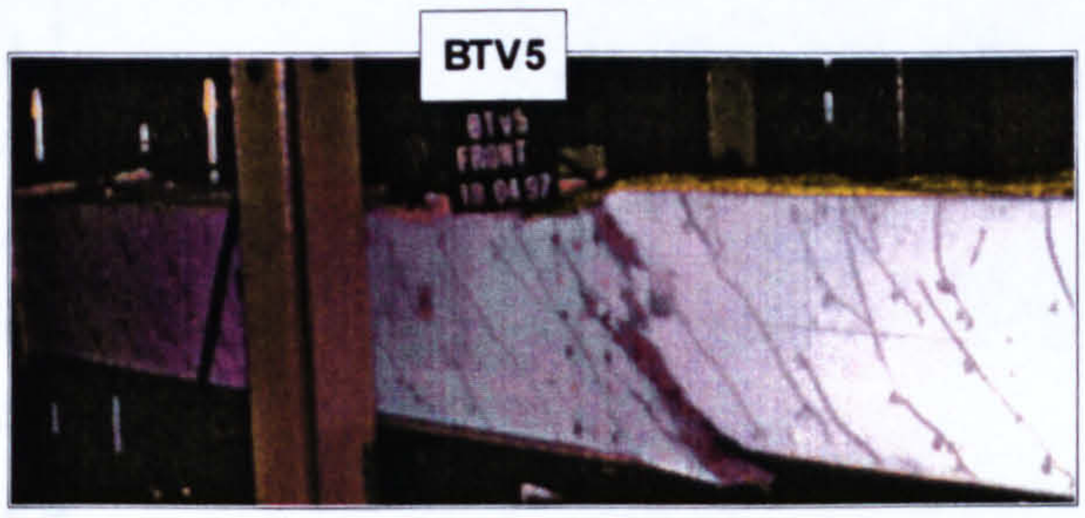

Fig. 5.20: Crack development in the front web (BTV5)

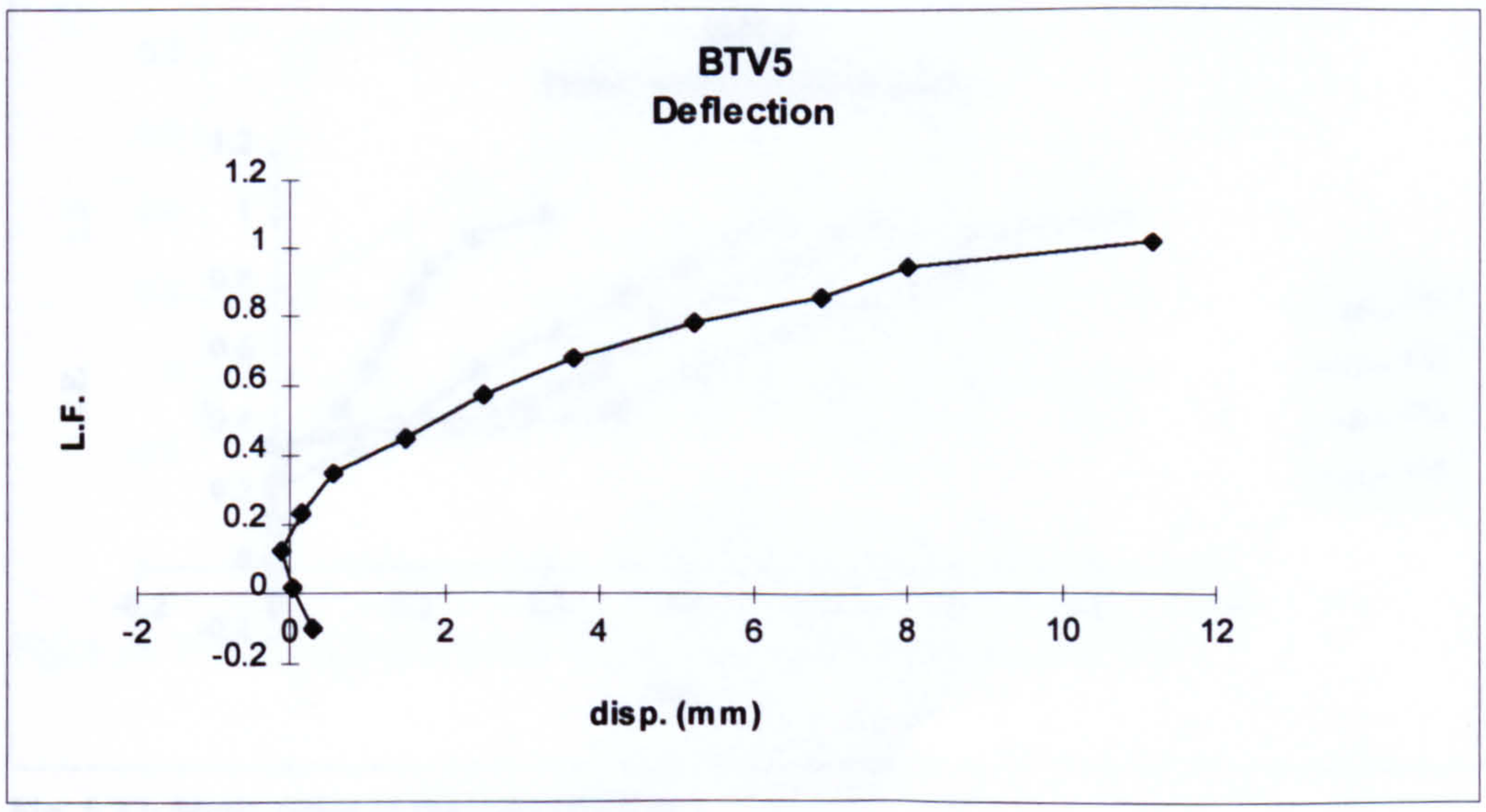

Fig. 5.21: Vertical displacement at mid-span of the bottom flange (BTV5)

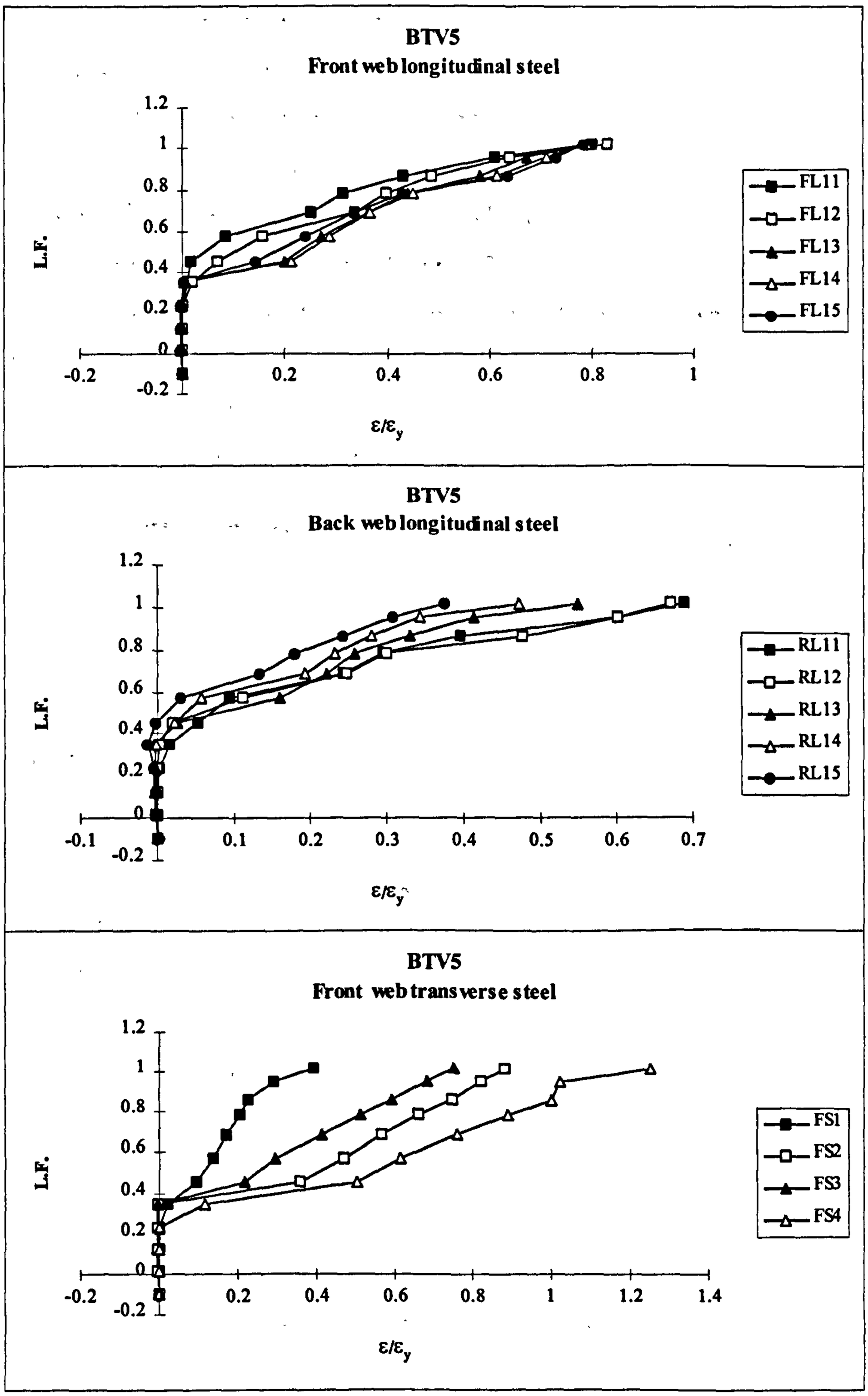

Fig. 5.22: Strain ratios in the steel (BTV5)

BTV6: T_d=26kNm, M_d=32.89kNm, V_d=41.08kN, T_d/M_d=0.79, τ_{tor}/τ_{shr}=2.34

Almost vertical cracks started in the bottom flange and the bottom of the webs at 50% of load level. Inclined cracks followed until 80% of load when cracks appeared in the top flange. The average crack width at this stage was 0.5mm. Failure happened at 92% of load by a major 60° inclined crack starting in the front web and quickly spiralling round the beam. Figure 5.23 shows crack development at the front web. Figure 5.24 shows the displacement and figure 5.25 shows strain in the reinforcement. The average strain ratio in the longitudinal steel front web was 0.75 and in the back web was 0.39. In the stirrups, the average strain ratio in the front web was 0.67 and in the back web was 0.36.

Fig. 5.23: Crack development in the front web (BTV6)

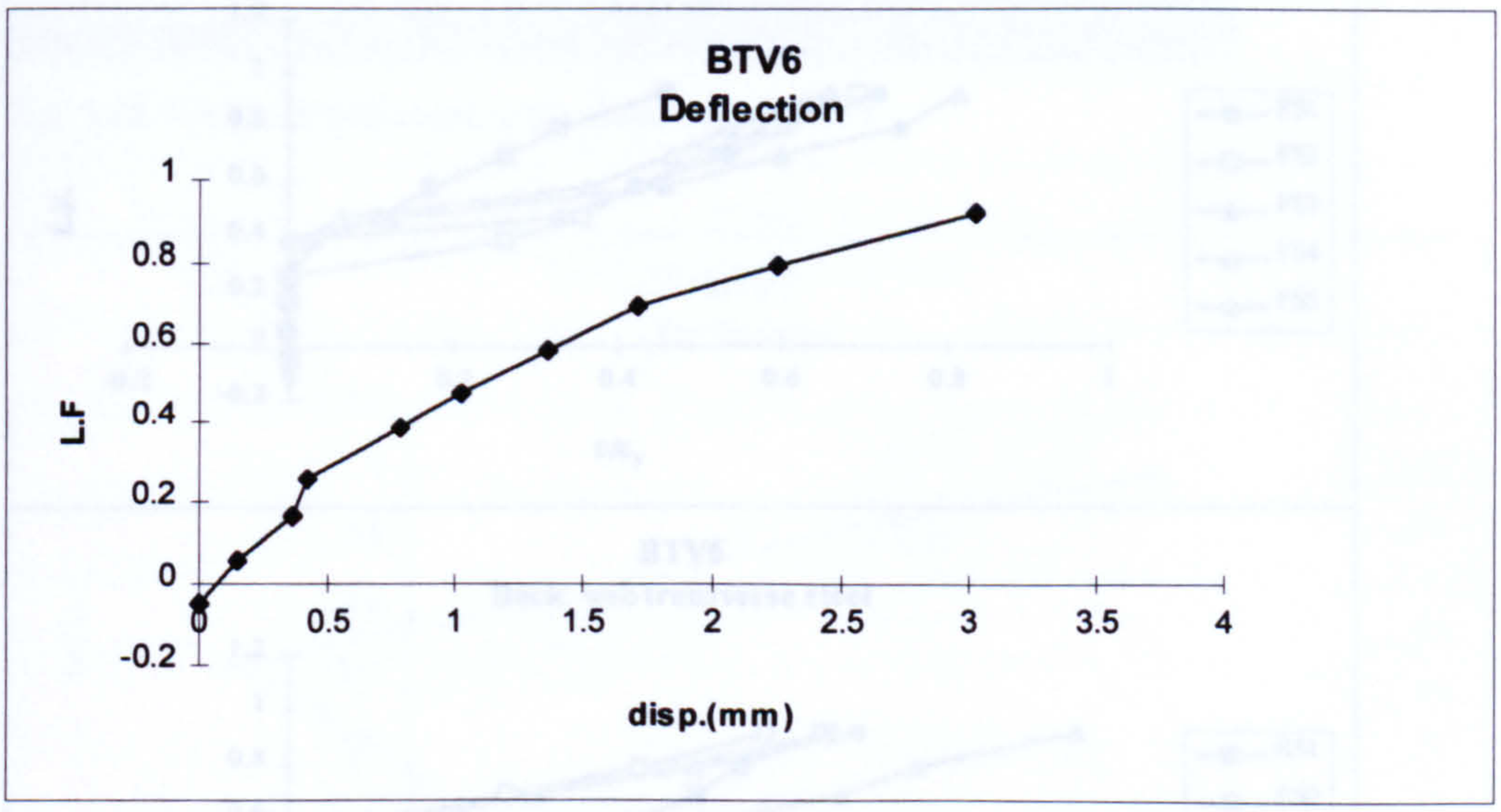

Fig. 5.24: Vertical displacement at mid-span of the bottom flange (BTV6)

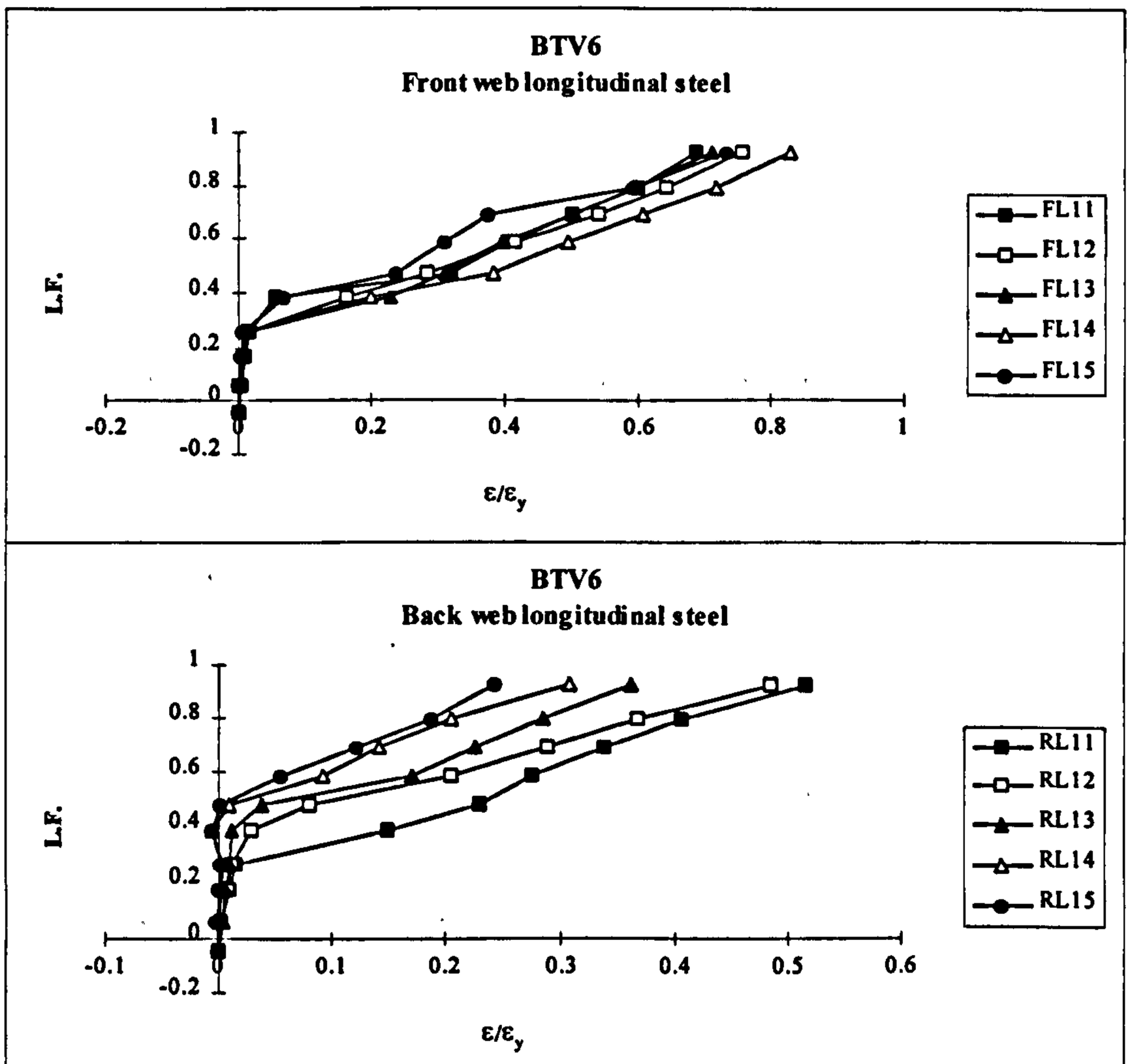

Fig. 5.25: Strain ratios in the steel (BTV6)

BTV7: T_d=39kNm, M_d=14.89kNm, V_d=21.08kN, T_d/M_d=2.62, τ_{tor}/τ_{shr}=6.84

At 30% of load, 45° inclined cracks started in the webs. At 40% of load, cracks appeared in the bottom flange and at 70% of load, cracks appeared in the top flange. The average crack width at this stage was 0.4mm. Displacement limit of span/250 was reached at 90% of load. Failure happened at 101% of load by 45° inclined major crack starting at 400mm to the right of mid-span in the front web and a concrete punch in the top flange near the point load. Figure 5.26 shows crack development at the front web. Figure 5.27 shows the displacement with some negative readings due a lateral shift in the beam position which was ratified after the sixth load step. Figure 5.28 shows strain in the reinforcement. The average strain ratio in the longitudinal steel front web was 0.84 and in the back web was 0.68. In the stirrups, the average strain ratio in the front web was 0.83 and in the back web was 0.82.

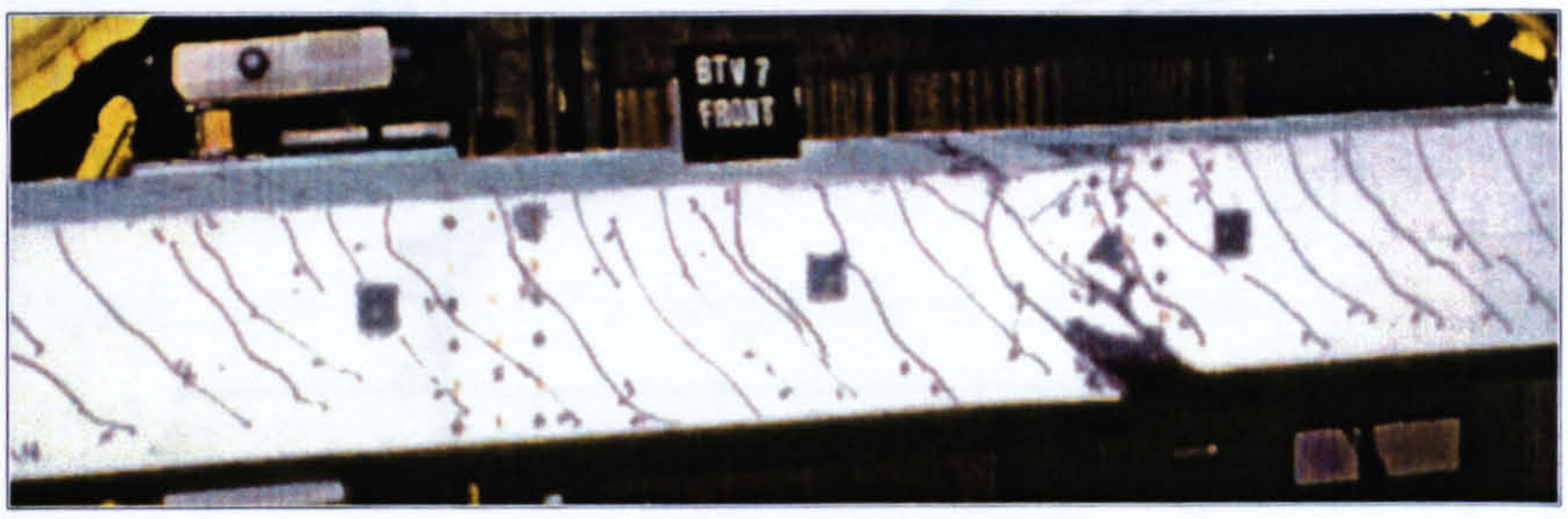

Fig. 5.26: Crack development in the front web (BTV7)

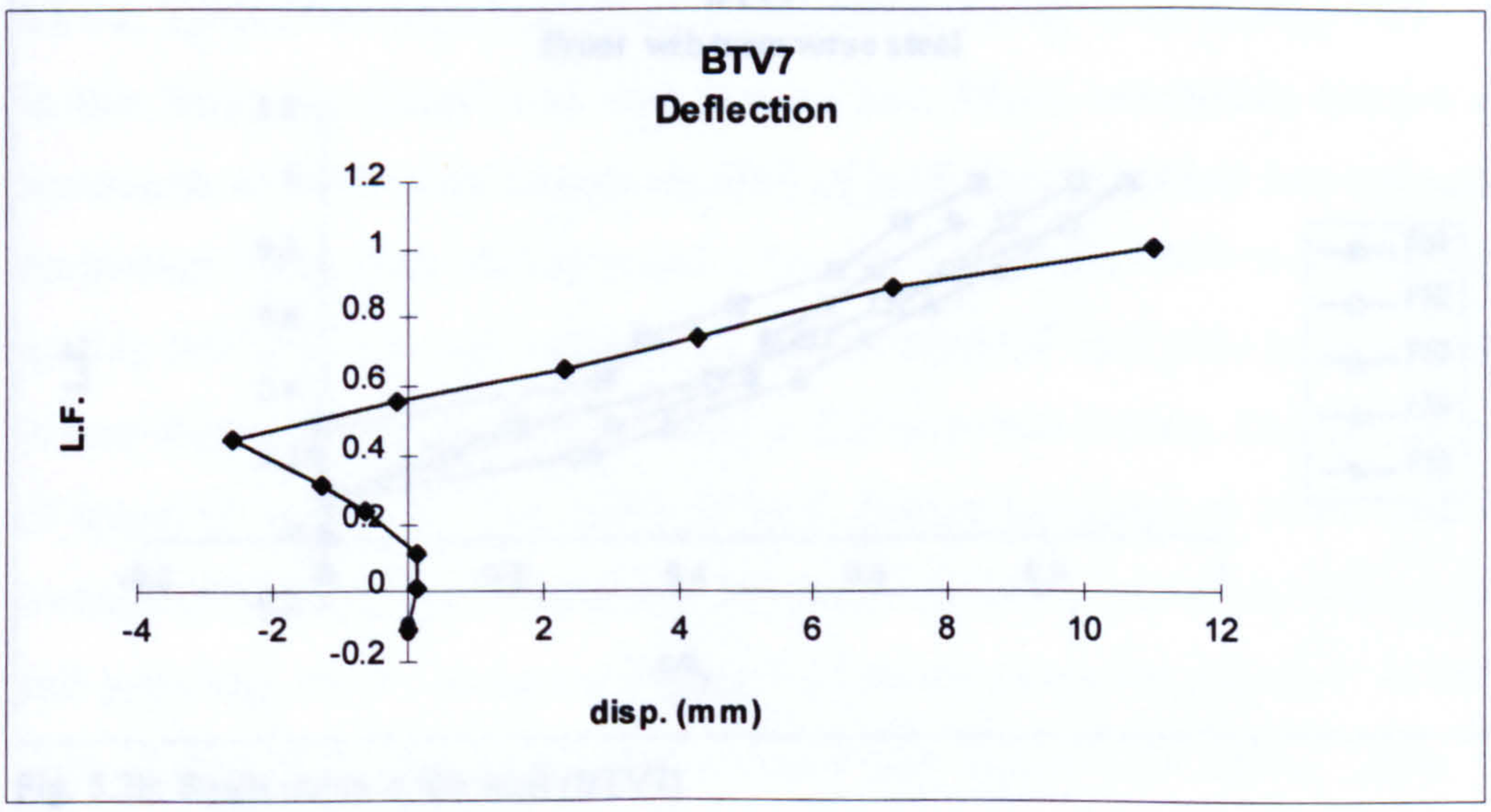

Fig. 5.27: Vertical displacement at mid-span of the bottom flange (BTV7)

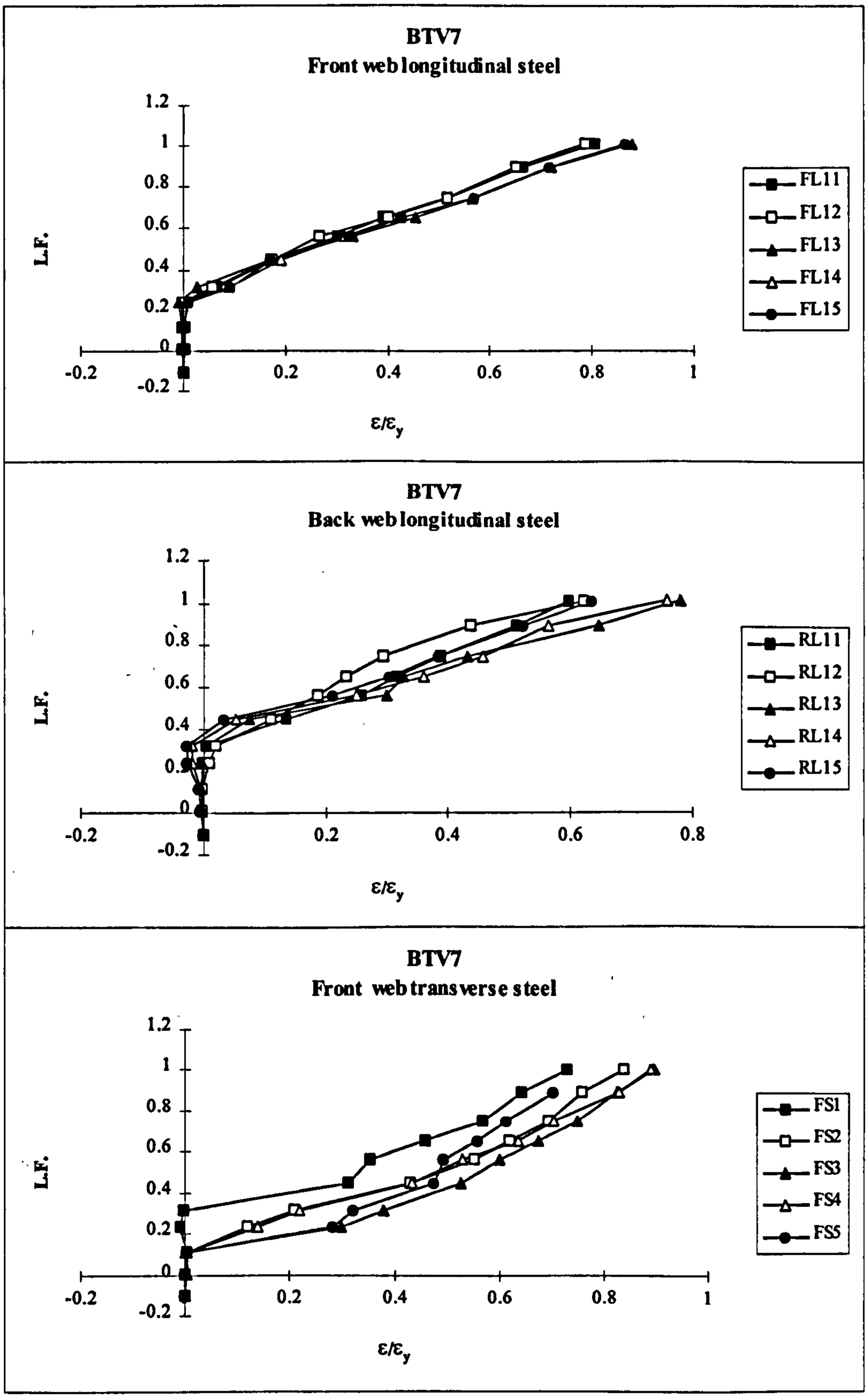

Fig. 5.28: Strain ratios in the steel (BTV7)

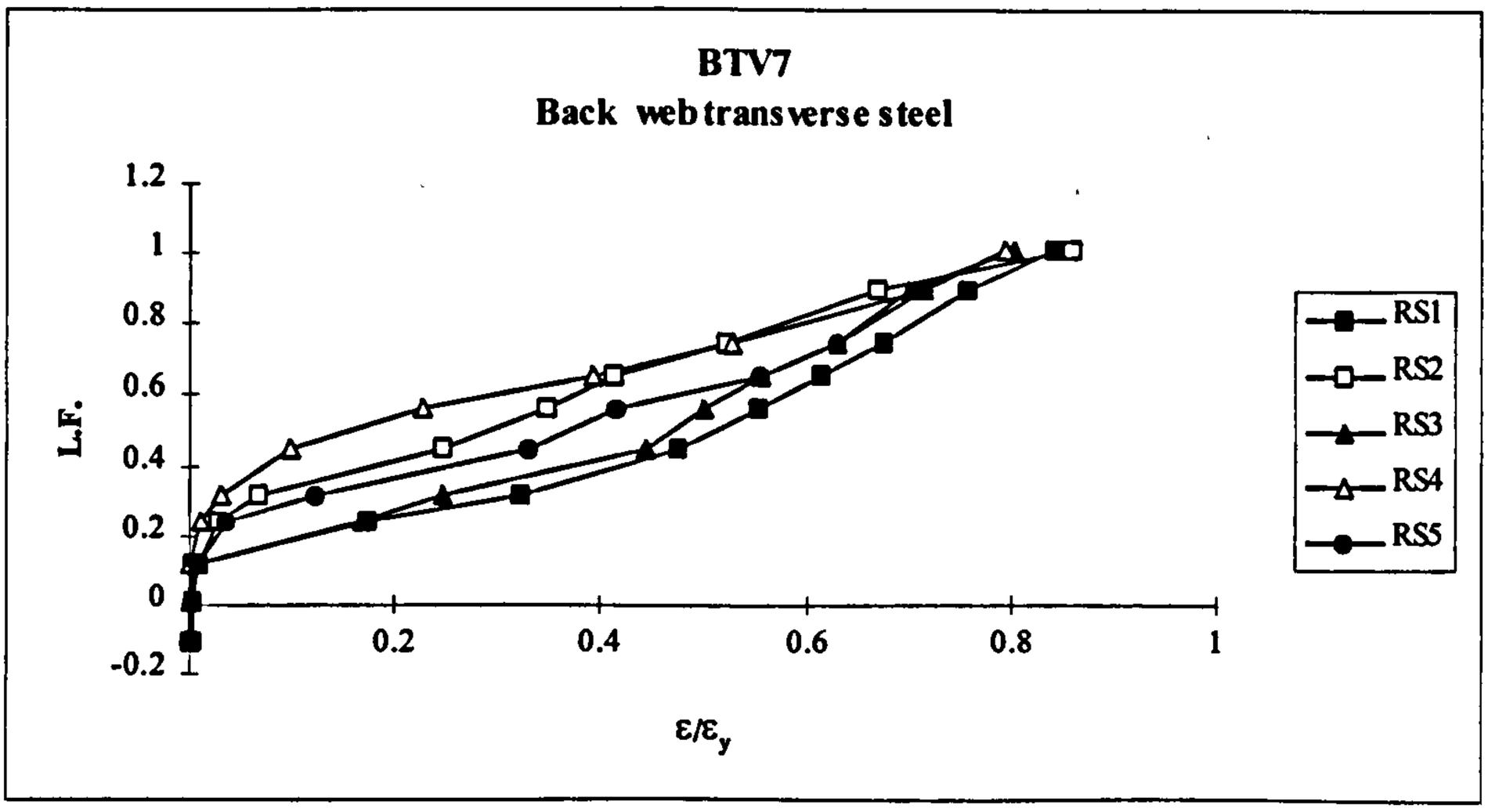

Fig. 5.28: Continued

BTV8: T_d=39kNm, M_d=32.89kNm, V_d=41.08kN, T_d/M_d=1.19, τ_{tor}/τ_{shr}=3.51

The crack development of this beam was similar to beam BTV7 except that the cracks started at a larger angle (80°) at the bottom of the webs and the failure occurred at 91% of load. Figure 5.29 shows crack development at the front web. Figure 5.30 shows the displacement and figure 5.31 shows strain in the reinforcement. The average strain ratio in the longitudinal steel front web was 0.68 and in the back web was 0.40. In the stirrups, the average strain ratio in the front web was 0.74 and in the back web was 0.48.

BTV9: T_d=18kNm, M_d=50.89kNm, V_d=61.08kN, T_d/M_d=0.35, τ_{tor}/τ_{shr}=1.09

In this beam the design load was divided into fifteen increments instead of ten increments as in all other beams. At 40% of load, almost vertical hair line crack in the bottom flange near mid-span and a few inclined cracks (60°) to the left of mid-span in the back web were noticed. At 80% of load 50° inclined cracks appeared in the top flange. The average crack width at this stage was 0.4mm. Displacement limit of span/250 was reached at 110% of load. Failure happened at 116% load by an inclined (50°) major crack starting at 300mm to the left of mid-span in the back web and spiralling round the beam. Figure 5.32 shows crack development in the back web. Figure 5.33 shows the displacement and figure 5.34 shows strain in the prestressing wires and the stirrups. The average strain ratio in the prestressing wire

in the front side was 2.05 and in the rear side was 1.08. In the stirrups, the average strain ratio in the front web was 1.06 and in the back web was 0.39.

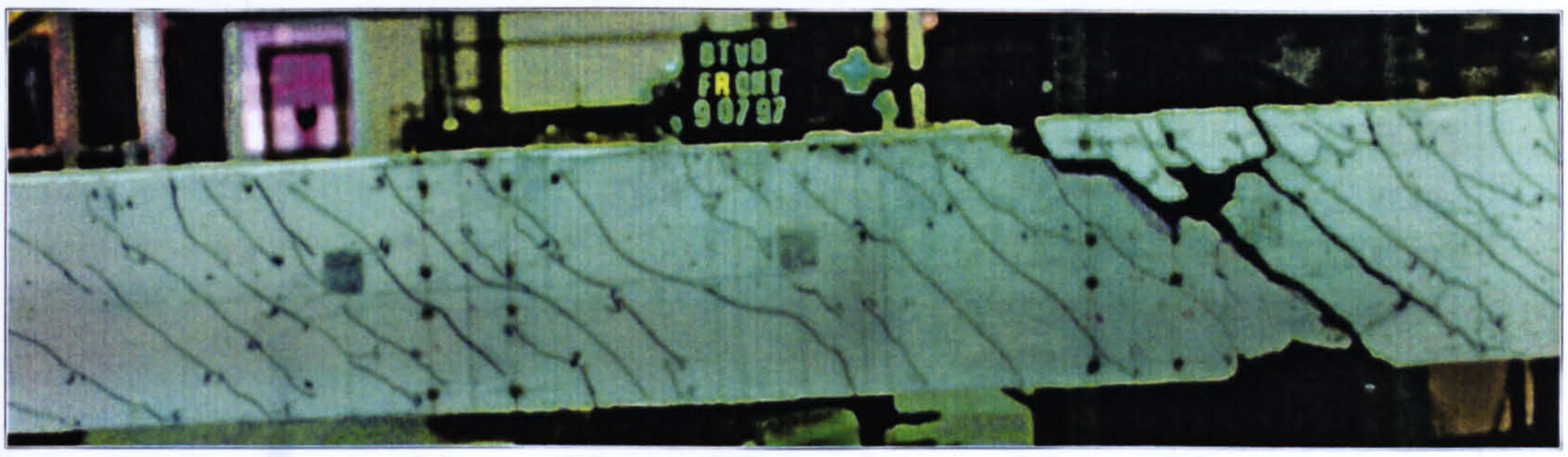

Fig. 5.29: Crack development in the front web (BTV8)

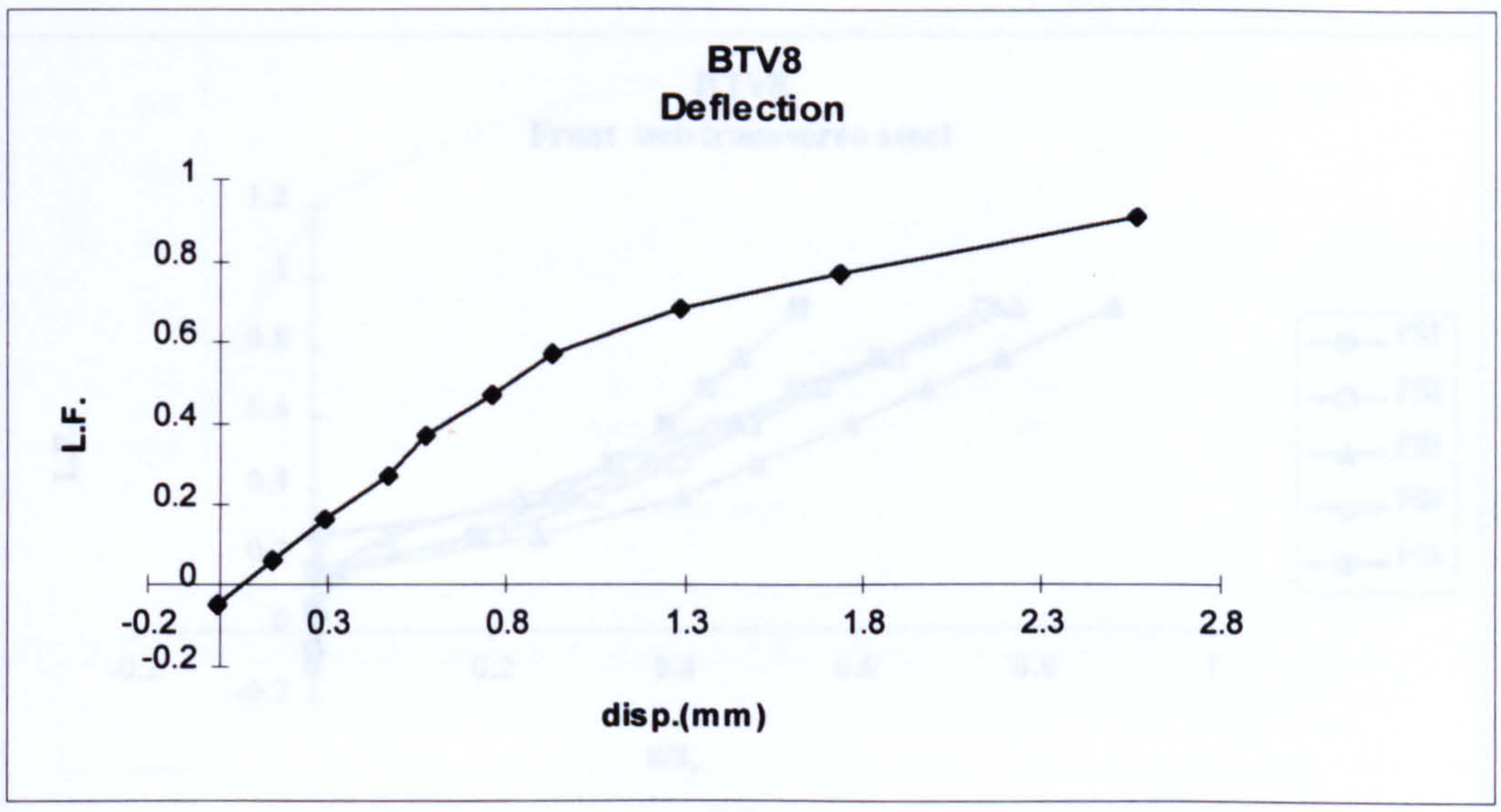

Fig. 5.30: Vertical displacement at mid-span of the bottom flange (BTV8)

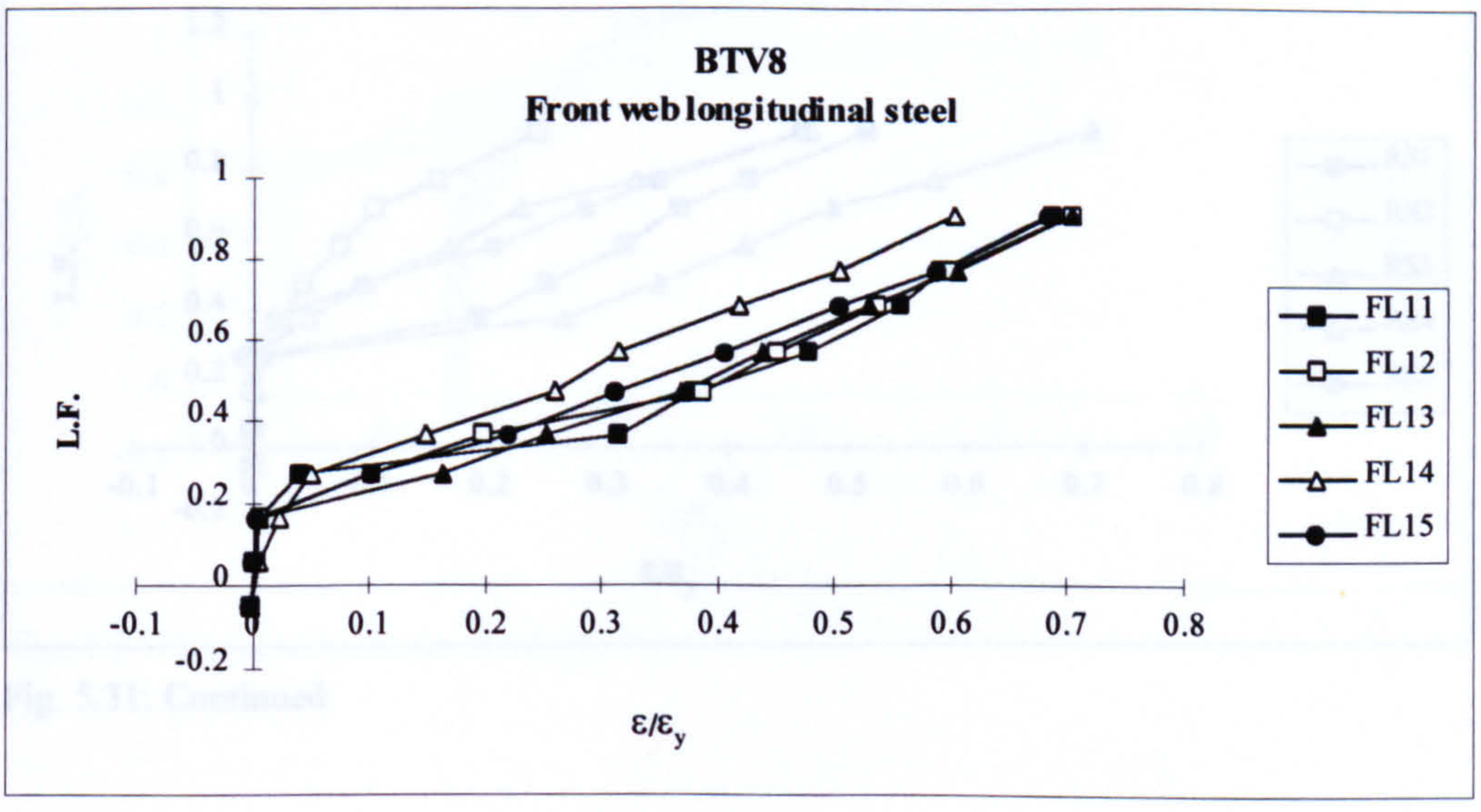

Fig. 5.31: Strain ratios in the steel (BTV8)

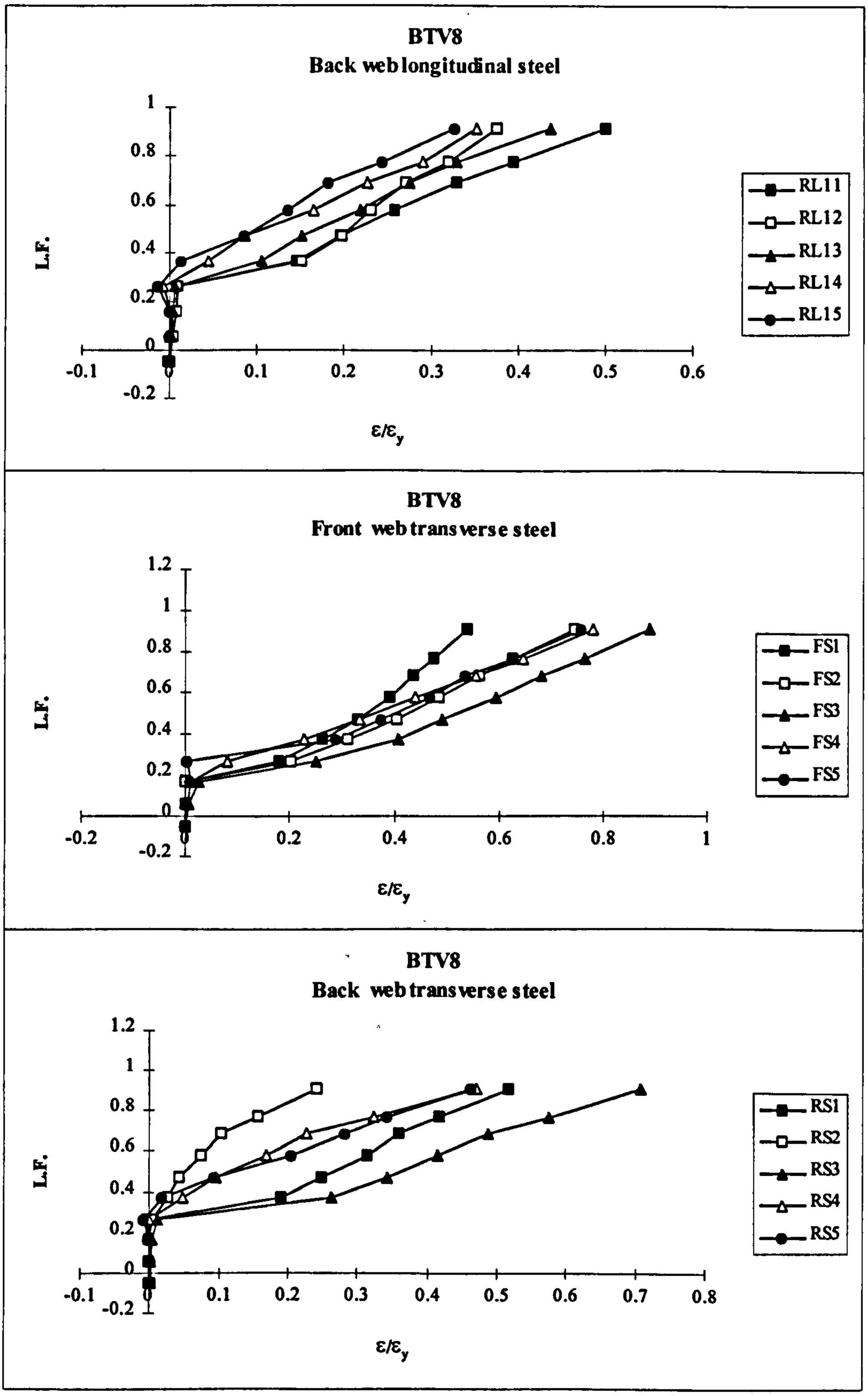

Fig. 5.31: Continued

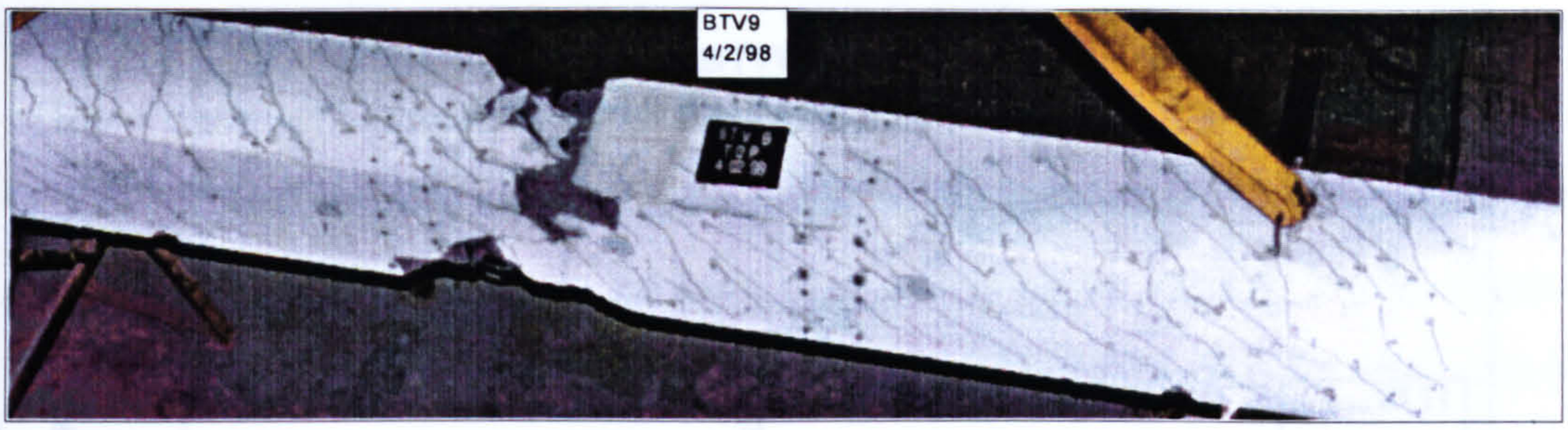

Fig. 5.32: Crack development in beam (BTV9)

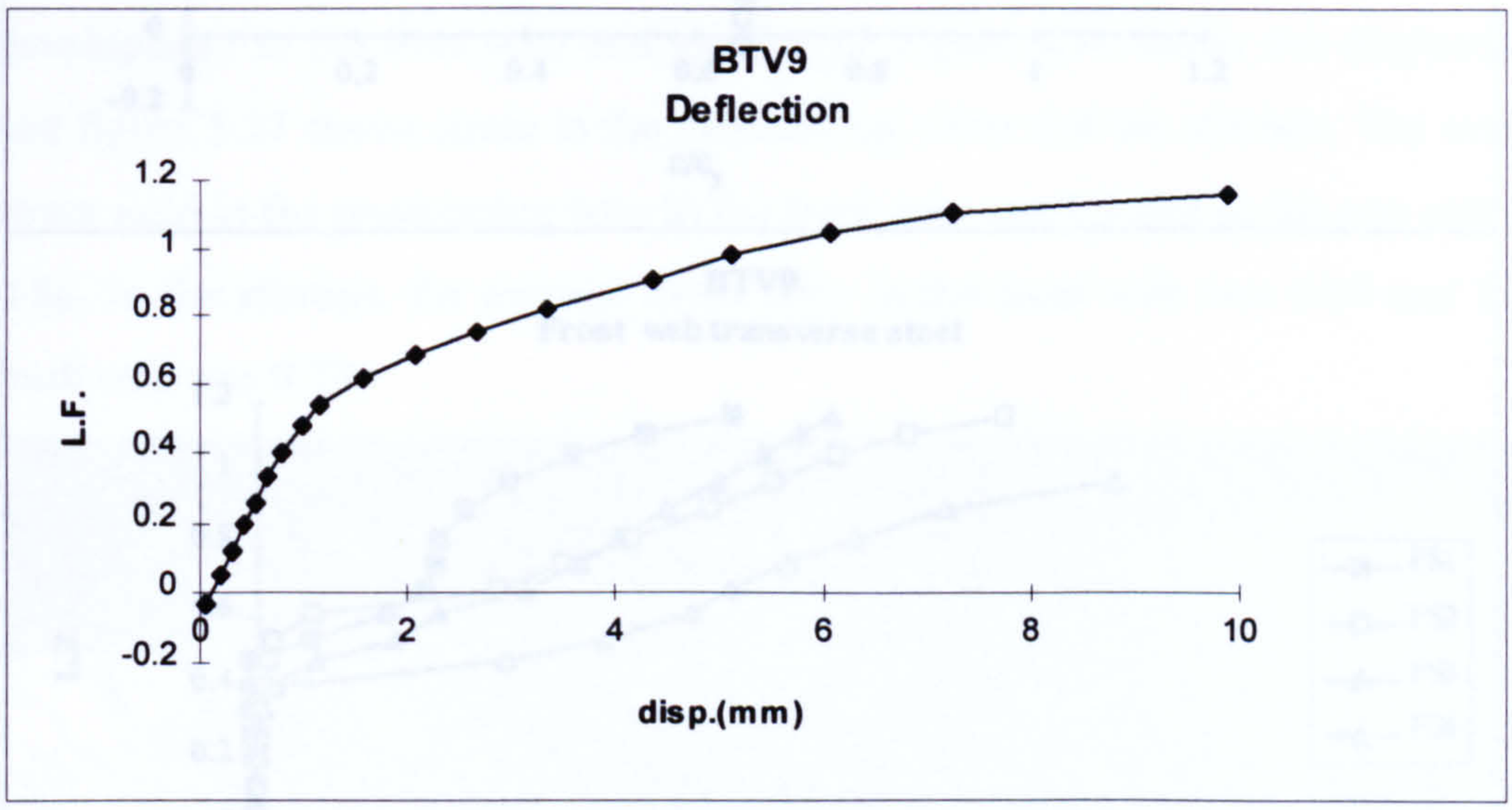

Fig. 5.33: Vertical displacement at mid-span of the bottom flange (BTV9)

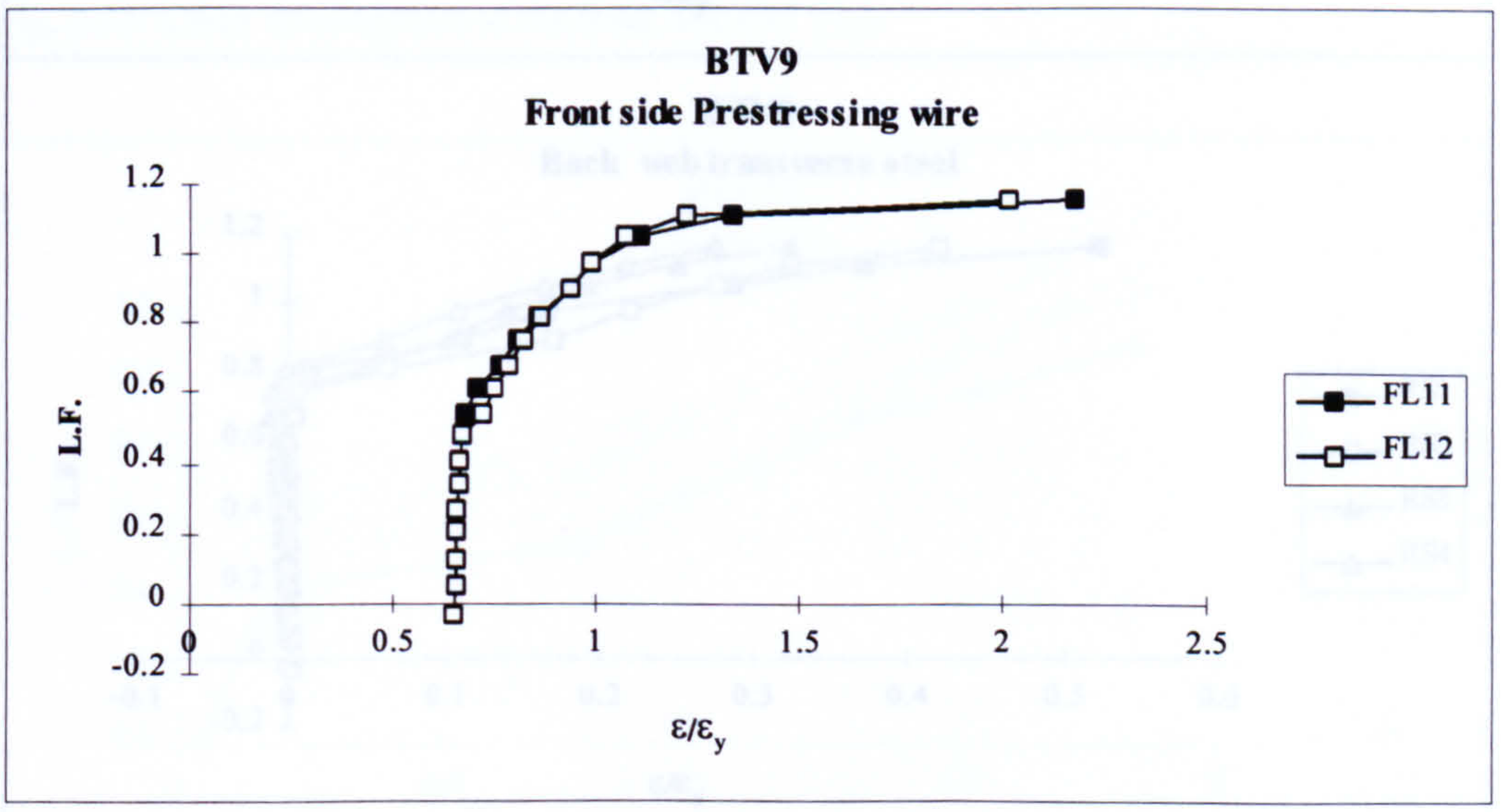

Fig. 5.34: Strain ratios in the steel (BTV9)

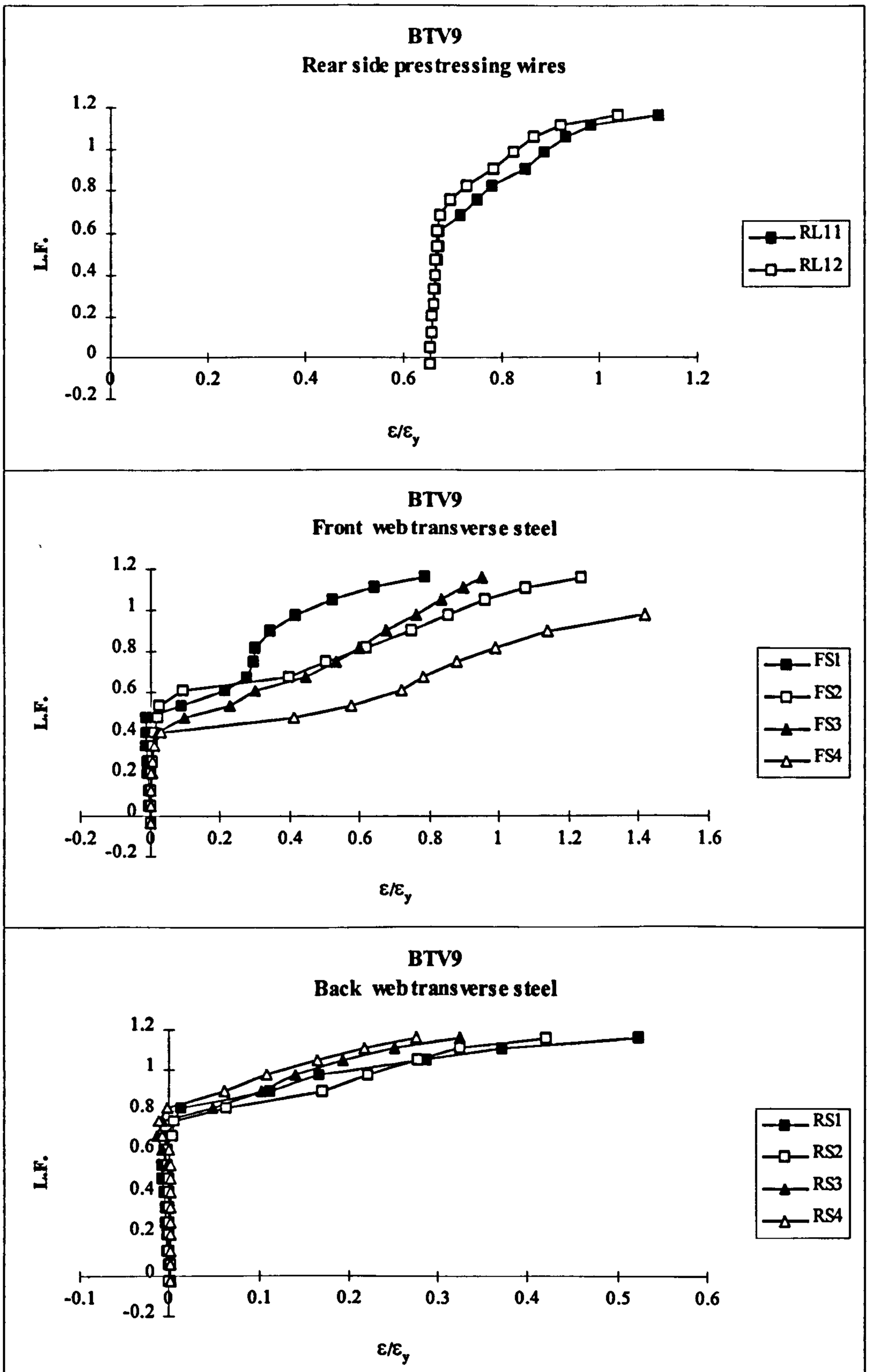

Fig. 5.34: Continued

BTV10: T_d=26kNm, M_d=14.89kNm, V_d=21.08kN, T_d/M_d=1.75, τ_{tor}/τ_{shr}=4.56

Inclined cracks (50°) appeared in the webs and in the bottom flange at 40% of load. At 50% of load, similar cracks were noticed in the top flange. The average crack width at this stage was 0.4mm. At 90% of load two major inclined cracks opened up, one was in the front web at 300mm to the right of mid-span and the other was in the back web at 200mm to the left of mid-span. Failure happened at 110% of load by the major cracks joining in the top and bottom flanges. Figure 5.35 shows crack development in the front web and top flange. Figure 5.36 shows the displacement and figure 5.37 shows strain in the prestressing wires and the stirrups. The average strain ratio in the prestressing wire in the front side was 1.0 and in the rear side was 0.86. In the stirrups, the average strain ratio in the front web was 0.87 and in the back web was 0.70.

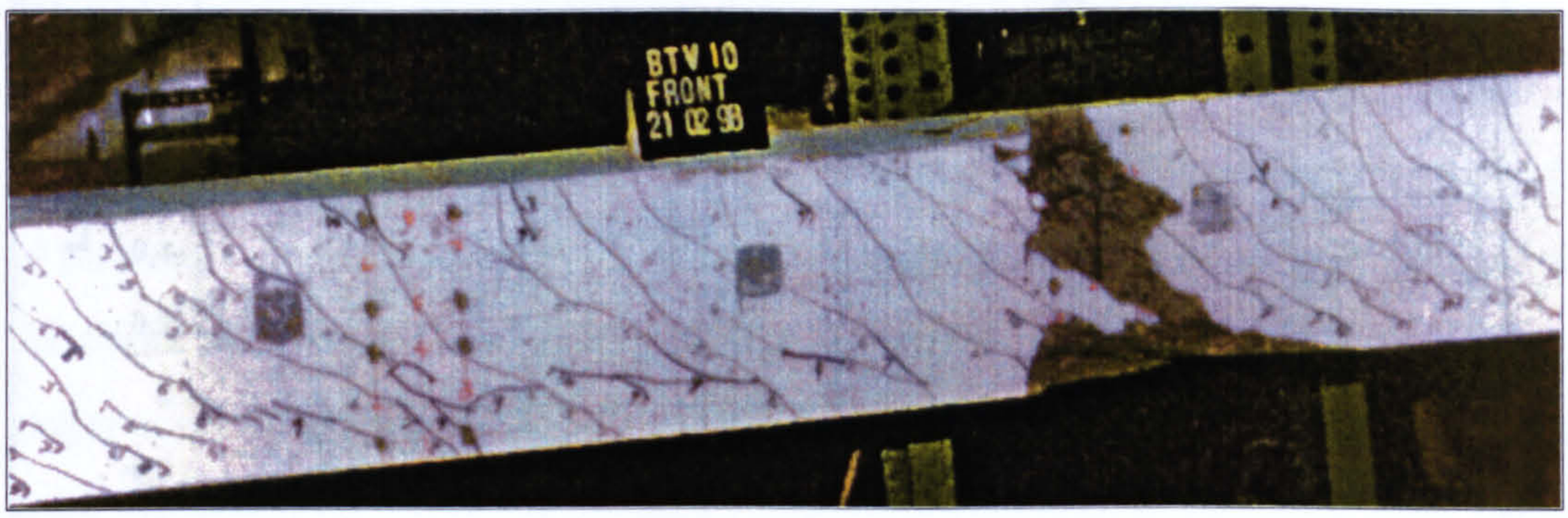

Fig. 5.35: Crack development in the front web (BTV10)

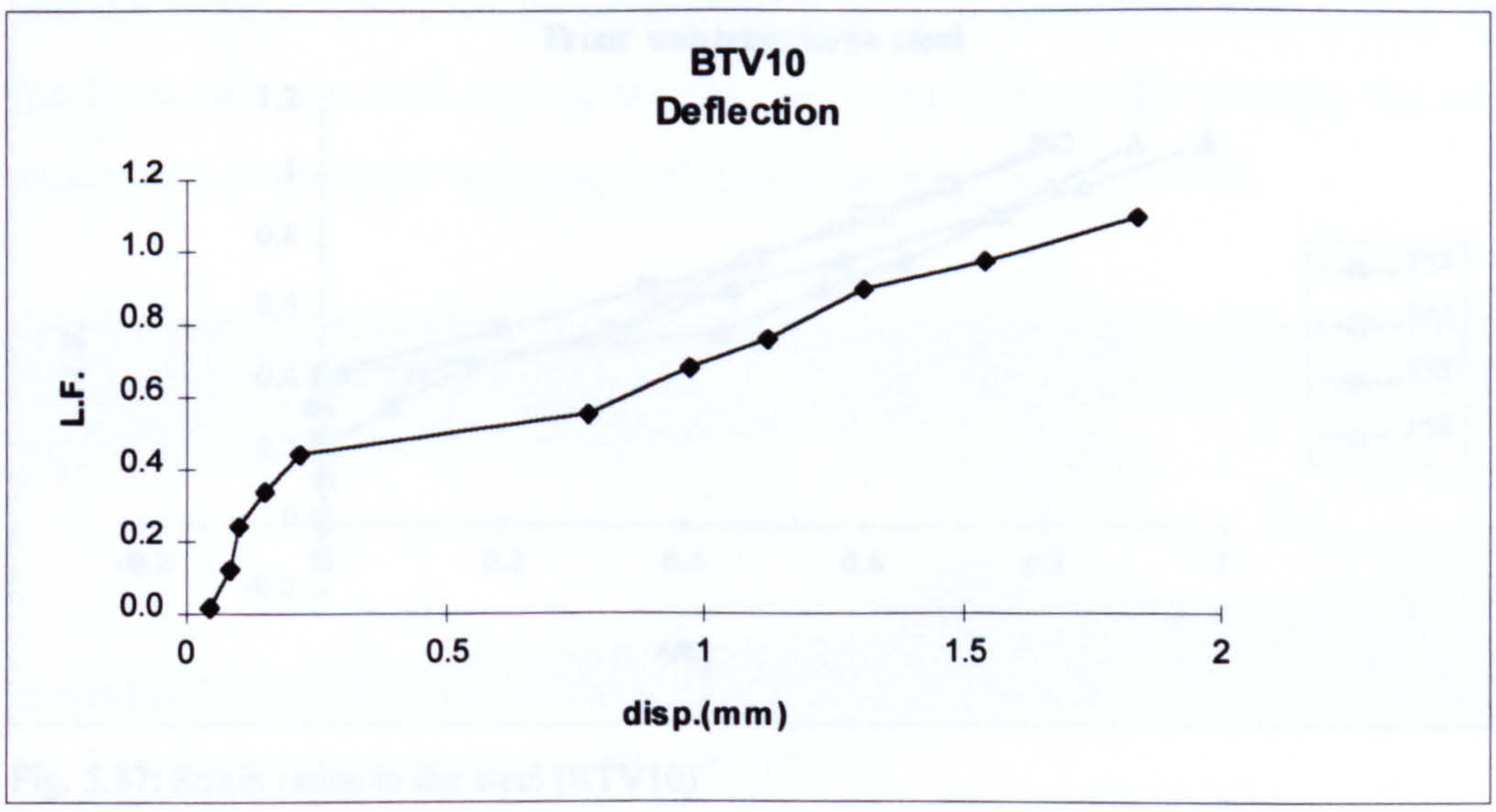

Fig. 5.36: Vertical displacement at mid-span of the bottom flange (BTV10)

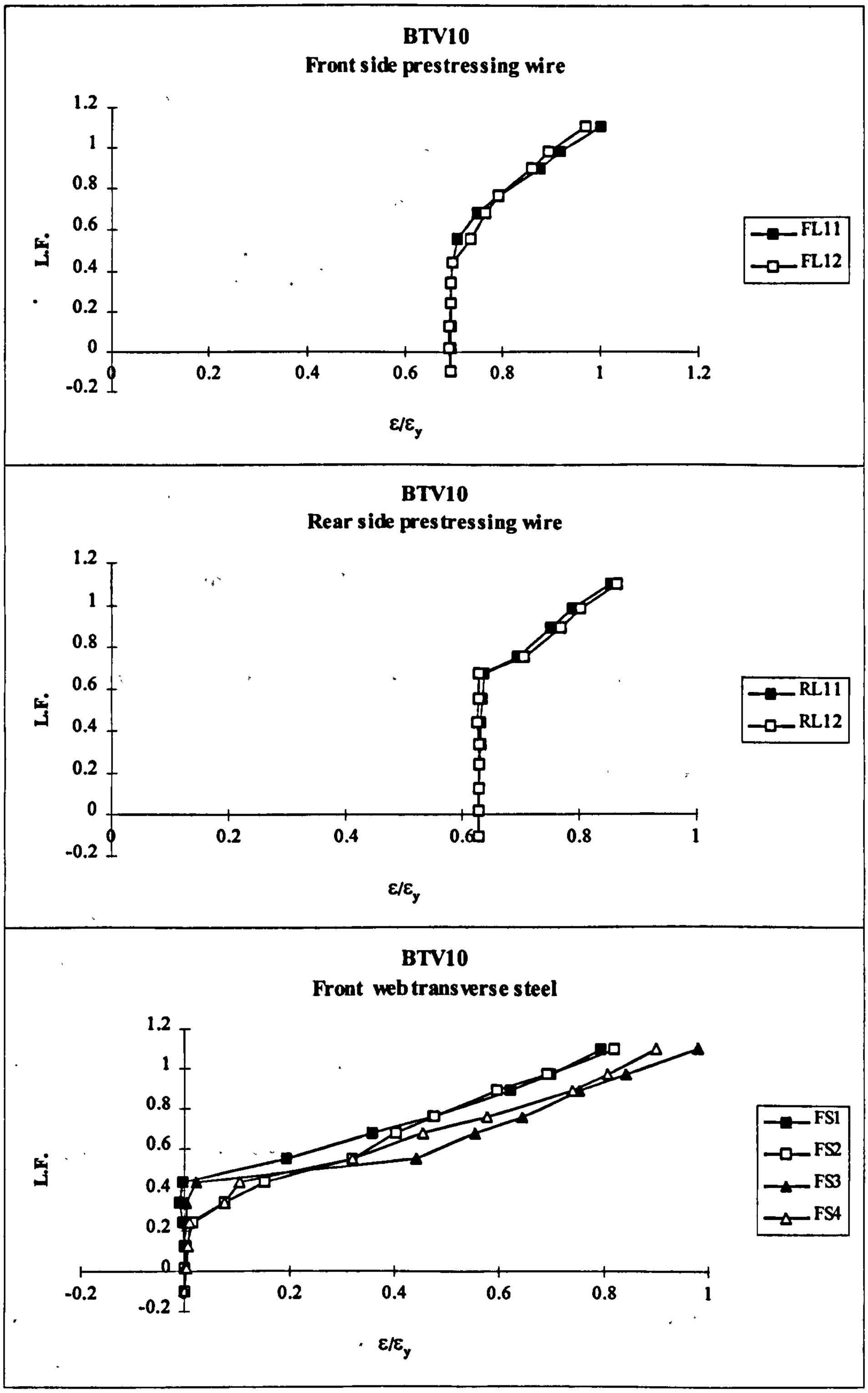

Fig. 5.37: Strain ratios in the steel (BTV10)

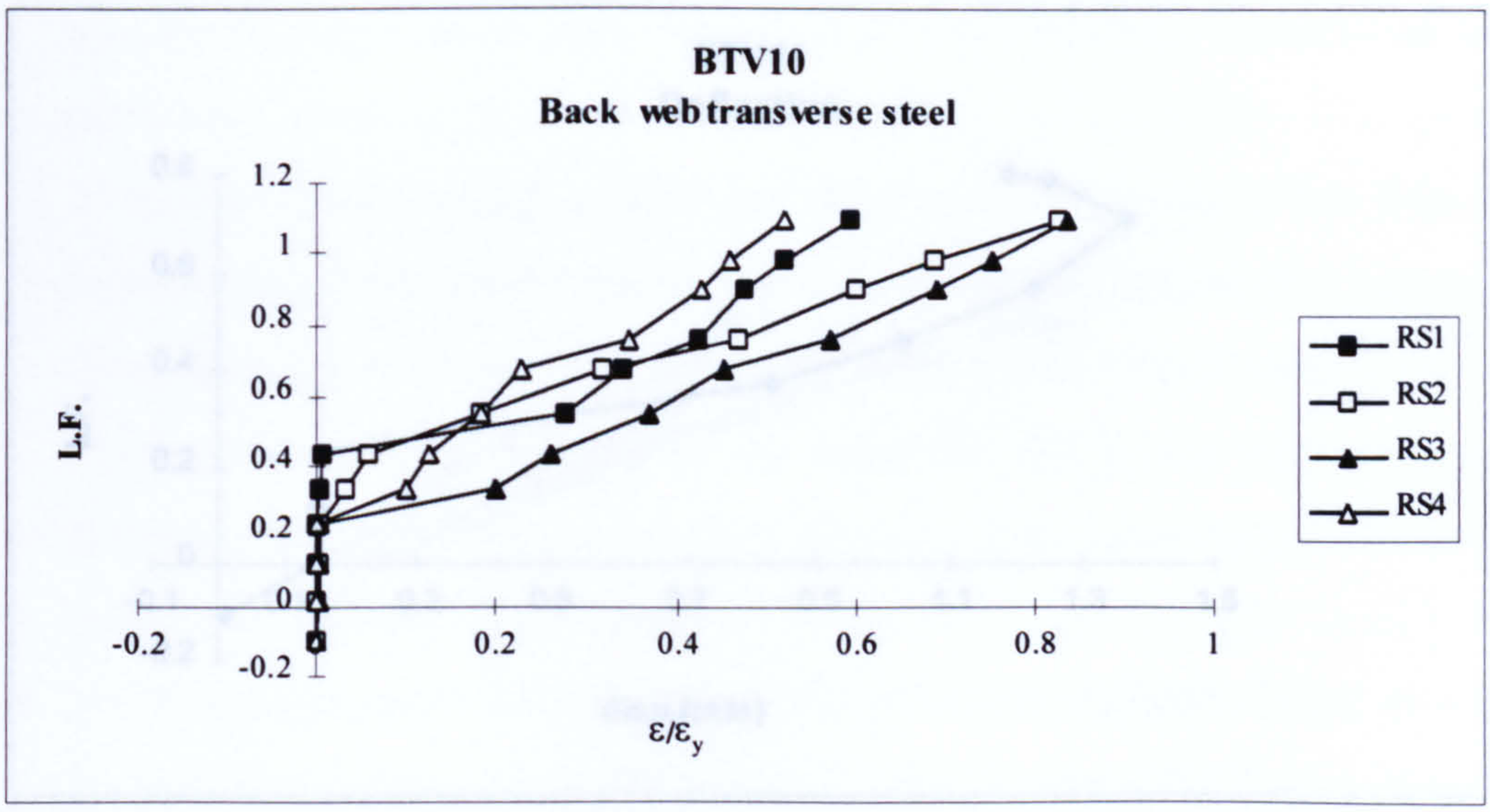

Fig. 5.37: Continued

BTV11: T_d=39kNm, M_d=14.89kNm, V_d=21.08kN, T_d/M_d=2.62, τ_{tor}/τ_{shr}=6.84

At 30% of load, 45° inclined cracks appeared in the webs and bottom flange. At 40% of load, similar cracks were noticed in the top flange. The average crack width at this stage was 0.3mm. At 80% of load, a major crack opened up in the front web. At about 90% of load, a sudden failure happened while applying the load by a major crack quickly spiralling round the beam. The readings for the this increment were not recorded. Figure 5.38 shows crack development in the front web. Figure 5.39 shows the displacement and figure 5.40 shows strain in the prestressing wires and the stirrups. The average strain ratio at 80% of load in the prestressing wire in the front side was 0.71 and in the rear side was 0.70. In the stirrups, the average strain ratio in the front web was 0.65 and in the back web was 0.62.

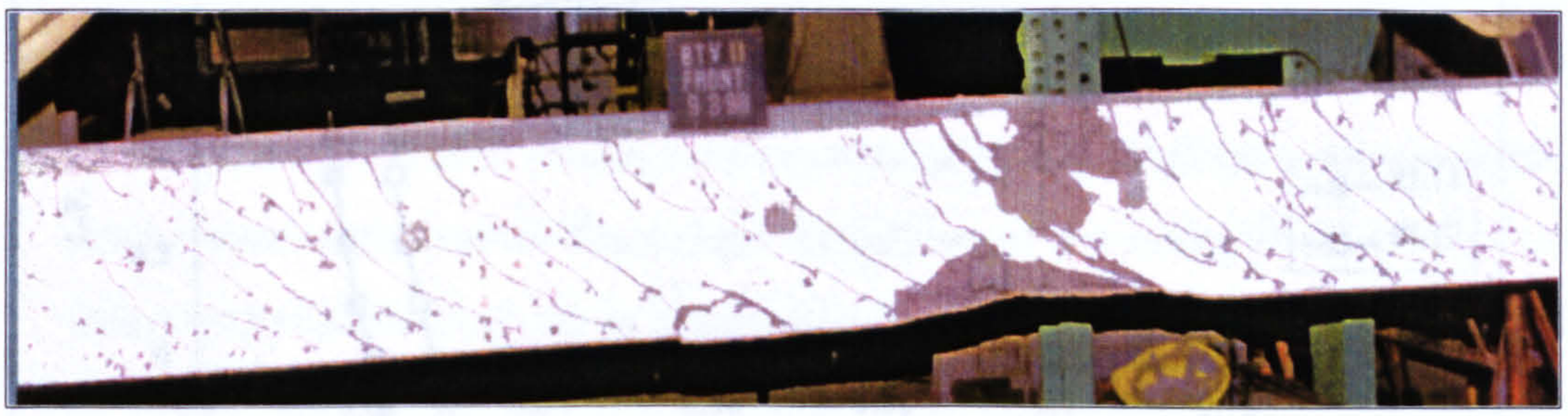

Fig. 5.38: Crack development in the front web (BTV11)

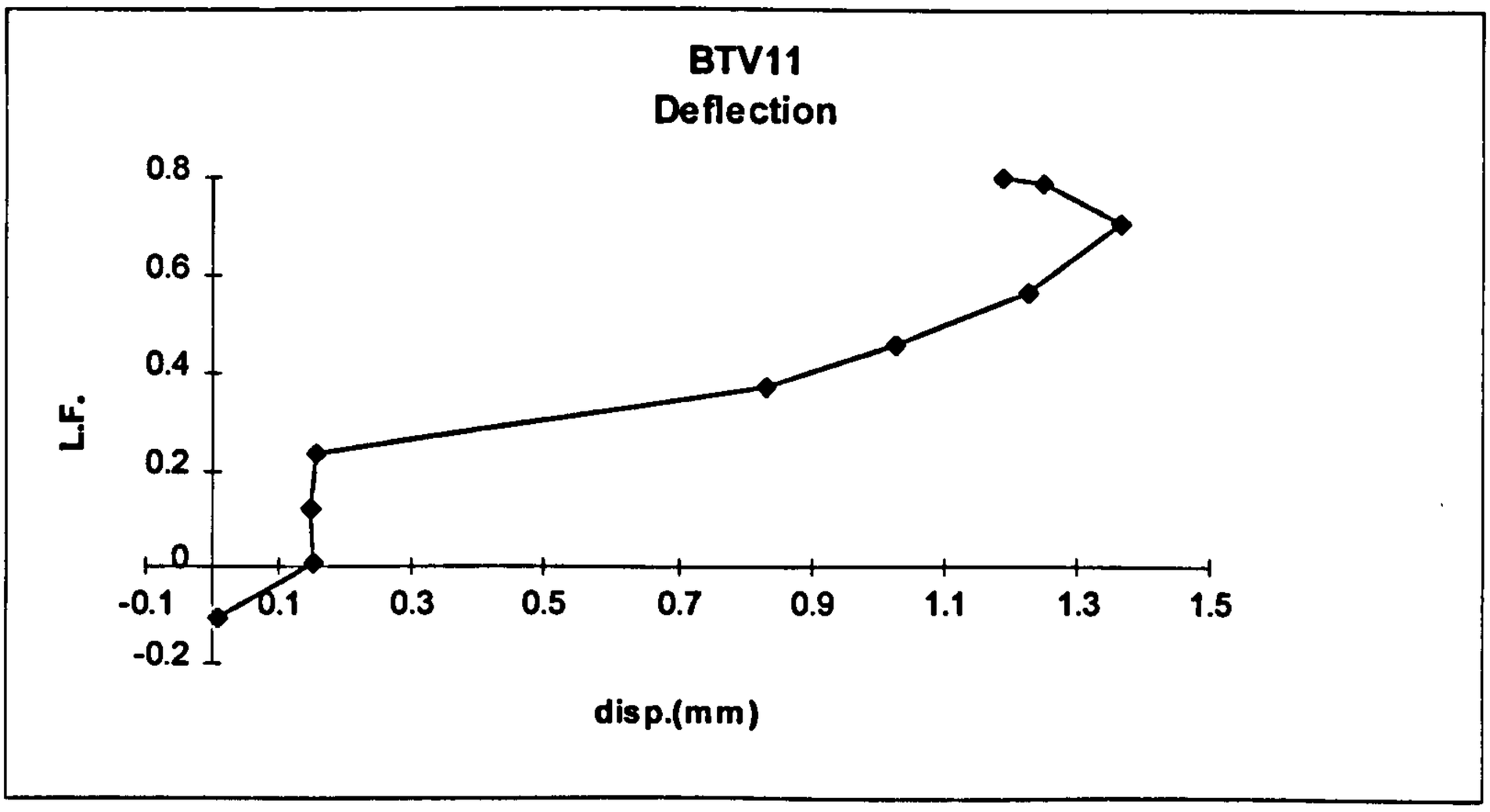

Fig. 5.39: vertical displacement at mid-span of the bottom flange (BTV11)

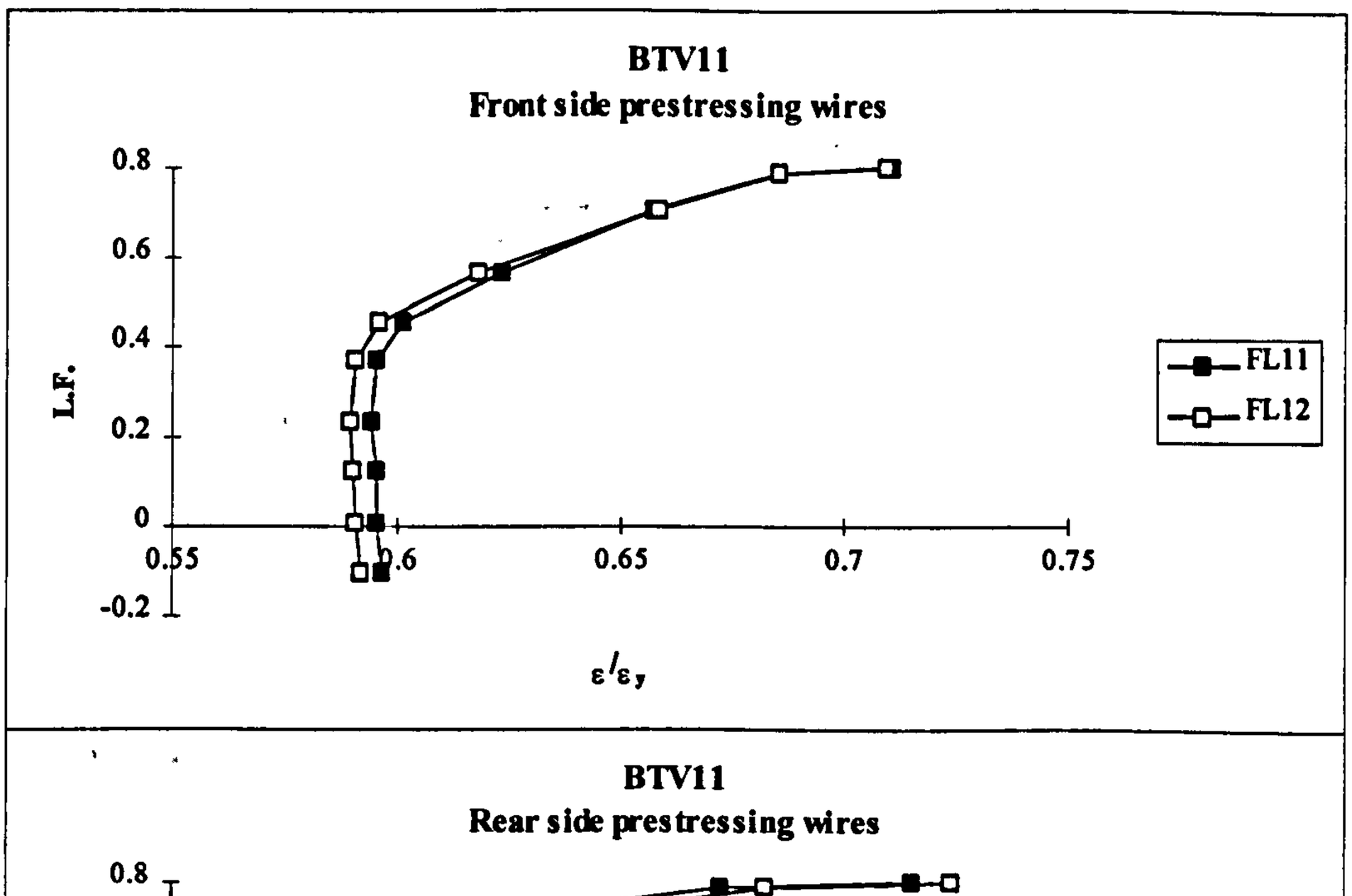

Fig. 5.40: Strain ratios in the steel (BTV11)

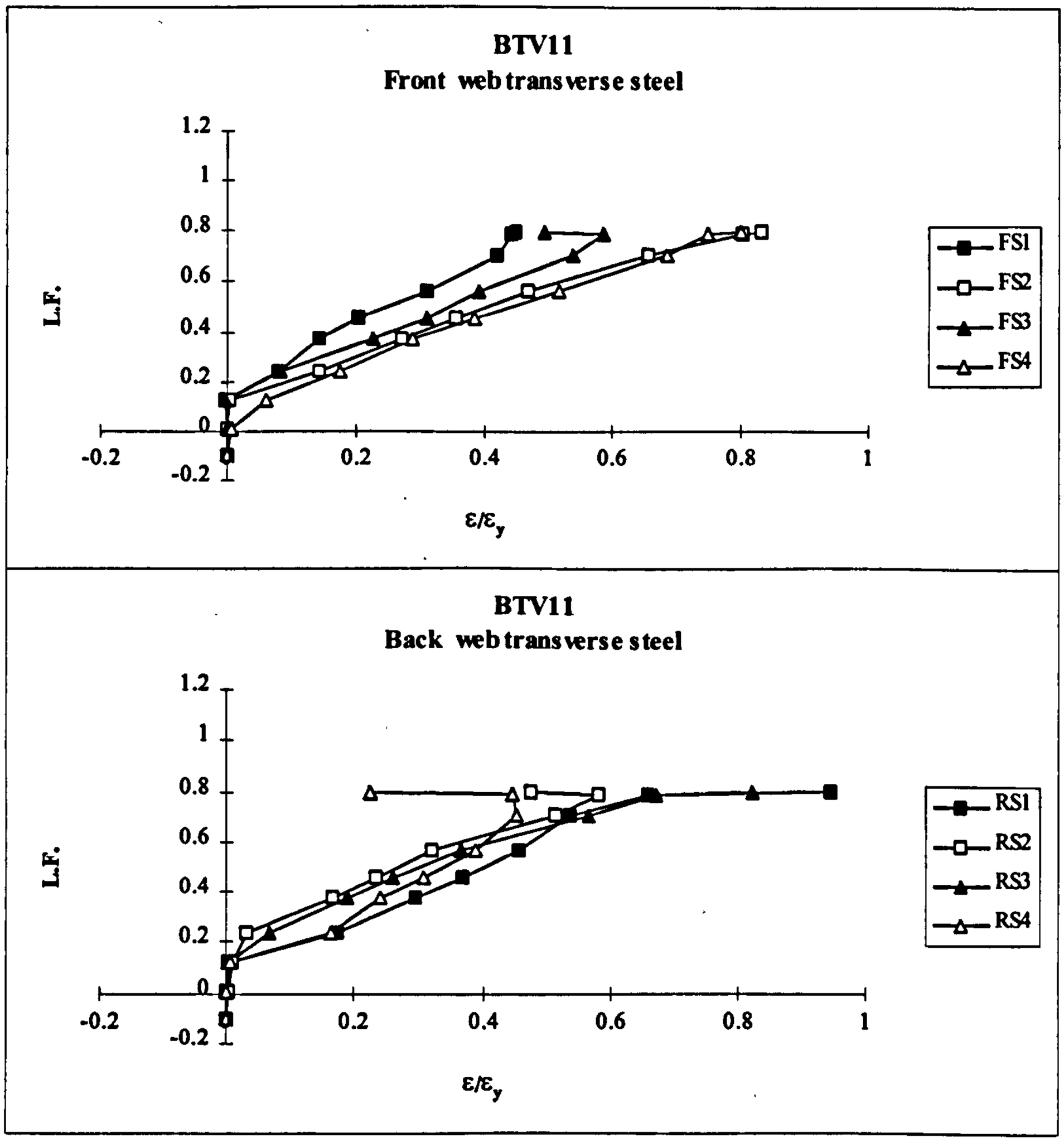

Fig. 5.40: Continued

Summary:

In general, the above behaviour can be summarised as follows:

1. Table 5.7 shows some test results related to steel strain and table 5.8 shows test results related to deflection and failure load.

2. In the case of beams in which bending was dominant ($T_d/M_d<1$) almost vertical cracks start in the bottom flange and the bottom of the webs. These cracks were followed by inclined cracks in succeeding load increments until they first appear in the top flange at about 80% of failure load. In the beams where torsion was dominant ($T_d/M_d>1$), inclined cracks extend into the bottom flange one increment after they are formed in the webs. In both groups, the smaller the ratio T_d/M_d, the closer is the angle of crack to vertical. In all beams, if vertical cracks occur, they

are present only near the mid-span in the bottom flange and at the lower half of the webs.

3. In beams where bending is dominant, the number of cracks is less than in the beams where torsion is dominant. This is due to the fact that torsion was constant throughout the entire length while maximum bending moment was present over a small distance in the middle of the beam. In the beams where bending is dominant cracks start at about 40% of load while when torsion is dominant cracks start at about 30% of load.
4. The maximum crack width in the reinforced beams is slightly larger than in the partially prestressed ones for the same load combination (BTV5 with BTV10 and BTV7 with BTV11). The average crack width when the first crack appeared in the top flange in the reinforced beams was 0.51mm and in the partially prestressed beams was 0.36mm.
5. For the same load combination, reinforced beams undergo larger displacement than the partially prestressed beams (BTV5 with BTV10 and BTV7 with BTV11). The average displacement in the reinforced beams was 6.5mm while in the partially prestressed beams was 4.3mm. With the exception of BTV1, BTV2 and BTV10, all beams which failed above design load reached the displacement limit span/250 at about 90% of failure load, while the other beams did not reach this limit.
6. In all reinforced beams, the longitudinal steel in the front web yielded or reached near yield strain. The strain in the back web longitudinal steel reached about 75% yield at failure load. However, in the beams (BTV1 and BTV6) with large τ_{tor}/τ_{shr} ratios and the beams (BTV5, BTV7 and BTV8) with large T_d/M_d ratios, the strain in the back web longitudinal steel was relatively less than in the other beams. The transverse steel in the front web yielded or reached near yield strain in most beams. In the back web, the stirrups did not yield in all cases. However, in the beams which were torsion dominant, the stirrups reached near yield strain (about 80% yield strain) but in the beams with bending dominant the strain was much less (about 30% yield strain).
7. In the partially prestressed beams, the wires in beams BTV9 and BTV10 yielded or reached near yield at failure load. However, in beam BTV11 which had a large

T_d/M_d ratio, the wires reached less than 75% of yield strain. The yield strain was reached in most cases in the front web stirrups while slightly less strain was recorded in the back web stirrups.

8. Most of the beams failed at about the design load (90-115% of load). However, beams BTV2 (122%) and BTV3 (126%) resisted slightly more load than designed for. Both beams had very small T_d/M_d ratios.
9. It was found during testing that reinforced beams undergo more ductile behaviour than partially prestressed beams. Generally, in both groups, beams with low T_d/M_d ratio experienced more ductile failure mode than the ones with large T_d/M_d ratios. Sudden failure was observed in beam BTV11 only.

Table 5.7: test results related to steel strain

Beam No.	First yield data				Maximum strain measured data			
	FYL	LFL	FYS	LFS	$(\varepsilon/\varepsilon_y)$MFL	MFL	$(\varepsilon/\varepsilon_y)$MFS	MFS
Group A: Reinforced concrete hollow beams								
BTV1	-	-	FS4	0.9	0.84	FL12	1.3	FS4
BTV2	FL12	1.1	FS4	1.1	1.67	FL12	1.1	FS4
BTV3	FL12	1.1	-	-	1.34	FL14	0.93	FS2
BTV4	FL13	1.0	-	-	1.3	FL12	0.8	FS2
BTV5	-	-	FS4	0.95	0.83	FL12	1.25	FS4
BTV6	-	-	-	-	0.83	FL14	0.82	FS3
BTV7	-	-	-	-	0.88	FL13	0.9	FS3
BTV8	-	-	-	-	0.91	FL11	0.89	FS3
Group B: Partially prestressed concrete hollow beams								
BTV9	FL11	1.0	FS4	0.82	2.2	FL11	1.23	FS2
BTV10	FL11	1.1	-	-	1	FL11	0.98	FS3
BTV11	NR	NR	NR	NR	NR	NR	NR	NR

FYL, FYS = Location of the first yield in the longitudinal steel or stirrup respectively

LFL, LFS = Load factor at which first yield was recorded in longitudinal steel or stirrup respectively

$(\varepsilon/\varepsilon_y)$MFL, $(\varepsilon/\varepsilon_y)$MFS = Maximum strain ratios in front web longitudinal steel and stirrups respectively

MFL, MFS = Location of maximum strain in front web longitudinal steel and stirrups respectively

NR = Not recorded

Table 5.8: Test results related to deflection and failure load

Beam No.	LFCR Ratio	LFCW Ratio	Δ mm	L_e/L_d Ratio
Group A: Reinforced concrete hollow beams				
BTV1	0.3	0.7	1.7	1.04
BTV2	0.5	0.7	6.0	1.22
BTV3	0.4	0.6	8.3	1.26
BTV4	0.4	0.7	8.2	1.06
BTV5	0.3	0.4	8.0	1.02
BTV6	0.5	0.6	3.1	0.92
BTV7	0.3	0.5	11.0	1.01
BTV8	0.3	0.5	2.6	0.91
Group B: Partially prestressed concrete hollow beams				
BTV9	0.4	0.7	9.9	1.16
BTV10	0.4	0.4	1.8	1.10
BTV11	0.3	0.4	1.2	0.90
Mean	0.37	0.56	5.62	1.05

LFCR = Load factor when first crack was noticed

LFCW = Load factor when the average crack width was 0.3mm

Δ = Maximum vertical displacement at mid-span of bottom flange

L_e/L_d = Experimental to design failure load

5.7: Conclusion

From the results presented in this chapter, it can be said that the direct design method has proved to be a very good tool for the design of reinforced and partially prestressed hollow beams. Most of the beams failed near the design load. Minor effects were noticed due to variations of τ_{tor}/τ_{shr} and T_d/M_d ratios. The elastic stress distribution used in the calculation of reinforcement and largest required reinforcement provided in the test span have given an acceptable results for hollow beams.

6: Material behaviour and modelling

6.1: Introduction

This chapter gives a summary of behaviour of reinforced concrete and how to model it. This will pave the way for finite element programming and 2-D model development in the following two chapters.

Concrete is a heterogeneous material composed of aggregate, sand and cement which has microcracks even before the application of any load. When reinforcement is added, the composite becomes even more complex. However, at macroscopic level, reinforced concrete can be considered as having two major components: steel reinforcements and concrete. In the modelling of its non-linear stress-strain behaviour, a general approach is to treat the response of each component separately, then obtain their combined effects by imposing the condition of material continuity. There are several approaches used to model the linear and non-linear responses of concrete as a continuum. These approaches have been evaluated by Chen and Ting (1980) and Chen and Saleeb (1994). In this study the non-linear elasticity approach is adopted. In this approach the bulk modulus, shear modulus, Poisson's ratio and Young's modulus of concrete are expressed in terms of stress/strain variables, such as deviatoric stresses or strains, stress or strain invariants, normal and octahedral strain ... etc. These relationships are obtained from experimental data. The moduli are usually used to formulate an isotropic matrix to represent the behaviour of concrete at a certain load level.

6.2: Concrete in compression

6.2.1: Uniaxial stress

The uniaxial cube compressive strength of concrete f_{cu} is usually determined by testing 150mm cubes after 28 days of casting. The size effect of cubes can be seen in Tokyay and Ozdemir (1997). The uniaxial cylinder compressive strength of concrete $f_c^{'}$ is evaluated by the strength of 152 x 305mm cylinder specimens. Other sizes were also tried [Nasser and Kenyon (1984) and Iravani (1996)]. The cylinder compressive strength $f_c^{'}$ is usually 70-90% of the cube strength f_{cu}. The difference is due to the frictional forces which develop between the platen of the testing machine and the contact face of the test specimen. These end forces produce a multiaxial stress state which increase the apparent cube compressive strength of

concrete. This is not the case with the cylinder specimen because the specific height width ratio minimises this effect.

The shape of the uniaxial stress-strain diagram is affected by many factors related to testing procedure or concrete property i.e. size and shape of the specimen, casting direction, water-cement ratio, cement characteristics and content, concrete unit weight, aggregate characteristics and content, type of curing and age when tested. In a typical stress-strain curve (Fig. 6.1a) for concrete under uniaxial compression, the axial stress-strain law is essentially linear up to approximately 30% of the concrete compressive strength $f_c^{'}$. Beyond this stress range, a gradual increase in curvature of the stress-strain curve up to 70-90% of $f_c^{'}$, after which it bends more sharply when approaching the peak strength $f_c^{'}$. At this stage, the strain ε_{cc} is about 0.002, the concrete is crushed and the stress-strain curve starts its descending branch until failure occurs at some ultimate strain ε_{max} about 0.0035. The lateral strain goes into a similar fashion (Fig. 6.1a).

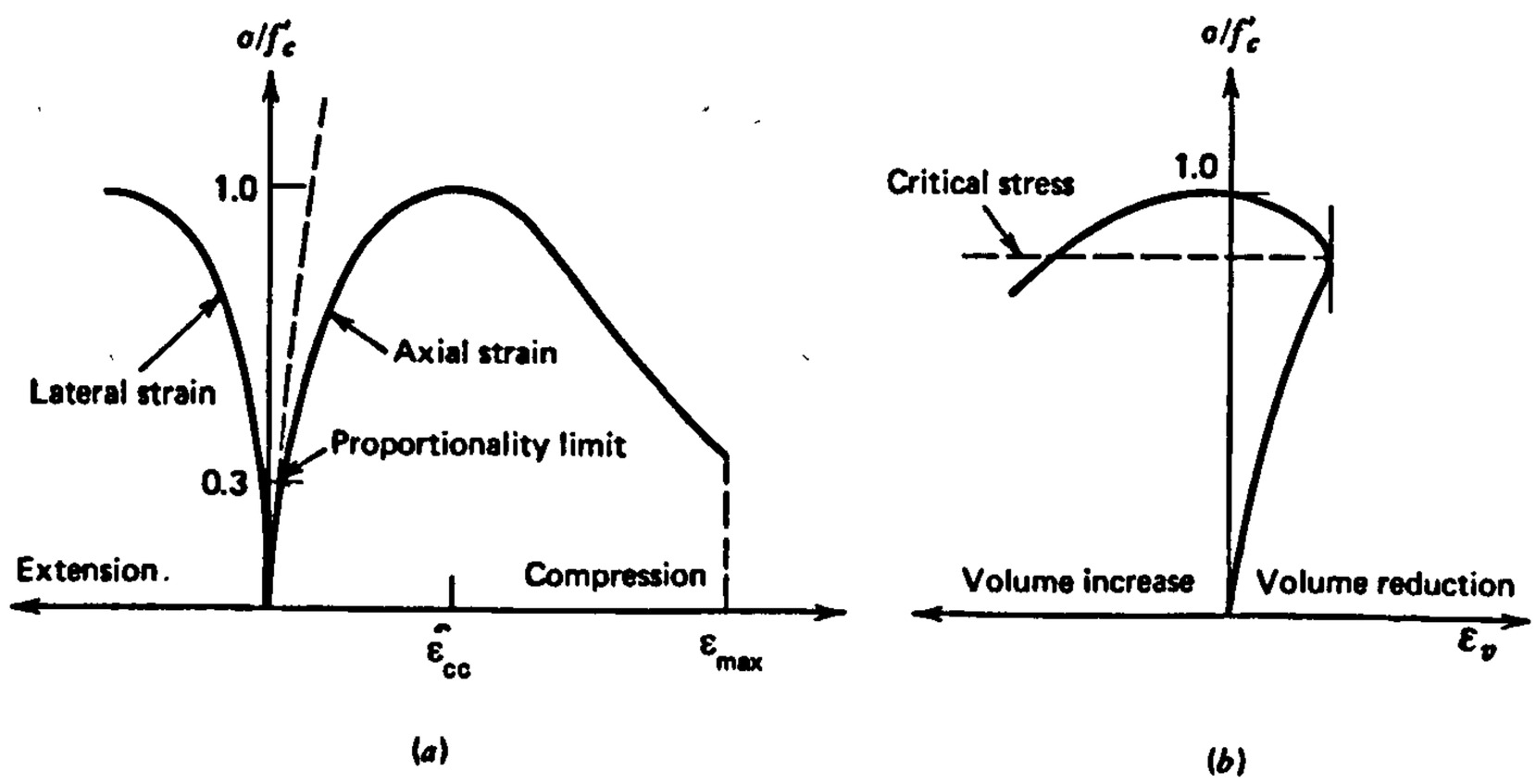

Fig. 6.1: Typical stress-strain curves for concrete in uniaxial compression test

The volumetric strain ε_v (Fig. 6.1b) is found to be almost linear up to 75-90% of maximum compressive strength $f_c^{'}$, after which the direction of the volumetric strain is reversed, resulting in a volume expansion near $f_c^{'}$. The formation and propagation of microcracks due to shrinkage and under uniaxial stress is described in many references. A few examples are shown in figure 6.2.

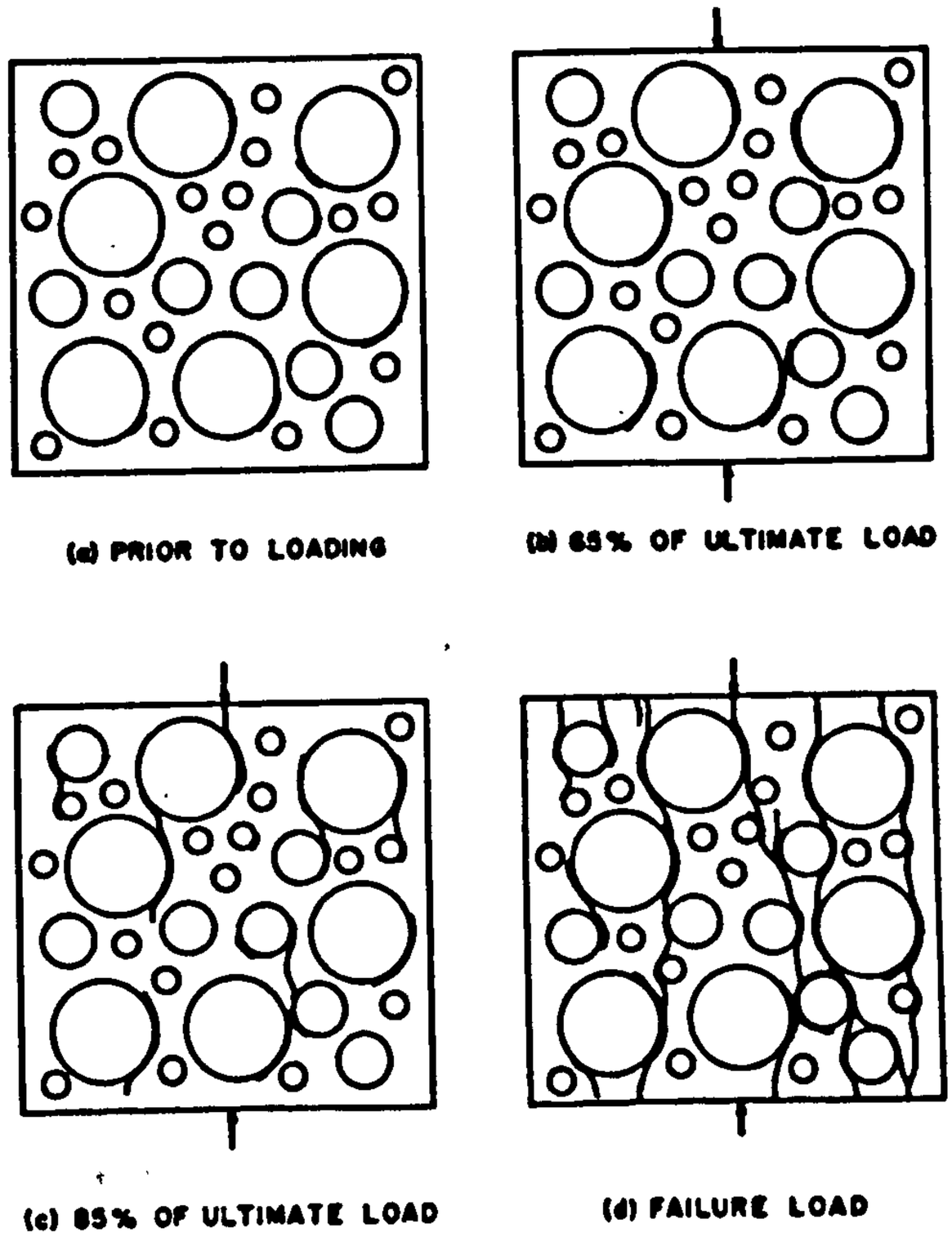

(a): Crack pattern obtained from x-ray examination [Liu et al. (1972)]

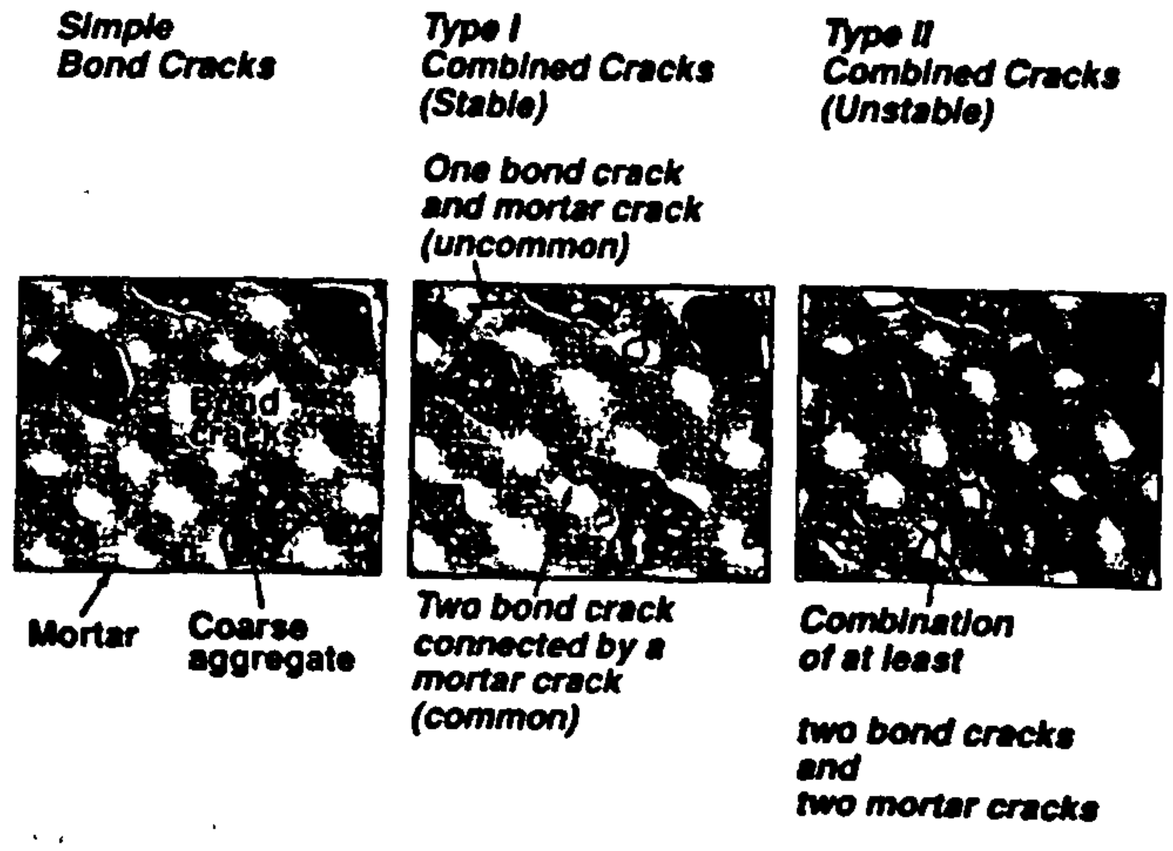

(b): Types of cracks [Hearn (1999)]

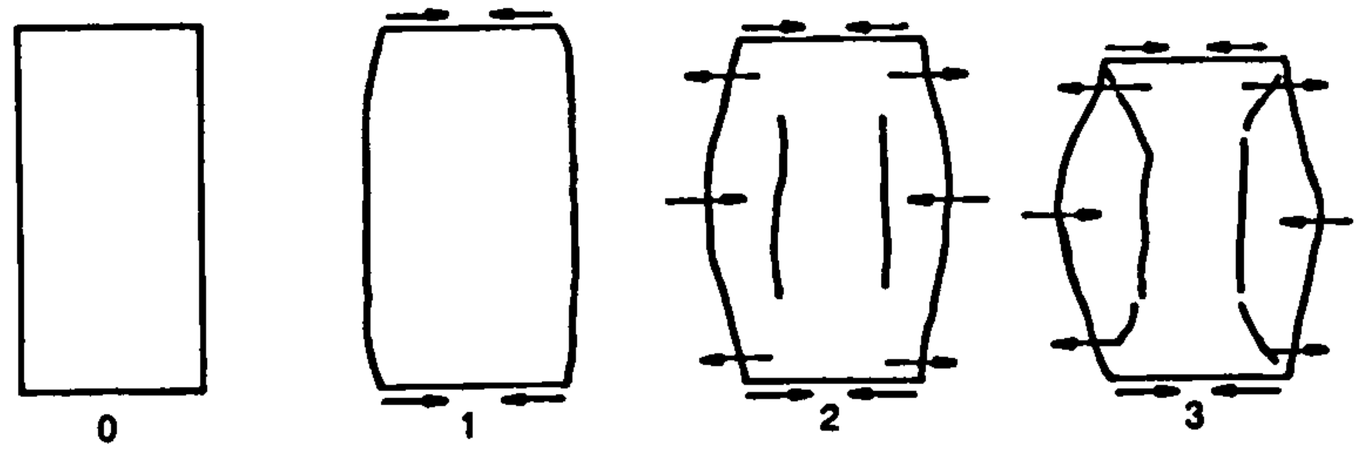

(c): Behaviour of concrete under increasing uniaxial compression [Kotsovos & Pavlovic (1995)]

Fig. 6.2: Formation of cracks due to shrinkage and under uniaxial stress

Figure 6.3 shows axial stress-strain curves for concrete of different compressive strengths. The shape of the ascending part of the stress-strain curve is more linear and steeper for high-strength concrete, and the strain at maximum stress is slightly higher for high-strength concrete, but all close to a strain value ε_{cc} of 0.002. The slope of the descending part becomes steeper for high strength concrete. An explanation to this behaviour can be expressed as follows [Neville (1997) and Darwin (1997)]:

Although the stress-strain curve of the cement paste (mortar) alone and the aggregate alone are almost linear in the major part of the ascending portion, the stress-strain curve of the concrete is non-linear (Fig. 6.4). One main reason for this non-linear stress-strain relation of the concrete is the presence of interfaces in the bond between the aggregate and the hardened cement paste in which microcracks develop even under modest loading condition. Upon loading these microcracks propagate and new ones form which leads to bond failure. If the modulus of elasticity of the concrete is considered to be made up of the modulus of elasticity of the paste and the modulus of elasticity of the aggregate in their joint condition, then the greater the difference between the moduli, the greater the non-linear behaviour of the composite. In the high strength concrete, the strength of the hardened cement paste is, by definition high because a very low water-cement ratio is used and the porosity of the hardened cement paste is low. There is therefore a smaller difference between the modulus of elasticity of the cement paste and the modulus of elasticity of the aggregate. This situation leads to a better stress transfer between the aggregate and the paste which means a less chance of bond failure to occur. The result is a longer linear region of the stress-strain curve. The fracture surfaces pass through the aggregate particles as well as through the hardened cement paste. This allows a fast development of the cracks after the yield stress is nearly reached which explains the brittle behaviour of the high strength concrete. In normal concrete the modulus of elasticity of the aggregate is much higher than the modulus of elasticity of the cement paste. This big difference causes a more non-linear behaviour of the concrete. This is so because the aggregate particles act as crack arresters due to strength difference.

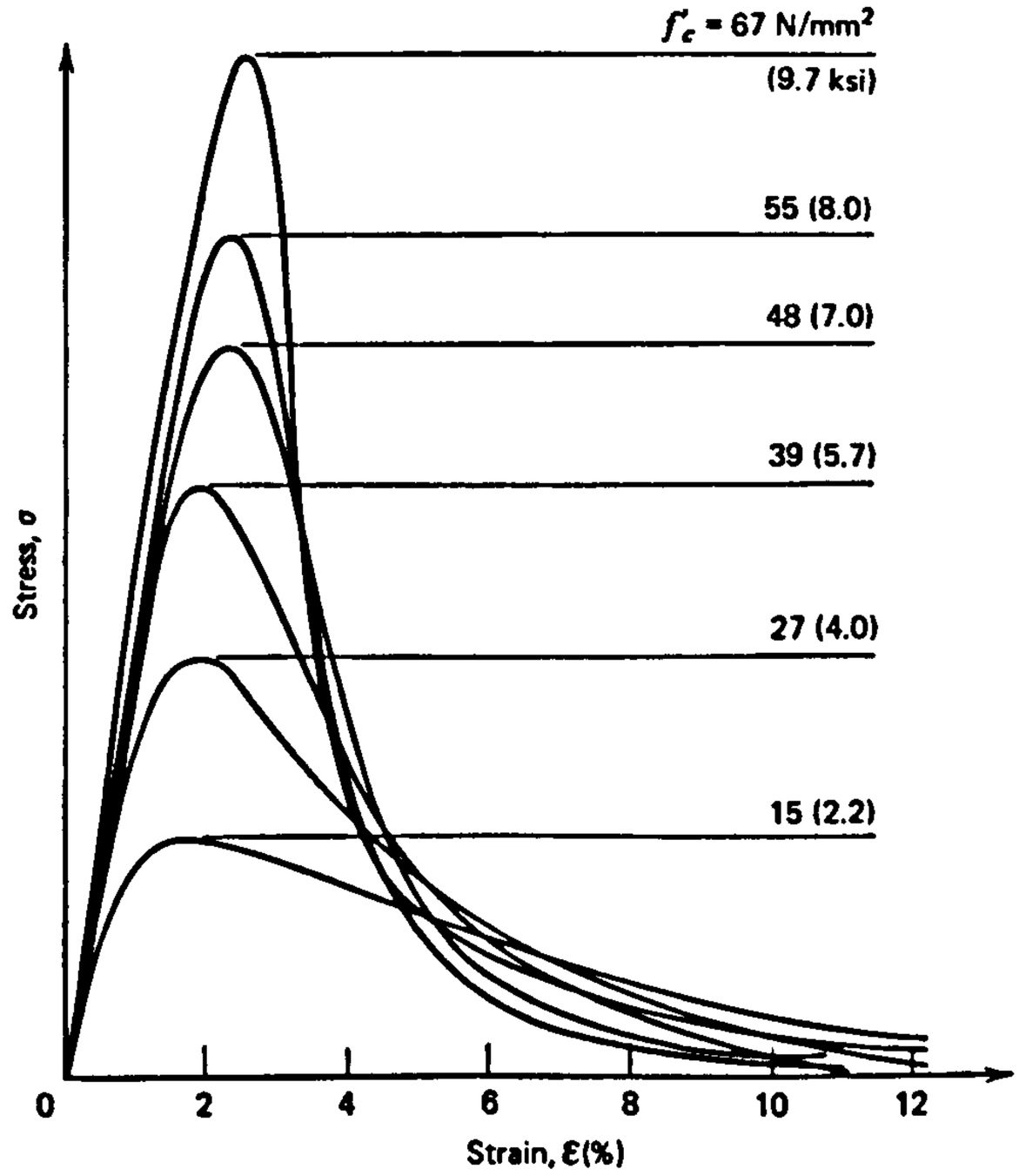

Fig. 6.3: Uniaxial stress-strain curves for concrete with different strengths

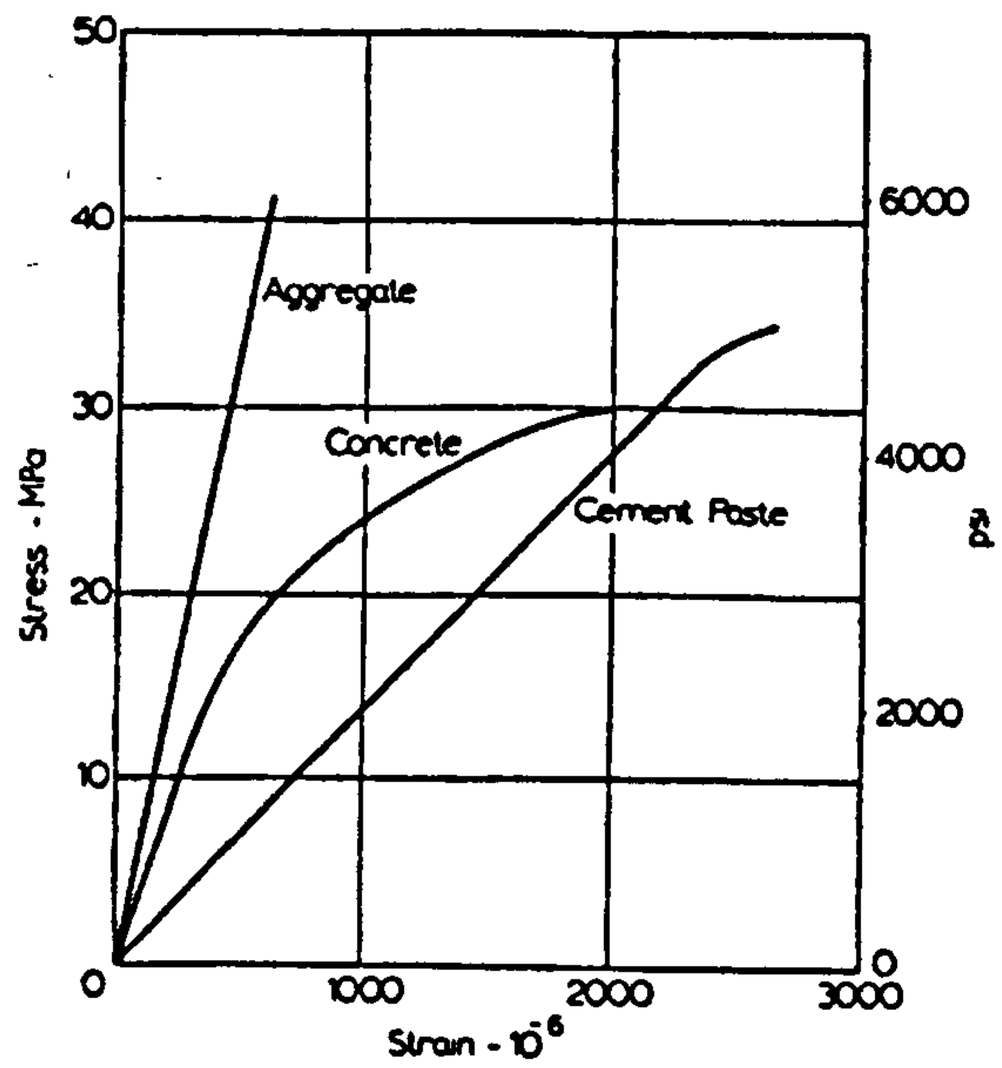

Fig. 6.4: Stress-strain relation for cement paste, aggregate, and concrete

Many numerical formulae have been proposed to describe the shape of the compressive stress-strain curve of the concrete under uniaxial stress. As examples Kotsovos and Cheong (1984) suggested the use of the ascending portion alone (until the point where the volume is minimum) of the stress-strain curve to describe the

behaviour of concrete assuming that the post peak relationship is only test method effect as shown in figure 6.5a. Figure 6.5b shows the stress-strain relationships for the loading and boundary conditions shown in figure 6.5a. Carreira and Chu (1985) proposed an equation to describe the ascending and descending portions of the curve. This equation was defined in terms of the concrete cylinder compressive` strength $f_c^{'}$, the strain ε_{cc} corresponding to $f_c^{'}$ and the initial modulus of elasticity E_c. They tested their equation against several experimental results of which one is shown in figure 6.5c. Almusallam and Alsayed (1995) proposed a stress-strain curve which includes ascending and descending parts. The only unknown in the equation forming this curve is the concrete compressive strength $f_c^{'}$ (Fig. 6.5d). Their model was checked against various experimental results and provided good agreement with measured values.

In this study equation 6.1 was used to represent the ascending portion of the uniaxial compressive stress-strain curve (Fig. 6.6). In this equation the initial slope and values of peak stress and corresponding strain may be entered as independent variables. This equation was originally proposed by Saenz (1964) and tested by Darwin and Pecknold (1977) on many experimental results. It was also used by Bhatt and Abdel-kader (1995) to numerically analyse many reinforced and prestressed concrete beams from different experimental investigations.

$$\sigma = \frac{E_c.\varepsilon}{1+\left(\frac{E_c}{E_s}-2\right)\frac{\varepsilon}{\varepsilon_p}+\left(\frac{\varepsilon}{\varepsilon_p}\right)^2} \qquad 6.1$$

where:

ε_p is the strain at the peak (maximum) compressive stress of the concrete σ_p.

E_c is the initial modulus of elasticity of concrete for uniaxial loading.

E_s is the secant modulus of elasticity at the peak stress and given by the expression $E_s = \sigma_p / \varepsilon_p$.

σ and ε are the current stress and strain in uniaxial loading.

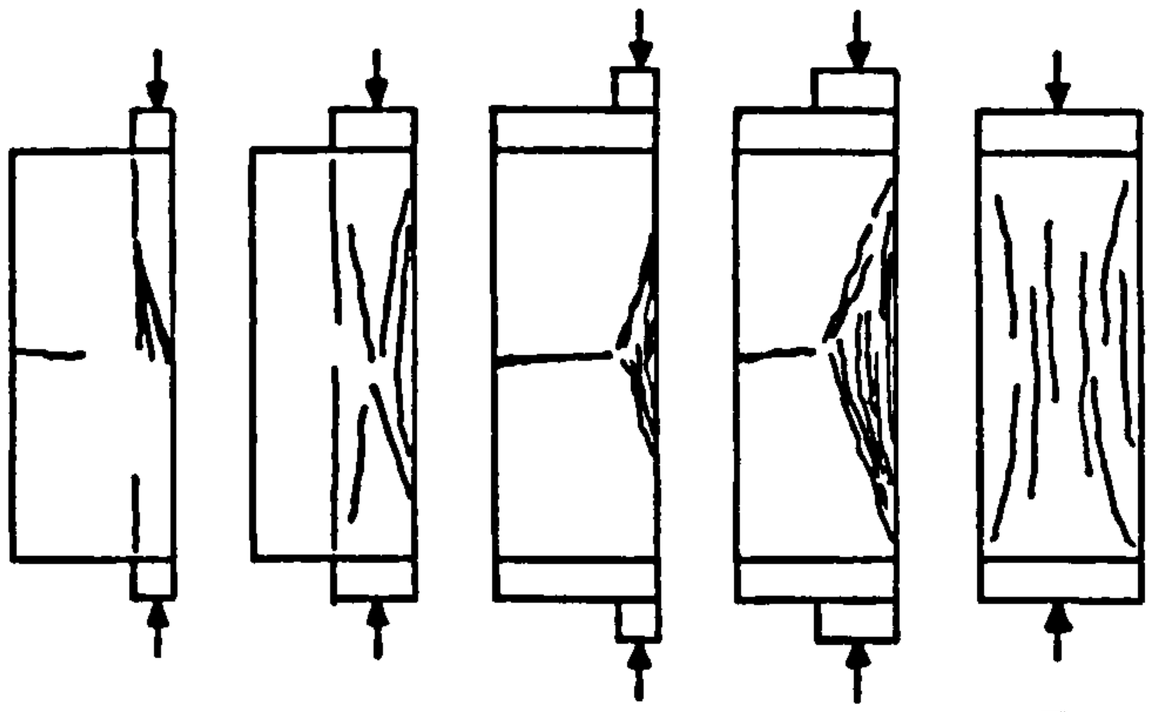

(a): Typical failure modes of prisms under eccentric loading [Kotsovos and Cheong (1984)]

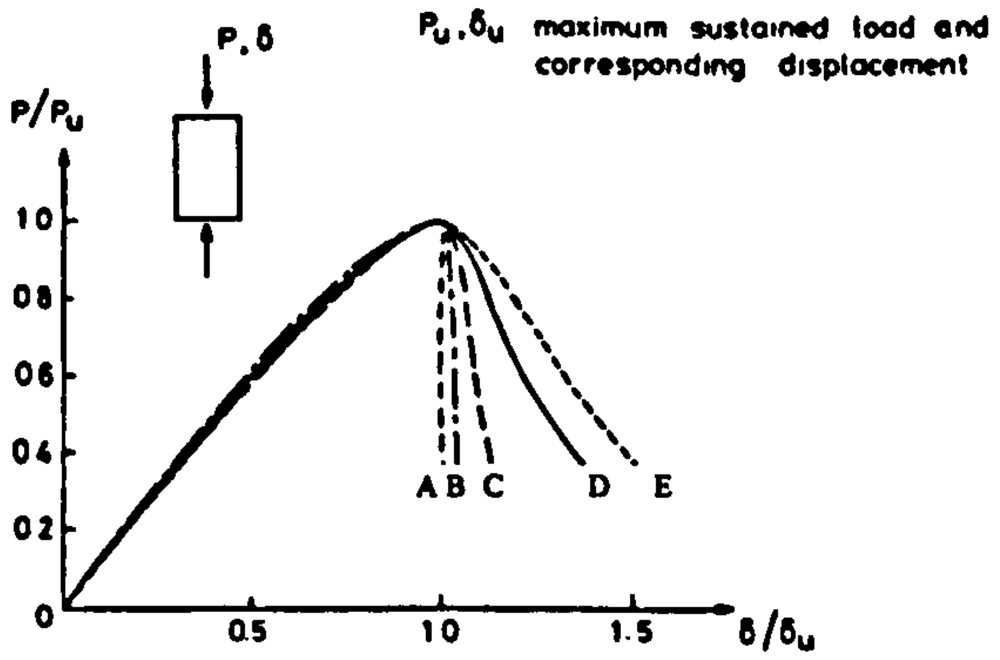

(b): Stress-strain relationships of prisms in (a)

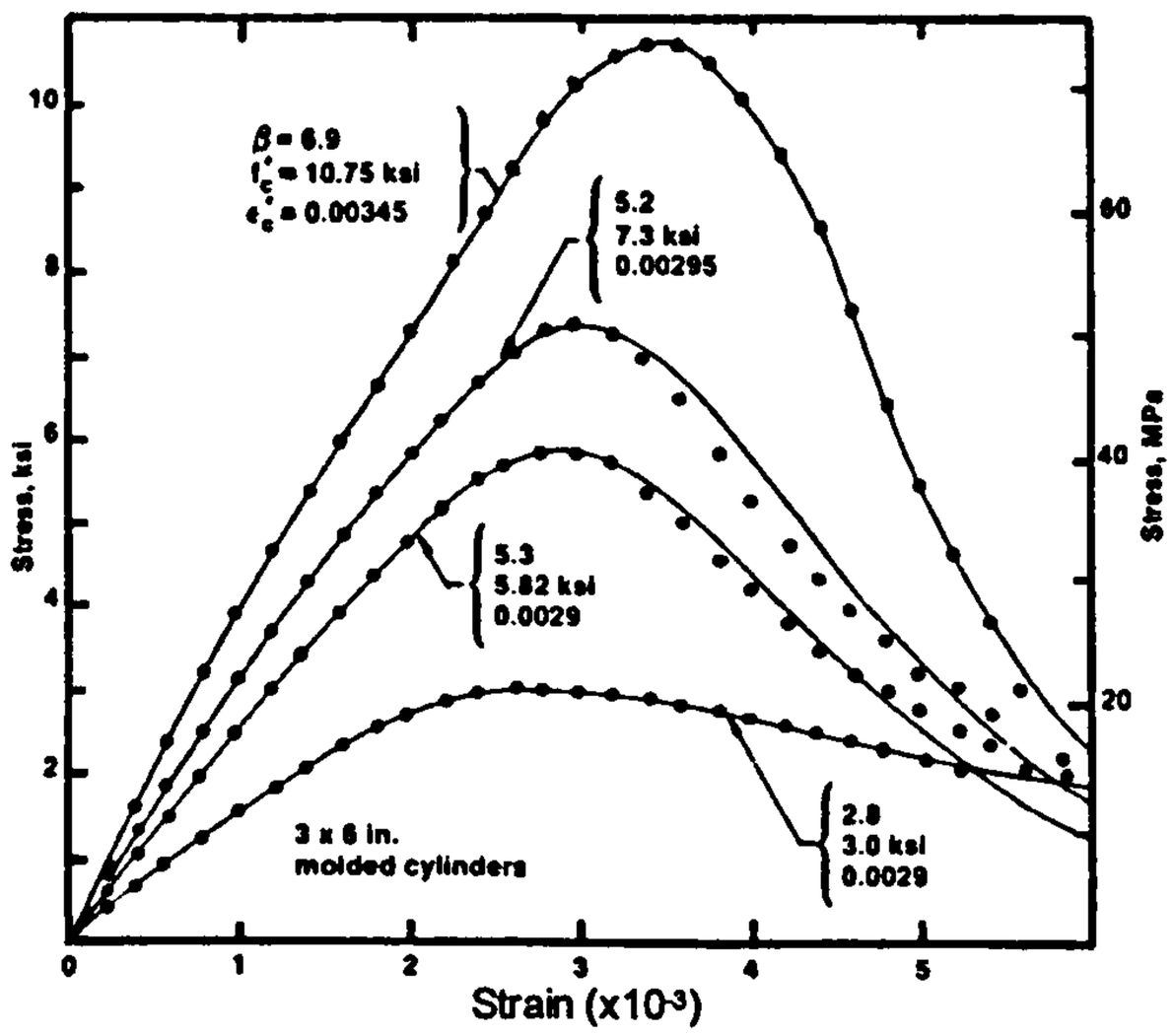

(C): Stress-strain relationship for normal concrete [Carreira and Chu (1985)]

Fig. 6.5: Stress-strain curves as suggested by different researchers for concrete in compression

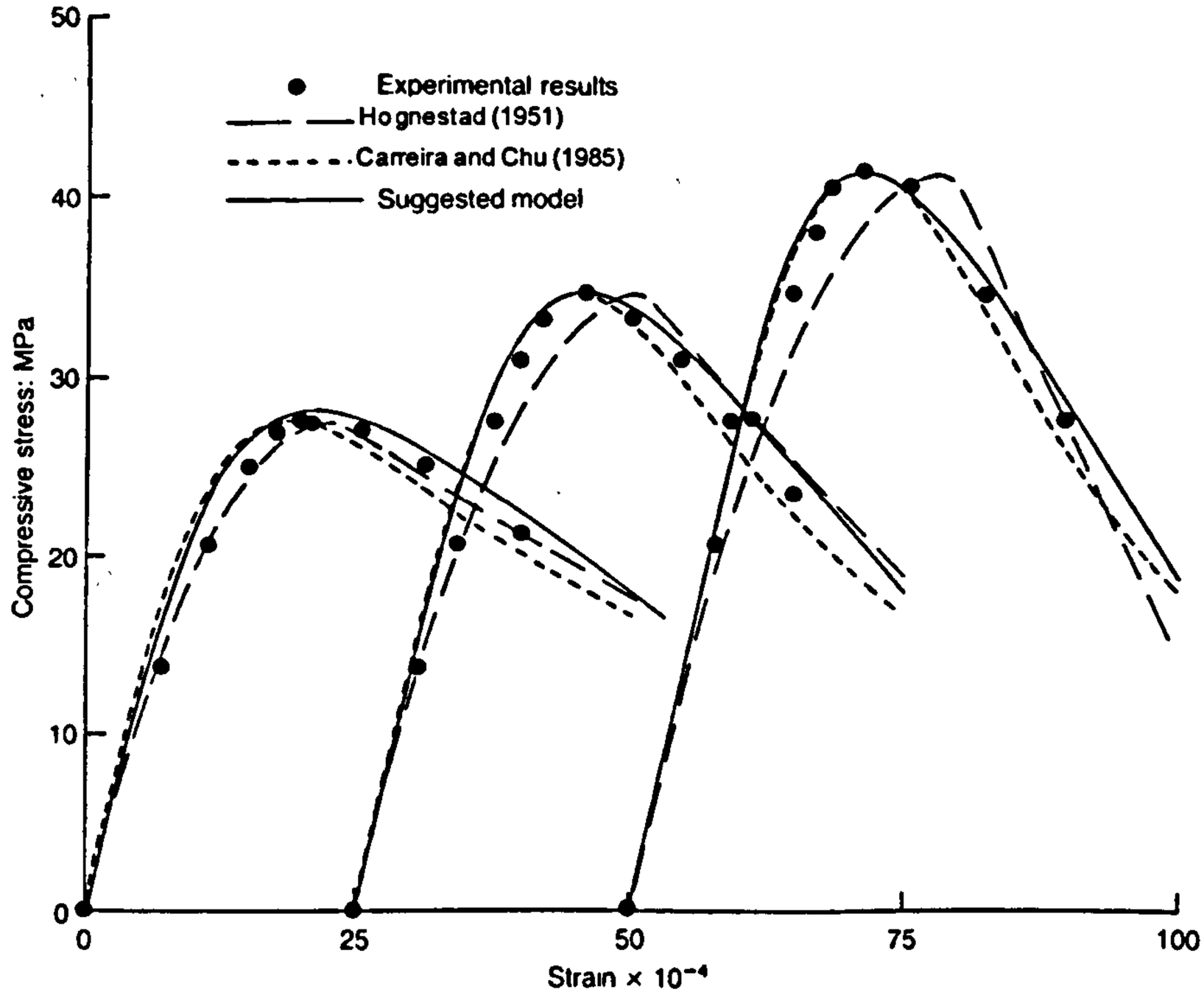

(d): Stress-strain relationship for normal concrete [Almusallam and Alsayed (1995)]

Fig. 6.5: Continued

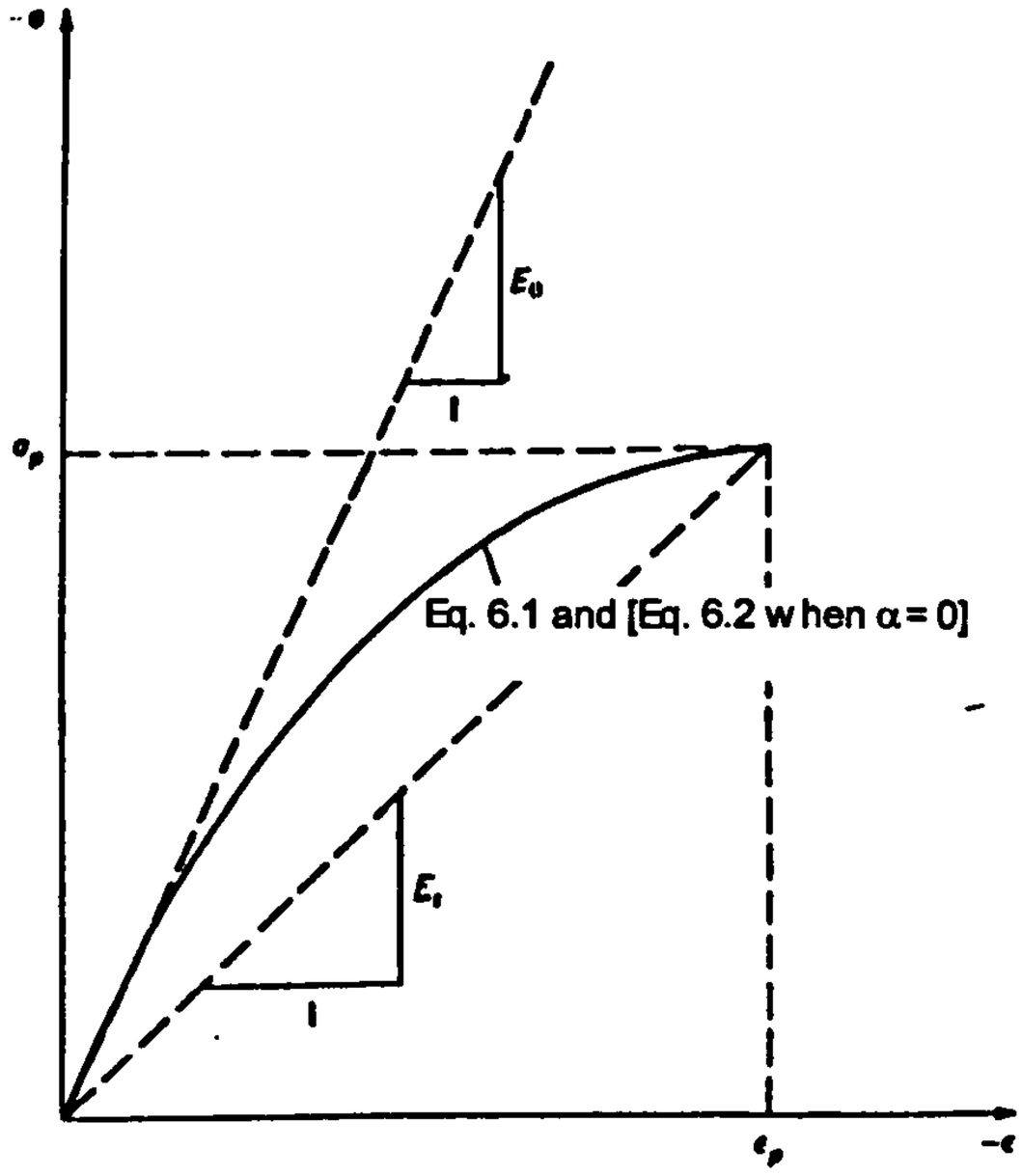

Fig. 6.6: Equivalent uniaxial stress-strain curve

Figure 6.7 shows a comparison between the stress-strain curves proposed by Saenz, Almusallam and Alsayed, and Bhatt and Abdel-Kader. It is clear that almost no difference between the curves in the ascending part. In the ascending part, the curves of Saenz and Bhatt and Abdel-Kader are identical while in the descending portion of Bhatt and Abdel-Kader curve, equation 6.3 was used. The parameters used in Almusallam and Alsayed curve are explained in the quoted reference. The parameters used in Saenz, and Bhatt and Abdel-kader curves are as follows:

$$E_c = 5000\sqrt{f_c'} \text{ N/mm}^2$$

$$\varepsilon_p = \frac{\sqrt{f_c'}}{2500}$$

More about the effect of these parameters is discussed in chapter 8.

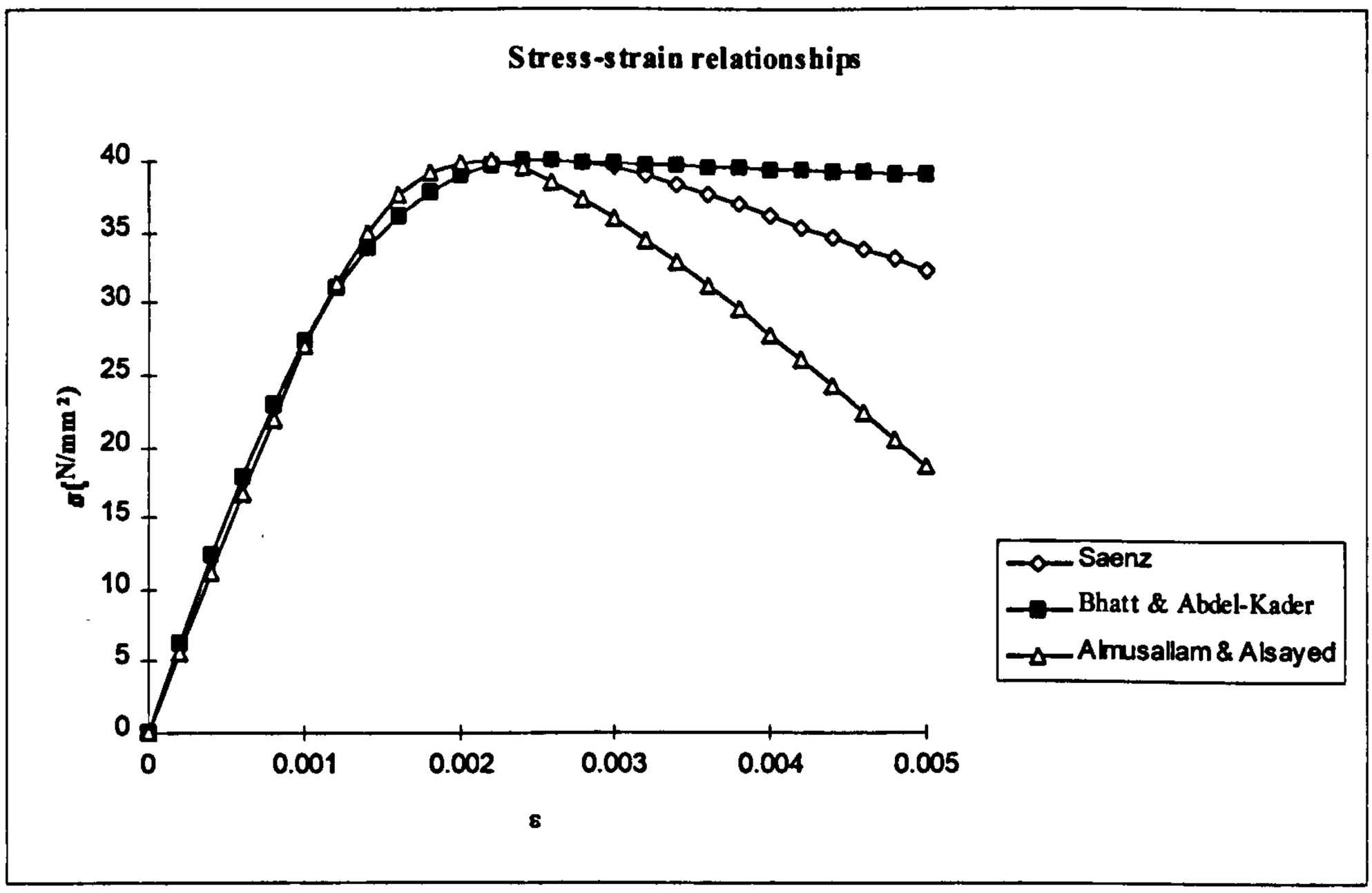

Fig. 6.7: Concrete stress-strain relationships in uniaxial compression

6.2.2: Biaxial stress

"Micro-cracks observations indicate that a main cause of the increase in both strength and stiffness in biaxial compression is the confinement of potential micro-cracking in the presence of biaxial compression." [Liu et al. (1972)]. Figure 6.8a shows the stress-strain curves for different state of biaxial compression. The lateral strain behaviour is also shown in this figure.

The volumetric strains $\frac{\Delta V}{V} = e = \varepsilon_1 + \varepsilon_2 + \varepsilon_3$ is shown in figure 6.8b. "Up to stresses $\sigma = 0.35 f_c^{'}$ volumetric strain and applied stress are approximately proportional. If the stress increases beyond this value the rate of volume reduction increases until 80 to 90 percent of the ultimate a point of inflection is reached. The minimum volume was observed at approximately 95 percent of the failure stress. Further straining of the specimen resulted in a volume increase and eventually in positive values for $\frac{\Delta V}{V}$" [Kupfer et al. (1969)]. Figure 6.8c shows modes of failure of biaxially loaded concrete.

In modelling the non-linear stress-strain relationship of the concrete in the principal stress direction, equation describing concrete in elastic stage is adopted as proposed by Liu et al. (1972) and used by Abdel Kader (1993). This equation accounts for non-linear behaviour of concrete in biaxial compression and takes the form:

$$\sigma = \frac{E_c . \varepsilon}{(1 - v\alpha)\left[1 + (\frac{1}{1 - v\alpha}\frac{E_c}{E_s} - 2)\frac{\varepsilon}{\varepsilon_p} + \left(\frac{\varepsilon}{\varepsilon_p}\right)^2\right]} \qquad 6.2$$

where:

σ_p is the ultimate strength of concrete in compression, equal $f_c^{'}$.

ε_p is the strain at maximum compressive strength of concrete.

E_c is the initial modulus of elasticity of concrete for uniaxial loading.

E_s is the secant modulus of elasticity at peak stress $E_s = \sigma_p / \varepsilon_p$.

v is the Poisson's ratio.

α is the ratio of the principal stresses $= \sigma_2 / \sigma_1$ (if $\alpha = 0$, i.e. for uniaxial state of stress, equations 6.1 and 6.2 become identical).

σ and ε are stress and strain in biaxial loading.

Equation 6.2 is used to generate the stress-strain behaviour of concrete in biaxial compression up to peak strain ε_p, after which this equation ceases to be valid due to softening deformation.

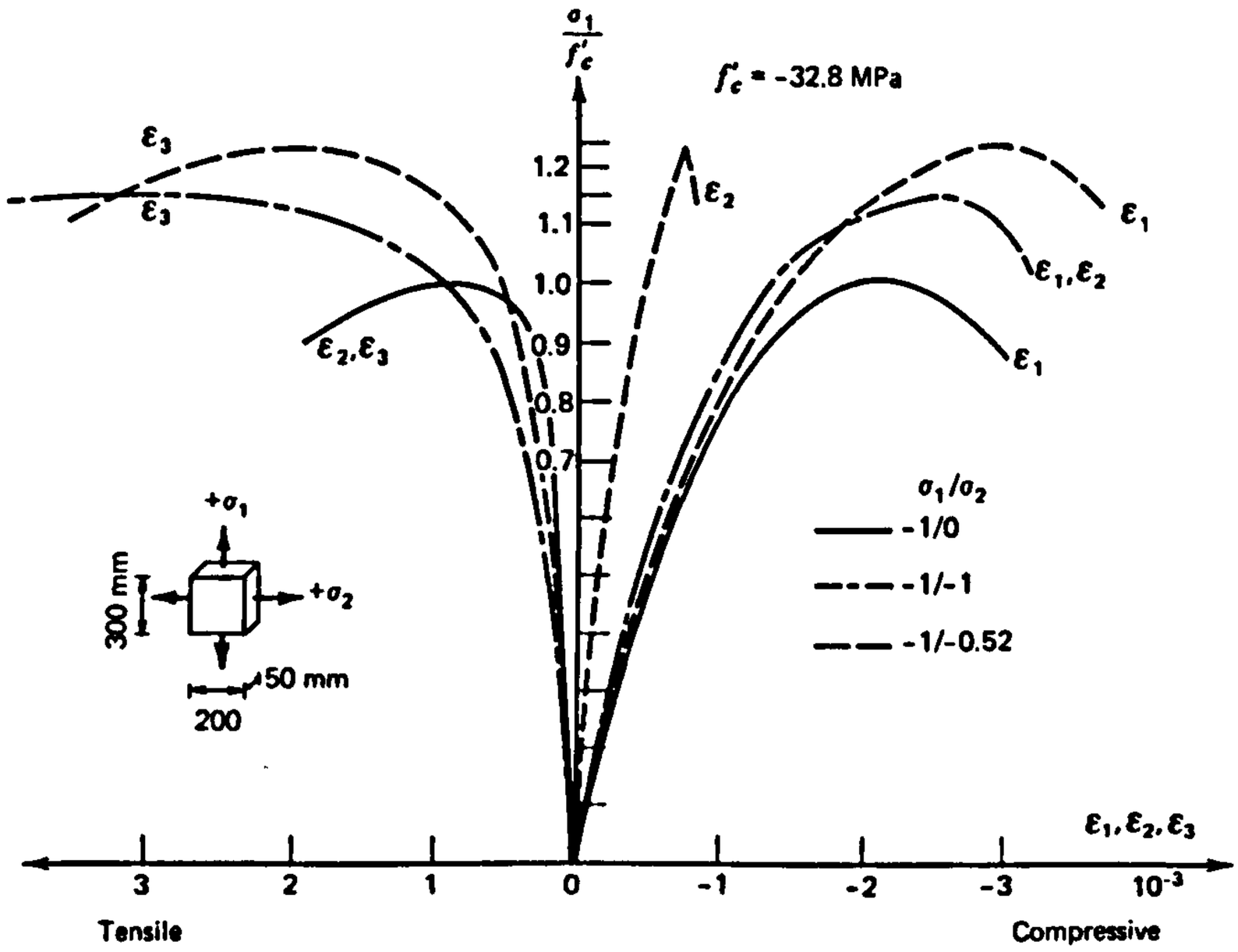

Fig. 6.8a: Stress-strain relationships of concrete under biaxial compression

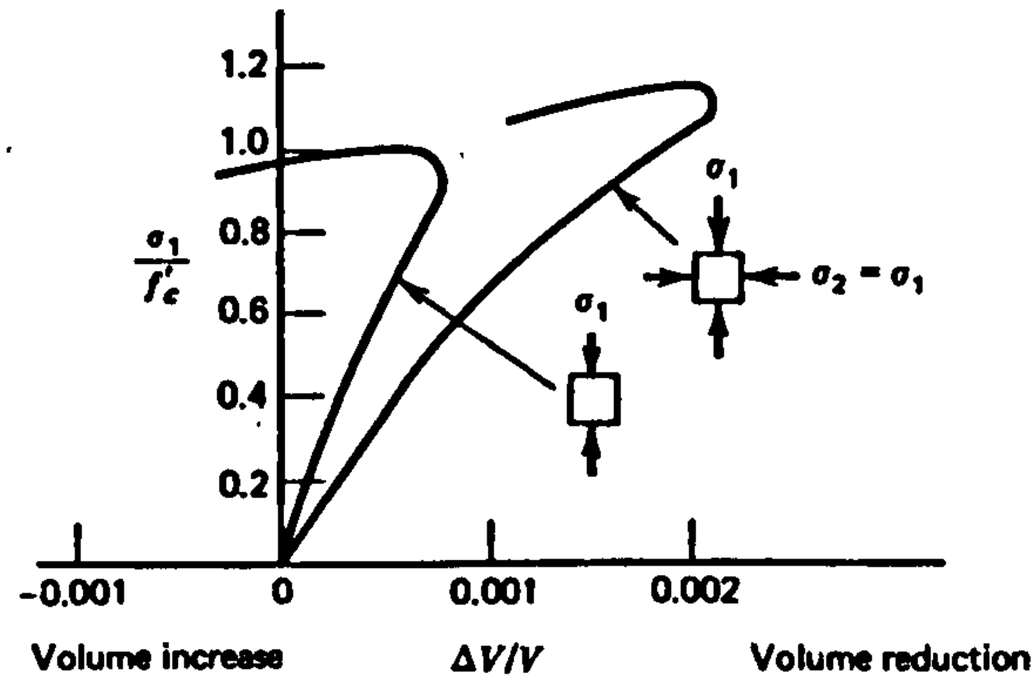

Fig. 6.8b: Stress-strain curve for concrete volume change under biaxial compression

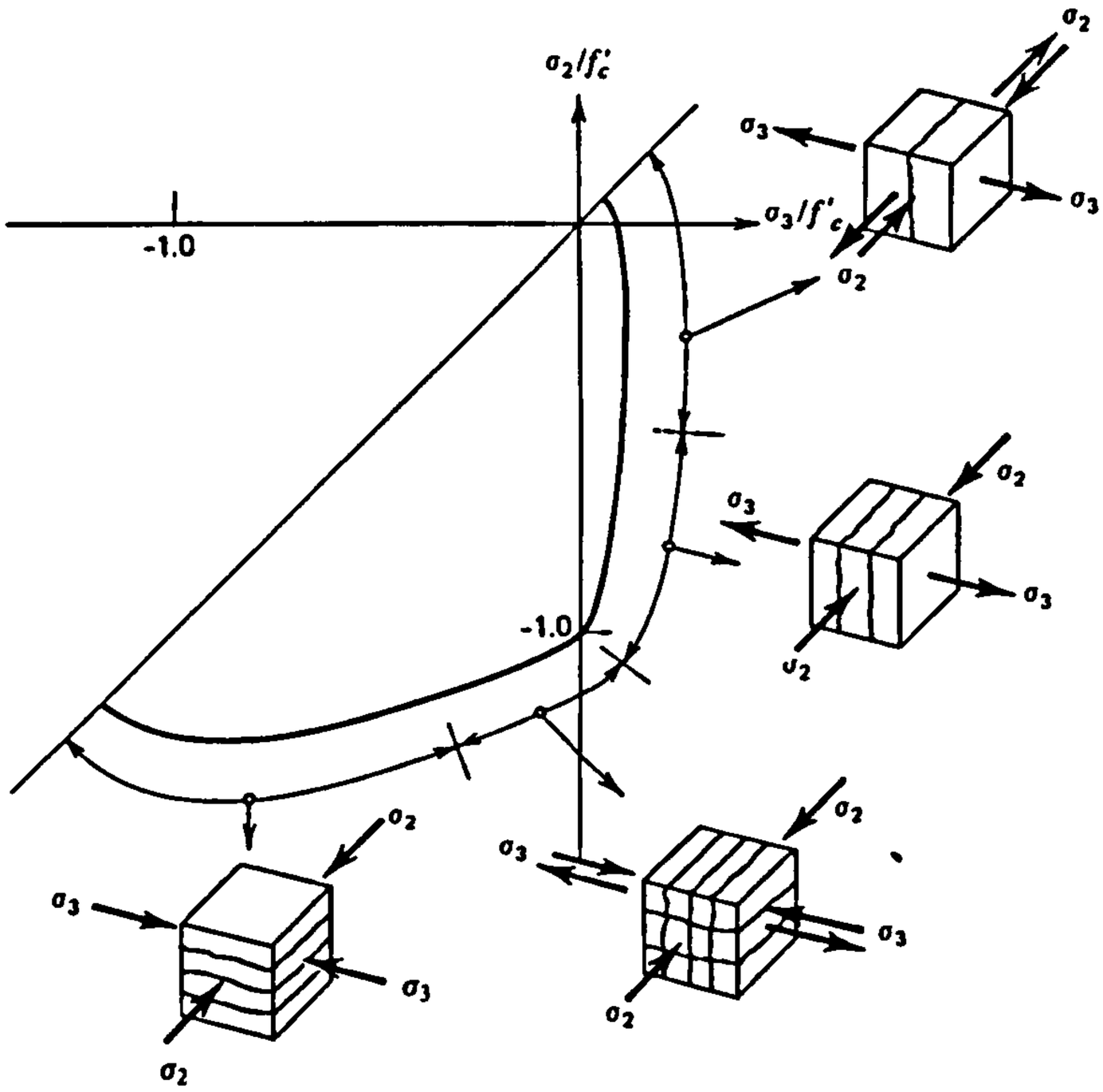

Fig. 6.8c: Failure modes of biaxially loaded concrete

6.2.3: Triaxial stress

It is well known that concrete could withstand very high stresses if it was in a state of triaxial compression. It behaves as a ductile material rather than a brittle one. This is because of the reduction in the possibility of bond cracking to occur and failure mode changing to crushing of the concrete rather than a cleavage one, which is due to suppression of micro-cracks development. The ultimate axial strength is found to increase considerably with increasing confining stress specially under hydrostatic stress condition. Figure 6.9a shows triaxial stress-strain relationship for concrete under different confining stresses ($\sigma_2 = \sigma_3$) while the axial load (σ_1) is increased. This figure shows linear behaviour up to about 30-40% of the ultimate load. Thereafter the behaviour depends on the confining pressure (σ_2, σ_3). Figure 6.9b shows the volumetric behaviour of concrete under hydrostatic stress.

More about the behaviour of concrete under triaxial stress can be found in the literature [e.g. Palaniswamy and Shah (1974), Kotsovos and Newman (1977, 1978), Hobbs et al. (1977), Cedolin et al. (1977), Elwi and Murray (1979), Ahmad and Shah (1982), Van Mier (1986), Imran and Pantazopoulou (1996), Lan and Guo (1997) and Ansari and Li (1998)].

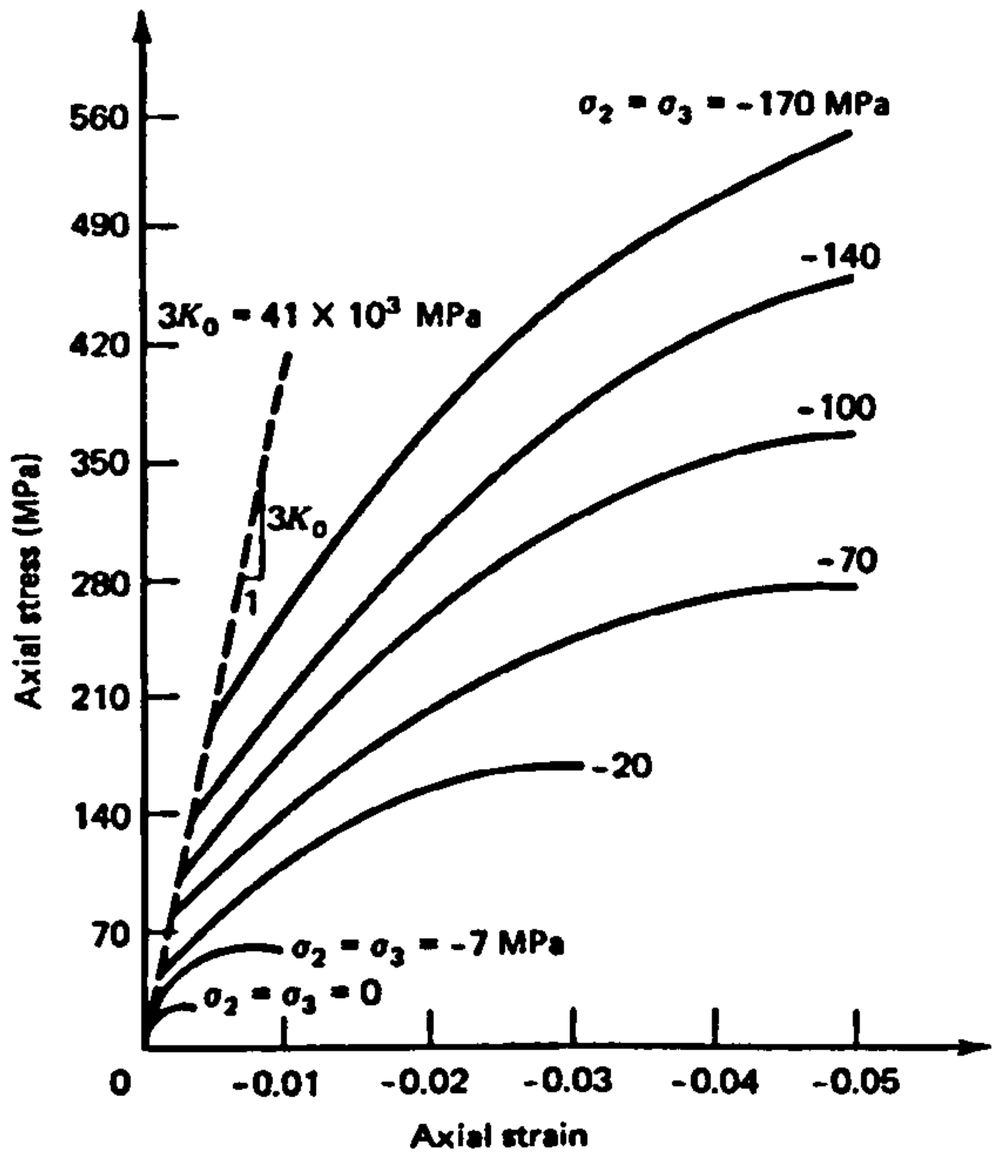

Fig. 6.9a: Triaxial stress-strain relationship for concrete

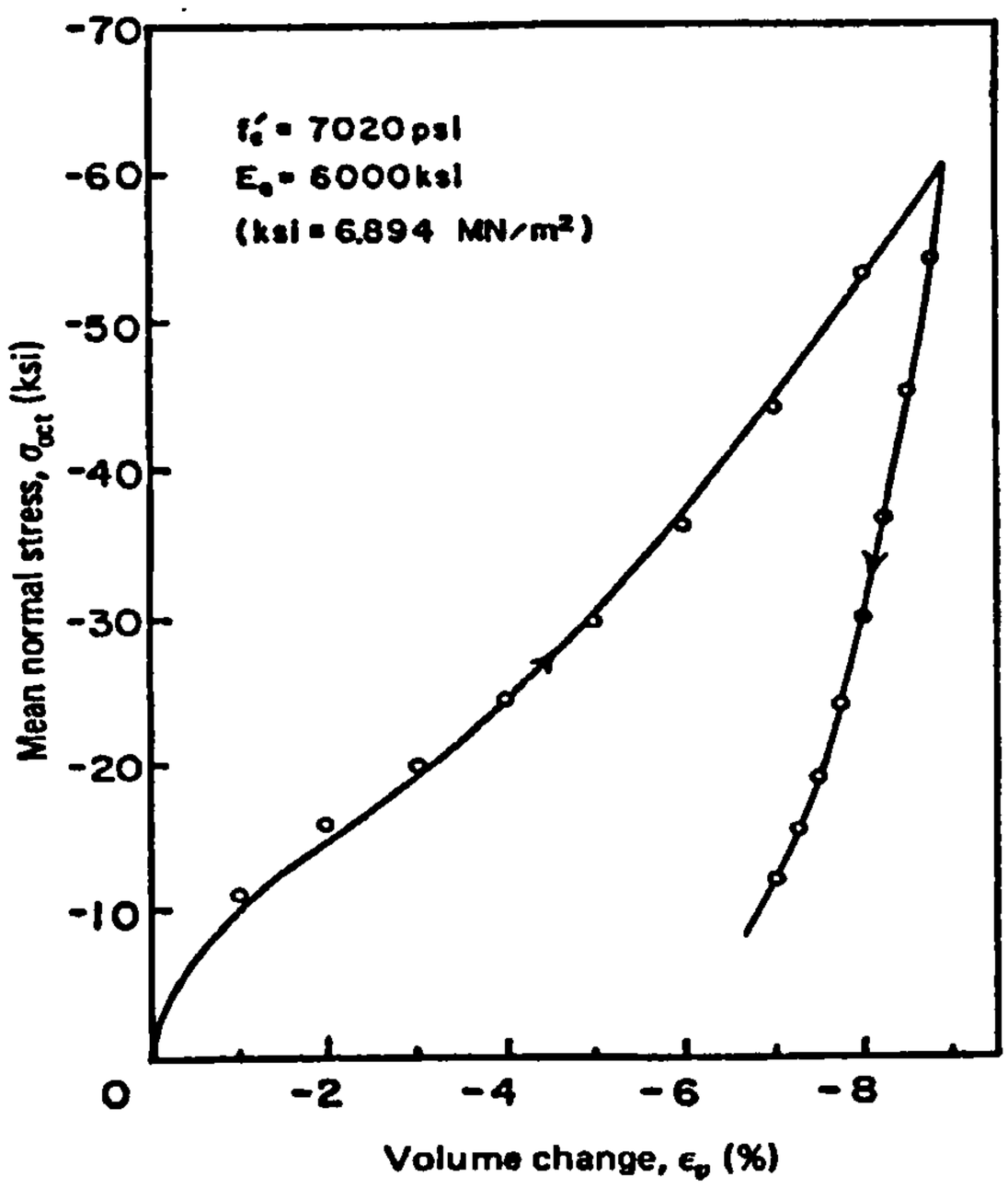

Fig. 6.9b: Behaviour of concrete in hydrostatic compression test

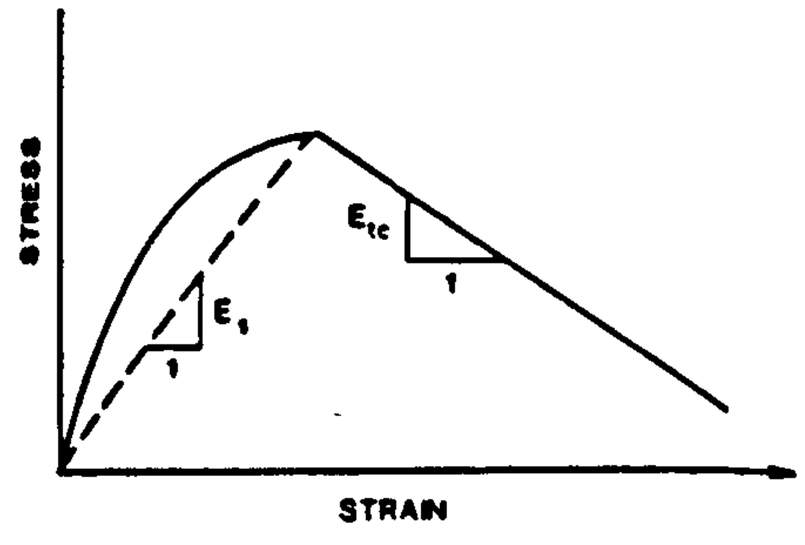

(a): Gajer and Dux (1990)

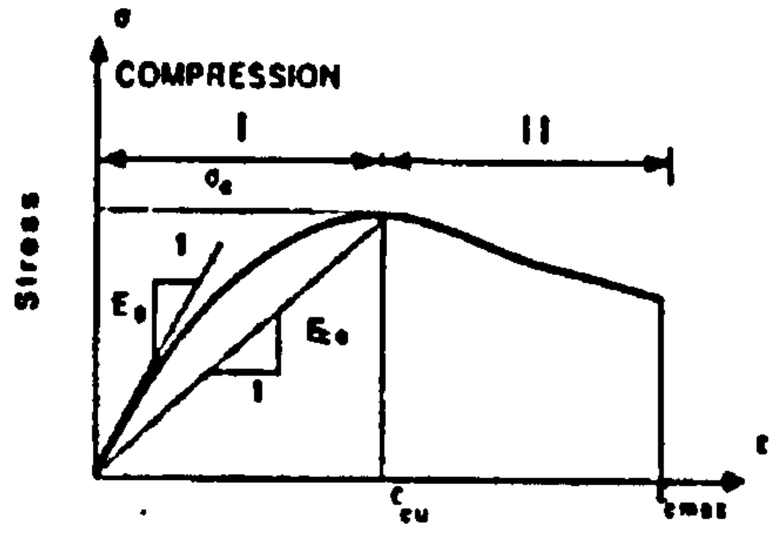

(b): Razaqpur and Nofal (1990)

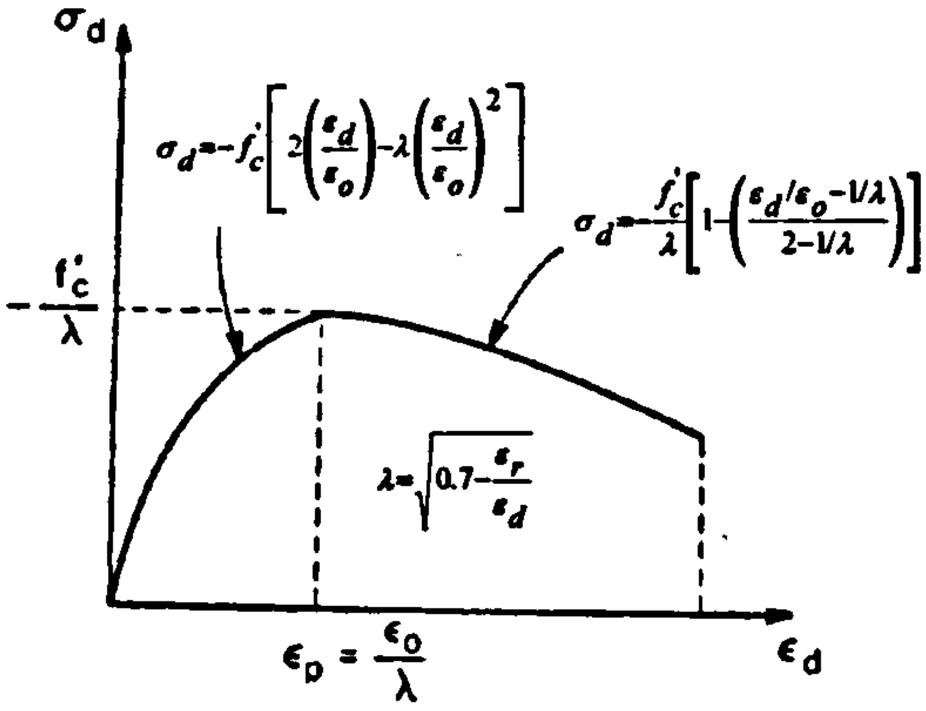

(c): Mau and Hsu (1987)

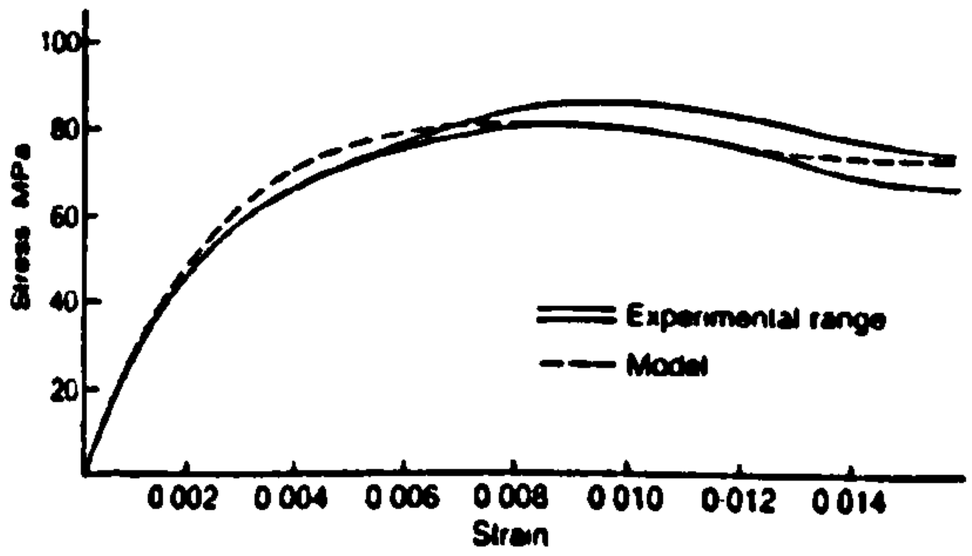

(d): Ahmad and Abdel-Fattah (1991)

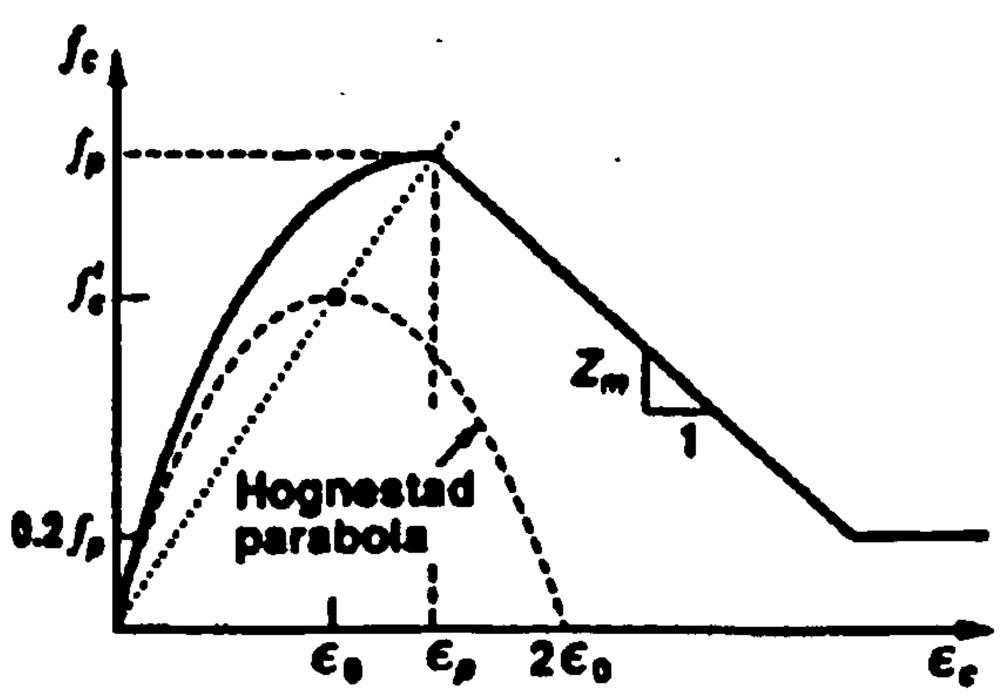

(e): Vecchio (1992)

Fig. 6.10: Compression softening curves as suggested by different researchers for non-linear analysis

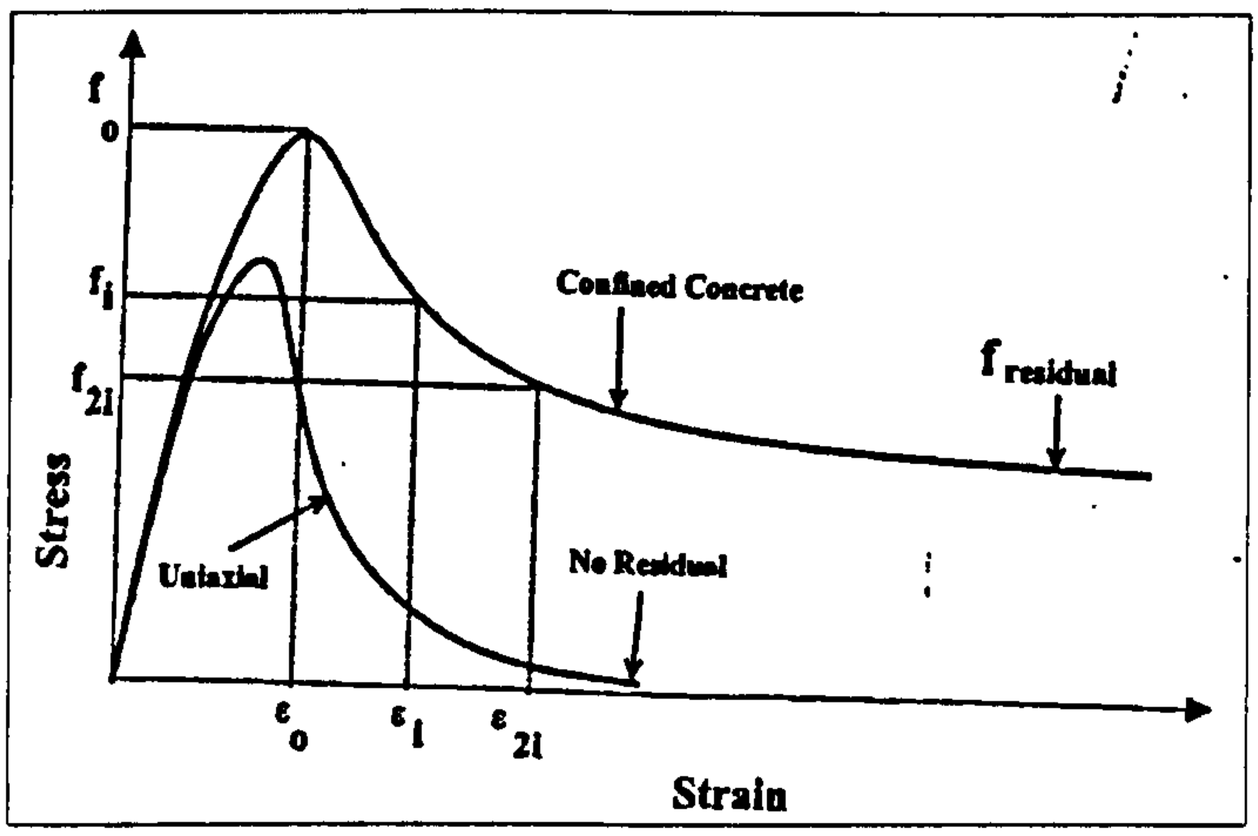

(f): Attard and Setunge (1996)

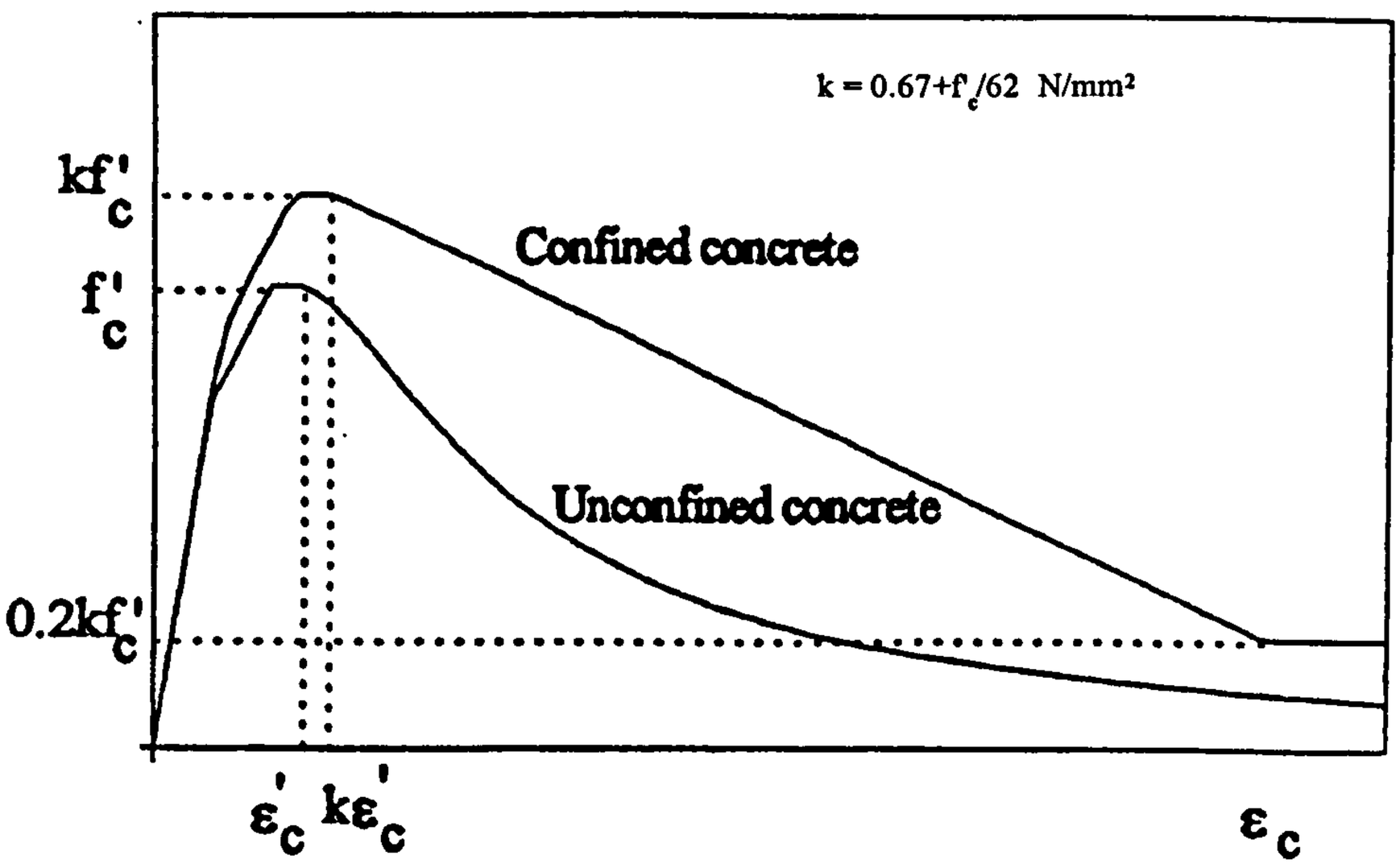

(g): Elmorsi et al. (1998)

Fig. 6.10: Continued

6.2.4: Compression softening

This term is used to describe the strain of the concrete after the peak stress in the compressive stress-strain curve which is important in the case of over reinforced concrete. There seems to be no agreement among the researchers on the shape of this portion (Fig. 6.10): "Only the ascending branch of stress-strain curves obtained from tests on concrete specimens in compression describe material behaviour; the descending branch expresses the interaction between specimen and testing machine" [Kotsovos (1987)]. "..... the concrete confinement plays an important role in the post-crushing behaviour of concrete. The better confined the concrete, the more gradual unloading" [Meyer and Bathe (1982)]. Choi et al. (1996) studied the effects

of several factors affecting the descending portion of the stress-strain curve for normal and high strength concrete. They concluded that the normal strength concrete is more ductile than the high strength concrete.

In our model a linear descending curve is adopted [Bhatt and Abdel-Kader (1995)] as given by equation 6.3 after the maximum stress is reached:

$$\sigma = \frac{(0.1-\varepsilon)}{(0.1-\varepsilon_{cc})} f_c' \quad \varepsilon < 0.005 \qquad 6.3$$

6.3: Concrete in Tension

Tensile strength of concrete f_t' (Fig. 6.11) is relatively low when compared with its compressive strength ($f_t' = 8\text{-}10\%\ f_c'$) and it does not effect the ultimate strength of the member. Therefore, in many design cases it is neglected. However, in finite element modelling the tensile behaviour of concrete is taken into account mainly to predict the load-deflection characteristics of structures.

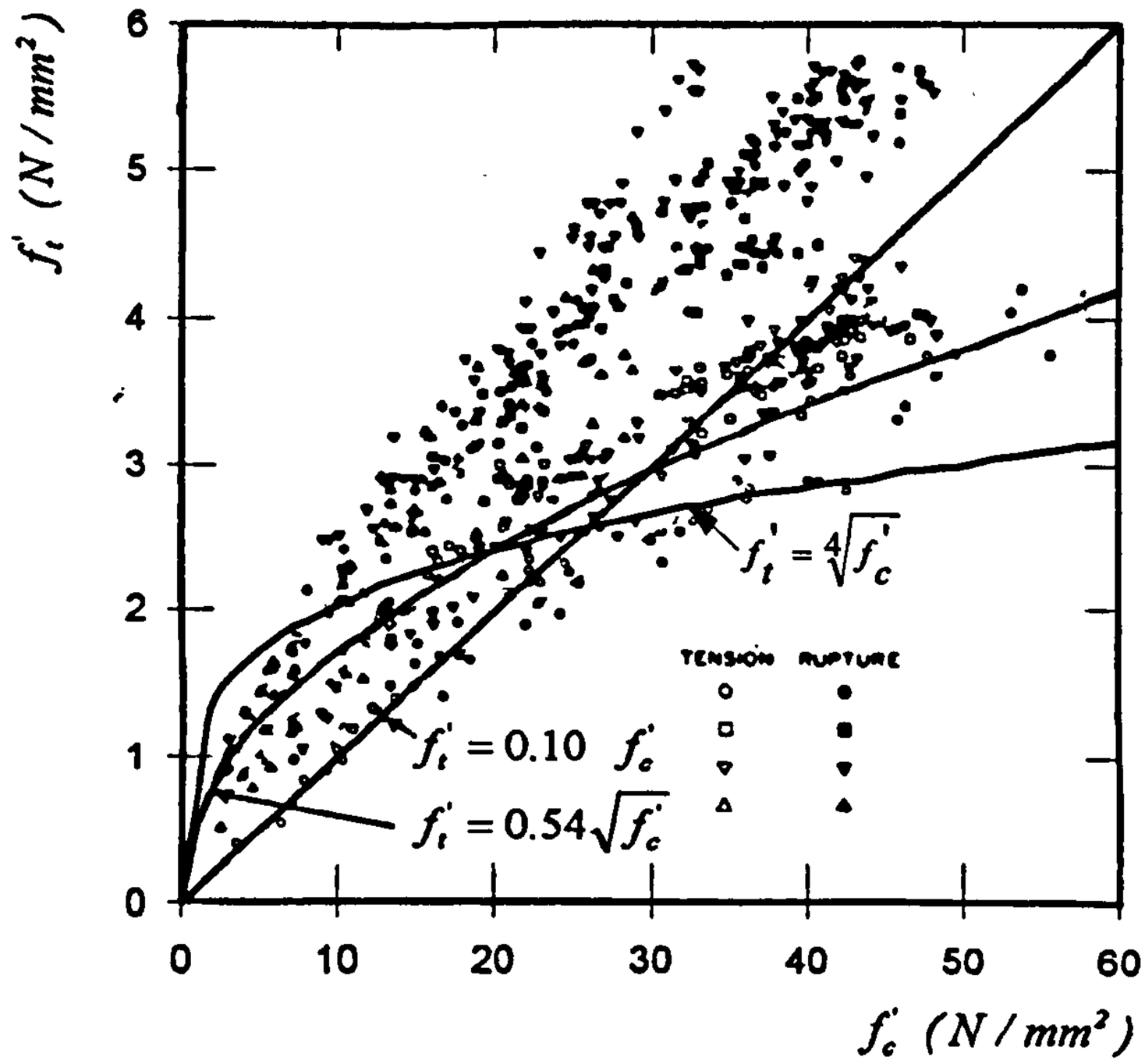

Fig. 6.11: Estimating tensile strength f'$_t$ from compressive strength f'$_c$

6.3.1: Tensile strength of concrete

Figure 6.12 shows typical tensile stress-strain curve for concrete.

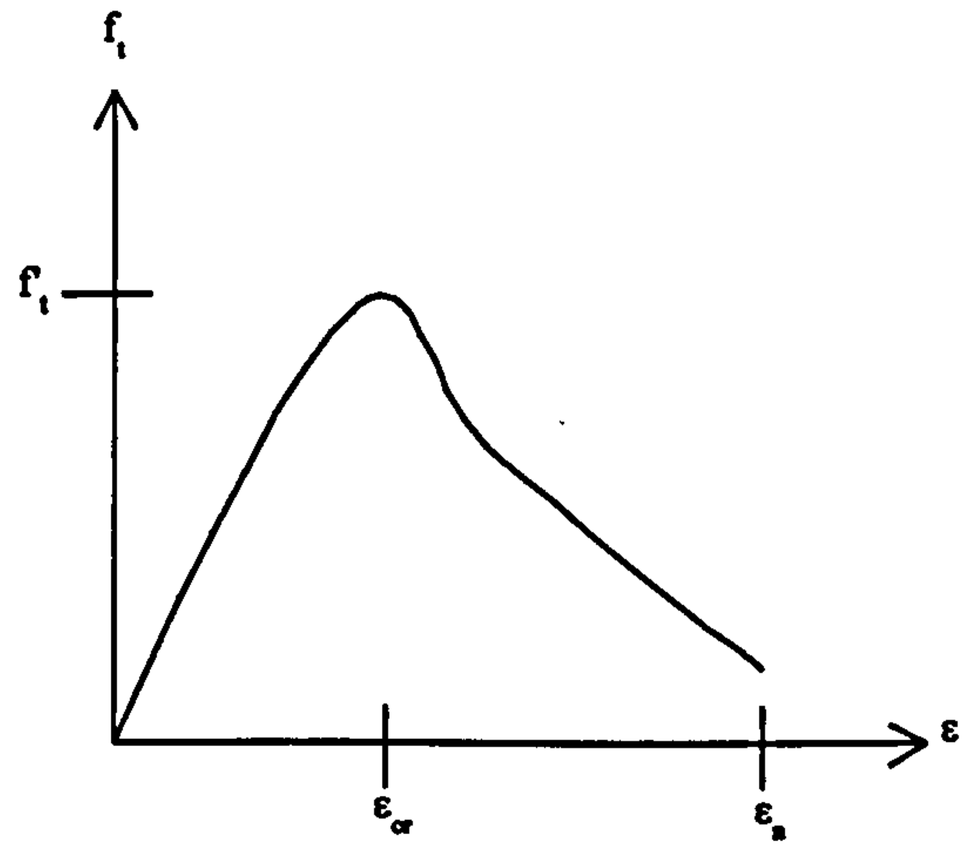

Fig. 6.12: Typical tensile stress-strain curve for concrete

In the laboratory, there are three methods of tests used to find the tensile strength of concrete f_t' (Fig. 6.13): the direct tension test, the beam bending test and the cylinder splitting test. In the direct tension, the specimen is gripped at its ends and pulled apart in tension. Because of the difficulties associated with applying a pure tensile force to a plain concrete specimen, there are no standard tests for direct tension. In the beam bending, a rectangular beam of plain concrete (usually 100x100x400mm or 150x150x600mm depending on the size of aggregate) is simply supported and loaded at third points. The tensile stress at failure is called the modulus of rupture f_r. In finding the splitting tensile strength f_{sp}, a cylinder (usually 150mm dia. x 300mm long) is loaded in compression on two diametrically opposite elements, failing in tension on the plane between the loaded elements. Raphael (1984) studied some results from these tests and suggested that $f_t' = 0.75 f_r$ (N/mm^2) or $f_t' = 0.44(f_c')^{2/3}$ (N/mm^2) for the concrete strength f_c' up to 62 N/mm^2. Gettu et al. (1996) studied the damage in high-strength concrete due to monotonic and cyclic compression. They concluded that "The tensile strength of concrete can be reduced by 25 percent due to compressive loads applied along a perpendicular direction, even in high-strength concrete". Tasdemir et al. (1996) reported that the tensile strength of concrete decreases with increase in the volume of coarse aggregate (Fig. 6.14). They used the term 'tensile strain capacity' to

identify the strain at which first crack was developed.

In finite element modelling, the tensile strength of concrete is very often inferred from the compressive strength $f_c^{'}$, because the latter is normally measured. ACI formula for the tensile strength $f_t^{'} = 0.54\sqrt{f_c^{'}}$ N/mm^2 and $f_t^{'} = \sqrt[4]{f_C^{'}}$ N/mm^2 which was suggested by Abdel-Kader (1993) (Fig. 6.11) were studied in chapter 8. The ascending part of the tensile stress-strain curve was considered as linear similar to any elastic stress-strain curve.

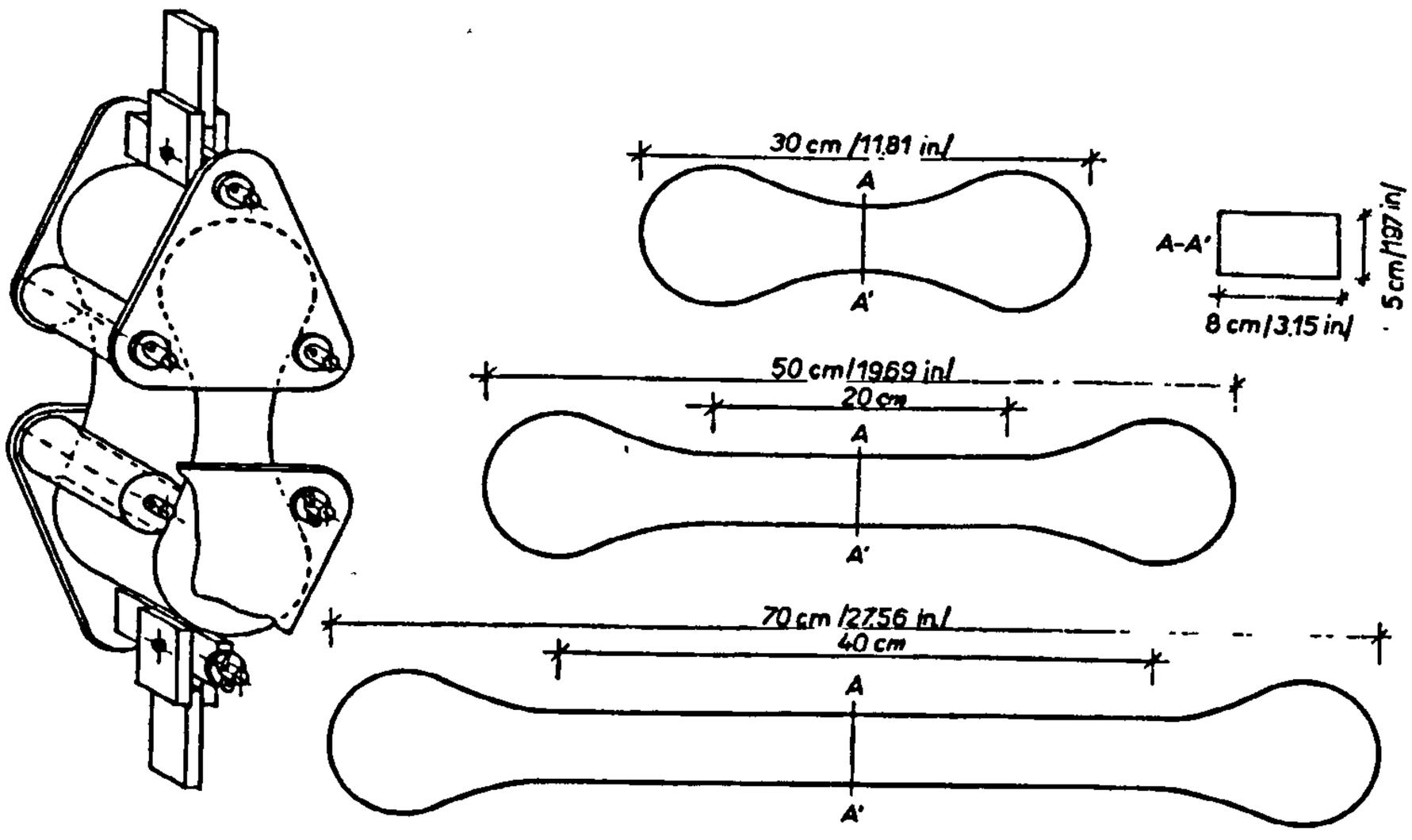

(a): direct tension test

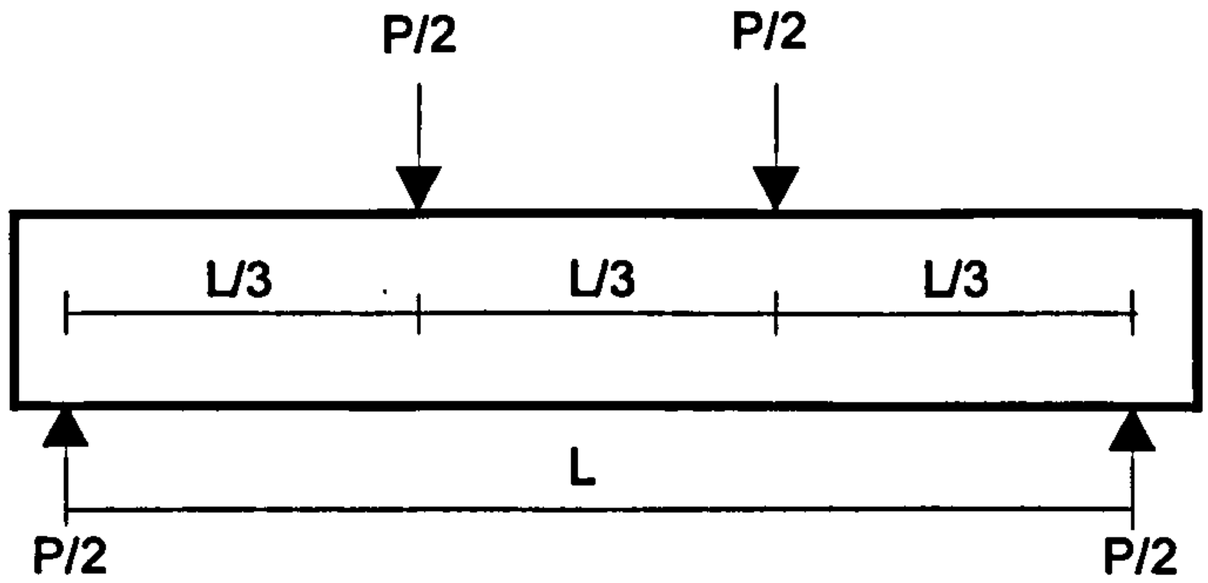

(b): Beam bending test

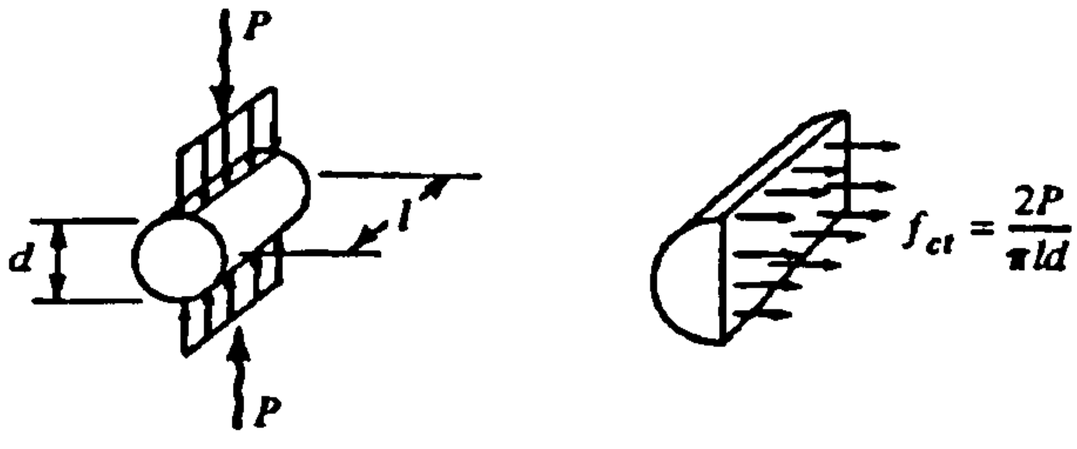

(c): Cylinder splitting test

Fig. 6.13: Methods for testing concrete tensile strength

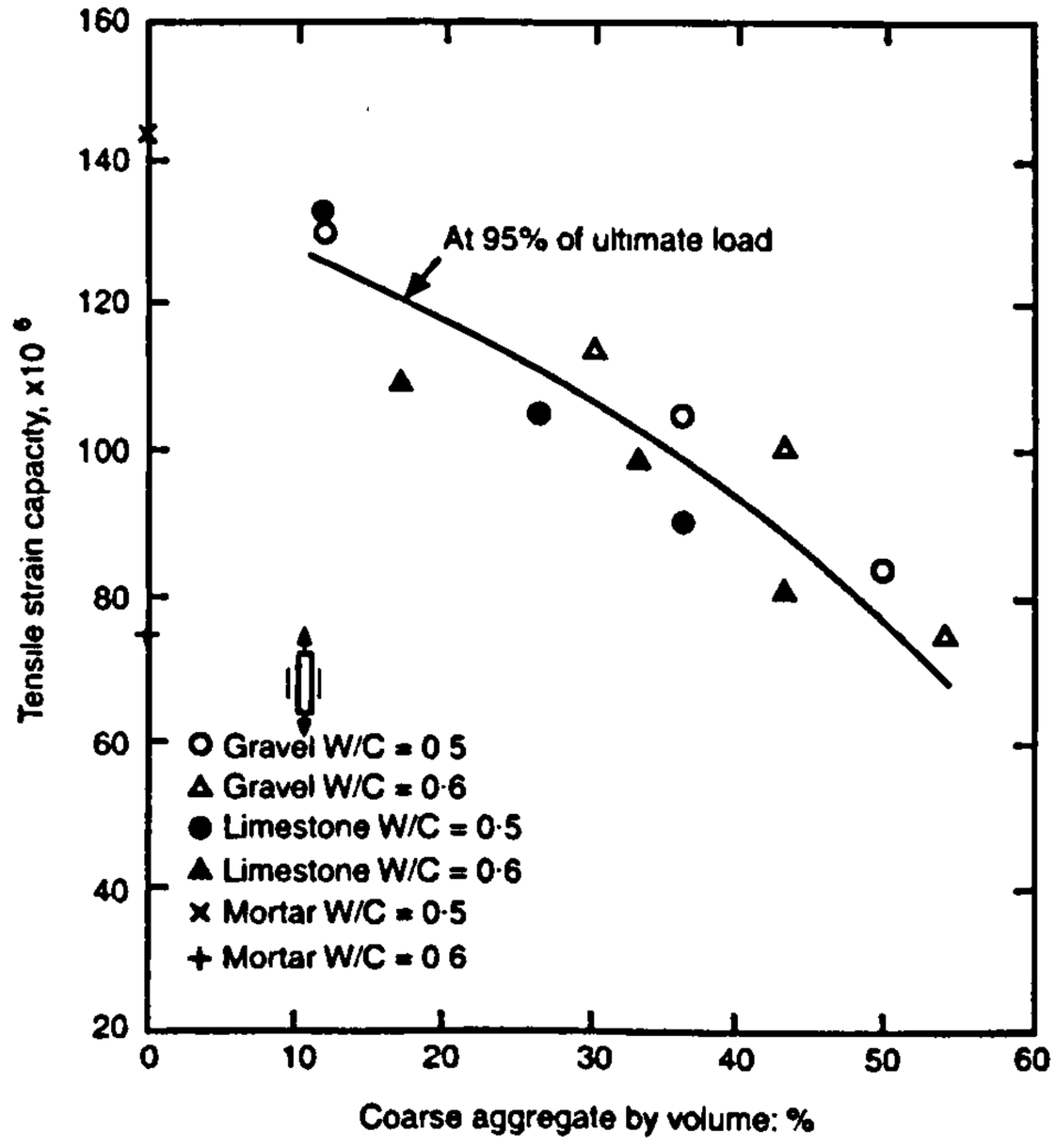

Fig. 6.14: Relation between tensile strain capacity and aggregate concentration [Tasdemir et al. (1996)]

6.3.2: Tension stiffening

When a reinforced concrete member is subjected to a tensile stress exceeding its tensile strength, the concrete cracks at discrete locations. The total tensile force is then transferred across the crack by the tensile steel, but between the cracks the concrete continues to carry stress locally, mainly in the direction of the bar due to the bond between concrete and reinforcement. This is called tension stiffening. As the stress in reinforcement and concrete vary along the bar normal to cracks, the tension stiffening effect is usually treated by assuming a relationship between the average concrete tensile stress and average concrete tensile strain over a long-gauge length in the direction normal to cracks. Similarly, the stress-strain relationship of reinforcement is taken on average basis. "The tensile stiffening effect must, in general, be inferred from the behaviour of concrete acting in combination with steel since the concrete by it self is unstable beyond its maximum strength capacity" [Murray et al. (1979)]. Several models to represent the tension stiffening have been proposed by different researchers (Fig. 6.15). Scanlon and Murray (1974) proposed a stepped piece-wise linear stress-strain relation, while Lin and Scordelis (1975) suggested a smooth unloading curve. Gilbert and Warner (1978) used several variations of Scanlon-Murray and Lin-Scordelis curves. In addition, they

employed a new curve consisting of a small drop in strength immediately after cracking followed by piece-wise linear unloading.

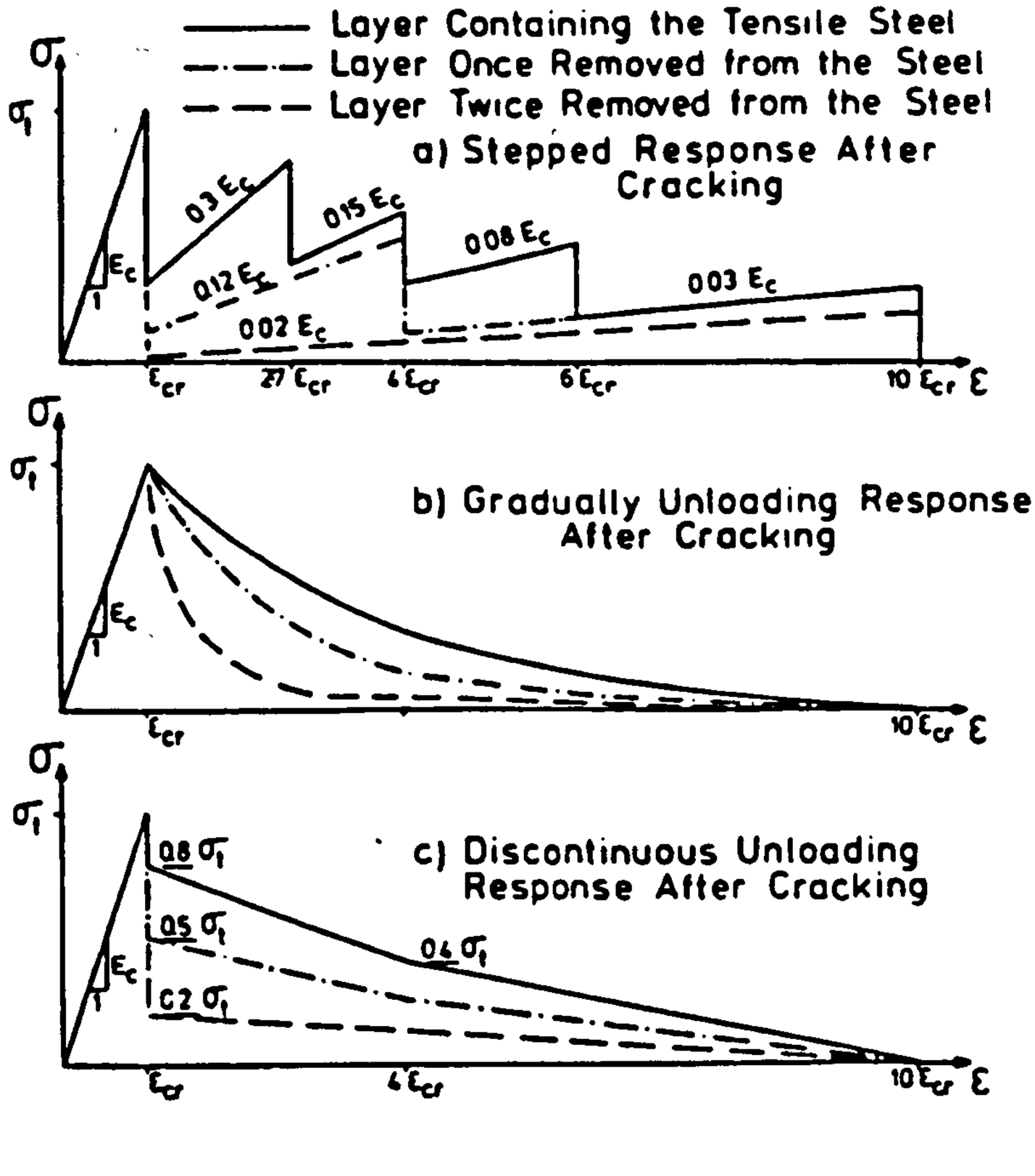

Fig. 6.15: Alternative stress-strain diagrams for concrete in tension

Gopalaratnam and Shah (1985) presented what was called the concrete softening for plain concrete. They assumed that the post cracking resistance of plain concrete in tension is due to discontinuities in cracking and to bridging of cracked surfaces by aggregates and fibrous crystals. Gupta and Maestrini (1990) included the effects of the bond between the bar and the concrete, area of the bar and yield strengths of the concrete and steel in the stress-strain relationship. Abrishami and Mitchell (1996) studied the effects of the presence of longitudinal splitting cracks caused by a bar on the tension stiffening using a uniaxial tensile stress on a specimen reinforced with a single bar. They concluded that the splitting cracks increases as the bar diameter increases. This results in a significant reduction in tension stiffening. Hsu and Zhang (1996) proposed a set of constitutive laws for reinforced concrete. The laws vary from neglecting the tensile strength of concrete with elastic-perfectly plastic stress-

strain relationship of reinforcement to employing both the average tensile stress-strain relationship of concrete and the average stress-strain curve of reinforcement.

In the present study, the descending part of the tensile stress-strain curve was considered as shown in figure 6.16. These curves were proposed by Abdel Kader (1993) and were tried in chapter 8. They are similar to a stress-strain curve proposed by Massicotte et al. (1990) with a certain maximum strain after which the tensile stress equals zero. This maximum strain has been suggested by Bazant and Lin (1988) to correspond to a point where the tensile stress normal to crack reduces to 5% of the tensile strength.

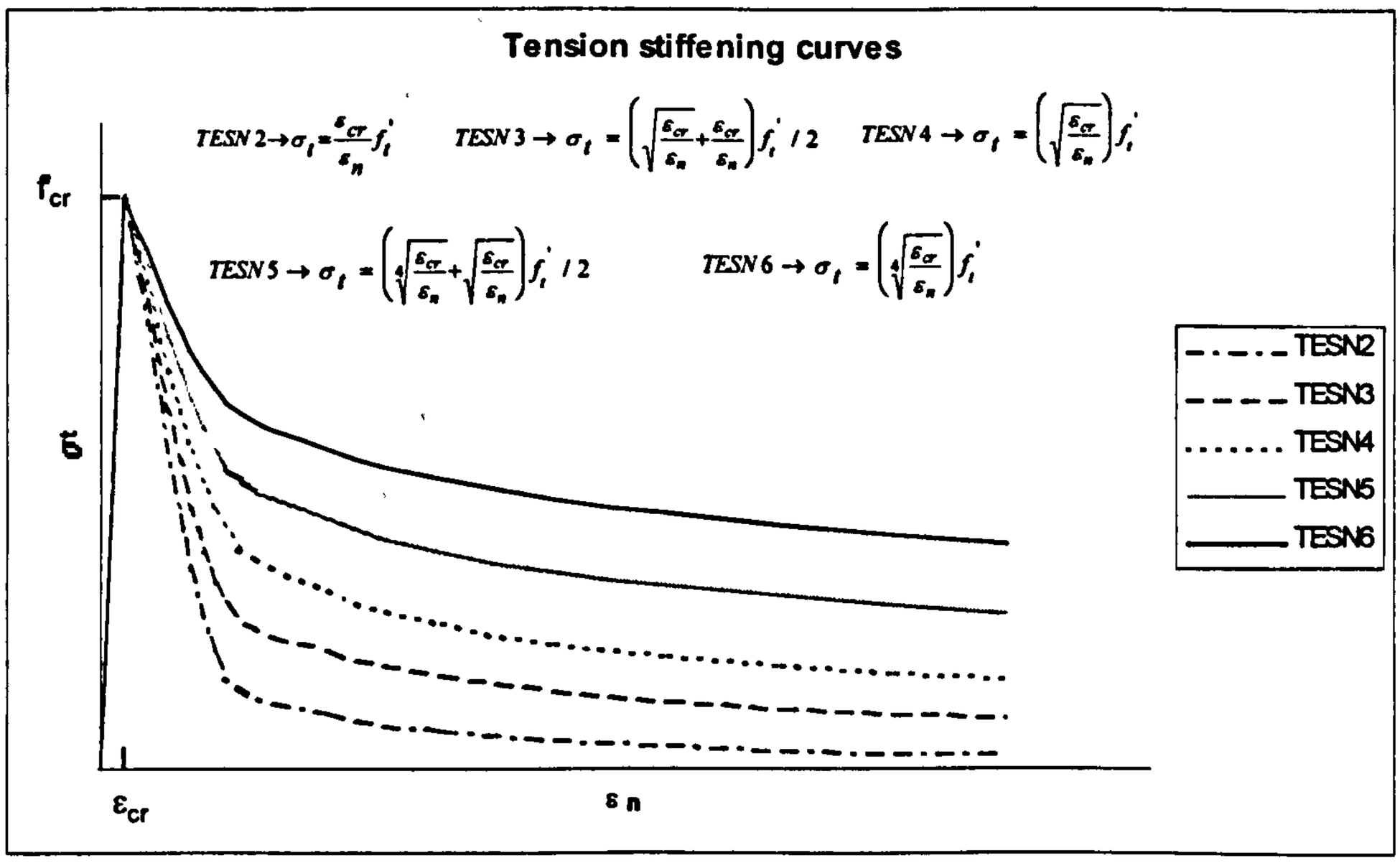

Fig. 6.16: Tension stiffening curves

6.4: Concrete in Shear

As discussed in chapter two, shear is resisted by concrete before cracking. Shear cracking happens when the major principal tensile stress exceeds the tensile strength of concrete. After cracking the reinforced concrete structures can still resist some shear across cracks due to internal truss action or compression field. The shear strength of concrete is mainly affected by the crack width and the amount and orientation of reinforcement crossing the cracks. The maximum size and shape of aggregate which causes interlocking, has also some influence on the shear stiffness.

6.4.1: Shear retention factor

In normal strength concrete, cracks usually occur along the interface between the cement paste and the aggregate particles. This results in a rough surface on each side of the crack which can provide a resisting force through the interlocking action of the aggregate. In the high strength concrete, cracks go across the paste and through the aggregate particles, resulting in a smoother surfaces along the crack, which reduces the post cracking shear stiffness for these concretes. The aggregate interlock action is controlled by crack width, the shear capacity being reduced by the increase of crack width. The reinforcement normal to the crack reduces the ability of the separated pieces to move apart which improves the interlock action in transmitting shear force along the crack.

In finite element, the reduction of the elastic shear modulus G across the plane of the crack is usually defined by what is called the shear retention factor β. This factor is related to the contribution of the aggregate interlock to the shear capacity of the section after cracking and takes the form: $G^* = \beta G$, where $1 > \beta > 0.0$ and G^* is the shear modulus for the cracked section.

On the amount of this factor's effect there are mainly two groups of opinions. Some consider it plays a negligible role in the load carrying capacity [Bedard and Kotsovos (1985) and Vidosa et al. (1991)], they take β as a constant (non-zero) only to avoid excessive deterioration of the stiffness matrix. Others [Cedolin and Poli (1977), Arnesen et al. (1980), Chang et al. (1987), Cervera et al. (1987) and Balakrishnan and Murray (1988)] consider it has a larger effect on behaviour. In the present study, the effect of the shear retention factor is considered as:

$$\beta = B\varepsilon_{cr} / \varepsilon_n \qquad \geq \beta_{\min} \qquad 6.4$$

where ε_{cr} is the tensile crack strain (corresponds to the peak tensile stress), ε_n is a fictitious strain normal to the crack plane and B and $\beta_{\min}$ are numerical constants (Fig. 6.17). Effect behaviour of several combination values for these constants are studied in chapter 8.

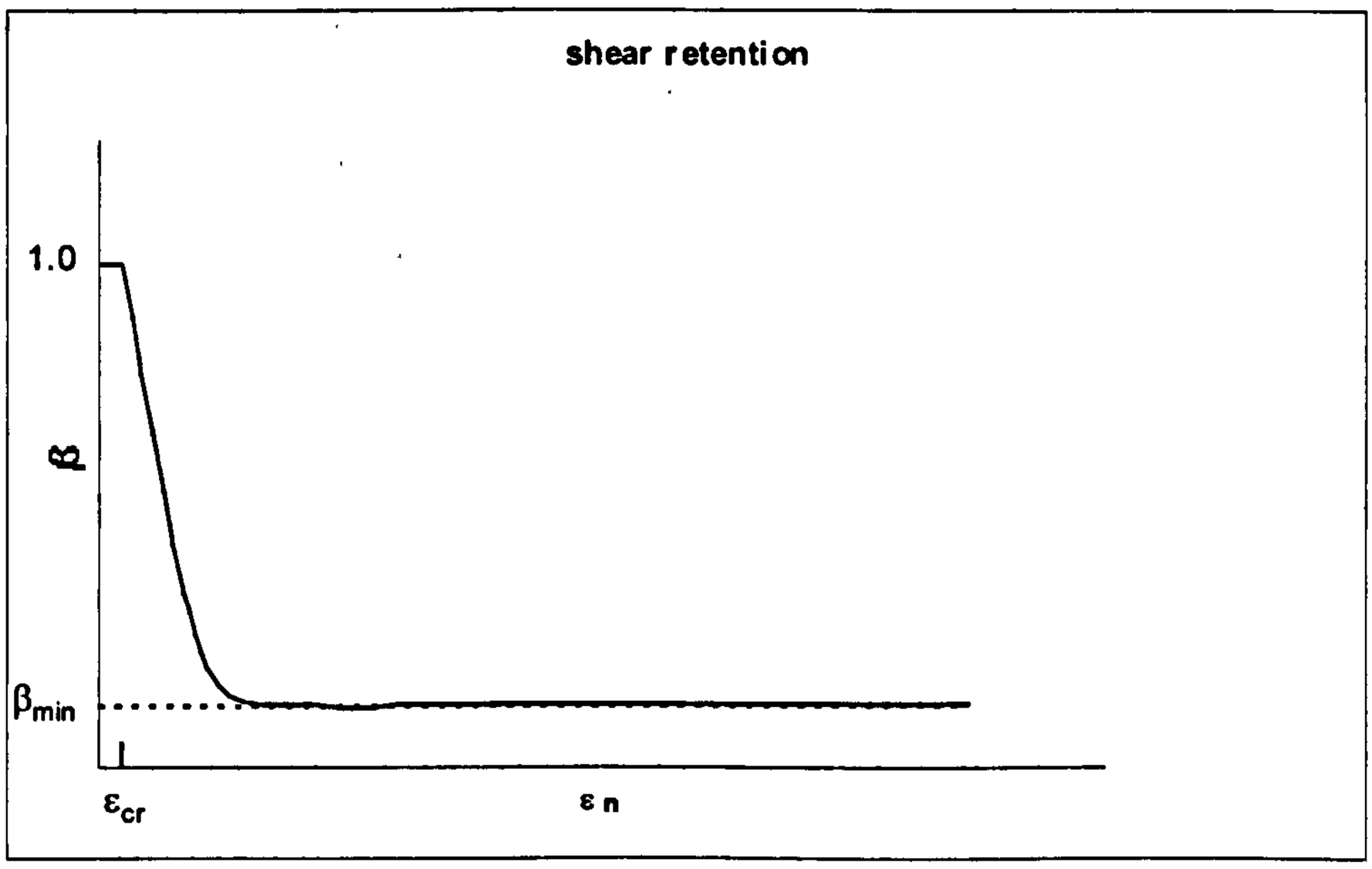

Fig. 6.17: Shear retention factor β used in this research

6.5: Concrete cracking

Non-linear behaviour of reinforced concrete is mainly caused by the progressive cracking. Nanakorn and Horii (1996) presented a model for the fracture process zone (Fig. 6.18) which consists of a micro-cracking zone and a bridging zone. The micro-cracking zone is a zone where the initiation of micro-cracks and their growth are dominant. The bridging zone is a part of a macro-crack along which the stress is transmitted partially by aggregate or fibres.

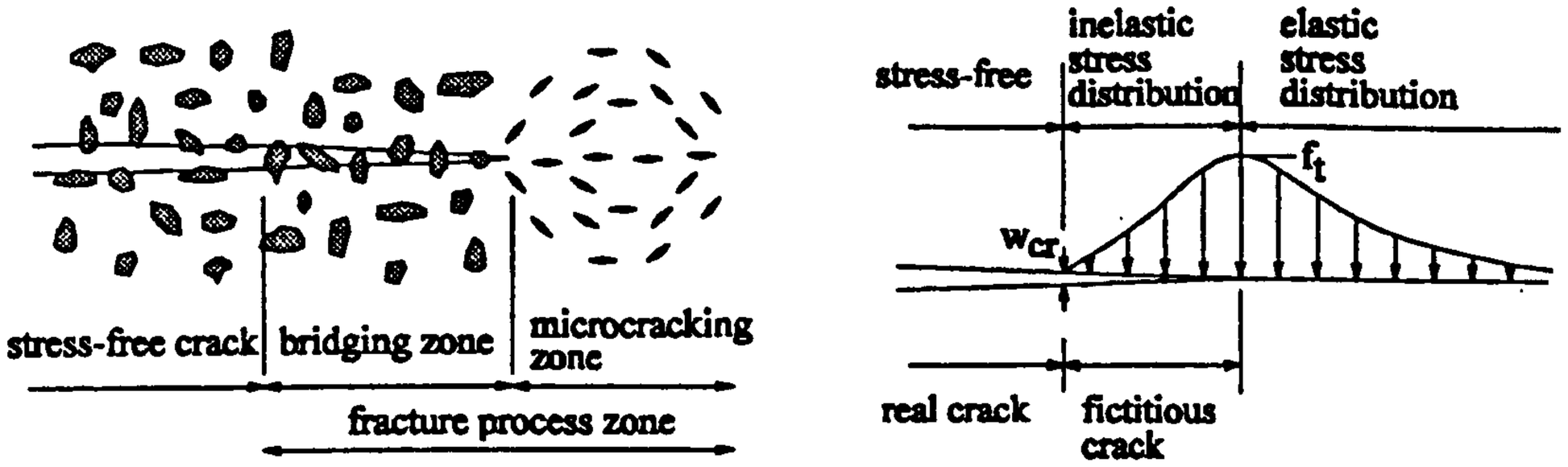

Fig. 6.18: Schematic illustration of fracture process zone [Nanakorn and Horii (1996)]

In finite element modelling of concrete cracking, extensive research has been carried out. Two distinct models: the discrete cracking model, originated by Ngo and Scordelis (1967) and the smeared cracking model established by Rashid (1968) are briefly discussed in the following sub-sections.

6.5.1: Discrete crack model

The discrete crack model was the first model used to represent the cracking for finite element method (Fig. 6.19). In this model, the elements are initially rigidly joined by linkage nodes until a crack is detected. This happens when the average stress in two adjacent elements violates the yield criterion (section 6.6). The crack propagation is simulated by allowing cracks to follow element boundaries. This is done by introducing new nodes on the element boundaries which make twins with the original ones. This approach requires a pre-determined element mesh which suits an assumed location and orientation of the cracks (geometrical restraints). Also, the introduction of the new nodes leads to a more expensive analysis (wide bandwidth in the global stiffness matrix). For these reasons the discrete crack model is rarely used.

6.5.2: Smeared crack model

In the smeared crack model, it is assumed that, before cracking the concrete is a homogeneous, isotropic and linear elastic material and after cracking the concrete remains a continuum but becomes orthotropic with one of the material axis orientated along the direction of the crack as shown in figure 6.20. In this model the idea of orthogonal cracks was adopted, where cracks are allowed to open only in directions orthogonal to the existing cracks. These fixed orthogonal cracks are governed by the direction of the first principal (tensile) stress that exceeds the cracking strength. When a first crack occurs, it is assumed that direct tensile stresses cannot be supported in the direction normal to the crack and therefore, the modulus of elasticity corresponding to this direction (normal to crack) is reduced to zero unless tension stiffening is considered (section 6.3.2). The reduced shear stiffness due to aggregate interlock is accounted for by a reduced shear modulus of elasticity, G^* (section 6.4.1). On further loading, orthogonal cracks occur when the tensile stress parallel to the first cracks becomes greater than the concrete tensile strength f_t'.

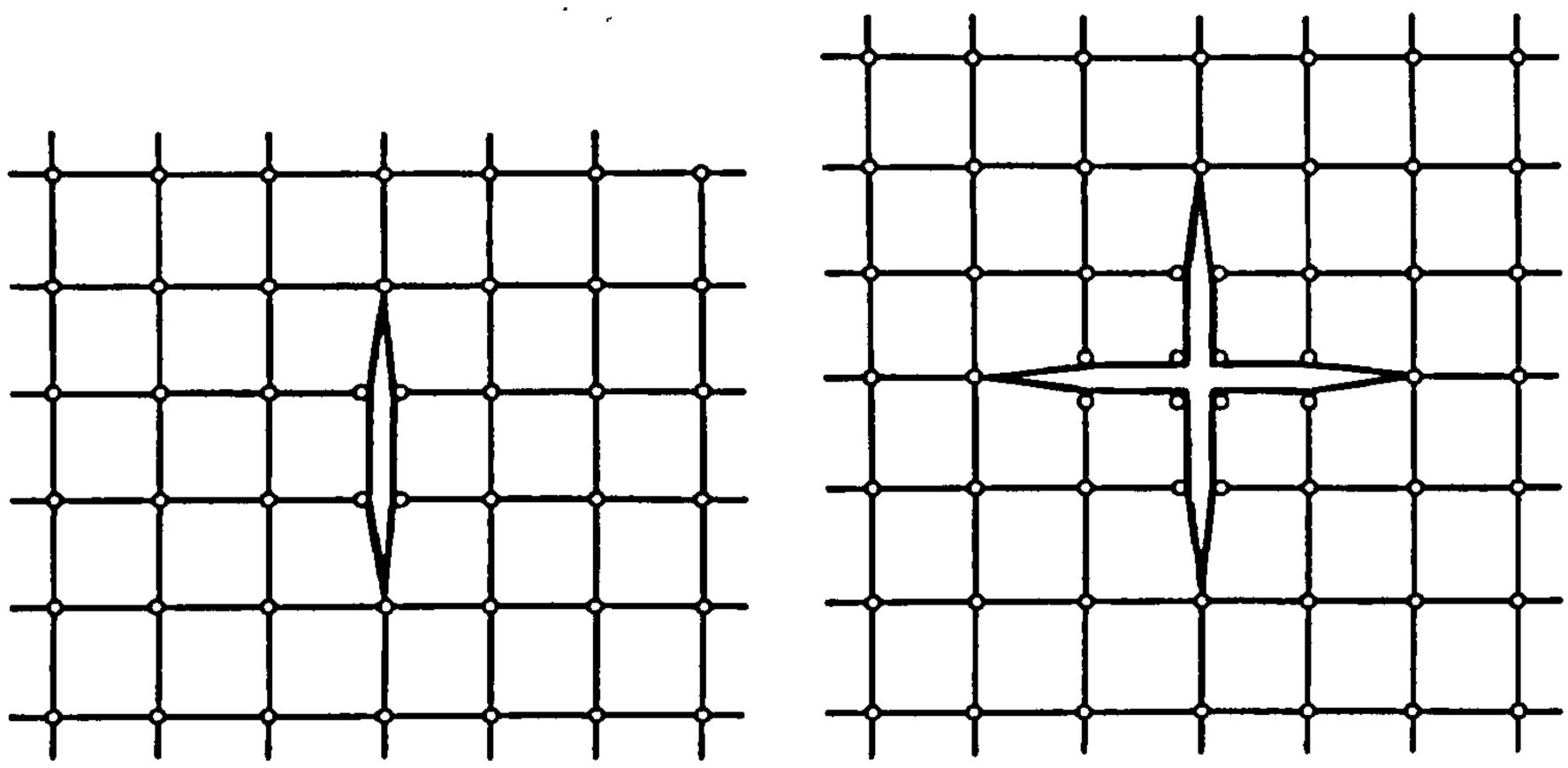

(a): One directional cracking (b): Two directional cracking

Fig. 6.19: Crack representation in discrete crack modelling approach

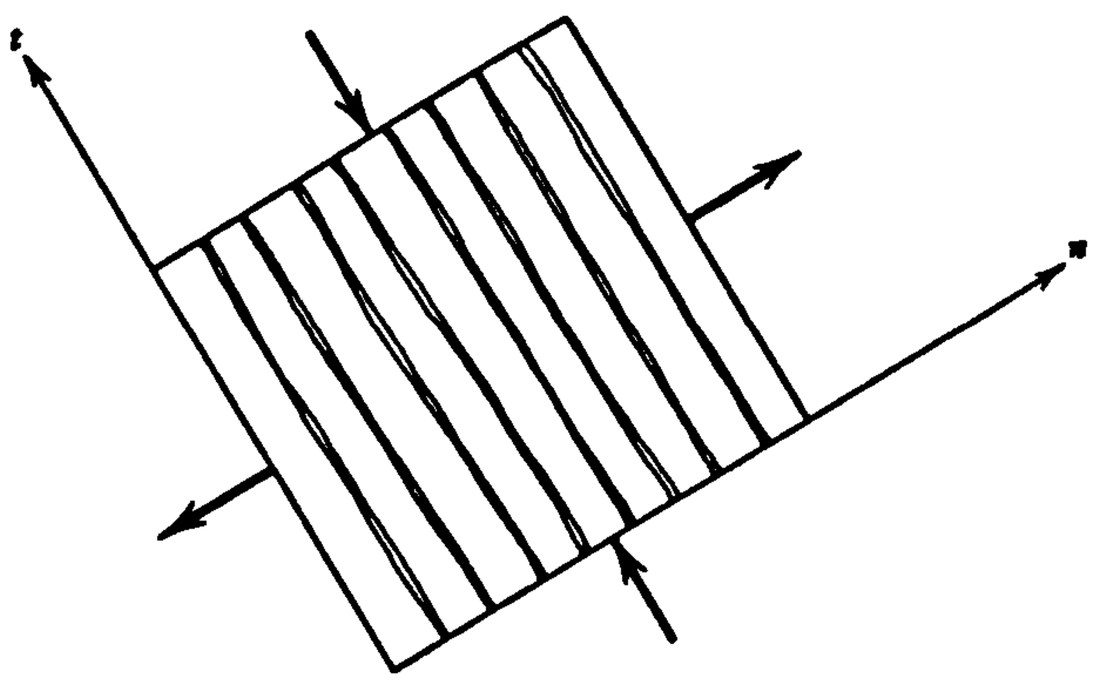

Fig. 6.20: Idealised representation of a single crack in the smeared cracking modelling approach

6.6: Concrete yield criterion

Because of the complexity of the reinforced concrete behaviour and its heterogeneous nature, it is difficult to completely describe its behaviour under all conditions. A large number of failure criteria have been proposed in the literature. One of them, for biaxial stress conditions based on experimental work of Kupfer et al. (1969) is discussed here. For triaxial state of stress Kotsovos and Newman (1979) introduced a constitutive equations used in 3-D finite element modelling. Kotsovos and Pavlovic (1995) developed a mathematical description of the ultimate strength envelope of concrete under axi-symetric stress states.

6.6.1: 2-D yield criterion

Figure 6.21 shows the failure curve in biaxial stresses. This curve was originally constructed by Kupfer et al. (1969) based on experimental results on three different concrete strengths. The three types of concrete behaved almost identically. This

curve is based on the non-dimensionalised values of the principal stresses σ_1 and σ_2 with respect to the uniaxial cylinder strength of the concrete f_c'.

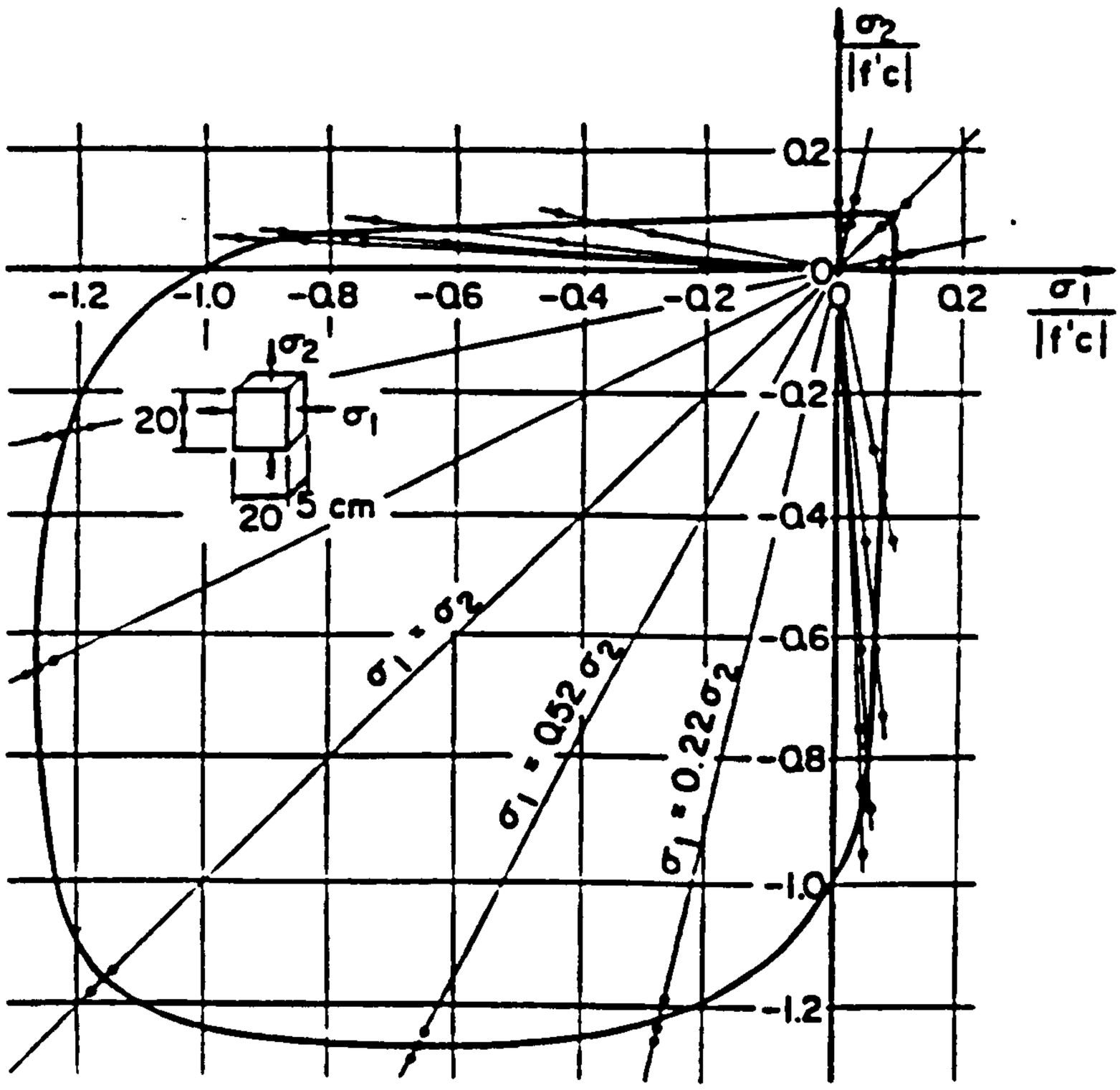

Fig. 6.21: Biaxial strength of concrete [Kupfer et al. (1969)]

The following points can be inferred from this curve:

- The ultimate strength of concrete under biaxial compression is greater than that under uniaxial compression. This is so because of the confinement of cracks. The concrete strength in this region is dependent on the ratio of the principal stresses (σ_1 / σ_2), and it appears that the maximum strength difference, 25%, is reached when the ratio is 0.52, decreasing to 16% as the ratio σ_1 / σ_2 increased to 1.0.
- The compressive strength decreases simultaneously with the increase of the tensile stress in the case of combined compression and tension stresses.
- The biaxial tensile strength of concrete is approximately equal to its uniaxial tensile strength, and the stress-strain curves are similar in shape in both uniaxial and biaxial tension.

6.6.1.1: Approximation of yield criteria

The general octahedral normal σ_{oct} and shear τ_{oct} stresses are given by the following equations:

$$\sigma_{oct} = \frac{\sigma_x + \sigma_y + \sigma_z}{3} \qquad 6.5$$

$$\tau_{oct} = \frac{1}{3}\sqrt{(\sigma_x - \sigma_y)^2 + (\sigma_y - \sigma_z)^2 + (\sigma_z - \sigma_x)^2 + 6(\tau_{xy}^2 + \tau_{yz}^2 + \tau_{zx}^2)} \qquad 6.6$$

For two dimensional stresses these equations reduce to:

$$\sigma_{oct} = \frac{\sigma_x + \sigma_y}{3} \qquad 6.7$$

$$\tau_{oct} = \frac{\sqrt{2}}{3}\sqrt{\sigma_x^2 + \sigma_y^2 - \sigma_x\sigma_y + 3\tau_{xy}^2} \qquad 6.8$$

From the investigations by Bresler and Pister (1958) , the relationship between octahedral normal stress σ_{oct} and octahedral shear stress τ_{oct} for 2-D stresses can be approximated to the form:

$$\tau_{oct} = a + b\sigma_{oct} \qquad 6.9$$

where σ_{oct} and τ_{oct} are as given in equations 6.7 and 6.8 respectively.

The factors a and b are determined using the boundary conditions as follows:

Compression yield

1. For uniaxial compression: $\sigma_y = \tau_{xy} = 0.0$ and failure occurs when $\sigma_x = -f_c'$.

Substituting into equations 6.7 and 6.8 leads to:

$$\sigma_{oct} = \frac{-f_c'}{3} \quad \text{and} \quad \tau_{oct} = \frac{\sqrt{2}}{3}f_c'$$

Thus equation 6.9 becomes:

$$\frac{\sqrt{2}}{3}f_c' = a - b\frac{f_c'}{3} \qquad 6.10$$

2. For biaxial compression:

For equal principal stresses, $\sigma_x = \sigma_y = -nf_c'$ and $\tau_{xy} = 0.0$

where $n = 1.16$

Substitution into equations 6.7 and 6.8 leads to:

$$\sigma_{oct} = -\frac{2}{3}(nf_c') \quad \text{and} \quad \tau_{oct} = \frac{\sqrt{2}}{3}(nf_c')$$

Thus equation (6.9) can be written as:

$$\frac{\sqrt{2}}{3}(nf_c^{'}) = a - \frac{2}{3}(nf_c^{'})b \qquad 6.11$$

Solving equations 6.10 and 6.11 for a and b we get:

$$a = \frac{\sqrt{2}f_c^{'}}{3}(1+\frac{n-1}{1-2n}) \text{ and } b = \frac{\sqrt{2}(n-1)}{1-2n}$$

Substituting into equation 6.11, the compression yield criterion is given as:

$$\frac{\tau_{oct}}{f_c^{'}} + \frac{\sqrt{2}(n-1)}{2n-1}\frac{\sigma_{oct}}{f_c^{'}} - \frac{\sqrt{2}}{3}\frac{n}{2n-1} = 0.0$$

when the value of $n = 1.16$ is substituted we get:

$$\frac{\tau_{oct}}{f_c^{'}} + 0.1714\frac{\sigma_{oct}}{f_c^{'}} - 0.4143 = 0.0 \qquad 6.12$$

Tension-compression yield

1. For uniaxial compression equation 6.10 applies.

2. For uniaxial tension $\sigma_y = \tau_{xy} = 0.0$ and failure occurs when $\sigma_x = f_t^{'} = mf_c^{'}$.

where $m = \frac{f_t^{'}}{f_c^{'}} = 0.1$

Substitution into equations 6.7 and 6.8 we get:

$$\sigma_{oct} = \frac{mf_c^{'}}{3} \text{ and } \tau_{oct} = \frac{\sqrt{2}}{3}mf_t^{'}$$

Thus equation 6.9 becomes:

$$\frac{\sqrt{2}}{3}mf_c^{'} = a + b\frac{mf_c^{'}}{3} \qquad 6.13$$

Solving equations 6.10 and 6.13 for a and b we get:

$$a = \frac{\sqrt{2}f_c^{'}}{3}(\frac{2m}{1+m}) \text{ and } b = \frac{\sqrt{2}(m-1)}{1+m}$$

Substituting into equation 6.13 we get:

$$\frac{\tau_{oct}}{f_c^{'}} + \frac{\sqrt{2}(1-m)}{(1+m)}\frac{\sigma_{oct}}{f_c^{'}} - \frac{2\sqrt{2}}{3}\frac{m}{(1+m)} = 0.0$$

Substituting the value of $m = 0.1$ we get:

$$\frac{\tau_{oct}}{f_c^{'}} + 1.1571\frac{\sigma_{oct}}{f_c^{'}} - 0.0857 = 0.0 \qquad 6.14$$

Tension-Tension yield

For biaxial tension the simple circular criterion is adopted because there is no significant change in the ultimate tensile strength due to biaxial tension:

$$\left(\frac{\sigma_1}{f_t'}\right)^2+\left(\frac{\sigma_2}{f_t'}\right)^2=1.0 \qquad 6.15$$

where σ_1 and σ_2 are the principal stresses.

6.6.1.2: Zoning of yield surfaces

The equations derived above define the 2-D failure surface for concrete in different state of stresses. However, well before this surface has been reached the concrete cracks and the non-linearity starts. To accommodate this behaviour into analysis, intermediate loading surfaces have been considered as shown in figure 6.22. In this figure the loading surface is divided into initial, subsequent and limiting yield surfaces. The initial yield surface ($\sigma = 0.5f_c'$) is regarded as the limit of elastic behaviour. For a state of stress within this yield surface, concrete is assumed to be linear and the linear elastic constitutive relations apply. When the state of stress goes beyond the initial yield surface, an intermediate concrete strength f_{cc} is calculated as in equation 6.16 [Johanry (1979) and Duncan and Johanry (1979)] for subsequent yielding surfaces (Fig. 6.23).

$$f_{cc} = f_{co} - f_t' + (E_c / E_i) f_t' \qquad 0.5f_c' < f_{cc} \le f_c' \qquad 6.16$$

where f_{cc} = the intermediate concrete strength, $f_{co} = 0.5f_c'$, f_t' = tensile strength of concrete, E_c = initial modulus of elasticity of concrete and E_i = instantaneous modulus of elasticity of concrete. The concrete instantaneous modulus is computed as in equation 6.17 and 6.18.

$$E_i = E_c(1-\varepsilon_i / 0.0025) \qquad \varepsilon_i \le 0.003 \qquad 6.17$$

$$E_i = 0 \qquad \varepsilon_i > 0.003 \qquad 6.18$$

Where ε_i is the instantaneous strain.

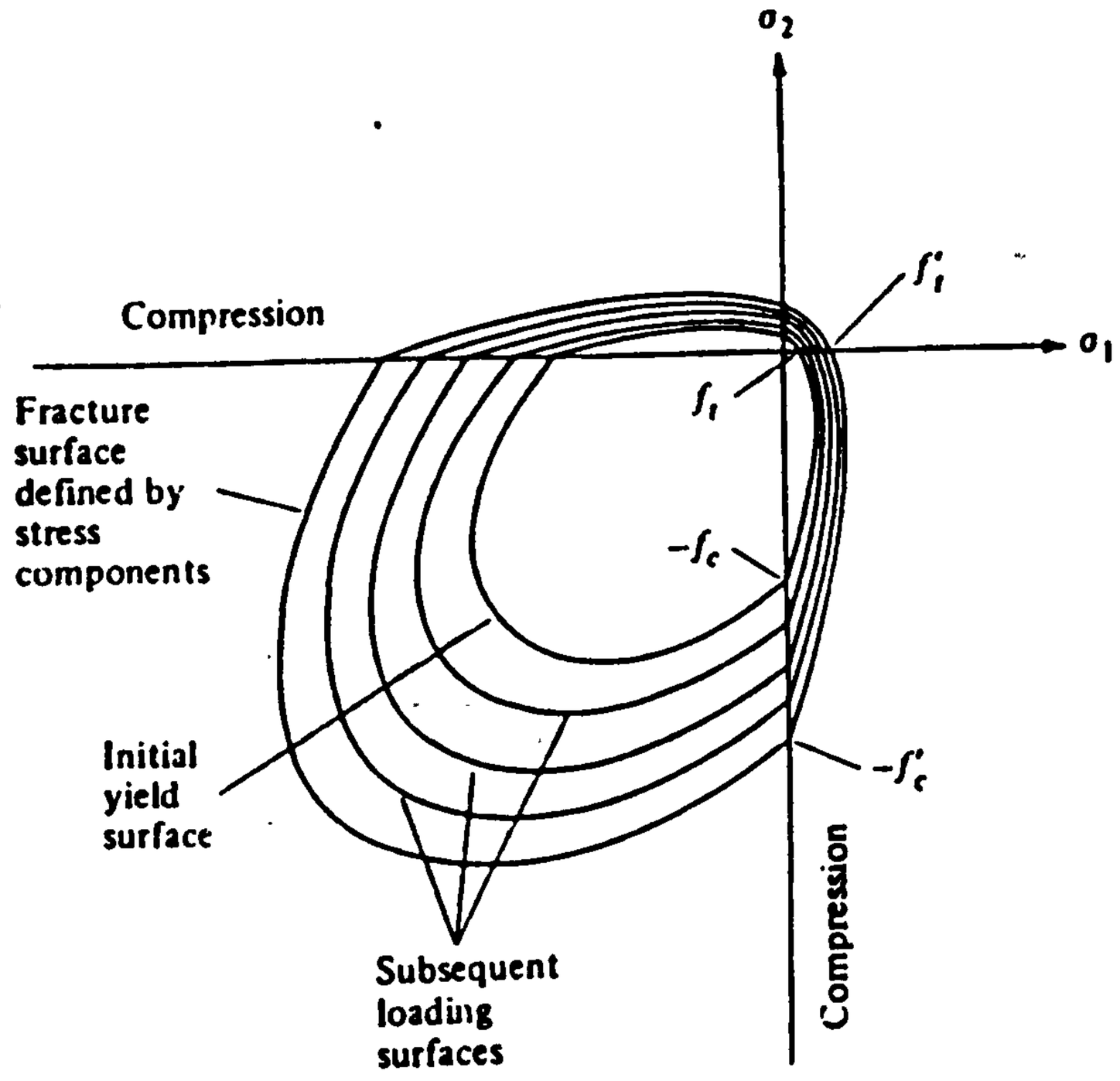

Fig. 6.22: Yield surface zones, initial, intermediate and failure envelop

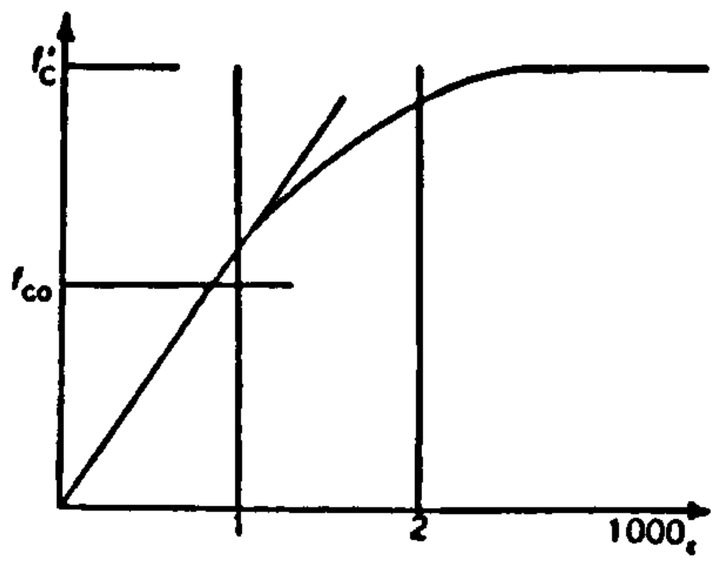

Fig. 6.23: Stress-strain curve for concrete [Duncan and Johanry (1979)]

6.7: Modelling of reinforcement

Modelling reinforcing steel is straight forward because the material behaviour is essentially uniaxial and well-known. There are three approaches to model the reinforcement in reinforced concrete: smeared model, discrete model and embedded model (Fig. 6.24).

6.7.1: Smeared model

In this model [Wegmuller (1974)] reinforcing steel is represented as an equivalent uniformly distributed steel layer. Each steel layer is assumed to resist stresses only in the direction of the original bar. This model is convenient for reinforced

concrete plate and shell structures, or where a large number of reinforcing bars is used.

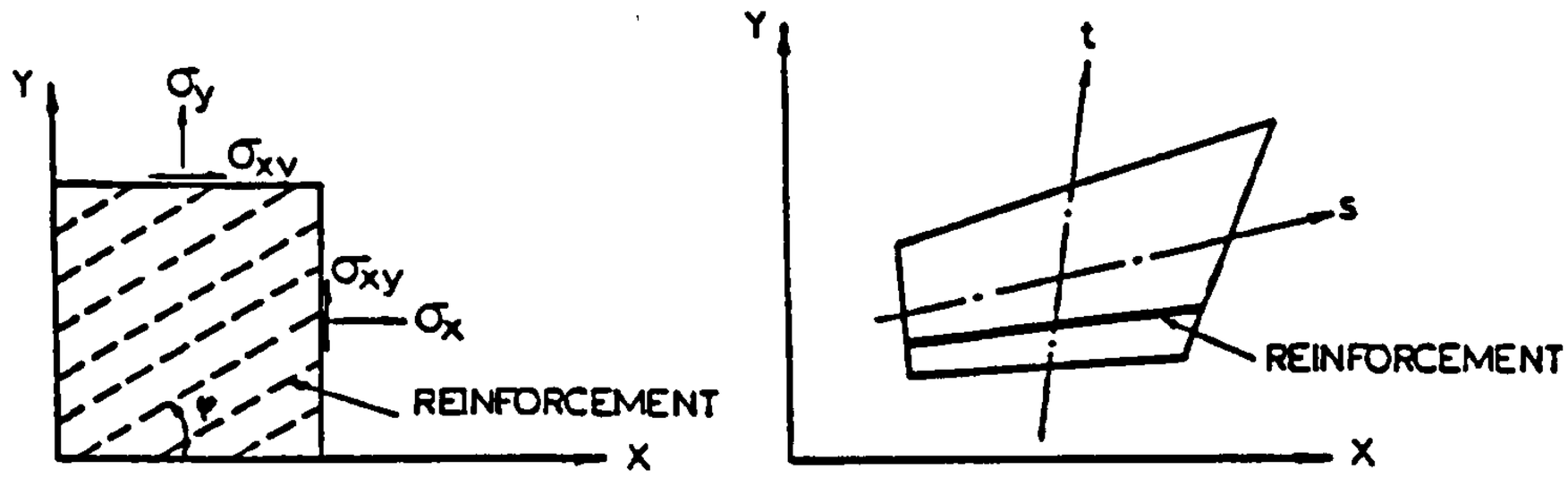

(a): smeared approach (b): Embedded bar

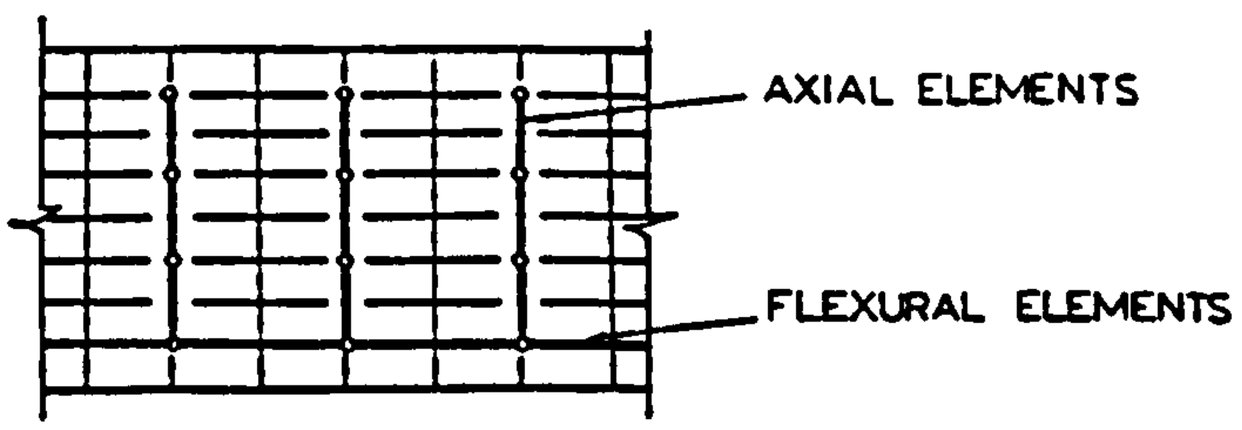

(C): Discrete representation

Fig. 6.24: Modelling of reinforcement

6.7.2: Discrete model

In this model reinforcing bar is represented by one-dimensional axial force element in the direction of the bar. The element is pin connected to the concrete two dimensional element nodal points with two degrees of freedom. The disadvantage of this model is that the finite element mesh is restricted by the locations of the bars which leads to an increase in the size of the stiffness matrix. For more information on this model see Cedolin and Poli (1977) , Ngo and Scordelis (1967) and El-Mezaini and Citipitioglu (1991).

6.7.3: Embedded model

In this model steel is idealised as a line element built into the finite element model such that its displacements are consistent (compatible) with those of the concrete element. The bar can be aligned with the concrete element axis [Phillips and Zienkiewcz (1976)] or inclined [Ranjbaran (1991)]. Also, it can account for bond-slip and arbitrarily oriented embedded reinforcing layers [Chang et al. (1987)].

The advantage of using the embedded model is that there is no limitation for representing the locations or distribution of reinforcement. The contribution of the

reinforcement to the element stiffness can be evaluated independently for each steel bar and added to the concrete stiffness.

In this study this model was used and reinforcing bars were oriented in the x and/or y axes.

6.8: Interaction between concrete and reinforcement

6.8.1: Bond-slip

The bond between concrete and reinforcing bars allows forces to be transferred between the two materials. It results from chemical adhesion, friction and mechanical interaction between concrete and reinforcement. The stronger the bond the larger the transferred force. Bond is influenced by concrete strength, embedment length, concrete cover, bar spacing and bar deformation or lugs. Figure 6.25 shows primary and secondary cracks in reinforced concrete tension member.

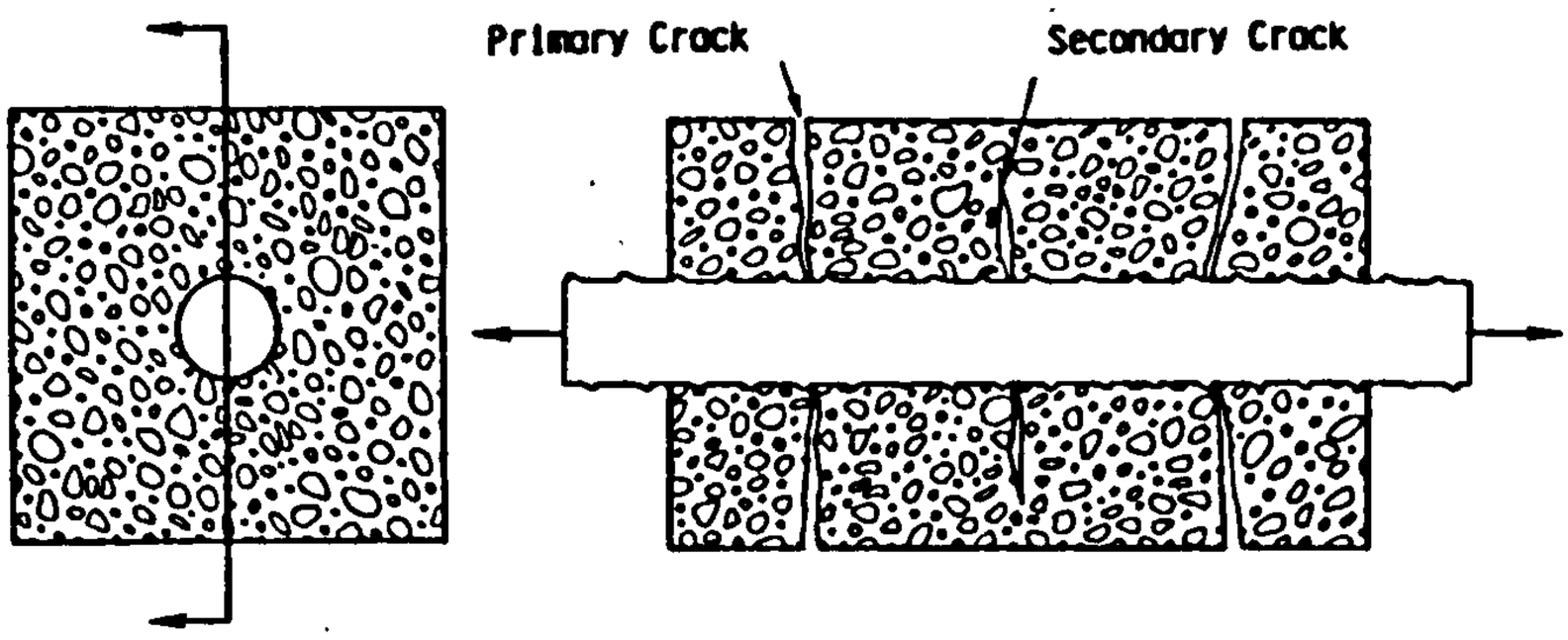

Fig. 6.25: Cracking of concrete

The primary cracks are widest at the surface and narrowest at the surface of reinforcing bar. The deformation of the reinforcing bar tends to control the crack width by limiting the slip between concrete and steel. The secondary cracks increase in width with distance away from the reinforcement before narrowing and closing prior to reaching the concrete surface. Fu and Chung (1998) studied the effects of water-cement ratio, curing age, silica fume, polymer admixtures, steel surface treatments, and corrosion on bond between concrete and steel reinforcing bars. They used electromechanical pull-out testing that involved measuring the shear bond strength and contact electrical resistivity. Polak and Blackwell (1998) assumed that, the bond is mainly due to bearing of concrete on the reinforcing bar lugs and, therefore, their model ignores other factors like the chemical adhesion, friction

and mechanical interlock between the bar and concrete. They divided the member cross-section into concrete and steel layers. As the reinforcing bar undergoes tensile strain, its perimeter decreases due to Poisson effect. Therefore, both the cross-sectional area of the reinforcing bar and the outer perimeter of lugs decrease. This leads to reduction in the contact between the concrete and the bar (Fig. 6.26). Salem and Maekawa (1997) assumed that the bond is maximum midway between cracks, decreases linearly towards the cracks and drops to zero at a distance 2.5 times bar diameter from the crack surface due to splitting and crushing of concrete around the bar near the crack surface.

In this study a full bond between concrete and steel is assumed.

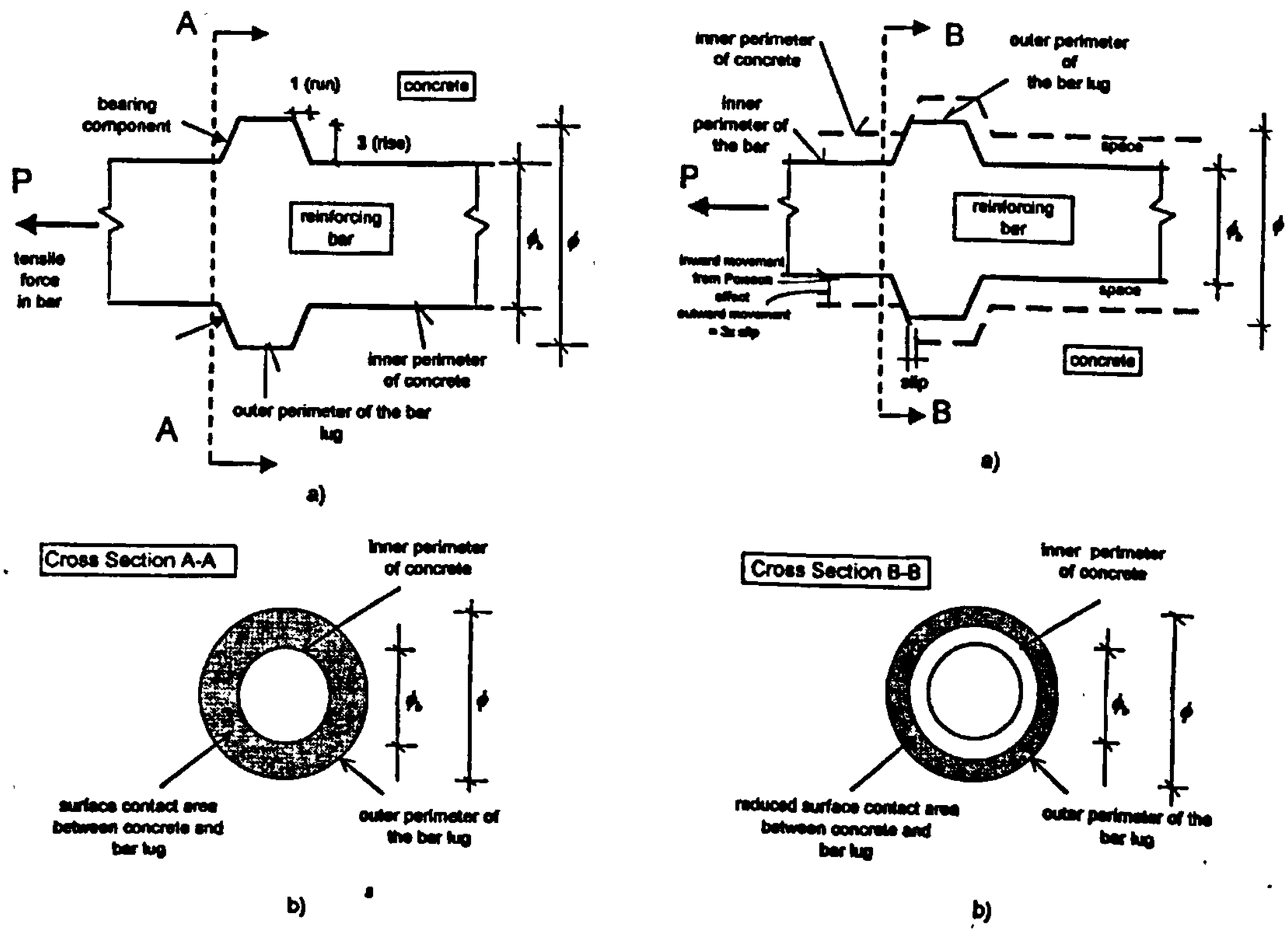

Fig. 6.26: (a): Reinforcing bar and concrete geometry before cracking, (b): Contact area between concrete and reinforcement after cracking, (c): Reinforcing bar and concrete geometry after cracking, (d): Contact area between concrete and reinforcement after cracking

6.8.2: Dowel action

Reinforcing bars crossing shear cracks are subject to concentrated shear forces. These bars act as dowels and play a major role in resisting the shear forces, especially when the resistance from the aggregate interlock has diminished due to crack opening (Fig. 6.27). Dowel action resistance may account for 30 percent of

the applied shear force [Kemp (1986)]. The dowel force capacity of a member is increased significantly by increasing the clear cover and the amount of stirrups. The bigger the cover the less chance of spalling of concrete which leads to a larger stress transfer to concrete. Also, large number of stirrups restrain the concrete against splitting and thus increase the ultimate bond stress. However, contradicting results were reported by Jelic et al. (1999) who concluded that the bar size plays no role in the beam ultimate shear capacity and that the dowel action cannot be considered as a viable component in the shear mechanism of cracked reinforced concrete section. The dowel action of steel is not considered in this study because it happens at very late stages of loading. Another reason for this is to avoid two dimensional representation of steel bar.

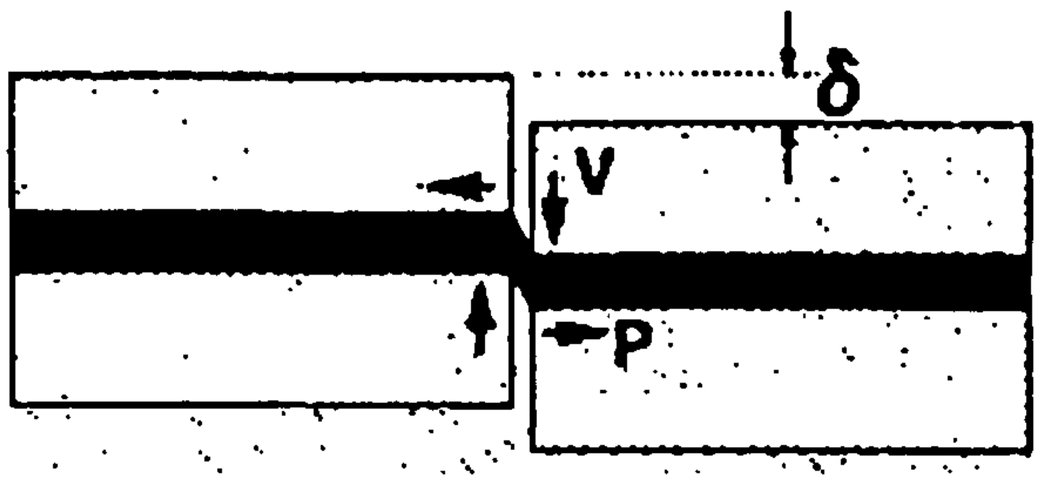

Fig. 6.27: Dowel action and kinking of steel bar

6.8.3: Kinking of steel bars

In the presence of shear, steel bars crossing the tensile cracks are often subjected to kinking due to perpendicular displacement to the axis of the bar (Fig. 6.27). This is in addition to the tension caused by crack opening. The bar at the crack interface is subjected to general condition of coupled axial pullout and transverse displacement. The local bending of a steel bar causes further damage of bond between concrete and steel increasing the yield zone of the bar at the crack. This longer yield zone contributes additional deformation to the average elongation of a steel bar. These effects lower the average stress-strain curve than the bare bar. Pang and Hsu (1995) found that, due to kinking of steel bars in concrete shear panels, the yield stress of the steel bar is significantly lower than the yield strength of the bare bar and that the post-yield branch lies significantly below the strain hardening curve of a bare bar. They proposed a bilinear stress-strain relationship as shown in figure 6.28. This is in contrary to the case where the bar is subjected to pure axial load (no transverse

displacement) in which it follows the bare bar stress-strain relationship. Similar findings were reported by Maekawa and Qureshi (1996) while testing beams subjected to a pure shear loading. In addition they found that the maximum strain in the bar occurs within the concrete at a location depending on the bar diameter, typically two times the bar diameter from the crack surface (Fig. 6.29).

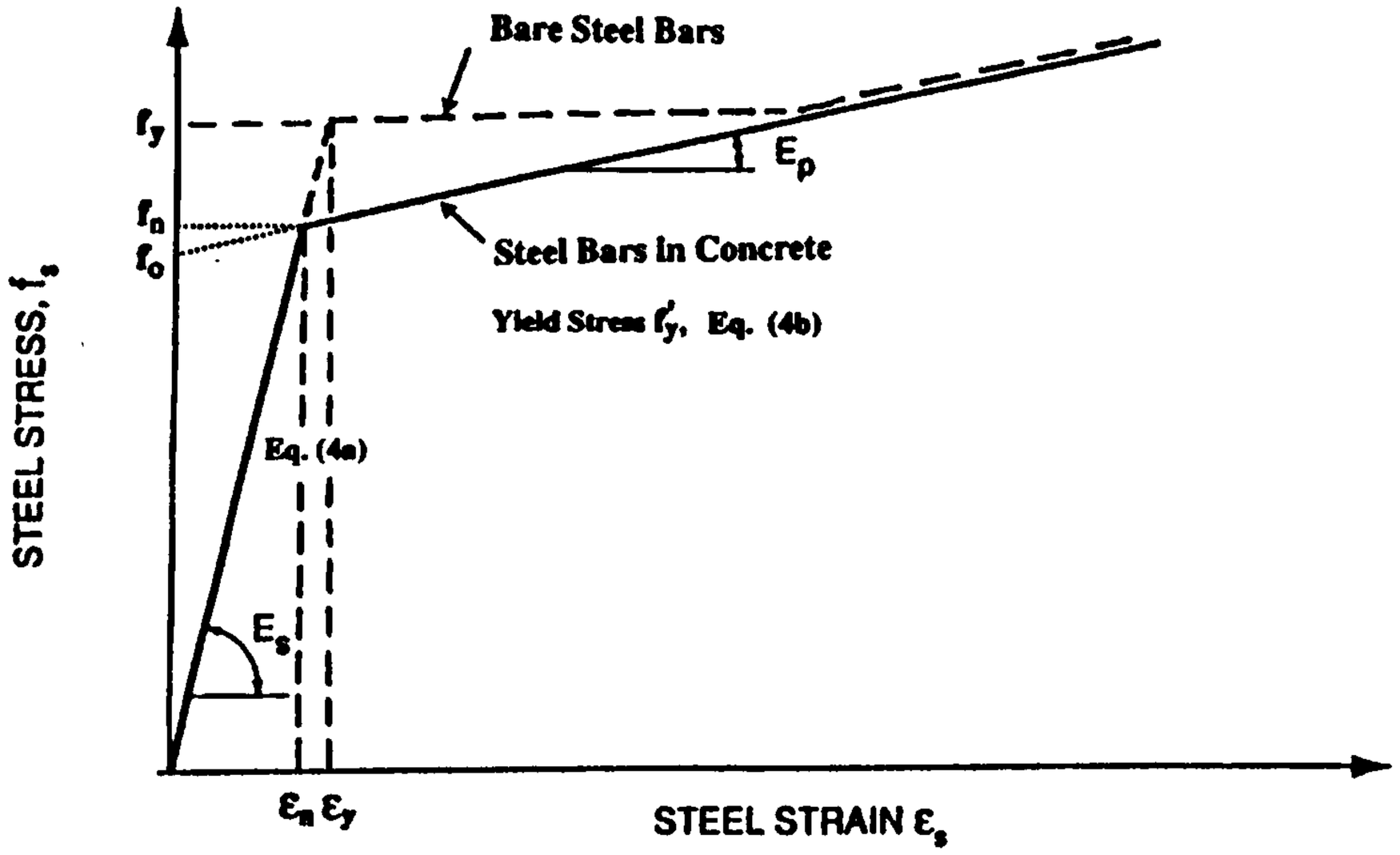

Fig. 6.28: Average stress-strain curves of mild steel bars using bilinear model [Pang and Hsu (1995)]

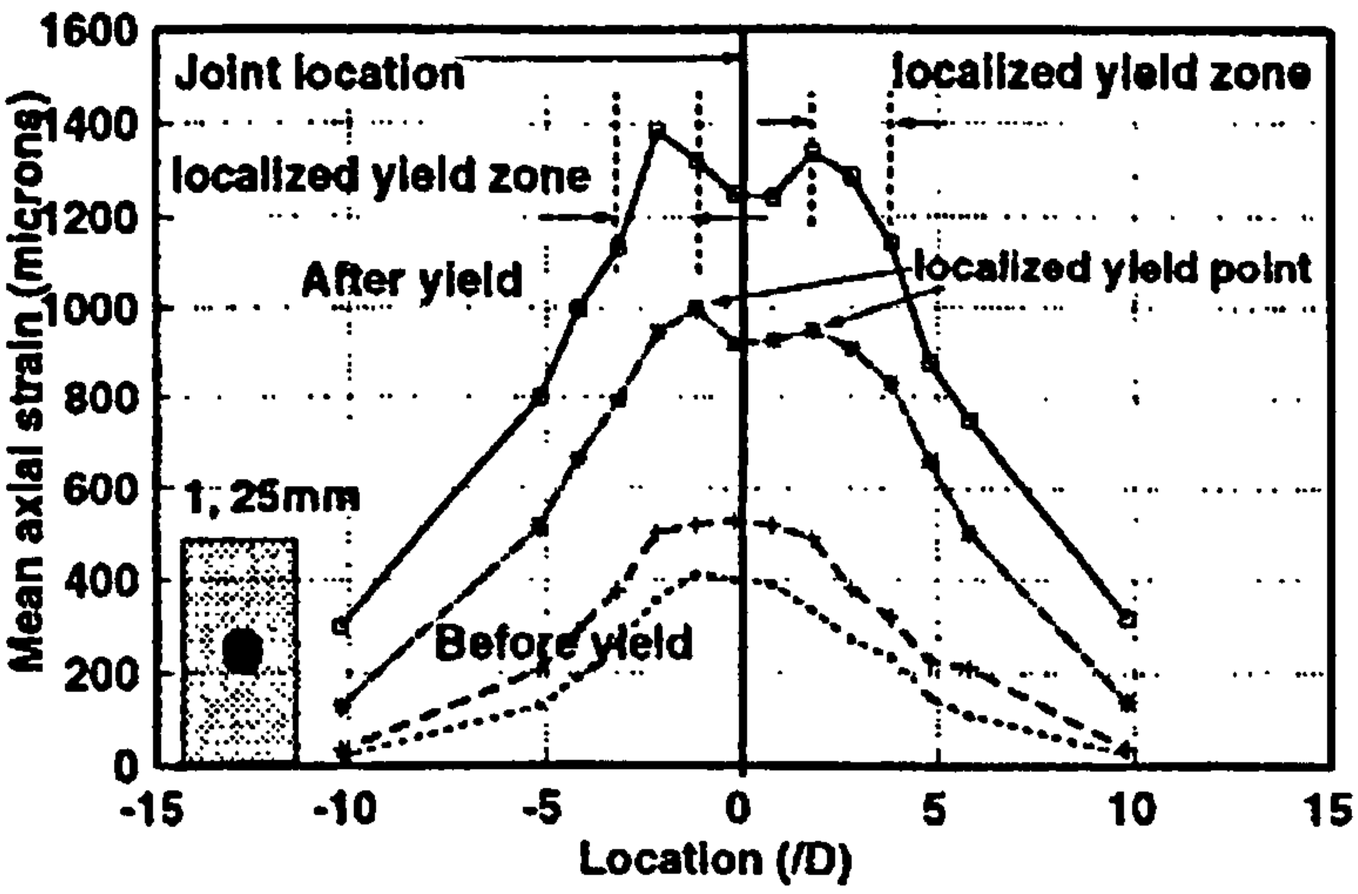

Fig. 6.29: Stress in steel bar around a vertical crack [Maekawa and Qureshi (1996)]

7: Modelling of hollow beams and 2-D finite element program

7.1: Introduction

In this chapter an in-house finite element program, originally developed for carrying out non-linear 2-D analysis [Abdel-Kader (1993)], used for the analysis of hollow beams is described. The method of ensuring compatibility between the plates using two dimensional model to analyse this type of structures is discussed. This program is used in a parametric study reported in chapter 8 to develop a finite element model which is used for the analysis of hollow beams tested in this research (Chapter 9). A brief review of the finite element displacement method is also presented.

7.2: Modelling of hollow beams

Figure 7.1 shows a typical rectangular hollow concrete beam. The biaxial state of stress that each plate is subjected to due to combined loading was discussed in section 3.7.1 of chapter 3.

7.2.1: Idealisation of the problem

Considering the complex behaviour of hollow beams, a detailed analysis would normally require a full three dimensional finite element model. However, a study of the structural behaviour of thin-walled concrete beams indicates that the main stress conditions are those of direct stresses in the plates of the box girder. The forces involved in out-of-plane bending are very small and can be ignored. The distortion of cross-section is prevented by the use of reasonably thick plates and diaphragms. This suggests that the main stresses are in-plane ones and, therefore, a plane stress element can be used to account for the major stresses. A zero stiffness is assumed for out-of-plane bending action of the component plates. Figure 3.11, which is repeated here for convenience, shows the state of stress in a box beam subjected to bending, torsion and shear. Figure 7.2 shows the plane stress element with two degrees of freedom per node which can be used in 2-D finite element modelling. The advantage of this approach over a full three-dimensional finite element solution is that it leads to cheaper computations while at the same time the main stresses are obtained with reasonable accuracy. This was proved later in chapter nine when the results were compared with tested beams.

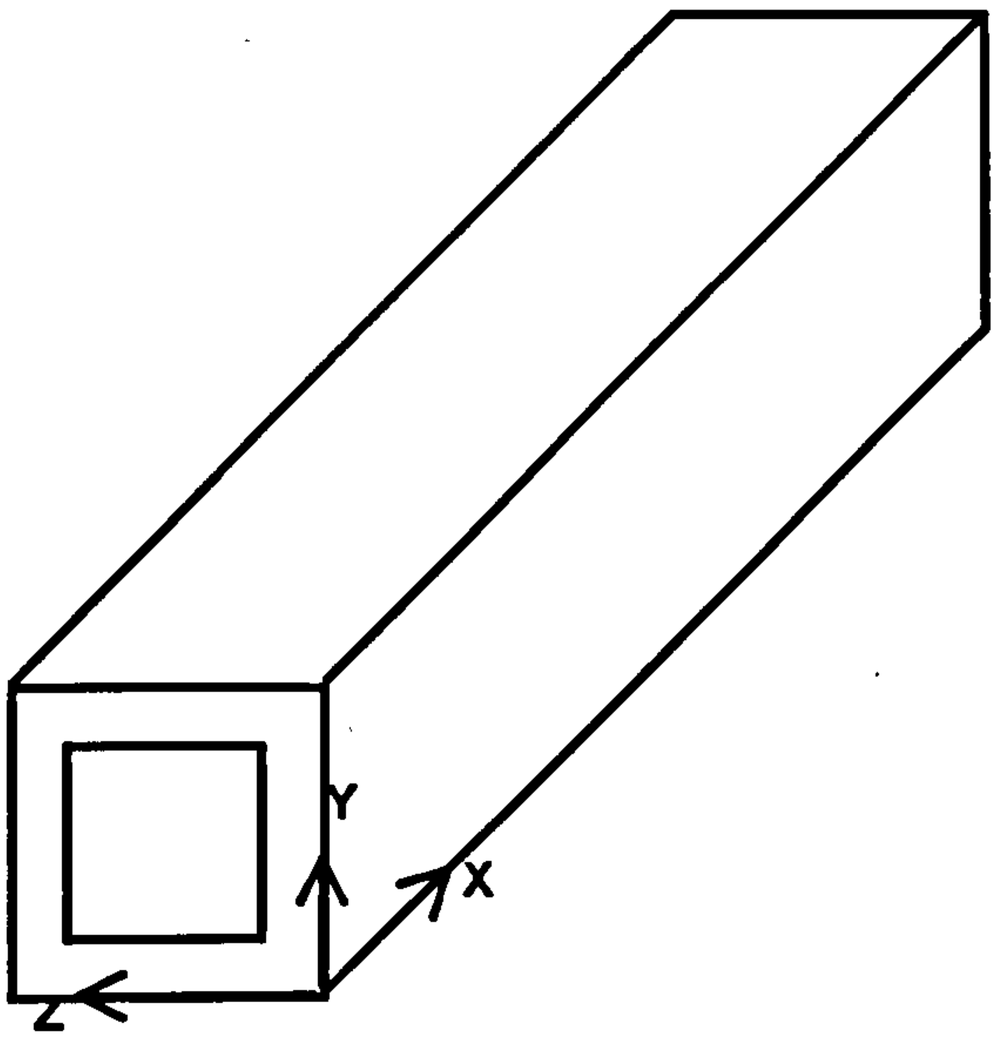

Fig. 7.1: Typical hollow beam used in this research

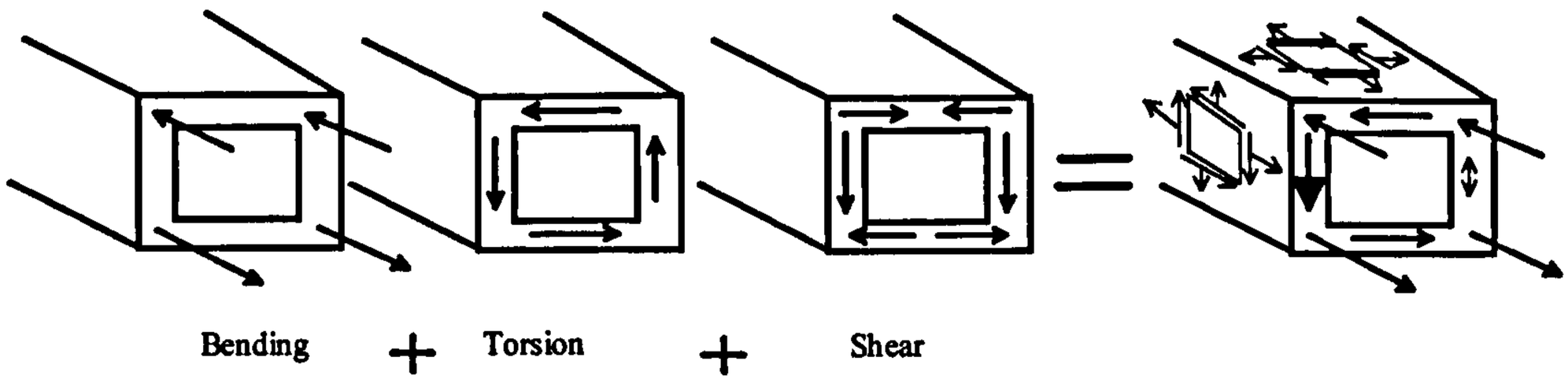

Fig. 3.11: State of stress in a typical beam

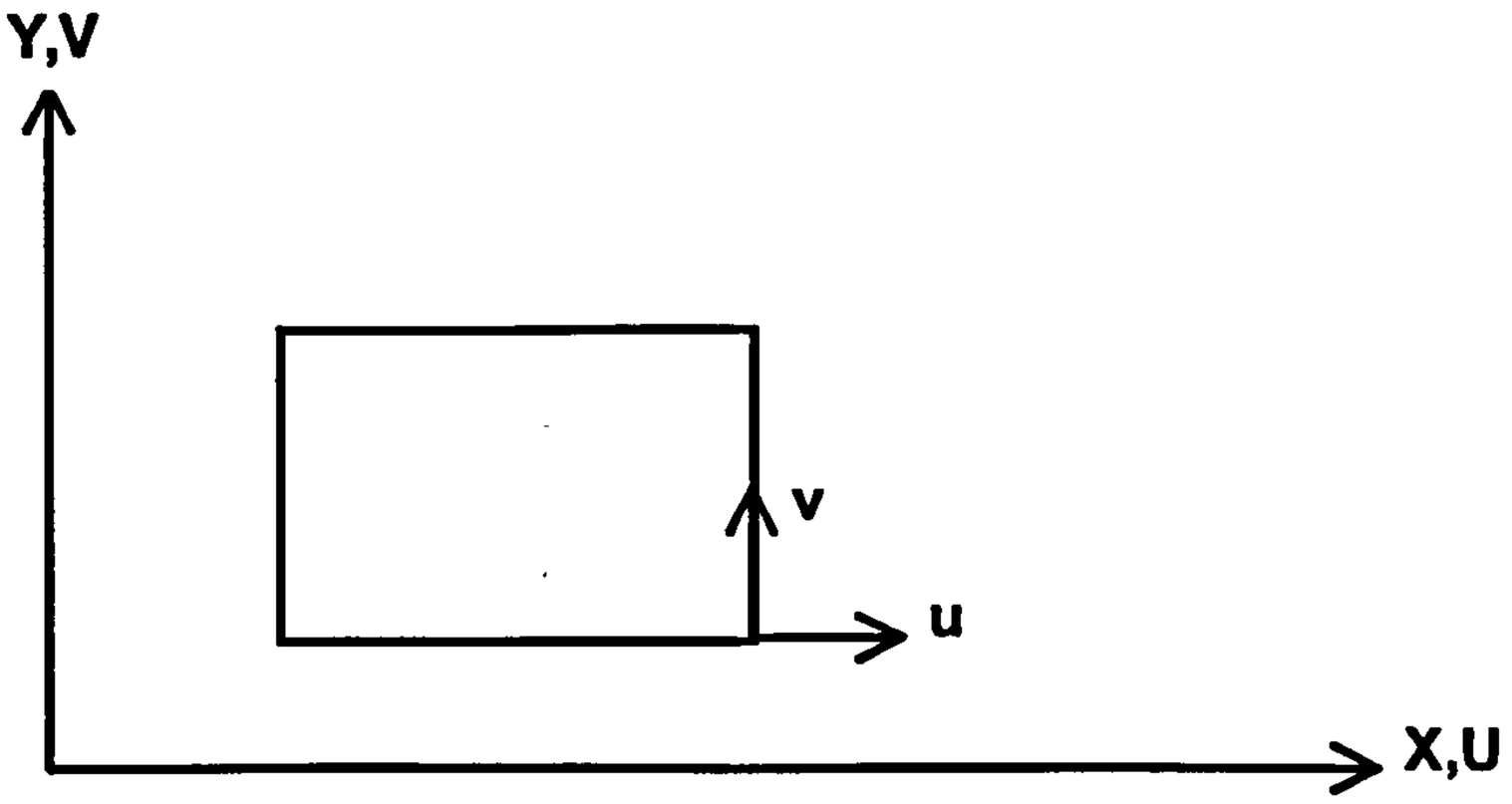

Fig. 7.2: Simplified plane stress element

7.2.2: Geometrical relationship between displacements

The two-dimensional idealisation of box girders is adequate provided compatibility of displacement between adjoining plates along the line of intersection is maintained and cross-sectional distortion is reduced to a minimum. To achieve these objectives, the following steps were adopted as shown in figure 7.3:

1. To ensure shear transfer between adjoining plates of the beam, compatibility of displacement along the line of intersection at the common edge of adjoining plates is maintained by introducing geometrical constraints.
2. To reduce cross-sectional distortion, end diaphragms are introduced into the analysis.

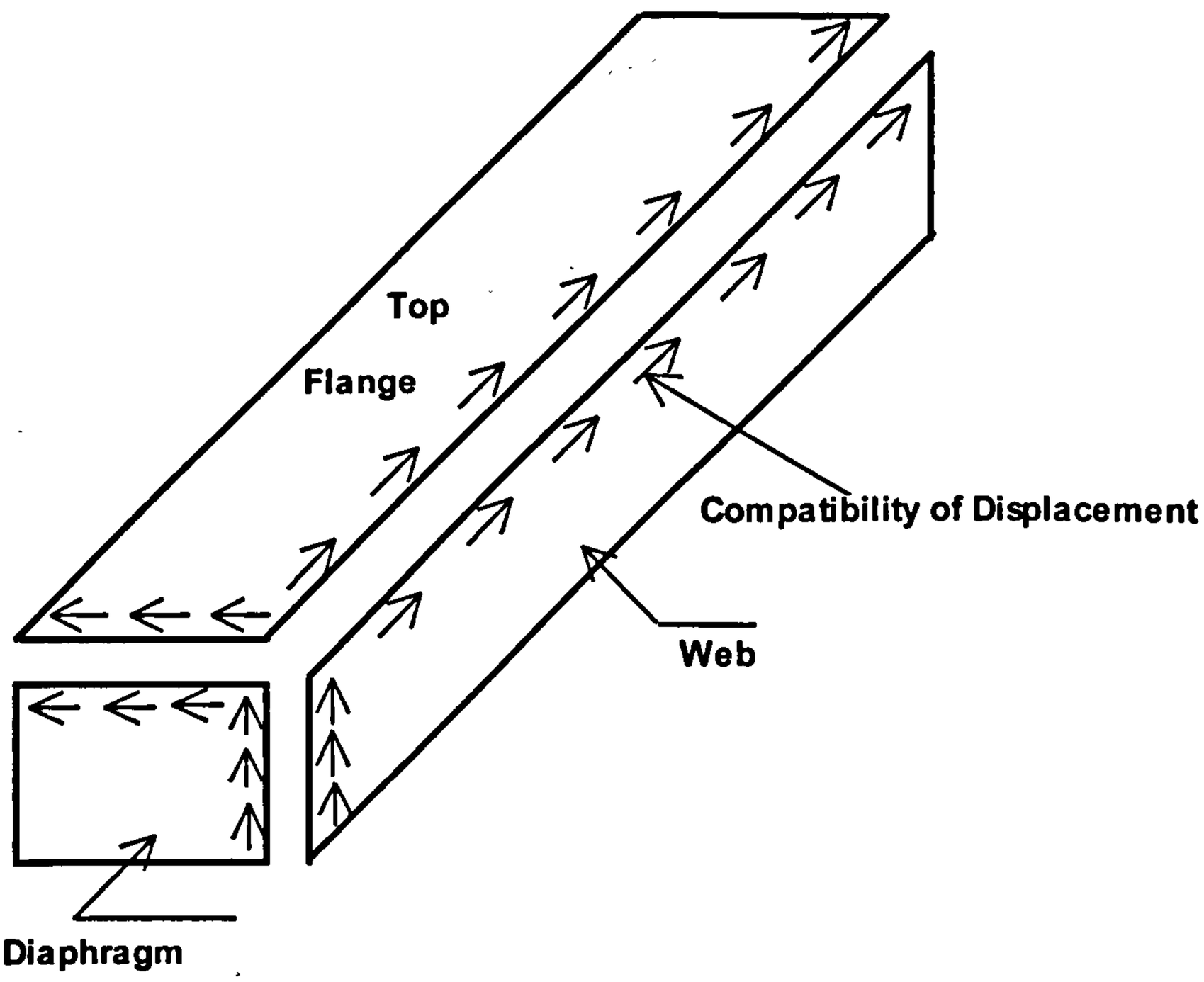

Fig. 7.3: Imposed displacement constraint

To illustrate this technique, consider top flange, front web and left diaphragm of a typical beam as shown in figure 7.4. For ease, only some element corner nodes are shown in this illustration.

If the out-of-plane bending is ignored, then the web and the flange can be considered as thin plates in a state of plane stress. However, the displacements of both plates along the joining line are equal to each other. The displacements perpendicular to the joining line are independent of each other. The same applies to the lines joining the plates with the diaphragm. It is therefore, necessary in this analysis to enforce geometrical constraints to ensure compatibility along the lines of intersections. This is done by giving the same freedom number for those equal displacements. Other freedoms which are independent are given different numbers.

In other words, every pair of displacements in the x-direction (direction of the beam axis) of the joining line between the flange and the web will be having the same freedom number and, therefore, the same displacement value for that pair. The displacements perpendicular to this line will have different numbers.

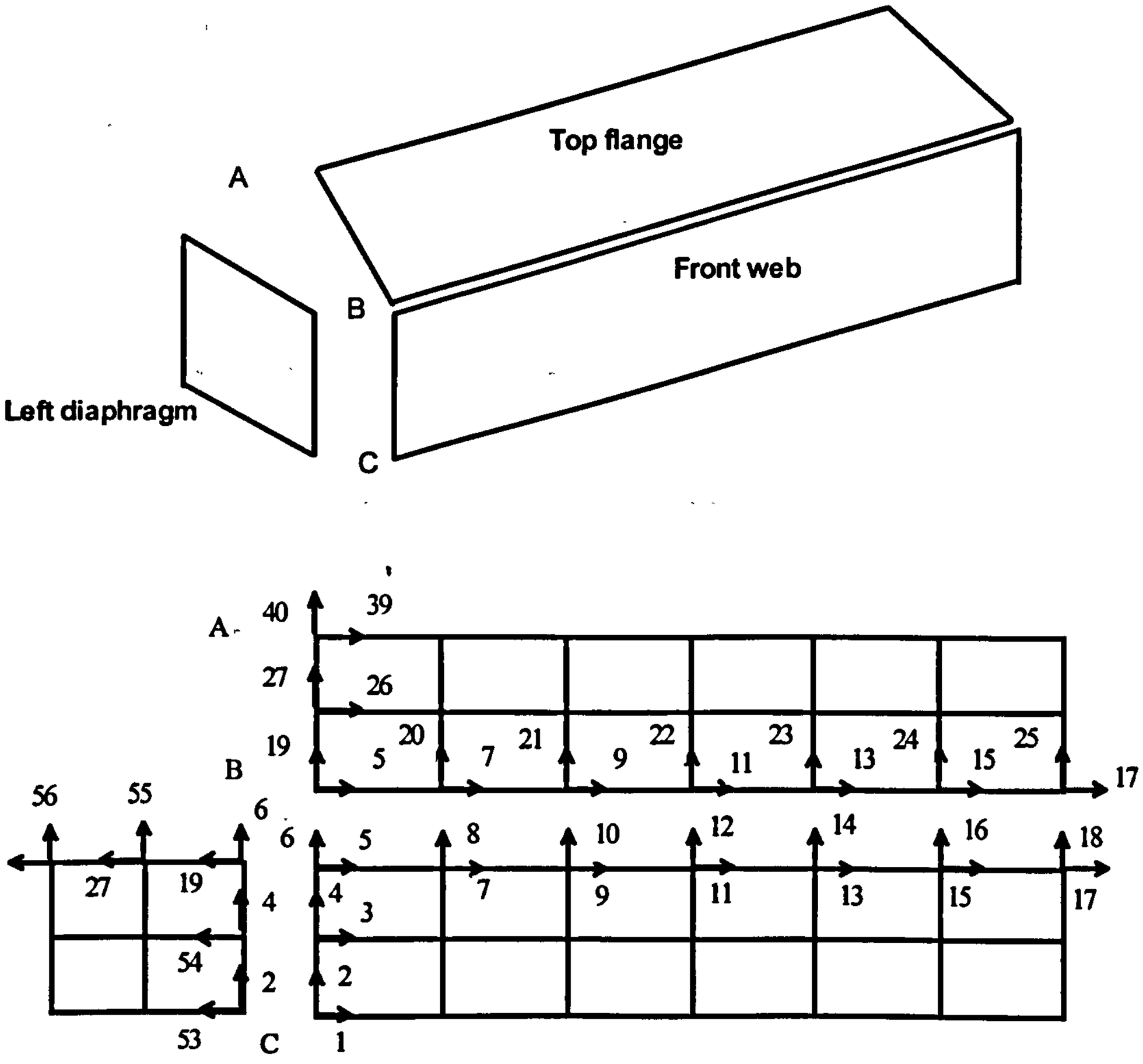

Fig. 7.4: Freedom constraints

In addition to the freedom numbering, attention should be given to plate orientation when the whole structure is assembled, to prevent contradicting directions of displacements. This is best done by selecting a 3-D axis system for the whole structure and expressing the local co-ordinates of each plate in such a way that it is compatible. So when all plates are put together they make sense in representing the actual structure. An example of this is shown in figure 7.5. In this figure only local co-ordinates are used and the plate origins are where the arrows intersect. The displacements on the intersection line along x-axis of a flange are equal to the displacements along the x-axis of a web. On the line intersecting the web and the

diaphragm, the y-axis displacements of a web are equal to the y-axis displacements of diaphragm. On the line intersecting the flange and the diaphragm, the y-axis displacements of a flange are equal to x-axis displacements of a diaphragm. The rigid body movement is prevented by a proper restraints which are dependent on the load conditions and support locations.

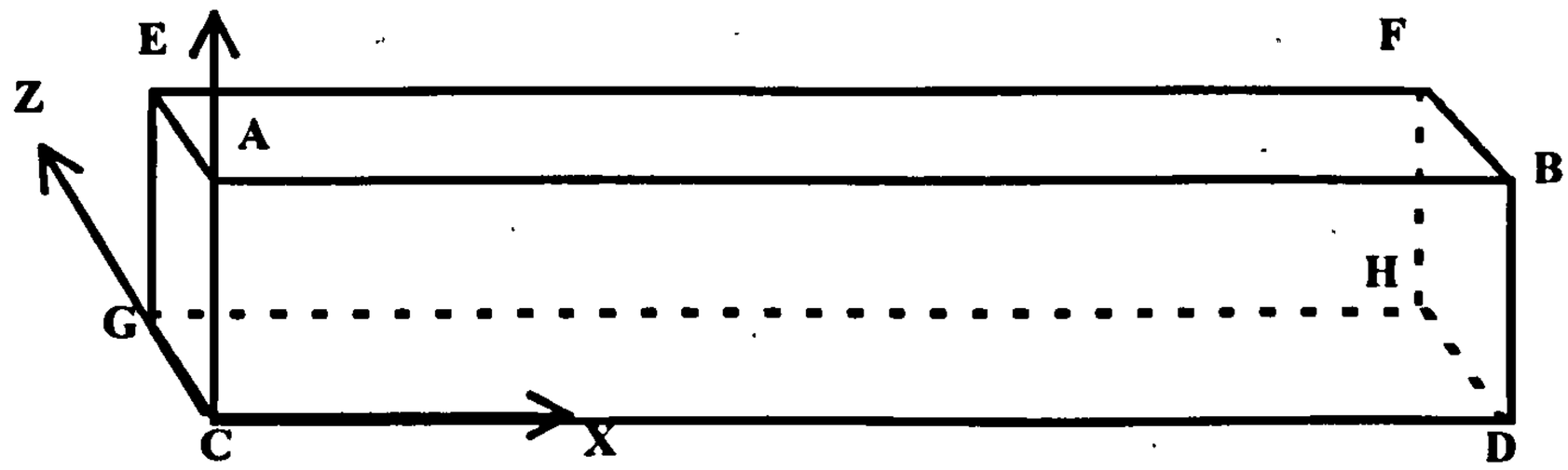

(a): 3-D co-ordinate system

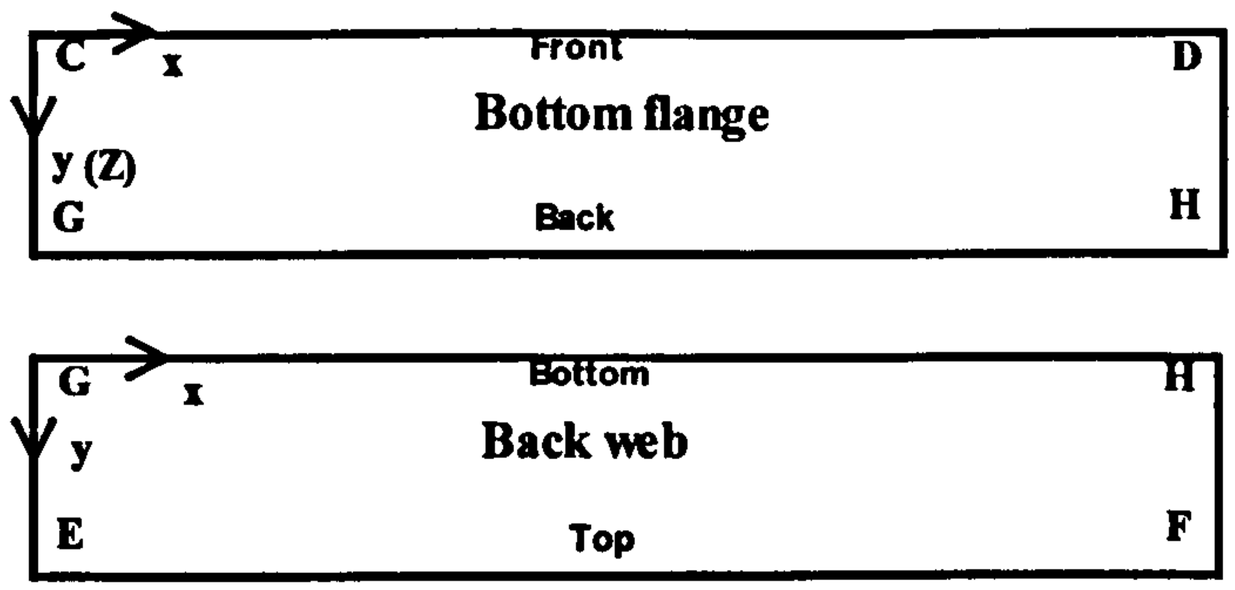

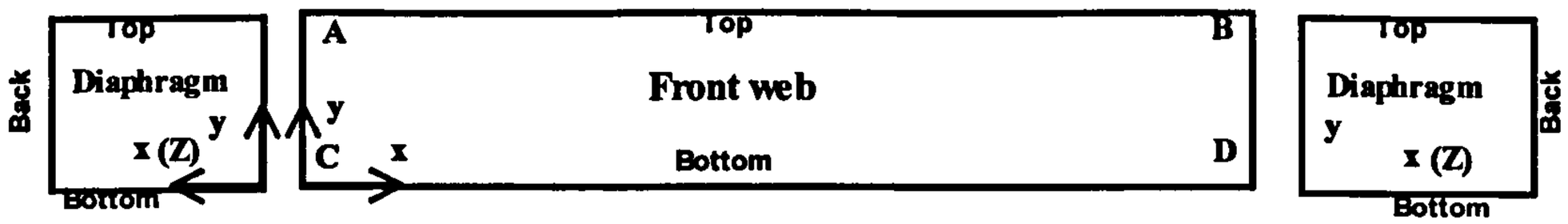

(b): Plate orientation using local co-ordinates

Fig. 7.5: Hollow beam idealisation

7.3: Finite element method

In this section a brief review of the finite element displacement method (the displacements are the prime unknowns, with the stresses being determined from the calculated displacement field) is presented. Detailed information about the finite element method and its applications can be found in the literature [e.g. Bathe

(1982), Hinton and Owen (1986), Hinton and Owen (1989), Zienkiewicz and Taylor (1989), MacLeod (1990) and Kotsovos and Pavlovic (1995)].

7.3.1: Concept and formulation

The differential equations governing the solution of elastic stress problems are linear. However, for the plastic stress problems the solution is non-linear and involves the solving of a series of linear problems.

In the finite element method the non-linear problems are solved satisfying the basic laws of continuum mechanics, equilibrium, compatibility and constitutive relationship of materials. For this purpose the continuum (structure) is divided into a series of distinct non-overlapping regions known as elements. These elements are connected at a finite number of points along their periphery known as nodal points. Within the element, there are points at which functions are calculated for integration purposes (Gauss Points). The shape of the element, the number of the nodal points and the Gauss points are arbitrary. To ensure adequate convergence to the exact solutions, in finite element displacement models, continuity of displacement between adjoining elements should be satisfied. Further, material constitutive relation must be maintained as well as preserving equilibrium in the structure. This can be achieved by ensuring that at any load level, stresses are consistent with displacement field and material constitutive relationship. This is generally obtained by successive linear solutions until specified accuracy is reached. If the material is within the elastic region, the relationship between the nodal forces and the displacement is linear and the stiffness matrix is un-changed. However, if the material yields then the relationship is non-linear and the stiffness matrix has to be updated. This is done by a succession of linear approximations considering the new material law. These piece-wise linearisations are used to form a global non-linear solution for the problem.

7.3.2: Discretisation by finite elements

The numerical solution to any problem is attempted by assuming that the behaviour of the continuum can be represented by a finite number of unknowns. For structural applications, the governing equilibrium equations can be obtained by minimising the total potential Π of the system which can be expressed as:

$$\Pi = \frac{1}{2}\int_V [\sigma]^T \{\varepsilon\} dV - \int_V [\delta]^T \{p\} dV - \int_S [\delta]^T \{q\} ds \qquad 7.1$$

where σ and ε are the stress and strain vectors respectively, δ is the displacements at any point, p is the body force per unit volume and q is the applied surface tractions. Integrations are taken over the volume V of the structure and loaded surface area S. The first term on the right hand side of equation 7.1 represents the internal strain energy and the other terms are the work contributions of the external forces p and q respectively.

In the finite element displacement method, the displacement is assumed to have unknown values only at the nodal points, so that the variation within any element is described in terms of the nodal values by means of interpolation functions. Thus:

$$\{\delta\} = [N]\{\delta^e\} \qquad 7.2$$

where N is the vector of interpolation functions termed as shape functions, and δ^e is the vector of nodal displacements of the element. The strains within the element can be expressed in terms of the element nodal displacement as:

$$\{\varepsilon\} = [B]\{\delta^e\} \qquad 7.3$$

where B is the strain matrix generally composed of derivatives of shape functions. The stresses σ may be related to the strains ε by the use of the elasticity matrix D as:

$$\{\sigma\} = [D]\{\varepsilon\} \qquad 7.4$$

The total potential of the continuum will be the sum of the energy contributions of the individual elements. Thus:

$$\Pi = \sum \Pi_e \qquad 7.5$$

where Π_e represents the total potential of an element e. By using equation 7.1, Π_e can be written as follows:

$$\Pi_e = \frac{1}{2}\int_{V_e} \{\delta^e\}^T [B]^T [D][B]\{\delta^e\} dV - \int_{V_e} \{\delta^e\}^T [N]^T \{p\} dV - \int_{S_e} \{\delta^e\}^T [N]^T \{q\} dS \quad 7.6$$

where V_e is the element volume and S_e is the loaded element surface area.

7.3.3: Element stiffness matrix

The performance of the minimisation for element e with respect to the nodal displacement δ^e of the element results in:

$$\frac{\partial \Pi_e}{\partial \delta^e} = \int_{V_e} [B]^T [D][B]\{\delta^e\} dV - \int_{V_e} [N]^T \{p\} dV - \int_{S_e} [N]^T \{q\} dS$$

$$= [K^e]\{\delta^e\} - \{F^e\} \qquad 7.7$$

where: $\{F^e\} = \int_{V_e} [N]^T \{p\} dV + \int_{S_e} [N]^T \{q\} dS$ 7.8

are the equivalent nodal forces for the element and:

$$[K^e] = \int_{V_e} [B]^T [D][B] dV \qquad 7.9$$

is termed the element stiffness matrix.

7.3.4: Continuum stiffness matrix

The summation of terms in equation 7.7 over all the elements, when equated to zero, results in a system of equilibrium equations for the complete continuum, i.e.

$$\{F\} = [K]\{\delta\} \qquad 7.10$$

where $\{F\}$ is the equivalent nodal forces for the continuum, $[K]$ is the stiffness matrix of the continuum and $\{\delta\}$ is the nodal displacements of the continuum.

These equations are then solved by any standard technique to yield the nodal displacements. Once this is done, the strains and thereafter the stresses in each element can be evaluated using equations 7.3 and 7.4 respectively.

7.3.5: Two-dimensional isoparametric element

Isoparametric elements are versatile, good performers and well tried and tested. In these elements, the interpolation function used for defining the displacement variation within the element is also used to define the element geometry. This simultaneous description of element geometry and displacement variation by the shape functions leads to efficient computing effort. The basic procedure is to express the element co-ordinates and element displacements by functions expressed in terms of the natural co-ordinates of the element. The natural co-ordinate system used in the isoparametric elements is a local system defined by the element and not by the element orientation in the global system. Figure 7.6 shows this type of element and its natural co-ordinate system.

7.3.6: Shape functions

The fundamental property of the shape (interpolation) function N_i is that its value in the natural co-ordinate system is unity at node i and zero at all other nodes.

Polynomials are often selected as shape functions because they are relatively easy to manipulate mathematically, particularly with regard to integration and differentiation. The degree of polynomial chosen depends on the number of nodes and degree of freedom associated with the element.

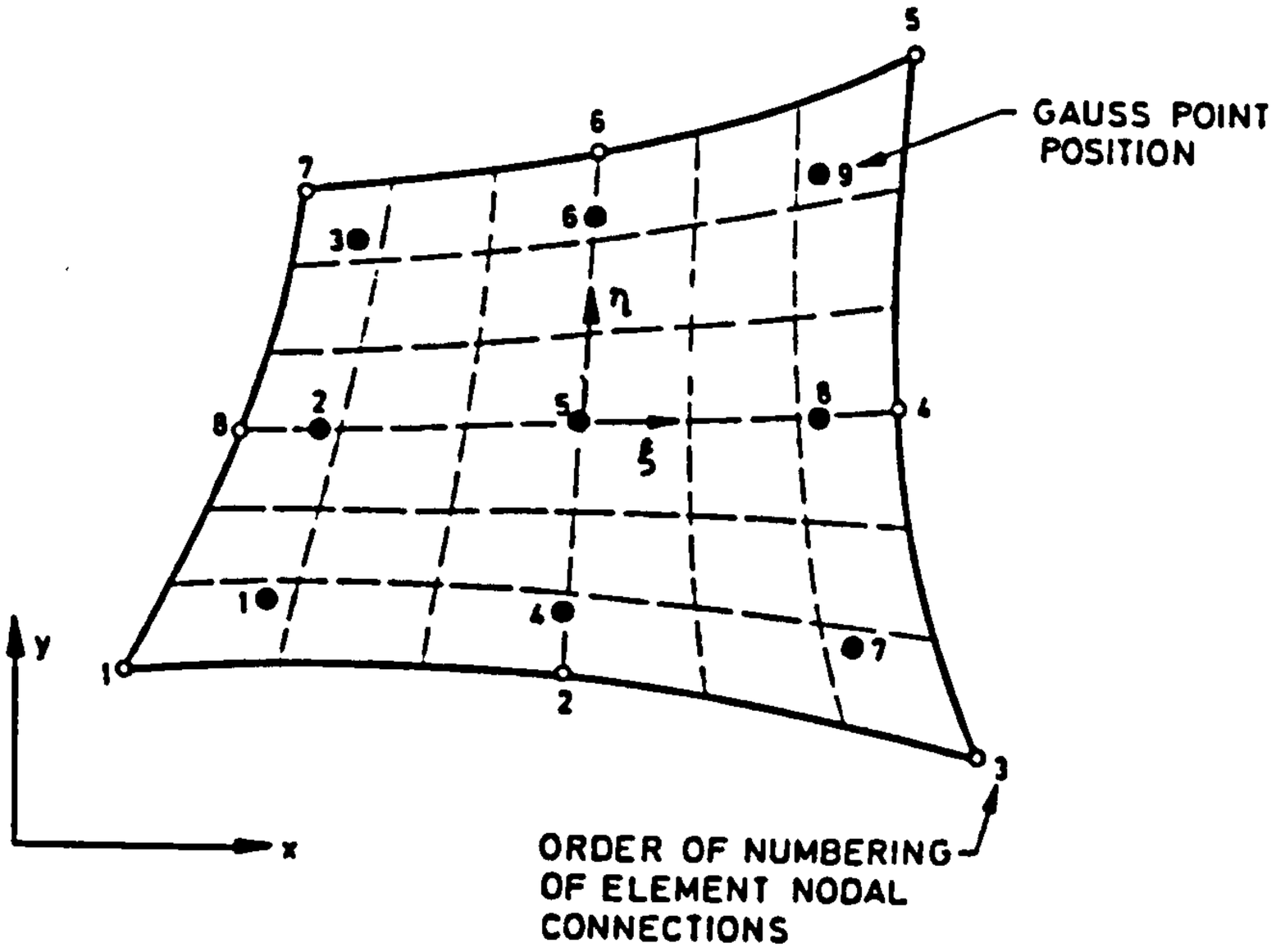

Fig. 7.6: Typical 8-nodded isoparametric element

Figure 7.7 shows the shape functions for 8-nodded isoparametric element. The shape functions for the eight-nodded element is given by the following equations in curvilinear co-ordinates ζ and η:

For corner nodes: $N_i = \frac{1}{4}(1+\zeta\zeta_i)(1+\eta\eta_i)(\zeta\zeta_i+\eta\eta_i-1)$ 7.11

For mid-side nodes: $N_i = \frac{1}{2}\{\zeta_i(1+\zeta\zeta_i)(1-\eta^2)+\eta_i(1+\eta\eta_i)(1-\zeta^2)\}$ 7.12

where ζ and η are the intrinsic co-ordinates of any point within the element. By definition, ζ and η have values in the interval [-1,1]. Since each element has two degrees of freedom at each node, namely u_i and v_i, then it has a total of 16 degrees of freedom, and the element nodal displacement vector $\{\delta^e\}$ can be written as:

$\{\delta^e\} = \{\{\delta_1\},\{\delta_2\},.....\{\delta_8\}\}$

$\{\delta_i\}$ = the displacement components at the i^{th} node.

$= \{u_i, v_i\}$

Having established the nodal displacements, the displacements at any point inside the element, u and v, can be expressed in terms of these shape functions as follows:

$$u = \sum_{i=1}^{8} N_i(\zeta,\eta)u_i \qquad 7.13$$

$$v = \sum_{i=1}^{8} N_i(\zeta,\eta)v_i \qquad 7.14$$

or $\{\delta\} = \{u,v\}$

$$= [N(\zeta,\eta)]^T\{\delta^e\} = \sum_{i=1}^{8} N_i(\zeta,\eta)^T\{\delta_i\}$$

where $[N(\zeta,\eta)]^T = \begin{bmatrix} N_1 & 0 & N_2 & 0 & \ldots\ldots\ldots\ldots N_8 & 0 \\ 0 & N_1 & 0 & N_2 & 0 & \ldots\ldots\ldots\ldots N_8 \end{bmatrix}$

= shape function matrix

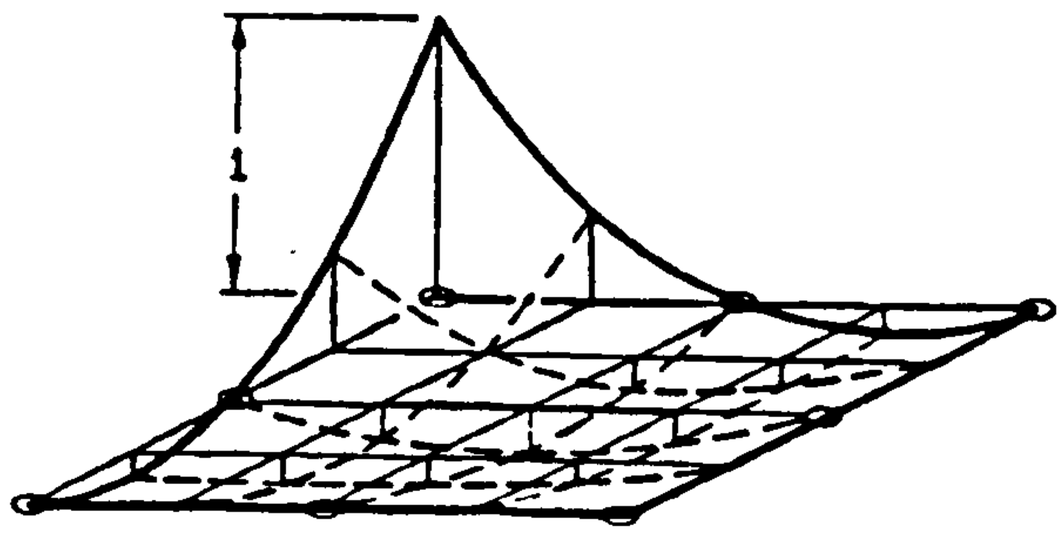

Fig. 7.7: Shape function for 8-nodded isoparametric element

7.3.7: Stress-strain relationships

The strains within the elements are expressed in terms of the derivations of the displacements, i.e.:

$$\{\varepsilon\} = \{\varepsilon_{xx} \quad \varepsilon_{yy} \quad \gamma_{xy}\}^T$$

$$= \left\{\frac{\partial u}{\partial x} \quad \frac{\partial v}{\partial y} \quad \left(\frac{\partial u}{\partial y}+\frac{\partial v}{\partial x}\right)\right\}^T \qquad 7.15$$

Substituting equations 7.13 and 7.14 into equation 7.15 leads to:

$$\{\varepsilon\} = [B]\{\delta^e\} \qquad 7.16$$

where $\{\delta^e\}^T = \{u_1 \quad v_1 \quad u_2 \quad v_2 \ldots\ldots\ldots\ldots u_8 \quad v_8\}$ and

$[B] = [B_1(\zeta,\eta) \quad B_2(\zeta,\eta) \ldots\ldots\ldots\ldots\ldots\ldots B_8(\zeta,\eta)]$

= Strain matrix.

in which:

$$[B_i(\zeta,\eta)] = \begin{bmatrix} \frac{\partial N_i}{\partial x} & 0 \\ 0 & \frac{\partial N_i}{\partial y} \\ \frac{\partial N_i}{\partial y} & \frac{\partial N_i}{\partial x} \end{bmatrix}$$

For linear analysis of uncracked concrete, and in the absence of initial stresses and strains, the incremental form of stress-strain relationship in global direction in plane stress case is given by the following equation:

$$\Delta\{\sigma\} = [D_T]\Delta\{\varepsilon\} \qquad 7.17$$

where $[D_T]$ is the tangential elasticity matrix given by:

$$[D_T] = \frac{E}{(1-\upsilon^2)} \begin{bmatrix} 1 & \upsilon & 0 \\ \upsilon & 1 & 0 \\ 0 & 0 & \frac{(1-\upsilon)}{2} \end{bmatrix} \qquad 7.18$$

where E is Young's modulus of elasticity and υ is Poisson's ratio. The onset of the cracking will introduce orthotropic conditions, and new incremental constitutive relationships will apply for the material parallel to and normal to the cracks. Normal stress across the crack is either reduced to zero in the case of tension cut-off, or

follows the descending portion of the tensile stress-strain curve when tension stiffening is taken into account. A new elasticity matrix in crack directions takes place and is given by:

$$[D_T]^* = \begin{bmatrix} E_n & 0 & 0 \\ 0 & \mathrm{E}_t & 0 \\ 0 & 0 & \beta\mathrm{G} \end{bmatrix} \qquad 7.19$$

where β is the shear retention factor, and E_n and E_t are the module of elasticity normal and parallel to the crack plane, respectively.

Using the tension cut-off criterion, when single crack has occurred, then:

$$E_n = 0.0 \qquad \text{and} \qquad E_t = E$$

For double cracking:

$$E_n = 0.0 \qquad \text{and} \qquad E_t = 0.0$$

It is essential, for reasons of numerical stability, to avoid zero values on the diagonals of the stiffness matrix. Thus instead of putting E equal to zero it takes a comparatively small value (e.g. $E = 1.0E-20$).

When tension stiffening is taken into account and a single crack has occurred, then:

$$E_n = \sigma_n / \varepsilon_n \qquad \text{and} \qquad E_t = E$$

For double cracking:

$$E_n = \sigma_n / \varepsilon_n \qquad \text{and} \qquad E_t = \sigma_t / \varepsilon_t$$

where ε_n and ε_t are the tensile strains normal and tangential to the crack plane, and σ_n and σ_t are the corresponding tensile stresses calculated from the tension stiffening curve.

7.3.8: Stiffness matrix of embedded bar

Due to the assumption of perfect bond (full compatibility) between steel and concrete, the displacements $\{u,v\}$ of any point on the bar are obtained from the displacement field of the isoparametric element as:

$$\begin{Bmatrix} u \\ v \end{Bmatrix} = [N(\zeta,\eta)]\{\delta\}^e \qquad 7.20$$

where N is the shape function of the concrete element and $\{\delta\}^e$ is the nodal displacement vector. In plane stress, bars lie in the plane of the analysis and only

strain in the bar direction is required. The virtual work of reinforcing element can be written as:

$$\Delta U = A_s \int_l \Delta\varepsilon_l . \sigma_l . dl \qquad 7.21$$

in which ΔU = internal virtual work in the reinforcement, A_s = cross-sectional area, dl = line segment along the reinforcement and σ_l and ε_l are the longitudinal stress and strain along the line segment respectively. For bar parallel to the x-axis:

$$\sigma_l = \sigma_x, \qquad \varepsilon_l = \varepsilon_x, \qquad dl = dx$$

Equation 7.21 becomes:

$$\Delta U = A_s \int_x \Delta\varepsilon_x . \sigma_x . dx \qquad 7.22$$

The strain in the bar can be calculated as follows:

$$\varepsilon_x = \frac{\partial u}{\partial x} = \frac{\partial (N(\zeta,\eta).u_i}{\partial x}$$

$$\begin{Bmatrix} \varepsilon_x \\ \varepsilon_y \end{Bmatrix} = [\frac{\partial N_i(\zeta,\eta)}{\partial x}, 0] \begin{Bmatrix} u_i \\ v_i \end{Bmatrix}$$

$$\varepsilon = B\delta^e$$

where B is the nodal displacement-strain matrix. The relation between the stress and strain in the bar is:

$$\sigma = E_s \varepsilon \quad \text{because } [D]_s = E_s$$

And the stiffness of embedded bar in x direction can be expressed as:

$$K_s = A_s E_s \int_s B^T B dx$$

$$dx = \frac{dx}{d\zeta} d\zeta = J_s . d\zeta$$

$$K_s = A_s E_s \int_{-1}^{1} B^T B \frac{d\zeta}{J_s} \qquad 7.23$$

where E_s = the bar Young's modulus and J_s = Jacobian for steel element. The same steps can be repeated for a bar in the y-axis.

The final expression for the composite element stiffness is simply evaluated by adding the stiffness matrices for concrete and steel together as follows:

$$K_e = K_c + K_s$$

in which K_e is the stiffness matrix for the composite element and K_c and K_s are the element and steel stiffness matrices respectively.

7.3.9: Numerical integration

Since it is difficult or perhaps impossible to perform a closed form of integrations in evaluating the element matrix, some form of numerical integration is essential. In this study, Gauss-Legender quadrature rules is used because of their higher efficiency over other forms of quadrature. These rules are particularly suitable for isoparametric elements since the limits of integration are ±1 which coincide with local co-ordinate system ±1 on element boundary. In this study a 3x3 Gauss rule is adopted. The general form of the integral using Gauss-Legender for two dimensions where double integral exist is:

$$\int_{-1}^{1}\int_{-1}^{1} f(\zeta,\eta)d\zeta d\eta = \sum_{i=1}^{m}\sum_{j=1}^{m} W_i W_j f(\zeta_i,\eta_j) \qquad 7.24$$

where W_i and W_j are the i^{th} and j^{th} weighting factors, ζ_i and η_i are the co-ordinates of the i^{th} integration point and m is the total number of integration points.

7.3.10: Equation solution technique

In this study the simultaneous equations are solved using the direct Gaussian elimination algorithms in conjunction with the frontal method of equation assembly and reduction. The main features of this method is that it assembles the equations and eliminates the variable at the same time. Hence the complete structural stiffness is never formed. This reduces computer storage significantly. The stiffnesses are evaluated using a secant rigidity matrix. The program used has several choices for updating the stiffness matrix as will be shown in chapter 8.

7.3.11: Numerical methods of analysis

The finite element method uses one of the following procedures for solution of non-linear problems:

1. Incremental procedure.
2. Iterative procedure.
3. Incremental-iterative procedure.

1: Incremental procedure

This approach consists of linearisation of equation 7.10. The external load $\{F\}$ is usually applied in small increments $\{\Delta F\}$.

$$[K_T]\{\Delta\delta\} - \{\Delta F\} = 0 \qquad 7.25$$

Where $[K_T]$ is the tangent stiffness matrix at the beginning of the increment and $\{\Delta\delta\}$ is the incremental displacement. The behaviour of the structure within each increment is assumed to be linear. For each load increment $[K_T]$ is assumed to be constant but changes for subsequent increments. The system of linear equations given by equation 7.25 is then solved to obtain unknown incremental displacement. The solution tends to drift away from the equilibrium curve as shown in figure 7.8. The degree of error resulting from this piece-wise linearisation depends mainly on the size of the load increment. The smaller the increment size the better the prediction but the analysis becomes expensive. In highly non-linear problems such as reinforced concrete structures, the accumulation of errors over several increments could lead to incorrect solution. This occurs due to the fact that the actual state of stress after each load increment does not correspond to the applied load as a result of non-linear effects. Hence, equilibrium violation occurs. To overcome this problem, the difference between actual resisting load and applied load, known as residual load, is calculated and added to the next load increment. This method is called the corrected incremental method and leads to better performance.

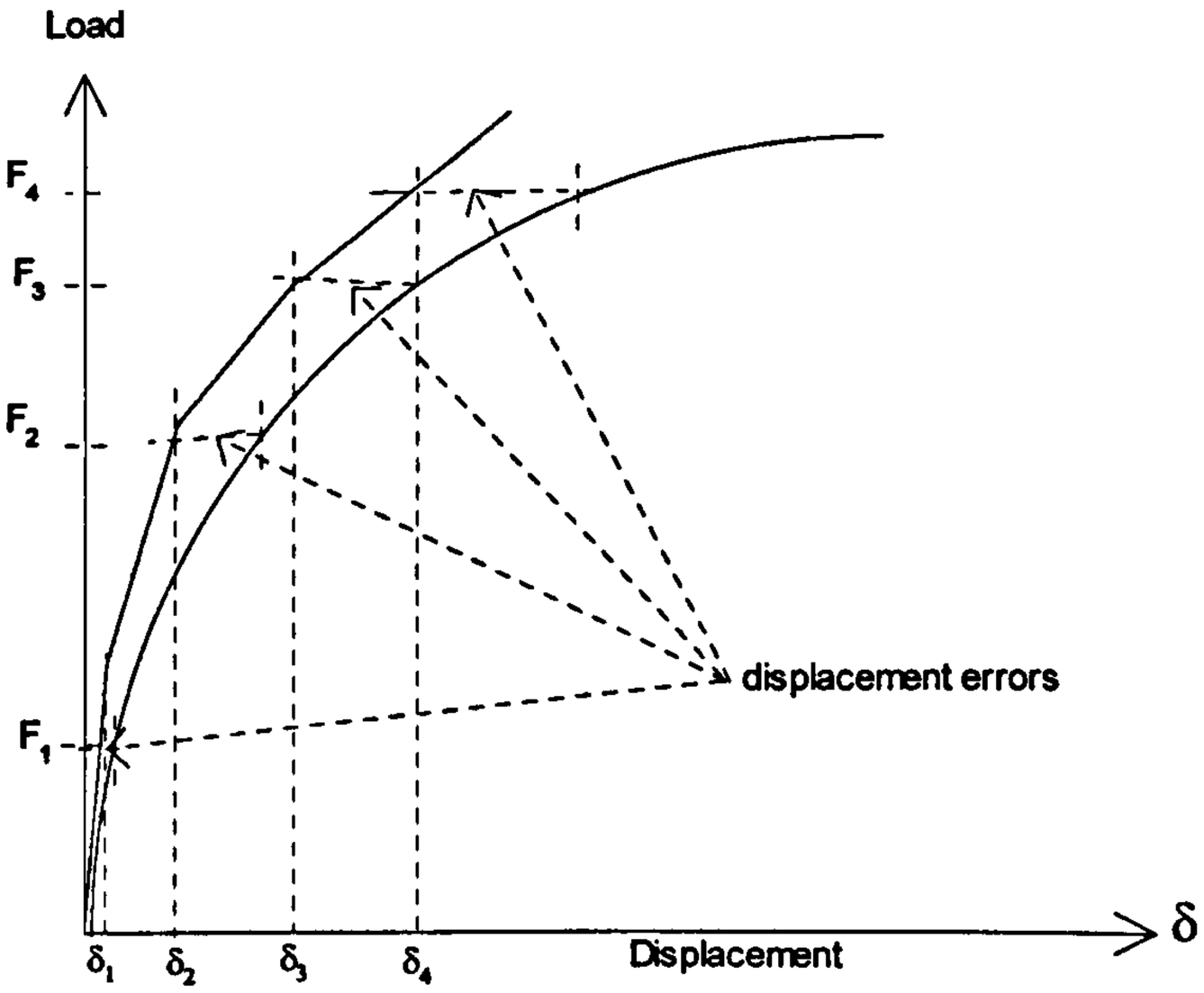

Fig. 7.8: Incremental method

2: Iteration procedure

In this approach the solution of equation 7.10 is obtained from a single load step (Fig. 7.9). After obtaining the displacements, the corresponding stresses are evaluated according to the prevailing material constitutive relations. Due to possible lack of equilibrium between the applied and internal resisting forces because of non-linear effects, residual or out of balance nodal forces occur. These out of balance forces are applied to the structure and solved for unknown additional displacements. Subsequently, new set of equivalent nodal forces are obtained. This process of successive iteration is continued until a chosen level of convergence is achieved. The total displacement is then obtained by summation of displacements from each iteration. This approach is convenient if only ultimate load capacity of the structure is desired. The main disadvantages of the iterative procedure are: there is no guarantee of convergence to exact solution because of large residual forces, the displacement, strains and stresses are obtained from only one load increment and gives no response history of the structure.

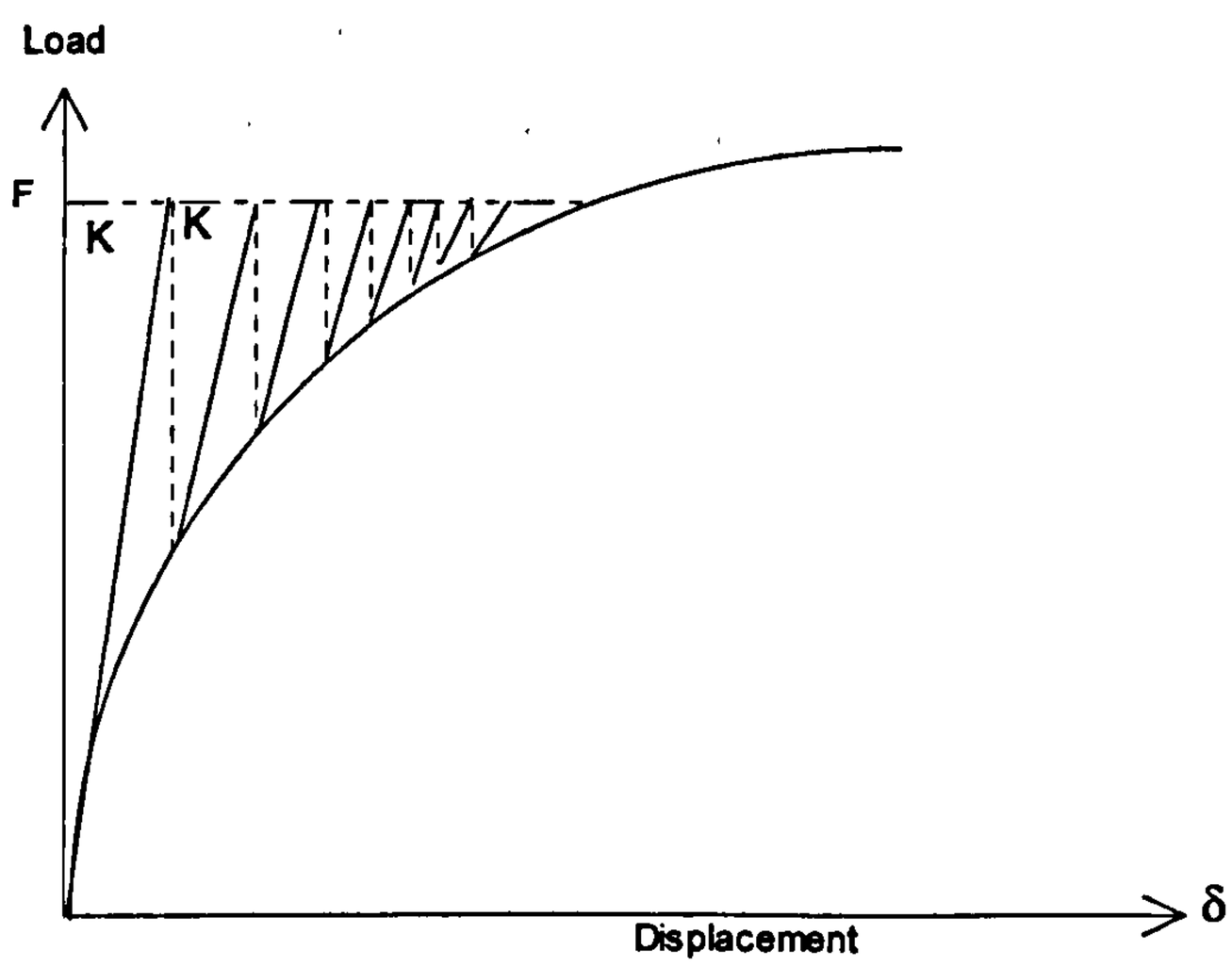

(a): Iteration method with constant stiffness

Fig. 7.9: Iteration method

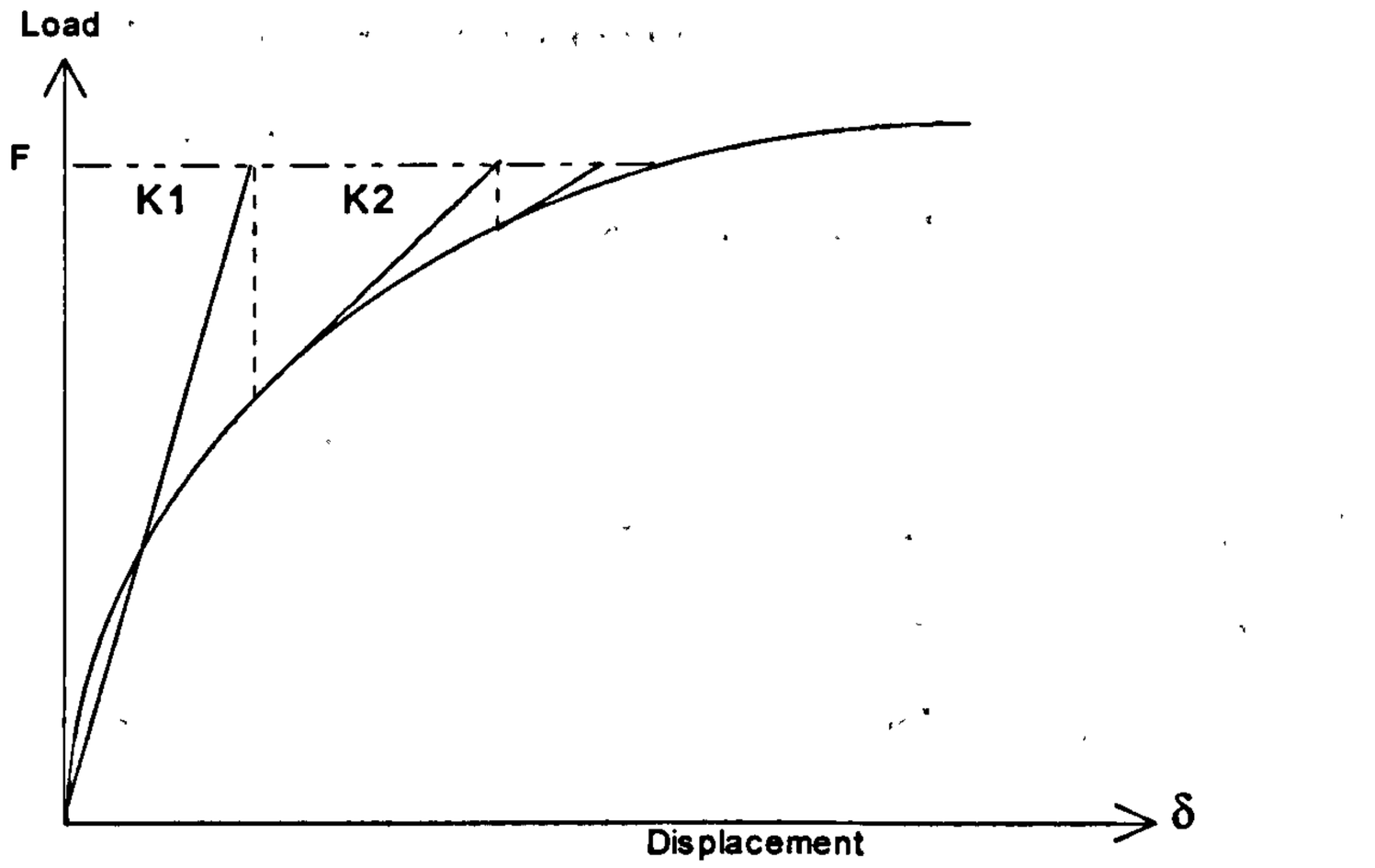

(b): Iteration method with variable stiffness

Fig. 7.9: Continued

3: Incremental-Iterative procedure

In this approach the advantages of the incremental and iteration methods are combined. In this method the total load is divided into a number of load increments and the solutions are obtained iteratively until equilibrium is achieved to an acceptable level of accuracy (Fig. 7.10). For every increment the stiffness matrix can be updated for every iteration, or after several iterations or kept constant during that increment. The mixed incremental-iteration procedure is adopted in this study.

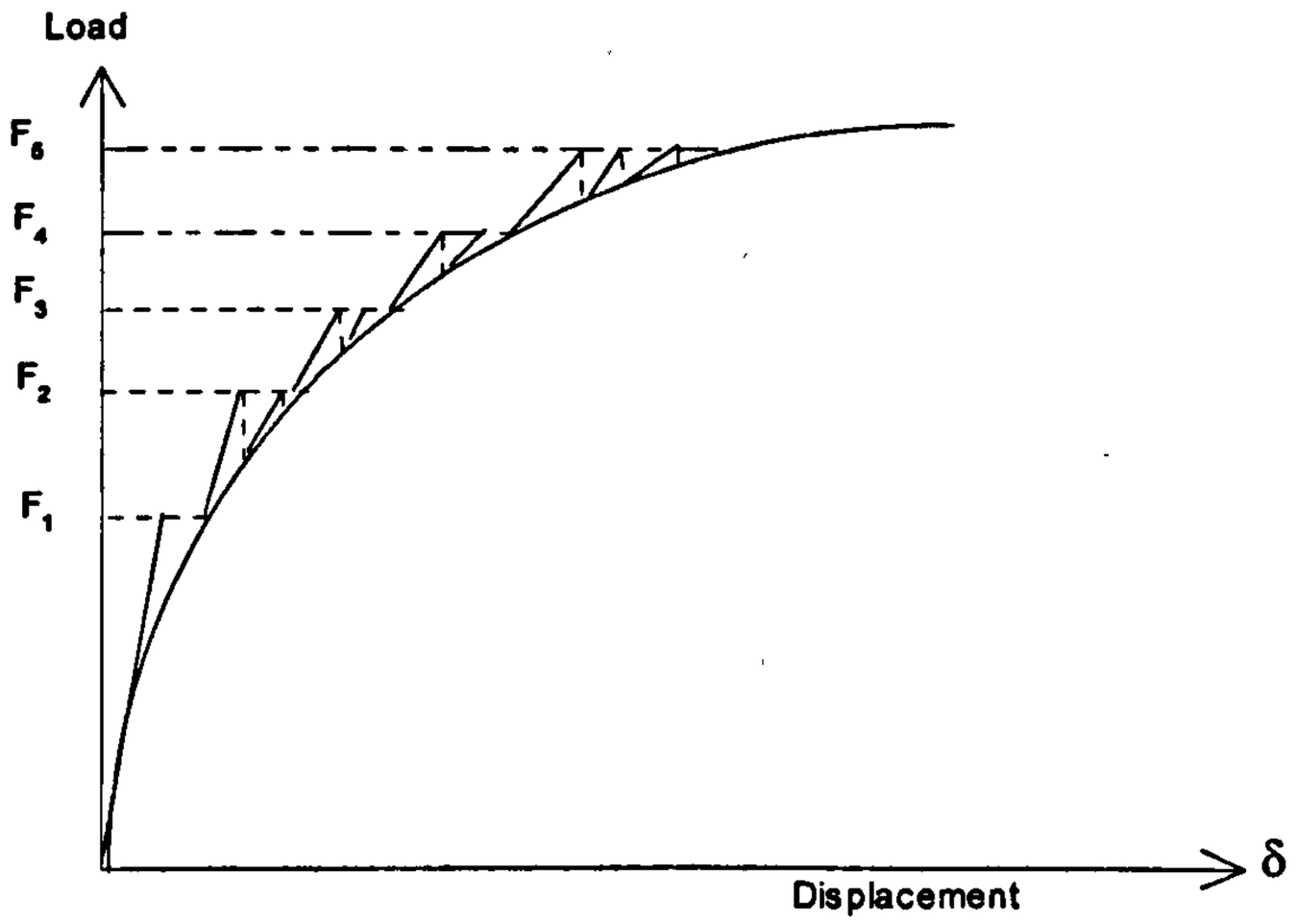

Fig. 7.10: Incremental-Iteration method

7.3.12: Convergence criterion

Since the numerical solutions do not usually lead to an exact equilibrium, criteria to determine convergence have to be established. The main purpose of the convergence criterion is to ensure gradual elimination of the out-of-balance (residual) forces and to terminate the iterative process when the desired accuracy has been achieved. In this study the convergence criterion is based on the out-of-balance load norms. They indicate directly how well equilibrium requirements are met. Since it is difficult and expensive to check the decay of residual forces for every degree of freedom, an overall evaluation of convergence is used. This is done by using the (residual) force norm. This criterion assumes that convergence is achieved if:

$$\frac{\Delta R_i^*}{F_i^*} \leq Toler \qquad 7.26$$

where:

$$\Delta R_i^* = \sqrt{\{R_i\}^T \{R_i\}}$$

= the norm of residuals.

$\{R_i\}$ = the residual force vector at i^{th} iteration,

$$F_i^* = \sqrt{\{F_i\}^T \{F_i\}}$$

= the norm of the applied loads,

$\{F_i\}$ = the total applied load vector,

Toler = specified convergence tolerance.

It should be noted that fine tolerance is desirable because it leads to closer solution to the exact but it can be very expensive to obtain due to large number of iterations. In some cases it causes divergence in the highly non-linear analysis. The rate of convergence very much depends on the method used in the solution. For example, the constant stiffness will lead to slow convergence and this leads to many iterations which is very costly. Discontinuities in material (cracks, yielding ...) causes large residuals and these residuals need to be distributed which leads to more discontinuities in other parts of the structure.

7.4: Basic steps in non-linear program

The major steps in the linear and non-linear analysis of a typical finite element program are:

1. Subdivision of the structure and representing different parts by appropriate types of finite elements.
2. Generation and assembly of load vector $\{F\}$.
3. Generation of element stiffness $[K^e]$.
4. Assembly of the structure stiffness $[K]$.
5. Solution for the nodal displacements $\{\delta_i\} = [K]^{-1}\{F_i\}$ and hence the strain $\{\varepsilon\} = \int [B]^T \{\delta_i\}$.
6. Determination of element stresses $\{\sigma\} = [D]\{\varepsilon\}$

   For non-linear analysis, add:
7. Check for cracking, yielding and failure.
8. Determination of unbalanced nodal forces.
9. Check for convergence

   (a). if not converged apply the unbalanced nodal forces again to the structure and go to step 3 if the stiffness is to be updated, or to step 5 if constant stiffness solution is adopted.

   (b). if converged apply the next load increment and go to step 2.
10. Stop when failure occurs or when full loading has been applied.

8: Parameteric study on the computational behaviour hollow beams

8.1: Introduction

The computational parameters affecting the final results of a finite element model for reinforced or prestressed concrete structures can be classified into two groups: The first contains material property parameters such as tension stiffening factor, shear retention factor, compressive and tensile strengths, stress-strain relationships, Young's modulus of concrete and yield strength of reinforcement. The second contains "numerical" factors such as the solution techniques used to solve non-linear equations, mesh size, number and size of increments, maximum number of iterations in each increment, convergence criteria, the type of element used in the analysis, the number of Gauss points per element and other parameters such as simulation of supports and applied loads.

The aim of this chapter is to report on some computational experiments conducted to study the effects of some of the above parameters on the predicted behaviour and the final failure load of the beams, using the program described in chapters 6 and 7. The results will help to gain a general understanding of the program response to change of each parameter and thus to choose a general model which gives good prediction of the behaviour of all tested hollow beams. The part of the beam between the supports (1800mm) is modelled with the effect of the outside sections being loaded on this internal segment. As there are many variables, the computation was confined to two typical reinforced concrete beams, BTV2 and BTV4 and one partially prestressed beam, BTV10 (Table 5.4). In Beam BTV4 the shear stress due to shear force is dominant, BTV10 has the torsion stress dominant and BTV2 has almost equal stresses due to torsion and shear. Also, in beams BTV2 and BTV4 bending is dominant while in BTV10 torsion is dominant. The parameters were varied one at a time. The final choice of parameters is that which gave closest values to the actual experimental results presented in chapter 5. The selected parameter values were fixed at the optimum value and were used in the next stage of analysis. After having chosen the most suitable set of parameters, a comparison between experimental and computational results is carried out in chapter 9. The element type, node numbers and Gauss points were shown in figures 7.6-7. Only one element

through the plate thickness was used. The maximum number of load increments was fixed at 30 and the maximum number of iterations in each increment was fixed at 100. Load increment was 10% for the first five increments and 5% for the remaining ones. Concrete compressive strength f_{cu} was the measured value for each beam (Table 5.6), the other values were taken as follows: concrete cylinder compressive strength $f_c^{'} = 0.8 f_{cu}$ N/mm^2, Young's modulus $E_c = 5000\sqrt{f_c^{'}}$ N/mm^2 and Poisson's ratio $\nu = 0.15$. The computational failure load was considered to be the load corresponding to the last converged increment. However, if the residual force for un-converged increment was very close to that of the allowed tolerance ratio, the analysis was continued for a few more increments. Only results at converged load increments were considered for analysis.

The effect of each parameter was judged on the basis of the following computed responses when compared with measured values:

- Load-deflection response at mid-depth at mid-span of the front web.
- Strain in the longitudinal steel at a selected point as follows:

BTV2: 420mm to the right of mid-span at 25mm from the bottom of the front web.

BTV4: 84mm to the right of mid-span at 25mm from the bottom of the front web.

BTV10: 93mm to the right of mid-span at 25mm from the bottom of the front web.

- Strain in the stirrup steel at a selected point as follows:

BTV2: 280 mm to the right of mid-span at half depth of the front web.

BTV4: 126 mm to the right of mid-span at half depth of the front web.

BTV10: 46 mm to the right of mid-span at half depth of the front web.

- Failure load.
- Convergence and cost of analysis.

8.2: Material parameters

In this section, numerical parameters were fixed as follows:

1. Non-Linear solution algorithm:

The stiffness matrix was calculated at the beginning of the first increment and unchanged thereafter except if the steel yields or concrete cracks at any point. The change can take place at any iteration and any increment.

2. The element size was 84x84mm.

3. Convergence tolerance was 5%.

Five parameters were studied in this part:

I. Tension stiffening factor.

II. Shear retention factor.

III. Tensile strength of concrete.

IV. Value of compressive strain at peak stress.

V. Compressive strength of concrete.

The analysis started with the following initial values and were varied as explained later:

- concrete tensile strength $f_t^{'} = 0.54\sqrt{f_c^{'}}\ N/mm^2$.
- shear retention factor, $\beta = B\frac{\varepsilon_{cr}}{\varepsilon_n} > \beta_{\min}$, $B = 0.4$ and $\beta_{\min} = 0.0$.
- maximum compressive strain $\varepsilon_{\max} = 0.0035$.
- compressive strain at peak stress $\varepsilon_{cc} = \frac{\sqrt{f_c^{'}}}{2500}$.

8.2.1: Effects of tension stiffening

The first parameter to be varied was tension stiffening factor. The descending portion of the stress-strain curve is considered as a function of the strain normal to the crack plane (Ch.6). Five equations were studied (Fig. 6.16) using the designations TESN2 to TESN6 as follows:

$$\sigma_t = \frac{\varepsilon_{cr}}{\varepsilon_n} f_t^{'} \qquad \text{TESN2}$$

$$\sigma_t = \left(\sqrt{\frac{\varepsilon_{cr}}{\varepsilon_n}} + \frac{\varepsilon_{cr}}{\varepsilon_n}\right) f_t^{'}/2 \qquad \text{TESN3}$$

$$\sigma_t = \left(\sqrt{\frac{\varepsilon_{cr}}{\varepsilon_n}}\right) f_t^{'} \qquad \text{TESN4}$$

$$\sigma_t = \left[\sqrt[4]{\frac{\varepsilon_{cr}}{\varepsilon_n}} + \sqrt{\frac{\varepsilon_{cr}}{\varepsilon_n}}\right] f_t^{'}/2 \qquad \text{TESN5}$$

$$\sigma_t = \left(\sqrt[4]{\frac{\varepsilon_{cr}}{\varepsilon_n}}\right) f_t^{'} \qquad \text{TESN6}$$

Results are presented in figures 8.1 to 8.3 from which it is clear that the above equations used for the tension stiffening gave similar results for the displacement and steel strain with TESN6 being the closest to the experimental results in most cases. Table 8.1 shows the percentage of the residual (un-balanced) forces by the

end of each increment which have been affected by the change in the tension stiffening values with TESN6 being the only equation which in all cases attained the largest number of converged increments.

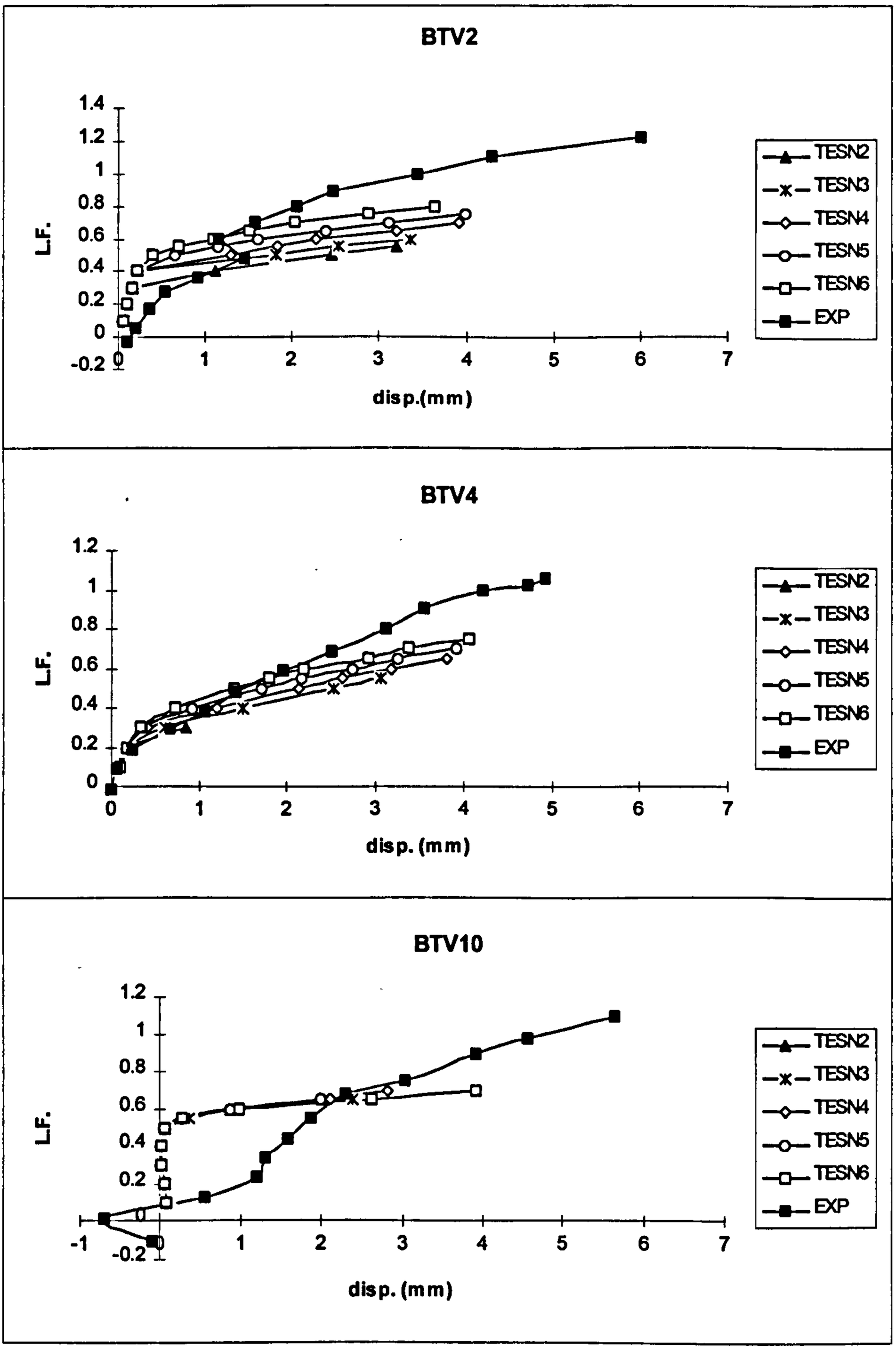

Fig. 8.1: Effect of the tension stiffening on the displacement

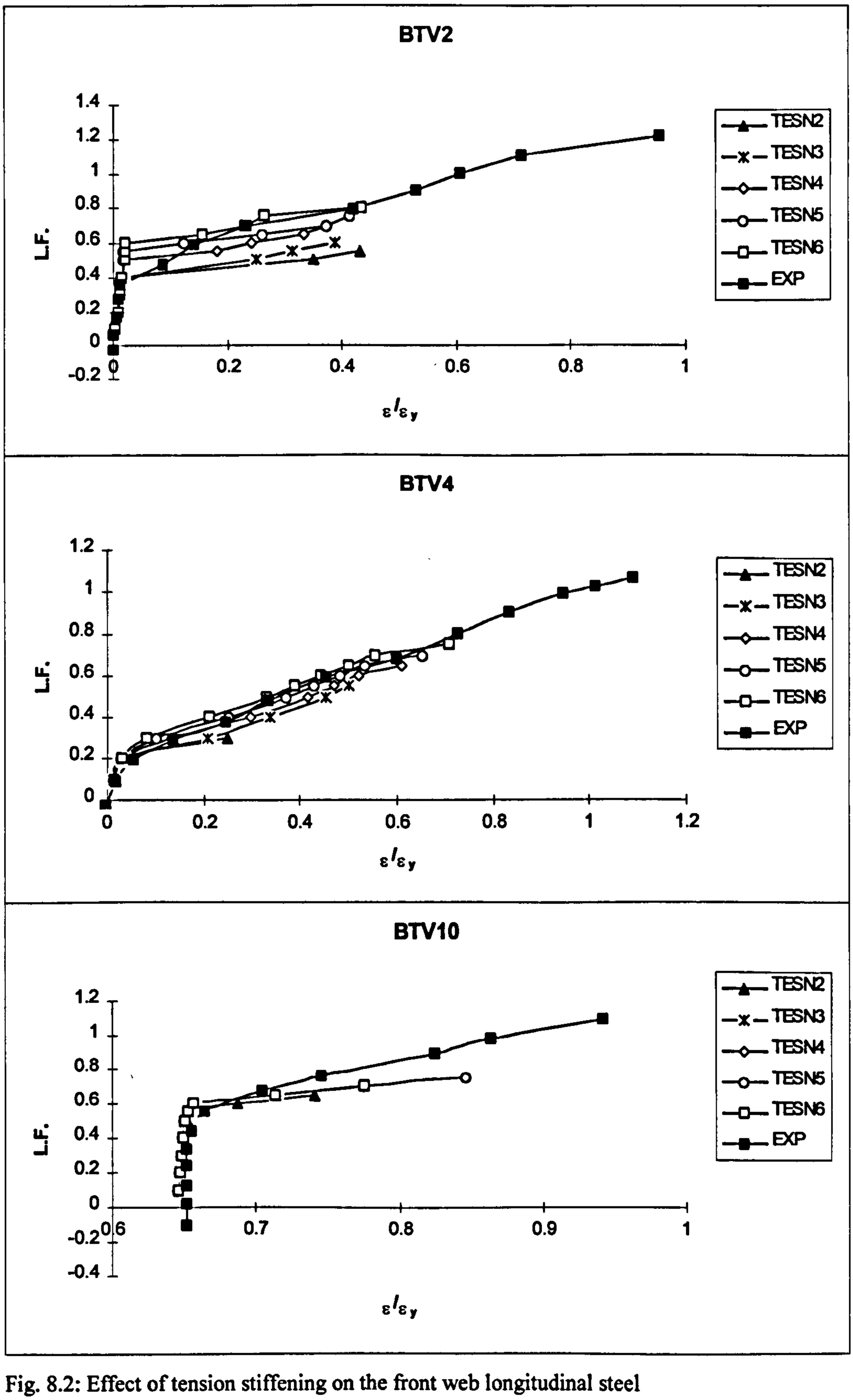

Fig. 8.2: Effect of tension stiffening on the front web longitudinal steel

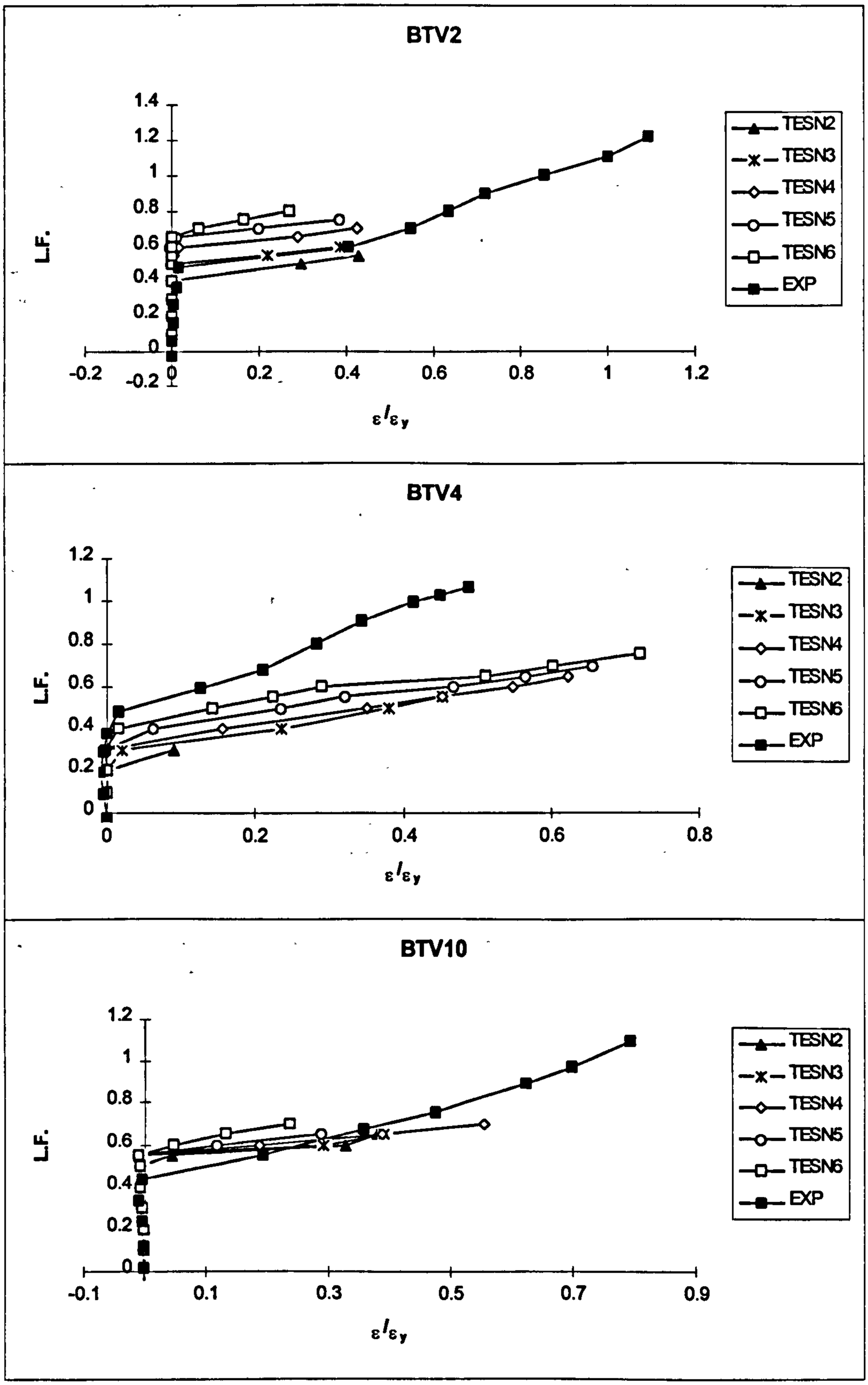

Fig. 8.3: Effect of tension stiffening on the front web transverse steel

Table 8.1: Effect of tension stiffening on the residual forces

Beam	TESN2		TESN3		TESN4		TESN5		TESN6	
L.F.	No.iter.	% R.F.	No.iter.	% R.F.	No.iter.	% R.F.	No.iter.	% R.F.	No.iter.	% R.F.
0.1	1	0.1	1	0.1	1	0.1	1	0.1	1	0.1
0.2	1	0.1	1	0.1	1	0.1	1	0.1	1	0.1
0.3	1	0.1	1	0.1	1	0.1	1	0.1	1	0.2
0.4	81	4.6	3	4.4	3	2.6	3	2.0	3	1.9
0.5	73	5.0	70	4.7	74	4.9	25	4.3	20	5.0
0.55	35	3.9	51	4.4	47	4.8	34	5.0	55	4.9
0.6	48	*****	40	4.6	12	5.0	25	4.9	79	4.9
0.65			53	*****	53	4.7	21	4.8	67	5.0
0.7					22	4.9	44	4.9	71	4.3
0.75					42	*****	38	3.8	78	4.3
0.8							44	*****	100	7.9

(a): BTV2

Beam	TESN2		TESN3		TESN4		TESN5		TESN6	
L.F.	No.iter	% R.F.	No.iter	% R.F.	No.iter	% R.F.	No.iter	% R.F.	No.iter	% R.F.
0.1	1	0.1	1	0.1	1	0.1	1	0.1	1	0.1
0.2	1	0.1	1	0.1	1	0.1	1	0.1	1	0.1
0.3	100	9.8	91	5.0	18	4.9	12	5.0	9	4.4
0.4			100	7.1	80	5.0	46	5.0	26	4.9
0.5			100	5.7	90	4.9	58	5.0	43	4.9
0.55			82	5.0	64	5.0	42	5.0	33	5.0
0.6			100	12.9	67	5.0	77	5.0	27	4.9
0.65					93	5.0	54	4.9	100	6.1
0.7					100	15.0	84	5.0	43	4.9
0.75							100	10.9	80	5.0
0.8									100	16.8

(b): BTV4

Beam	TESN2		TESN3		TESN4		TESN5		TESN6	
L.F.	No.iter.	% R.F.	No.iter.	% R.F.	No.iter.	% R.F.	No.iter.	% R.F.	No.iter.	% R.F.
0.1	1	0.1	1	0.1	1	0.1	1	0.1	1	0.2
0.2	1	0.1	1	0.1	1	0.1	1	0.1	1	0.1
0.3	1	0.1	1	0.1	1	0.1	1	0.1	1	0.1
0.4	1	0.1	1	0.1	1	0.1	1	0.1	1	0.1
0.5	1	1.5	1	1.4	1	1.3	1	1.2	1	2.5
0.55	1	3.1	1	2.7	1	2.3	1	2.1	1	2.7
0.6	1	4.3	1	2.9	1	2.5	1	2.2	1	3.6
0.65	3	4.6	2	4.5	1	4.4	1	3.9	2	4.6
0.7	100	43.4	100	32.8	1	4.8	100	37.3	7	5.0
0.75					100	45.7			100	11.1

(c): BTV10

**** = very large number

%RF = % of residual force

Table 8.2 shows a significant effect of the tension stiffening on the failure load in all cases, again, with TESN6 being closest to the failure load in all cases. From the

above it is possible to say that equation TESN6 has shown the best performance among this group and, therefore, selected for the next stage of analysis.

Table 8.2: Effect of tension stiffening on the failure load

Beam	TESN2	TESN3	TESN4	TESN5	TESN6	EXP
BTV2	0.55	0.6	0.7	0.75	0.75	1.22
BTV4	0.2	0.55	0.65	0.7	0.75	1.06
BTV10	0.65	0.65	0.7	0.65	0.7	1.1

8.2.2: Effects of the shear retention factor

Having fixed the tension stiffening factor as defined by TESN6, the next stage was to vary the shear retention factor β which was taken as a function of the tensile strain normal to the crack (Ch.6) as follows:

$$\beta = B\frac{\varepsilon_{cr}}{\varepsilon_n} \geq \beta_{\min}$$

Where ε_{cr} is the tensile crack strain; ε_n is a fictitious strain normal to the crack plane and B and $\beta_{\min}$ are numerical constants (Fig. 6.17e). Six pairs of values for these two constants were studied as designated below:

$B = 0.1$	$\beta_{\min} = 0.0$	SR10
$B = 0.1$	$\beta_{\min} = 0.05$	SR15
$B = 0.4$	$\beta_{\min} = 0.0$	SR40
$B = 0.4$	$\beta_{\min} = 0.05$	SR45
$B = 0.6$	$\beta_{\min} = 0.0$	SR60
$B = 0.6$	$\beta_{\min} = 0.05$	SR65

Figure 8.4 shows that change in shear retention factor had some effect on the deflection behaviour of the beams specially beam BTV10 with SR45 being the closest to the experiment. Figures 8.5-6 indicate that the shear retention had insignificant effect on the longitudinal steel strains but some effect on the transverse steel strain in beam BTV10. Table 8.3 shows that SR45 was the only combination which in all cases managed to attain the largest converged number of increments. This is reflected in table 8.4 which shows that, in all cases, SR45 gave the closest failure load to the experiment. In general, it can be seen that beams with $\beta_{\min} = 0.05$ gave less residual forces, required less number of iterations to converge and gave higher failure load than those with $\beta_{\min}$ =0.0.

From the above discussion, the shear retention factor parameters (B= 0.4 and $\beta_{min} = 0.05$) used in SR45 was adopted for next stage of the analysis.

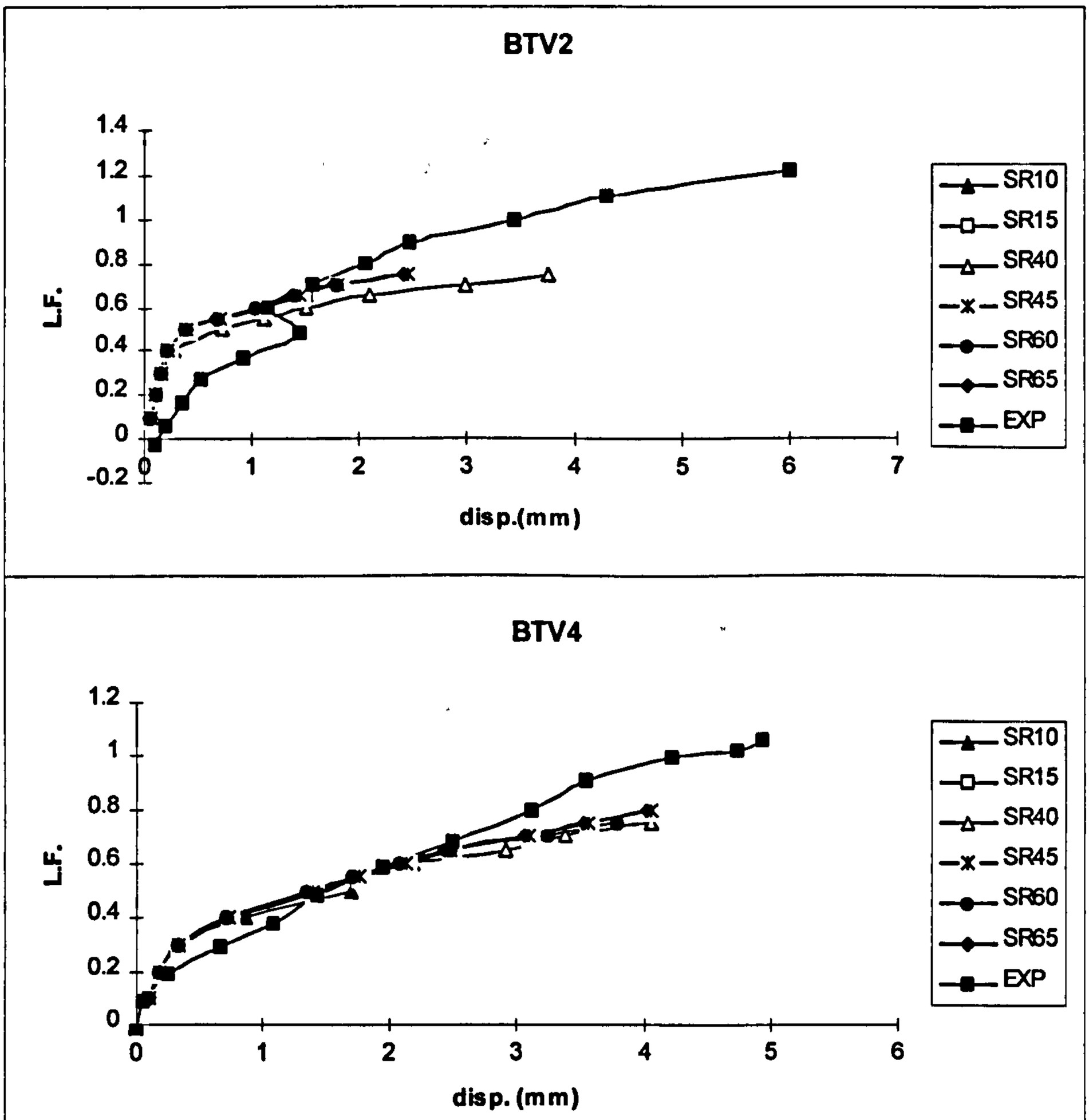

Fig. 8.4: Effect of the shear retention on the displacement

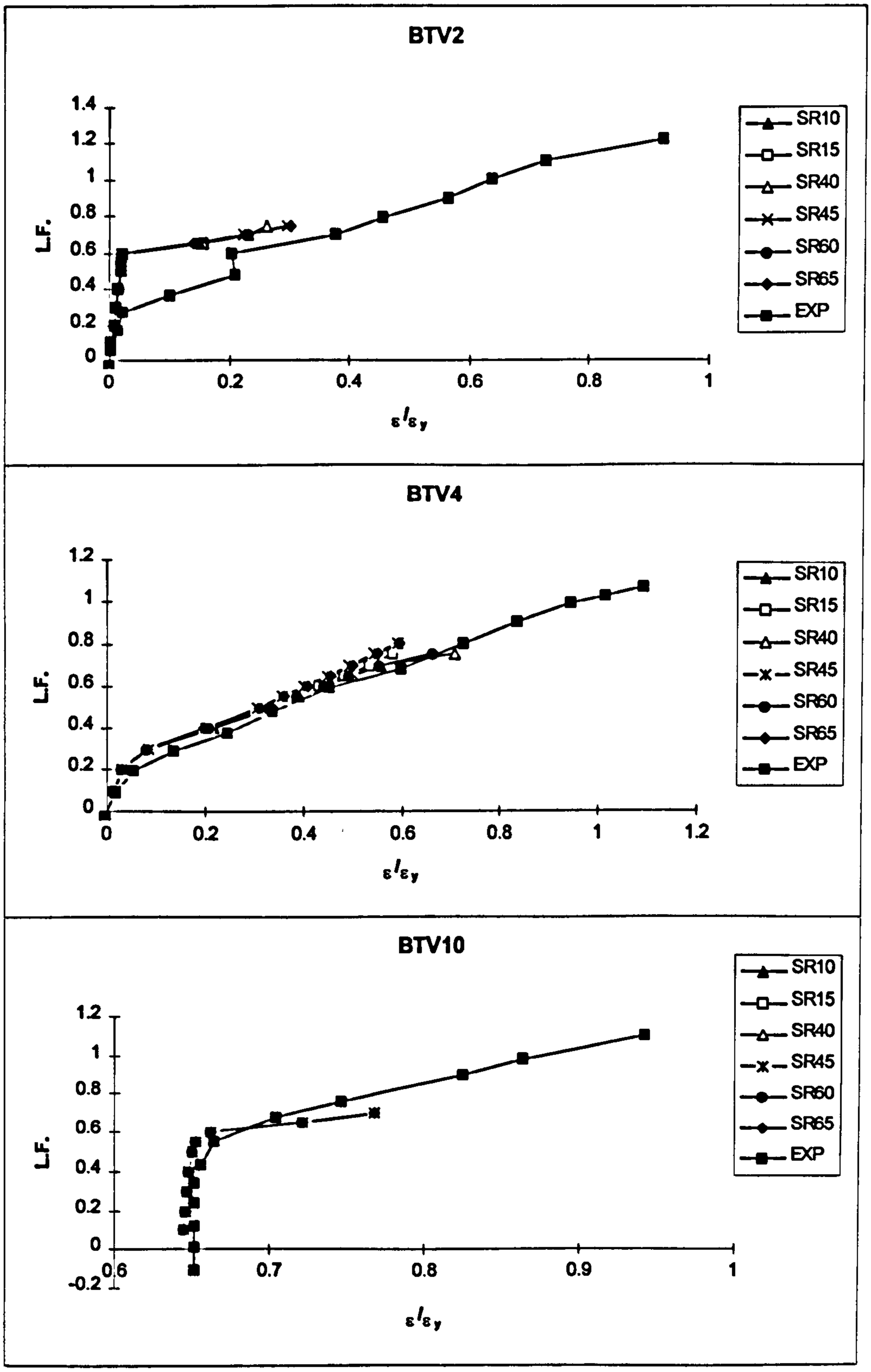

Fig. 8.5: Effect of the shear retention on the front web longitudinal steel

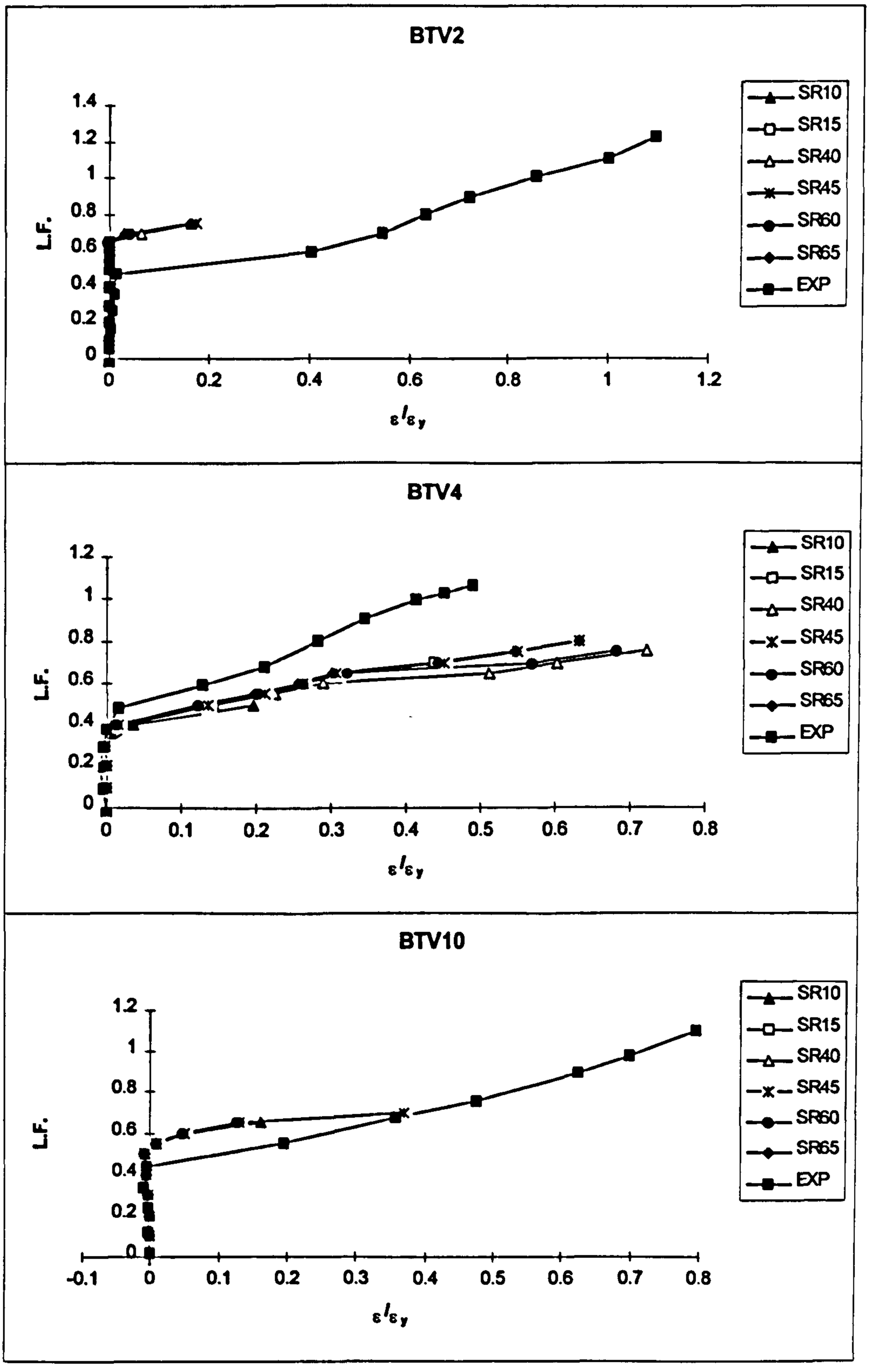

Fig. 8.6: Effect of the shear retention on the front web transverse steel

Table 8.3: Effect of the shear retention on the residual forces

Beam	SR10		SR15		SR40		SR45		SR60		SR65	
L.F.	No. iter.	%R.F.	No. iter.	%R.F.	No. iter.	%R.F.	No. iter.	%R.F.	No. iter.	%R.F.	No. iter.	%R.F.
0.1	1	0.1	1	0.1	1	0.1	1	0.1	1	0.8	1	0.1
0.2	1	0.1	1	0.1	1	0.1	1	0.1	1	1.2	1	0.1
0.3	1	0.2	1	0.2	1	0.2	1	0.2	1	1.4	1	0.2
0.4	3	1.9	3	1.9	3	1.9	3	1.9	3	1.9	3	1.8
0.5	20	5.0	20	5.0	20	5.0	20	5.0	19	4.7	18	4.9
0.55	55	4.9	55	4.9	55	4.9	55	4.9	48	5.0	47	4.9
0.6	79	4.9	79	4.9	79	4.9	75	5.0	64	5.0	66	4.8
0.65	79	5.0	79	5.0	67	5.0	70	4.9	59	5.0	54	4.9
0.7	100	13.3	100	13.3	71	4.3	57	4.8	61	4.9	54	5.0
0.75					78	4.3	61	4.9	100	8.6	59	4.8
0.8					100	7.9	100	9.0	100	9.8	100	7.3

(a): BTV2

Beam	SR10		SR15		SR40		SR45		SR60		SR65	
L.F.	No. iter.	%R.F.	No. iter.	%R.F.	No. iter.	%R.F.	No. iter.	%R.F.	No. iter.	%R.F.	No. iter.	%R.F.
0.1	1	0.1	1	0.1	1	0.1	1	0.1	1	0.1	1	0.1
0.2	1	0.1	1	0.1	1	0.1	1	0.1	1	0.1	1	0.1
0.3	11	5.0	11	4.9	9	4.4	9	4.4	8	4.9	8	4.9
0.4	53	5.0	32	4.9	26	4.9	26	4.9	22	5.0	22	5.0
0.5	70	5.0	43	4.9	43	4.9	41	4.9	37	4.9	37	4.9
0.55	100	6.5	32	4.9	33	5.0	32	4.9	31	4.8	30	5.0
0.6	100	10.4	26	4.9	27	4.9	25	5.0	24	5.0	24	4.9
0.65			22	4.8	100	6.1	21	5.0	24	4.7	20	5.0
0.7			64	4.8	43	4.9	75	5.0	86	4.8	65	4.9
0.75			50	4.9	80	5.0	47	5.0	57	4.8	47	4.9
0.8			100	13.8	100	16.8	45	5.0	100	5.7	42	5.0
0.85							100	11.3	100	13.8	100	11.6

(b): BTV4

Beam	SR10		SR15		SR40		SR45		SR60		SR65	
L.F.	No. iter.	%R.F.	No. iter.	%R.F.	No. iter.	%R.F.	No. iter.	%R.F.	No. iter.	%R.F.	No. iter.	%R.F.
0.1	1	0.2	1	0.2	1	0.2	1	0.2	1	0.2	1	0.2
0.2	1	0.1	1	0.1	1	0.1	1	0.1	1	0.1	1	0.1
0.3	1	0.1	1	0.1	1	0.1	1	0.1	1	0.1	1	0.1
0.4	1	0.1	1	0.1	1	0.1	1	0.1	1	0.1	1	0.1
0.5	1	2.5	1	2.5	1	2.5	1	2.5	1	2.5	1	2.5
0.55	1	2.7	1	2.7	1	2.7	1	2.7	1	2.7	1	2.7
0.6	1	3.6	1	3.6	1	3.6	1	3.6	1	3.6	1	3.6
0.65	2	4.6	2	4.6	2	4.6	2	4.6	2	4.6	2	4.6
0.7	100	15.2	100	12.1	7	5.0	3	4.6	100	10.0	100	10.2
0.75					100	11.1	100	11.1				

(c): BTV10

Table 8.4: Effect of the shear retention on the failure load

Beam	SR10	SR15	SR40	SR45	SR60	SR65	EXP
BTV2	0.65	0.65	0.75	0.75	0.7	0.75	1.22
BTV4	0.5	0.75	0.75	0.8	0.75	0.8	1.06
BTV10	0.65	0.65	0.7	0.7	0.65	0.65	1.1

8.2.3: Effects of tensile strength of concrete

Using TESN6 and SR45 as tension stiffening and shear retention factors respectively, the next parameter investigated was the tensile strength of concrete.

Two empirical equations for uni-axial tensile strength of concrete were tried (Fig. 6.11) namely $f_t^{'} = 0.54\sqrt{f_c^{'}}$ N/mm^2 and $f_t^{'} = \sqrt[4]{f_c^{'}}$ N/mm^2.

$f_t^{'} = 0.54\sqrt{f_c^{'}}$ N/mm^2 used in FT1

$f_t^{'} = \sqrt[4]{f_c^{'}}$ N/mm^2 used in FT2

From figures 8.7-9 it is obvious that FT1 gave displacement and steel strain values slightly closer to the experiment than FT2. Beam FT2 cracked at lower load levels than FT1 as shown in these figures and in table 8.5. This table also shows that FT1 has shown better convergence values and larger number of converged increments.

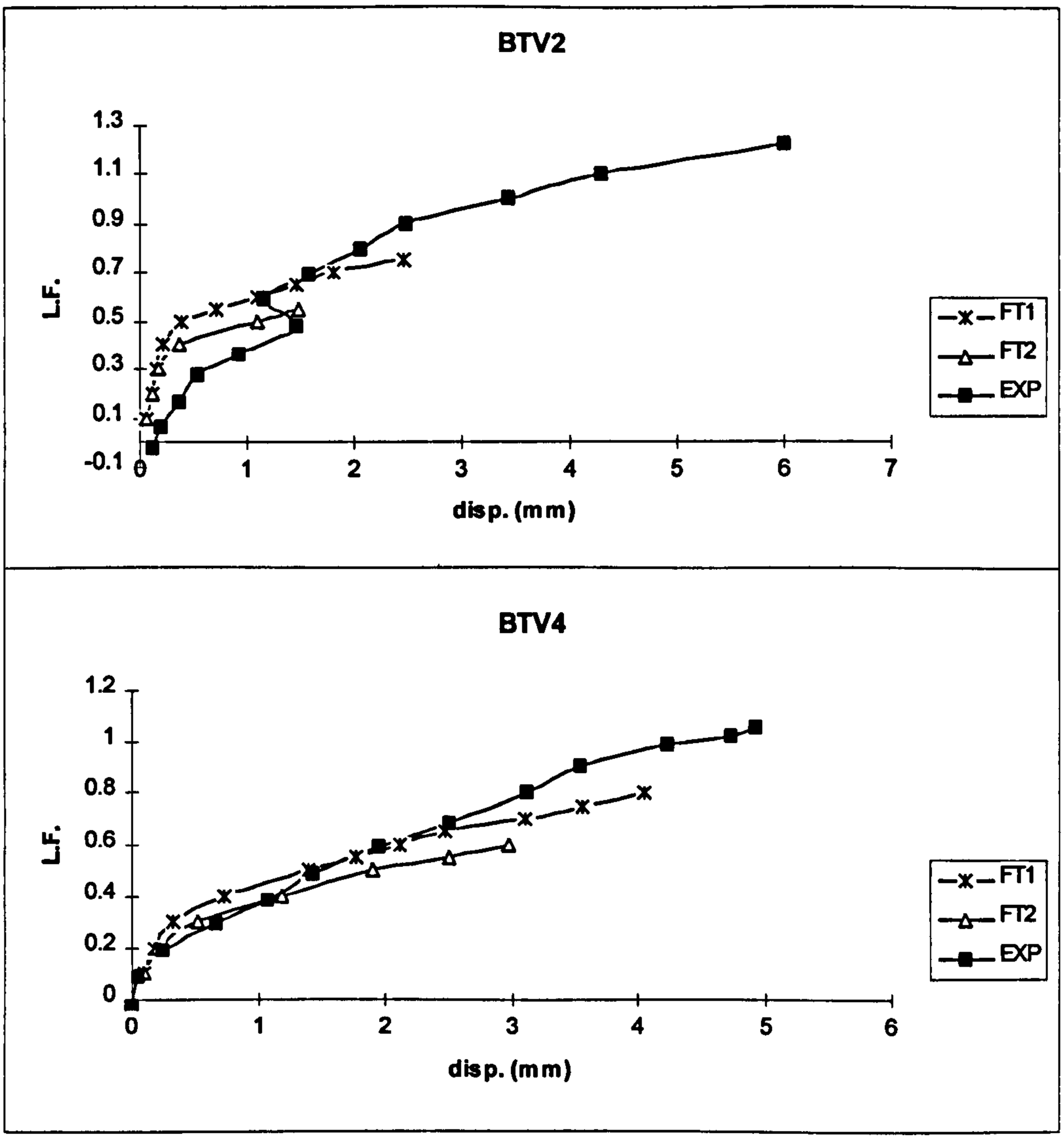

Fig. 8.7: Effect of the concrete tensile strength on the displacement

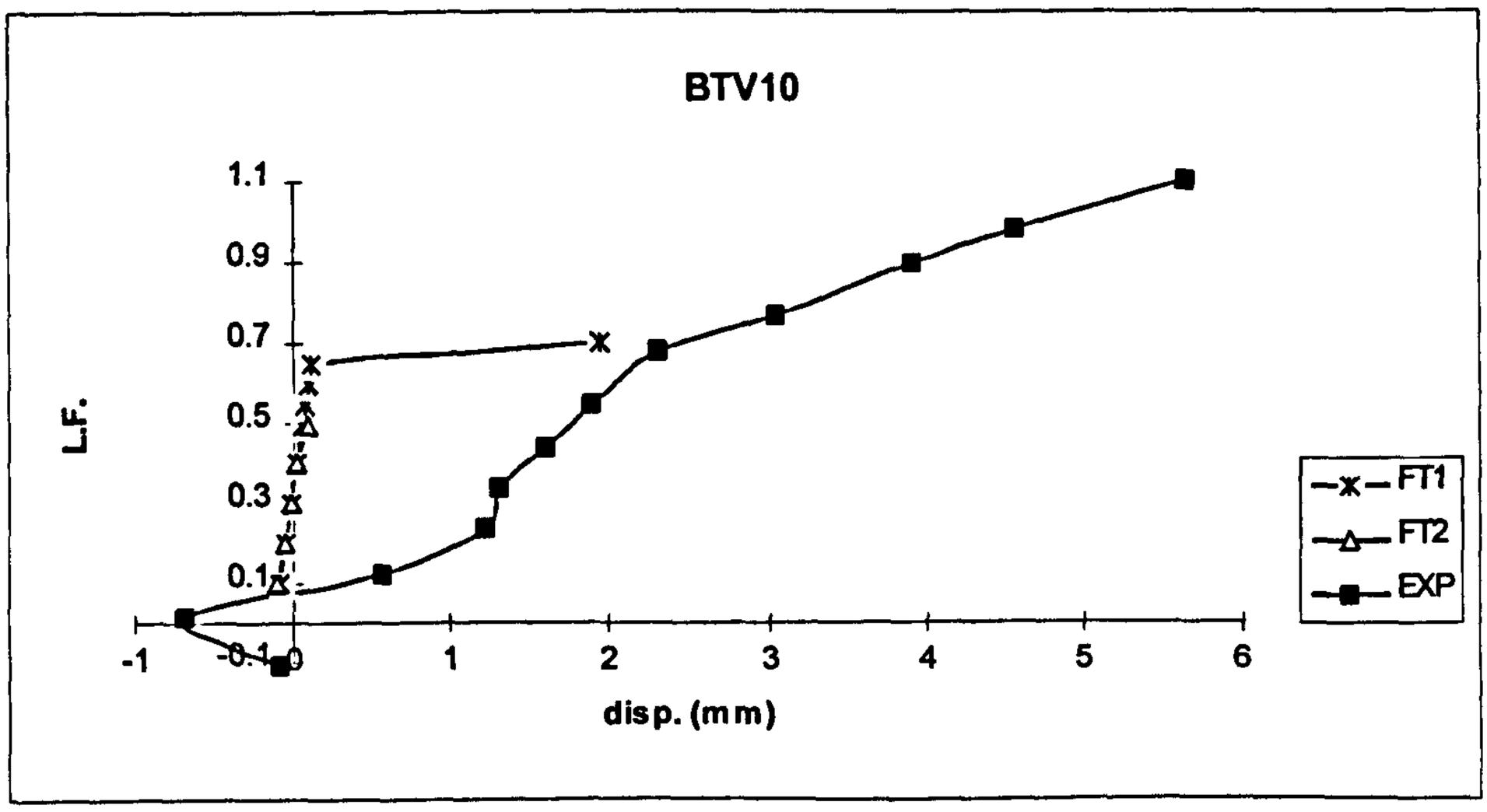

Fig. 8.7: Continued

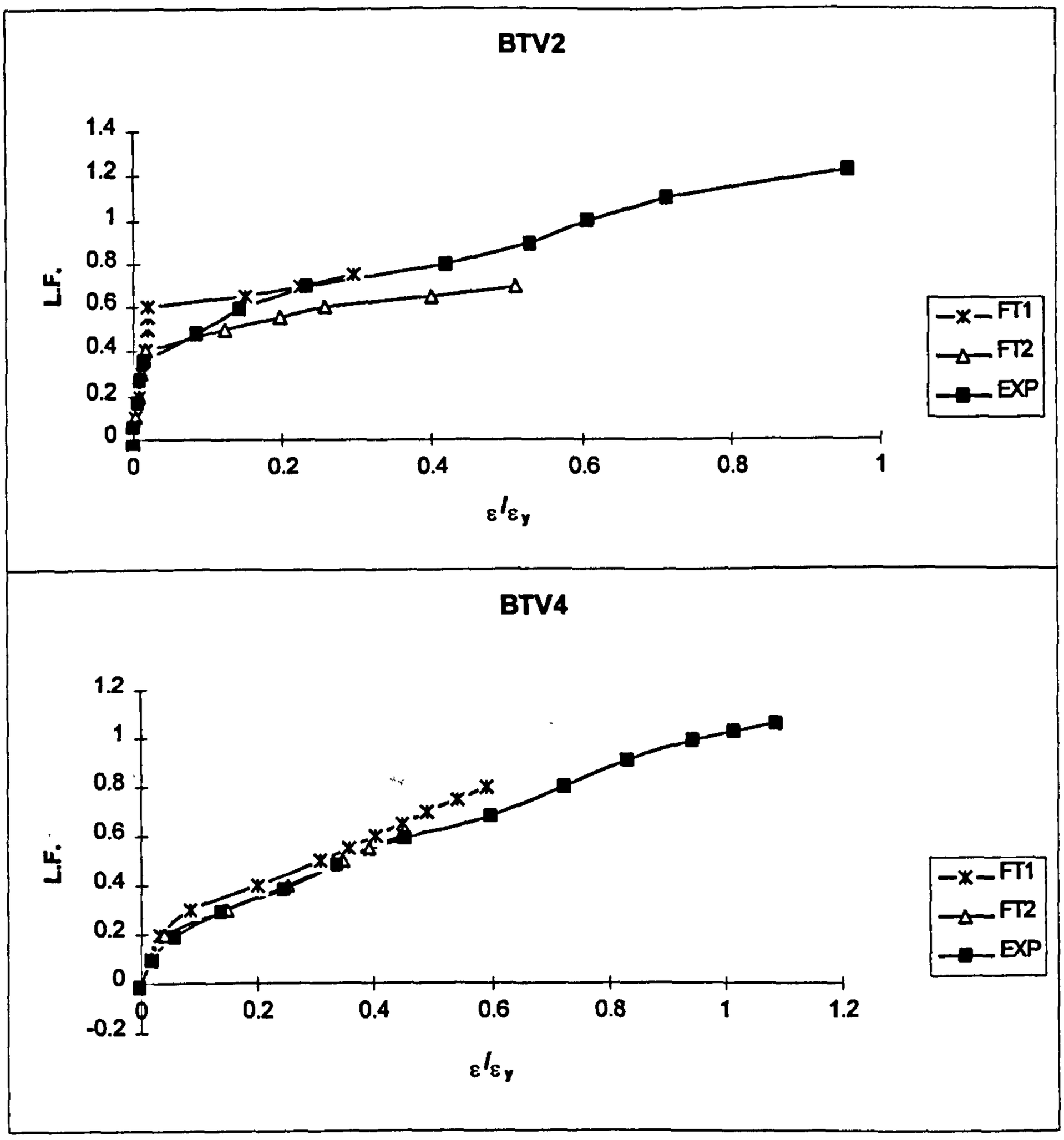

Fig. 8.8: Effect of the concrete tensile strength on the front web longitudinal steel

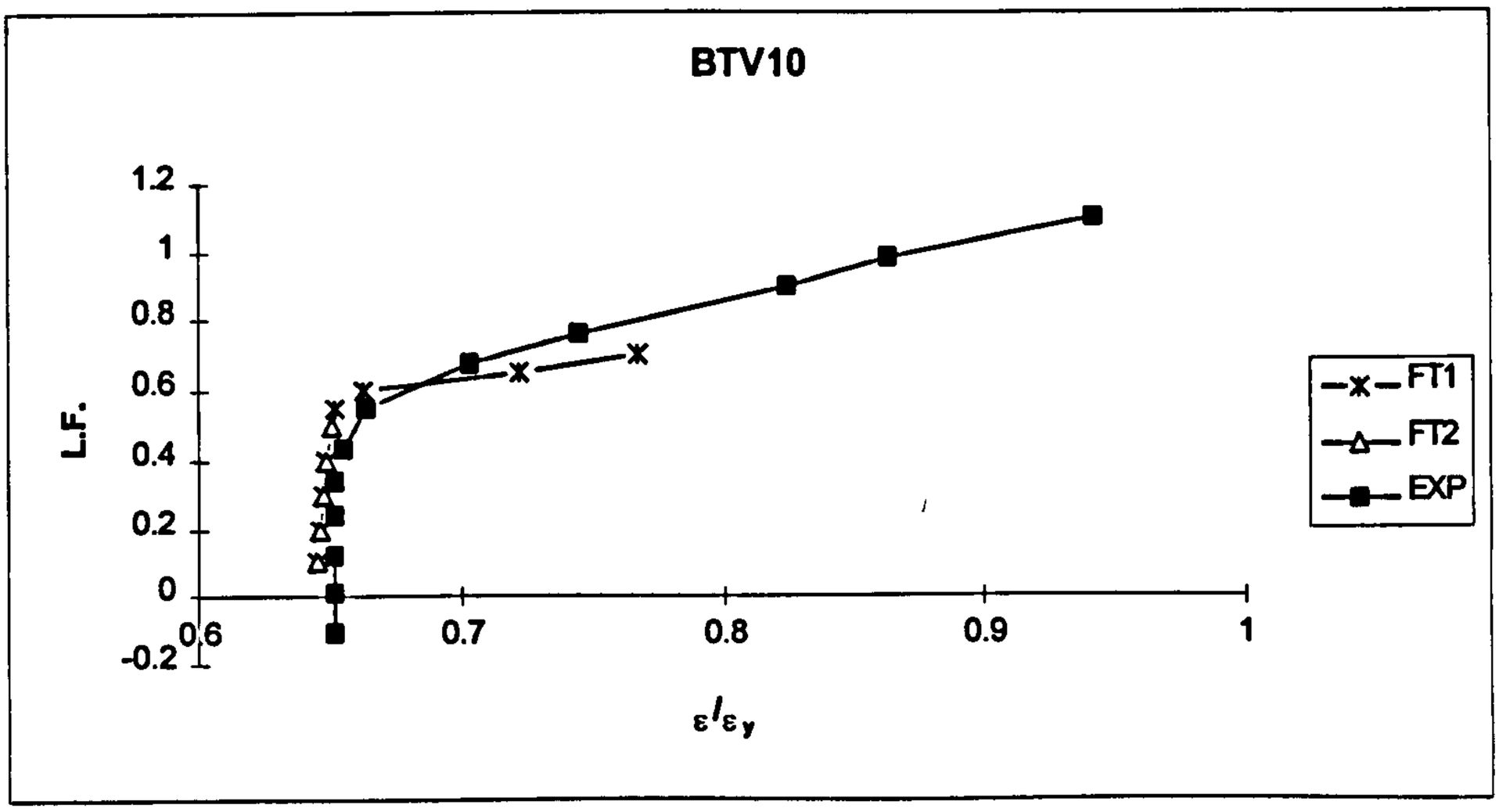

Fig. 8.8: Continued

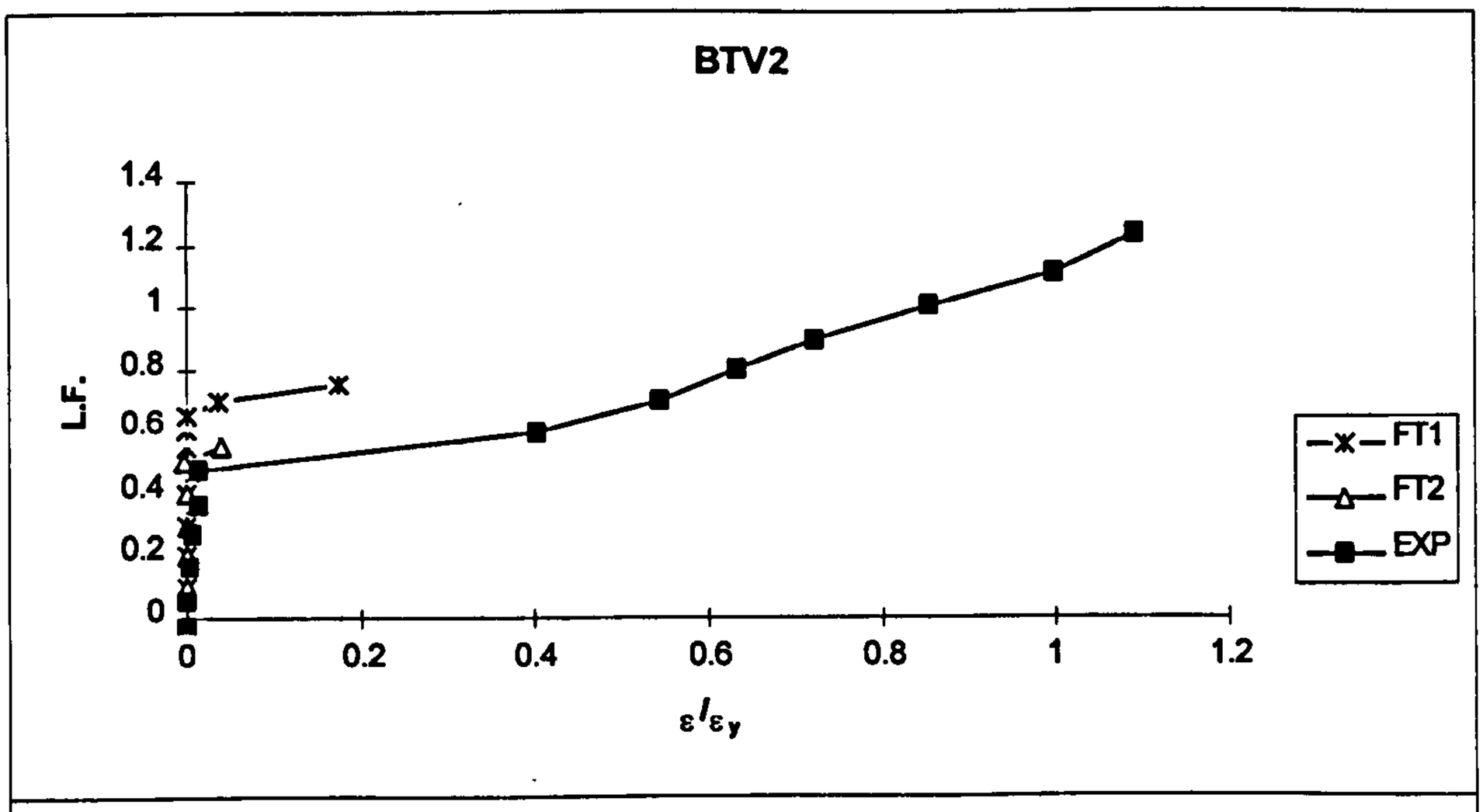

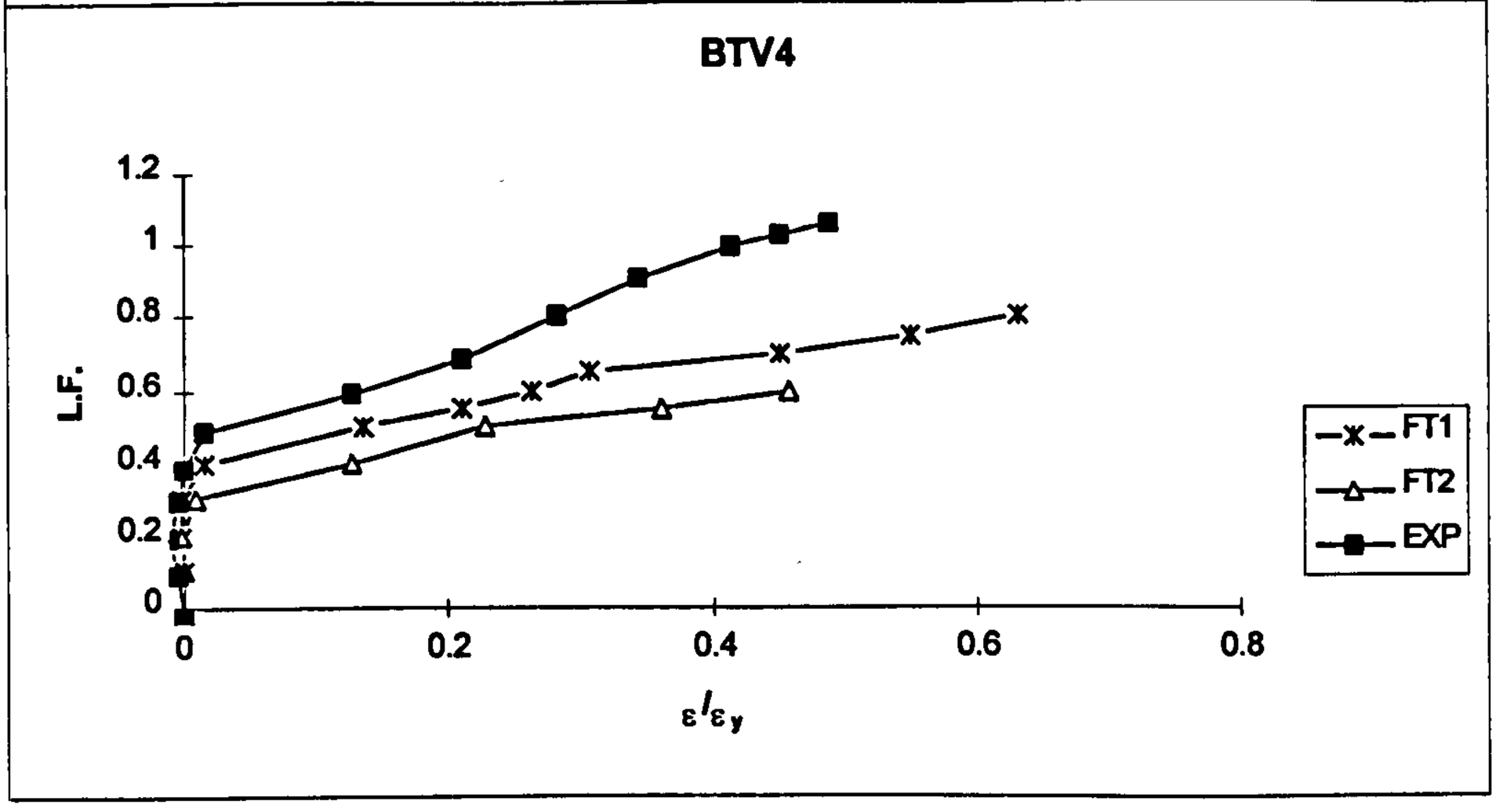

Fig. 8.9: Effect of the concrete tensile strength on the front web transverse steel

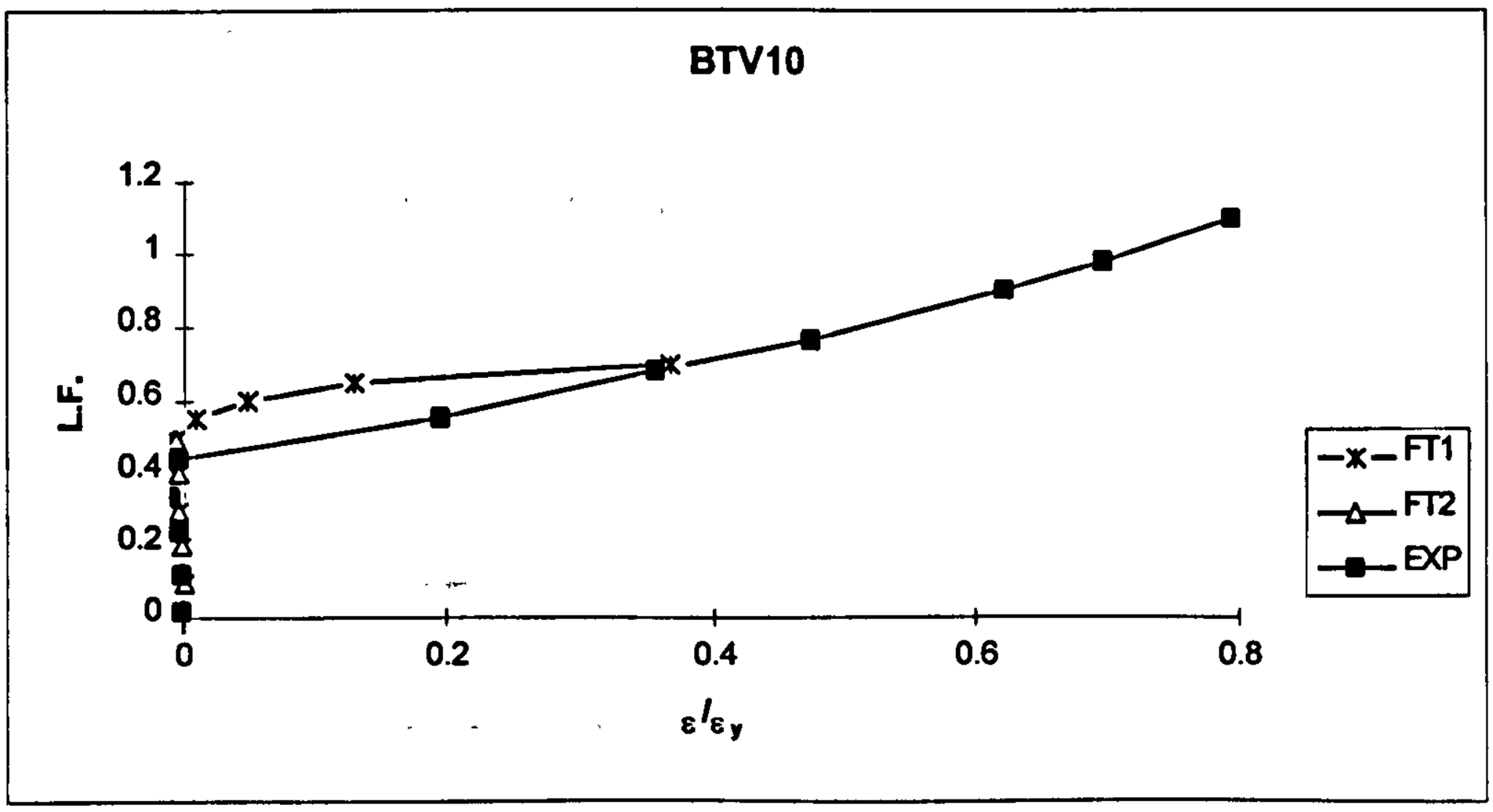

Fig. 8.9: Continued

Table 8.5: Effect of concrete tensile strength on the residual forces

Beam	FT1		FT2	
L.F	No. iter.	%R.F.	No .iter.	%R.F.
0.1	1	0.1	1	0.1
0.2	1	0.1	4	4.2
0.3	9	4.4	24	4.8
0.4	26	4.9	45	4.9
0.5	41	4.9	36	4.9
0.55	32	4.9	73	4.8
0.6	25	5.0	49	4.8
0.65	21	5.0	100	13.3
0.7	75	5.0		
0.75	47	5.0		
0.8	45	5.0		
0.85	100	11.3		

(b): BTV4

Beam	FT1		FT2	
L.F	No. iter.	%R.F.	No .iter.	%R.F.
0.1	1	0.1	1	0.1
0.2	1	0.1	4	4.2
0.3	9	4.4	24	4.8
0.4	26	4.9	45	4.9
0.5	41	4.9	36	4.9
0.55	32	4.9	73	4.8
0.6	25	5.0	49	4.8
0.65	21	5.0	100	13.3
0.7	75	5.0		
0.75	47	5.0		
0.8	45	5.0		
0.85	100	11.3		

(b): BTV4

Beam	FT1		FT2	
L.F	No. iter.	%R.F.	No .iter.	%R.F.
0.1	1	0.2	1	0.2
0.2	1	0.1	1	0.1
0.3	1	0.1	1	0.1
0.4	1	0.1	1	2.4
0.5	1	2.5	1	4.7
0.55	1	2.7	100	10.1
0.6	1	3.6		
0.65	2	4.6		
0.7	3	4.6		
0.75	100	11.1		

(c): BTV10

Table 8.6 shows that FT1 has resisted more load than FT2.

From this discussion it is clear that the tensile strength of concrete had significant effect on the ultimate load carrying capacity and some effect on the displacement and the steel strain.

Since beam FT1 behaved closer to the experiments, it was considered for next stage of the analysis.

Table 8.6: Effect of concrete tensile strength on the failure load

Beam	FT1	FT2	EXP
BTV2	0.75	0.55	1.22
BTV4	0.8	0.6	1.06
BTV10	0.7	0.5	1.1

8.2.4: Effects of the value of maximum compressive strain

Having fixed the tension stiffening factor as TESN6, the shear retention factor as SR45 and the tensile strength as $f_t^{'} = 0.54\sqrt{f_c^{'}}$ N/mm^2, the next step was to examine the effect of maximum compressive strain. In the previous computational experiments, the strain at peak stress was taken as a function of the concrete compressive strength ($\varepsilon_{cc} = \frac{\sqrt{f_c^{'}}}{2500}$) and the maximum strain at failure was considered as a constant value ($\varepsilon_{max} = 0.0035$). In this section the effect of having both strains made equal to the strain at peak stress ($\varepsilon_{max} = \varepsilon_{cc} = \frac{\sqrt{f_c^{'}}}{2500}$) was investigated. This means that there was no softening in the stress-strain curve. The two values coincide when $f_c^{'} = 76.6$ N/mm^2, a value well beyond the cylinder strength of beams tested in this work.

$\varepsilon_{max} = 0.0035$ and $\varepsilon_{cc} = \frac{\sqrt{f_c^{'}}}{2500}$ used in EMAX1

$\varepsilon_{max} = \varepsilon_{cc} = \frac{\sqrt{f_c^{'}}}{2500}$ used in EMAX2

Although the value for ε_{max} in EMAX1 was about 44% higher than that of EMAX2, both beams followed almost the same path for displacement and steel strains with EMAX1 being slightly closer to experiment in some cases (Figs. 8.10-12). Table 8.7 shows that EMAX1 has performed better than EMAX2 (less residual

forces and better convergence). Table 8.8 indicates that beam EMAX2 failed earlier than beam EMAX1.

From the above it is clear that the ε_{max} has some effect on the beam behaviour and ultimate failure load. Since the equations used in beam EMAX1 gave closer results to the experiments it was decided to use a separate equations for ε_{max} and ε_{cc} as in this beam for the next stage of analysis.

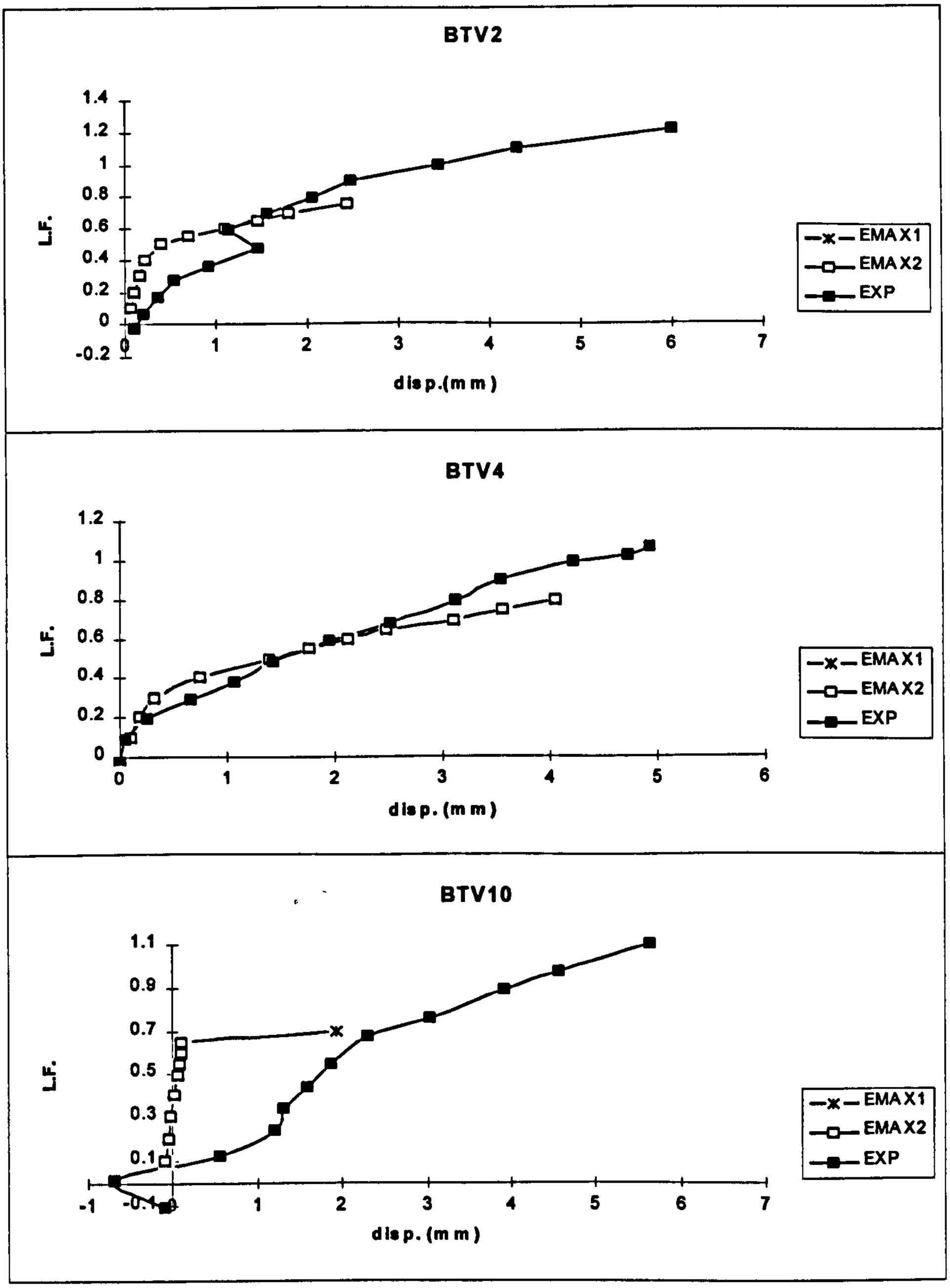

Fig. 8.10: Effect of the value of the compressive strain at peak stress on the displacement

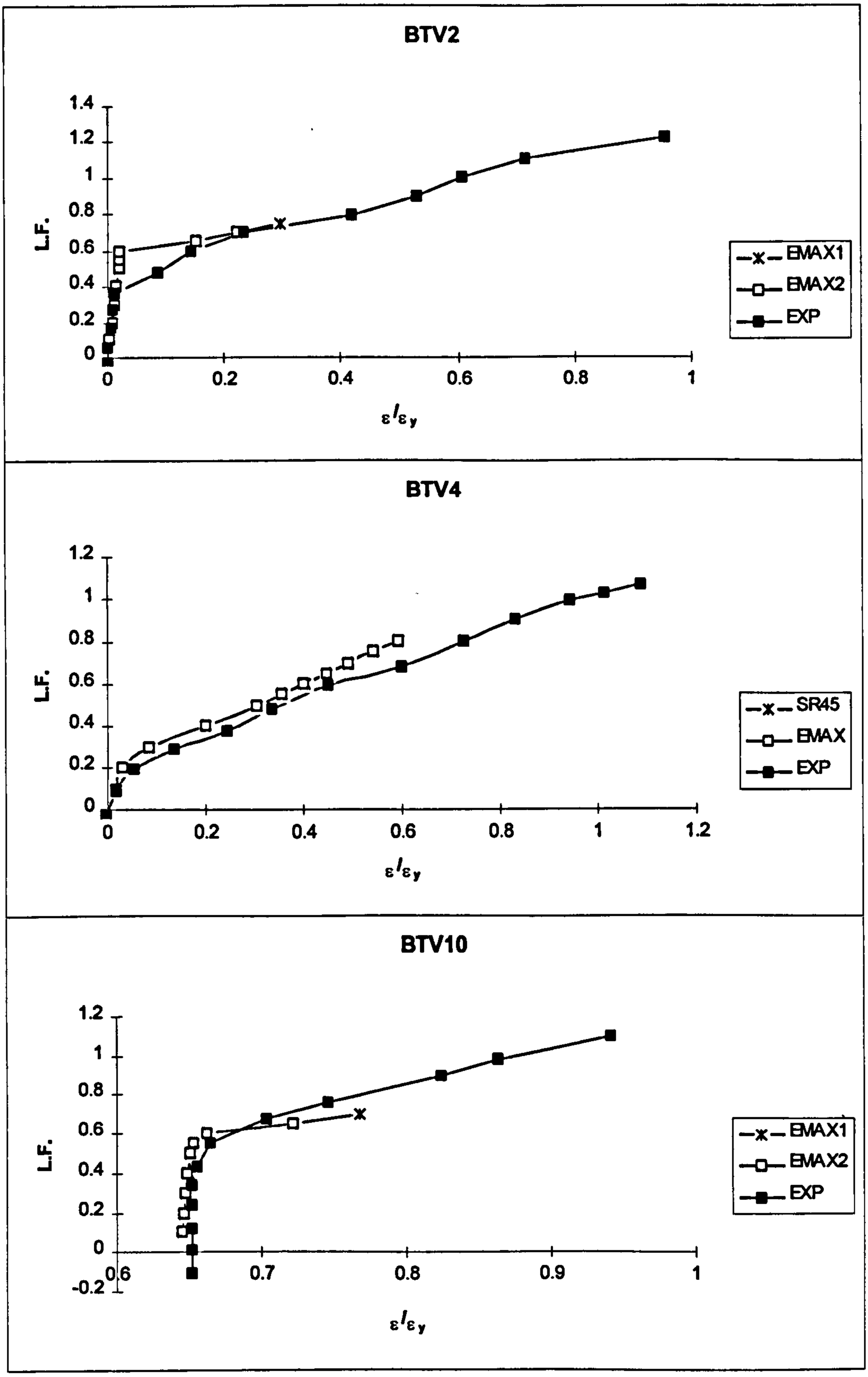

Fig. 8.11: Effect of the compressive strain at peak stress on the front web longitudinal steel

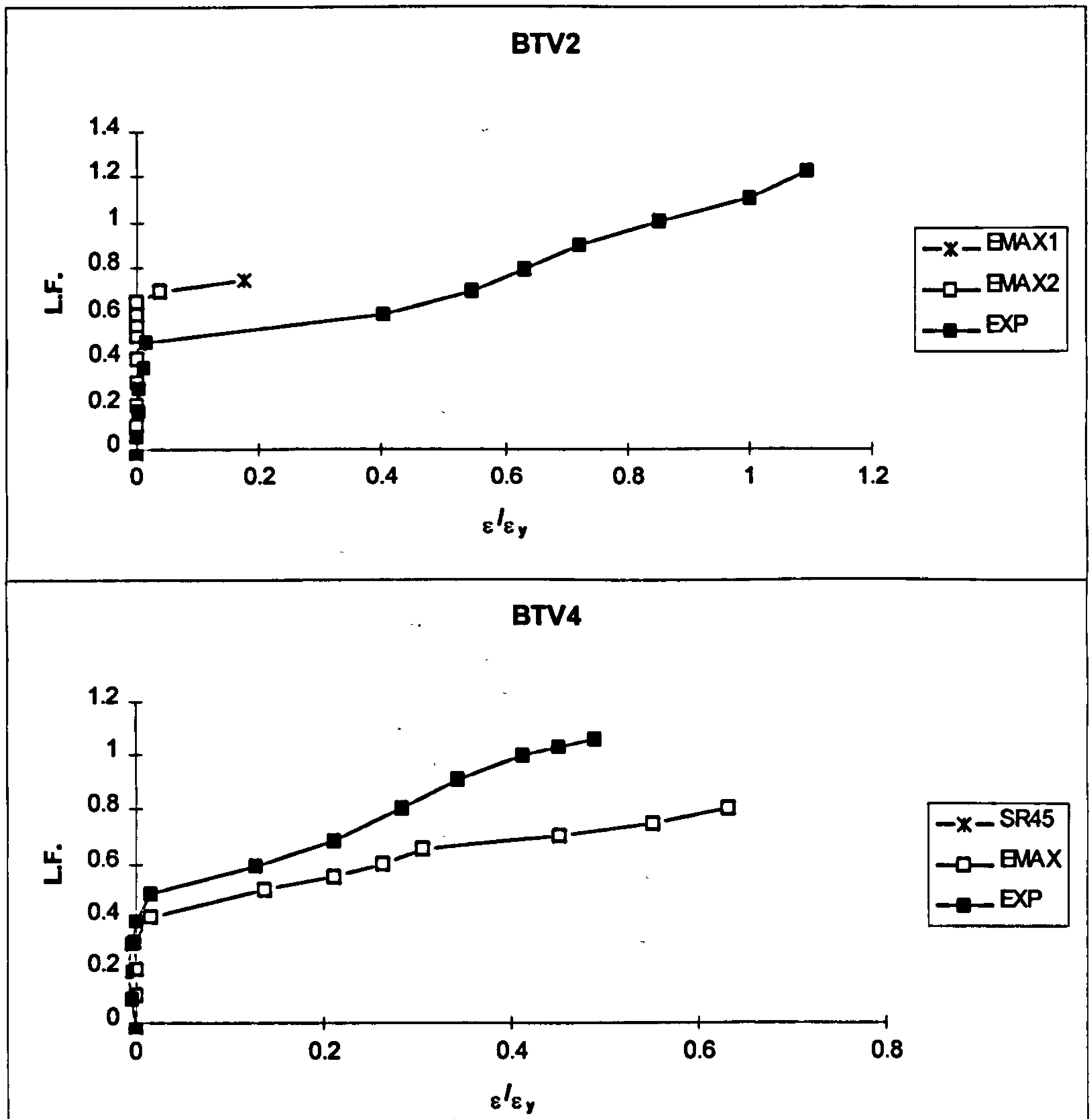

Fig. 8.12: Effect of the value of compressive strain at peak stress on the front web transverse steel

Table 8.7: Effect of the value of the compressive strain at peak stress on the residual forces

Beam	EMAX1		EMAX2	
L.F	No. iter.	%R.F.	No .iter.	%R.F.
0.1	1	0.1	1	0.1
0.2	1	0.1	1	0.1
0.3	1	0.2	1	0.2
0.4	3	1.9	3	1.9
0.5	20	5.0	20	5.0
0.55	55	4.9	55	4.9
0.6	75	5.0	75	5.0
0.65	70	4.9	70	4.9
0.7	57	4.8	57	4.8
0.75	61	4.9	100	8.4
0.8	100	9.0		

(a): BTV2

Beam	EMAX1		EMAX2	
L.F	No. iter.	%R.F.	No .iter.	%R.F.
0.1	1	0.1	1	0.1
0.2	1	0.1	1	0.1
0.3	9	4.4	9	4.4
0.4	26	4.9	26	4.9
0.5	41	4.9	41	4.9
0.55	32	4.9	32	4.9
0.6	25	5.0	25	5.0
0.65	21	5.0	21	5.0
0.7	75	5.0	75	5.0
0.75	47	5.0	47	5.0
0.8	45	5.0	45	5.0
0.85	100	11.3	100	74.0

(b): BTV4

Beam	EMAX1		EMAX2	
L.F	No. iter.	%R.F.	No .iter.	%R.F.
0.1	1	0.2	1	0.2
0.2	1	0.1	1	0.1
0.3	1	0.1	1	0.1
0.4	1	0.1	1	0.1
0.5	1	2.5	1	2.5
0.55	1	2.7	1	2.7
0.6	1	3.6	1	3.6
0.65	2	4.6	2	4.6
0.7	3	4.6	100	11.1
0.75	100	11.1		

(c): BTV10

Table 8.8: Effect of the value of the compressive strain at peak stress on the failure load

Beam	EMAX1	EMAX2	EXP
BTV2	0.75	0.7	1.22
BTV4	0.8	0.8	1.06
BTV10	0.7	0.65	1.1

8.2.5: Effects of concrete compressive strength

After having fixed: Tension stiffening = TESN6, shear retention = SR45, tensile strength of concrete = FT1 and compressive strain as in EMAX1, the next stage was to investigate the effect of the concrete compressive strength $f_c^{'}$. The effect of 25% increase in the actual concrete compressive strength was tried. This was helpful to see how accurate one can be in taking the average of cube strength results for each beam and in a way this was an indication of sensitivity of results to cube strength.

Two values for $f_c^{'}$ were examined for each beam designated as:

$f_c^{'}$ = as measured used in beam COMP1

$f_c^{'} = 1.25 f_c^{'}$ N/mm^2 used in beam COMP2

It is worth mentioning that a 25% change in compressive strength of concrete in beam COMP2 led to about 12% changes in compressive strain at peak stress, Young's modulus and tensile strength of concrete due to the following relations:

$$\varepsilon_{cc} = \frac{\sqrt{f_c'}}{2500}$$

$$E_c = 5000\sqrt{f_c'} \quad \text{N/mm}^2$$

$$f_t' = 0.54\sqrt{f_c'} \quad \text{N/mm}^2$$

From figures 8.13-15 it is clear that both beams have given very similar results for displacements and steel strains. Tables 8.9-10 show that the two beams behaved in a similar fashion except that in beam BTV4, COMP2 failed at a load of 5% larger than COMP1.

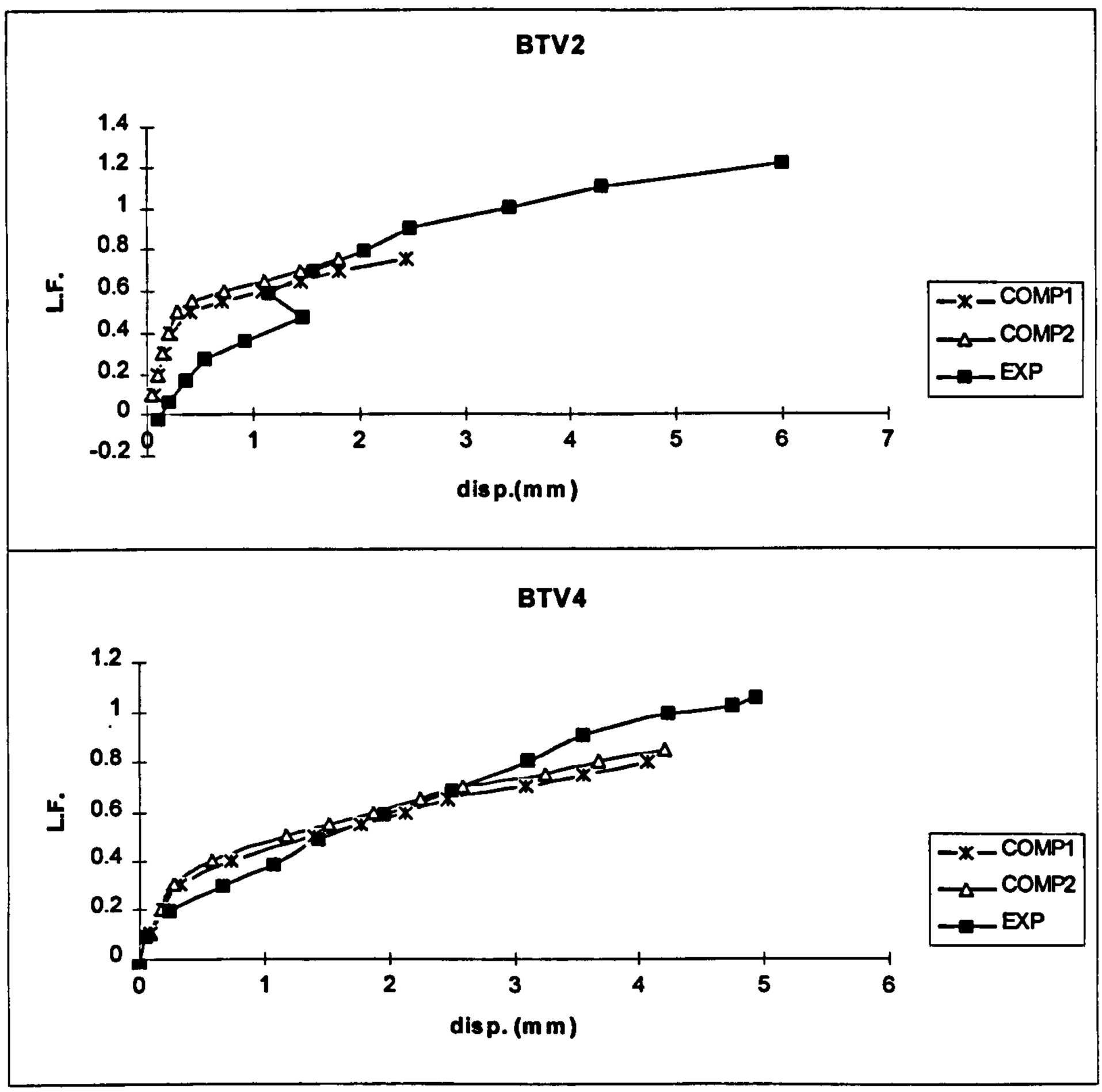

Fig. 8.13: Effect of the concrete compressive strength on the displacement

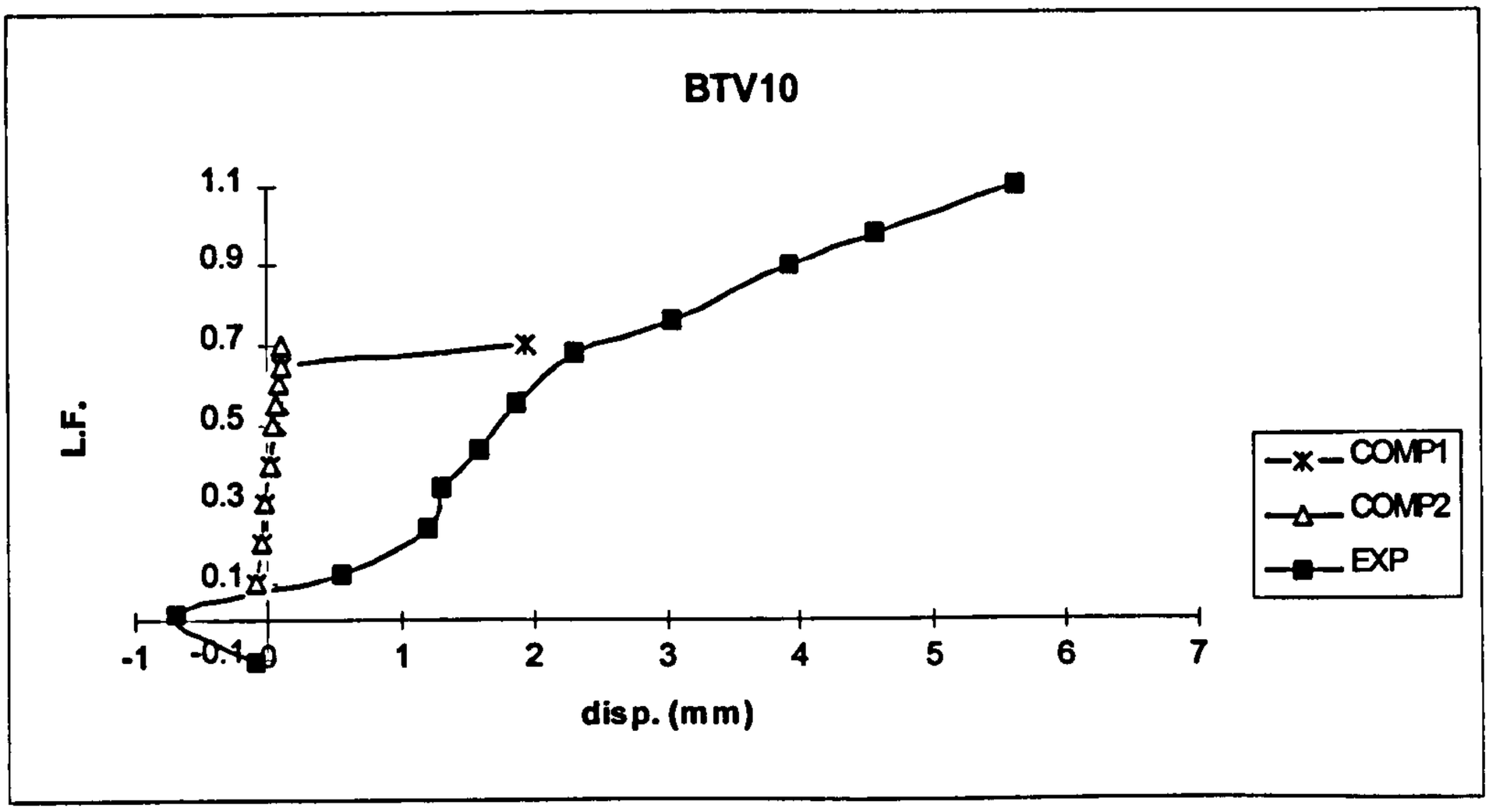

Fig. 8.13: Continued

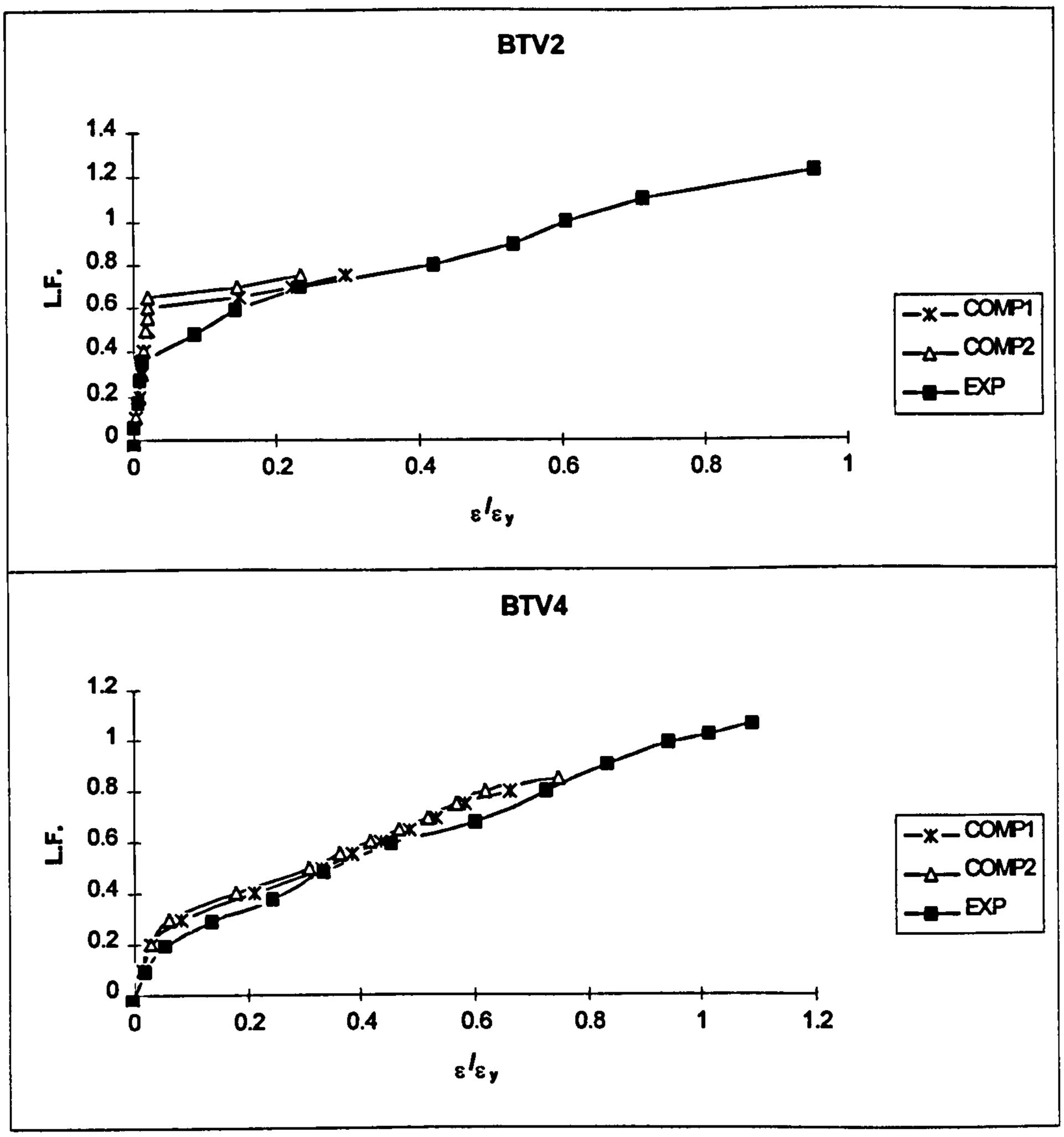

Fig. 8.14: Effect of the concrete compressive strength on the front web longitudinal steel

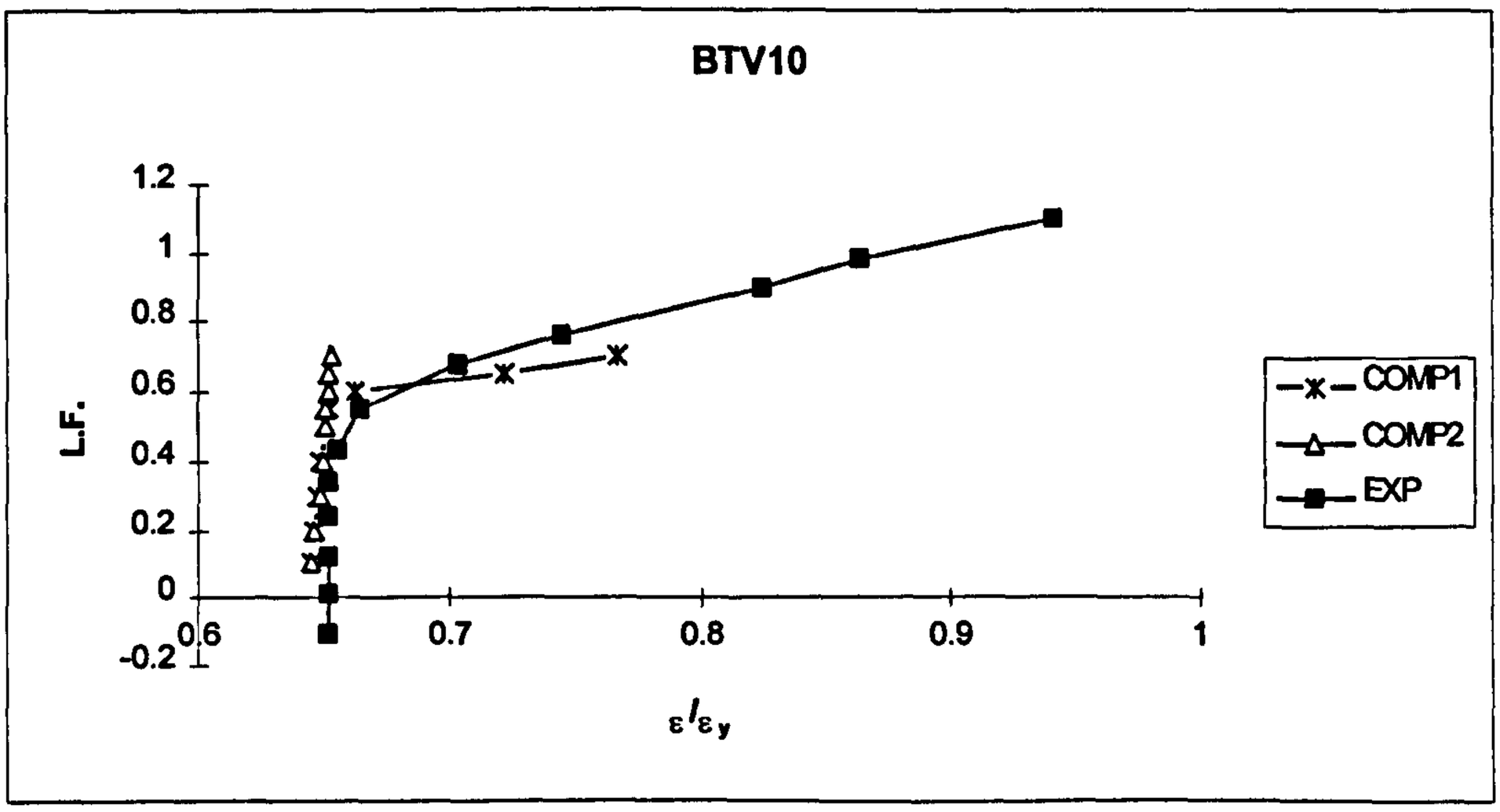

Fig. 8.14: Continued

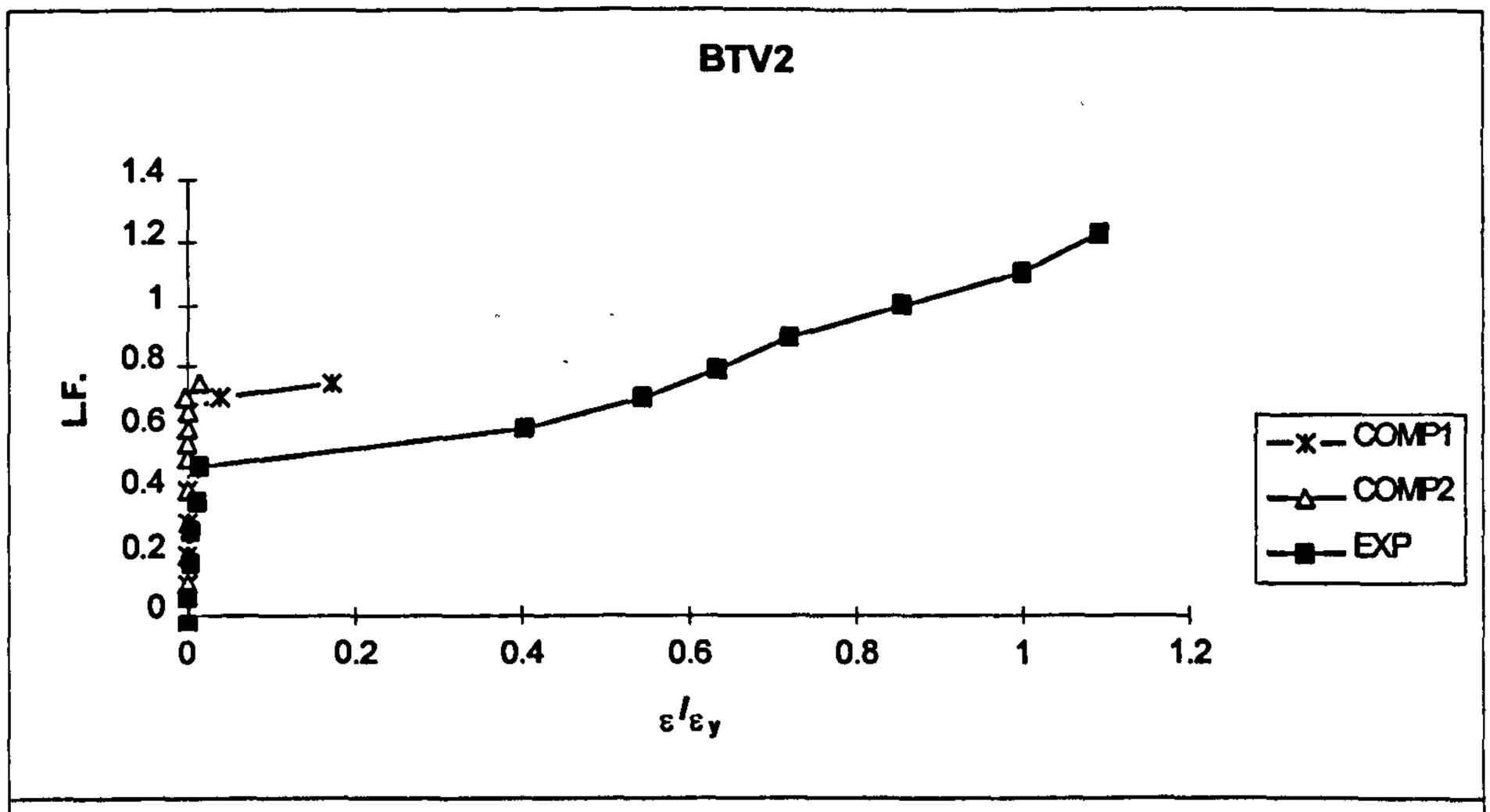

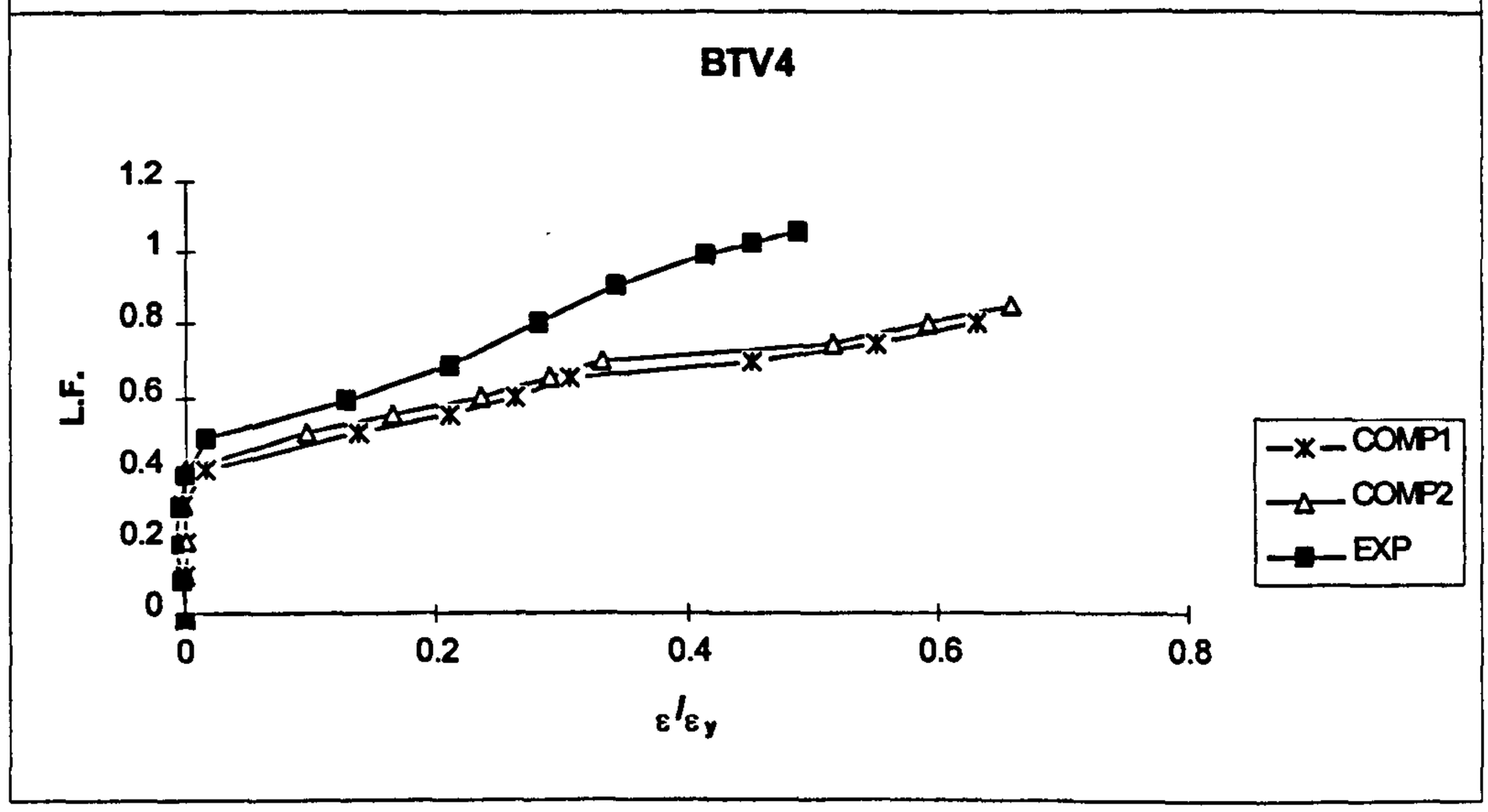

Fig. 8.15: Effect of the compressive strength on the front web transverse steel

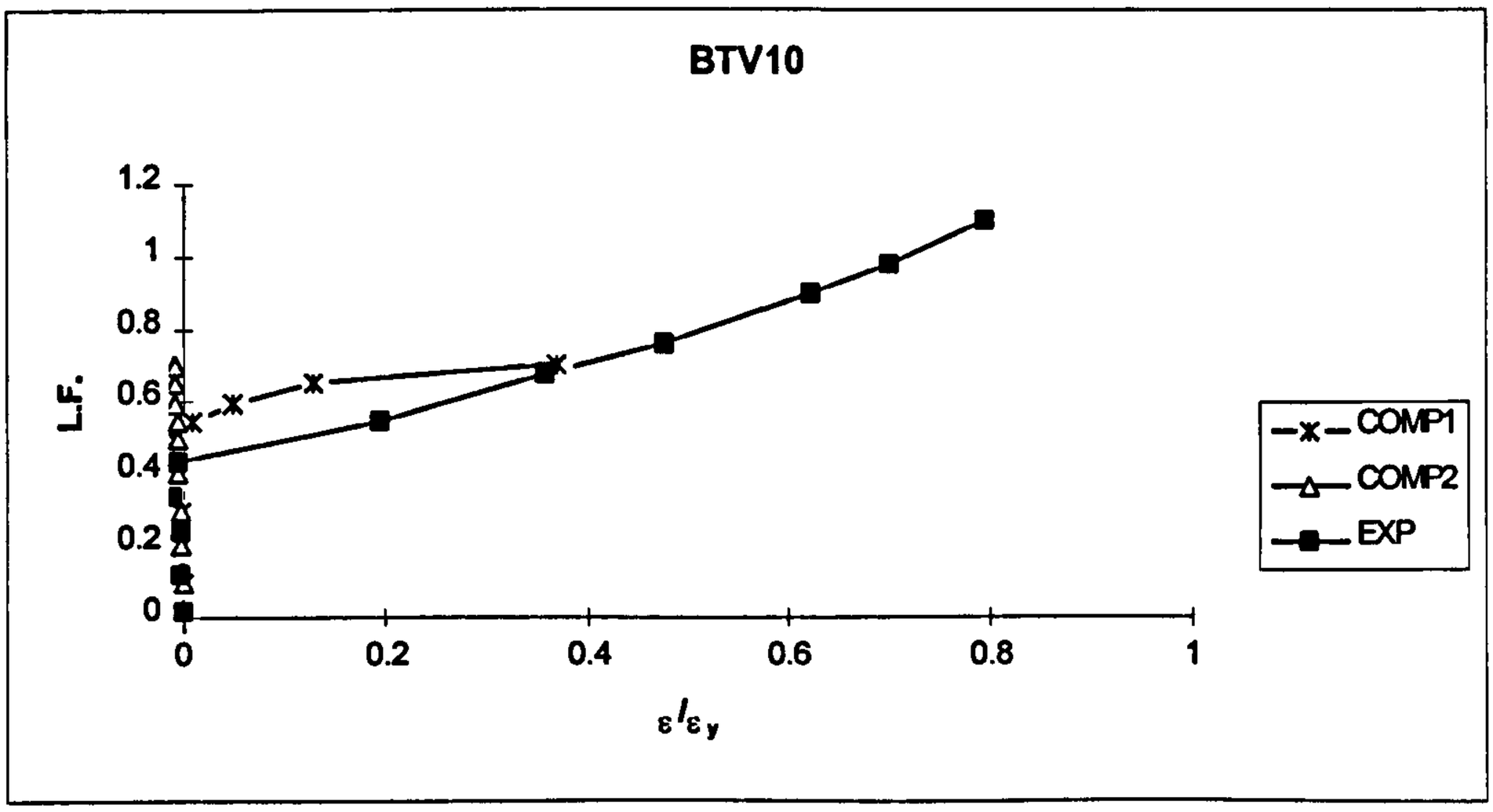

Fig. 8.15: Continued

Table 8.9: Effect of the concrete compressive strength on the residual forces

Beam	COMP1		COMP2	
L.F	No. iter.	%R.F.	No .iter.	%R.F.
0.1	1	0.1	1	0.1
0.2	1	0.1	1	0.0
0.3	1	0.2	1	0.1
0.4	3	1.9	1	0.1
0.5	20	5.0	15	5.0
0.55	55	4.9	25	4.7
0.6	75	5.0	61	5.0
0.65	70	4.9	77	4.9
0.7	57	4.8	65	4.9
0.75	61	4.9	63	5.0
0.8	100	9.0	100	8.7

(a): BTV2

Beam	COMP1		COMP2	
L.F.	No. iter.	%R.F.	No .iter.	%R.F.
0.1	1	0.1	1	0.1
0.2	1	0.1	1	0.2
0.3	9	4.4	7	4.7
0.4	26	4.9	20	4.8
0.5	41	4.9	41	4.9
0.55	32	4.9	30	5.0
0.6	25	5.0	34	5.0
0.65	21	5.0	29	5.0
0.7	75	5.0	24	4.9
0.75	47	5.0	82	4.9
0.8	45	5.0	39	5.0
0.85	100	11.3	60	4.9
0.9			100	8.7

(b): BTV4

Beam	COMP1		COMP2	
L.F.	No. iter.	%R.F.	No .iter.	%R.F.
0.1	1	0.2	1	0.0
0.2	1	0.1	1	0.0
0.3	1	0.1	1	0.0
0.4	1	0.1	1	0.1
0.5	1	2.5	1	1.6
0.55	1	2.7	1	1.6
0.6	1	3.6	1	1.9
0.65	2	4.6	1	3.6
0.7	3	4.6	1	3.8
0.75	100	11.1	100	13.5

(c): BTV10

Table 8.10: Effect of the concrete compressive strength on the failure load

Beam	SR45	COMP	EXP
BTV2	0.75	0.75	1.22
BTV4	0.8	0.85	1.06
BTV10	0.7	0.7	1.1

From the above it is possible to state that the concrete compressive strength (in the range considered) had very little effect on the displacement and steel strain but some effect on the ultimate load carrying capacity and the convergence values. In other words, some differences in concrete strength from the actual values will not cause large changes in the beam behaviour or ultimate load. This was perhaps an indication that the failures were all ductile and governed by steel yield. Therefore, the analysis was continued using the laboratory cube tests f_{cu}.

8.3: Numerical parameters

As a result of the analysis in section 8.2, the following material parameters were selected and kept fixed:

1. Concrete compressive strength: as measured.
2. Tension stiffening: $\sigma_t = (\sqrt[4]{\frac{\varepsilon_{cr}}{\varepsilon_n}}) f_t^{'}$.
3. Shear retention parameters: $B = 0.4 \qquad \beta_{\min} = 0.05$.
4. Tensile strength of concrete: $f_t^{'} = 0.54\sqrt{f_c^{'}}$ N/mm^2.
5. Maximum compressive strain, cracking strain and Young's modulus: $\varepsilon_{\max} =$ 0.0035, $\varepsilon_{cc} = \frac{\sqrt{f_c^{'}}}{2500}$ and $E_c = 5000\sqrt{f_c^{'}}$ N/mm^2 respectively.

Three numerical parameters were studied in this part of analysis:

I. Non-linear solution algorithm.

II. Mesh size.

III. Size of convergence tolerance.

Initially all beams were tested for 84x84mm mesh size and convergence tolerance of 5%.

8.3.1: Effects of non-linear solution algorithm

The mixed incremental-iterative procedure (Ch.7) was adopted in this study. In this procedure, the load is applied in increments and the solution is obtained iteratively until equilibrium is achieved in each increment to an acceptable level of accuracy. The stiffness matrix was updated at various values of iteration and/or increment. Five different methods of updating the stiffness matrix were examined at this stage. The equilibrium conditions were checked by evaluating the residual force norms. The methods of updating the stiffness matrix were:

1. Stiffness matrix was computed at the beginning of the first increment and unchanged thereafter except if the steel yielded or concrete cracked at any point. This method was used in beam NALGO1.
2. Stiffness matrix was re-computed for each iteration in each increment. This was applied in beam NALGO2.
3. Stiffness matrix was computed for the first iteration of each increment. This was introduced in beam NALGO3.
4. Stiffness matrix was calculated for the first iteration of the first increment and then for the second iteration of each of the following increments. This was tested in beam NALGO4.
5. Stiffness matrix was calculated for the first iteration of the first increment and for iteration numbers 2,5,10,20,25,30,.....etc., of any increment. This was explored in beam NALGO5.

Figures 8.16-18 show that all beams have followed almost the same path for displacement and steel strain. However, by examining tables 8.11 it is clear that beam NALGO2 was the best in achieving convergence. The second best was NALGO5. Table 8.12 shows the failure loads which indicate that beams NALGO2 and NALGO5 were the closest to the test failure loads. No major cost differences between NALGO2 and NALGO5 were encountered, as both beams took almost same time.

The above analysis indicate that the solution algorithm played almost no role on the beam behaviour. Nevertheless, it had some effect on the ultimate load carrying capacity and solution convergence.

Since beam NALGO2 has shown the best numerical behaviour, it was considered for subsequent analysis.

8.3.2: Effects of the mesh size

Having chosen the solution algorithm as NALGO2, the next step was to study the effect of the mesh size. Two element sizes were examined (Fig. 8.19):

1. 84x84 mm. used in MSH1 (22x12 elements excluding the diaphragms). This mesh size was used in all previous computational experiments
2. 126x126 mm. used in MSH2 (14x8 elements excluding the diaphragms).

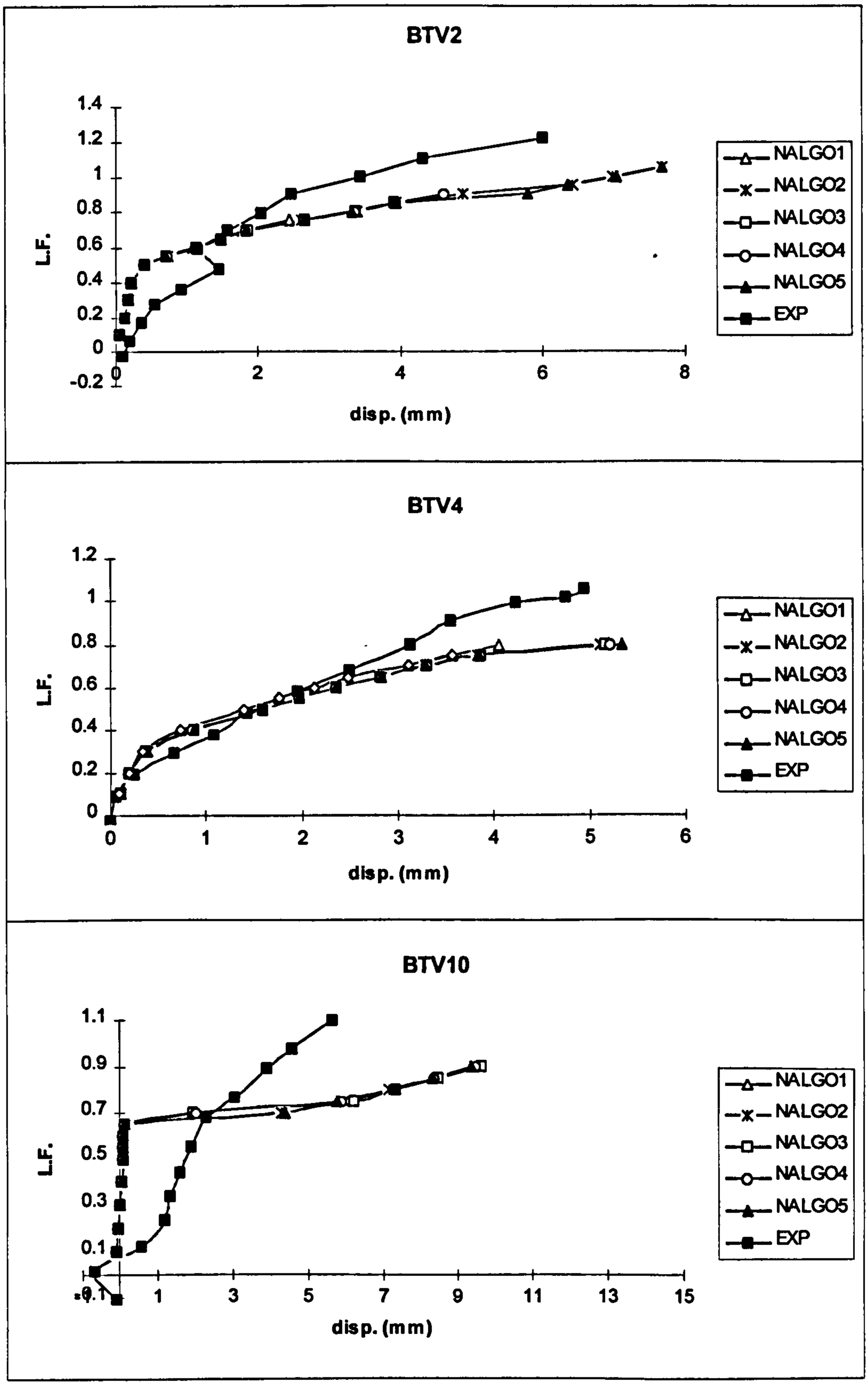

Fig. 8.16: Effect of the solution algorithm on the displacement

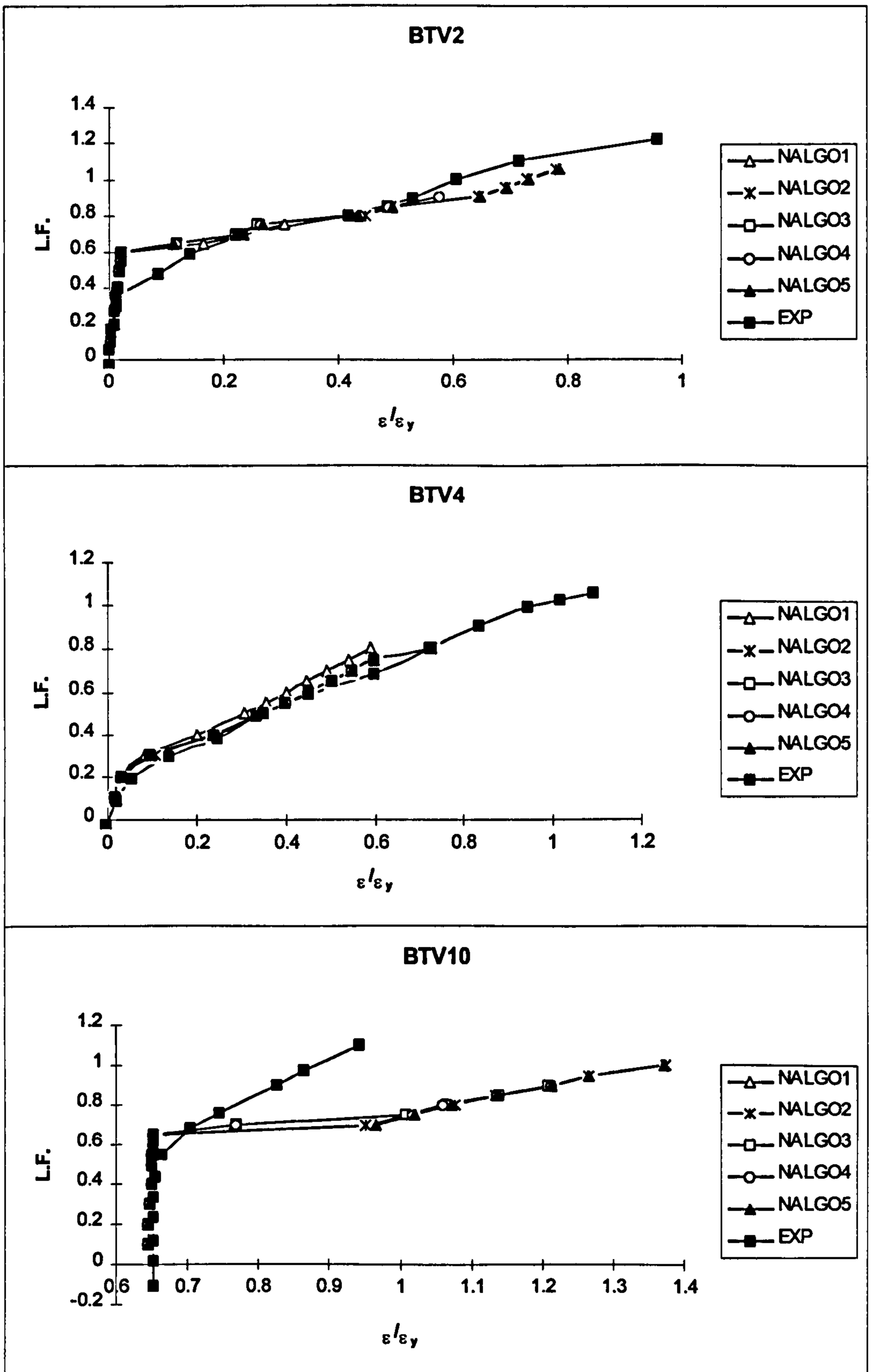

Fig. 8.17: Effect of the solution algorithm on the front web longitudinal steel

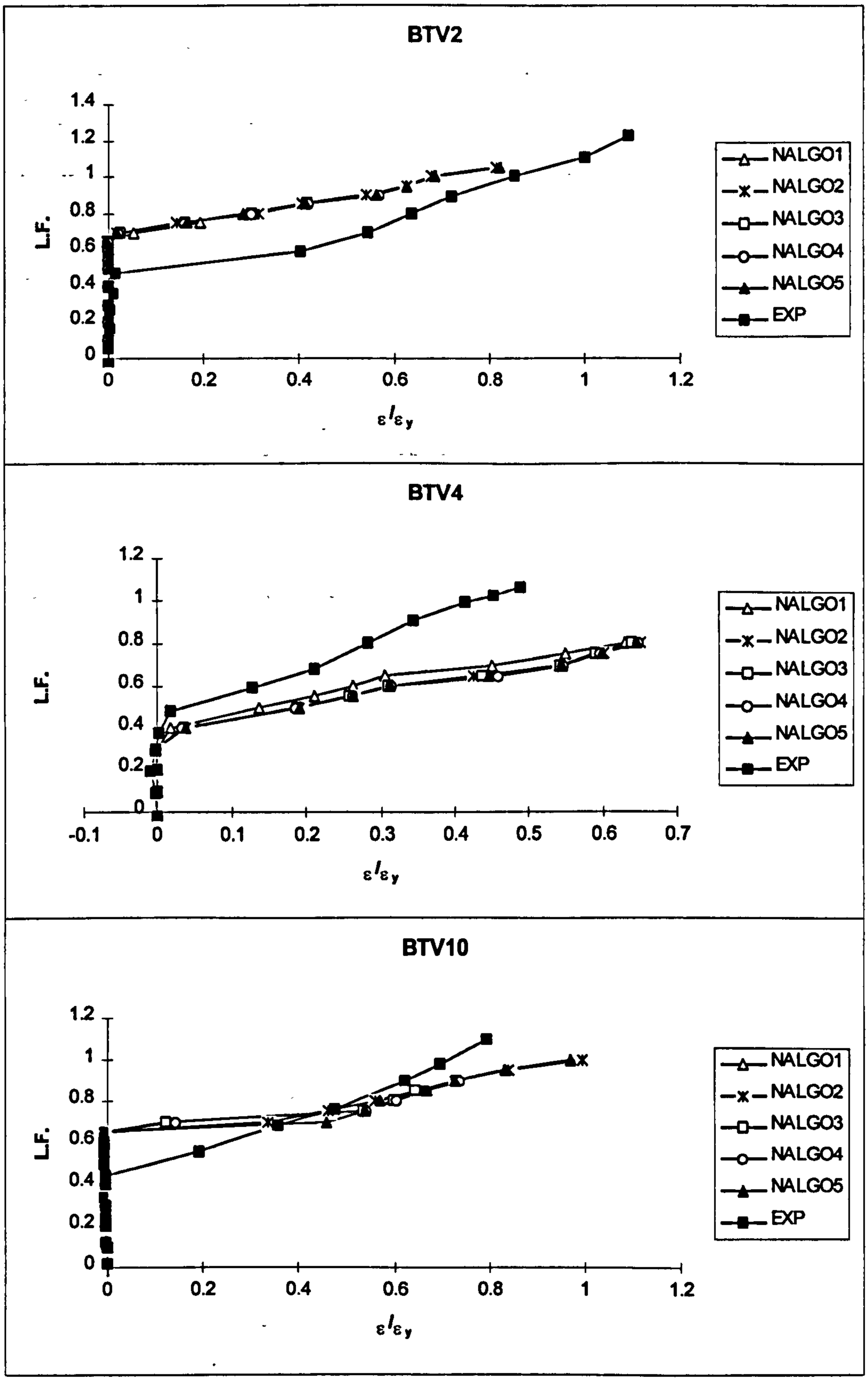

Fig. 8.18: Effect of the solution algorithm on the front web transverse steel

Table 8.11: Effect of the solution algorithm on the residual forces

Beam	NALGO1		NALGO2		NALGO3		NALGO4		NALGO5	
L.F	No. iter.	%R.F.	No .iter.	%R.F.	No. iter.	%R.F.	No .iter.	%R.F.	No. iter.	%R.F.
0.1	1	0.1	1	0.0	1	0.0	1	0.0	1	0.0
0.2	1	0.1	1	0.1	1	0.1	1	0.1	1	0.1
0.3	1	0.2	1	0.1	1	0.1	1	0.2	1	0.2
0.4	3	1.9	2	4.9	3	1.9	2	4.9	2	4.9
0.5	20	5.0	10	4.9	19	4.8	16	4.6	11	4.8
0.55	55	4.9	20	4.6	40	5.0	38	4.9	21	4.9
0.6	75	5.0	25	4.6	58	4.9	55	4.9	26	4.9
0.65	70	4.9	21	4.9	45	4.9	44	4.9	23	5.0
0.7	57	4.8	14	4.7	28	4.9	25	5.0	16	4.9
0.75	61	4.9	18	4.9	65	4.9	63	4.9	31	4.9
0.8	100	9.0	23	4.0	30	4.9	30	4.8	20	4.3
0.85			11	4.1	15	5.0	13	4.8	13	4.2
0.9			34	4.8	100	10.2	28	5.0	95	3.4
0.95			32	4.5			100	14.8	9	4.2
1			9	3.8					15	4.7
1.05			15	4.8					15	4.9
1.1			49	*****					85	*****

(a): BTV2

Beam	NALGO1		NALGO2		NALGO3		NALGO4		NALGO5	
L.F	No. iter.	%R.F.	No .iter.	%R.F.	No. iter.	%R.F.	No .iter.	%R.F.	No. iter.	%R.F.
0.1	1	0.1	1	0.1	1	0.1	1	0.1	1	0.1
0.2	1	0.1	1	0.1	1	0.1	1	0.1	1	0.1
0.3	9	4.4	7	3.6	9	4.4	7	5.0	7	5.0
0.4	26	4.9	11	4.9	27	4.9	20	4.8	13	4.5
0.5	41	4.9	13	4.8	34	4.9	26	5.0	15	4.9
0.55	32	4.9	11	4.8	19	4.9	17	4.9	13	4.7
0.6	25	5.0	10	4.5	15	5.0	15	4.9	11	4.4
0.65	21	5.0	10	4.0	13	4.9	12	5.0	10	4.6
0.7	75	5.0	7	4.2	8	4.7	7	4.8	7	4.3
0.75	47	5.0	9	4.8	16	4.9	16	4.9	11	4.5
0.8	45	5.0	7	4.0	8	5.0	7	5.0	7	4.7
0.85	100	11.3	16	******	100	82.0	100	80.6	29	******

(b): BTV4

Beam	NALGO		NALGO2		NALGO3		NALGO4		NALGO5	
L.F	No. iter.	%R.F.	No .iter.	%R.F.	No. iter.	%R.F.	No .iter.	%R.F.	No. iter.	%R.F.
0.1	1	0.2	1	0.2	1	0.2	1	0.2	1	0.2
0.2	1	0.1	1	0.1	1	0.1	1	0.1	1	0.1
0.3	1	0.1	1	0.1	1	0.1	1	0.1	1	0.1
0.4	1	0.1	1	0.1	1	0.1	1	0.1	1	0.1
0.5	1	2.5	1	2.5	1	2.5	1	2.5	1	2.5
0.55	1	2.7	1	2.5	1	2.5	1	2.7	1	2.7
0.6	1	3.6	1	3.3	1	3.3	1	3.6	1	3.6
0.65	2	4.6	1	5.0	1	5.0	2	4.2	2	4.2
0.7	3	4.6	71	4.1	100	11.6	100	16.8	82	4.4
0.75	100	11.1	35	2.1	100	16.2	100	13.8	35	4.4
0.8			19	4.4	100	11.5	100	16.1	28	4.7
0.85			22	4.5	54	4.9	60	4.3	29	5.0
0.9			21	4.8	55	4.7	68	5.0	28	4.5
0.95			28	4.5	100	7.7	100	10.5	26	4.9
1			27	4.5					24	4.9
1.05			45	****					56	****

(c): BTV10

Table 8.12: Effect of the solution algorithm on the failure load

Beam	NALGO1	NALGO2	NALGO3	NALGO4	NALGO5	EXP
BTV2	0.75	1.05	0.85	0.9	1.05	1.22
BTV4	0.8	0.8	0.8	0.8	0.8	1.06
BTV10	0.7	1.0	0.9	0.9	1.0	1.1

These mesh sizes were suitable for the analysis of most of the actual beams in this research because the locations of strain gauges in these beams could be easily represented by Gauss points using these meshes. The mesh used in MSH2 gave its best results only with algorithm number 1 (NALGO1) explained in section 8.3.1. With other algorithms the beam could carry up to only 60% of the load, therefore, only the results with this algorithm (number 1) is compared with beam MSH1.

Figure 8.20 shows that beam MSH2 has slightly closer displacement results to the experiment than beam MSH1 compared to the experimental results of beams BTV2 and BTV4. In the case of beam BTV10, MSH1 was softer than the experiment and MSH2 was stiffer. The longitudinal steel strains shown in figure 8.21 indicate that as compared to the experimental results of beams BTV2 and BTV4 MSH1 showed closer results to the experiments than those of MSH2. In BTV10, MSH1 was more flexible than the experiment and MSH2 was stiffer. In the case of transverse steel, MSH1 showed better results than MSHS2 in all beams (Fig. 8.22). Tables 8.13-14 show that MSH2 has given over-stiff response to beam BTV2 and under-stiff response for BTV10. For all beams MSH1 has shown better convergence and less residual forces.

It is clear from this stage that the mesh size has some effect on the beam behaviour and ultimate load carrying capacity. Since beam MSH1 has finer mesh, worked well with all solution algorithm in all three beams examined and was not expensive to run, it was used in the analysis of all beams tested.

8.3.3: Effects of convergence tolerance

Having chosen NALGO2 and MSH1 for solution algorithm and mesh size respectively, the next step was to examine the value of convergence tolerance. The acceptable value to judge convergence of a solution, is using the ratio of the norm of the residual force to the applied force (Ch.7). This ratio was used to monitor the gradual elimination of these out-of-balance forces until a desired level of accuracy (tolerance) was achieved. As stated in section 8.2 the tolerance used up to now was 5%. In this section effect of three more tolerance values were studied:

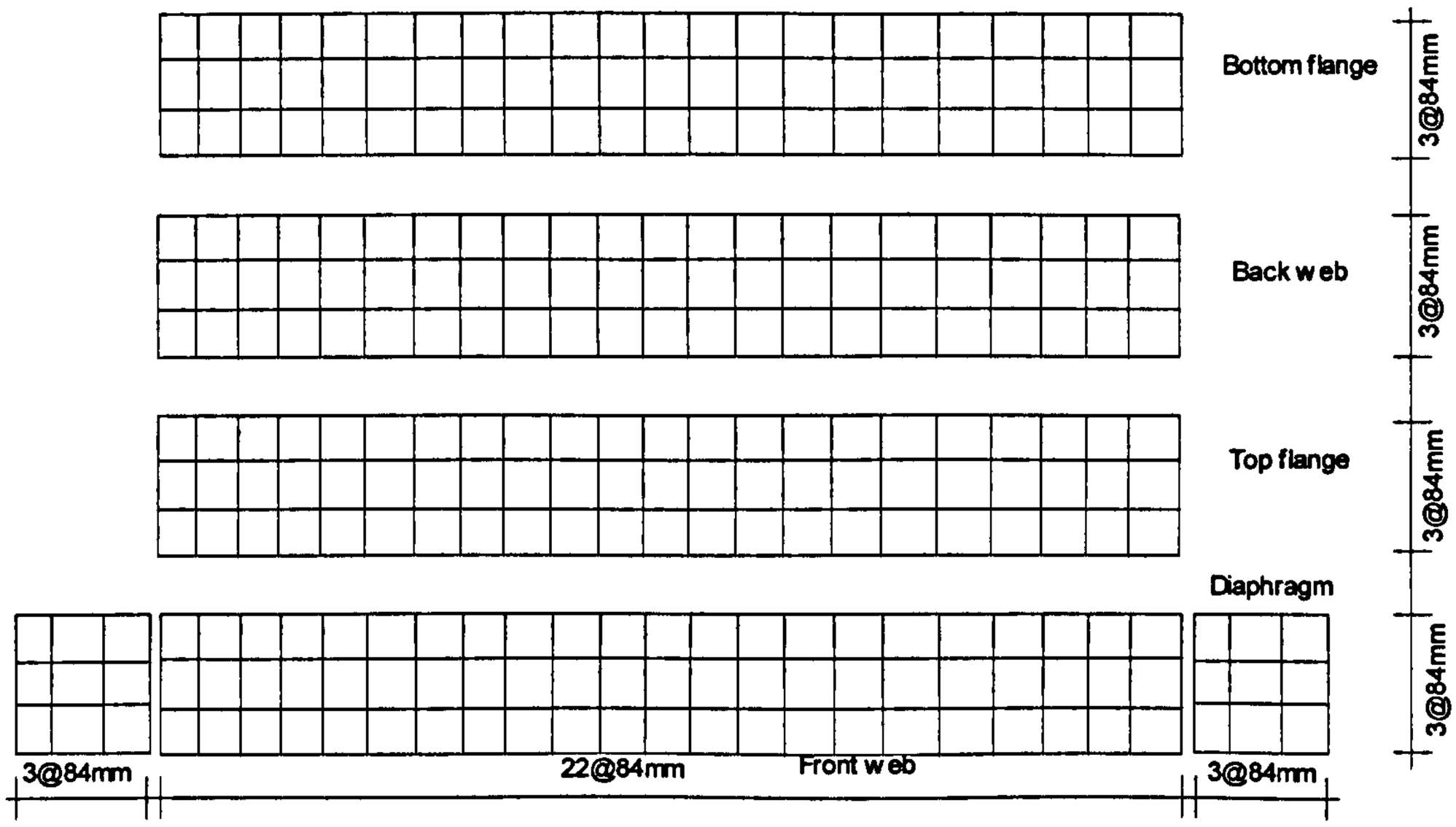

(a): MSH1 (84x84mm)

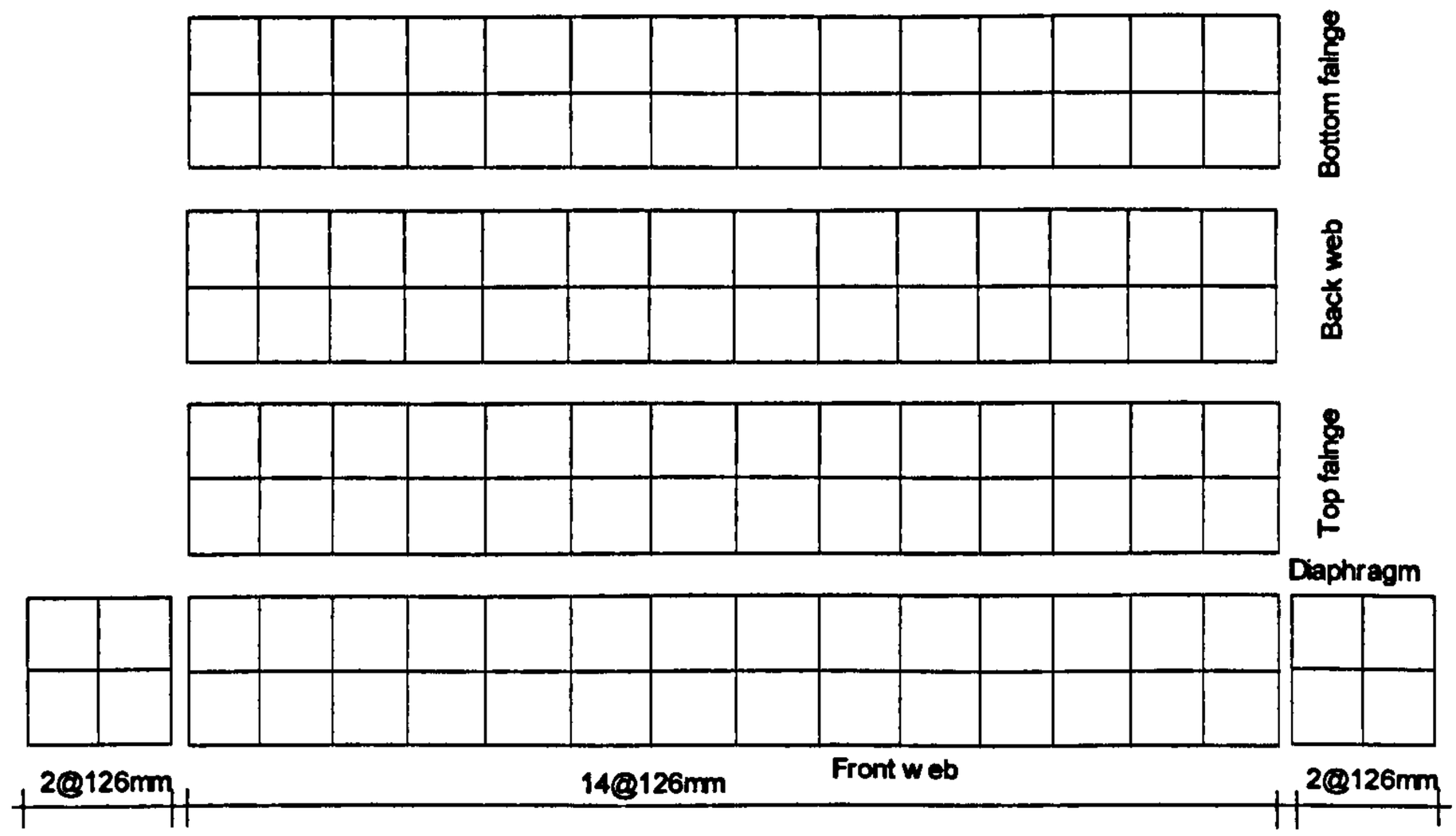

(b): MSH2 (126x126mm)

Fig 8.19: Mesh sizes used in this parametric study

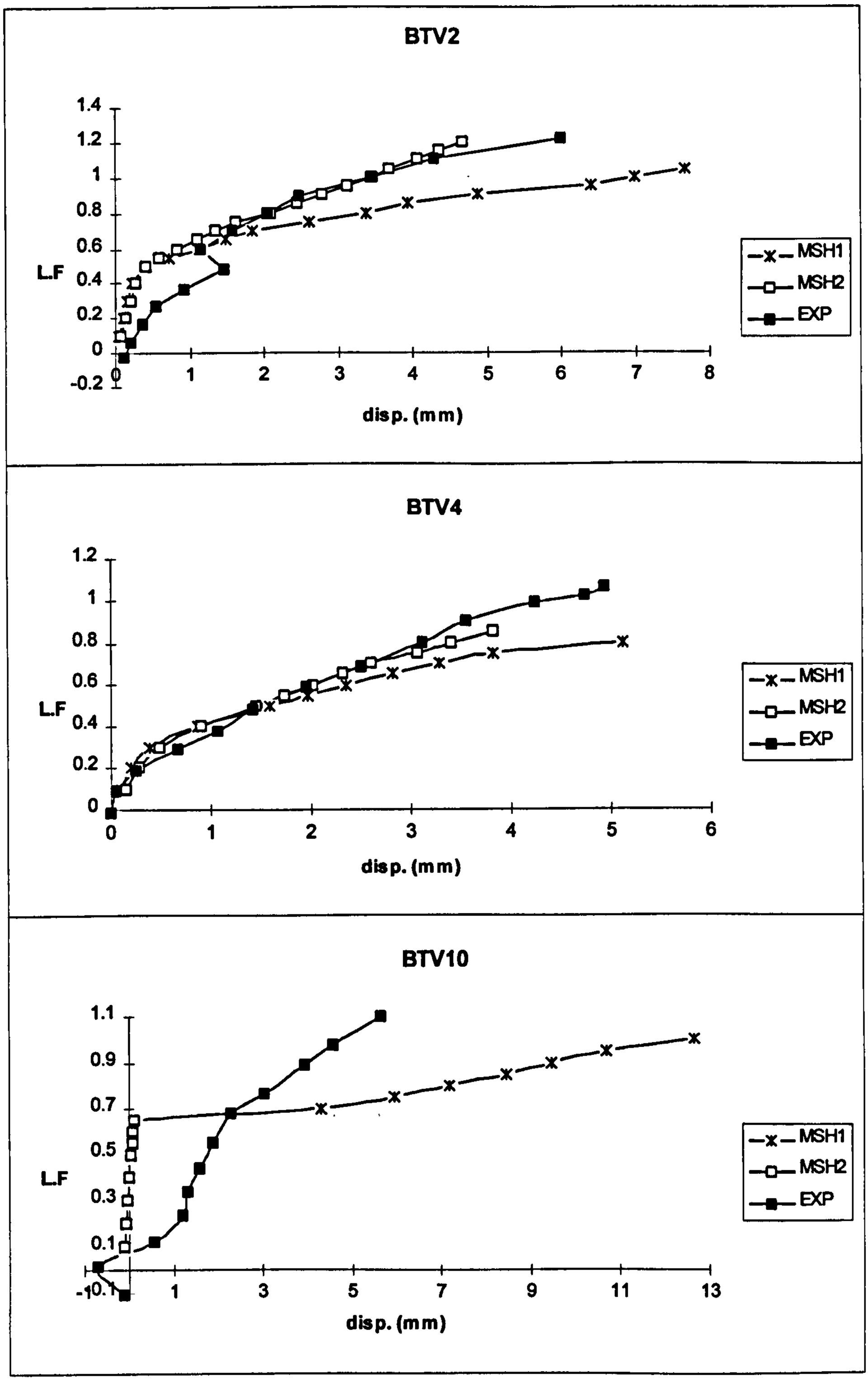

Fig. 8.20: Effect of the mesh size on the displacement

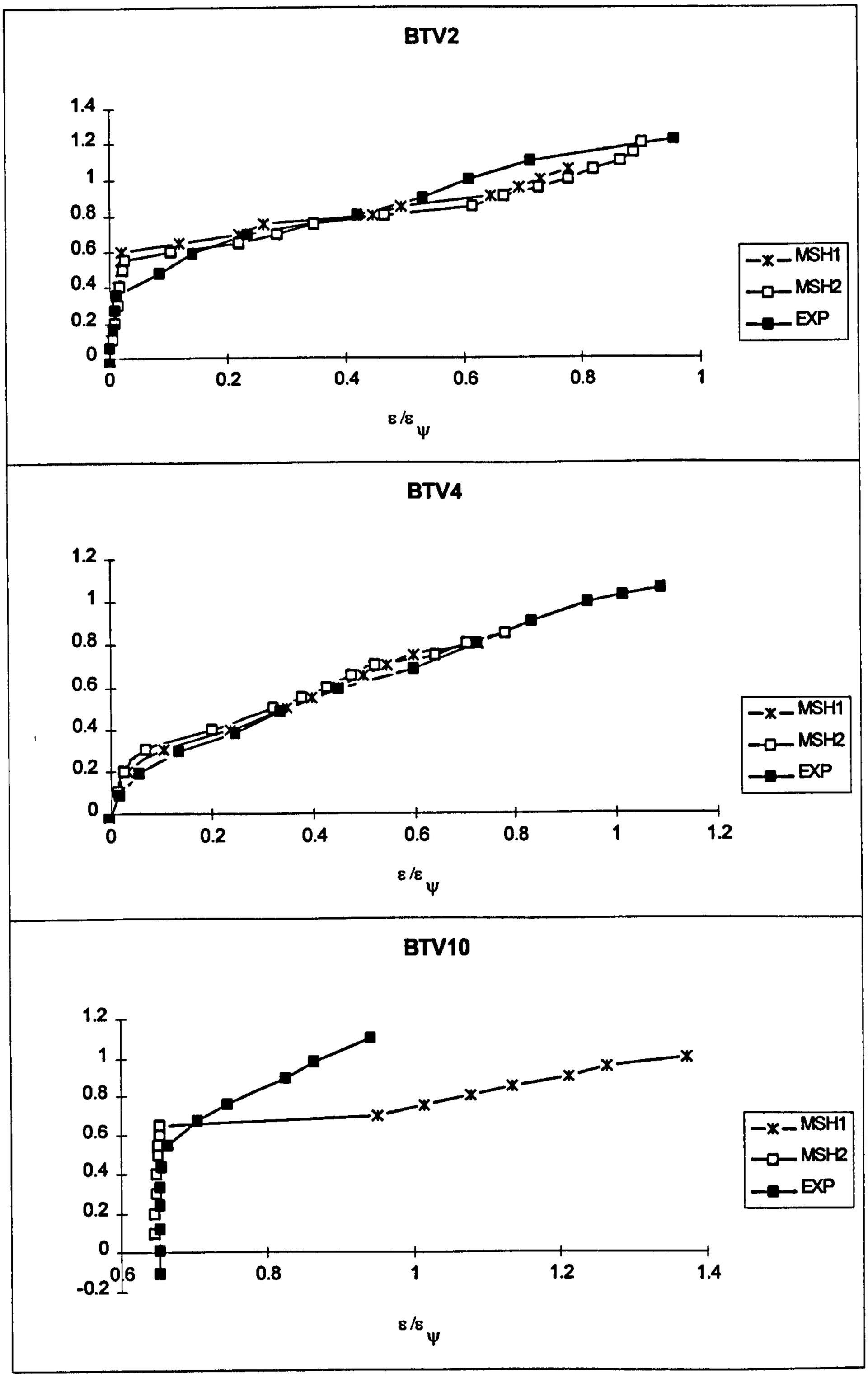

Fig. 8.21: Effect of the mesh size on the front web longitudinal steel

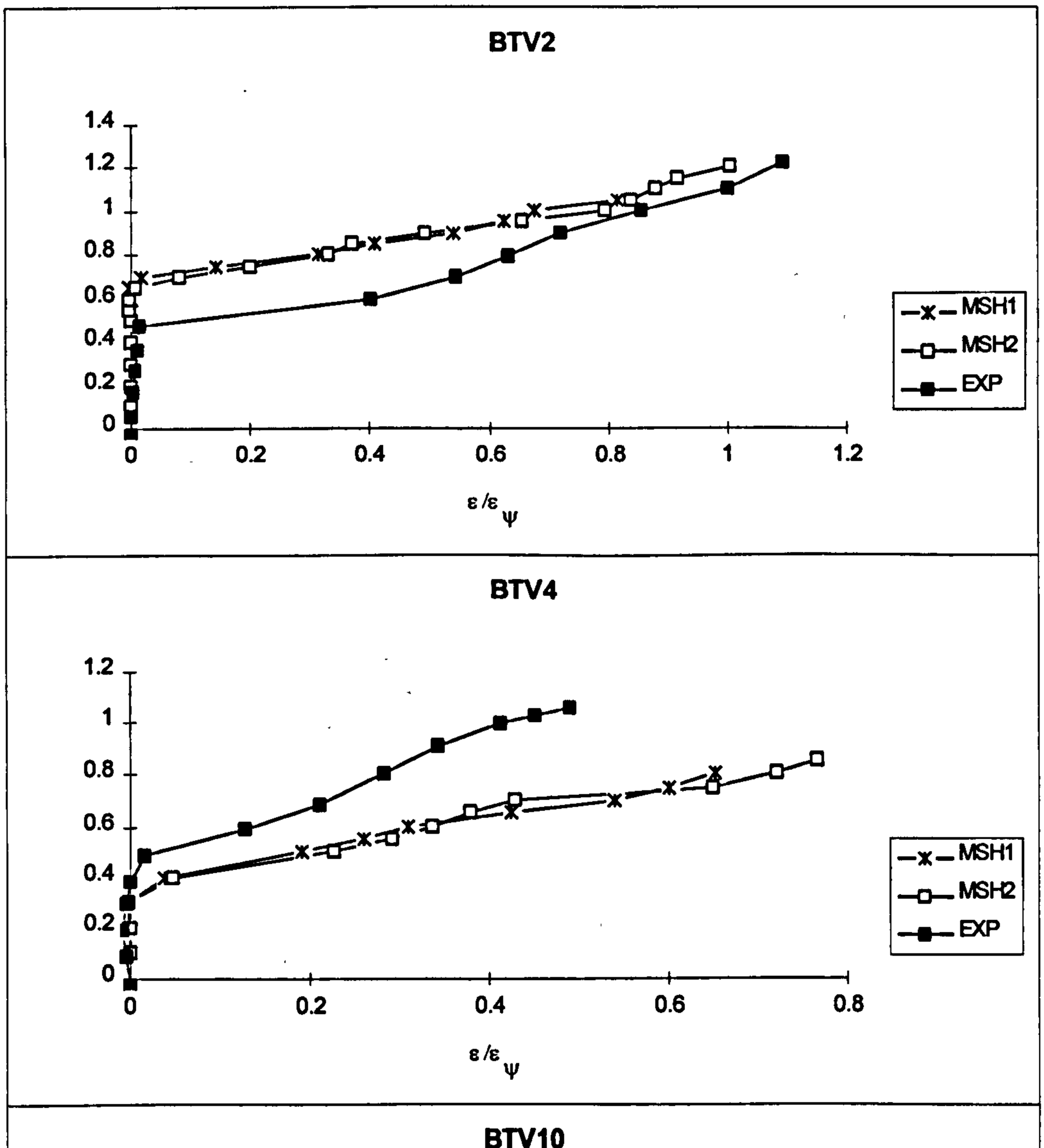

Fig. 8.22: Effect of the mesh size on the front web transverse steel

Table 8.13: Effect of the mesh size on the residual forces

Beam	MSH1		MSH2	
L.F	No .iter.	%R.F.	No. iter.	%R.F.
0.1	1	0.0	1	0.1
0.2	1	0.1	1	0.1
0.3	1	0.1	1	0.3
0.4	2	4.9	2	3.1
0.5	10	4.9	18	5.0
0.55	20	4.6	37	4.9
0.6	25	4.6	59	5.0
0.65	21	4.9	65	4.9
0.7	14	4.7	55	4.8
0.75	18	4.9	52	5.0
0.8	23	4.0	100	7.0
0.85	11	4.1	70	4.9
0.9	34	4.8	74	4.8
0.95	32	4.5	79	4.9
1	9	3.8	91	4.8
1.05	15	4.8	48	4.9
1.1	49	****	100	8.4
1.15			89	5.0
1.2			99	5.0
1.25			100	8.5

(a): BTV2.

Beam	MSH1		MSH2	
L.F	No .iter.	%R.F.	No. iter.	%R.F.
0.1	1	0.1	1	0.1
0.2	1	0.1	1	0.4
0.3	7	3.6	9	4.9
0.4	11	4.9	28	4.9
0.5	13	4.8	39	5.0
0.55	11	4.8	27	4.9
0.6	10	4.5	24	5.0
0.65	10	4.0	23	4.8
0.7	7	4.2	21	5.0
0.75	9	4.8	53	4.8
0.8	7	4.0	39	4.8
0.85	16	******	49	5.0
0.9			100	12.8

(b):BTV4

Beam	MSH1		MSH2	
L.F	No .iter.	%R.F.	No. iter.	%R.F.
0.1	1	0.2	1	0.3
0.2	1	0.1	1	0.1
0.3	1	0.1	1	0.1
0.4	1	0.1	1	0.1
0.5	1	2.5	1	0.2
0.55	1	2.5	1	0.1
0.6	1	3.3	1	0.1
0.65	1	5.0	2	4.6
0.7	71	4.1	100	7.5
0.75	35	2.1		
0.8	19	4.4		
0.85	22	4.5		
0.9	21	4.8		
0.95	28	4.5		
1	27	4.5		
1.05	45	*****		

(c): BTV10

Table 8.14 Effect of mesh size on the failure load

Beam	MSH1	MSH2	EXP
BTV2	1.05	1.2	1.22
BTV4	0.8	0.85	1.06
BTV10	1.0	0.65	1.1

1. 1% for all increments used in beam TOL1.
2. 4% for all increments used in beam TOL4.
3. 5% for all increments used in beam TOL5.
4. 6% for all increments used in beam TOL6

It is obvious from figures 8.23-25 that results for load-deflection and steel strain were very similar for the different values of tolerance. Tables 8.15 indicate that TOL1 was more expensive to run. Table 8.16 shows that TOL4 gave the results which were closest to the experimental results for failure loads in all beams. Generally speaking, with smaller tolerance, computational cost was naturally increased and the results of analysis were not much different from that of a reasonably larger tolerance. From the above it can be seen that a 4% tolerance is a suitable value for our purpose. Therefore, a tolerance of 4% was used in the analysis of all tested beams.

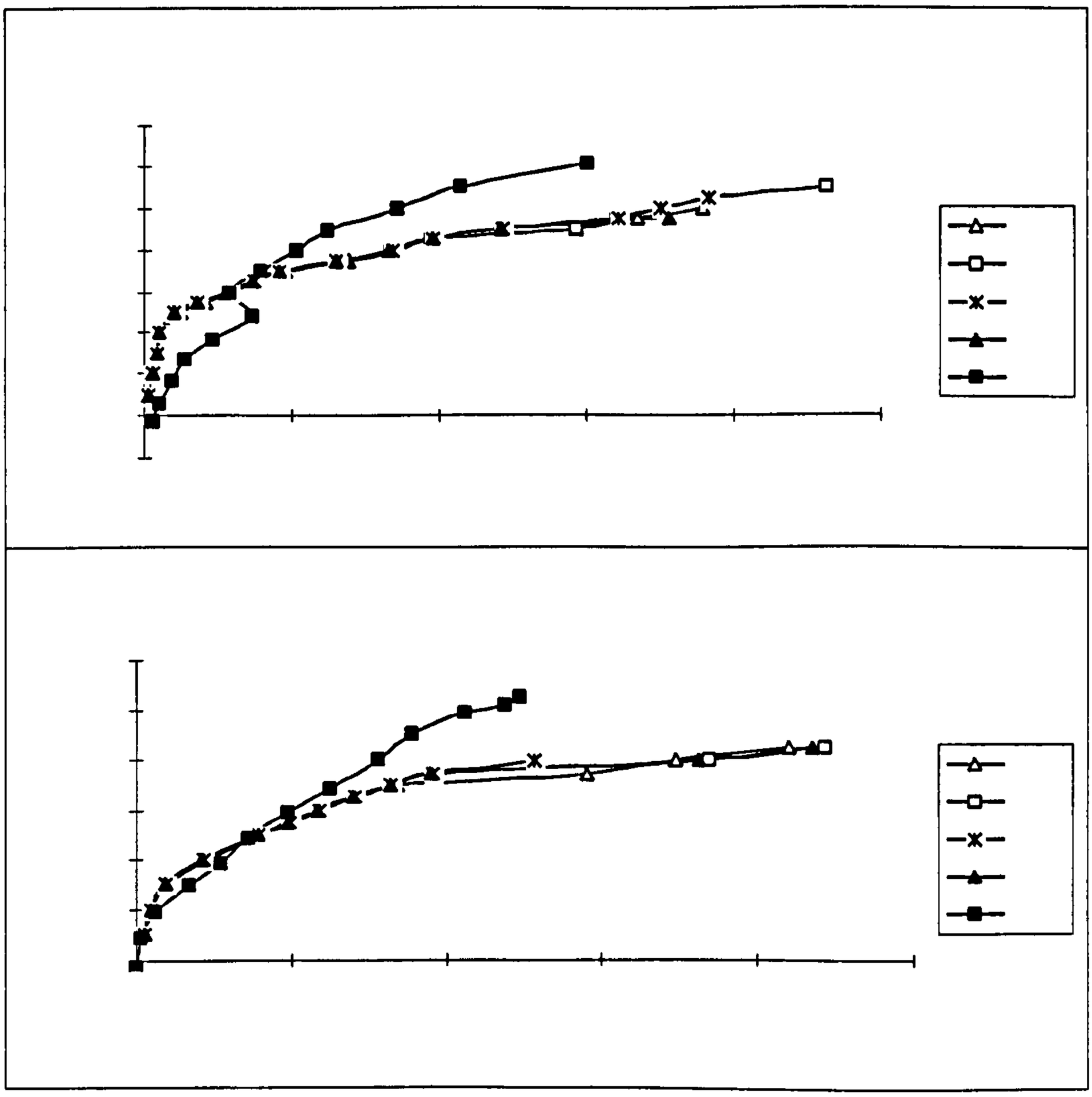

Fig. 8.23: Effect of the convergence tolerance on the displacement

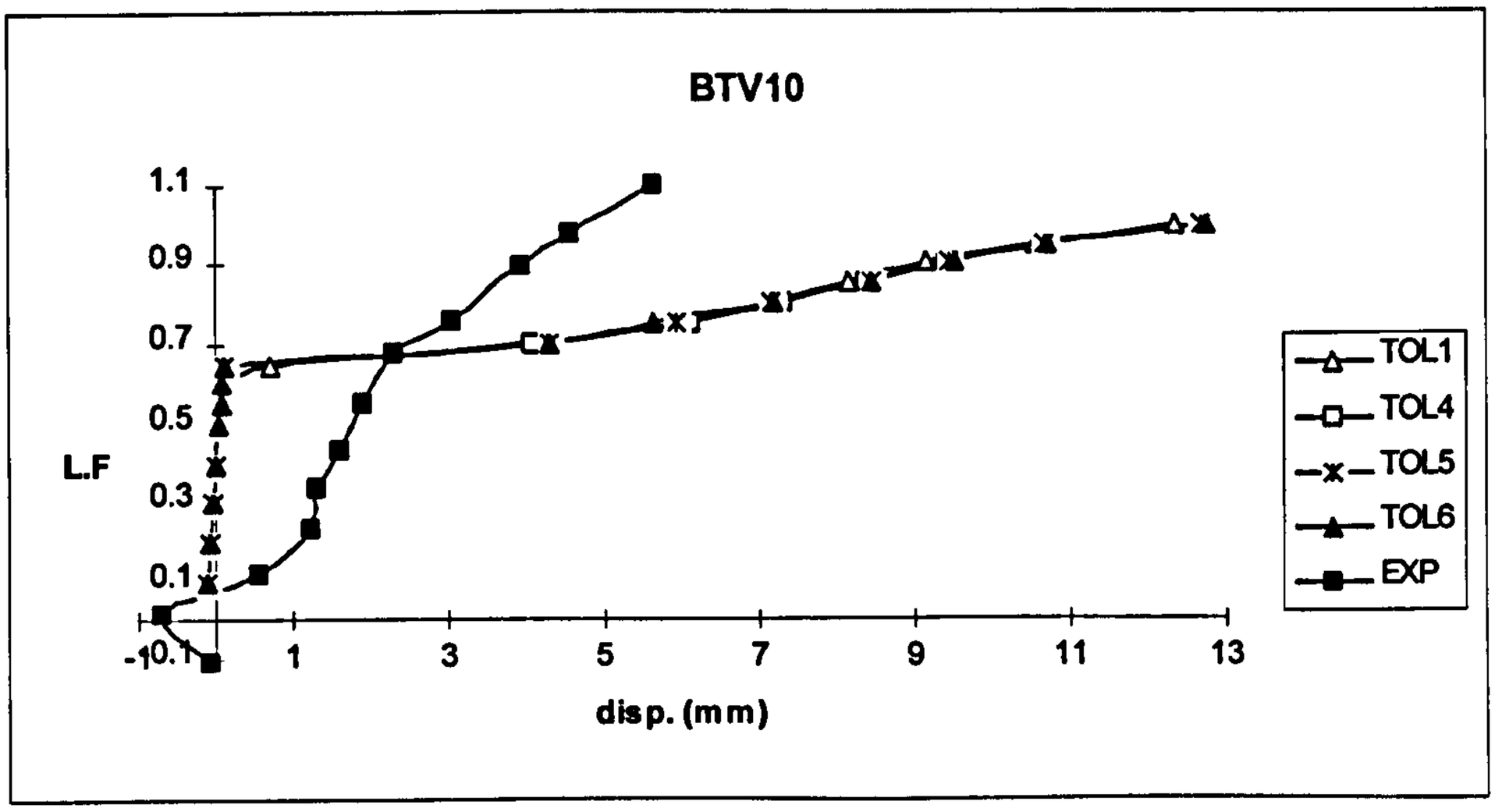

Fig. 8.23: Continued

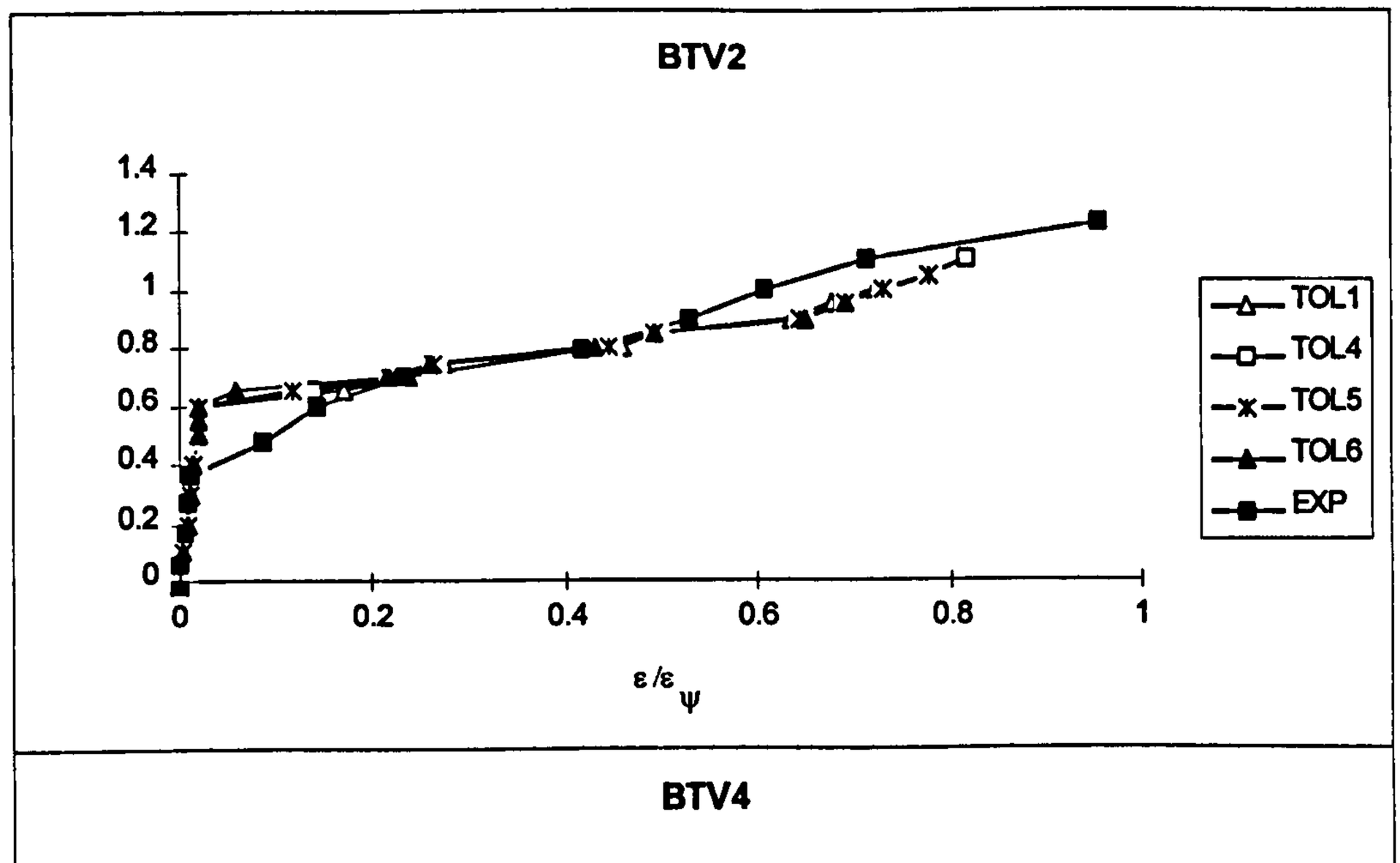

Fig. 8.24: Effect of the convergence tolerance on the front web longitudinal steel

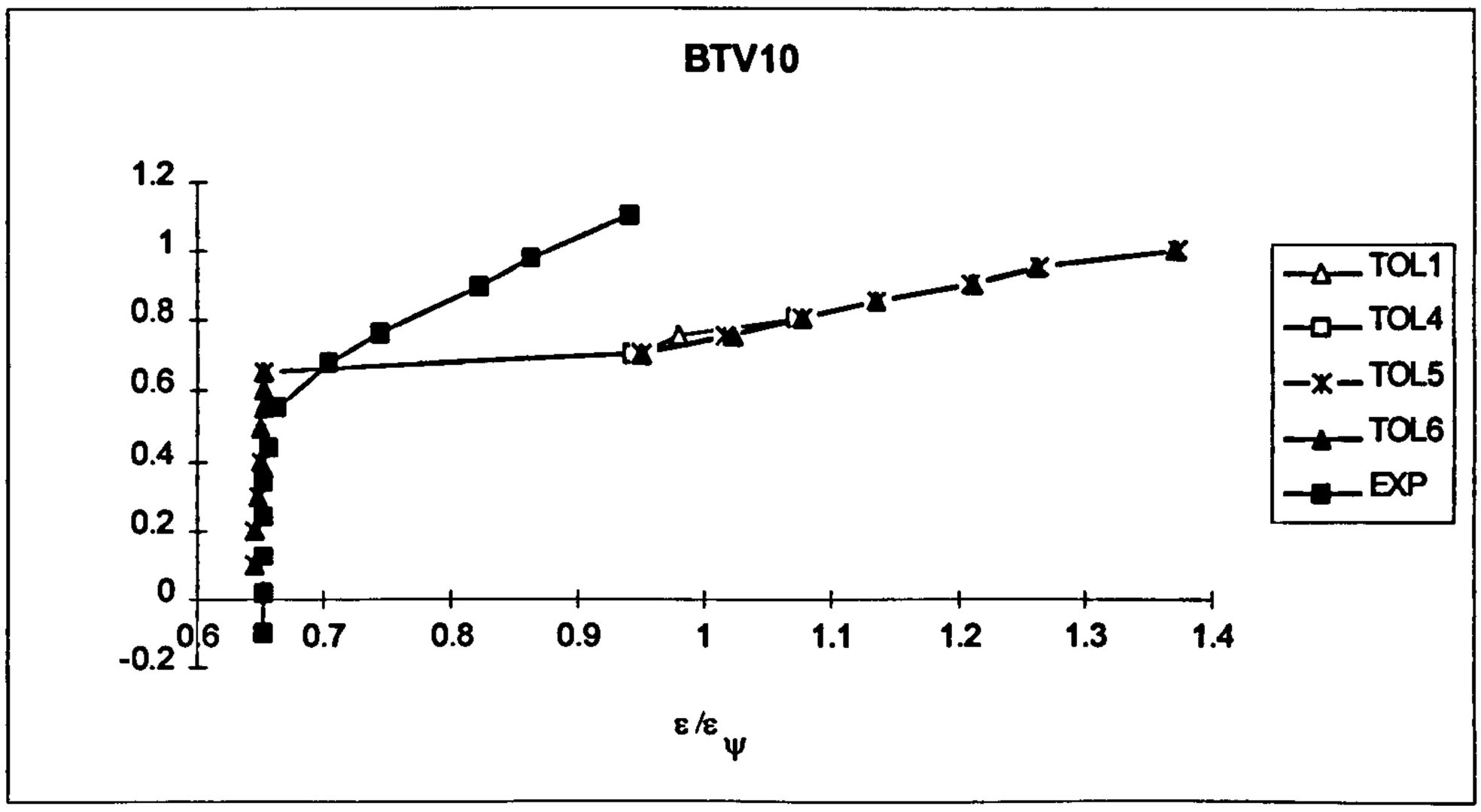

Fig. 8.24: Continued

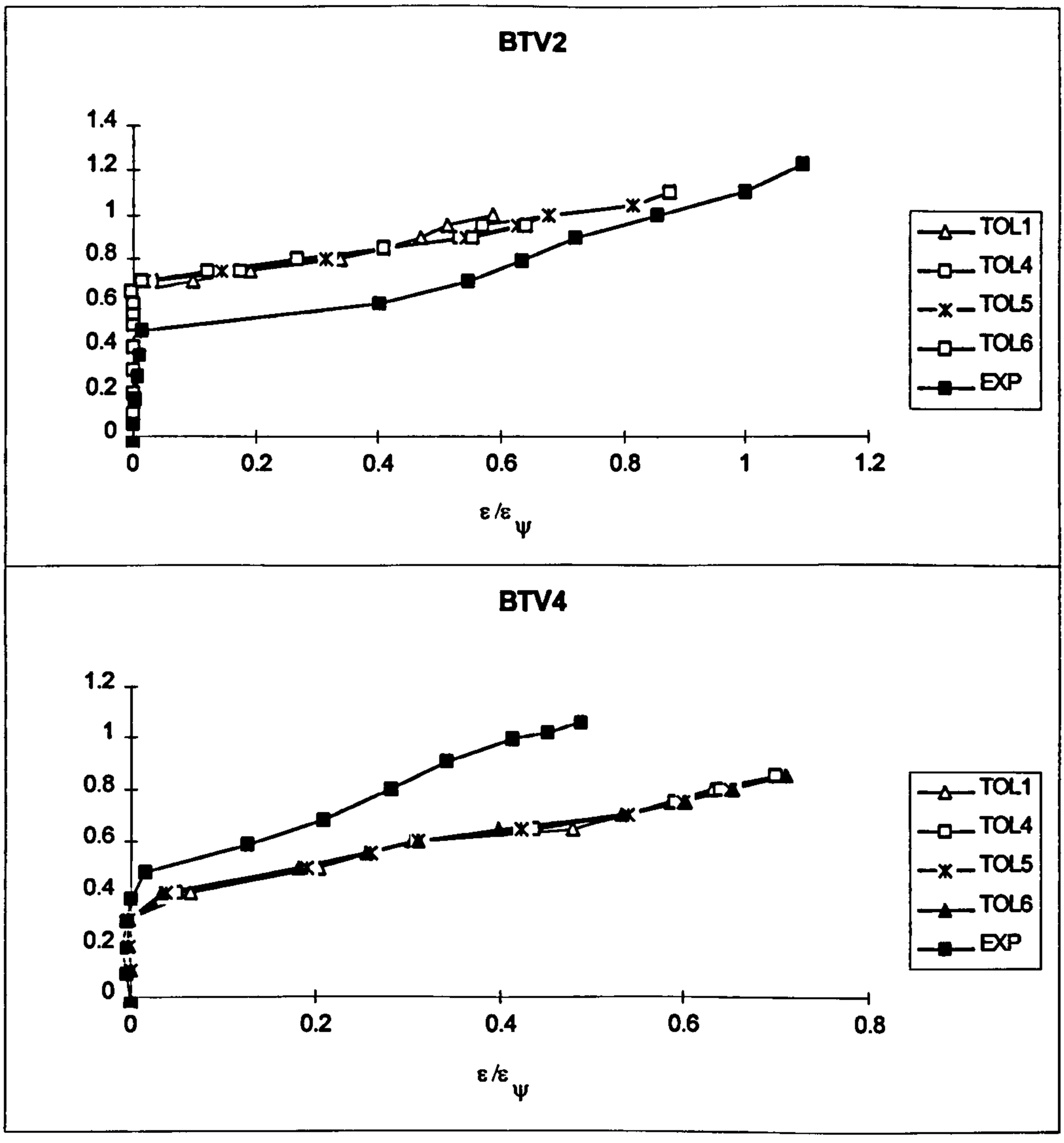

Fig. 8.25: Effect of the convergence tolerance on the front web transverse steel

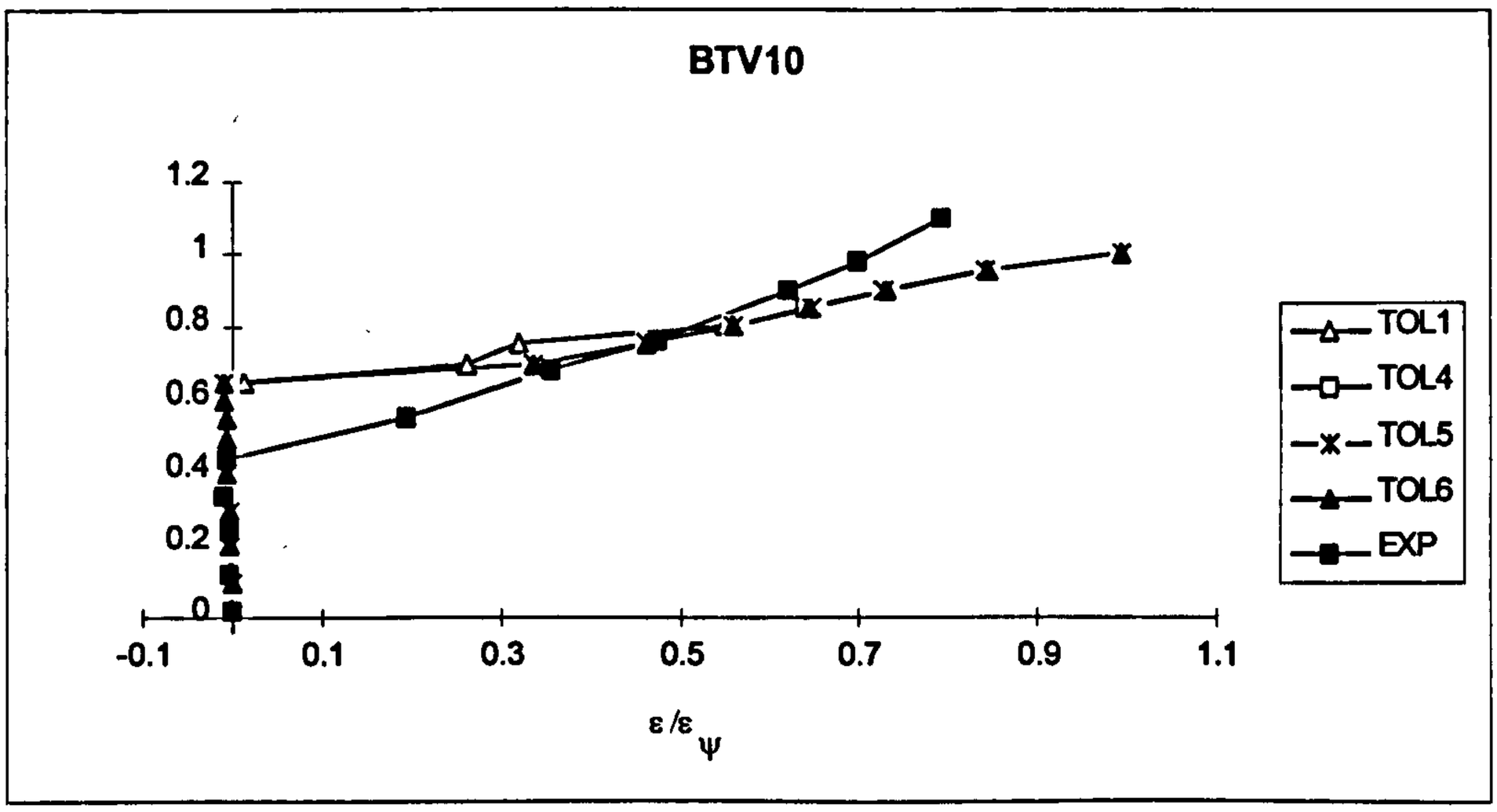

Fig. 8.25: Continued

8.4: Conclusion

To get results close to experimental results, one could consider a separate parametric study for each test. Since the aim was to choose a general model which suited all hollow beams tested, some accuracy was sacrificed and the following parameter values were selected and were used for the analysis of tested beams in chapter 9:

- Concrete cube compressive strength: f_{cu} as measured for each beam.
- Concrete cylinder compressive strength: $f_c^{'} = 0.8 f_{cu}$ N/mm^2.
- Young's modulus: $E_c = 5000\sqrt{f_c^{'}} N/mm^2$.
- Compressive strain at peak stress: $\varepsilon_{cc} = \frac{\sqrt{f_c^{'}}}{2500}$.
- Maximum compressive strain: $\varepsilon_{max} = 0.0035$.
- Tensile strength of concrete: $f_t^{'} = 0.54\sqrt{f_C^{'}}$ N/mm^2.
- Tension stiffening: $\sigma_t = (\sqrt[4]{\frac{\varepsilon_{cr}}{\varepsilon_n}}) f_t^{'}$ N/mm^2.
- Shear retention numerical constants: $B = 0.4$ $\beta_{min} = 0.05$.
- Poisson's ratio: $v = 0.15$.
- The stiffness matrix is re-computed for each iteration in each increment.
- Mesh size: 84x84mm.
- Convergence tolerance: 4%.
- Maximum number of increments: 30.

- Load increment: 10% for the first five increments and 5% thereafter.
- Maximum number of iterations per increment: 100.

Table 8.15: Effect of the convergence tolerance on the residual forces

Beam	TOL1		TOL4		TOL5		TOL6	
L.F.	No .iter.	%R.F.	No. iter.	%R.F.	No. iter.	%R.F.	No. iter.	%R.F.
0.1	1	0.0	1	0.0	1	0.0	1	0.0
0.2	1	0.1	1	0.1	1	0.1	1	0.1
0.3	1	0.1	1	0.1	1	0.1	1	0.1
0.4	8	0.8	3	1.5	2	4.9	2	4.9
0.5	37	0.7	15	3.5	10	4.9	10	4.9
0.55	69	0.9	32	3.8	20	4.6	17	6.0
0.6	35	0.9	27	4.0	25	4.6	19	6.0
0.65	47	1.0	24	3.9	21	4.9	14	6.0
0.7	48	1.0	17	3.9	14	4.7	15	5.9
0.75	45	0.9	31	3.9	18	4.9	14	5.7
0.8	31	0.9	20	3.8	23	4.0	18	5.9
0.85	26	1.0	11	3.4	11	4.1	10	5.7
0.9	75	0.7	70	2.9	34	4.8	32	5.8
0.95	43	0.9	12	3.4	32	4.5	45	5.8
1	67	0.9	10	3.7	9	3.8	49	****
1.05	52	****	16	3.8	15	4.8		
1.1			37	3.9	49	****		
1.15			57	****				

(a): BTV2

Beam	TOL1		TOL4		TOL5		TOL6	
L.F.	No .iter.	%R.F.	No. iter.	%R.F.	No. iter.	%R.F.	No. iter.	%R.F.
0.1	1	0.1	1	0.1	1	0.1	1	0.1
0.2	1	0.3	1	0.3	1	0.1	1	0.3
0.3	14	0.9	8	3.4	7	3.6	6	5.0
0.4	27	1.0	14	3.5	11	4.9	10	5.7
0.5	32	0.9	15	3.9	13	4.8	11	5.7
0.55	28	0.8	11	3.8	11	4.8	8	5.7
0.6	17	1.0	9	3.8	10	4.5	7	5.4
0.65	21	0.9	10	3.9	10	4.0	8	5.4
0.7	33	0.9	9	3.9	7	4.2	5	5.8
0.75	100	6.6	10	3.9	9	4.8	7	5.9
0.8	43	0.8	77	3.8	7	4.0	72	5.7
0.85	36	0.9	20	3.3	16	****	13	5.8
0.9	12	****	11	****			13	****

(b): BTV4

Table 8.15: Continued

Beam	TOL1		TOL4		TOL5		TOL6	
L.F.	No .iter.	%R.F.	No. iter.	%R.F.	No. iter.	%R.F.	No. iter.	%R.F.
0.1	1	0.2	1	0.2	1	0.2	1	0.2
0.2	1	0.1	1	0.1	1	0.1	1	0.1
0.3	1	0.1	1	0.1	1	0.1	1	0.1
0.4	1	0.1	1	0.1	1	0.1	1	0.1
0.5	3	0.5	1	2.5	1	2.5	1	2.5
0.55	3	0.9	1	2.5	1	2.5	1	2.5
0.6	4	0.4	1	3.3	1	3.3	1	3.3
0.65	100	7.6	8	3.8	1	5.0	1	5.0
0.7	100	1.6	66	2.8	71	4.1	70	5.2
0.75	50	1.0	31	3.6	35	2.1	18	5.3
0.8	44	1.0	21	3.6	19	4.4	16	4.9
0.85	51	0.9	24	4.0	22	4.5	23	5.4
0.9	36	1.0	30	3.9	21	4.8	17	5.5
0.95	72	1.0	24	3.4	28	4.5	23	5.9
1	71	1.0	20	****	27	4.5	28	5.3
1.05	24	****			45	****	48	****

(c): BTV10

Table 8.16: Effect of the convergence tolerance on the failure load

Beam	TOL1	TOL4	TOL5	TOL6	EXP
BTV2	1.0	1.1	1.05	0.95	1.22
BTV4	0.85	0.85	0.8	0.85	1.06
BTV10	1.0	0.95	1.0	1.0	1.1

9: Comparison between experimental and computational results of hollow beams

9.1: Introduction

In this chapter the 2-D finite element model finalised in chapter 8 was used for the non-linear analysis of the hollow beams described in chapter 5. The experimental and computational results were compared and the validity of the direct design method was further examined. Values of concrete cube strength and steel tensile strength used in the analysis were those obtained from tests. All other parameters used were as recommended in the preceding chapter. The comparison was carried out using the following criteria:

- Load-displacement relationship.
- Strain in longitudinal steel.
- Strain in transverse (links) steel.
- Relative angle of twist.
- Failure load.
- Crack pattern and mode of failure.

In this chapter, only a few typical results were shown in this chapter. However, appendix B contains a complete set of measured and computed values of strain in reinforcement.

9.2: Comparison between experimental and computational results

9.2.1: Load-displacement relationship

Figure 9.1 shows the displacements at mid-span of the front web. It is clear from this figure that, in general, an acceptable agreement between experimental and computational results was achieved in most cases of reinforced and partially prestressed beams. However, in beams BTV6 and BTV10 the computed displacements were slightly larger than the observed ones in the last few load increments.

9.2.2: Strain in the longitudinal steel

Figures 9.2-3 and the related figures in appendix B show that a very good agreement between the experimental and computational results was obtained for longitudinal steel strains in the front and back webs. However, in beams BTV8 and BTV10 the

computed strains were larger than observed. In BTV8, the average difference in the bottom layer of the front web was 26% and in the back web was 28%. In BTV10, the difference in the front side was 28% and in the rear side was 23%.

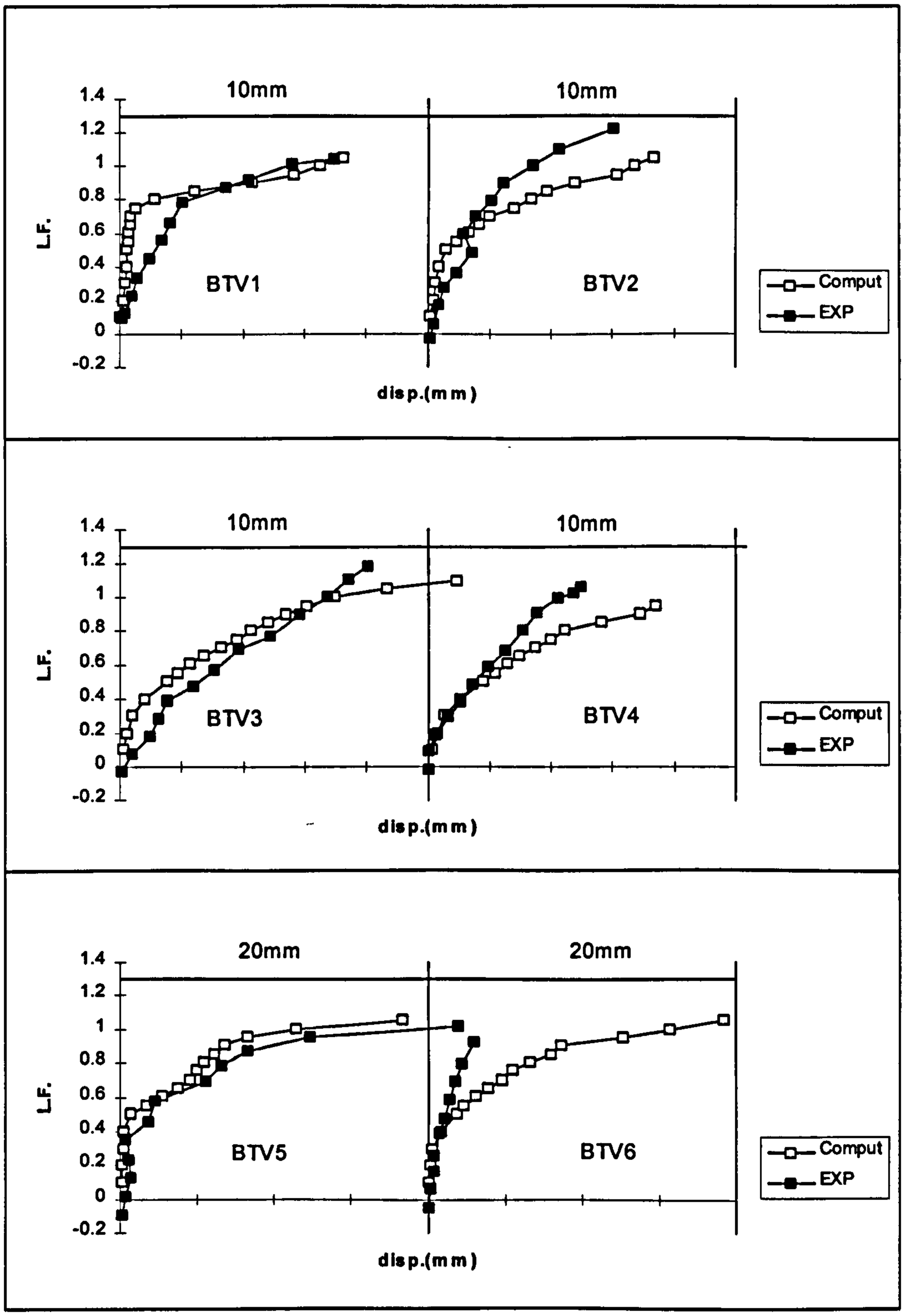

Fig. 9.1: Vertical displacement at mid-span of the front web

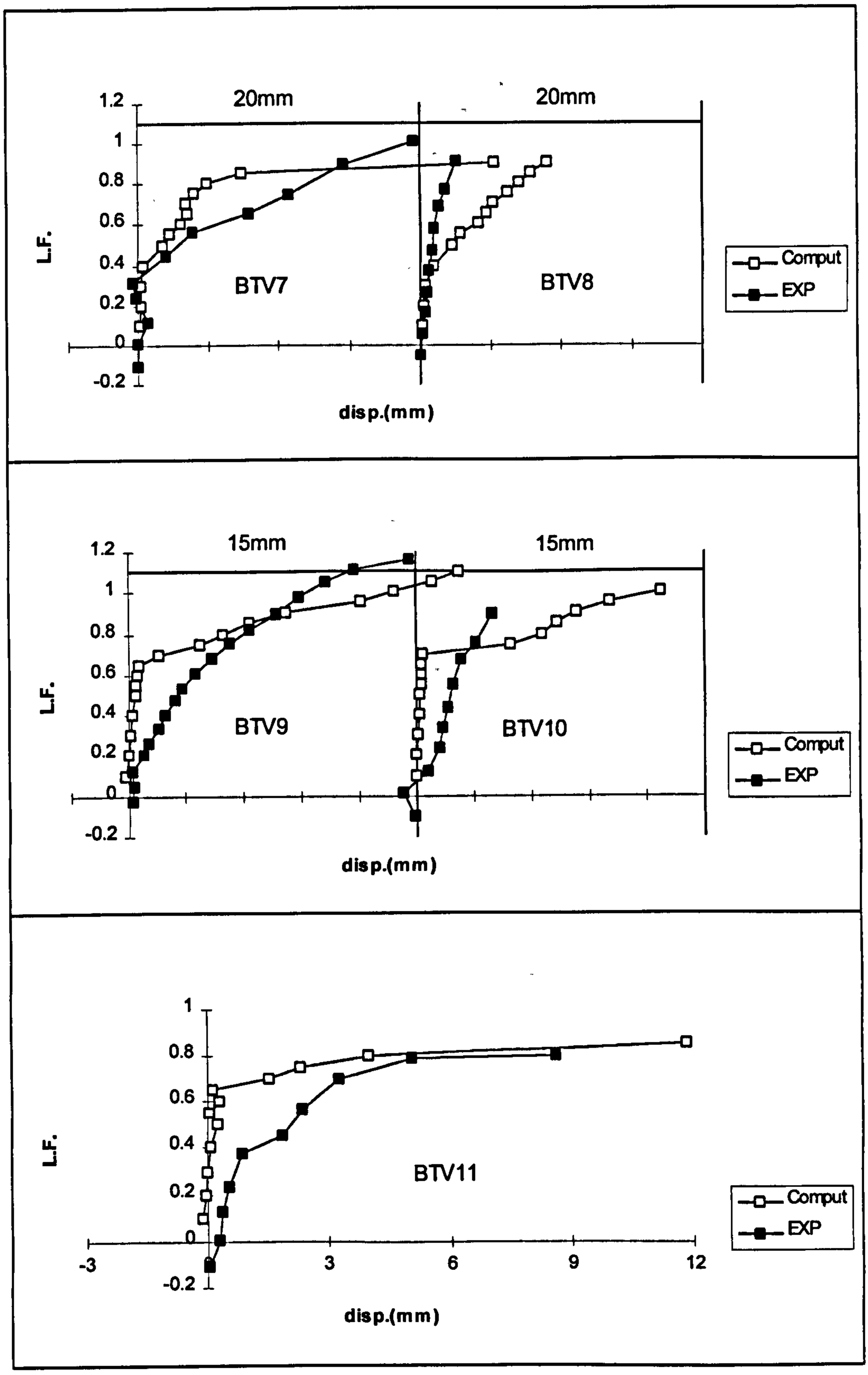

Fig. 9.1: Continued

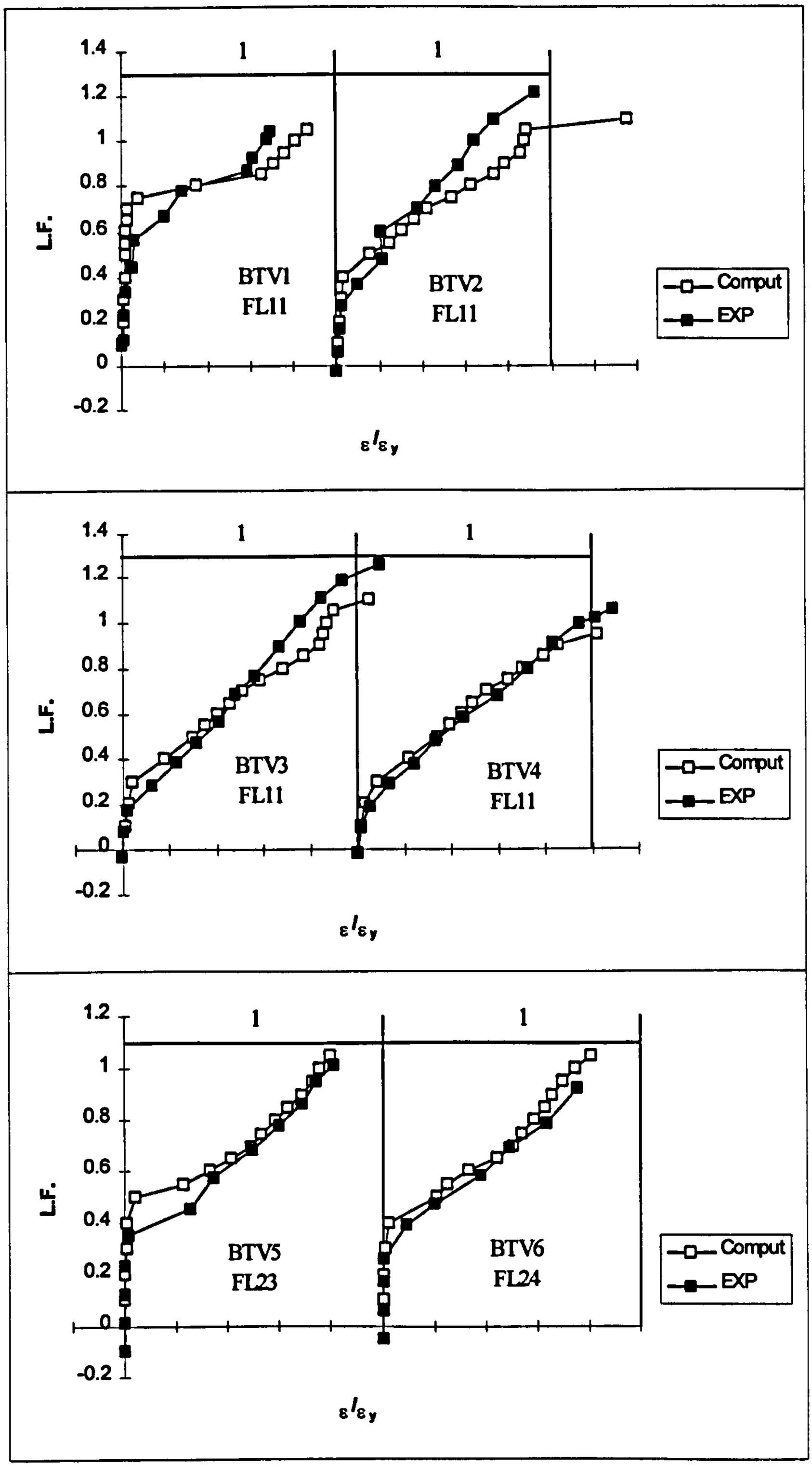

Fig. 9.2: Strain at a selected point in a longitudinal bar (Front web)

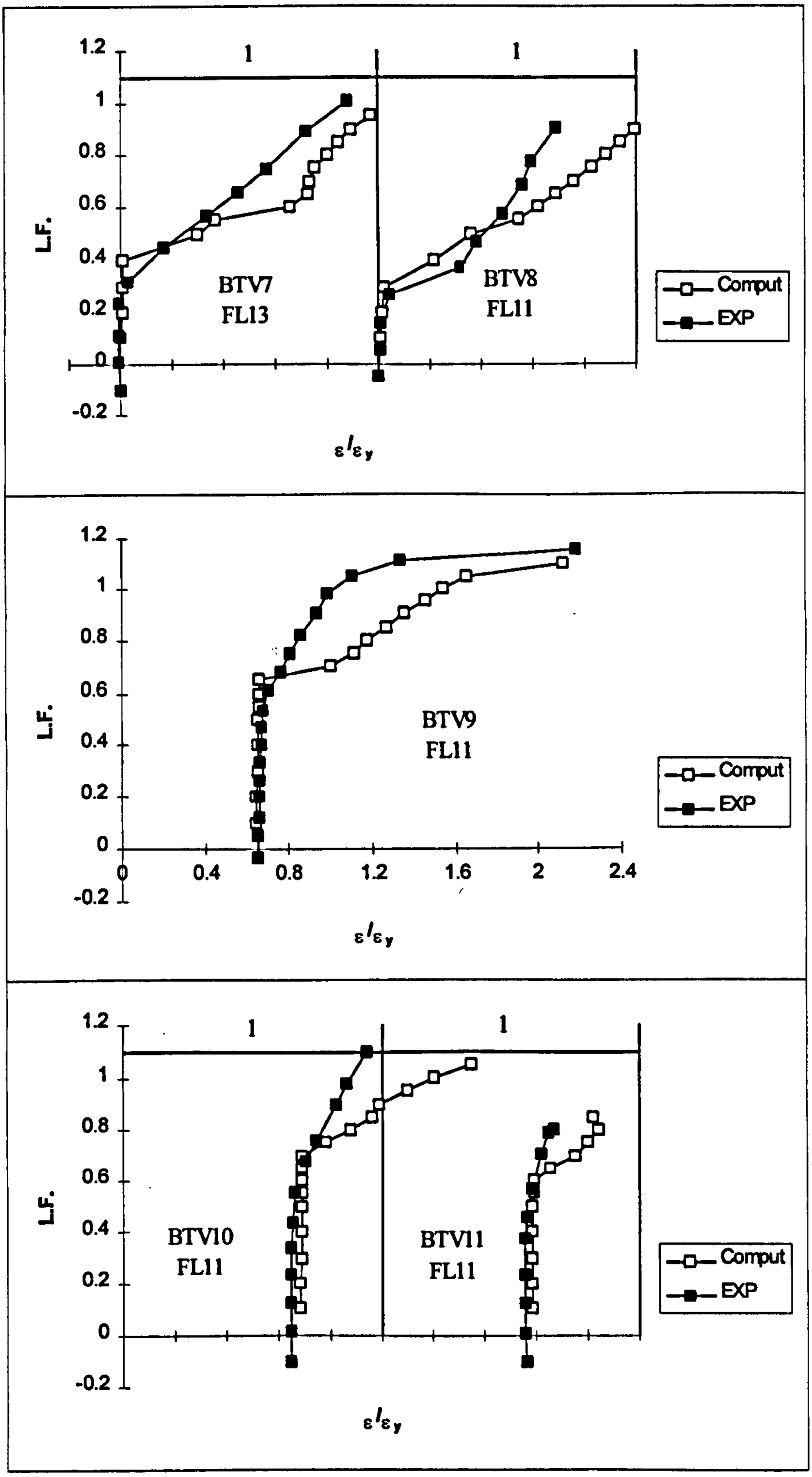

Fig. 9.2: Continued

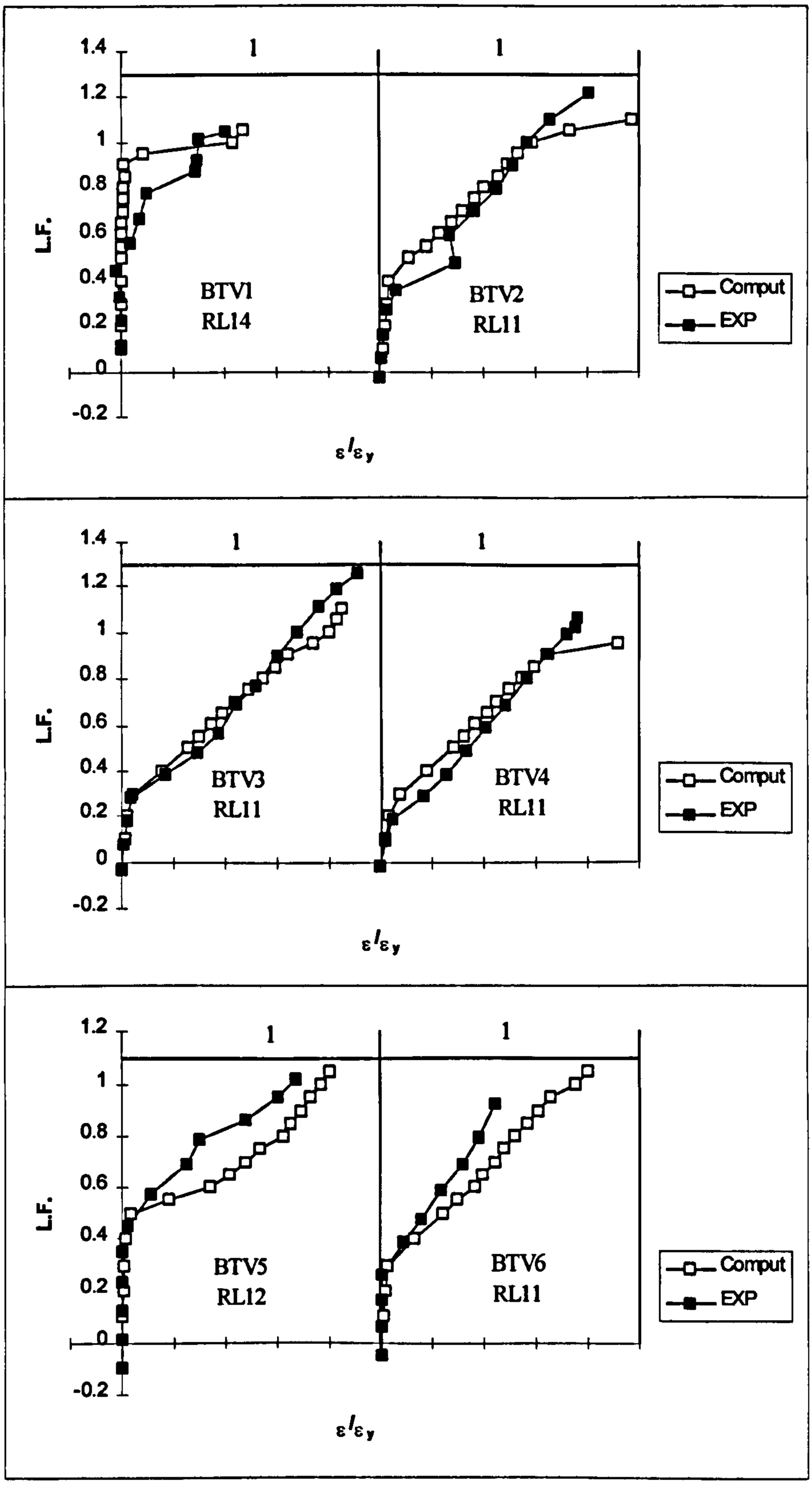

Fig. 9.3: Strain ratio at a selected point in a longitudinal bar (Back web)

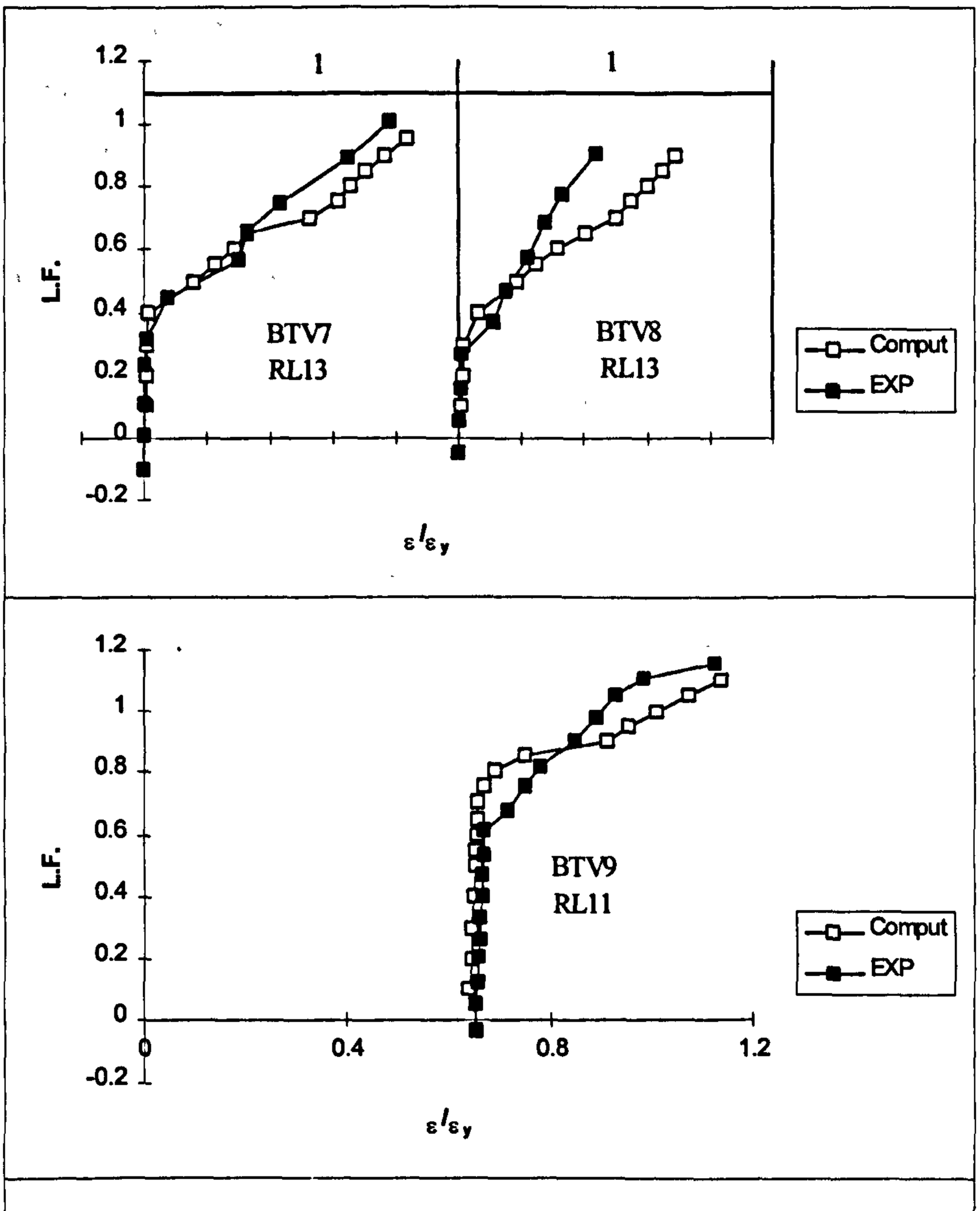

Fig. 9.3: Continued

9.2.3: Strain in the transverse steel

Figures 9.4-5 and the related figures in appendix B show good agreement between experimental and computational results in the transverse steel strain specially for the stirrups in the front web. However, in beams BTV2 and BTV6 the computed strains in the front web stirrups were larger than the observed. In BTV2 the average difference was 19% and in BTV6 the difference was 22%.

In the back web stirrups in beams BTV3 and BTV4, the observed strains were larger than the computed one. In BTV3 the average difference was 11% and in BTV4 it was 7%.

9.2.4: Relative angle of twist

Figure 9.6 shows experimental and computational relative angles of twist. The method of calculating the angle of twist and the relative angle of twist was explained in chapter 4. It can be seen that there is a good agreement between experimental and computational results.

9.2.5: Failure load

Table 9.1 shows the ratio of experimental to design failure load L_e/L_d, the ratio of computational to design L_c/L_d failure load and experimental to computational failure load L_e/L_c. In general, very good agreement was attained in failure loads. In most cases the experimental results were slightly larger than the computed ones. The mean experimental and computational failure loads were just above the 100% of design loads.

9.2.6: Crack pattern and mode of failure

Figures 9.7-11 show typical observed and computed crack patterns of the tested beams. It can be seen that good agreement was achieved between the experimental and computational results on the crack orientation and concentration of cracks in the regions where shear stresses are additive.

9.3: Conclusion

From the results in this chapter it can be said that the prediction of the 2-D finite element model discussed in the previous chapters has compared well with the experimental results of the hollow beams designed using the direct design method.

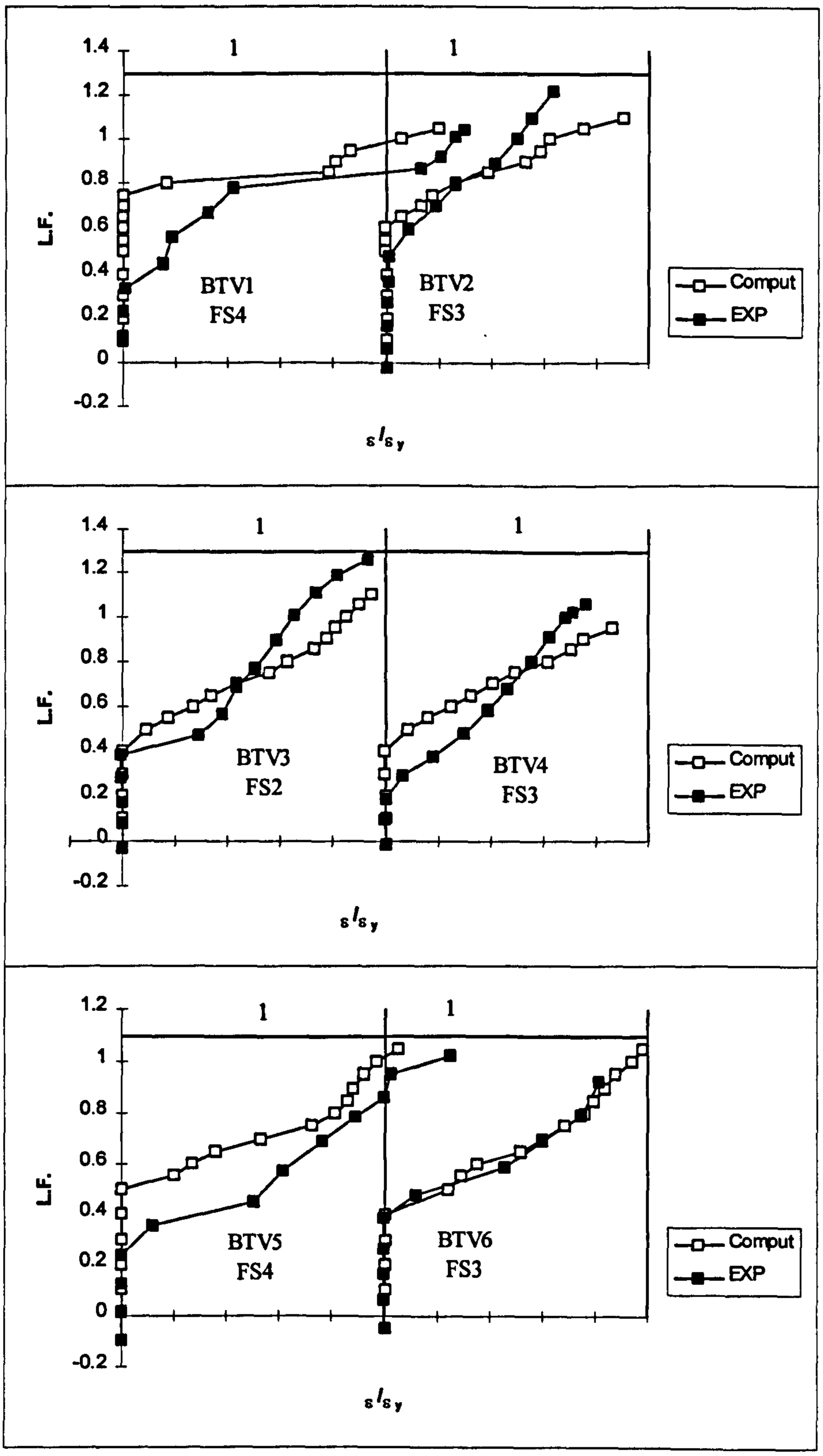

Fig. 9.4: Strain ratio at a selected point in a transverse bar (Front web)

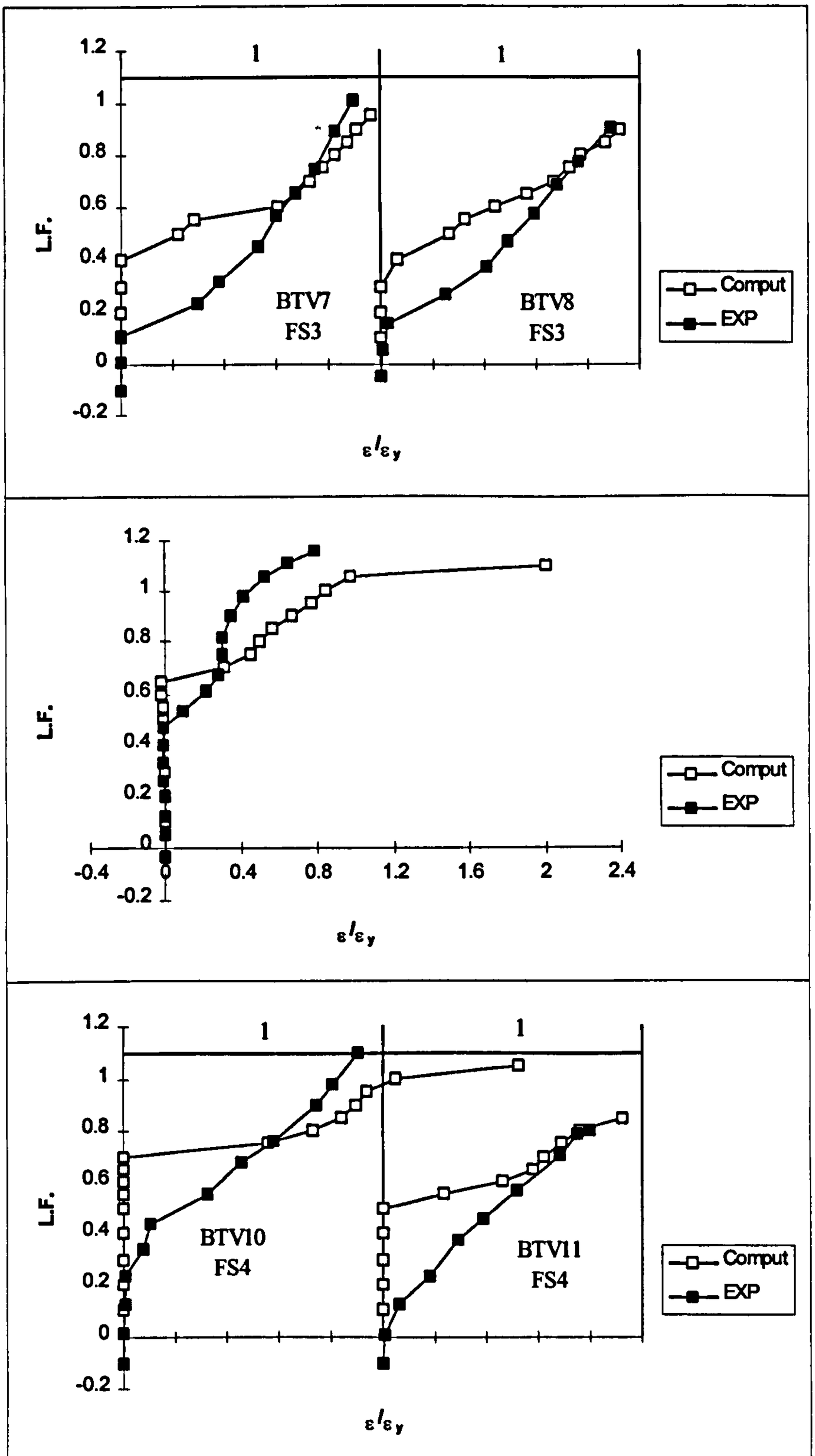

Fig. 9.4: Continued

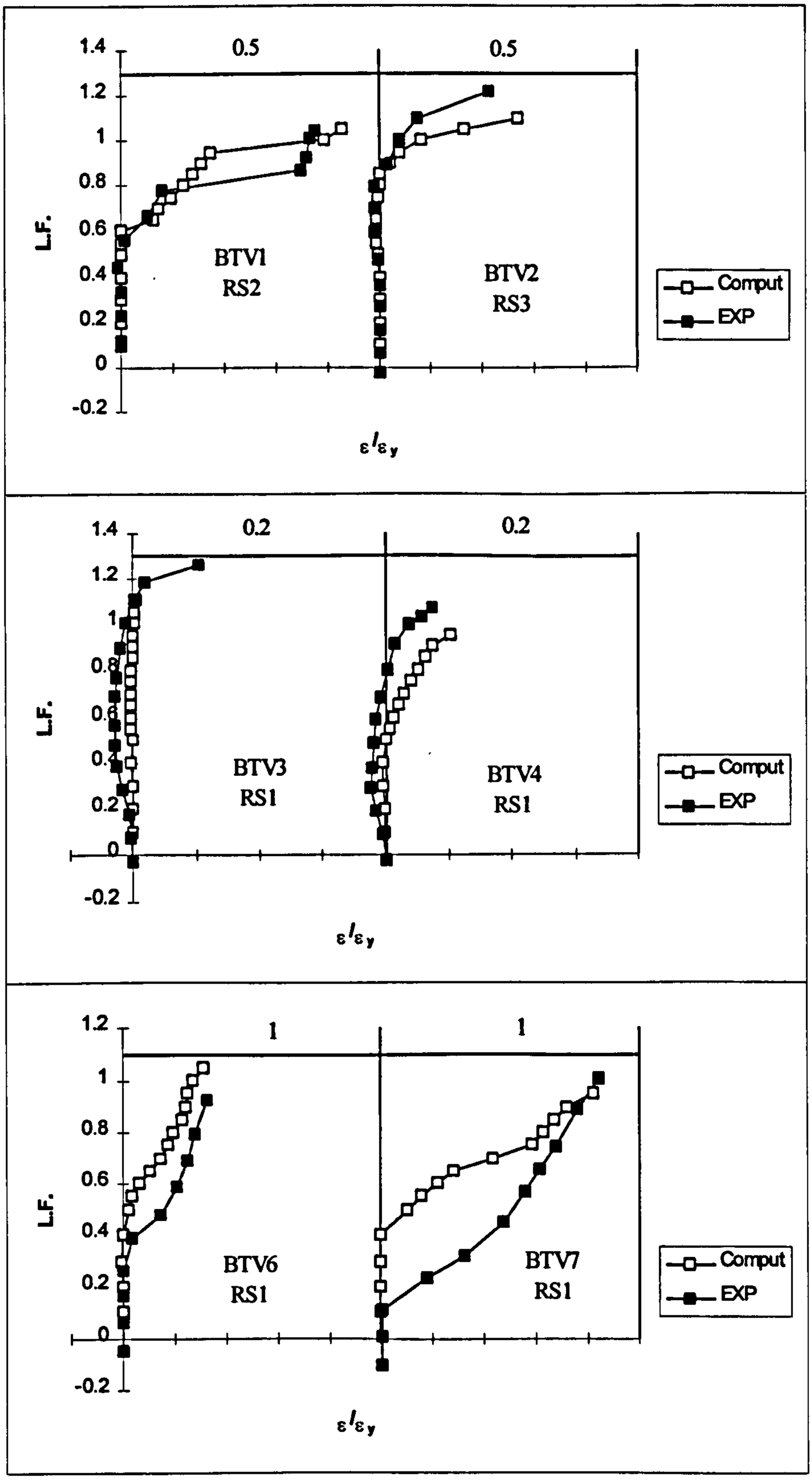

Fig. 9.5: Strain ratio at a selected point in a transverse bar (Back web)

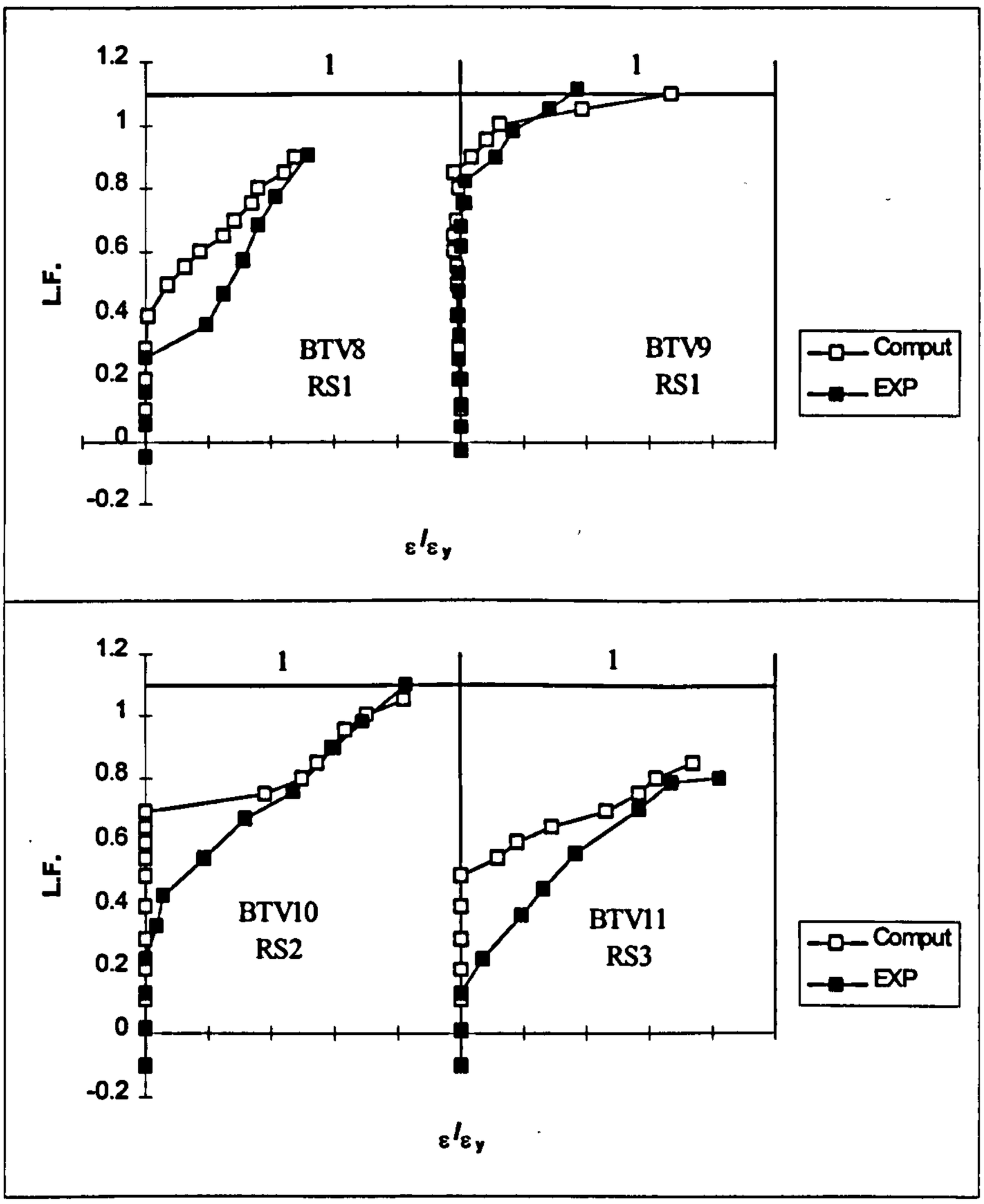

Fig. 9.5: Continued

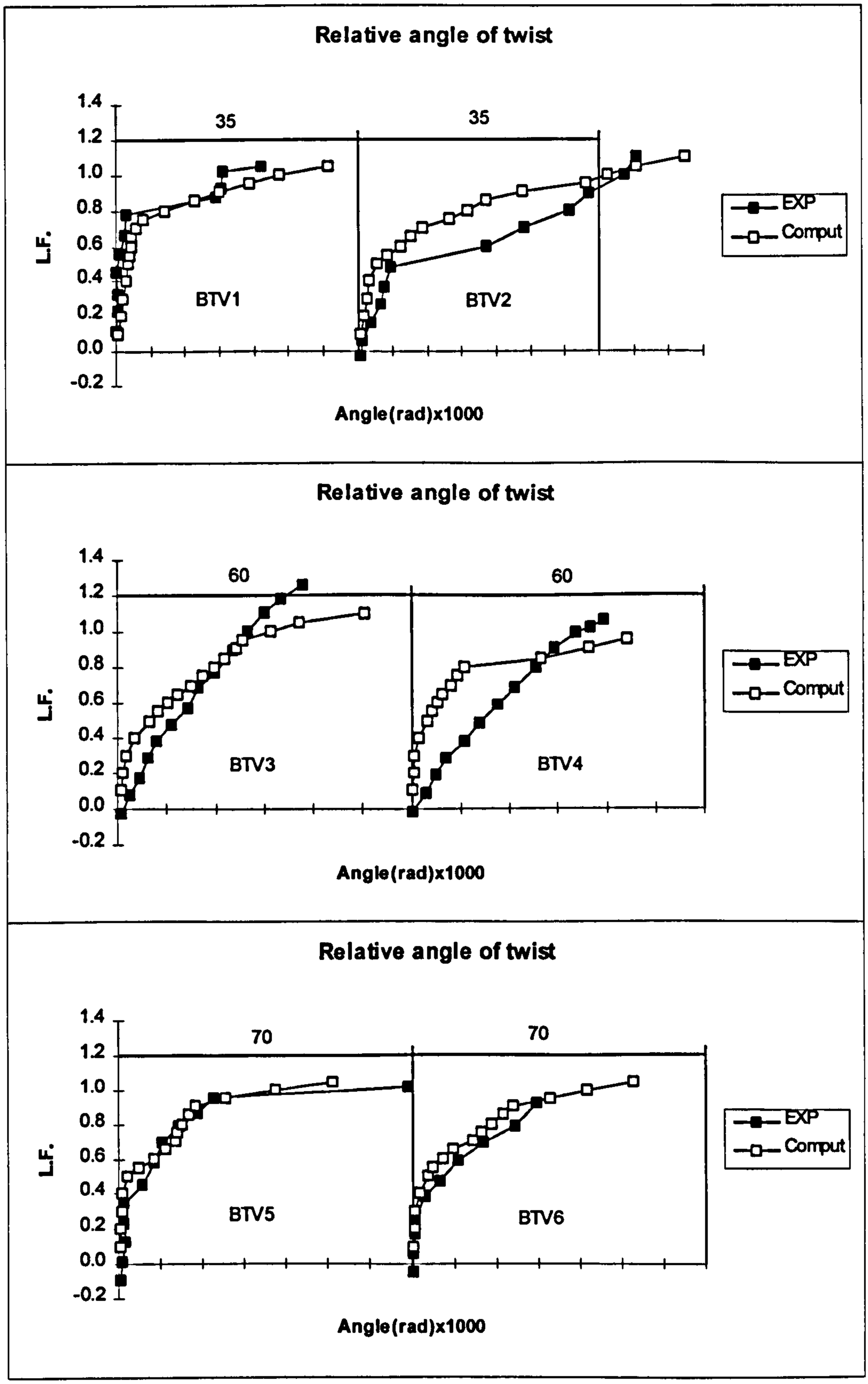

Fig. 9.6: Relative angle of twist

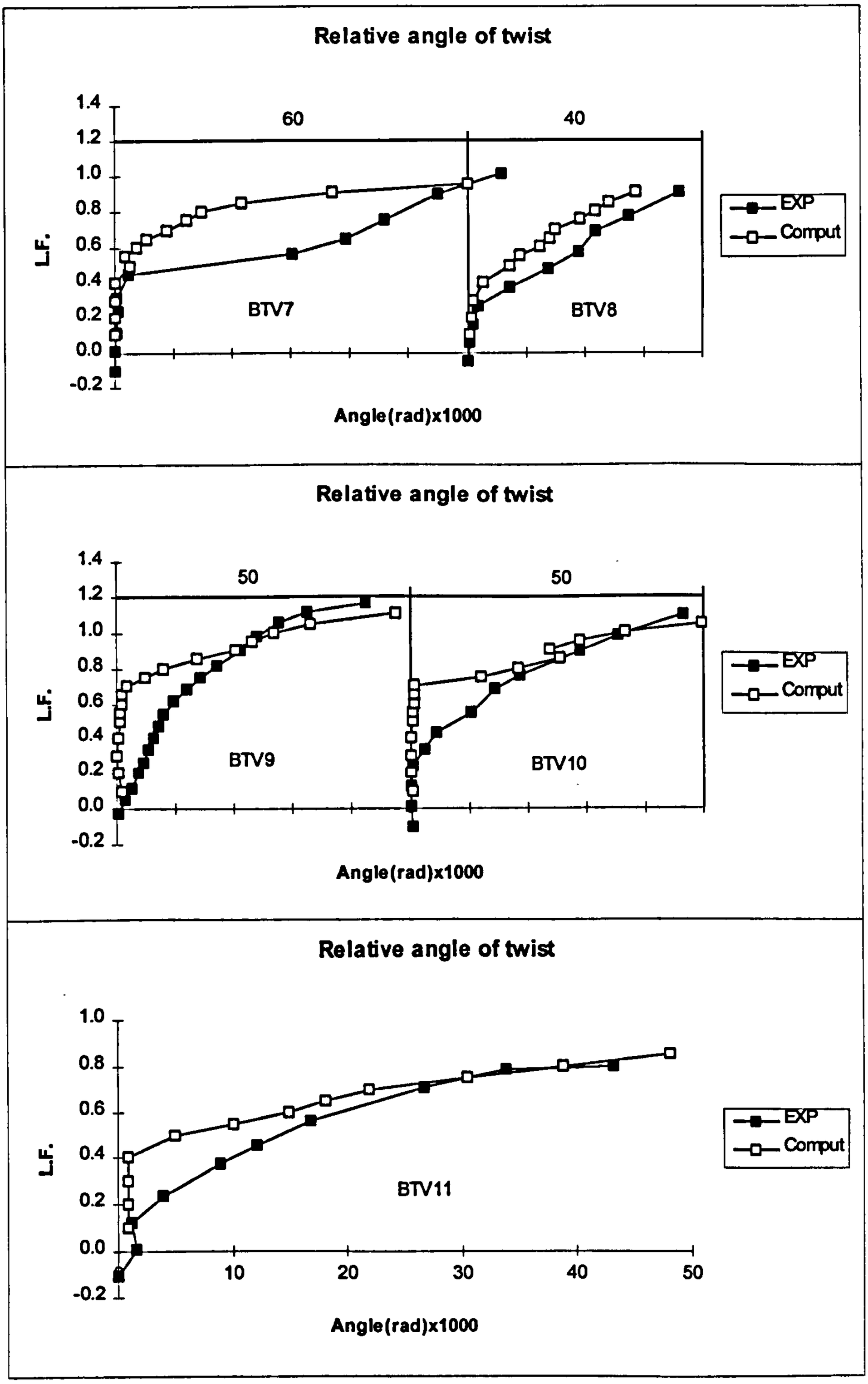

Fig. 9.6: Continued

Table 9.1: Experimental/design and computational/design failure ratios

Beam No.	$\tau_{tor.}/\tau_{shr}$ Ratio.	T_d/M_d Ratio.	Test Result Ratios L_e/L_d	L_c/L_d	L_e/L_c
Group A: Reinforced concrete hollow beams					
BTV1	2.28	0.87	1.04	1.05	0.99
BTV2	1.17	0.40	1.22	1.10	1.10
BTV3	0.79	0.26	1.26	1.10	1.14
BTV4	0.59	0.19	1.06	0.95	1.12
BTV5	4.56	1.75	1.02	1.05	0.97
BTV6	2.34	0.79	0.92	1.05	0.88
BTV7	6.84	2.62	1.01	0.95	1.06
BTV8	3.51	1.19	0.91	0.90	1.01
Group B: Partially prestressed hollow beams					
BTV9	1.09	0.35	1.16	1.10	1.05
BTV10	4.56	1.75	1.10	1.05	1.04
BTV11	6.84	2.62	0.90	0.85	1.06
Mean			1.05	1.01	1.04

L_d, L_e, L_c= Design, experimental and computational failure loads

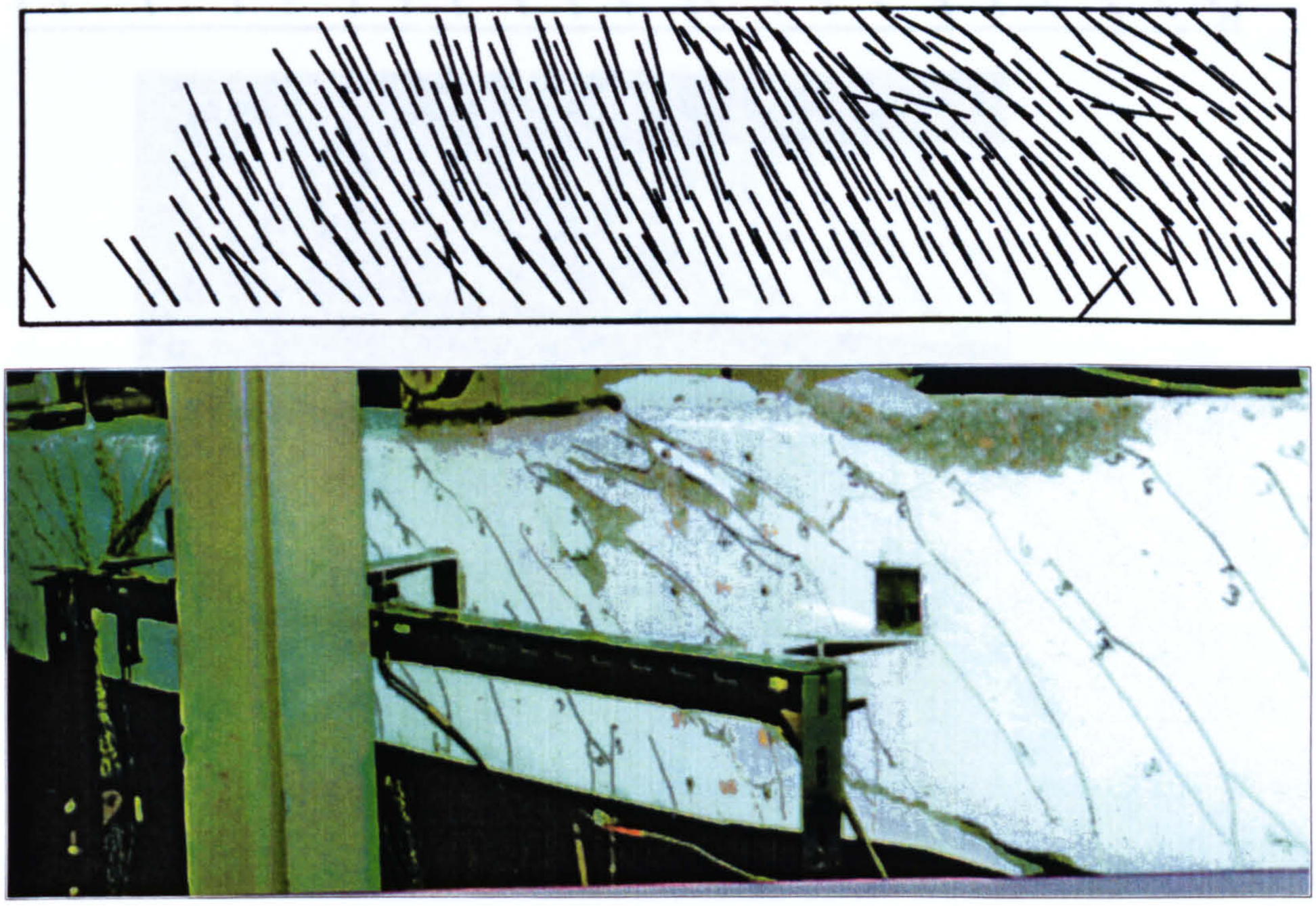

Fig. 9.7: Crack development in the back web (BTV1)

Fig. 9.8a: Crack development in the front web (BTV3)

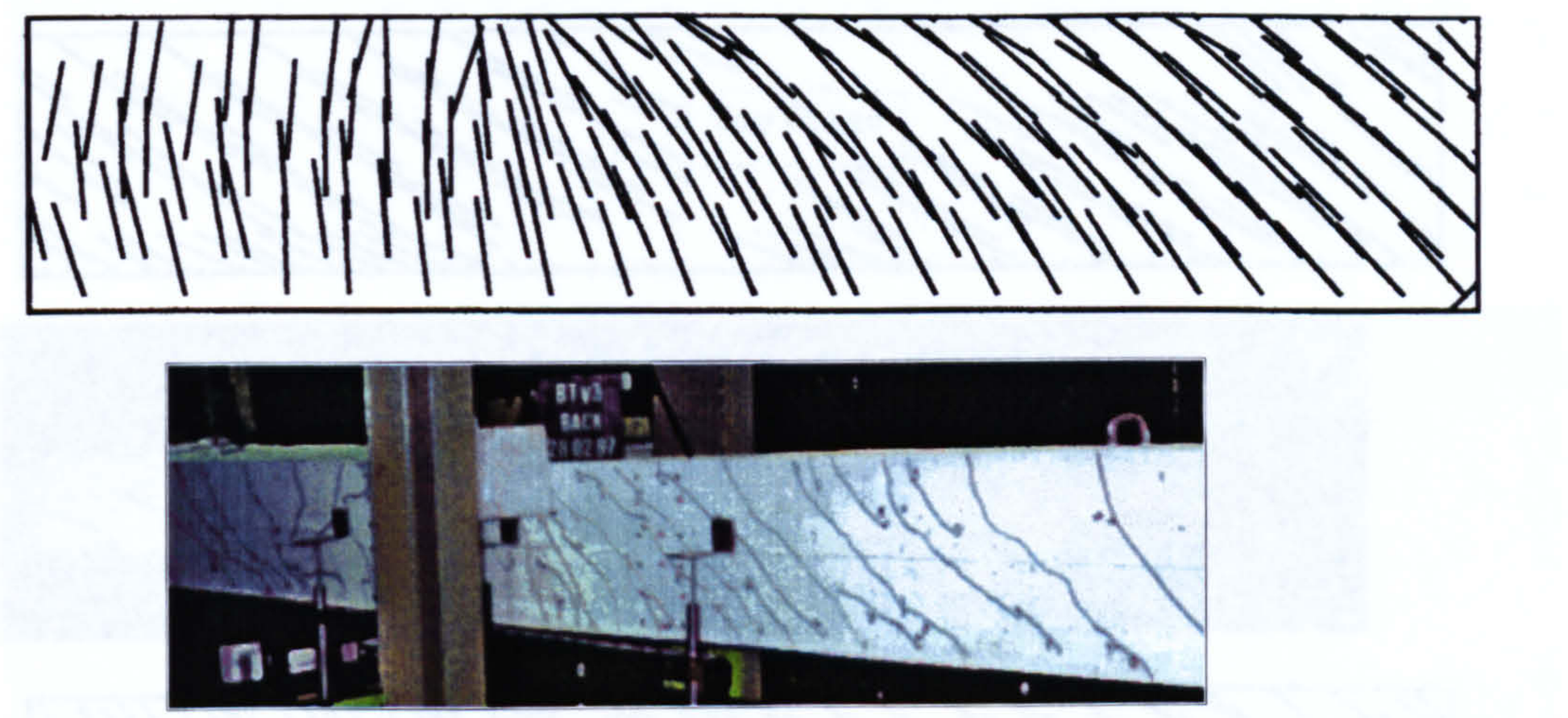

Fig. 9.8b: Crack development in the back web (BTV3)

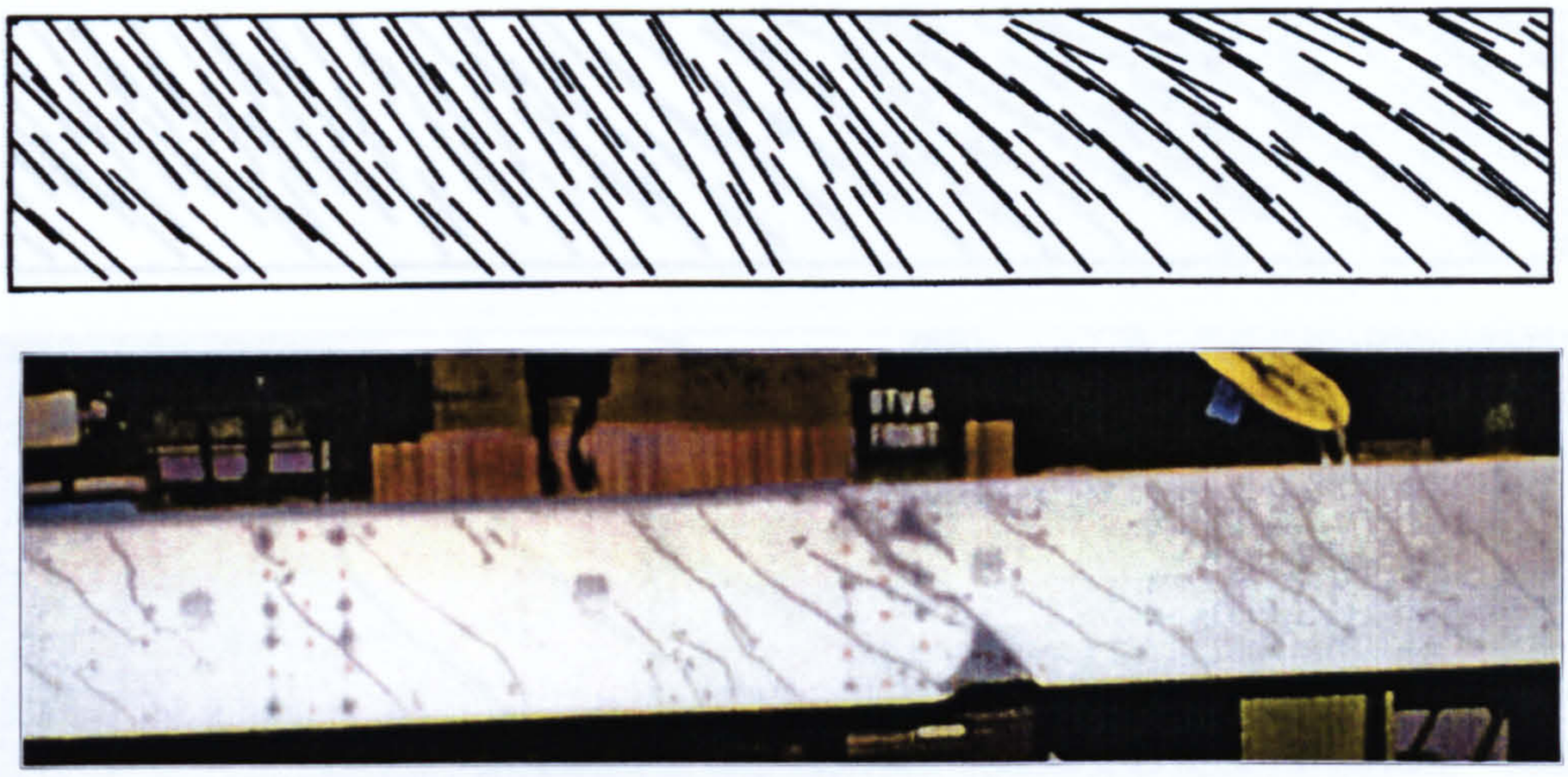

Fig. 9.9a: Crack development in the front web (BTV6)

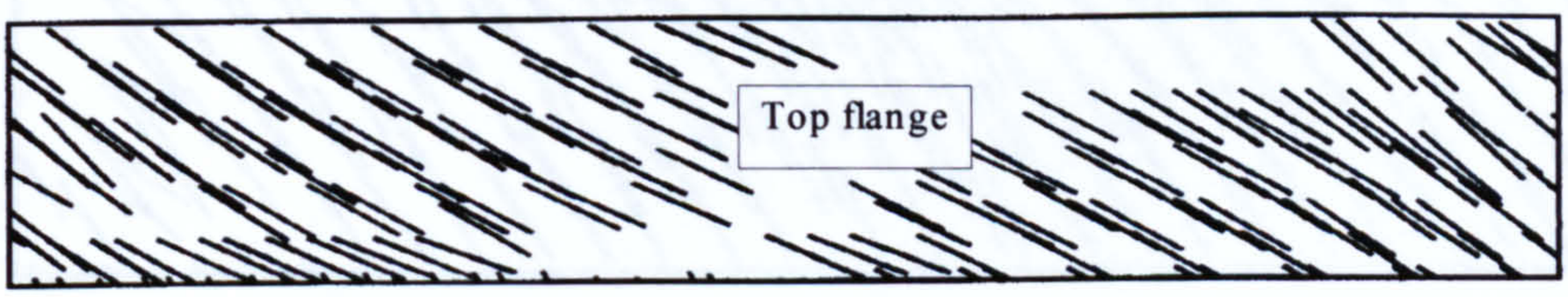

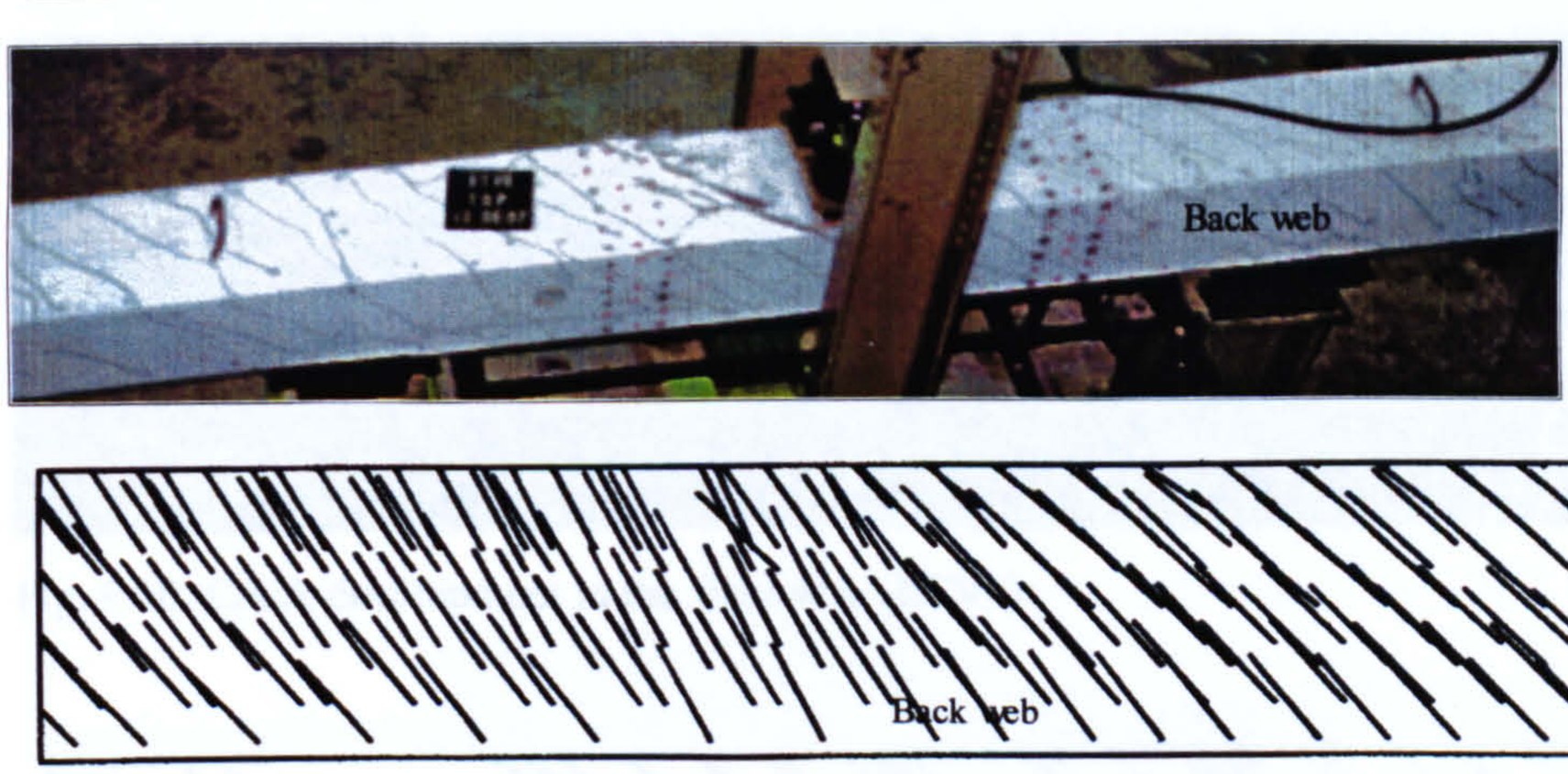

Fig. 9.9b-c: Crack development in the top flange and back web (BTV6)

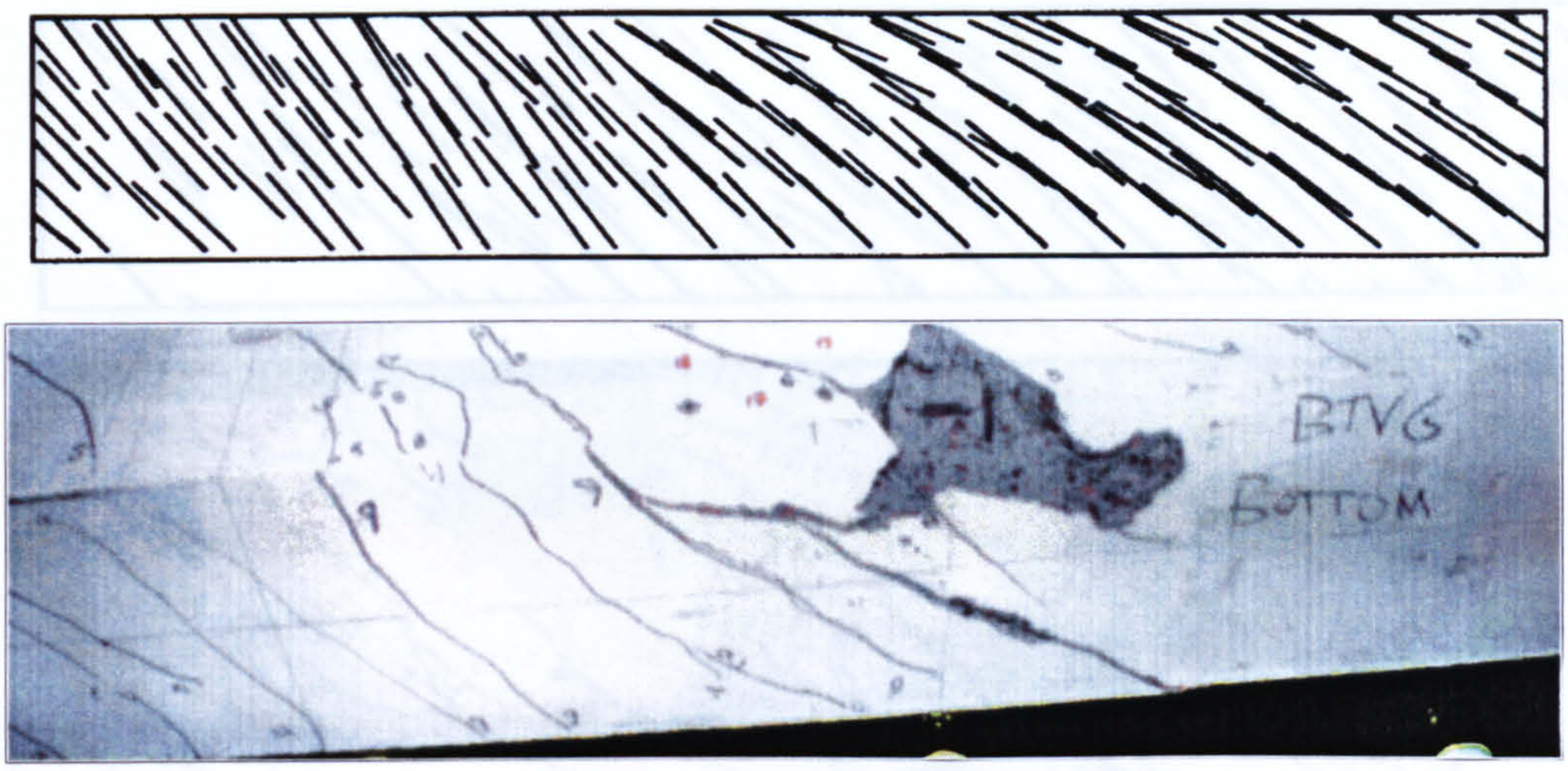

Fig. 9.9d: Crack development in the bottom flange (BTV6)

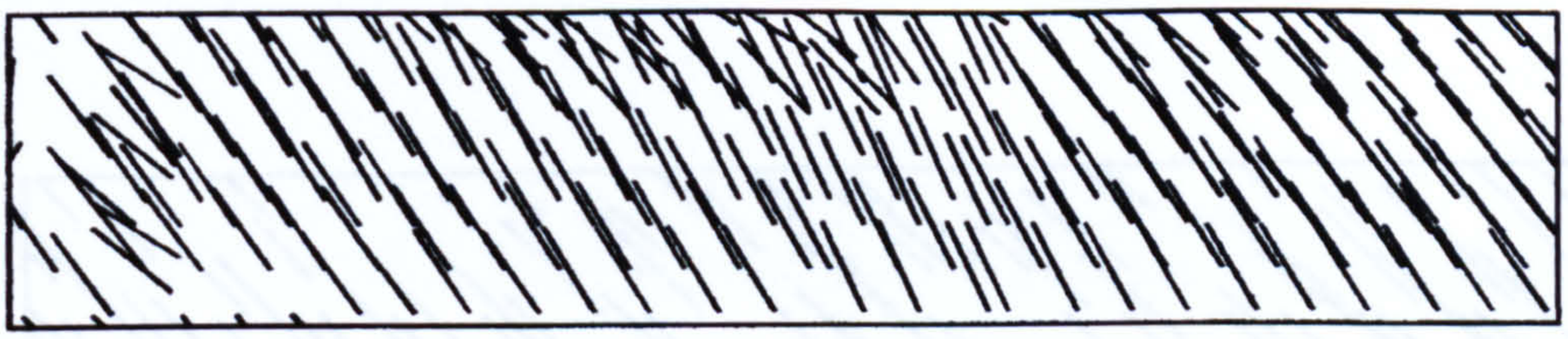

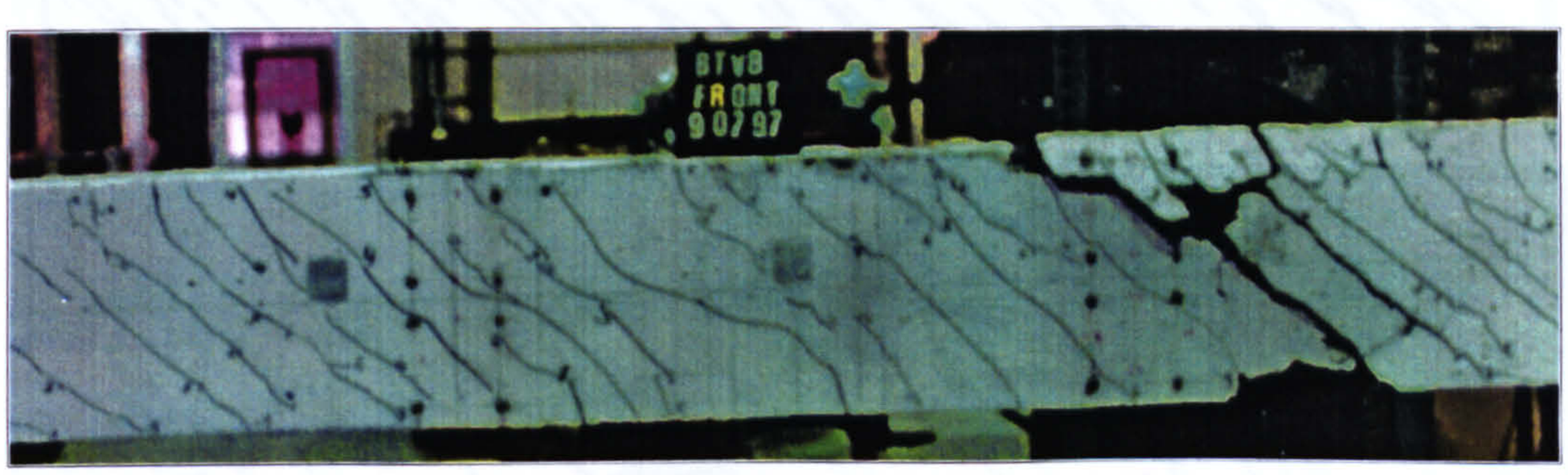

Fig. 9.10: Crack development in the front web (BTV8)

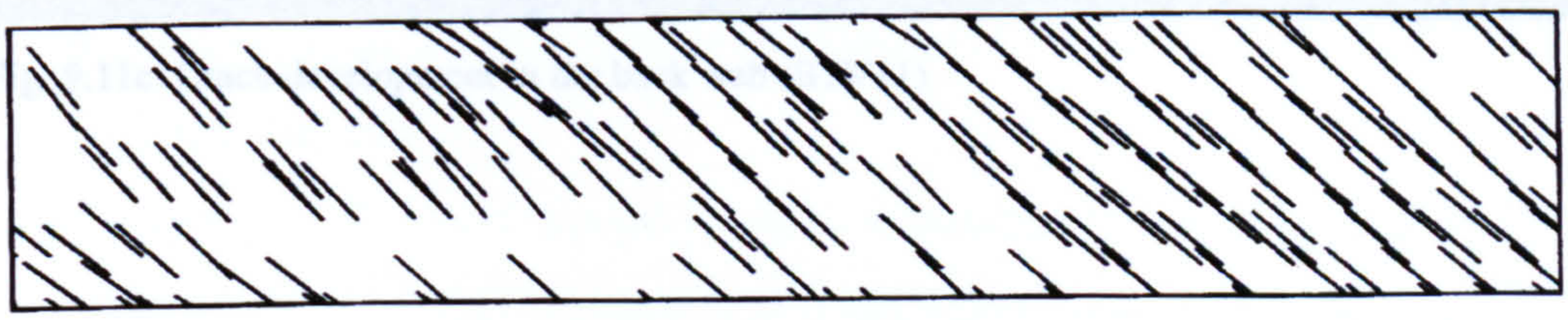

Fig. 9.11a: Crack development in the front web (BTV11)

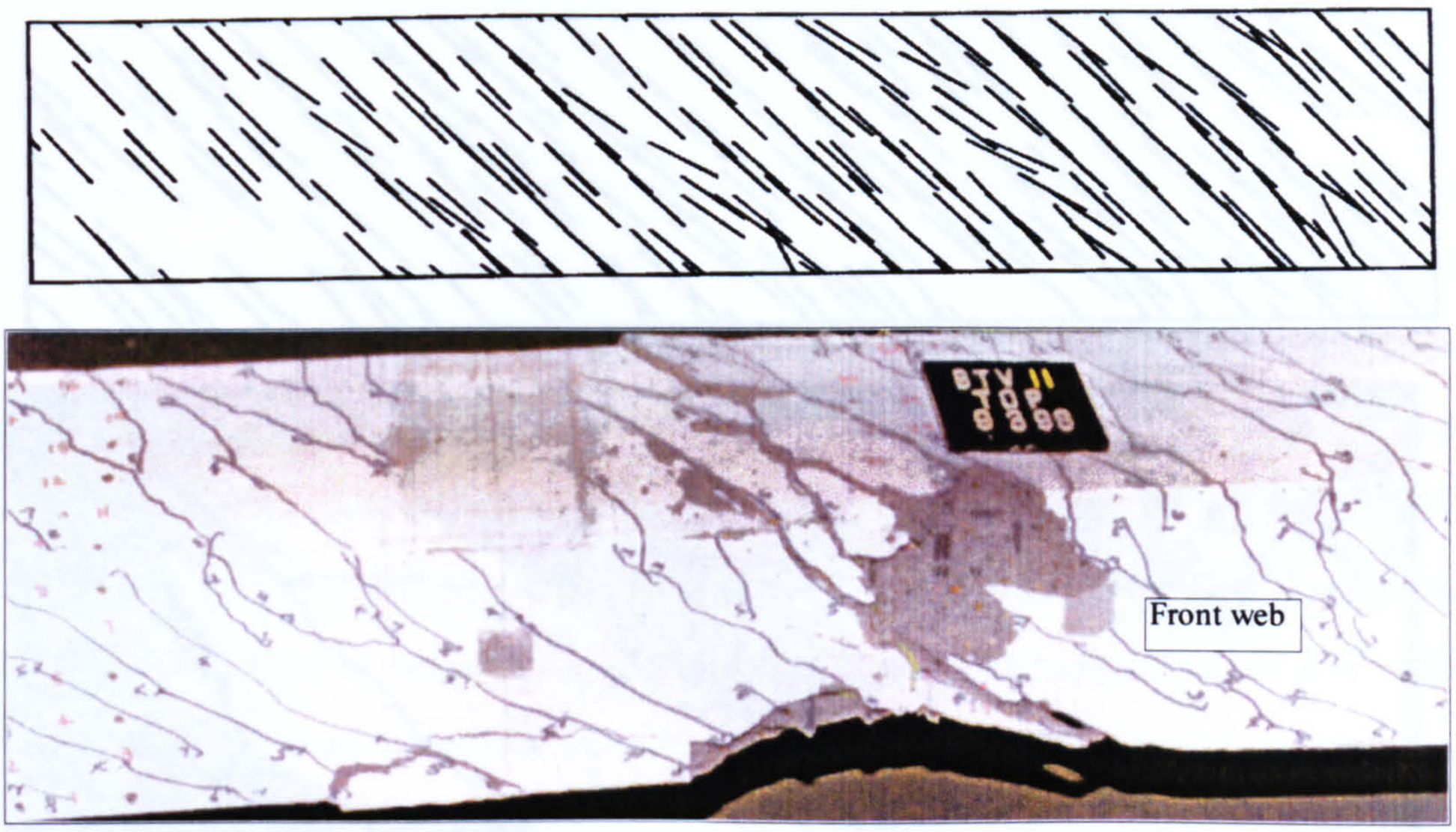

Fig. 9.11b: Crack development in the top flange (BTV11)

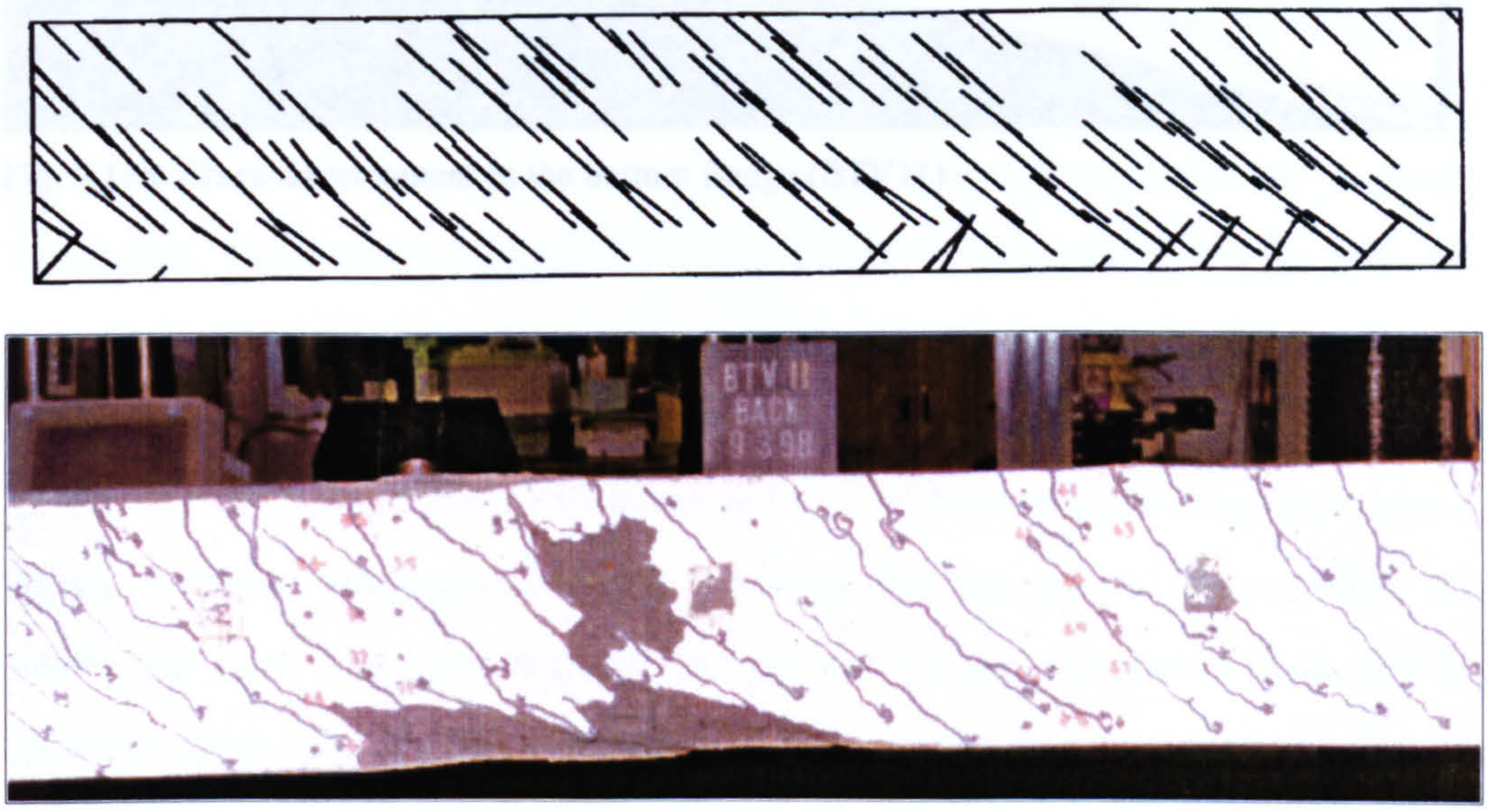

Fig. 9.11c: Crack development in the back web (BTV11)

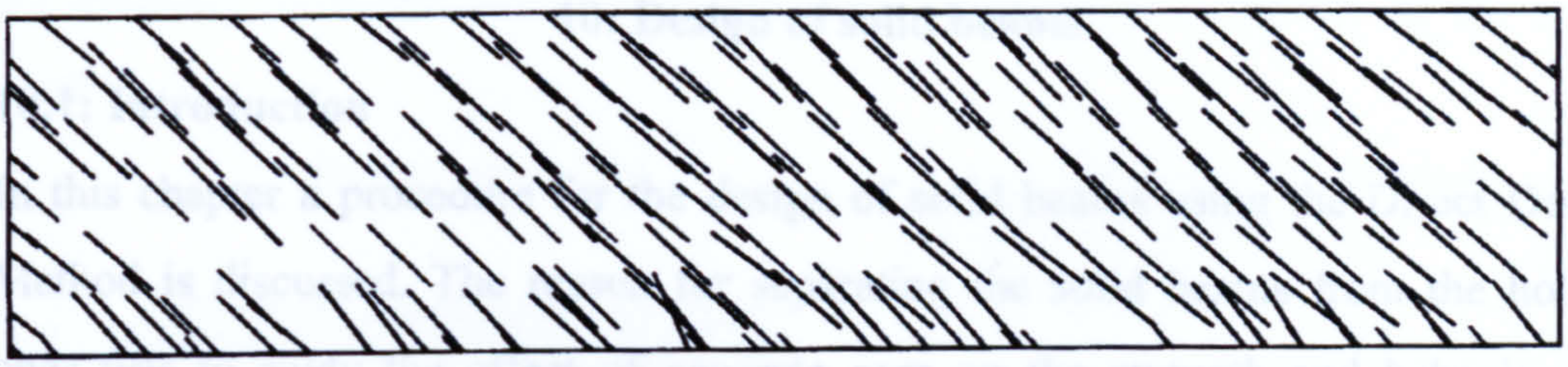

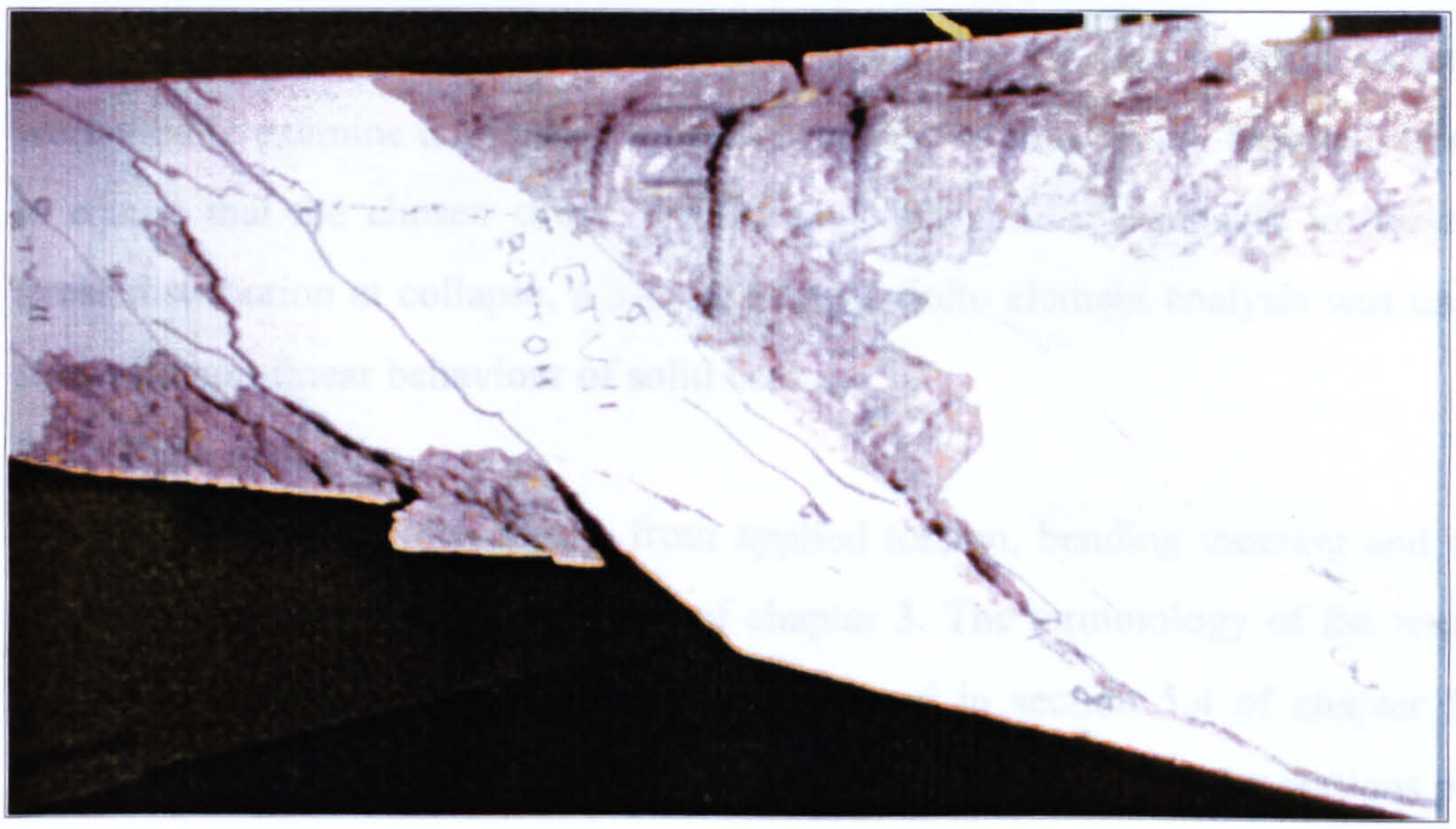

Fig. 9.11d: Crack development in the bottom flange (BTV11)

10: Design of solid beams

10.1: Introduction

In this chapter a procedure for the design of solid beams using the Direct Design Method is discussed. The reason for separating the solid beams from the hollow ones was to study the effect of concrete core on the strength and behaviour of beams. Different stress distributions combined with the direct design procedure were used to examine their effect on the quantity of reinforcement required. In order to ensure that the chosen stress distribution corresponds reasonably to the actual stress distribution at collapse, a 3-D non-linear finite element analysis was used to study the non-linear behaviour of solid beams.

10.2: Back ground

The state of stress which results from applied torsion, bending moment and shear force was explained in section 3.7.2 of chapter 3. The terminology of the required and provided reinforcement which was discussed in section 5.4 of chapter 5 for hollow beams applies to solid beams as well. Figure 10.1a shows the sections of the beam where the shear stresses are added and that where the shear stresses are subtracted. The steel in the 600mm region to the right of the mid-span (Fig. 10.1b) was strain gauged in both front and rear sides. In this region the shear stresses are added in the front side and subtracted in the rear side as can be seen in figure 10.1c. In the hollow beams and solid beam BTV12 (which will be discussed later) the largest required reinforcement was provided for the whole cross-section in the whole test span. The term 'largest' corresponds to the mid-span section and to the location where the shear stresses are added. Providing the largest reinforcement, of course, leads to some sections being over designed.

10.2.1: Pilot test beam

Solid beam BTV12 was designed to resist a combined load consisting of 13kNm torsion, 50.9kNm bending moment and 61kN shear force. This load combination was the same as that used for the design of hollow beam BTV3. In the design, for bending moment and shear force, elastic stress distribution in a solid section was used. However, shear stress due to torsion was calculated as for a hollow section. The reason for modelling the beam as a hollow one for torsion is because most of

the torsional resistance comes from the shear stress at the periphery of the cross-section.

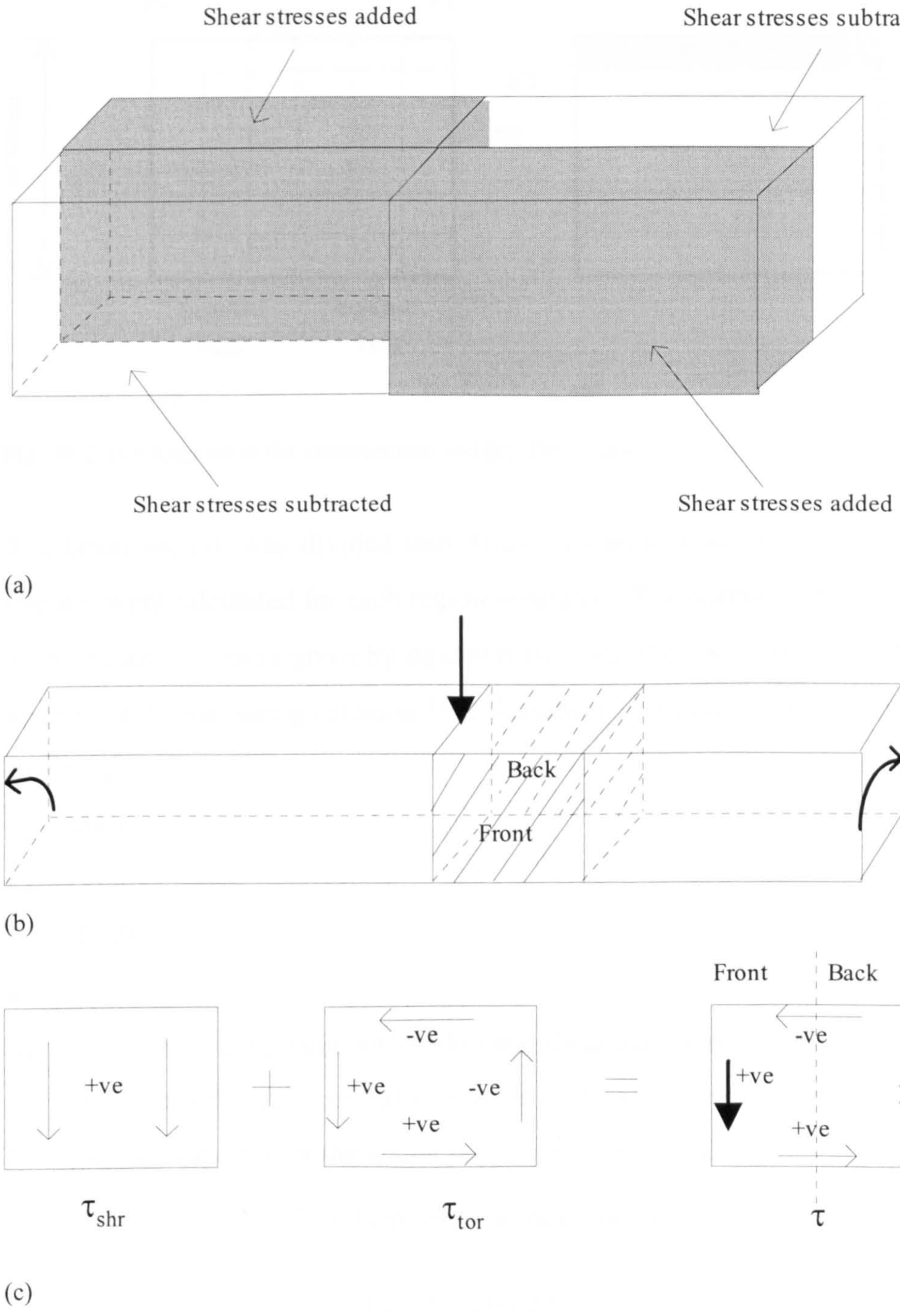

Fig. 10.1: (a): Regions of addition and subtraction of shear stresses, (b): Location of strain gauged reinforcement and (c): Shear stress sign convention

The design procedure was as follows:

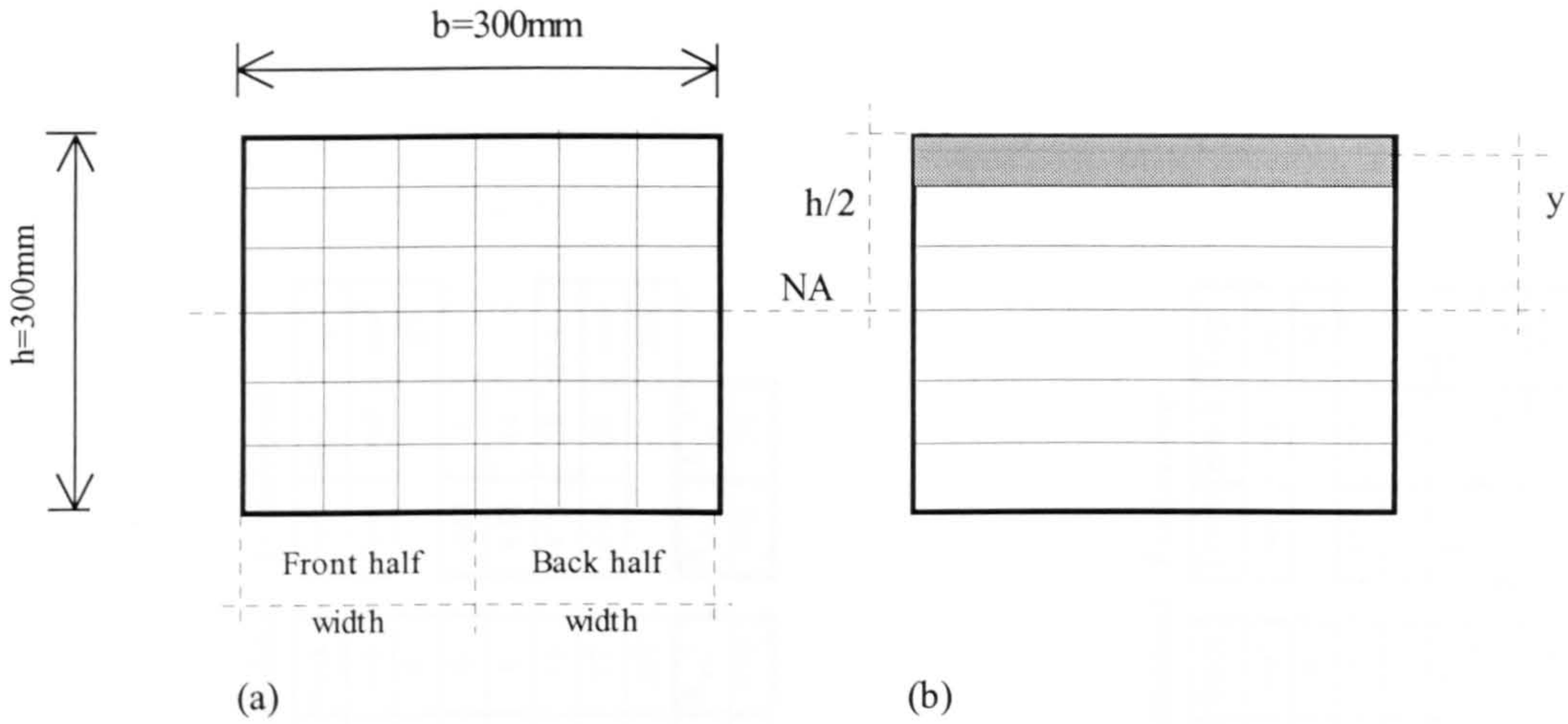

Fig. 10.2: (a): Regions in the cross-section and (b): Dimensions

The beam section was divided into 50x50mm regions as in figure 10.2a and the stresses were calculated for each region separately. The normal stress σ_x at any point of the beam section is given by equation 10.1 and the shear stress τ_{shr} due to shear force is calculated using equation 10.2. Equation 10.3 is used for the torsional shear stress τ_{tor}.

$$\sigma_x = My/I \qquad 10.1$$

$$\tau_{shr} = VQ/(bI) \qquad 10.2$$

$$\tau_{tor} = T/(2tA_o) \qquad 10.3$$

where:

M, T and V = bending moment, torsion and shear force respectively.

y = the distance from the neutral axis to the centroid of each region (Fig. 10.2b).

I = Moment of inertia for the whole solid section ($bh^3/12$).

$Q = \int_{area} ydA$. The statical moment of area about the neutral axis of the area above the section where the shear stress is required.

b = breadth of the cross section.

h = the height (depth) of the whole section.

t = the thickness in which the torsional shear stress is circulating.

A_o = The area enclosed by the centre line of the hollow section.

The normal stress and the shear stress due to shear force from equations 10.1 and 10.2 are uniformly distributed across the beam width and varying through the

Table 10.1: Comparison between required steel areas using elastic stress distribution

σ_x	σ_x	σ_x	σ_x	σ_x	σ_x
N/mm²	N/mm²	N/mm²	N/mm²	N/mm²	N/mm²
-11.7	-11.7	-11.7	-11.7	-11.7	-11.7
-7.0					-7.0
-2.3					-2.3
2.3					2.3
7.0					7.0
11.7	11.7	11.7	11.7	11.7	11.7

τ_{shr}	τ_{shr}	τ_{shr}	τ_{shr}	τ_{shr}	τ_{shr}
N/mm²	N/mm²	N/mm²	N/mm²	N/mm²	N/mm²
0.4	0.4	0.4	0.4	0.4	0.4
2.4					2.4
2.6					2.6
2.6					2.6
2.4					2.4
0.4	0.4	0.4	0.4	0.4	0.4

τ_{tor}	τ_{tor}	τ_{tor}	τ_{tor}	τ_{tor}	τ_{tor}
N/mm²	N/mm²	N/mm²	N/mm²	N/mm²	N/mm²
-2.1	-2.1	-2.1	-2.1	-2.1	-2.1
2.1					-2.1
2.1					-2.1
2.1					-2.1
2.1					-2.1
2.1	2.1	2.1	2.1	2.1	2.1

τ	τ	τ	τ	τ	τ
N/mm²	N/mm²	N/mm²	N/mm²	N/mm²	N/mm²
-2.1	-2.1	-2.1	-2.1	-2.1	-2.1
4.4					0.3
4.7					0.6
4.7					0.6
4.4					0.3
2.1	2.1	2.1	2.1	2.1	2.1

A_x	A_x	A_x	A_x	A_x	A_x
mm²	mm²	mm²	mm²	mm²	mm²
0	0	0	0	0	0
0					0
12					0
35					15
57					37
69	69	69	69	69	69
				ΣA_x	570

A_t	A_t	A_t	A_t	A_t	A_t
mm²/m	mm²/m	mm²/m	mm²/m	mm²/m	mm²/m
37	37	37	37	37	37
280					1
472					14
472					56
444					28
208	208	208	208	208	208

Reinforced hollow elastic

Longitudinal

Front	Back
mm²	mm²
0	0
0	0
12	0
35	15
57	37
207	207
A_{sx}^{f}	A_{sx}^{b}
312	258

Transverse

Front	Back	Top
mm²	mm²	mm²
		37
280	1	
472	14	
472	56	Bot.
444	28	mm²
		208

A_{sy}^{f}	A_{sy}^{b}
472	56

σ_x	σ_x	σ_x	σ_x	σ_x	σ_x
N/mm²	N/mm²	N/mm²	N/mm²	N/mm²	N/mm²
-9.4	-9.4	-9.4	-9.4	-9.4	-9.4
-5.6	-5.6	-5.6	-5.6	-5.6	-5.6
-1.9	-1.9	-1.9	-1.9	-1.9	-1.9
1.9	1.9	1.9	1.9	1.9	1.9
5.6	5.6	5.6	5.6	5.6	5.6
9.4	9.4	9.4	9.4	9.4	9.4

τ_{shr}	τ_{shr}	τ_{shr}	τ_{shr}	τ_{shr}	τ_{shr}
N/mm²	N/mm²	N/mm²	N/mm²	N/mm²	N/mm²
0.3	0.3	0.3	0.3	0.3	0.3
0.8	0.8	0.8	0.8	0.8	0.8
1.0	1.0	1.0	1.0	1.0	1.0
1.0	1.0	1.0	1.0	1.0	1.0
0.8	0.8	0.8	0.8	0.8	0.8
0.3	0.3	0.3	0.3	0.3	0.3

τ_{tor}	τ_{tor}	τ_{tor}	τ_{tor}	τ_{tor}	τ_{tor}
N/mm²	N/mm²	N/mm²	N/mm²	N/mm²	N/mm²
-2.1	-2.1	-2.1	-2.1	-2.1	-2.1
2.1					-2.1
2.1					-2.1
2.1					-2.1
2.1					-2.1
2.1	2.1	2.1	2.1	2.1	2.1

τ	τ	τ	τ	τ	τ
N/mm²	N/mm²	N/mm²	N/mm²	N/mm²	N/mm²
-2.1	-2.1	-2.1	-2.1	-2.1	-2.1
2.8	0.8	0.8	0.8	0.8	-1.3
3.1	1.0	1.0	1.0	1.0	-1.1
3.1	1.0	1.0	1.0	1.0	-1.1
2.8	0.8	0.8	0.8	0.8	-1.3
2.1	2.1	2.1	2.1	2.1	2.1

A_x	A_x	A_x	A_x	A_x	A_x
mm²	mm²	mm²	mm²	mm²	mm²
0	0	0	0	0	0
0	0	0	0	0	0
6	0	0	0	0	0.0
25	14	14	14	14	15
42	32	32	32	32	35
57	57	57	57	57	57
				ΣA_x	653

A_t	A_t	A_t	A_t	A_t	A_t
mm²/m	mm²/m	mm²/m	mm²/m	mm²/m	mm²/m
46	46	46	46	46	46
143	10	10	10	10	31
307	52	52	52	52	63
307	99	99	99	99	109
284	76	76	76	76	132
208	208	208	208	208	208

Reinforced solid elastic

Longitudinal

Front	Back
mm²	mm²
0	0
0	0
6	0
53	44
107	99
172	172
A_{sx}^{f}	A_{sx}^{b}
338	315

Transverse

Front	Back	Top
mm²	mm²	mm²
		46
164	51	
411	167	
505	307	Bot.
437	284	mm²
		208

A_{sy}^{f}	A_{sy}^{b}
505	307

depth. The shear stress due to torsion is assumed to be circulating in the outer 50mm periphery. The net shear stress is the algebraic sum of the shear stress due to torsion and the shear stress due to shear force.

As an alternative, the beam was also designed as a hollow beam with elastic stress distribution as described in chapter 5. The effect of the core was thus totally ignored. In calculating the steel areas, steel yield stress through out this chapter was arbitrarily taken as $500N/mm^2$.

Table 10.1 shows that the required reinforcement in the case of modelling the beam as being hollow and also as solid. In this table, σ_x is positive when tensile while τ_{shr} and τ_{tor} are as shown in figure 10.1c. The A_x and A_t are the required reinforcement for each region in the longitudinal X and transverse Y or Z directions respectively. It is clear that in the top and bottom strips of the beam, A_x and A_t are constant over the whole width. However, in the regions between these strips, each cell requires different area of A_x and A_t. For each half of the beam width between the top and bottom strips, the stirrup leg area shown is the summation of all areas in the cells at that level. This results in four stirrup leg areas for each half, the largest leg area among the areas in the front half where the stresses are added is called A_{sy}^f while A_{sy}^b is the one opposite to A_{sy}^f at the same level in the rear half. In the case of longitudinal reinforcement, A_{sx}^f is the summation of steel areas for all the cells in the front half of the beam width, including the top and bottom strips and A_{sx}^b is the corresponding value in the rear half.

Table 10.1 shows that when solid beam is modelled as a hollow beam it requires slightly less reinforcement in both longitudinal and transverse directions than when the beam is designed as a solid one. This suggests that including the core does not reduce the required steel area. The reason for this unexpected result is not clear at this stage. However, in order to experimentally investigate the effect of the 200x200mm concrete core on the strength and behaviour of the beam and to have test data for future analysis, beam BTV12 was designed as a hollow section but constructed as solid.

Although A_{sx}^f was the largest longitudinal steel required in one half of the beam, the same steel area was provided in the other half as well. Also the largest transverse

steel A_{sy}^{f} was used for the whole cross-section. These areas were provided in the whole 1.2m test span. Outside the test-span, more reinforcement was provided to ensure failure in the test-span.

The concrete cube compressive strength was 50N/mm^2 and the average yield stress for longitudinal steel was 500N/mm^2 and for the transverse steel was 530N/mm^2. The steel arrangement was as shown figure 10.3.

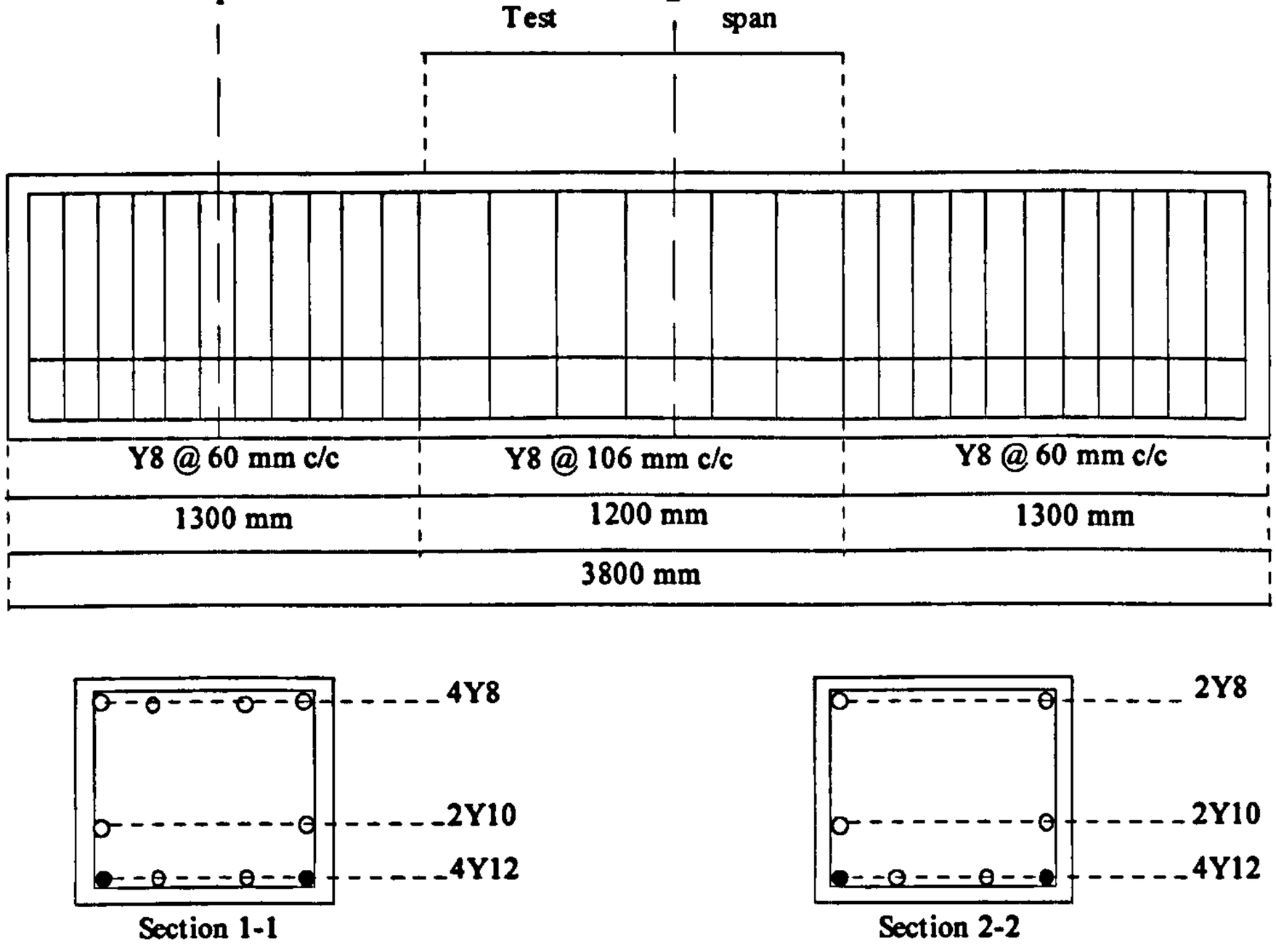

Fig. 10.3: Reinforcement arrangement for beam BTV12

The test result presented in table 10.2 shows that beam BTV12 resisted about 85% more load than the design load or 46% more than the corresponding hollow beam BTV3. A non-linear analysis using the 2-D program developed for the hollow beams and a new 3-D one (discussed later) revealed that the former under estimates the strength of the solid beams while the latter naturally predicts load closer to the experiment (Fig. 10.4). These results raise the question why does a solid beam resist more load than a hollow one with same reinforcement?. To answer this question the following theoretical investigation was under taken, particularly to see whether a more reasonable stress distribution can be used for designing the steel.

Table 10.2: Ratios of experimental to design and computed to design failure load

Beam No.	EXP/DSGN	COMPUT/DSGN	
	L_e/L_d	2-D	3-D
BTV3	1.26	1.1	-
BTV12	1.85	1.25	1.65

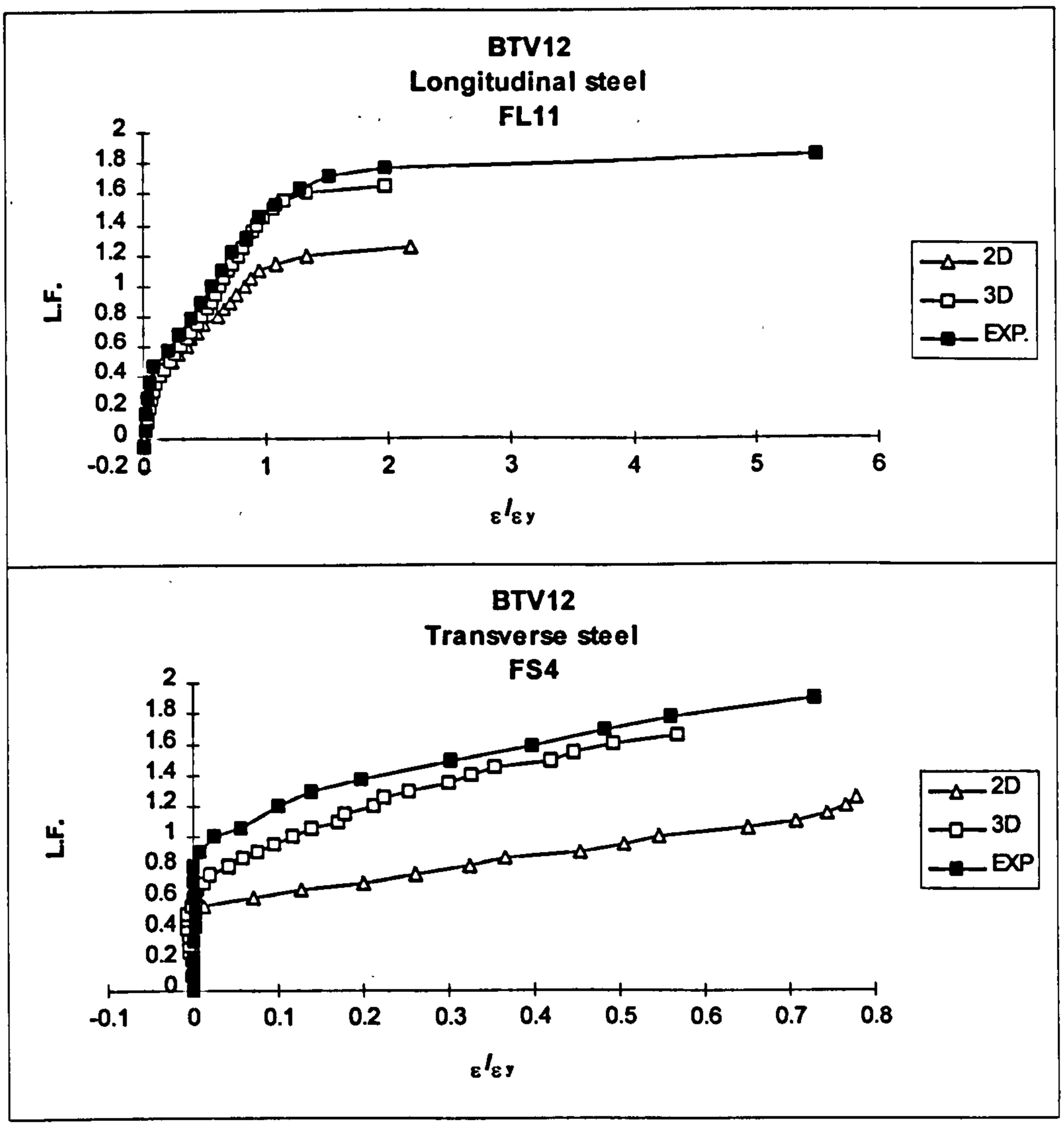

Fig. 10.4: Comparison between observed and computed 2d and 3D results

10.3: 3-D finite element program

The 3-D finite element program used for non-linear analysis of this computational study was developed by El-Nounu 1985 using Kotsovs' concrete model. This model was based on experimental data obtained at Imperial College London from tests on the behaviour of concrete under complex stress states [Kotsovos and Newman (1979) and Kotsovos (1979)]. The testing techniques used to obtain this data were validated by comparing them with those obtained in an international co-operative programme of research into the effect of different test methods on the behaviour

of concrete. This model is capable of describing the behaviour of concrete under uniaxial, biaxial and triaxial stress conditions. It requires only the concrete cube compressive strength f_{cu} to define the behaviour of concrete under different stress states. More information about this model is given in Kotsovos M.D. and Pavlovic' M.N.(1995). In the 3-D program a twenty node iso-parametric solid element with twenty seven Gauss points was used. The concrete cylinder compressive strength f_c' is taken as $f_c' = 0.8 f_{cu}$ N/mm^2, the Young's modulus $E_c = 5000\sqrt{f_c'}$ N/mm^2, the split cylinder tensile strength $f_t' = 0.54\sqrt{f_c'}$ N/mm^2 and the Poisson's ratio is set at a constant value of 0.15. Before cracking or crushing, the concrete behaviour is assumed to be non-linear elastic isotropic. After cracking, smeared crack approach with simple tension stiffening and shear retention equations are employed to represent the post cracking behaviour of concrete (Fig. 10.5). The stress-strain relationship in tension was assumed to be linear up to f_t' and immediately after cracking the tensile stress f_t is reduced to $0.8 f_t'$. Thereafter, f_t decreases linearly with strain and is zero at the maximum strain of 0.003 which roughly corresponds to yield strain of steel of 0.0025. Transfer of shear stresses across cracks is modelled by means of the 'shear retention' factor β which defines the shear modulus of cracked concrete as βG, where G is the elastic shear modulus of the un-cracked concrete. The shear retention factor $\beta = 0.25\varepsilon_{cr}/\varepsilon_n$, where ε_{cr} = cracking strain ($\varepsilon_{cr} = \frac{f_t'}{E_c}$) and ε_n = average of the three principal strains at any cracked point ($\varepsilon_n = \frac{\varepsilon_1 + \varepsilon_2 + \varepsilon_3}{3}$). In the case of concrete crushing, complete loss of strength is assumed i.e. no compression softening is allowed for. The reinforcement is modelled as one dimensional element embedded in the solid concrete elements. Elasto-plastic stress-strain behaviour with or without strain hardening can be allowed for (model without strain hardening was only used in this research). Only uniaxial resistance is considered with no provision for kinking or dowel action.

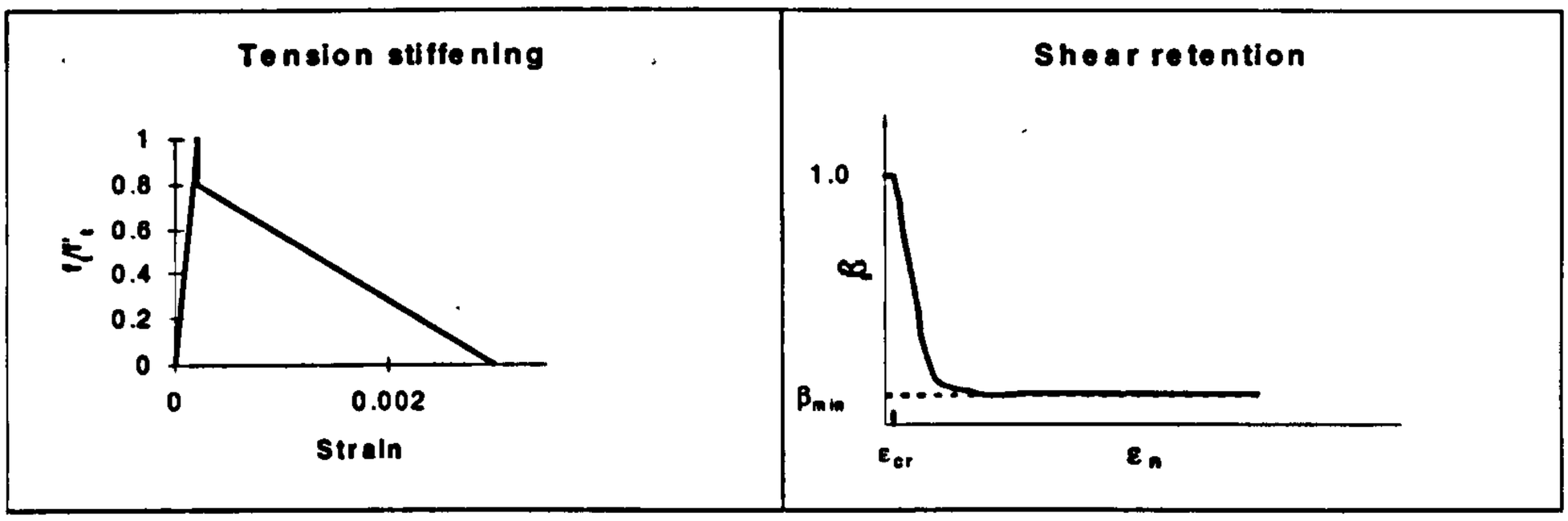

Fig. 10.5: Tension stiffening and shear retention curves

10.4: Theoretical investigation

In this section the results of the use of 3-D finite element program to study the stress distribution due to different load combinations, load levels and ratios of torsion to bending moment T/M and shear force to bending moment V/M is presented. The material properties and steel area used are as for beam BTV12 and are kept fixed throughout the analysis. In order to have a complete control on the applied loads, the self weight of the beam and torsional arms was ignored. The beam cross section was modelled as four 150x150x150mm elements. The convergence tolerance based on the ratio of residual forces to applied load was 5.0%, the number of increments was 50 and the maximum number of iterations in each increment was 200. All other parameters were calculated as explained in section 10.3. Load increment of 10% of the design load was applied for the first two increments and then the load was increased by 5% for each increment until failure. The stresses in the cross-section at 17mm to the right of mid-span were analysed. In each vertical strip, stresses at six Gauss points were calculated. The Gauss points used in the analysis are shown in figure 10.6. The stress distribution at the last converged increment was used for the analysis.

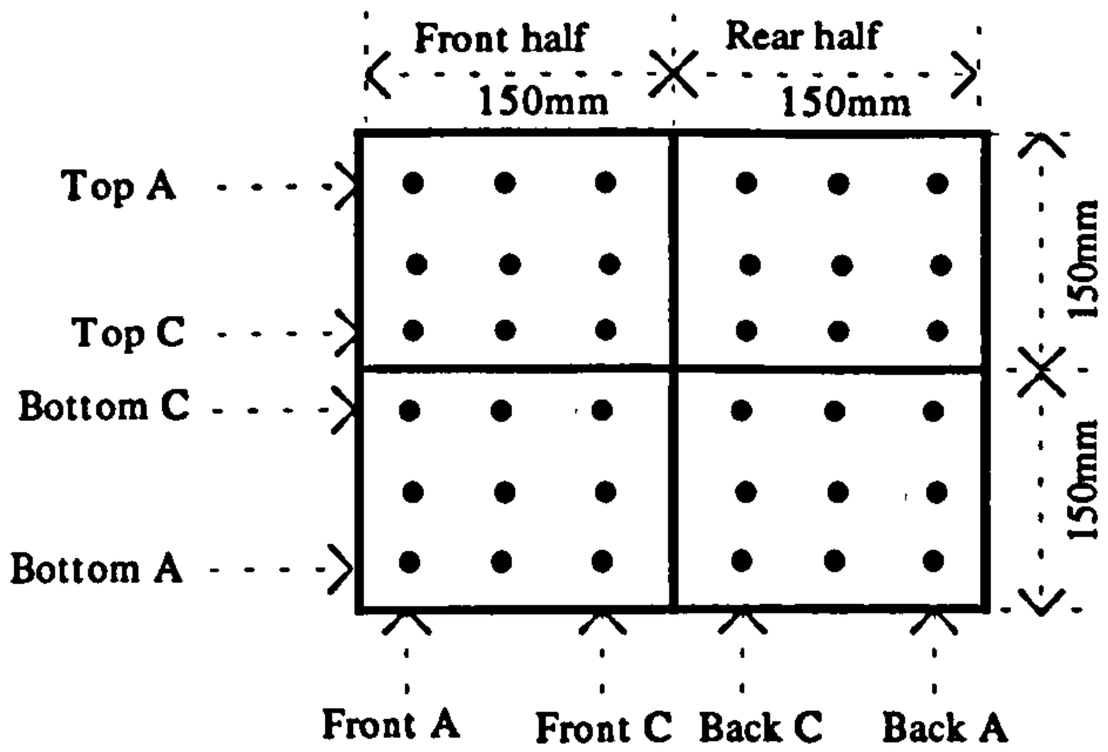

Fig. 10.6: Gauss points

10.4.1: Effect of load combination

Load values of T=13kNm, M=51kNm and V=60kN were imposed in five load combinations as follows. In each case only proportional loading was used.

1. **Pure bending:** Figure 10.7 shows the normal compressive stress distribution in the case of pure bending. Compressive stress in concrete exists in the top 27% (80x300 mm) of the beam.
2. **Bending moment and shear force:** Figure 10.8 shows the normal and shear stresses in the beam when subjected to combined loading of bending moment and shear force. The normal compressive stress is still concentrated in the top 27% of the cross section while the shear stress exists in the top 45% of the cross section. Very little shear stress exists in the cracked zones.
3. **Pure Torsion:** The shear stress distribution for reinforced concrete solid beams in the case of pure torsion is shown in figures 10.9. It is clear that most of the shear stress due to pure torsion circulates in the outer shell as expected with minimal stress in the core. Quantitatively, the outer 22% (33 mm) shell of the cross section resists about 90% of the total torsion.
4. **Torsion and bending moment:** The normal and shear stresses for the combined load of torsion and bending moment is presented in figures 10.10. These figures show that compressive normal stress is still in the top 27% of the cross section and the shear stress is still concentrated in the outer 22% shell. However, a change in behaviour is visible in the distribution of compressive stress where the outer shell is having a lower neutral axis than the inner part.
5. **Torsion, bending moment and shear force:** Figures 10.11 show the normal and shear stress distributions for this load combination. The normal stress distribution is similar to that for torsion and bending moment alone except for the presence of a large stress variation across the beam width. As is to be expected more shear stress exists at the section where the shear stresses due to torsion and shear force are added than that where the stresses are subtracted. Contribution of the core in resisting the shear stress is quit evident.

From the above discussion it is possible to say that the normal stress and the shear stress due to shear force are partly resisted by the core. The shear stress due to torsion is resisted by the outer shell. The presence of normal compressive stress in

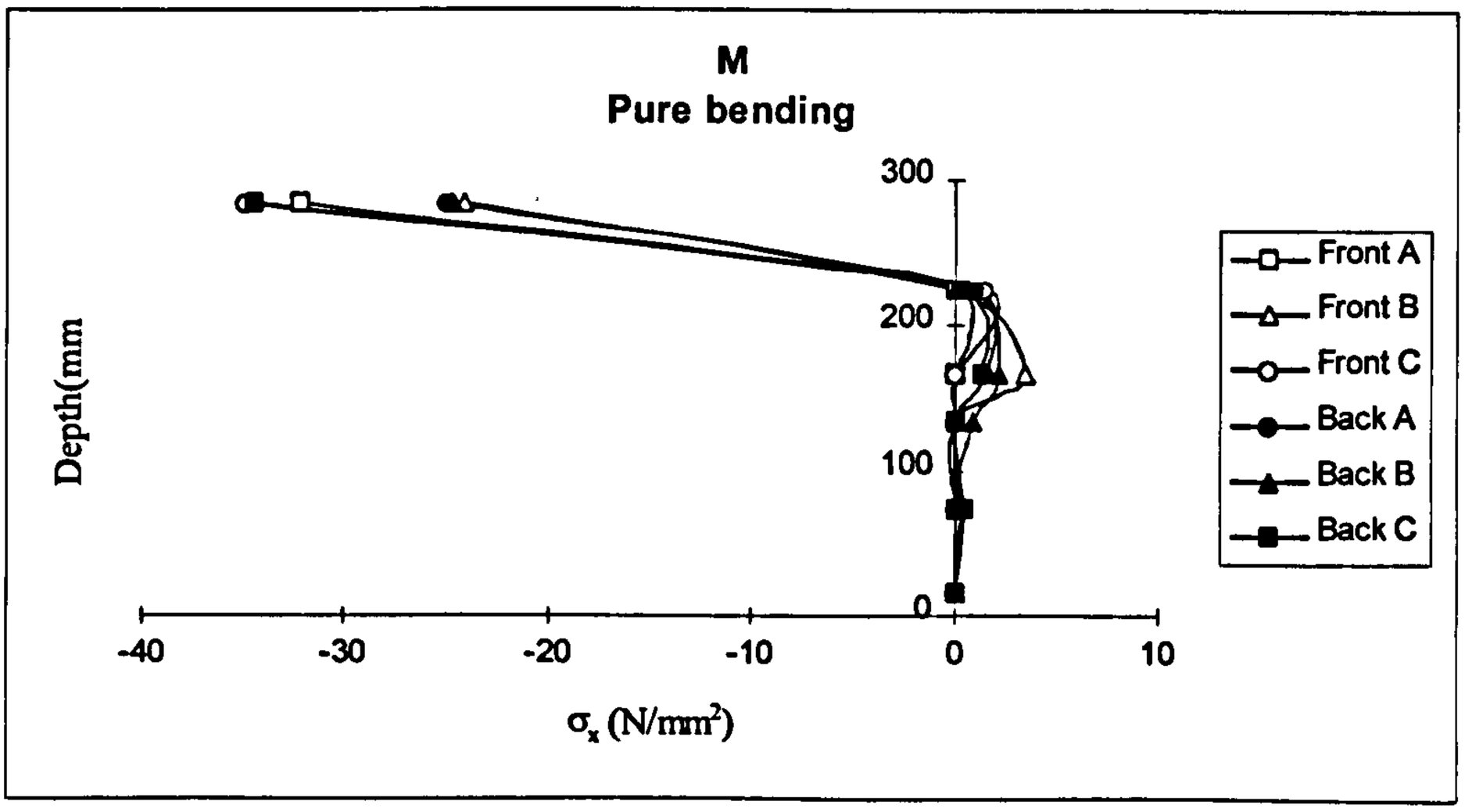

Fig. 10.7: Normal stress distribution in the case of pure bending moment

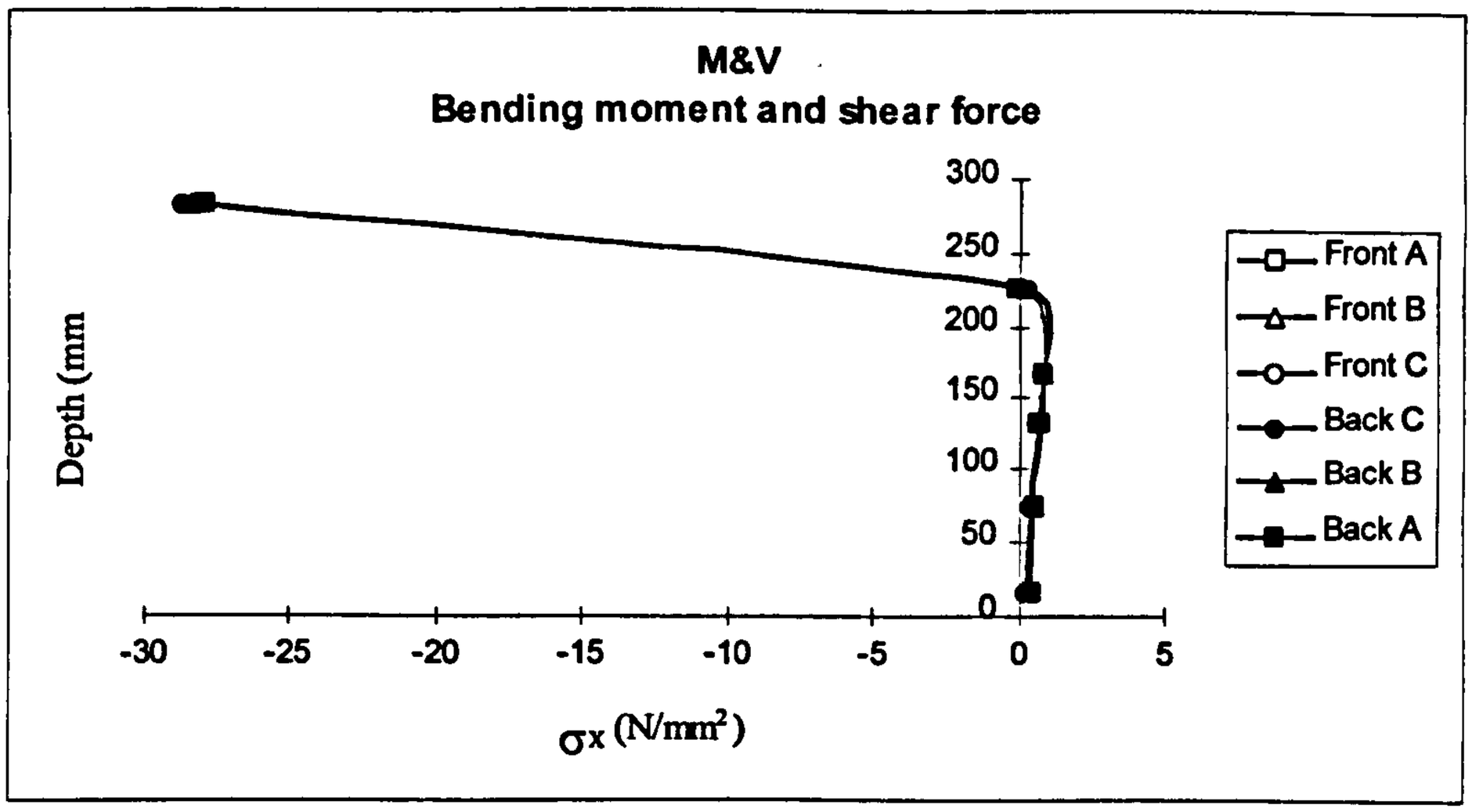

Fig. 10.8a: Normal stress distributions due to combined bending and shear

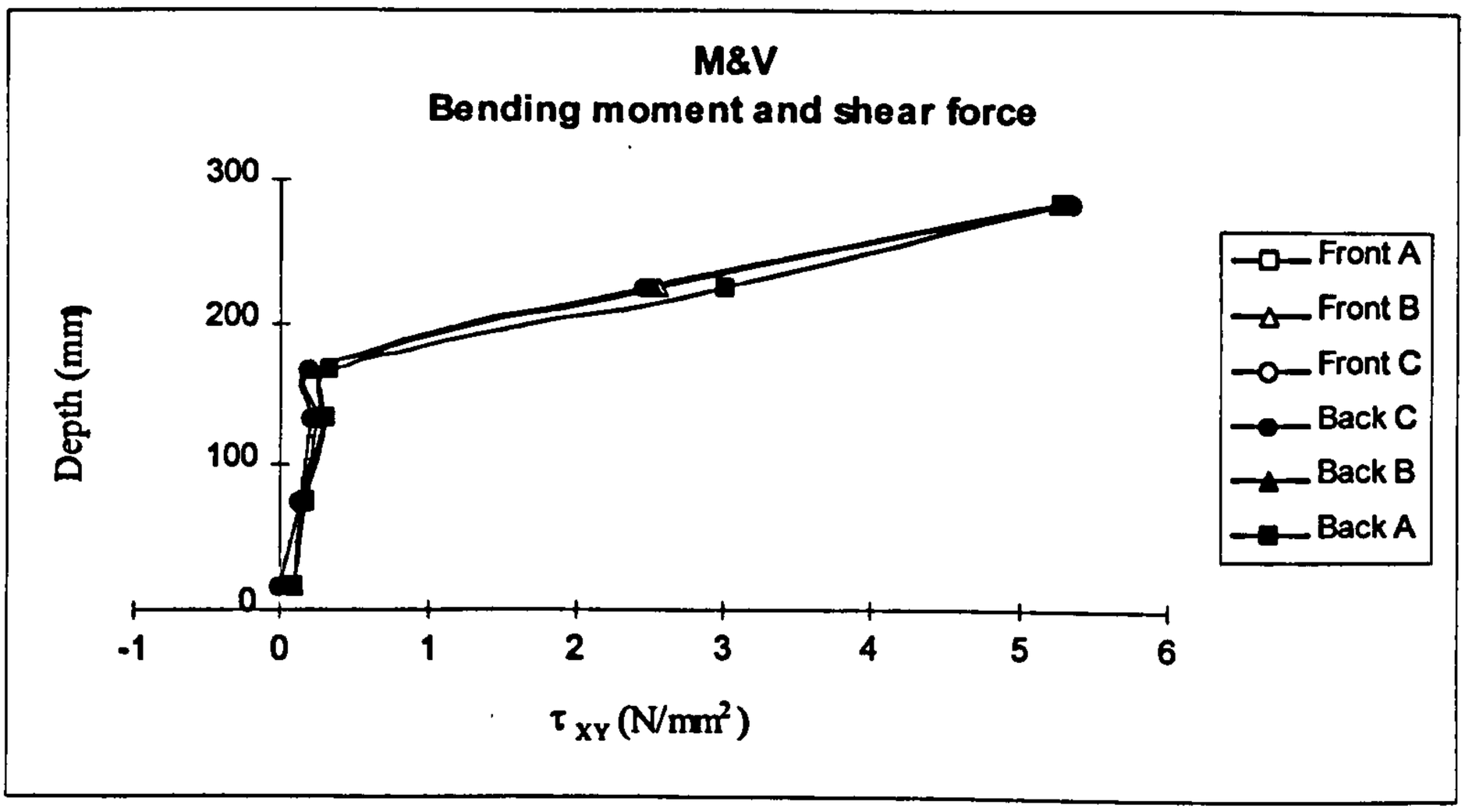

Fig. 10.8b: Shear stress distribution due to combined bending and shear

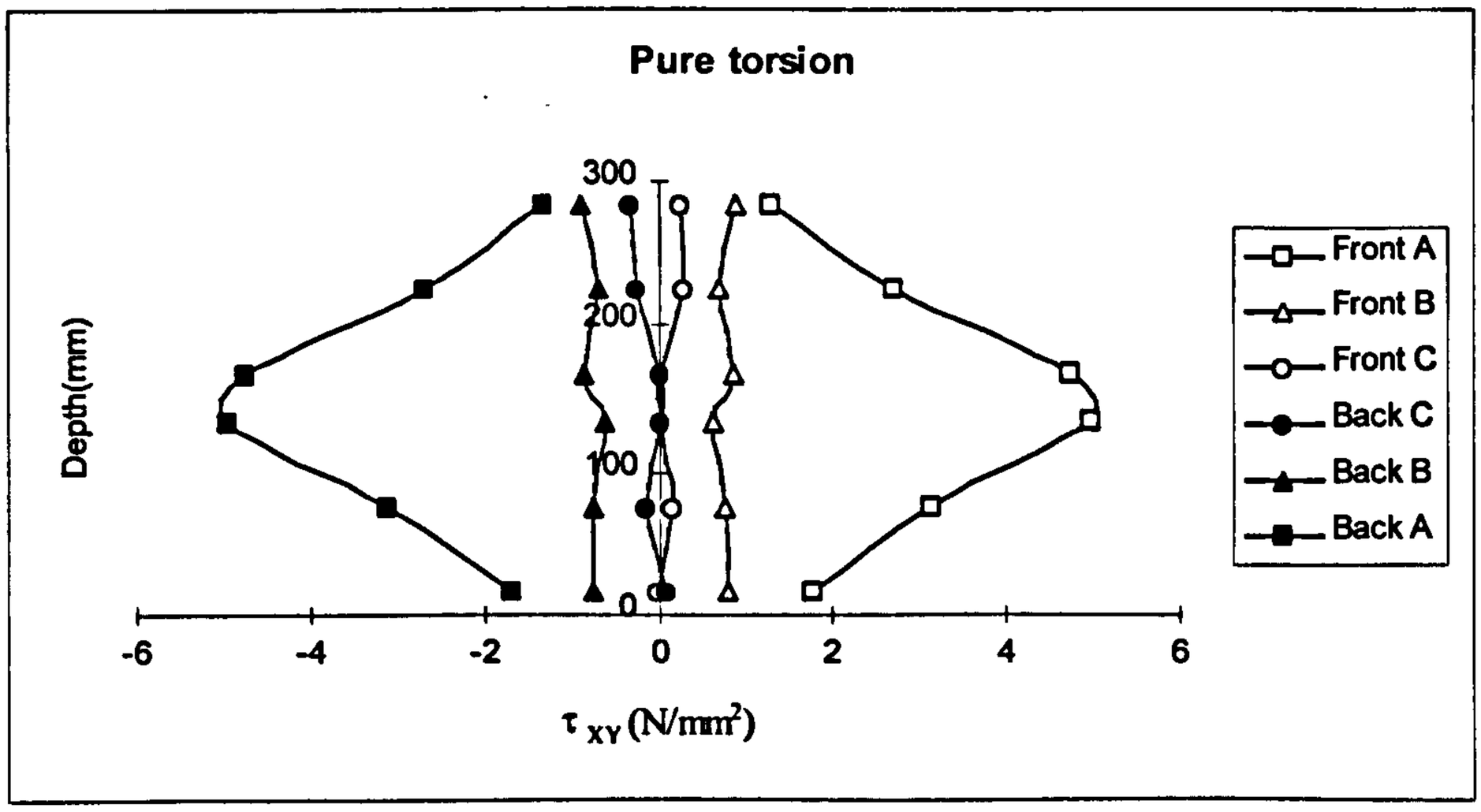

Fig. 10.9a: Shear stress distribution (τ_{xy}) in the case of pure torsion

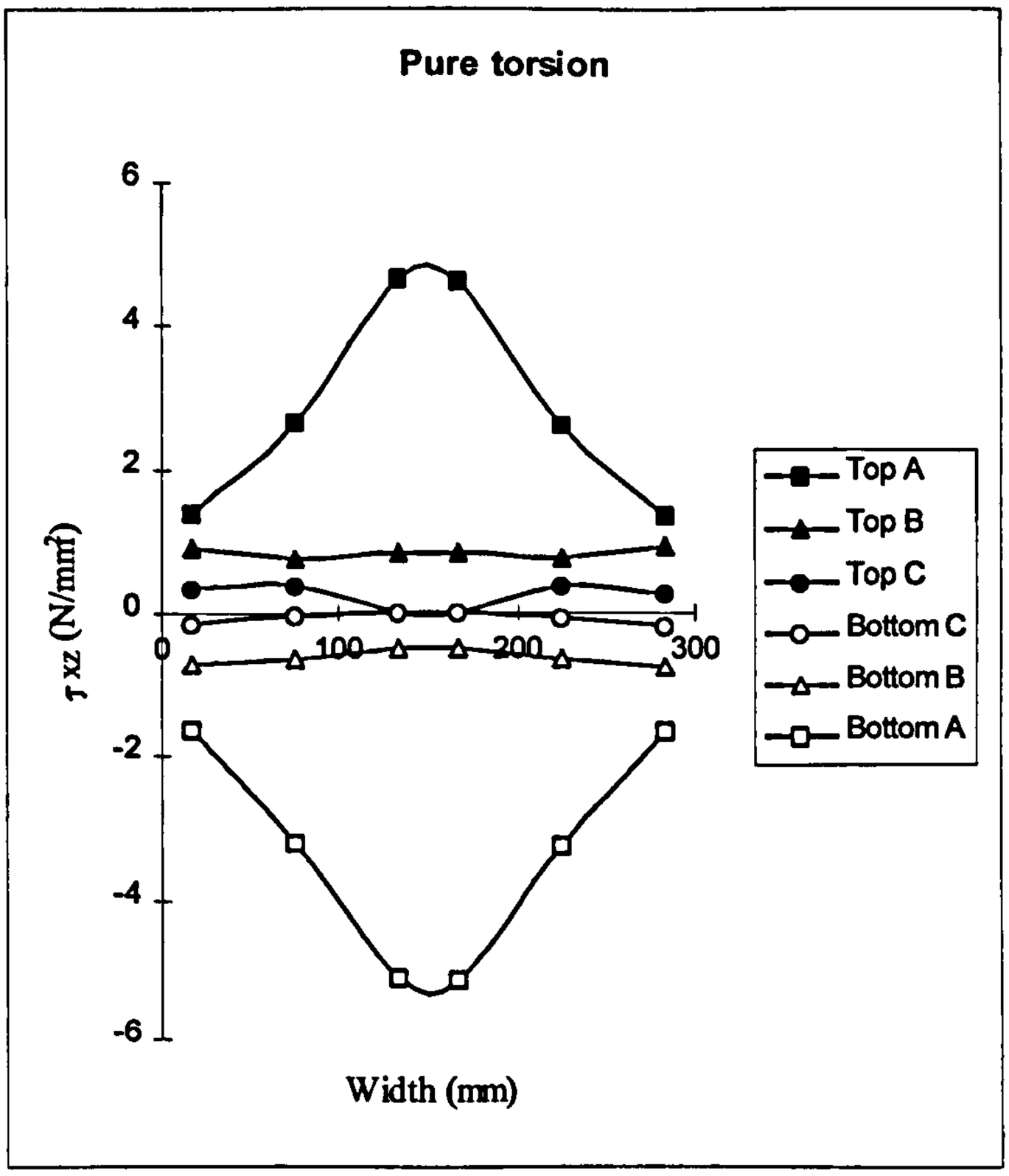

Fig. 10.9b: Shear stress distribution (τ_{xz}) in the case of pure torsion

the core allows it to resist some shear stress by reducing the principal tensile stress. On the other hand, the concentration of shear stress in the region where they are added causes cracks to develop which leads to some loss of normal stress in this region at later stages of loading.

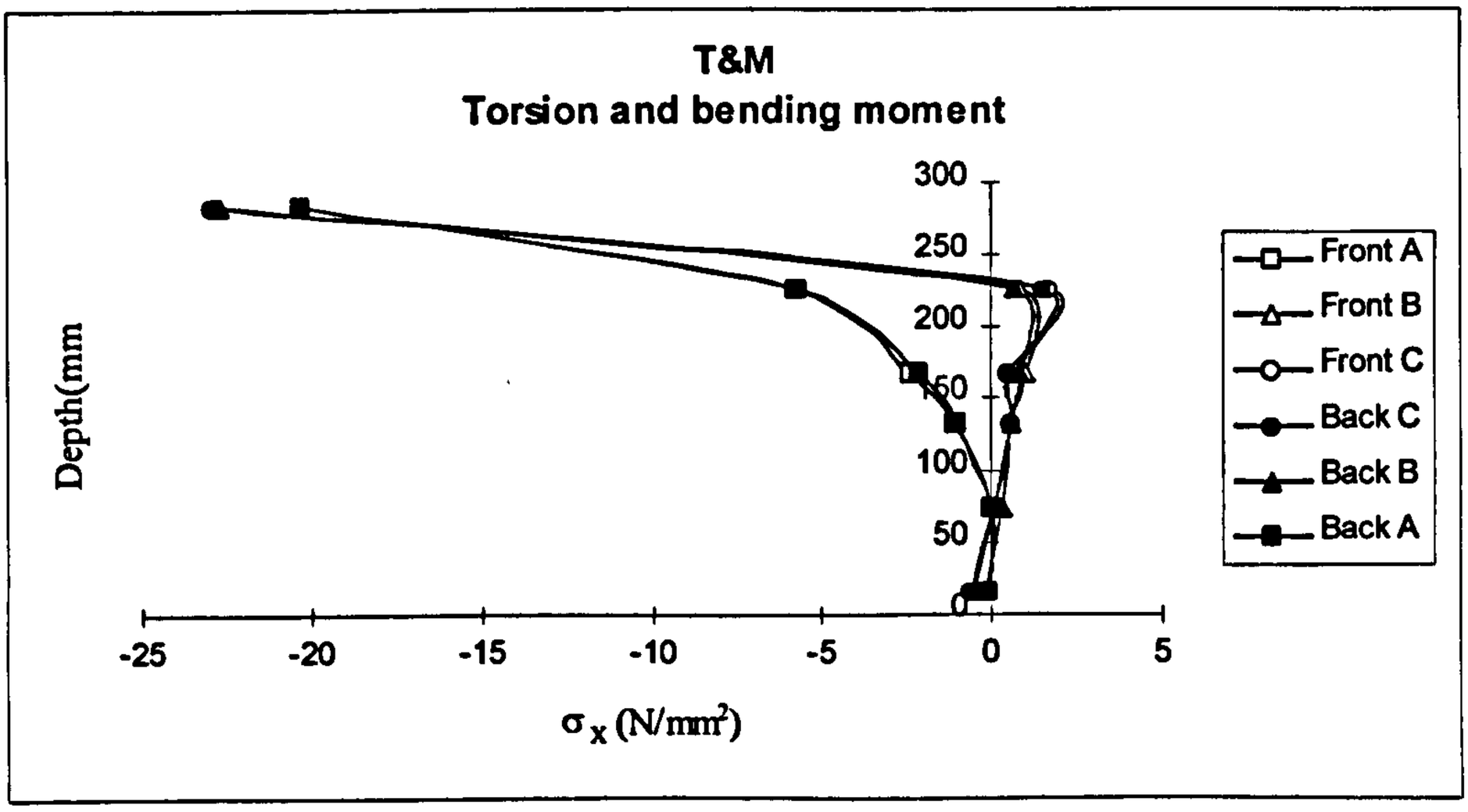

Fig. 10.10a: Normal stress distributions due to combined torsion and bending

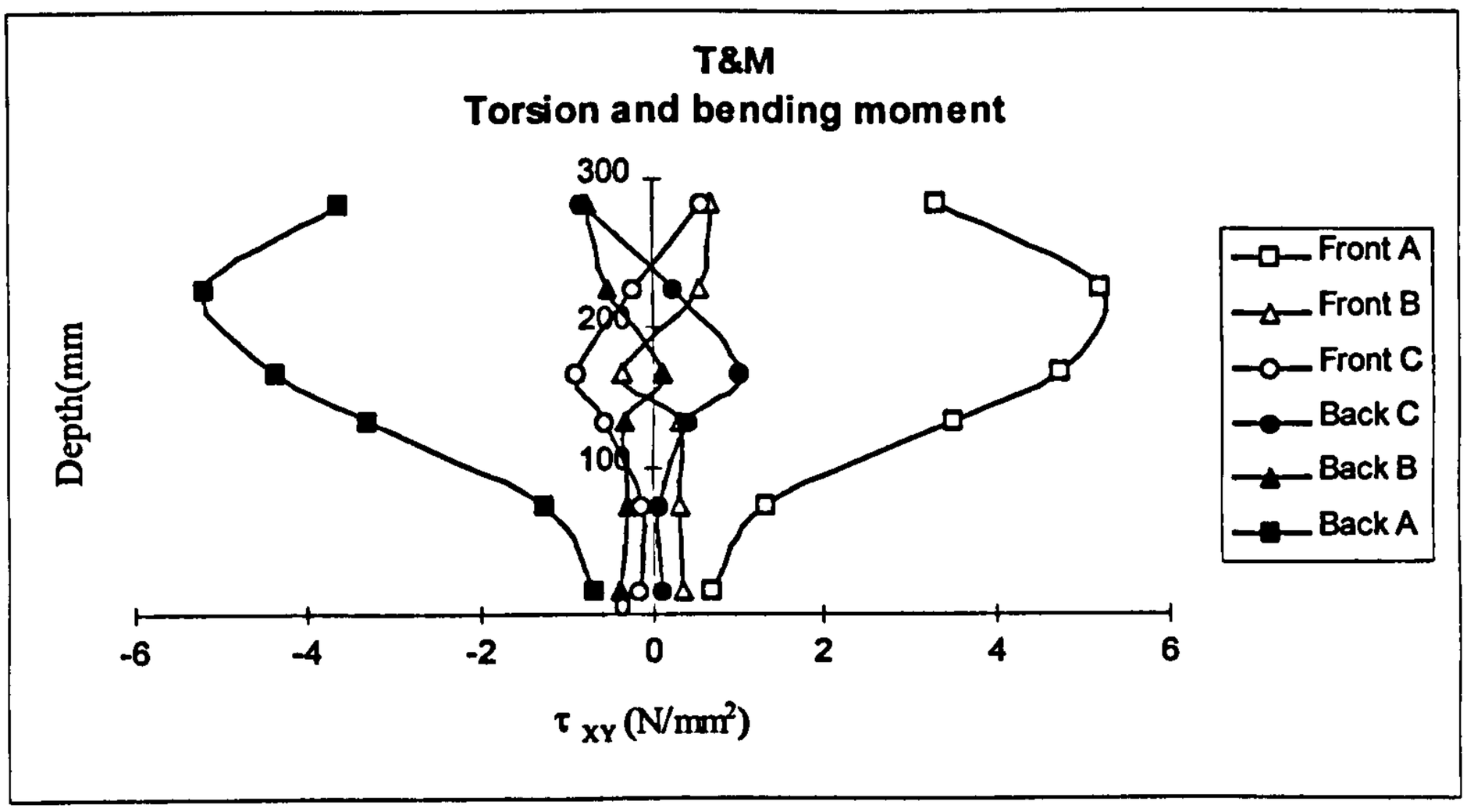

Fig. 10.10b: Shear stress distributions due to combined torsion and bending

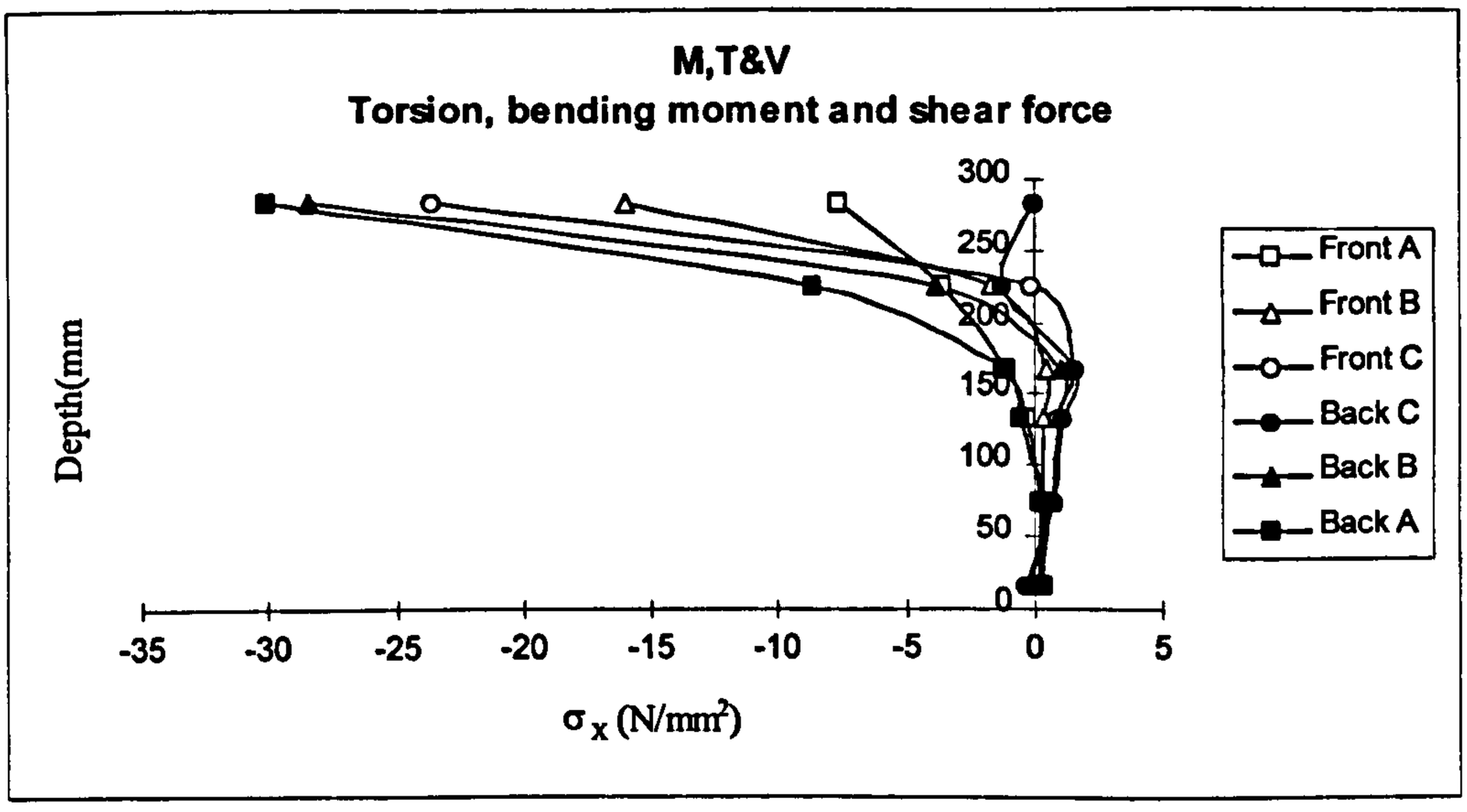

Fig. 10.11a: Normal stress distributions due to combined torsion, bending and shear

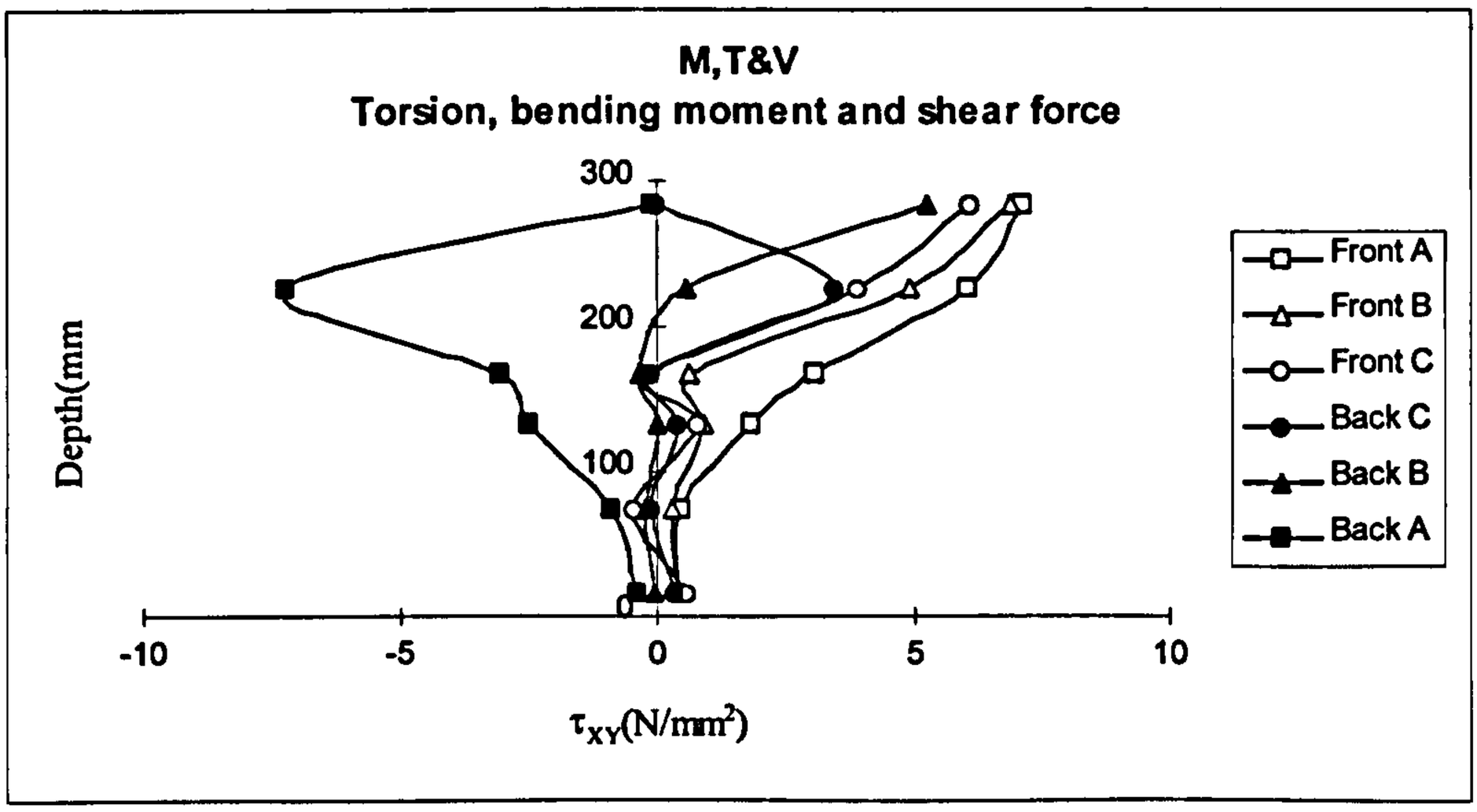

Fig. 10.11b: Shear stress distributions due to combined torsion, bending and shear

10.4.2: Effect of torsion to bending moment ratio

In this sub-section was examined the effect of T/M ratio on the stress in the core when the beam was subjected to combined loading of torsion and bending moment alone. Concrete and steel arrangement were fixed as above while T/M ratio was varied as in table 10.3. Again the stresses at the last converged increment was used for the analysis.

Table 10.3: Torsion and bending ratios

Beam No.	T kN.m.	M kN.m.	T/M Ratio
M1	13	51	0.25
M2	26	23.81	1.09
M3	39	10.31	3.78

From figures 10.12, it appears that as T/M ratio increases, in the outer layers compressive stress is concentrated at the mid-depth of the beam. However, in the inner layers, compressive stress is concentrated towards the top and bottom of the beam depth. No such large changes were noticed in the distribution of the shear stress due to torsion (Fig. 10.13). When the ratio of the torsion to bending moment becomes very large the difference in stress distribution between the outer shell and the core became pronounced. At this stage the whole section participates in resisting stress with mainly compression in the outer shell and tension in the inner part. If the tensile resistance of concrete is ignored then the beam behaves as a hollow one.

Shear stress curves in figure 10.13 show that with the increase of the torsion, only minor changes noticed in the stresses in the core.

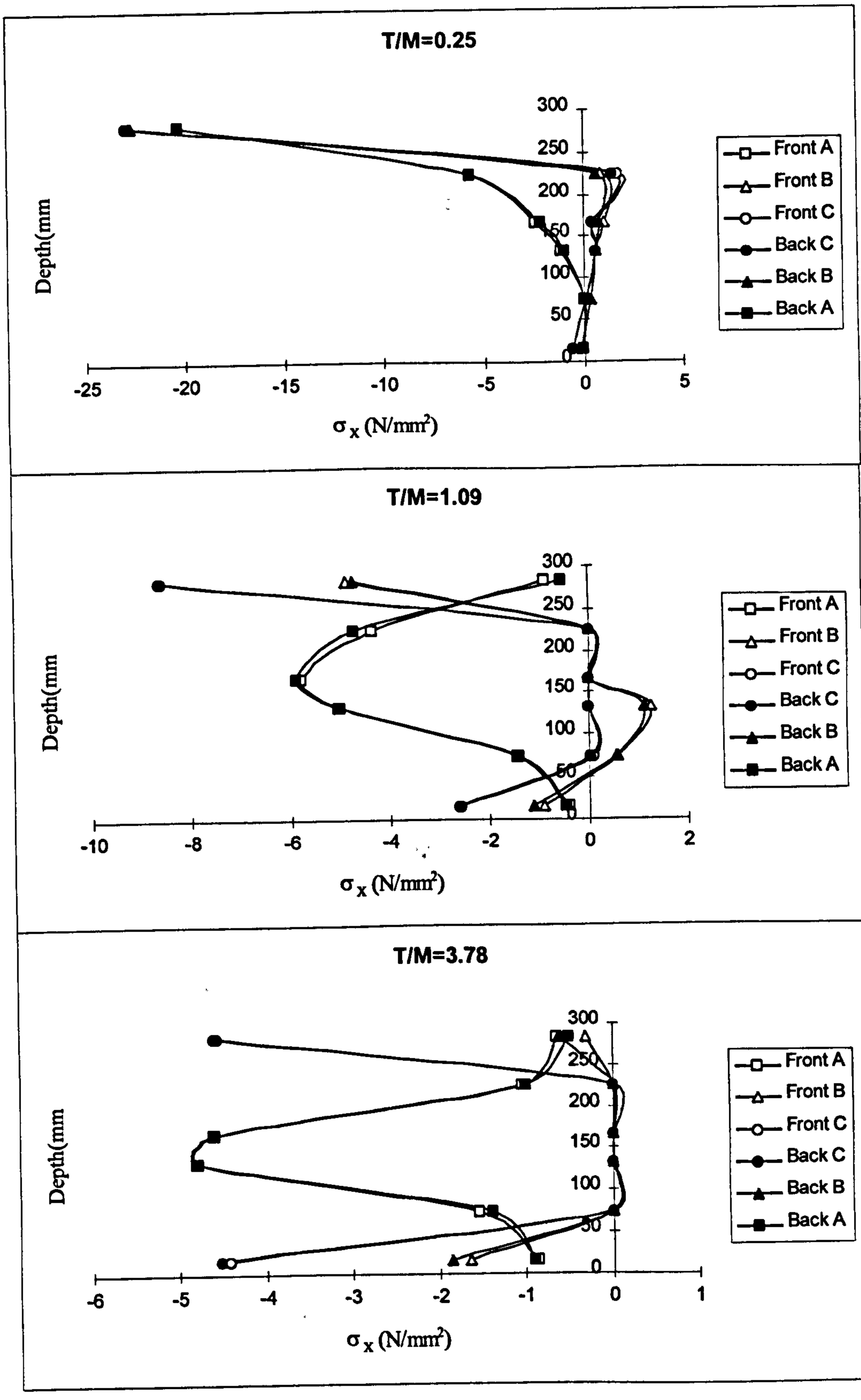

Fig. 10.12: Effect of the ratio of torsion to bending on the normal stress distribution

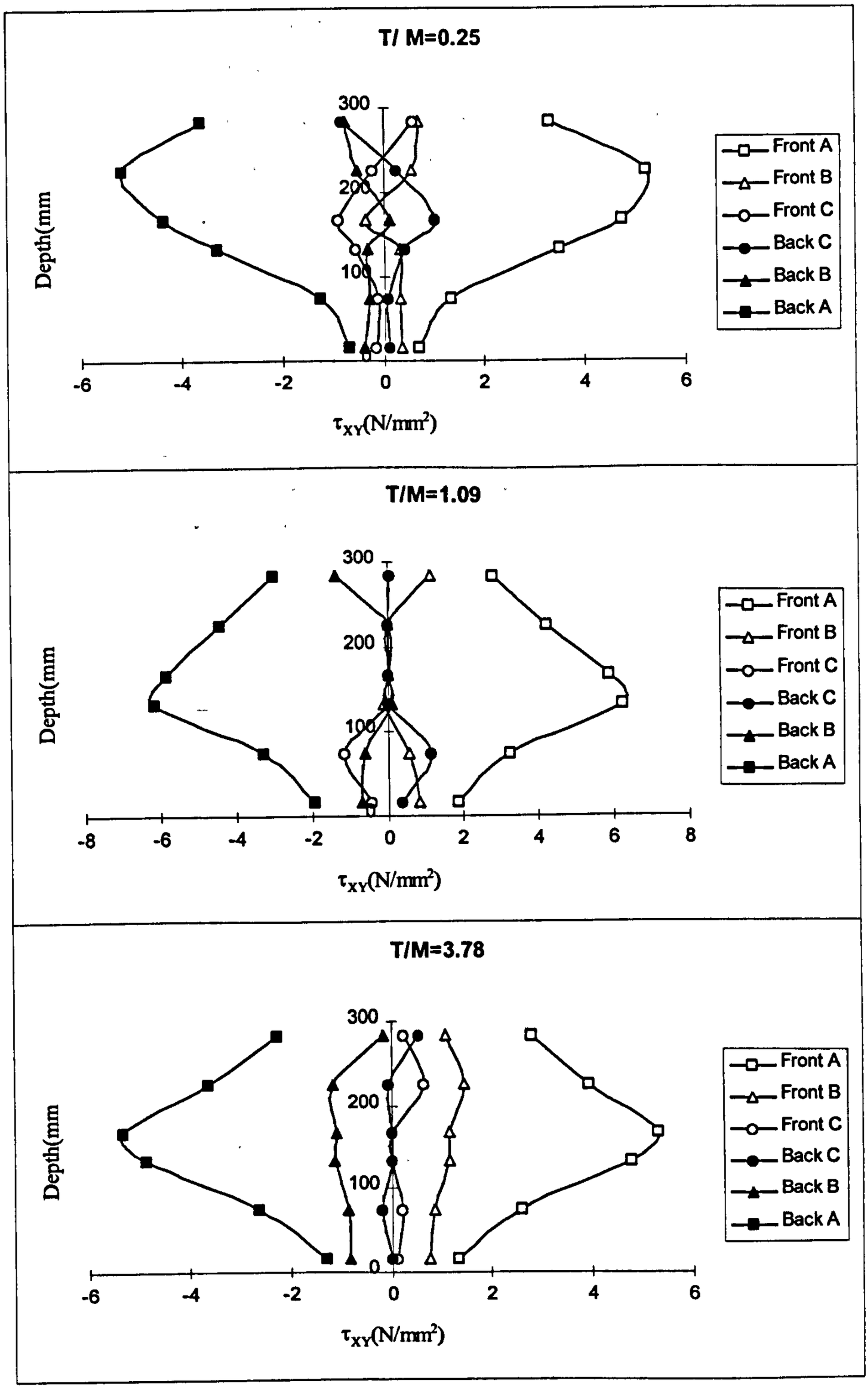

Fig. 10.13: Effect of the ratio of torsion to bending on the shear stress distribution

10.4.3: Effect of shear force to bending moment ratio

Table 10.4 shows three different V/M ratios for which the beam was analysed. Figures 10.14-15 show that when the beam is subjected to bending moment and shear force alone there is almost no effect of the V/M ratio on the normal or shear stress distributions.

Table 10.4: Shear force and bending moment ratios

Beam No.	V_d kN.	M_d kN.m.	V_d/M_d m^{-1}
J1	50	90.00	0.56
J2	50	42.5	1.18
J3	50	21.15	2.36

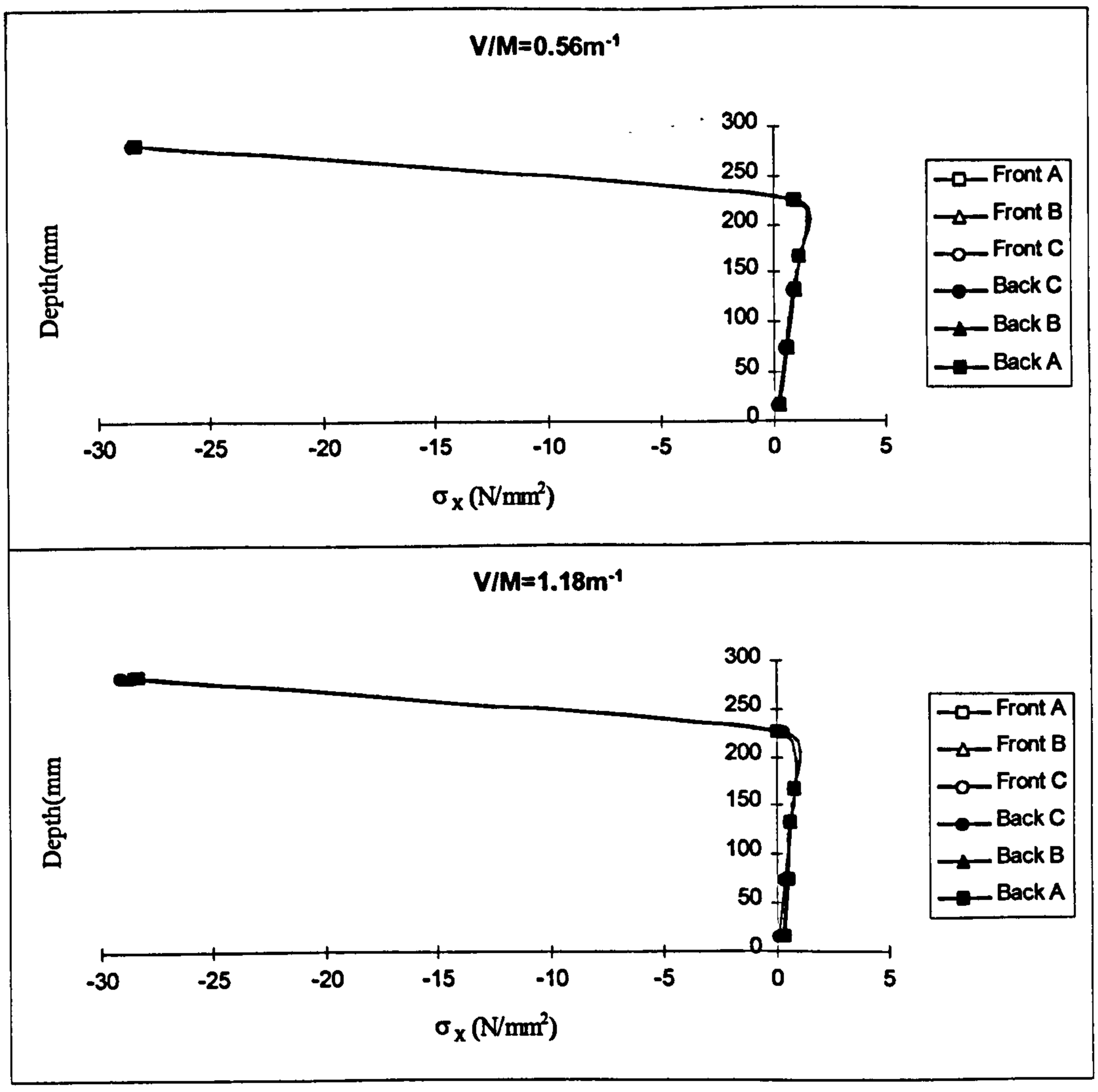

Fig. 10.14: Effect of the ratio of shear to bending on the normal stress distribution

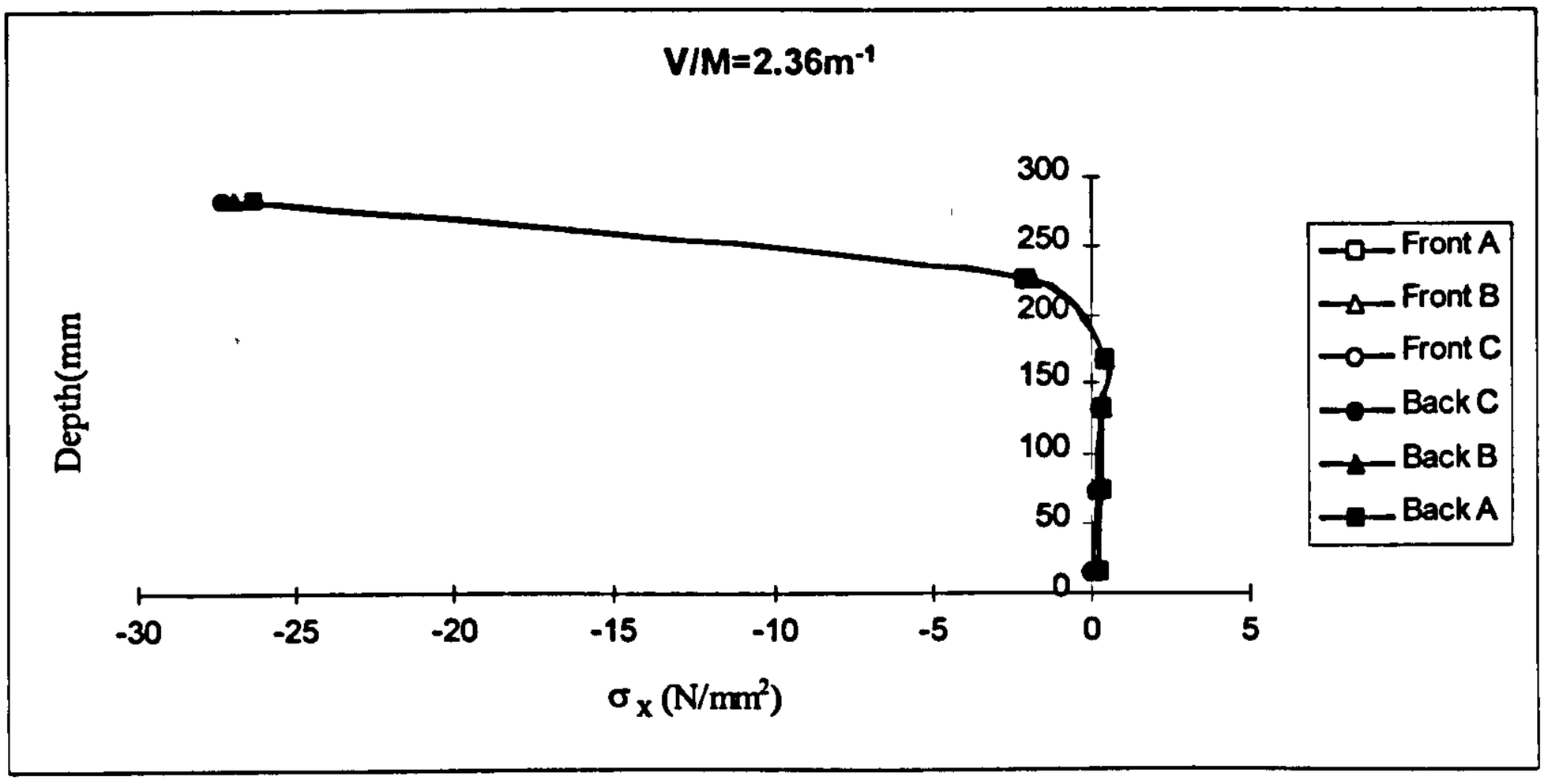

Fig. 10.14: Continued

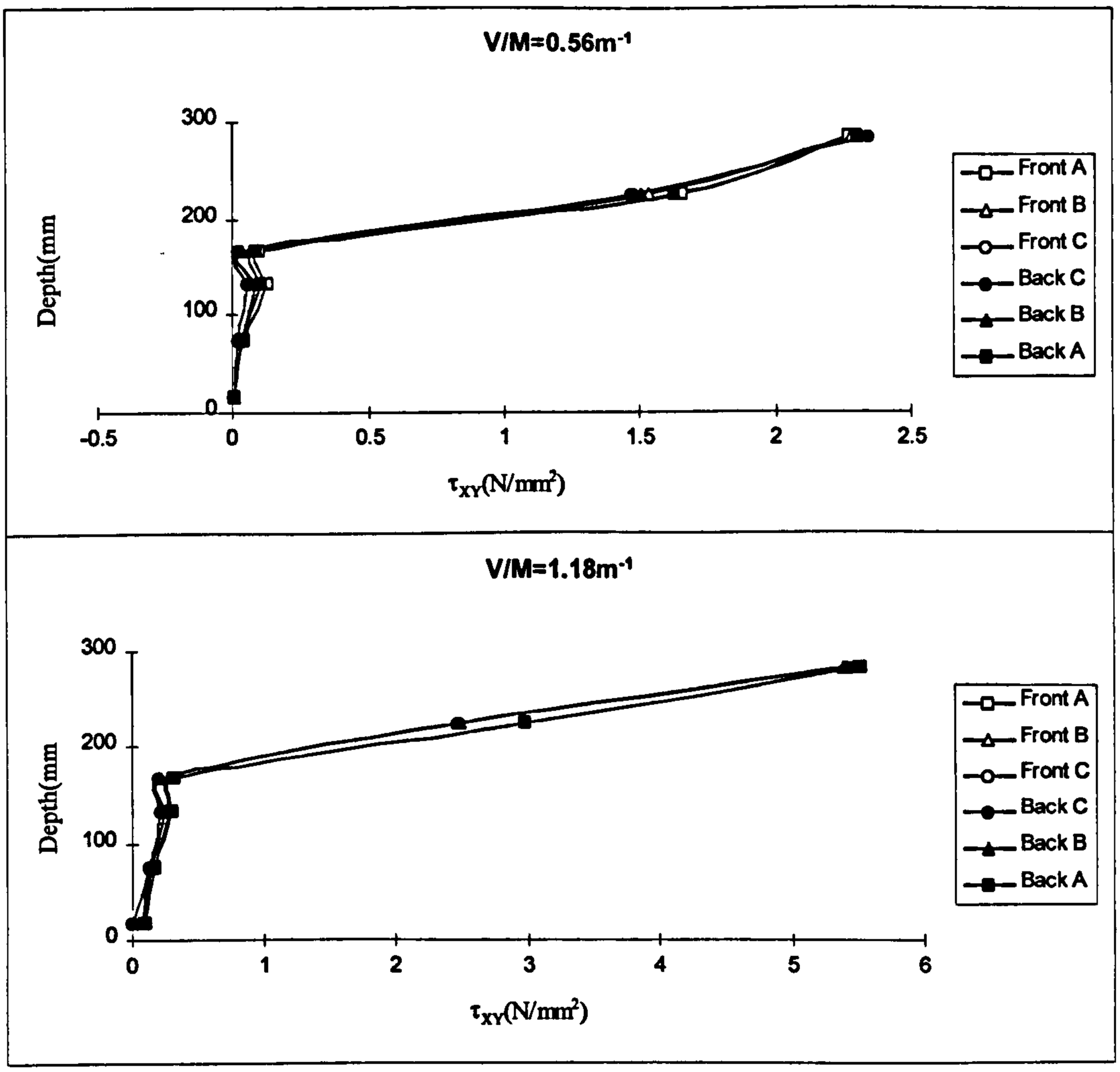

Fig. 10.15: Effect of the ratio of shear to bending on the shear stress distribution

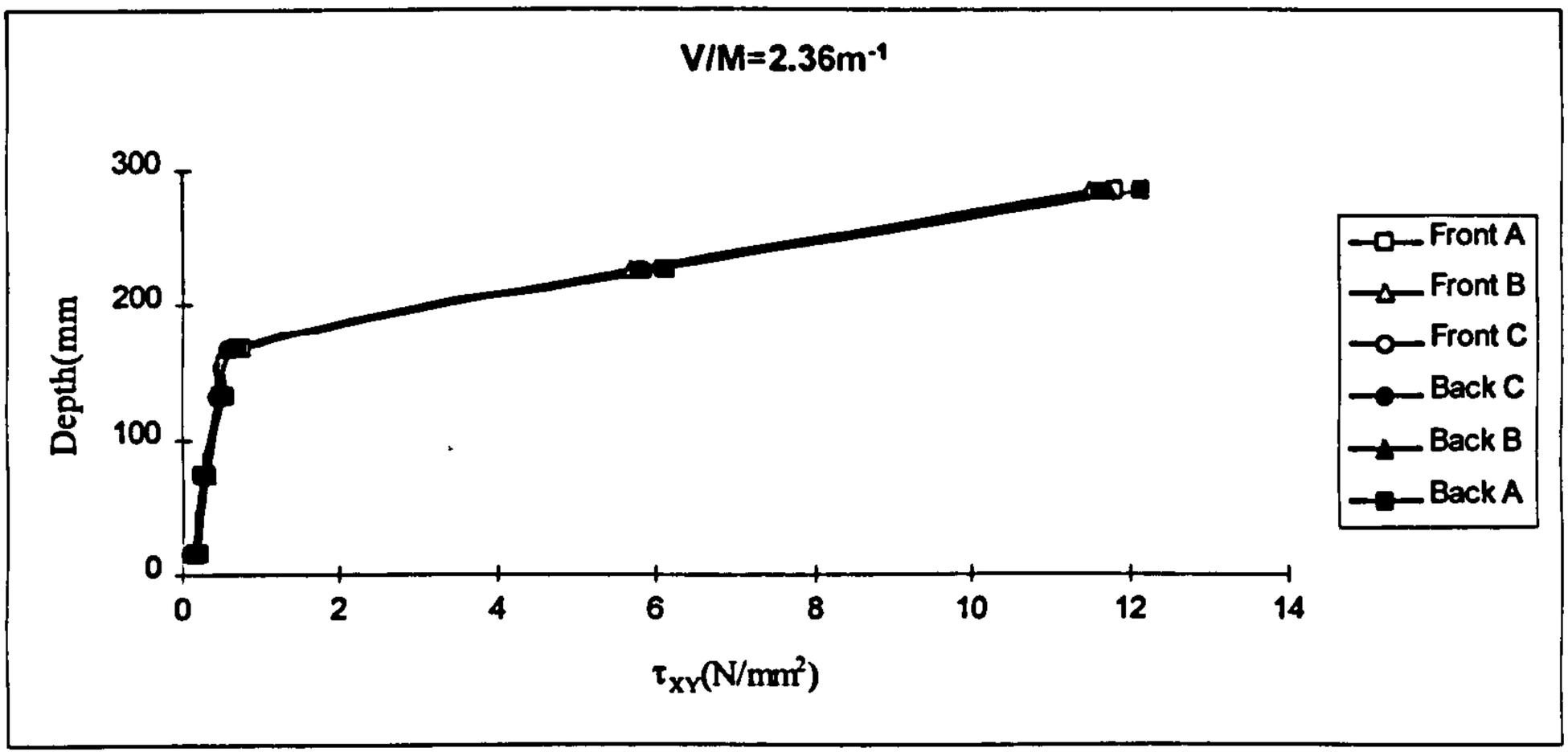

Fig. 10.15: Continued

10.4.4: Effect of load level

In this sub-section the behaviour of the beam under several load levels starting from elastic to failure load was studied. The beam was subjected to combined loading of 26kNm torsion, 23.81kNm bending moment and 28kN shear force.

It is clear from figures 10.16 that the normal stress distribution changes from elastic linear before cracking to non-linear with an increase in compression in the outer shell until failure. However, in the upper part of the beam compressive stress was maintained with slightly different values across the beam width.

Figures 10.17 show that uniform shear stress across the width exists at the elastic stage, changing to more concentration in the outer shell when the load was increased until failure.

From the results in this section it can be said that although the core participates in the load resistance, it is, however, difficult to quantitatively describe this resistance in a very simple manner. One reason for this difficulty is that the contribution of the core is affected by the load combination. The positive effect of the normal compressive stress in increasing the load resistance is reduced by the concentration of the shear stresses in one side of the section. In other words, presence of large value of torsion leads to a solid beam acting like a hollow one, while presence of large bending moment activates the core resistance. Another reason is that, not the whole core participates in stress resistance. The participation is affected by the location of the neutral axis which is dependent on the load level and load combination. Finally, the core resistance may be affected by the material properties

i.e. tensile stress in the core concrete reduces the load on the steel which leads to a stronger beam, and strain hardening of steel gives extra strength.

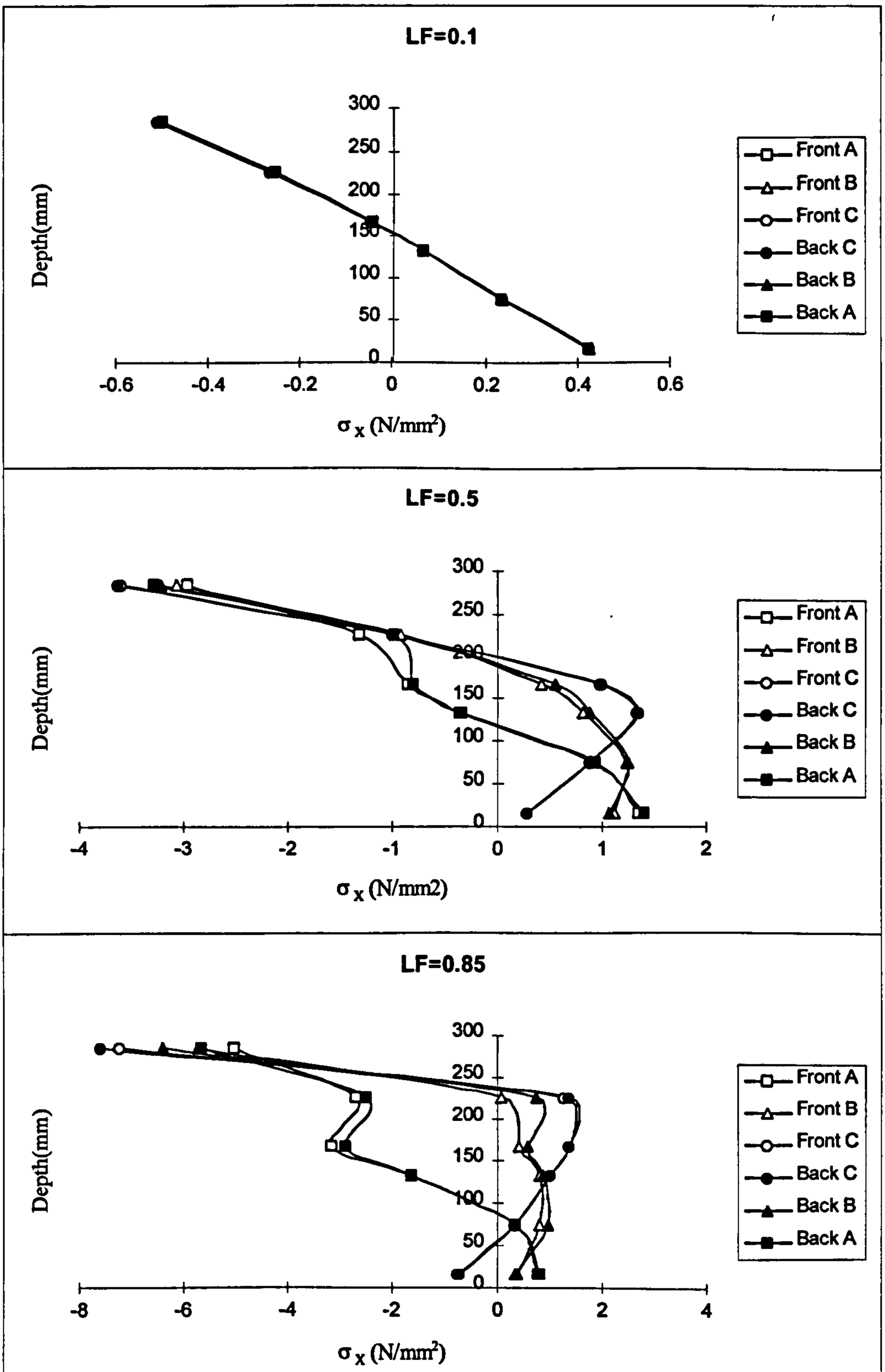

Fig. 10.16: Normal stress in different load levels

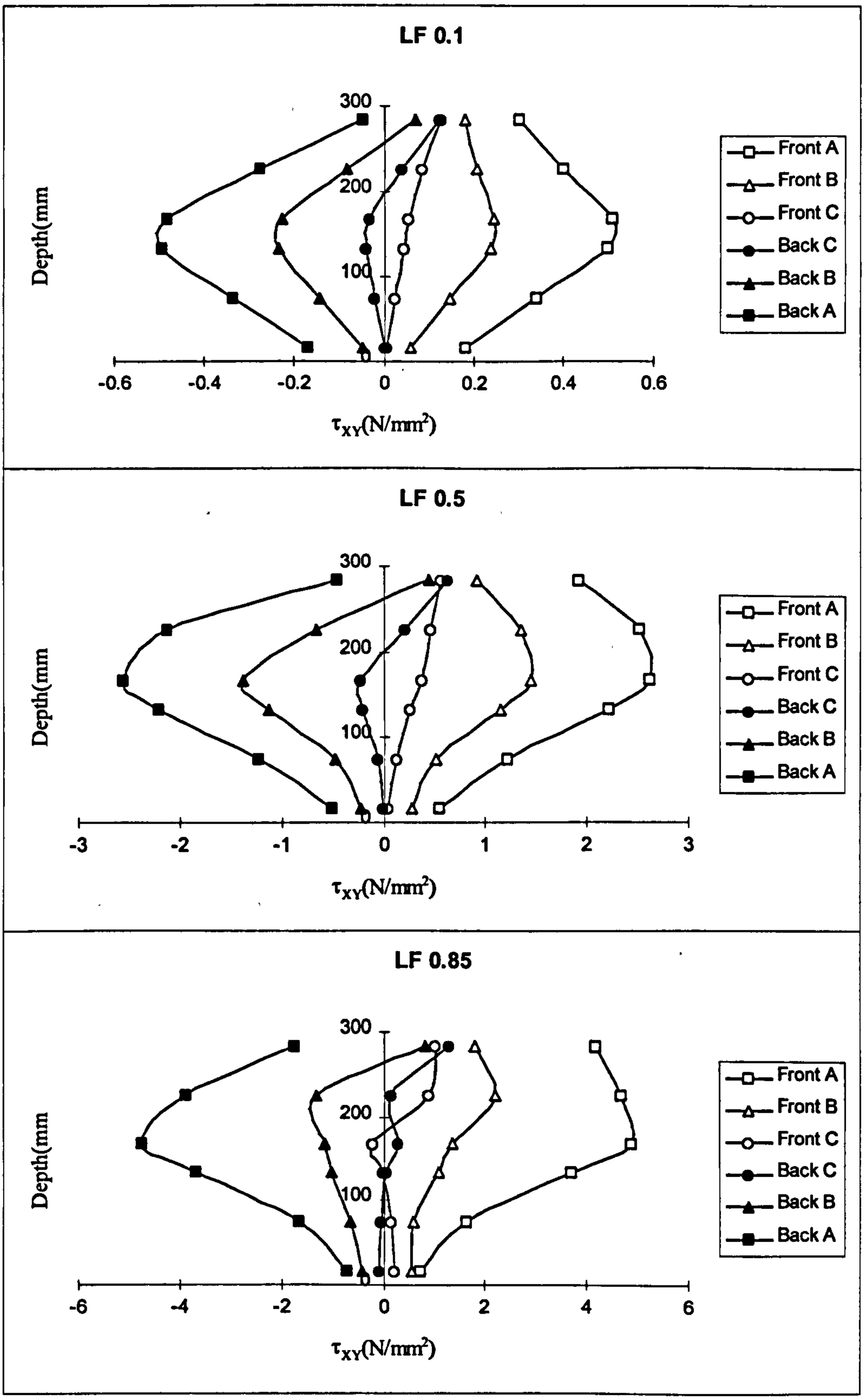

Fig. 10.17: Shear stress in different load levels

10.5: Design trials

The findings from the stress analysis in section 10.4 can be summarised as follows:

1. The torsion is resisted by the outer 50 mm shell.
2. The direct shear and bending moment are partially resisted by the core.
3. Large torsion combined with bending moment alone or with shear force causes the presence of two separate neutral axes for the outer shell and the core, with more compressive stress in the outer shell.
4. Large bending moment increases the participation of the core in the stress resistance.

In an attempt to produce a safe and economical design, these points were considered in a search for a reasonable stress distribution for the calculation of reinforcement. The design stress distribution must comply with the Lower Bound Theorem. This theorem allows any stress distribution to be used in the design as long as it does not violate equilibrium and material yield conditions. The highest load that can be resisted by a member while still satisfying these conditions is the best lower bound to ultimate load. In addition, the design stress distribution should be easy to implement and gives acceptable results for different load combinations. Hence, several stress distributions were tried for reinforced and partially prestressed beams using the load combination of T=13kNm, M=51kNm and V=60kN. All of these trials satisfy the Lower Bound Theorem. The resulting normal and shear stresses in each region were used in the direct design procedure to calculate the required steel areas.

The beam was again divided into 36 cells, the required longitudinal reinforcement in the front half of the beam, where the shear stresses are added, is called A_{sx}^{f} and in the back half, where the stresses are subtracted, is called A_{sx}^{b}. However, in order to reduce the provided longitudinal reinforcement, the average of $(A_{sx}^{f} + A_{sx}^{b})$ is provided in each half width of the beam. This implies that one half of the section, where the stresses are added, will be under designed and the other is over designed. This is less than providing A_{sx}^{f} in each half as was done for the hollow beams and BTV12. The difference in the longitudinal steel areas between the two methods is discussed later in section 10.6. The transverse steel is still based on the largest

required stirrup leg area A_{sy}^{l}.

As the aim was to optimise the usage of material, the trial which gives least reinforcement was adopted as a model for computational experiments in section 10.6. The computational experiments were carried out using the 3-D program to examine the beam behaviour and failure load for different load combinations.

10.5.1: Reinforced concrete beams

Four design trials for reinforced concrete beams were studied (Fig 10.18). Plastic stress distribution was used with different shape and size of stress blocks (shaded areas) as follows:

1. **Trial R1:** The normal stress was resisted by the top and bottom 50x300mm blocks, the shear stress due to shear force was taken by the 200x50mm side blocks and the torsional shear stress was calculated using the shear flow as in a hollow section.
2. **Trial R2:** Similar to trial R1 except that the depth of the compressive stress in the outer shell was doubled.
3. **Trial R3:** Similar to trial R1 except that the shear stress due to shear force was resisted by the middle 200mm across the whole width.
4. **Trail R4:** Similar to trial R3 except that the shear stress due to shear force was resisted by the 200x200mm core.

The stress values and required steel areas, calculated based on each trial, are presented in table 10.5. It is clear from this table that no major differences exist between these trials in calculating the steel areas because all different stress distributions assume a "plastic state". However, trial R1 required the least reinforcement among this group.

10.5.2: Partially prestressed concrete beams

Two design trials were studied for the partially prestressed beams. Four prestressing wires were used carrying 20kN axial force each. The eccentricity for each pair was 125 and 75mm respectively, and the yield stress f_{py} was 1570N/mm^2.

1. **Trial P1:** Elastic stress distribution combined with the direct design procedure was used for the calculation of required reinforcement. The beam was again divided as in figure 10.2 and equations 10.1 to 10.3 were used for the calculation of external stresses. The normal stresses due to bending moment

and due to the eccentric axial loads caused by prestressing were calculated separately and algebraically summed. Similarly the shear stresses from shear force and torsion were algebraically added.

2. **Trial P2:** Plastic stress distribution was considered as follows:

The shear stresses were calculated as in trial R1 in section 10.4.1. The normal stresses from the external bending moment and the axial forces were combined and assumed to be acting as one axial force through the centroid and a net bending moment acting about the centroidal axis XX as shown in figure 10.19. In this figure, a = the distance between the neutral axis and centroidal axis, b and d = the breadth and depth of the cross section and σ_x = normal stress in the direction of the beam axis.

For the given load combination, the value of a was found to be 20mm and therefore, for convenience the depths of the regions in figure 10.2 were used as 50,60,60,40,40 and 50mm from top to bottom respectively. The width, however, was kept at 50mm for each region.

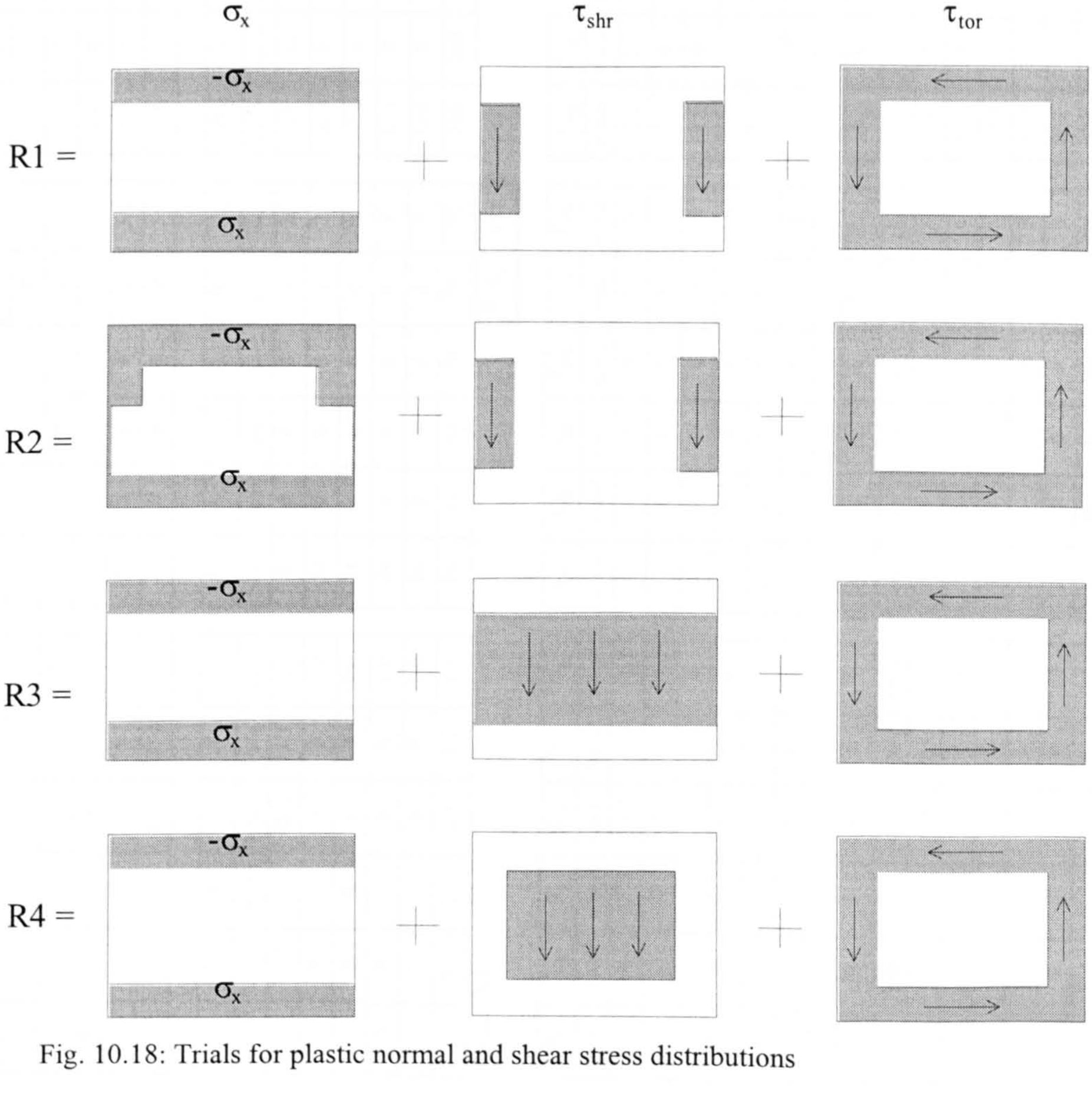

Fig. 10.18: Trials for plastic normal and shear stress distributions

Table 10.5: Stresses and reinforcement in each region

σ_x	σ_x	σ_x	σ_x	σ_x	σ_x
N/mm²	N/mm²	N/mm²	N/mm²	N/mm²	N/mm²
-13.5	-13.5	-13.5	-13.5	-13.5	-13.5
0	0	0	0	0	0
0	0	0	0	0	0
0	0	0	0	0	0
0	0	0	0	0	0
13.5	13.5	13.5	13.5	13.5	13.5

τ_{shr}	τ_{shr}	τ_{shr}	τ_{shr}	τ_{shr}	τ_{shr}
N/mm²	N/mm²	N/mm²	N/mm²	N/mm²	N/mm²
0	0	0	0	0	0
3.1	0	0	0	0	3.1
3.1	0	0	0	0	3.1
3.1	0	0	0	0	3.1
3.1	0	0	0	0	3.1
0	0	0	0	0	0

τ_{tor}	τ_{tor}	τ_{tor}	τ_{tor}	τ_{tor}	τ_{tor}
N/mm²	N/mm²	N/mm²	N/mm²	N/mm²	N/mm²
-2.1	-2.1	-2.1	-2.1	-2.1	-2.1
2.1	0	0	0	0	-2.1
2.1	0	0	0	0	-2.1
2.1	0	0	0	0	-2.1
2.1	0	0	0	0	-2.1
2.1	2.1	2.1	2.1	2.1	2.1

τ	τ	τ	τ	τ	τ
N/mm²	N/mm²	N/mm²	N/mm²	N/mm²	N/mm²
-2.1	-2.1	-2.1	-2.1	-2.1	-2.1
5.1	0	0	0	0	1.0
5.1	0	0	0	0	1.0
5.1	0	0	0	0	1.0
5.1	0	0	0	0	1.0
2.1	2.1	2.1	2.1	2.1	2.1

A_x	A_x	A_x	A_x	A_x	A_x
mm²	mm²	mm²	mm²	mm²	mm²
0	0	0	0	0	0
26	0	0	0	0	5
26	0	0	0	0	5
26	0	0	0	0	5
26	0	0	0	0	5
78	78	78	78	78	78
				ΣA_x	591

A_t	A_t	A_t	A_t	A_t	A_t
mm²/m	mm²/m	mm²/m	mm²/m	mm²/m	mm²/m
32	32	32	32	32	32
513	0	0	0	0	97
513	0	0	0	0	97
513	0	0	0	0	97
513	0	0	0	0	97
208	208	208	208	208	208

Trial R1

Longitudinal

Front	Back
mm²	mm²
0	0
25.67	4.87
26	5
26	5
26	5
234.4	234.4
A_{sx}^f	A_{sx}^b
337	254

Transverse

Front	Back	Top
mm²	mm²	mm²
		32
513	97	
513	97	
513	97	Bot.
513	97	mm²
		208

A_{sy}^f	A_{sy}^b
513	97

σ_x	σ_x	σ_x	σ_x	σ_x	σ_x
N/mm²	N/mm²	N/mm²	N/mm²	N/mm²	N/mm²
-11.3	-11.3	-11.3	-11.3	-11.3	-11.3
-11.3	0	0	0	0	-11.3
0	0	0	0	0	0
0	0	0	0	0	0
0	0	0	0	0	0
15.1	15.1	15.1	15.1	15.1	15.1

τ_{shr}	τ_{shr}	τ_{shr}	τ_{shr}	τ_{shr}	τ_{shr}
N/mm²	N/mm²	N/mm²	N/mm²	N/mm²	N/mm²
0	0	0	0	0	0
3.1	0	0	0	0	3.1
3.1	0	0	0	0	3.1
3.1	0	0	0	0	3.1
3.1	0	0	0	0	3.1
0	0	0	0	0	0

τ_{tor}	τ_{tor}	τ_{tor}	τ_{tor}	τ_{tor}	τ_{tor}
N/mm²	N/mm²	N/mm²	N/mm²	N/mm²	N/mm²
-2.1	-2.1	-2.1	-2.1	-2.1	-2.1
2.1	0	0	0	0	-2.08
2.1	0	0	0	0	-2.08
2.1	0	0	0	0	-2.08
2.1	0	0	0	0	-2.08
2.1	2.1	2.1	2.1	2.1	2.1

τ	τ	τ	τ	τ	τ
N/mm²	N/mm²	N/mm²	N/mm²	N/mm²	N/mm²
-2.1	-2.1	-2.1	-2.1	-2.1	-2.1
5.1	0	0	0	0	1.0
5.1	0	0	0	0	1.0
5.1	0	0	0	0	1.0
5.1	0	0	0	0	1.0
2.1	2.1	2.1	2.1	2.1	2.1

A_x	A_x	A_x	A_x	A_x	A_x
mm²	mm²	mm²	mm²	mm²	mm²
0	0	0	0	0	0
0	0	0	0	0	0
26	0	0	0	0	5
26	0	0	0	0	5
26	0	0	0	0	5
86	86	86	86	86	86
				ΣA_x	606

A_t	A_t	A_t	A_t	A_t	A_t
mm²/m	mm²/m	mm²/m	mm²/m	mm²/m	mm²/m
38	38	38	38	38	38
233	0	0	0	0	233
513	0	0	0	0	97
513	0	0	0	0	97
513	0	0	0	0	97
208	208	208	208	208	208

Trial R2

Longitudinal

Front	Back
mm²	mm²
0	0
0	0
26	4.87
26	5
26	5
257	257
A_{sx}^f	A_{sx}^b
334	272

Transverse

Front	Back	Top
mm²	mm²	mm²
		38
233	233	
513	97	
513	97	Bot.
513	97	mm²
		208

A_{sy}^f	A_{sy}^b
513	97

Table 10.5: Continued

σ_x	σ_x	σ_x	σ_x	σ_x	σ_x
N/mm²	N/mm²	N/mm²	N/mm²	N/mm²	N/mm²
-13.5	-13.5	-13.5	-13.5	-13.5	-13.5
0	0	0	0	0	0
0	0	0	0	0	0
0	0	0	0	0	0
0	0	0	0	0	0
13.5	13.5	13.5	13.5	13.5	13.5

τ_{shr}	τ_{shr}	τ_{shr}	τ_{shr}	τ_{shr}	τ_{shr}
N/mm²	N/mm²	N/mm²	N/mm²	N/mm²	N/mm²
0	0	0	0	0	0
1.0	1.0	1.0	1.0	1.0	1.0
1.0	1.0	1.0	1.0	1.0	1.0
1.0	1.0	1.0	1.0	1.0	1.0
1.0	1.0	1.0	1.0	1.0	1.0
0	0	0	0	0	0

τ_{tor}	τ_{tor}	τ_{tor}	τ_{tor}	τ_{tor}	τ_{tor}
N/mm²	N/mm²	N/mm²	N/mm²	N/mm²	N/mm²
-2.08	-2.08	-2.08	-2.08	-2.08	-2.08
2.1	0	0	0	0	-2.08
2.1	0	0	0	0	-2.08
2.1	0	0	0	0	-2.08
2.1	0	0	0	0	-2.08
2.1	2.1	2.1	2.1	2.1	2.1

τ	τ	τ	τ	τ	τ
N/mm²	N/mm²	N/mm²	N/mm²	N/mm²	N/mm²
-2.1	-2.1	-2.1	-2.1	-2.1	-2.1
3.1	1.0	1.0	1.0	1.0	-1.1
3.1	1.0	1.0	1.0	1.0	-1.1
3.1	1.0	1.0	1.0	1.0	-1.1
3.1	1.0	1.0	1.0	1.0	-1.1
2.1	2.1	2.1	2.1	2.1	2.1

Trial R3

A_x	A_x	A_x	A_x	A_x	A_x
mm²	mm²	mm²	mm²	mm²	mm²
0	0	0	0	0	0
15	5	5	5	5	5
15	5	5	5	5	5
15	5	5	5	5	5
15	5	5	5	5	5
78	78	78	78	78	78
				ΣA_x	633

A_t	A_t	A_t	A_t	A_t	A_t
mm²/m	mm²/m	mm²/m	mm²/m	mm²/m	mm²/m
32	32	32	32	32	32
310	102	102	102	102	106
310	102	102	102	102	106
310	102	102	102	102	106
310	102	102	102	102	106
208	208	208	208	208	208

Longitudinal

Front	Back
mm²	mm²
0	0
25.67	15.49
26	15
26	15
26	15
234.4	234.4
A_{sx}^{f}	A_{sx}^{b}
337	296

Transverse

Front	Back	Top
mm²	mm²	mm²
		32
513	310	
513	310	
513	310	Bot.
513	310	mm²
		208

A_{sy}^{f}	A_{sy}^{b}
513	310

σ_x	σ_x	σ_x	σ_x	σ_x	σ_x
N/mm²	N/mm²	N/mm²	N/mm²	N/mm²	N/mm²
-13.5	-13.5	-13.5	-13.5	-13.5	-13.5
0	0	0	0	0	0
0	0	0	0	0	0
0	0	0	0	0	0
0	0	0	0	0	0
13.5	13.5	13.5	13.5	13.5	13.5

τ_{shr}	τ_{shr}	τ_{shr}	τ_{shr}	τ_{shr}	τ_{shr}
N/mm²	N/mm²	N/mm²	N/mm²	N/mm²	N/mm²
0	0	0	0	0	0
0	1.5	1.5	1.5	1.5	0
0	1.5	1.5	1.5	1.5	0
0	1.5	1.5	1.5	1.5	0
0	1.5	1.5	1.5	1.5	0
0	0	0	0	0	0

τ_{tor}	τ_{tor}	τ_{tor}	τ_{tor}	τ_{tor}	τ_{tor}
N/mm²	N/mm²	N/mm²	N/mm²	N/mm²	N/mm²
-2.1	-2.08	-2.08	-2.08	-2.08	-2.08
2.1	0	0	0	0	-2.08
2.1	0	0	0	0	-2.08
2.1	0	0	0	0	-2.08
2.1	0	0	0	0	-2.08
2.1	2.1	2.1	2.1	2.1	2.1

τ	τ	τ	τ	τ	τ
N/mm²	N/mm²	N/mm²	N/mm²	N/mm²	N/mm²
-2.1	-2.1	-2.1	-2.1	-2.1	-2.1
2.1	1.5	1.5	1.5	1.5	-2.1
2.1	1.5	1.5	1.5	1.5	-2.1
2.1	1.5	1.5	1.5	1.5	-2.1
2.1	1.5	1.5	1.5	1.5	-2.1
2.1	2.1	2.1	2.1	2.1	2.1

Trial R4

A_x	A_x	A_x	A_x	A_x	A_x
mm²	mm²	mm²	mm²	mm²	mm²
0	0	0	0	0	0
10	8	8	8	8	10
10	8	8	8	8	10
10	8	8	8	8	10
10	8	8	8	8	10
78	78	78	78	78	78
				ΣA_x	674

A_t	A_t	A_t	A_t	A_t	A_t
mm²/m	mm²/m	mm²/m	mm²/m	mm²/m	mm²/m
32	32	32	32	32	32
208	153	153	153	153	208
208	153	153	153	153	208
208	153	153	153	153	208
208	153	153	153	153	208
208	208	208	208	208	208

Longitudinal

Front	Back
mm²	mm²
0	0
25.67	25.67
26	25.67
26	26
26	26
234	234
A_{sx}^{f}	A_{sx}^{b}
337	337

Transverse

Front	Back	Top
mm²	mm²	mm²
		32
513	513	
513	513	
513	513	Bot.
513	513	mm²
		208

A_{sy}^{f}	A_{sy}^{b}
513	513

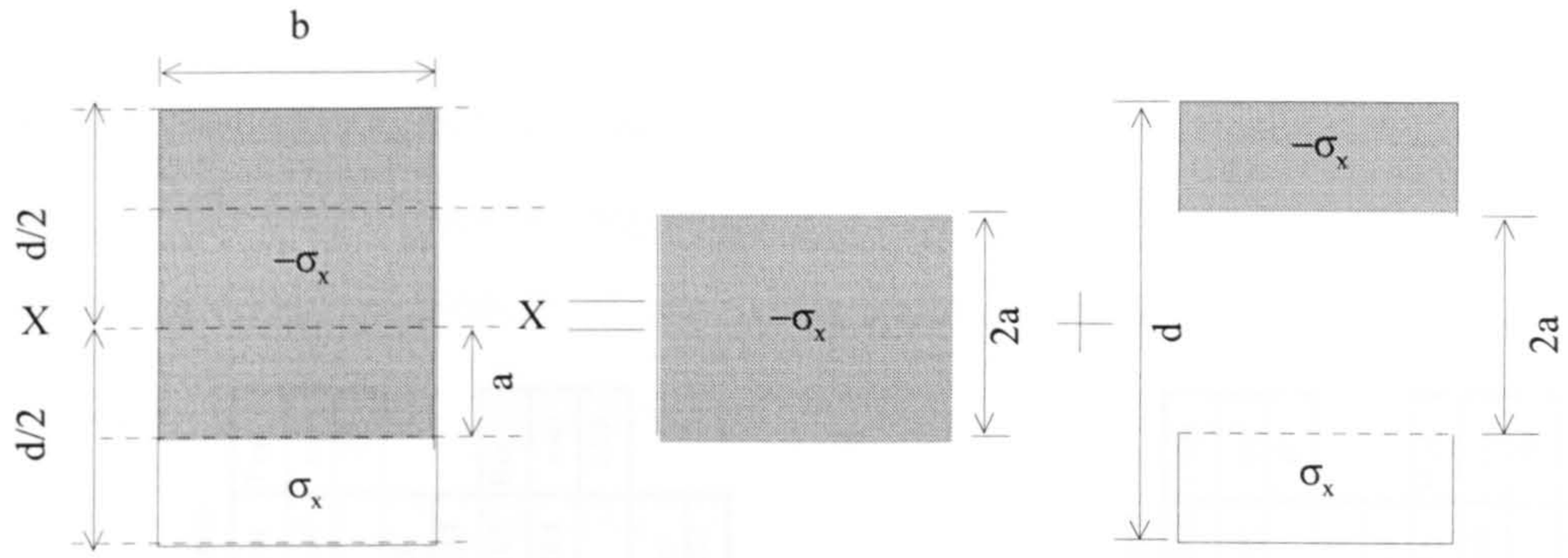

Fig. 10.19: Plastic stress distribution in the presence of axial load

Table 10.6 shows that the elastic stress distribution leads to less longitudinal reinforcement than the plastic stress distribution. This is because the plastic stress distribution gives more total tensile force than the elastic stress distribution due to the shorter lever arm length in the case of plastic stress distribution.

As shown in table 10.7, trials R1 and P1 required the least reinforcement for reinforced and partially prestressed beams respectively, they were used for the design of beams in the following section.

Table 10.7: Summary of required reinforcement based on the design trials

Trial No	$A_{xs}^{f}+A_{sx}^{b}$ mm^2	A_{ys}^{f} mm^2/m
Reinforced beam.		
R1	591	513
R2	606	513
R3	633	513
R4	674	513
Partially prestressed beam		
P1	383	505
P2	509	489

Table 10.6: Stresses and reinforcement in each region

σ_x	σ_x	σ_x	σ_x	σ_x	σ_x
N/mm²	N/mm²	N/mm²	N/mm²	N/mm²	N/mm²
-8.8	-8.8	-8.8	-8.8	-8.8	-8.8
-5.6	-5.6	-5.6	-5.6	-5.6	-5.6
-2.5	-2.5	-2.5	-2.5	-2.5	-2.5
0.7	0.7	0.7	0.7	0.7	0.7
3.9	3.9	3.9	3.9	3.9	3.9
7.0	7.0	7.0	7.0	7.0	7.0

τ_{shr}	τ_{shr}	τ_{shr}	τ_{shr}	τ_{shr}	τ_{shr}
N/mm²	N/mm²	N/mm²	N/mm²	N/mm²	N/mm²
0.3	0.3	0.3	0.3	0.3	0.3
0.8	0.8	0.8	0.8	0.8	0.8
1.0	1.0	1.0	1.0	1.0	1.0
1.0	1.0	1.0	1.0	1.0	1.0
0.8	0.8	0.8	0.8	0.8	0.8
0.3	0.3	0.3	0.3	0.3	0.3

τ_{tor}	τ_{tor}	τ_{tor}	τ_{tor}	τ_{tor}	τ_{tor}
N/mm²	N/mm²	N/mm²	N/mm²	N/mm²	N/mm²
-2.1	-2.08	-2.08	-2.08	-2.08	-2.08
2.1	0	0	0	0	-2.08
2.1	0	0	0	0	-2.08
2.1	0	0	0	0	-2.08
2.1	0	0	0	0	-2.08
2.1	2.1	2.1	2.1	2.1	2.1

τ	τ	τ	τ	τ	τ
N/mm²	N/mm²	N/mm²	N/mm²	N/mm²	N/mm²
-2.1	-2.1	-2.1	-2.1	-2.1	-2.1
2.8	0.8	0.8	0.8	0.8	-1.3
3.1	1.0	1.0	1.0	1.0	-1.1
3.1	1.0	1.0	1.0	1.0	-1.1
2.8	0.8	0.8	0.8	0.8	-1.3
2.1	2.1	2.1	2.1	2.1	2.1

A_x	A_x	A_x	A_x	A_x	A_x
mm²	mm²	mm²	mm²	mm²	mm²
0	0	0	0	0	0
0	0	0	0	0	0
3	0	0	0	0	0
19	8	8	8	8	9
7	23	23	23	23	-1
46	19	46	46	19	46
				ΣA_x	383

A_t	A_t	A_t	A_t	A_t	A_t
mm²/m	mm²/m	mm²/m	mm²/m	mm²/m	mm²/m
49	49	49	49	49	49
143	10	10	10	10	31
307	40	40	40	40	48
307	99	99	99	99	109
284	76	76	76	76	132
208	208	208	208	208	208

Trial P1

Longitudinal

Front	Back
mm²	mm²
0	0
0	0
3	0
36	26
53	45
110	110
A_{sx}^{f}	A_{sx}^{b}
202	181

Transverse

Front	Back	Top
mm²	mm²	mm²
		49
164	51	
386	127	
505	307	Bot.
437	284	mm²
		208

A_{sy}^{f}	A_{sy}^{b}
505	307

σ_x	σ_x	σ_x	σ_x	σ_x	σ_x
N/mm²	N/mm²	N/mm²	N/mm²	N/mm²	N/mm²
-6.5	-6.5	-6.5	-6.5	-6.5	-6.5
-6.5	-6.5	-6.5	-6.5	-6.5	-6.5
-6.5	-6.5	-6.5	-6.5	-6.5	-6.5
6.5	6.5	6.5	6.5	6.5	6.5
6.5	6.5	6.5	6.5	6.5	6.5
6.5	6.5	6.5	6.5	6.5	6.5

τ_{shr}	τ_{shr}	τ_{shr}	τ_{shr}	τ_{shr}	τ_{shr}
N/mm²	N/mm²	N/mm²	N/mm²	N/mm²	N/mm²
0	0	0	0	0	0
3.1	0	0	0	0	3.1
3.1	0	0	0	0	3.1
3.1	0	0	0	0	3.1
3.1	0	0	0	0	3.1
0	0	0	0	0	0

τ_{tor}	τ_{tor}	τ_{tor}	τ_{tor}	τ_{tor}	τ_{tor}
N/mm²	N/mm²	N/mm²	N/mm²	N/mm²	N/mm²
-2.08	-2.08	-2.08	-2.08	-2.08	-2.08
2.1	0	0	0	0	-2.08
2.1	0	0	0	0	-2.08
2.1	0	0	0	0	-2.08
2.1	0	0	0	0	-2.08
2.1	2.1	2.1	2.1	2.1	2.1

τ	τ	τ	τ	τ	τ
N/mm²	N/mm²	N/mm²	N/mm²	N/mm²	N/mm²
-2.1	-2.1	-2.1	-2.1	-2.1	-2.1
5.1	0	0	0	0	1.0
5.1	0	0	0	0	1.0
5.1	0	0	0	0	1.0
5.1	0	0	0	0	1.0
2.1	2.1	2.1	2.1	2.1	2.1

A_x	A_x	A_x	A_x	A_x	A_x
mm²	mm²	mm²	mm²	mm²	mm²
0	0	0	0	0	0
0	0	0	0	0	0
0	0	0	0	0	0
46	26	26	26	26	30
20	26	26	26	26	3
43	16	43	43	16	43
				ΣA_x	509

A_t	A_t	A_t	A_t	A_t	A_t
mm²/m	mm²/m	mm²/m	mm²/m	mm²/m	mm²/m
67	67	67	67	67	67
489	0	0	0	0	18
489	0	0	0	0	18
411	0	0	0	0	78
411	0	0	0	0	208
208	208	208	208	208	208

Trial P2

Longitudinal

Front	Back
mm²	mm²
0	0
0	0
0	0
98	82
71	55
101	101
A_{sx}^{f}	A_{sx}^{b}
271	238

Transverse

Front	Back	Top
mm²	mm²	mm²
		67
489	18	
489	18	
411	78	Bot.
411	208	mm²
		208

A_{sy}^{f}	A_{sy}^{b}
411	78

10.6: Computational experiments

In this section models R1 and P1 were used for the design of reinforced and partially prestressed beams respectively and the 3-D program was used to study the behaviour of these models. It should be emphasised that in these models the total provided longitudinal reinforcement is the summation ($\sum A_x = A_{sx}^f + A_{sx}^b$) of all required steel areas in this direction. This is less than twice A_{sx}^f as was provided for hollow beams and solid beam BTV12. Table 10.8 shows a comparison between these steel areas for several load combinations. It can be seen that the difference is larger in the case of reinforced beams (up to 19%).

The transverse steel is still based on the largest required stirrup leg area A_{sy}^f.

Table 10.8: Comparison between summation and largest longitudinal reinforcement

Load combination			R1			P1		
T	M	V	$A_{xs}^f+A_{sx}^b$	$2A_{xs}^f$	$(A_{xs}^f+A_{xs}^b)/(2A_{sx}^f)$	$A_{xs}^f+A_{sx}^b$	$2A_{xs}^f$	$(A_{xs}^f+A_{xs}^b)/(2A_{sx}^f)$
kN.m.	kN.m.	kN.	mm^2	mm^2	Ratio	mm^2	mm^2	Ratio
13	51	60	590	675	0.87	383	400	0.96
26	70	82	699	864	0.81	699	736	0.95
39	70	82	845	1009	0.84	822	860	0.96

10.6.1: Effect of the τ_{tor}/τ_{shr} ratio on the computed steel stress and failure load

Three reinforced (N1-N3) and two partially prestressed (N4-N5) beams designed for different τ_{tor}/τ_{shr} ratios are shown in table 10.9. The shear force V and the ratio of torsion to bending moment T/M were kept constant. The bending moment was varied by varying the distance between the supports. This table also shows the ratios of computed to design failure loads L_c/L_d. It is clear that, for the load combination tested here, the smaller the ratio τ_{tor}/τ_{shr} the larger the failure load ratio for both reinforced and partially prestressed beams. Figure 10.20 shows that in all reinforced beams the longitudinal steel in the front face yielded near the failure load. However, in the partially prestressed beams and in the rear face of the reinforced beams, the longitudinal steel did not reach yield. In all cases the transverse steel did not reach yield but the larger the τ_{tor}/τ_{shr} ratio the larger the stirrup stress.

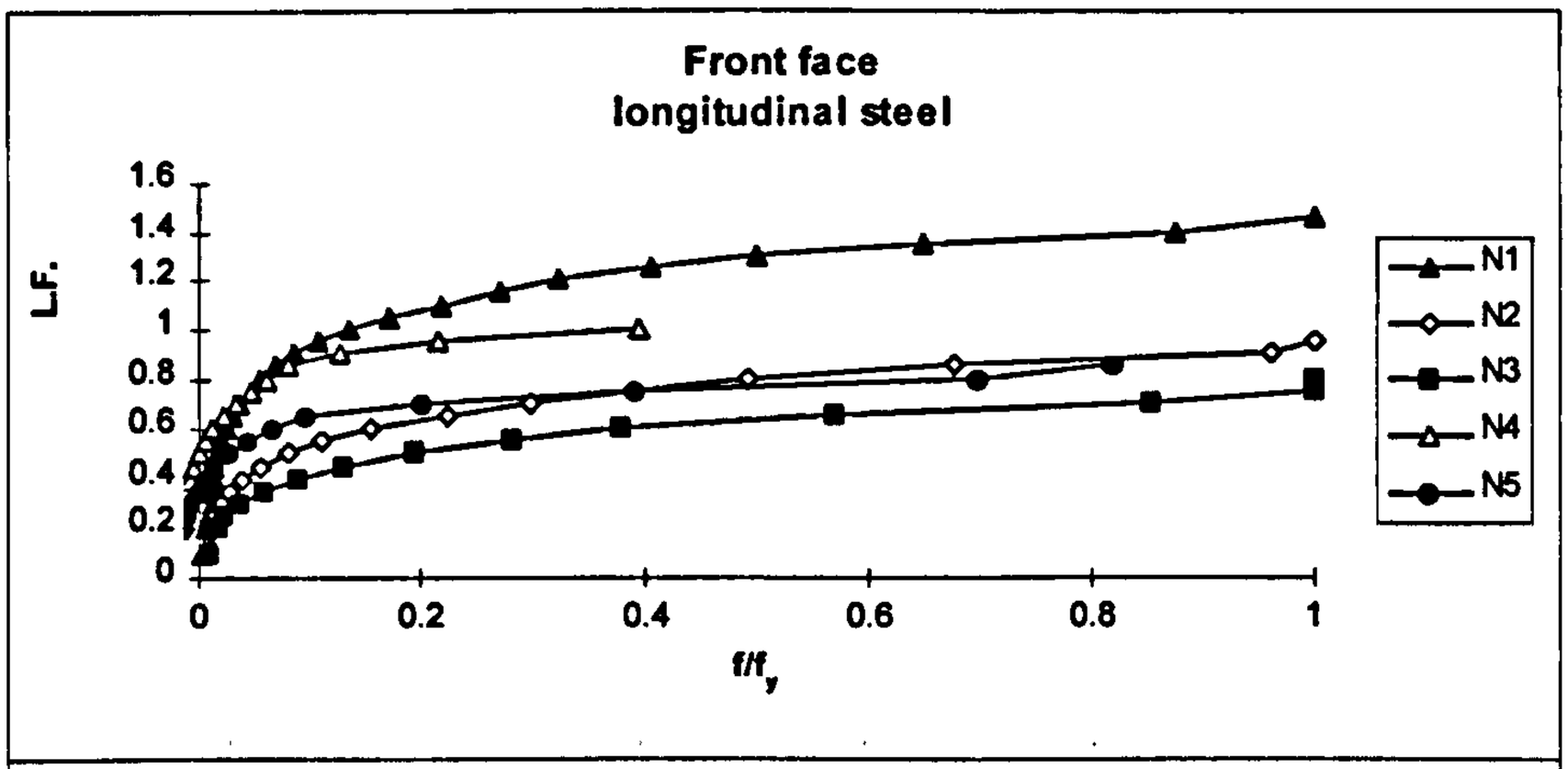

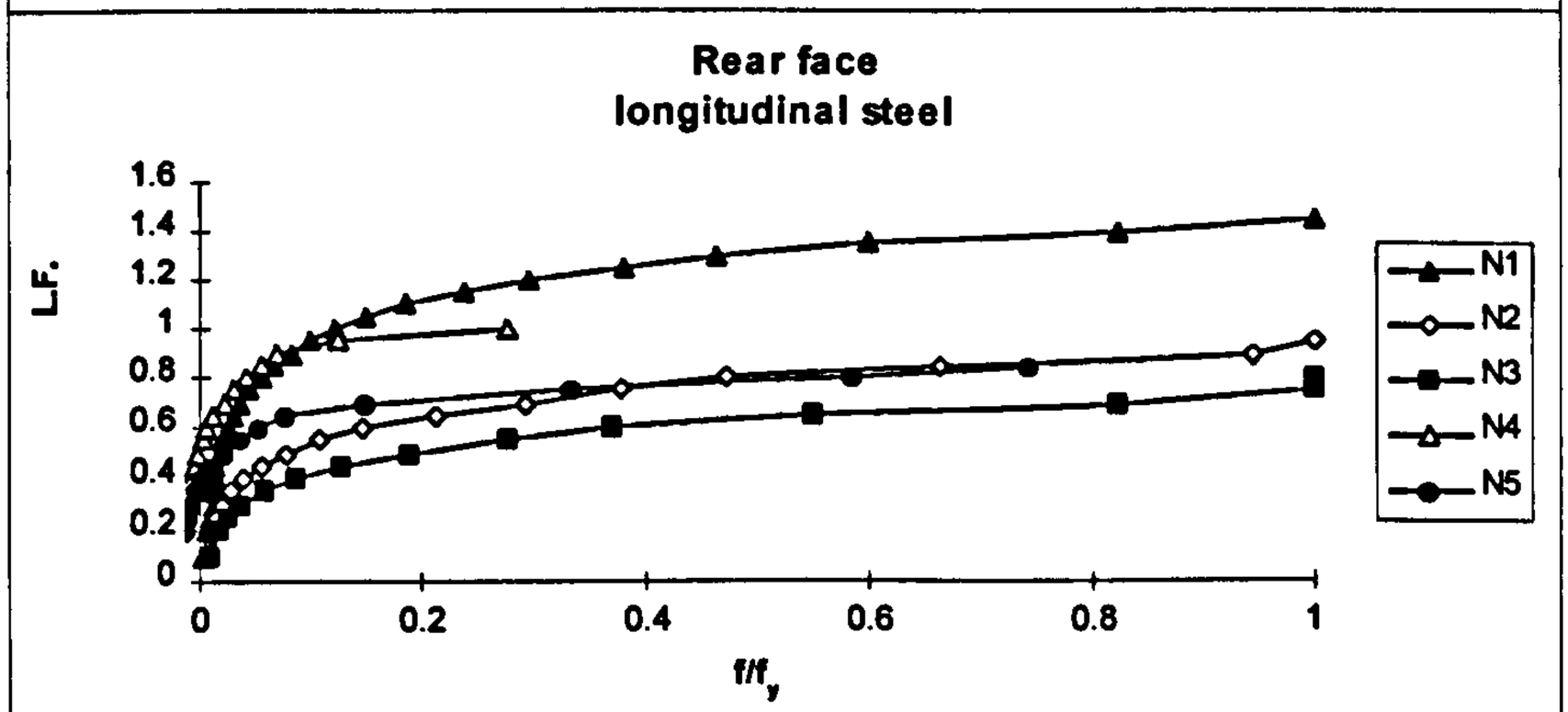

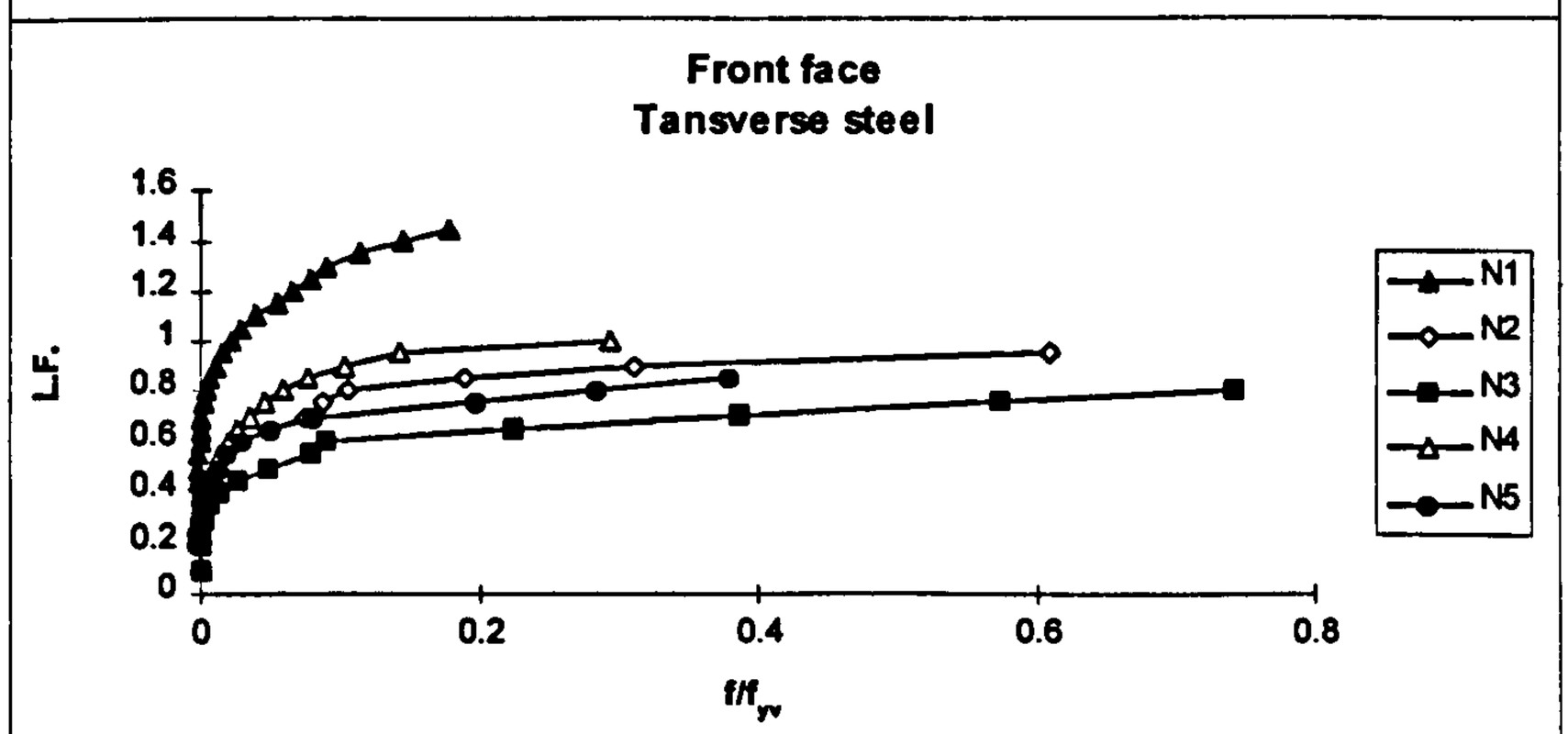

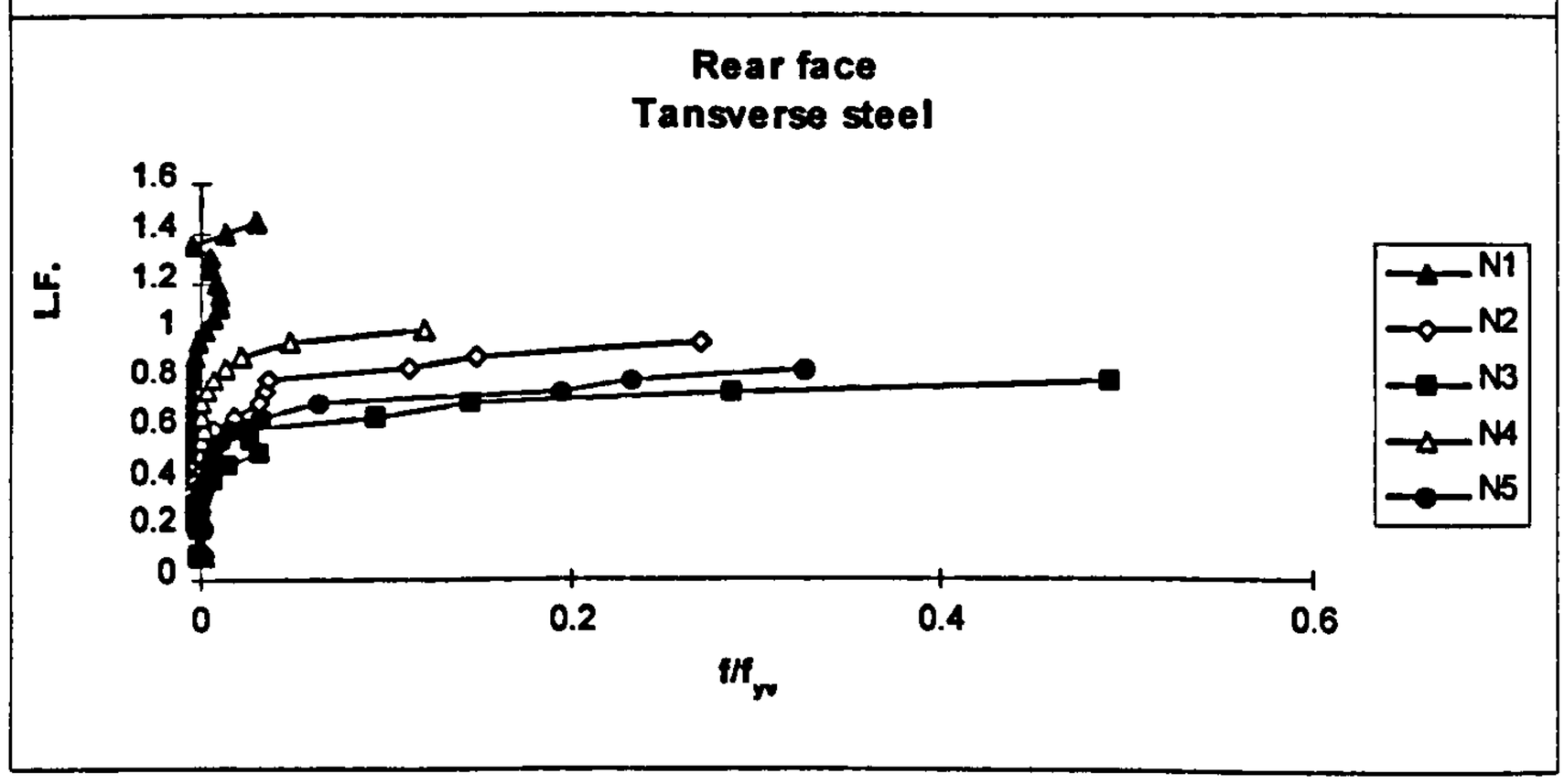

Fig. 10.20: Effect of τ_{tor}/τ_{shr} ratio on steel stress (N1-N5 see Table 10.9)

Table 10.9: Effect of τ_{tor}/τ_{shr} ratio on failure load

Beam No.	T_d kN.m.	V_d kN.	M_d kN.m.	T_d/M_d Ratio	τ_{tor}/τ_{shr} Ratio	L_c/L_d Ratio
Reinforced models						
N1	13	61	13	1.0	0.68	1.45
N2	26	61	26	1.0	1.36	0.95
N3	39	61	39	1.0	2.05	0.80
Partially prestressed models						
N4	26	61	26	1.0	1.40	1.00
N5	39	61	39	1.0	2.10	0.85

10.6.2: Effect of T/M ratio on the computed steel stress and failure load

Similar to sub-section 10.6.1 five beams (K1-K5) were designed for different T/M ratios as in table 10.10. The beams were subjected to bending and torsion alone. Results show that, the smaller the T/M ratio, the larger the failure load for both the reinforced and partially prestressed beams. Figures 10.21 show that the longitudinal steel in all beams except K5 reached yield near failure load. The transverse steel did not reach yield in all cases but the larger the T/M the larger the stress in the stirrups. From the results in this section it can be seen that the selected design models R1 and P1 have shown acceptable agreement between the design and non-linear analysis on the failure load and longitudinal steel yield. However, there is poor agreement in the case of stress in the transverse steel specially when τ_{tor}/τ_{shr} or T/M are small. The use of the summation of reinforcement in the longitudinal direction $(\sum A_x = A_{sx}^f + A_{sx}^b)$ results in acceptable predicted failure load and steel behaviour in this direction.

Table 10.10: Effect of T_d/M_d ratio on failure load

Beam No.	T_d kN.m.	V_d kN.	M_d kN.m.	T_d/M_d Ratio	L_c/L_d Ratio
Reinforced models					
K1	13	0	51	0.25	1.10
K2	26	0	51	0.51	0.95
K3	39	0	34	1.15	0.80
Partially prestressed models					
K4	13	0	51	0.25	1.25
K5	39	0	34	1.15	0.80

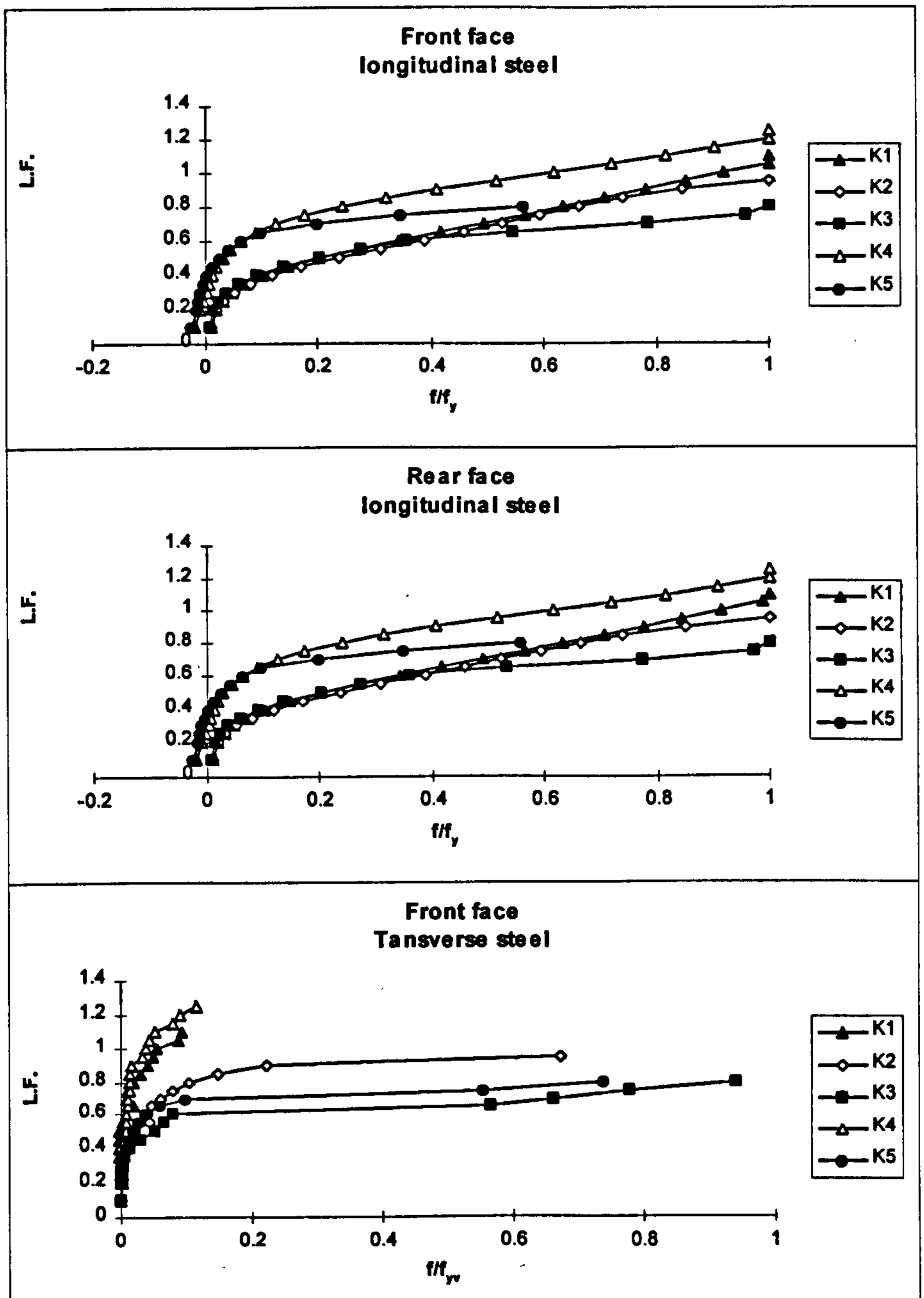

Fig. 10.21: Effect of T_d/M_d ratio on steel stress (K1-K5 see table 10.10)

10.7 Effect of using average transverse steel on beam behaviour

Since in the previous computational experiments, the transverse steel did not yield, the average of the transverse steel areas $(A_{sy}^f + A_{sy}^b)/2$ was used in the following computational experiments instead of using the largest required stirrup leg area A_{sy}^f as in all previous work. The longitudinal steel was kept as the summation of the whole steel areas. This was done to study the effect of reducing the transverse steel on the beam behaviour and failure load. Two beams having different τ_{tor}/τ_{shr} and T/M ratios as in table 10.11 were analysed. Each beam was designed for the same load combinations twice, once with A_{sy}^f and another with $(A_{sy}^f + A_{sy}^b)/2$. In this table, L_c/L_d indicates the failure load ratio for the case when the A_{sy}^f was used and L_c^*/L_d represents the failure load ratio when the average transverse steel $(A_{sy}^f + A_{sy}^b)/2$ was used. Figure 10.22 shows the strain ratios in the longitudinal and transverse steel. The * in this figure represents the strain ratio for the case when $(A_{sy}^f + A_{sy}^b)/2$ was used and the those graphs without * are for the case when the A_{sy}^f was used.

From this table and these figures it can be seen that there was no change in the failure loads or the stresses in the longitudinal steel. The stresses in the transverse steel have slightly increased in beam F2* but it did not yield.

Table 10.11: Effect of average transverse steel on failure load

Beam No.	τ_{tor}/τ_{shr} Ratio	T_d/M_d Ratio	Failure Ratios L_c/L_d	L_c^*/L_d
Reinforced model				
F1	0.69	0.25	1.45	1.45
Partially prestressed model				
F2	1.56	0.56	1.15	1.15

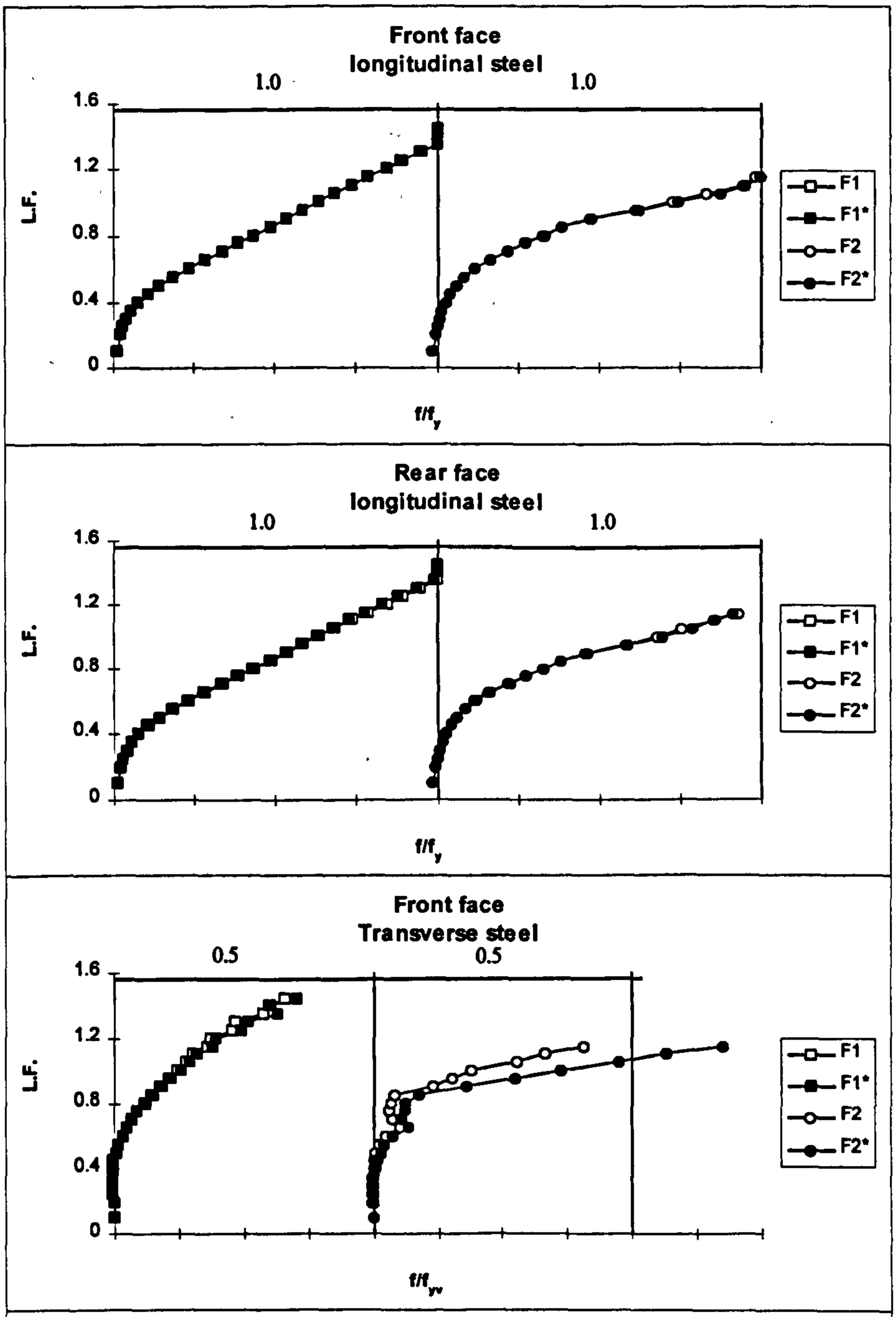

Fig. 10.22: Effect of average transverse steel on steel stress

10.8 Conclusion

From the study in this chapter it can be concluded that the concrete in the core participates in the beam strength and behaviour and cannot be ignored. Its participation depends partly on the ratio of the torsion to bending moment and the ratio of the shear stress due to torsion to shear stress due to shear force. The assumed stress distribution has little effect on the amount of calculated reinforcement. One way of reducing the excess reinforcement is using the summation of longitudinal steel instead of the area based on the largest stress combination, and using the average stirrup leg area instead of the largest leg area. The finite element program used for the non-linear analysis predicts an acceptable theoretical failure load and longitudinal steel response for the beams designed using models R1 and P1 explained in section 10.5. The transverse steel, however, did not reach yield even when average transverse steel was used.

In order to experimentally examine these design models and agreement between test results and predicted results from the finite element program, five beams were designed based on these models with average transverse steel as discussed in section 10.7. The experimental test results and non-linear analysis are presented in the following chapter.

11: Experimental and computational investigation of solid beams

11.1: Introduction

Based on the recommendations presented in the preceding chapter, three reinforced and two partially prestressed solid beams were tested. The 3-D finite element program was used for the non-linear analysis. The experimental and computational results are compared and the validity of the stress distributions used, the direct design method and the prediction of the 3-D finite element program are examined. The comparison is carried out using the following criteria:

- Load displacement relationship.
- Strain in longitudinal steel.
- Strain in transverse (links) steel.
- Relative angle of twist.
- Crack pattern and mode of failure.
- Failure load.
- Crack pattern and mode of failure.

As the data is very large, only a few typical results are shown in this chapter. Appendix B contains a complete set of experimental and computational steel strain.

Table 11.1: Load combinations

Beam No.	T_d kN.m.	τ_{tor} N/mm^2	V_d kN	τ_{shr} N/mm^2	τ_{tor}/τ_{shr} Ratio	M_d kN.m.	T_d/M_d Ratio
Group C: Reinforced concrete solid beams							
BTV13	26	4.16	61.08	3.00	1.39	50.89	0.51
BTV14	13	2.08	61.08	3.00	0.69	50.89	0.26
BTV15	39	6.24	41.08	2.05	3.04	32.89	1.19
Group D: Partially prestressed hollow beams							
BTV16	13	2.08	61.08	3.00	0.69	50.89	0.26
BTV17	39	6.24	41.08	2.05	3.04	32.89	1.19

11.2: Experimental investigation

11.2.1: Test beams

Plastic stress distribution Trial R1 (chapter 10) was used for the design of reinforced concrete beams while elastic stress distribution Trial P1 was adopted for the partially prestressed ones. Table 11.1 shows the load combination used in the tests. The main differences between these beams are the ratio of the shear stress due to torsion to shear stress due to shear force τ_{tor}/τ_{shr} which varied between 0.69 and 3.04

and the ratio of the torsion to bending moment T/M which varied between 0.26 to 1.19. The beam cross-section was 300x300mm and the length was 3.8m. The beams were loaded, tested and monitored as described in chapter 4. The typical arrangement of reinforcement and the vertical distances between longitudinal layers of reinforcement were as for the hollow beams (Figs. 5.5-6). Figure 11.1 shows the reinforcement provided for each beam inside the test span and outside it. The steel bar diameters were as shown in the figures while the diameter of the prestressing wires was 5 mm. The filled circles represent the strain gauged bars or prestressing wires while the unfilled circles represent the rest.

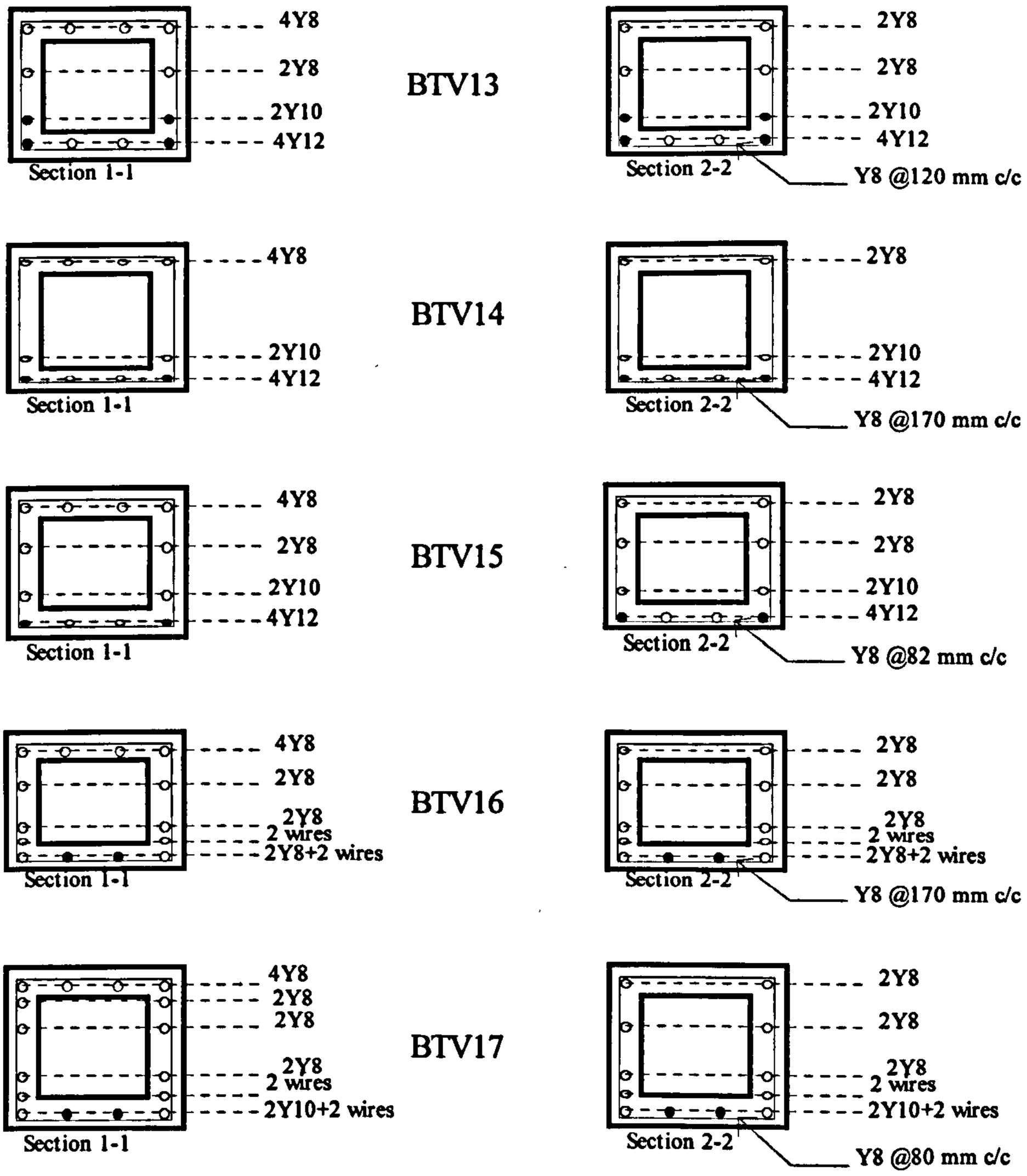

Fig. 11.1: Reinforcement in solid beams

Table 11.2 shows the measured average material properties. The cube f_{cu} and cylinder f'_c concrete compressive strengths in this table were for the samples cured under the same conditions as for the beam.Table 11.3 shows the locations of strain gauges. This table has to be read in conjunction with figure 5.4 which is repeated here for convenience.

Table 11.2: Average material properties

Beam	f_{cu}	f'_c	f_y	f_{yv}	f_{py}	Age
No.	N/mm^2	N/mm^2	N/mm^2	N/mm^2	N/mm^2	days
Group C: Reinforced concrete solid beams						
BTVI3	40	28.5	500	500	-	9
BTVI4	37	25.7	500	500	-	8
BTVI5	61	38.2	500	500	-	8
Group D: Partially prestressed solid beams						
BTVI6	52	36	500	500	1570	8
BTVI7	53	36	500	500	1570	10

Table 11.3: Location of strain gauges (To be read in conjunction with Fig. 5.4)

Space	a	b	c	d	e	f	g	h	j	k
Beam	mm	mm	mm	mm	mm	mm	mm	mm	mm	mm
BTVI3	120	120	120	120	-	60	120	120	120	-
BTVI4	170	170	170	170	-	85	170	170	170	-
BTVI5	82	82	82	82	-	41	82	82	82	-
BTVI6	170	170	-	-	-	85	170	170	170	-
BTVI7	80	80	80	-	-	40	80	80	80	-

11.2.2: Experimental observations

This sub-section summaries the observed behaviour in the test span region of the tested solid beams at significant stages in the behaviour. The data presented is as in the case of hollow beam discussed in chapter 5.

BTV13: T_d=26kN.m., M_d=50.89kN.m., V_d=61.08kN., T_d/M_d=0.51, τ_{tor}/τ_{shr}=1.36

At 50% of design load, almost vertical cracks were first noticed at the bottom and front faces near mid-span. At 60% of load, the first crack was noticed in the back face. At 70% of load, inclined (50°) cracks appeared in the top face as an extension of the inclined cracks at the front and back faces. The average crack width at this stage was 0.5mm. Displacement limit of span/250 was reached just before failure load. Failure happened at 108% of load by a major inclined (50°) crack opening up

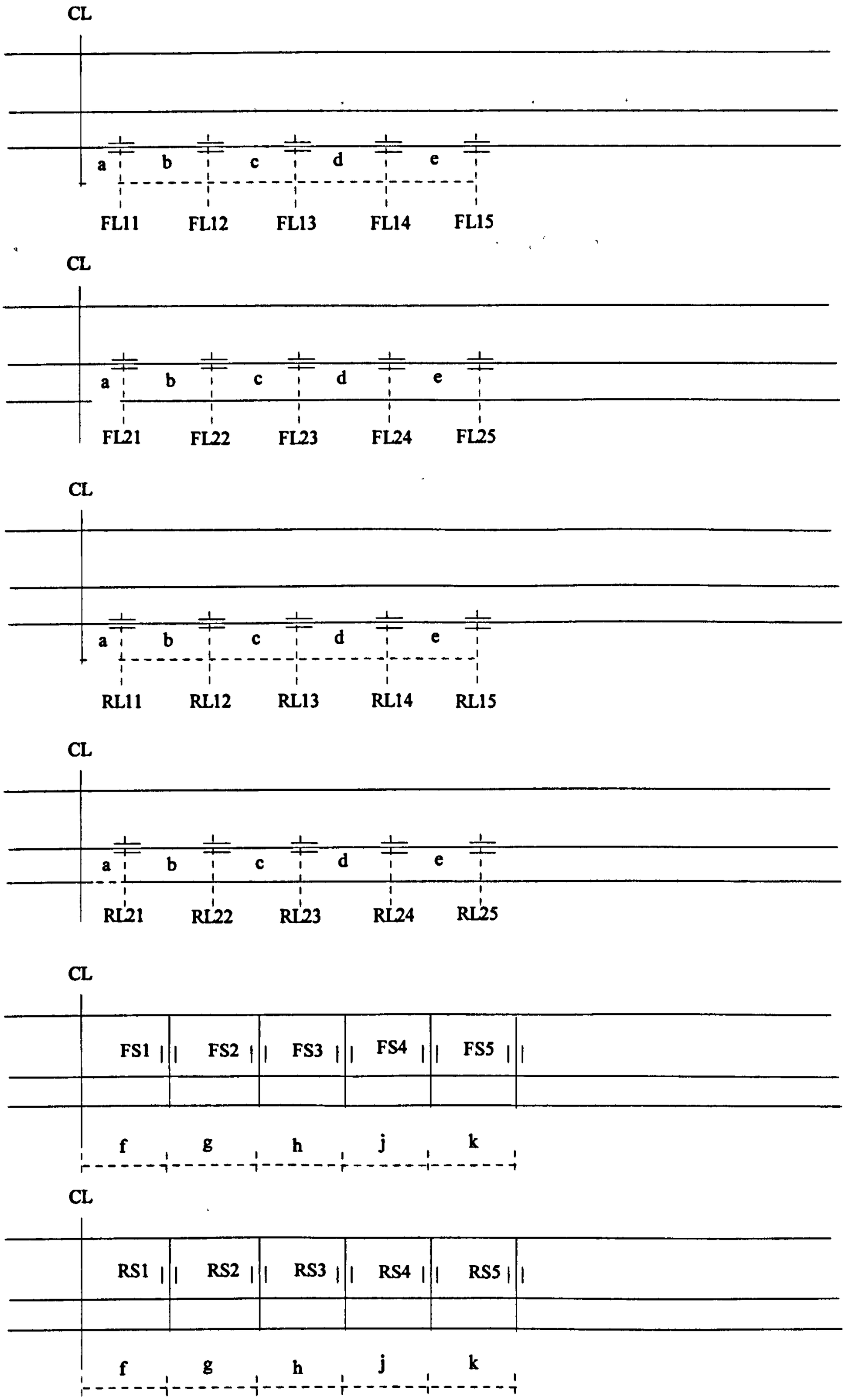

Fig. 5.4: Legend for strain gauge locations

on the front face at about 400mm to the right of mid-span and spiralling round the beam. Figure 11.2 shows crack development. Figure 11.3 shows the steel strain. The average steel strain ratio on the front face was 1.04 and in the back face 0.62. In the stirrups, the average steel strain ratio in the front face was 0.90 and in the rear face was 0.35.

Fig. 11.2: Crack development in the front web (BTV13)

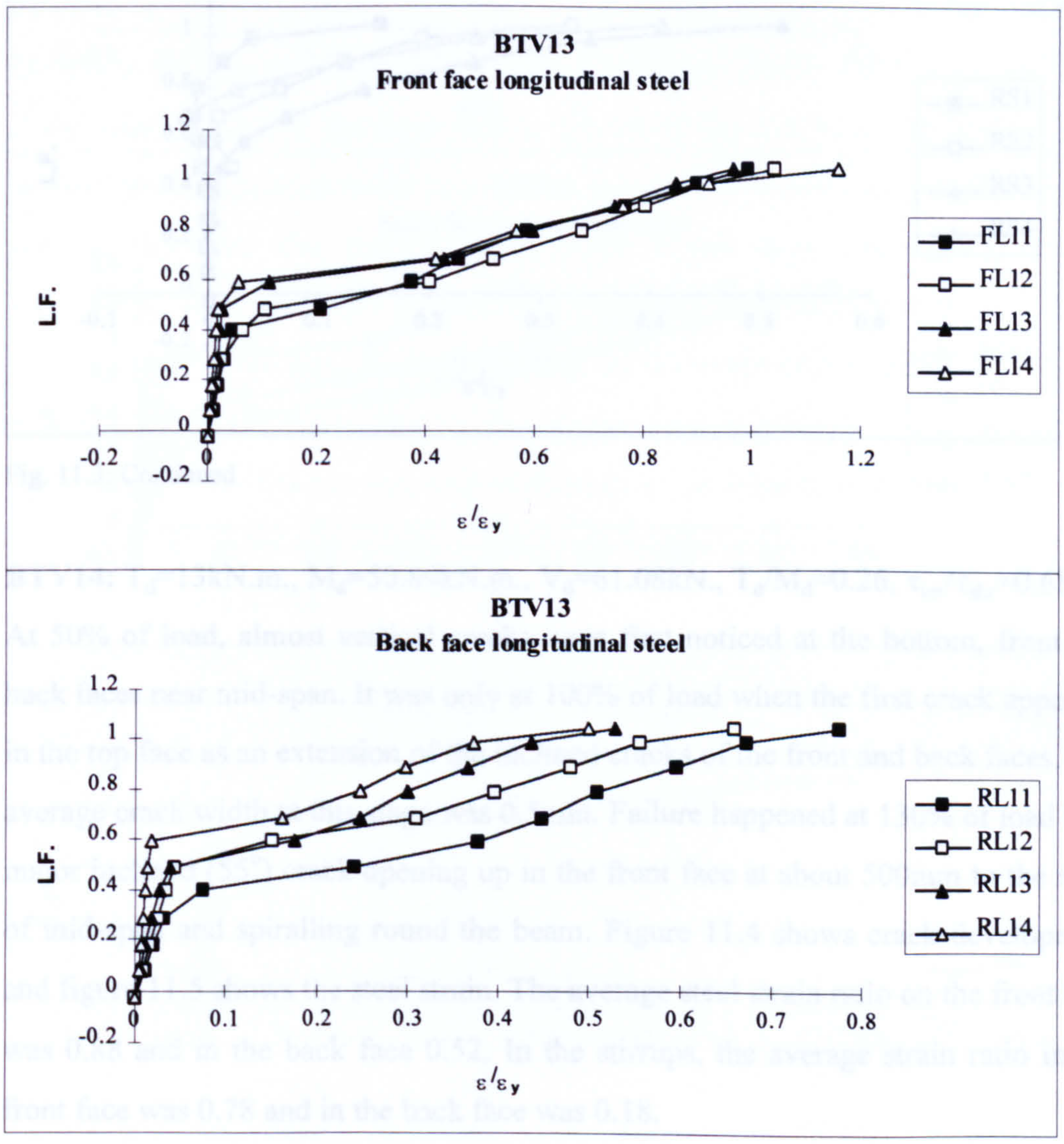

Fig. 11.3: Strain ratios in the steel (BTV13)

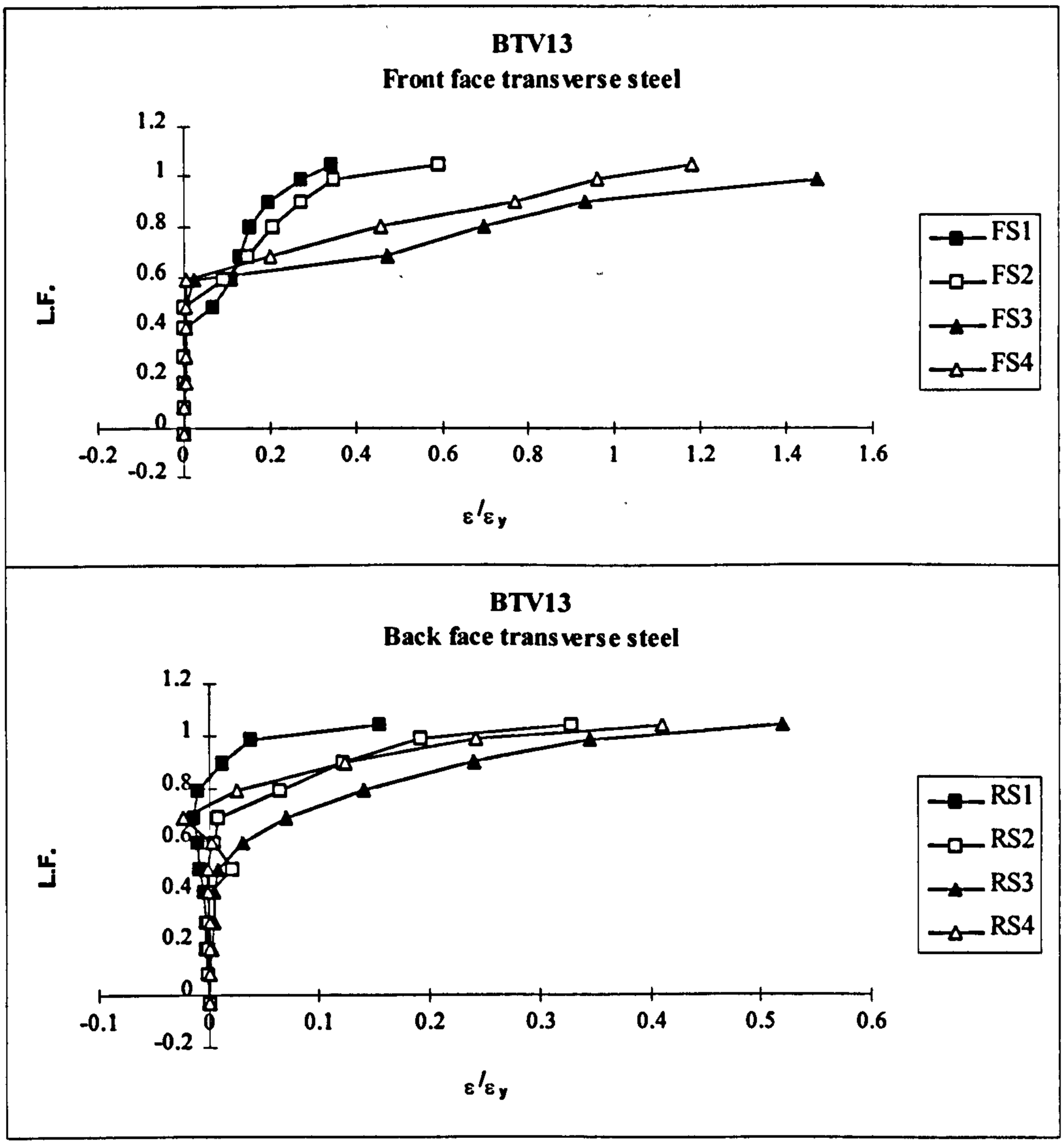

Fig. 11.3: Continued

BTV14: T_d=13kN.m., M_d=50.89kN.m., V_d=61.08kN., T_d/M_d=0.26, τ_{tor}/τ_{shr}=0.68

At 50% of load, almost vertical cracks were first noticed at the bottom, front and back faces near mid-span. It was only at 100% of load when the first crack appeared in the top face as an extension of the inclined cracks of the front and back faces. The average crack width at this stage was 0.5mm. Failure happened at 130% of load by a major inclined (55°) crack opening up in the front face at about 500mm to the right of mid-span and spiralling round the beam. Figure 11.4 shows crack development and figure 11.5 shows the steel strain. The average steel strain ratio on the front face was 0.88 and in the back face 0.52. In the stirrups, the average strain ratio in the front face was 0.78 and in the back face was 0.18.

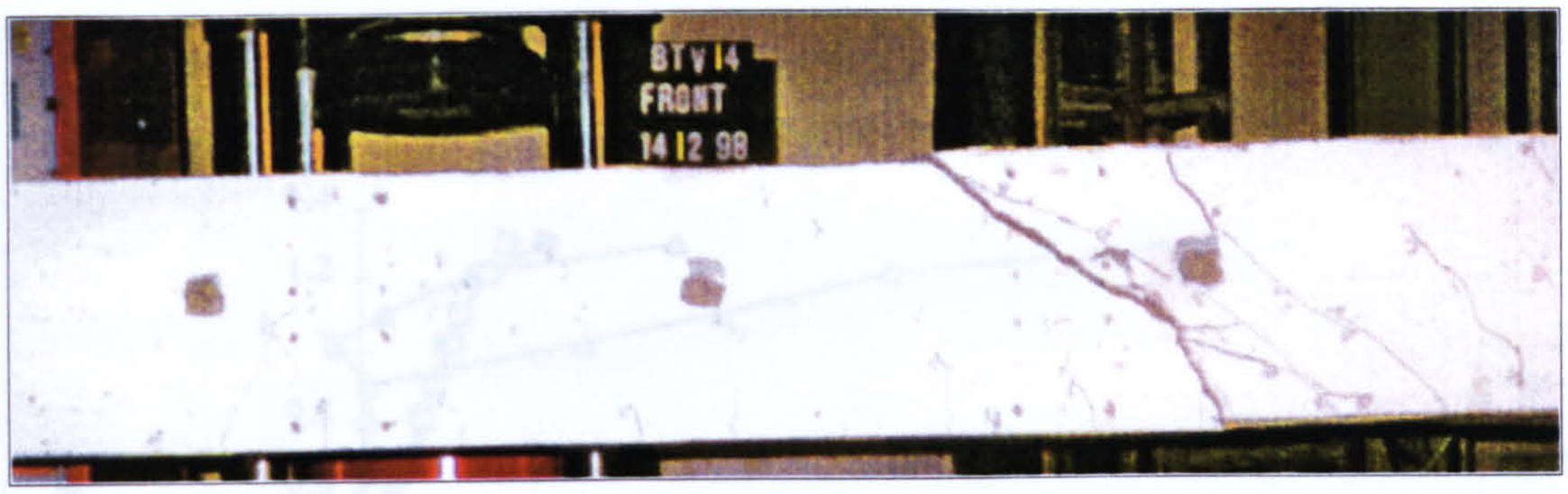

Fig. 11.4: Crack development in the front web (BTV14)

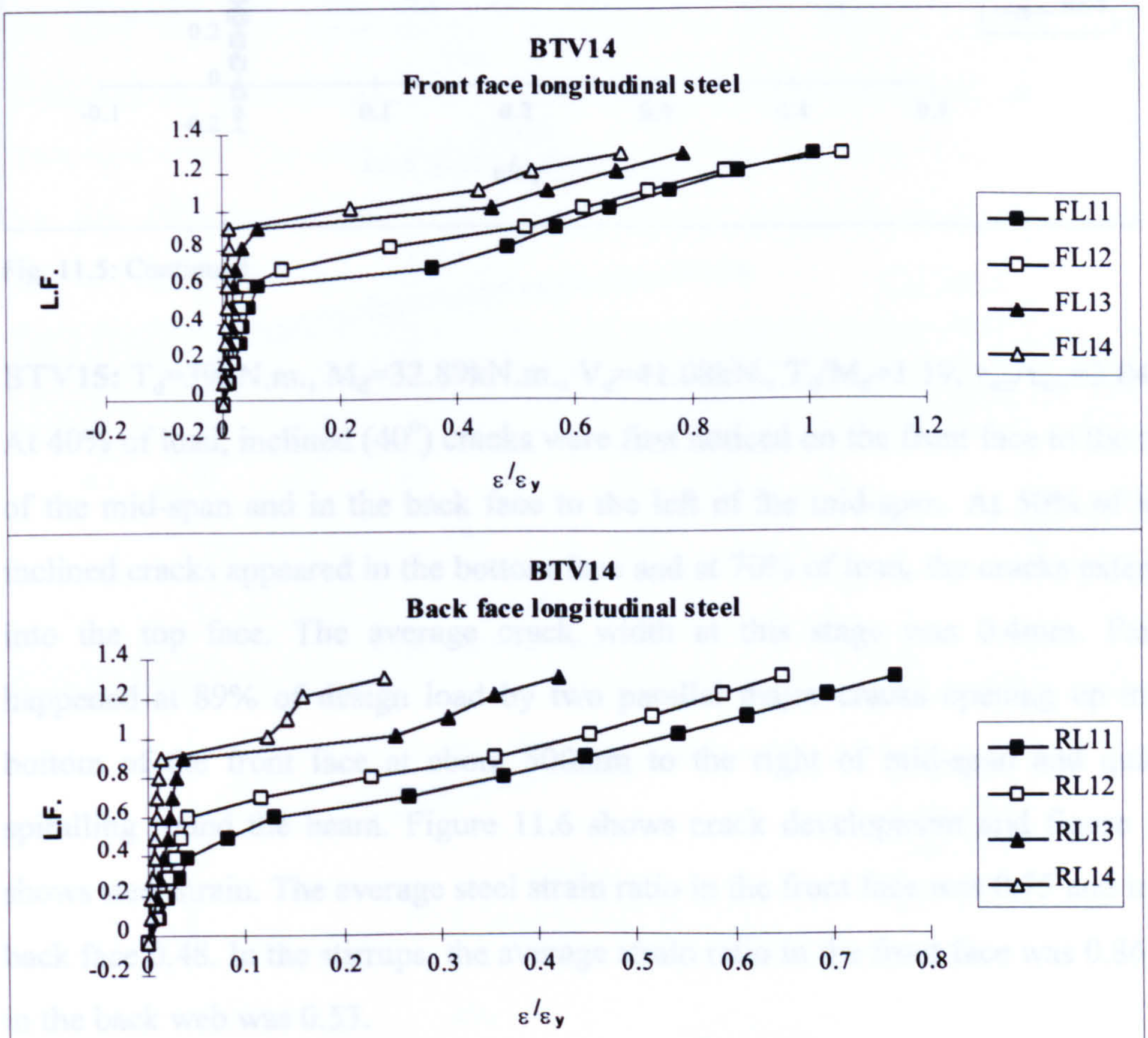

Fig. 11.5: Strain ratios in the steel (BTV14)

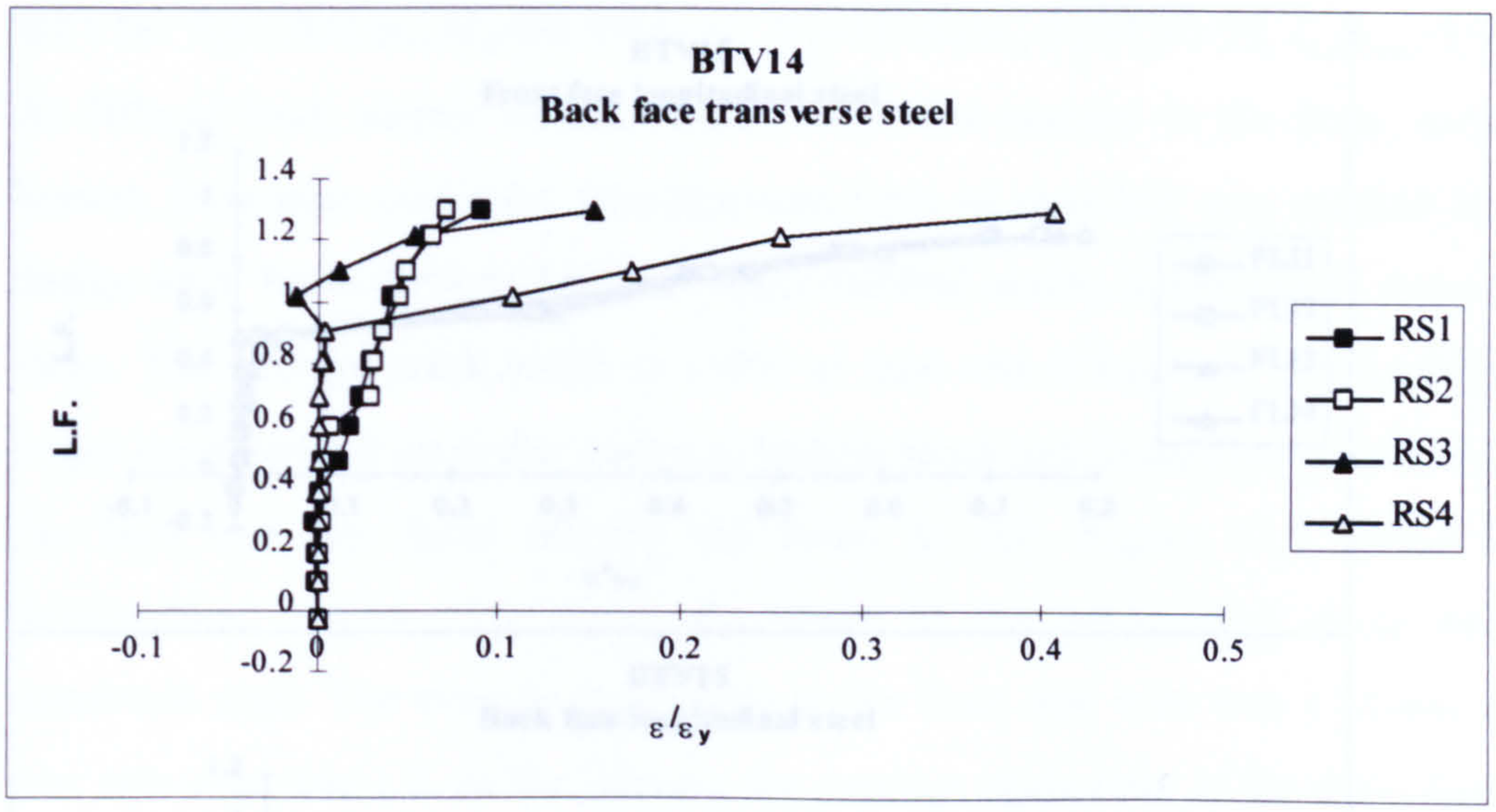

Fig. 11.5: Continued

BTV15: T_d=39kN.m., M_d=32.89kN.m., V_d=41.08kN., T_d/M_d=1.19, τ_{tor}/τ_{shr}=3.04

At 40% of load, inclined (40°) cracks were first noticed on the front face to the right of the mid-span and in the back face to the left of the mid-span. At 50% of load, inclined cracks appeared in the bottom face and at 70% of load, the cracks extended into the top face. The average crack width at this stage was 0.4mm. Failure happened at 89% of design load by two parallel major cracks opening up in the bottom of the front face at about 500mm to the right of mid-span and quickly spiralling round the beam. Figure 11.6 shows crack development and figure 11.7 shows steel strain. The average steel strain ratio in the front face was 0.75 and in the back face 0.48. In the stirrups, the average strain ratio in the front face was 0.86 and in the back web was 0.53.

Fig. 11.6: Crack development in the front web (BTV15)

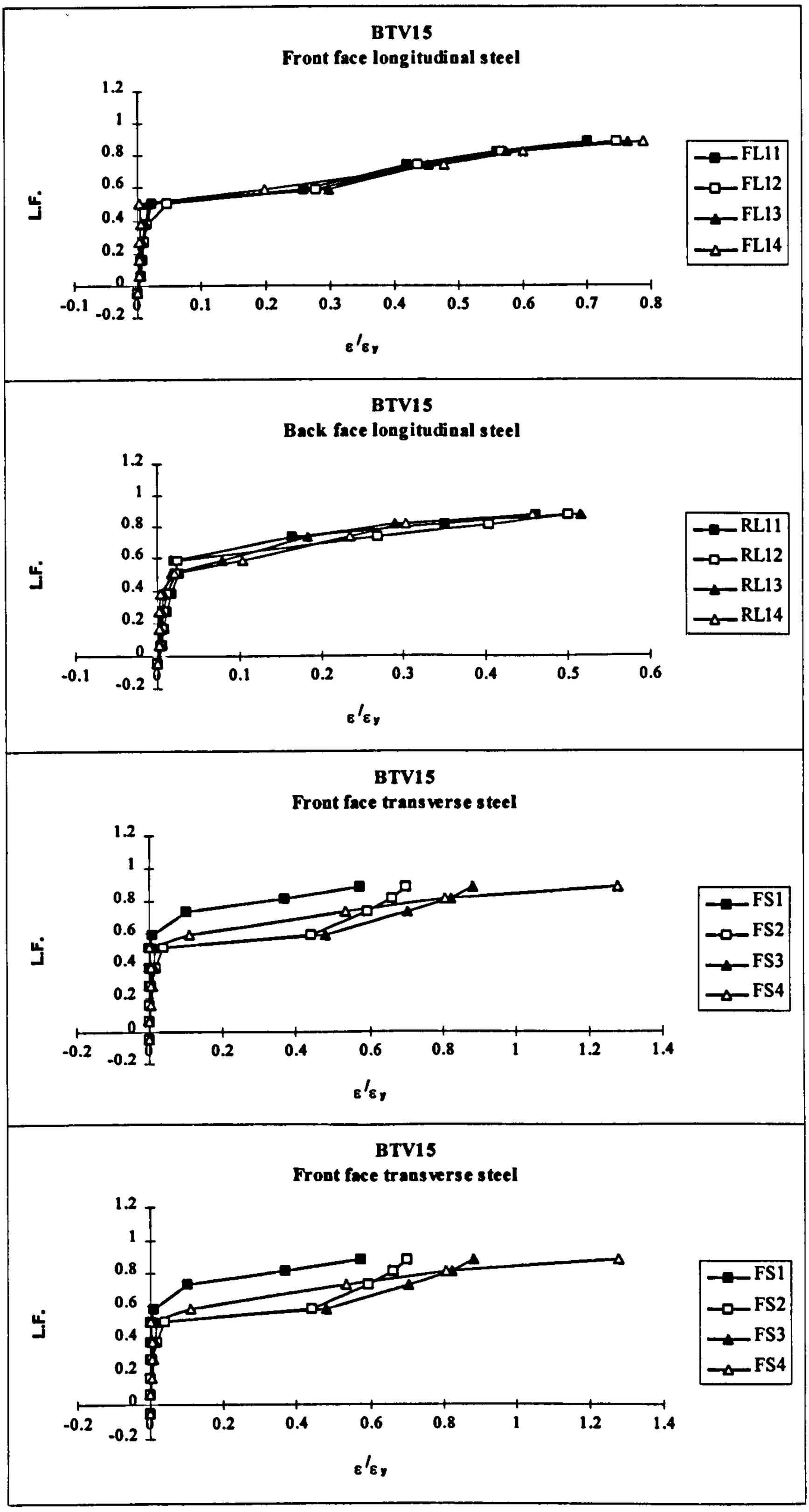

Fig. 11.7: Strain ratios in the steel (BTV15)

BTV16: T_d=13kN.m., M_d=50.89kN.m., V_d=61.08kN., T_d/M_d=0.26, τ_{tor}/τ_{shr}=0.68

At 70% of load, almost vertical cracks were first noticed in the front, back and bottom faces near mid-span. Displacement limit of span/250 was reached at 80% design load. From 80% to 110% of load, inclined cracks developed in these three faces. The average crack width at 110% of load was 0.4mm. At 120% of load, a major crack opened up in the front and bottom faces and immediately extended into the back and top faces causing the beam to fail. Figure 11.8 shows crack development. Figure 11.9 shows the strain in the prestressing wires and the transverse steel. The average strain ratio in the front side wire was 1.34 and in the rear side wire was 1.2. In the stirrups, the average strain ratio in the front face was 0.43 and in the back face was 0.13.

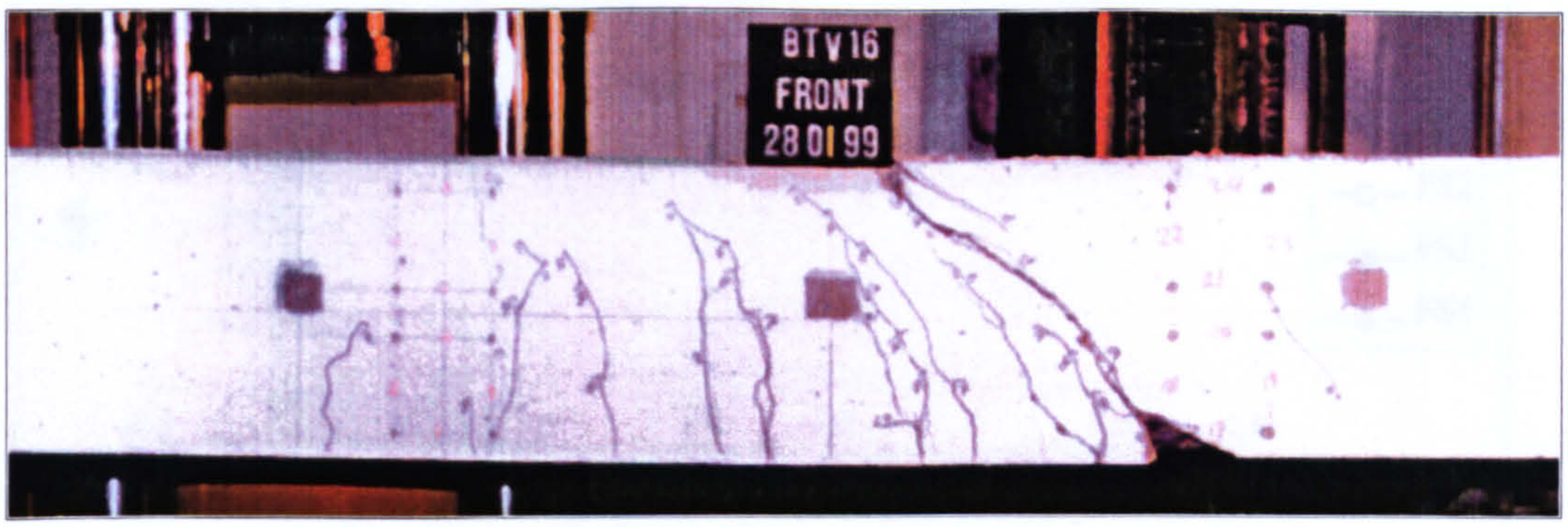

Fig. 11.8: Crack development in the front face (BTV16)

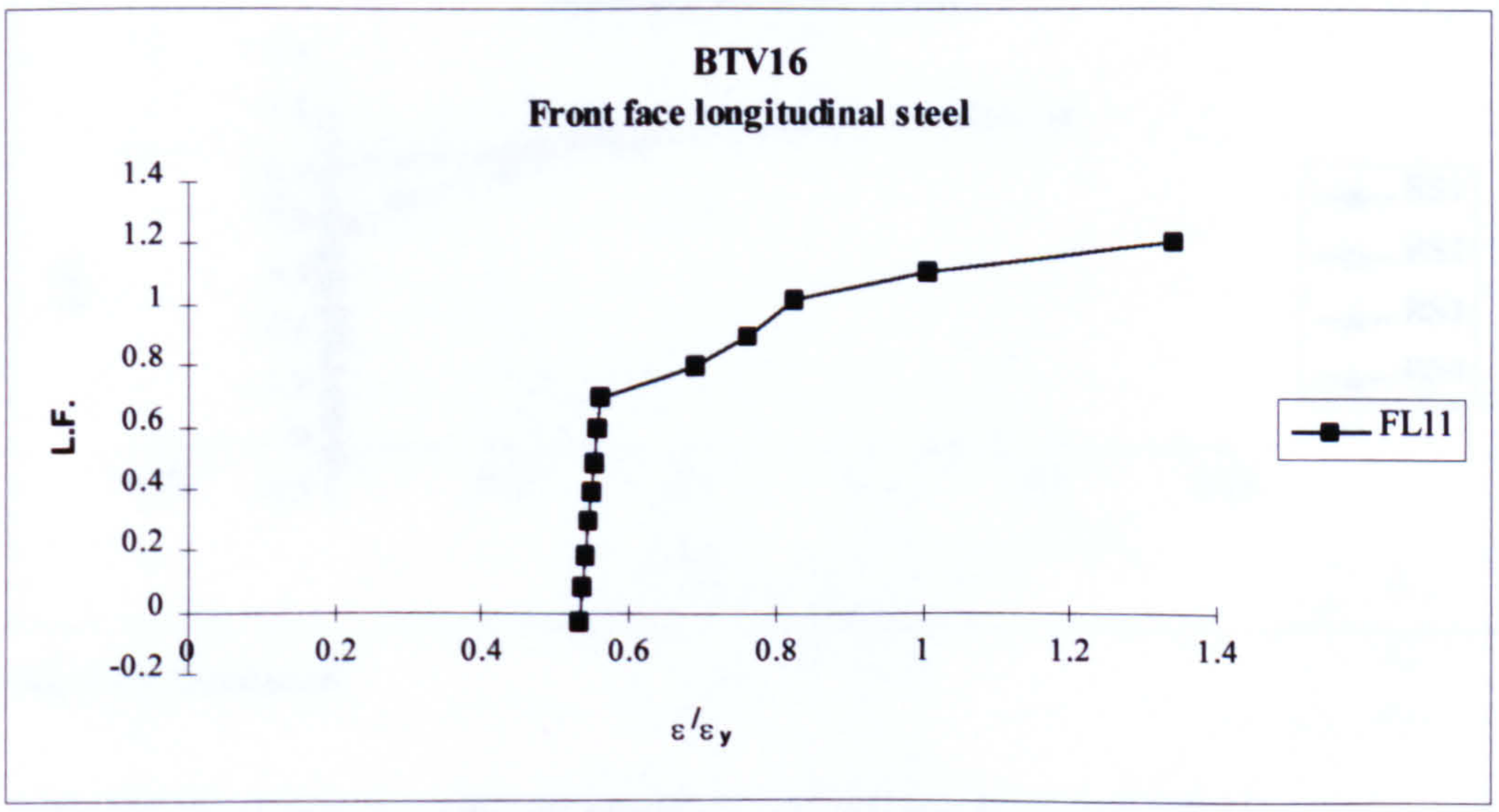

Fig. 11.9: Strain ratios in the steel (BTV16)

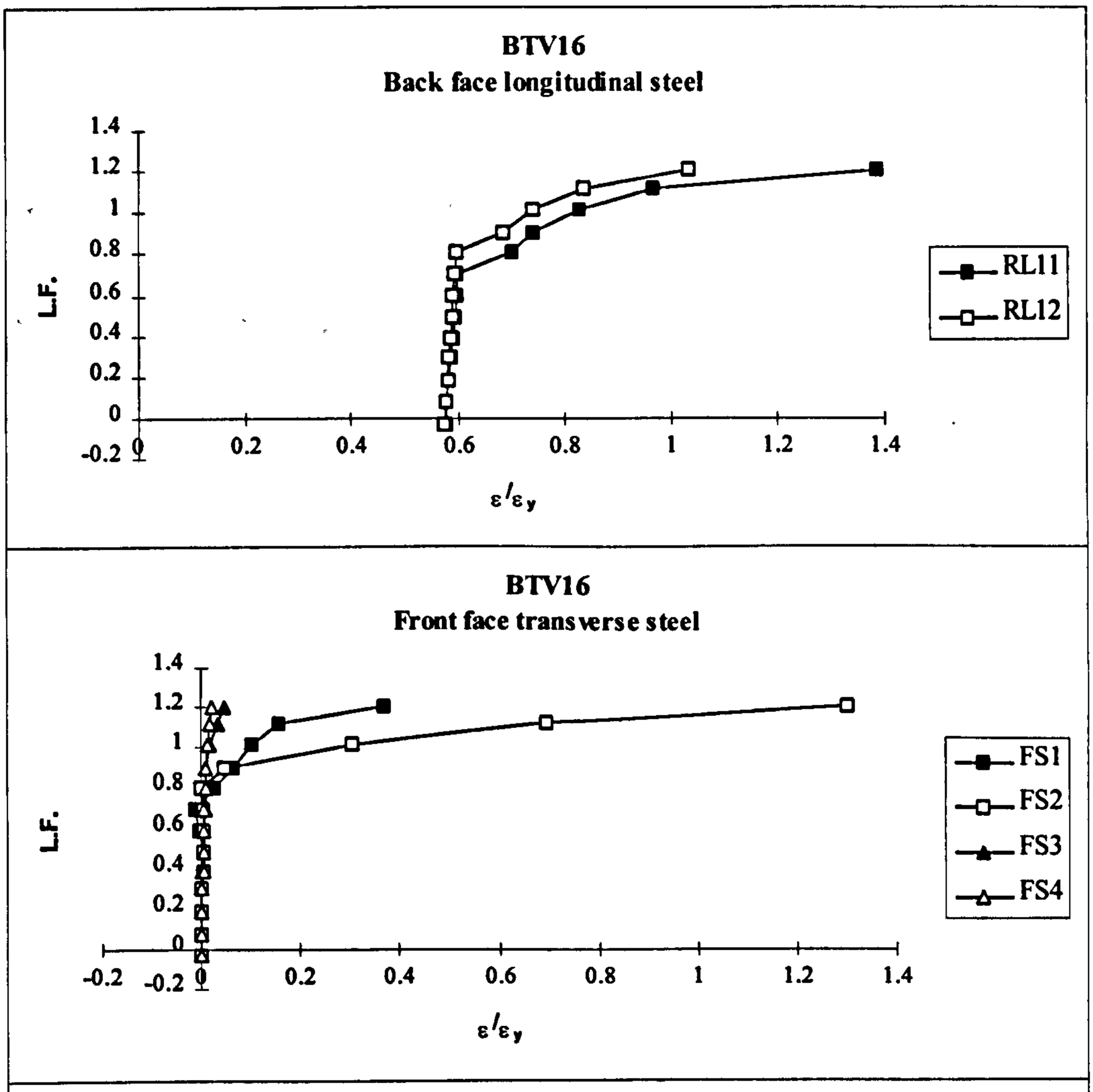

Fig. 11.9: Continued

BTV17: T_d=39kN.m., M_d=32.89kN.m., V_d=41.08kN., T_d/M_d=1.19, τ_{tor}/τ_{shr}=3.04

Inclined (50°) cracks appeared on all faces at 50% of design load. With an increase of load, more cracks developed until failure happened at 97% of load by a major crack opening in the bottom, back and top faces. The average crack width

before failure load was 0.4mm. Figure 11.10 shows crack development and figure 11.11 shows strain in the prestressing wires and transverse steel. The average strain ratio in the front side wire was 0.85 and in the rear side wire was 0.71. In the stirrups, the average strain ratio in the front face was 0.59 and in the back face was 0.41.

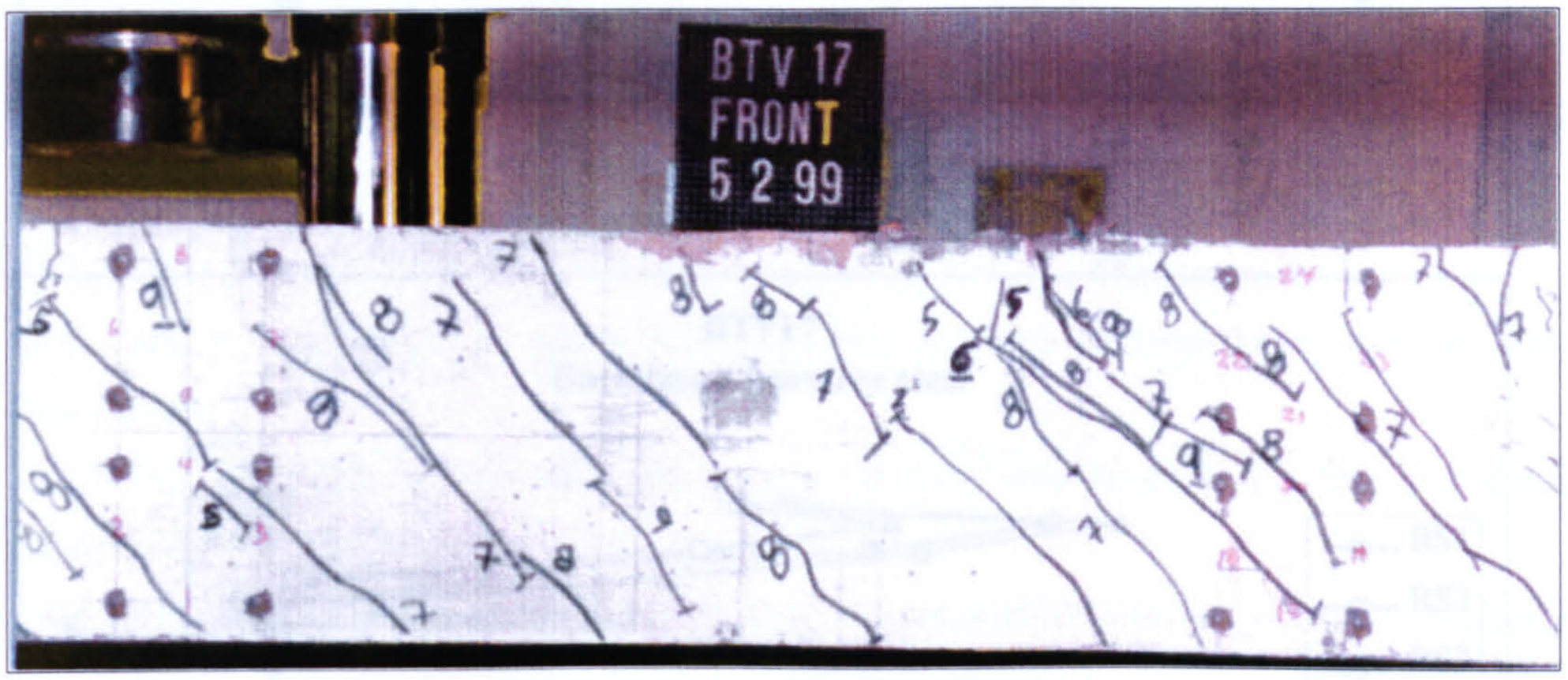

Fig. 11.10: Crack development in the front face (BTV17)

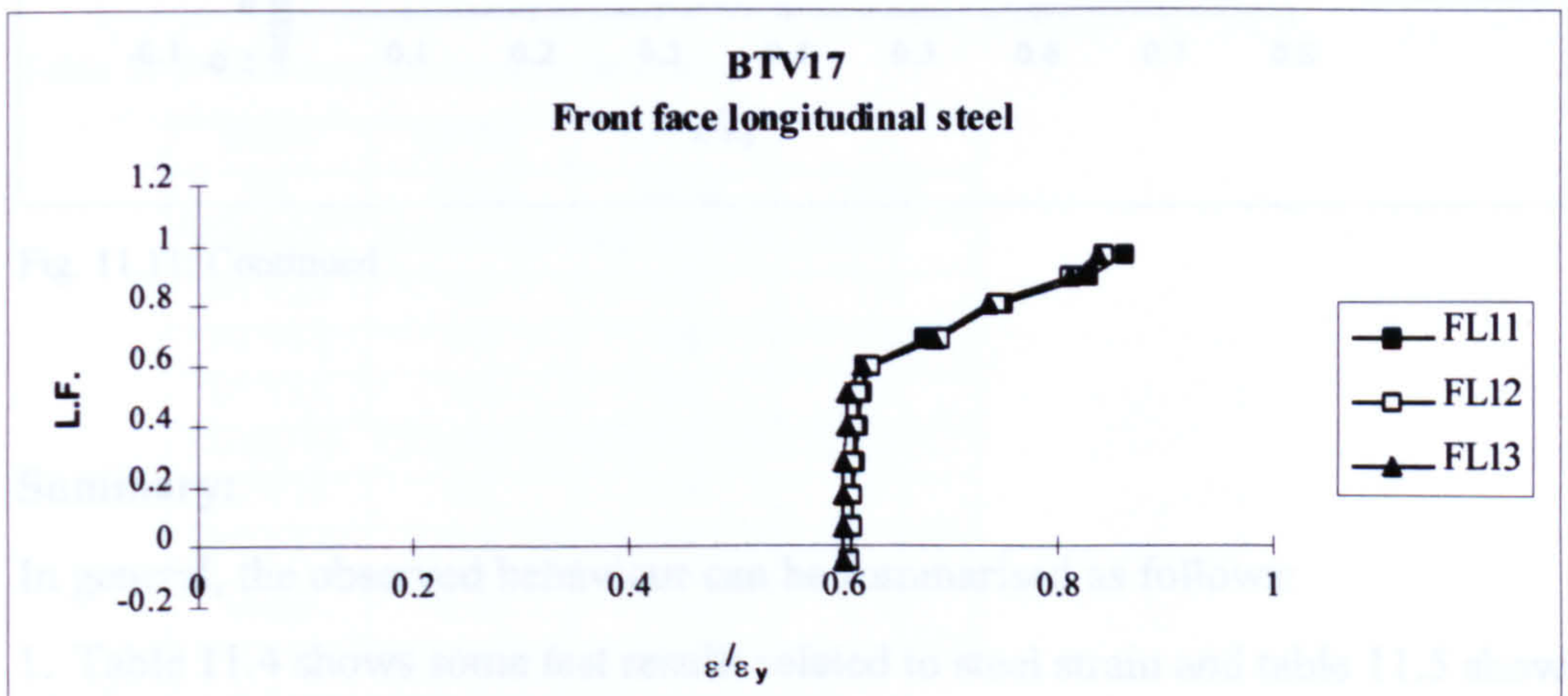

Fig. 11.11: Strain ratios in the steel (BTV17)

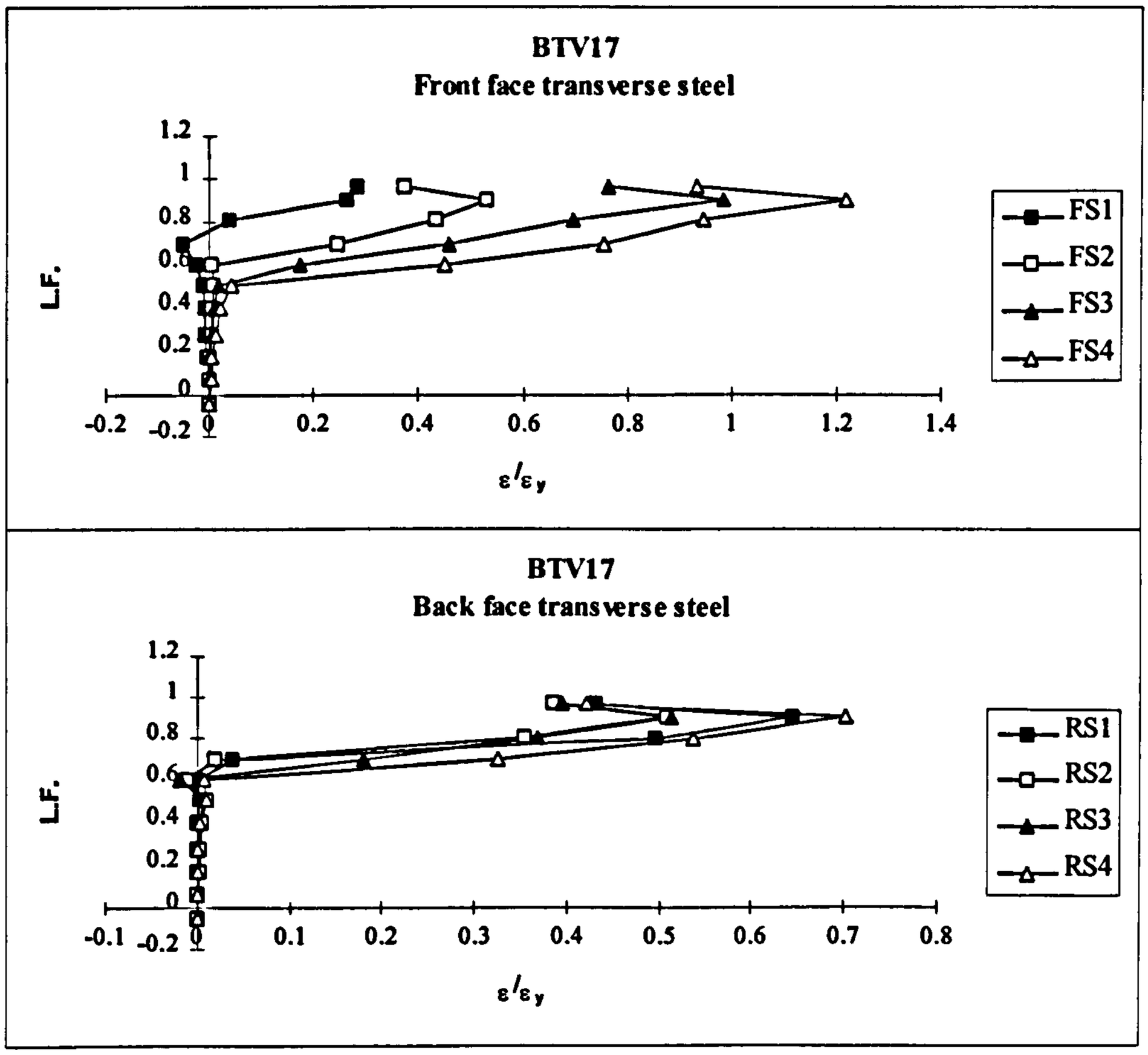

Fig. 11.11: Continued

Summary:

In general, the observed behaviour can be summarised as follows:

1. Table 11.4 shows some test results related to steel strain and table 11.5 shows test results related to deflection.
2. In the case of beams in which bending was dominant ($T_d/M_d<1$) almost vertical cracks started in the bottom face and at the lower half of the front and rear sides. These cracks were followed by inclined cracks in succeeding load increments until they first appear in the top flange at about 80% of failure load. In the beams where torsion was dominant ($T_d/M_d>1$), inclined cracks extended into the bottom face one increment after they were formed in the front and rear sides. In both groups, the smaller the ratio T_d/M_d, the closer is the angle of crack to vertical. In all beams, if vertical cracks occur, they are present only in the bottom face and at the lower half of the front and rear sides.

Table 11.4: Test results related to steel strain

Beam No.	First yield data				Maximum strain measured data			
	FYL	LFL	FYS	LFS	$(\varepsilon/\varepsilon_y)$MFL	MFL	$(\varepsilon/\varepsilon_y)$MFS	MFS
Group C: Reinforced concrete solid beams								
BTV13	FL14	1.1	FS3	1	1.6	FL14	1.5	FS3
BTV14	FL11	1.3	FS4	1.3	1.67	FL12	1.2	FS4
BTV15	-	-	FS4	0.89	0.79	FL13	1.3	FS4
Group D: Partially prestressed concrete solid beams								
BTV16	FL11	1.2	FS2	1.2	1.4	FL11	1.3	FS2
BTV17	-	-	-	-	0.86	FL11	1.2	FS4

FYL, FYS = Location of the first yield in the longitudinal steel or stirrup respectively

LFL, LFS = Load factor at which first yield was recorded in longitudinal steel or stirrup respectively

$(\varepsilon/\varepsilon_y)$MFL, $(\varepsilon/\varepsilon_y)$MFS = Maximum strain ratios in front web longitudinal steel and stirrups respectively

MFL, MFS = Location of maximum strain in front web longitudinal steel and stirrups respectively

Table 11.5: Test results related to deflection

Beam No.	LFCR Ratio	LFCW Ratio	Δ mm
Group C: Reinforced concrete solid beams			
BTV13	0.5	0.6	7.2
BTV14	0.5	0.8	7.0
BTV15	0.4	0.6	0.3
Group D: Partially prestressed solid beams			
BTV16	0.7	0.9	13.2
BTV17	0.5	0.8	0.9
Mean	0.52	0.74	5.72

LFCR = Load factor when first crack was noticed

LFCW = Load factor when the average crack width was 0.3mm

Δ = Maximum vertical displacement at mid-span of bottom flange

3. The average crack width when the first crack appeared in the top face in the reinforced beams was 0.47mm and in the partially prestressed beams was 0.40mm.
4. All beams with bending dominant (T_d/M_d<1) reached the displacement limit span/250 while the ones with torsion dominant (T_d/M_d>1) experienced relatively smaller displacement.
5. In the beams with T_d/M_d<1, the longitudinal steel or prestressing wires in the front face yielded or reached yield strain while slightly less strain was recorded in the ones with T_d/M_d>1. In the back face, only the prestressing wires in BTV16 yielded. With exception to BTV16, the transverse steel in the front face yielded or reached near yield strain. In the stirrups of the back face, negligible strain was recorded in all beams.
6. Both beams BTV15 and BTV17 (T_d/M_d=1.19) failed slightly below design load while beams BTV14 and BTV16 (T_d/M_d=0.26) failed above the design load and BTV13 (T_d/M_d=0.51) failed just above design load. The experimental to design failure load L_e/L_d is shown in table 11.6.

Table 11.6: Ratios of loads

Beam No.	T_d/M_d Ratio	τ_{tor}/τ_{shr} Ratio	Test Result Ratios		
			L_e/L_d	L_c/L_d	L_e/L_c
Group C: Reinforced concrete solid beams					
BTVI3	0.51	1.39	1.08	1.10	0.98
BTVI4	0.26	0.69	1.30	1.35	0.96
BTVI5	1.19	3.04	0.89	0.95	0.93
Group D: Partially prestressed concrete solid beams					
BTVI6	0.26	0.69	1.20	1.20	1.00
BTVI7	1.19	3.04	0.97	0.95	1.02
Mean			1.09	1.11	0.98

L_e, L_d, L_c = Experimental, design and computed failure loads.

11.3: Comparison between the experimental and computational results

In order to obtain a finite element solution for the tested beams, the 3-D program was used for the non-linear analysis. Measured values of concrete cube compressive strength and steel tensile strength were used. The concrete cylinder compressive strength, Young's modulus, Poisson's ratio, concrete tensile strength, shear retention and tension stiffening were used as explained in chapter 10.

11.3.1: Load displacement relationship

Figure 11.12 shows the vertical displacement at the centre of the bottom face of each beam. It is clear from this figure that, in general, a good agreement was achieved between experimental and computational results in most cases except beams BTV13 and BTV16. In these two beams, observed displacements were larger than computed.

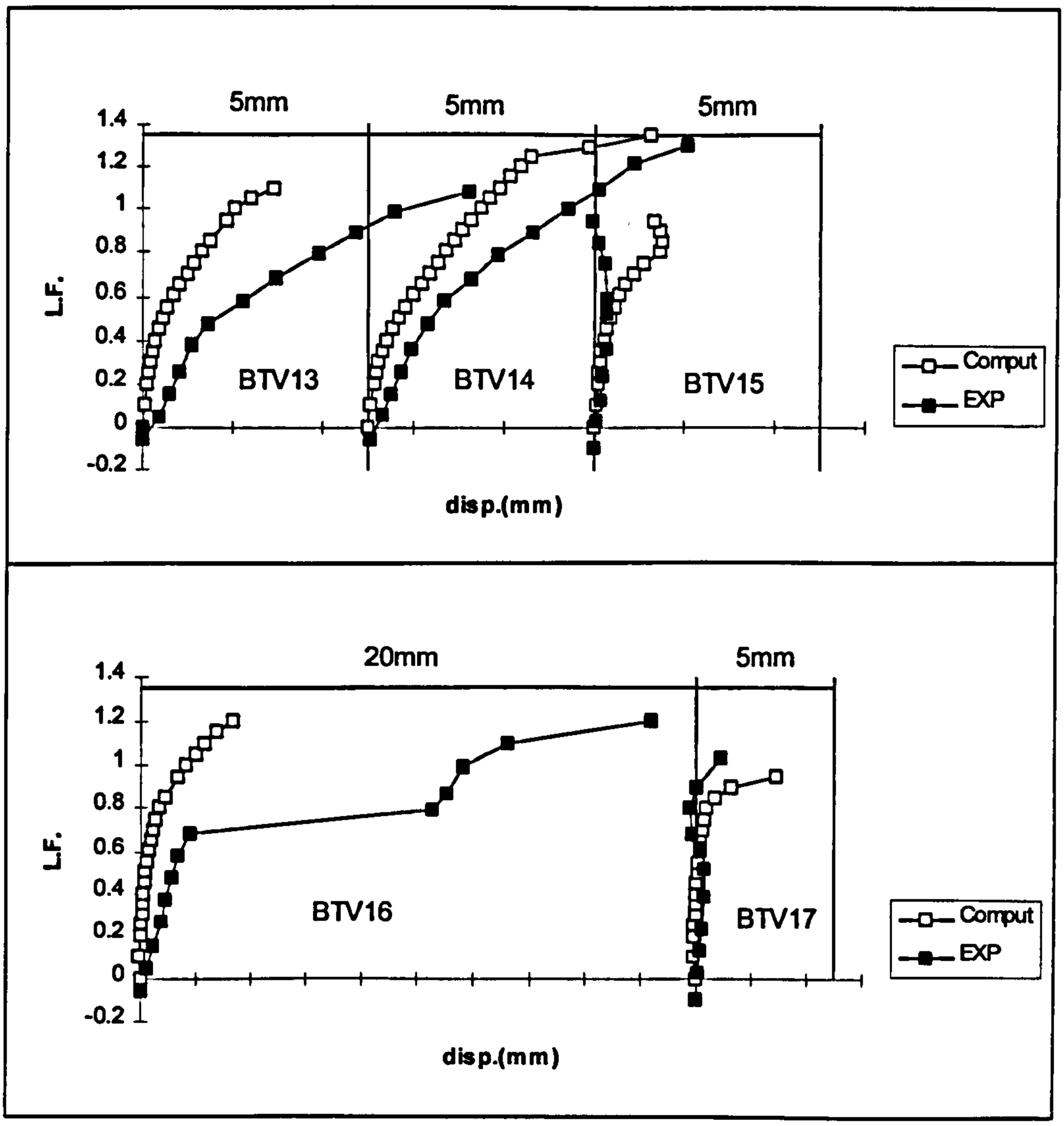

Fig. 11.12: Vertical displacement at mid-span of the bottom face

11.3.2: Strain in longitudinal steel

Figures 11.13-14 and the related figures in appendix B show very good agreement between the experimental and computational results in most cases for the longitudinal steel in the front and back faces. However, in beam BTV13 the observed strain in front face longitudinal steel was 24% larger than computed.

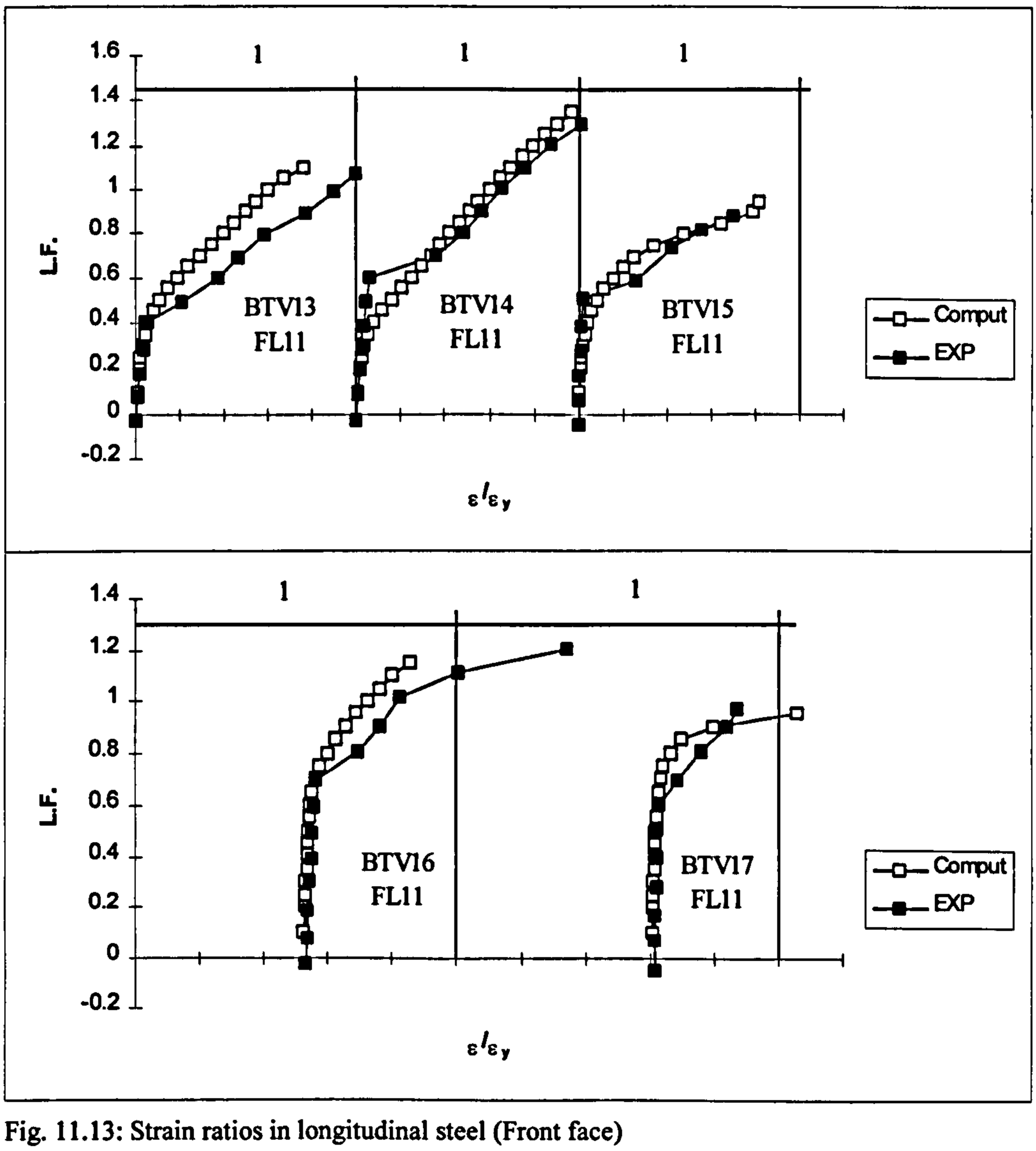

Fig. 11.13: Strain ratios in longitudinal steel (Front face)

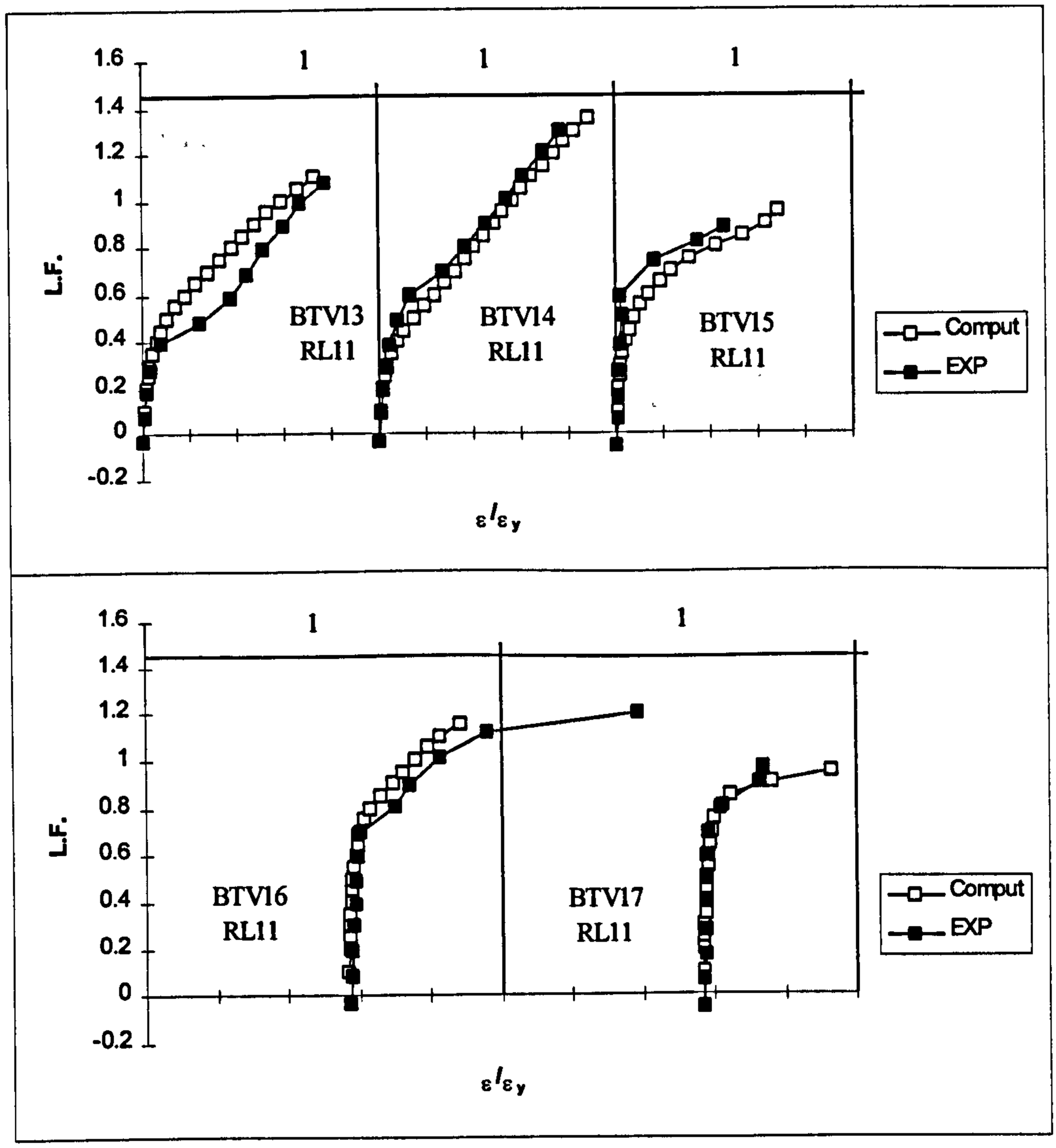

Fig. 11.14: Strain ratios in longitudinal steel (Rear face)

11.3.3: Strain in transverse steel

Figures 11.15-16 and the figures in appendix B show that, in general, an acceptable agreement between experimental and computational results was achieved.

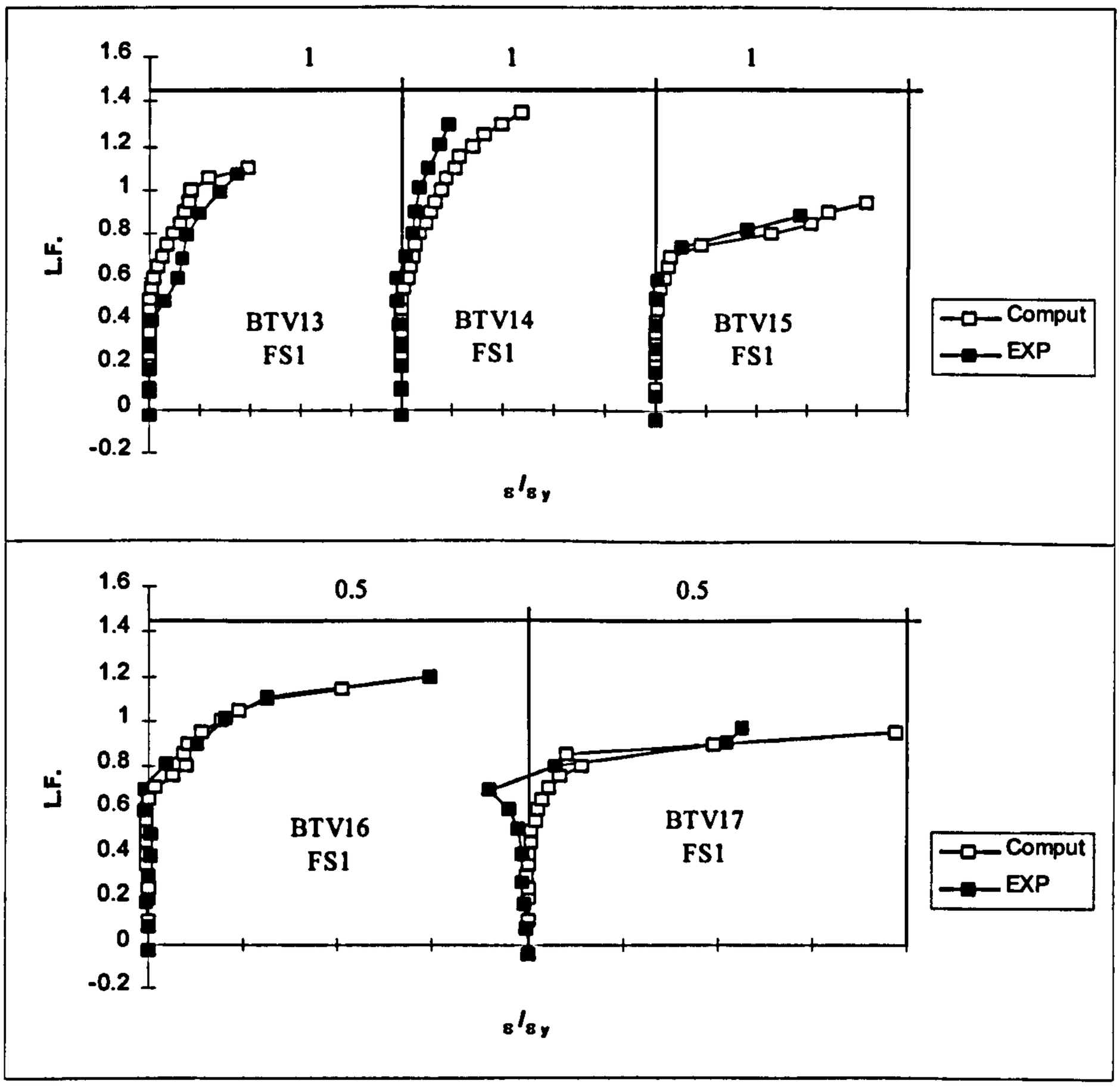

Fig. 11.15: Strain ratio in transverse steel (Front face)

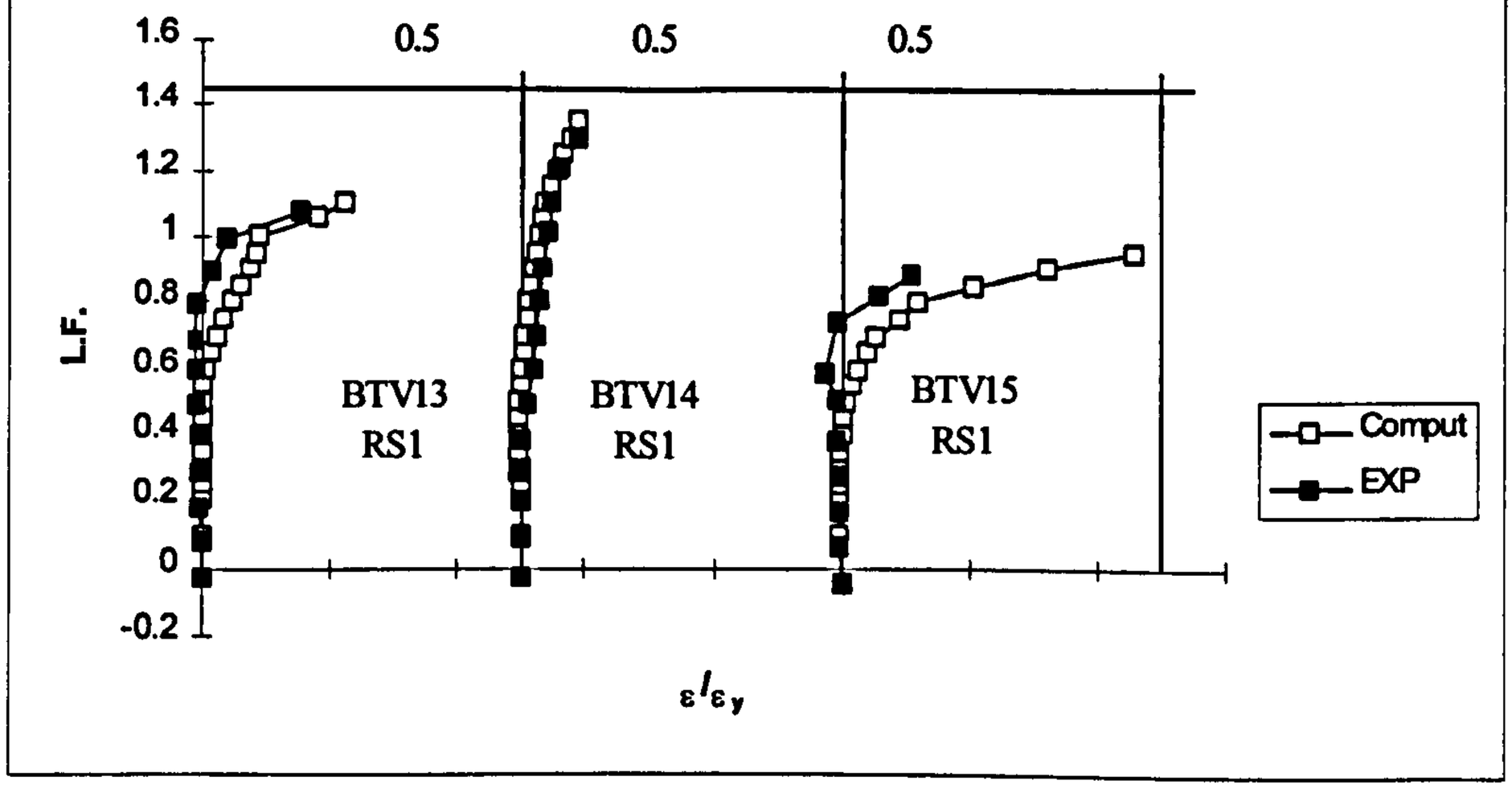

Fig. 11.16: Strain ratios in transverse steel (Back face)

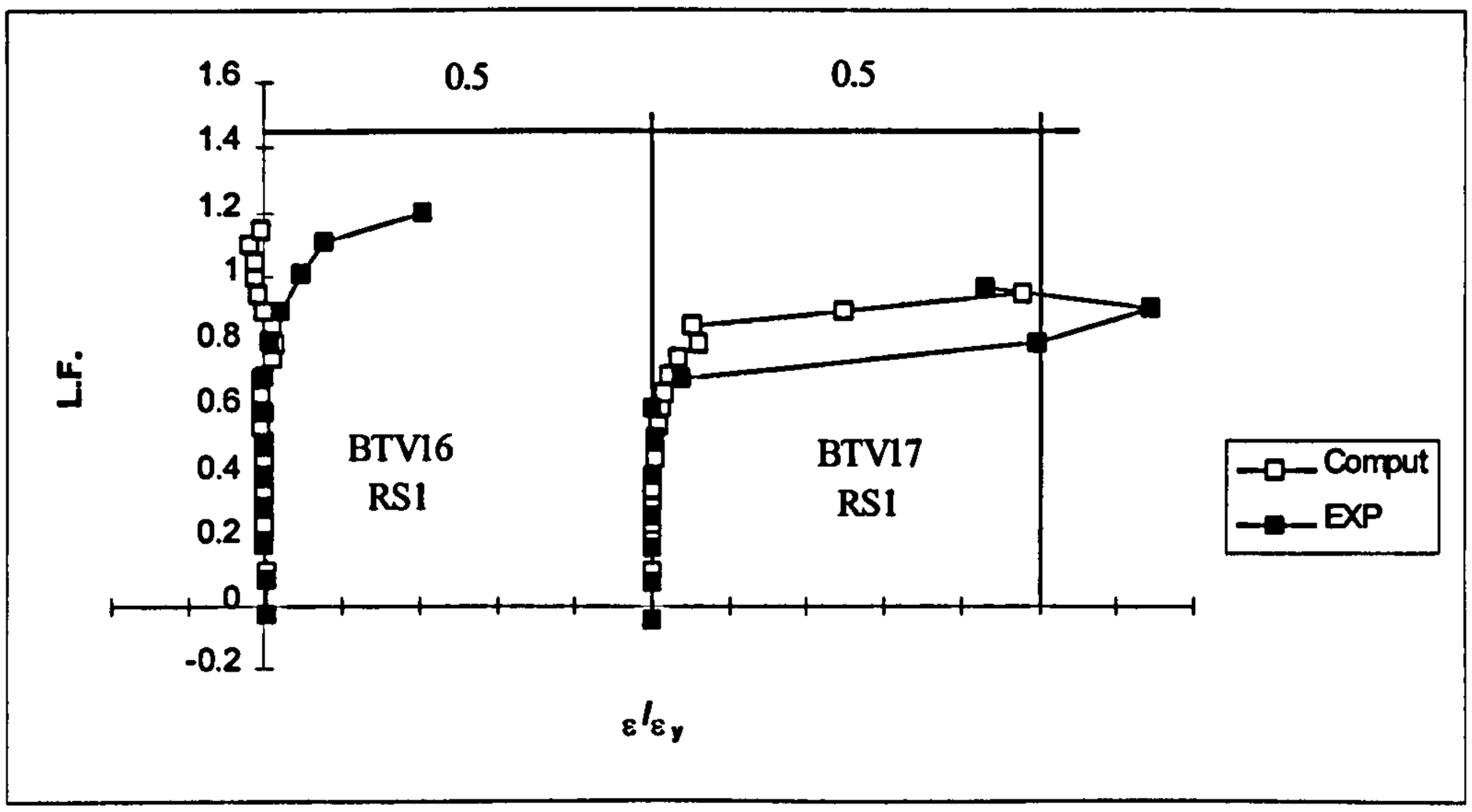

Fig. 11.16: Continued

11.3.4: Relative angle of twist

Figure 11.17 shows the experimental and computational relative angles of twist. These angles were calculated as explained in section 4.5.2.2 of chapter 4. It can be seen that, a good agreement has been achieved between experimental and computational results in most cases. However, in beam BTV17 the observed angle was larger than the computed one. In beams where torsion was dominant ($T_d/M_d>1$) the relative angle of twist was relatively larger than when the bending was dominant ($T_d/M_d<1$). For the same load combination, the partially prestressed beam BTV16 experienced smaller twist than the reinforced beam BTV14. However, the difference in the case of beams BTV15 and BTV17 was negligible.

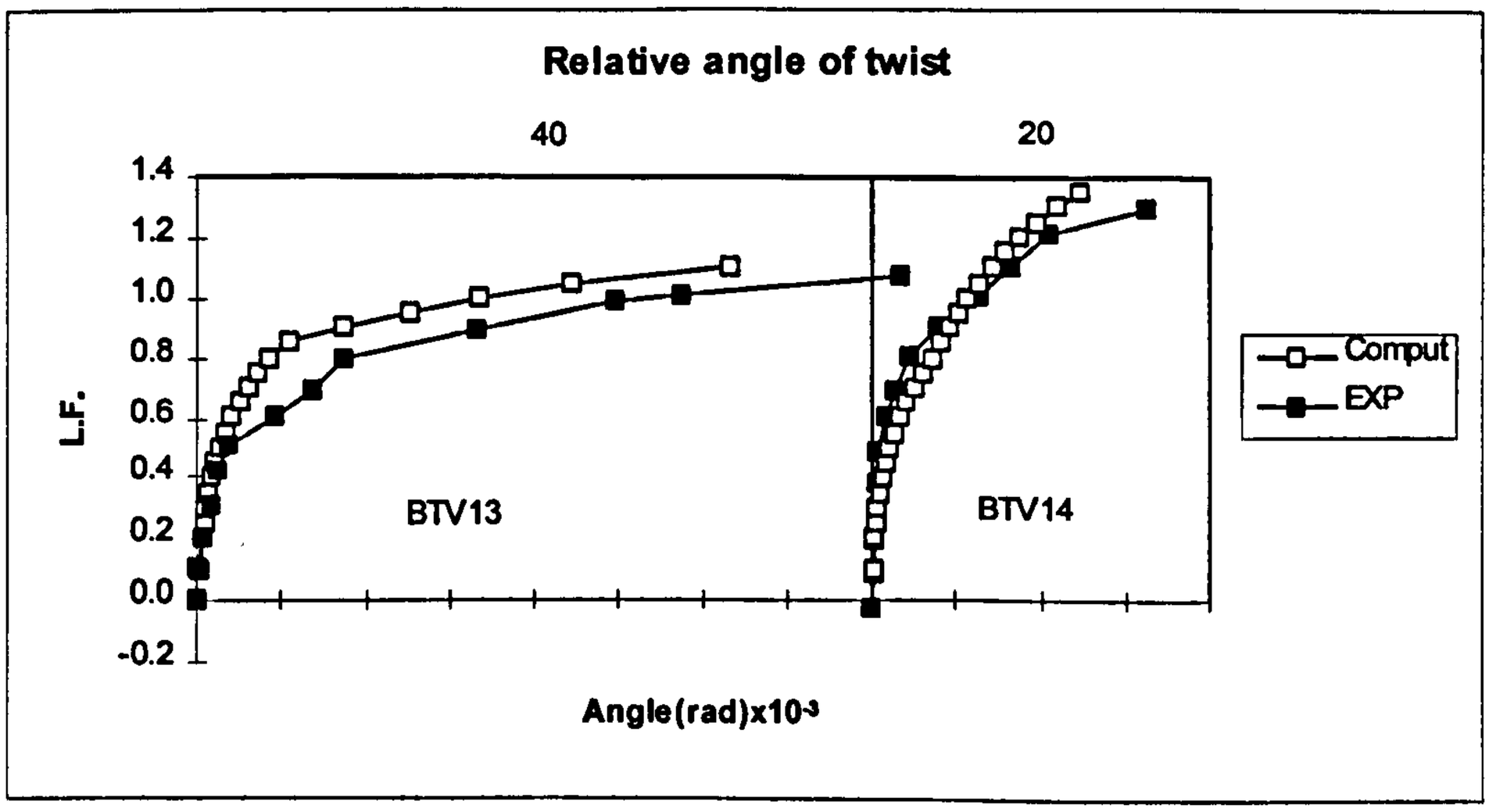

Fig. 11.7: Relative angle of twist

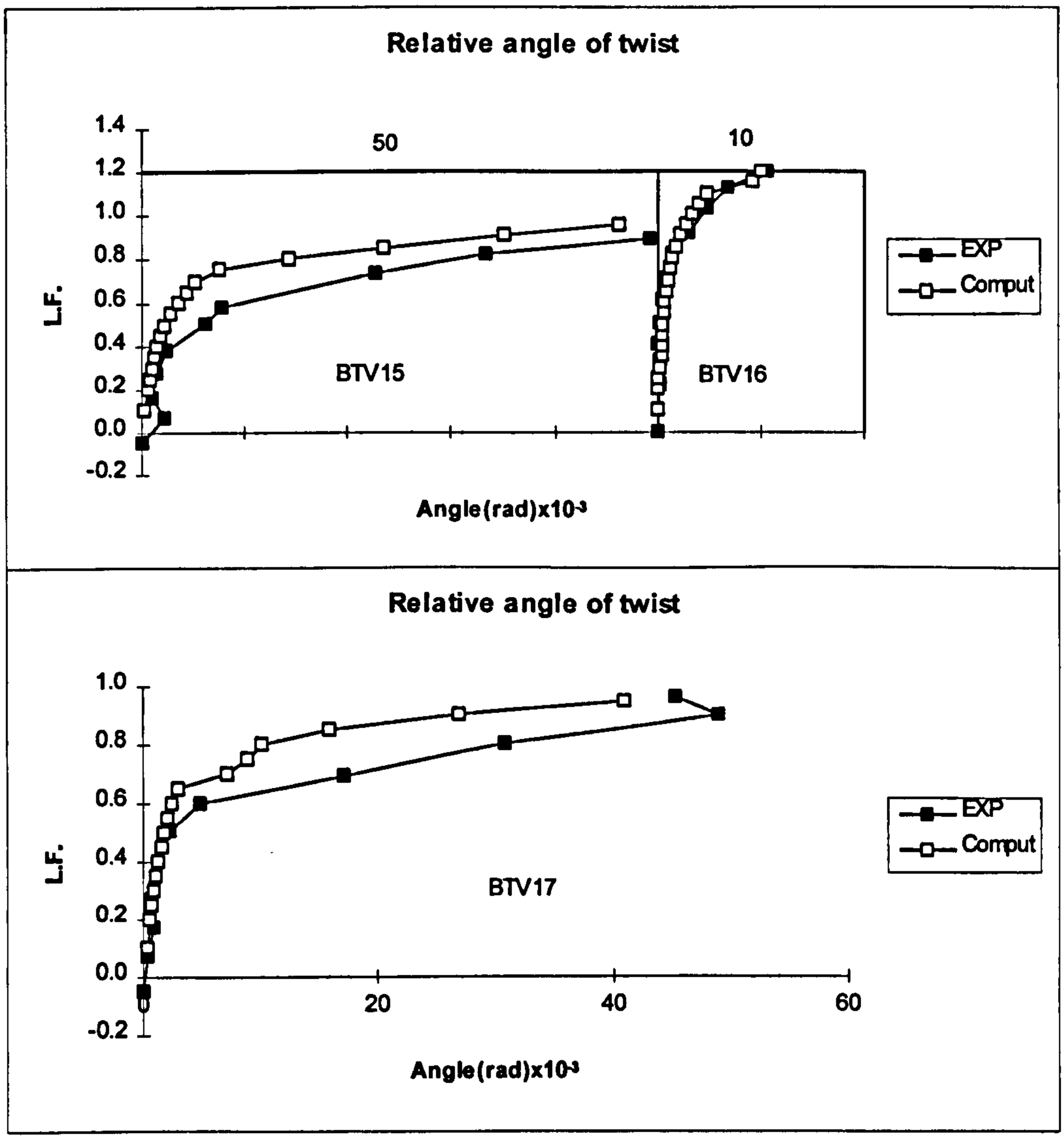

Fig. 11.7: Continued

11.3.5: Failure load

Table 11.6 shows good agreement between experimental L_e and computational L_c failure loads. However, Beams BTV14 and BTV16 (T_d/M_d=0.26) failed at 30% and 20% above design load respectively and beam BTV15 (T_d/M_d=1.19) failed at 11% below design load. In general beams with T_d/M_d<1 failed at slightly above design load and beams with T_d/M_d>1 failed at slightly below design load.

11.3.6: Crack pattern and mode of failure

Figures 11.18-21 show typical computed and observed crack development of the tested beams. In beams BTV13, BTV14 and BTV16 the mode of failure was mostly flexural where the beam experienced relatively large displacement and the flexural steel yielded. A small number of large cracks caused failure at the time of flexural

steel yielding. Beams BTV15 and BTV17 failed by diagonal cracking due to high torsional shear stress and the failure mode was less ductile with small displacement, less longitudinal steel strain and larger transverse steel strain than the bending dominant beams.

11.4: Conclusion

From the results presented in this chapter it can be concluded that the direct design procedure produces a good design for solid beams subjected to general loading conditions. However, in the case of very large torsion, beams fail slightly below the design load. The plastic stress distribution used for the design of reinforced solid beams and the elastic stress distribution adopted for the partially prestressed beams gave good results for beam failure load and steel yield. The average transverse steel used in the design of solid beams showed acceptable results with regards to economy knowing that excess steel is practically difficult to avoid. The steel in the regions where the shear stresses are additive, yielded or reached yield stress. The results from the 3-D finite element program was shown to be in a good agreement with the experimental results and therefore, proven to be a good tool for the prediction of beam behaviour and ultimate load of solid beams.

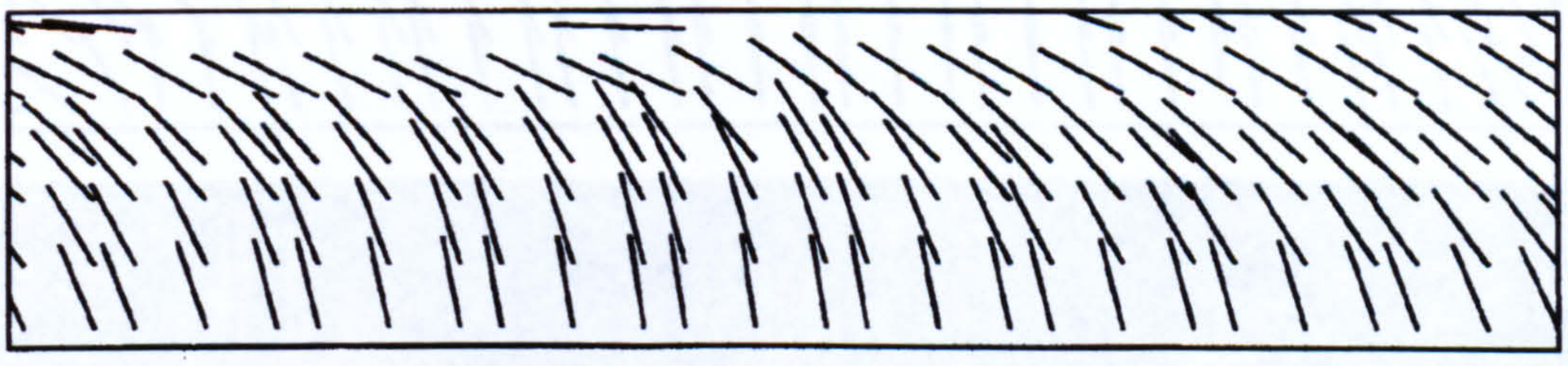

Fig. 11.18a: Crack development in the front face (BTV14)

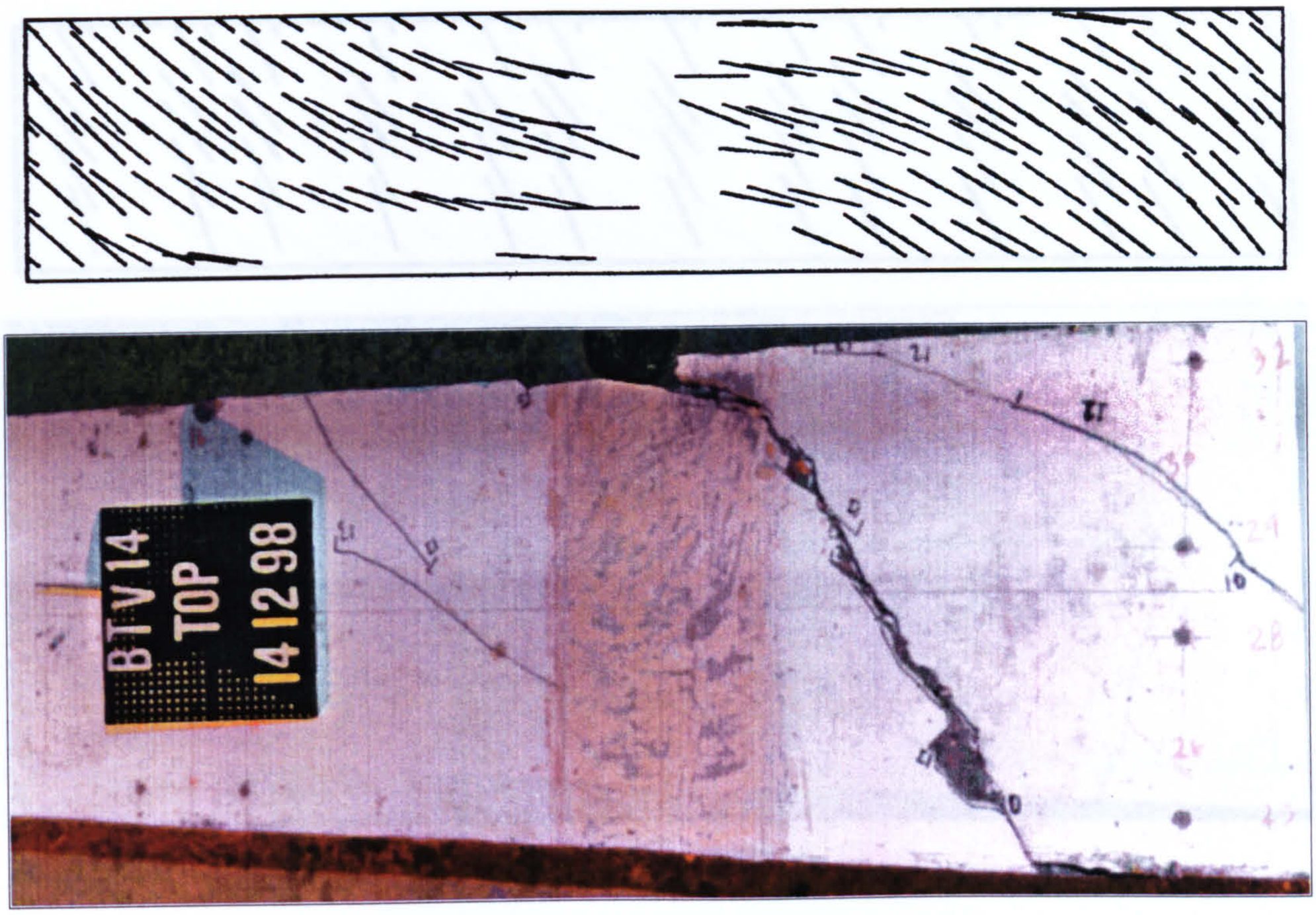

Fig. 11.18b: Crack development in the top face (BTV14)

Fig. 11.18c: Crack development in the rear face (BTV14)

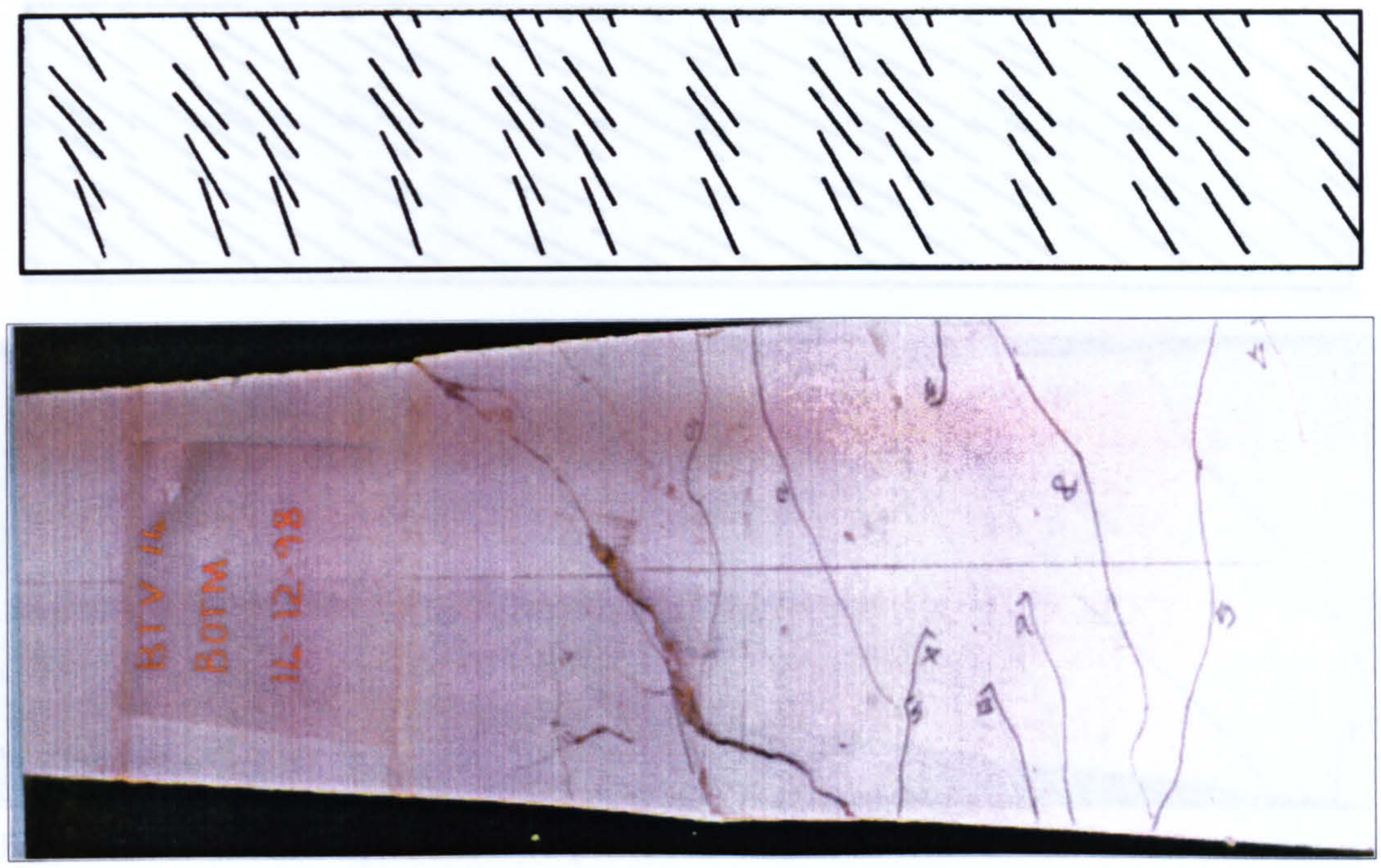

Fig. 11.18d: Crack development in the bottom face (BTV14)

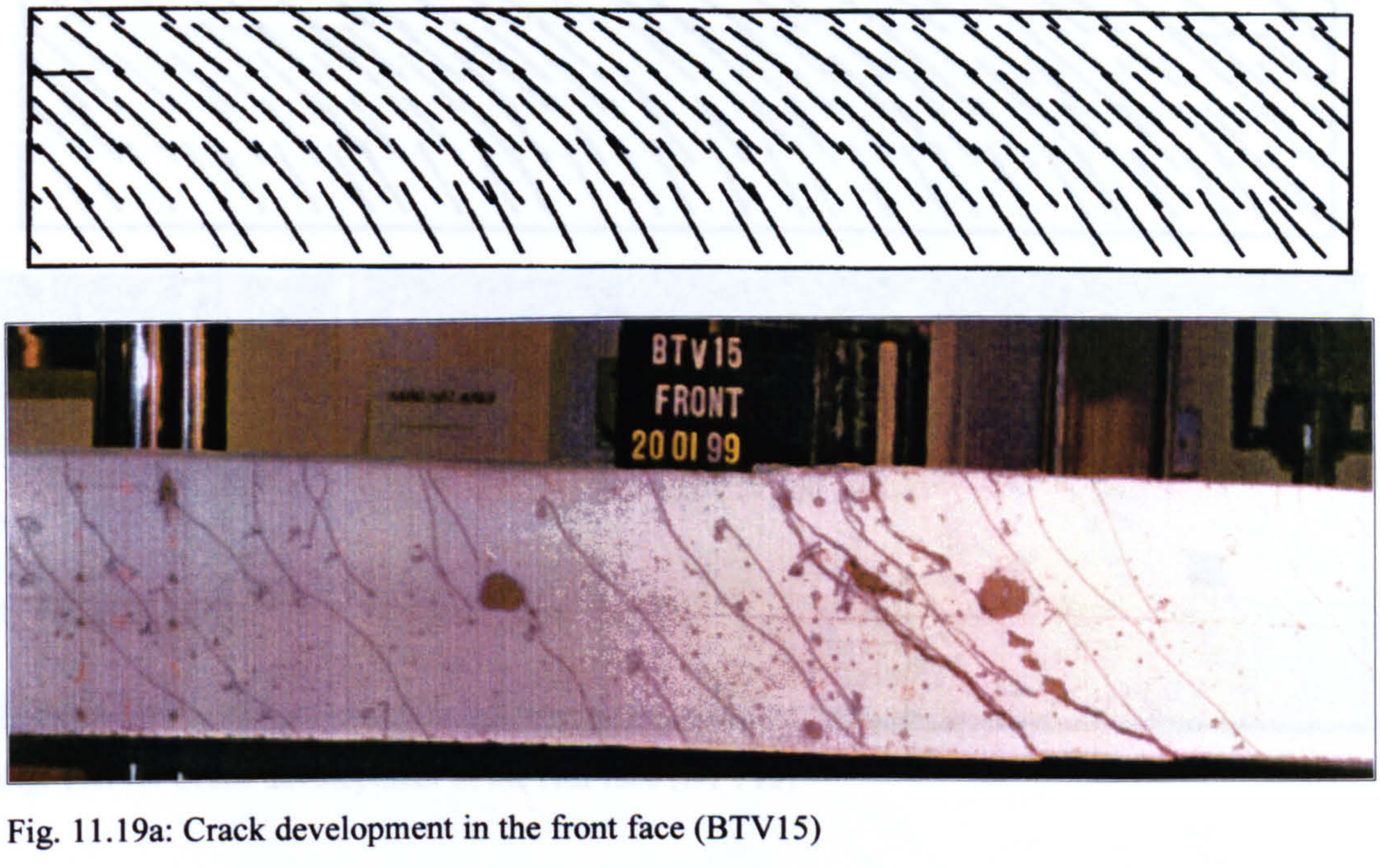

Fig. 11.19a: Crack development in the front face (BTV15)

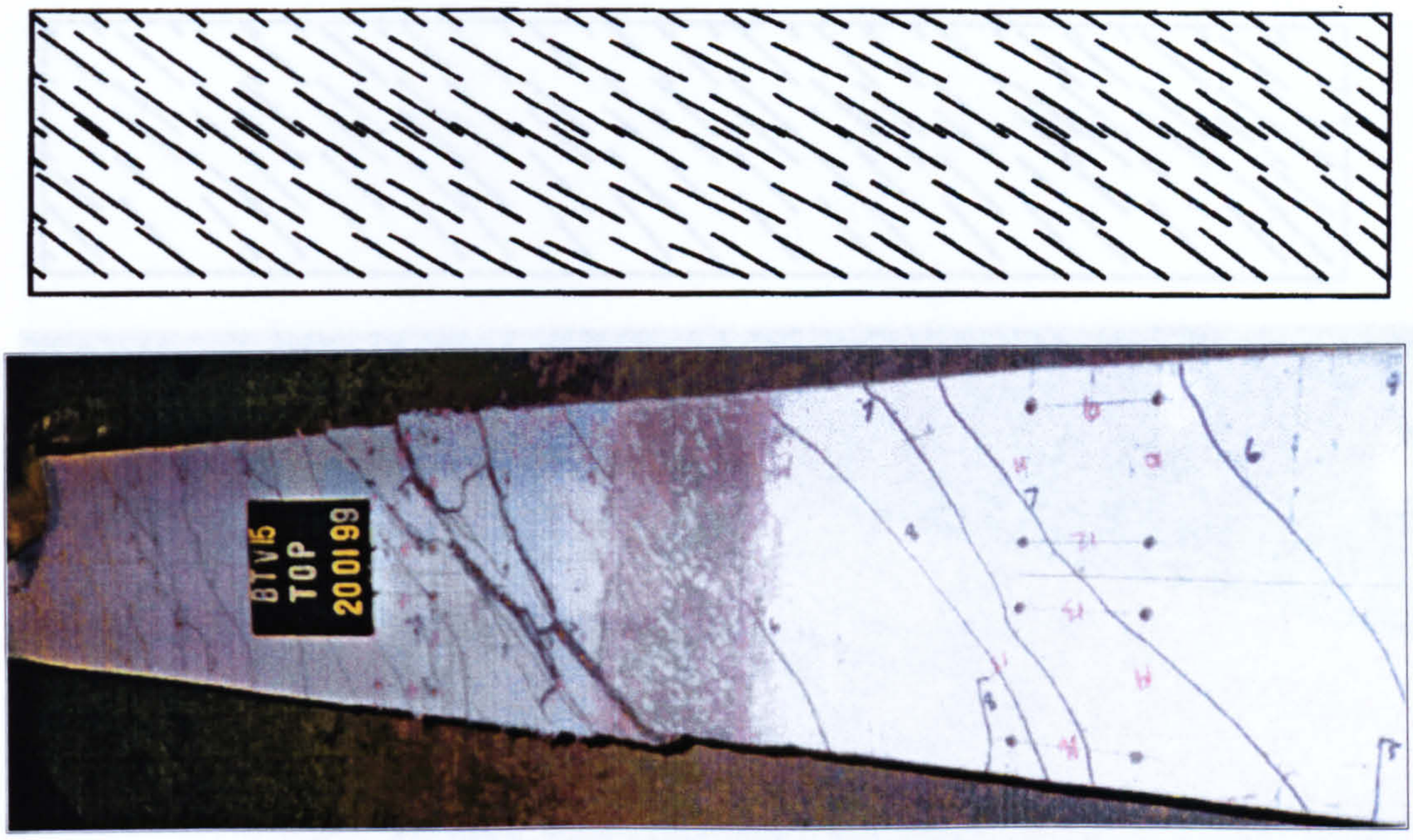

Fig. 11.19b: Crack development in the top face (BTV15)

Fig. 11.19c: Crack development in the rear face (BTV15)

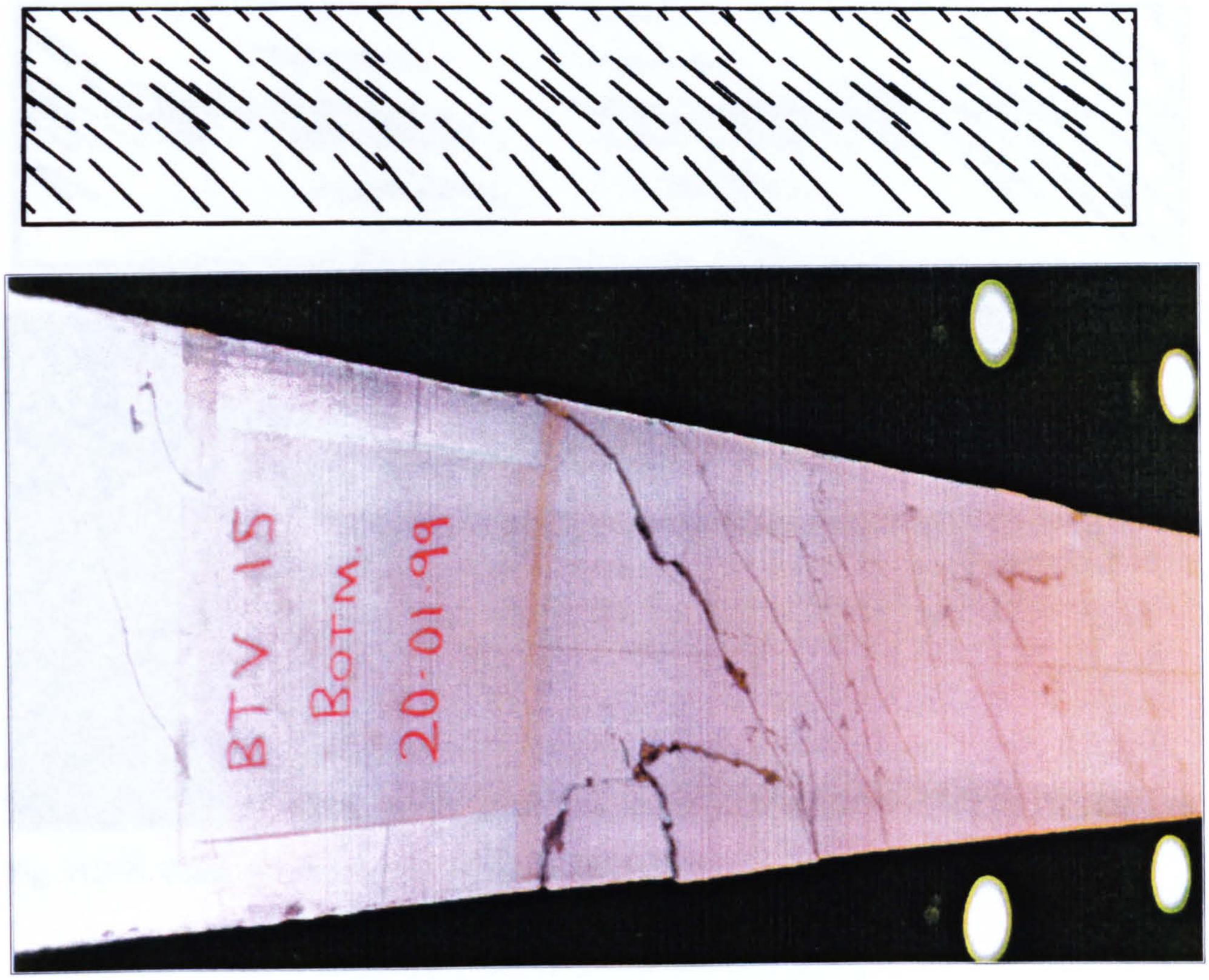

Fig. 11.19d: Crack development in the bottom face (BTV15)

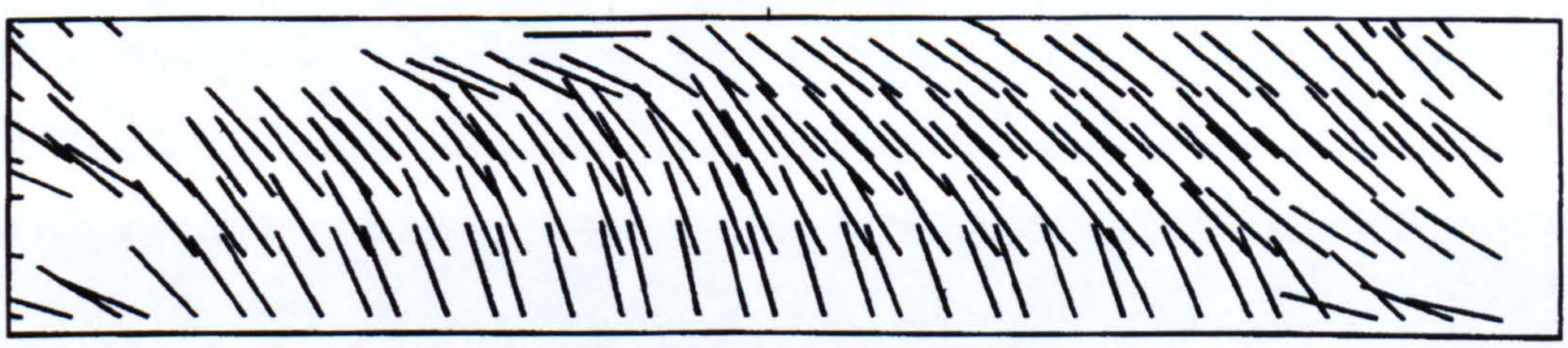

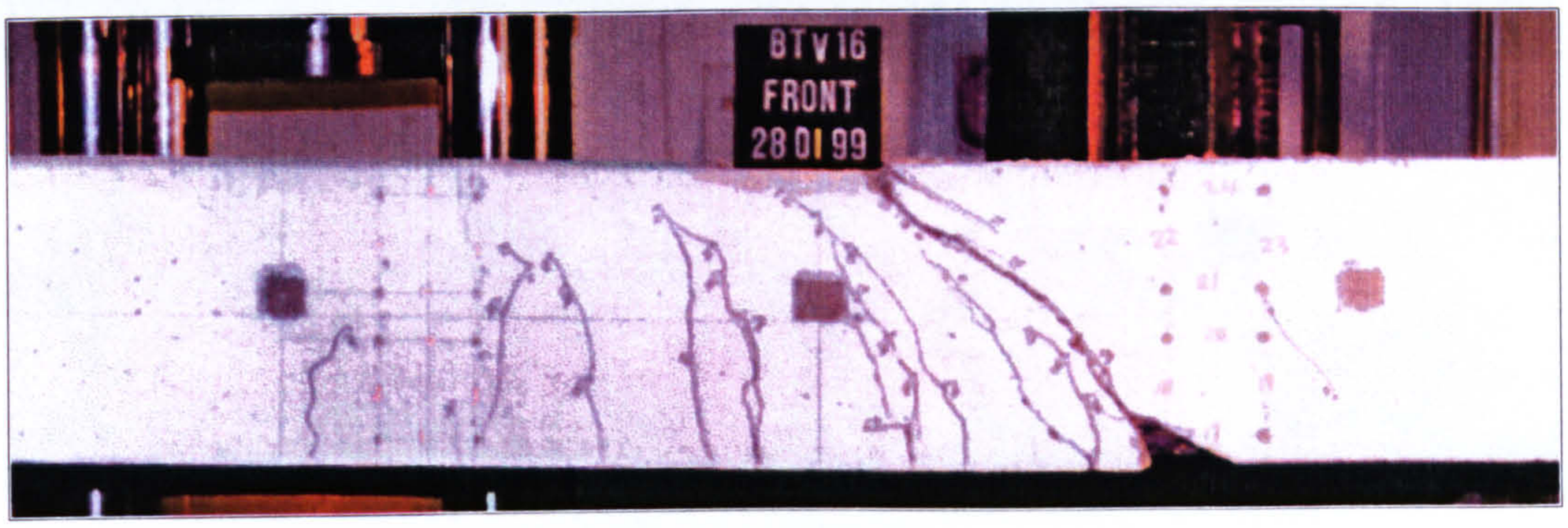

Fig. 11.20a: Crack development in the front face (BTV16)

Fig. 11.20b: Crack development in the top face (BTV16)

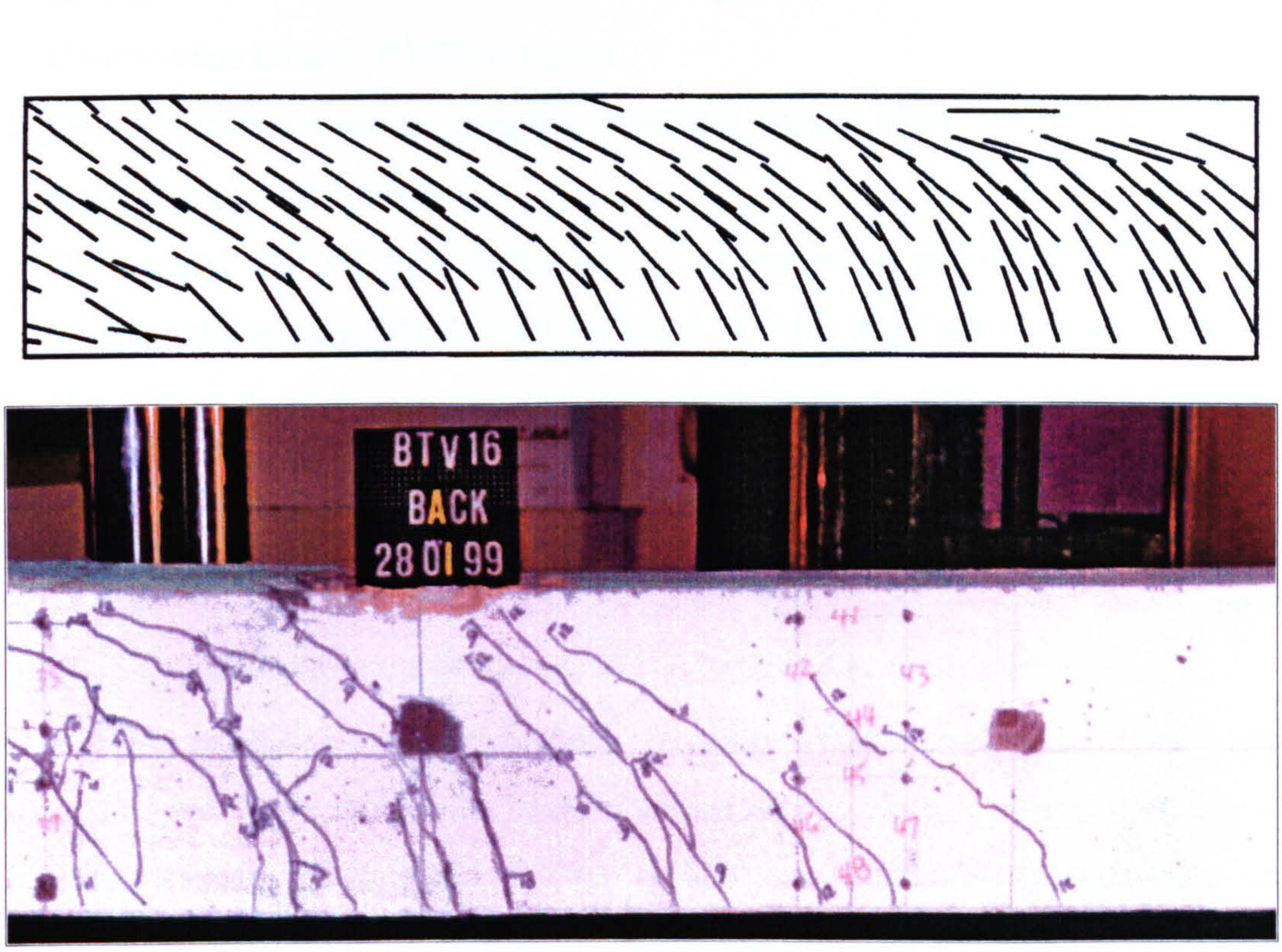

Fig. 11.20c: Crack development in the rear face (BTV16)

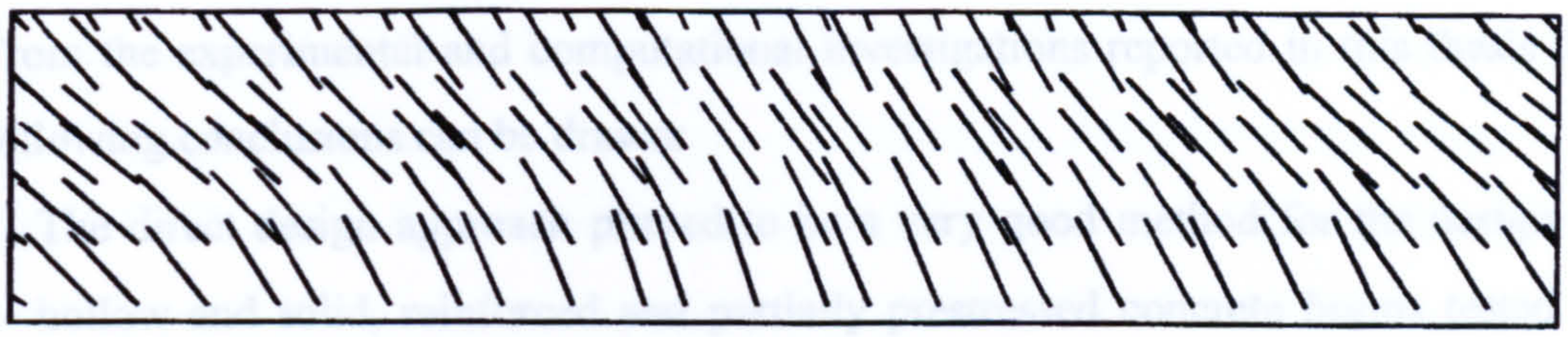

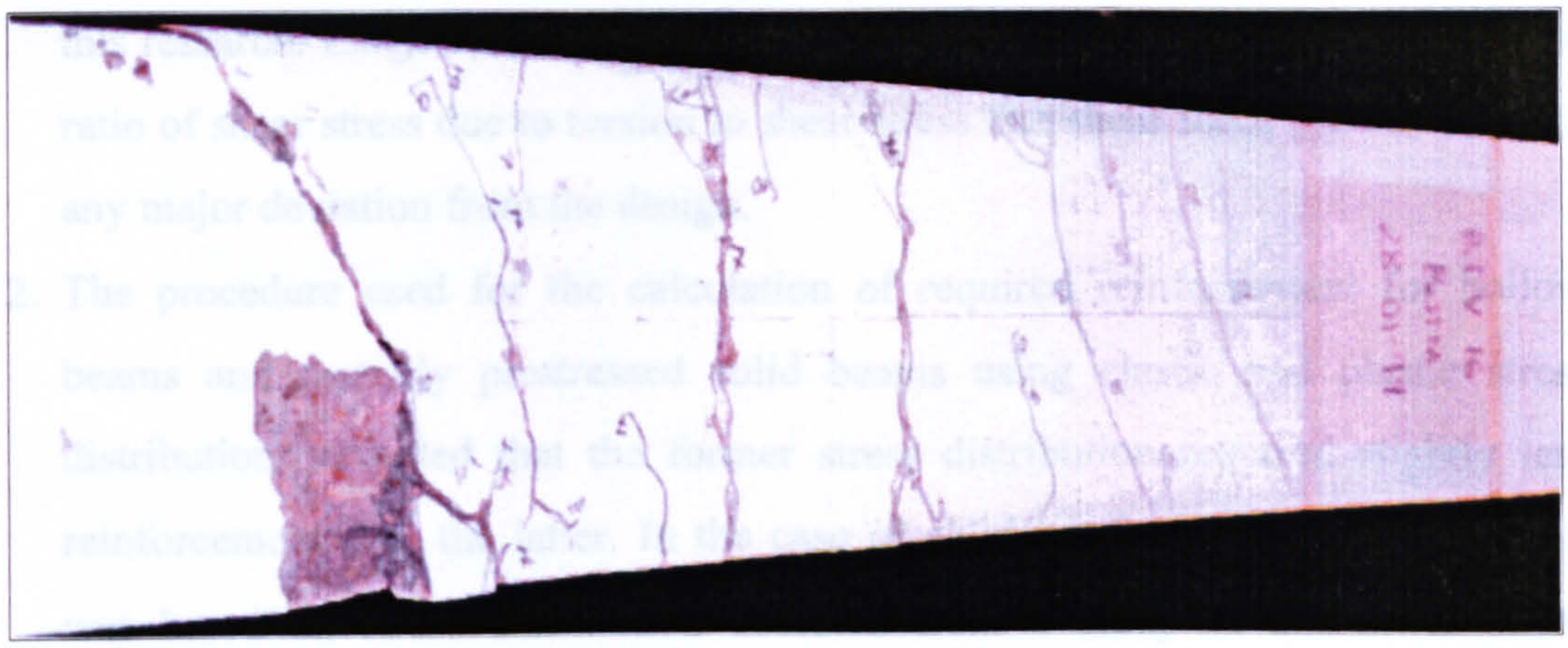

Fig. 11.20d: Crack development in the bottom face (BTV16)

12: Conclusions and recommendations

12.1: Conclusions

From the experimental and computational investigations reported in this thesis the following conclusions can be drawn:

1. The direct design approach proved to be a very good method for the design of hollow and solid, reinforced and partially prestressed concrete beams tested in this research. Large variations in the ratio of torsion to bending moment and the ratio of shear stress due to torsion to shear stress due shear force did not result in any major deviation from the design.
2. The procedure used for the calculation of required reinforcement for hollow beams and partially prestressed solid beams using elastic and plastic stress distributions revealed that the former stress distribution required slightly less reinforcement than the latter. In the case of solid reinforced beams, the design was based on stress distribution obtained from a study of non-linear stress analysis carried out in chapter 10.
3. Results from the 2-D finite element program showed good agreement with experimental results of hollow beams.
4. The 3-D finite element program predicted results close to the experimental behaviour of solid beams.
5. The method used for the construction of hollow beams proved to be particularly good in maintaining almost exact thickness of walls and location of steel cage.
6. The simple method used for constructing partially prestressed beams was very successful.

12.2: Recommendations for further work

Further research is needed to solve problems encountered in this study and to expand the use of the direct design method to different type of structures.

1. A study is needed to experimentally investigate the reason for the beams with large T/M ratio failing at slightly below design loads. The use of longer centreline in calculating the enclosed area of cross-section A_o for torsional shear stress results in less steel area which may cause premature failure load in the case of beams resisting large torsion. Some numerical examples are shown in appendix C.

2. The design of solid beams needs further investigation on the selection of a reasonable stress distribution which can be used in the direct design method. The present approach clearly leads to excessive shear links.

12.3: Design procedure

Appendix D shows design recommendations for hollow and solid reinforced and partially prestressed beams.

Appendix A

Numerical design example using the Truss Analogy.

Calculate the longitudinal and transverse reinforcement required to resist 32kNm bending moment, 40kN shear force and 13kNm torsion, using the truss analogy. The cross-section is 300x300mm with 50mm wall thickness. Assume under reinforced section and the longitudinal and transverse steel yield stress is 500N/mm^2.

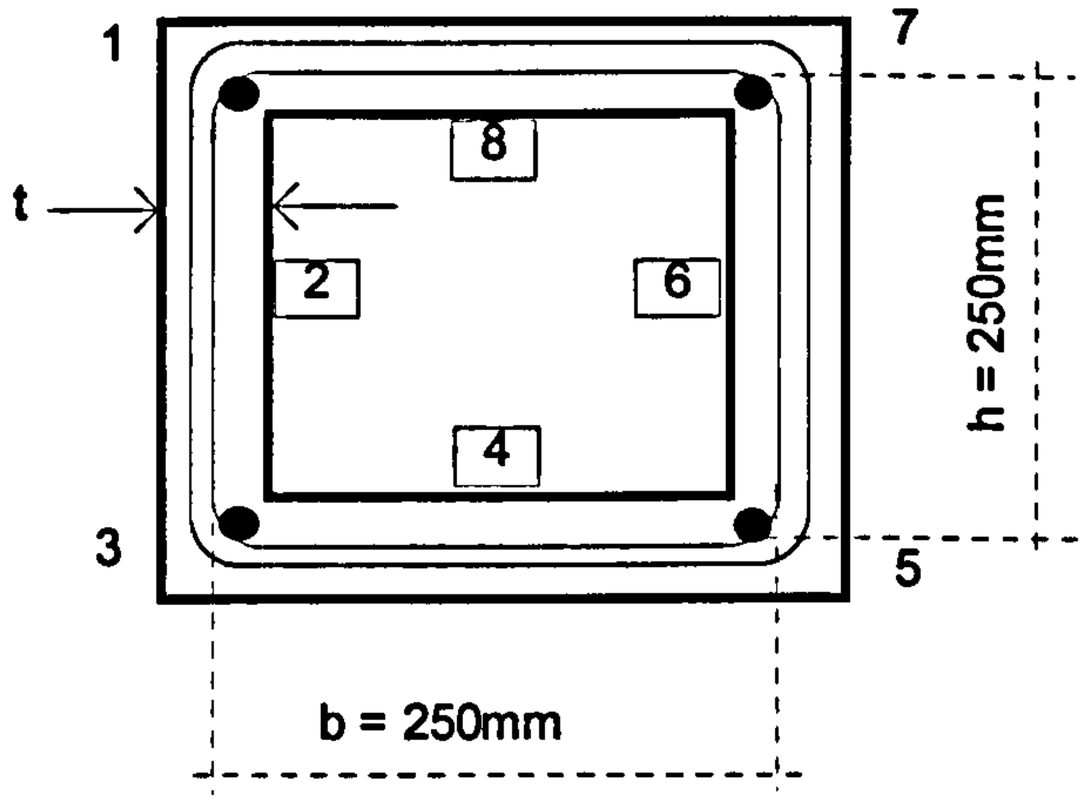

Fig. A1: Definitions and dimensions

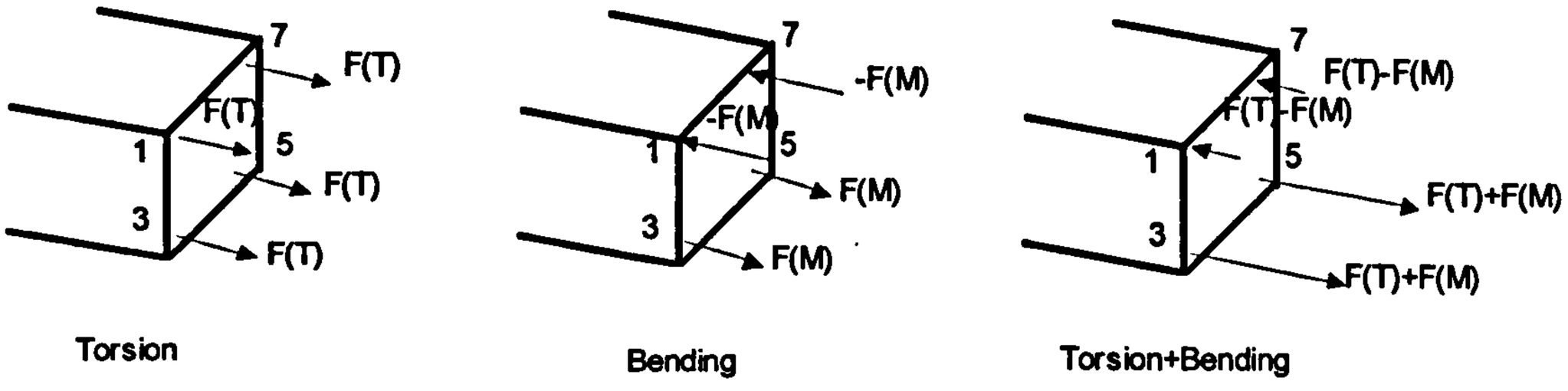

Fig. A2: Superposition of normal forces due to torsion and bending

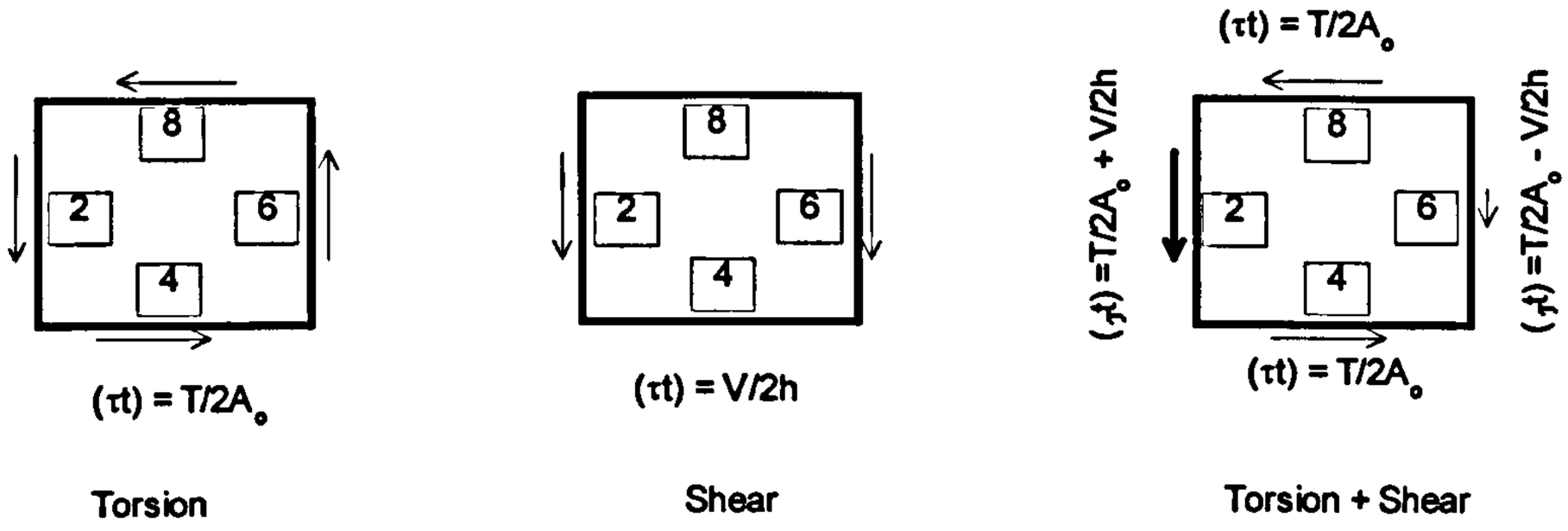

Fig. A3: Superposition of shear stresses due to torsion and shear force

Solution:

$M = 32\text{kNm}.$

$V = 40\text{kN}.$

$T = 13\text{kNm}.$

$h = b = 250\text{mm}.$

$f_y = f_{yv} = 500\text{N/mm}^2.$

$A_o = 250\text{x}250 = 62500\text{mm}^2.$

The bare numbers represent the corners and the numbers in the squares represent the sides (Fig. A1). The normal stress due to bending and that due to torsion are added at side 4 and subtracted at side 8 (Fig. A2). The shear stress due to torsion and that due to shear force are added at side 2 and subtracted at side 6 (Fig. A3).

Longitudinal Reinforcement:

For ease, assume four corner longitudinal bars.

Due to Bending:

$$A_s(M)_3 = A_s(M)_5 = \frac{M}{2hf_y} = \frac{32x10^6}{2x250x500} = 128mm^2.$$

Due to Torsion and Shear:

Side2: (Shear stresses added)

$$A_s(T,V)_1 = A_s(T,V)_3 = \frac{1}{2f_y}\left(\frac{Th}{2A_o} + \frac{V}{2}\right)\cot\alpha$$

$$= \frac{1}{2x500}\left(\frac{13x10^6x250}{2x62500} + \frac{40x10^3}{2}\right)\cot\alpha$$

$$= 46\cot\alpha\, mm^2.$$

Side6: (Shear stresses subtracted)

$$A_s(T,V)_5 = A_s(T,V)_7 = \frac{1}{2f_y}\left(\frac{Th}{2A_o} - \frac{V}{2}\right)\cot\alpha$$

$$= \frac{1}{2x500}\left(\frac{13x10^6 x250}{2x62500} - \frac{40x10^3}{2}\right)\cot\alpha$$

$$= 6\cot\alpha\, mm^2 .$$

Sides 4 & 8: (Effect of torsion alone)

$$A_s(T,V)_3 = A_s(T,V)_5 = A_s(T,V)_7 = A_s(T,V)_1 = \frac{1}{2f_y}\left(\frac{Tb}{2A_o}\right)\cot\alpha$$

$$= \frac{1}{2x500}\left(\frac{13x10^6 x250}{2x62500}\right)\cot\alpha$$

$$= 26\cot\alpha\, mm^2 .$$

Total Longitudinal Reinforcement:

Corner 1: (The tensile stress due to torsion and shear is reduced by the compressive stress due to bending.)

$$A_s(1) = \Sigma A_s(T,V)_1 - \frac{M}{2hf_y}$$

$$= (46\cot\alpha + 26\cot\alpha - 128)mm^2$$

$$= (72\cot\alpha - 128)mm^2 .$$

Corner 3: (The tensile stress due to torsion and shear is added to the tensile stress due to bending.)

$$A_s(3) = \Sigma A_s(T,V)_3 + \frac{M}{2hf_y}$$

$$= (46\cot\alpha + 26\cot\alpha + 128)mm^2$$

$$= (72\cot\alpha + 128)mm^2 .$$

Corner 5: (The tensile stress due to torsion and shear is added to the tensile stress due to bending.)

$$A_s(5) = \sum A_s(T,V)_5 + \frac{M}{2hf_y}$$

$$= (6\cot\alpha + 26\cot\alpha + 128)mm^2$$

$$= (32\cot\alpha + 128)mm^2 .$$

Corner 7: (The tensile stress due to torsion and shear is reduced by the compressive stress due to bending.)

$$A_s(7) = \sum A_s(T,V)_7 - \frac{M}{2hf_y}$$

$$= (6\cot\alpha + 26\cot\alpha - 128)mm^2$$

$$= (32\cot\alpha - 128)mm^2 .$$

Transverse Reinforcement:

The general equation for transverse reinforcement in each side is:

$$A_{sv} = \frac{S}{f_{yv}} = \left(\frac{(\tau t)1000}{f_{yv}}\right)\tan\alpha\,(mm^2/m).$$

where S = stirrup force, τ = shear stress and t = wall thickness.

The shear flow (τt) value is different for each side as follows:

side 2: $(\tau t)_2 = \frac{T}{2A_o} + \frac{V}{2h}$

side 6: $(\tau t)_6 = \frac{T}{2A_o} - \frac{V}{2h}$

sides 4 & 8: $(\tau t)_4 = (\tau t)_8 = \frac{T}{2A_o}$

Side 2: (Shear stresses added)

$$A_{sv}(2) = \left[\frac{1}{f_{yv}}\left(\frac{T}{2A_o} + \frac{V}{2h}\right)1000\right]\tan\alpha$$

$$= \left[\frac{1}{500}\left(\frac{13x10^6}{2x62500} + \frac{40x10^3}{2x250}\right)1000\right]\tan\alpha$$

$$= (368\tan\alpha)mm^2/m .$$

Side 6: (Shear stresses subtracted)

$$A_{sv}(6) = \left[\frac{1}{f_{yv}}\left(\frac{T}{2A_o} - \frac{V}{2h}\right)1000\right]\tan\alpha$$

$$= \left[\frac{1}{500}\left(\frac{13x10^6}{2x62500} - \frac{40x10^3}{2x250}\right)1000\right]\tan\alpha$$

$$= (48\tan\alpha)mm^2 / m.$$

Side 4 and 8: (Torsion alone)

$$A_{sv}(4) = A_{sv}(8) = \left[\frac{1}{f_{yv}}\left(\frac{T}{2A_o}\right)1000\right]\tan\alpha$$

$$= \left[\frac{1}{500}\left(\frac{13x10^6}{2x62500}\right)1000\right]\tan\alpha$$

$$= (208\tan\alpha)mm^2 / m.$$

SUMMARY:

Longitudinal Reinforcement: (mm^2)

Corner	1	3	5	7
$\alpha = 26.57^\circ$	16	272	192	0
$\alpha = 45.00^\circ$	0	200	160	0
$\alpha = 63.43^\circ$	0	164	144	0

Transverse Reinforcement: (mm^2/m)

Side	2	4	6	8
$\alpha = 26.57^\circ$	184	104	24	104
$\alpha = 45.00^\circ$	368	208	48	208
$\alpha = 63.43^\circ$	736	416	96	416

Appendix B

Experimental and computational steel strain ratios

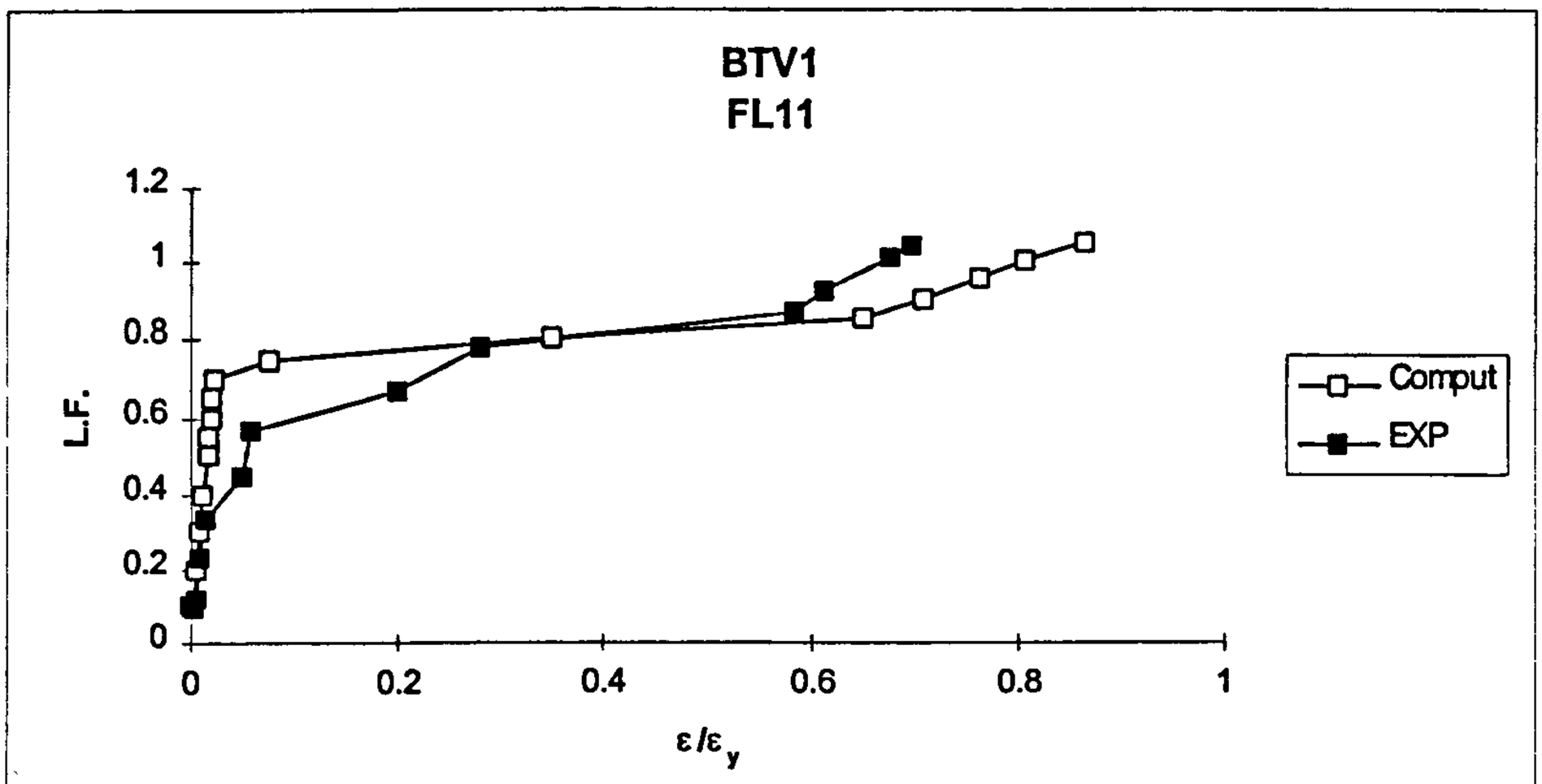
BTV1
FL11
L.F.
1.2
1
0.8
0.6
0.4
0.2
0
0
0.2
0.4
0.6
0.8
1
ε/ε y
Comput
EXP

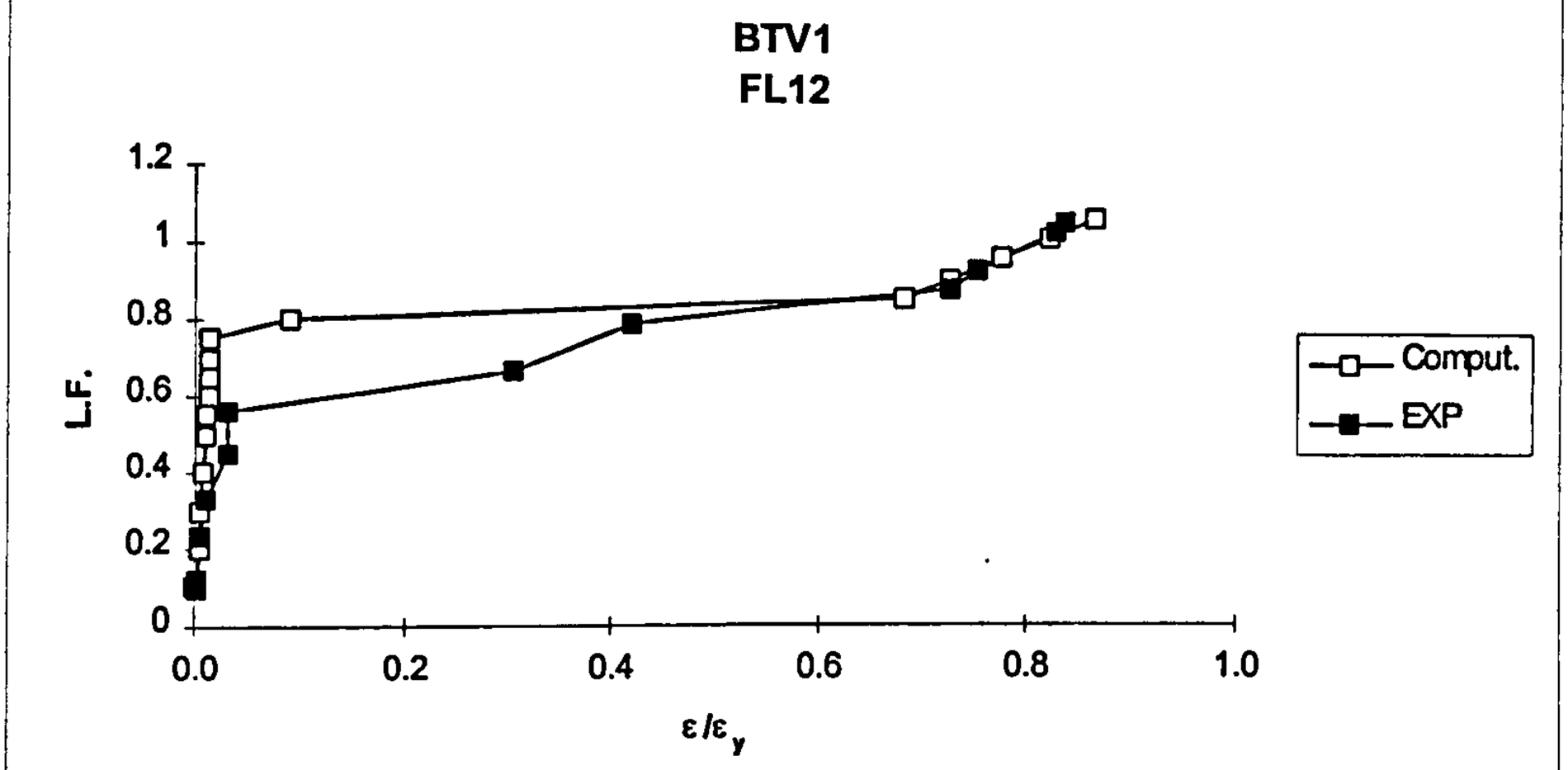
BTV1
FL12
L.F.
1.2
1
0.8
0.6
0.4
0.2
0
0.0
0.2
0.4
0.6
0.8
1.0
ε/ε y
Comput.
EXP

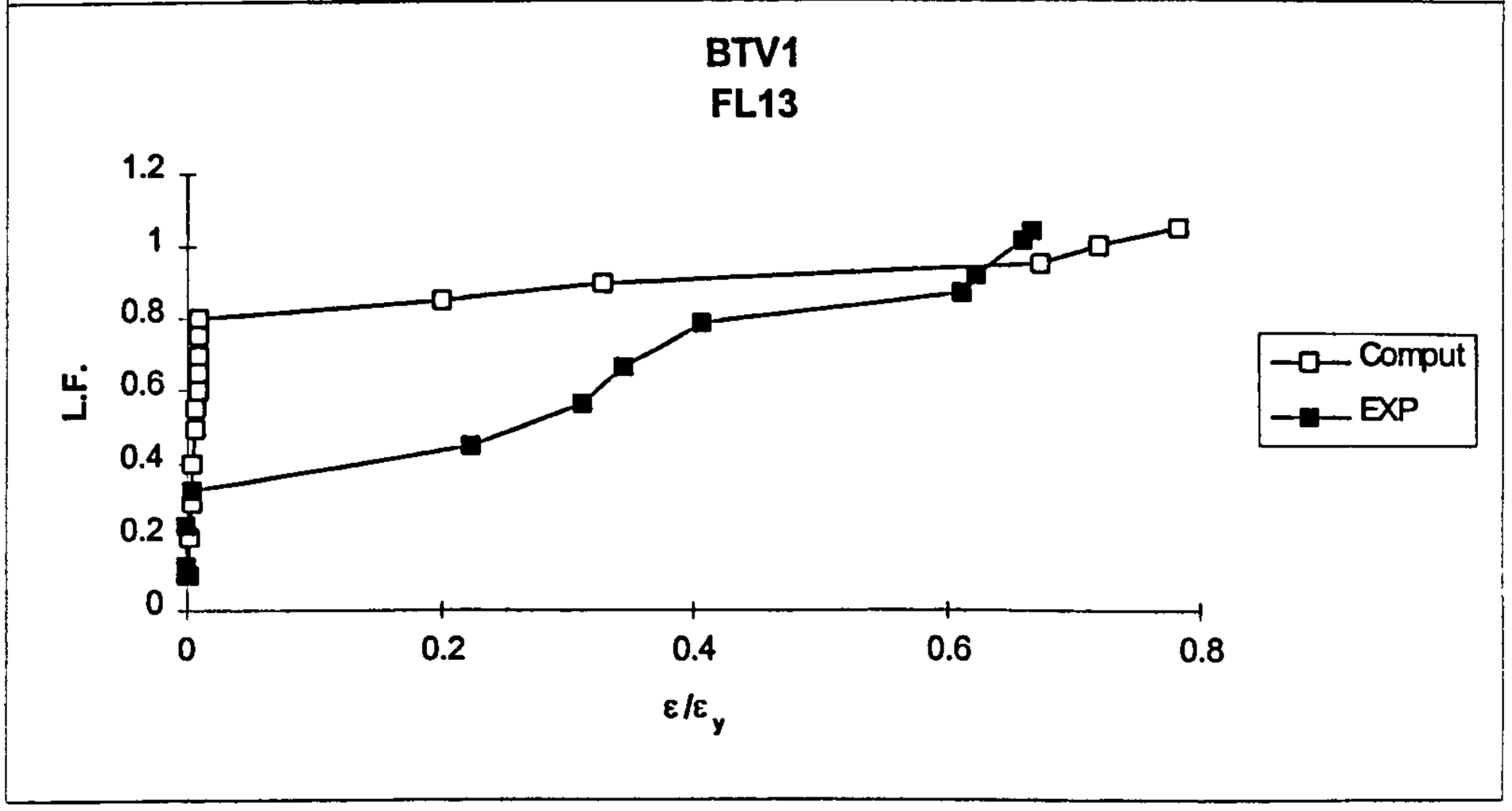
BTV1
FL13
L.F.
1.2
1
0.8
0.6
0.4
0.2
0
0
0.2
0.4
0.6
0.8
ε/ε y
Comput
EXP

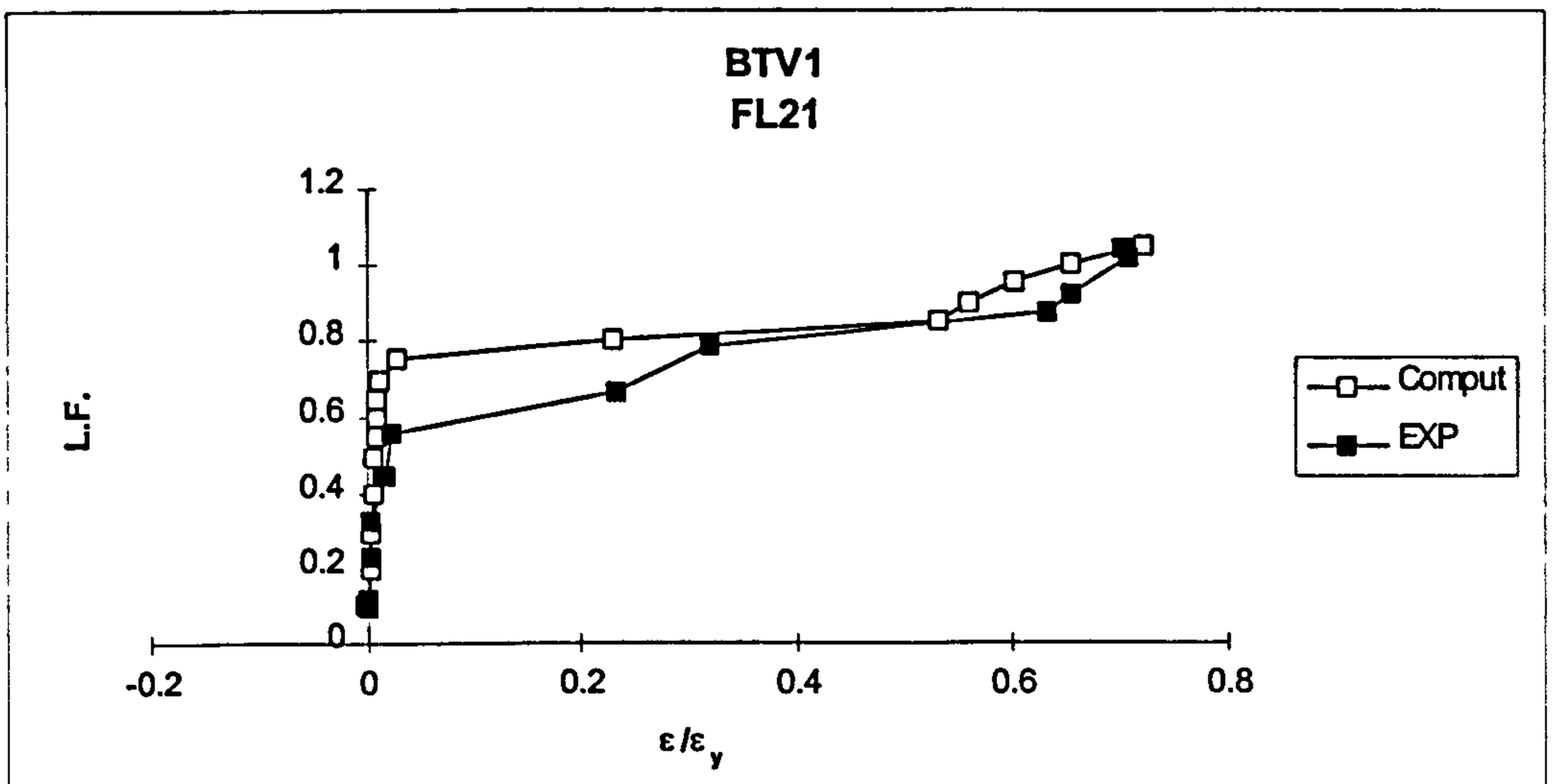
BTV1
FL21
L.F.
1.2
1
0.8
0.6
0.4
0.2
0
-0.2
0
0.2
0.4
0.6
0.8
Comput
EXP
ε/ε y

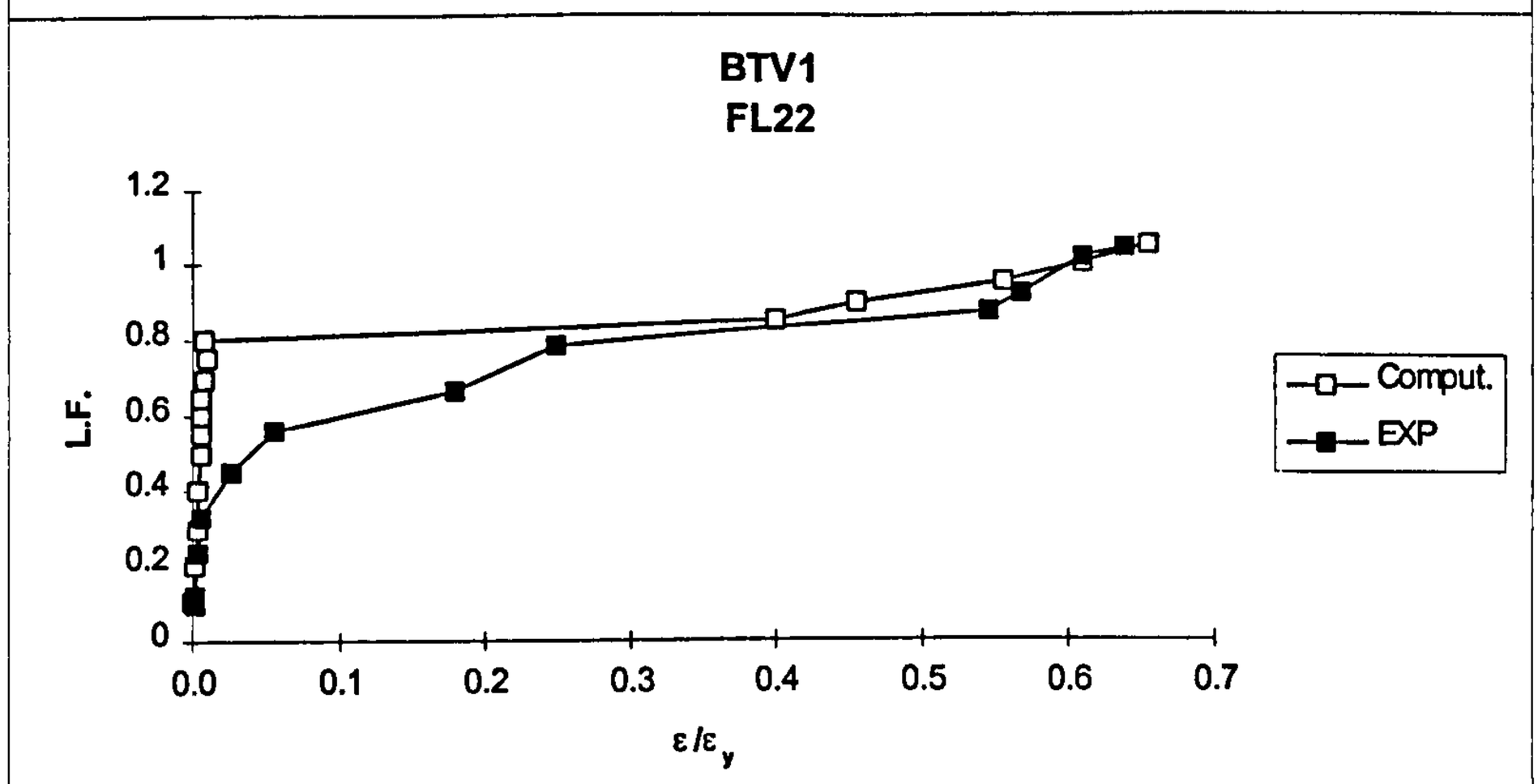
BTV1
FL22
L.F.
1.2
1
0.8
0.6
0.4
0.2
0
0.0
0.1
0.2
0.3
0.4
0.5
0.6
0.7
Comput.
EXP
ε/ε y

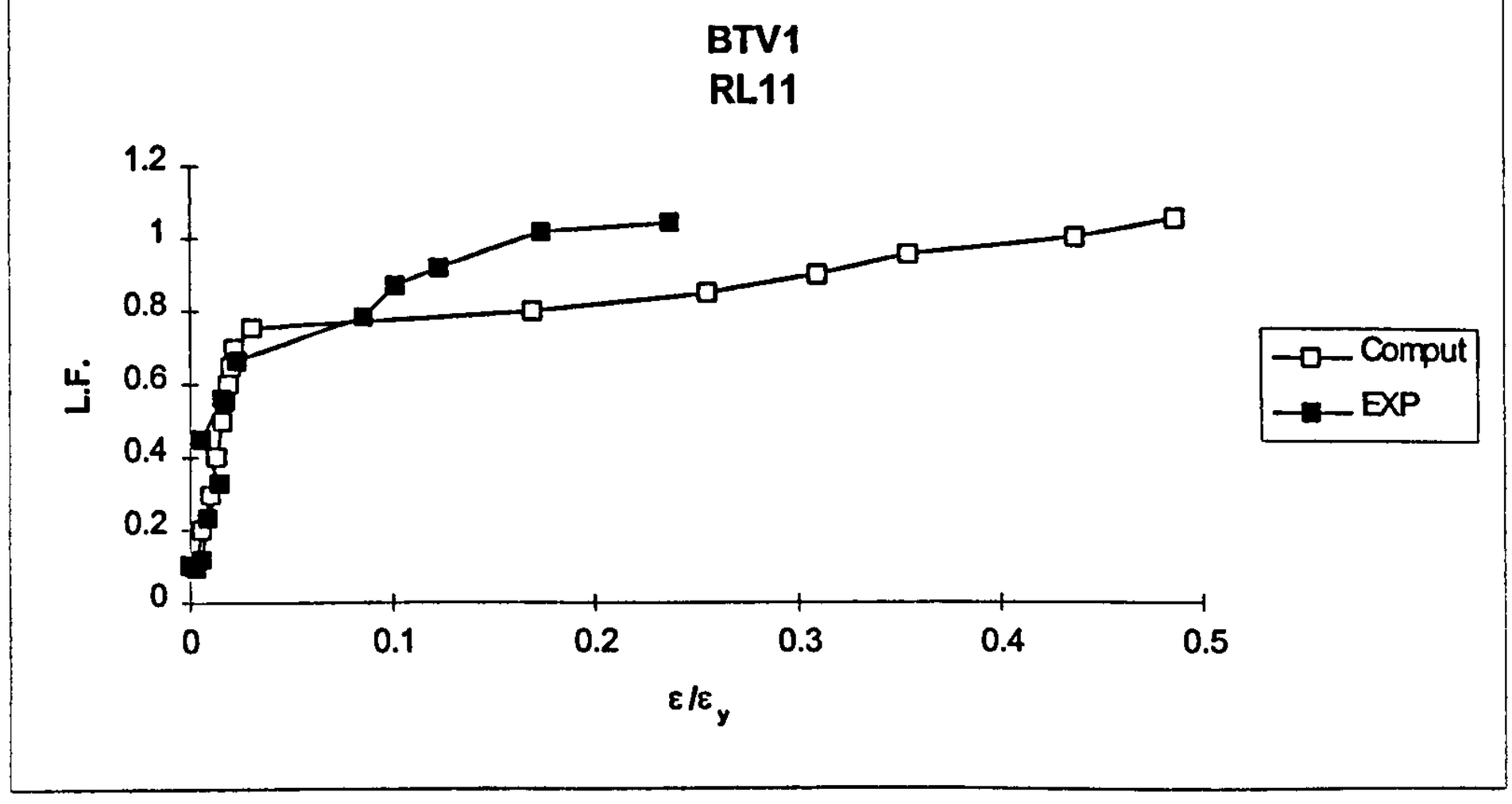
BTV1
RL11
L.F.
1.2
1
0.8
0.6
0.4
0.2
0
0
0.1
0.2
0.3
0.4
0.5
Comput
EXP
ε/ε y

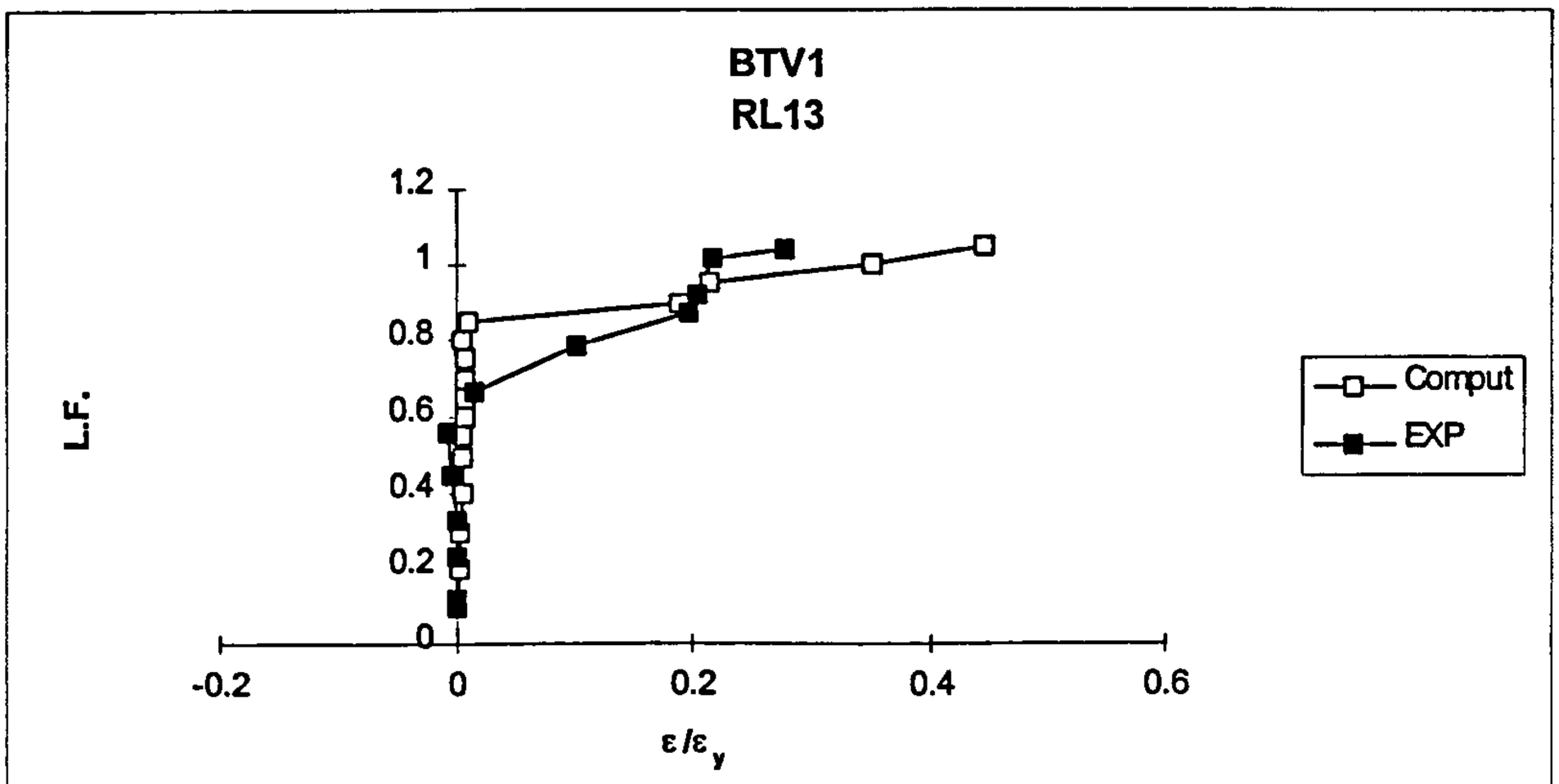
BTV1
RL13
L.F.
1.2
1
0.8
0.6
0.4
0.2
0
-0.2
0
0.2
0.4
0.6
ε /ε y
Comput
EXP

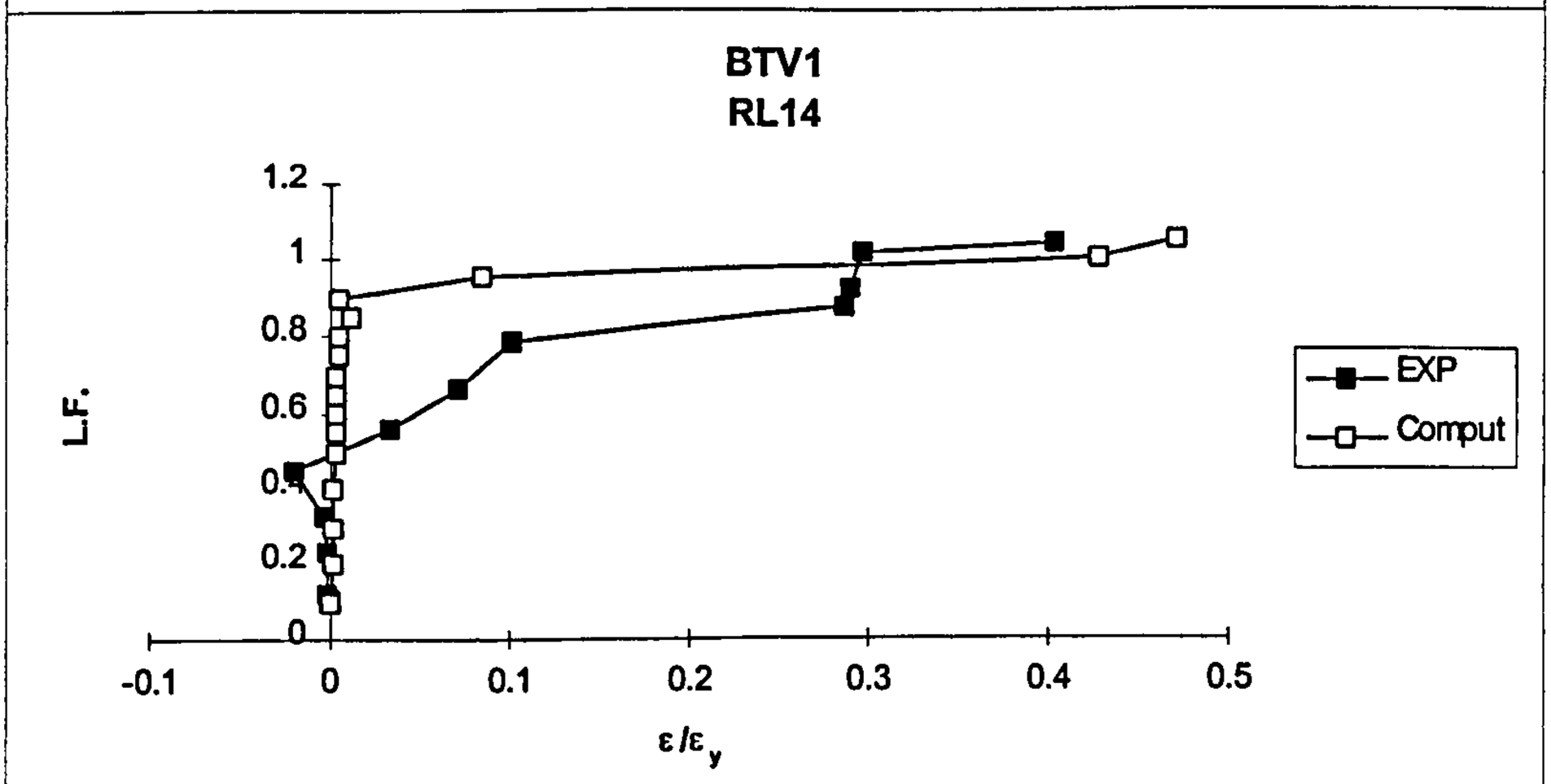
BTV1
RL14
L.F.
1.2
1
0.8
0.6
0.2
0
-0.1
0
0.1
0.2
0.3
0.4
0.5
ε /ε y
EXP
Comput

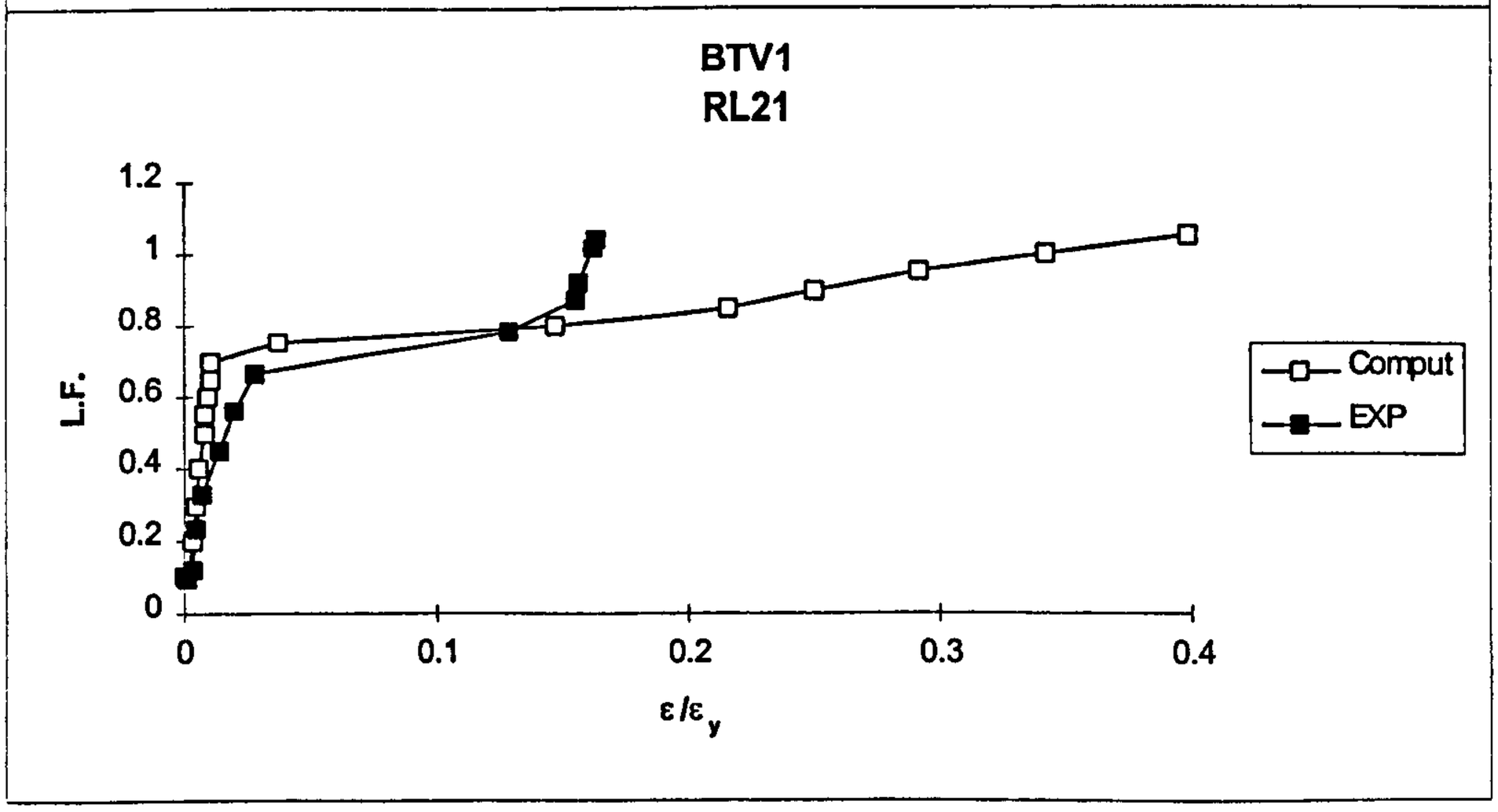
BTV1
RL21
L.F.
1.2
1
0.8
0.6
0.4
0.2
0
0
0.1
0.2
0.3
0.4
ε /ε y
Comput
EXP

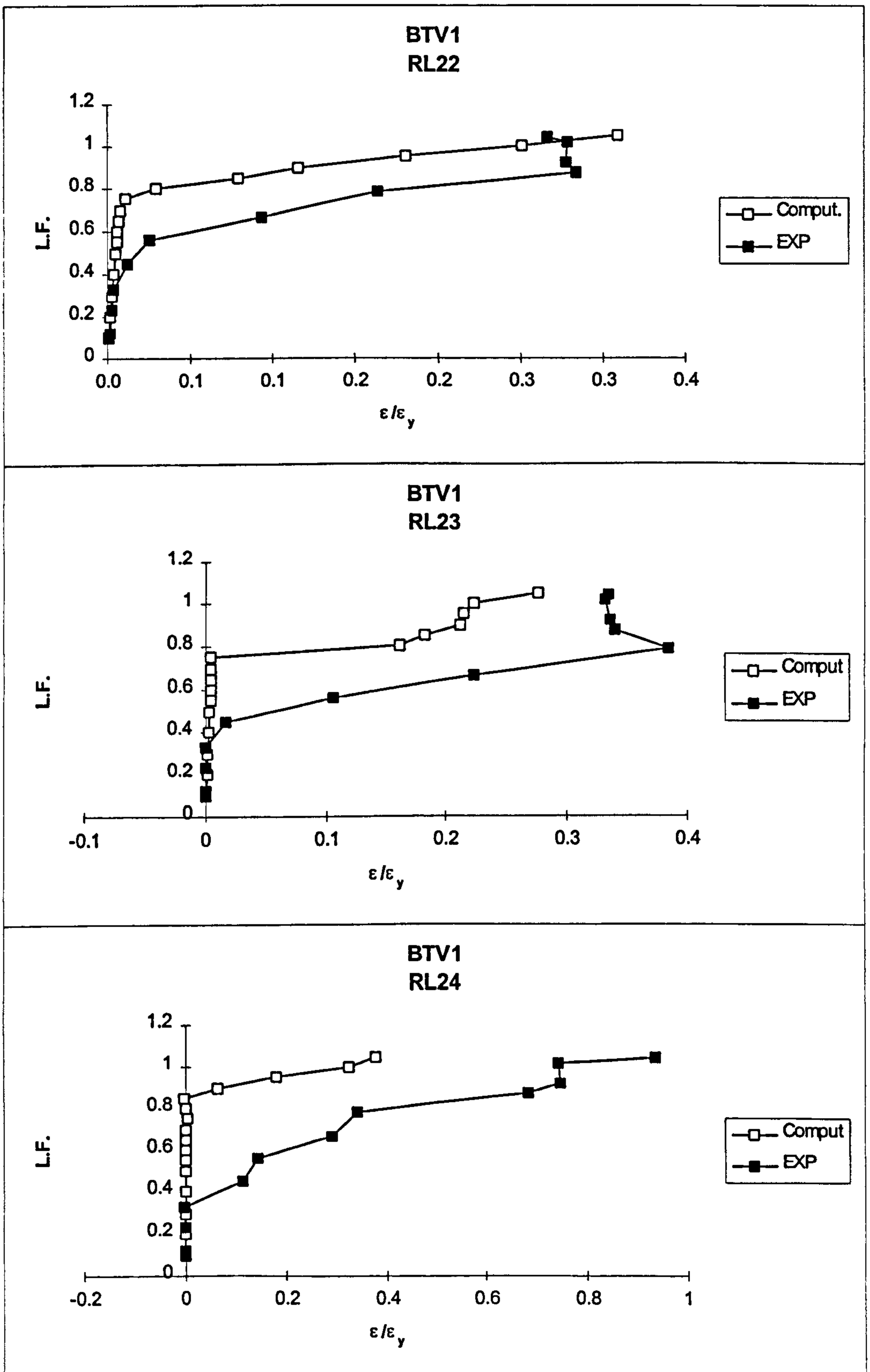
BTV1
RL22
L.F.
1.2
1
0.8
0.6
0.4
0.2
0
0.0
0.1
0.1
0.2
0.2
0.3
0.3
0.4
ε/ε y
Comput.
EXP
BTV1
RL23
L.F.
1.2
1
0.8
0.6
0.4
0.2
0
-0.1
0
0.1
0.2
0.3
0.4
ε/ε y
Comput
EXP
BTV1
RL24
L.F.
1.2
1
0.8
0.6
0.4
0.2
0
-0.2
0
0.2
0.4
0.6
0.8
1
ε/ε y
Comput
EXP

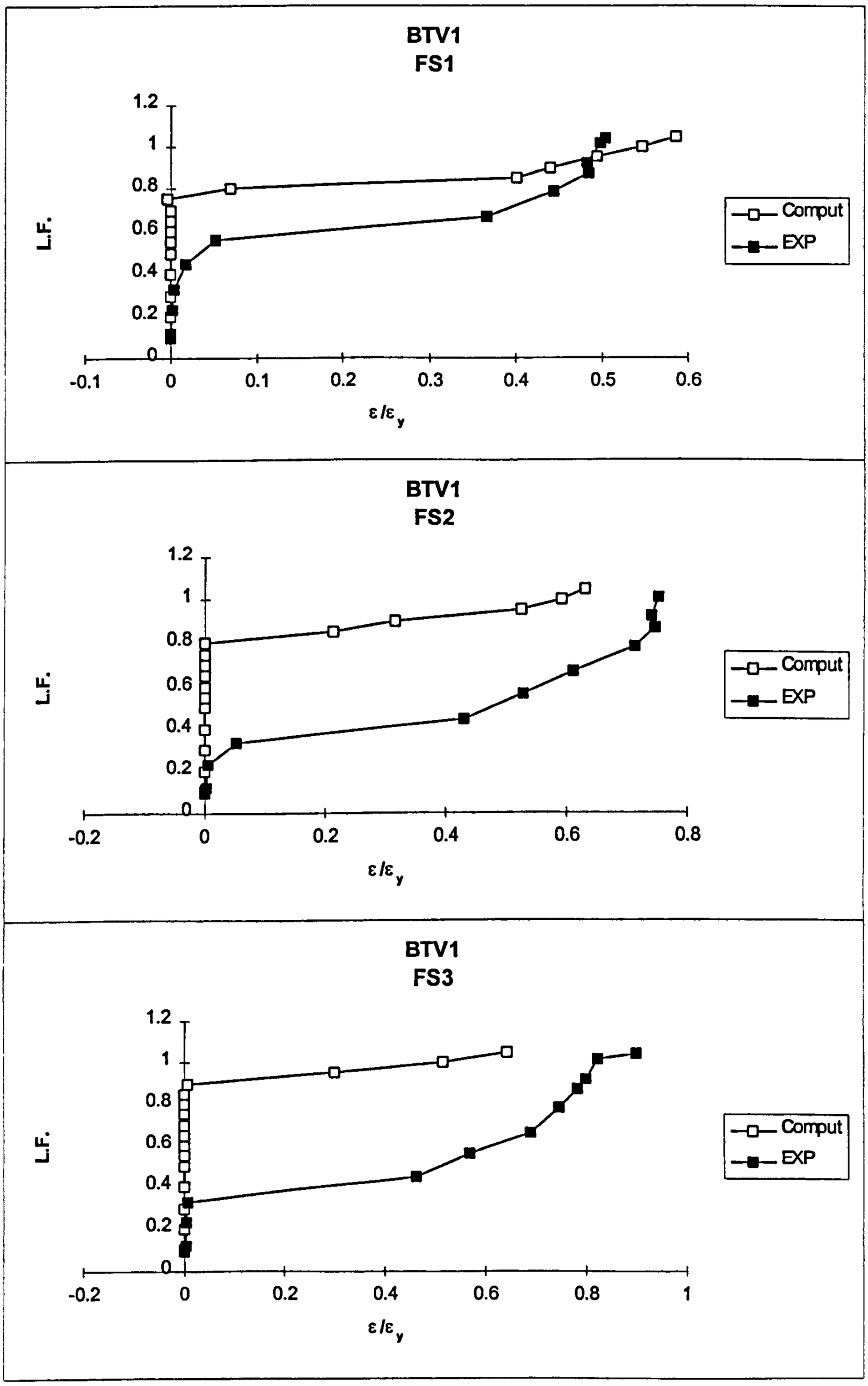
BTV1
FS1
L.F.
1.2
1
0.8
0.6
0.4
0.2
0
-0.1
0
0.1
0.2
0.3
0.4
0.5
0.6
ε/ε_y
Comput
EXP
BTV1
FS2
L.F.
1.2
1
0.8
0.6
0.4
0.2
0
-0.2
0
0.2
0.4
0.6
0.8
ε/ε_y
Comput
EXP
BTV1
FS3
L.F.
1.2
1
0.8
0.6
0.4
0.2
0
-0.2
0
0.2
0.4
0.6
0.8
1
ε/ε_y
Comput
EXP

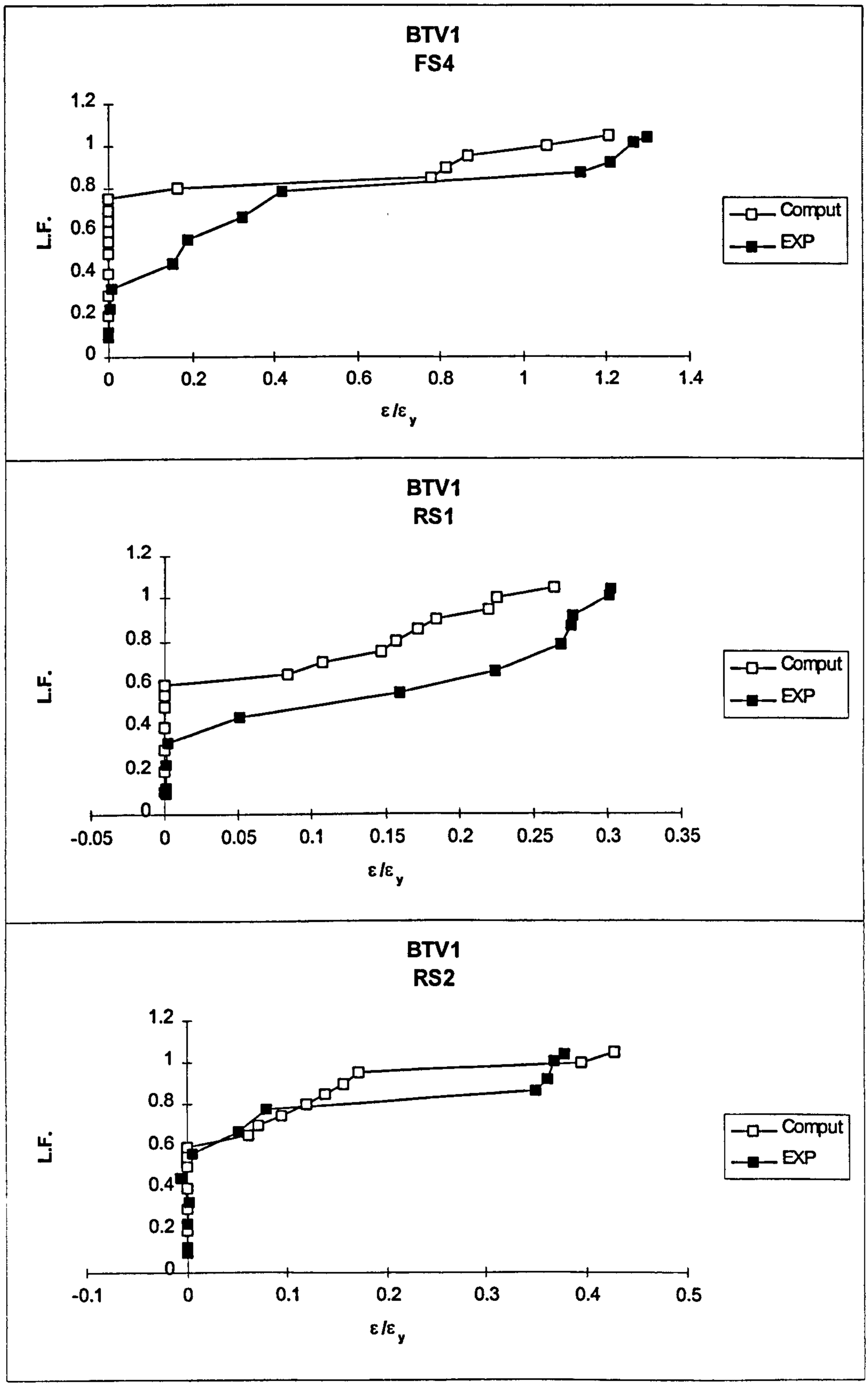
BTV1
FS4
L.F.
1.2
1
0.8
0.6
0.4
0.2
0
0
0.2
0.4
0.6
0.8
1
1.2
1.4
ε/ε y
Comput
EXP
BTV1
RS1
L.F.
1.2
1
0.8
0.6
0.4
0.2
0
-0.05
0
0.05
0.1
0.15
0.2
0.25
0.3
0.35
ε/ε y
Comput
EXP
BTV1
RS2
L.F.
1.2
1
0.8
0.6
0.4
0.2
0
-0.1
0
0.1
0.2
0.3
0.4
0.5
ε/ε y
Comput
EXP

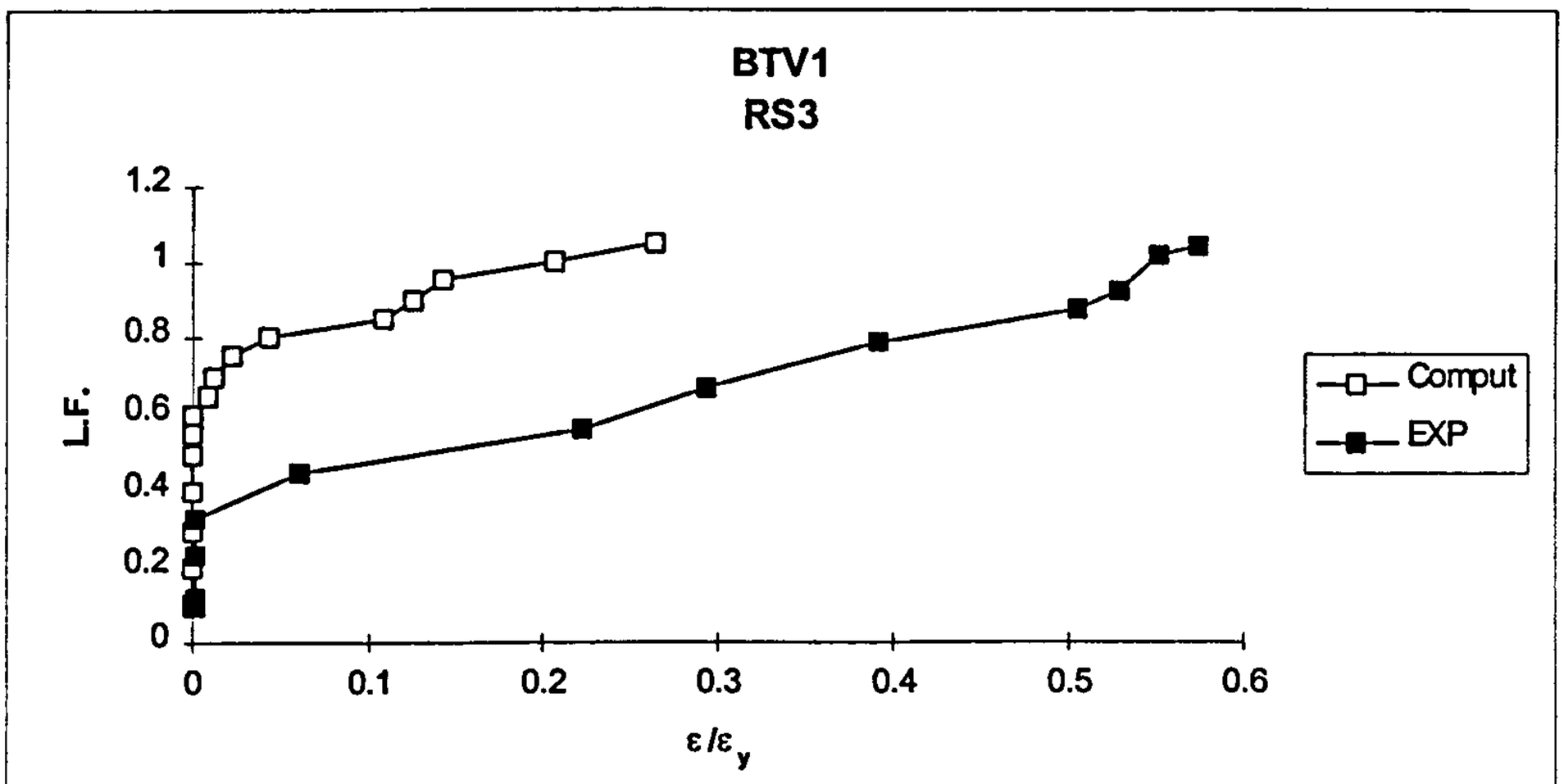
BTV1
RS3
L.F.
1.2
1
0.8
0.6
0.4
0.2
0
0
0.1
0.2
0.3
0.4
0.5
0.6
ε /ε y
Comput
EXP

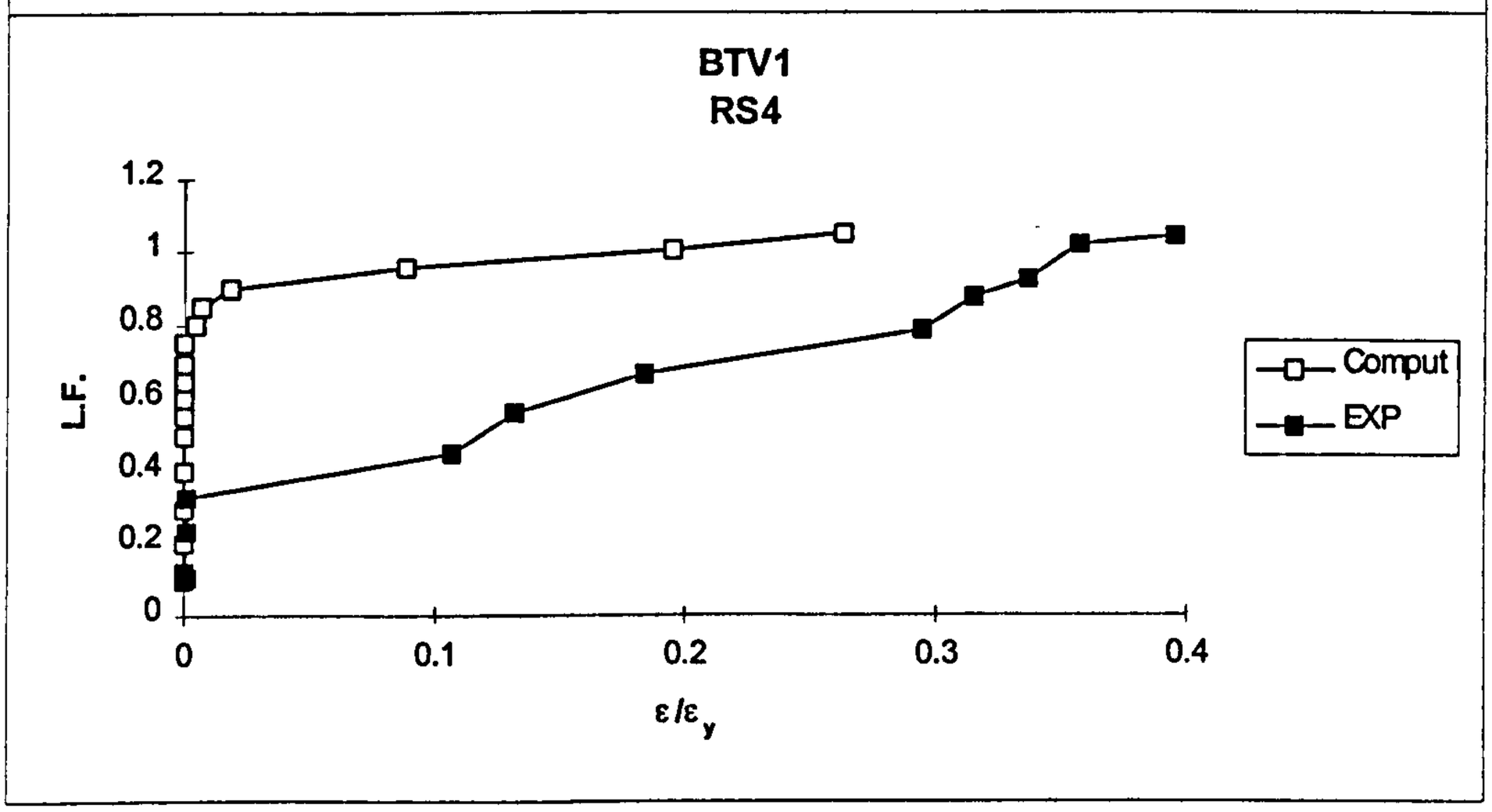
BTV1
RS4
L.F.
1.2
1
0.8
0.6
0.4
0.2
0
0
0.1
0.2
0.3
0.4
ε /ε y
Comput
EXP

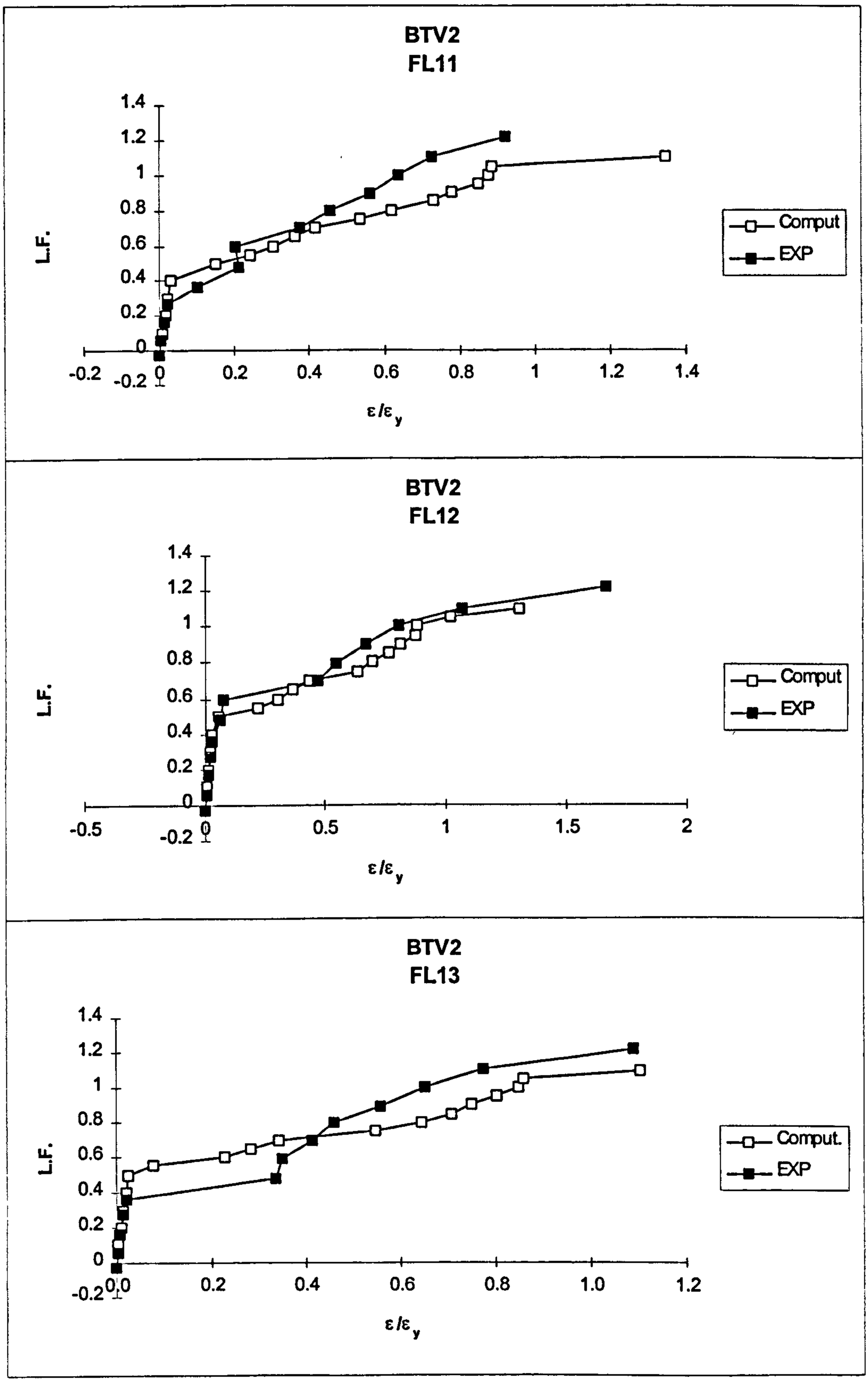
BTV2
FL11
L.F.
1.4
1.2
1
0.8
0.6
0.4
0.2
0
-0.2
-0.2
0
0.2
0.4
0.6
0.8
1
1.2
1.4
ε/ε y
Comput
EXP
BTV2
FL12
L.F.
1.4
1.2
1
0.8
0.6
0.4
0.2
0
-0.5
-0.2
0
0.5
1
1.5
2
ε/ε y
Comput
EXP
BTV2
FL13
L.F.
1.4
1.2
1
0.8
0.6
0.4
0.2
0
-0.2
0.0
0.2
0.4
0.6
0.8
1.0
1.2
ε/ε y
Comput.
EXP

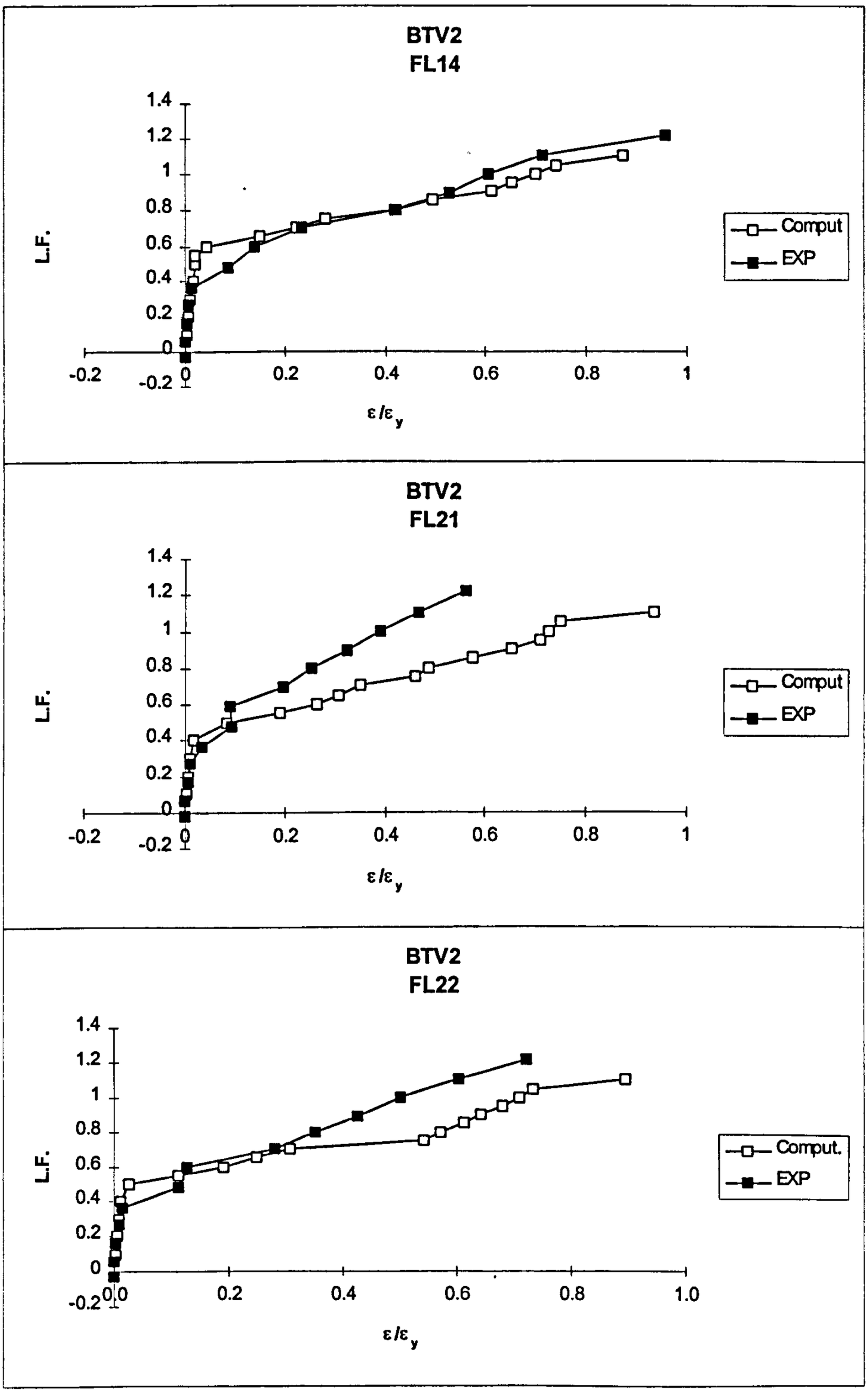
BTV2
FL14
L.F.
1.4
1.2
1
0.8
0.6
0.4
0.2
0
-0.2
-0.2
0
0.2
0.4
0.6
0.8
1
ε/ε_y
Comput
EXP
BTV2
FL21
L.F.
1.4
1.2
1
0.8
0.6
0.4
0.2
0
-0.2
-0.2
0
0.2
0.4
0.6
0.8
1
ε/ε_y
Comput
EXP
BTV2
FL22
L.F.
1.4
1.2
1
0.8
0.6
0.4
0.2
0
-0.2
0.0
0.2
0.4
0.6
0.8
1.0
ε/ε_y
Comput.
EXP

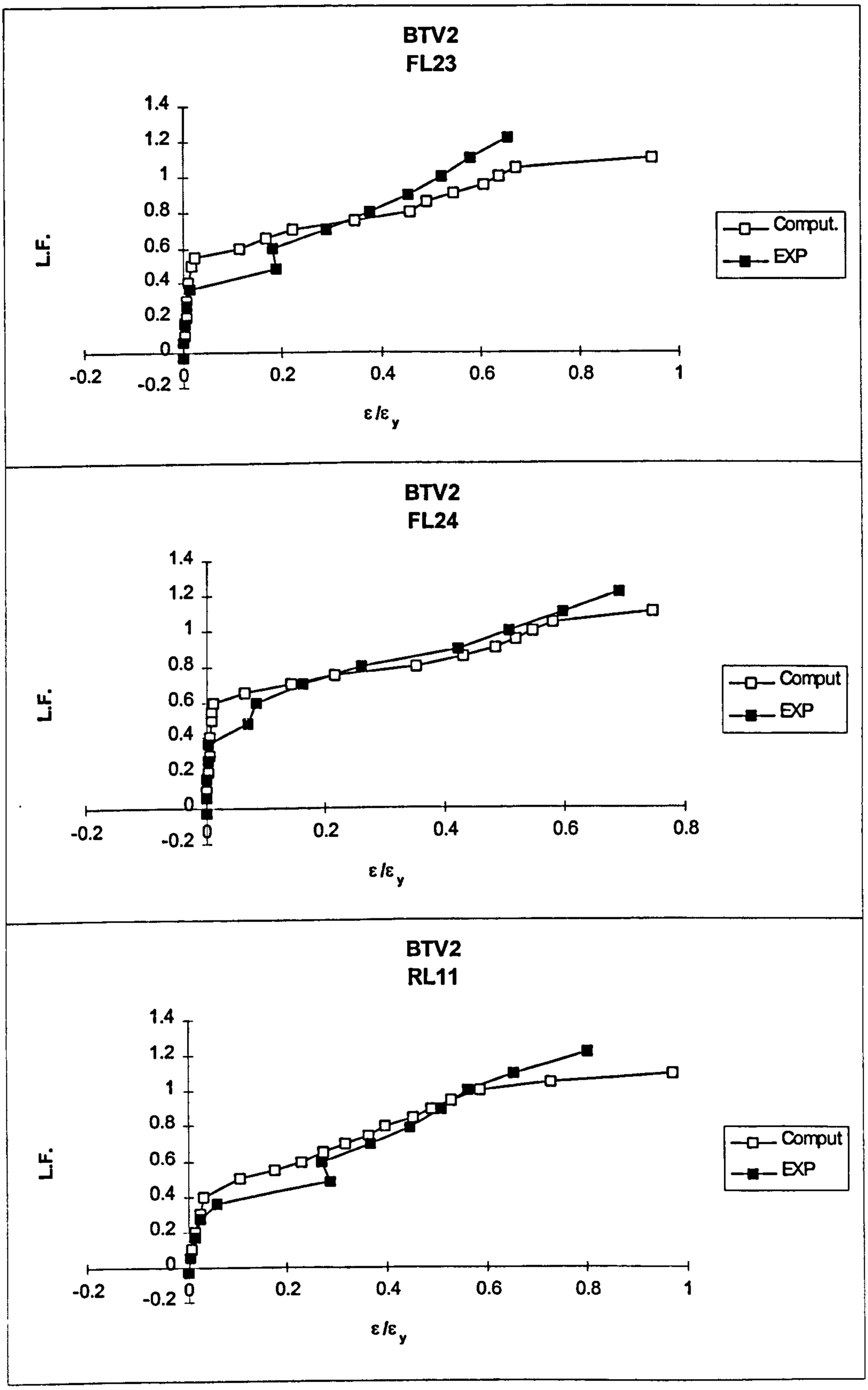
BTV2
FL23
L.F.
1.4
1.2
1
0.8
0.6
0.4
0.2
0
-0.2
-0.2
0
0.2
0.4
0.6
0.8
1
ε/ε_y
Comput.
EXP
BTV2
FL24
L.F.
1.4
1.2
1
0.8
0.6
0.4
0.2
0
-0.2
-0.2
0
0.2
0.4
0.6
0.8
ε/ε_y
Comput
EXP
BTV2
RL11
L.F.
1.4
1.2
1
0.8
0.6
0.4
0.2
0
-0.2
-0.2
0
0.2
0.4
0.6
0.8
1
ε/ε_y
Comput
EXP

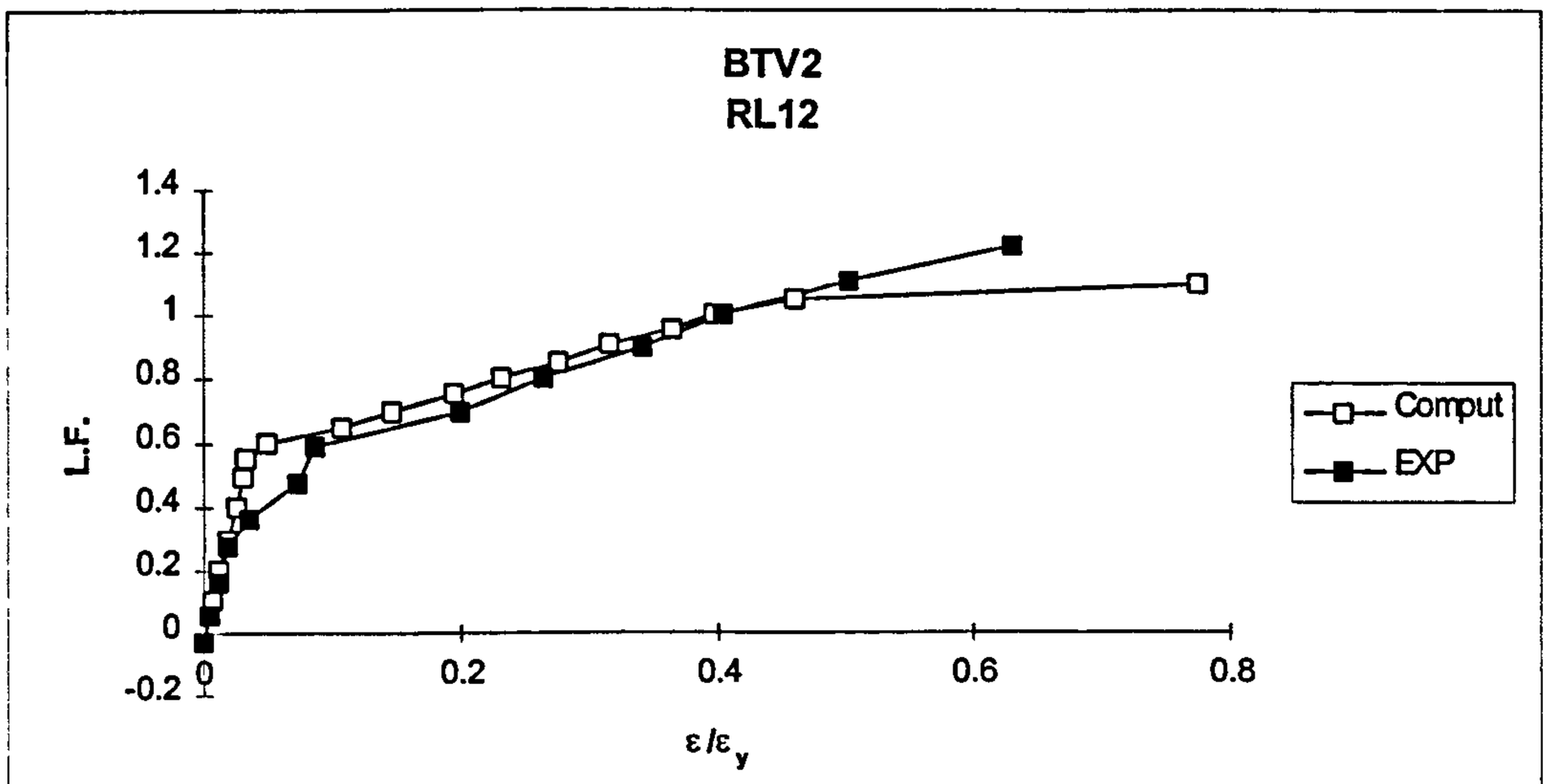
BTV2
RL12
L.F.
1.4
1.2
1
0.8
0.6
0.4
0.2
0
-0.2
0
0.2
0.4
0.6
0.8
Comput
EXP
ε/ε y

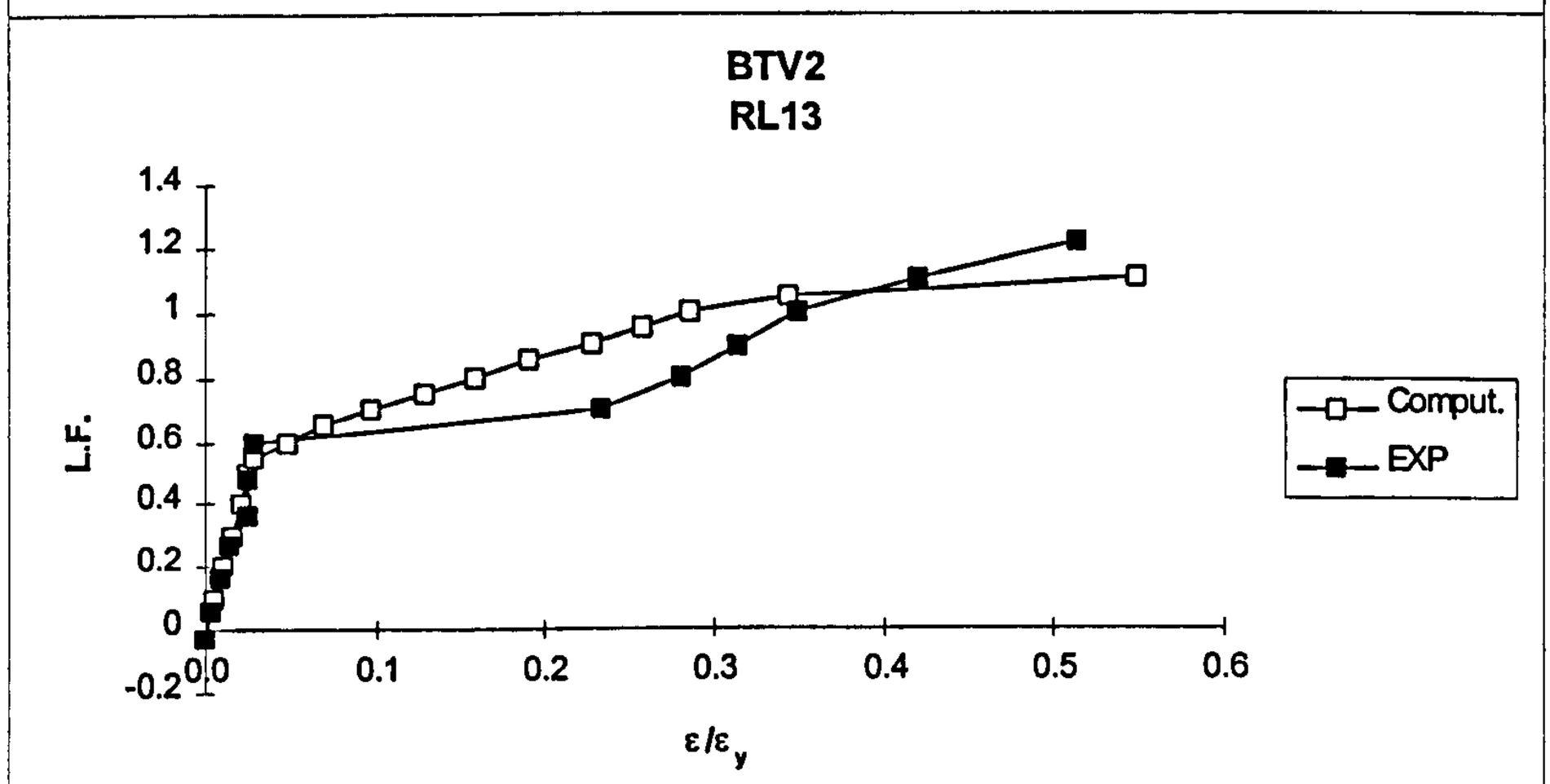
BTV2
RL13
L.F.
1.4
1.2
1
0.8
0.6
0.4
0.2
0
-0.2
0.0
0.1
0.2
0.3
0.4
0.5
0.6
Comput.
EXP
ε/ε y

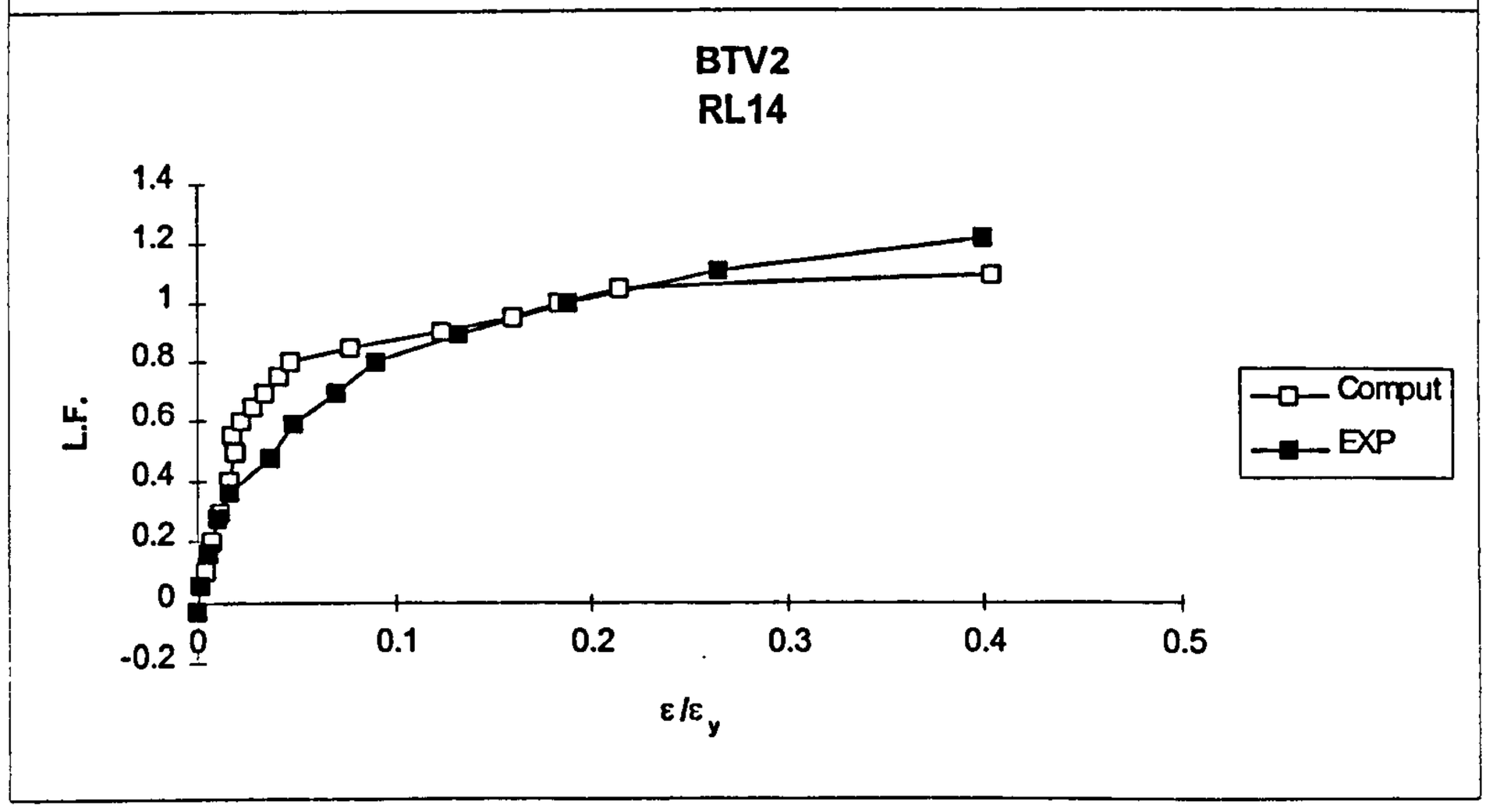
BTV2
RL14
L.F.
1.4
1.2
1
0.8
0.6
0.4
0.2
0
-0.2
0
0.1
0.2
0.3
0.4
0.5
Comput
EXP
ε/ε y

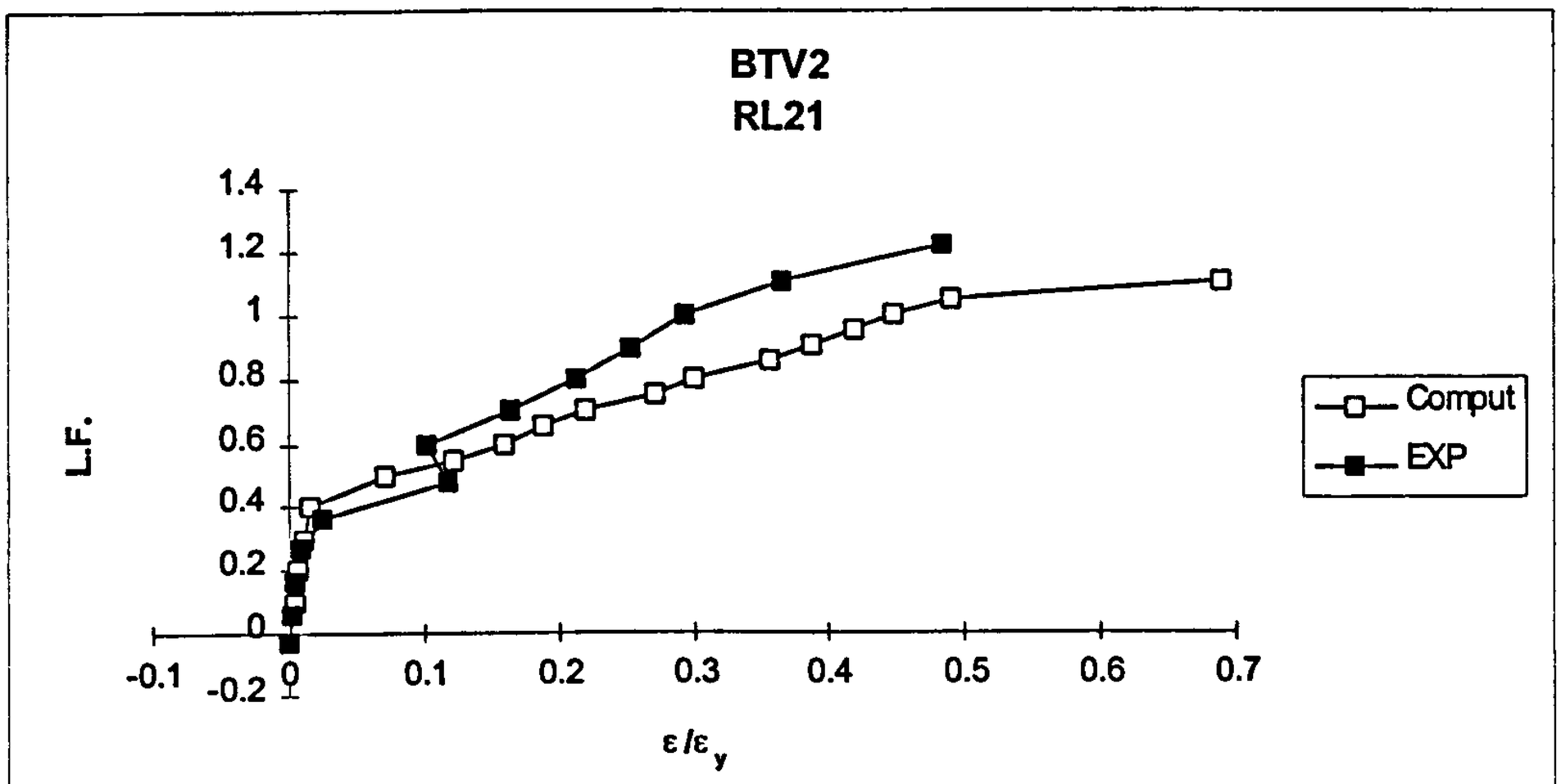
BTV2
RL21
L.F.
1.4
1.2
1
0.8
0.6
0.4
0.2
0
-0.2
-0.1
0
0.1
0.2
0.3
0.4
0.5
0.6
0.7
ε /ε y
Comput
EXP

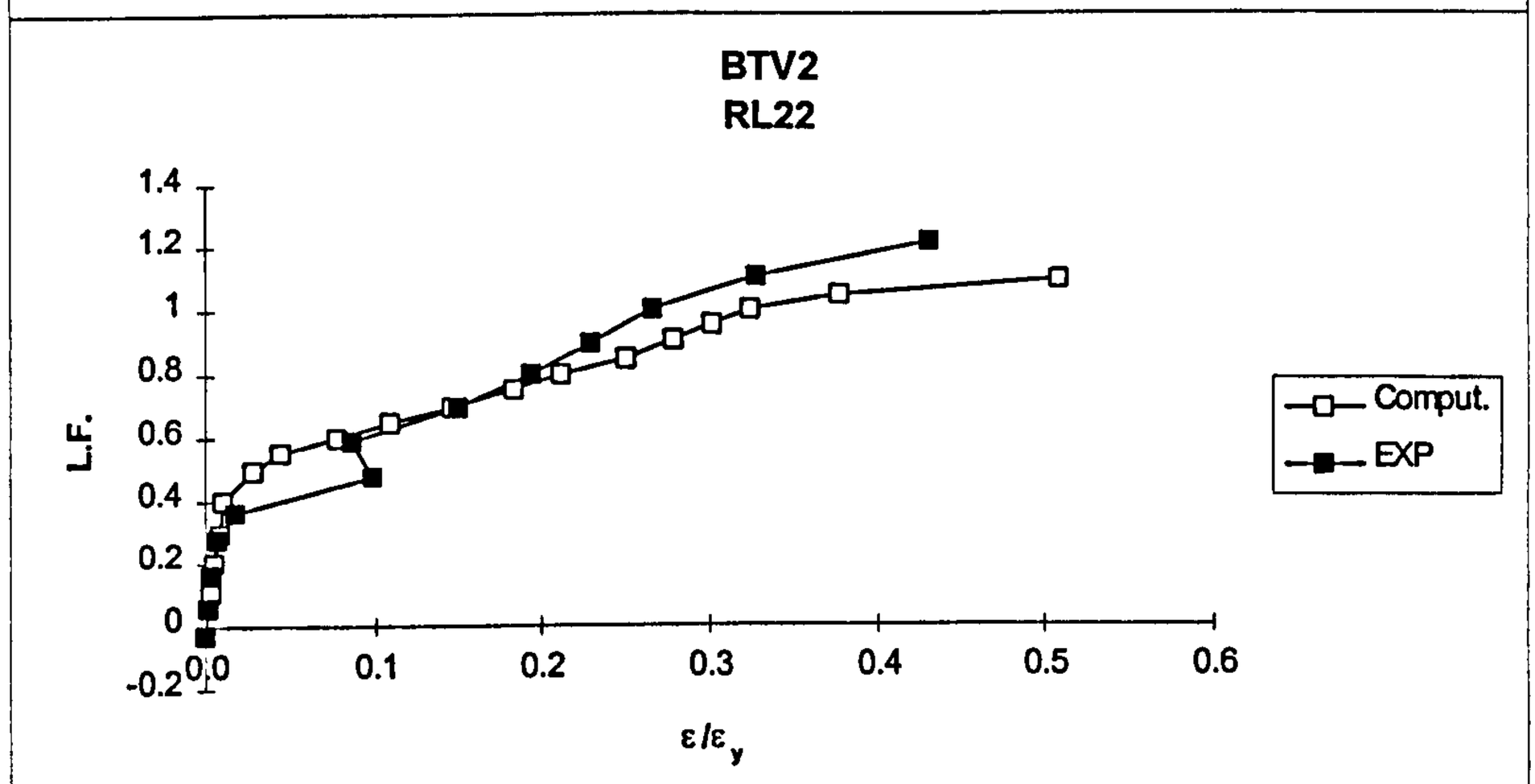
BTV2
RL22
L.F.
1.4
1.2
1
0.8
0.6
0.4
0.2
0
-0.2
0
0.1
0.2
0.3
0.4
0.5
0.6
ε /ε y
Comput.
EXP

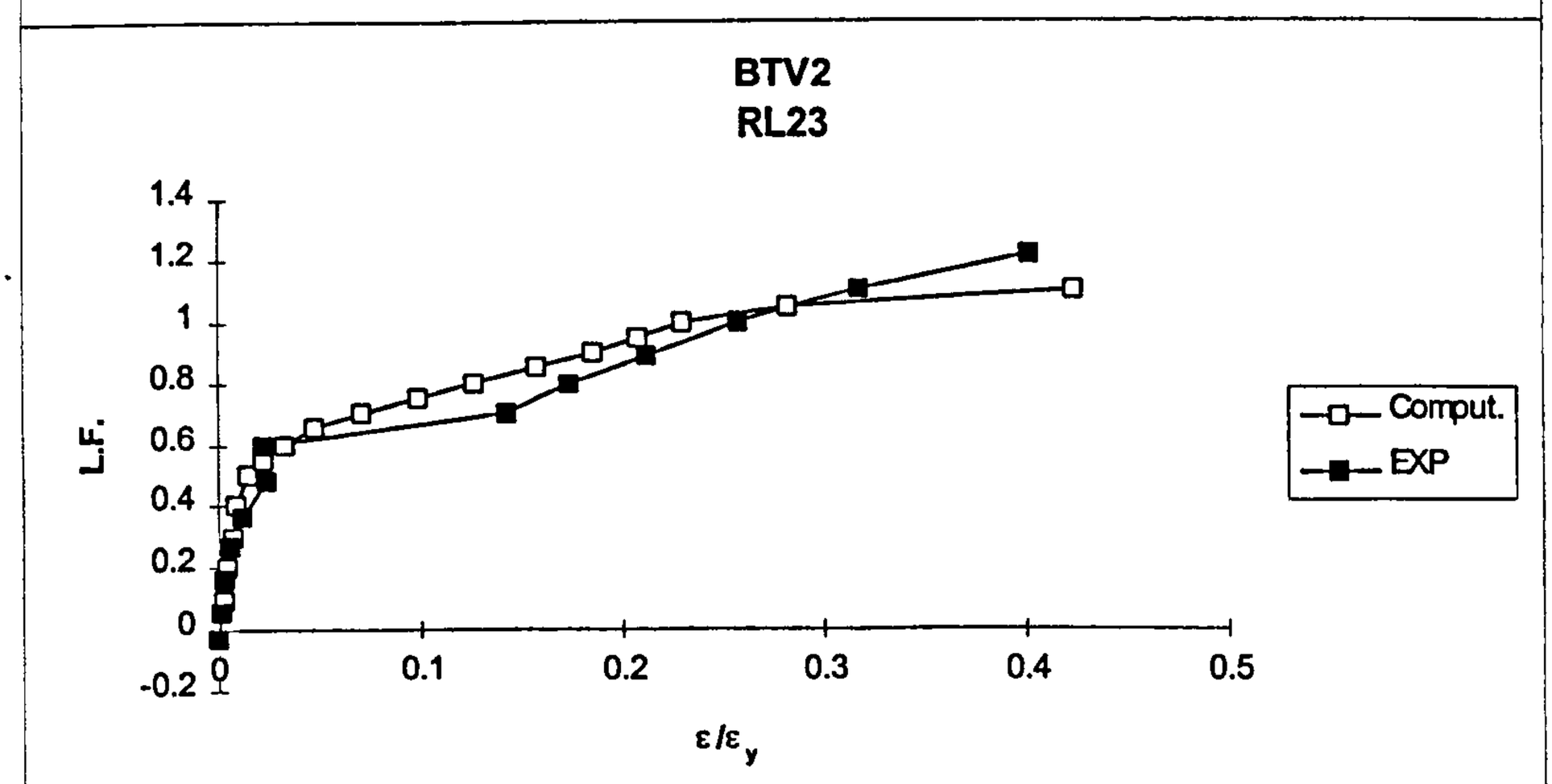
BTV2
RL23
L.F.
1.4
1.2
1
0.8
0.6
0.4
0.2
0
-0.2
0
0.1
0.2
0.3
0.4
0.5
ε /ε y
Comput.
EXP

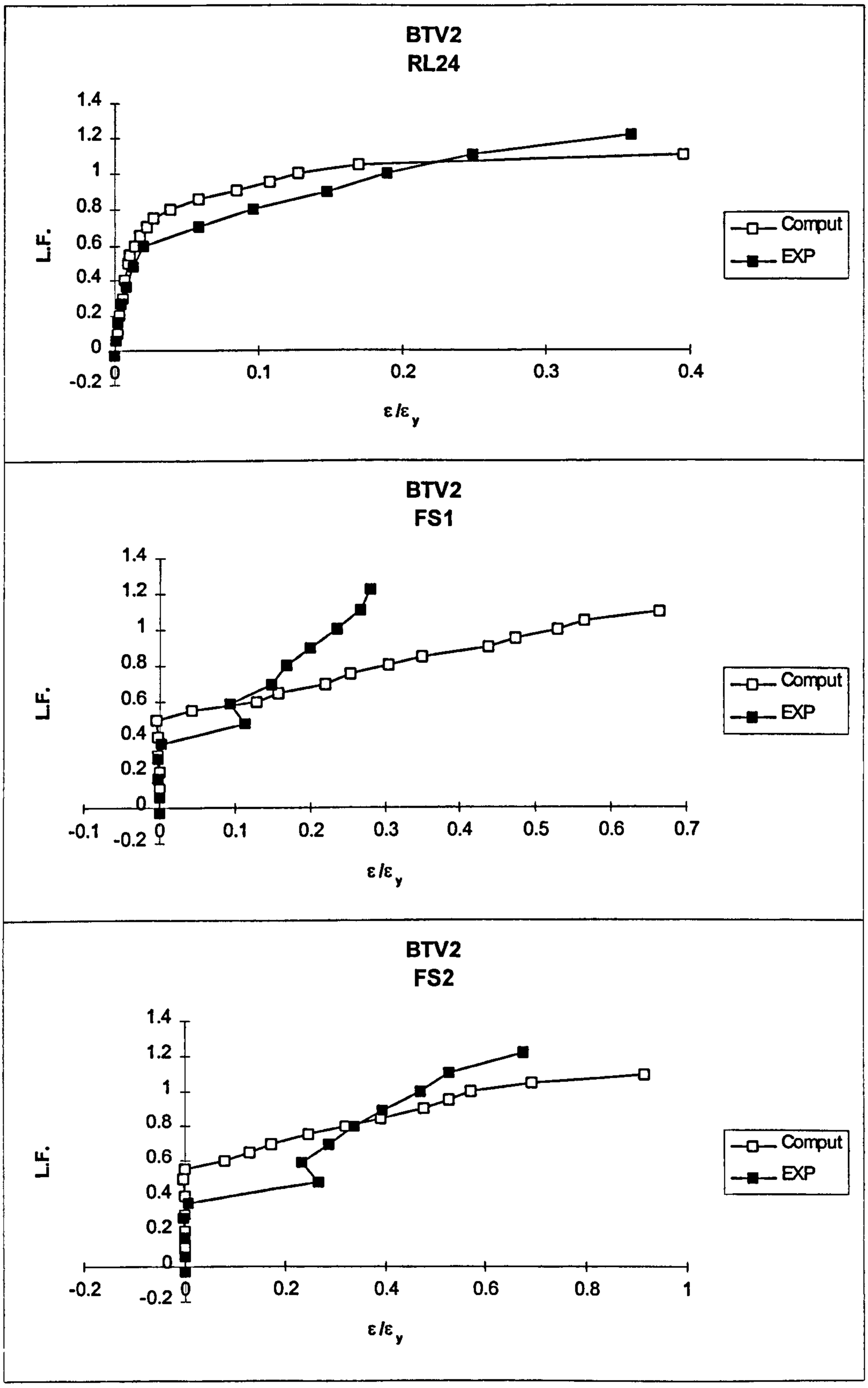
BTV2
RL24
L.F.
1.4
1.2
1
0.8
0.6
0.4
0.2
0
-0.2
0
0.1
0.2
0.3
0.4
ε/ε y
Comput
EXP
BTV2
FS1
L.F.
1.4
1.2
1
0.8
0.6
0.4
0.2
0
-0.1
-0.2
0
0.1
0.2
0.3
0.4
0.5
0.6
0.7
ε/ε y
Comput
EXP
BTV2
FS2
L.F.
1.4
1.2
1
0.8
0.6
0.4
0.2
0
-0.2
-0.2
0
0.2
0.4
0.6
0.8
1
ε/ε y
Comput
EXP

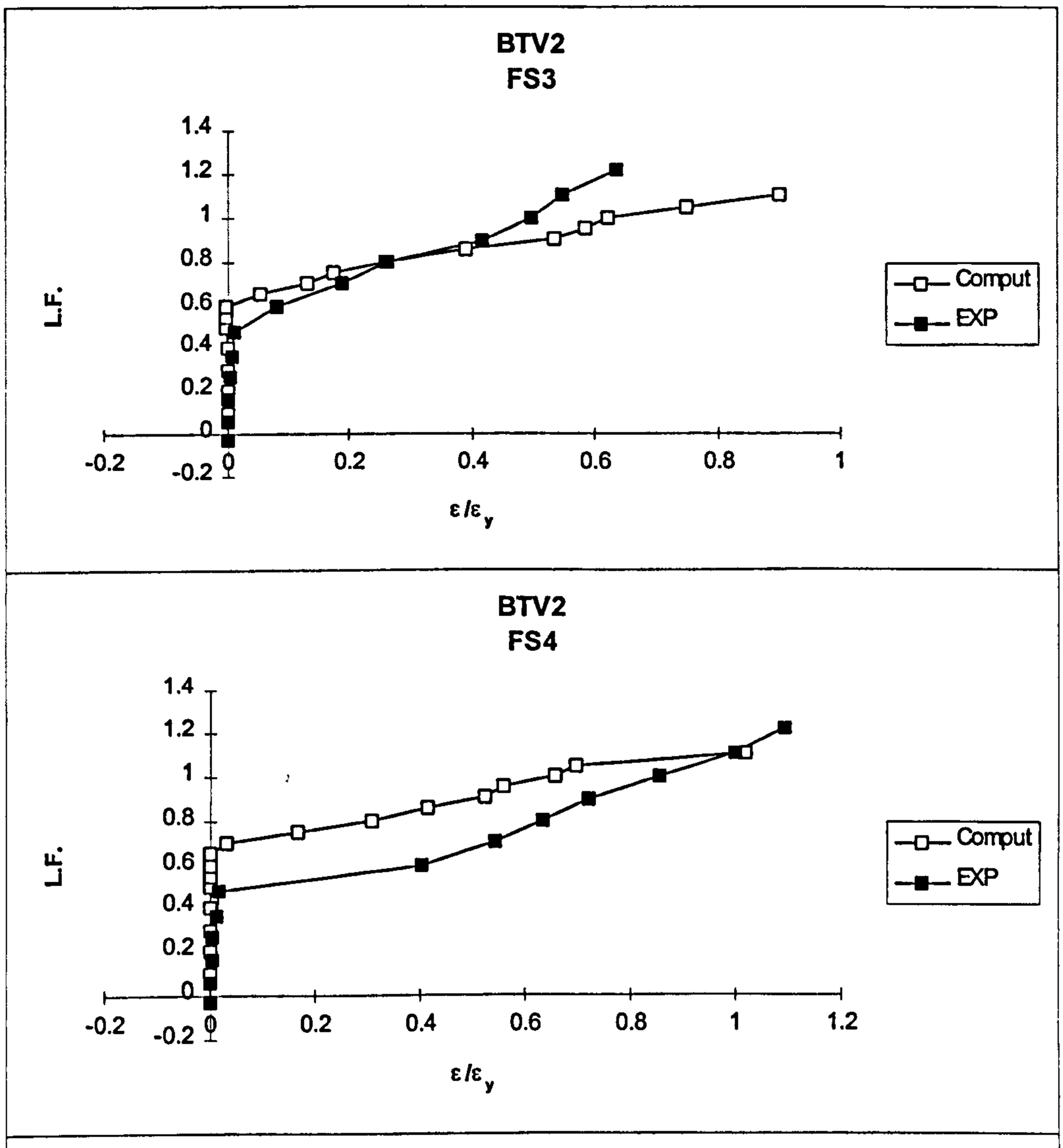
BTV2
FS3
L.F.
1.4
1.2
1
0.8
0.6
0.4
0.2
0
-0.2
-0.2
0
0.2
0.4
0.6
0.8
1
ε/ε_y
Comput
EXP
BTV2
FS4
L.F.
1.4
1.2
1
0.8
0.6
0.4
0.2
0
-0.2
-0.2
0
0.2
0.4
0.6
0.8
1
1.2
ε/ε_y
Comput
EXP
BTV2
RS1
L.F.
1.4
1.2
1
0.8
0.6
0.4
0.2
0
-0.05
-0.2
0
0.05
0.1
0.15
0.2
ε/ε_y
Comput
EXP

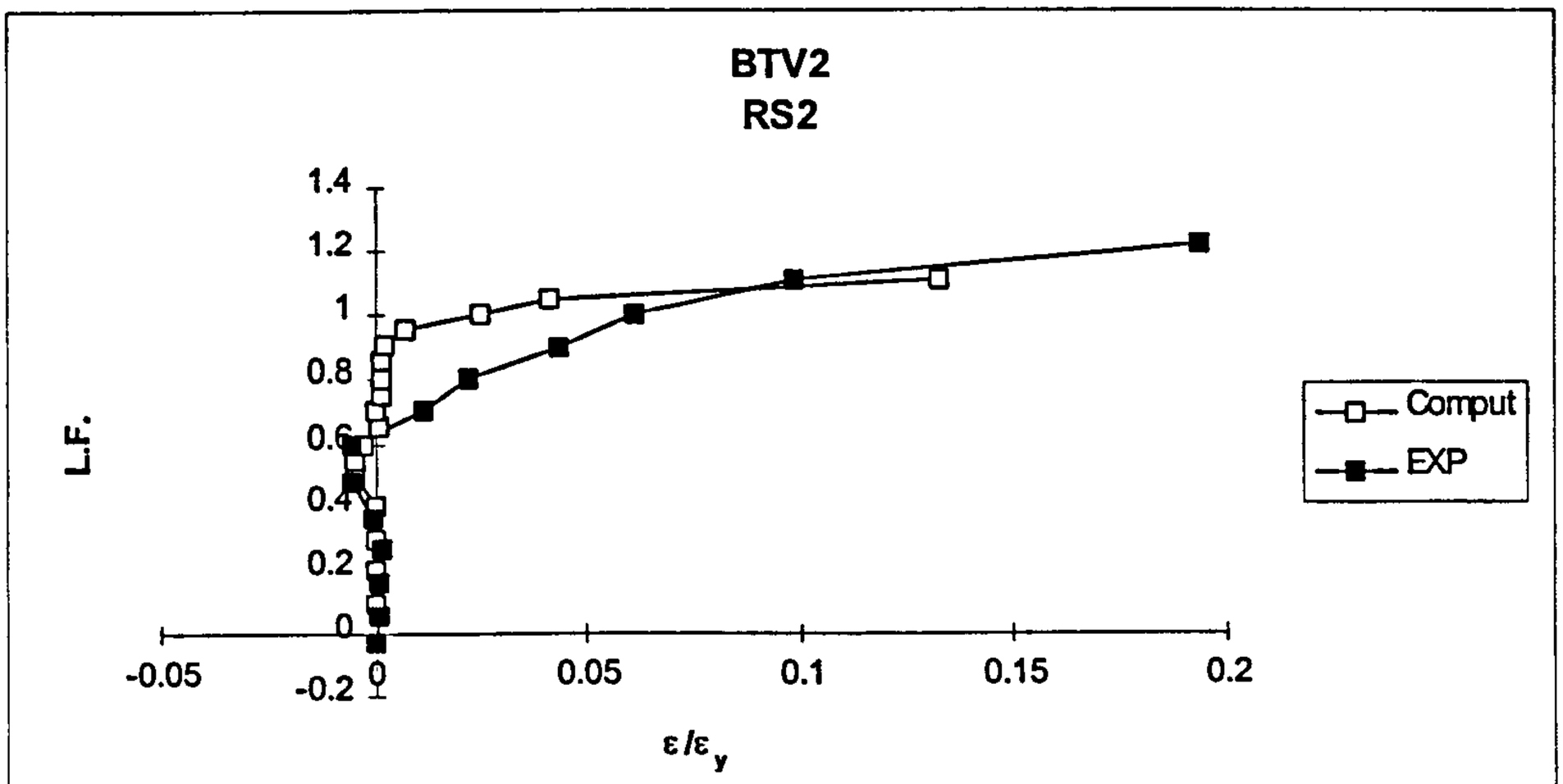
BTV2
RS2
L.F.
1.4
1.2
1
0.8
0.6
0.4
0.2
0
-0.2
-0.05
0
0.05
0.1
0.15
0.2
Comput
EXP
ε/ε y

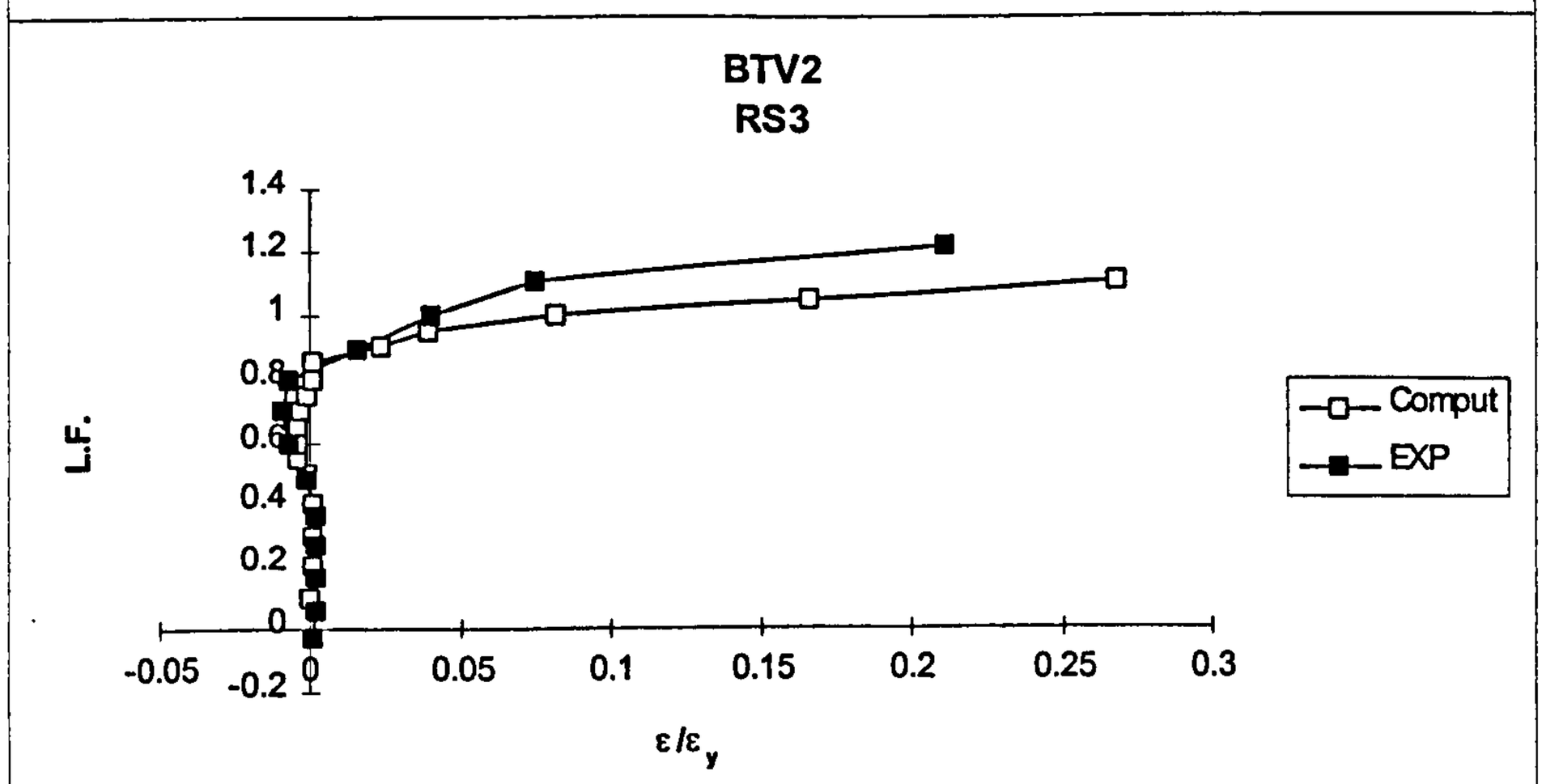
BTV2
RS3
L.F.
1.4
1.2
1
0.8
0.6
0.4
0.2
0
-0.2
-0.05
0
0.05
0.1
0.15
0.2
0.25
0.3
Comput
EXP
ε/ε y

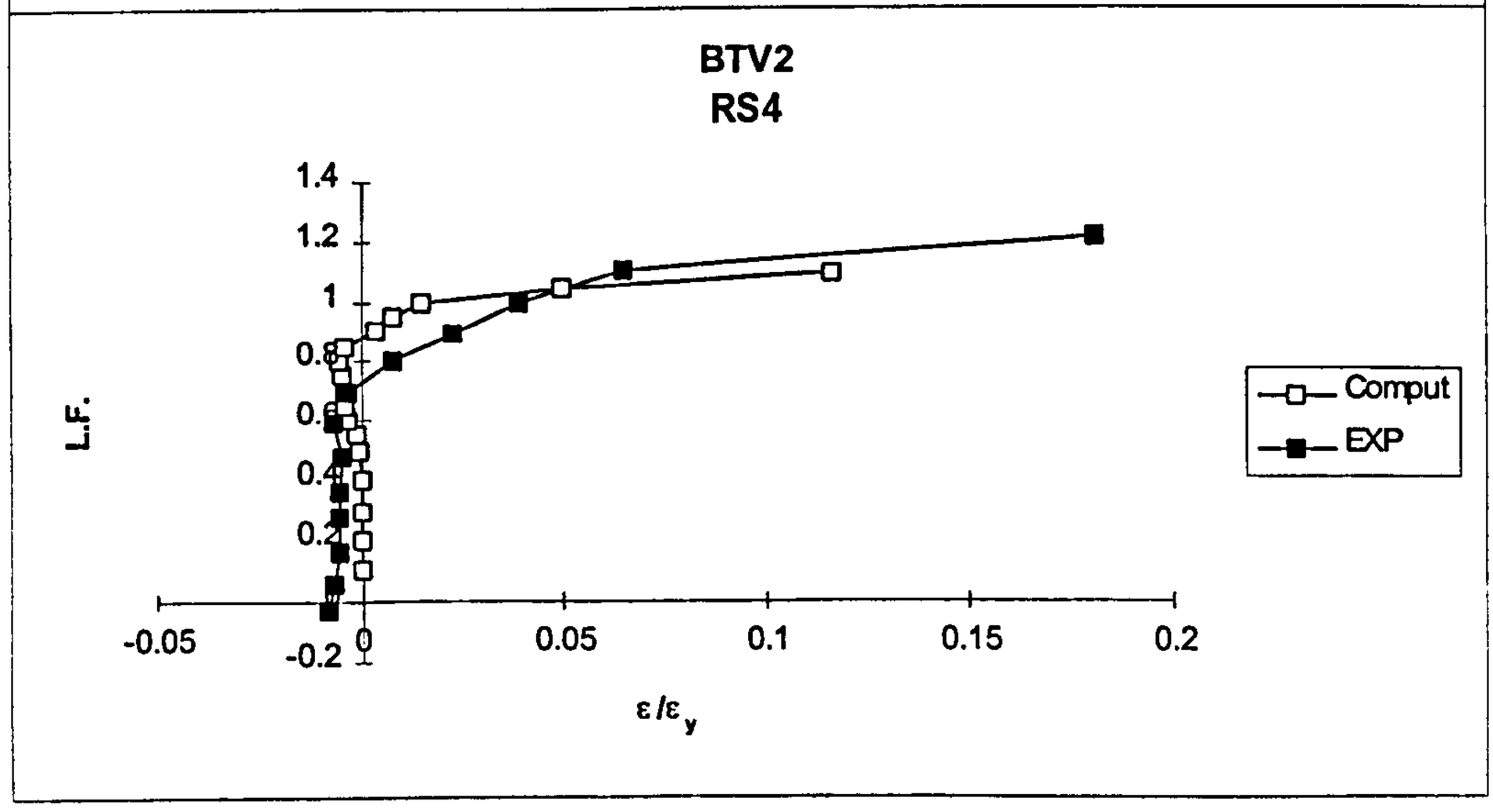
BTV2
RS4
L.F.
1.4
1.2
1
0.8
0.6
0.4
0.2
-0.2
-0.05
0
0.05
0.1
0.15
0.2
Comput
EXP
ε/ε y

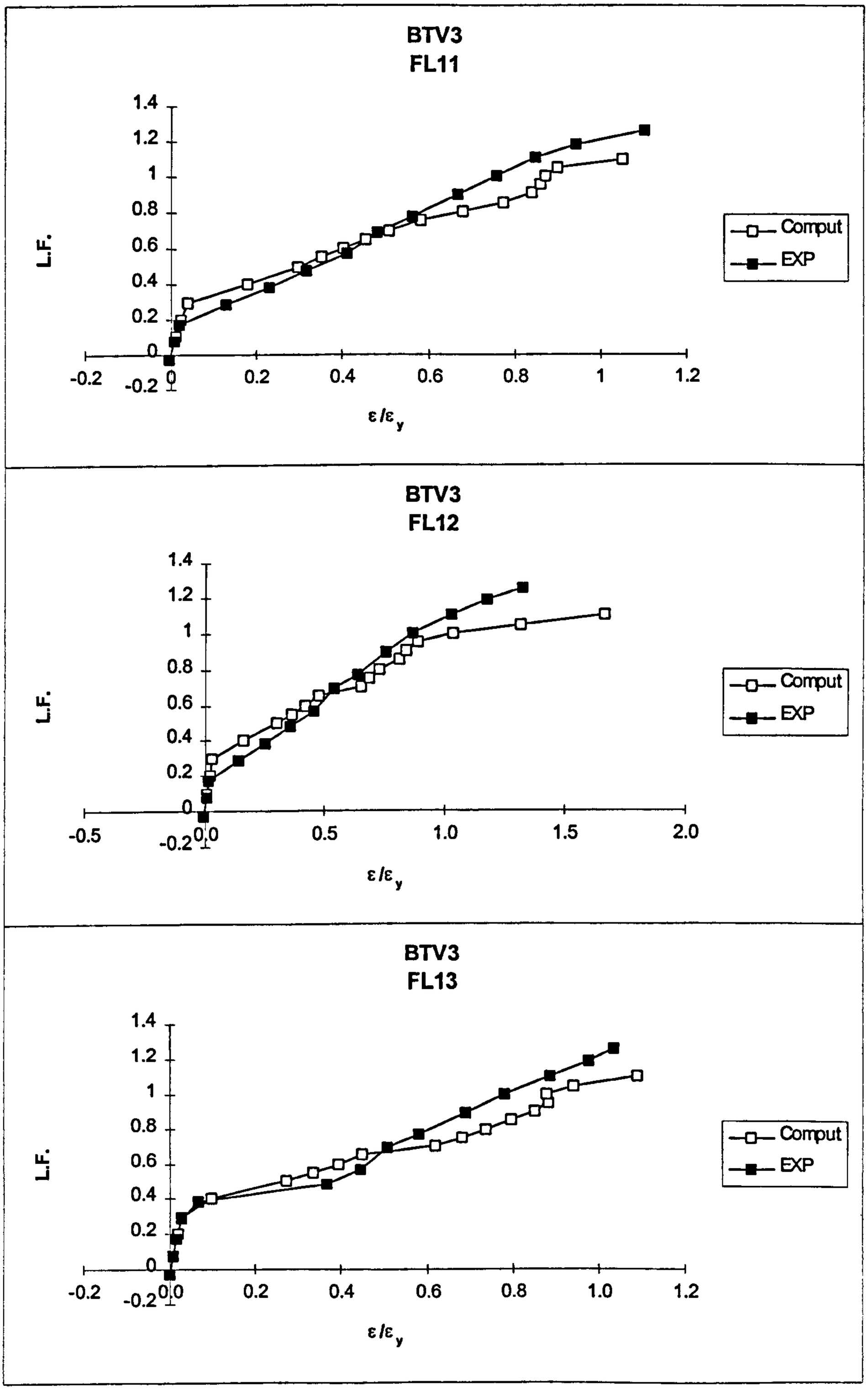
BTV3
FL11
L.F.
1.4
1.2
1
0.8
0.6
0.4
0.2
0
-0.2
-0.2
0
0.2
0.4
0.6
0.8
1
1.2
ε/ε y
Comput
EXP
BTV3
FL12
L.F.
1.4
1.2
1
0.8
0.6
0.4
0.2
0
-0.5
-0.2
0.0
0.5
1.0
1.5
2.0
ε/ε y
Comput
EXP
BTV3
FL13
L.F.
1.4
1.2
1
0.8
0.6
0.4
0.2
0
-0.2
-0.2
0.0
0.2
0.4
0.6
0.8
1.0
1.2
ε/ε y
Comput
EXP

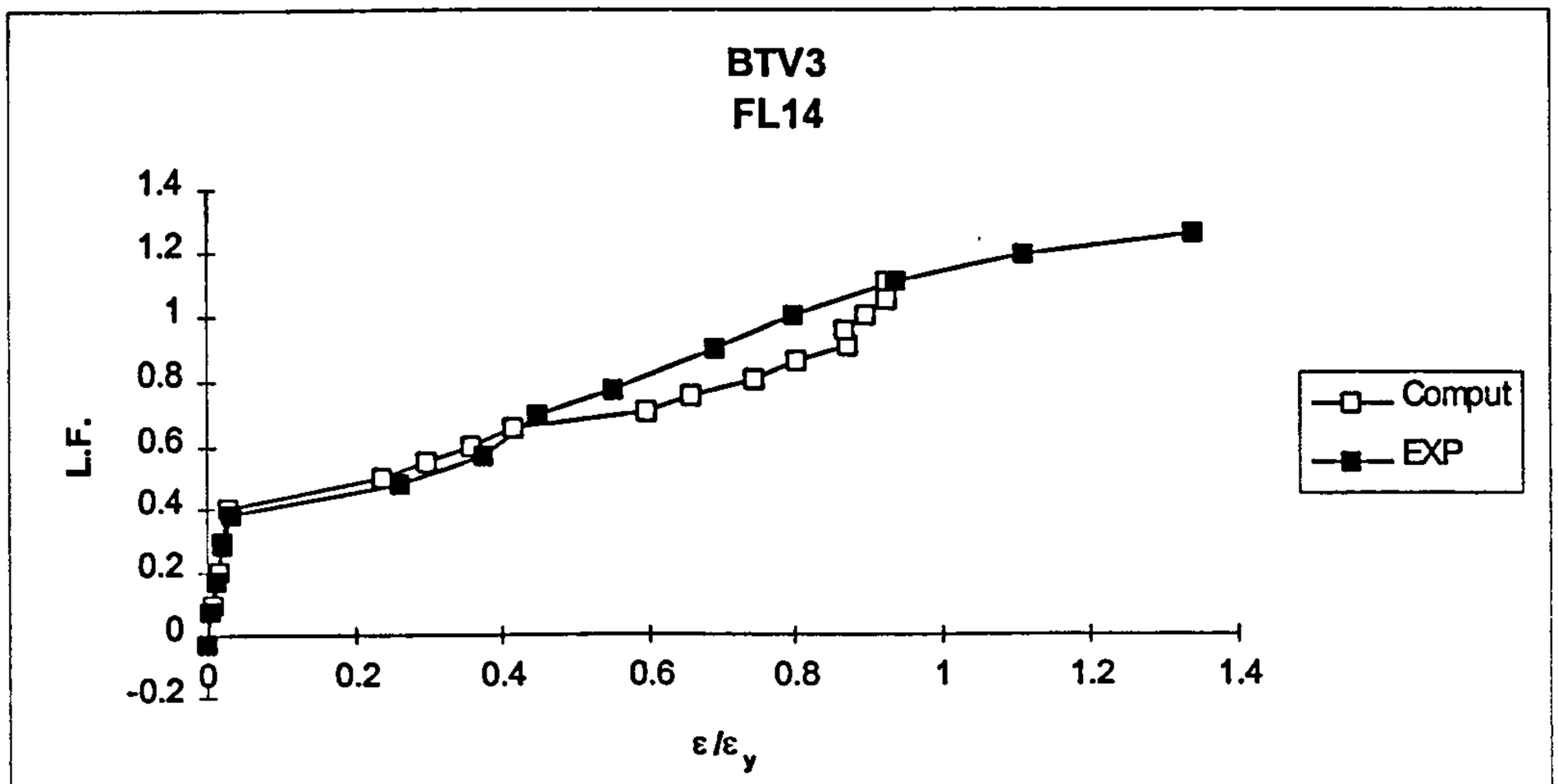
BTV3
FL14
L.F.
1.4
1.2
1
0.8
0.6
0.4
0.2
0
-0.2
0
0.2
0.4
0.6
0.8
1
1.2
1.4
ε /ε y
Comput
EXP

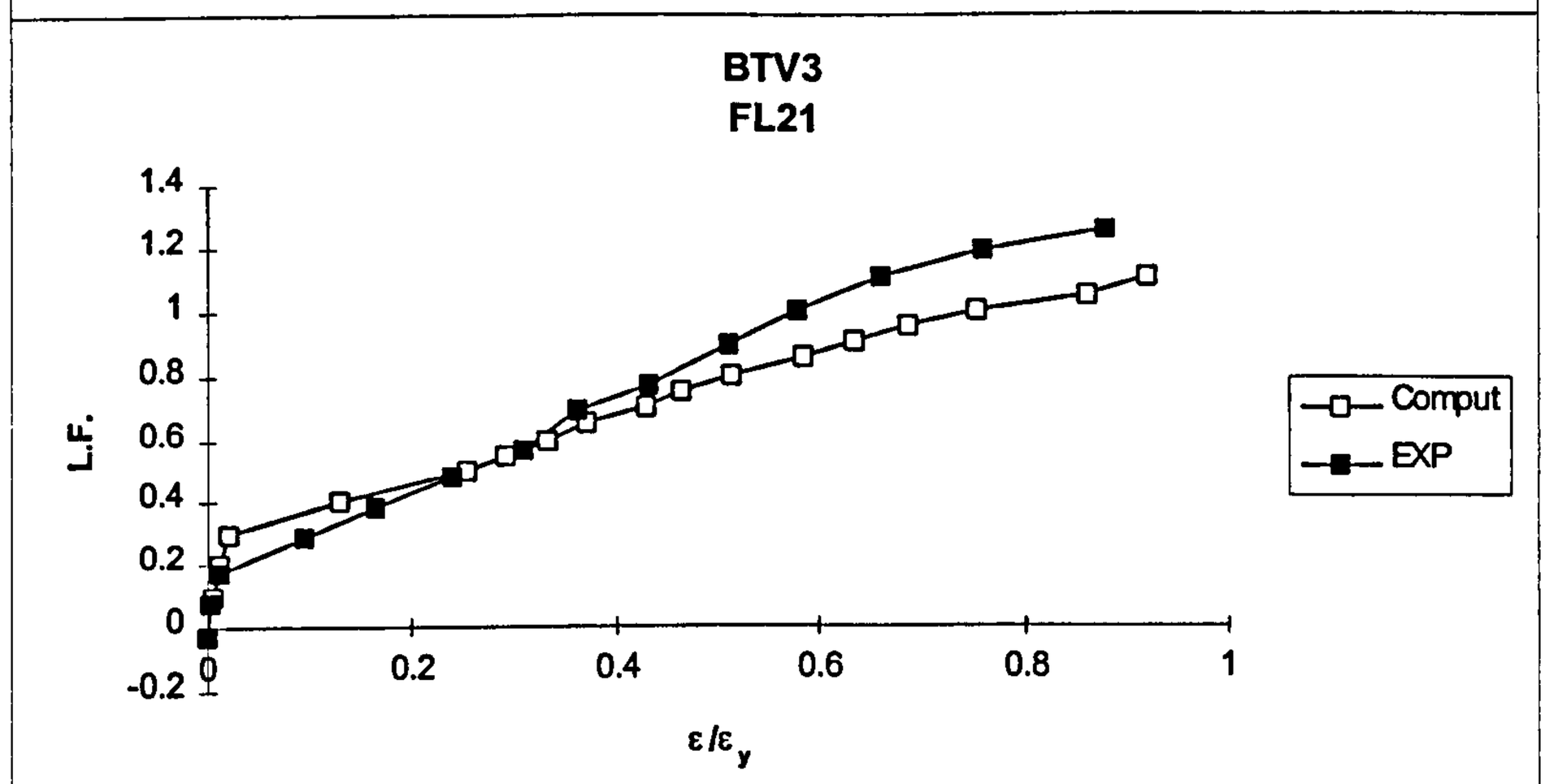
BTV3
FL21
L.F.
1.4
1.2
1
0.8
0.6
0.4
0.2
0
-0.2
0
0.2
0.4
0.6
0.8
1
ε /ε y
Comput
EXP

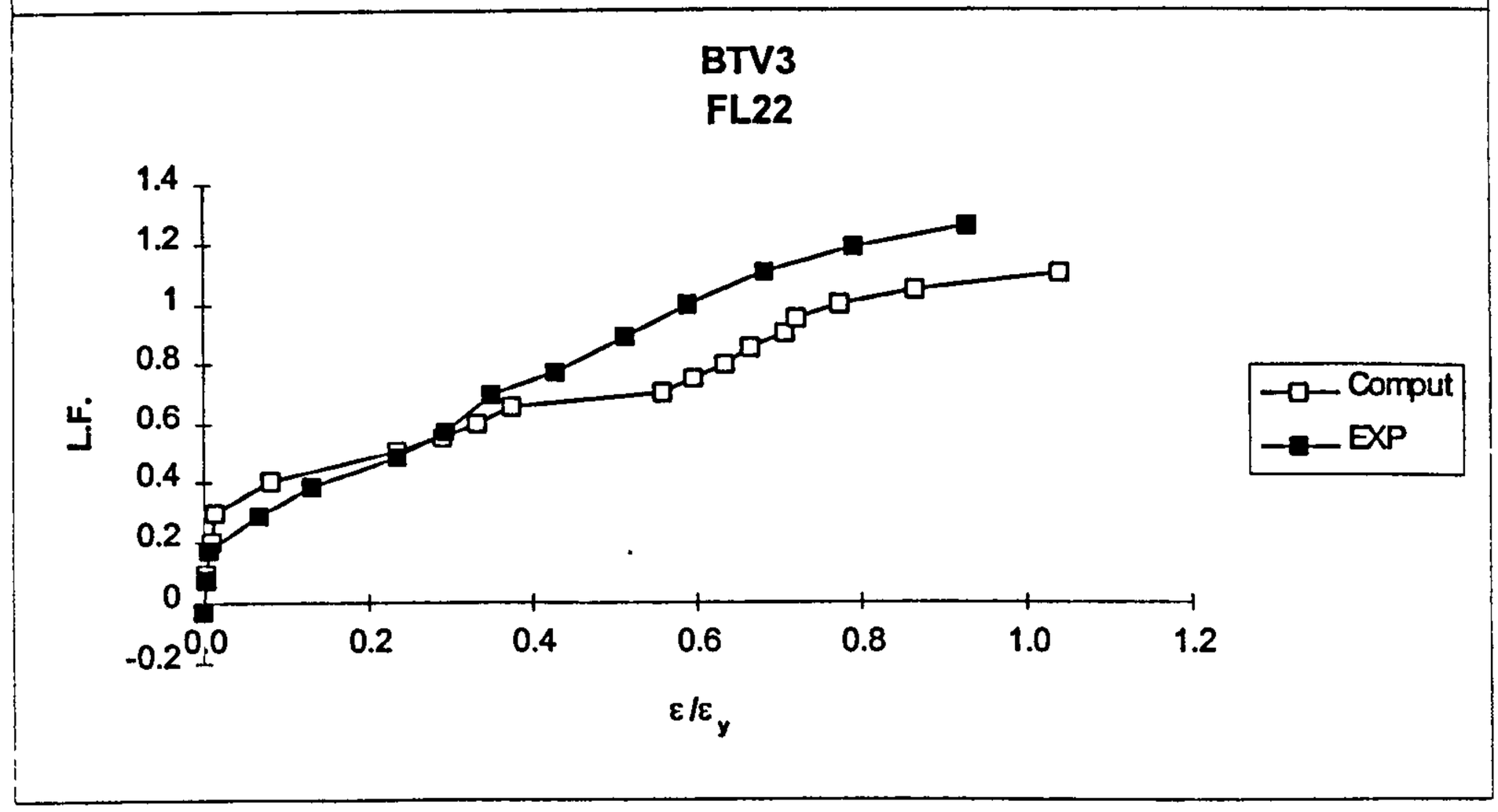
BTV3
FL22
L.F.
1.4
1.2
1
0.8
0.6
0.4
0.2
0
-0.2
0,0
0.2
0.4
0.6
0.8
1.0
1.2
ε /ε y
Comput
EXP

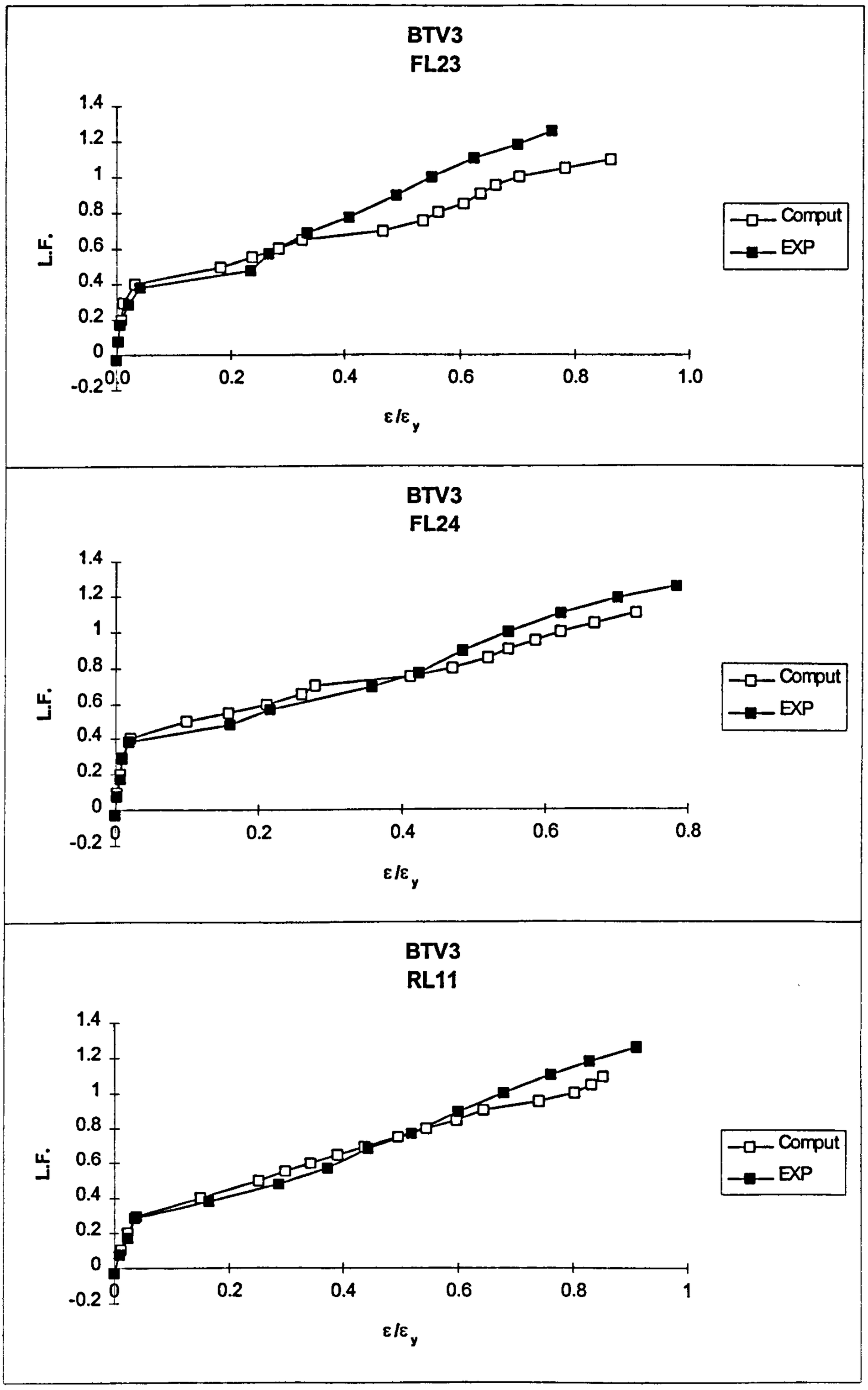
BTV3
FL23
L.F.
1.4
1.2
1
0.8
0.6
0.4
0.2
0
-0.2
0.0
0.2
0.4
0.6
0.8
1.0
ε/ε y
Comput
EXP
BTV3
FL24
L.F.
1.4
1.2
1
0.8
0.6
0.4
0.2
0
-0.2
0
0.2
0.4
0.6
0.8
ε/ε y
Comput
EXP
BTV3
RL11
L.F.
1.4
1.2
1
0.8
0.6
0.4
0.2
0
-0.2
0
0.2
0.4
0.6
0.8
1
ε/ε y
Comput
EXP

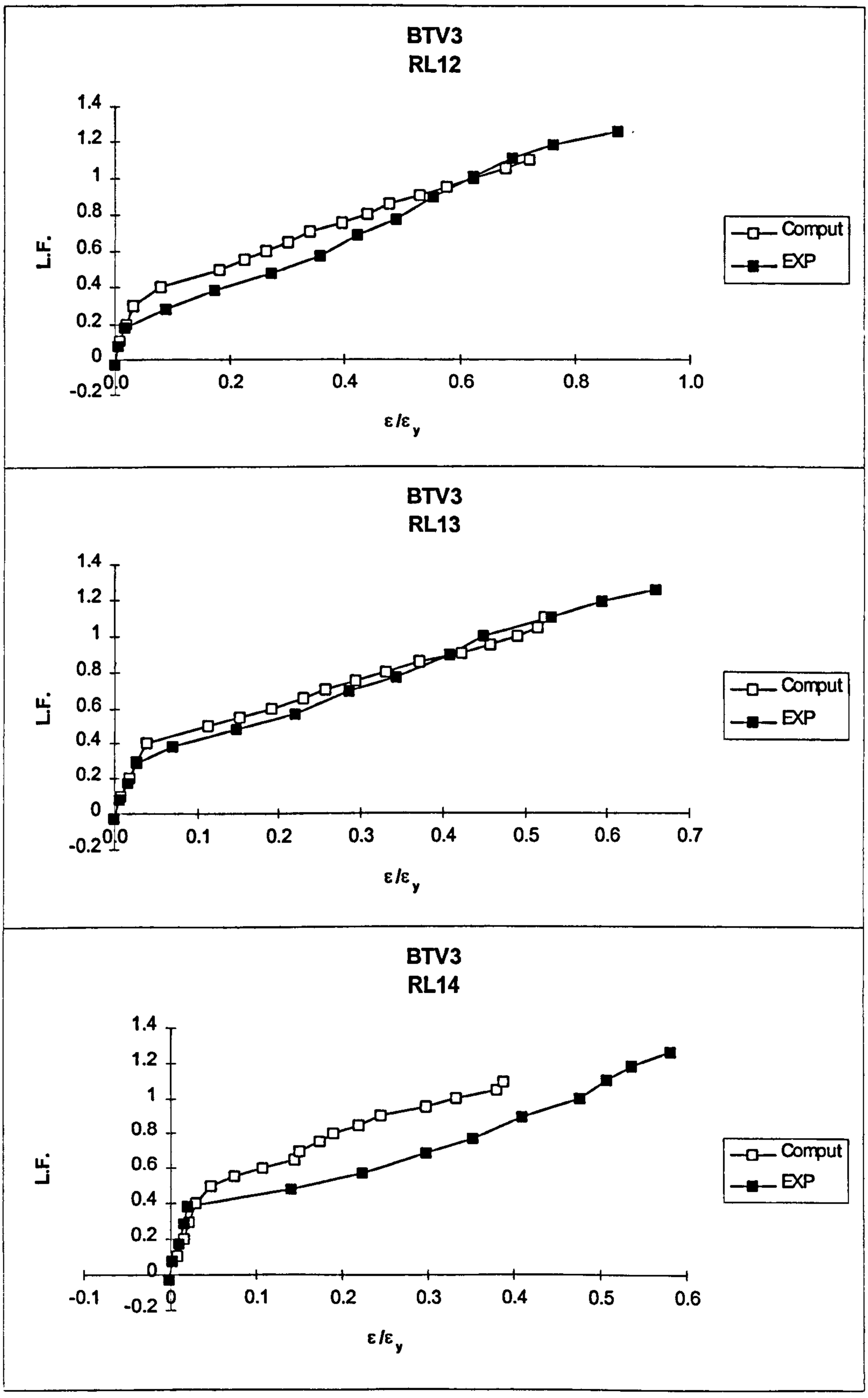
BTV3
RL12
L.F.
1.4
1.2
1
0.8
0.6
0.4
0.2
0
-0.2
0.0
0.2
0.4
0.6
0.8
1.0
ε/ε y
Comput
EXP
BTV3
RL13
L.F.
1.4
1.2
1
0.8
0.6
0.4
0.2
0
-0.2
0.0
0.1
0.2
0.3
0.4
0.5
0.6
0.7
ε/ε y
Comput
EXP
BTV3
RL14
L.F.
1.4
1.2
1
0.8
0.6
0.4
0.2
0
-0.2
-0.1
0
0.1
0.2
0.3
0.4
0.5
0.6
ε/ε y
Comput
EXP

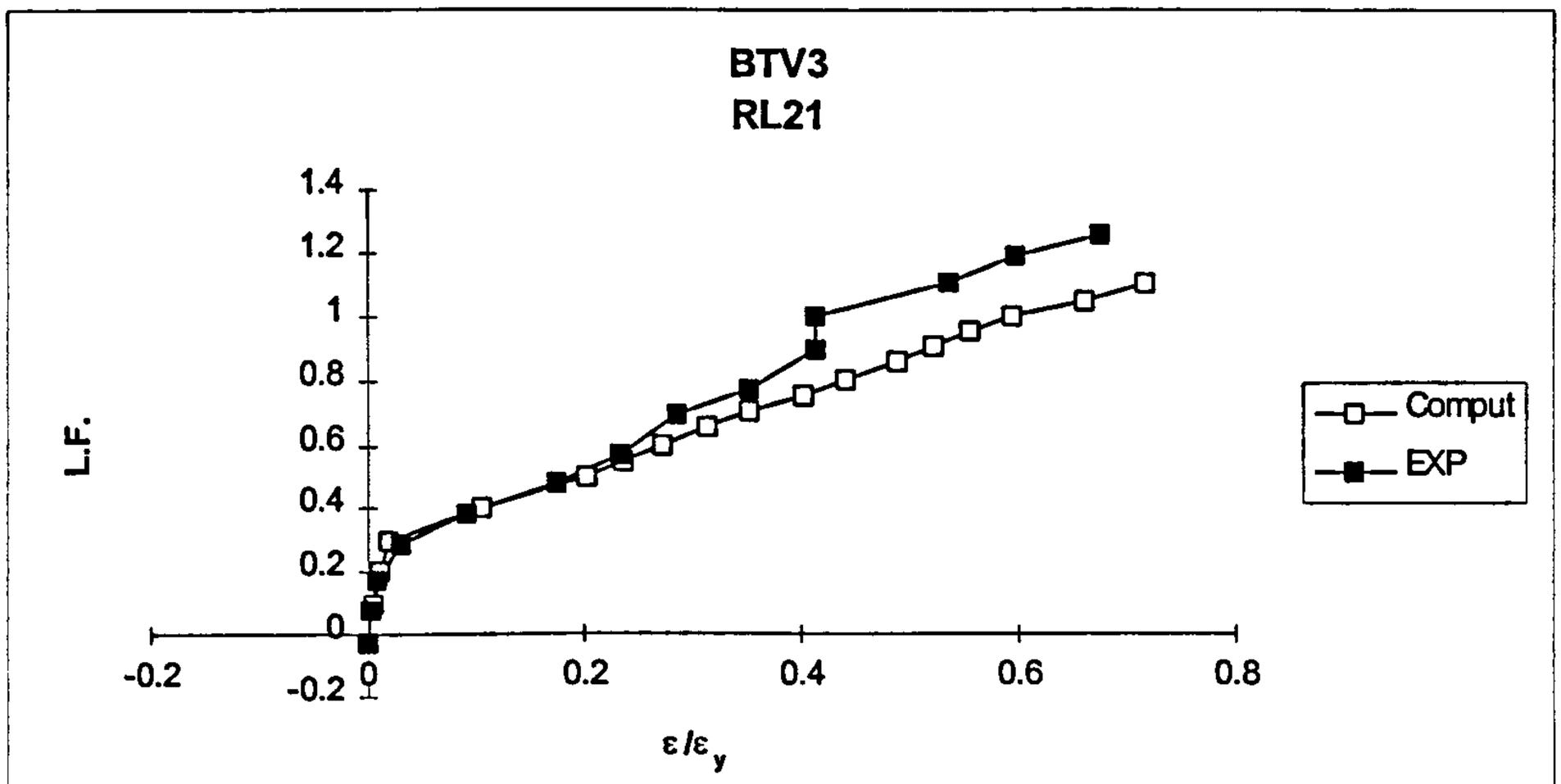
BTV3
RL21
L.F.
1.4
1.2
1
0.8
0.6
0.4
0.2
0
-0.2
0
0.2
0.4
0.6
0.8
Comput
EXP
ε/ε y

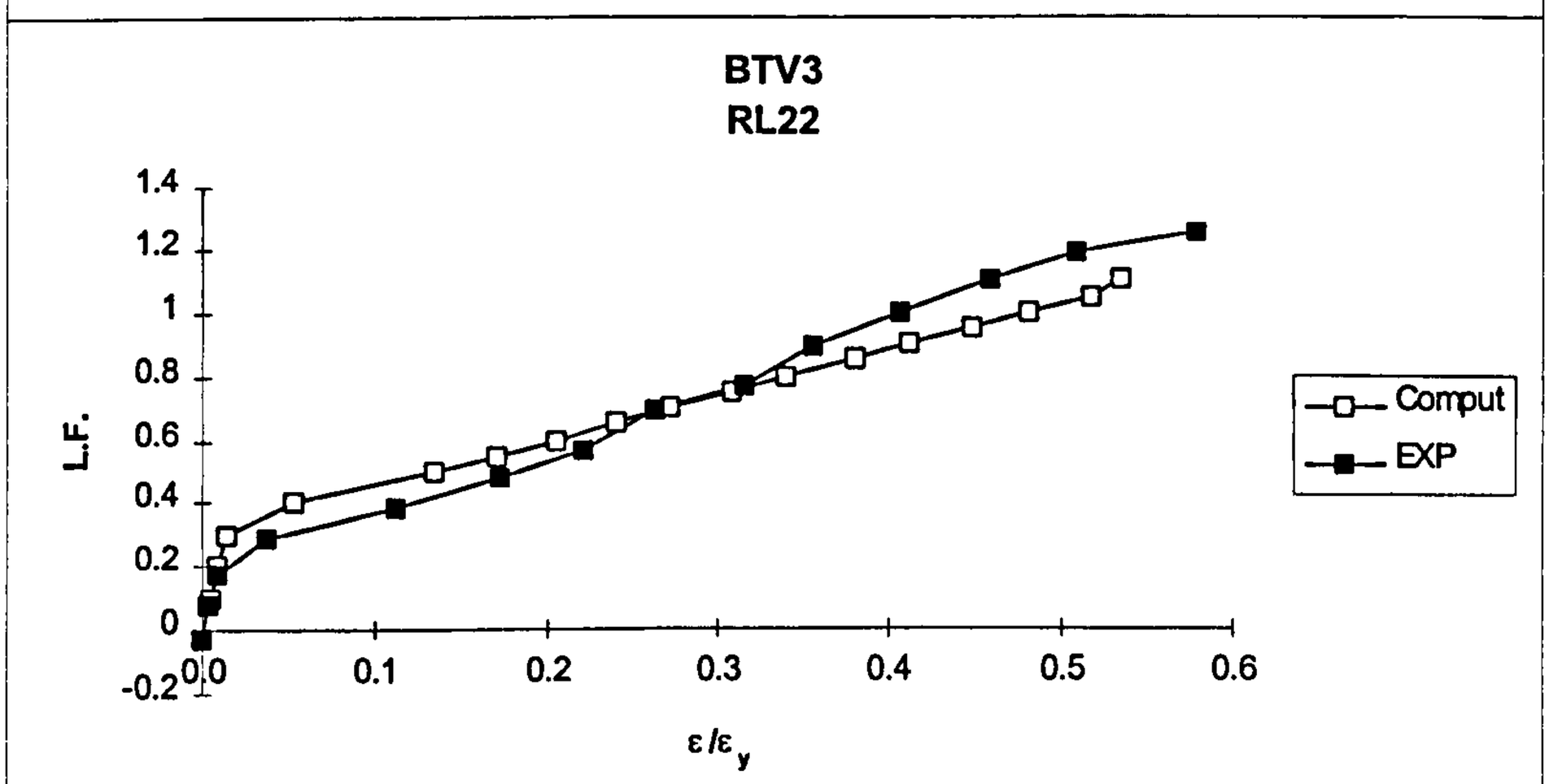
BTV3
RL22
L.F.
1.4
1.2
1
0.8
0.6
0.4
0.2
0
-0.2
0.0
0.1
0.2
0.3
0.4
0.5
0.6
Comput
EXP
ε/ε y

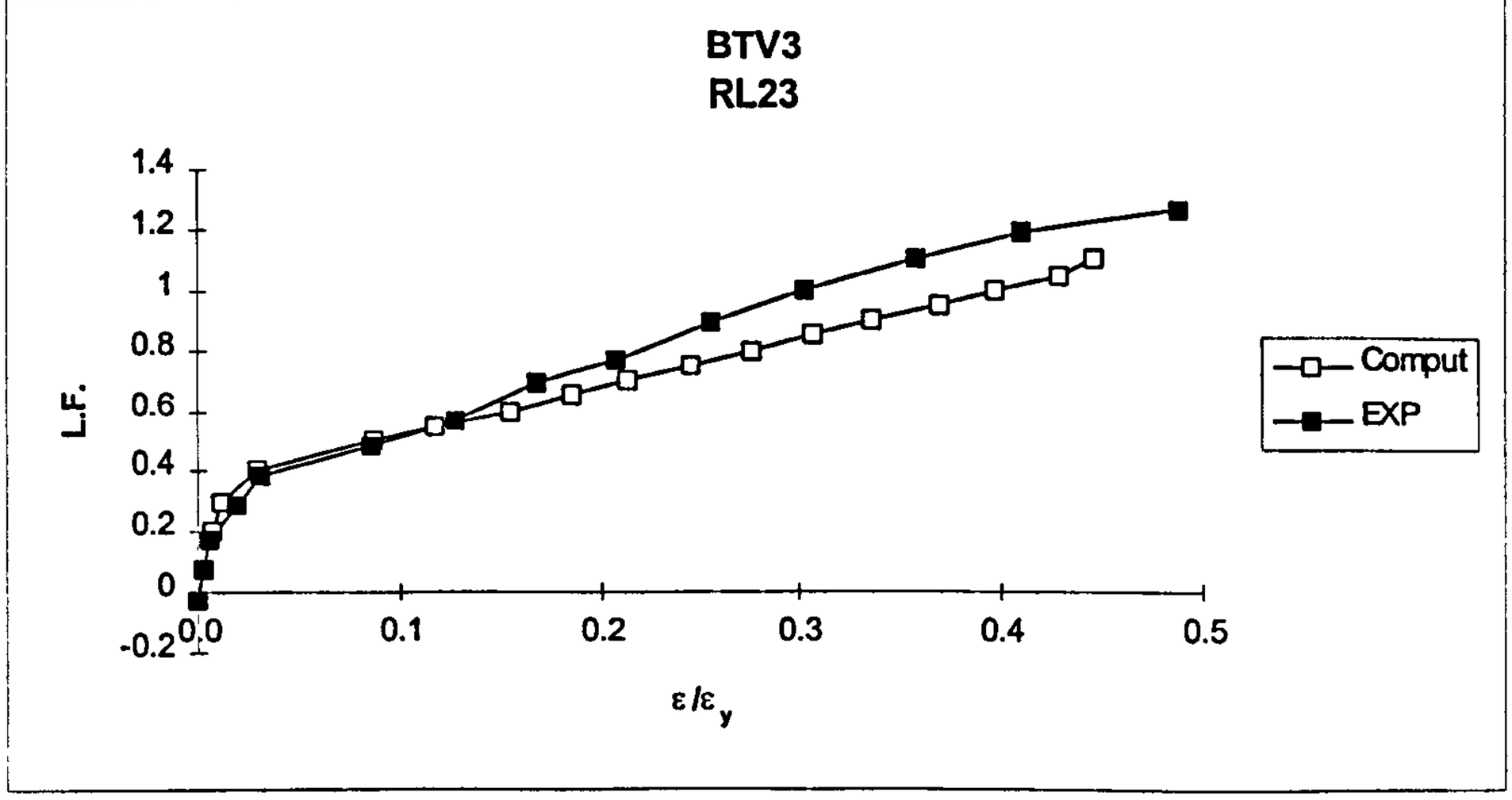
BTV3
RL23
L.F.
1.4
1.2
1
0.8
0.6
0.4
0.2
0
-0.2
0.0
0.1
0.2
0.3
0.4
0.5
Comput
EXP
ε/ε y

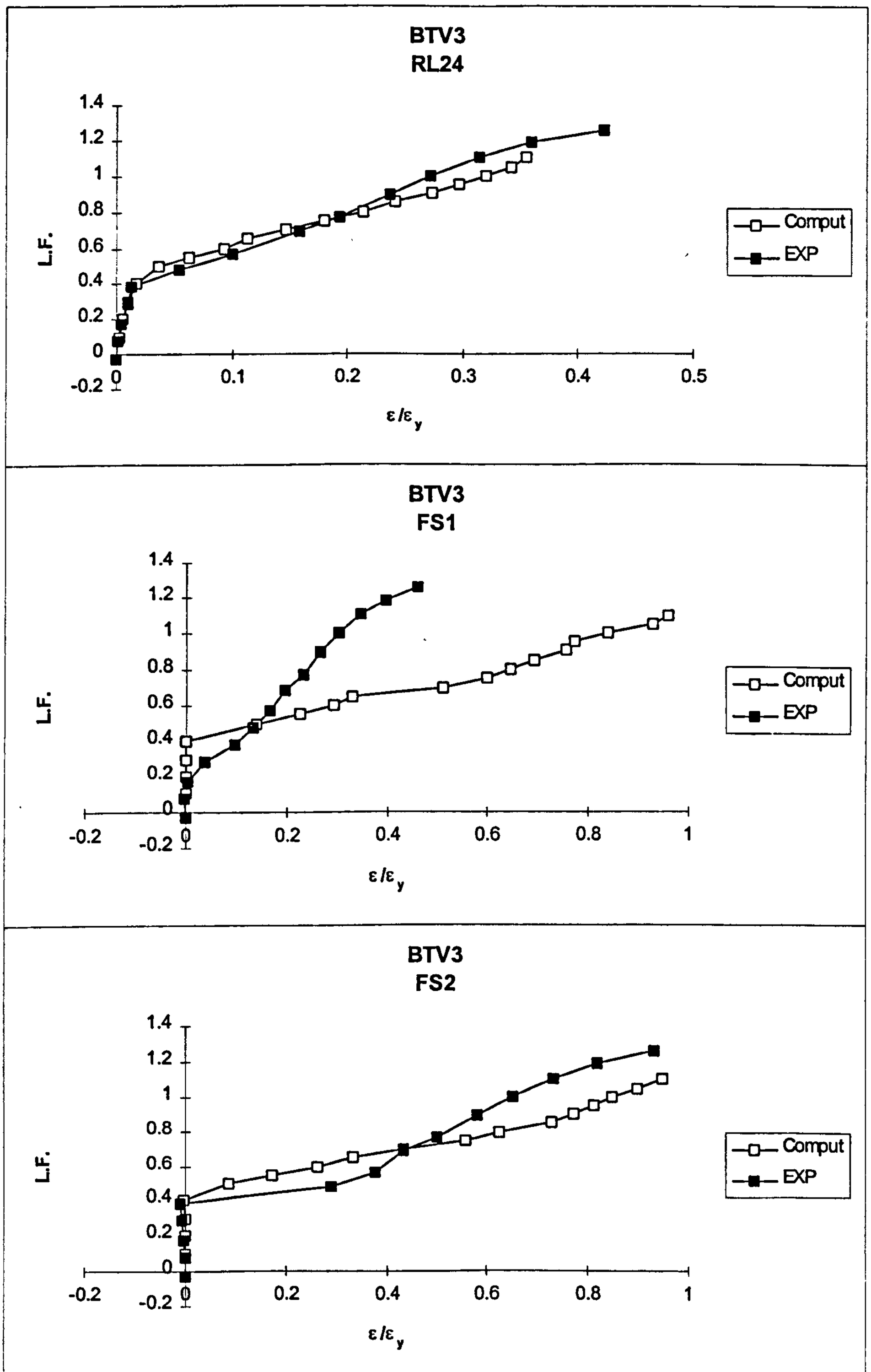
BTV3
RL24
L.F.
1.4
1.2
1
0.8
0.6
0.4
0.2
0
-0.2
0
0.1
0.2
0.3
0.4
0.5
ε/ε y
Comput
EXP
BTV3
FS1
L.F.
1.4
1.2
1
0.8
0.6
0.4
0.2
0
-0.2
-0.2
0
0.2
0.4
0.6
0.8
1
ε/ε y
Comput
EXP
BTV3
FS2
L.F.
1.4
1.2
1
0.8
0.6
0.4
0.2
0
-0.2
-0.2
0
0.2
0.4
0.6
0.8
1
ε/ε y
Comput
EXP

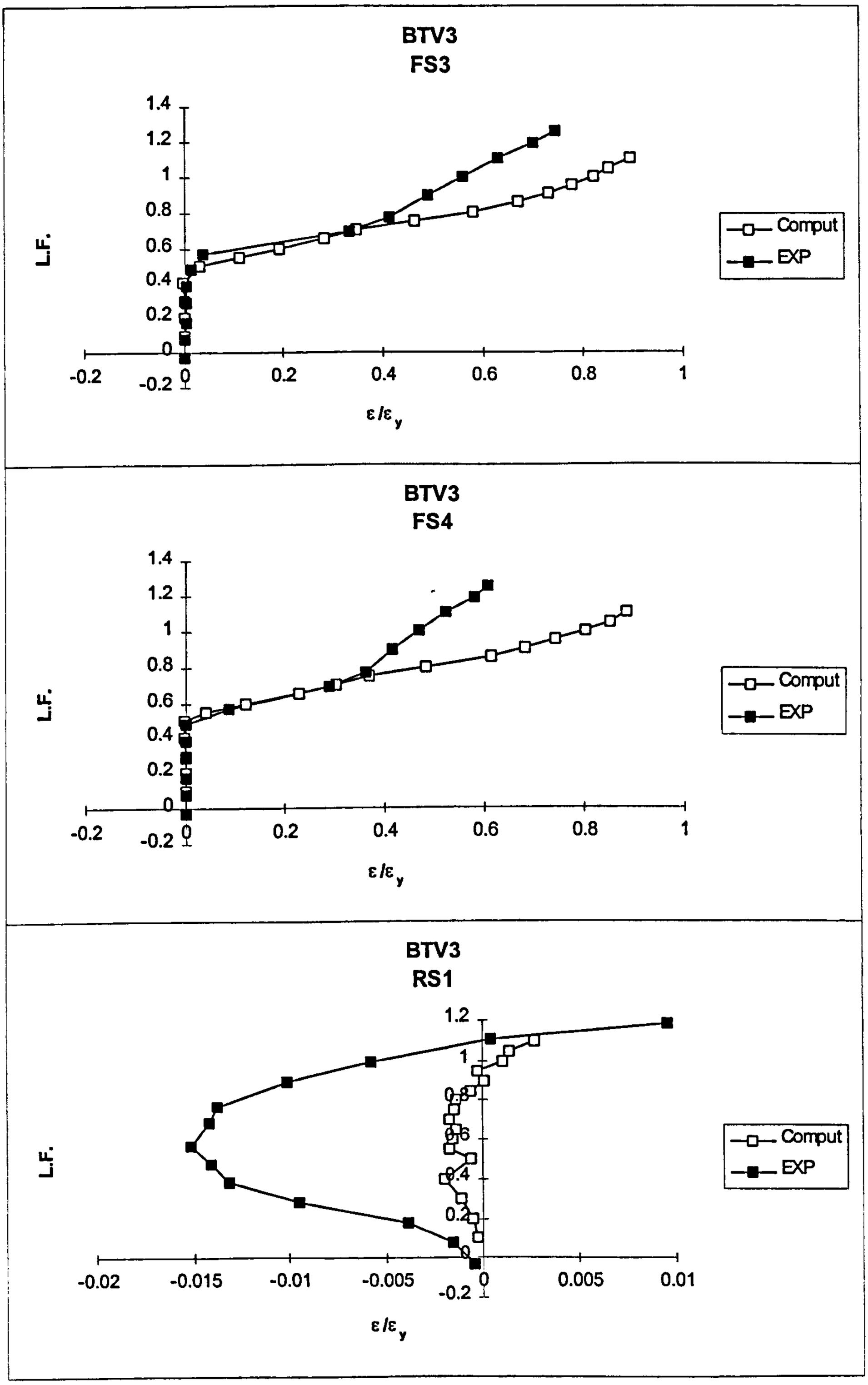
BTV3
FS3
L.F.
1.4
1.2
1
0.8
0.6
0.4
0.2
0
-0.2
-0.2
0
0.2
0.4
0.6
0.8
1
ε/ε y
Comput
EXP
BTV3
FS4
L.F.
1.4
1.2
1
0.8
0.6
0.4
0.2
0
-0.2
-0.2
0
0.2
0.4
0.6
0.8
1
ε/ε y
Comput
EXP
BTV3
RS1
L.F.
1.2
1
0.8
0.6
0.4
0.2
0
-0.02
-0.015
-0.01
-0.005
-0.2
0
0.005
0.01
ε/ε y
Comput
EXP

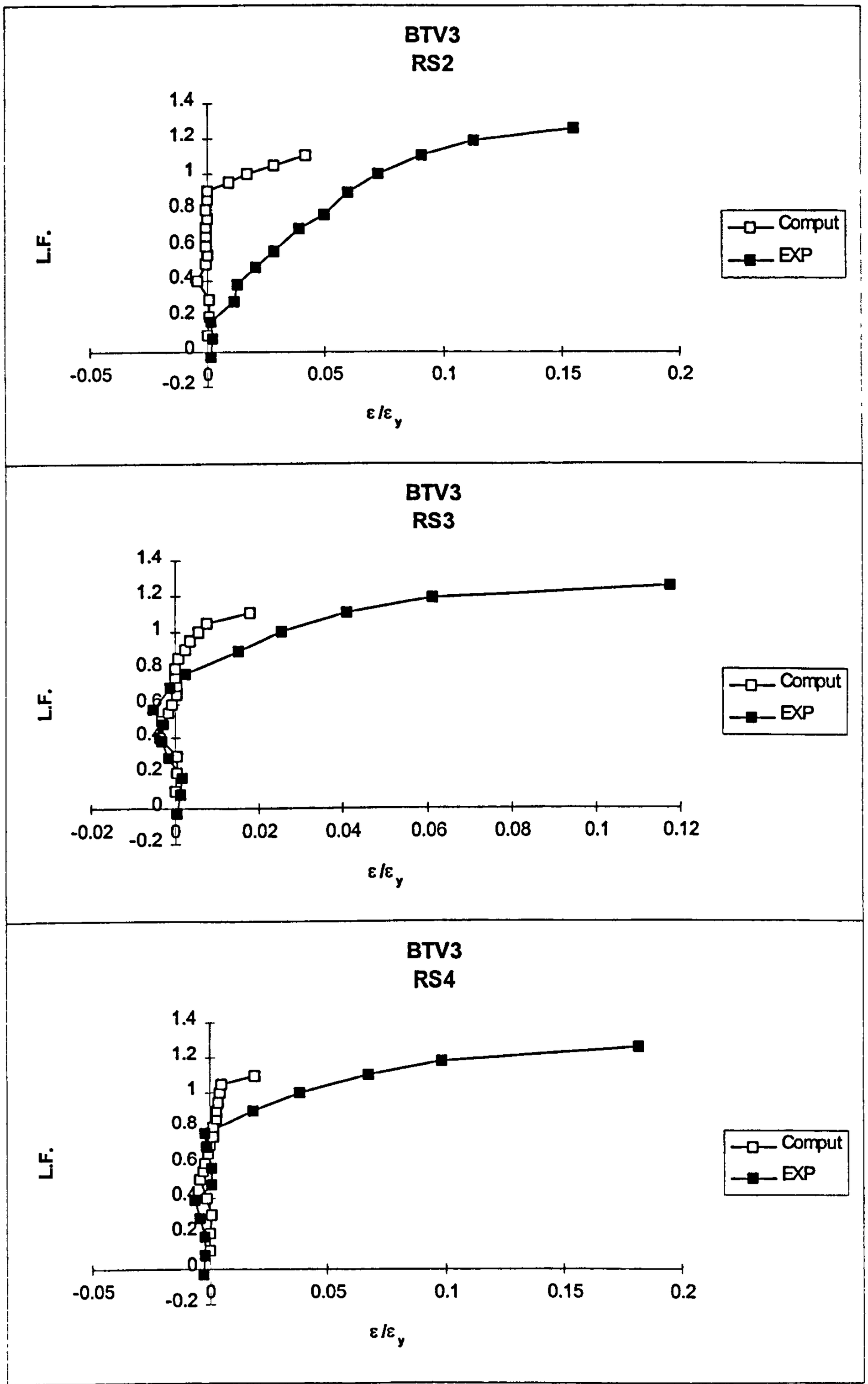
BTV3
RS2
L.F.
1.4
1.2
1
0.8
0.6
0.4
0.2
0
-0.2
-0.05
0
0.05
0.1
0.15
0.2
ε /ε y
Comput
EXP
BTV3
RS3
L.F.
1.4
1.2
1
0.8
0.6
0.4
0.2
0
-0.2
-0.02
0
0.02
0.04
0.06
0.08
0.1
0.12
ε /ε y
Comput
EXP
BTV3
RS4
L.F.
1.4
1.2
1
0.8
0.6
0.4
0.2
0
-0.2
-0.05
0
0.05
0.1
0.15
0.2
ε /ε y
Comput
EXP

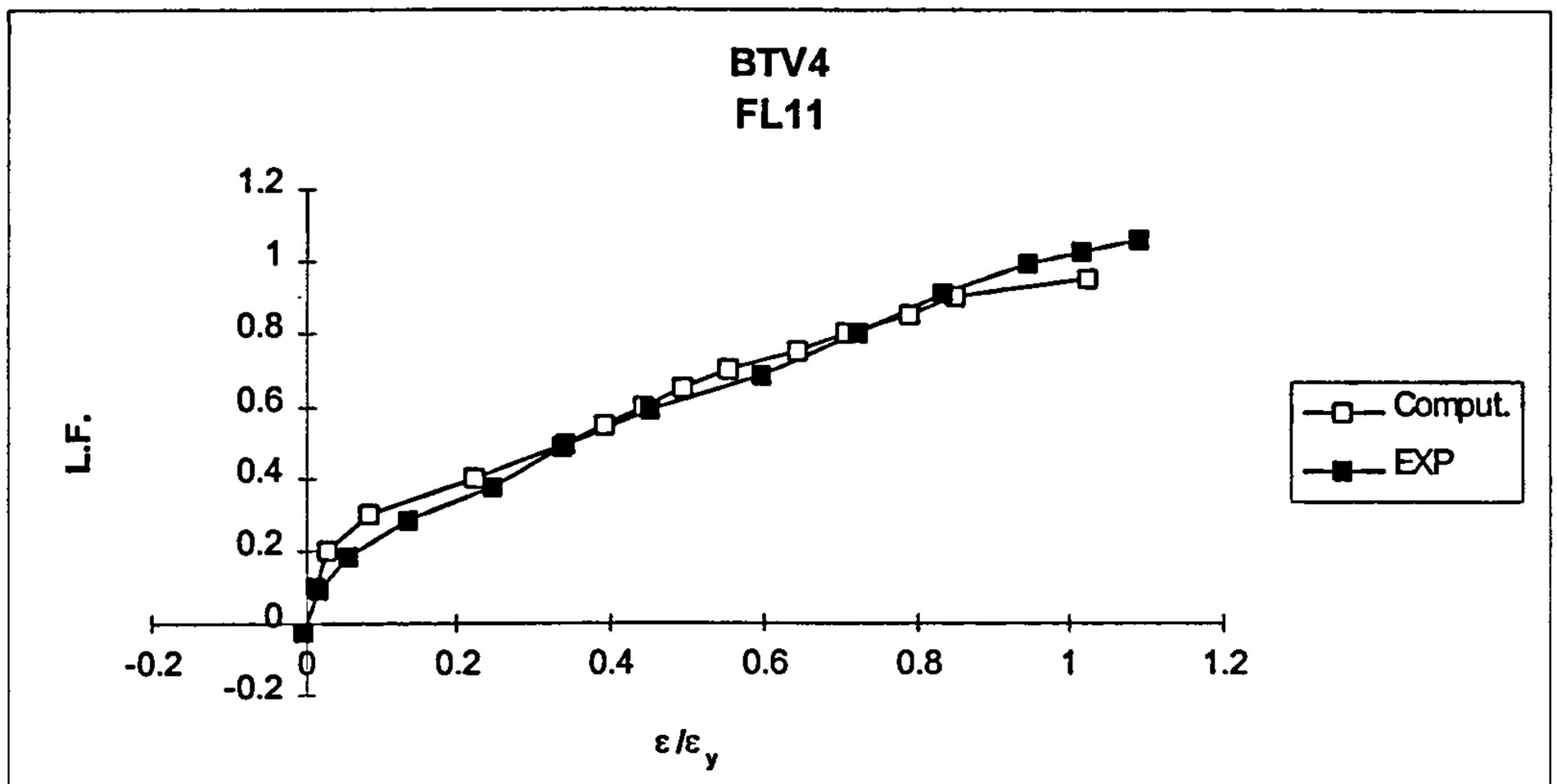
BTV4
FL11
L.F.
1.2
1
0.8
0.6
0.4
0.2
0
-0.2
-0.2
0
0.2
0.4
0.6
0.8
1
1.2
Comput.
EXP
ε /ε y

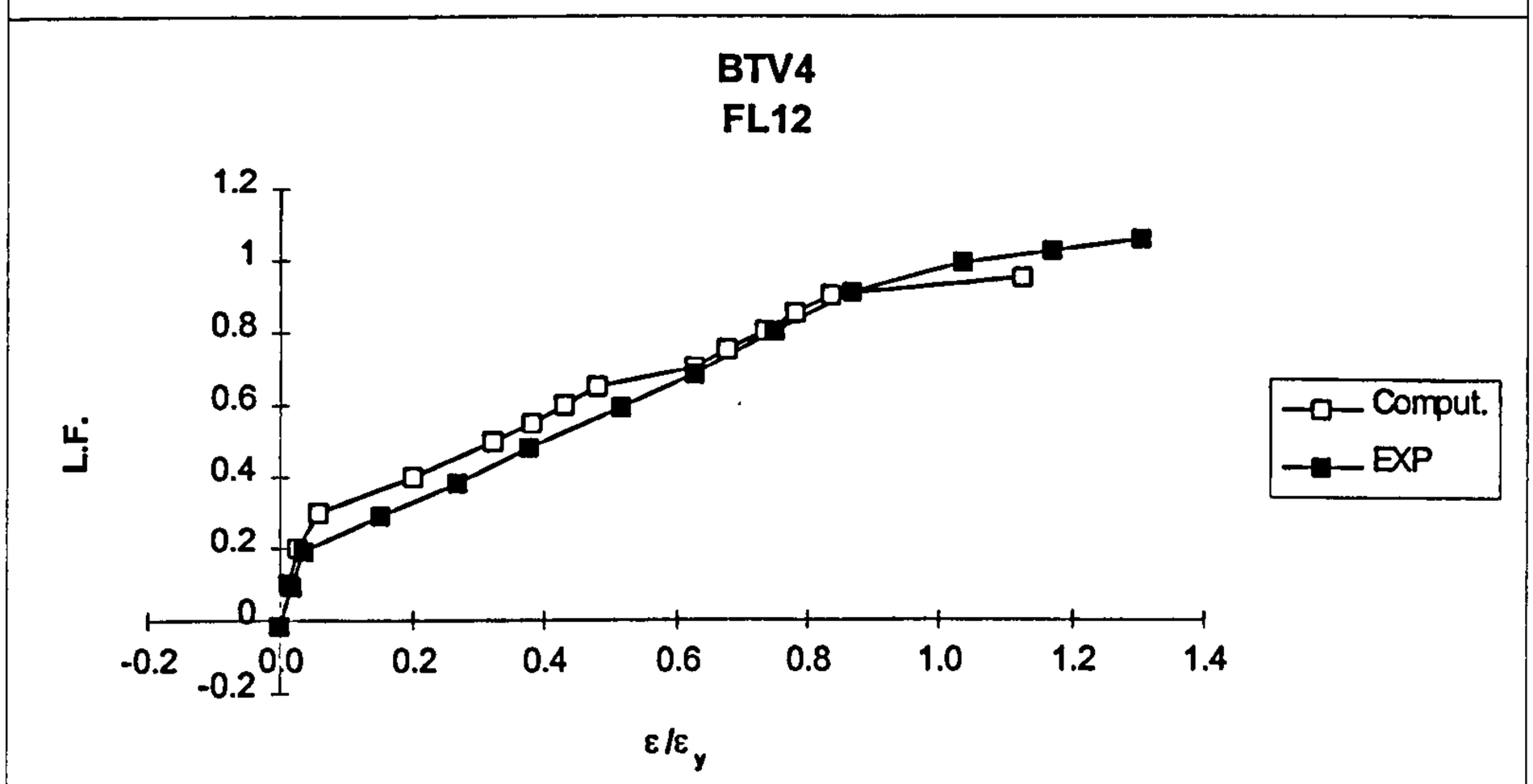
BTV4
FL12
L.F.
1.2
1
0.8
0.6
0.4
0.2
0
-0.2
-0.2
0.0
0.2
0.4
0.6
0.8
1.0
1.2
1.4
Comput.
EXP
ε /ε y

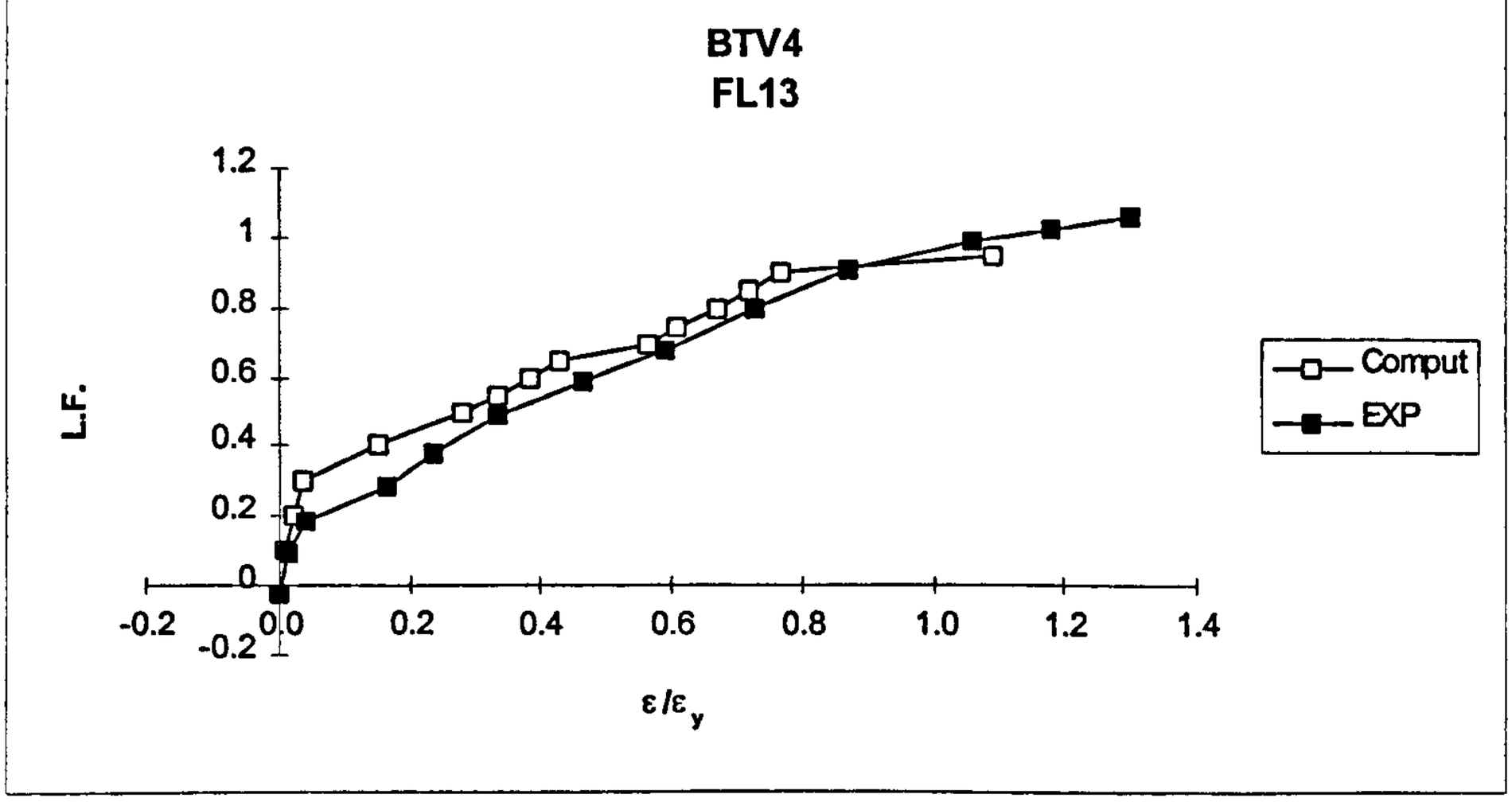
BTV4
FL13
L.F.
1.2
1
0.8
0.6
0.4
0.2
0
-0.2
-0.2
0.0
0.2
0.4
0.6
0.8
1.0
1.2
1.4
Comput
EXP
ε /ε y

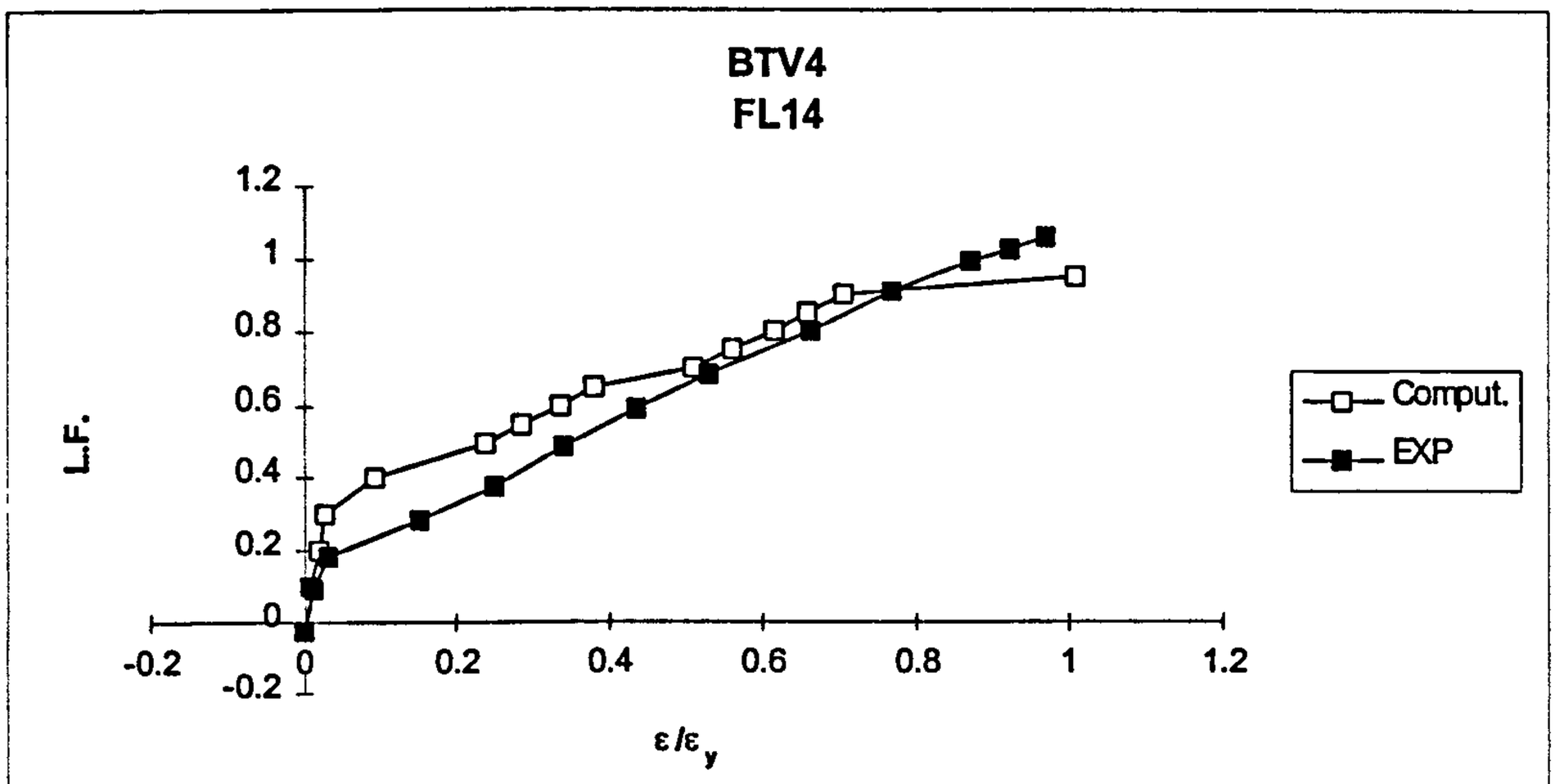
BTV4
FL14
L.F.
1.2
1
0.8
0.6
0.4
0.2
0
-0.2
-0.2
0
0.2
0.4
0.6
0.8
1
1.2
ε/ε y
Comput.
EXP

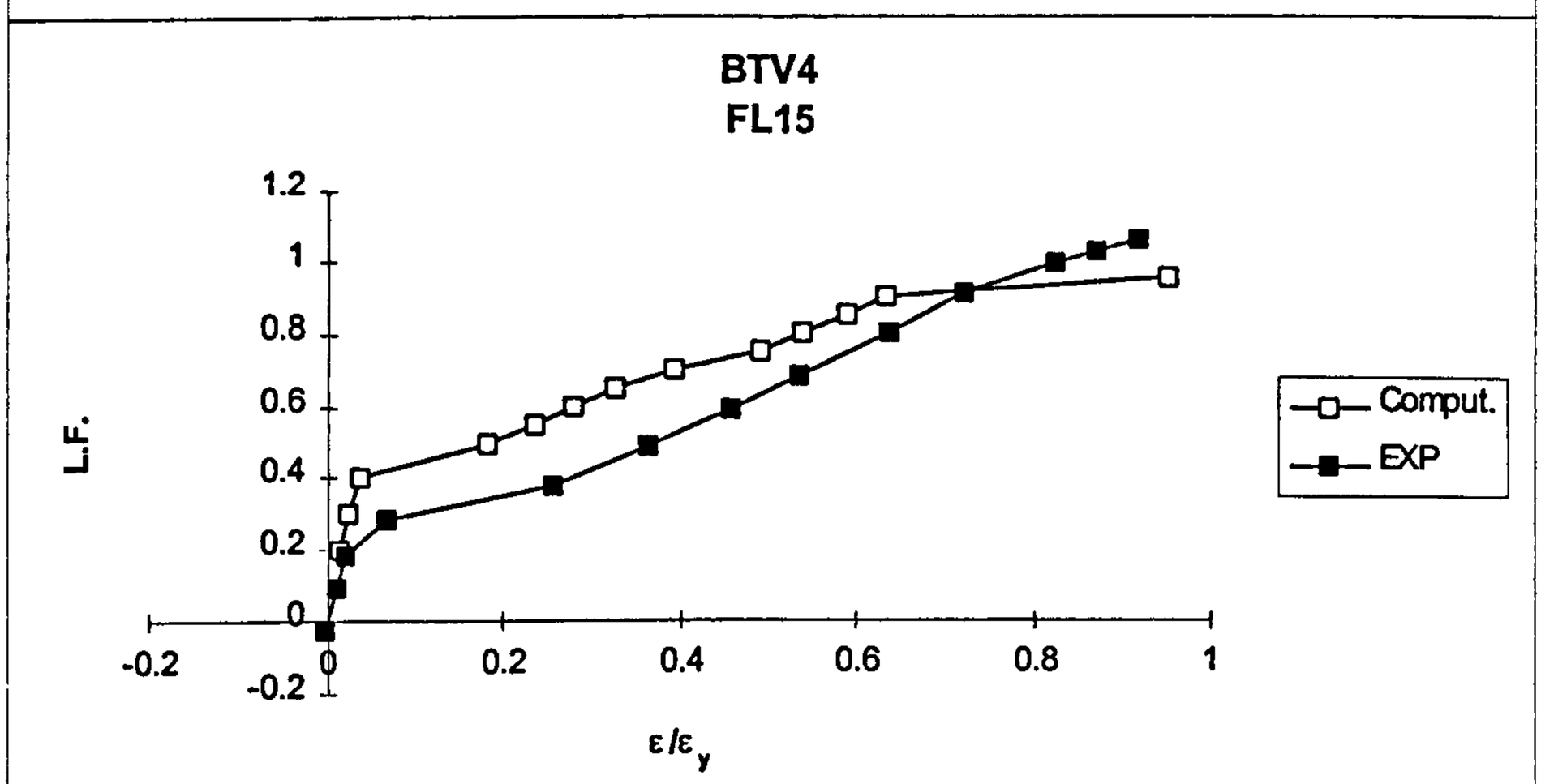
BTV4
FL15
L.F.
1.2
1
0.8
0.6
0.4
0.2
0
-0.2
-0.2
0
0.2
0.4
0.6
0.8
1
ε/ε y
Comput.
EXP

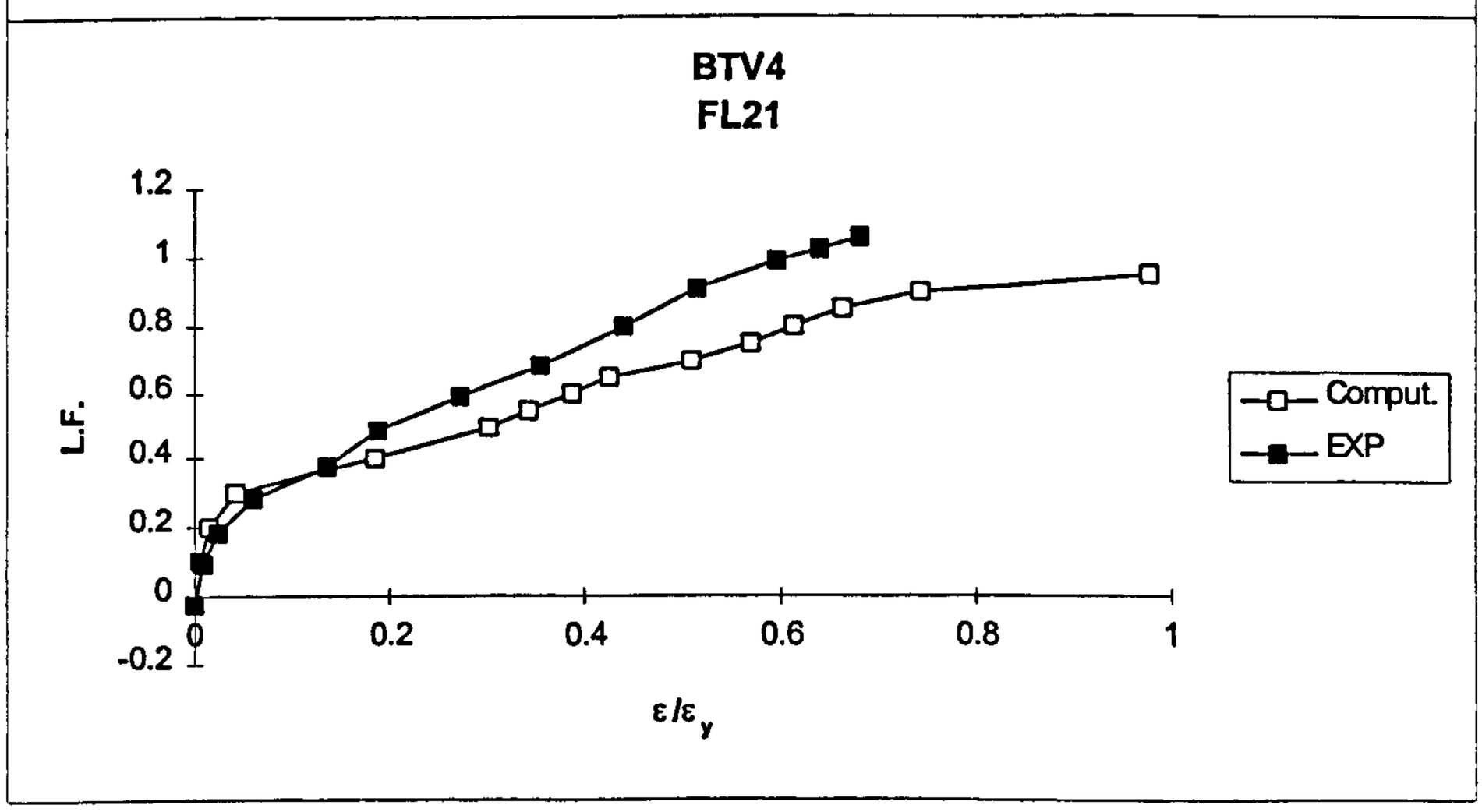
BTV4
FL21
L.F.
1.2
1
0.8
0.6
0.4
0.2
0
-0.2
0
0.2
0.4
0.6
0.8
1
ε/ε y
Comput.
EXP

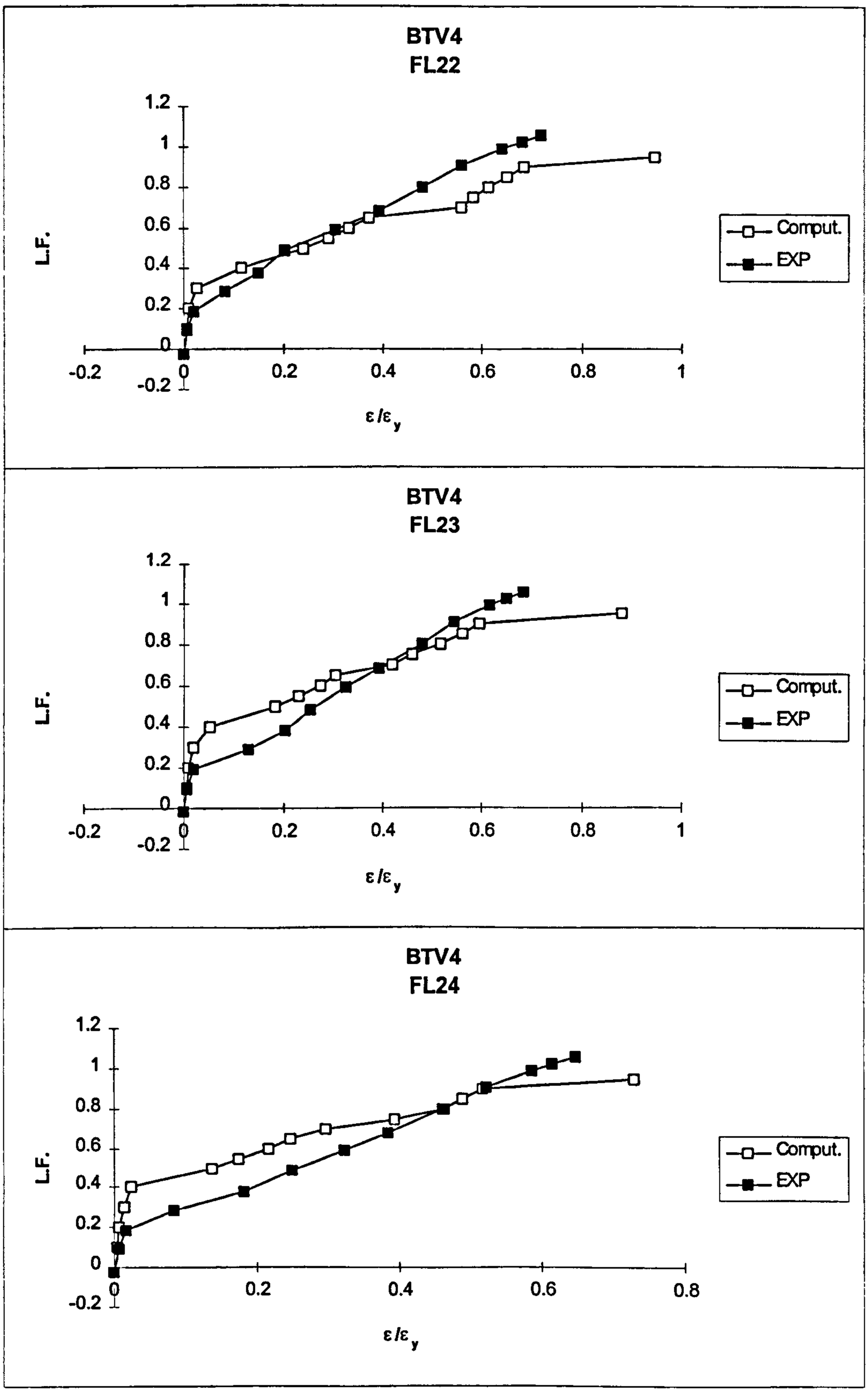
BTV4
FL22
L.F.
1.2
1
0.8
0.6
0.4
0.2
0
-0.2
-0.2
0
0.2
0.4
0.6
0.8
1
ε/ε y
Comput.
EXP
BTV4
FL23
L.F.
1.2
1
0.8
0.6
0.4
0.2
0
-0.2
-0.2
0
0.2
0.4
0.6
0.8
1
ε/ε y
Comput.
EXP
BTV4
FL24
L.F.
1.2
1
0.8
0.6
0.4
0.2
0
-0.2
0
0.2
0.4
0.6
0.8
ε/ε y
Comput.
EXP

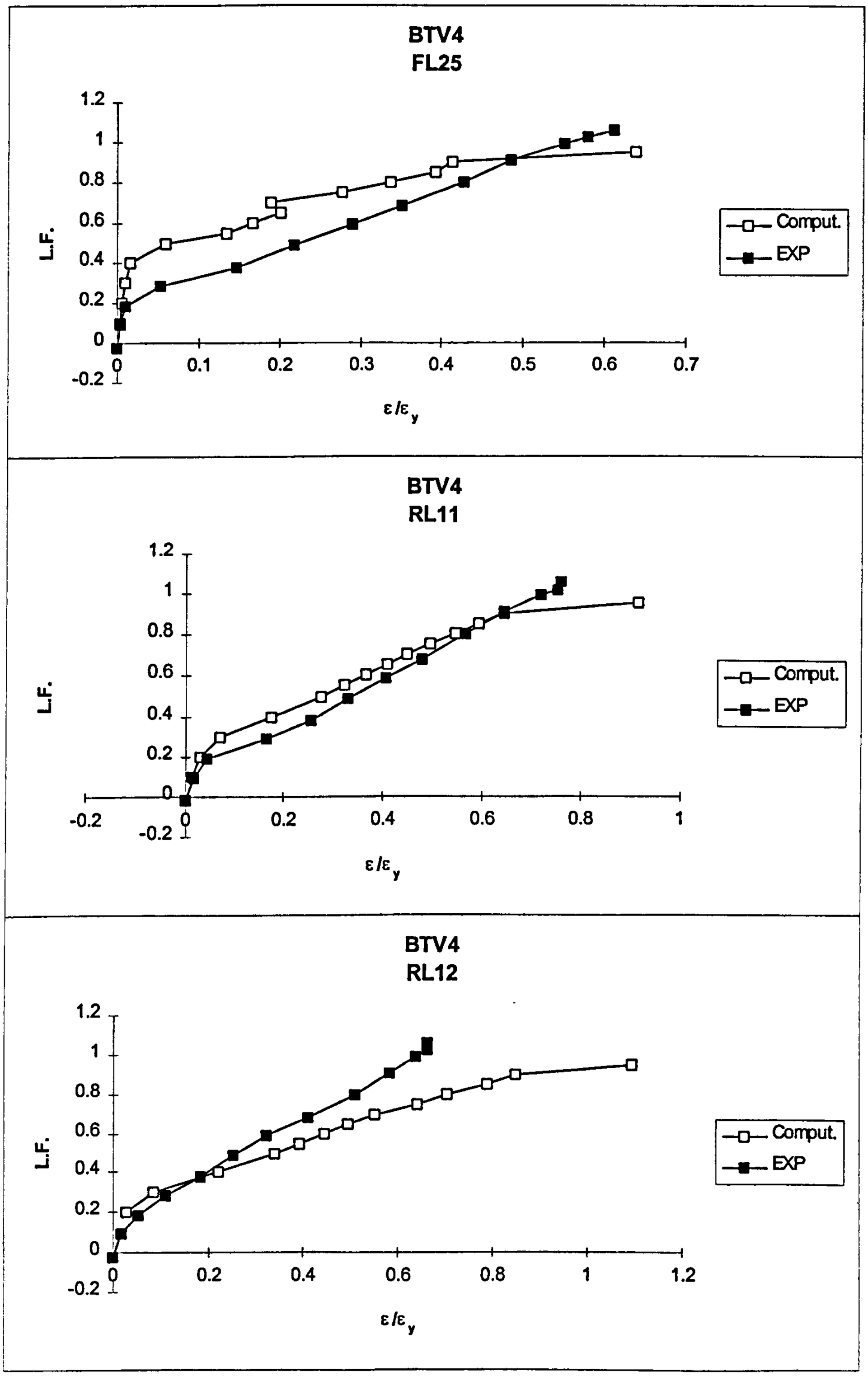
BTV4
FL25
L.F.
1.2
1
0.8
0.6
0.4
0.2
0
-0.2
0
0.1
0.2
0.3
0.4
0.5
0.6
0.7
ε/ε_y
Comput.
EXP
BTV4
RL11
L.F.
1.2
1
0.8
0.6
0.4
0.2
0
-0.2
-0.2
0
0.2
0.4
0.6
0.8
1
ε/ε_y
Comput.
EXP
BTV4
RL12
L.F.
1.2
1
0.8
0.6
0.4
0.2
0
-0.2
0
0.2
0.4
0.6
0.8
1
1.2
ε/ε_y
Comput.
EXP

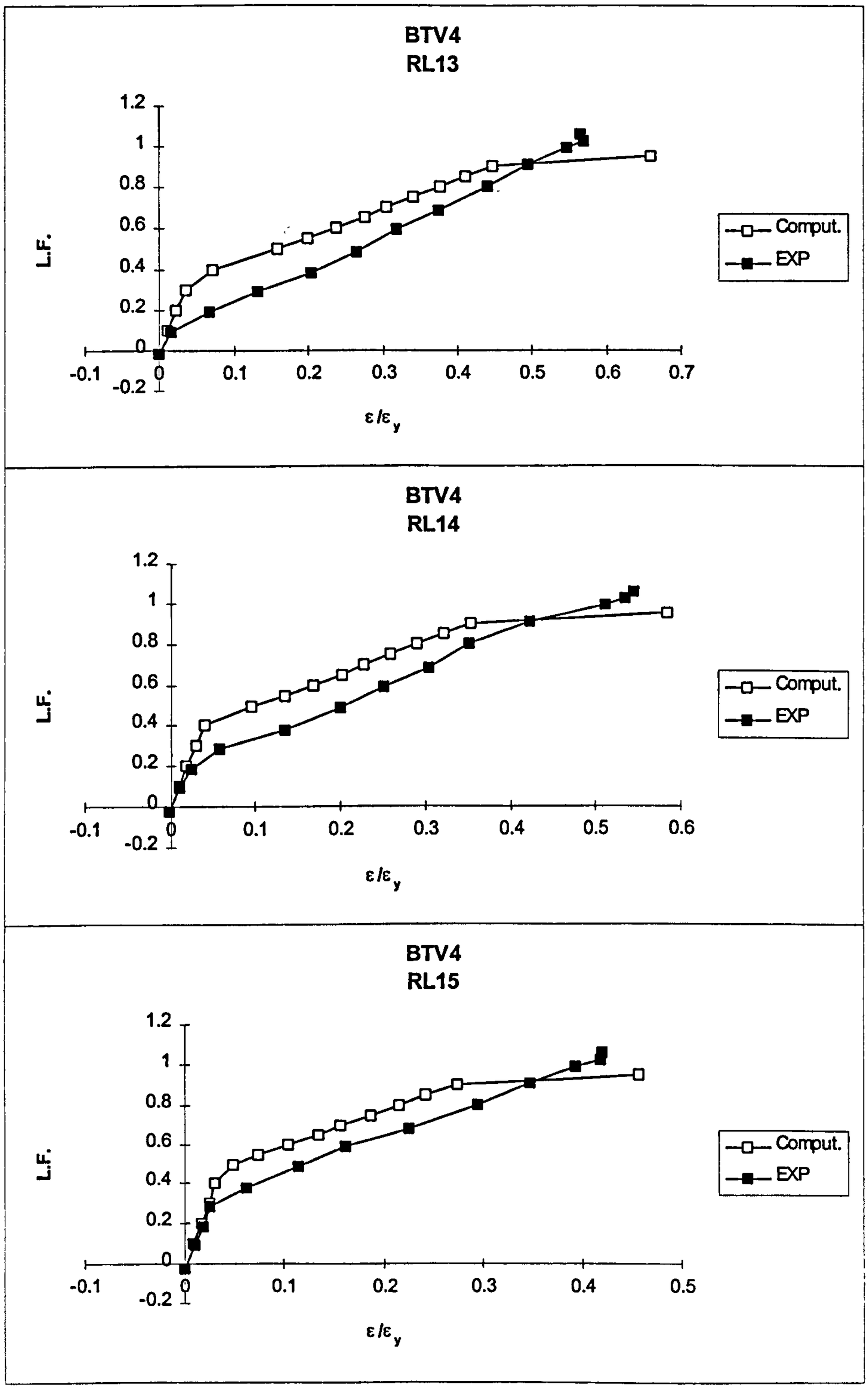
BTV4
RL13
L.F.
1.2
1
0.8
0.6
0.4
0.2
0
-0.2
-0.1
0
0.1
0.2
0.3
0.4
0.5
0.6
0.7
Comput.
EXP
ε/ε_y
BTV4
RL14
L.F.
1.2
1
0.8
0.6
0.4
0.2
0
-0.2
-0.1
0
0.1
0.2
0.3
0.4
0.5
0.6
Comput.
EXP
ε/ε_y
BTV4
RL15
L.F.
1.2
1
0.8
0.6
0.4
0.2
0
-0.2
-0.1
0
0.1
0.2
0.3
0.4
0.5
Comput.
EXP
ε/ε_y

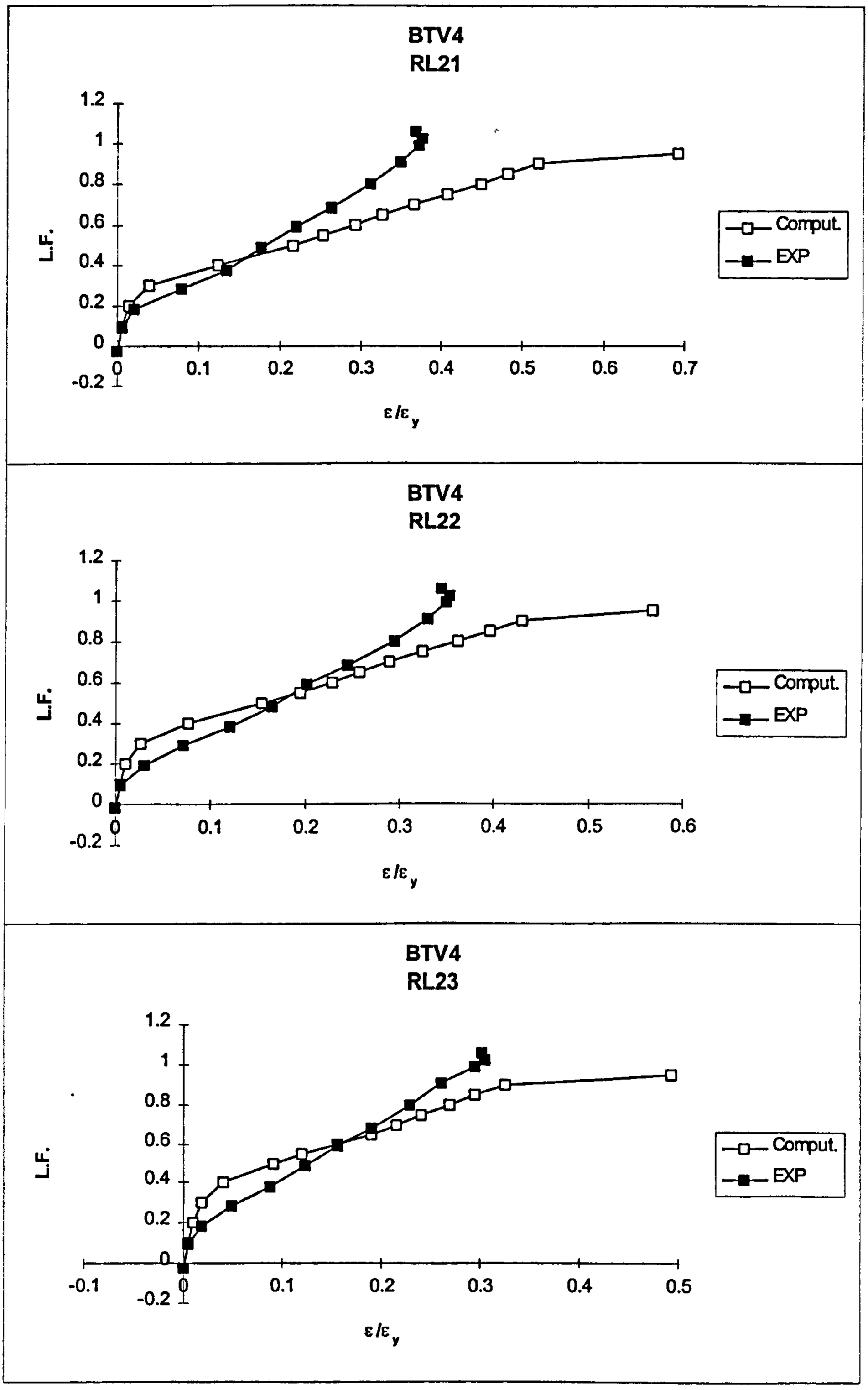
BTV4
RL21
L.F.
1.2
1
0.8
0.6
0.4
0.2
0
-0.2
0
0.1
0.2
0.3
0.4
0.5
0.6
0.7
ε/ε y
Comput.
EXP
BTV4
RL22
L.F.
1.2
1
0.8
0.6
0.4
0.2
0
-0.2
0
0.1
0.2
0.3
0.4
0.5
0.6
ε/ε y
Comput.
EXP
BTV4
RL23
L.F.
1.2
1
0.8
0.6
0.4
0.2
0
-0.2
-0.1
0
0.1
0.2
0.3
0.4
0.5
ε/ε y
Comput.
EXP

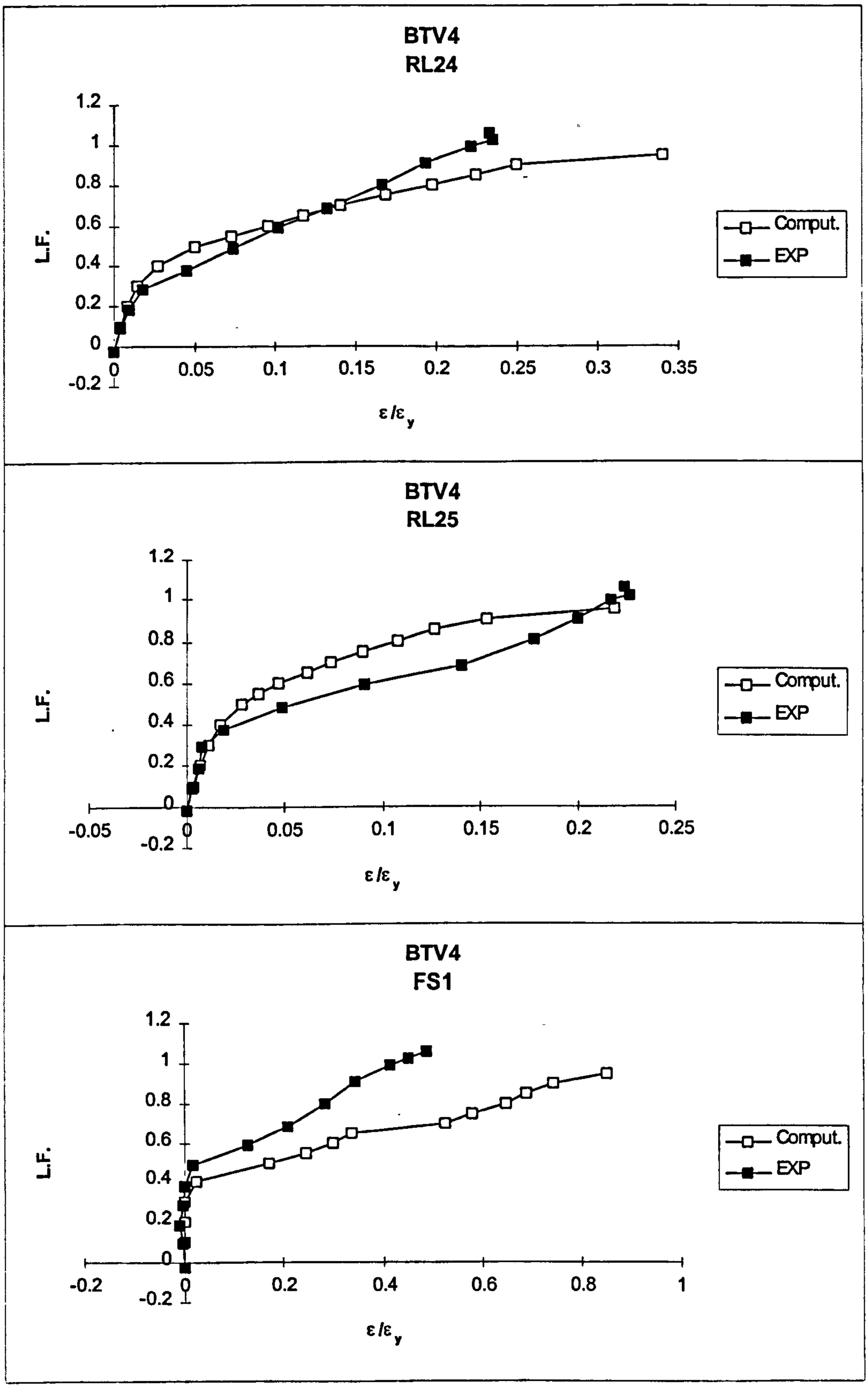
BTV4
RL24
L.F.
1.2
1
0.8
0.6
0.4
0.2
0
-0.2
0
0.05
0.1
0.15
0.2
0.25
0.3
0.35
ε /ε y
Comput.
EXP
BTV4
RL25
L.F.
1.2
1
0.8
0.6
0.4
0.2
0
-0.2
-0.05
0
0.05
0.1
0.15
0.2
0.25
ε /ε y
Comput.
EXP
BTV4
FS1
L.F.
1.2
1
0.8
0.6
0.4
0.2
0
-0.2
-0.2
0
0.2
0.4
0.6
0.8
1
ε /ε y
Comput.
EXP

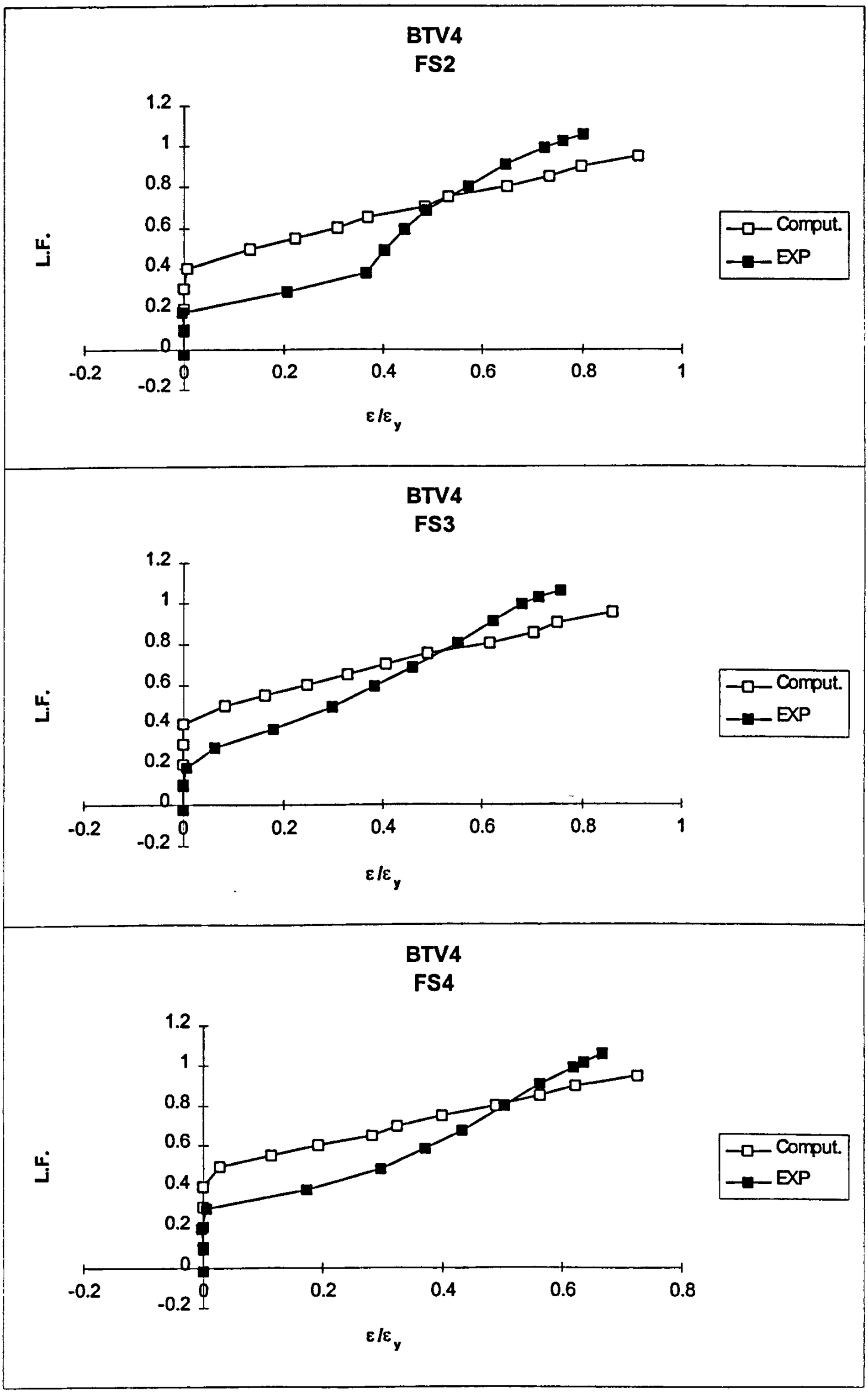
BTV4
FS2
L.F.
1.2
1
0.8
0.6
0.4
0.2
0
-0.2
0
0.2
0.4
0.6
0.8
1
ε/ε_y
Comput.
EXP
BTV4
FS3
L.F.
1.2
1
0.8
0.6
0.4
0.2
0
-0.2
0
0.2
0.4
0.6
0.8
1
ε/ε_y
Comput.
EXP
BTV4
FS4
L.F.
1.2
1
0.8
0.6
0.4
0.2
0
-0.2
0
0.2
0.4
0.6
0.8
ε/ε_y
Comput.
EXP

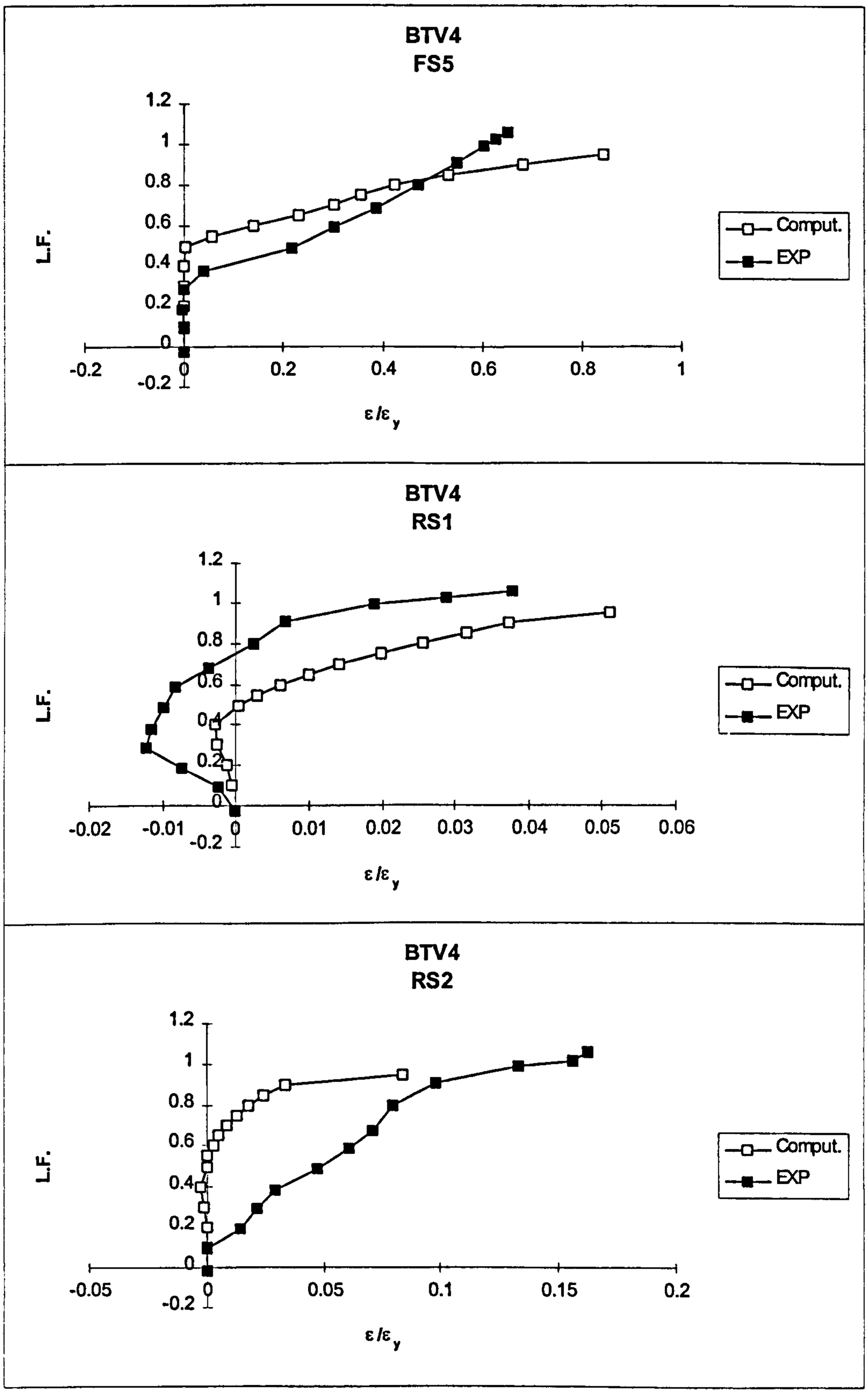
BTV4
FS5
L.F.
ε/ε_y
Comput.
EXP
BTV4
RS1
L.F.
ε/ε_y
Comput.
EXP
BTV4
RS2
L.F.
ε/ε_y
Comput.
EXP

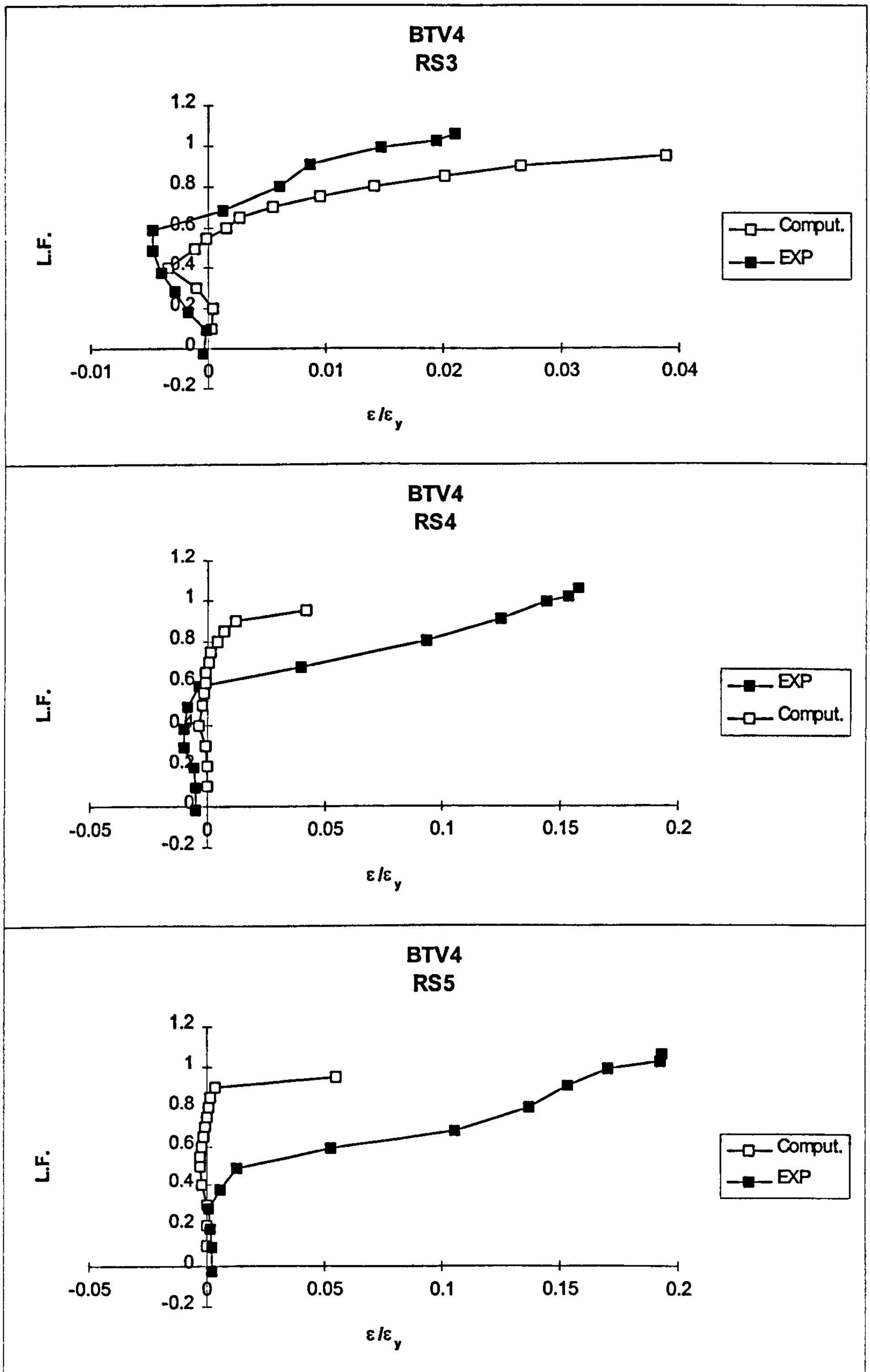
BTV4
RS3
L.F.
1.2
1
0.8
0.6
0.4
0.2
0
-0.2
-0.01
0
0.01
0.02
0.03
0.04
ε/ε y
Comput.
EXP
BTV4
RS4
L.F.
1.2
1
0.8
0.6
0.4
0.2
0
-0.2
-0.05
0
0.05
0.1
0.15
0.2
ε/ε y
EXP
Comput.
BTV4
RS5
L.F.
1.2
1
0.8
0.6
0.4
0.2
0
-0.2
-0.05
0
0.05
0.1
0.15
0.2
ε/ε y
Comput.
EXP

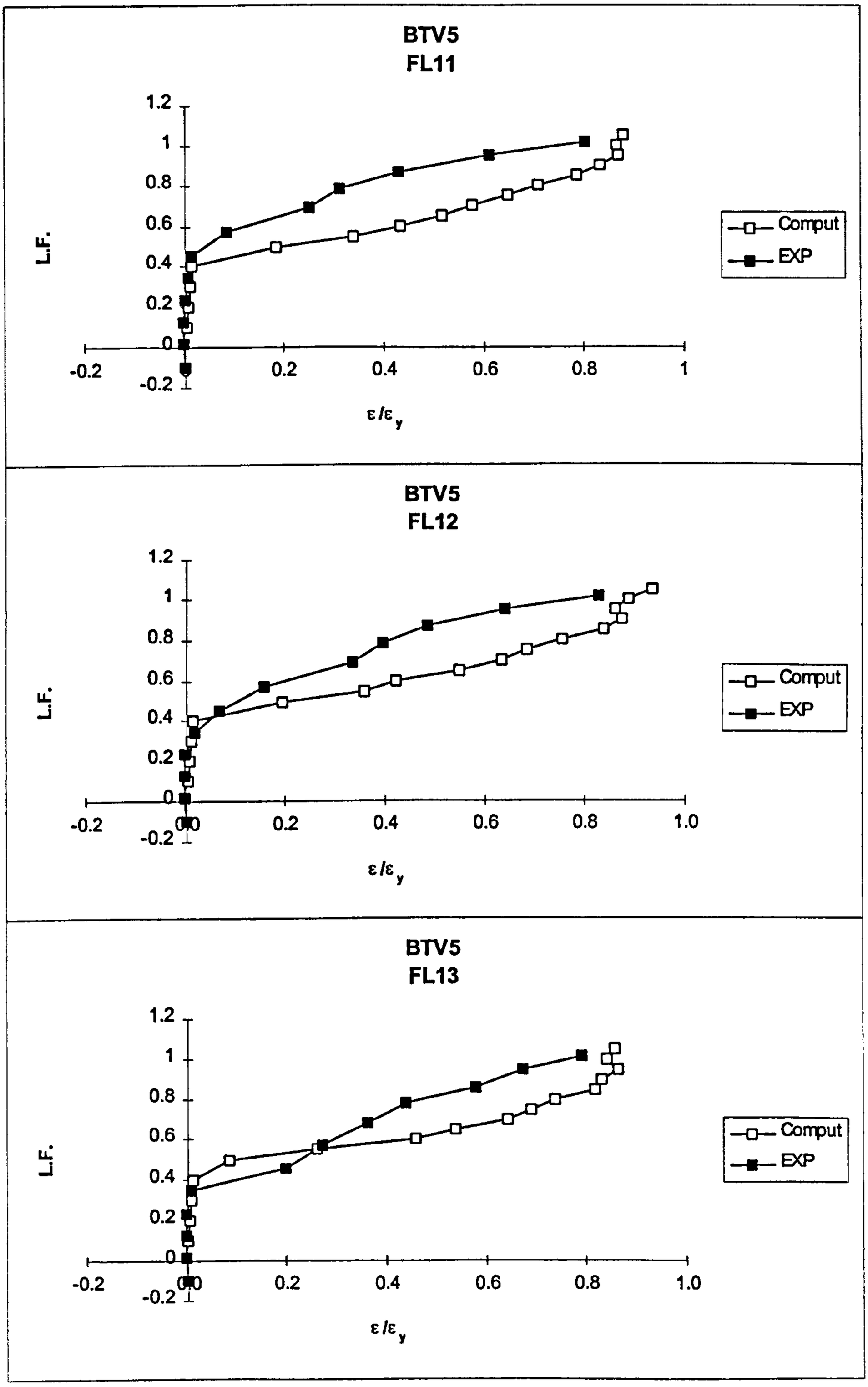
BTV5
FL11
L.F.
1.2
1
0.8
0.6
0.4
0.2
0
-0.2
-0.2
0.2
0.4
0.6
0.8
1
ε/ε y
Comput
EXP
BTV5
FL12
L.F.
1.2
1
0.8
0.6
0.4
0.2
0
-0.2
-0.2
0.2
0.4
0.6
0.8
1.0
ε/ε y
Comput
EXP
BTV5
FL13
L.F.
1.2
1
0.8
0.6
0.4
0.2
0
-0.2
-0.2
0.2
0.4
0.6
0.8
1.0
ε/ε y
Comput
EXP

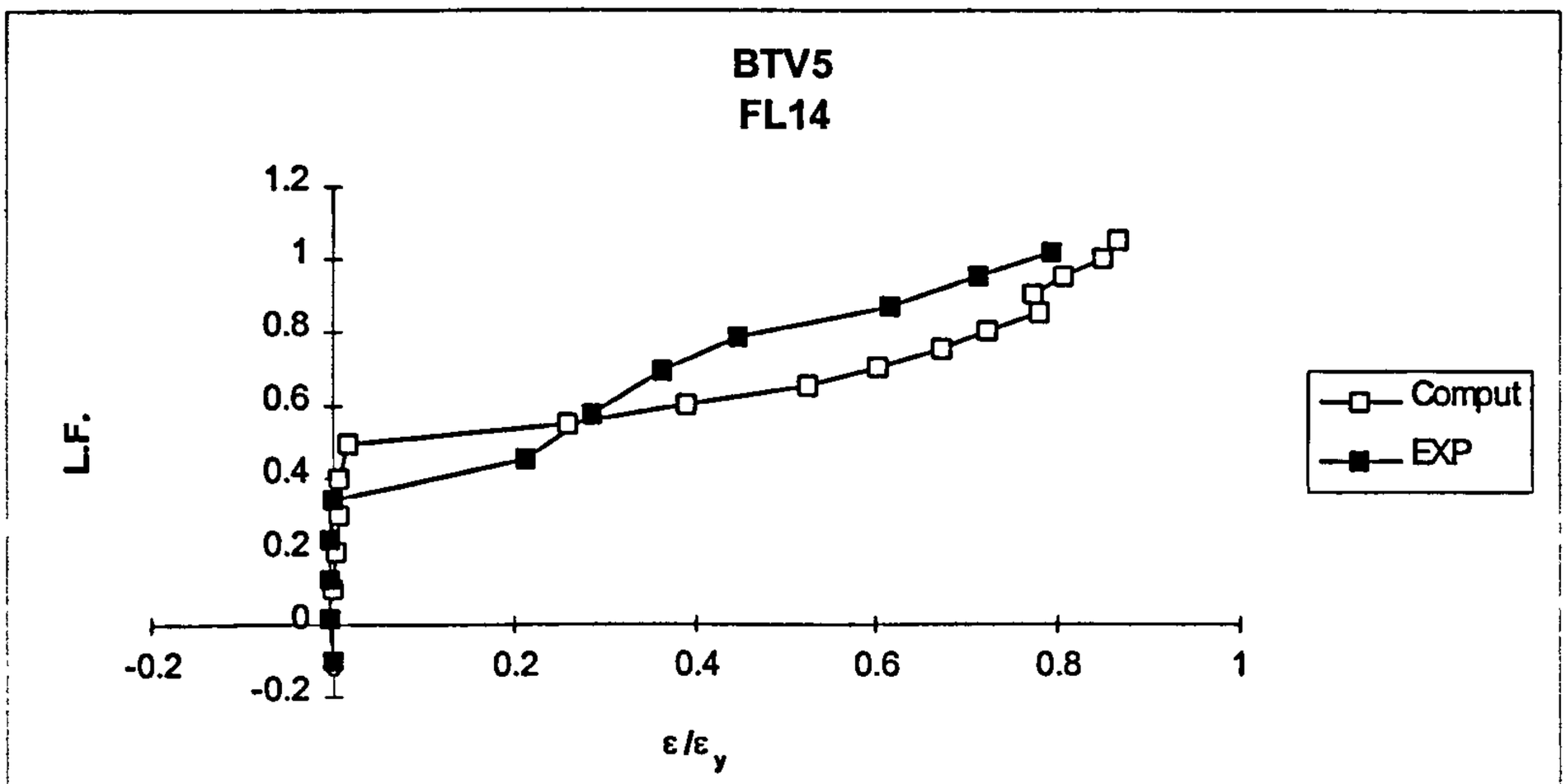
BTV5
FL14
L.F.
1.2
1
0.8
0.6
0.4
0.2
0
-0.2
-0.2
0.2
0.4
0.6
0.8
1
ε/ε y
Comput
EXP

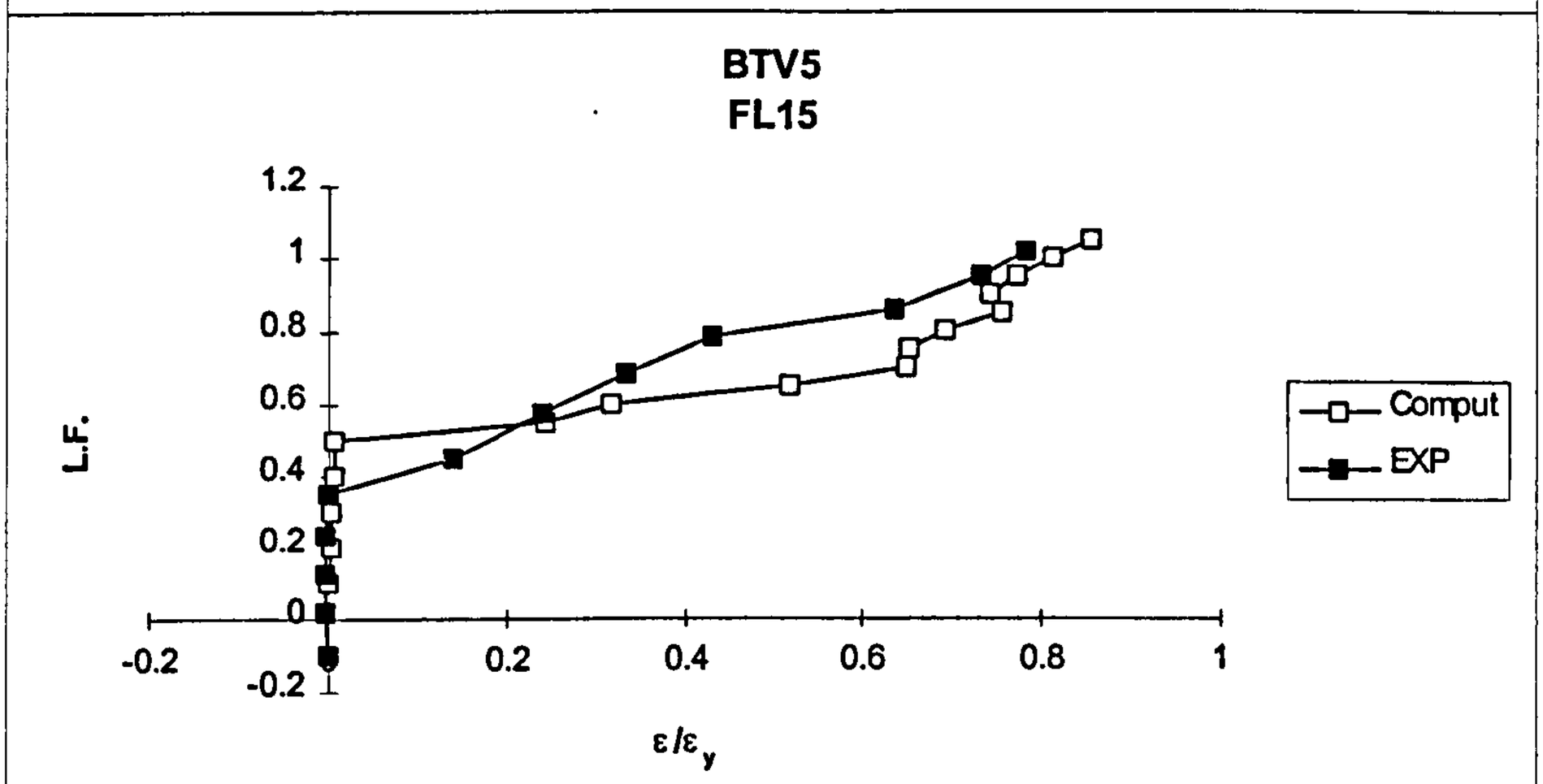
BTV5
FL15
L.F.
1.2
1
0.8
0.6
0.4
0.2
0
-0.2
-0.2
0.2
0.4
0.6
0.8
1
ε/ε y
Comput
EXP

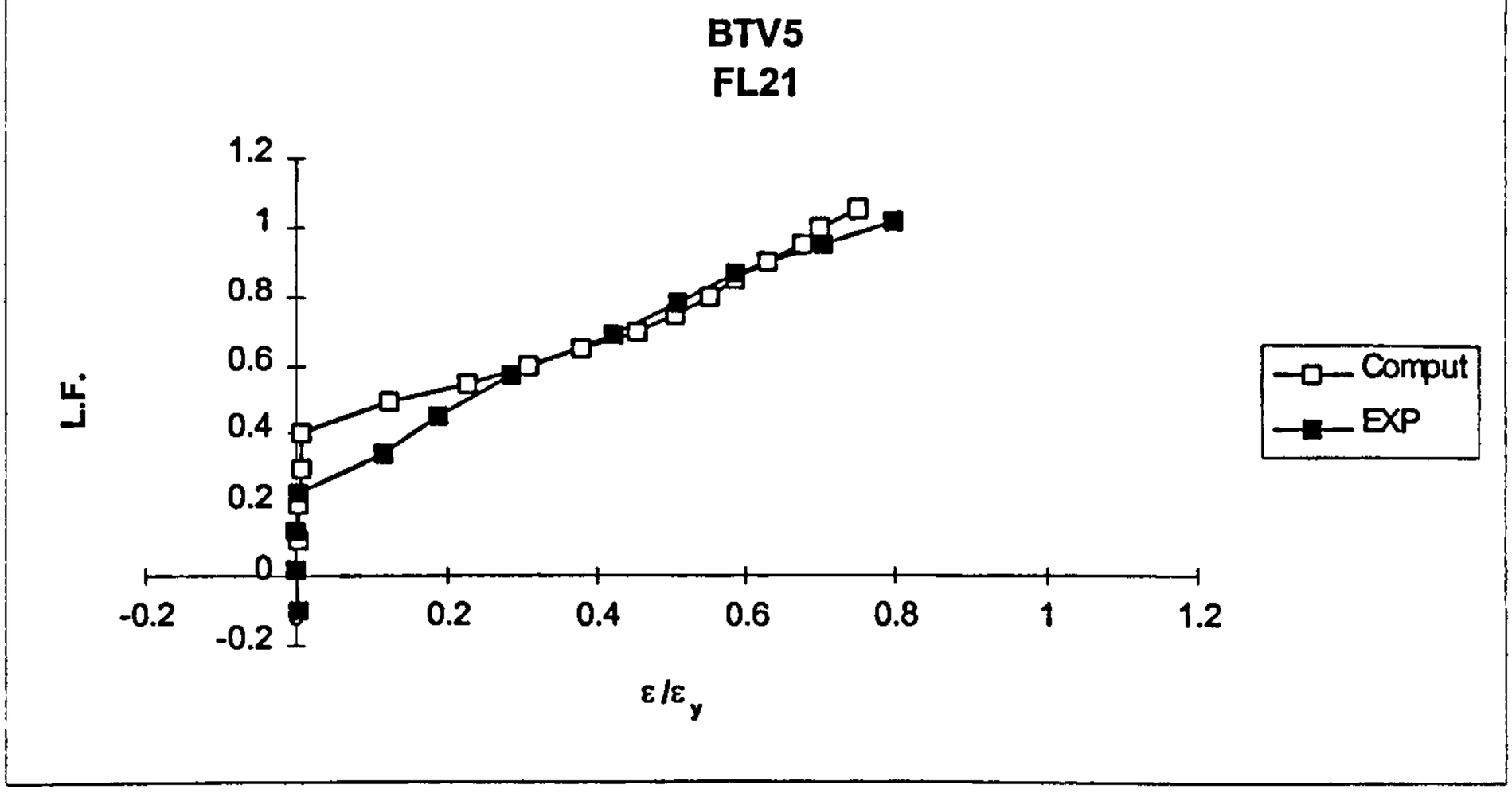
BTV5
FL21
L.F.
1.2
1
0.8
0.6
0.4
0.2
0
-0.2
-0.2
0.2
0.4
0.6
0.8
1
1.2
ε/ε y
Comput
EXP

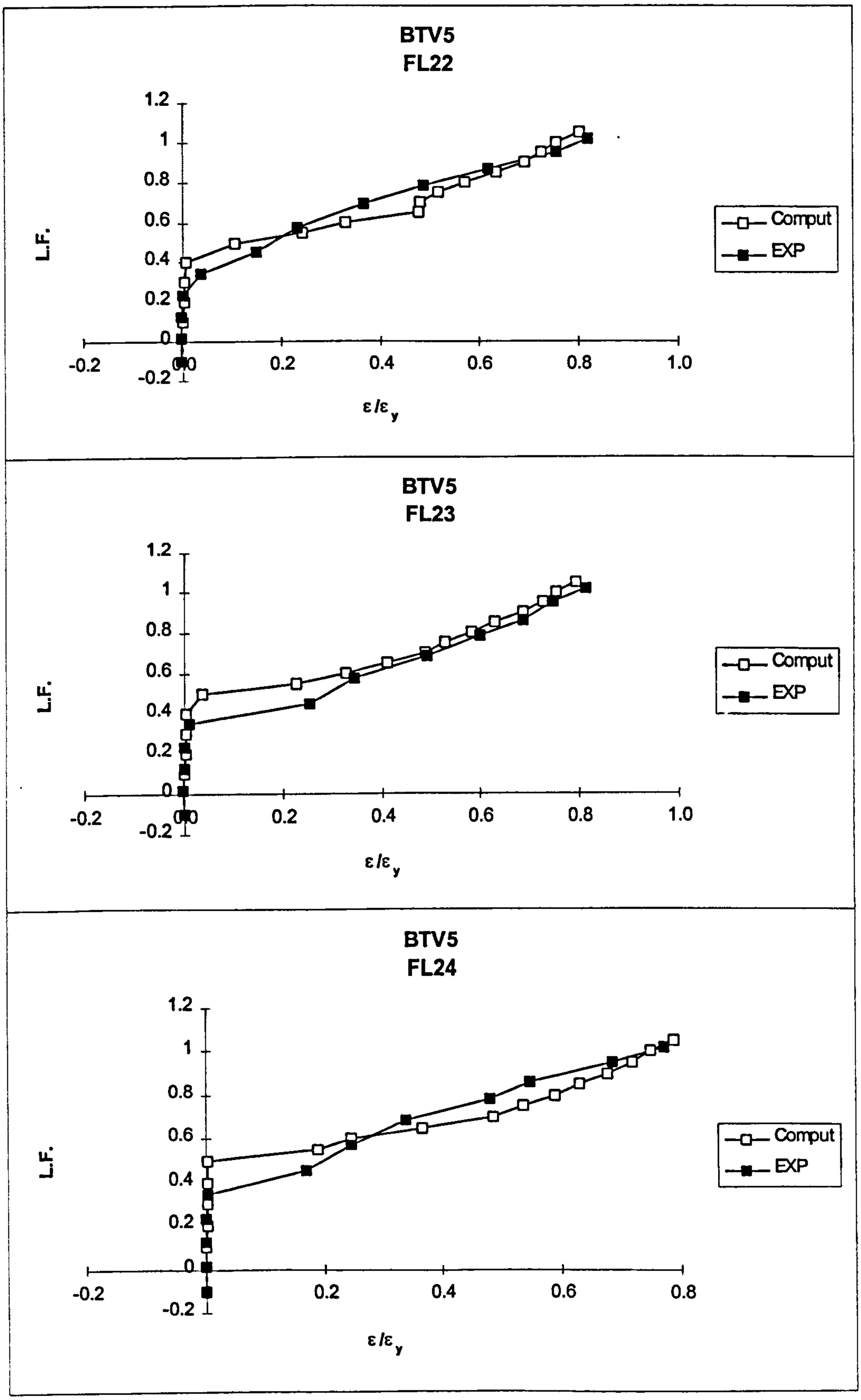
BTV5
FL22
L.F.
1.2
1
0.8
0.6
0.4
0.2
0
-0.2
-0.2
0.0
0.2
0.4
0.6
0.8
1.0
ε/ε y
Comput
EXP
BTV5
FL23
L.F.
1.2
1
0.8
0.6
0.4
0.2
0
-0.2
-0.2
0.0
0.2
0.4
0.6
0.8
1.0
ε/ε y
Comput
EXP
BTV5
FL24
L.F.
1.2
1
0.8
0.6
0.4
0.2
0
-0.2
-0.2
0.2
0.4
0.6
0.8
ε/ε y
Comput
EXP

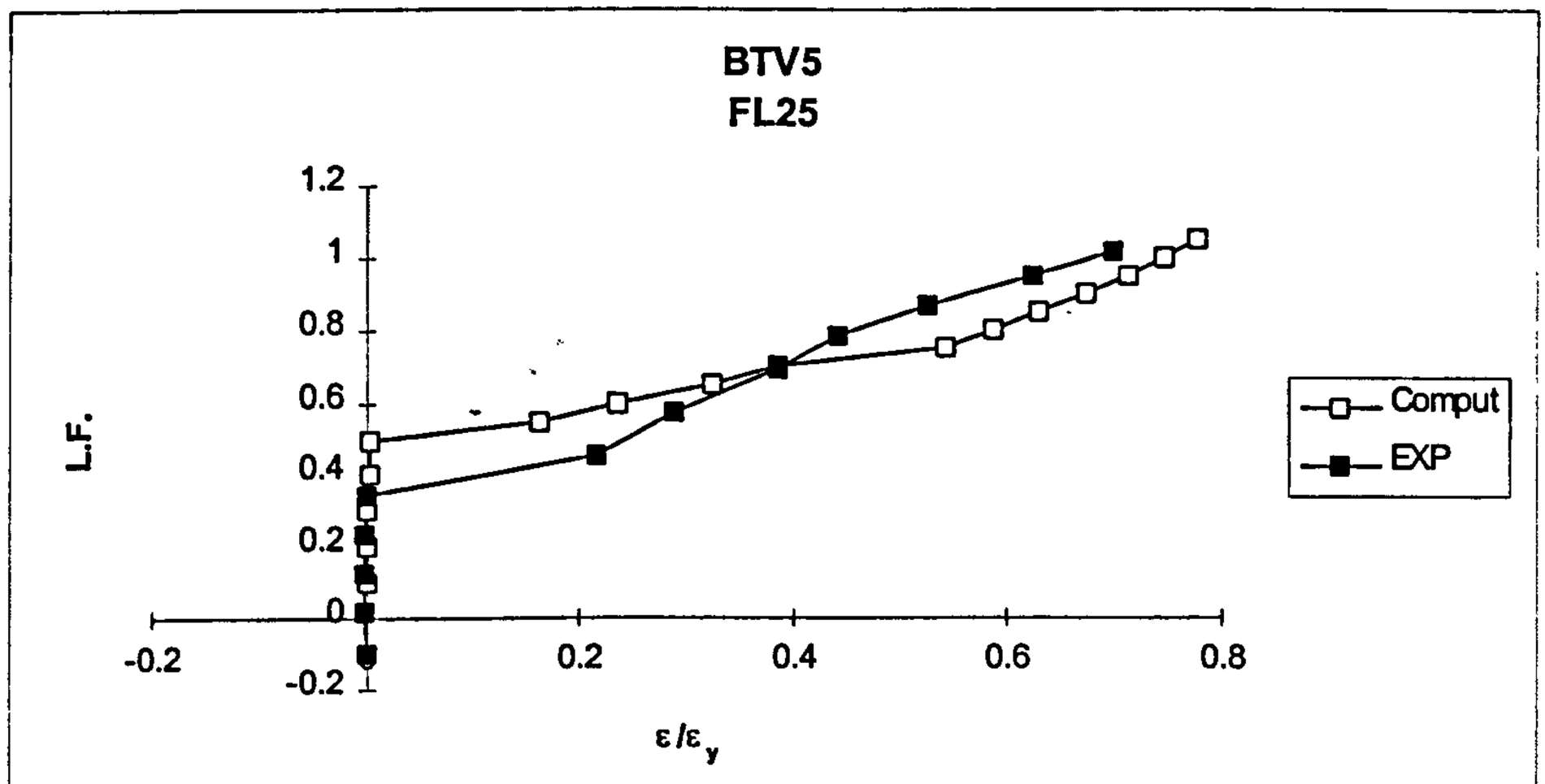
BTV5
FL25
L.F.
1.2
1
0.8
0.6
0.4
0.2
0
-0.2
0.2
0.4
0.6
0.8
Comput
EXP
ε/ε y

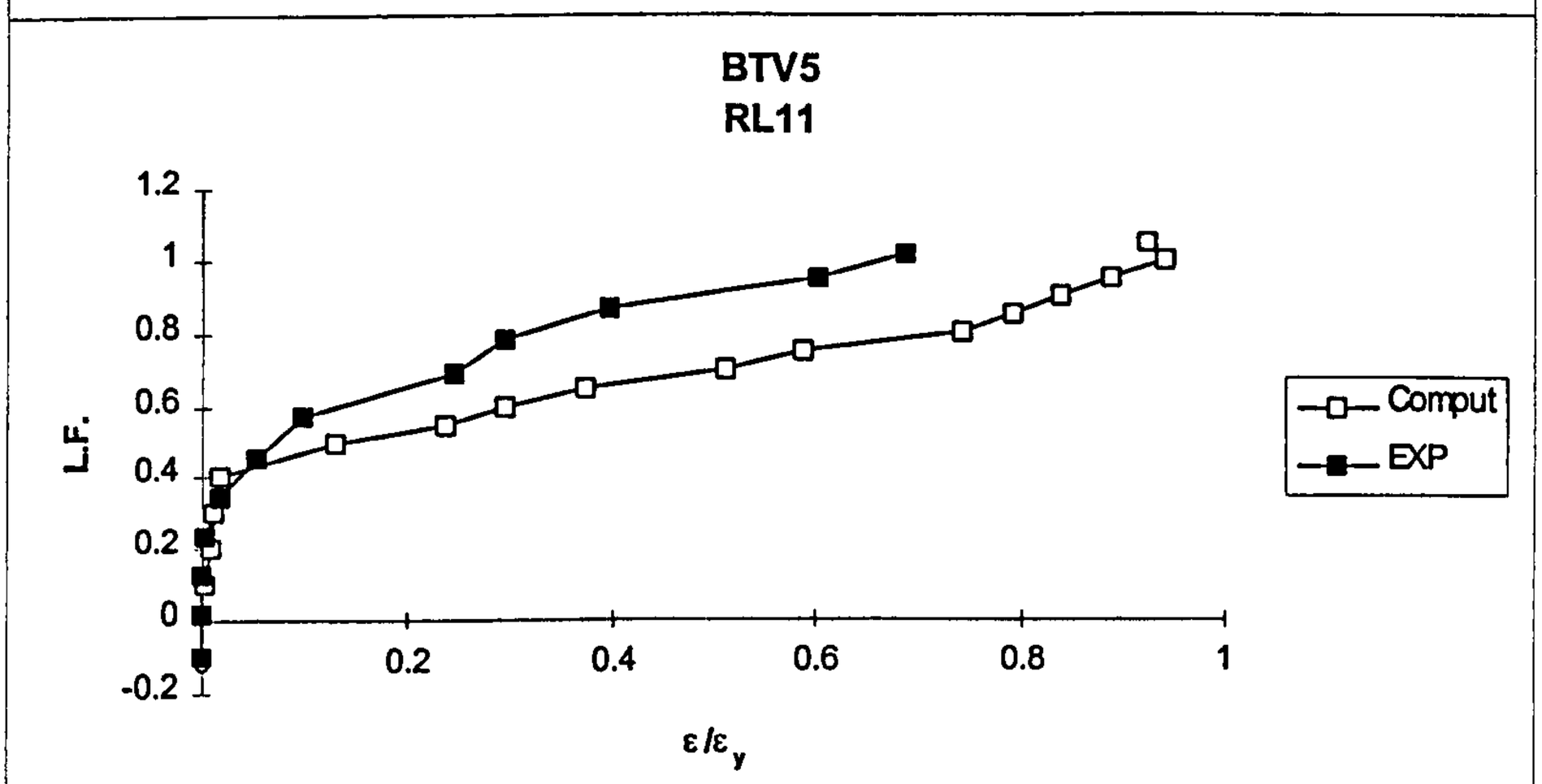
BTV5
RL11
L.F.
1.2
1
0.8
0.6
0.4
0.2
0
-0.2
0.2
0.4
0.6
0.8
1
Comput
EXP
ε/ε y

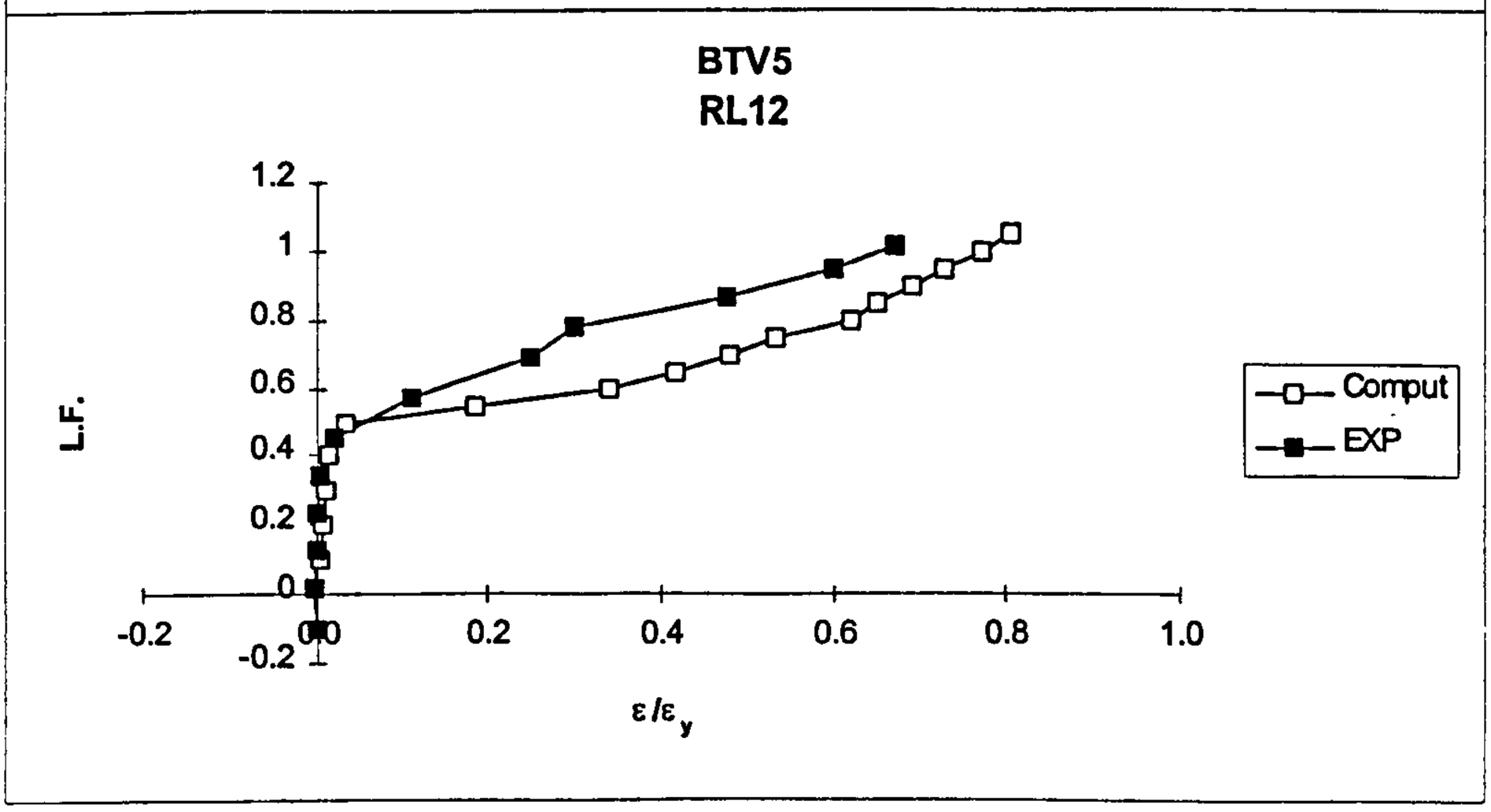
BTV5
RL12
L.F.
1.2
1
0.8
0.6
0.4
0.2
0
-0.2
0.2
0.4
0.6
0.8
1.0
Comput
EXP
ε/ε y

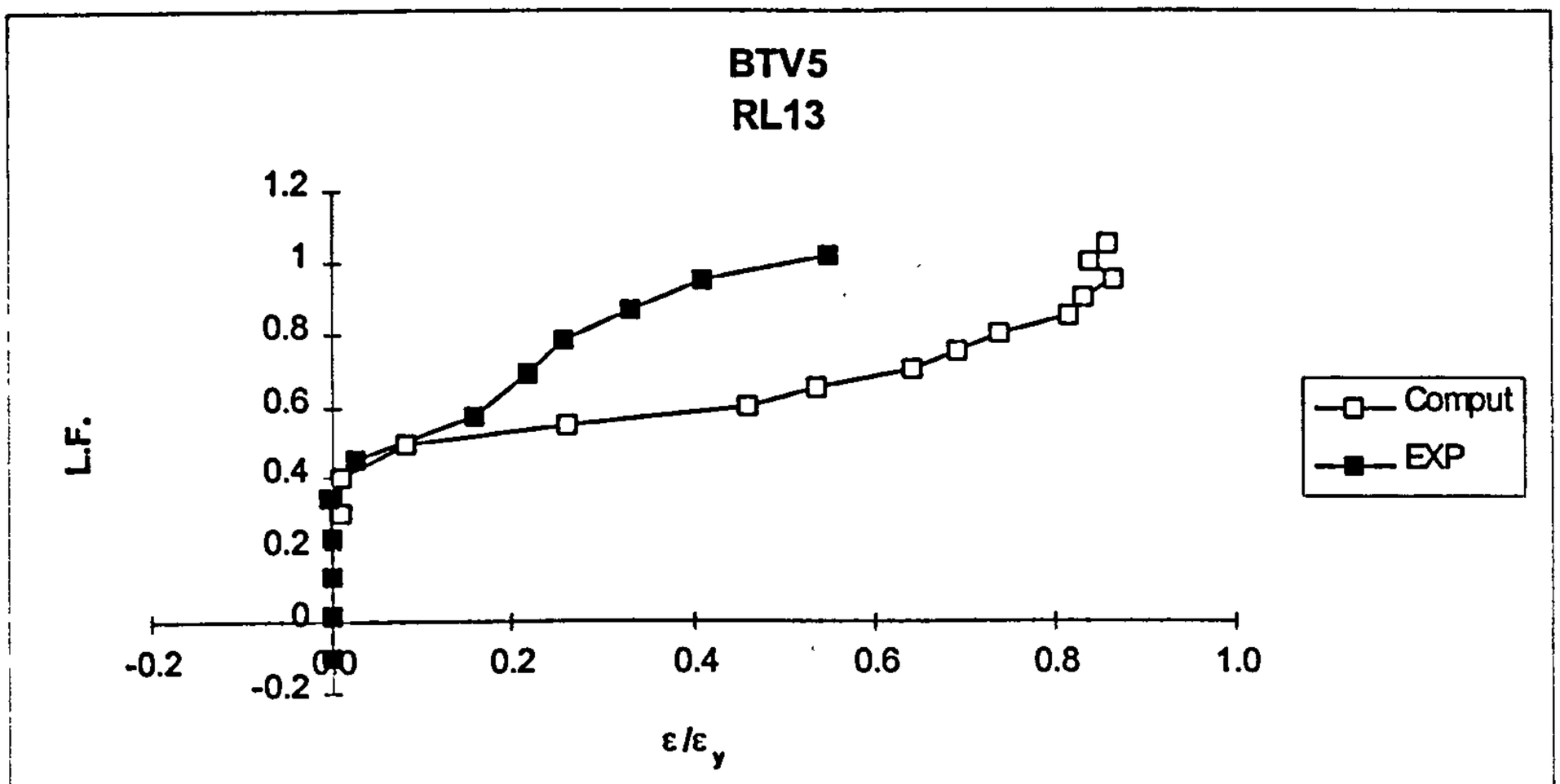
BTV5
RL13
L.F.
1.2
1
0.8
0.6
0.4
0.2
0
-0.2
0.0
0.2
0.4
0.6
0.8
1.0
-0.2
ε/ε y
Comput
EXP

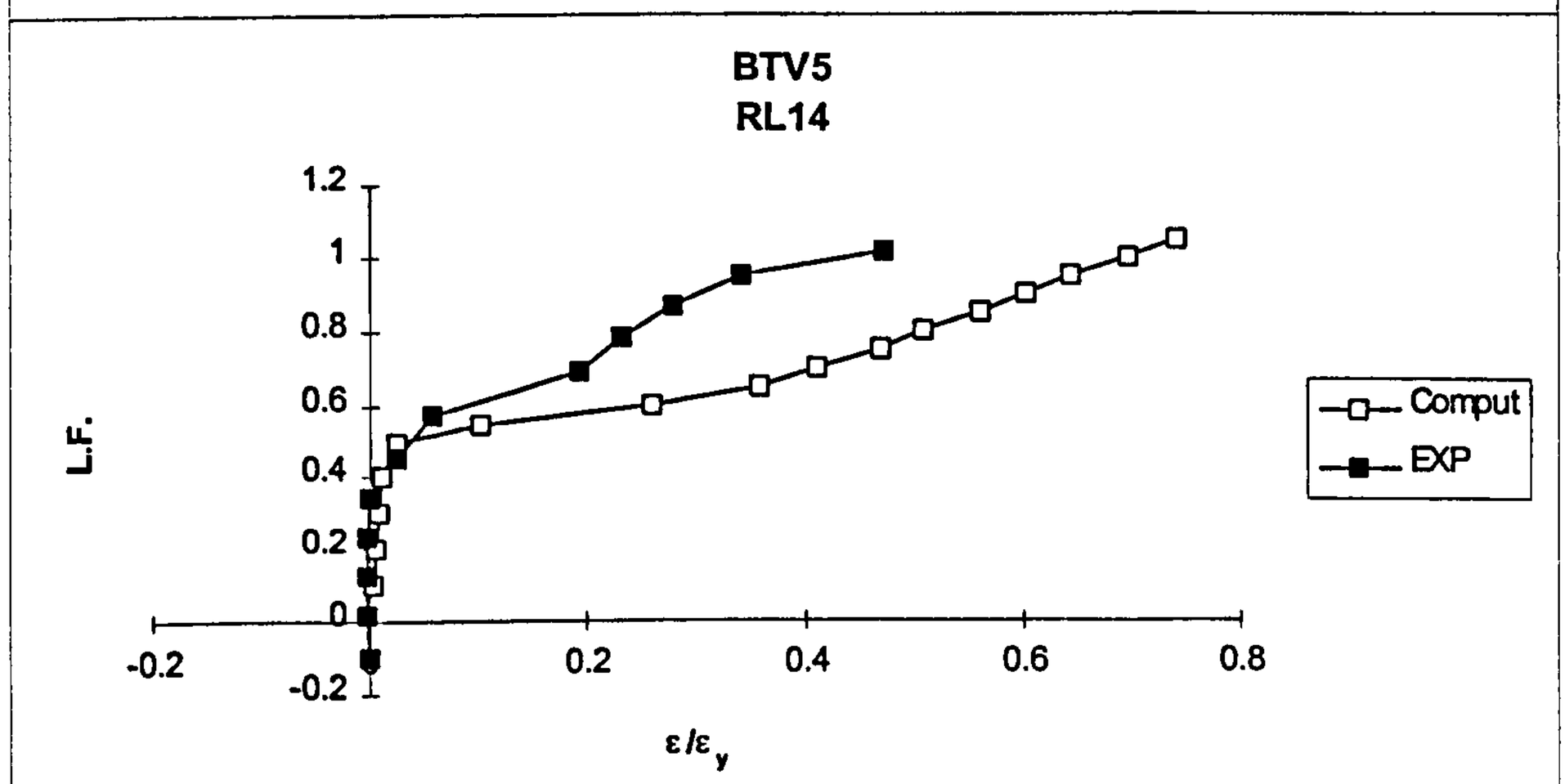
BTV5
RL14
L.F.
1.2
1
0.8
0.6
0.4
0.2
0
-0.2
0.2
0.4
0.6
0.8
-0.2
ε/ε y
Comput
EXP

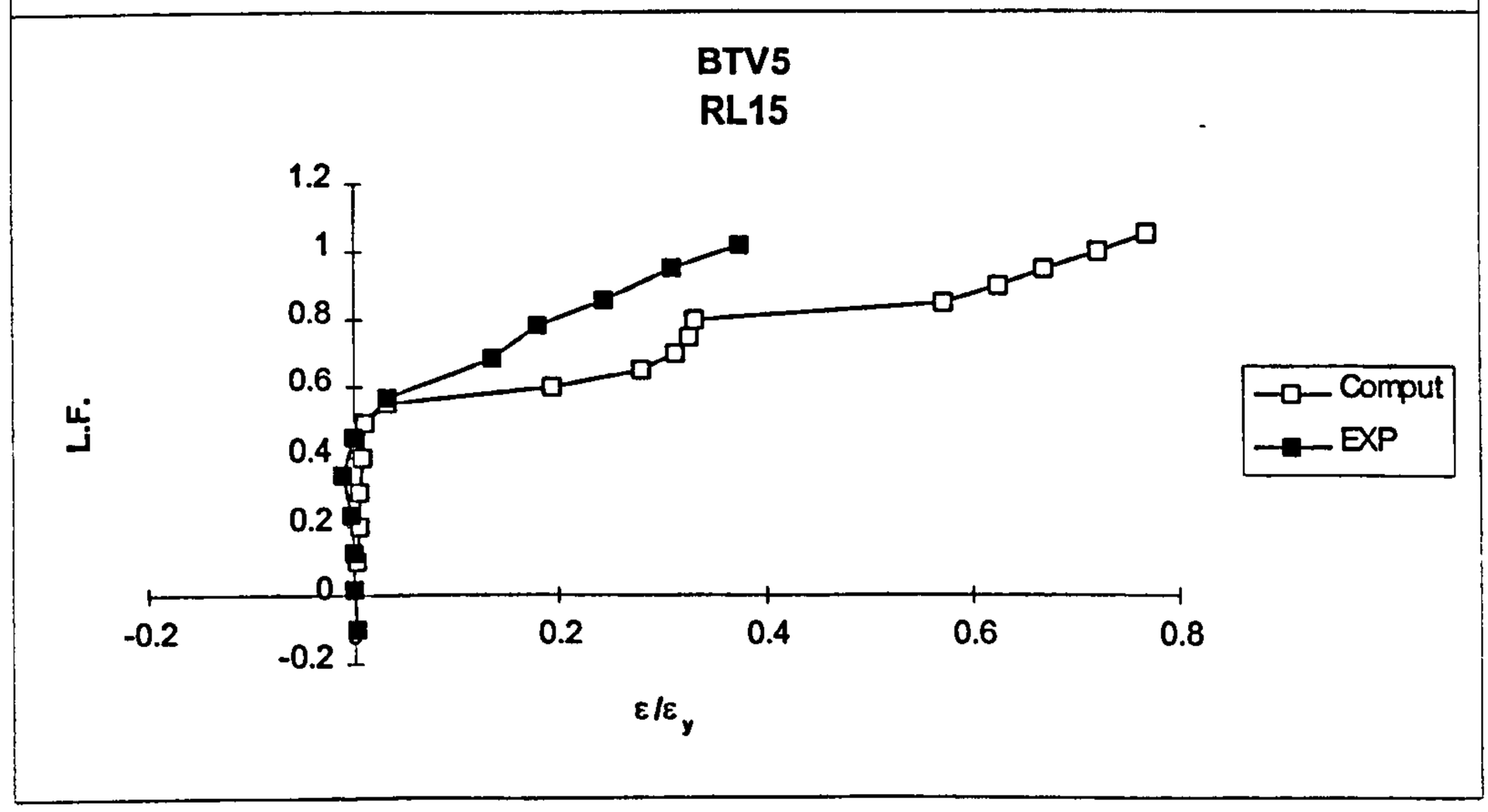
BTV5
RL15
L.F.
1.2
1
0.8
0.6
0.4
0.2
0
-0.2
0.2
0.4
0.6
0.8
-0.2
ε/ε y
Comput
EXP

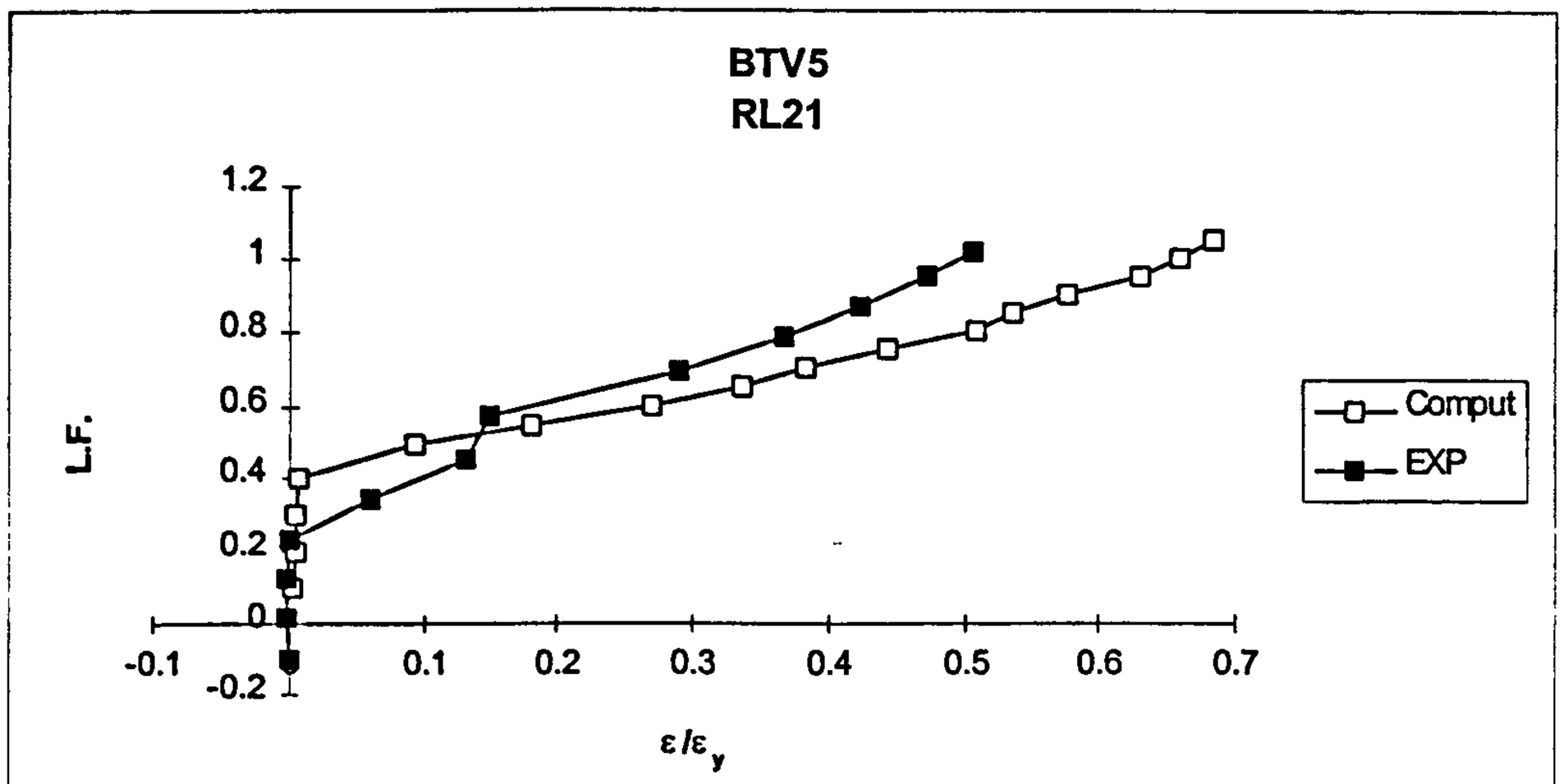
BTV5
RL21
L.F.
1.2
1
0.8
0.6
0.4
0.2
0
-0.2
-0.1
0.1
0.2
0.3
0.4
0.5
0.6
0.7
Comput
EXP
ε/ε y

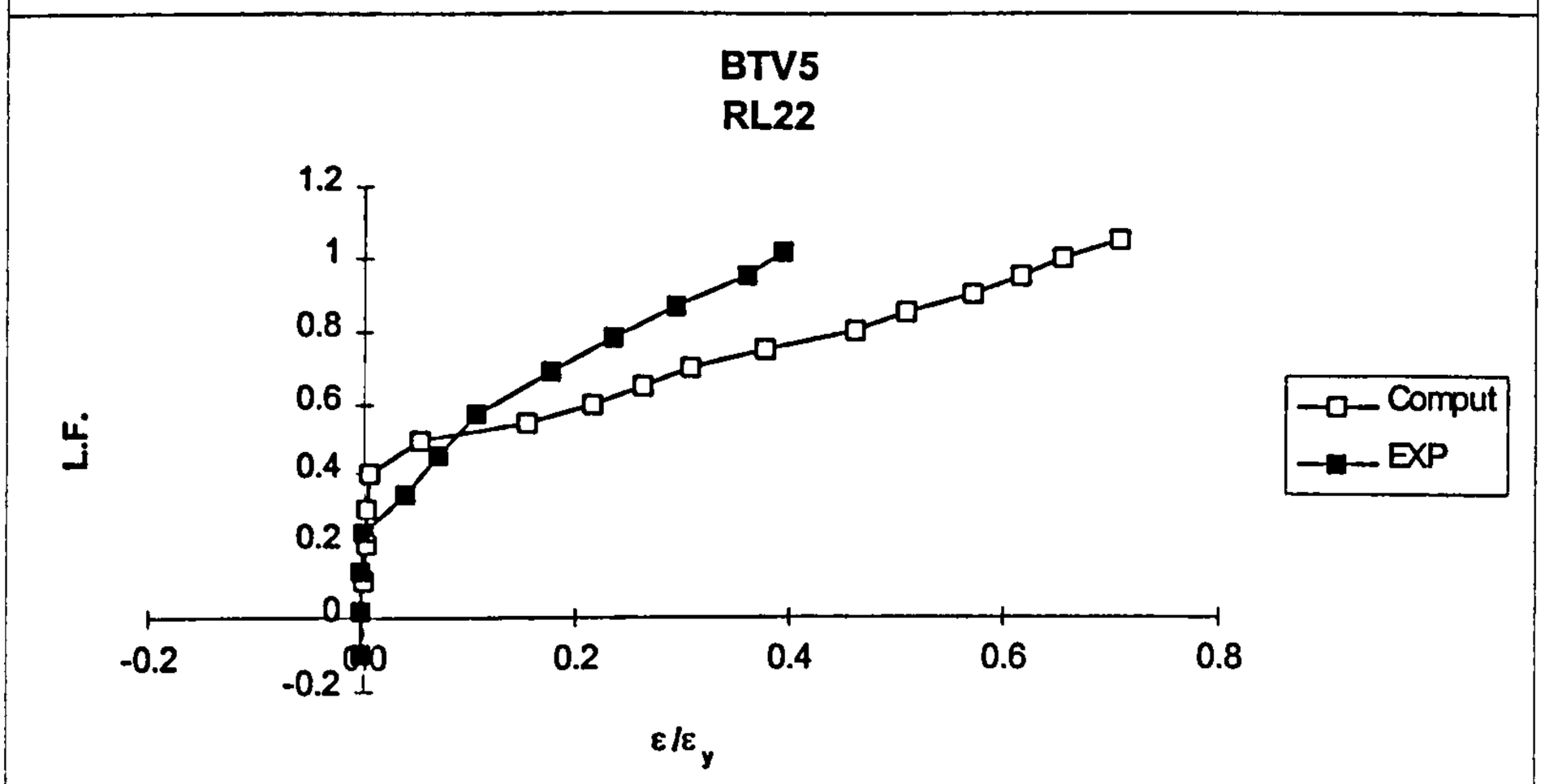
BTV5
RL22
L.F.
1.2
1
0.8
0.6
0.4
0.2
0
-0.2
-0.2
0
0.2
0.4
0.6
0.8
Comput
EXP
ε/ε y

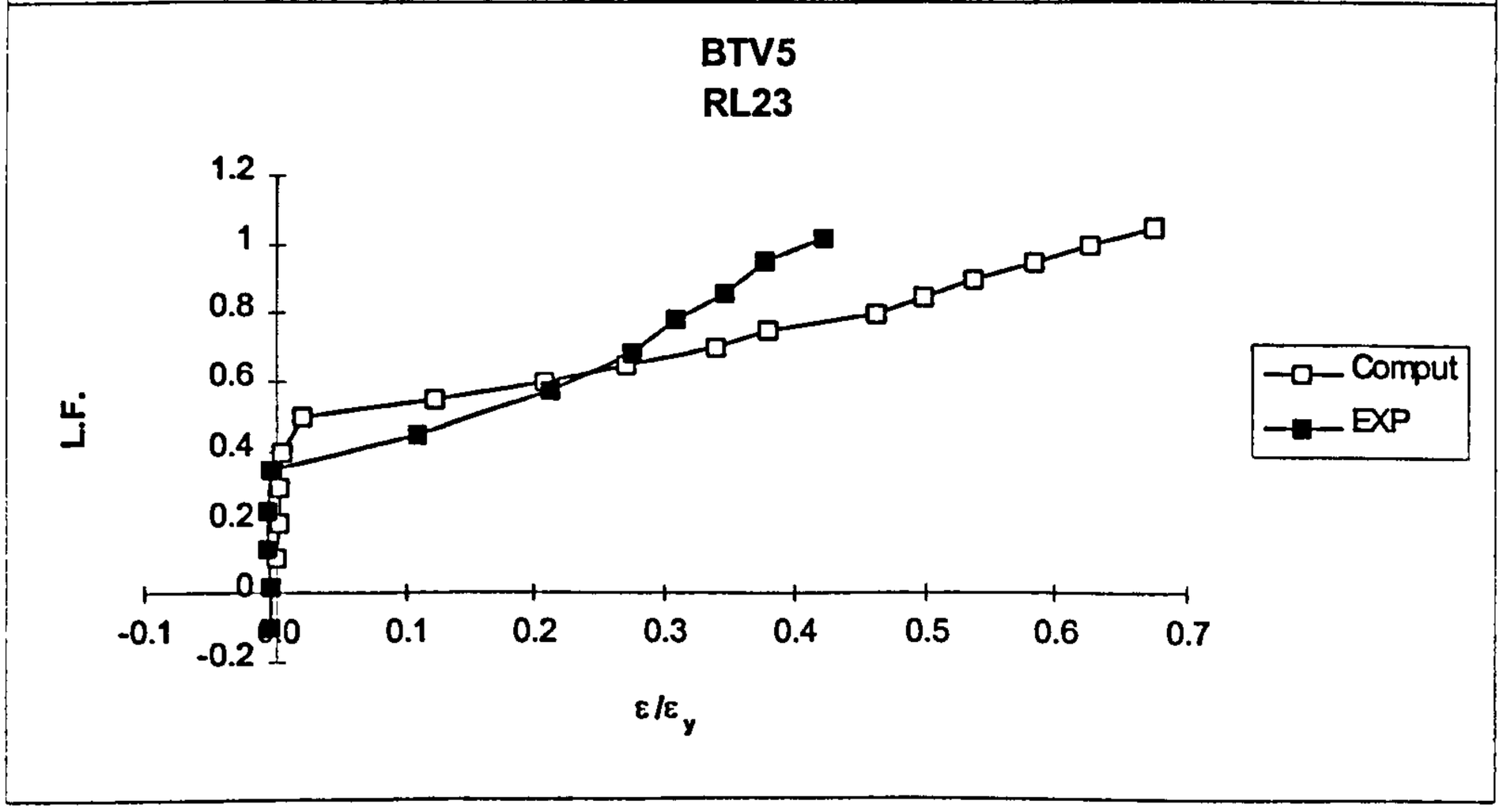
BTV5
RL23
L.F.
1.2
1
0.8
0.6
0.4
0.2
0
-0.2
-0.1
0.1
0.2
0.3
0.4
0.5
0.6
0.7
Comput
EXP
ε/ε y

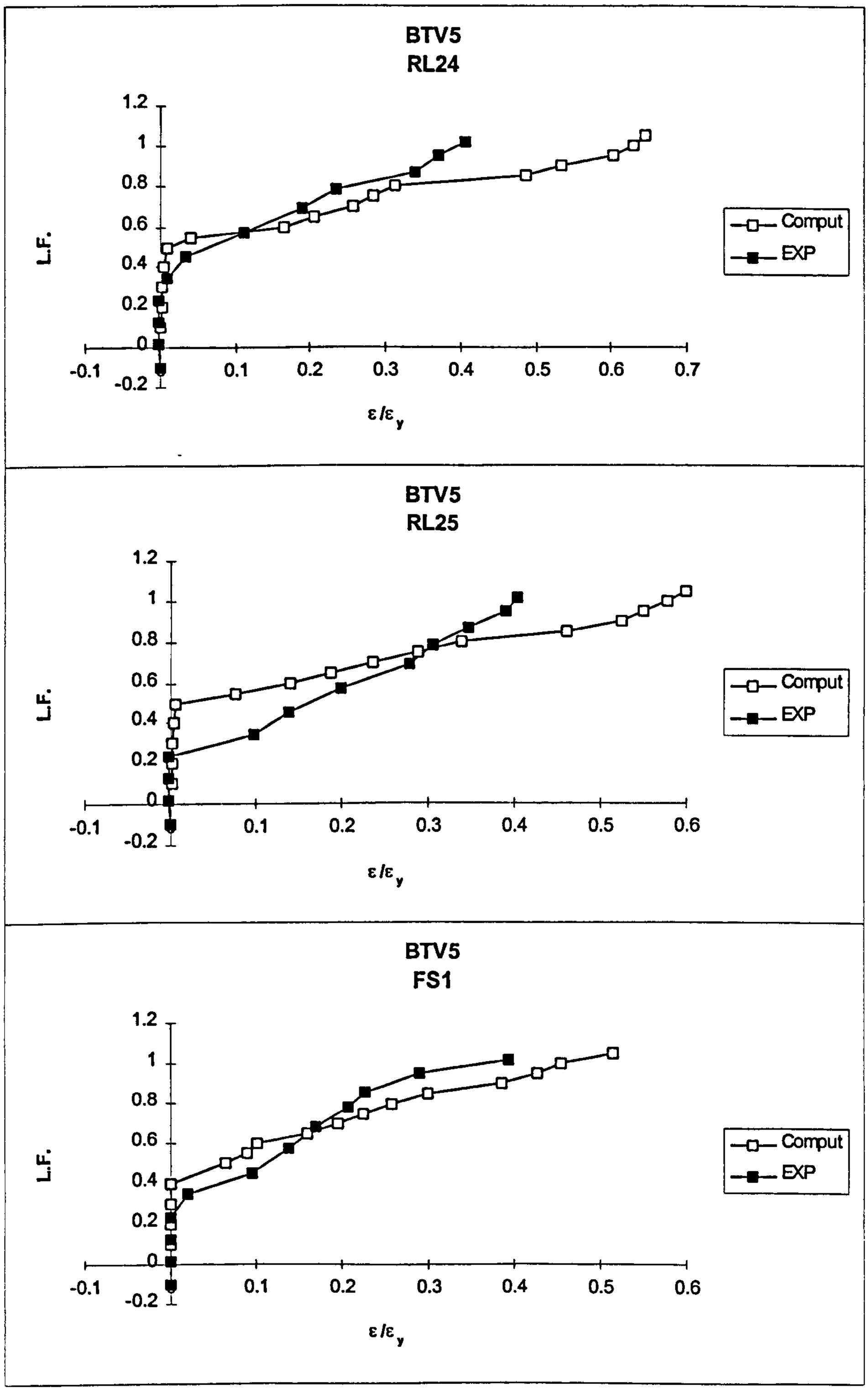
BTV5
RL24
L.F.
1.2
1
0.8
0.6
0.4
0.2
0
-0.2
-0.1
0.1
0.2
0.3
0.4
0.5
0.6
0.7
Comput
EXP
ε/ε y
BTV5
RL25
L.F.
1.2
1
0.8
0.6
0.4
0.2
0
-0.2
-0.1
0.1
0.2
0.3
0.4
0.5
0.6
Comput
EXP
ε/ε y
BTV5
FS1
L.F.
1.2
1
0.8
0.6
0.4
0.2
0
-0.2
-0.1
0.1
0.2
0.3
0.4
0.5
0.6
Comput
EXP
ε/ε y

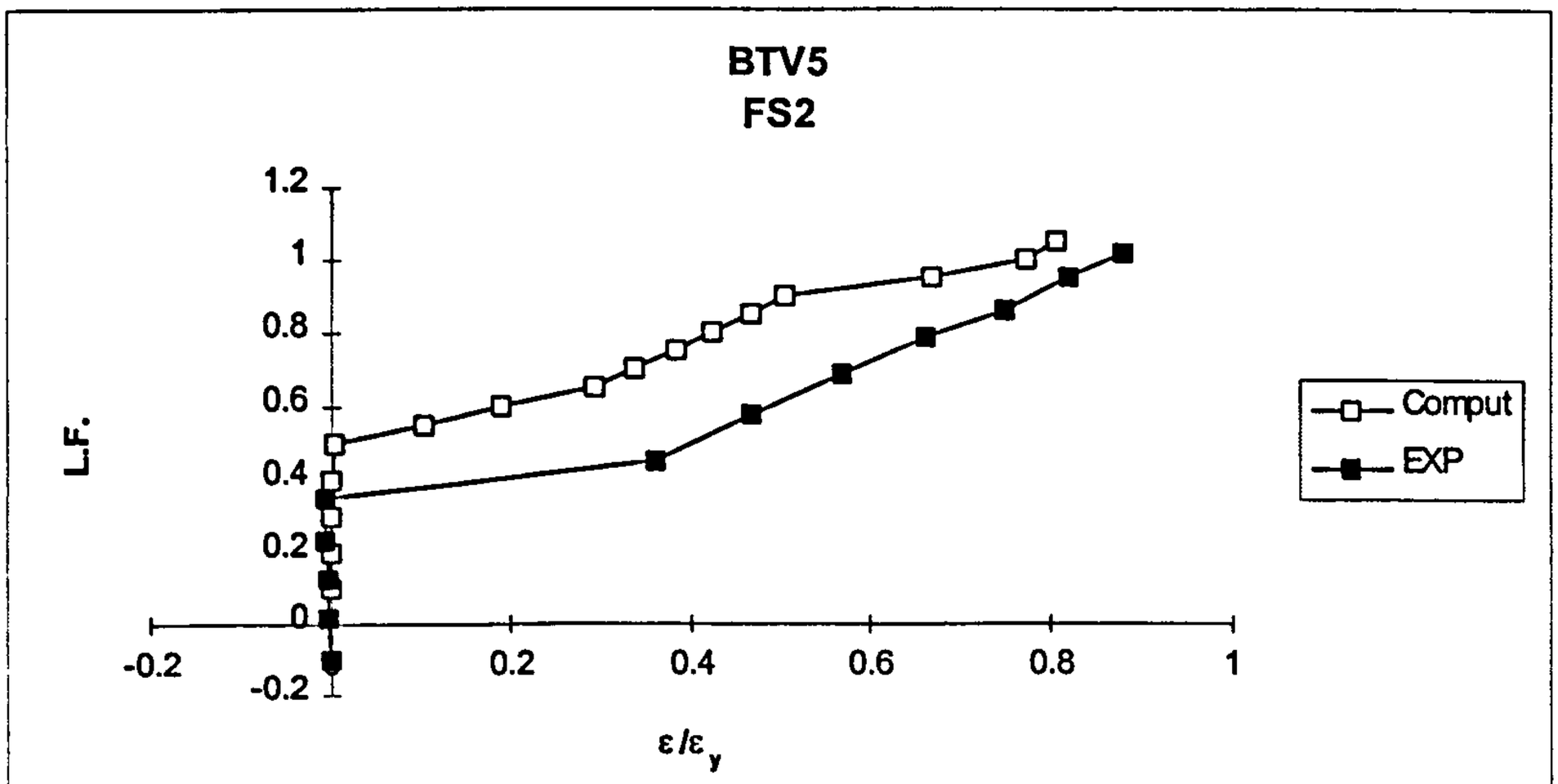
BTV5
FS2
L.F.
1.2
1
0.8
0.6
0.4
0.2
0
-0.2
-0.2
0.2
0.4
0.6
0.8
1
Comput
EXP
ε/ε y

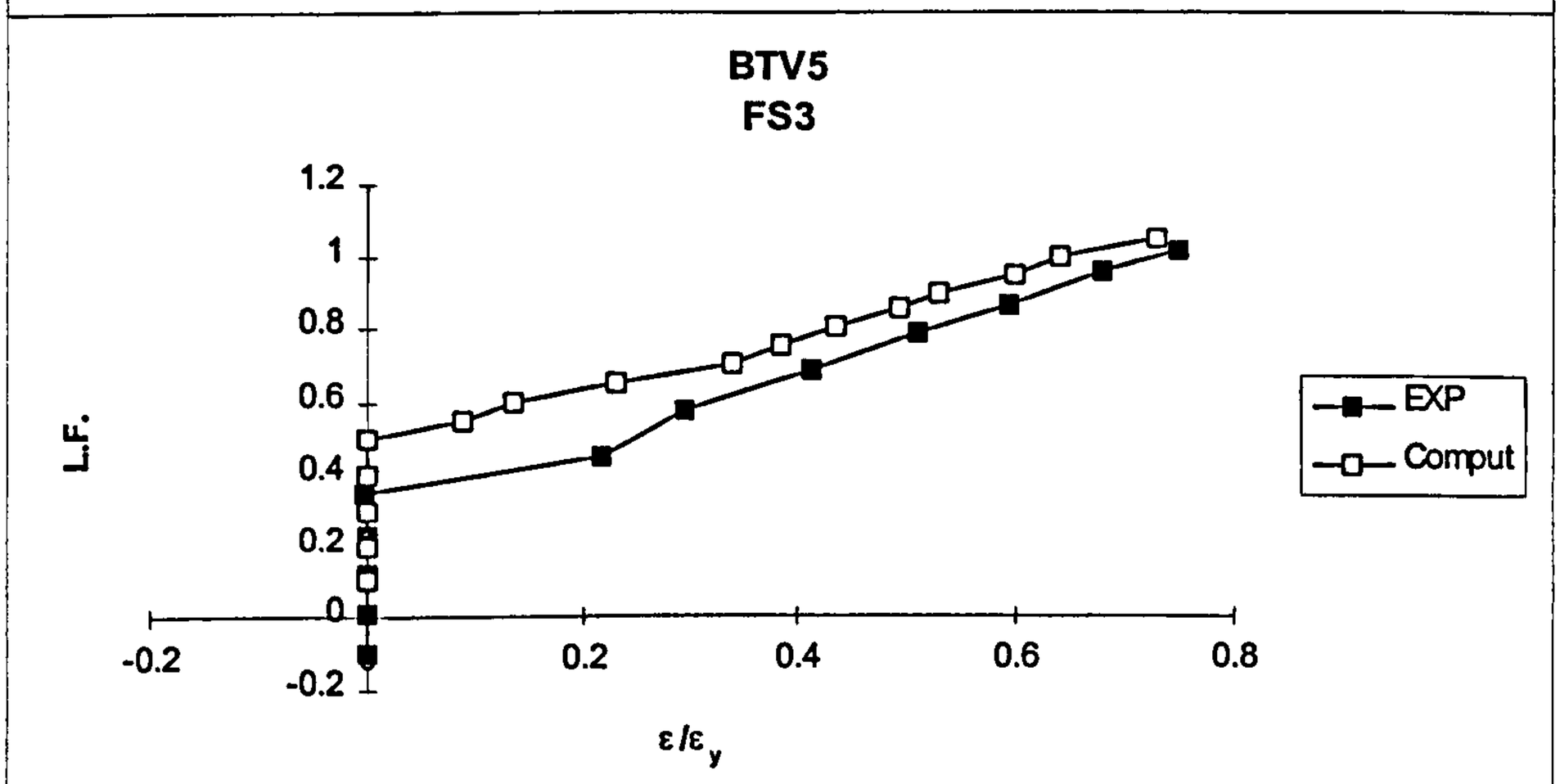
BTV5
FS3
L.F.
1.2
1
0.8
0.6
0.4
0.2
0
-0.2
-0.2
0.2
0.4
0.6
0.8
EXP
Comput
ε/ε y

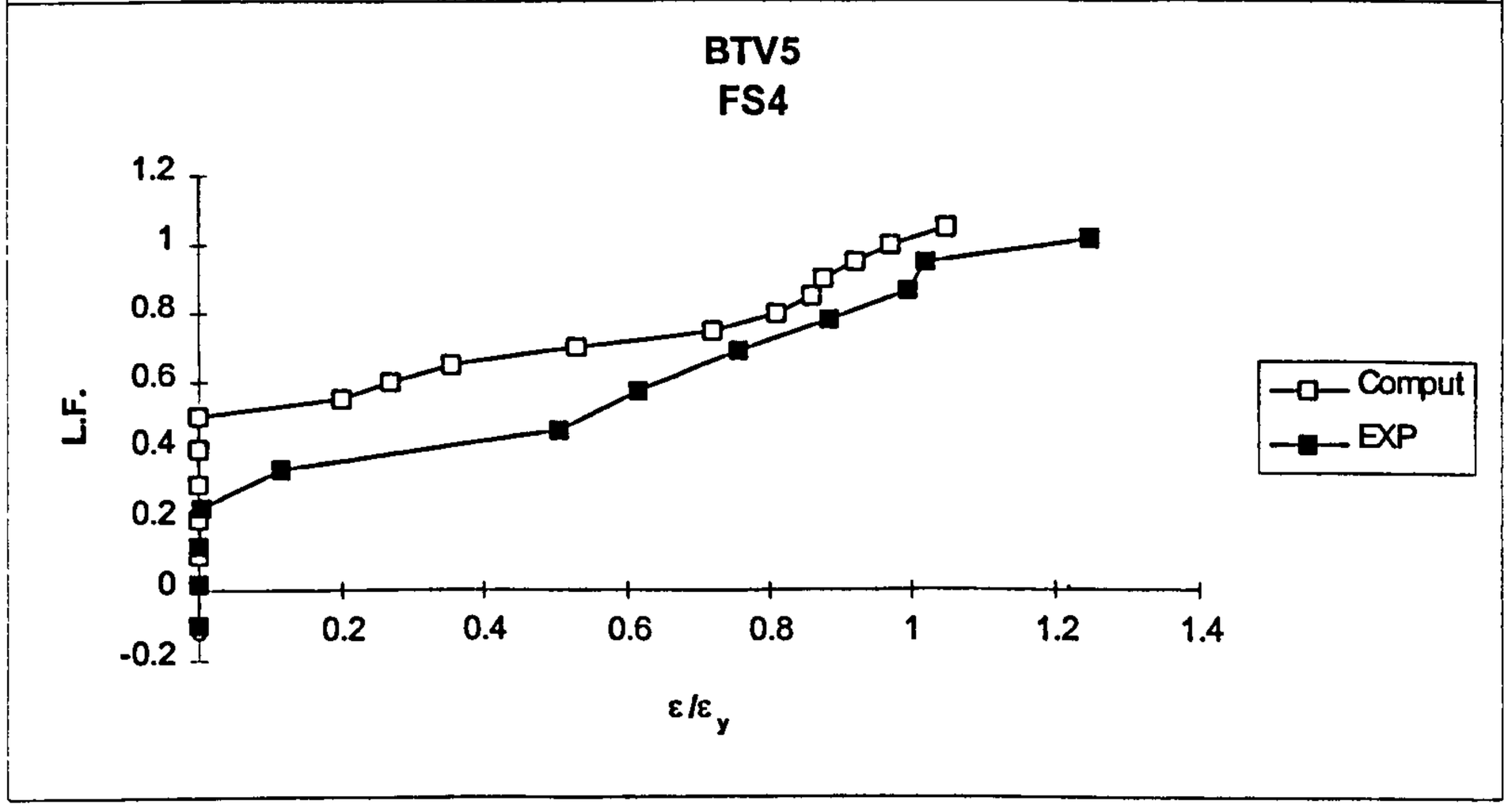
BTV5
FS4
L.F.
1.2
1
0.8
0.6
0.4
0.2
0
-0.2
0.2
0.4
0.6
0.8
1
1.2
1.4
Comput
EXP
ε/ε y

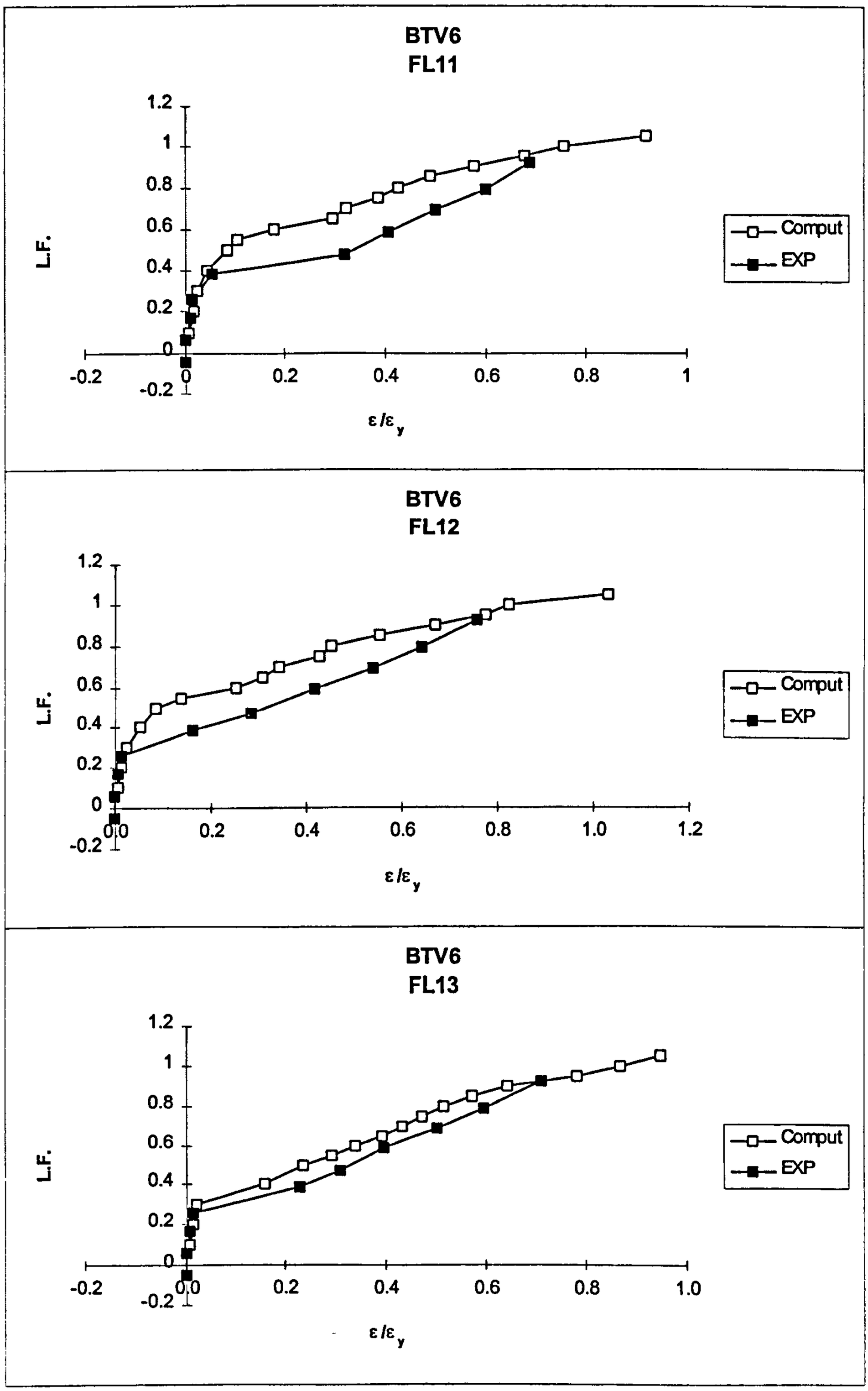
BTV6
FL11
L.F.
1.2
1
0.8
0.6
0.4
0.2
0
-0.2
-0.2
0
0.2
0.4
0.6
0.8
1
ε/ε_y
Comput
EXP
BTV6
FL12
L.F.
1.2
1
0.8
0.6
0.4
0.2
0
-0.2
0.0
0.2
0.4
0.6
0.8
1.0
1.2
ε/ε_y
Comput
EXP
BTV6
FL13
L.F.
1.2
1
0.8
0.6
0.4
0.2
0
-0.2
0.0
0.2
0.4
0.6
0.8
1.0
ε/ε_y
Comput
EXP

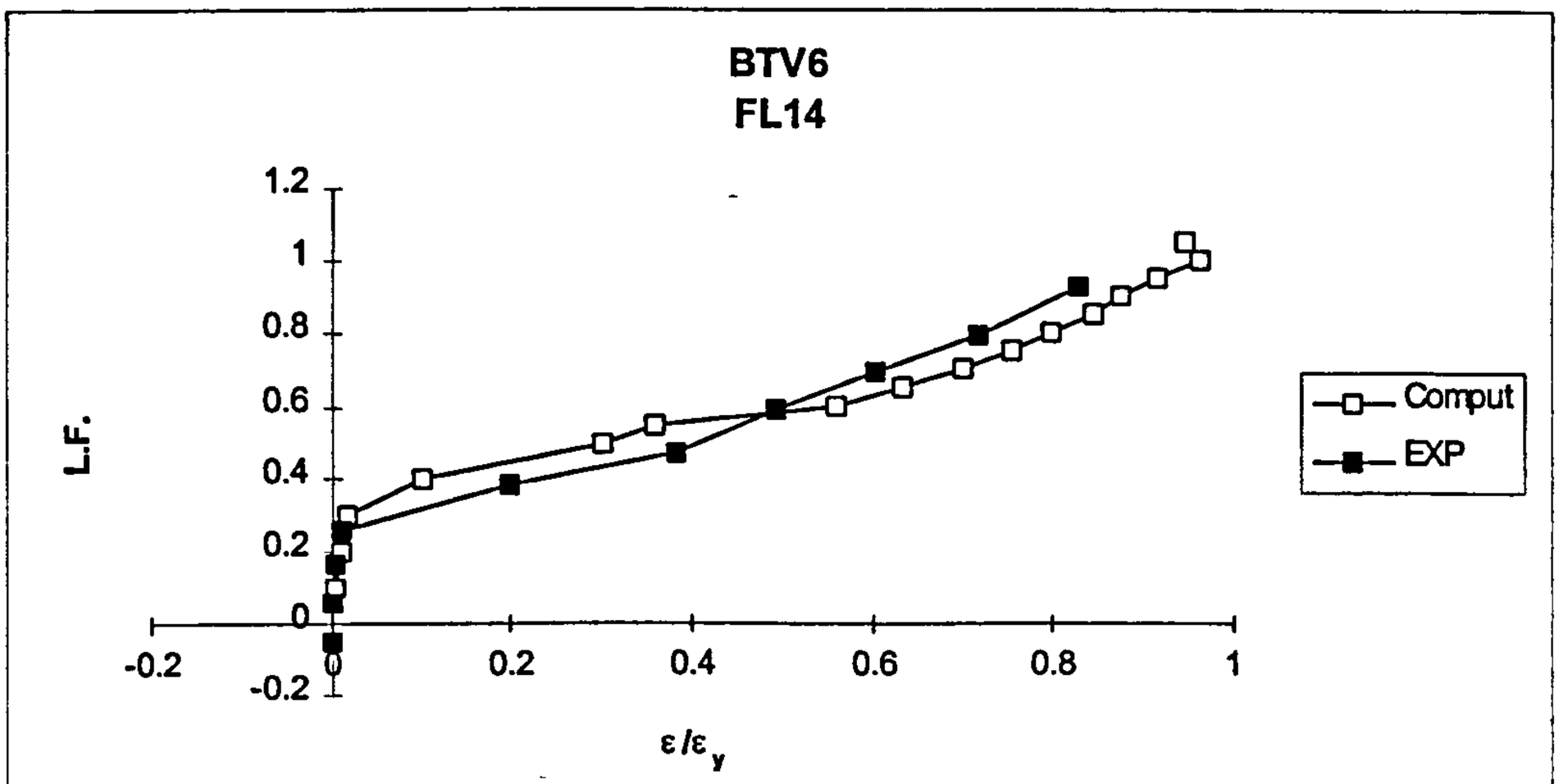
BTV6
FL14
L.F.
1.2
1
0.8
0.6
0.4
0.2
0
-0.2
-0.2
0
0.2
0.4
0.6
0.8
1
ε/ε y
Comput
EXP

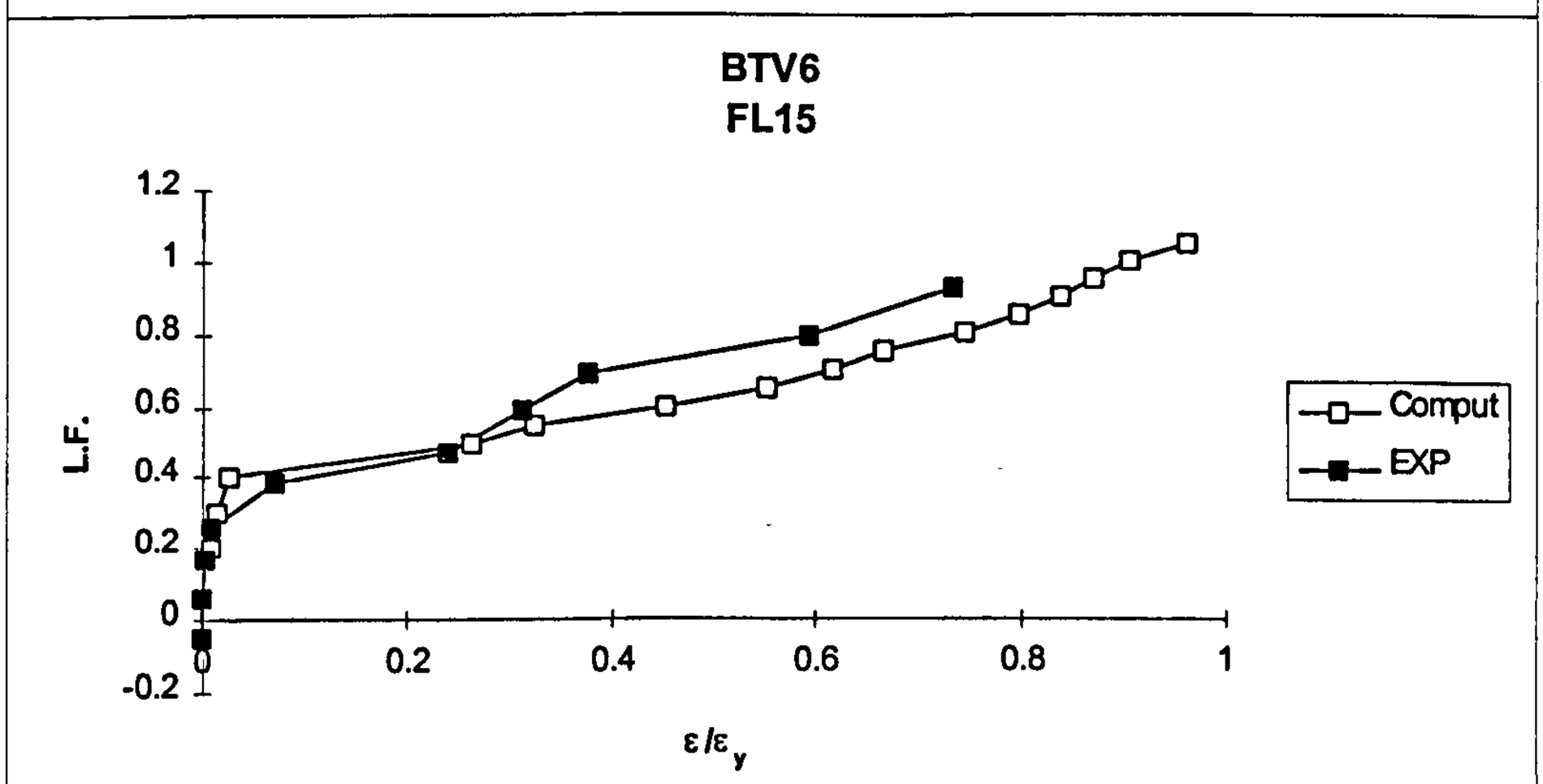
BTV6
FL15
L.F.
1.2
1
0.8
0.6
0.4
0.2
0
-0.2
0
0.2
0.4
0.6
0.8
1
ε/ε y
Comput
EXP

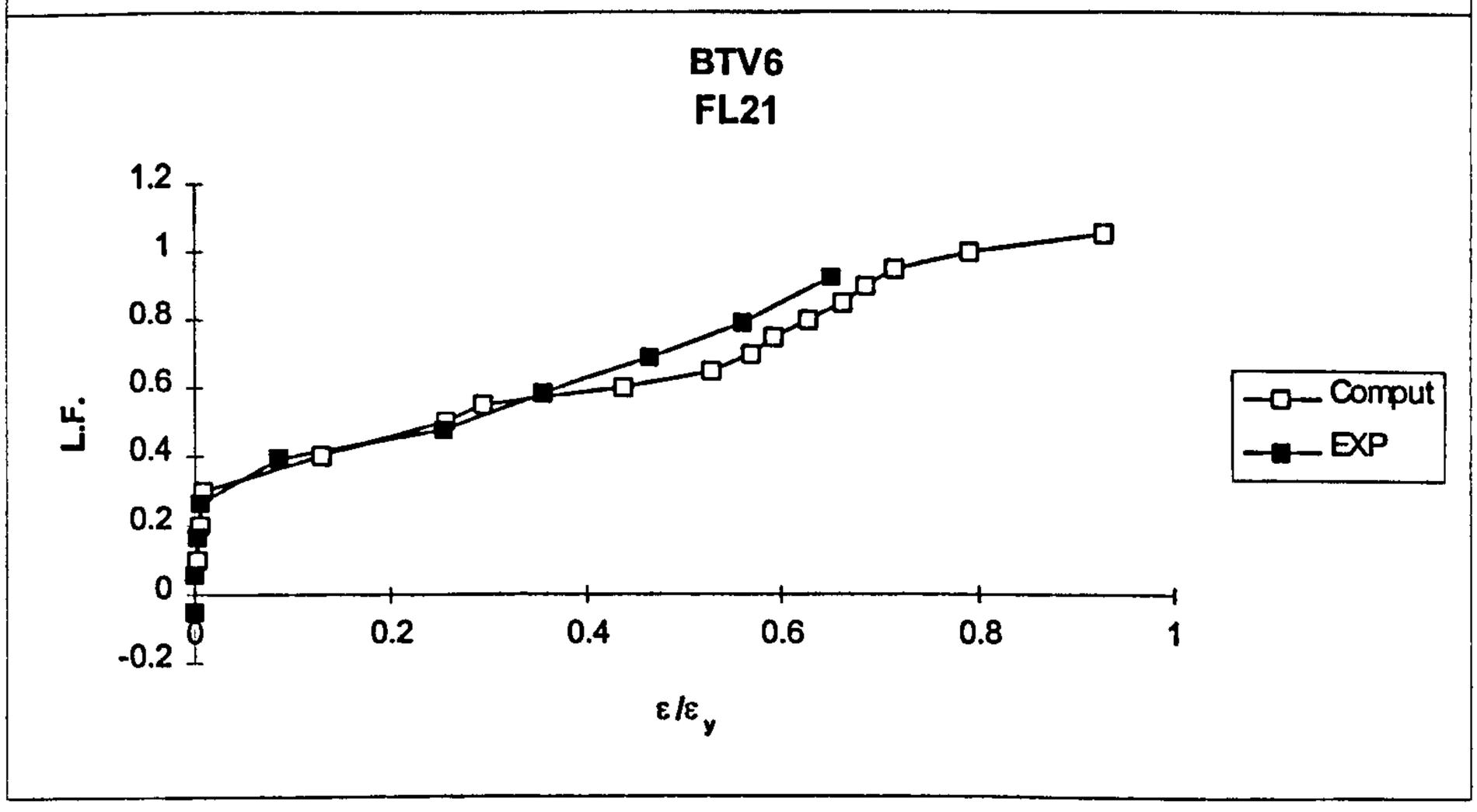
BTV6
FL21
L.F.
1.2
1
0.8
0.6
0.4
0.2
0
-0.2
0
0.2
0.4
0.6
0.8
1
ε/ε y
Comput
EXP

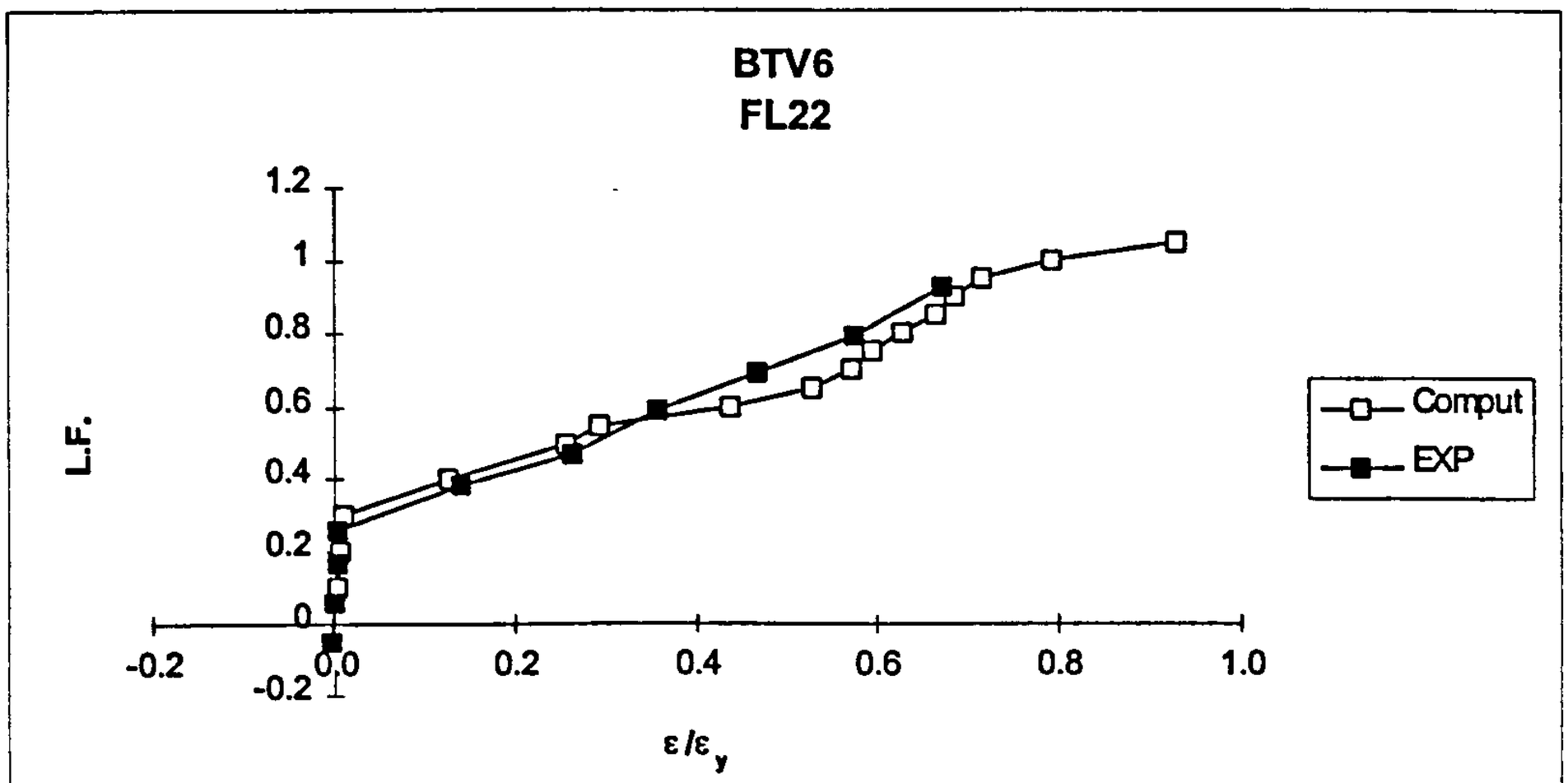
BTV6
FL22
L.F.
1.2
1
0.8
0.6
0.4
0.2
0
-0.2
-0.2
0.0
0.2
0.4
0.6
0.8
1.0
ε/ε y
Comput
EXP

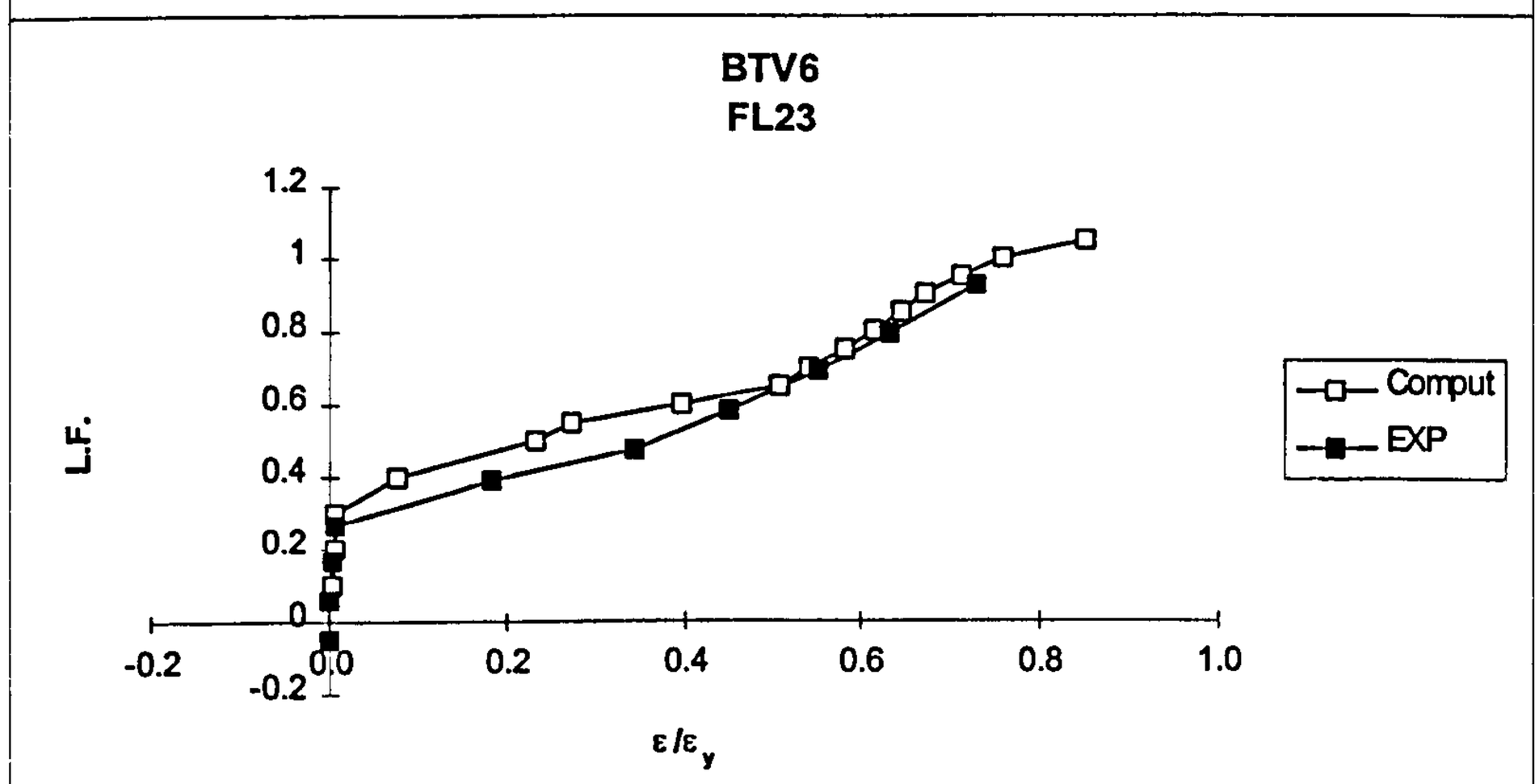
BTV6
FL23
L.F.
1.2
1
0.8
0.6
0.4
0.2
0
-0.2
-0.2
0.0
0.2
0.4
0.6
0.8
1.0
ε/ε y
Comput
EXP

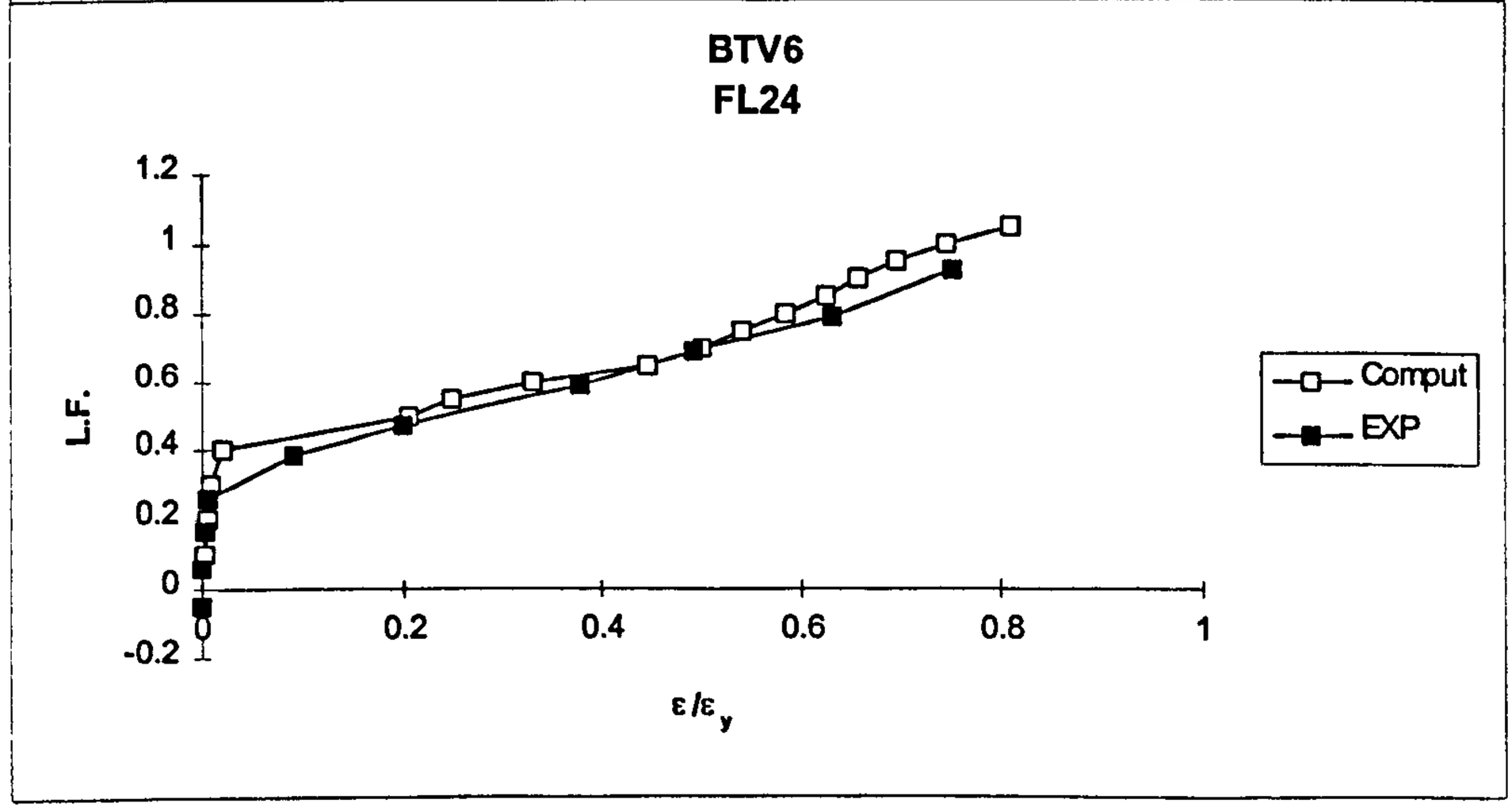
BTV6
FL24
L.F.
1.2
1
0.8
0.6
0.4
0.2
0
-0.2
0
0.2
0.4
0.6
0.8
1
ε/ε y
Comput
EXP

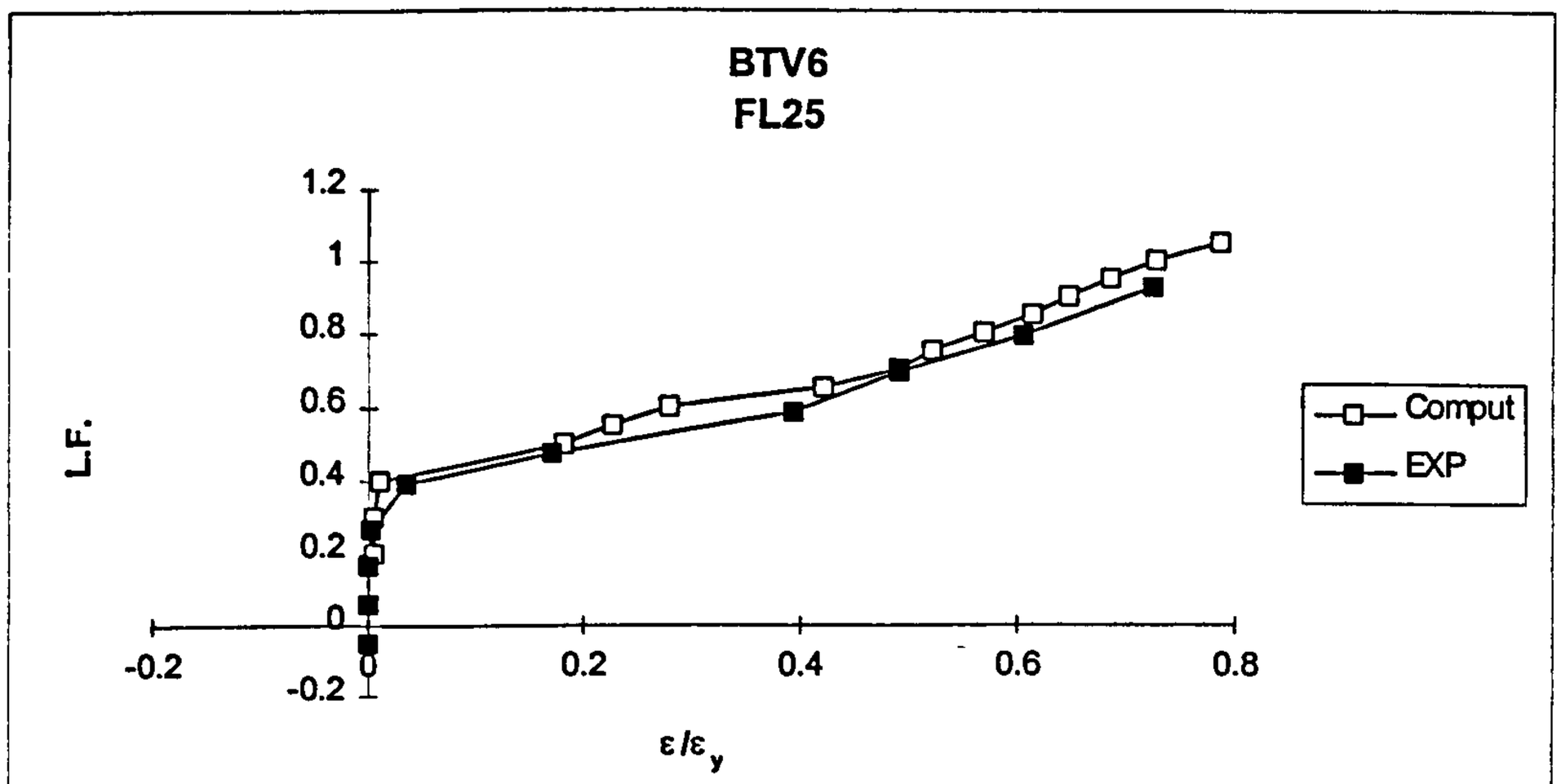
BTV6
FL25
L.F.
1.2
1
0.8
0.6
0.4
0.2
0
-0.2
-0.2
0
0.2
0.4
0.6
0.8
ε/ε_y
Comput
EXP

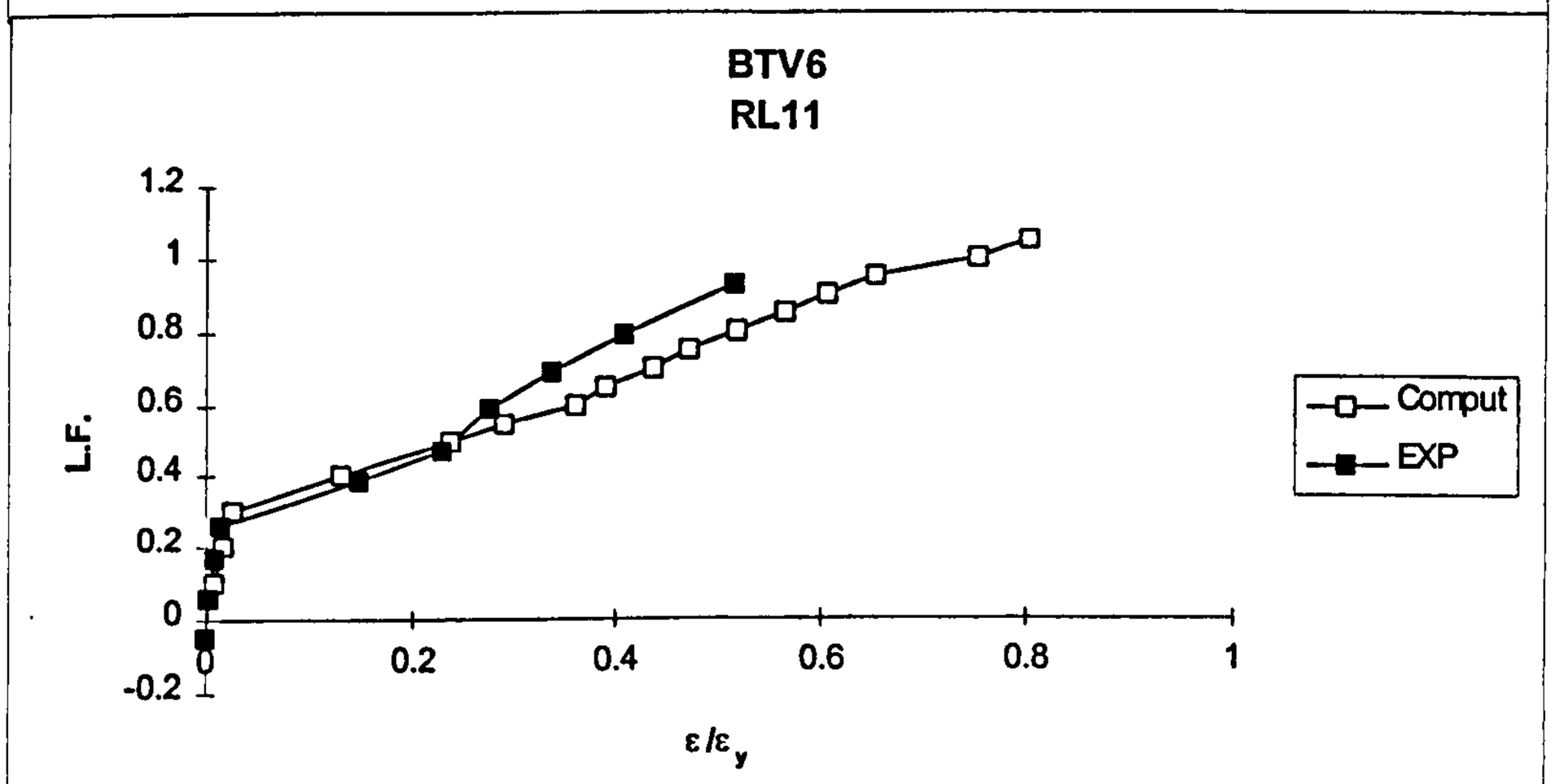
BTV6
RL11
L.F.
1.2
1
0.8
0.6
0.4
0.2
0
-0.2
0
0.2
0.4
0.6
0.8
1
ε/ε_y
Comput
EXP

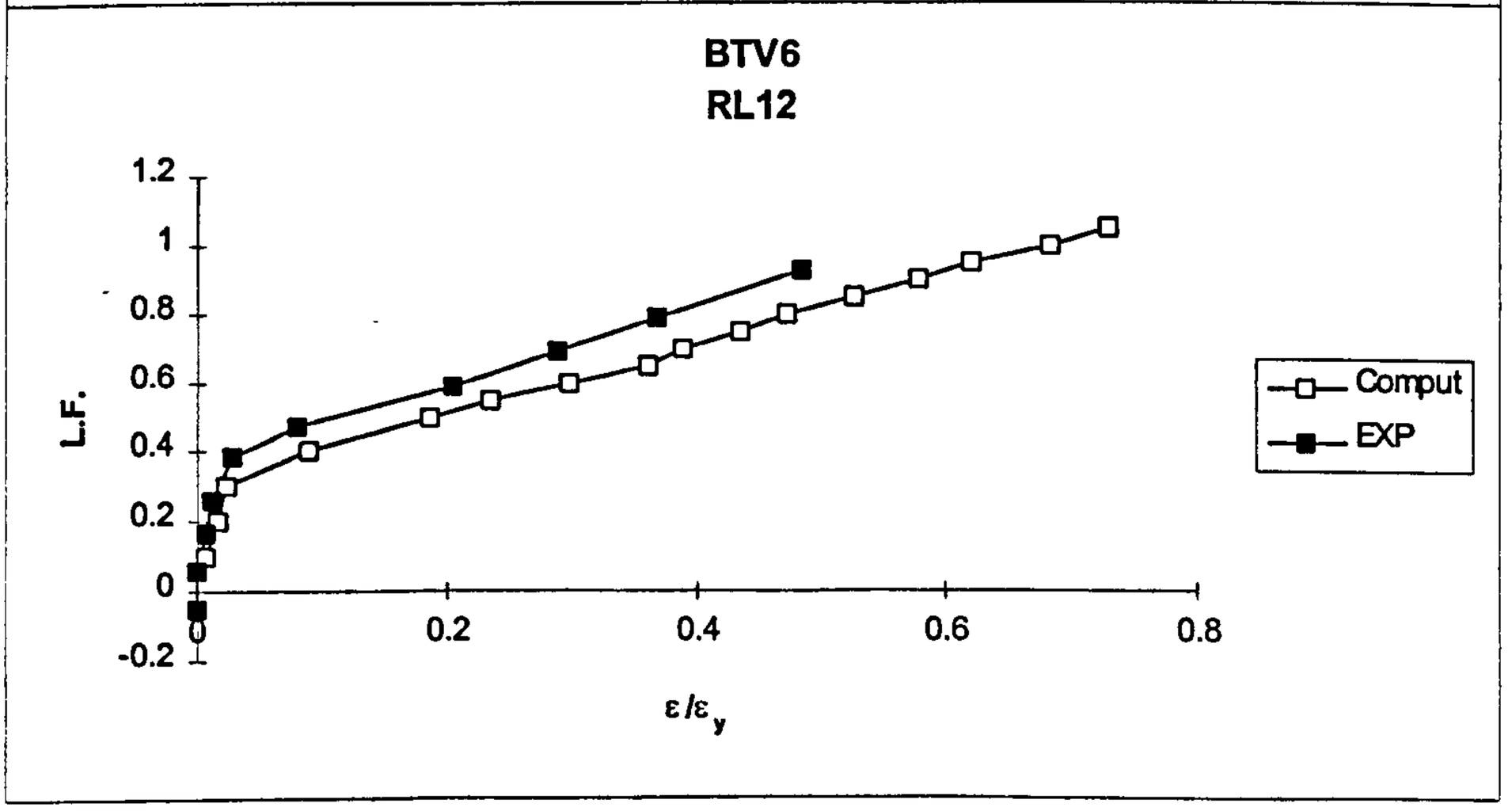
BTV6
RL12
L.F.
1.2
1
0.8
0.6
0.4
0.2
0
-0.2
0
0.2
0.4
0.6
0.8
ε/ε_y
Comput
EXP

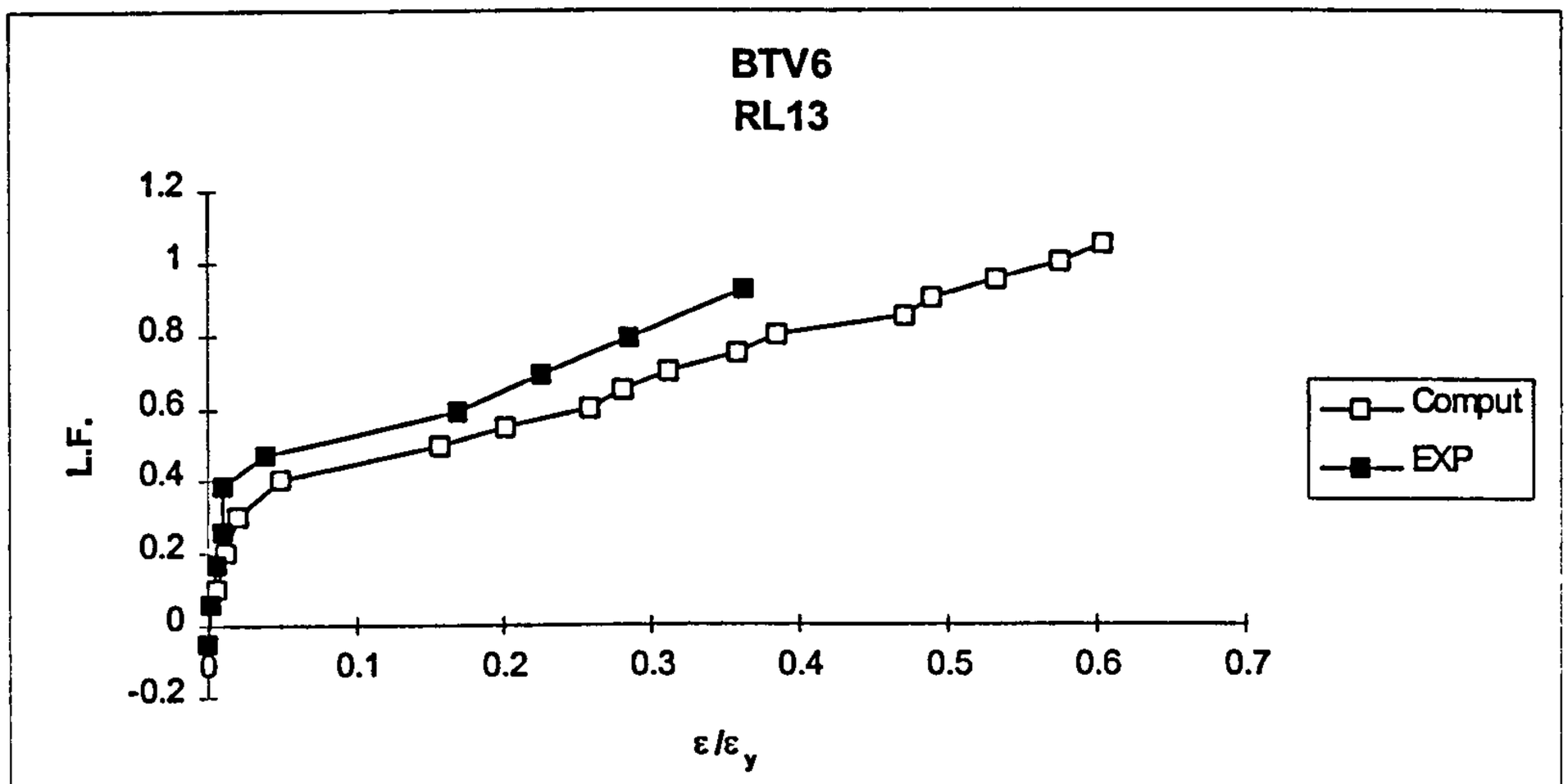
BTV6
RL13
L.F.
1.2
1
0.8
0.6
0.4
0.2
0
-0.2
0
0.1
0.2
0.3
0.4
0.5
0.6
0.7
ε /ε y
Comput
EXP

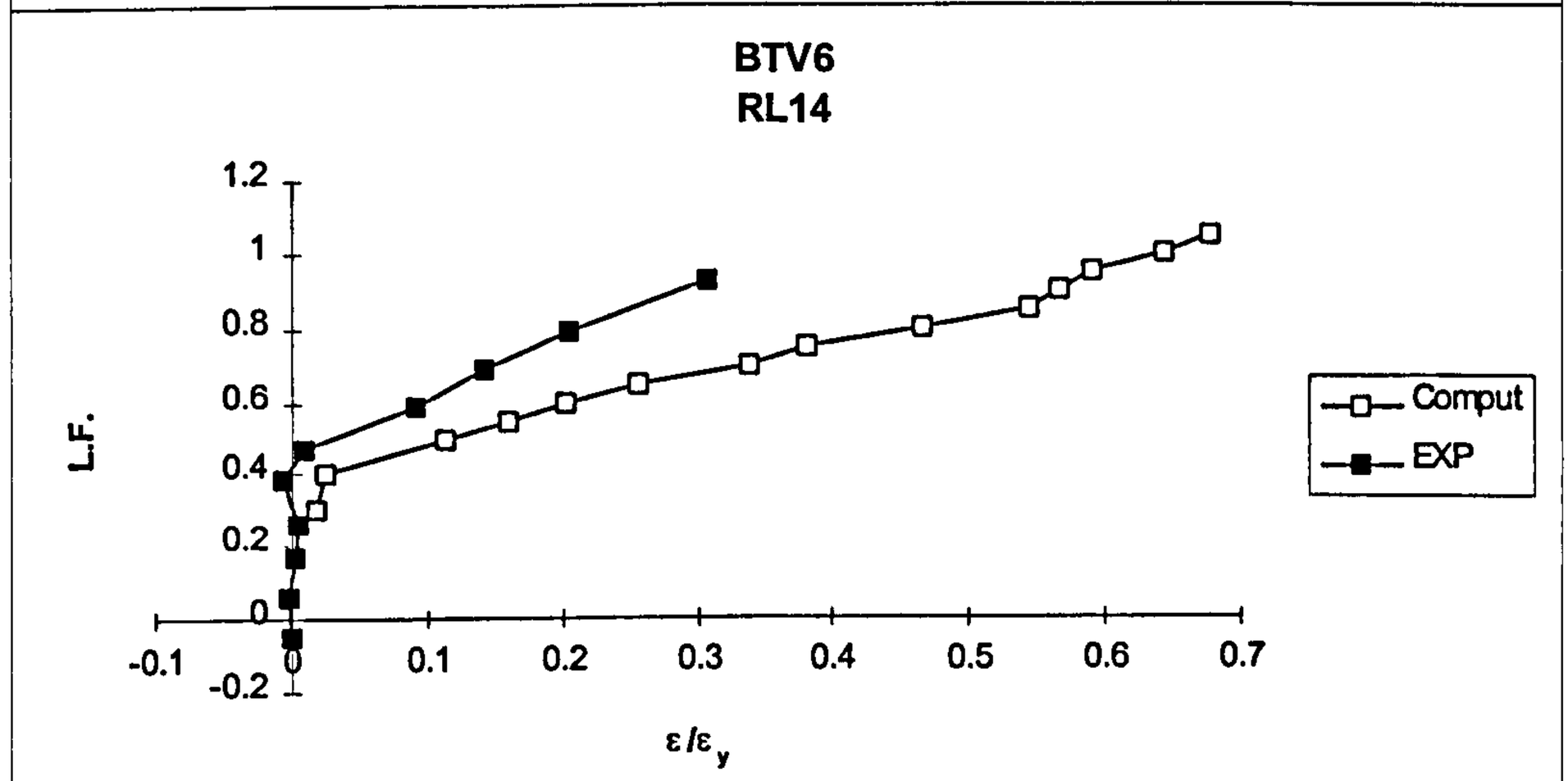
BTV6
RL14
L.F.
1.2
1
0.8
0.6
0.4
0.2
0
-0.2
-0.1
0
0.1
0.2
0.3
0.4
0.5
0.6
0.7
ε /ε y
Comput
EXP

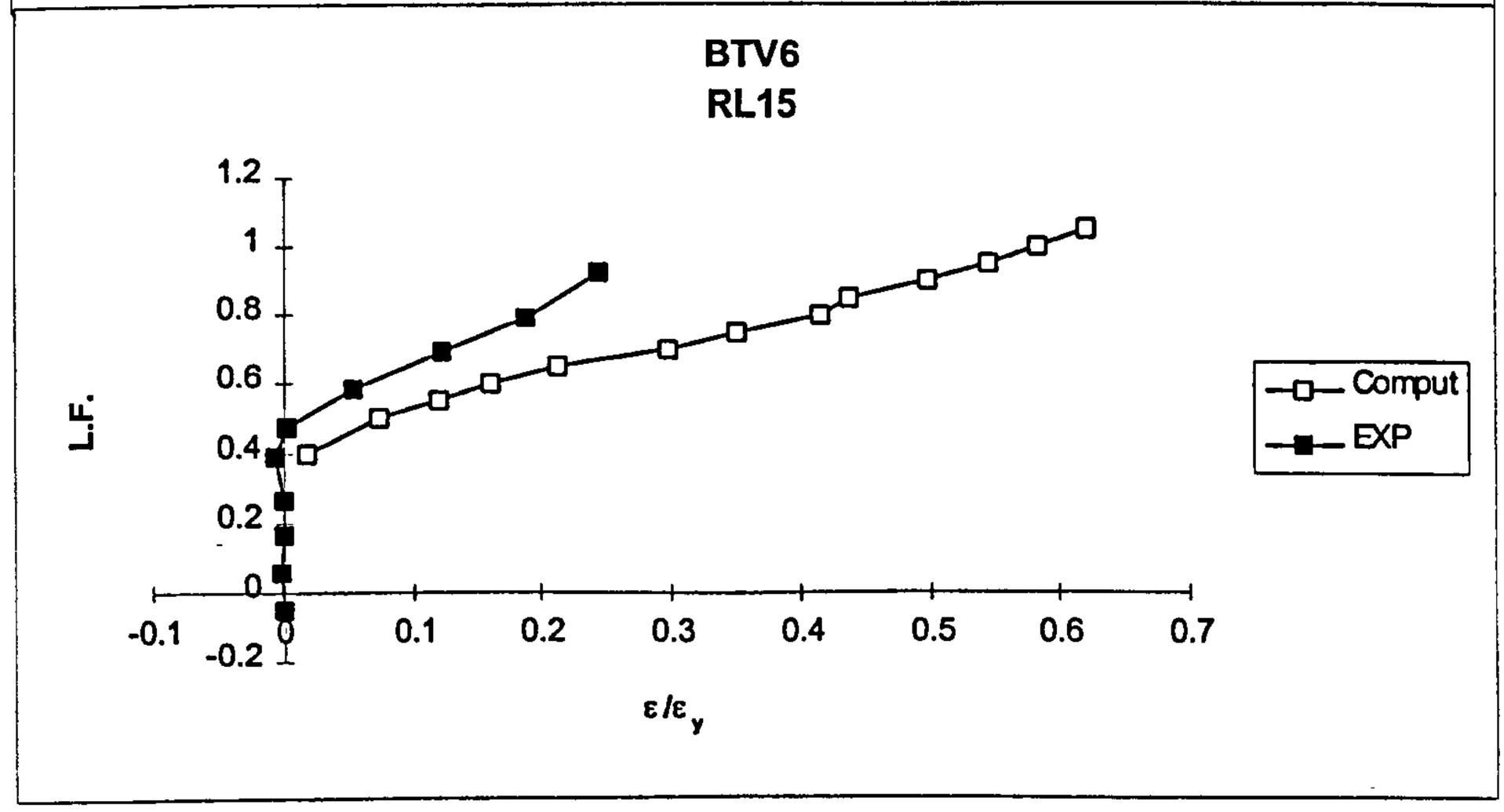
BTV6
RL15
L.F.
1.2
1
0.8
0.6
0.4
0.2
0
-0.2
-0.1
0
0.1
0.2
0.3
0.4
0.5
0.6
0.7
ε /ε y
Comput
EXP

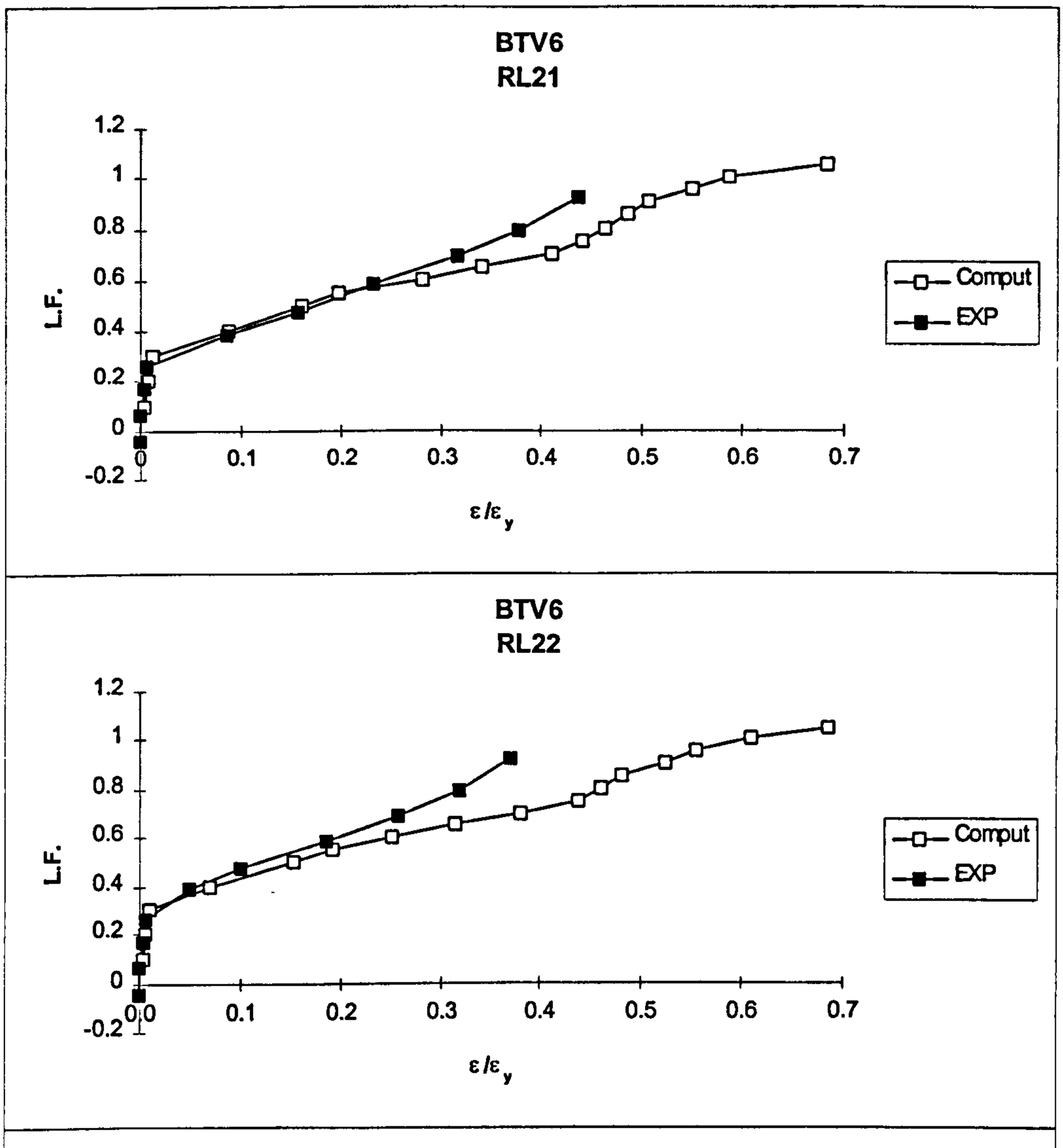
BTV6
RL21
L.F.
1.2
1
0.8
0.6
0.4
0.2
0
-0.2
0
0.1
0.2
0.3
0.4
0.5
0.6
0.7
ε/ε y
Comput
EXP
BTV6
RL22
L.F.
1.2
1
0.8
0.6
0.4
0.2
0
-0.2
0
0.1
0.2
0.3
0.4
0.5
0.6
0.7
ε/ε y
Comput
EXP
BTV6
RL23
L.F.
1.2
1
0.8
0.6
0.4
0.2
0
-0.2
-0.1
0
0.1
0.2
0.3
0.4
0.5
0.6
ε/ε y
Comput
EXP

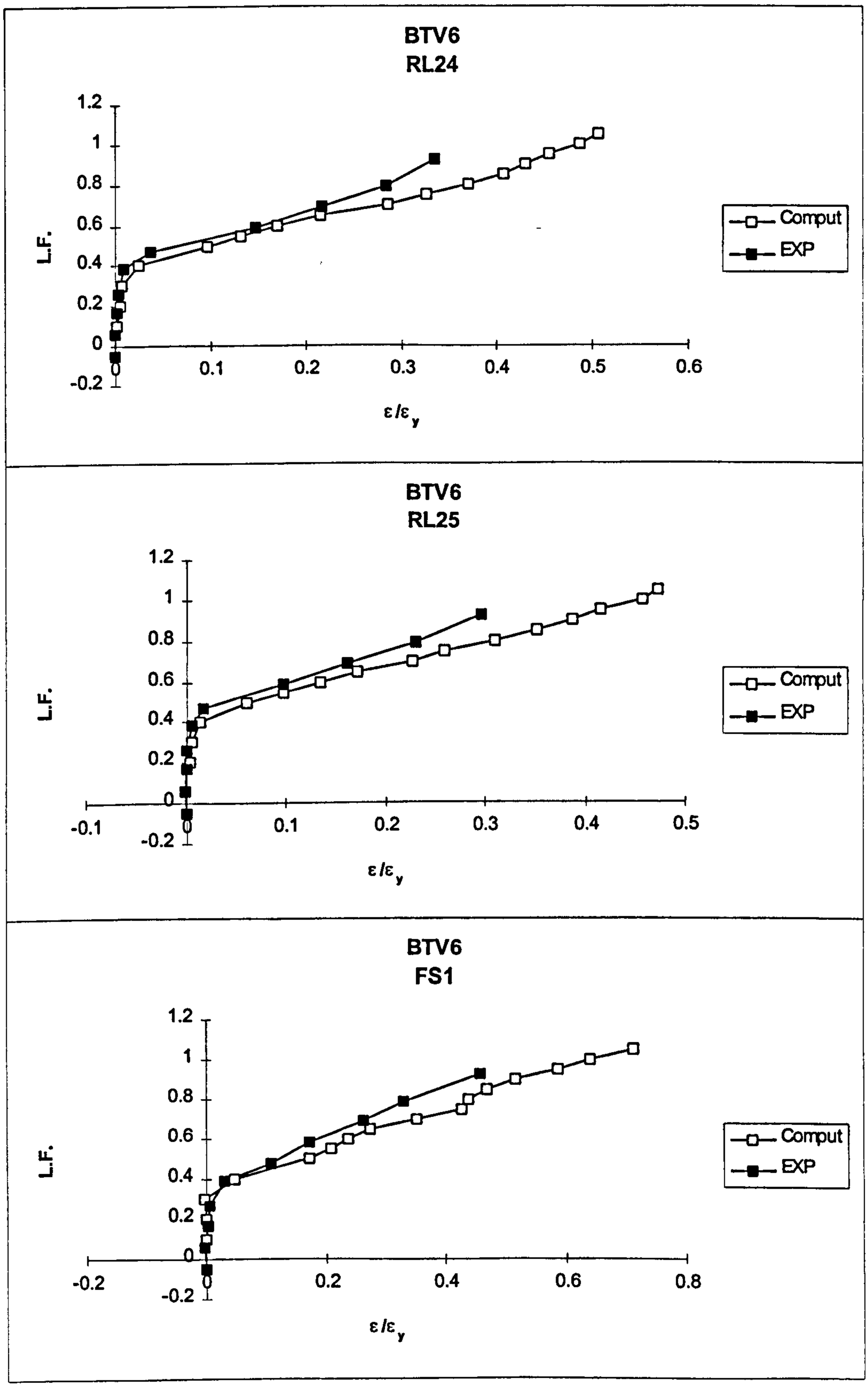
BTV6
RL24
L.F.
1.2
1
0.8
0.6
0.4
0.2
0
-0.2
0
0.1
0.2
0.3
0.4
0.5
0.6
ε/ε_y
Comput
EXP
BTV6
RL25
L.F.
1.2
1
0.8
0.6
0.4
0.2
0
-0.2
-0.1
0
0.1
0.2
0.3
0.4
0.5
ε/ε_y
Comput
EXP
BTV6
FS1
L.F.
1.2
1
0.8
0.6
0.4
0.2
0
-0.2
-0.2
0
0.2
0.4
0.6
0.8
ε/ε_y
Comput
EXP

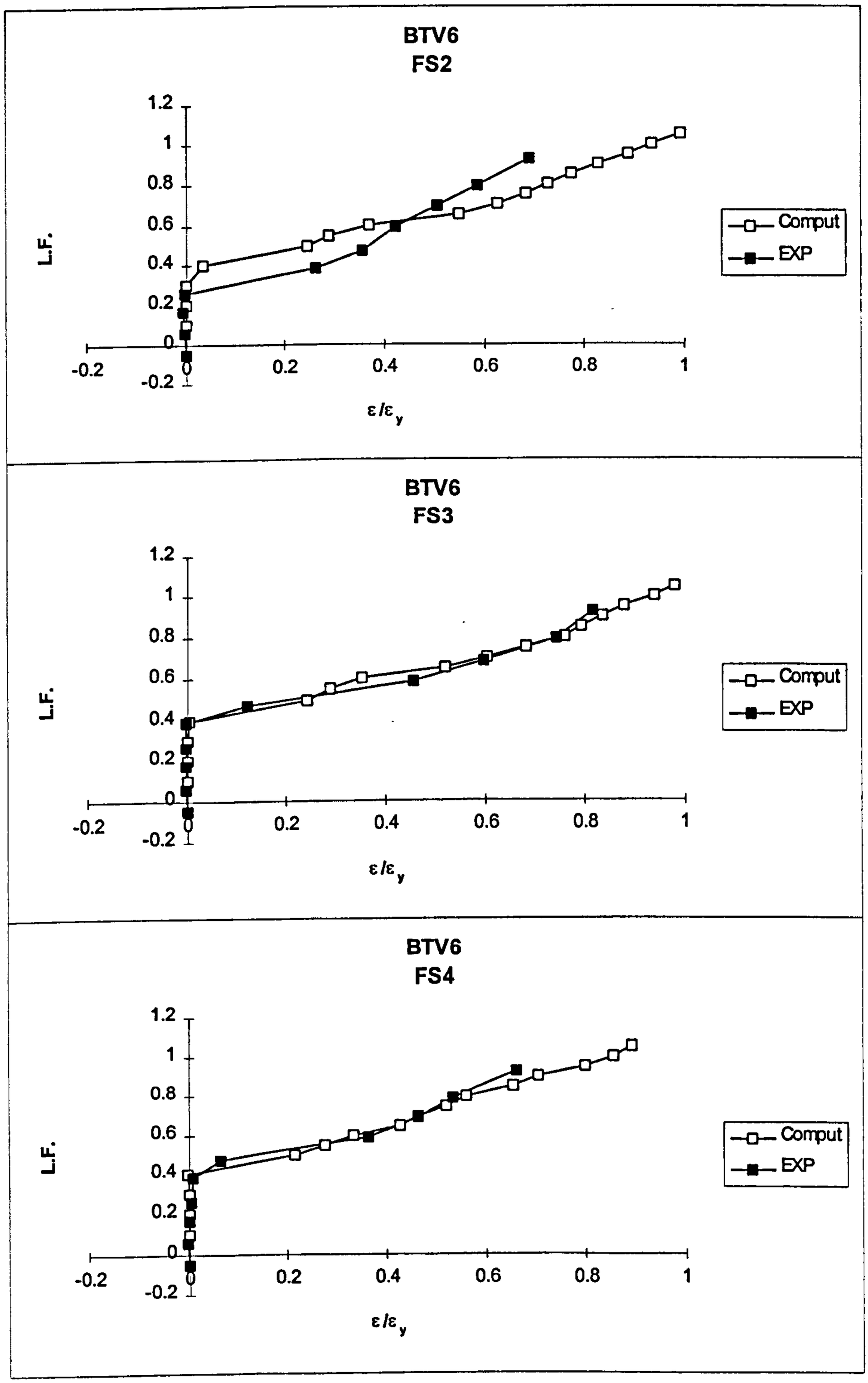
BTV6
FS2
L.F.
1.2
1
0.8
0.6
0.4
0.2
0
-0.2
-0.2
0
0.2
0.4
0.6
0.8
1
ε/ε y
Comput
EXP
BTV6
FS3
L.F.
1.2
1
0.8
0.6
0.4
0.2
0
-0.2
-0.2
0
0.2
0.4
0.6
0.8
1
ε/ε y
Comput
EXP
BTV6
FS4
L.F.
1.2
1
0.8
0.6
0.4
0.2
0
-0.2
-0.2
0
0.2
0.4
0.6
0.8
1
ε/ε y
Comput
EXP

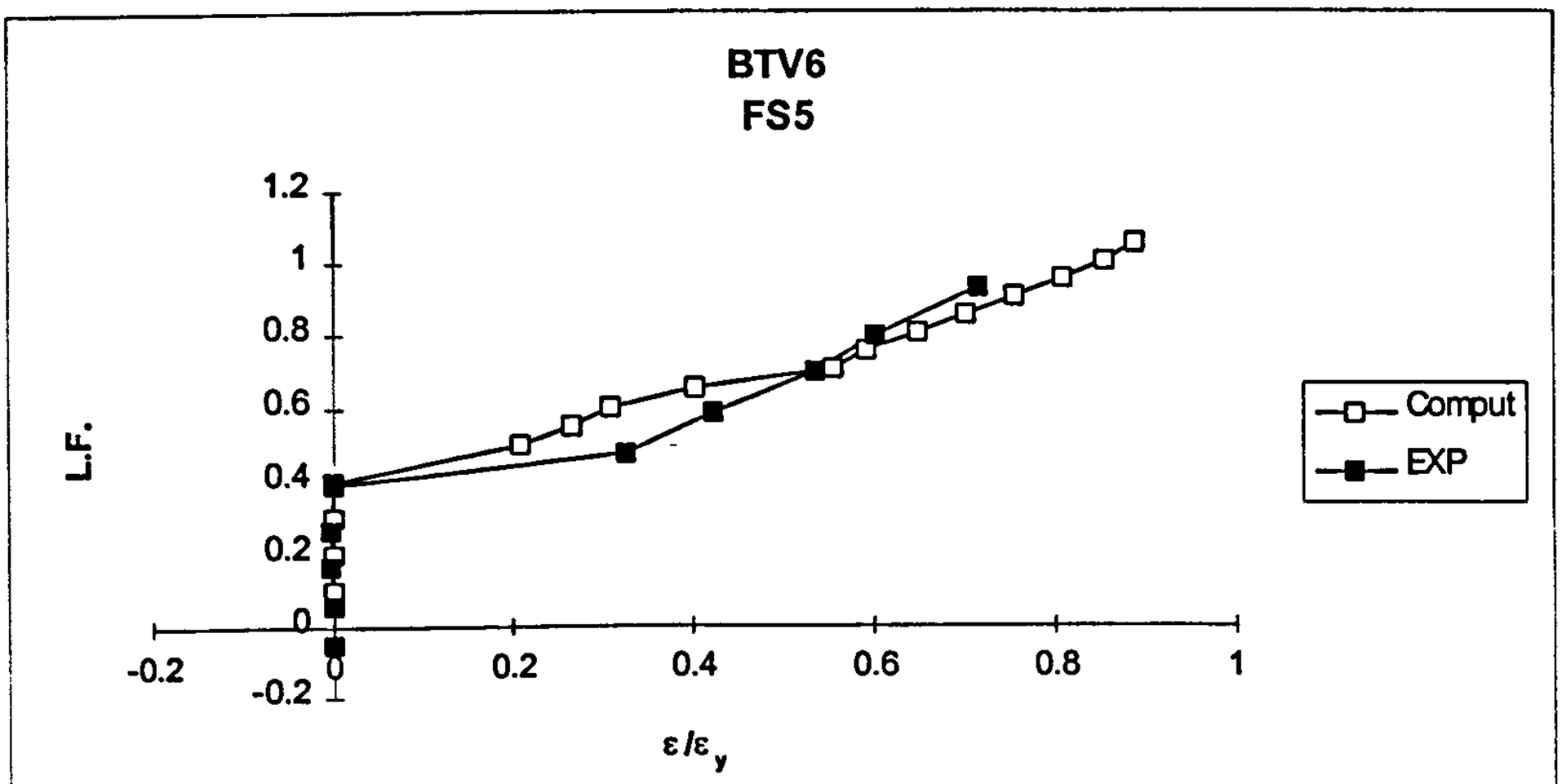
BTV6
FS5
L.F.
1.2
1
0.8
0.6
0.4
0.2
0
-0.2
-0.2
0
0.2
0.4
0.6
0.8
1
ε/ε y
Comput
EXP

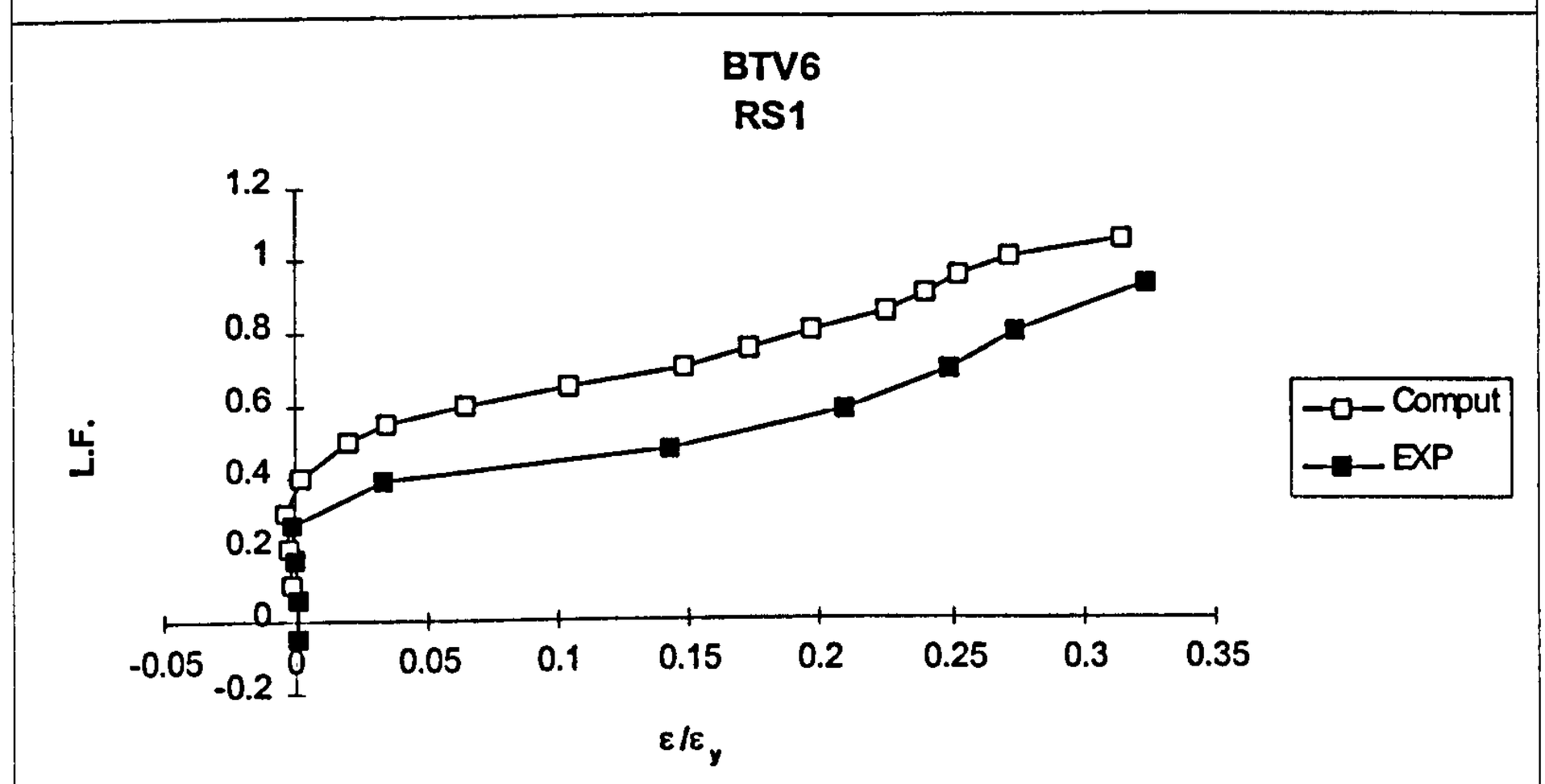
BTV6
RS1
L.F.
1.2
1
0.8
0.6
0.4
0.2
0
-0.2
-0.05
0
0.05
0.1
0.15
0.2
0.25
0.3
0.35
ε/ε y
Comput
EXP

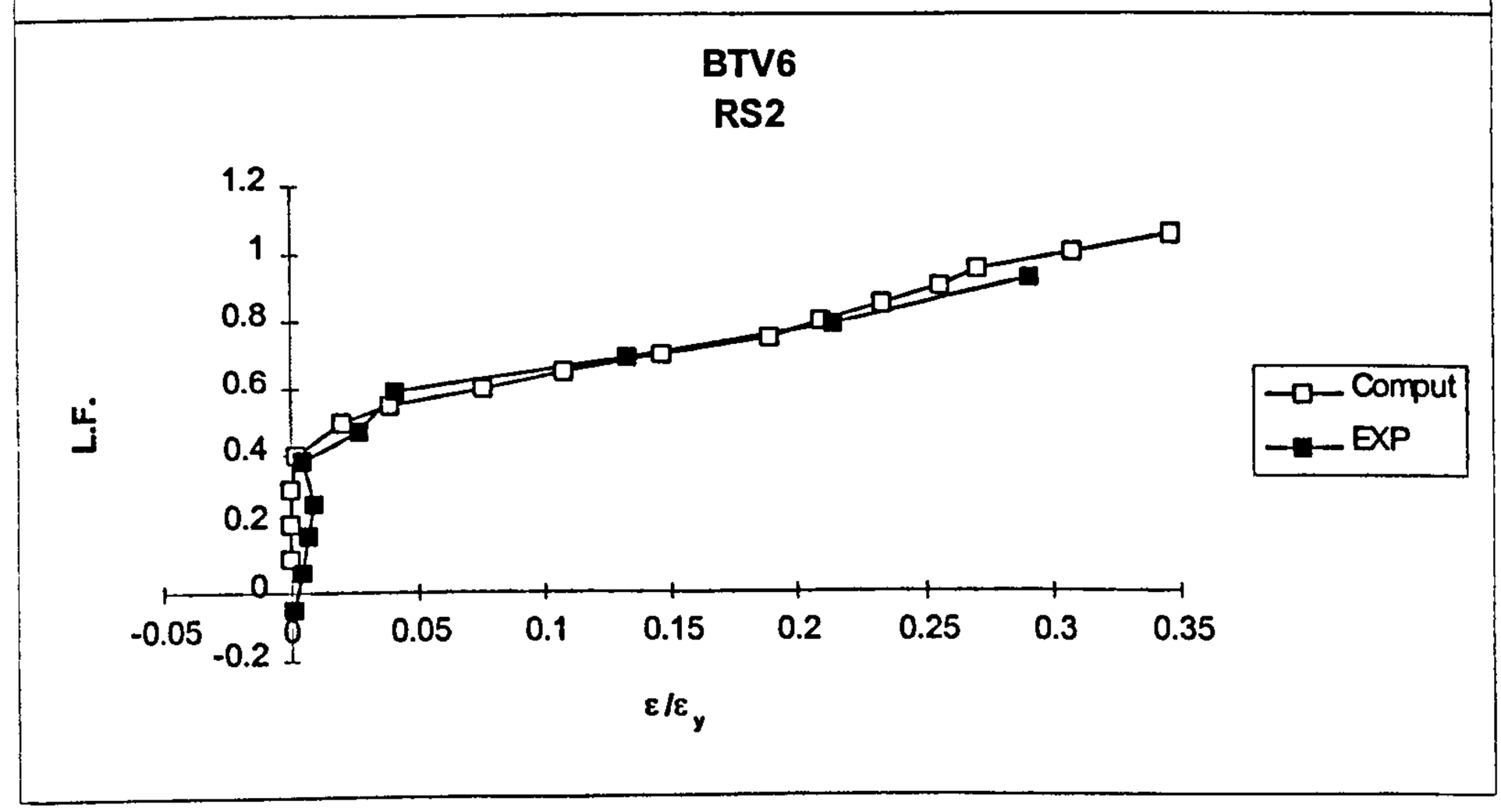
BTV6
RS2
L.F.
1.2
1
0.8
0.6
0.4
0.2
0
-0.2
-0.05
0
0.05
0.1
0.15
0.2
0.25
0.3
0.35
ε/ε y
Comput
EXP

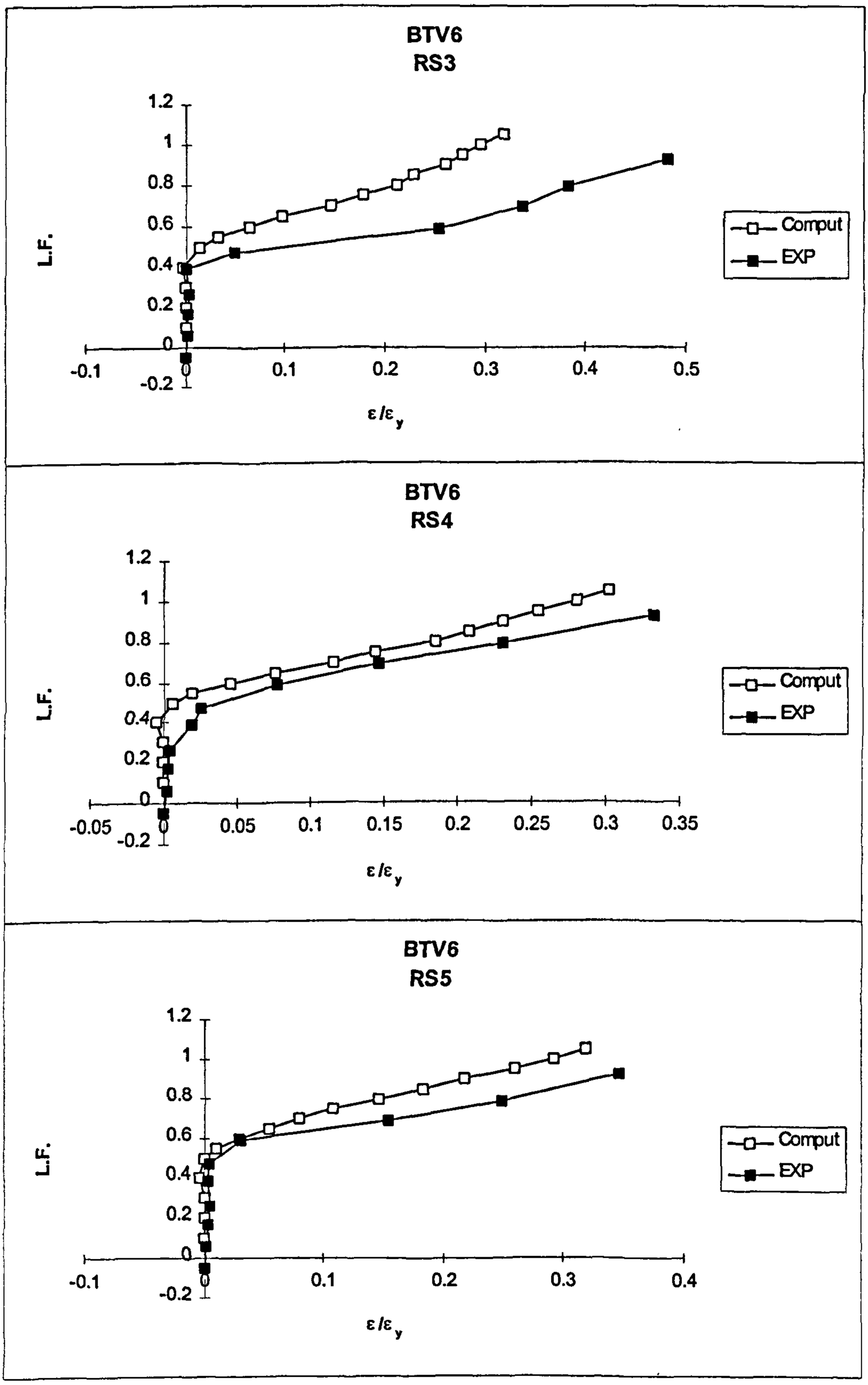
BTV6
RS3
L.F.
1.2
1
0.8
0.6
0.4
0.2
0
-0.2
-0.1
0
0.1
0.2
0.3
0.4
0.5
ε/ε_y
Comput
EXP
BTV6
RS4
L.F.
1.2
1
0.8
0.6
0.4
0.2
0
-0.2
-0.05
0
0.05
0.1
0.15
0.2
0.25
0.3
0.35
ε/ε_y
Comput
EXP
BTV6
RS5
L.F.
1.2
1
0.8
0.6
0.4
0.2
0
-0.2
-0.1
0
0.1
0.2
0.3
0.4
ε/ε_y
Comput
EXP

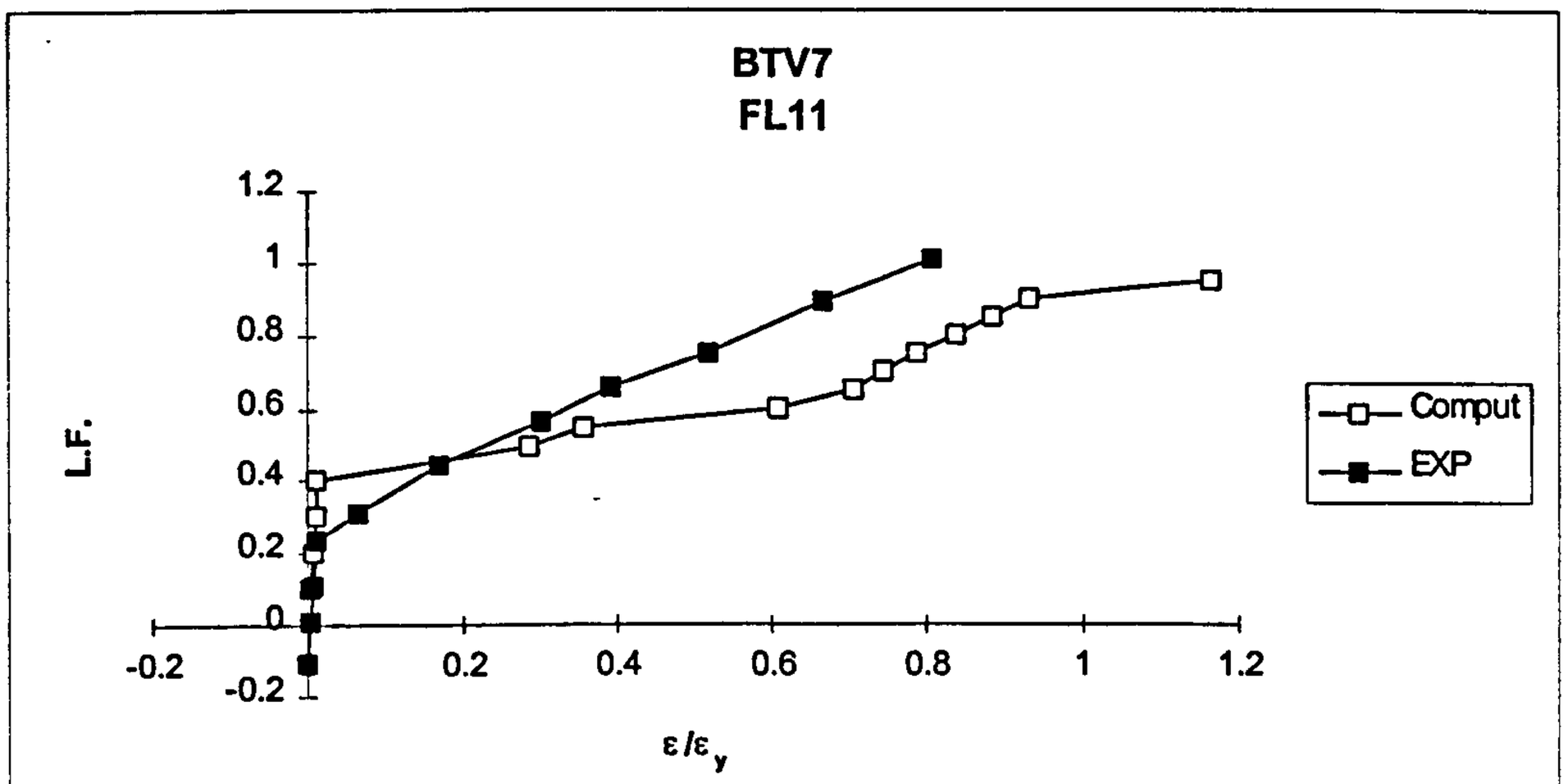
BTV7
FL11
L.F.
1.2
1
0.8
0.6
0.4
0.2
0
-0.2
-0.2
0.2
0.4
0.6
0.8
1
1.2
ε/ε y
Comput
EXP

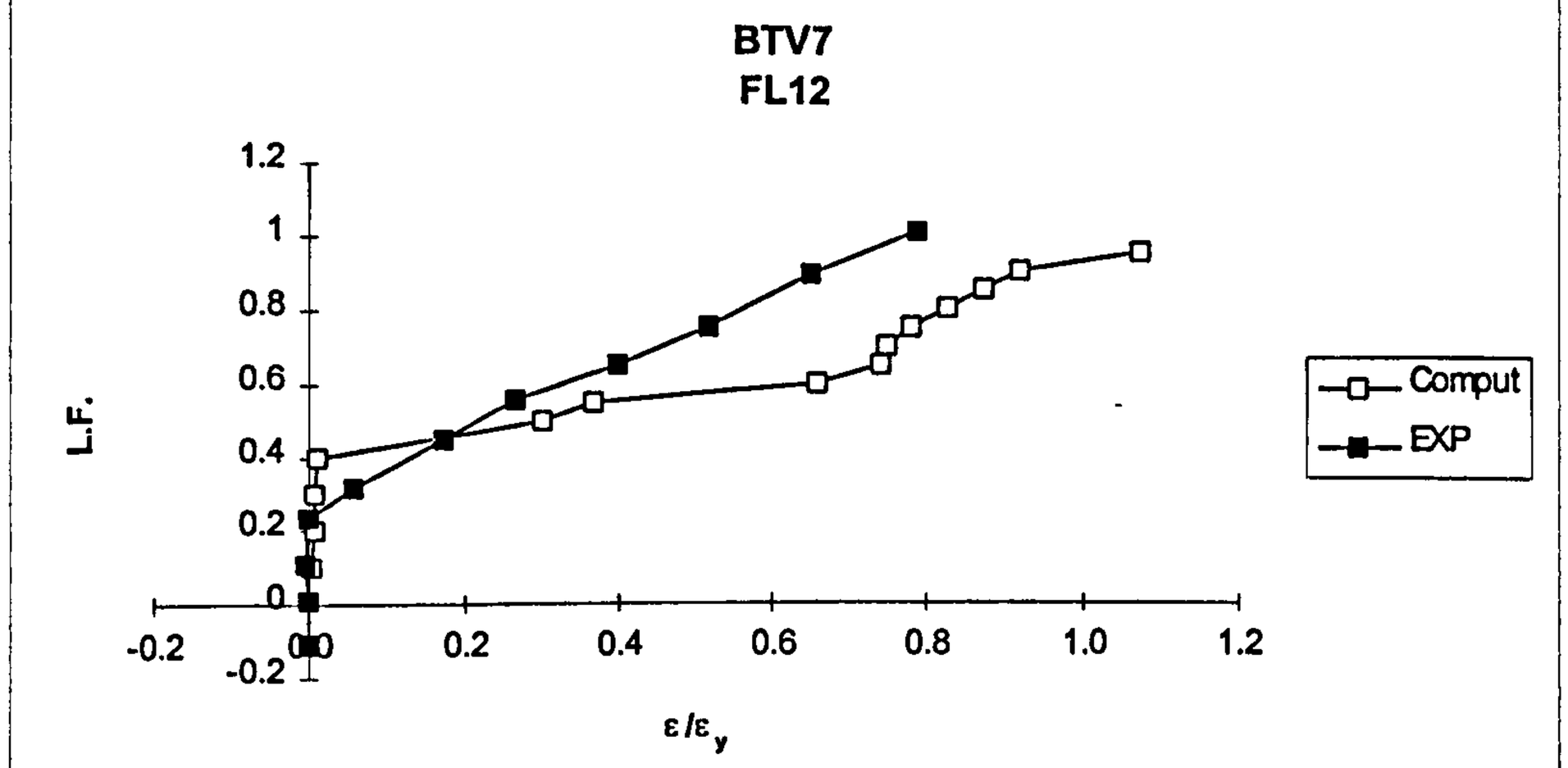
BTV7
FL12
L.F.
1.2
1
0.8
0.6
0.4
0.2
0
-0.2
-0.2
0.2
0.4
0.6
0.8
1.0
1.2
ε/ε y
Comput
EXP

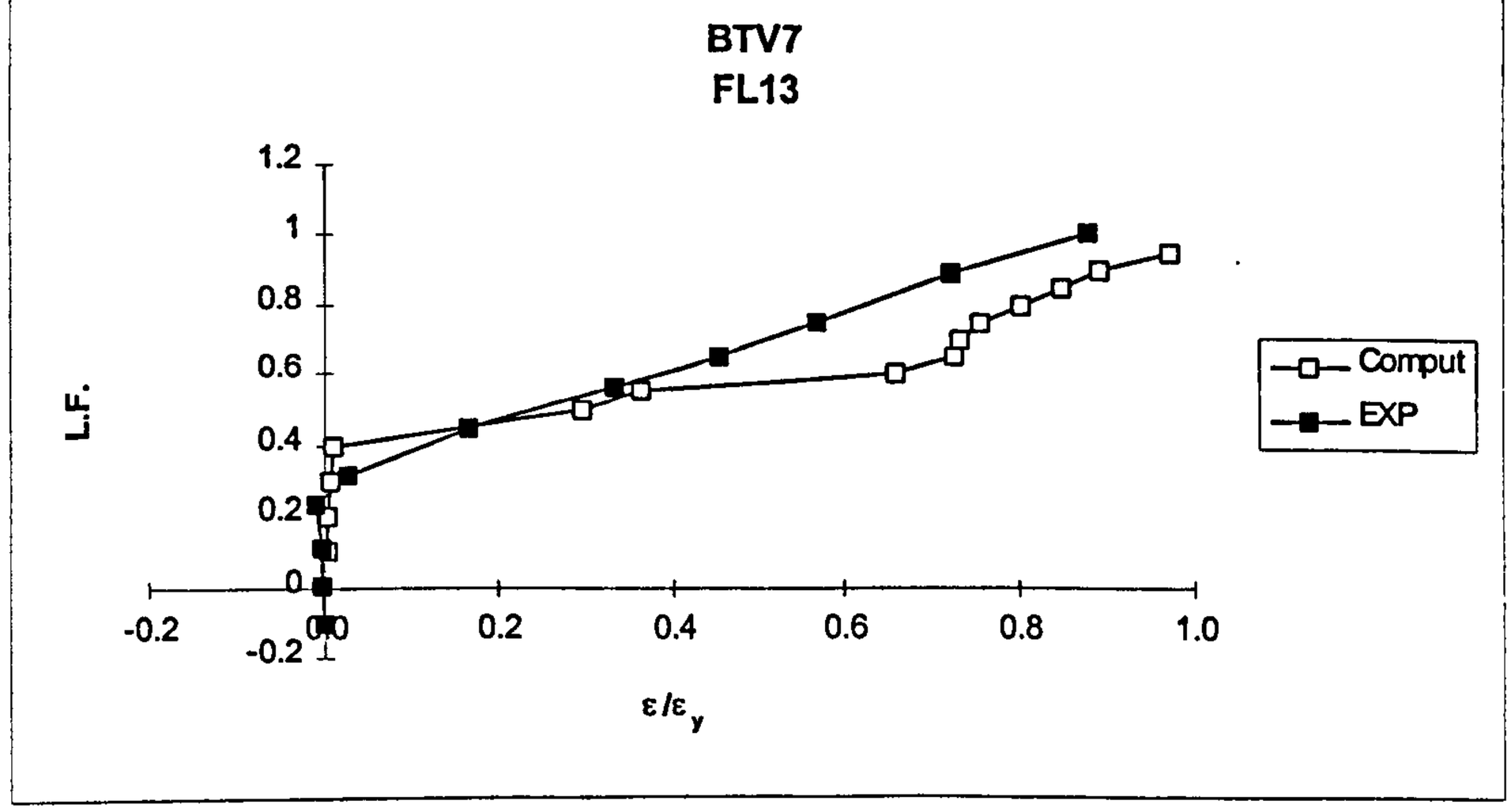
BTV7
FL13
L.F.
1.2
1
0.8
0.6
0.4
0.2
0
-0.2
-0.2
0.2
0.4
0.6
0.8
1.0
ε/ε y
Comput
EXP

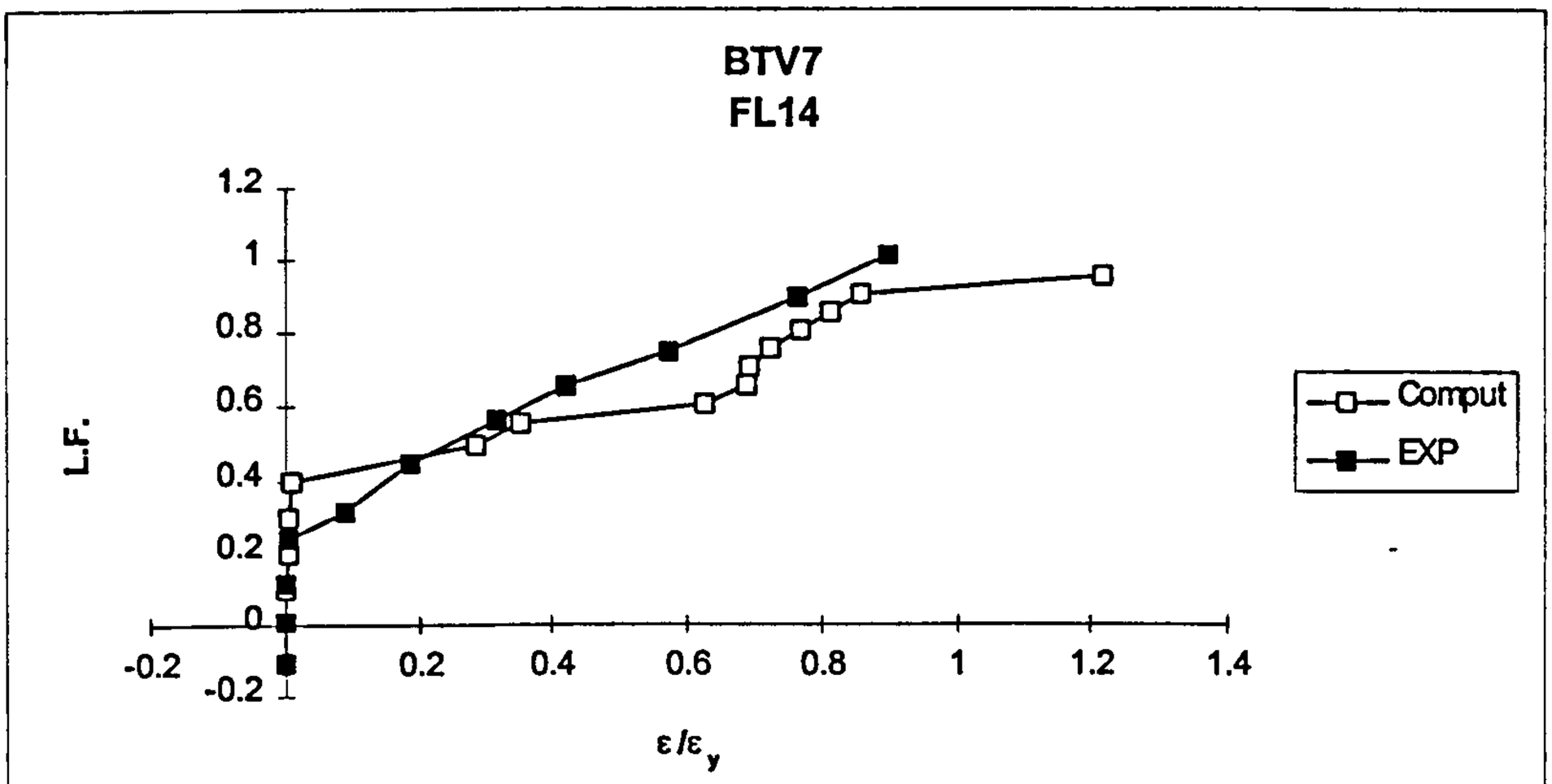
BTV7
FL14
L.F.
1.2
1
0.8
0.6
0.4
0.2
0
-0.2
-0.2
0.2
0.4
0.6
0.8
1
1.2
1.4
Comput
EXP
ε/ε y

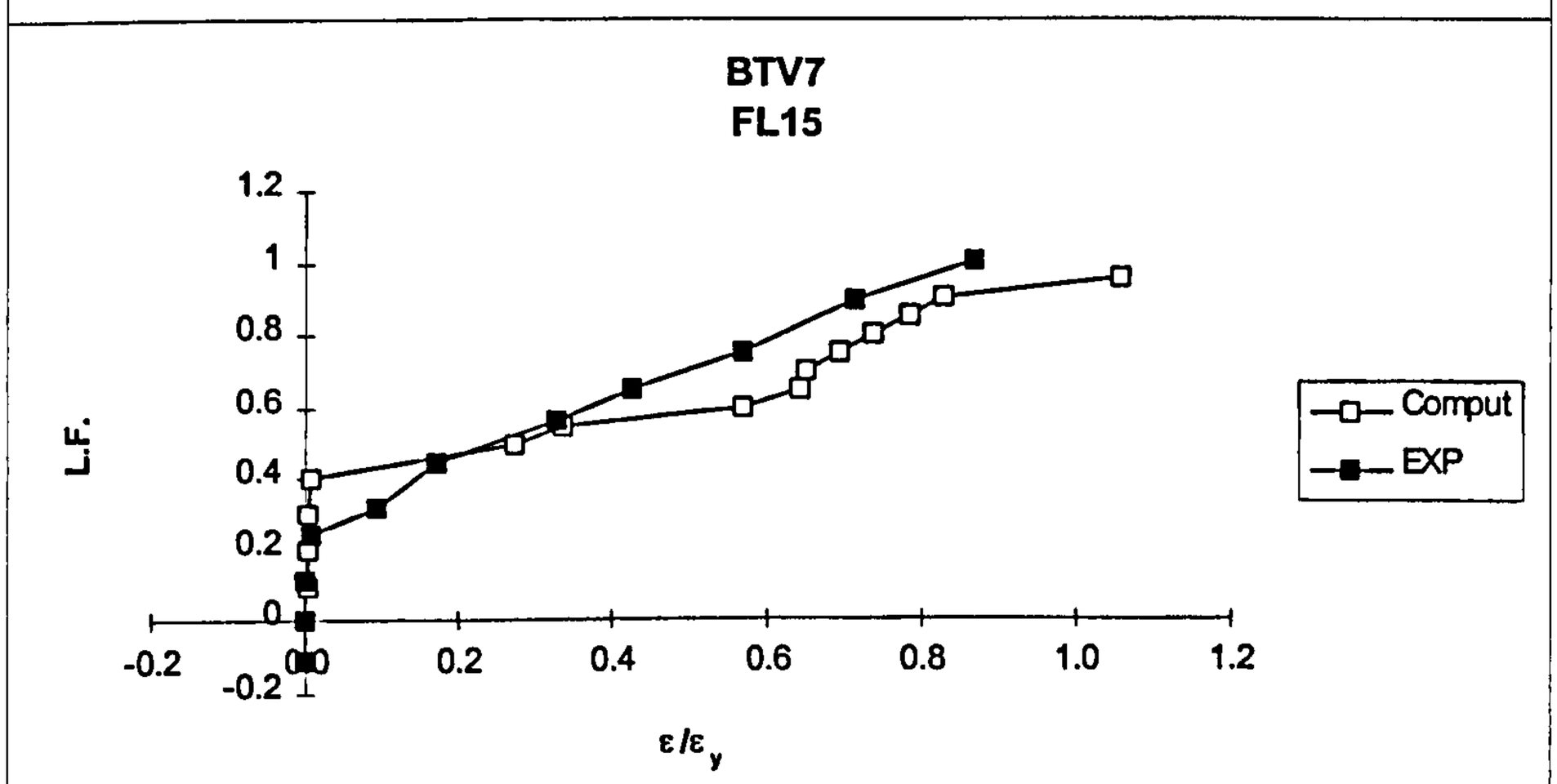
BTV7
FL15
L.F.
1.2
1
0.8
0.6
0.4
0.2
0
-0.2
-0.2
0.2
0.4
0.6
0.8
1.0
1.2
Comput
EXP
ε/ε y

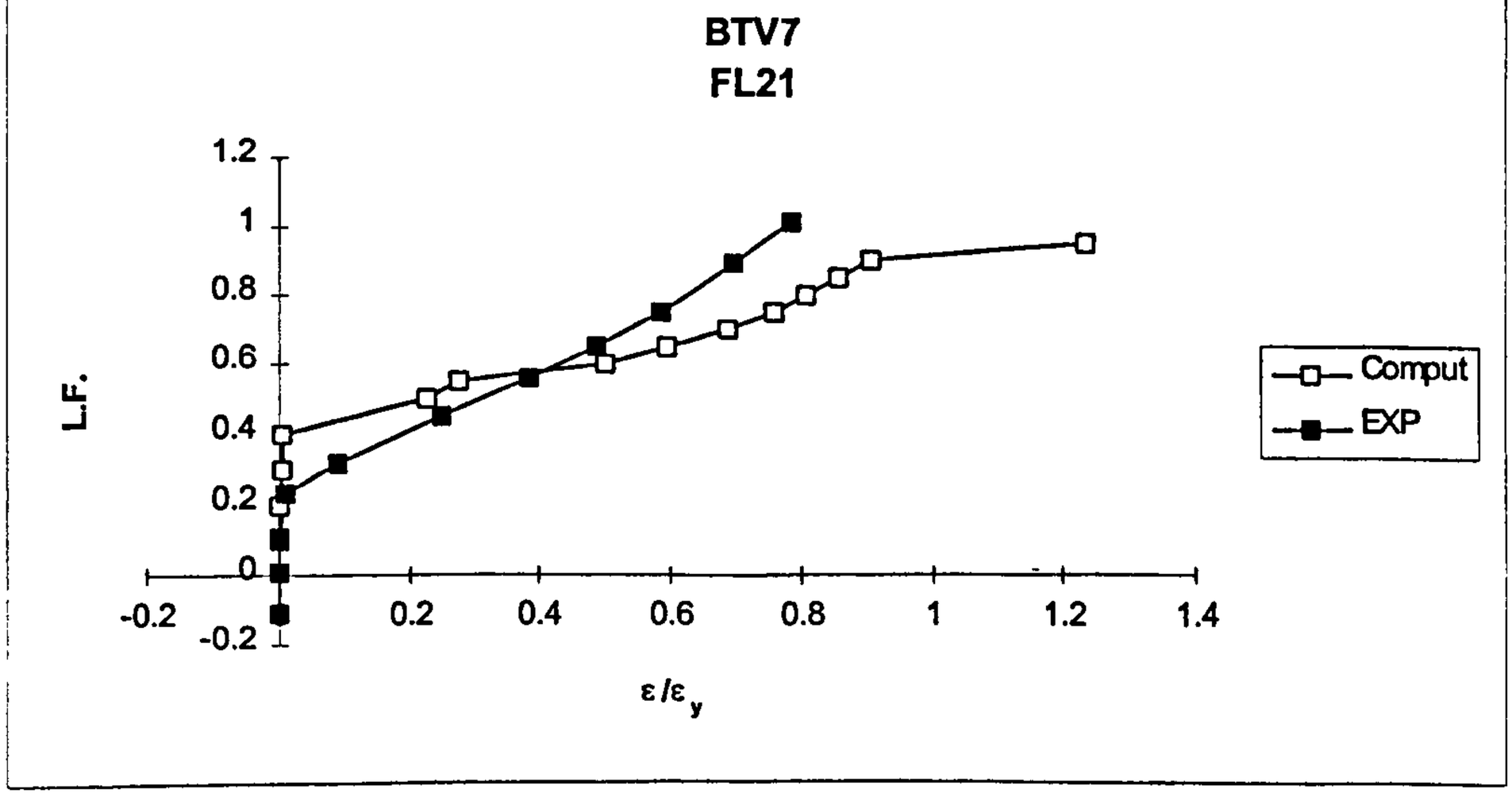
BTV7
FL21
L.F.
1.2
1
0.8
0.6
0.4
0.2
0
-0.2
-0.2
0.2
0.4
0.6
0.8
1
1.2
1.4
Comput
EXP
ε/ε y

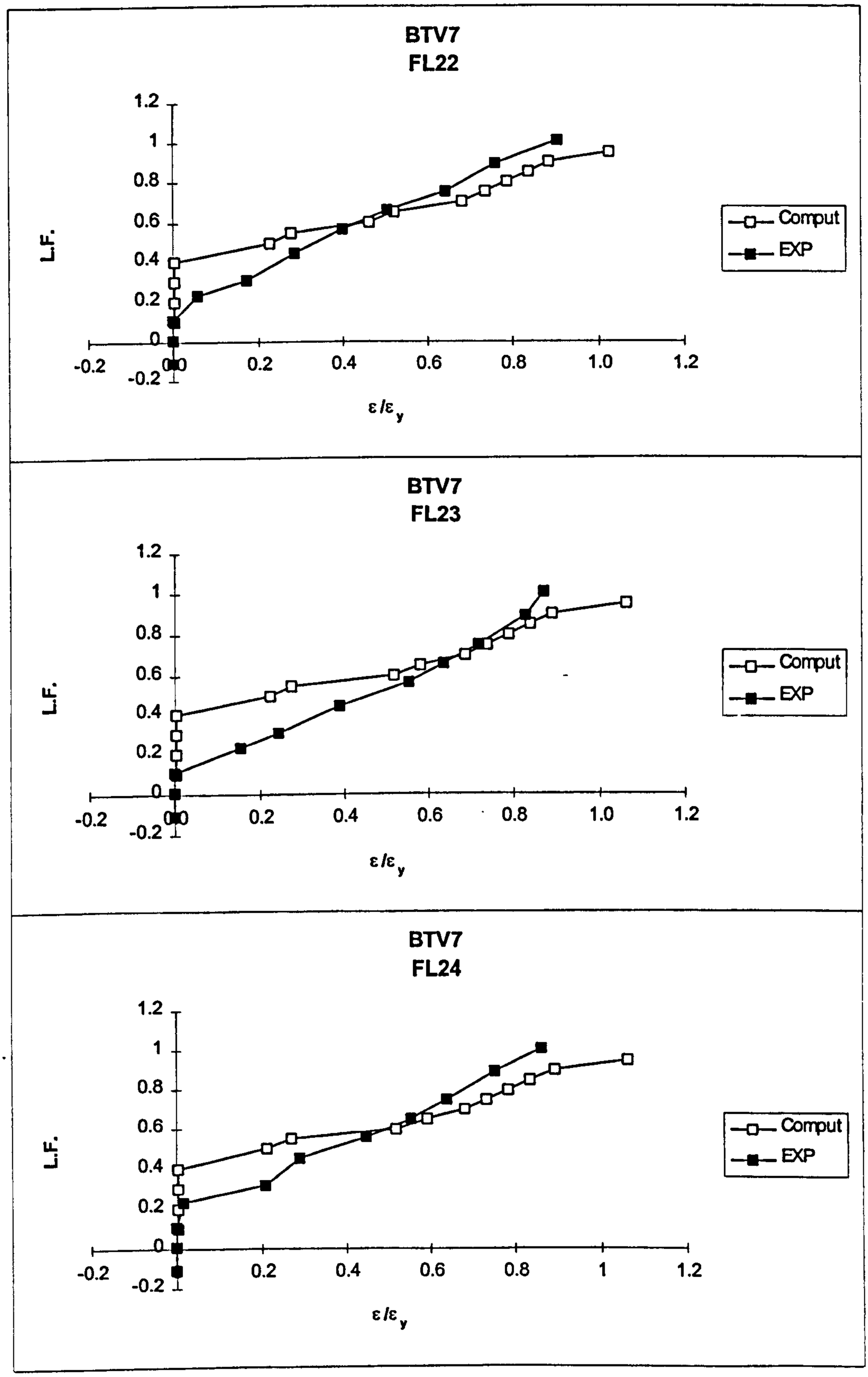
BTV7
FL22
L.F.
1.2
1
0.8
0.6
0.4
0.2
0
-0.2
-0.2
0.0
0.2
0.4
0.6
0.8
1.0
1.2
ε/ε y
Comput
EXP
BTV7
FL23
L.F.
1.2
1
0.8
0.6
0.4
0.2
0
-0.2
-0.2
0.0
0.2
0.4
0.6
0.8
1.0
1.2
ε/ε y
Comput
EXP
BTV7
FL24
L.F.
1.2
1
0.8
0.6
0.4
0.2
0
-0.2
-0.2
0.2
0.4
0.6
0.8
1
1.2
ε/ε y
Comput
EXP

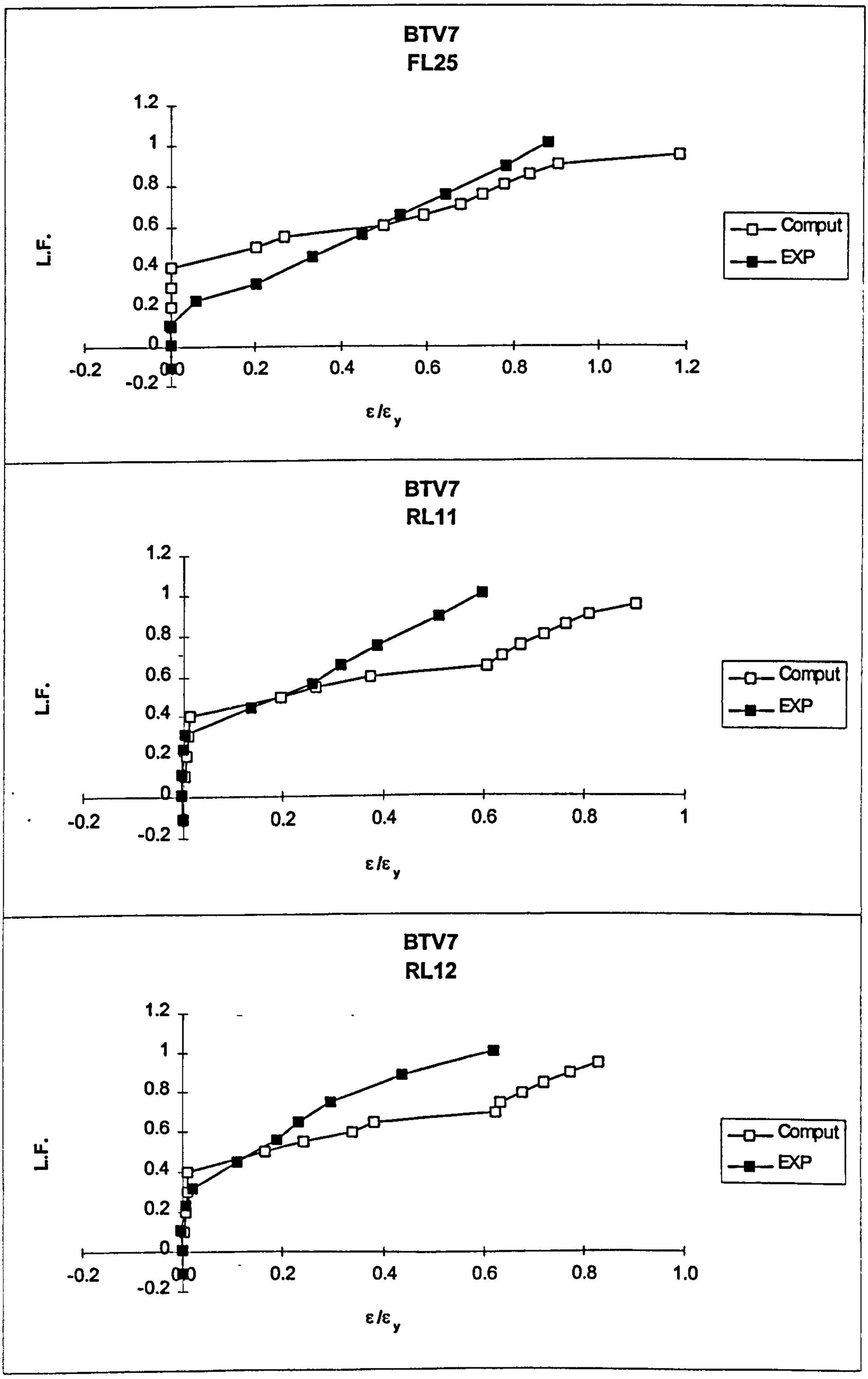
BTV7
FL25
L.F.
1.2
1
0.8
0.6
0.4
0.2
0
-0.2
-0.2
0
0.2
0.4
0.6
0.8
1.0
1.2
ε/ε y
Comput
EXP
BTV7
RL11
L.F.
1.2
1
0.8
0.6
0.4
0.2
0
-0.2
-0.2
0
0.2
0.4
0.6
0.8
1
ε/ε y
Comput
EXP
BTV7
RL12
L.F.
1.2
1
0.8
0.6
0.4
0.2
0
-0.2
-0.2
0
0.2
0.4
0.6
0.8
1.0
ε/ε y
Comput
EXP

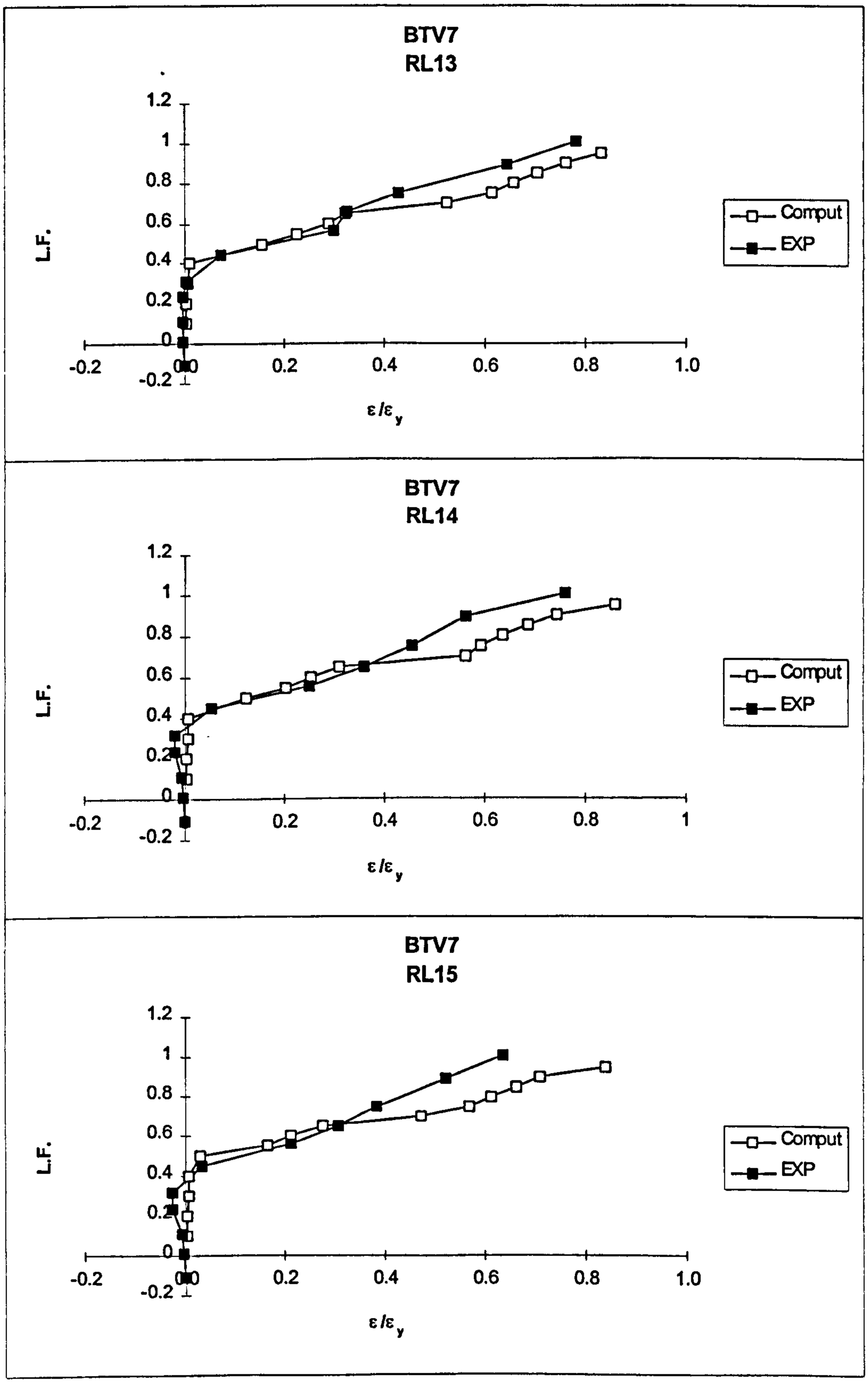
BTV7
RL13
L.F.
1.2
1
0.8
0.6
0.4
0.2
0
-0.2
0.2
0.4
0.6
0.8
1.0
Comput
EXP
ε/ε y
BTV7
RL14
L.F.
1.2
1
0.8
0.6
0.4
0.2
0
-0.2
0.2
0.4
0.6
0.8
1
Comput
EXP
ε/ε y
BTV7
RL15
L.F.
1.2
1
0.8
0.6
0.4
0.2
0
-0.2
0.2
0.4
0.6
0.8
1.0
Comput
EXP
ε/ε y

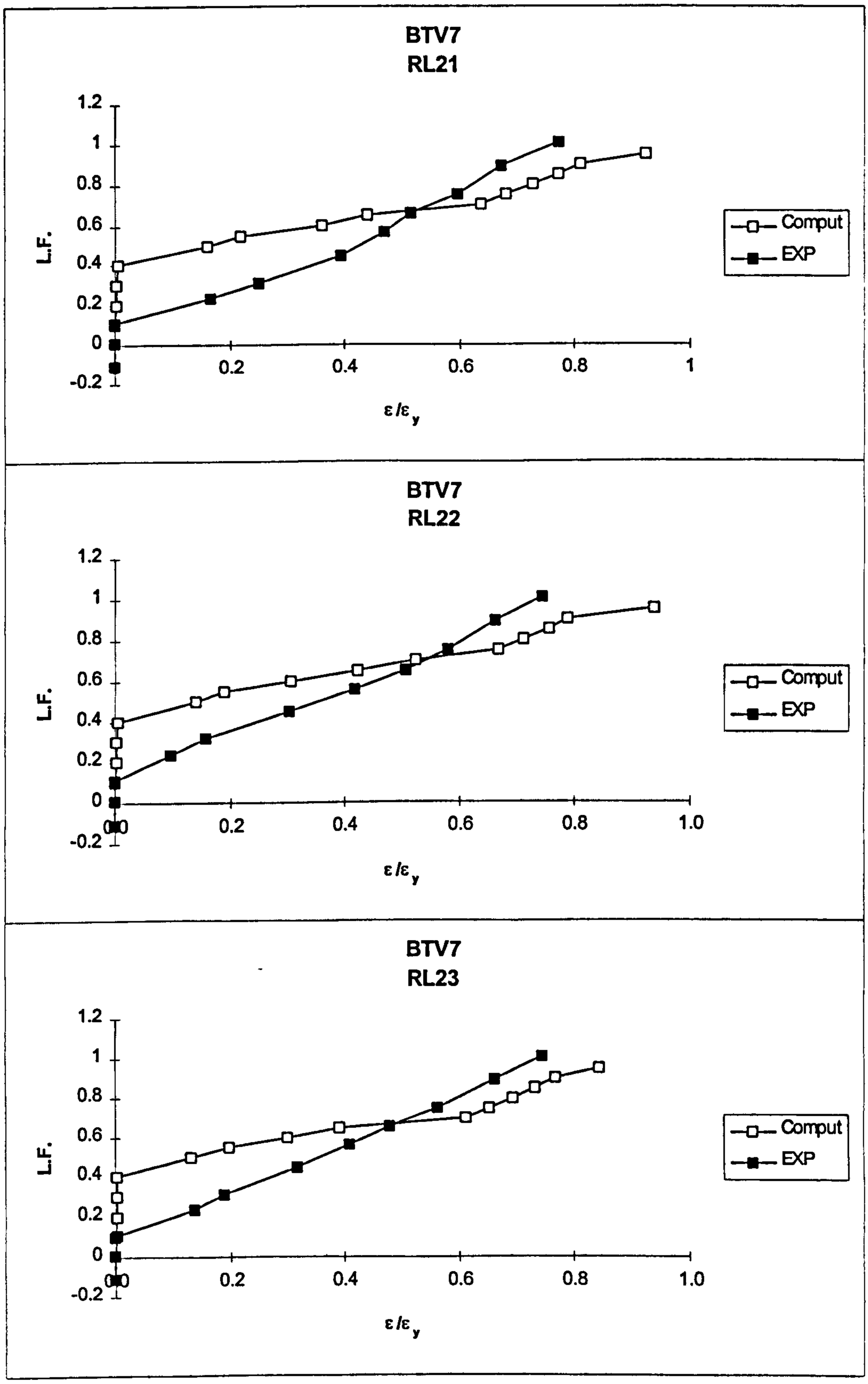
BTV7
RL21
L.F.
1.2
1
0.8
0.6
0.4
0.2
0
-0.2
0.2
0.4
0.6
0.8
1
Comput
EXP
ε /ε y
BTV7
RL22
L.F.
1.2
1
0.8
0.6
0.4
0.2
0
-0.2
0
0.2
0.4
0.6
0.8
1.0
Comput
EXP
ε /ε y
BTV7
RL23
L.F.
1.2
1
0.8
0.6
0.4
0.2
0
-0.2
0
0.2
0.4
0.6
0.8
1.0
Comput
EXP
ε /ε y

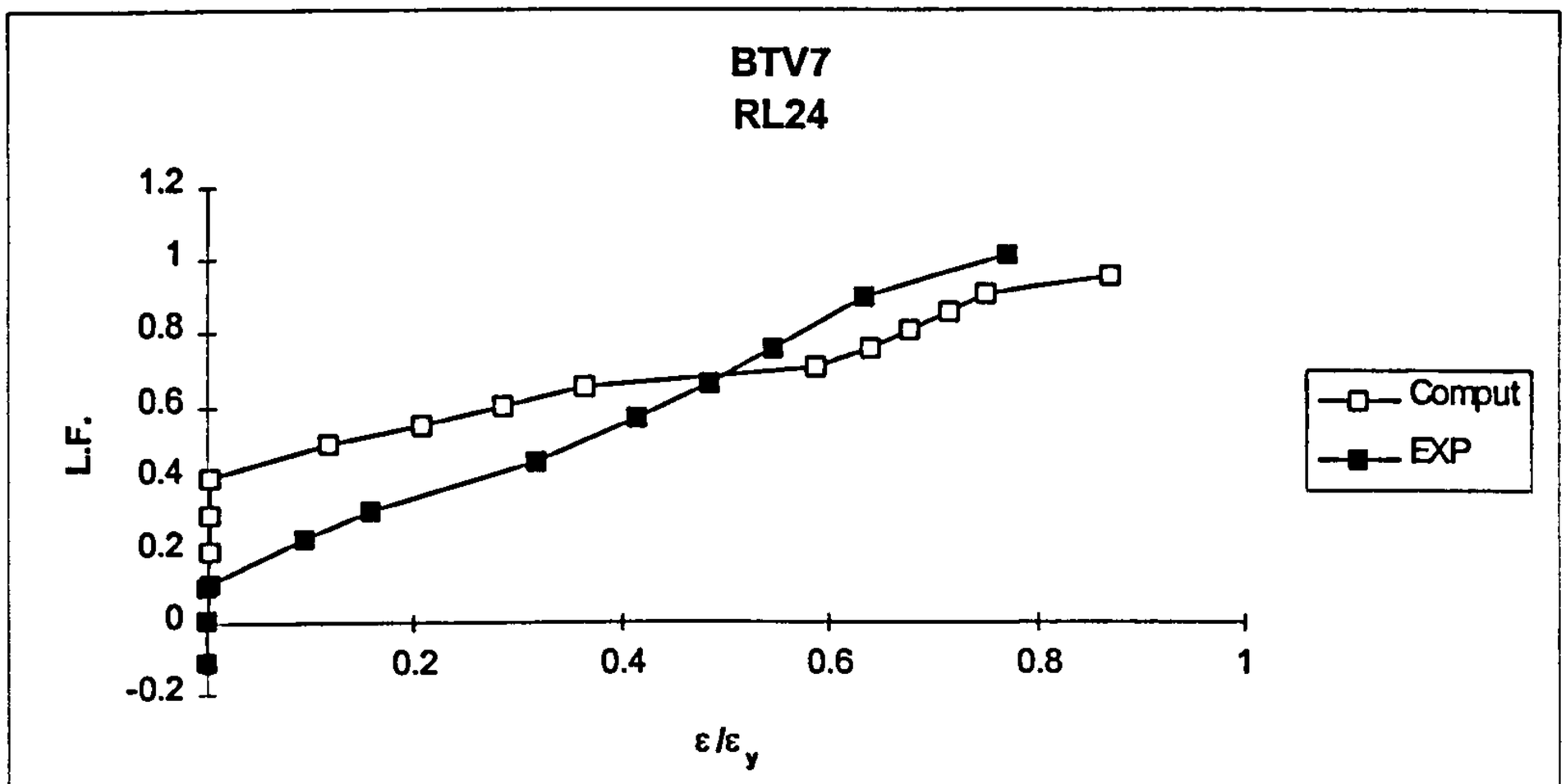
BTV7
RL24
L.F.
1.2
1
0.8
0.6
0.4
0.2
0
-0.2
0.2
0.4
0.6
0.8
1
ε/ε y
Comput
EXP

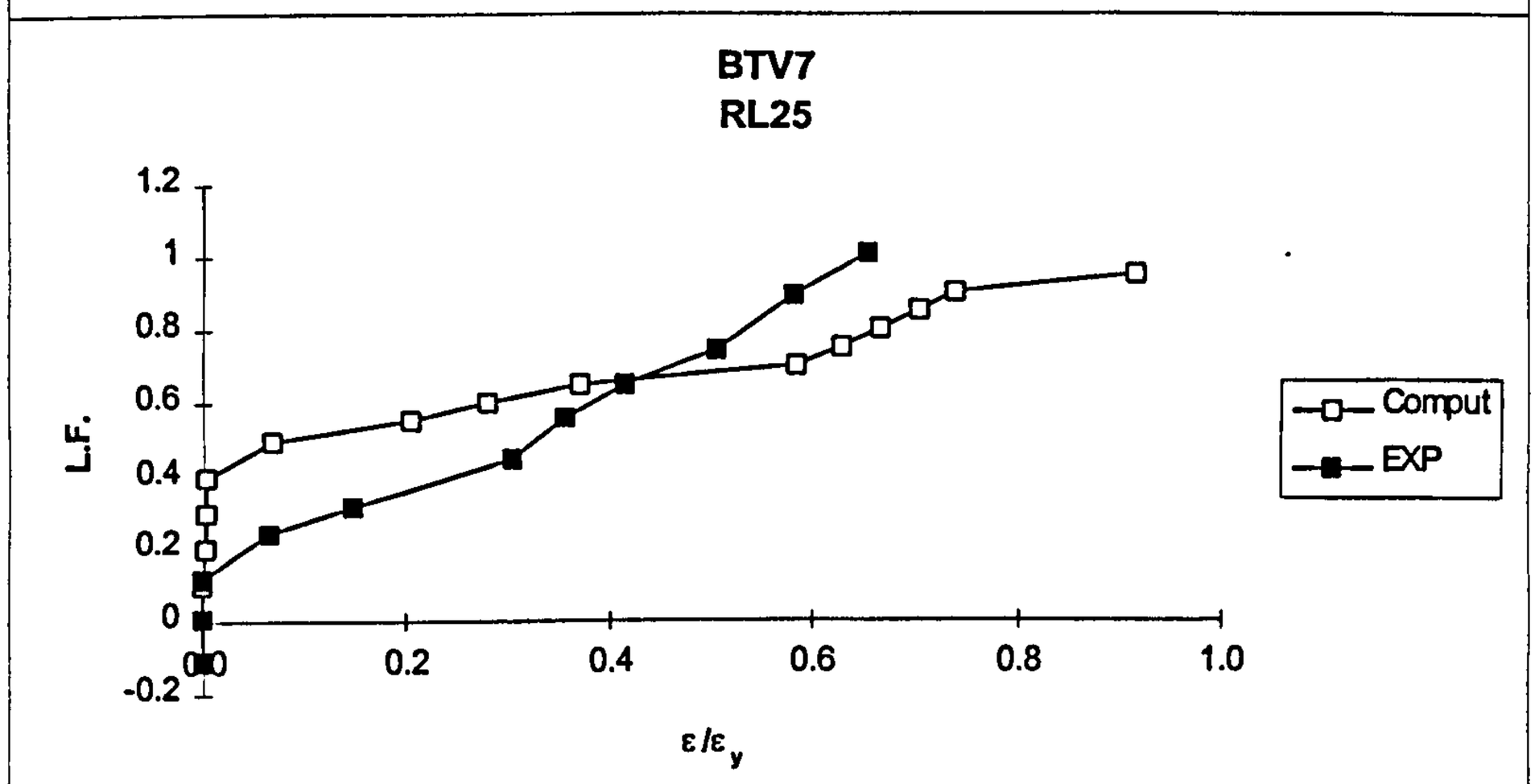
BTV7
RL25
L.F.
1.2
1
0.8
0.6
0.4
0.2
0
-0.2
0.2
0.4
0.6
0.8
1.0
ε/ε y
Comput
EXP

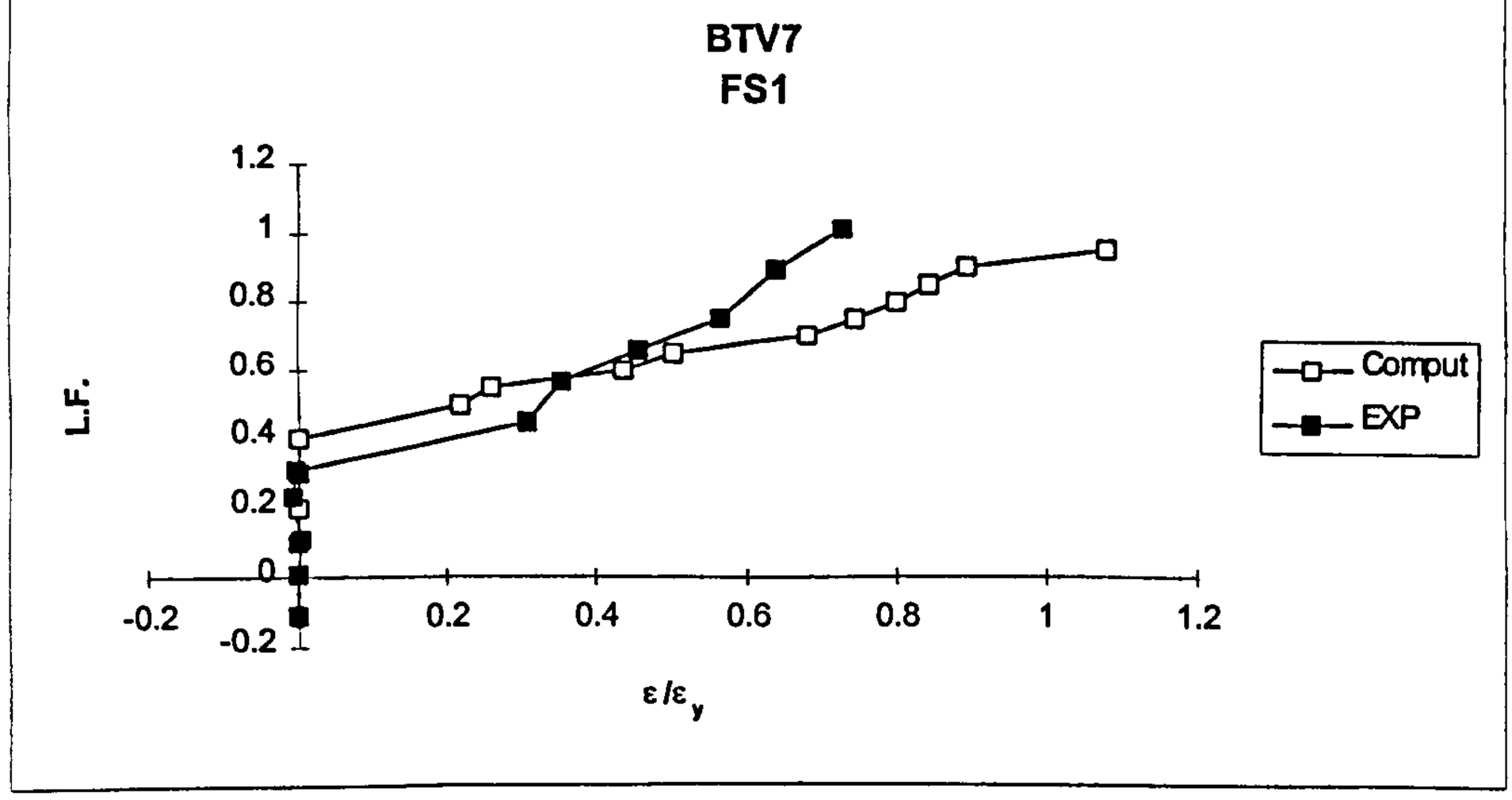
BTV7
FS1
L.F.
1.2
1
0.8
0.6
0.4
0.2
0
-0.2
-0.2
0.2
0.4
0.6
0.8
1
1.2
ε/ε y
Comput
EXP

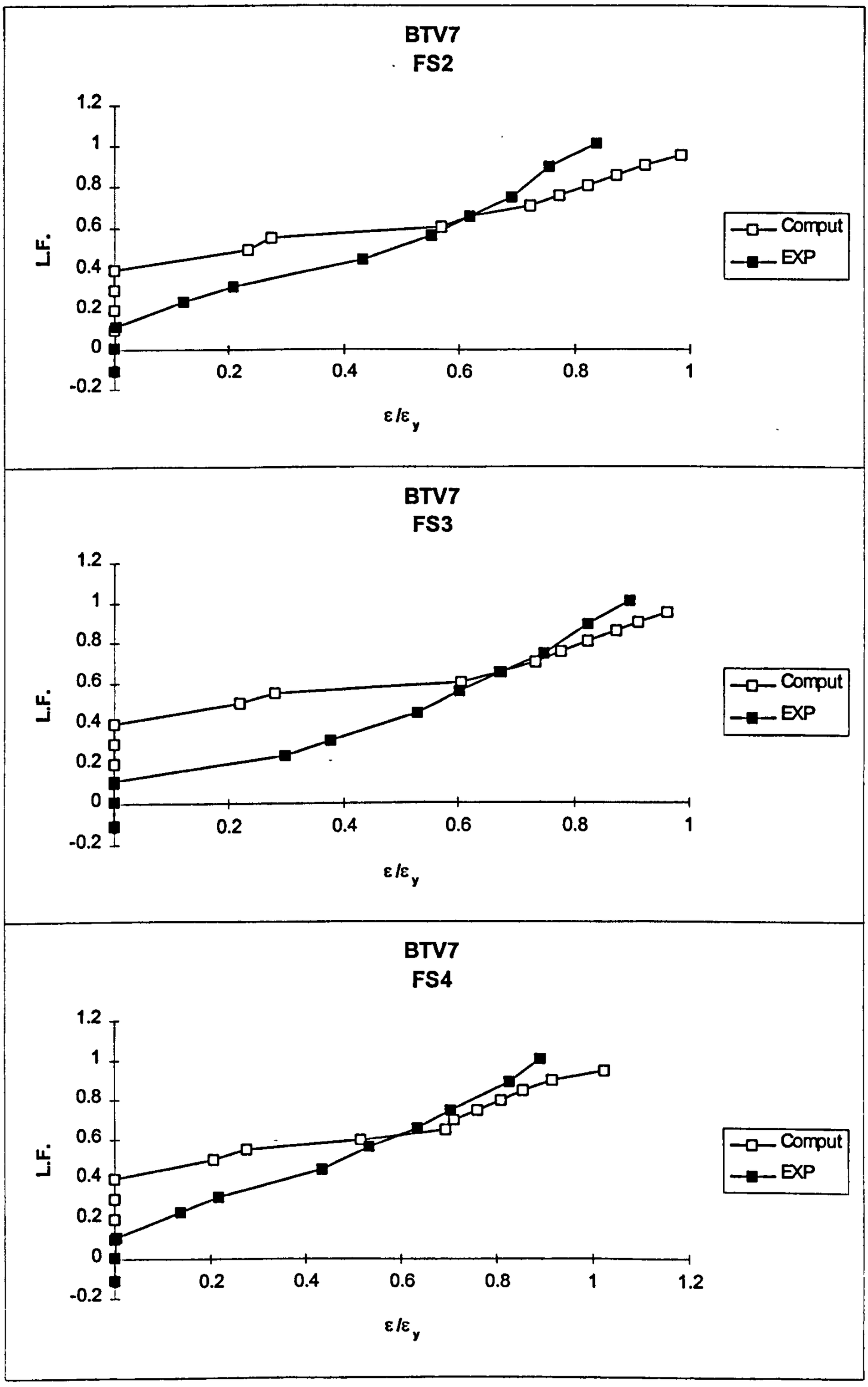
BTV7
FS2
L.F.
1.2
1
0.8
0.6
0.4
0.2
0
-0.2
0.2
0.4
0.6
0.8
1
ε /ε y
Comput
EXP
BTV7
FS3
L.F.
1.2
1
0.8
0.6
0.4
0.2
0
-0.2
0.2
0.4
0.6
0.8
1
ε /ε y
Comput
EXP
BTV7
FS4
L.F.
1.2
1
0.8
0.6
0.4
0.2
0
-0.2
0.2
0.4
0.6
0.8
1
1.2
ε /ε y
Comput
EXP

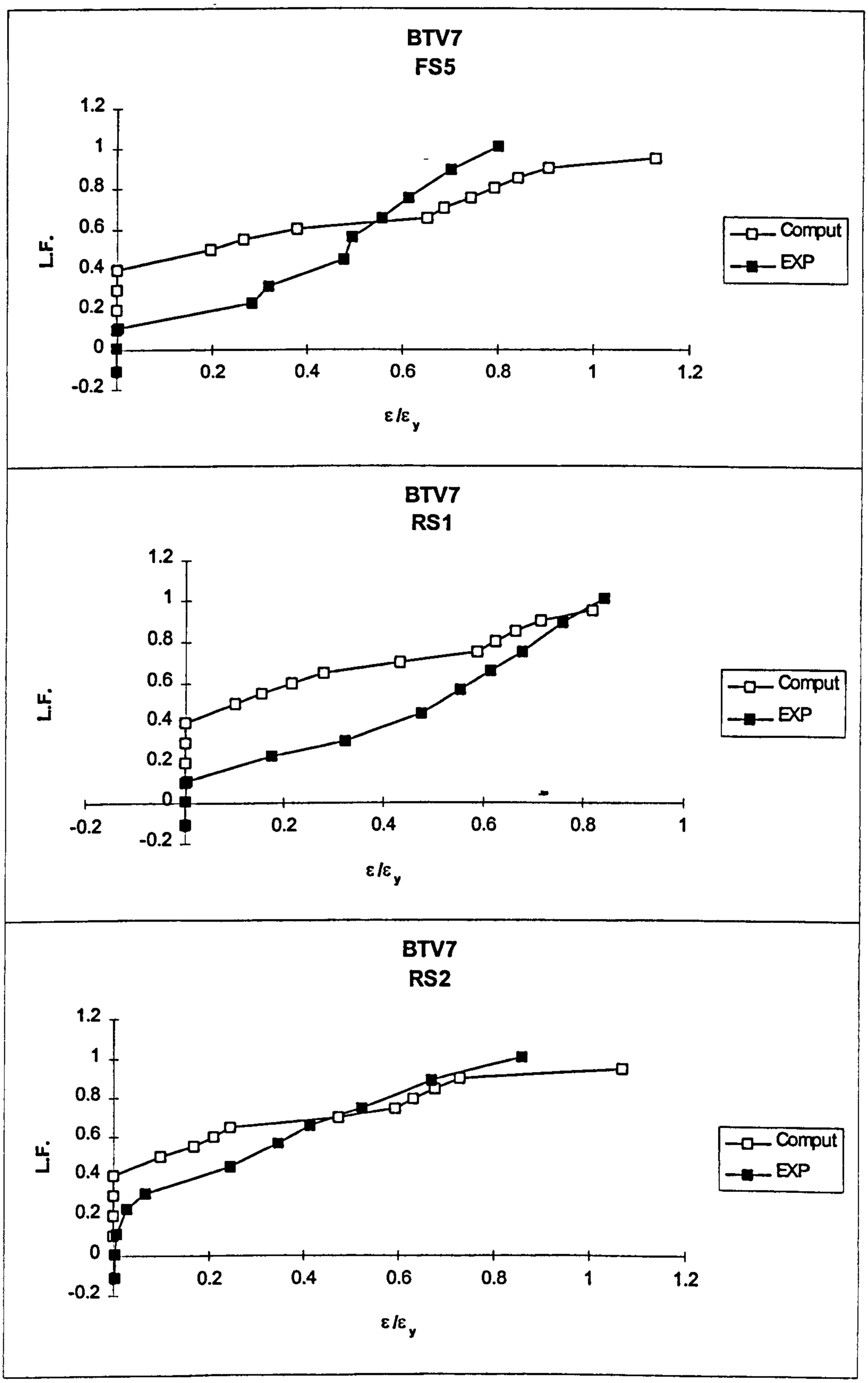
BTV7
FS5
L.F.
1.2
1
0.8
0.6
0.4
0.2
0
-0.2
0.2
0.4
0.6
0.8
1
1.2
ε/ε_y
Comput
EXP
BTV7
RS1
L.F.
1.2
1
0.8
0.6
0.4
0.2
0
-0.2
0.2
0.4
0.6
0.8
1
ε/ε_y
Comput
EXP
BTV7
RS2
L.F.
1.2
1
0.8
0.6
0.4
0.2
0
-0.2
0.2
0.4
0.6
0.8
1
1.2
ε/ε_y
Comput
EXP

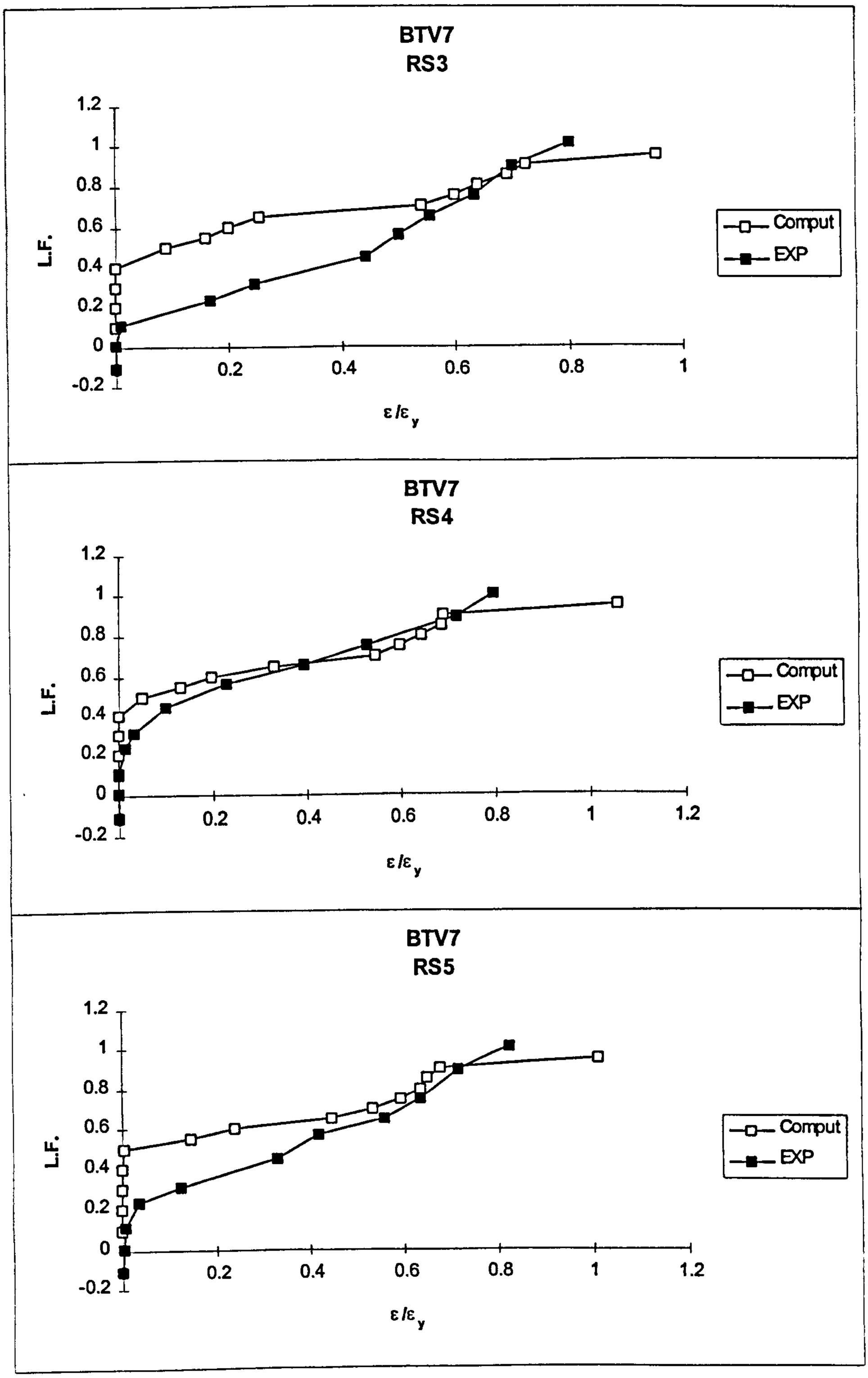
BTV7
RS3
L.F.
1.2
1
0.8
0.6
0.4
0.2
0
-0.2
0.2
0.4
0.6
0.8
1
ε /ε y
Comput
EXP
BTV7
RS4
L.F.
1.2
1
0.8
0.6
0.4
0.2
0
-0.2
0.2
0.4
0.6
0.8
1
1.2
ε /ε y
Comput
EXP
BTV7
RS5
L.F.
1.2
1
0.8
0.6
0.4
0.2
0
-0.2
0.2
0.4
0.6
0.8
1
1.2
ε /ε y
Comput
EXP

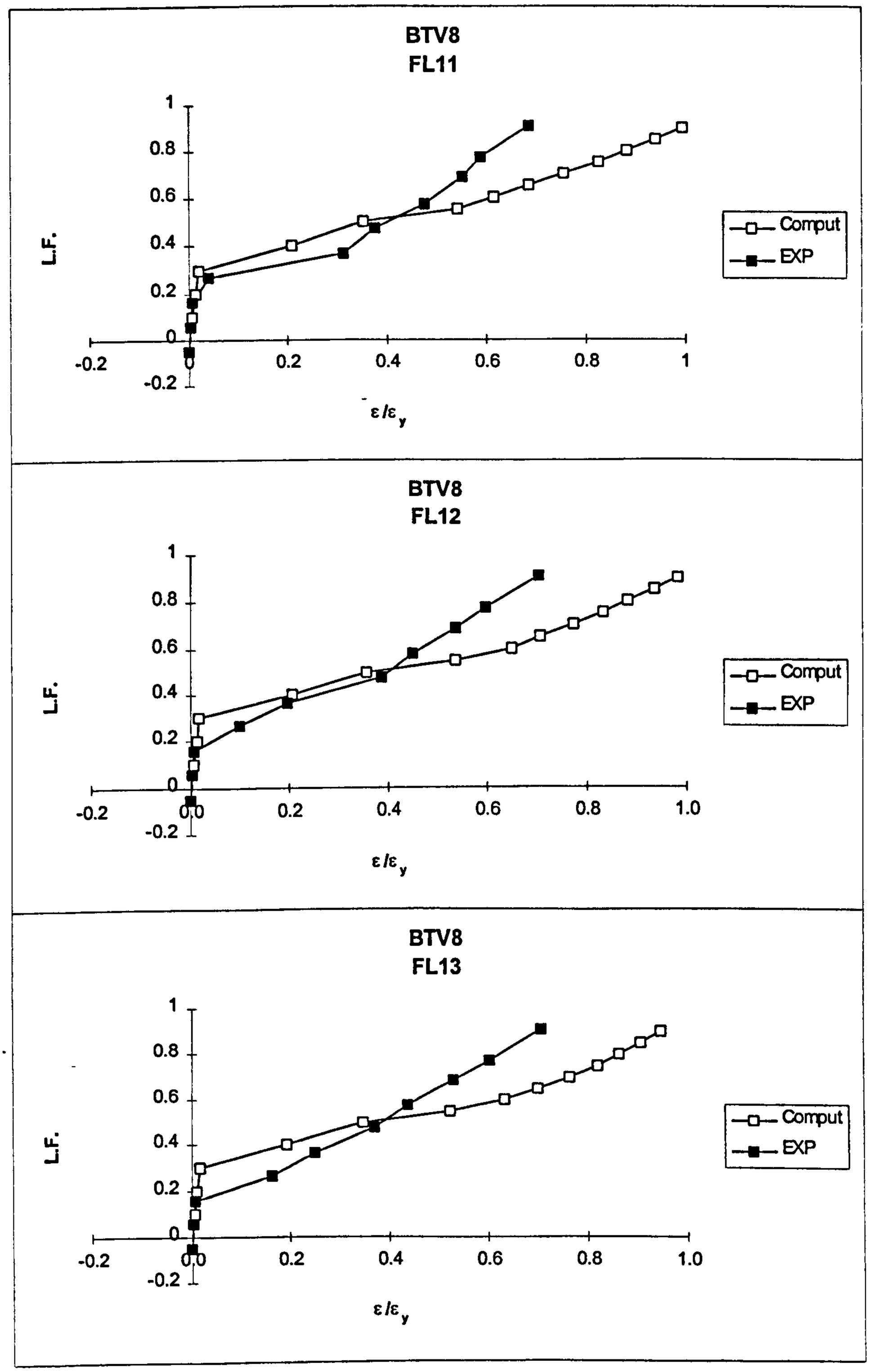
BTV8
FL11
L.F.
1
0.8
0.6
0.4
0.2
0
-0.2
0
0.2
0.4
0.6
0.8
1
Comput
EXP
ε/ε_y
BTV8
FL12
L.F.
1
0.8
0.6
0.4
0.2
0
-0.2
0.0
0.2
0.4
0.6
0.8
1.0
Comput
EXP
ε/ε_y
BTV8
FL13
L.F.
1
0.8
0.6
0.4
0.2
0
-0.2
0.0
0.2
0.4
0.6
0.8
1.0
Comput
EXP
ε/ε_y

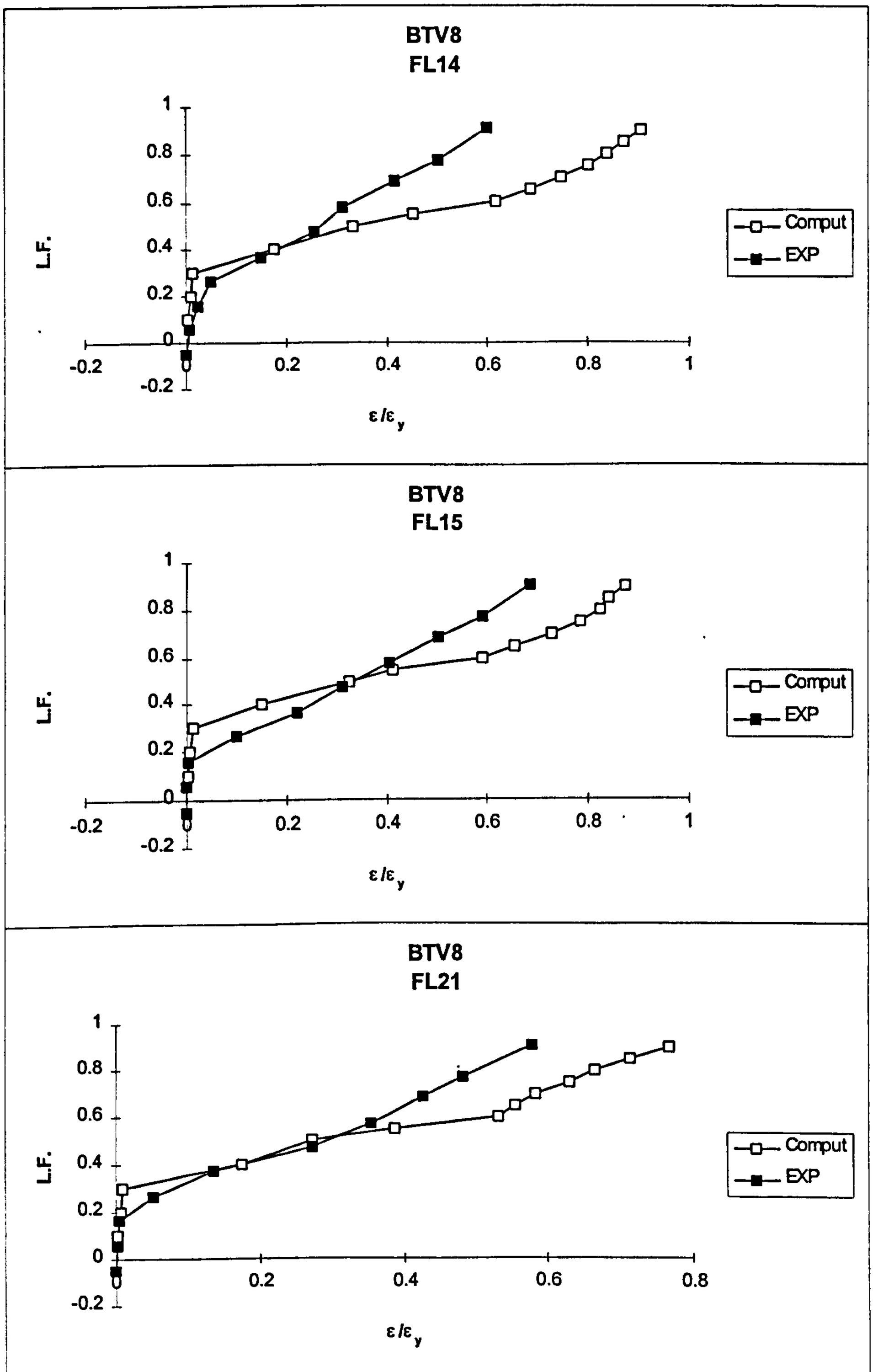
BTV8
FL14
L.F.
1
0.8
0.6
0.4
0.2
0
-0.2
0
0.2
0.4
0.6
0.8
1
ε/ε_y
Comput
EXP
BTV8
FL15
L.F.
ε/ε_y
Comput
EXP
BTV8
FL21
L.F.
ε/ε_y
Comput
EXP

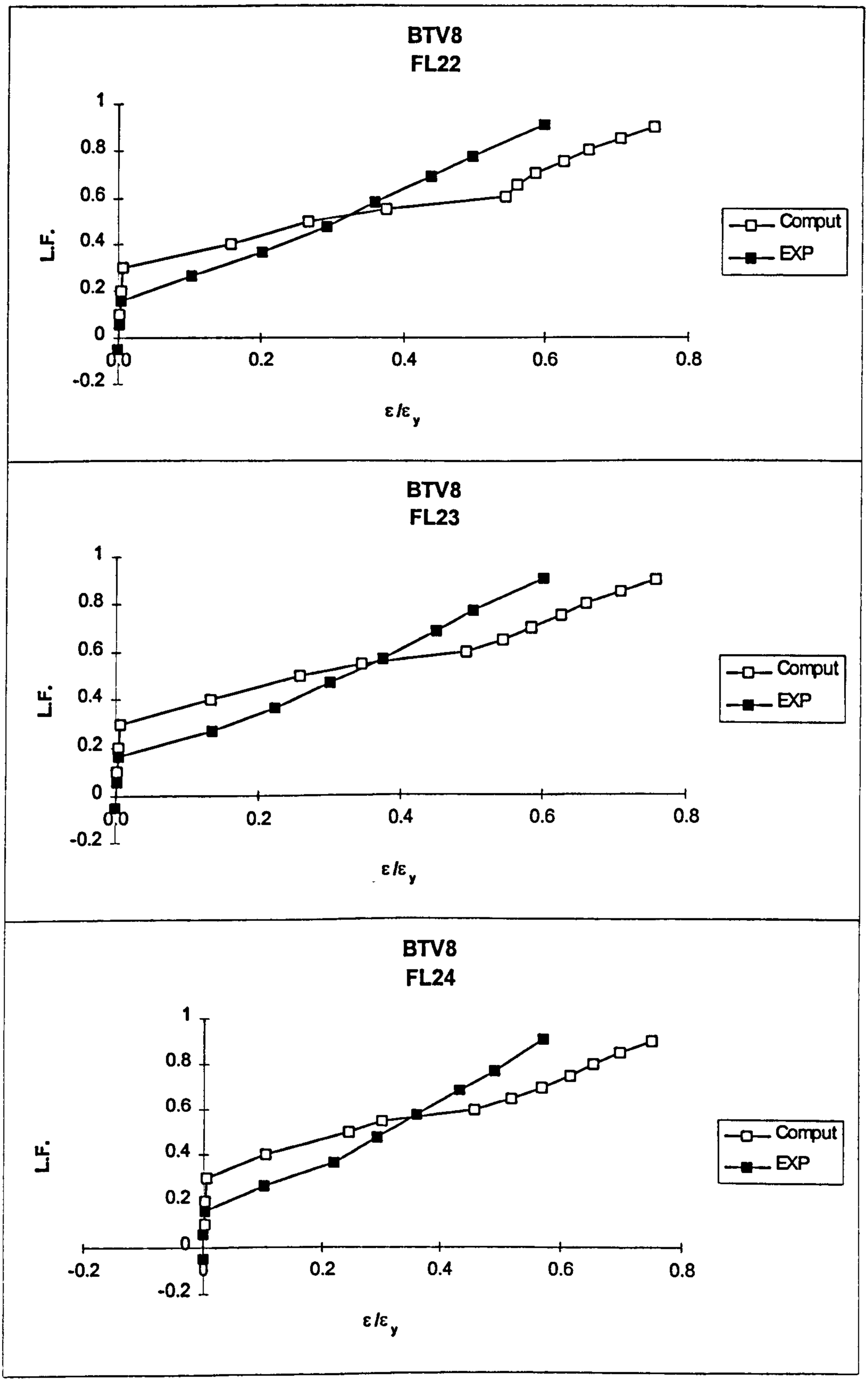
BTV8
FL22
L.F.
1
0.8
0.6
0.4
0.2
0
-0.2
0.0
0.2
0.4
0.6
0.8
ε/ε_y
Comput
EXP
BTV8
FL23
L.F.
ε/ε_y
Comput
EXP
BTV8
FL24
L.F.
ε/ε_y
Comput
EXP

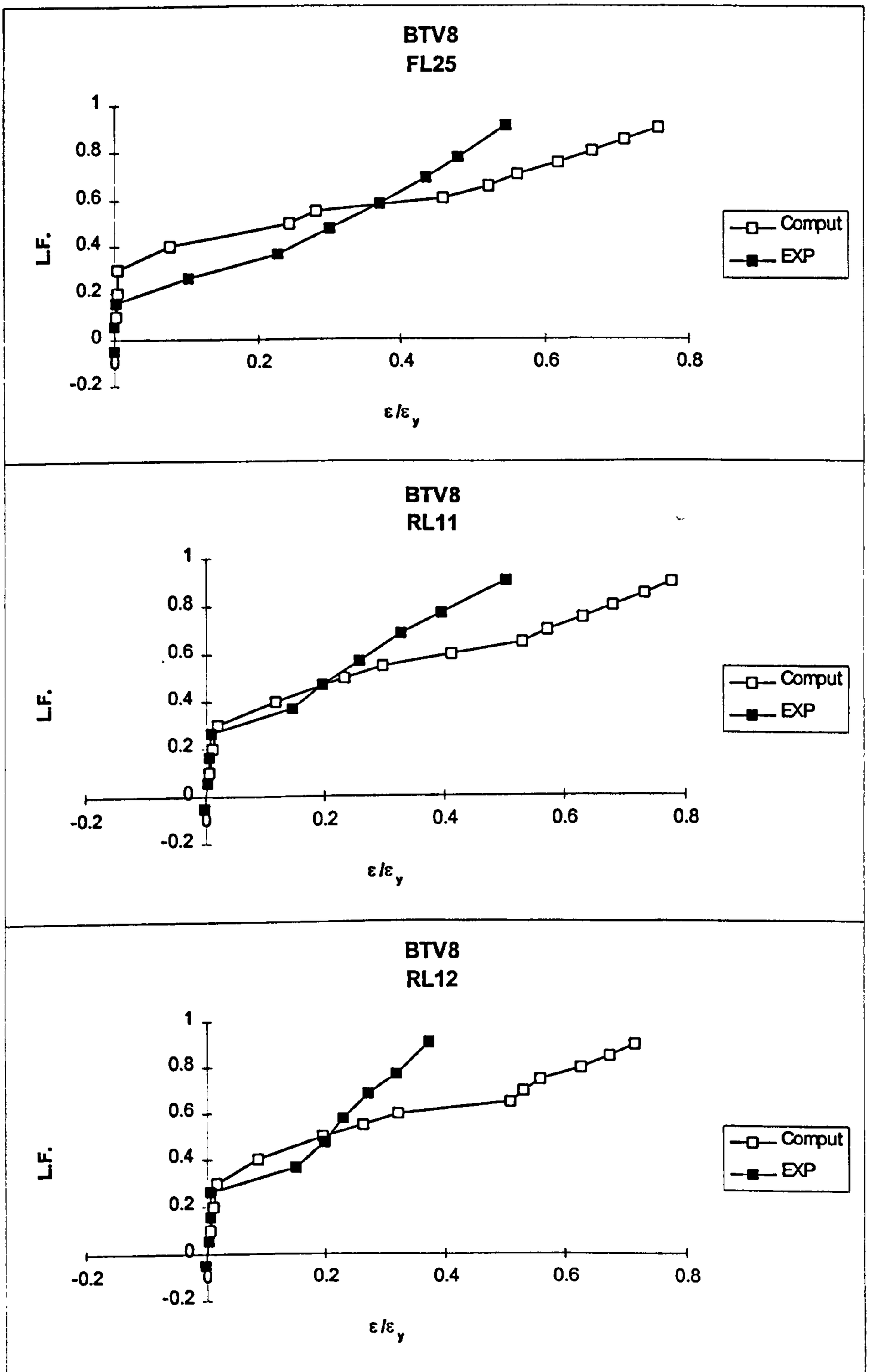
BTV8
FL25
L.F.
1
0.8
0.6
0.4
0.2
0
-0.2
0
0.2
0.4
0.6
0.8
ε/ε y
Comput
EXP
BTV8
RL11
L.F.
ε/ε y
Comput
EXP
BTV8
RL12
L.F.
ε/ε y
Comput
EXP

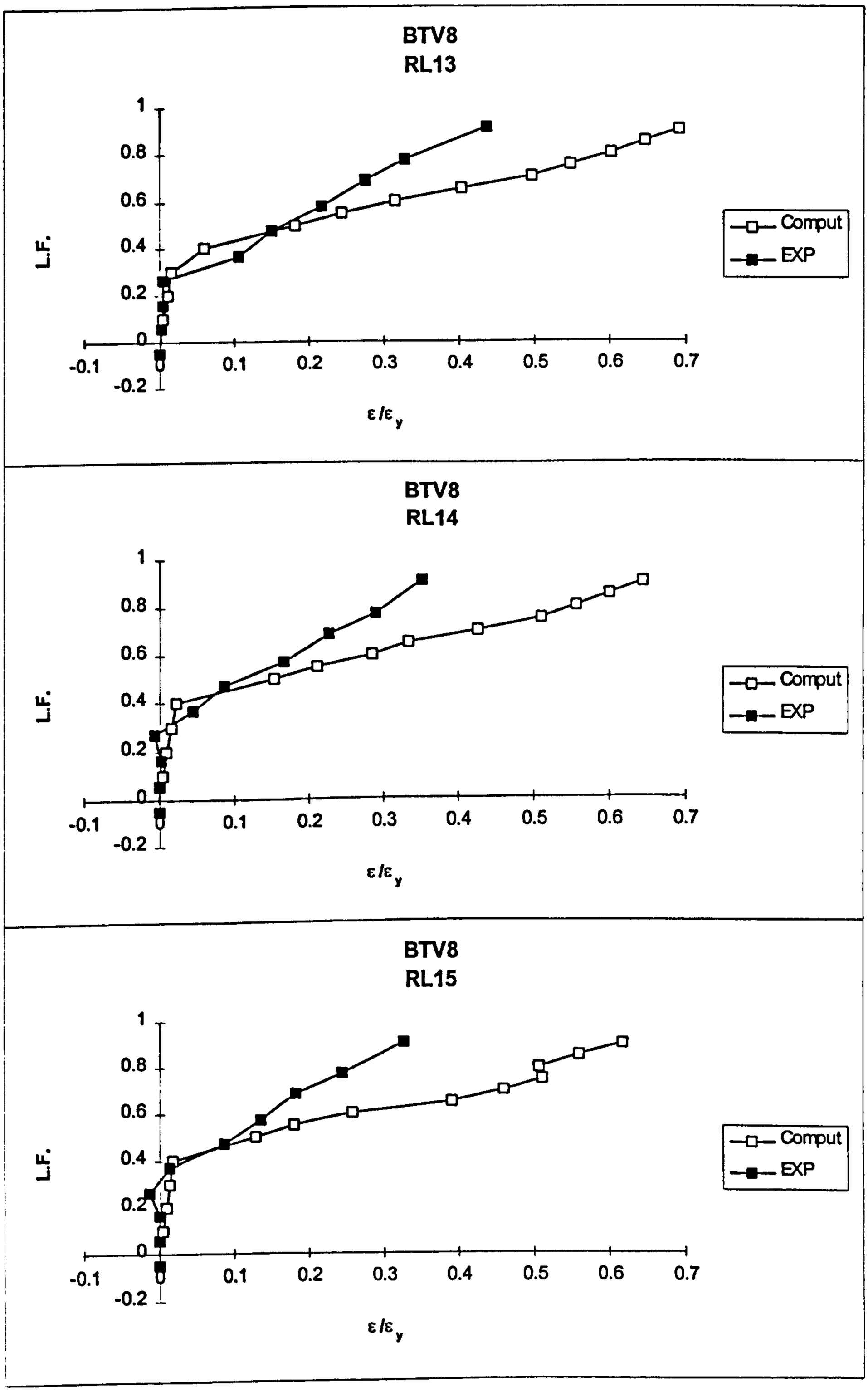
BTV8
RL13
L.F.
1
0.8
0.6
0.4
0.2
0
-0.2
-0.1
0
0.1
0.2
0.3
0.4
0.5
0.6
0.7
ε/ε y
Comput
EXP
BTV8
RL14
L.F.
ε/ε y
Comput
EXP
BTV8
RL15
L.F.
ε/ε y
Comput
EXP

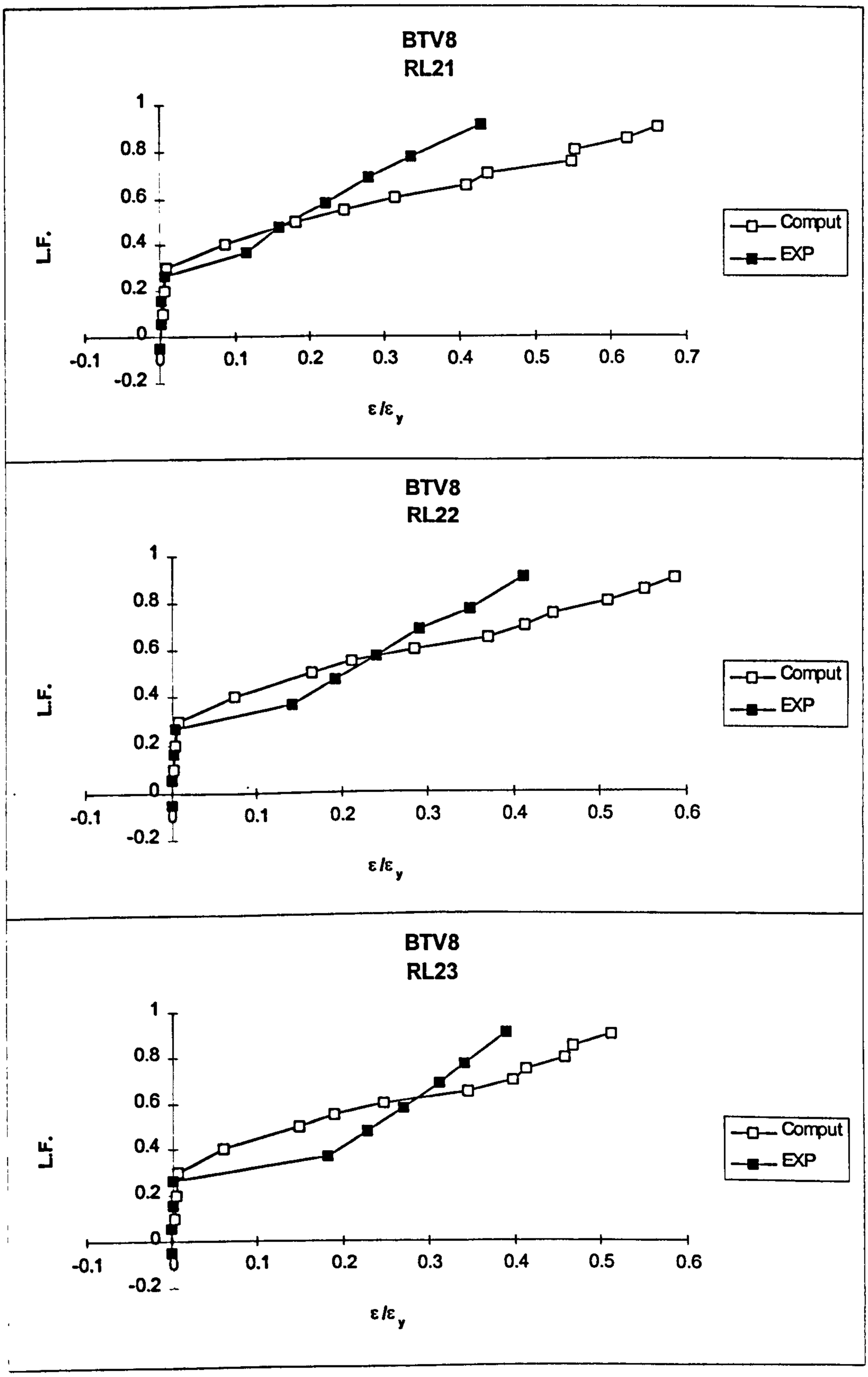
BTV8
RL21
L.F.
1
0.8
0.6
0.4
0.2
0
-0.2
-0.1
0
0.1
0.2
0.3
0.4
0.5
0.6
0.7
Comput
EXP
ε/ε_y
BTV8
RL22
L.F.
1
0.8
0.6
0.4
0.2
0
-0.2
-0.1
0
0.1
0.2
0.3
0.4
0.5
0.6
Comput
EXP
ε/ε_y
BTV8
RL23
L.F.
1
0.8
0.6
0.4
0.2
0
-0.2
-0.1
0
0.1
0.2
0.3
0.4
0.5
0.6
Comput
EXP
ε/ε_y

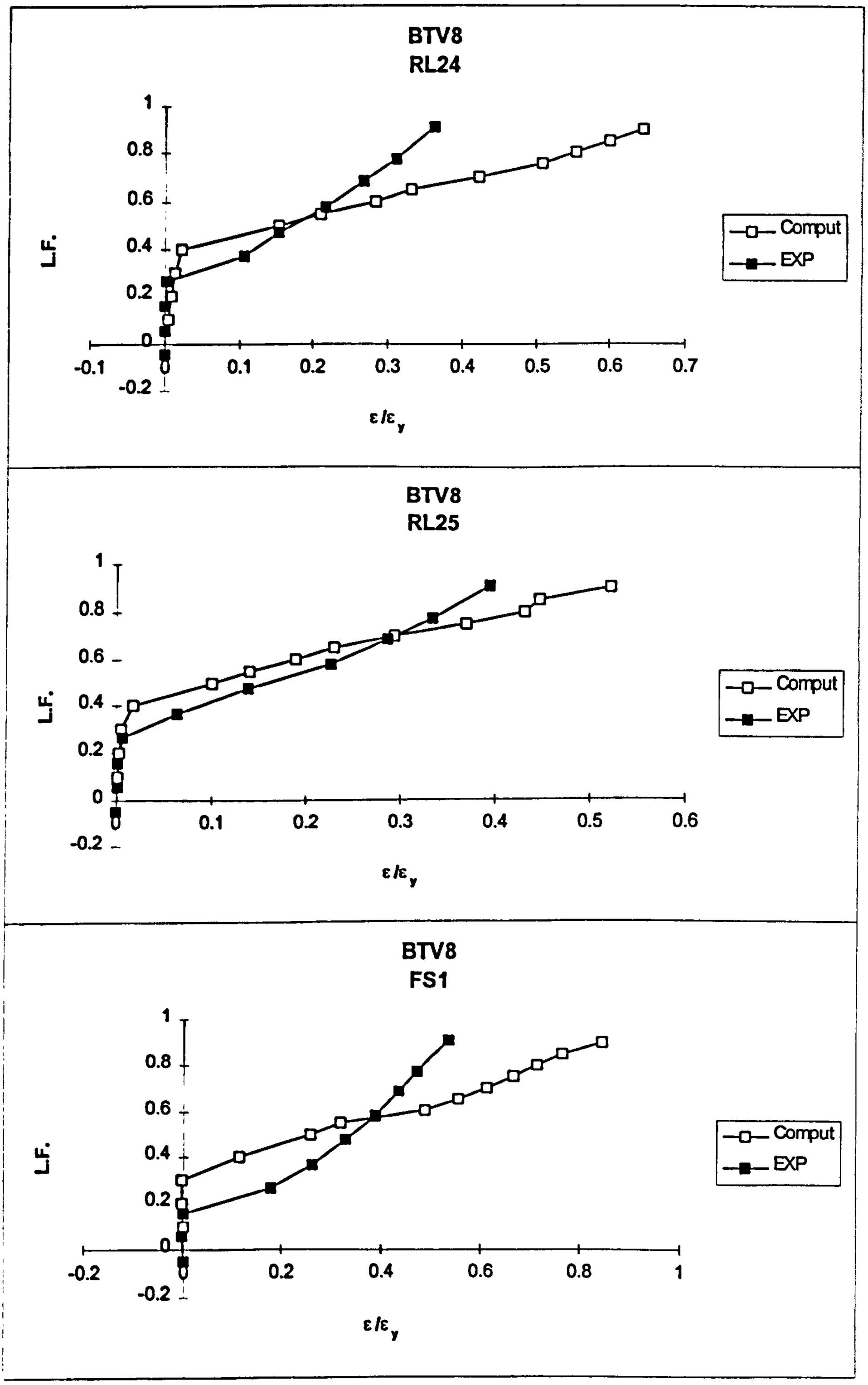
BTV8
RL24
L.F.
1
0.8
0.6
0.4
0.2
0
-0.2
-0.1
0
0.1
0.2
0.3
0.4
0.5
0.6
0.7
ε/ε_y
Comput
EXP
BTV8
RL25
L.F.
1
0.8
0.6
0.4
0.2
0
-0.2
0
0.1
0.2
0.3
0.4
0.5
0.6
ε/ε_y
Comput
EXP
BTV8
FS1
L.F.
1
0.8
0.6
0.4
0.2
0
-0.2
-0.2
0
0.2
0.4
0.6
0.8
1
ε/ε_y
Comput
EXP

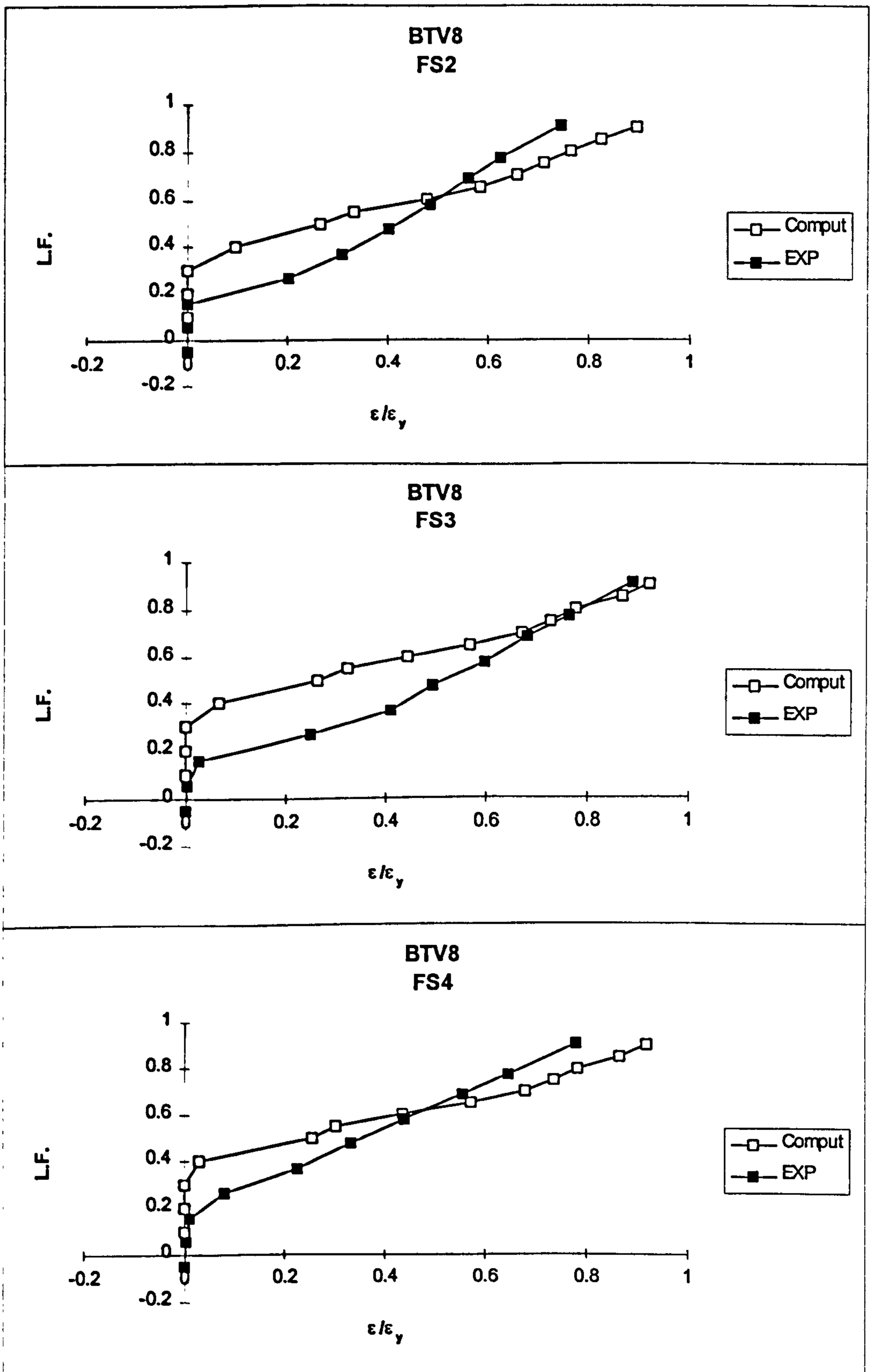
BTV8
FS2
L.F.
1
0.8
0.6
0.4
0.2
0
-0.2
-0.2
0
0.2
0.4
0.6
0.8
1
ε/ε_y
Comput
EXP
BTV8
FS3
L.F.
ε/ε_y
Comput
EXP
BTV8
FS4
L.F.
ε/ε_y
Comput
EXP

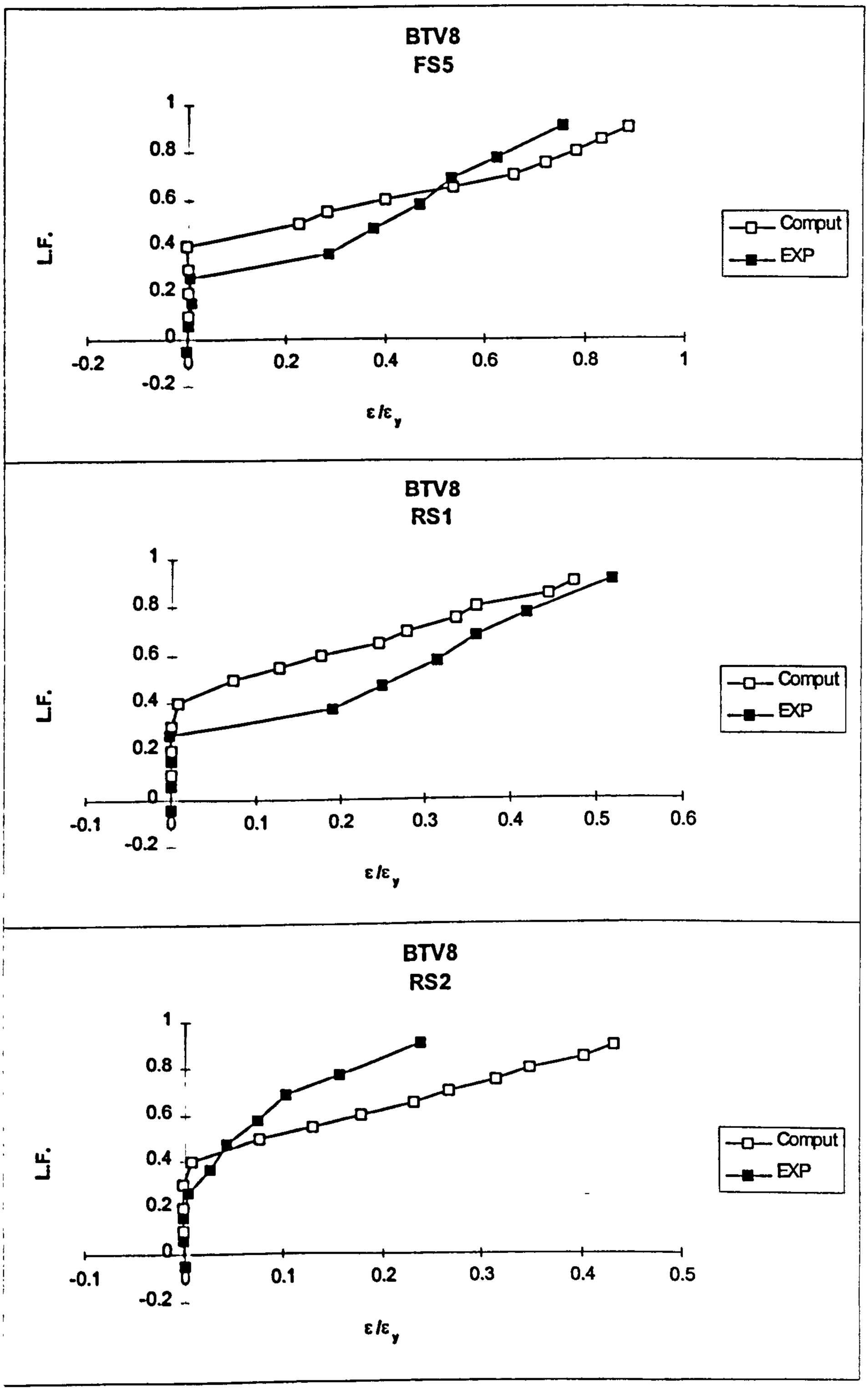
BTV8
FS5
L.F.
1
0.8
0.6
0.4
0.2
0
-0.2
-0.2
0
0.2
0.4
0.6
0.8
1
ε/ε_y
Comput
EXP
BTV8
RS1
L.F.
1
0.8
0.6
0.4
0.2
0
-0.2
-0.1
0
0.1
0.2
0.3
0.4
0.5
0.6
ε/ε_y
Comput
EXP
BTV8
RS2
L.F.
1
0.8
0.6
0.4
0.2
0
-0.2
-0.1
0
0.1
0.2
0.3
0.4
0.5
ε/ε_y
Comput
EXP

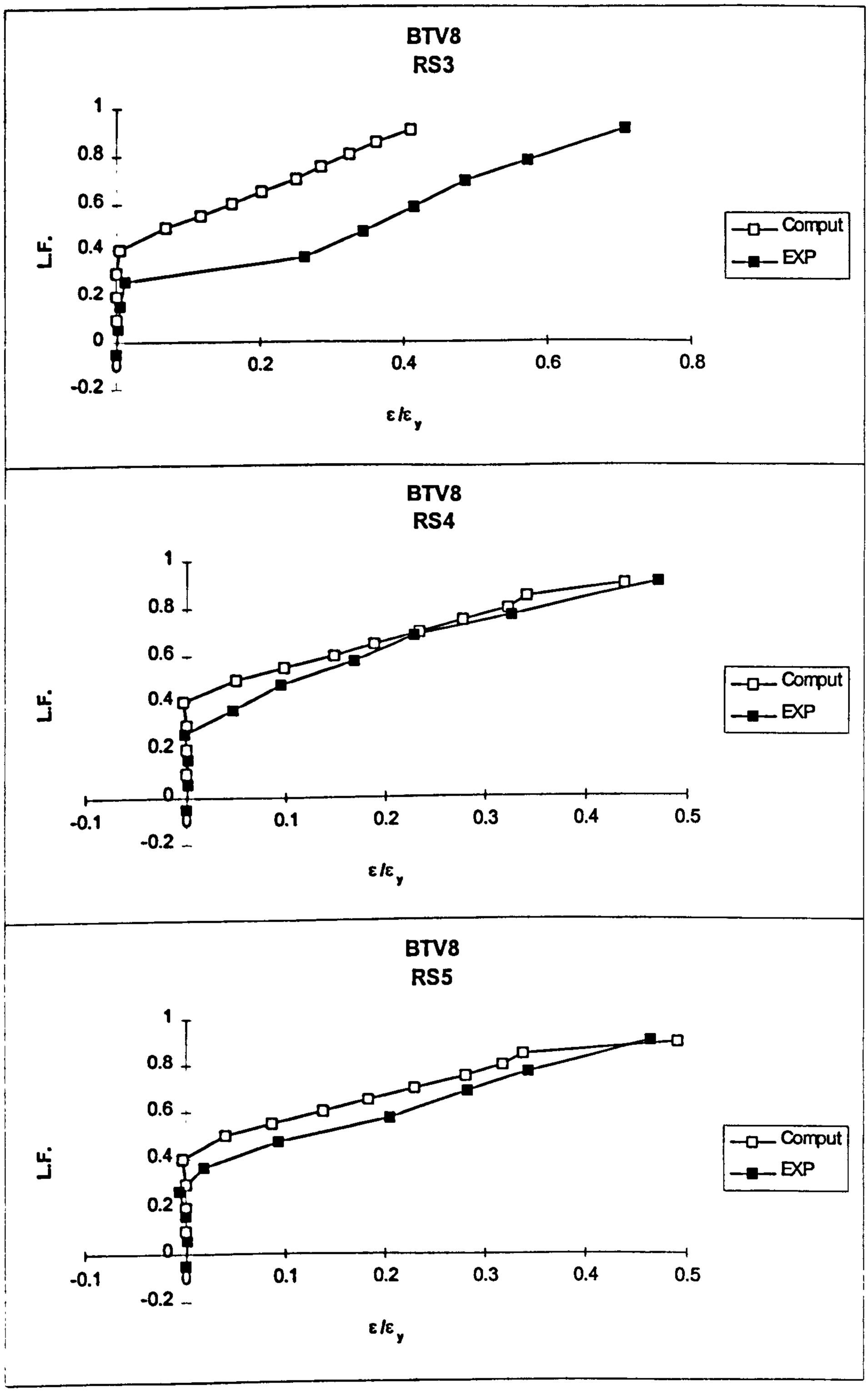
BTV8
RS3
L.F.
1
0.8
0.6
0.4
0.2
0
-0.2
0
0.2
0.4
0.6
0.8
ε/ε_y
Comput
EXP
BTV8
RS4
L.F.
1
0.8
0.6
0.4
0.2
0
-0.2
-0.1
0
0.1
0.2
0.3
0.4
0.5
ε/ε_y
Comput
EXP
BTV8
RS5
L.F.
1
0.8
0.6
0.4
0.2
0
-0.2
-0.1
0
0.1
0.2
0.3
0.4
0.5
ε/ε_y
Comput
EXP

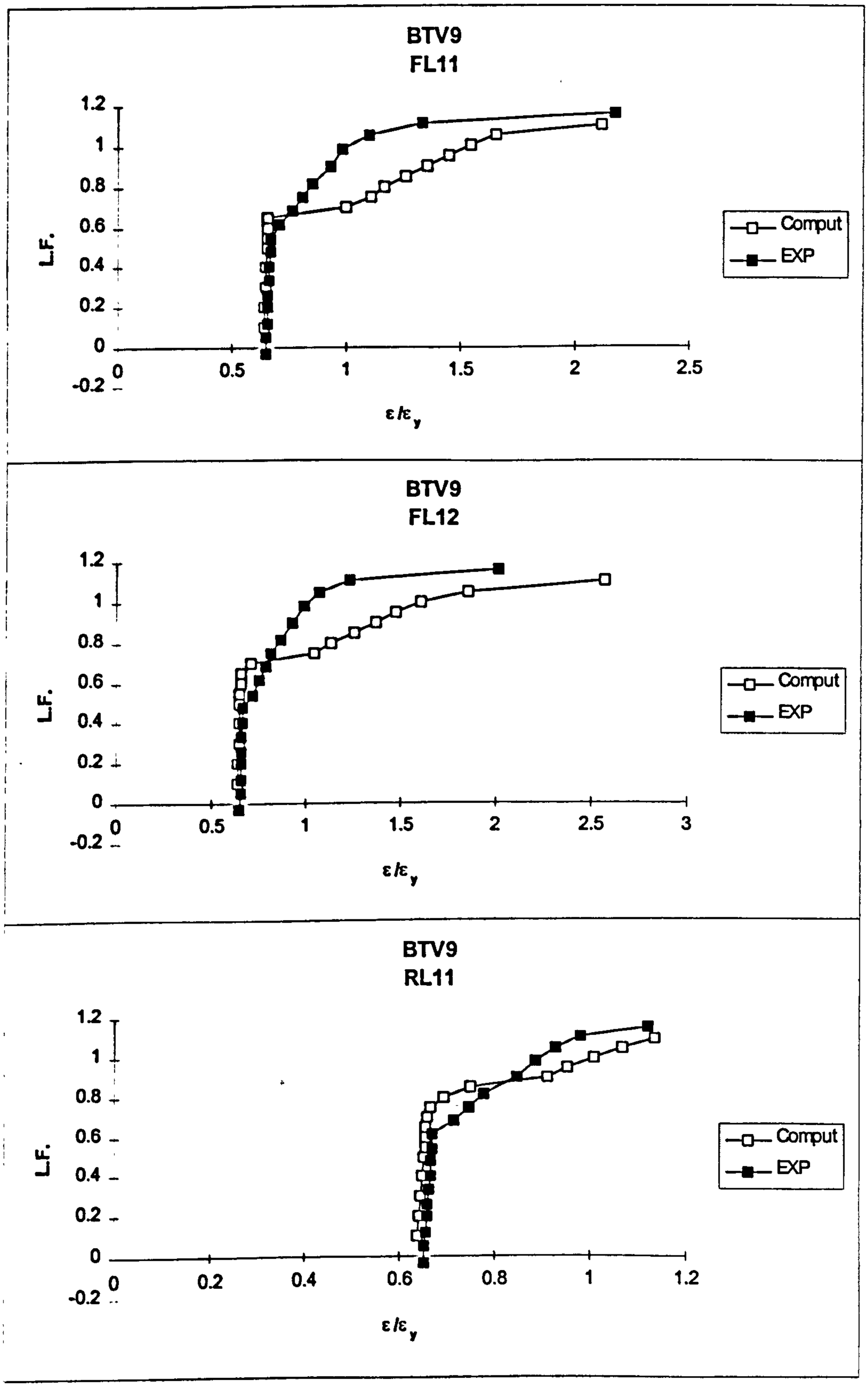
BTV9
FL11
L.F.
1.2
1
0.8
0.6
0.4
0.2
0
-0.2
0
0.5
1
1.5
2
2.5
ε/ε_y
Comput
EXP
BTV9
FL12
L.F.
1.2
1
0.8
0.6
0.4
0.2
0
-0.2
0
0.5
1
1.5
2
2.5
3
ε/ε_y
Comput
EXP
BTV9
RL11
L.F.
1.2
1
0.8
0.6
0.4
0.2
0
-0.2
0
0.2
0.4
0.6
0.8
1
1.2
ε/ε_y
Comput
EXP

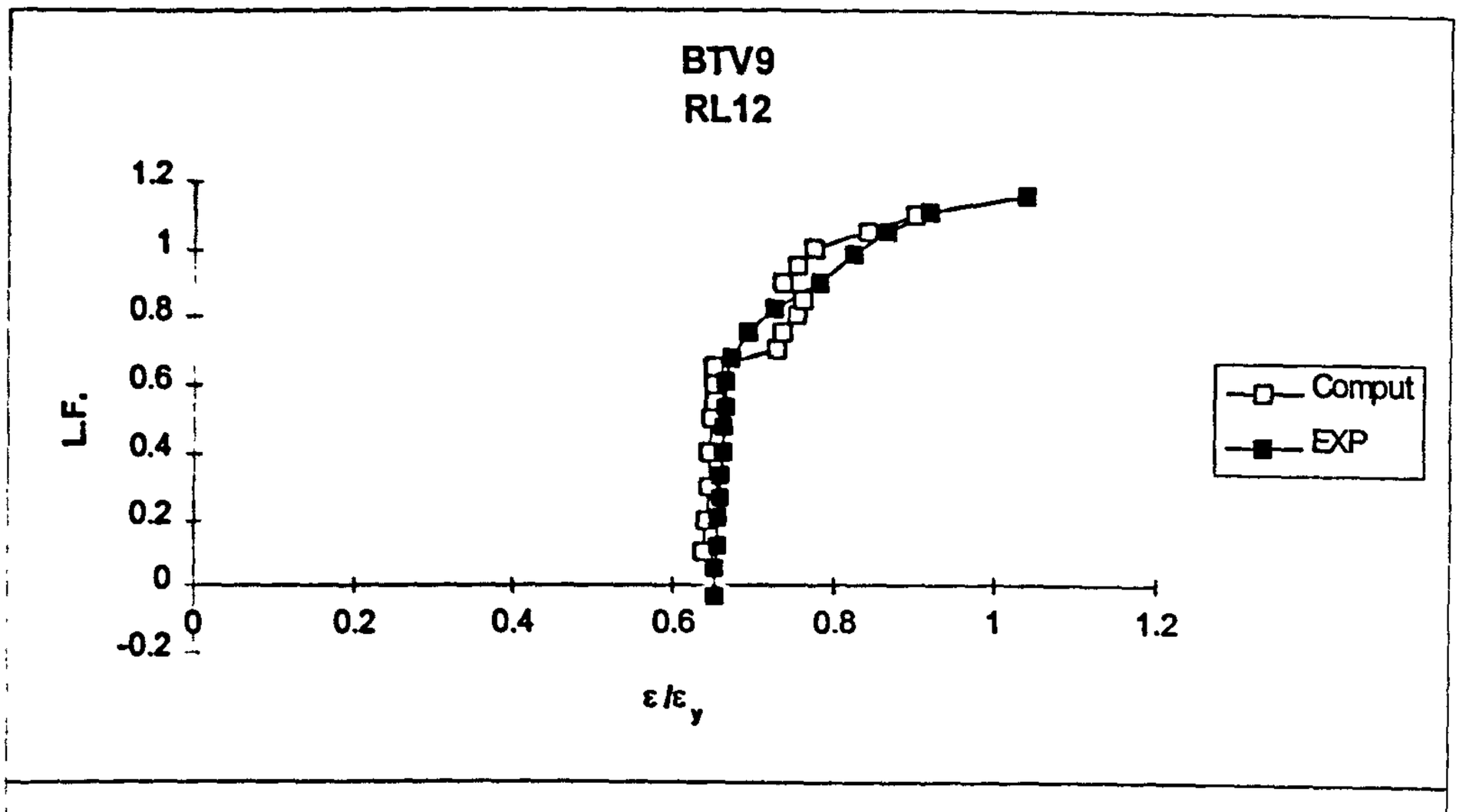
BTV9
RL12
L.F.
1.2
1
0.8
0.6
0.4
0.2
0
-0.2
0
0.2
0.4
0.6
0.8
1
1.2
ε /ε y
Comput
EXP

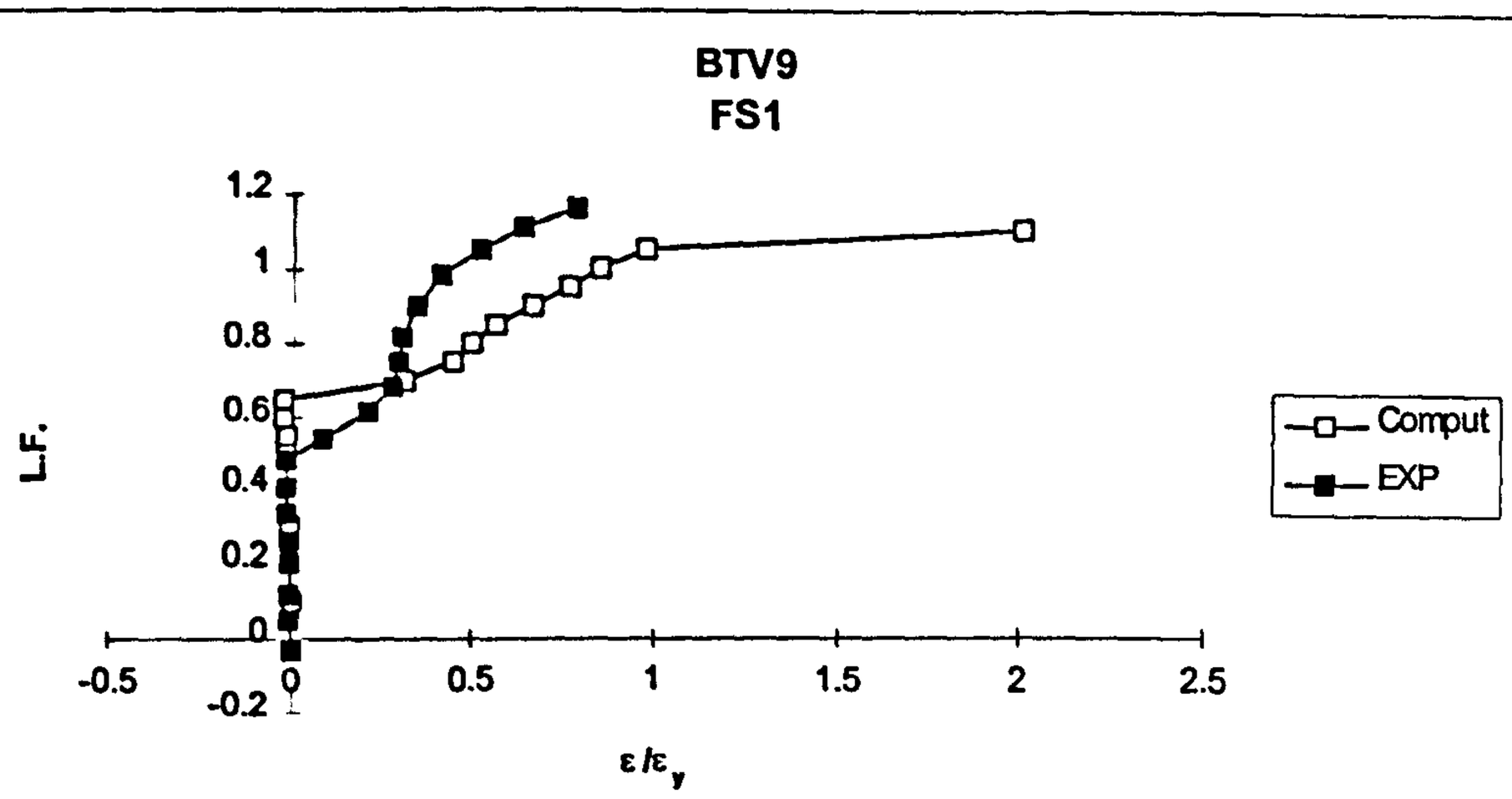
BTV9
FS1
L.F.
1.2
1
0.8
0.6
0.4
0.2
0
-0.2
-0.5
0
0.5
1
1.5
2
2.5
ε /ε y
Comput
EXP

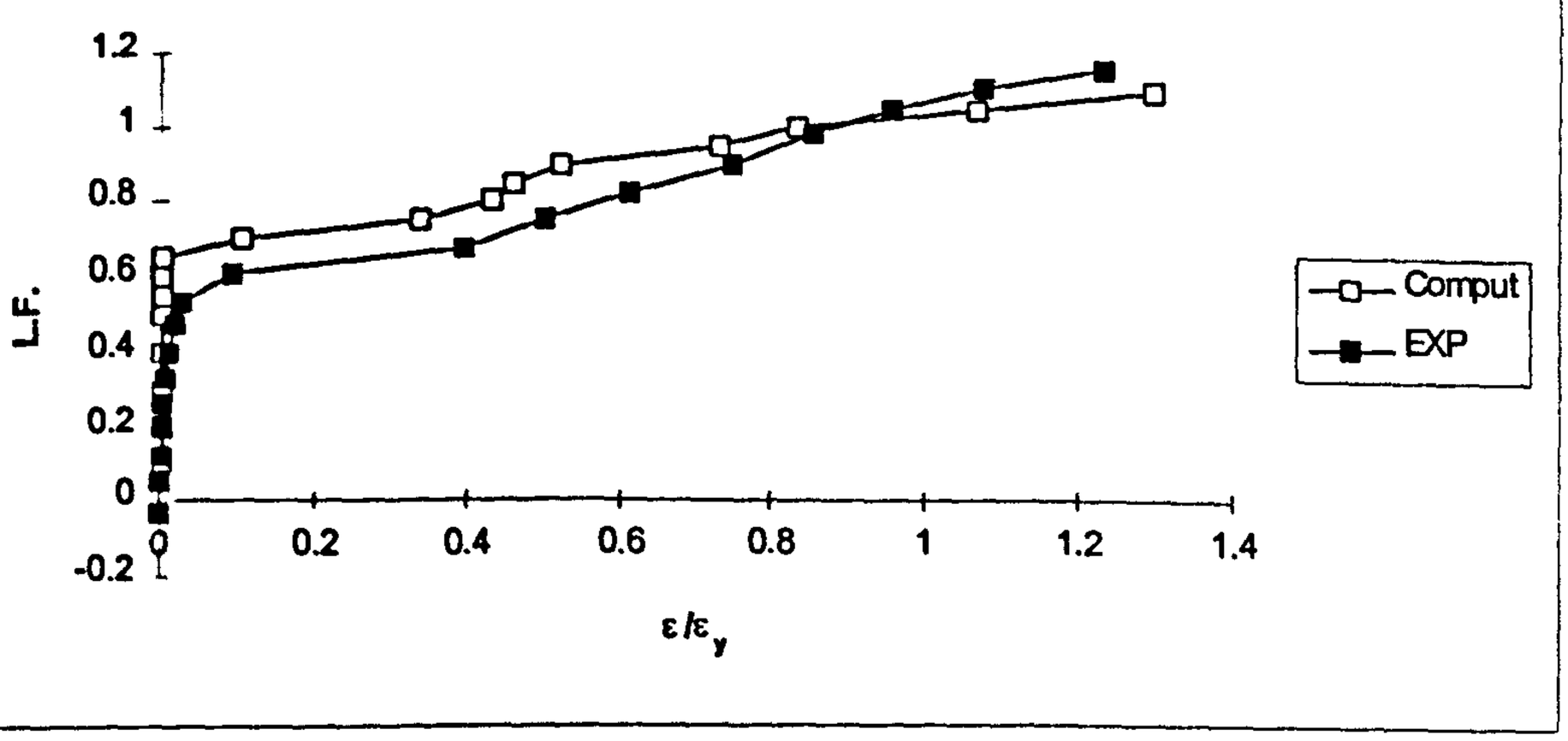
BTV9
FS2
L.F.
1.2
1
0.8
0.6
0.4
0.2
0
-0.2
0
0.2
0.4
0.6
0.8
1
1.2
1.4
ε /ε y
Comput
EXP

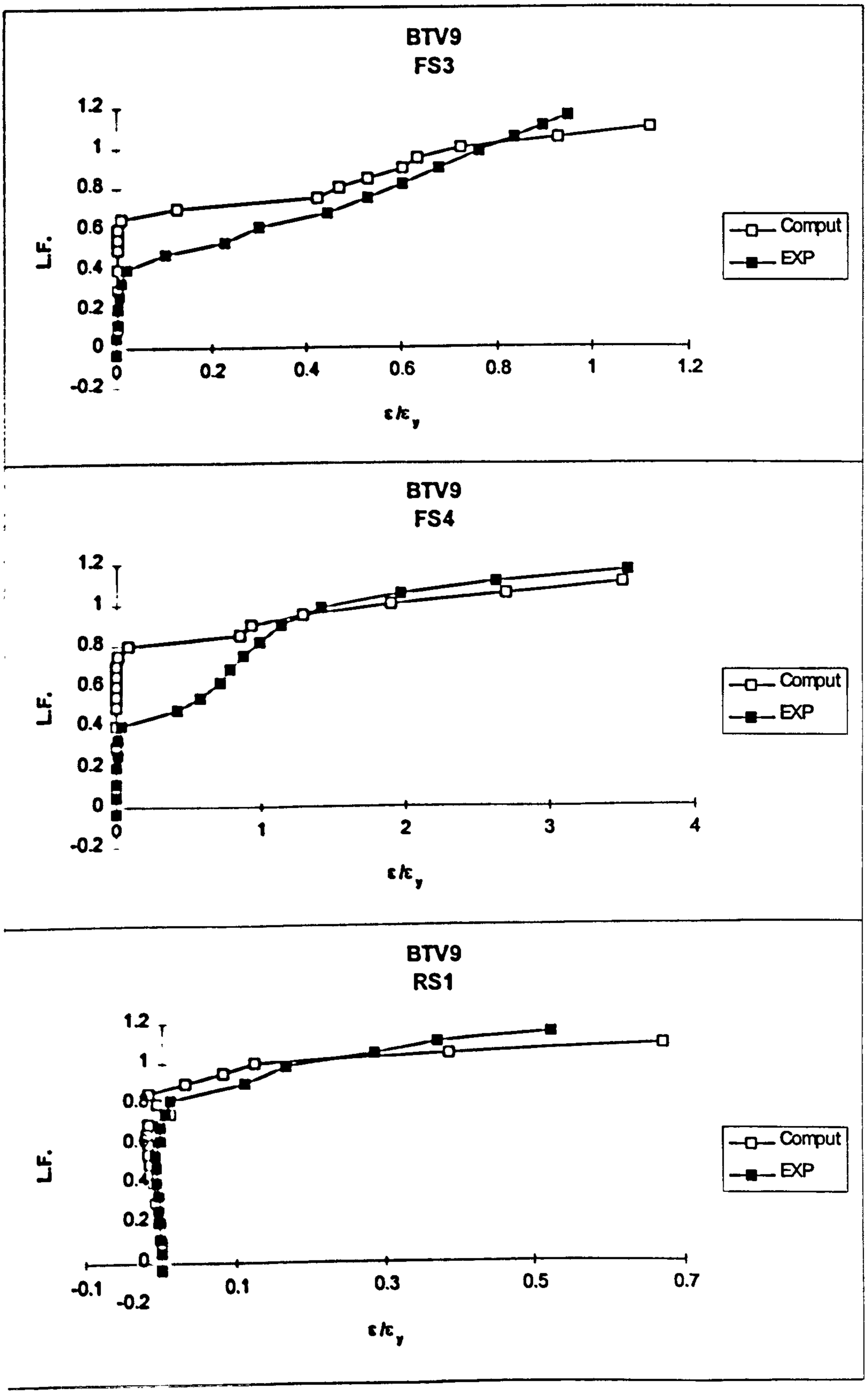
BTV9
FS3
L.F.
1.2
1
0.8
0.6
0.4
0.2
0
-0.2
0
0.2
0.4
0.6
0.8
1
1.2
ε/ε_y
Comput
EXP
BTV9
FS4
L.F.
1.2
1
0.8
0.6
0.4
0.2
0
-0.2
0
1
2
3
4
ε/ε_y
Comput
EXP
BTV9
RS1
L.F.
1.2
1
0.8
0.6
0.4
0.2
0
-0.2
-0.1
0.1
0.3
0.5
0.7
ε/ε_y
Comput
EXP

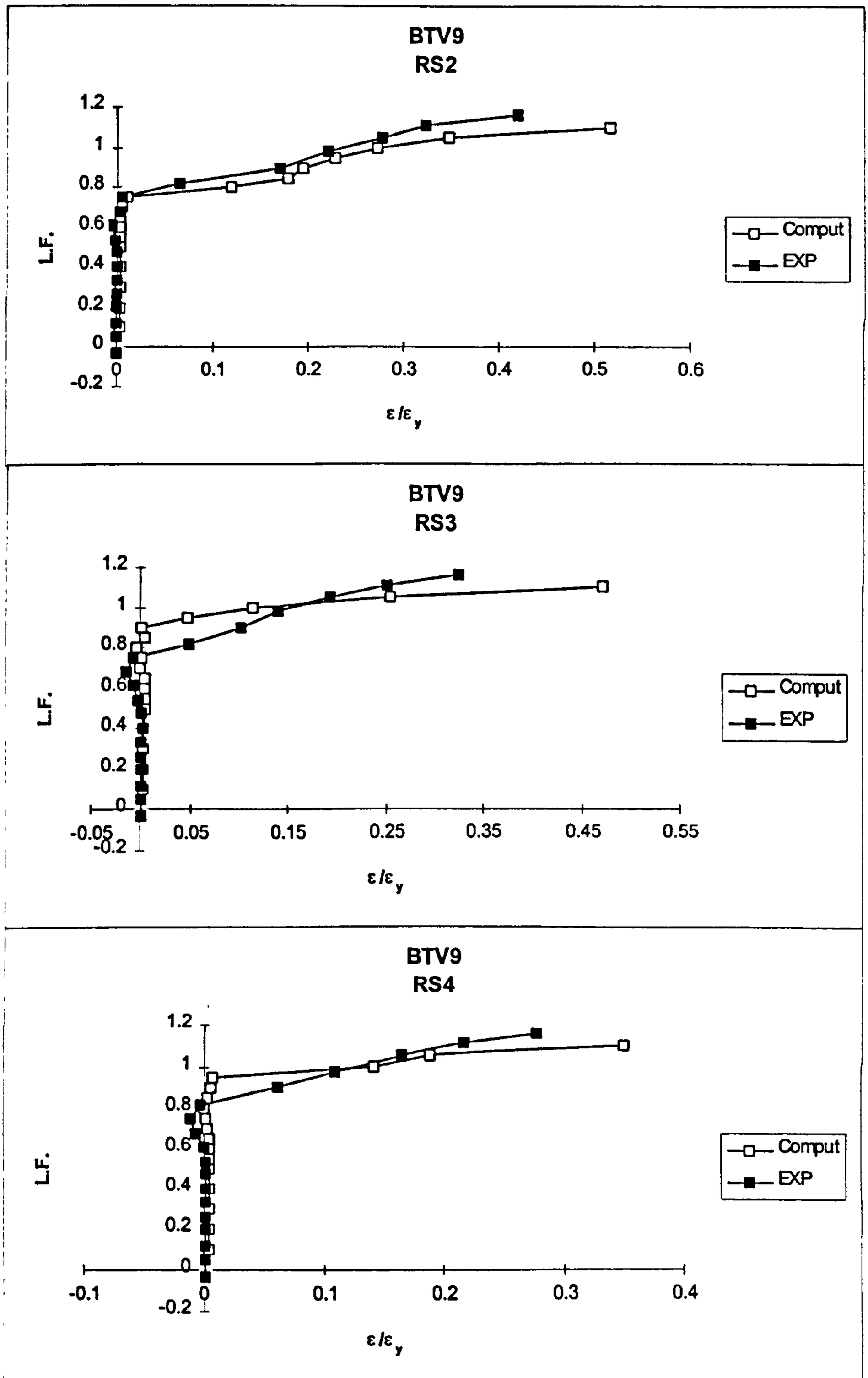
BTV9
RS2
L.F.
1.2
1
0.8
0.6
0.4
0.2
0
-0.2
0
0.1
0.2
0.3
0.4
0.5
0.6
ε/ε_y
Comput
EXP
BTV9
RS3
L.F.
1.2
1
0.8
0.6
0.4
0.2
0
-0.2
-0.05
0.05
0.15
0.25
0.35
0.45
0.55
ε/ε_y
Comput
EXP
BTV9
RS4
L.F.
1.2
1
0.8
0.6
0.4
0.2
0
-0.2
-0.1
0
0.1
0.2
0.3
0.4
ε/ε_y
Comput
EXP

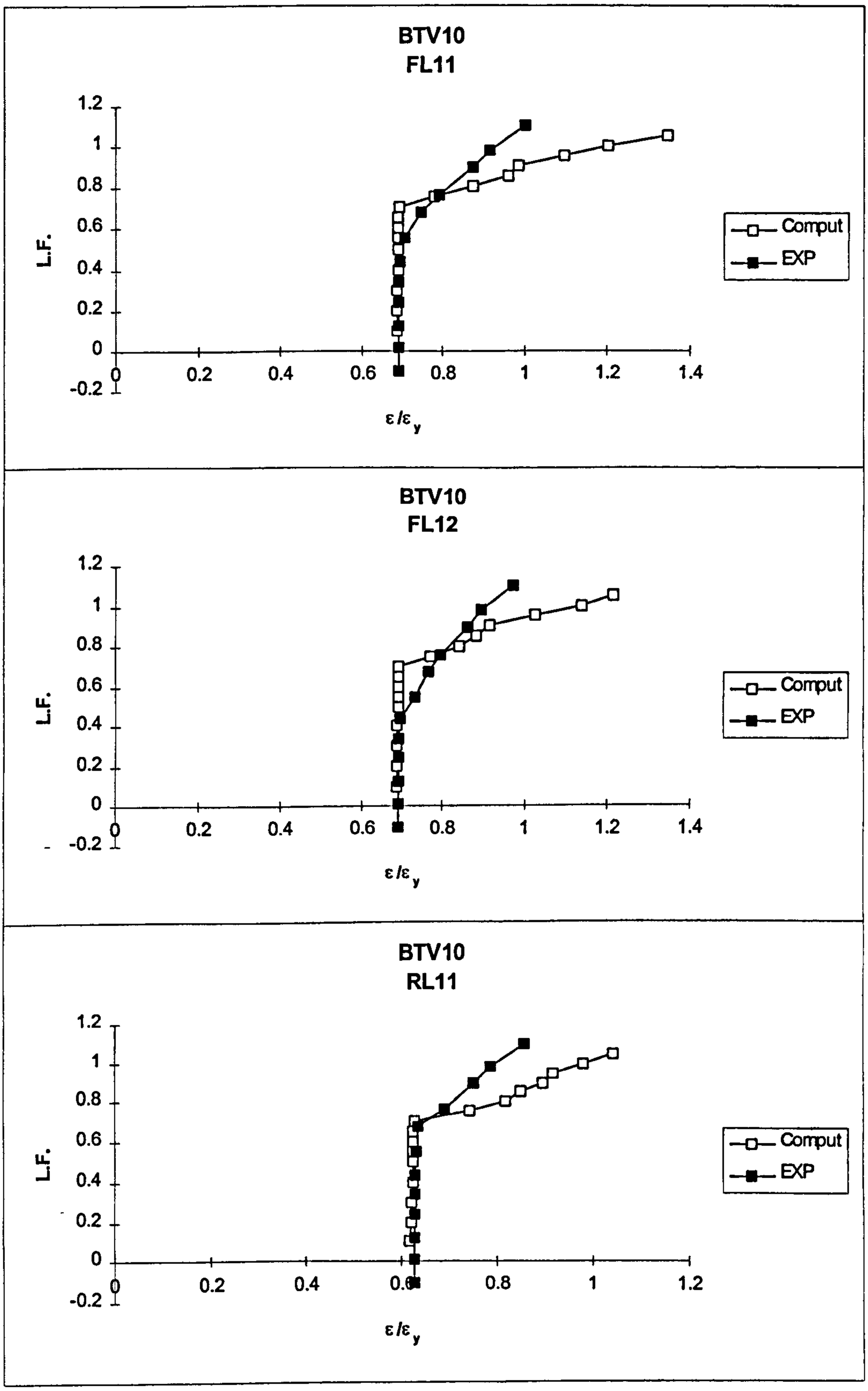
BTV10
FL11
L.F.
1.2
1
0.8
0.6
0.4
0.2
0
-0.2
0
0.2
0.4
0.6
0.8
1
1.2
1.4
ε /ε y
Comput
EXP
BTV10
FL12
L.F.
ε /ε y
Comput
EXP
BTV10
RL11
L.F.
ε /ε y
Comput
EXP

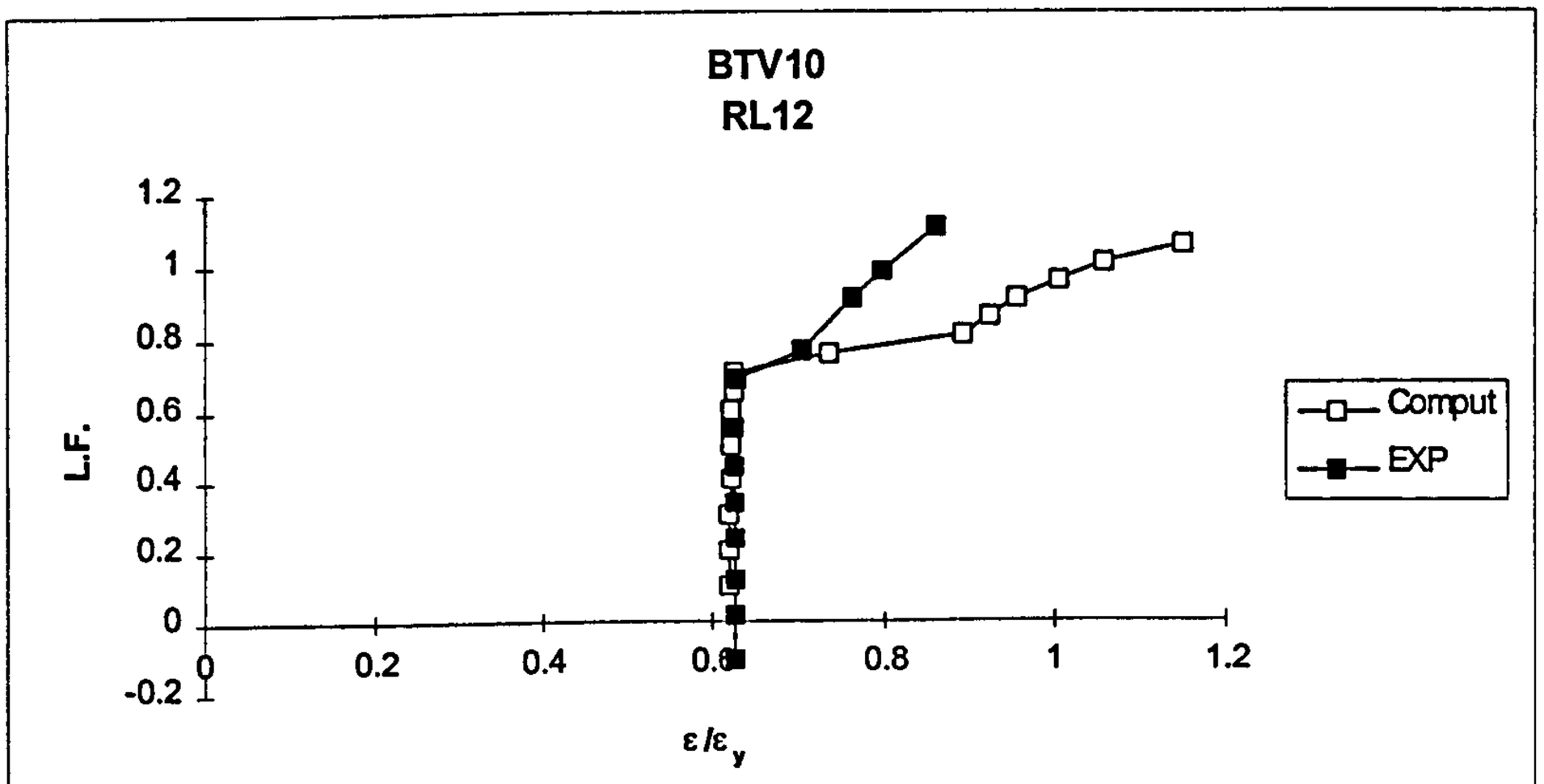
BTV10
RL12
L.F.
1.2
1
0.8
0.6
0.4
0.2
0
-0.2
0
0.2
0.4
0.8
1
1.2
Comput
EXP
ε/ε y

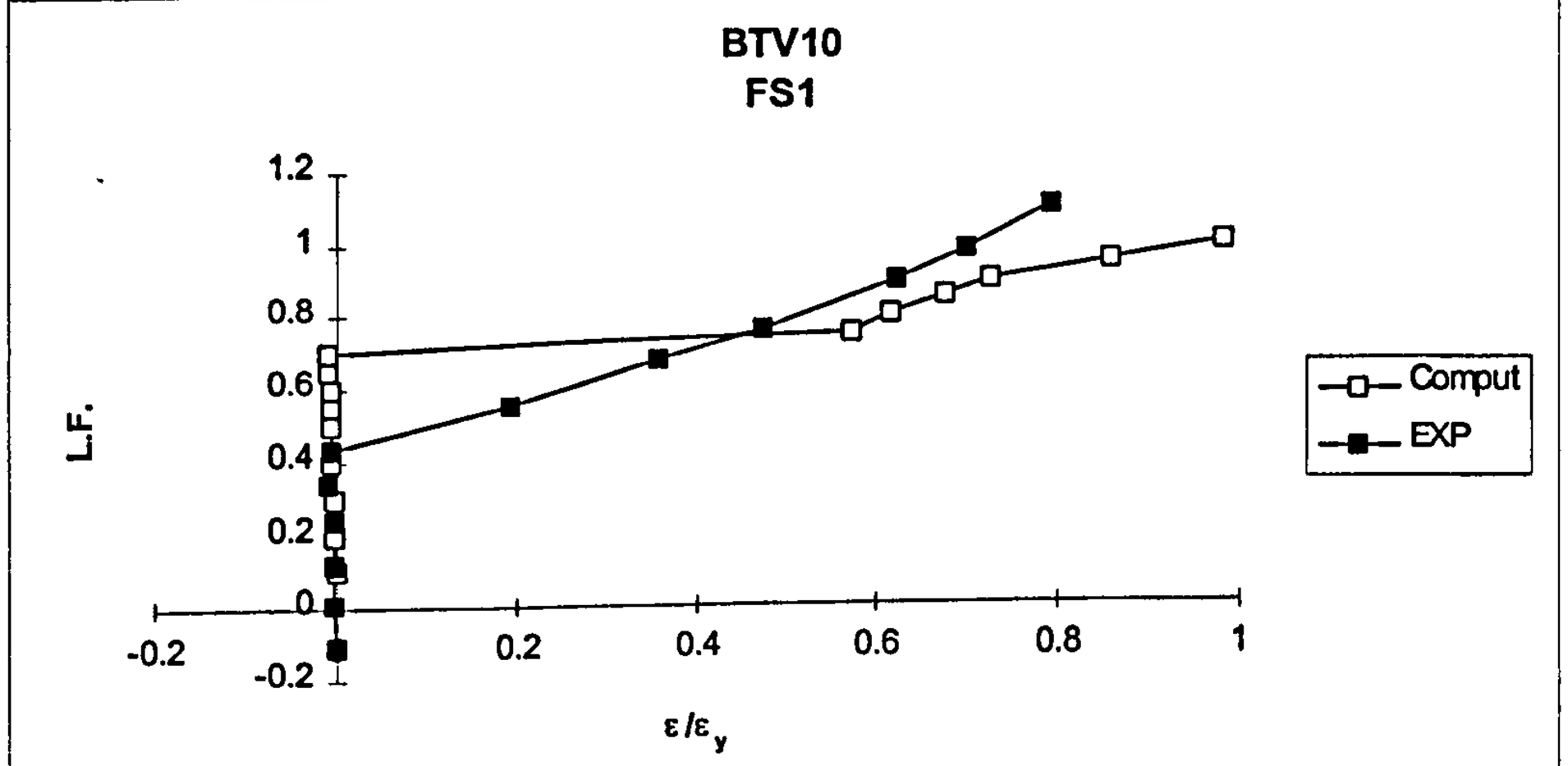
BTV10
FS1
L.F.
1.2
1
0.8
0.6
0.4
0.2
0
-0.2
-0.2
0.2
0.4
0.6
0.8
1
Comput
EXP
ε/ε y

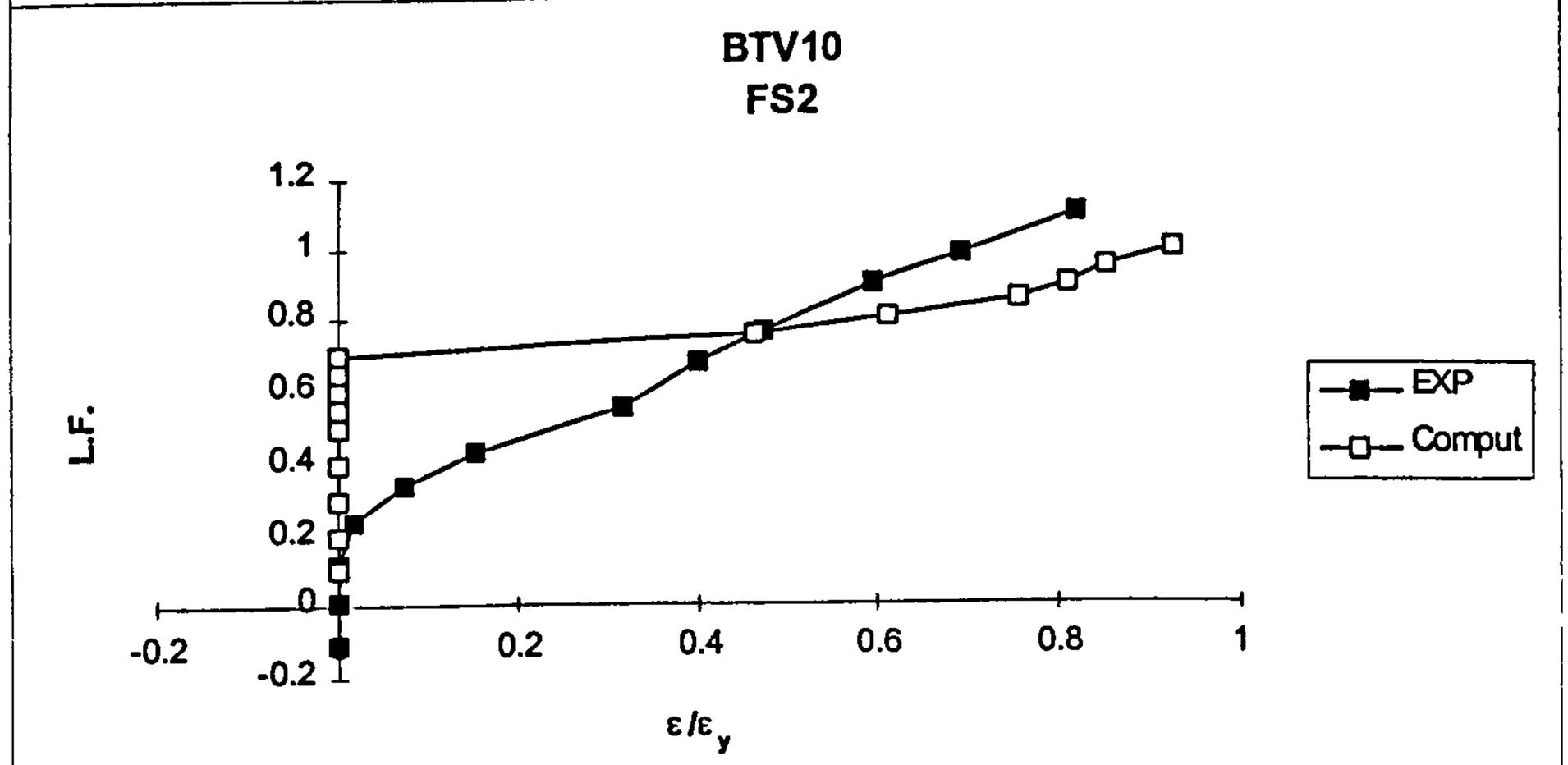
BTV10
FS2
L.F.
1.2
1
0.8
0.6
0.4
0.2
0
-0.2
-0.2
0.2
0.4
0.6
0.8
1
EXP
Comput
ε/ε y

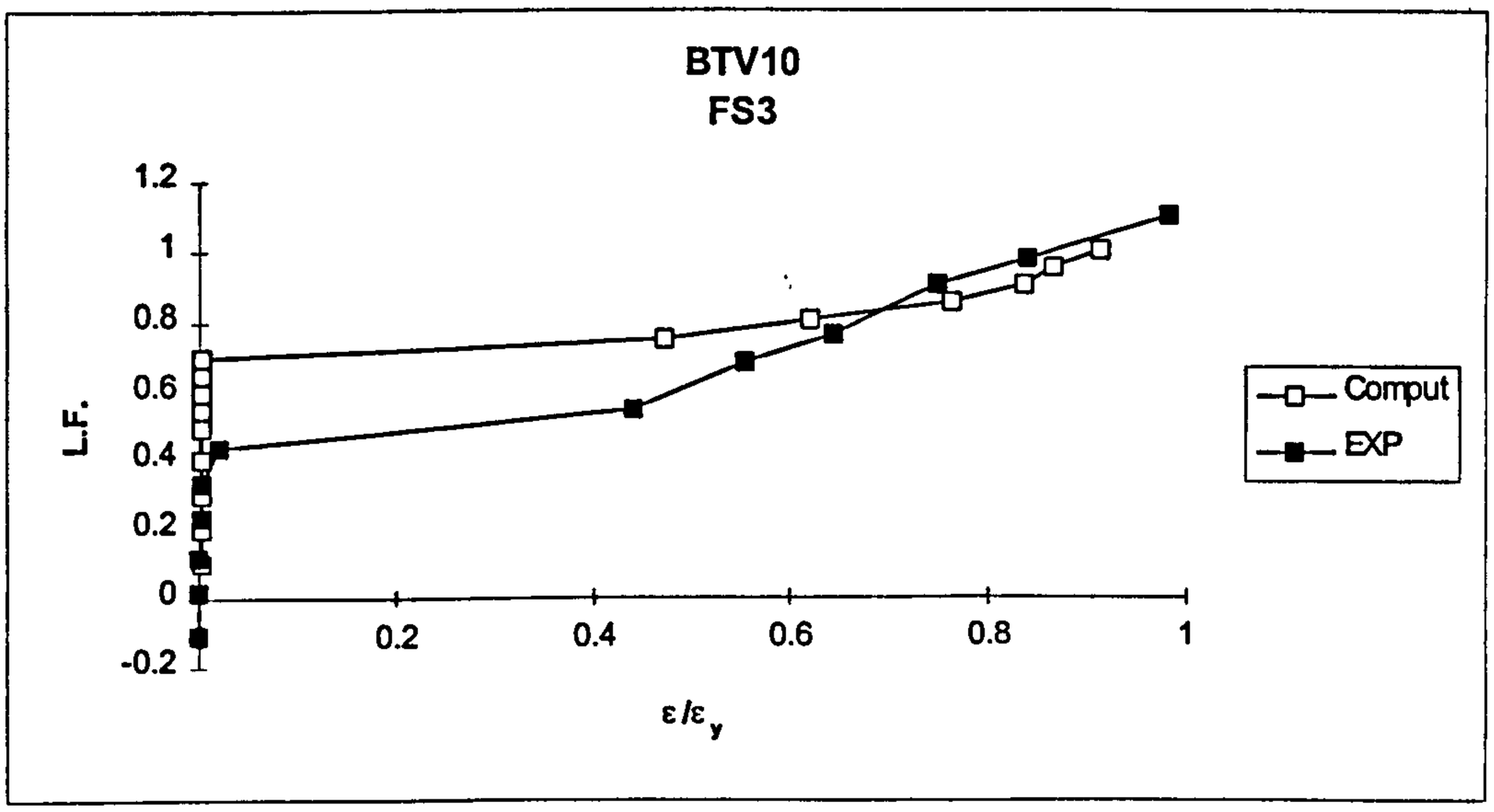
BTV10
FS3
1.2
1
0.8
0.6
0.4
0.2
0
-0.2
L.F.
0.2
0.4
0.6
0.8
1
Comput
EXP
ε/ε y

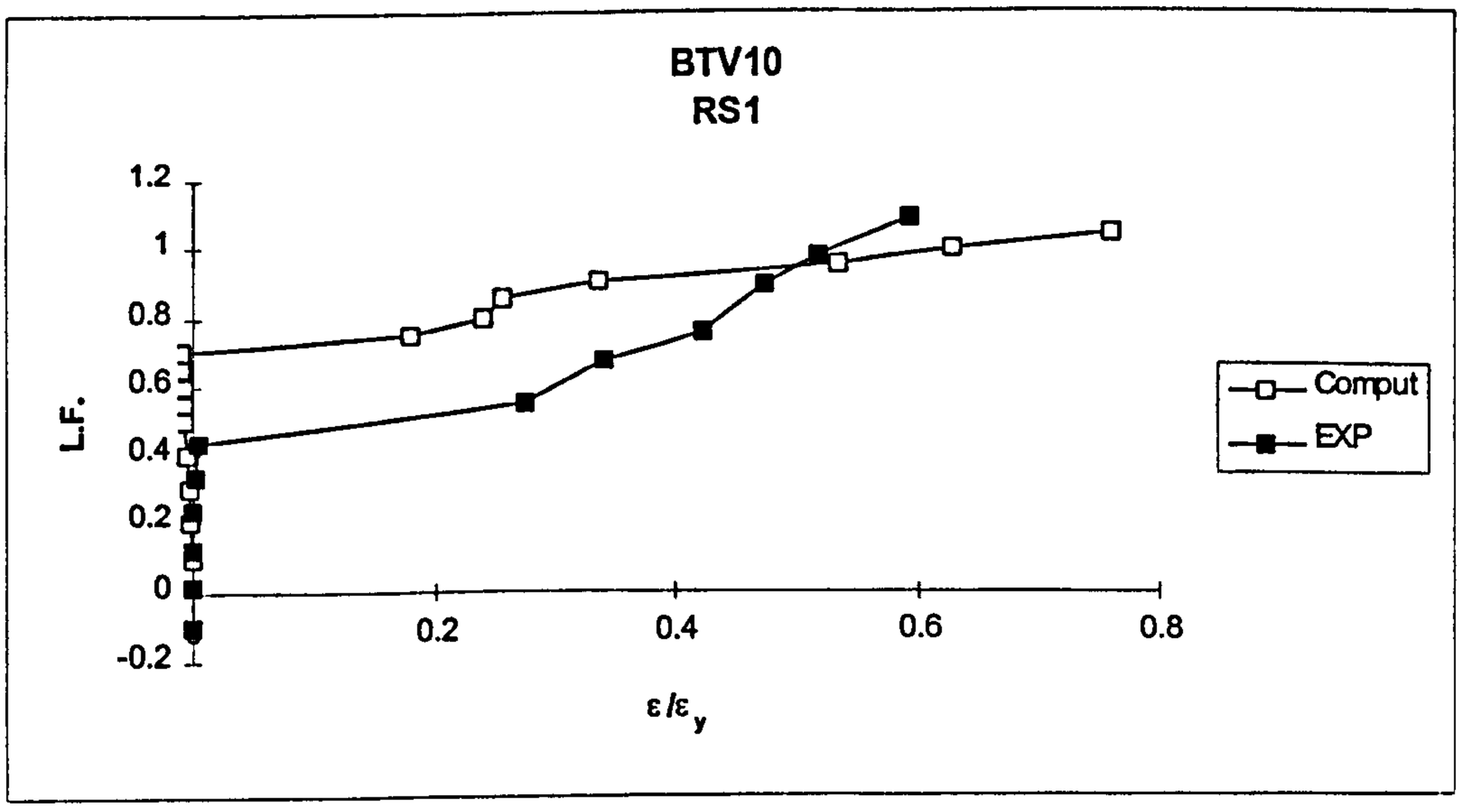
BTV10
RS1
1.2
1
0.8
0.6
0.4
0.2
0
-0.2
L.F.
0.2
0.4
0.6
0.8
Comput
EXP
ε/ε y

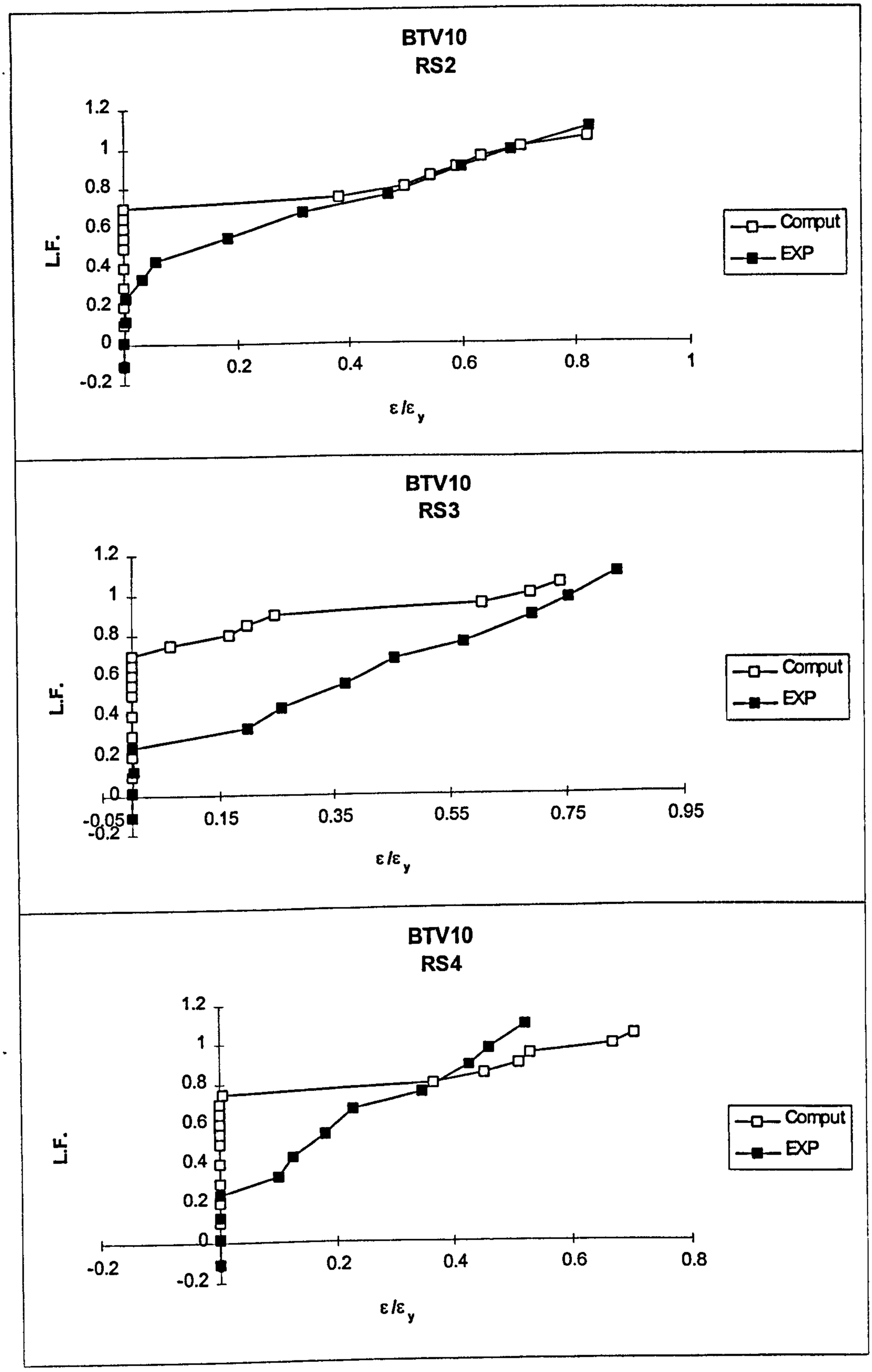
BTV10
RS2
L.F.
1.2
1
0.8
0.6
0.4
0.2
0
-0.2
0.2
0.4
0.6
0.8
1
ε/ε_y
Comput
EXP
BTV10
RS3
L.F.
1.2
1
0.8
0.6
0.4
0.2
0
-0.05
-0.2
0.15
0.35
0.55
0.75
0.95
ε/ε_y
Comput
EXP
BTV10
RS4
L.F.
1.2
1
0.8
0.6
0.4
0.2
0
-0.2
-0.2
0.2
0.4
0.6
0.8
ε/ε_y
Comput
EXP

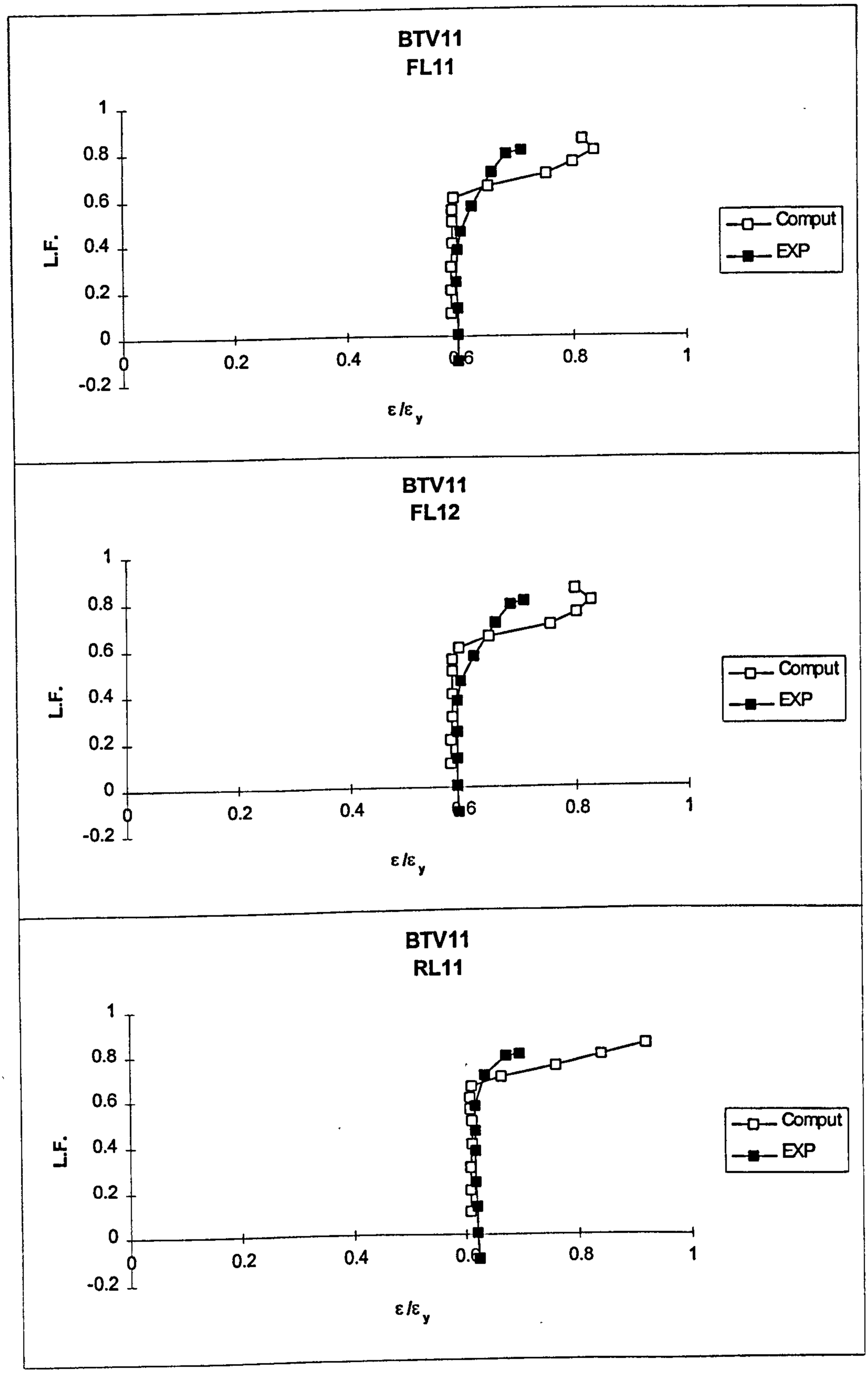
BTV11
FL11
L.F.
1
0.8
0.6
0.4
0.2
0
-0.2
0
0.2
0.4
0.6
0.8
1
ε /ε y
Comput
EXP
BTV11
FL12
L.F.
ε /ε y
Comput
EXP
BTV11
RL11
L.F.
ε /ε y
Comput
EXP

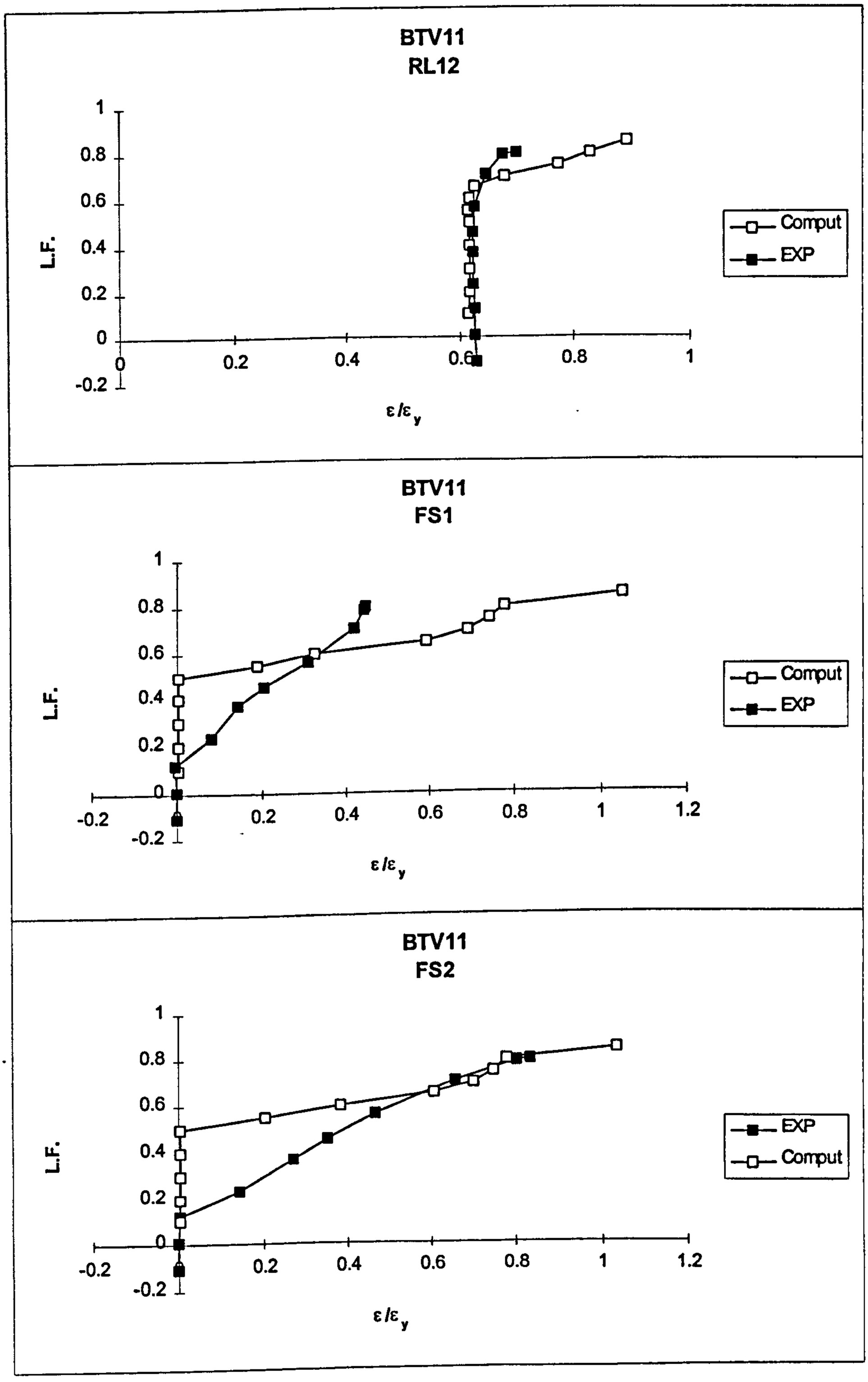
BTV11
RL12
L.F.
1
0.8
0.6
0.4
0.2
0
-0.2
0
0.2
0.4
0.6
0.8
1
ε/ε y
Comput
EXP
BTV11
FS1
L.F.
1
0.8
0.6
0.4
0.2
0
-0.2
-0.2
0.2
0.4
0.6
0.8
1
1.2
ε/ε y
Comput
EXP
BTV11
FS2
L.F.
1
0.8
0.6
0.4
0.2
0
-0.2
-0.2
0.2
0.4
0.6
0.8
1
1.2
ε/ε y
EXP
Comput

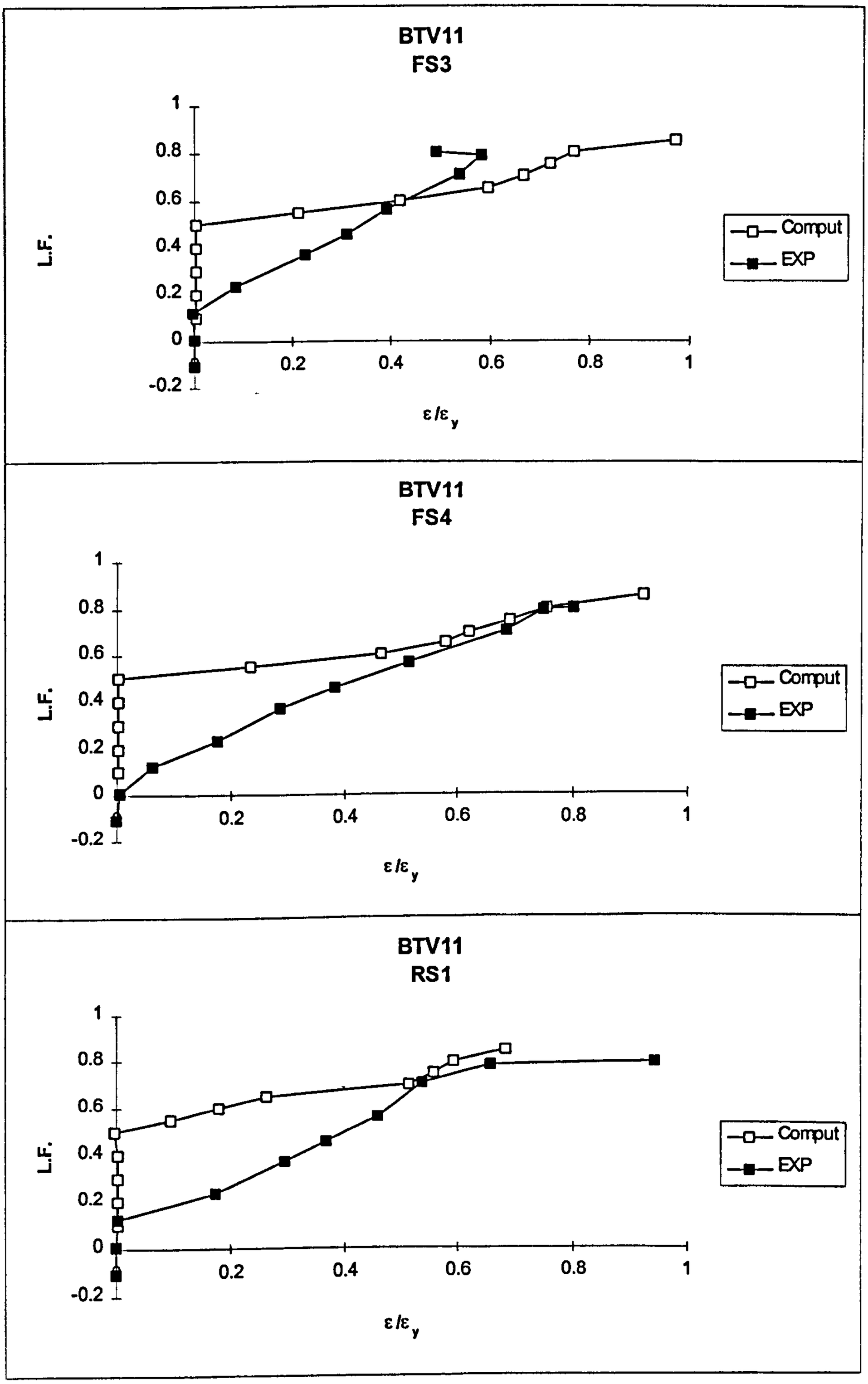
BTV11
FS3
L.F.
1
0.8
0.6
0.4
0.2
0
-0.2
0.2
0.4
0.6
0.8
1
ε/ε_y
Comput
EXP
BTV11
FS4
L.F.
1
0.8
0.6
0.4
0.2
0
-0.2
0.2
0.4
0.6
0.8
1
ε/ε_y
Comput
EXP
BTV11
RS1
L.F.
1
0.8
0.6
0.4
0.2
0
-0.2
0.2
0.4
0.6
0.8
1
ε/ε_y
Comput
EXP

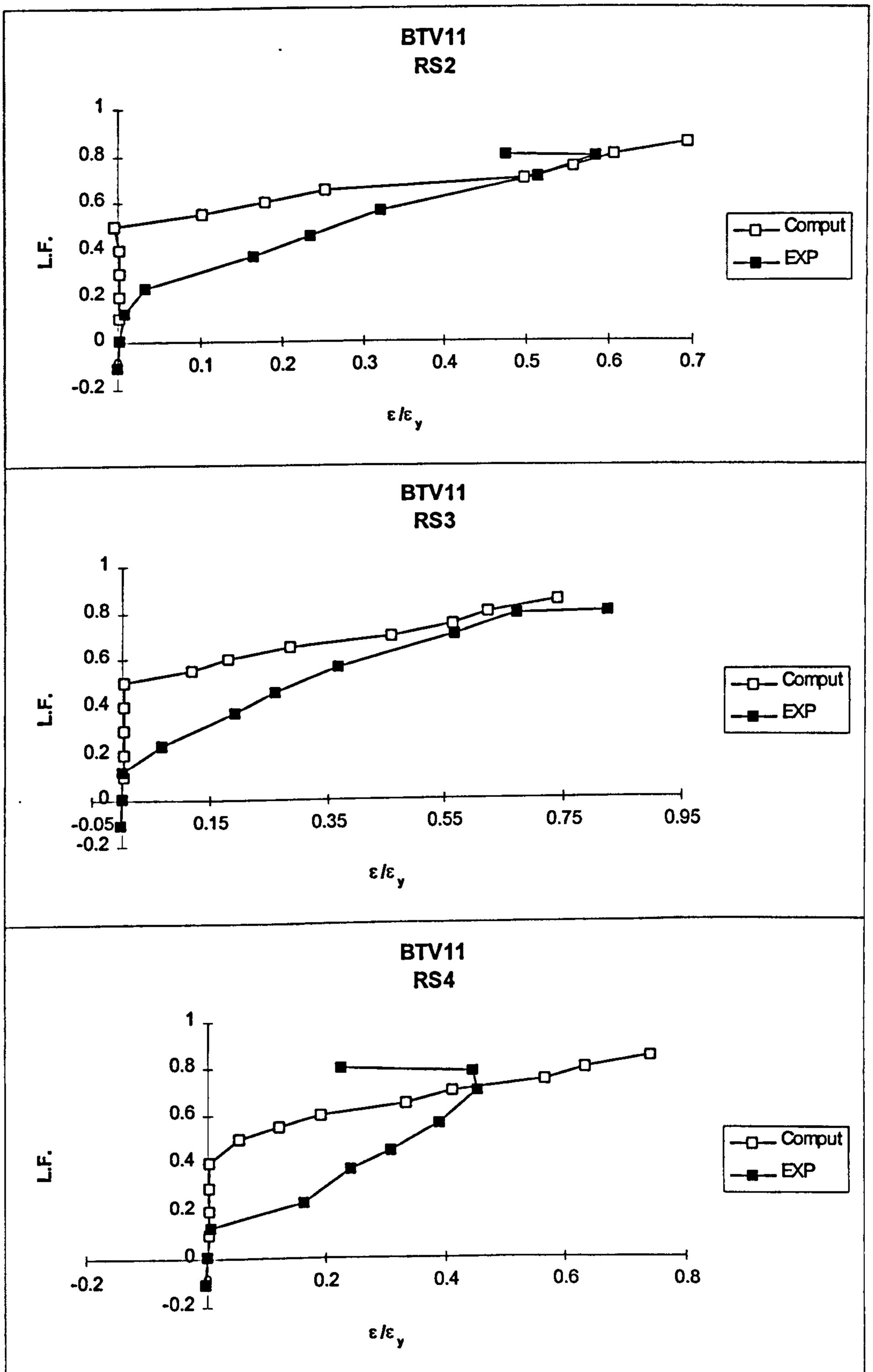
BTV11
RS2
L.F.
1
0.8
0.6
0.4
0.2
0
-0.2
0.1
0.2
0.3
0.4
0.5
0.6
0.7
ε/ε_y
Comput
EXP
BTV11
RS3
L.F.
1
0.8
0.6
0.4
0.2
0
-0.05
-0.2
0.15
0.35
0.55
0.75
0.95
ε/ε_y
Comput
EXP
BTV11
RS4
L.F.
1
0.8
0.6
0.4
0.2
0
-0.2
-0.2
0.2
0.4
0.6
0.8
ε/ε_y
Comput
EXP

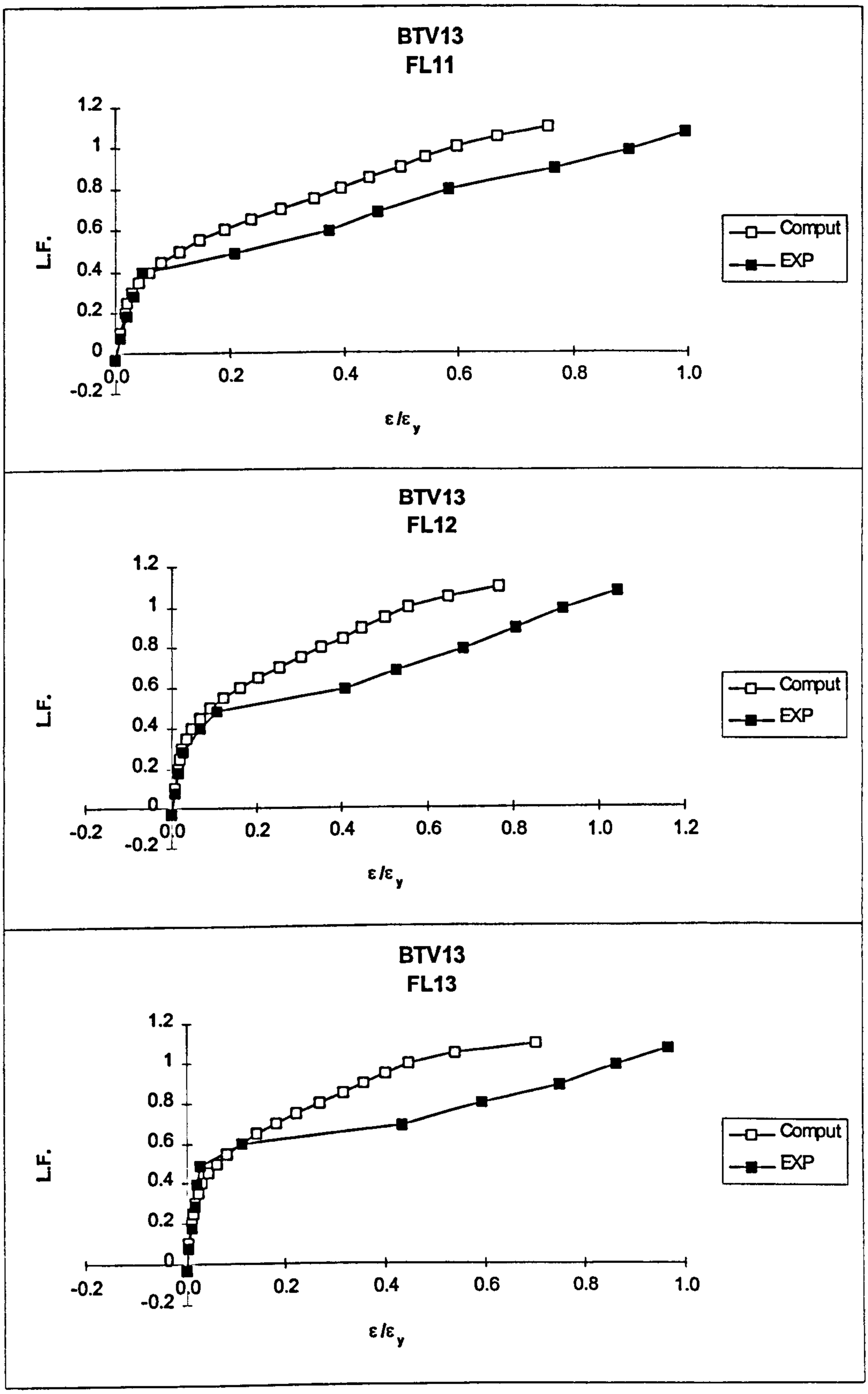
BTV13
FL11
L.F.
1.2
1
0.8
0.6
0.4
0.2
0
-0.2
0.0
0.2
0.4
0.6
0.8
1.0
ε/ε y
Comput
EXP
BTV13
FL12
L.F.
1.2
1
0.8
0.6
0.4
0.2
0
-0.2
0.0
0.2
0.4
0.6
0.8
1.0
1.2
ε/ε y
Comput
EXP
BTV13
FL13
L.F.
1.2
1
0.8
0.6
0.4
0.2
0
-0.2
0.0
0.2
0.4
0.6
0.8
1.0
ε/ε y
Comput
EXP

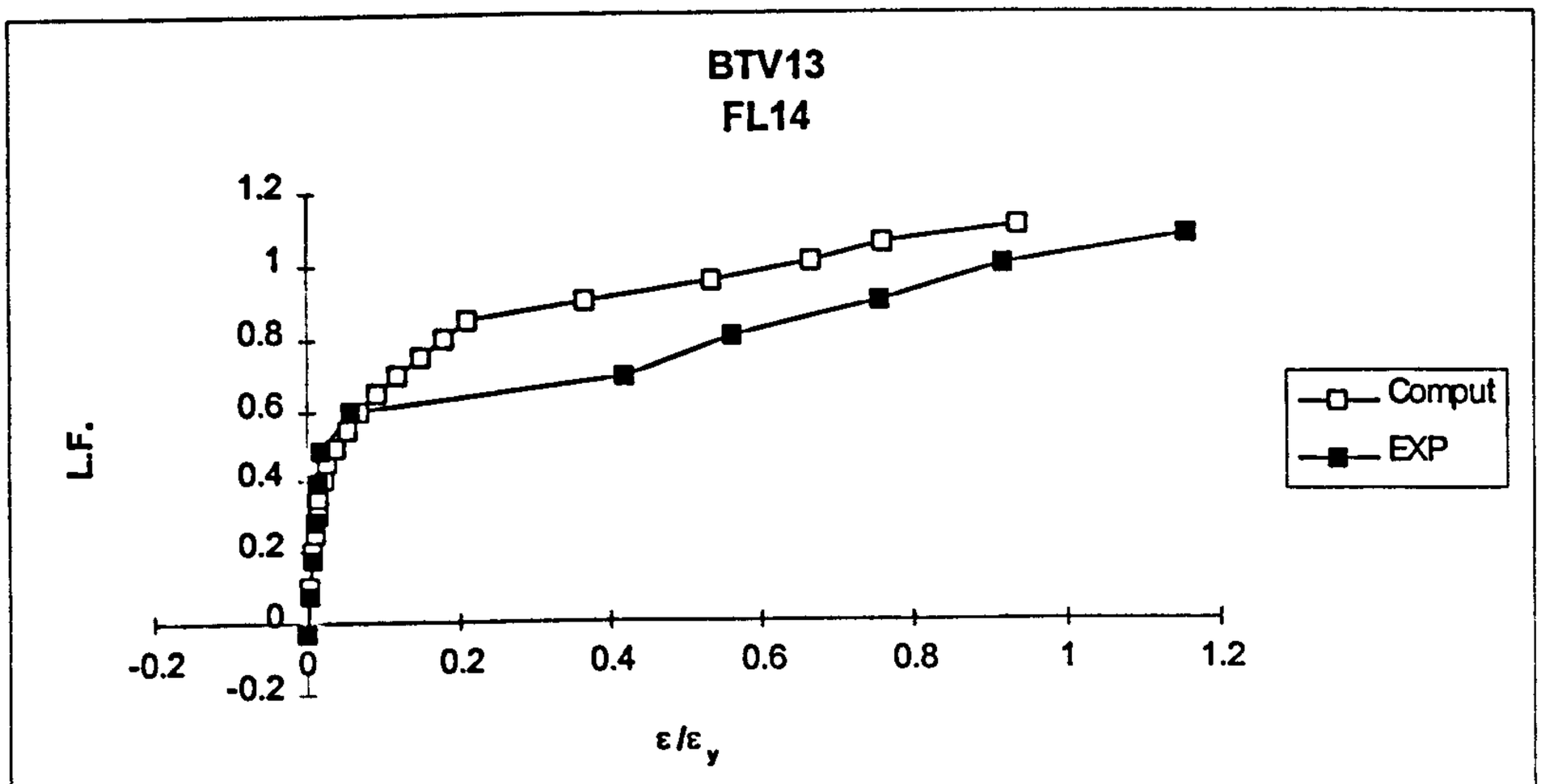
BTV13
FL14
L.F.
1.2
1
0.8
0.6
0.4
0.2
0
-0.2
0
0.2
0.4
0.6
0.8
1
1.2
Comput
EXP
ε/ε y

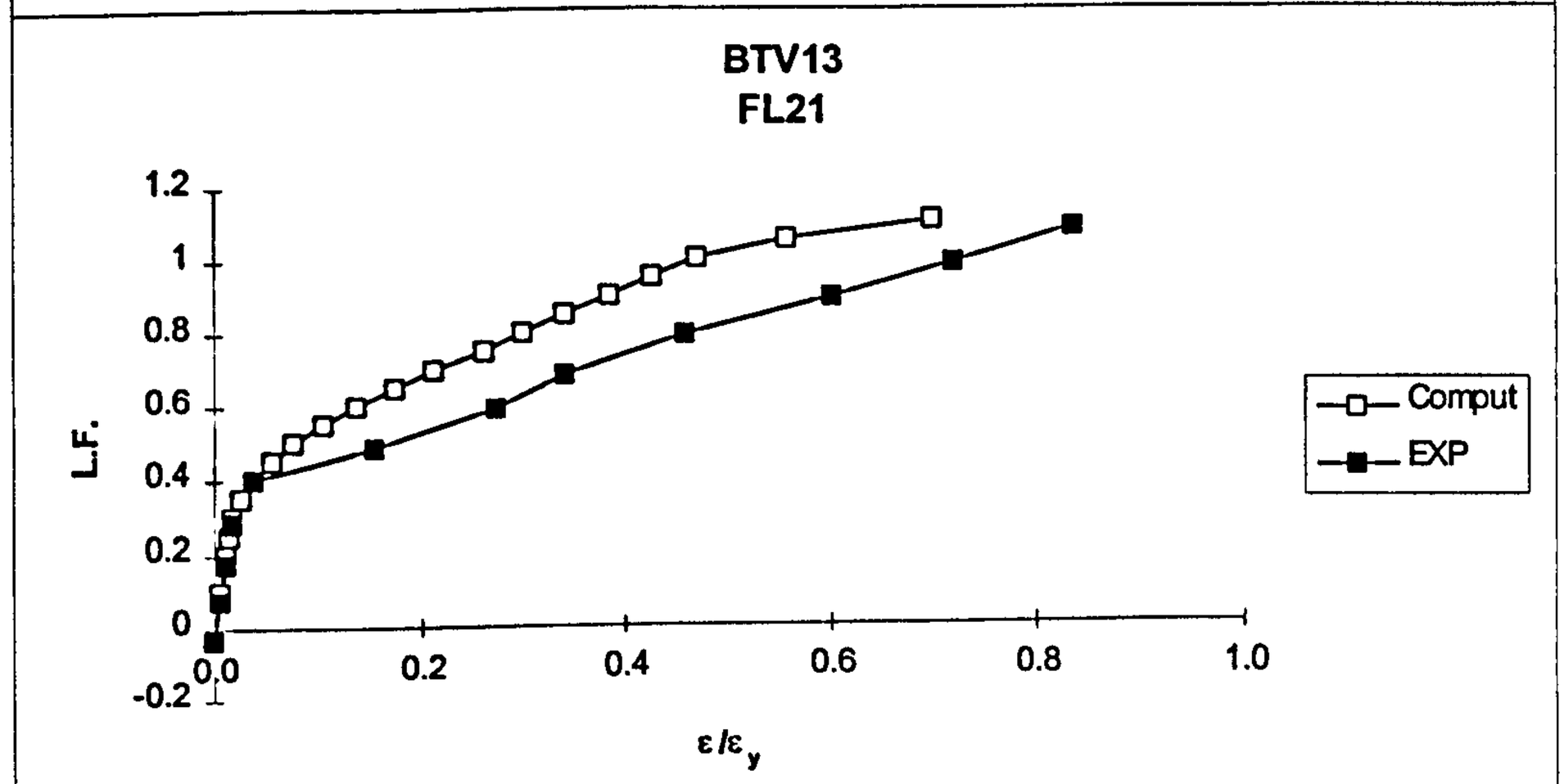
BTV13
FL21
L.F.
1.2
1
0.8
0.6
0.4
0.2
0
-0.2
0.0
0.2
0.4
0.6
0.8
1.0
Comput
EXP
ε/ε y

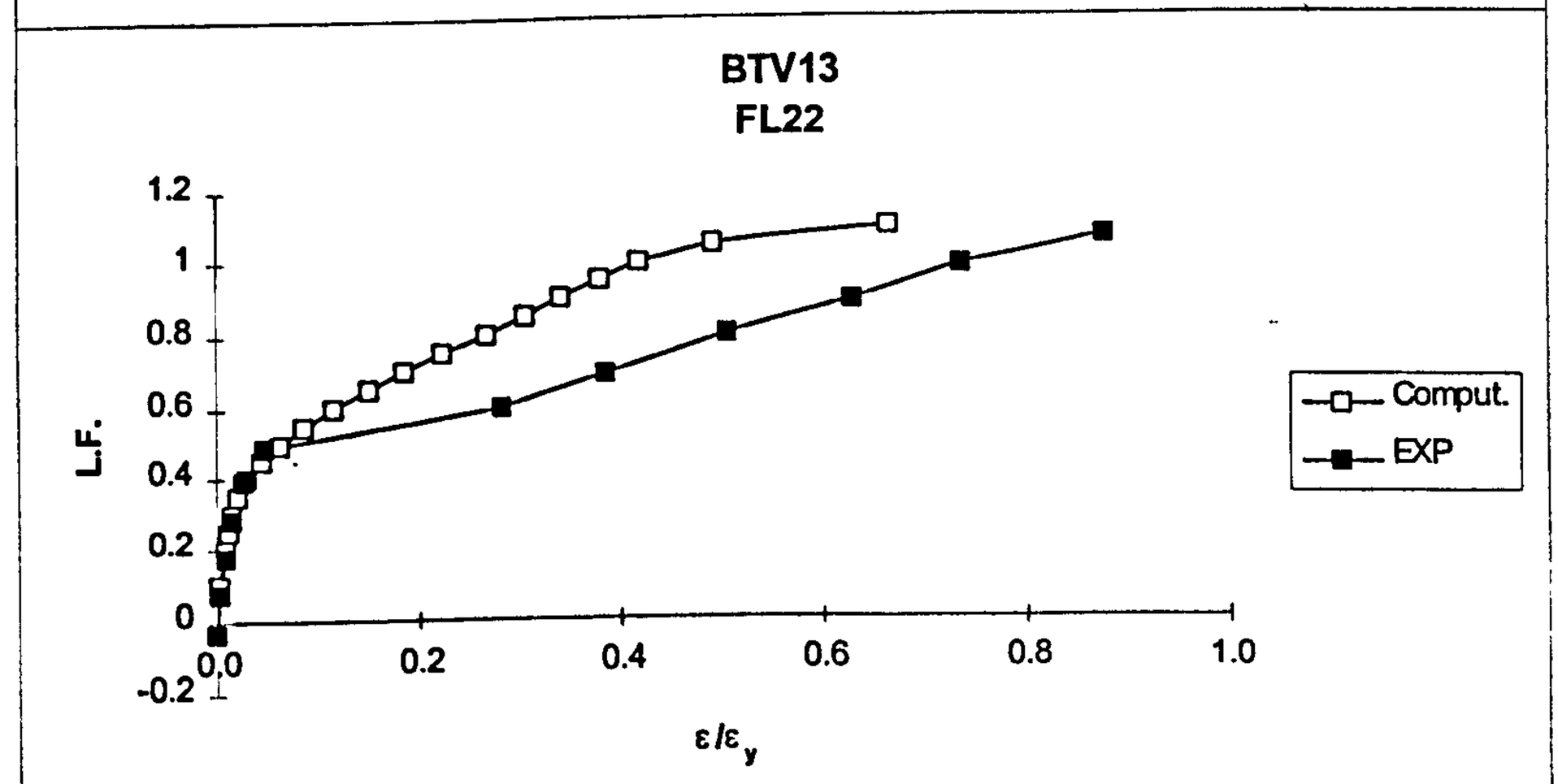
BTV13
FL22
L.F.
1.2
1
0.8
0.6
0.4
0.2
0
-0.2
0.0
0.2
0.4
0.6
0.8
1.0
Comput.
EXP
ε/ε y

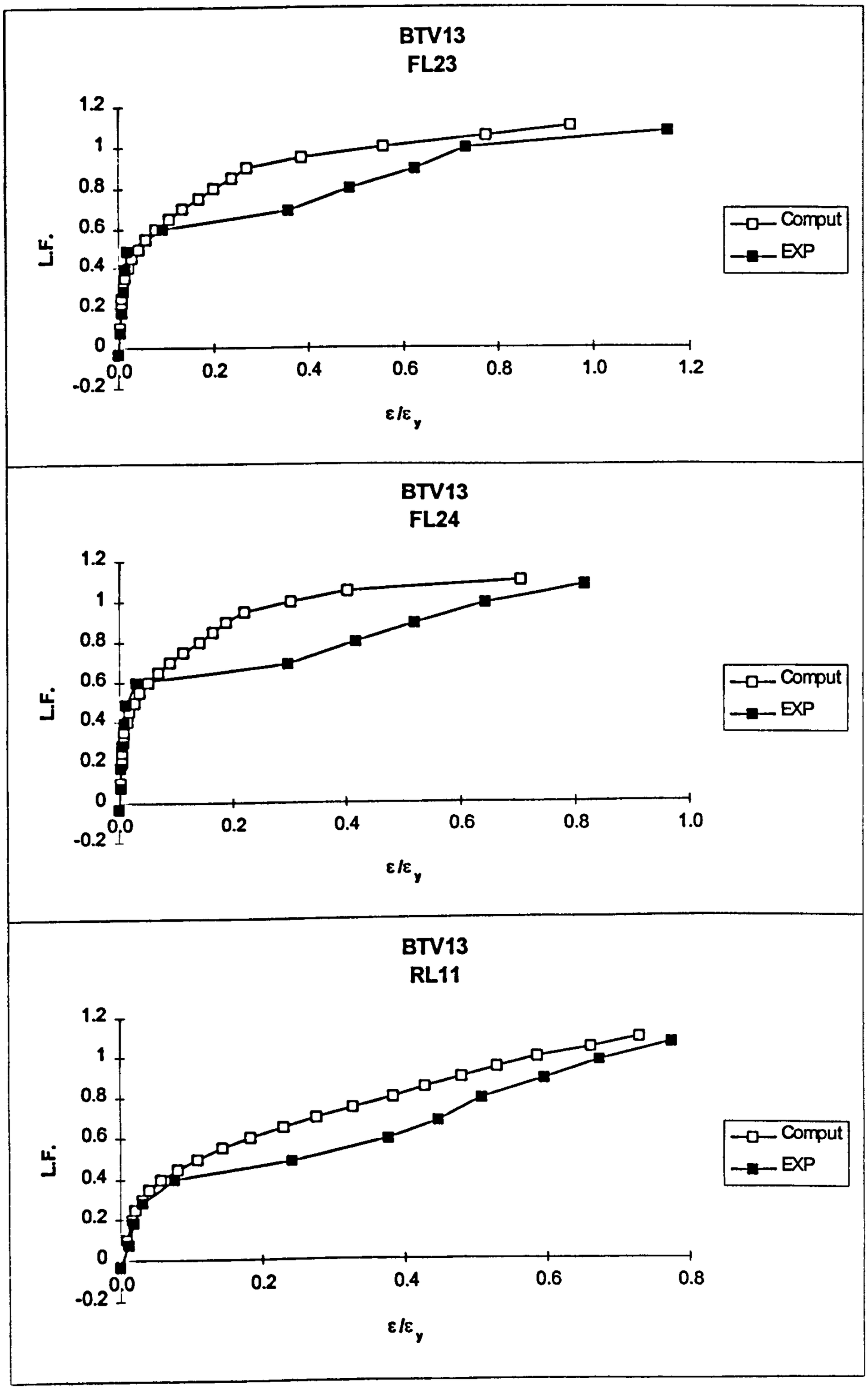
BTV13
FL23
L.F.
1.2
1
0.8
0.6
0.4
0.2
0
-0.2
0.0
0.2
0.4
0.6
0.8
1.0
1.2
ε/ε_y
Comput
EXP
BTV13
FL24
L.F.
1.2
1
0.8
0.6
0.4
0.2
0
-0.2
0.0
0.2
0.4
0.6
0.8
1.0
ε/ε_y
Comput
EXP
BTV13
RL11
L.F.
1.2
1
0.8
0.6
0.4
0.2
0
-0.2
0.0
0.2
0.4
0.6
0.8
ε/ε_y
Comput
EXP

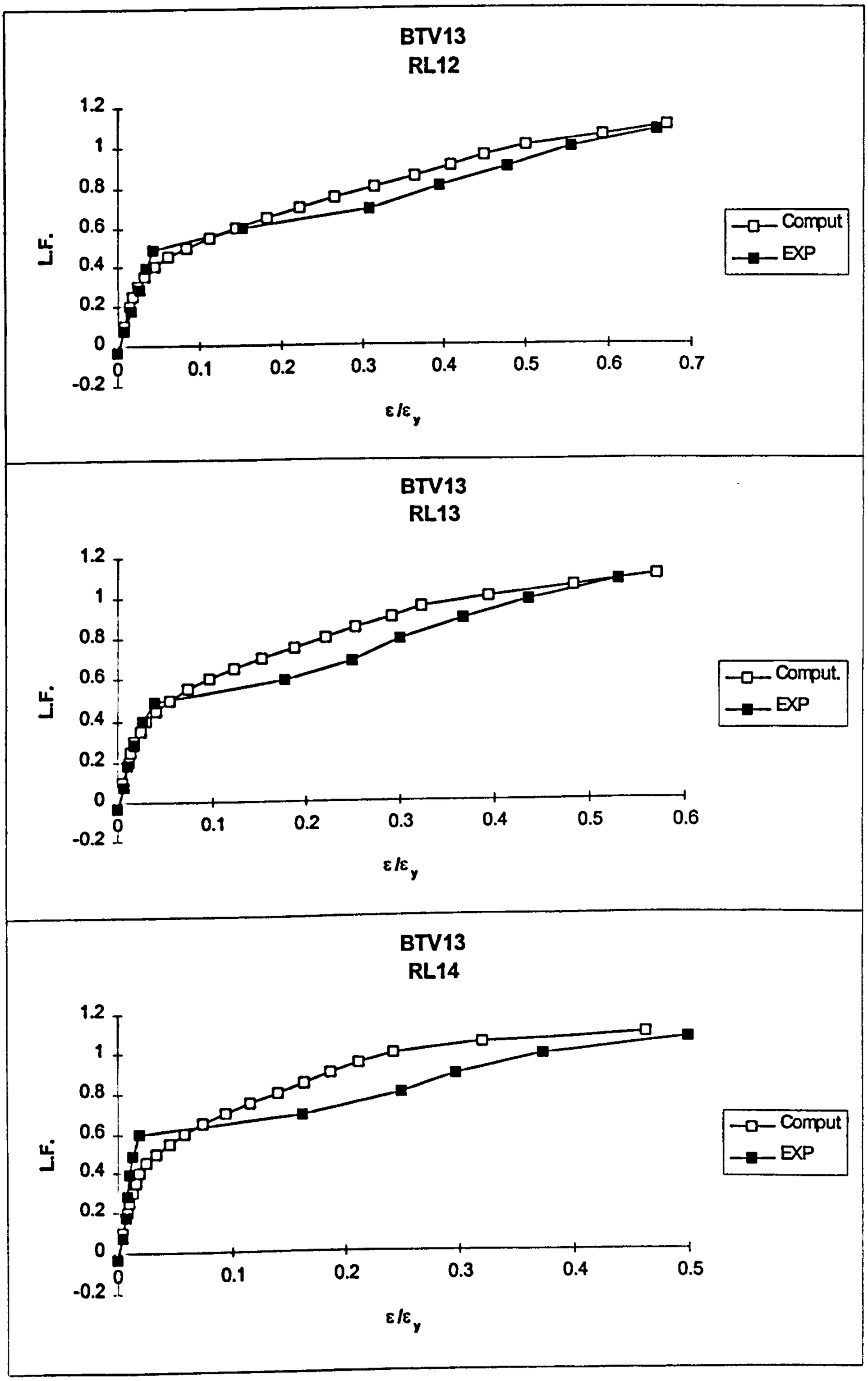
BTV13
RL12
L.F.
1.2
1
0.8
0.6
0.4
0.2
0
-0.2
0
0.1
0.2
0.3
0.4
0.5
0.6
0.7
ε/ε_y
Comput
EXP
BTV13
RL13
L.F.
1.2
1
0.8
0.6
0.4
0.2
0
-0.2
0
0.1
0.2
0.3
0.4
0.5
0.6
ε/ε_y
Comput.
EXP
BTV13
RL14
L.F.
1.2
1
0.8
0.6
0.4
0.2
0
-0.2
0
0.1
0.2
0.3
0.4
0.5
ε/ε_y
Comput
EXP

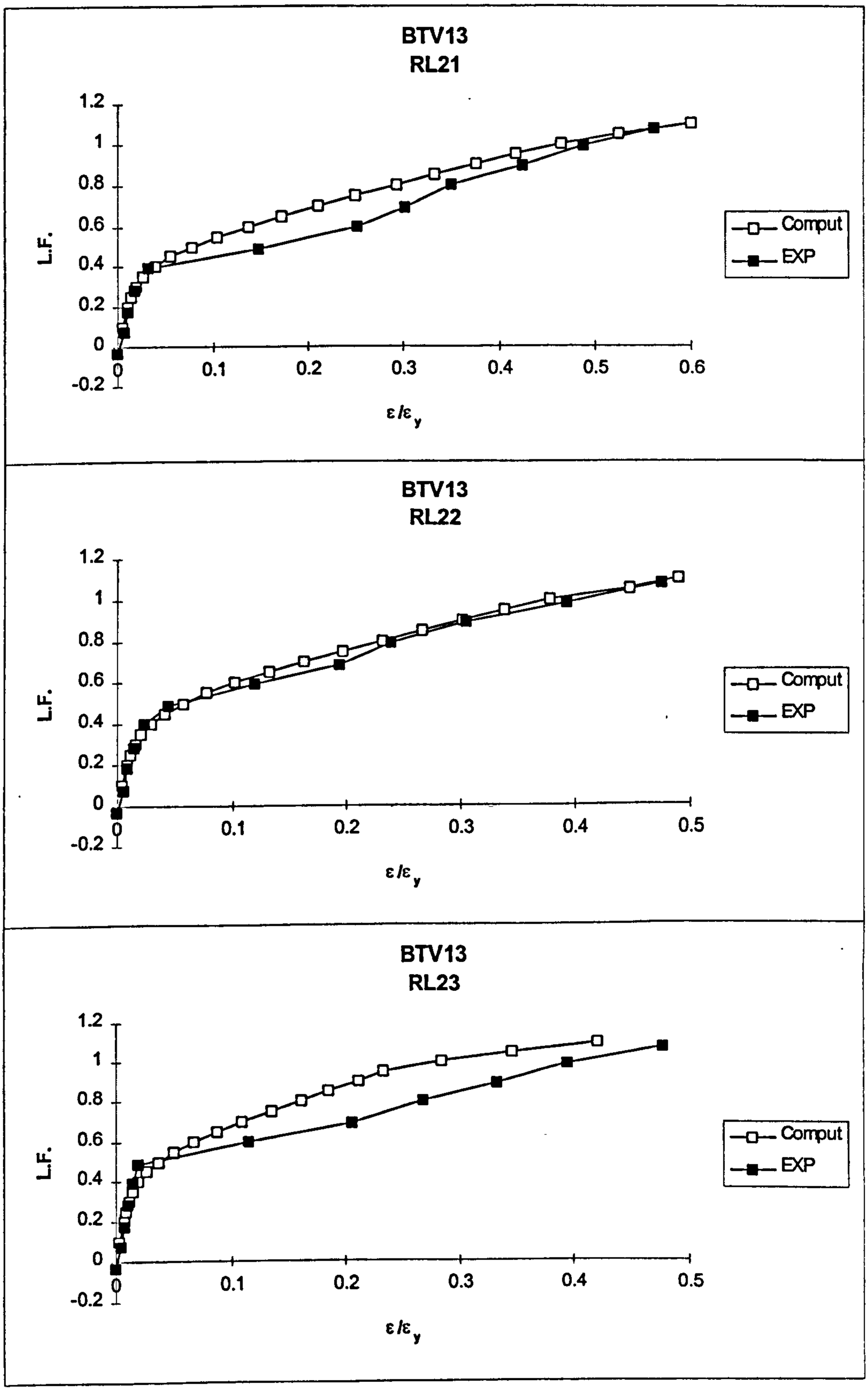
BTV13
RL21
L.F.
1.2
1
0.8
0.6
0.4
0.2
0
-0.2
0
0.1
0.2
0.3
0.4
0.5
0.6
ε/ε y
Comput
EXP
BTV13
RL22
L.F.
1.2
1
0.8
0.6
0.4
0.2
0
-0.2
0
0.1
0.2
0.3
0.4
0.5
ε/ε y
Comput
EXP
BTV13
RL23
L.F.
1.2
1
0.8
0.6
0.4
0.2
0
-0.2
0
0.1
0.2
0.3
0.4
0.5
ε/ε y
Comput
EXP

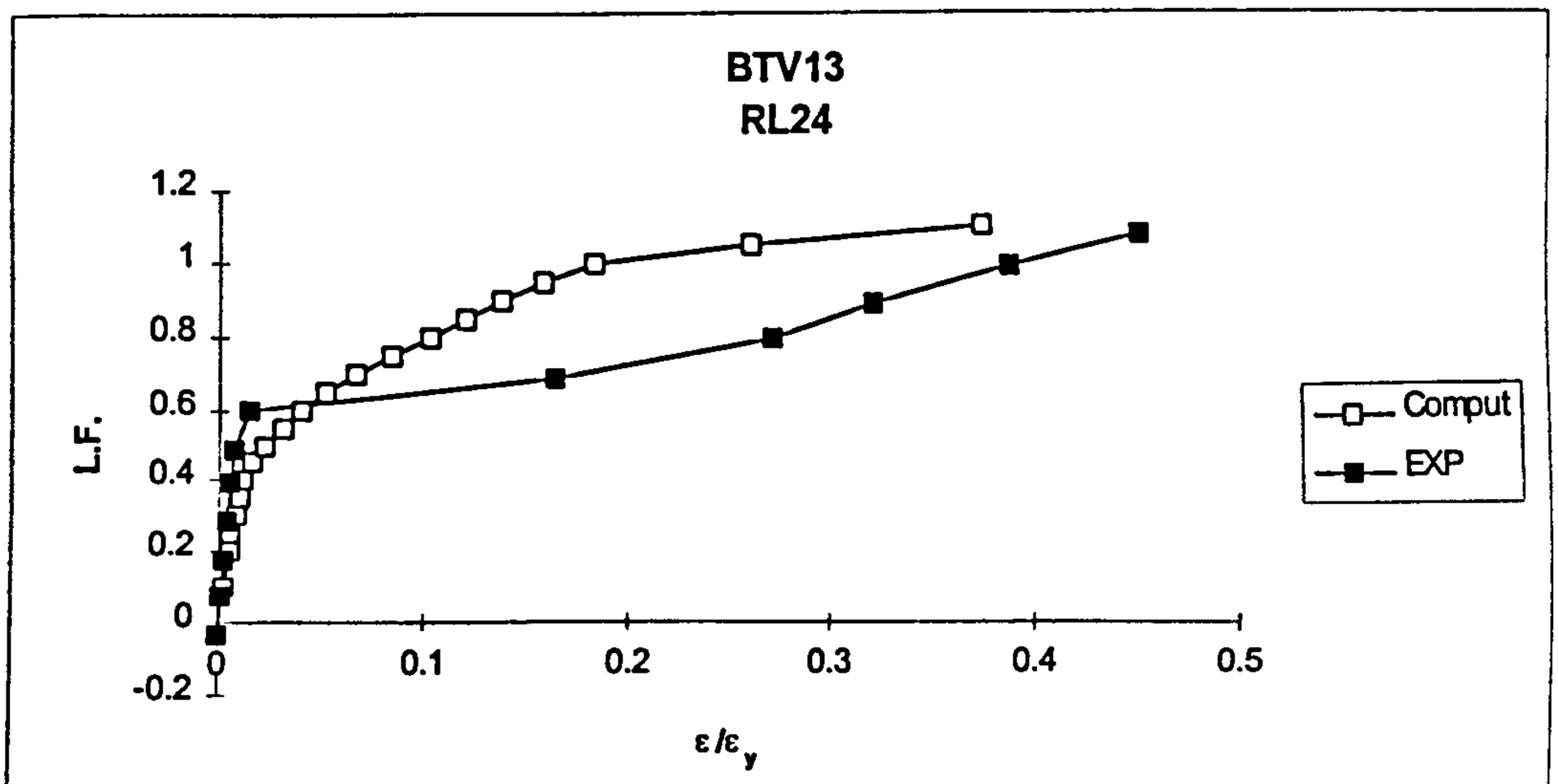
BTV13
RL24
L.F.
1.2
1
0.8
0.6
0.4
0.2
0
-0.2
0
0.1
0.2
0.3
0.4
0.5
Comput
EXP
ε/ε y

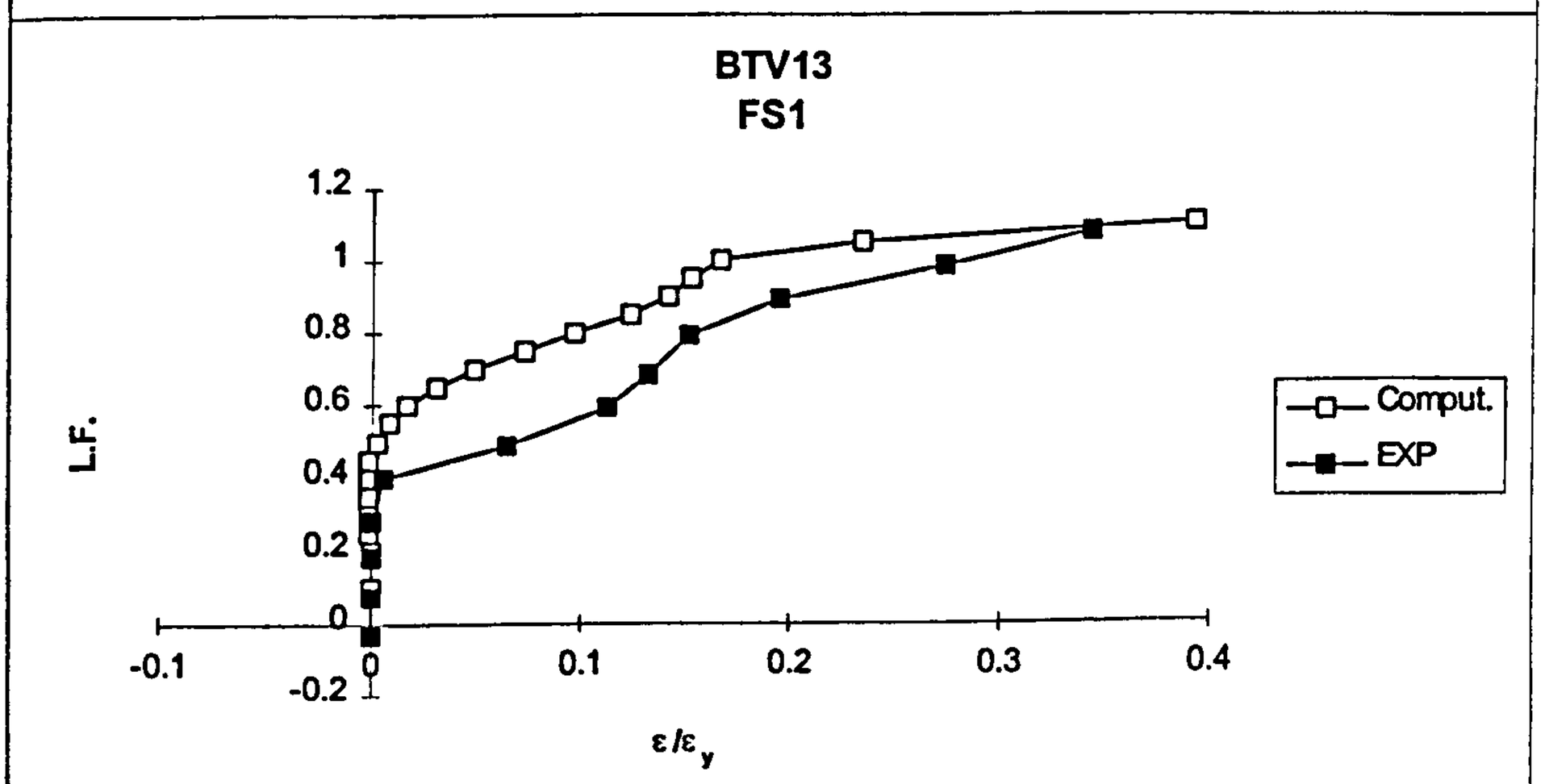
BTV13
FS1
L.F.
1.2
1
0.8
0.6
0.4
0.2
0
-0.2
-0.1
0
0.1
0.2
0.3
0.4
Comput.
EXP
ε/ε y

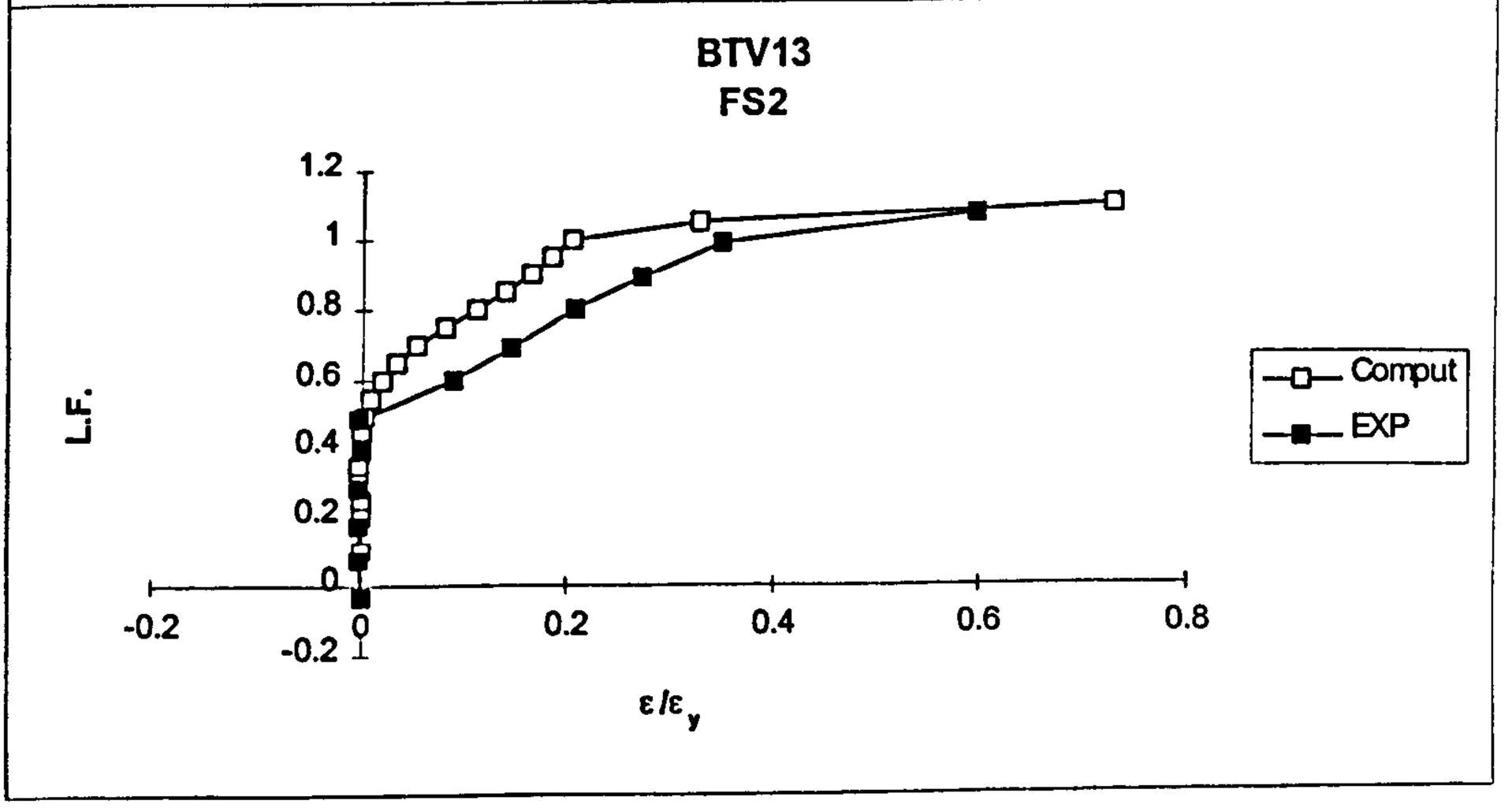
BTV13
FS2
L.F.
1.2
1
0.8
0.6
0.4
0.2
0
-0.2
-0.2
0
0.2
0.4
0.6
0.8
Comput
EXP
ε/ε y

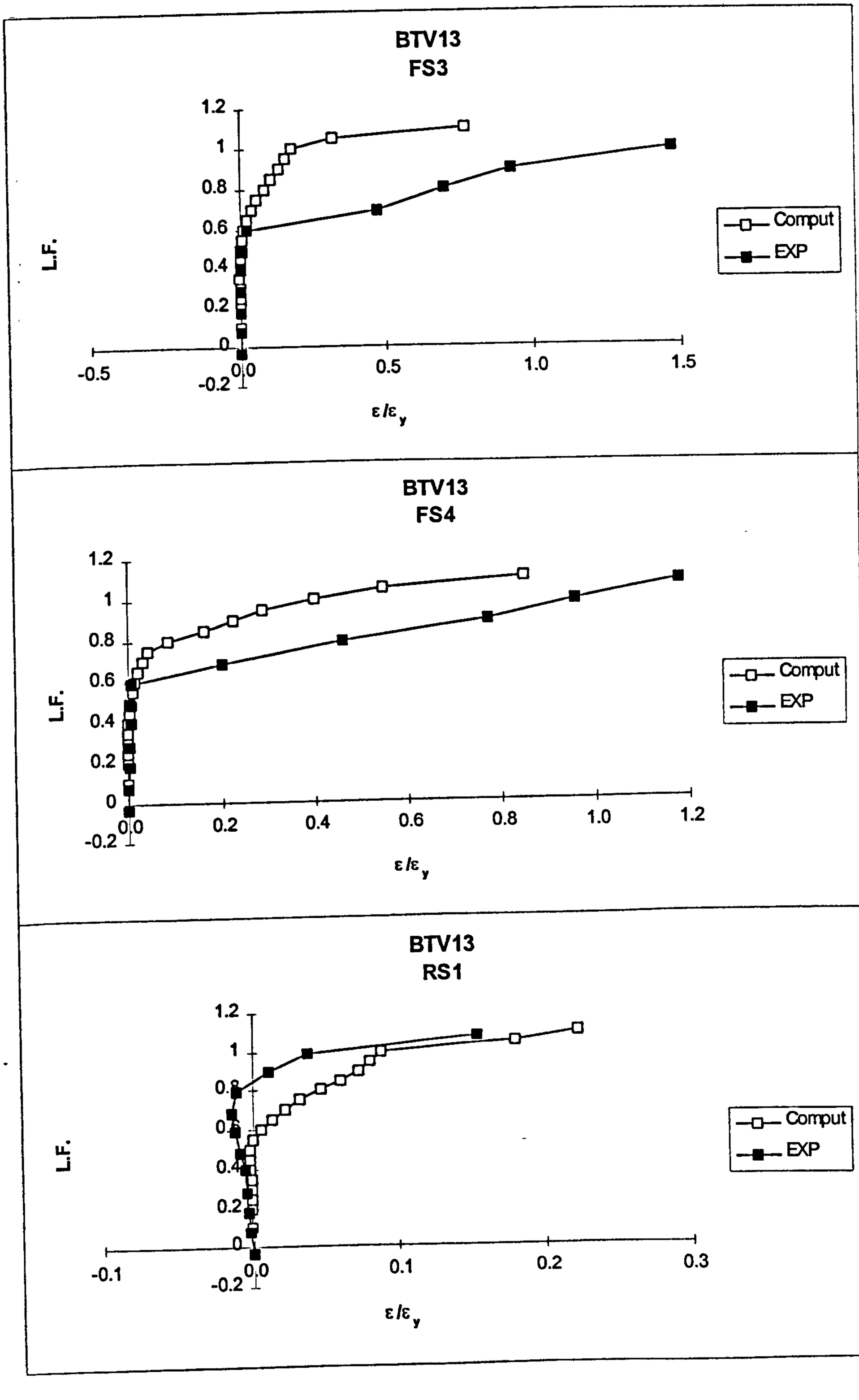
BTV13
FS3
L.F.
1.2
1
0.8
0.6
0.4
0.2
0
-0.2
-0.5
0.0
0.5
1.0
1.5
ε/ε_y
Comput
EXP
BTV13
FS4
L.F.
1.2
1
0.8
0.6
0.4
0.2
0
-0.2
0.0
0.2
0.4
0.6
0.8
1.0
1.2
ε/ε_y
Comput
EXP
BTV13
RS1
L.F.
1.2
1
0.8
0.6
0.4
0.2
0
-0.2
-0.1
0.0
0.1
0.2
0.3
ε/ε_y
Comput
EXP

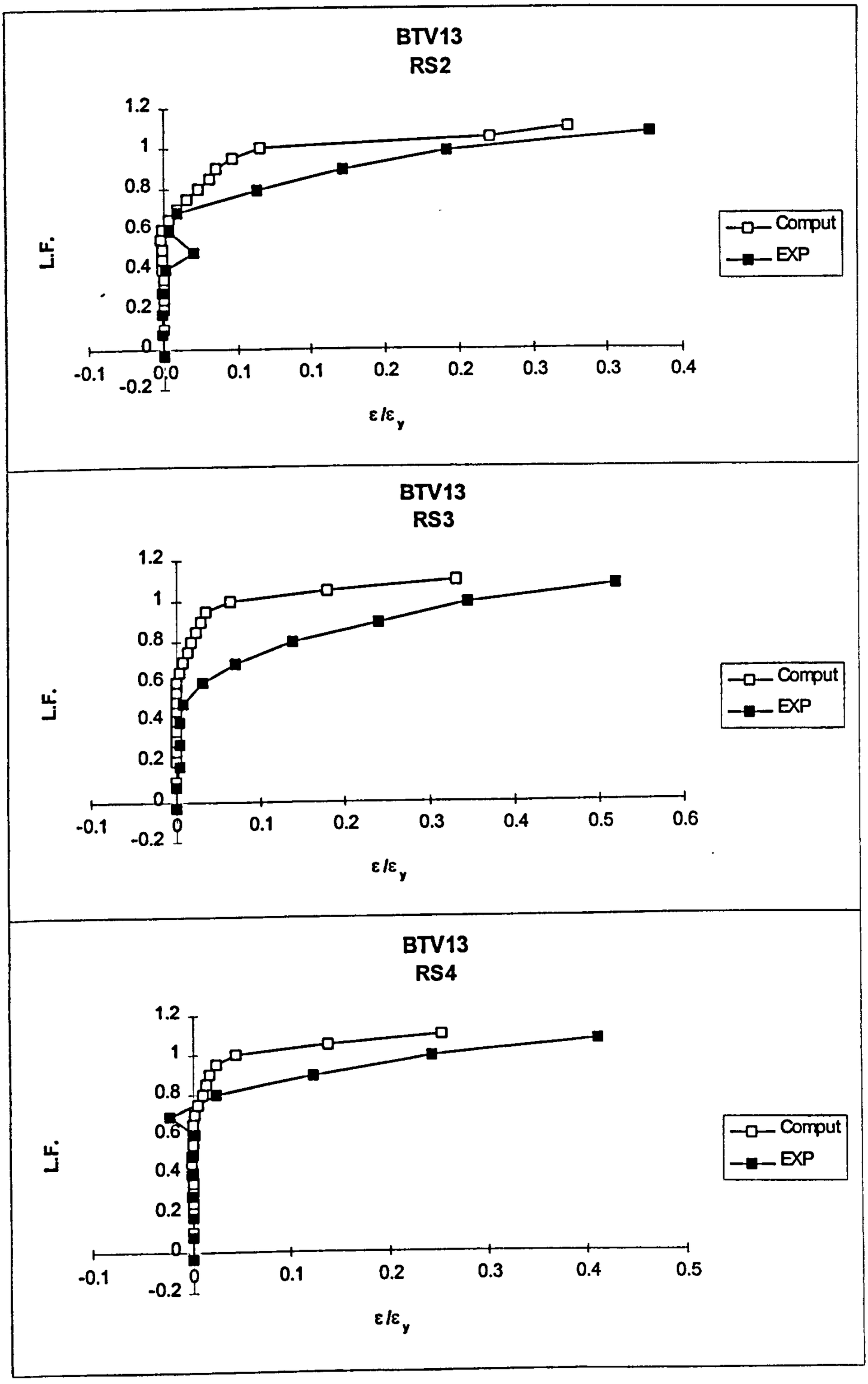
BTV13
RS2
L.F.
1.2
1
0.8
0.6
0.4
0.2
0
-0.2
-0.1
0.0
0.1
0.1
0.2
0.2
0.3
0.3
0.4
ε/ε_y
Comput
EXP
BTV13
RS3
L.F.
1.2
1
0.8
0.6
0.4
0.2
0
-0.2
-0.1
0
0.1
0.2
0.3
0.4
0.5
0.6
ε/ε_y
Comput
EXP
BTV13
RS4
L.F.
1.2
1
0.8
0.6
0.4
0.2
0
-0.2
-0.1
0
0.1
0.2
0.3
0.4
0.5
ε/ε_y
Comput
EXP

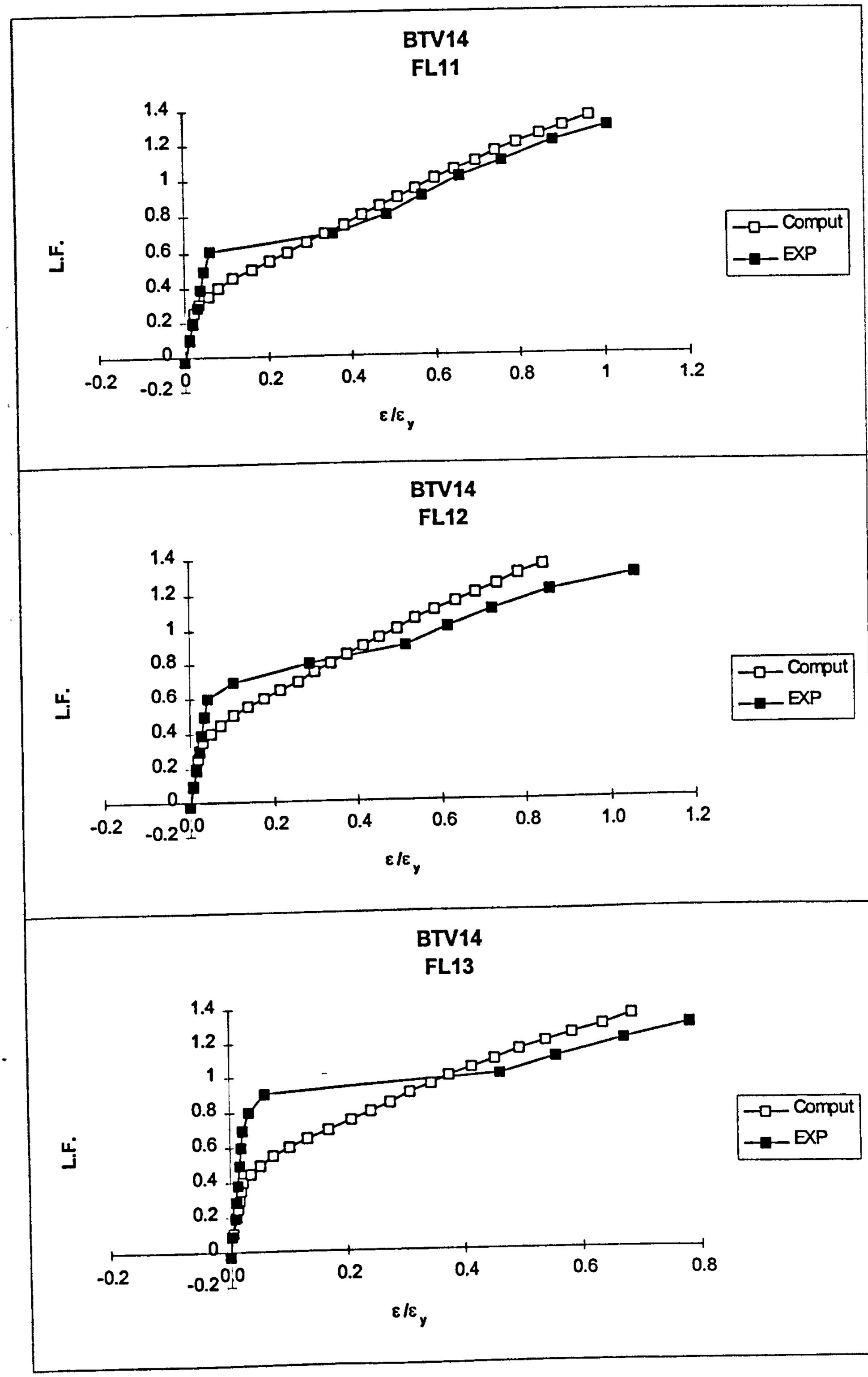
BTV14
FL11
L.F.
1.4
1.2
1
0.8
0.6
0.4
0.2
0
-0.2
-0.2
0
0.2
0.4
0.6
0.8
1
1.2
ε/ε y
Comput
EXP
BTV14
FL12
L.F.
1.4
1.2
1
0.8
0.6
0.4
0.2
0
-0.2
-0.2
0.0
0.2
0.4
0.6
0.8
1.0
1.2
ε/ε y
Comput
EXP
BTV14
FL13
L.F.
1.4
1.2
1
0.8
0.6
0.4
0.2
0
-0.2
-0.2
0.0
0.2
0.4
0.6
0.8
ε/ε y
Comput
EXP

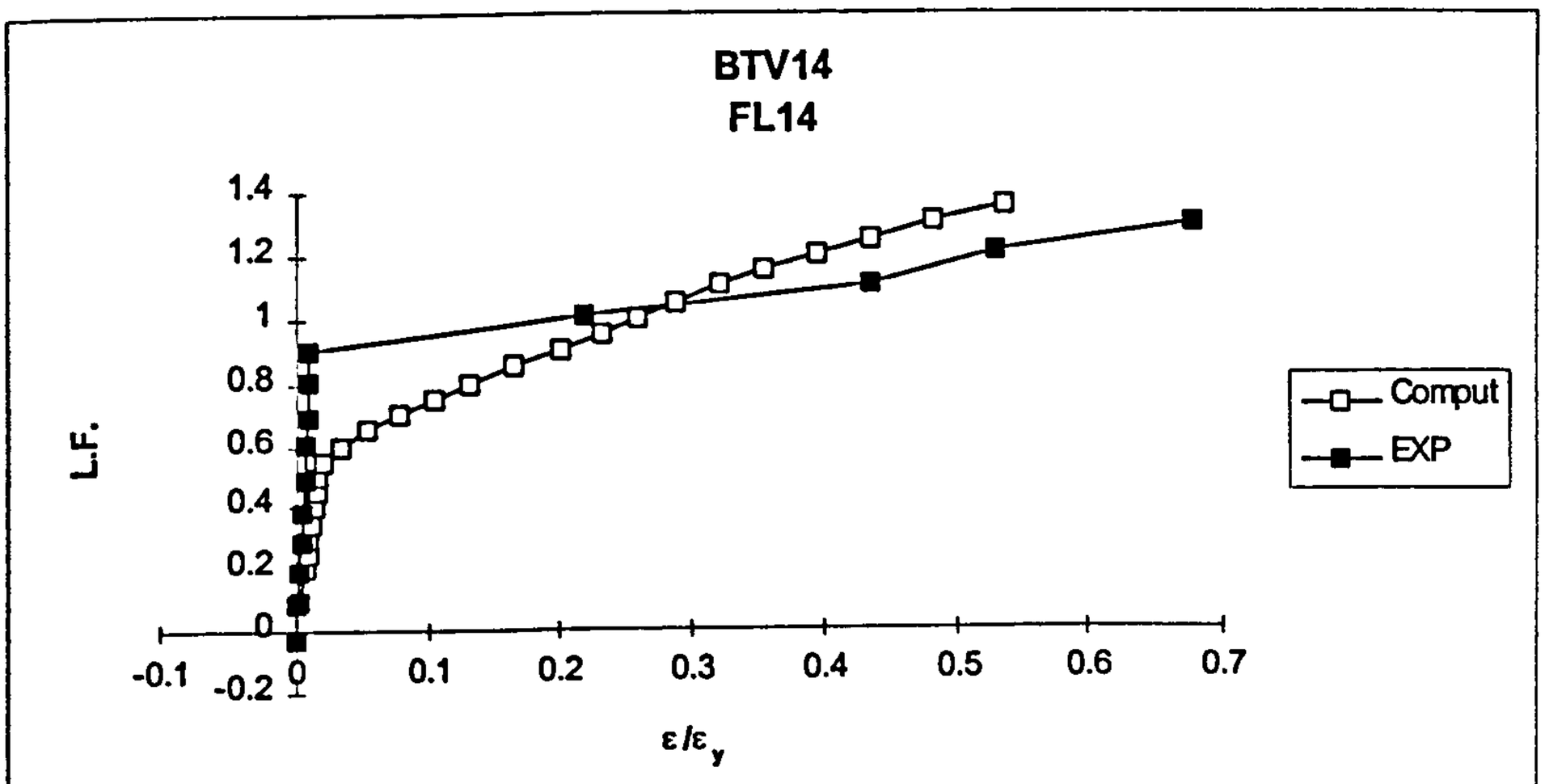
BTV14
FL14
L.F.
1.4
1.2
1
0.8
0.6
0.4
0.2
0
-0.2
-0.1
0
0.1
0.2
0.3
0.4
0.5
0.6
0.7
ε/ε_y
Comput
EXP

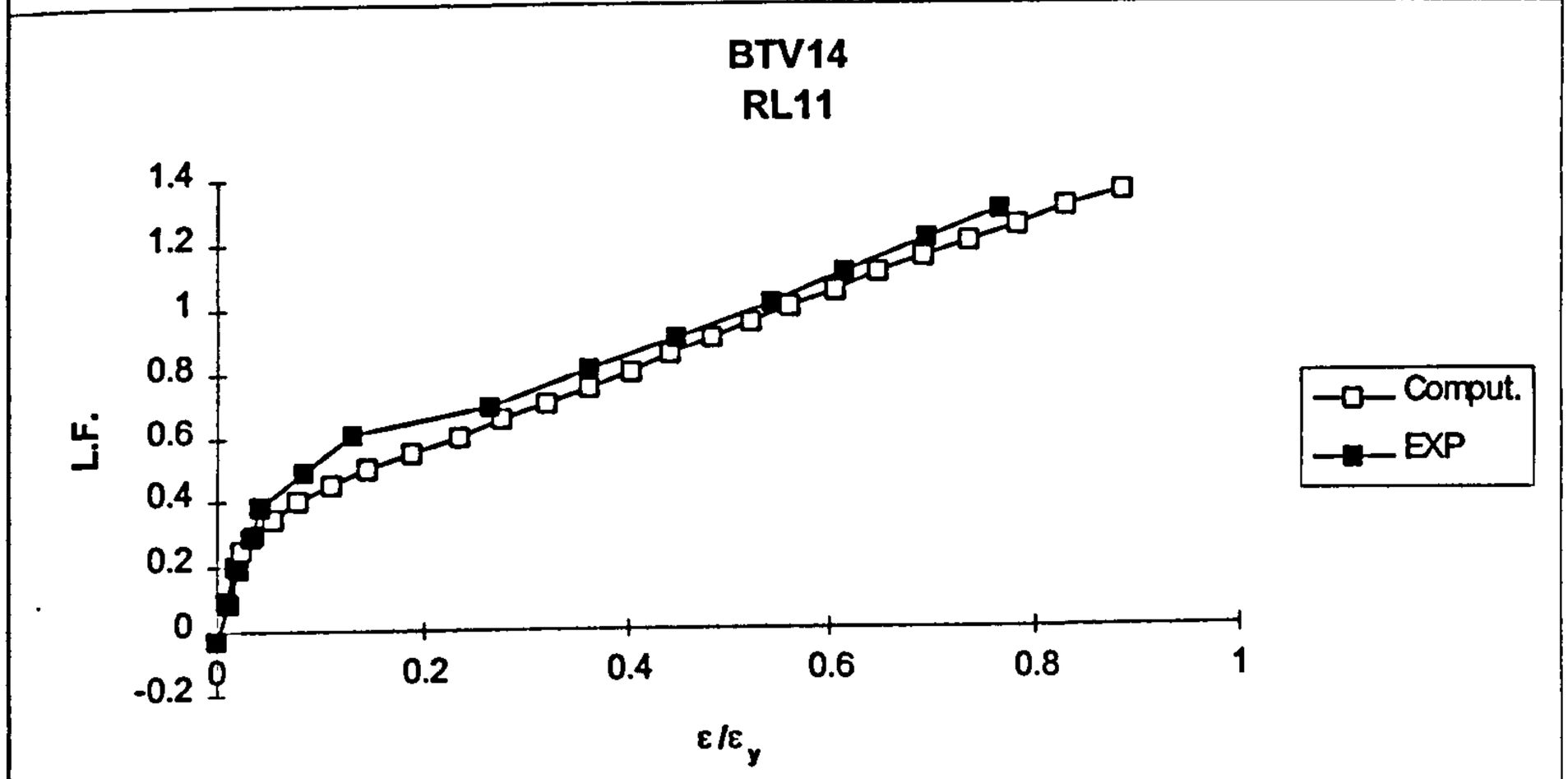
BTV14
RL11
L.F.
1.4
1.2
1
0.8
0.6
0.4
0.2
0
-0.2
0
0.2
0.4
0.6
0.8
1
ε/ε_y
Comput.
EXP

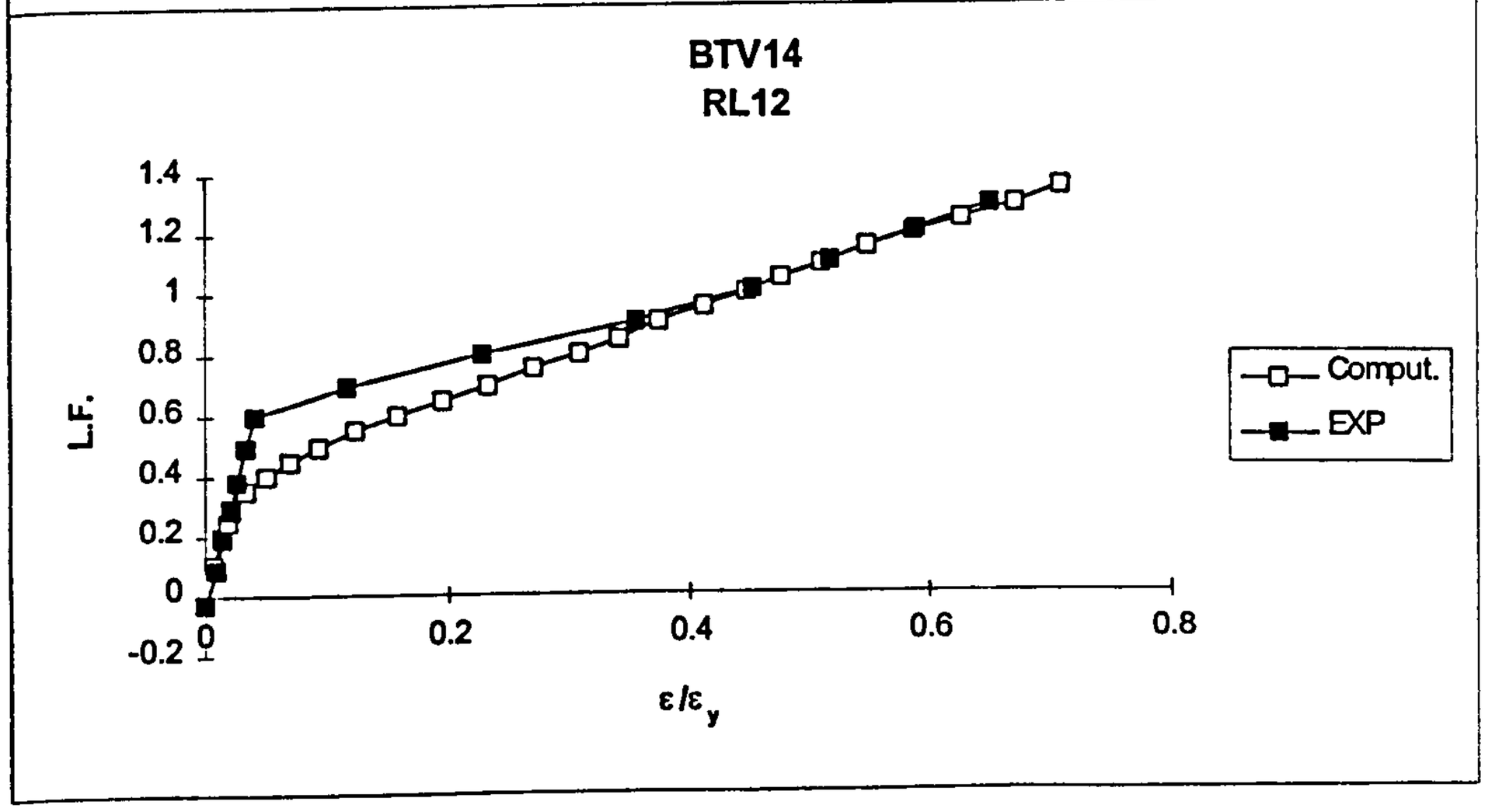
BTV14
RL12
L.F.
1.4
1.2
1
0.8
0.6
0.4
0.2
0
-0.2
0
0.2
0.4
0.6
0.8
ε/ε_y
Comput.
EXP

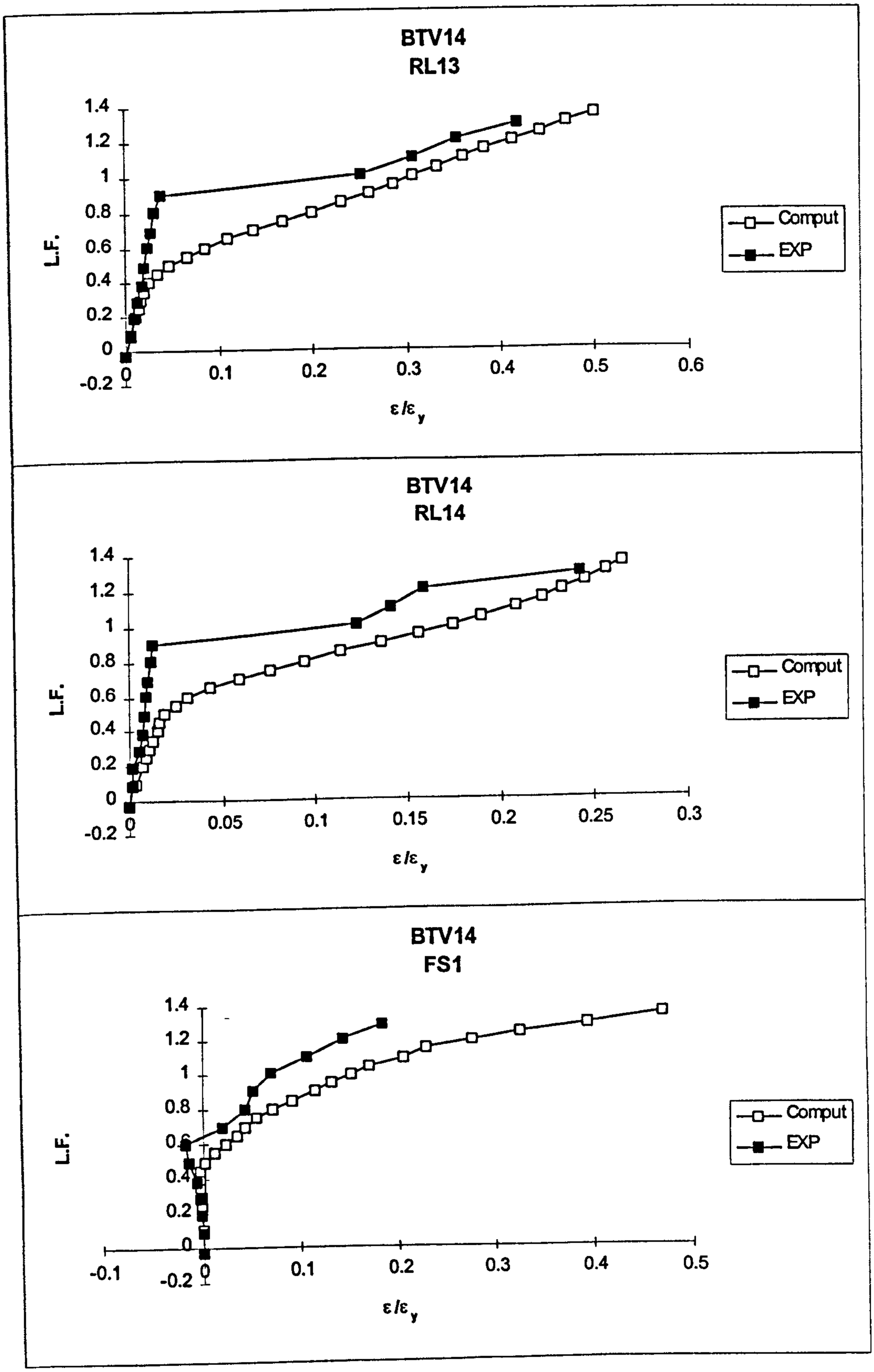
BTV14
RL13
L.F.
1.4
1.2
1
0.8
0.6
0.4
0.2
0
-0.2
0
0.1
0.2
0.3
0.4
0.5
0.6
ε/ε y
Comput
EXP
BTV14
RL14
L.F.
1.4
1.2
1
0.8
0.6
0.4
0.2
0
-0.2
0
0.05
0.1
0.15
0.2
0.25
0.3
ε/ε y
Comput
EXP
BTV14
FS1
L.F.
1.4
1.2
1
0.8
0.6
0.4
0.2
0
-0.2
-0.1
0
0.1
0.2
0.3
0.4
0.5
ε/ε y
Comput
EXP

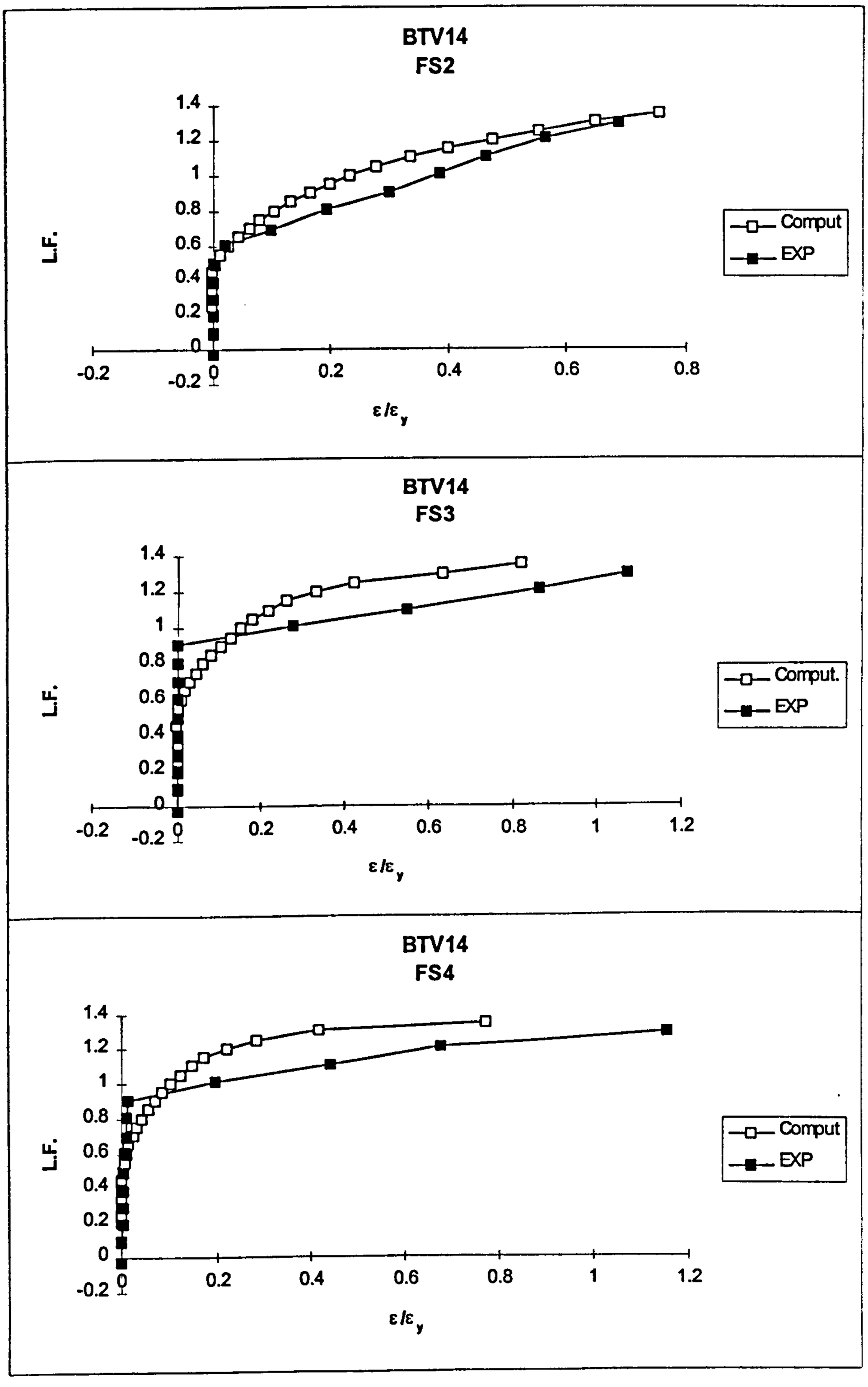
BTV14
FS2
L.F.
1.4
1.2
1
0.8
0.6
0.4
0.2
0
-0.2
-0.2
0
0.2
0.4
0.6
0.8
ε/ε_y
Comput
EXP
BTV14
FS3
L.F.
1.4
1.2
1
0.8
0.6
0.4
0.2
0
-0.2
-0.2
0
0.2
0.4
0.6
0.8
1
1.2
ε/ε_y
Comput.
EXP
BTV14
FS4
L.F.
1.4
1.2
1
0.8
0.6
0.4
0.2
0
-0.2
0
0.2
0.4
0.6
0.8
1
1.2
ε/ε_y
Comput
EXP

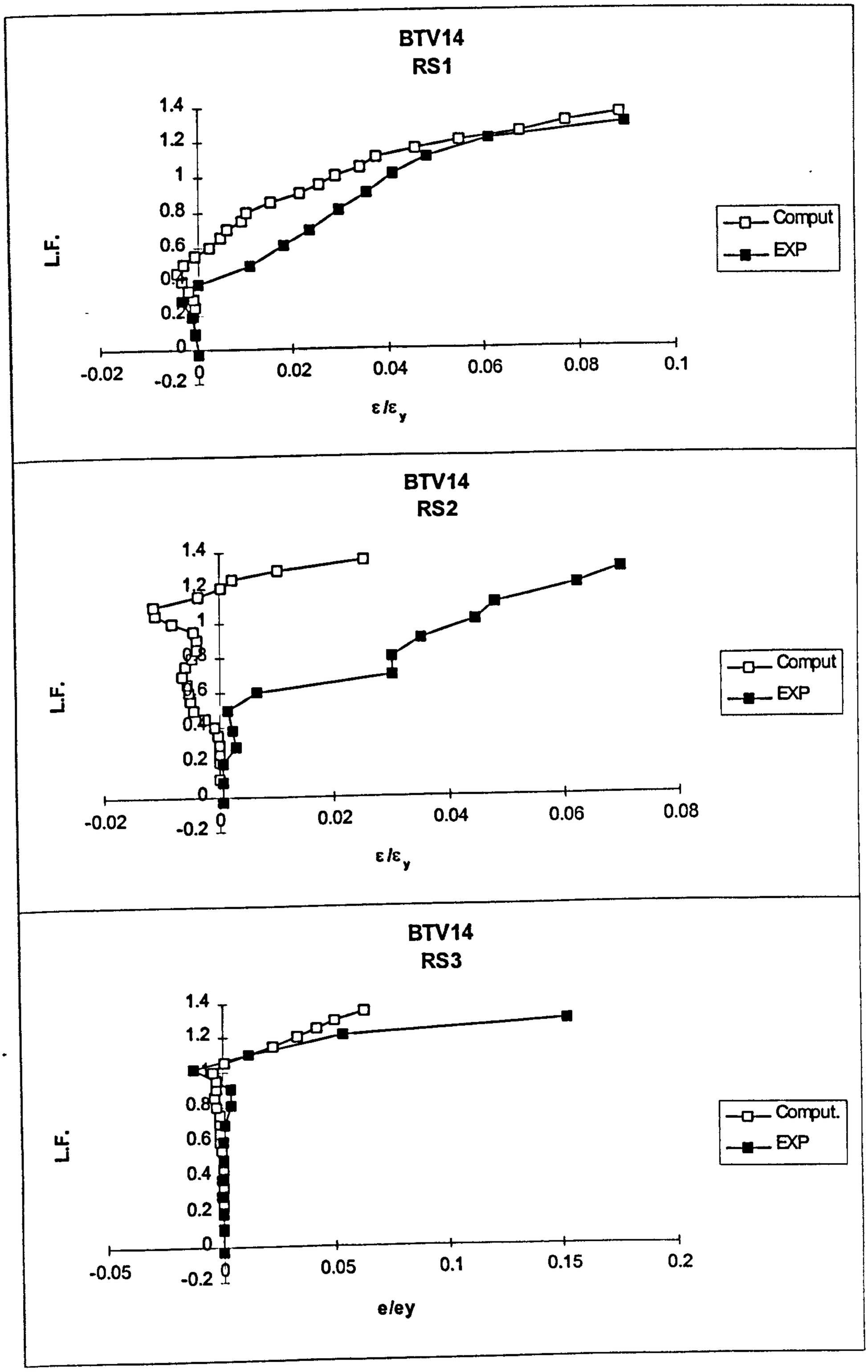
BTV14
RS1
L.F.
1.4
1.2
1
0.8
0.6
0.4
0.2
0
-0.2
-0.02
0
0.02
0.04
0.06
0.08
0.1
ε/ε_y
Comput
EXP
BTV14
RS2
L.F.
1.4
1.2
1
0.8
0.6
0.4
0.2
0
-0.2
-0.02
0
0.02
0.04
0.06
0.08
ε/ε_y
Comput
EXP
BTV14
RS3
L.F.
1.4
1.2
0.8
0.6
0.4
0.2
0
-0.2
-0.05
0
0.05
0.1
0.15
0.2
e/ey
Comput.
EXP

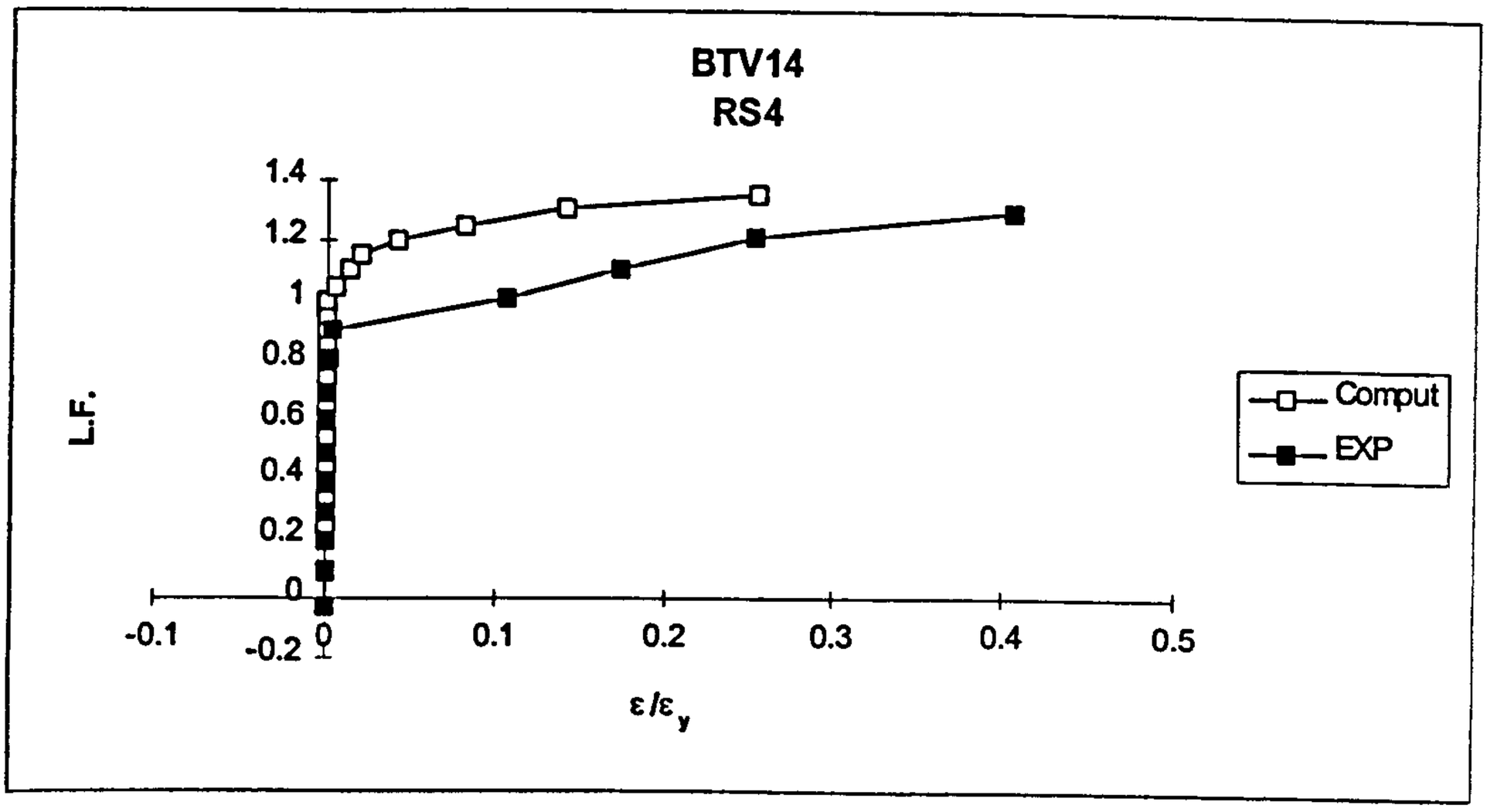
BTV14
RS4
L.F.
1.4
1.2
1
0.8
0.6
0.4
0.2
0
-0.1
-0.2
0.1
0.2
0.3
0.4
0.5
ε/ε_y
Comput
EXP

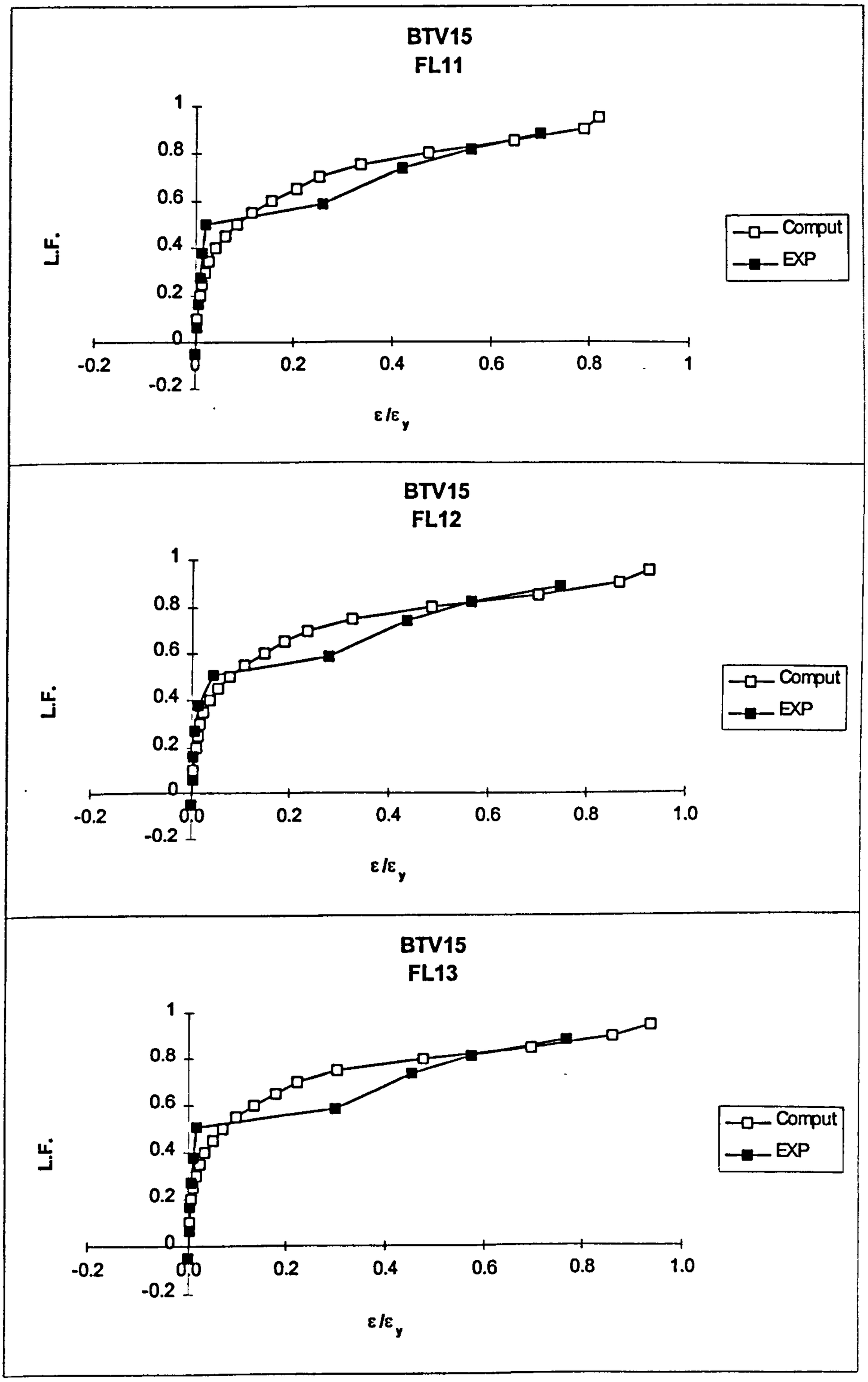
BTV15
FL11
L.F.
1
0.8
0.6
0.4
0.2
0
-0.2
-0.2
0
0.2
0.4
0.6
0.8
1
ε/ε_y
Comput
EXP
BTV15
FL12
L.F.
1
0.8
0.6
0.4
0.2
0
-0.2
-0.2
0.0
0.2
0.4
0.6
0.8
1.0
ε/ε_y
Comput
EXP
BTV15
FL13
L.F.
1
0.8
0.6
0.4
0.2
0
-0.2
-0.2
0.0
0.2
0.4
0.6
0.8
1.0
ε/ε_y
Comput
EXP

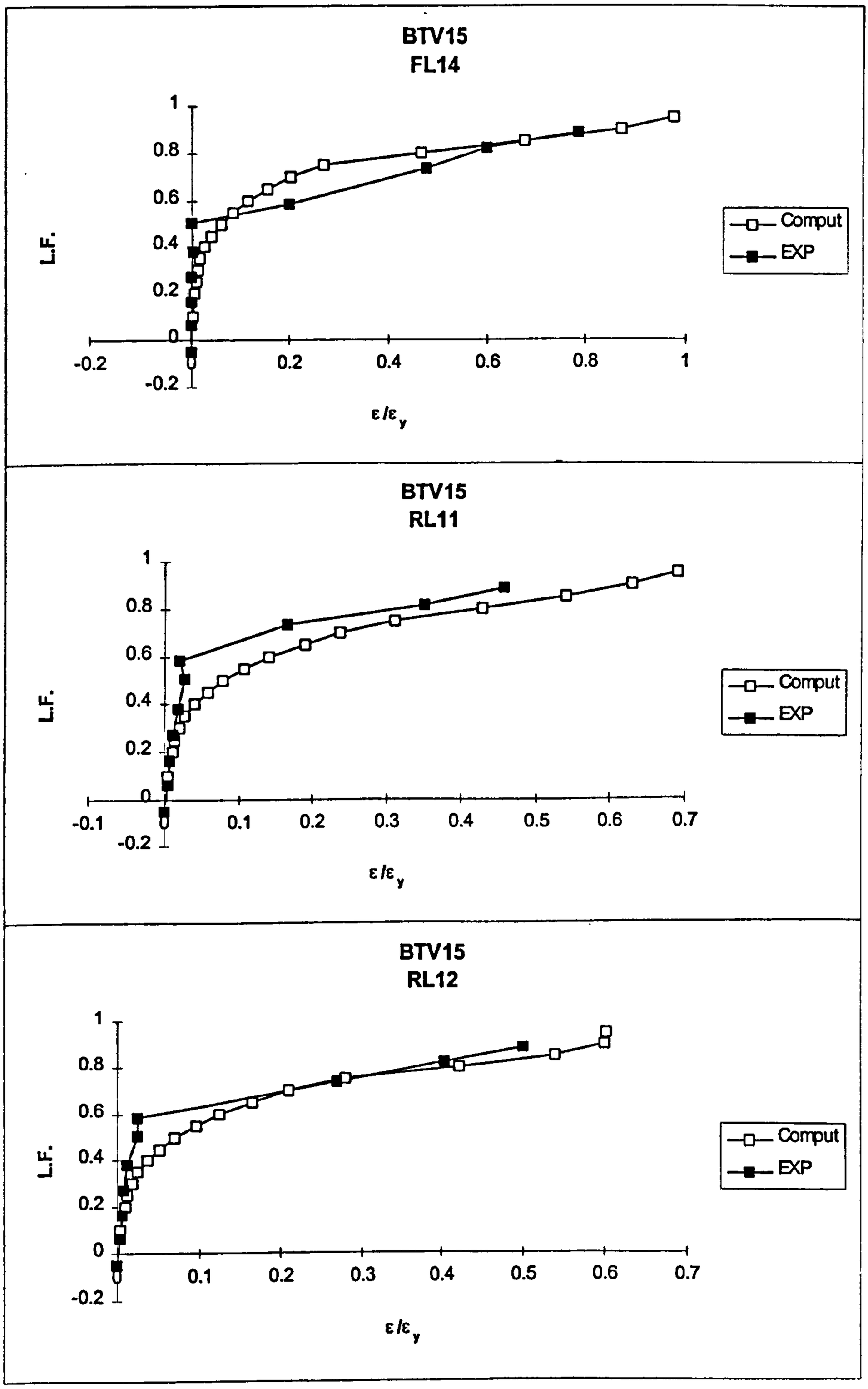
BTV15
FL14
L.F.
ε/ε_y
Comput
EXP
BTV15
RL11
L.F.
ε/ε_y
Comput
EXP
BTV15
RL12
L.F.
ε/ε_y
Comput
EXP

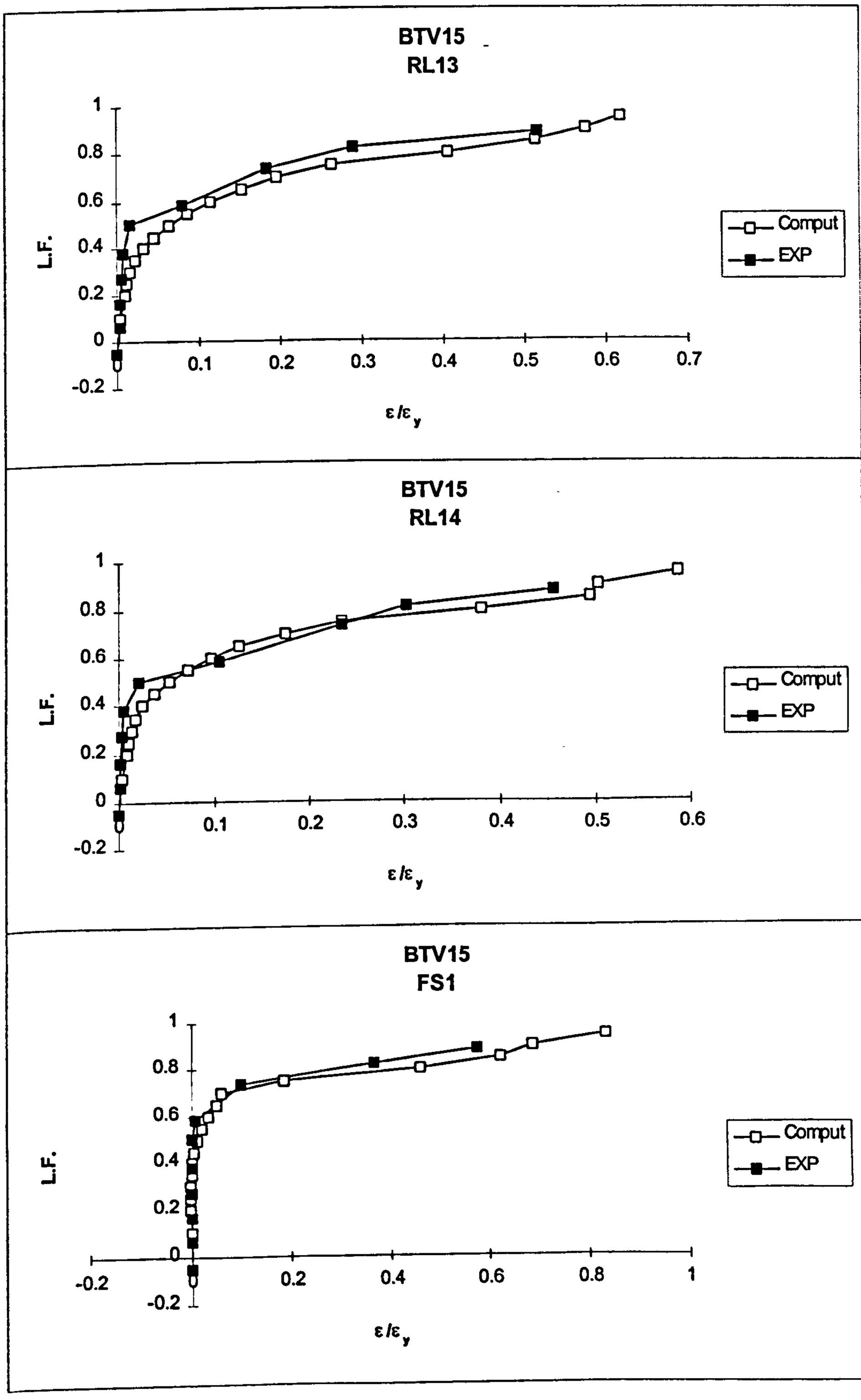
BTV15
RL13
L.F.
1
0.8
0.6
0.4
0.2
0
-0.2
0.1
0.2
0.3
0.4
0.5
0.6
0.7
ε/ε y
Comput
EXP
BTV15
RL14
L.F.
1
0.8
0.6
0.4
0.2
0
-0.2
0.1
0.2
0.3
0.4
0.5
0.6
ε/ε y
Comput
EXP
BTV15
FS1
L.F.
1
0.8
0.6
0.4
0.2
0
-0.2
0.2
0.4
0.6
0.8
1
ε/ε y
Comput
EXP

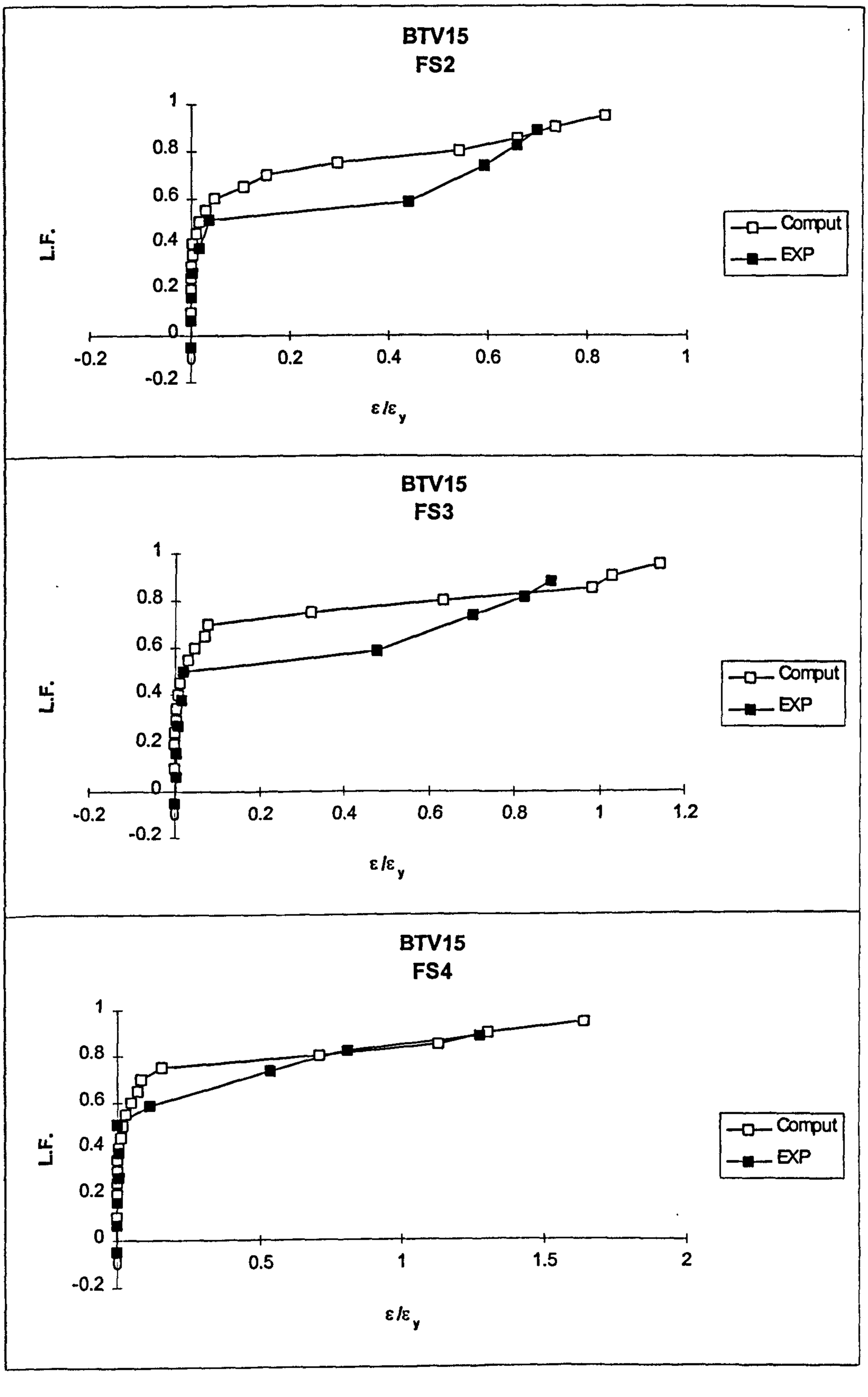
BTV15
FS2
L.F.
1
0.8
0.6
0.4
0.2
0
-0.2
-0.2
0.2
0.4
0.6
0.8
1
ε/ε y
Comput
EXP
BTV15
FS3
L.F.
1
0.8
0.6
0.4
0.2
0
-0.2
-0.2
0.2
0.4
0.6
0.8
1
1.2
ε/ε y
Comput
EXP
BTV15
FS4
L.F.
1
0.8
0.6
0.4
0.2
0
-0.2
0
0.5
1
1.5
2
ε/ε y
Comput
EXP

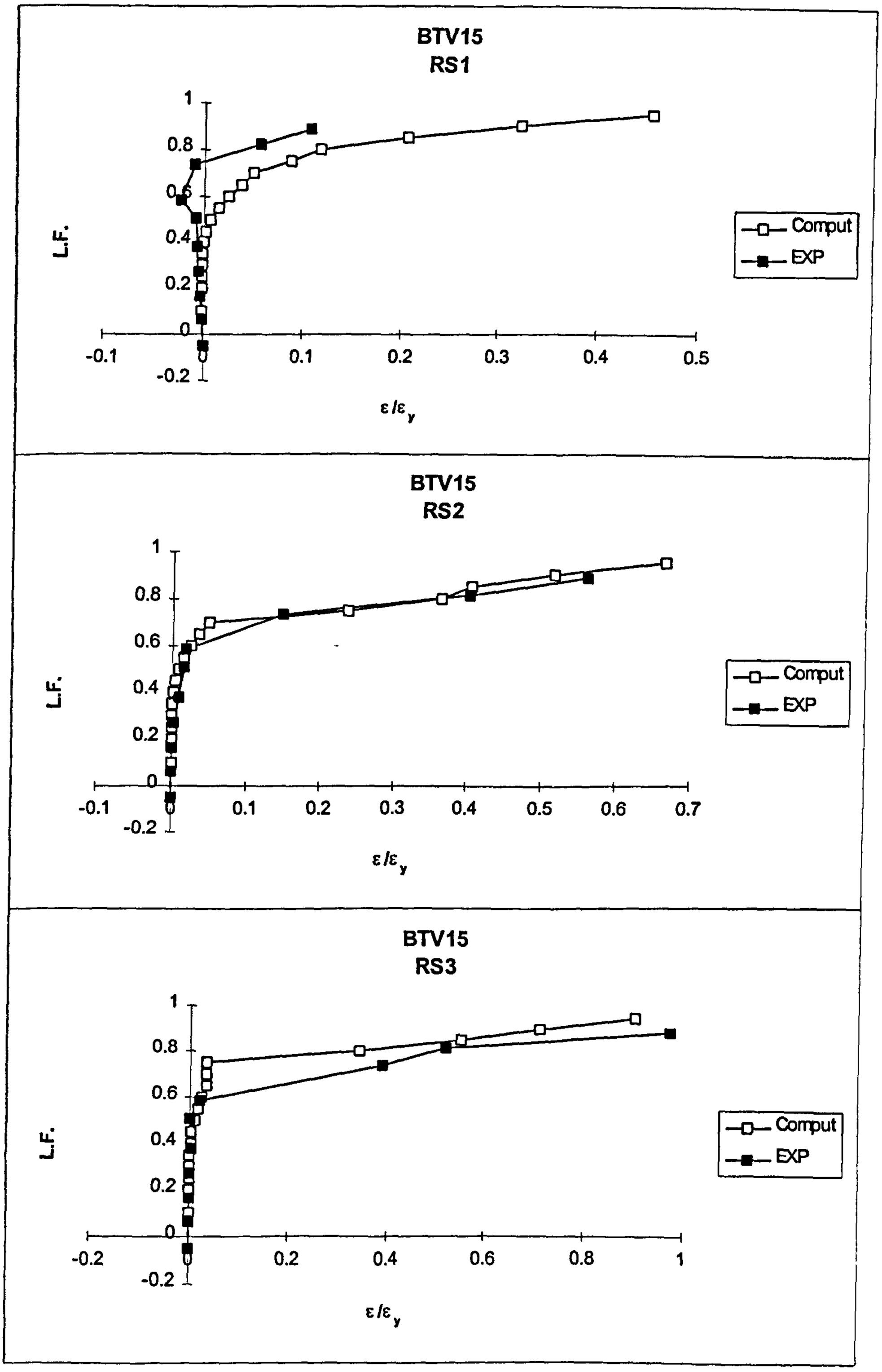
BTV15
RS1
L.F.
1
0.8
0.6
0.4
0.2
0
-0.2
-0.1
0
0.1
0.2
0.3
0.4
0.5
ε/ε_y
Comput
EXP
BTV15
RS2
L.F.
1
0.8
0.6
0.4
0.2
0
-0.2
-0.1
0
0.1
0.2
0.3
0.4
0.5
0.6
0.7
ε/ε_y
Comput
EXP
BTV15
RS3
L.F.
1
0.8
0.6
0.4
0.2
0
-0.2
-0.2
0
0.2
0.4
0.6
0.8
1
ε/ε_y
Comput
EXP

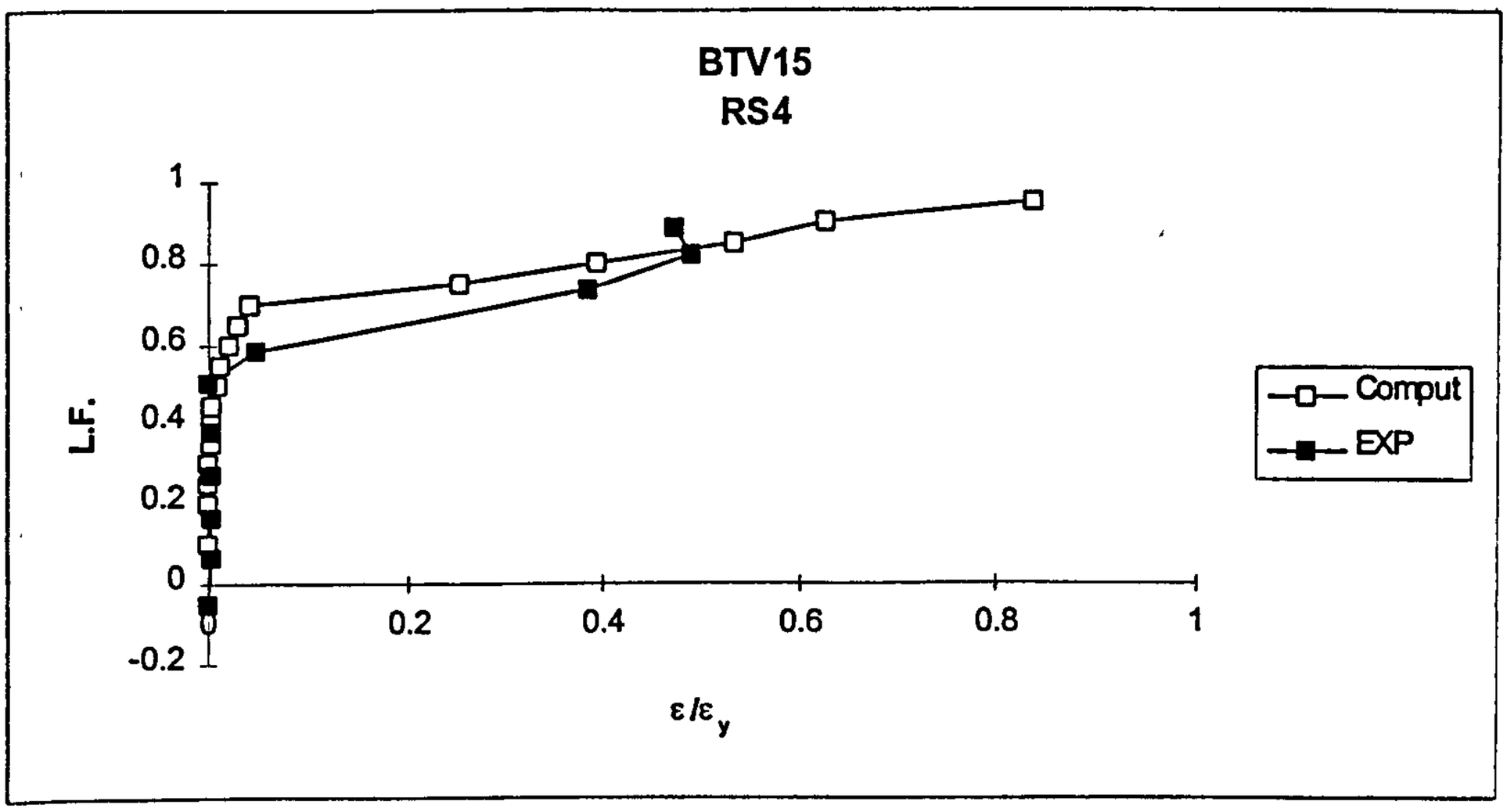
BTV15
RS4
L.F.
1
0.8
0.6
0.4
0.2
0
-0.2
0
0.2
0.4
0.6
0.8
1
Comput
EXP
ε/ε_y

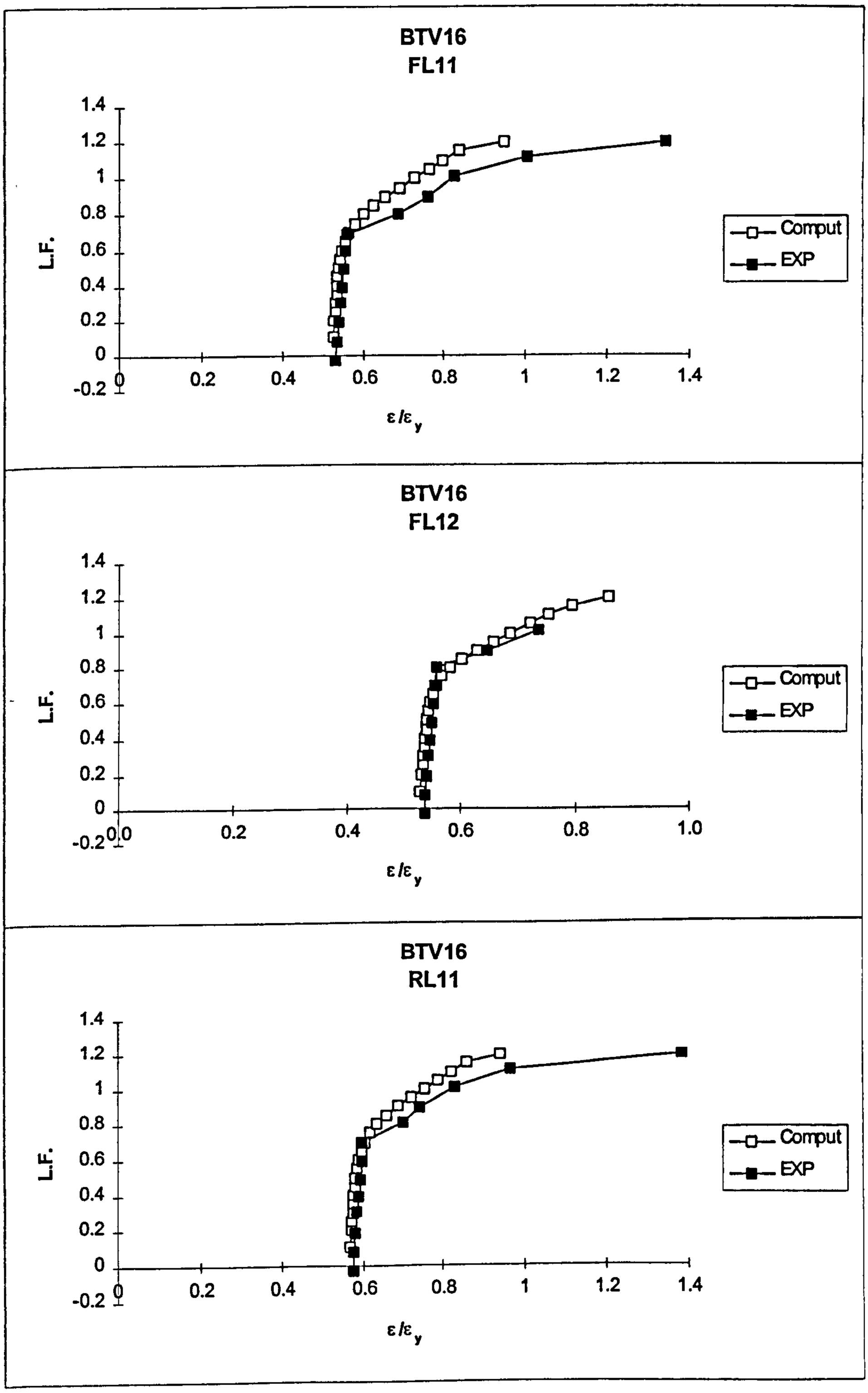
BTV16
FL11
L.F.
1.4
1.2
1
0.8
0.6
0.4
0.2
0
-0.2
0
0.2
0.4
0.6
0.8
1
1.2
1.4
ε/ε_y
Comput
EXP
BTV16
FL12
L.F.
1.4
1.2
1
0.8
0.6
0.4
0.2
0
-0.2
0.0
0.2
0.4
0.6
0.8
1.0
ε/ε_y
Comput
EXP
BTV16
RL11
L.F.
1.4
1.2
1
0.8
0.6
0.4
0.2
0
-0.2
0
0.2
0.4
0.6
0.8
1
1.2
1.4
ε/ε_y
Comput
EXP

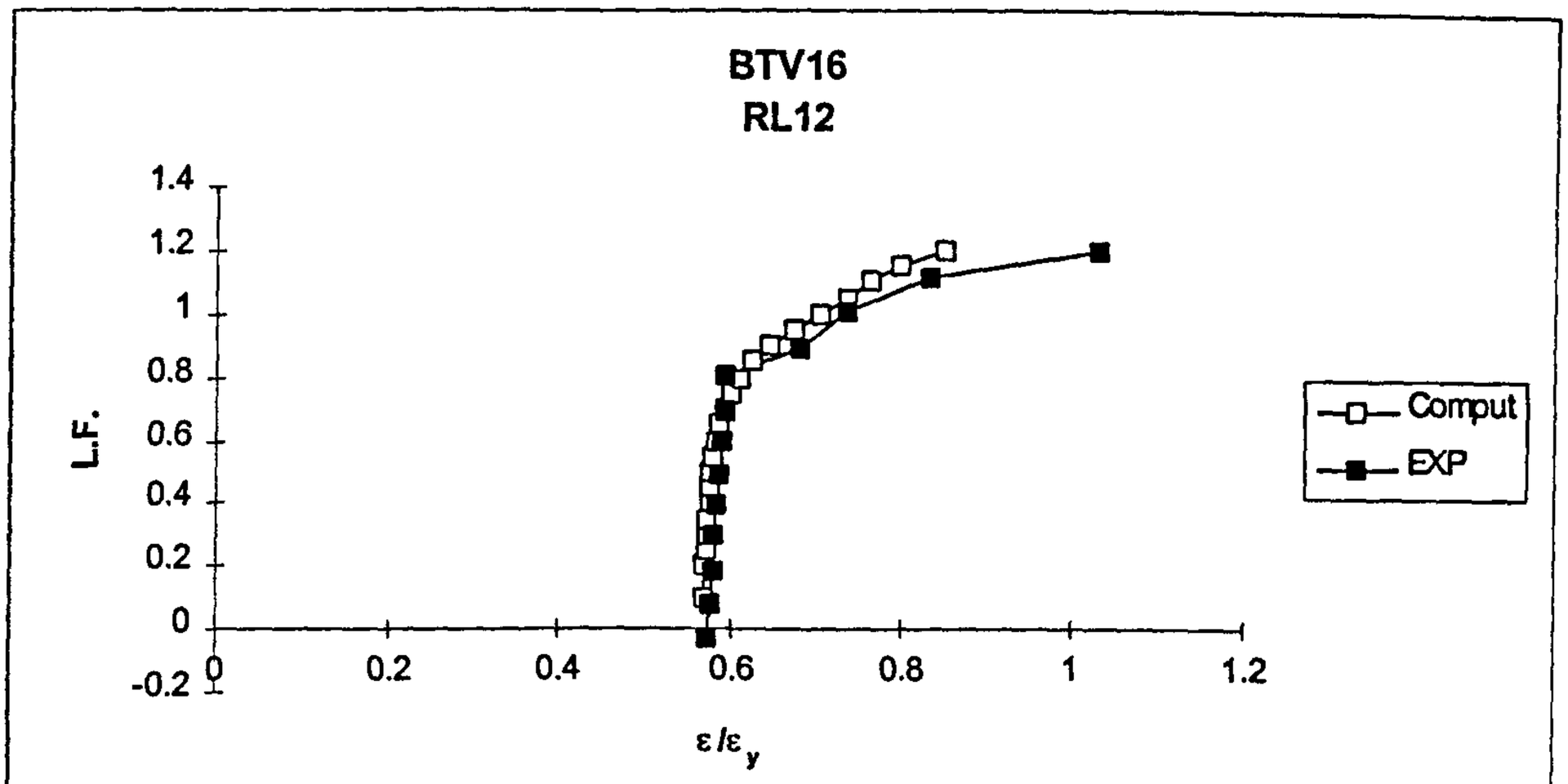
BTV16
RL12
L.F.
1.4
1.2
1
0.8
0.6
0.4
0.2
0
-0.2
0
0.2
0.4
0.6
0.8
1
1.2
ε/ε_y
Comput
EXP

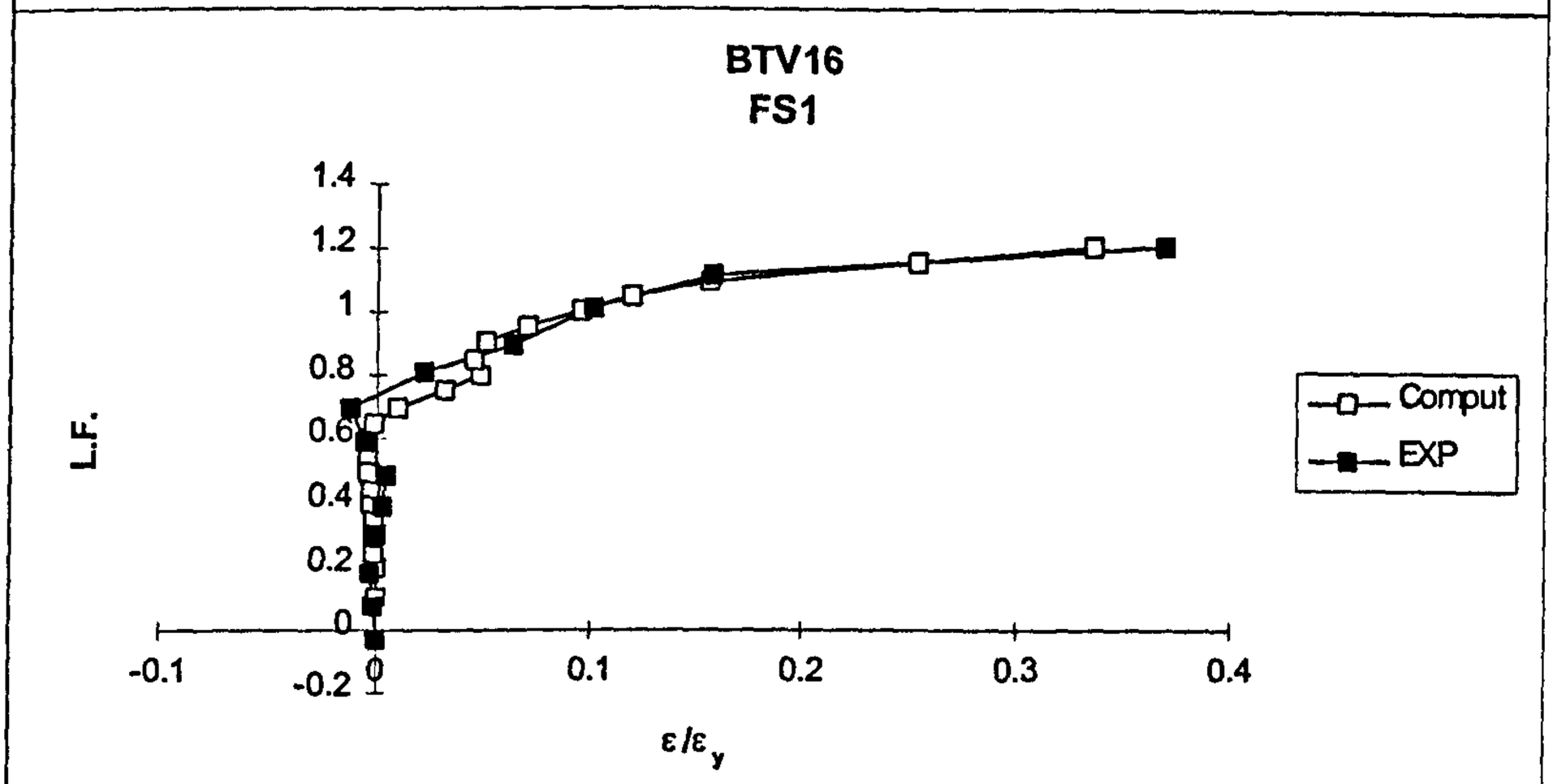
BTV16
FS1
L.F.
1.4
1.2
1
0.8
0.6
0.4
0.2
0
-0.2
-0.1
0
0.1
0.2
0.3
0.4
ε/ε_y
Comput
EXP

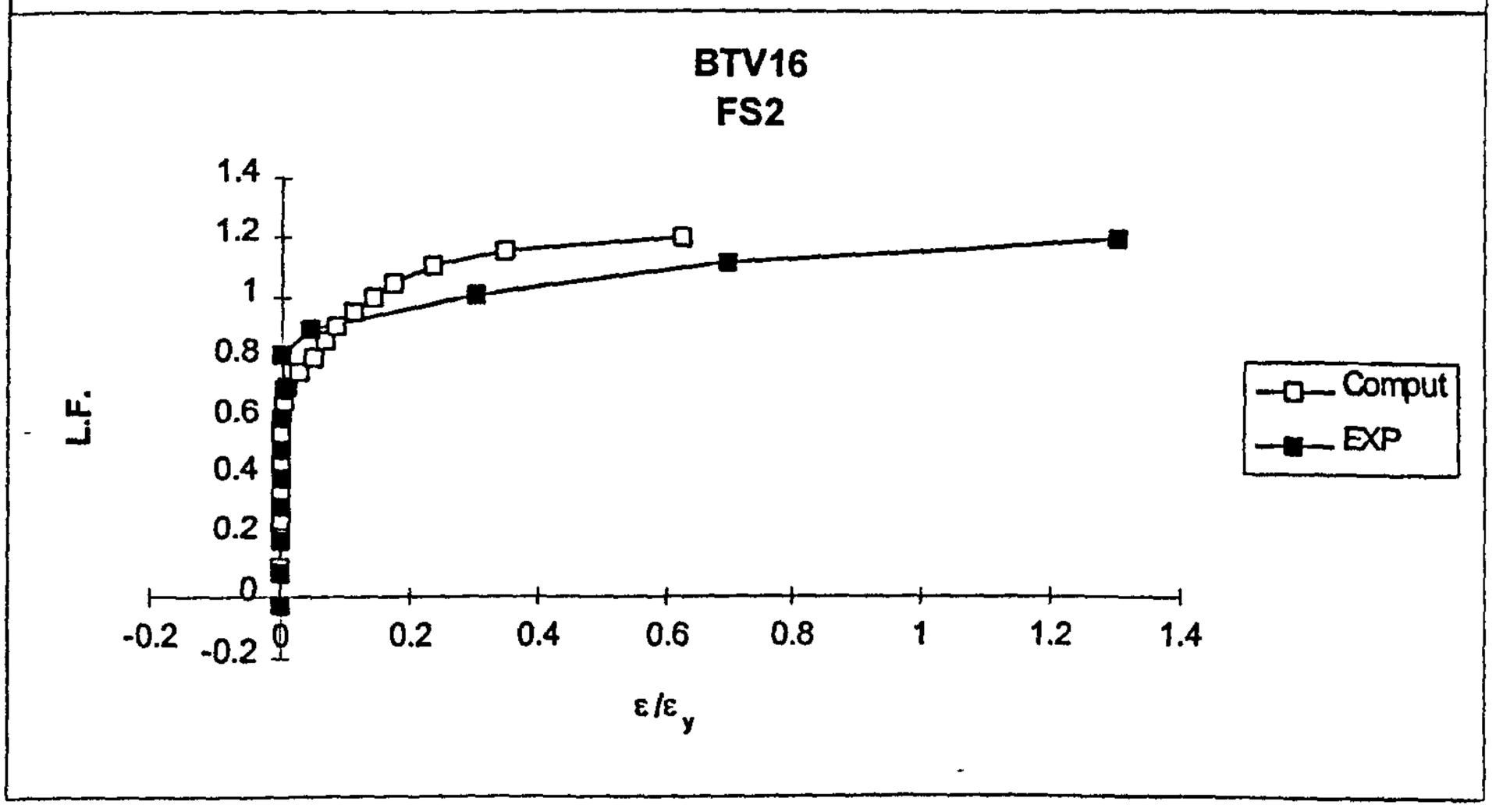
BTV16
FS2
L.F.
1.4
1.2
1
0.8
0.6
0.4
0.2
0
-0.2
-0.2
0
0.2
0.4
0.6
0.8
1
1.2
1.4
ε/ε_y
Comput
EXP

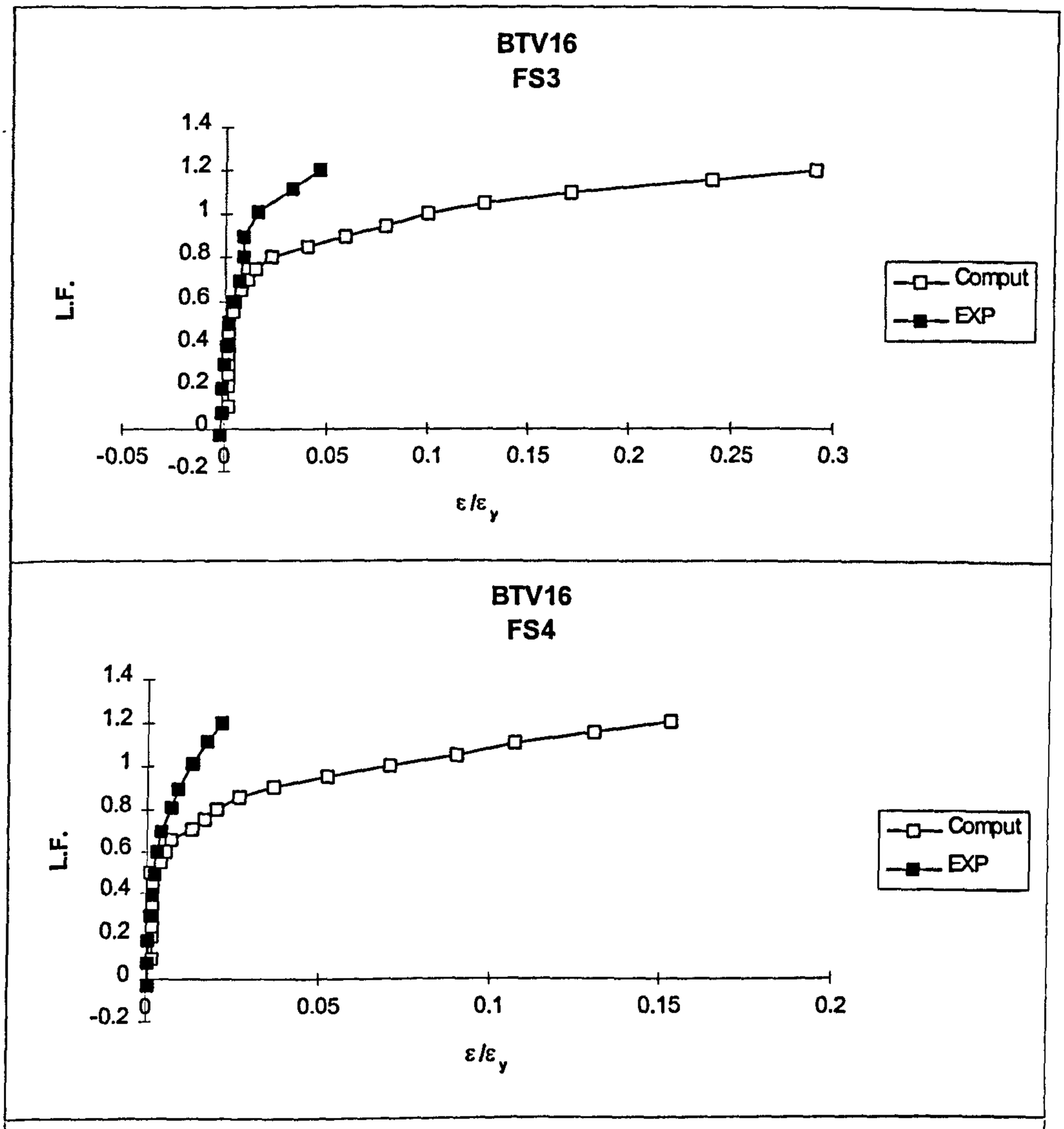
BTV16
FS3
L.F.
1.4
1.2
1
0.8
0.6
0.4
0.2
0
-0.2
-0.05
0
0.05
0.1
0.15
0.2
0.25
0.3
ε /ε y
Comput
EXP
BTV16
FS4
L.F.
1.4
1.2
1
0.8
0.6
0.4
0.2
0
-0.2
0
0.05
0.1
0.15
0.2
ε /ε y
Comput
EXP
BTV16
RS1
L.F.
1.4
1.2
1
0.8
0.6
0.4
0.2
0
-0.2
-0.05
0
0.05
0.1
0.15
0.2
0.25
ε /ε y
Comput
EXP

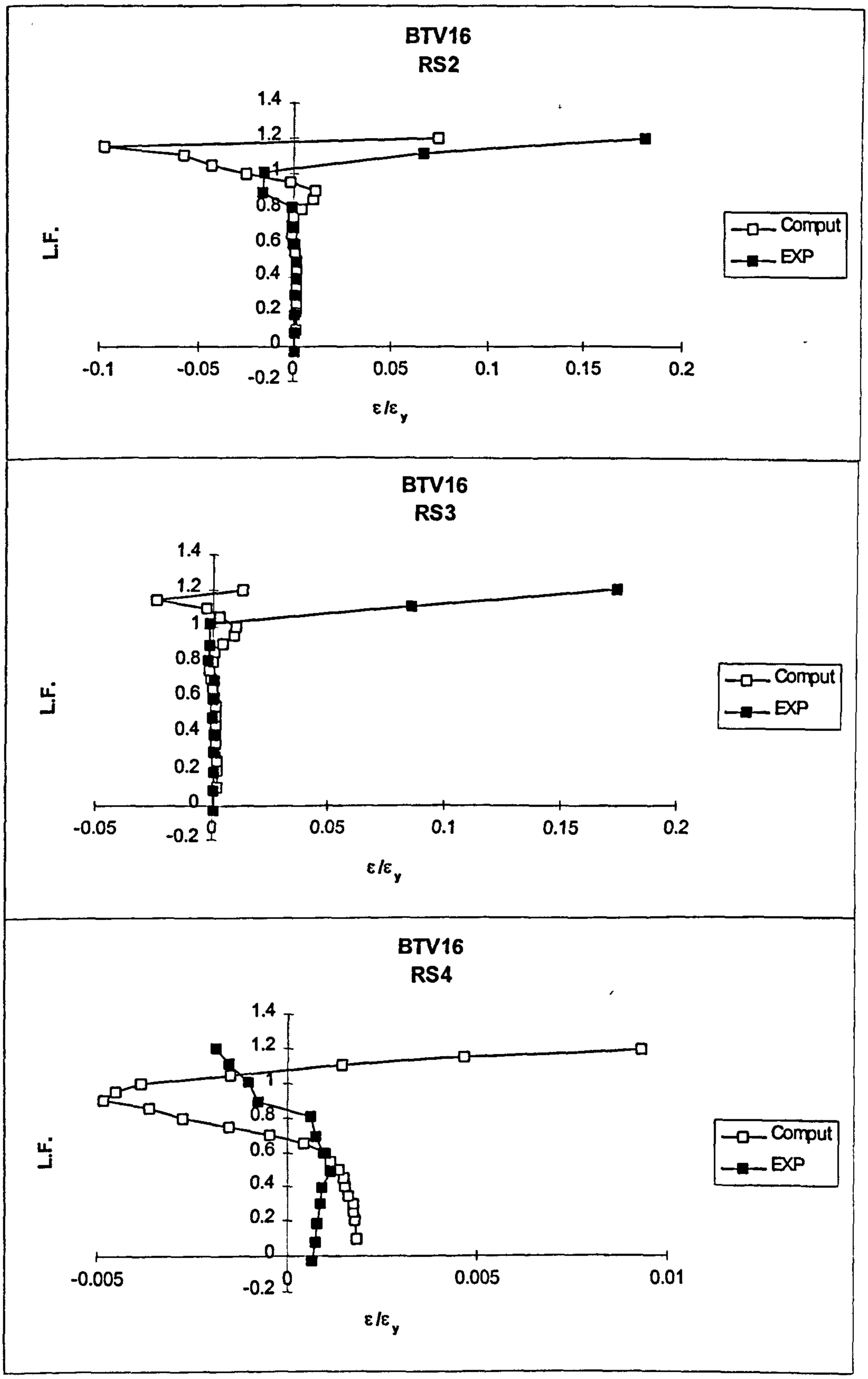
BTV16
RS2
L.F.
1.4
1.2
1
0.8
0.6
0.4
0.2
0
-0.2
-0.1
-0.05
0
0.05
0.1
0.15
0.2
ε/ε_y
Comput
EXP
BTV16
RS3
L.F.
1.4
1.2
1
0.8
0.6
0.4
0.2
0
-0.2
-0.05
0
0.05
0.1
0.15
0.2
ε/ε_y
Comput
EXP
BTV16
RS4
L.F.
1.4
1.2
1
0.8
0.6
0.4
0.2
0
-0.2
-0.005
0
0.005
0.01
ε/ε_y
Comput
EXP

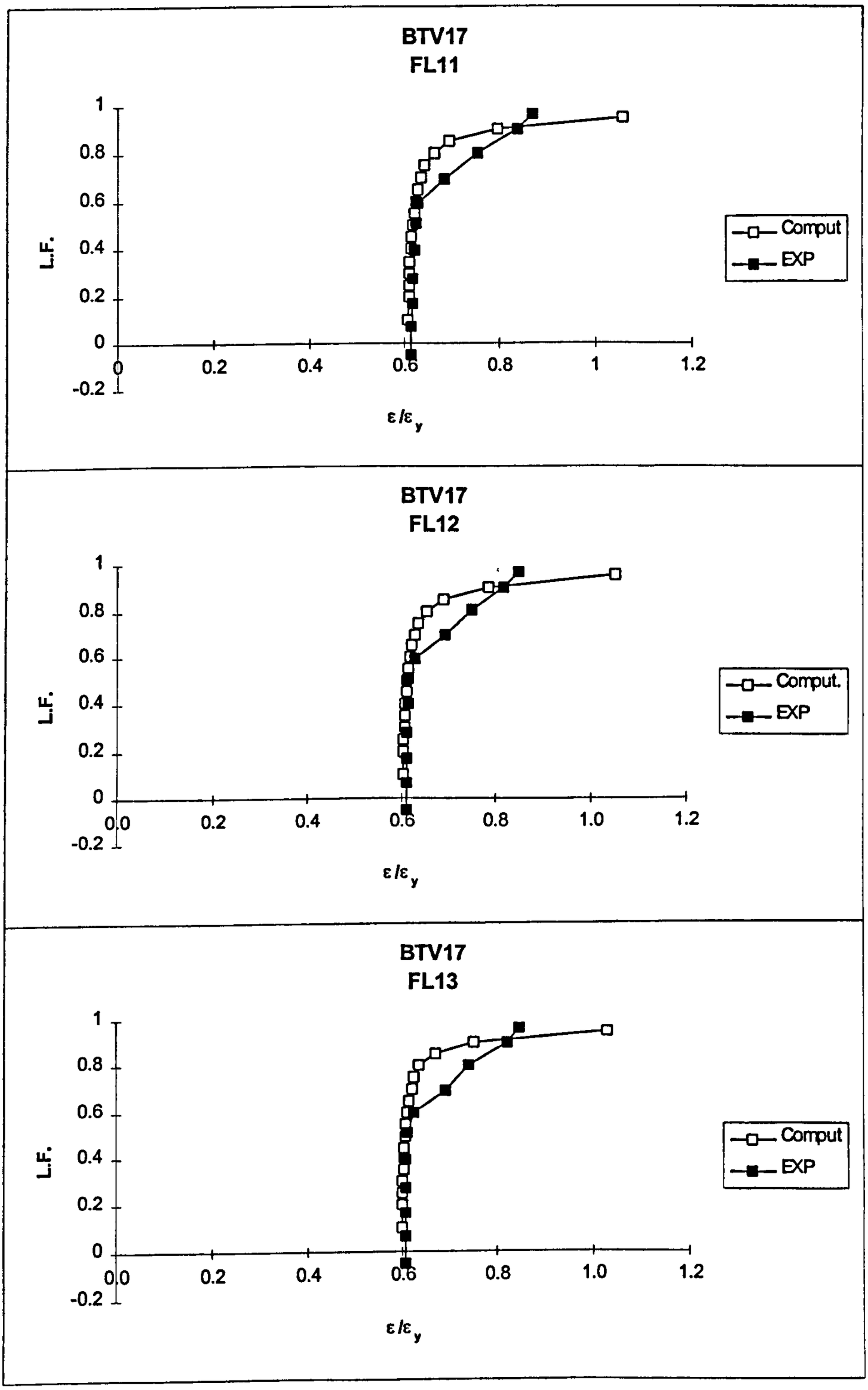
BTV17
FL11
L.F.
1
0.8
0.6
0.4
0.2
0
-0.2
0
0.2
0.4
0.6
0.8
1
1.2
ε/ε y
Comput
EXP
BTV17
FL12
L.F.
1
0.8
0.6
0.4
0.2
0
-0.2
0.0
0.2
0.4
0.6
0.8
1.0
1.2
ε/ε y
Comput.
EXP
BTV17
FL13
L.F.
1
0.8
0.6
0.4
0.2
0
-0.2
0.0
0.2
0.4
0.6
0.8
1.0
1.2
ε/ε y
Comput
EXP

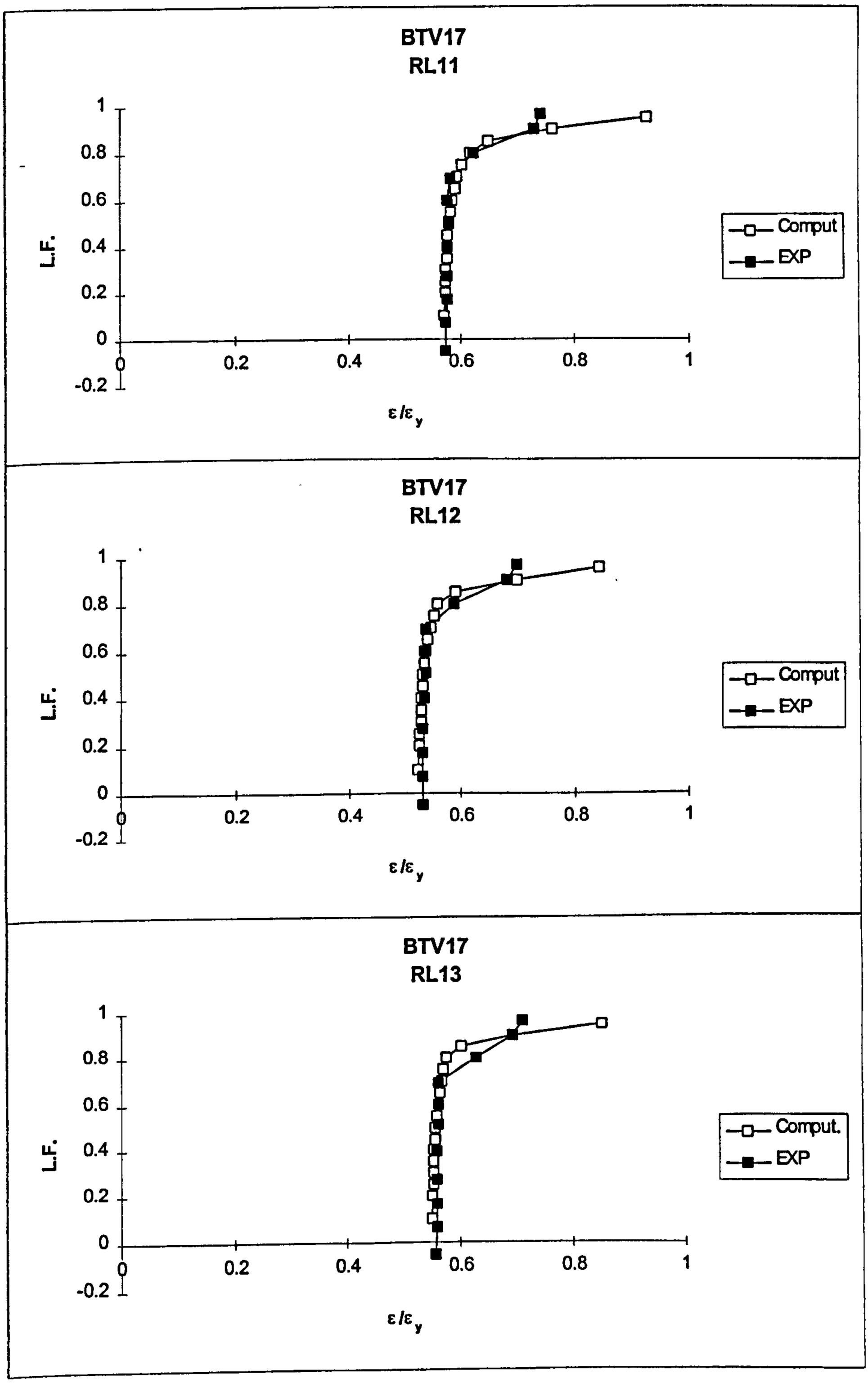
BTV17
RL11
L.F.
1
0.8
0.6
0.4
0.2
0
-0.2
0
0.2
0.4
0.6
0.8
1
ε/ε_y
Comput
EXP
BTV17
RL12
L.F.
ε/ε_y
Comput
EXP
BTV17
RL13
L.F.
ε/ε_y
Comput.
EXP

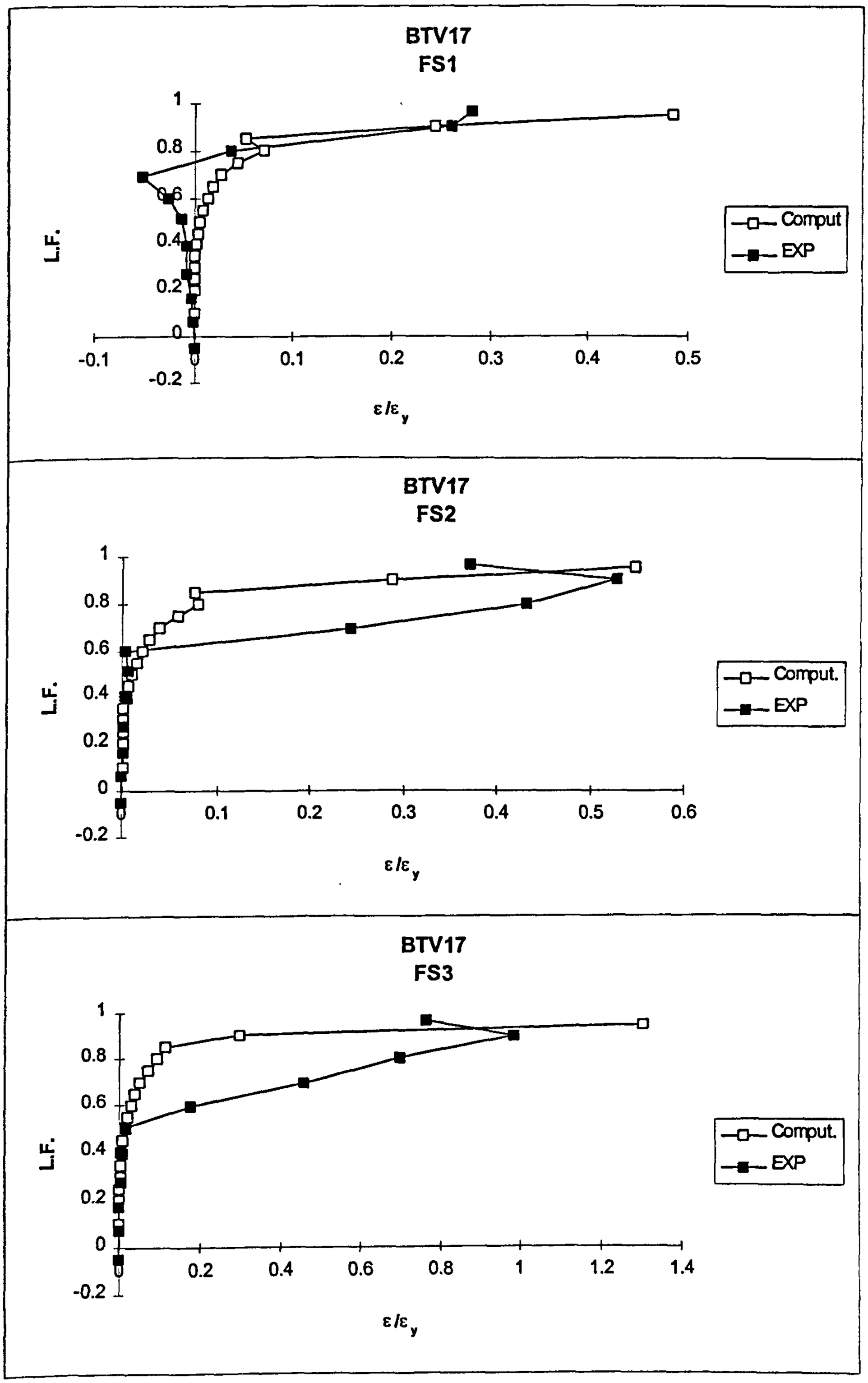
BTV17
FS1
L.F.
1
0.8
0.6
0.4
0.2
0
-0.2
-0.1
0.1
0.2
0.3
0.4
0.5
ε/ε_y
Comput
EXP
BTV17
FS2
L.F.
1
0.8
0.6
0.4
0.2
0
-0.2
0.1
0.2
0.3
0.4
0.5
0.6
ε/ε_y
Comput.
EXP
BTV17
FS3
L.F.
1
0.8
0.6
0.4
0.2
0
-0.2
0.2
0.4
0.6
0.8
1
1.2
1.4
ε/ε_y
Comput.
EXP

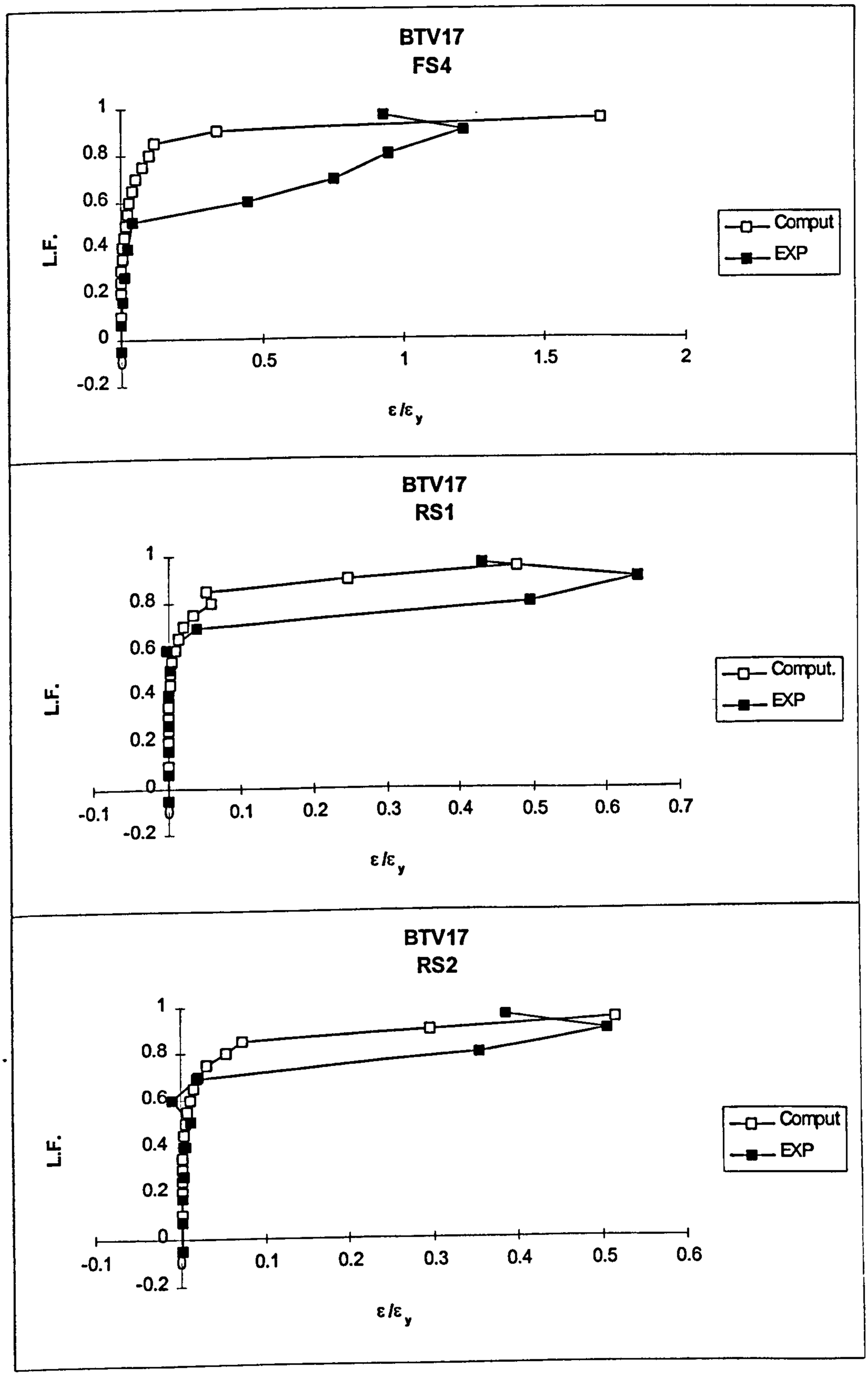
BTV17
FS4
L.F.
1
0.8
0.6
0.4
0.2
0
-0.2
0.5
1
1.5
2
ε/ε_y
Comput
EXP
BTV17
RS1
L.F.
1
0.8
0.6
0.4
0.2
0
-0.2
-0.1
0.1
0.2
0.3
0.4
0.5
0.6
0.7
ε/ε_y
Comput.
EXP
BTV17
RS2
L.F.
1
0.8
0.6
0.4
0.2
0
-0.2
-0.1
0.1
0.2
0.3
0.4
0.5
0.6
ε/ε_y
Comput
EXP

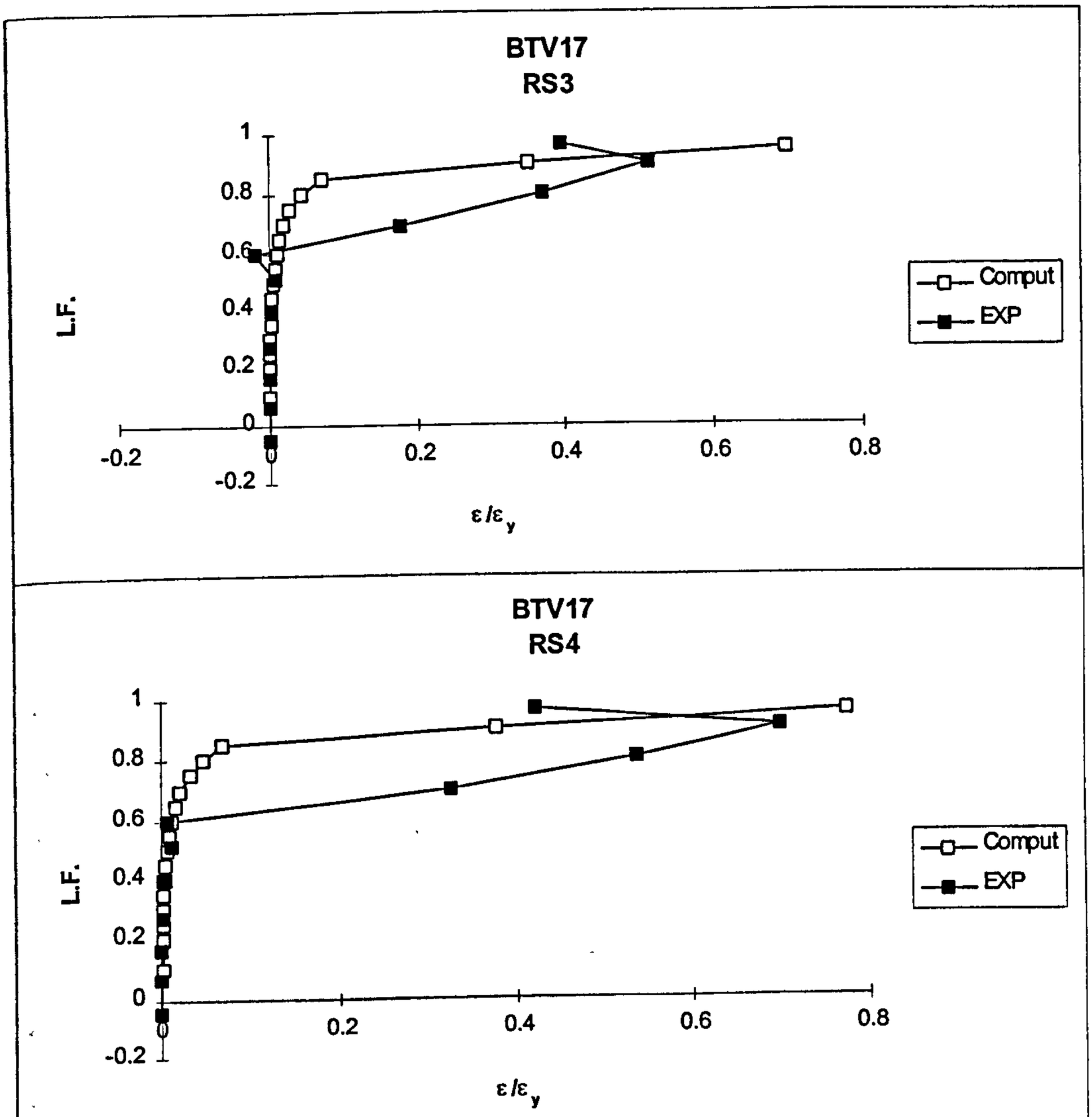
BTV17
RS3
L.F.
1
0.8
0.6
0.4
0.2
0
-0.2
-0.2
0
0.2
0.4
0.6
0.8
ε/ε_y
Comput
EXP
BTV17
RS4
L.F.
1
0.8
0.6
0.4
0.2
0
-0.2
0.2
0.4
0.6
0.8
ε/ε_y
Comput
EXP

Appendix C

Effect of the location of centre-line on the value of torsional stress in beams.

In this research, shear stress due to torsion in the hollow and solid beams was calculated using the following equation:

$$\tau = \frac{T}{2A_o t}$$

where; τ = shear stress due to torsion

T = applied torque

A_o = enclosed area by the centre-line

t = wall thickness of the beam

The shear stress due to torsion is directly effected by the enclosed area A_o. The larger the area the smaller the resulting stress and, therefore, the less steel required. In the case of large torsion, assumption of large A_o may lead to a premature beam failure due to insufficient steel provided. Figure C1 shows three different locations of centre-line which can be used for the calculation of A_o.

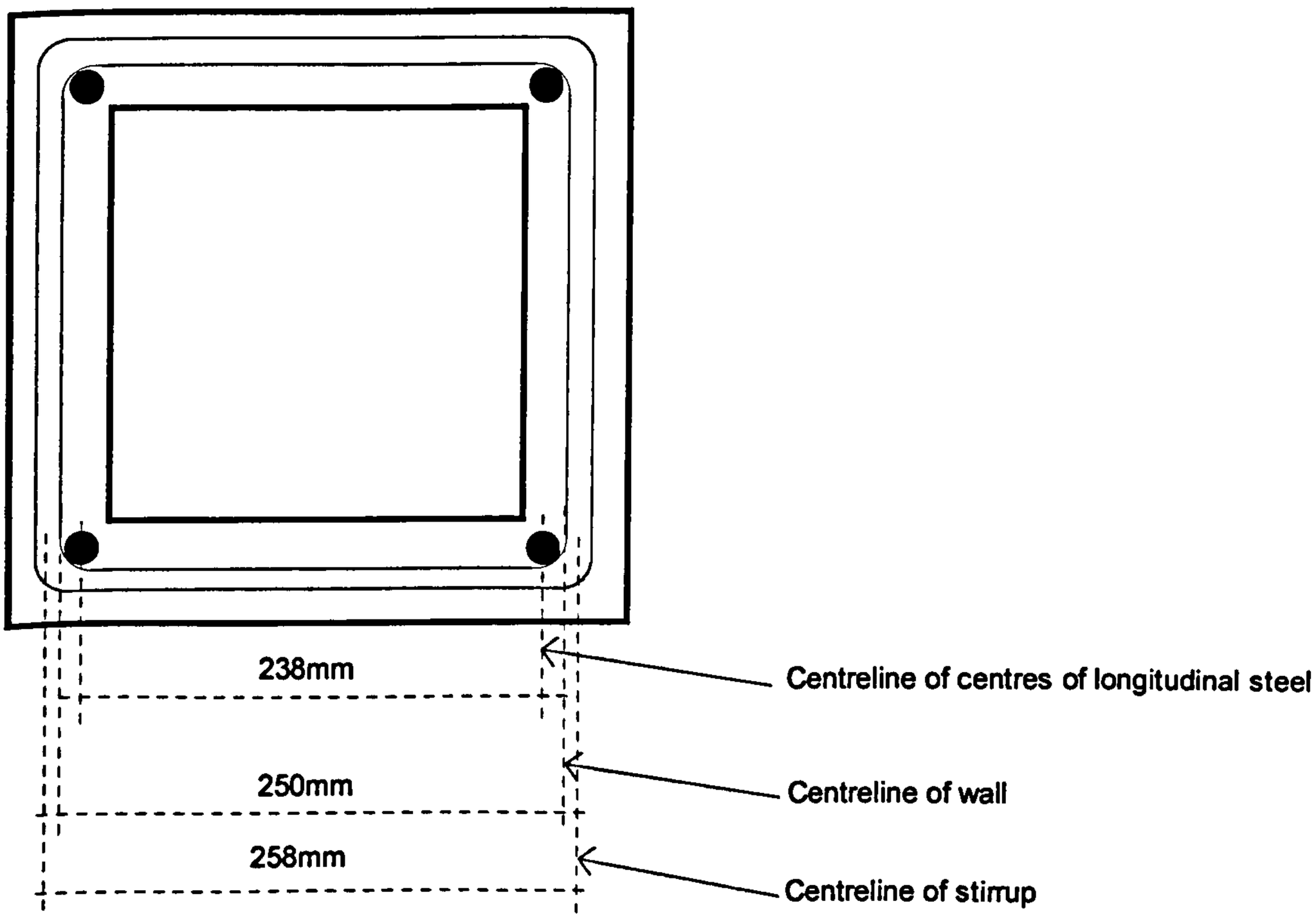

Fig. C1: Three possible centre-lines for A_o.

1. centreline connecting the centres of the longitudinal bars.
2. centreline of the wall thickness (this was used in the design of beams tested).
3. centreline of the stirrup.

For the 300x300x50mm section tested in this research, A_o can be:

1. $(A_o)_1 = (238)^2 mm^2$, in the case of using the centres of longitudinal bars.
2. $(A_o)_2 = (250)^2 mm^2$, in the case of using the centre of wall thickness.
3. $(A_o)_3 = (258)^2 mm^2$, in the case of using the centre line of the stirrup.

Table C1: Difference in stress due to change in A_o.

$T_{(kNm)}$	13	26	Ratio τ/τ_2
τ_1 (N/mm²)	2.30	4.59	1.1
τ_2 (N/mm²)	2.08	4.16	1
τ_3 (N/mm²)	1.95	3.91	0.94

Table C2 shows required reinforcement for two beams using three different centrelines.

Elastic stress distribution was used in the direct design method (DDM) and the angle of the compression diagonals in the truss analogy (TA) was used as 45°.

Table C2: Steel requirement for different A_o.

M kN.m.	T kN.m.	V kN.	b=h mm.	A_s(DDM) mm².	A_{sv}(DDM) mm²/m.	A_s(TA) mm².	A_{sv}(TA) mm²/m.
14.9	13	21	238	245	320	238	318
14.9	13	21	250	235	299	226	292
14.9	13	21	258	228	286	219	276
14.9	39	21	238	689	779	656	777
14.9	39	21	250	624	715	624	708
14.9	39	21	258	586	677	604	586

b and h are dimensions of the enclosed area A_o.

Appendix D

Design procedures

From the results in this research, the following design procedures are recommended:

D.1: Hollow reinforced beams (Elastic stress distribution)

Design these beams based on the largest stress where the shear stresses are added and where the bending moment and torsion are also largest.

1. Calculate the design bending moment M, torsion T and shear force V based on the loading condition, support locations and geometry of the beam.
2. Divide the cross-section into regions. (Fig. D1(a)).
3. Calculate normal stress σ_x due to applied load at the centre of each region ($\sigma_{xi} = My_i / I$, where i = region reference). (Fig. D1(b)).
4. Calculate the shear stress in each region i due to shear force ($\tau_{shri} = \frac{VQ}{Ib}$, where I = moment of inertia of the cross-section, b = total thickness of the webs, $Q = \int_{area} ydA$. The statical moment of area about the neutral axis of the area above the section where the stress is required). (Fig. D1(c)).
5. Calculate the shear stresses due to torsion ($\tau_{tor} = \frac{T}{2tA_o}$, where t = thickness of the web and A_o = the area enclosed by the centre line of the hollow section). (Fig. D1(d)).
6. Add the shear stresses to get the design shear stress for each region ($\tau_i = \tau_{shri} + \tau_{tor}$) .(Fig. D1(e)).
7. Calculate the ratio of the normal stress to the shear stress ($\frac{\sigma_{xi}}{\tau_i}, \frac{\sigma_{yi}}{\tau_i} = 0$)
8. Based on step 7 select the design case and equations from figure 3.8 which is repeated here for convenience.
9. Calculate the required reinforcement.
10. The largest value among the stirrup areas is used for the whole cross-section. Also, the longitudinal reinforcement required for the half of the cross-section where the shear stresses are added is used in the other half as well.

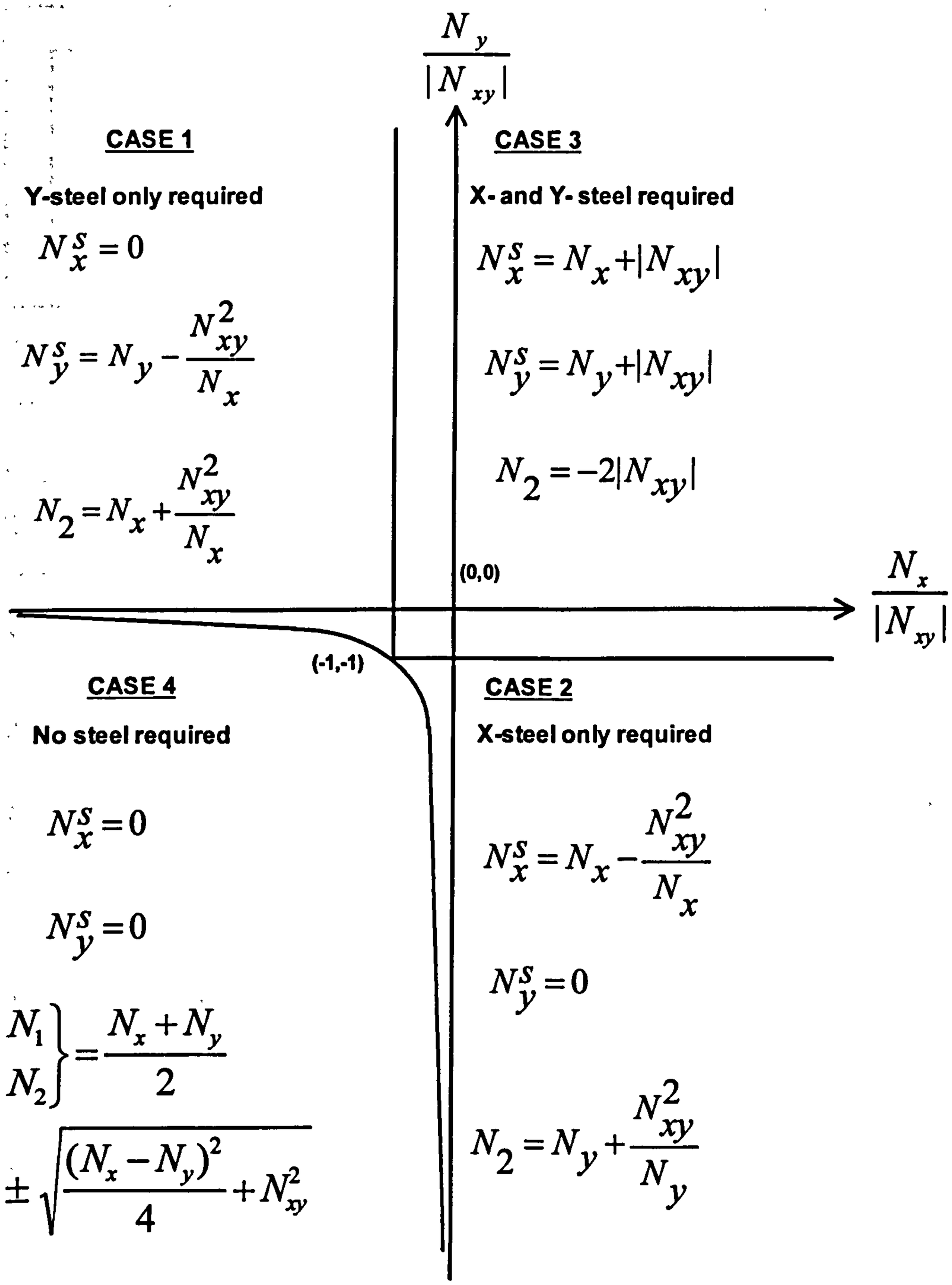

Fig. 3.8: Boundary graph for Nielsen's design equations

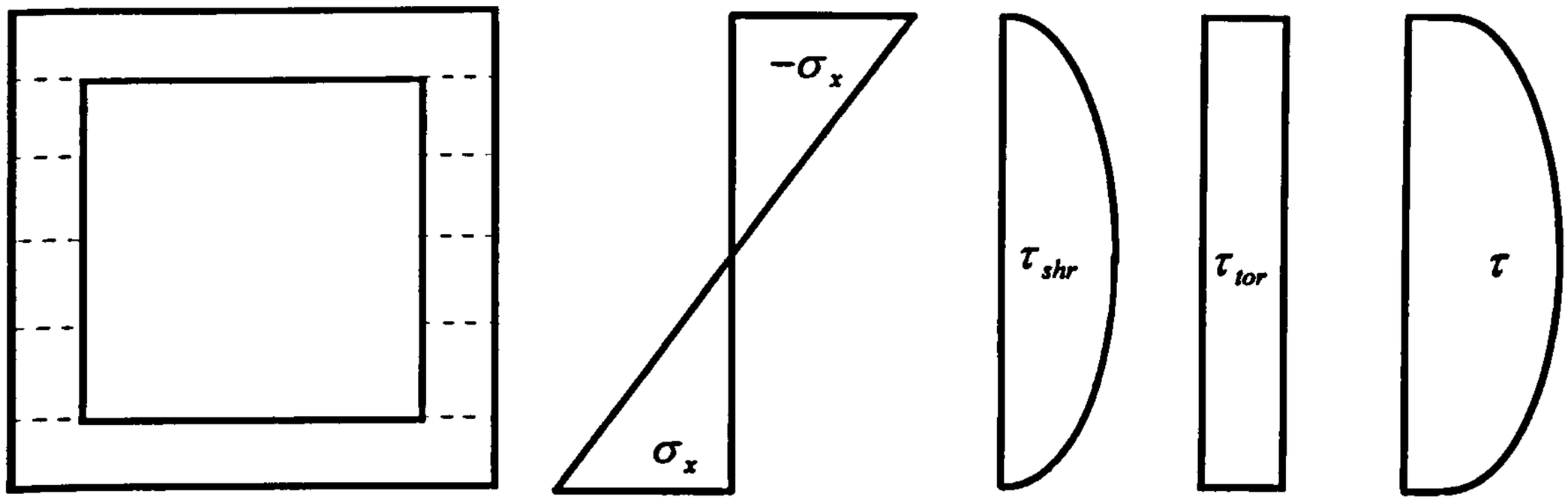

Fig. D1: Stress distribution in reinforced hollow beam

D.2: Hollow partially prestressed beams (Elastic stress distribution)

Design these beams based on the largest stress where the shear stresses are added and where the bending moment and torsion are also largest.

1. Calculate the design load (M, T and V) based on the loading condition, support locations and geometry of the beam.
2. Divide the cross-section into regions. (Fig. D2(a))
3. Calculate normal stresses due to direct prestressing forces ($\sigma_{xa} = \frac{\sum P_j}{A_c}$, where P_j = the individual axial forces in the prestressing wires after deducting all loses and A_c = concrete area. (Fig. D2(b)).
4. Calculate normal stresses due to eccentricities [$\sigma_{xe} = (\sum P_j e_j) Y / I$, where e_j = eccentricities of the axial forces and Y = distance between the neutral axis and the extreme fibre]. (Fig. D2(c)).
5. Add the stresses from steps 3 and 4. Check that large tensile stress is not present in the top flange. Also, check that the compressive stress in the bottom flange does not exceed f_c' otherwise increase the section or concrete compressive strength. (Fig. D2 (d)).
6. Calculate normal stresses σ_{xap} due to applied load at the centre of each region ($\sigma_{xapi} = My_i / I$, where i = region reference). (Fig. D2(e)).
7. Calculate the net (design) normal stresses σ_{xi} by algebraically summing all normal stresses (Fig. D2(f)). Check that the compressive stress in the top flange does not exceed f_c'.

8. Calculate the shear stress in each region i due to shear force ($\tau_{shri} = \frac{VQ}{Ib}$ where Q, I and b are as given in step 4 of section D1). (Fig. D1(c)).

9. Calculate the shear stresses due to torsion ($\tau_{tor} = \frac{T}{2tA_o}$, where all variables are as defined in section D1). (Fig. D1(d)).

10. Add the shear stresses to get the design shear stress for each region ($\tau_i = \tau_{shri} + \tau_{tor}$).(Fig. D1(e)).

11. Calculate the ratio of the normal stress to the shear stress ($\frac{\sigma_{xi}}{\tau_i}, \frac{\sigma_{yi}}{\tau_i} = 0$)

12. Based on step 11 select the design case and equations from figure 3.8.

13. Calculate the required reinforcement.

14. The largest value among the link areas is used for the whole cross-section. Also, the longitudinal reinforcement required for the half of the cross-section where the shear stresses are added is used in the other half as well.

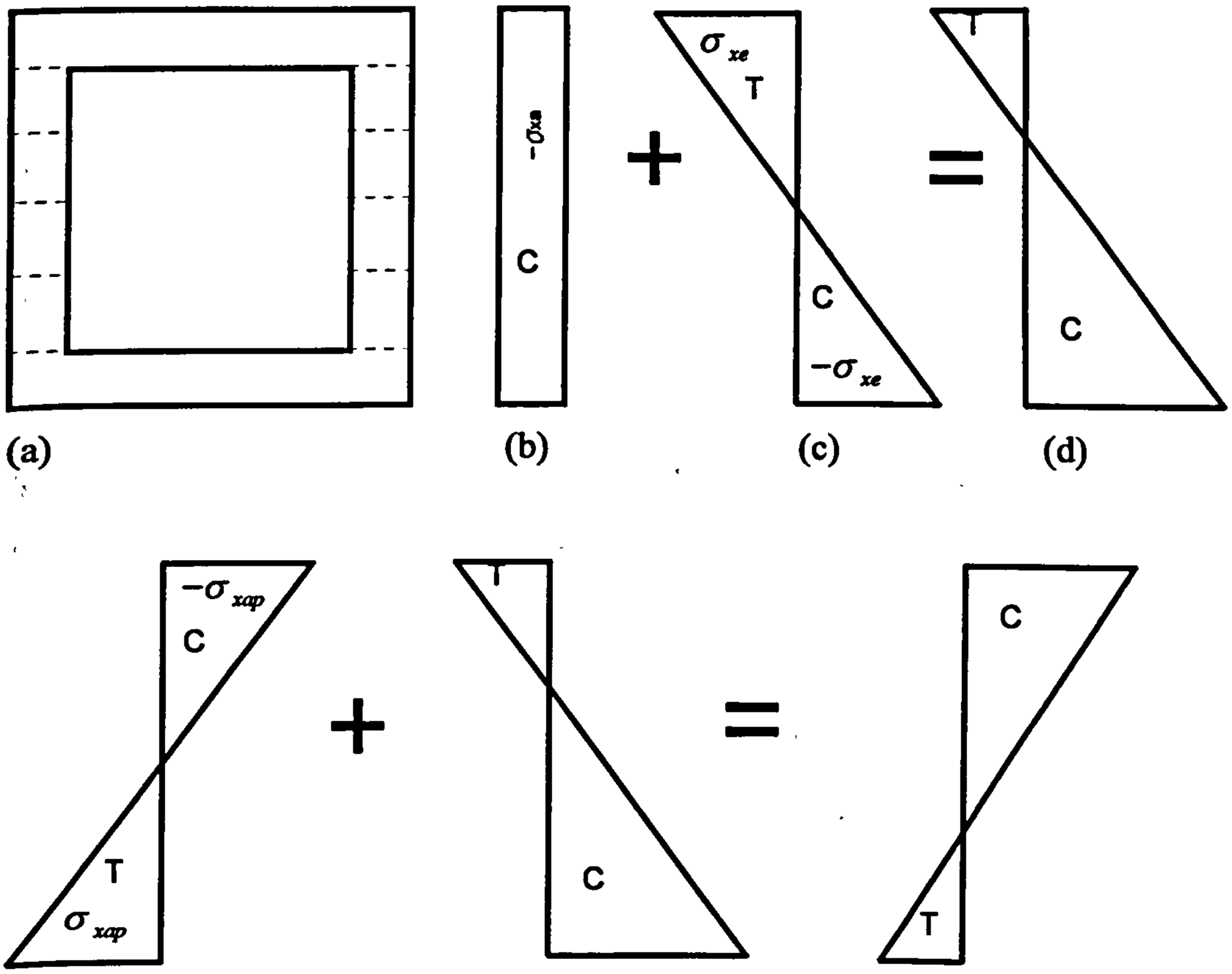

Fig. D2: Stress distribution in partially prestressed hollow beam

D.3: Solid Reinforced beams ("Plastic" stress distribution)

Design this type of beams using the stress distribution shown in figure D3.

1. Calculate the design load (M, T and V) based on the loading condition, support locations and geometry of the beam.
2. Divide the cross-section into regions. (Fig. D3(a)). Note that regions A_{comp} and A_{ten} have normal stresses and torsional shear stress (No shear stress due to shear force) and regions B_{add} and B_{sub} have no normal stress but combined shear stress. The depth of the A_{comp} and A_{ten} regions can be taken as 1/6 of the total beam depth and the width of the shear blocks B_{add} and B_{sub} can be taken as 1/6 of the total beam width.
3. Calculate the normal stresses at the top and bottom regions ($\sigma_x = \frac{M}{Ad}$, where A = area of the normal stress region (A_{comp} or A_{ten}) and d = lever arm between the centroids of the compressive and tensile regions (Fig D3(b).
4. Calculate the shear stress due to shear force ($\tau_{shr} = \frac{V}{A_w}$, where A_w = area of the B_{add} and B_{sub} shown in figure D3(c)).
5. Calculate the torsional shear stress ($\tau_{tor} = \frac{T}{2tA_o}$), (Fig. D3(d)).
6. Calculate the net shear stress in regions B_{add} and B_{sub} ($\tau_i = \tau_{shri} \pm \tau_{tori}$).
7. Calculate the ratio of the normal stress to the shear stress ($\frac{\sigma_{xi}}{\tau_i}, \frac{\sigma_{yi}}{\tau_i} = 0$)
8. Based on step 7 select the design case and equations from figure 3.8.
9. Calculate the required reinforcement in each region.
10. The stirrup area is the average of (the largest area in the region where the stresses are added and the corresponding area at the same level on the other side). The area of the longitudinal reinforcement in each half of the cross-section is the average of (the area in the half where the stresses are added and that where the stresses are subtracted).

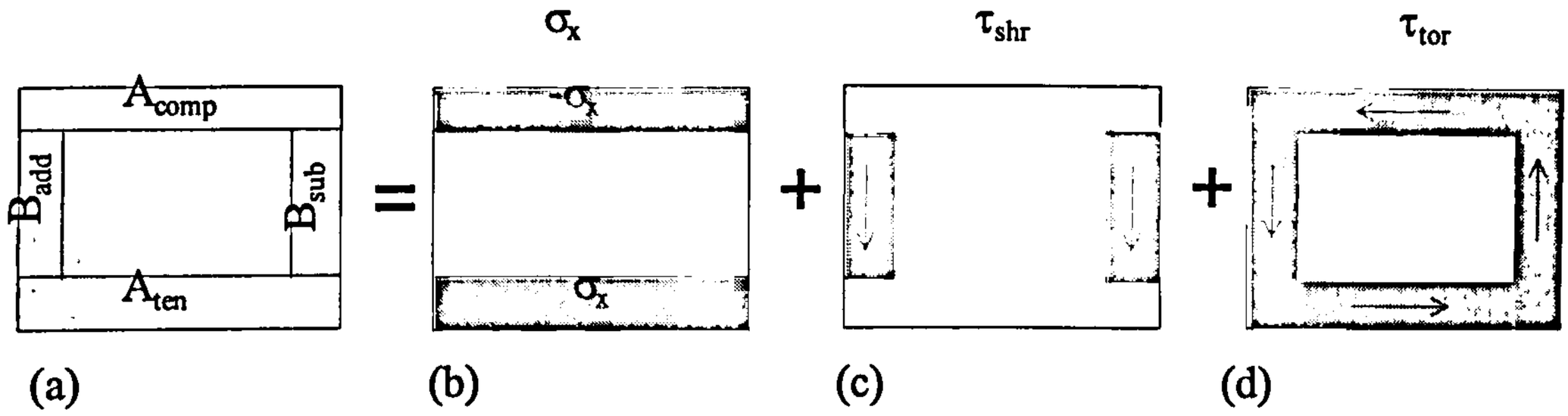

Fig. D3: Stress distribution in solid reinforced beams

D.4: Solid partially prestressed beams (Elastic stress distribution)

Design this type of beams using elastic stress distribution similar to hollow beams explained in section D2 with corresponding values for I, A_c as for solid section and the section is divided as in figure D4. The stirrup area is average of (the largest area in the region where the stresses are added and the area at the same level in the other side). The area of the longitudinal reinforcement in each half of the cross-section is the average of (the area in the half where the stresses are added and that where the stresses are subtracted).

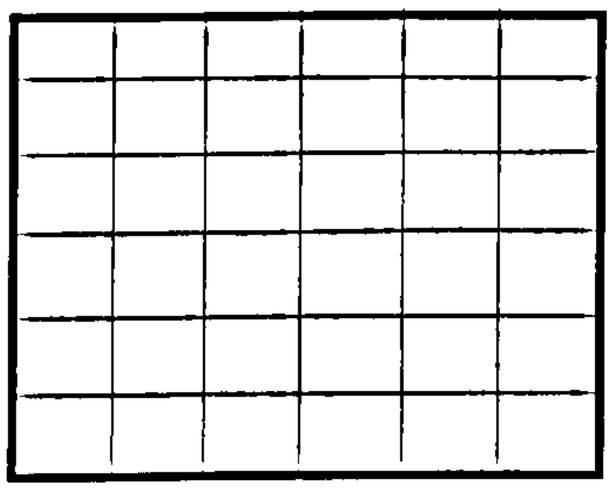

Fig. D4.

References

Abdel-Hafez Laila M. (1986)
Direct Design of Reinforced Concrete Skew Slab., Ph.D. thesis, University of Glasgow.

Abdel-Kader M. M. A. (1993)
Prediction of Shear Strength of Reinforced and Prestressed Concrete Beams by Finite Element method., Ph.D. Thesis, University of Glasgow.

Abrishami H. H. and Mitchell D. (1996)
"Influence of Splitting Cracks on Tension Stiffening.", ACI Structural Journal, Nov.-Dec., pp.703-710.

Ahmad S. H. and Abdel-Fattah (1991)
"A Rational Model for the Stress-Strain Relationship of Circular Hoop-Confined Concrete.", Magazine of Concrete Research, Vol.43, No.154, pp.23-28.

Ahmad S. H. and Shah S. P. (1982)
"Complete Triaxial Stress-Strain Curves for Concrete.", Journal of Structural Division, ASCE, Vol.108, No. ST4, April, pp.728-742.

Ali M. A. and White R. N. (1999)
"Toward a Rational Approach for Design of Minimum Torsion Reinforcement.", ACI Structural Journal, Jan.-Feb., pp.40-45.

Almusallam T. H. and Alsayed S. H. (1995)
"Stress-Strain Relationship of Normal, High-Strength and Lightweight Concrete.", Magazine of Concrete Research, Vol.47, No.170 Mar., pp.39-44.

Ansari F. and Li Q. (1998)
"High-Strength Concrete Subjected to Triaxial Compression.", ACI Materials Journal, Nov.-Dec., pp.747-755.

Arnesen A., Sorensen S. I. and Bergan P. G. (1980)
"Nonlinear Analysis of Reinforced Concrete.", Computers and Structures, Vol.12, pp.571-579.

Asghar M. Bhatti and Almughrabi A. (1996)
"Refined Model to Estimate Torsional Strength of Reinforced Concrete Beams.", ACI Structural Journal, Sept.-Oct., pp.614-622.

Attard M. M. and Setunge S. (1996)
"Stress-Strain Relationship of Confined and Unconfined Concrete.", ACI Materials Journal, Sep.-Oct., pp.432-442.

Balakrishnan S. and Murray D. W. (1988)
"Concrete Constitutive Model for NLFE Analysis of Structures.", Journal of Structural Engineering, ASCE, Vol.114, No.7, July, pp.1449-1466.

Bathe K. J. (1982)
The Finite Element Procedures in Engineering analysis., Printice-Hall Inc.

Bazant P. Z. and Lin F. B. (1988)
"Nonlinear Smeared Cracking Model for Concrete Fracture.", Journal of Structural Engineering, ASCE, Vol.114, No.11, Nov., pp.2493-2510.

Bedard C. and Kotsovos M. D. (1985)
"Application of NLFEA to Concrete Structures.", Journal of Structural Engineering, ASCE, Vol.111, No.12, Dec., pp.2691-2707.

Belarbi A. and Hsu T. T. C. (1990)
"Stirrup Stresses in Reinforced Concrete Beams." ACI Structural Journal, Sept.-Oct., pp.530-538.

Bensalem A. (1993)
Direct Design of Reinforced Concrete Structures using Non-Elastic Stress Fields., Ph.D. thesis, University of Glasgow.

Bhatt P. and Abdel-Kader M. (1995)
"Prediction of Shear Strength of Reinforced Concrete Beams By Nonlinear Finite Element Analysis.", Developments in Computational Techniques for Civil Engineering. CIVIL-COMP Press, Edinburgh, Scotland, UK. pp.191-204.

Bresler B. and Pister K. S. (1958)
"Strength of Concrete under Combined Stresses.", ACI Journal, Sep., pp.321-345.

Carreira D. J. and Chu K-H. (1985)
"Stress-Strain Relationship for Plain Concrete in Compression.", ACI Journal, Nov.-Dec., pp.797-804.

Cedolin B. L. and Poli S. D. (1977)
"Finite Element Studies of Shear-Critical R/C Beams.", Journal of the Engineering Mechanics Division, ASCE, Vol.193, No. EM3, June, pp.395-410.

Cedolin L., Crutzen Y. R. J. and Poli S. D. (1977)
"Triaxial Stress-Strain Relationship for Concrete.", Journal of the Engineering Mechanics Division, ASCE, Vol.103, No.EM3, June, pp.423-439.

Cervera M., Hinton E. and Hassen O. (1987)
"Nonlinear Analysis of Reinforced Concrete Plate and Shell Structures Using 20-Nodded Isoparametric Brick Elements.", Computer and Structures, Vol.25, No.6, pp.845-869.

Chang T. Y., Taniguchi H. and Chen W. F. (1987)
"Nonlinear Finite Element Analysis of Reinforced Concrete Panels.", Journal of Structural Engineering, ASCE, Vol.113, No.1, Jan., pp.122-140.

Chen W-F. and Saleeb A. F. (1994)
Constitutive Equations for Engineering Materials, Elsevier.

Chen W-F. and Ting E. C. (1980)
"Constitutive Models for Concrete Structures.", Journal of the Engineering Mechanics Division, ASCE, Vol.106, No.EM1, Feb., pp.1-19.

Choi S., Thienel K-C. and Shah S. P. (1996)
"Strain Softening of Concrete in Compression under Different end Constraints.", Magazine of Concrete Research, Vol.48, No.175, June, pp.103-115.

Chung W. and Ahmad S. H. (1994)
"Model for Shear Critical High-Strength Concrete Beams.", ACI Structural Journal, Jan.-Feb., pp.31-41.

Clark L.A. (1976)
"The Provision of Tension and Compression Reinforcement to Resist In-Plane Forces.", Magazine of concrete research., Vol. 28, No. 94. Mar., pp 3-12.

Collins M. P. and Mitchell D. (1980)
"Shear and Torsion Design of Prestressed and Non-Prestressed Concrete Beams.", PCI journal., Sep.-Oct., pp 32-100.

Collins M. P., Walsh P. F., Archer F. E., and Hall A. S. (1968)
"Ultimate Strength of Reinforced Concrete Beams subjected to Combined Torsion and Bending.", ACI Journal., Detroit, SP 18-14, pp.379 - 402.

Cowan H. J. (1965)
Reinforced and Prestressed concrete in Torsion., Edward Arnold Ltd.

Darwin D. (1997)
Discussion of "Aggregate Bond and Modulus of Elasticity of Concrete.", By Neville 1997, ACI Materials Journal, Nov.-Dec., pp.612-613.

Darwin D. and Pecknold D. A. (1977)
"Nonlinear Biaxial Stress-Strain Law for Concrete.", Journal of the Engineering Mechanics Division, ASCE, Vol.103, No.EM2, April, pp.229-241.

Duncan W. and Johnarry T. (1979)
"Further Studies on the Constant Stiffness Method of Non-Linear Analysis of Concrete Structures.", Proceeding. Institution of Civil Engineers, Part:2, Vol.67, Dec., pp.951-969.

Ebireri J. O. (1985)
Direct Design of Beams for Combined Bending and Torsion., Ph.D. thesis, University of Glasgow.

Elfren L., Karlsson I., and Losberg A. (1974)
"Torsion-Bending-Shear Interaction for Concrete Beams.", Journal of the Structural Division. ASCE, Vol.100, No. ST8., Aug., pp.1657-1677.

El-Hussein E. A. (1994)
"Finite Element and Direct Design Method in Combined Torsion, Bending and Shear of Reinforced Concrete.", Computational structural engineering for practice, Civil-Comp Ltd, Edinburgh, Scotland, pp.165-171.

El-Mezaini N. and Citipitioglu E. (1991)
"Finite Element Analysis of Prestressed and Reinforced Concrete Structures.", Journal of Structural Engineer, ASCE, Vol.117, No.10, Oct., pp.2851-2864.

Elmorsi M., Kianoush M. R. and Tso W. K. (1998)
"Nonlinear Analysis of Cyclically Loaded Reinforced Concrete Structures.", ACI Structural Journal, Nov.-Dec., pp.725-739.

El-Nuonu G. F. R. (1985)
Design of Shear Wall-Floor Slab Connections., Ph.D. thesis, University of Glasgow.

Elwi A. A. and Murray D. W. (1979)
"A 3D Hypoelastic Concrete Constitutive Relationship.", Journal of the Engineering Mechanics Division, ASCE, Vol.105, No.EM4, Aug., pp.623-641.

Ewida A. A. and McMullen A. E. (1981)
"Torsion-Shear-Flexure Interaction in Reinforced Concrete Members.", Magazine of Concrete Research. Vol. 33, No. 115 : June, pp.113-122.

Fu X. and Chung D. D. L. (1998)
"Effects of Water-Cement Ratio, Curing Age, Silica Fume, Polymer Admixtures, Steel Surface Treatments and Corrosion on Bond between Concrete and Steel Reinforcing Bars.", ACI Materials Journal, Nov.-Dec., pp.725-734.

Gajer G. and Dux P. F. (1990)
"Crack Band based Model for FEM Analysis of Concrete Structures.", Journal of Structural Engineering, ASCE, Vol.116, No.6, June, pp.1697-1714.

Gettu R., Aguado A. and Oliveira M. O. F. (1996)
"Damage in High-Strength Concrete due to Monotonic and Cyclic Compression - A Study Based on Splitting Tensile Strength.", ACI Materials Journal, Nov.-Dec., pp.519-523.

Gilbert R. I. and Warner R. F.(1978)
"Tension Stiffening in Reinforced Concrete Slabs.", Journal of the Structural Division, ASCE, Vol.104, No.ST12, Dec.,pp.1885-1900.

Goode C. D. and Helmy M. A. (1968a)
"Ultrimate Strength of Reinforced Concrete Beams in Combined Bending and Torsion.", ACI Journal, Detroit, SP 18-13, pp.357-377.

Goode C. D. and Helmy M. A. (1968b)
"Bending and Torsion of Reinforced Concrete Beams.", Magazine of Concrete Research, Vol.20, No.64, Sept., pp.155-166.

Gopalaratnam V. S. and Shah S. P.(1985)
"Softening Response of Plain Concrete in Direct Tension.", ACI Journal, May-June, pp.310-323.

Gupta A. K. and Maestrini S. R. (1990)
"Tension-Stiffness Model for Reinforced Concrete Bars.", Journal of Structural Engineering, ASCE, Vol.116, No.3, Mar., pp. 769-790.

Hago A. M. (1982)
Direct Design of Reinforced Concrete Slabs., Ph.D. thesis, University of Glasgow.

Hearn N. (1999)
"Effect of Shrinkage and Load-Induced Cracking on Water Permeability of Concrete.", ACI Materials Journal, Mar.-Apr., pp.234-241.

Hinton E. and Owen D. R. J. (1986)
Computational Modelling of Reinforced Concrete Structures., Pineridge Press Limited.

Hinton E. and Owen D. R. J. (1989)
Finite Element Programming., Academic Press.

Hobbs D. W., Pomeroy C. D. and Newman J. B. (1977)
"Design Stresses for Concrete Structures Subjected to Multi-Axial Stresses.", The Structural Engineer, Vol.55, No.4, April, pp.151-164.

Hognestad H. (1951)
"A study of Combined Bending and Axial Load in Reinforced Concrete Members.", University of Illinois Engineering Experimental Station, Bulletin Series No. 399. [Quoted by Almusallam and Alsayed (1995)]

Hsu T. T. C. (1968)
"Torsion of Structural Concrete-Behavior of Reinforced Concrete Rectangular Members.", Torsion of structural concrete, SP-18-10, American concrete institute, Detroit, pp.261-306.

Hsu T. T. C. (1988)
"Softened Truss Model Theory for Shear and Torsion.", ACI Structural Journal, Nov.-Dec., pp.624-635.

Hsu T. T. C. (1991a)
"Nonlinear Analysis of Concrete Membrane Elements.", ACI Structural Journal, Sep. Oct., pp.552-561.

Hsu T. T. C. (1991b)
"Nonlinear Analysis of Concrete Torsional Members.", ACI Structural Journal, Nov.-Dec., pp.674-682.

Hsu T. T. C. and Mo Y. L. (1985a)
"Softening of Concrete in Torsion Members-Theory and Tests.", ACI Journal, May-June, pp.290-303.

Hsu T. T. C. and Mo Y. L. (1985b)
"Softening of Concrete in Torsion Members-Design Recommendations.", ACI Journal, Jul.-Aug., pp.443-452.

Hsu T. T. C. and Mo Y. L. (1985c)
"Softening of Concrete in Torsional Members-Prestressed Concrete.", ACI Journal, Sept.-Oct., pp.603-615.

Hsu T. T. C. and Zhang L-X. (1996)
"Tension Stiffening in Reinforced Concrete Membrane Elements.", ACI Structural Journal, Jan.-Feb., pp.108-115.

Hsu T.T.C. (1984)
Torsion of Reinforced Concrete., Van Nostrand Reinhold Company Inc.

Imran I. and Pantazopoulou S. J. (1996)
"Experimental Study of Plain Concrete under Triaxial Stress.", ACI Materials Journal, Nov.-Dec., pp.589-601.

Iravani S. (1996)
"Mechanical Properties of High-Performance Concrete.", ACI Materials Journal, Sep.-Oct., pp.416-426.

Jelic I., Pavlovic M. N. and Kotsovos M. D. (1999)
"A Study of Dowel Action in Reinforced Concrete Beams.", Magazine of Concrete Research, Vol. 51, No. 2, Apr., pp. 131-141.

Johanry T. (1979)
Elastic-plastic Analysis of Concrete Structures using Finite Elements., Ph.D. thesis, University of Strathclyde.

Karlsson I. and Elfgren L. (1972)
"Torsional Stiffness of Reinforced Concrete Members Subjected to Pure Torsion.", Magazine of Concrete Research, Vol.24, No.80, sept., pp.149-156.

Kemp E. L. (1986)
"Bond in Reinforced Concrete: Behaviour and Design Criteria.", ACI Journal, Vol.83, Jan.-Fed., pp.50-57.

Kotsovos M. D. (1979)
"A Mathematical Description of the Strength Properties of Concrete under Generalized Stress.", Magazine of Concrete Research, Vol. 31, No. 108, Sep., pp. 151-158.

Kotsovos M. D. (1987)
"Consideration of Triaxial Stress Conditions in Design: A Necessity.", ACI Structural Journal, May-June, pp.266-273.

Kotsovos M. D. and Pavlovic M. N. (1995)
Structural Concrete., Thomas Telford Publications.

Kotsovos M. D. and Cheong H. K. (1984)
"Applicability of Test Specimen Results for the Description of the Behaviour of Concrete in a Structure.", ACI Journal, Jul.-Aug., pp.358-363.

Kotsovos M. D. and Newman J. B. (1977)
"Behaviour of Concrete Under Multiaxial Stress.", ACI Journal, Sep., pp.443-446.

Kotsovos M. D. and Newman J. B. (1978)
"Generalized Stress-Strain Relations for Concrete.", Journal of the Engineering Mechanics Division, ASCE, Vol.104, No.EM4, Aug., pp. 845-856.

Kotsovos M. D. and Newman J. B. (1979)
"A mathematical Description of the Deformation Behaviour of Concrete Under Complex Loading.", Magazine of Concrete Research, Vol. 31, No. 107, June, pp.77-90.

Kupfer H., Hilsdorf H. K. and Rusch H. (1969)
"Behavior of Concrete Under Biaxial Stresses.", ACI Journal, August, pp.656-666.

Kuyt B. (1971)
"A Theoretical Investigation of Ultimate Torque as calculated by Truss theory and by the Russian Ultimate Equilibrium Method.", Magazine of Concrete Research, Vol.23, No.77, Dec., pp.155-160.

Lampert P. and Thurlimann B. (1971)
"Ultimate Strength and Design of Reinforced Concrete Beams in Torsion and Bending.", International Association for Bridge and Structural Engineering, IABSE, Publication 31-I, pp.107-131.

Lan S. and Guo Z. (1997)
"Experimental Investigation of Multiaxial Compressive Strength of Concrete under Different Stress Paths.", ACI Materials Journal, Sep.-Oct., pp.427-434.

Lessig N. N. (1958)
"Theoretical and Experimental Investigation of Reinforced Concrete Beams Subjected to Combined Bending and Torsion.", Design and Construction of Reinforced Concrete Structures, Moscow, In Russian. [Quoted by Elfren et al. (1974)]

Lin C. S. and Scordelis A. C. (1975)
"Nonlinear Analysis of RC Shell of General Form.", Journal of the Structural Division, ASCE, Vol.101, No.ST3, Mar., pp.523-538.

Liu T. C. Y., Nilson A. H. and Slate F. O. (1972)
"Stress-Strain Response and Fracture of Concrete in Uniaxial and Biaxial Compression.", ACI Journal, May, pp. 291-295.

MacGregor J. G. and Ghoneim M. G. (1995)
"Design for Torsion.", ACI Structural Journal, Mar.- Apr., pp.211-218.

MacLeod I. A. (1990)
Analytical Modelling of Structural Systems., Ellis Horwood Ltd.

Maekawa K. and Qureshi (1996)
"Behavior of Embedded Bars in Concrete under Combined Axial Pullout and Transverse Displacement.", Journal of Materials, Concrete Structures and Pavements, Vol.30, No.532, pp.159-173.

Maekawa K. and Qureshi J. (1997)
"Stress Transfer across Interfaces in Reinforced Concrete due to Aggregate Interlock and Dowel Action.", J. Materials, Conc. Struct., Pavements., JSCE, No.557, Vol.34, Feb., pp.159-172.

Massicotte B., Elwi A. E. and MacGregor J. G. (1990)
"Tension-Stiffening Model for Planar Reinforced Concrete Members.", Journal of Structural Engineering, ASCE, Vol.116, No.11, Nov., pp.3039-3058.

Mattock A. H. (1968)
"How to Design for Torsion.", Torsion of structural concrete, SP-18, American concrete institute, Detroit, pp.469-495.

Mau S. T. and Hsu T. T. C. (1987)
"Shear Strength Prediction for Deep Beams with Web Reinforcement.", ACI Journal, Nov.-Dec., pp.513-523.

Memon M. (1984)
Strength and Stiffness of Shear Wall-Floor slab connections., Ph.D. thesis, University of Glasgow.

Meyer C. and Bathe K. J. (1982)
"Nonlinear Analysis of R/C Structures in Practice.", Journal of the Structural Division, ASCE, Vol.108, No.ST7, July, pp.1605-1622.

Mitchell D. and Collins M. P. (1974)
"Diagonal Compression Field Theory- A Rational Model for Structural Concrete in Pure Torsion." ACI Journal, Aug., pp.396-408.

Morsch E. (1902)
"Der Eisenbetonbau, seine Anwendung und Theorie.", 1st ed. Wayss and Freytag, A.G., Im Selbstverlag der Firma, Neustadt a. d. Haardt, May 1902, 118pp, "Der Eisenbetonbau, seine Theorie und Anwendung.", 2nd ed., Verlag von Konrad Wittmer, Stuttgart, 1906, 252pp, 3rd ed. translated into English by E.P. Goodrich, McGraw-Hill Book Co., New York 1909, 368pp. [Quoted by many references]

Moussa J. (1988)
Direct Design for Multiple Load Cases., M.Sc. thesis, University of Glasgow.

Murray D. W., Chitnuyanondh L., Rijub-Agha K. Y. and Wong C. (1979)
Concrete Plasticity Theory for Biaxial Stress Analysis.", Journal of the Engineering Mechanics Division, ASCE, Vol.105, No.EM6, Dec., pp.989-1006.

Nadai A. (1950)
Theory of Flow and Fracture of Solids., Vol.1, McGraw-Hill Book Co., New York.

Nanakorn P. and Horii H. (1996)
"Back Analysis of Tension-Softening Relationship of Concrete.", J. Materials, Conc. Struct., Pavements., JSCE, No.544, Vol.32, Aug., pp.265-275.

Nasser K. W. and Kenyon J. C. (1984)
"Why not 3x6 inch Cylinders for Testing Concrete Compressive Strength?.", ACI Journal, Jan.-Feb., pp.47-53.

Neville A. M. (1997)
"Aggregate Bond and Modulus of Elasticity of Concrete.", ACI Materials Journal, Jan.-Feb., pp.71-74.

Ngo D. and Scordelis A. C. (1967)
"Finite Element Analysis of Reinforced Concrete Beams.", ACI Journal Vol.64, No.3, pp.152-163.

Nielsen M. P. (1971)
"On the Strength of Reinforced Concrete Discs.", Aalborg, Denmarks Ingeniorakademi Bygninsafdelingen, 1971, Bulletin No.B2, Reprinted from: Acta Polytechnica Scandinavica, Civil Engineering and Building Construction Series, No.70, 1969, 254pp. [Quoted by Clark (1976)]

Nielsen M. P. (1974)
"Optimum Design of Reinforced Concrete Shells and Slabs.", Structural research laboratory, Technical University of Denmark, Report NR.R44, pp.190-200.

Nielsen M. P. (1979)
"Some Examples of Lower-Bound Design of Reinforcement in Plane Stress Problems.", IABSE colloquium., Copenhagen, Session V. Plasticity in Reinforced Concrete, Final report. Vol.29. Aug., pp. 317-324.

Nielsen M. P. (1984)
Limit Analysis and Concrete Plasticity., Prentice-Hall Inc.

Osburn D. L., Mayoglou B. and Mattock A. H. (1969)
"Strength of Reinforced Concrete Beams with Web Reinforcement in Combined Torsion, Shear and Bending.", ACI Journal, Jan., pp.31-41.

Palaniswamy R. and Shah S. P. (1974)
"Fracture and Stress-Strain Relationship of Concrete under Triaxial Compression.", Journal of the Structural Division, ASCE, Vol.100, No.ST5, May, pp.901-916.

Pang X-B and Hsu (1995)
"Behavior of Reinforced Concrete Membrane Elements in Shear.", ACI Structural Journal, Nov.-Dec., pp. 665-679.

Pang X-B. and Hsu T. T. C. (1996)
"Fixed Angle Softened Truss Model for Reinforced Concrete.", ACI Structural Journal, Mar.-Apr., pp.197-207.

Phillips D. V. and Zienkiewicz O. (1976)
"Finite Element Non-Linear Analysis of Concrete Structures.", Proceeding of Institution of Civil Engineers, Vol.61, Mar., No.2, pp.59-88.

Polak M. A. and Blackwell K. G. (1998)
"Modeling Tension in Reinforced Concrete Members Subjected to Bending and Axial Load.", Journal of Structural Engineering, ASCE, Vol.124, No.9, Sept., pp.1018-1024.

Ramirez J. A. and Breen J. E. (1991)
"Evaluation of a Modified Truss-Model Approach for Beams in Shear.", ACI structural journal, Sept.-Oct., pp.562-571.

Ranjbaran A. (1991)
"Embedding of Reinforcements in Reinforced Concrete Elements Implemented in DENA.", Computers and Structures, Vol.40, No.4, pp.925-930.

Raphael J. M. (1984)
"Tensile Strength of Concrete.", ACI Journal, Mar.-Apr., pp.158-165.

Rashid Y. R. (1968)
"Ultimate Strength Analysis of Prestressed Concrete Pressure Vessels.", Nuclear Engineering and Design, Vol.7, No.4, April, pp.334-344.

Rausch E. (1929)
"Berechnung des Eisenbetons gegen Verdrehung (Torsion) und Abscheren.", Julius Springer-Verlag, Berlin, 51pp. [Quoted by Collins and Mitchell (1980)]

Razaqpur A. G. and Nofal M. (1990)
"Analytical Modelling of Nonlinear Behavior of Composite Bridges.", Journal of Structural Engineering, ASCE, Vol.116, No.6, June, pp.1715-1733.

Ritter W. (1899)
"Die Bauweise Hennebique.", Schweizerishe Bauzeitung, Zurich, Feb. [Quoted by many references]

Saadi R. (1988)
Direct Design of Partially Prestressed Concrete Beams for Combined Bending and Torsion., M.Sc. thesis, University of Glasgow.

Saenz I. P. (1964)
Discussion of "Equation of the Stress-Strain Curve of Concrete." By Desayi P. and Krishnan S., ACI Journal, Sep., pp.1229-1235.

Salem M. H. and Maekawa K. (1997)
"Tension Stiffness Modelling for Cracked Reinforced Concrete Derived from Micro-Bond Characteristics.", University of Tokyo, Tokyo, Collected papers., Vol.35, pp.549-554.

Scanlon A. and Murray Y. D. (1974)
"Time Dependent Reinforced Concrete Slab Deflection.", Journal of Structural Division, ASCE, Vol.100, No.9, pp.1911-1924.

Stevens N. J., Uzumri S. M., Collins M. P. and Will G. T. (1991)
"Constitutive Model for Reinforced Concrete Finite Element Analysis.", ACI Structural Journal, Jan.-Feb., pp.49-59.

Tasdemir M. A., Lydon F. D. and Barr B. I. G. (1996)
"The Tensile Strain Capacity of Concrete.", Magazine of Concrete Research, Vol.48, No.176, Sep., pp.211-218.

Thurlimann B. (1979)
"Torsional Strength of Reinforced and Prestressed Concrete Beams-CEB Approach.", Institut fur Baustatik und konstruktion, ETH. Zurich., No.92., June, pp 117-143. Also can be found in: American concrete institute, Detroit, SP59.

Tokyay M. and Ozdemir (1997)
"Specimen Shape and Size effect on the Compressive Strength of Higher Strength Concrete.", Cement and Concrete Research, Vol. 27, No. 8, pp. 1281-1289.

Van Mier J. G. M. (1986)
"Fracture of Concrete under Complex Stress.", Heron, Vol.31, No.3, Delft University of Technology, Delft, The Netherlands.

Vecchio F. J. (1992)
"Finite Element Modeling of Concrete Expansion and Confinement.", Journal of Structural Engineering, ASCE, Vol.118, No.9, Sep., pp. 2390-2406.

Vecchio F. J. and Collins M. P. (1986)
"The Modified Compression-Field Theory for Reinforced Concrete Elements Subjected to Shear.", ACI Journal, Mar.-Apr., pp. 219-231.

Vecchio F. J. and Collins M. P. (1988)
"Predicting the Response of Reinforced Concrete Beams Subjected to Shear using Modified Compression Field Theory.", ACI Structural Journal, May-June, pp. 258-268.

Vidosa F. G., Kotsovos M. D. and Pavlovic M. N. (1991a)
"Three-Dimensional Non-Linear Finite Element Model for Structural Concrete.", Part 1, Main features and objectivity study., Proceeding of the Institution of civil engineers, Part 2, Vol.91, Sept., pp.517-544.

Vidosa F. G., Kotsovos M. D. and Pavlovic M. N. (1991b)
"Three-Dimensional Non-Linear Finite Element Model for Structural Concrete.", Part 2, Generality study, Proceeding of the Institution of Civil Engineers, Part 2, Vol.91, Sept., pp.545-560.

Vidosa F. G., Kotsovos M. D. and Pavlovic M. N. (1991c)
"Non-Linear Finite Element Analysis of Concrete Structures: Performance of a Fully Three-Dimensional Brittle Model.", Computers and Structures, Vol.40, No.5, pp.1287-1306.

Wegmuller A. W. (1974)
"Elastic-Plastic Finite Element Analysis of Plates.", Technical Notes TN99, Proceeding of the Institute of Civil Engineers, Vol.57(2), Sep., pp.535-543.

Zienkiewicz O. C. and Taylor R. L. (1989)
The Finite Element Method., McGraw-Hill Book Company.